



**DIVISION DE EDUCACION CONTINUA  
FACULTAD DE INGENIERIA U.N.A.M.**

LA MECANICA DE ROCAS APLICADAS A LA MINERIA  
Y A LA CONSTRUCCION

ETAPAS DE INVESTIGACION DEL SITIO

ING. JOSE LUIS ROSAS LOPEZ

MAYO. 1985

## 1. ETAPAS DE INVESTIGACION DEL SITIO.

### 1.1. INTRODUCCION.

En este capítulo se pretende establecer una secuencia ordenada y bien planeada de actividades para realizar un estudio geológico ingenieril, básico para prever o resolver cualquier problema de Mecánica de Rocas.

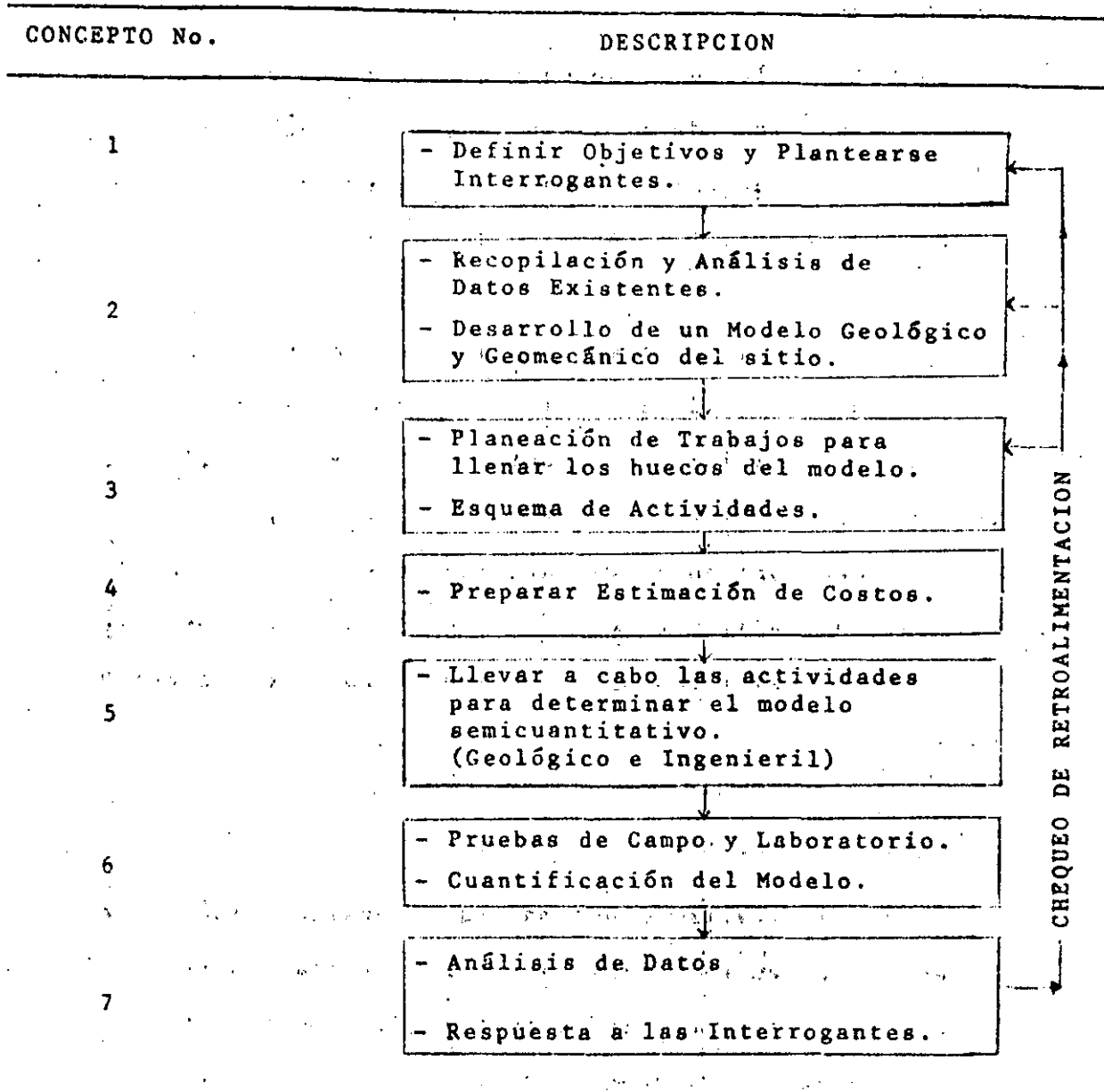
En primer lugar, se presentará un diagrama general, con las secuencias de distintas actividades para planear la investigación de un sitio; posteriormente, se establecerán las etapas que deben llevarse a cabo en un estudio geológico-ingenieril, mencionando brevemente sus objetivos, las actividades que se realizan en cada una de ellas y las herramientas o técnicas auxiliares para el desarrollo de estas actividades.

### 1.2. DIAGRAMA GENERAL DE ACTIVIDADES.

La figura 1 ilustra de una manera general el tipo de actividades que deben realizarse para planear una investigación de un sitio. El diagrama es idealizado y no representa una secuencia de actividades en orden rígido. El número y orden de conceptos varía de trabajo a trabajo.

A continuación se desarrolla con mayor detalle los alcances de los diversos conceptos de la figura 1.

FIGURA 1



## DESCRIPCION DE CONCEPTOS DE LA FIGURA 1

CONCEPTO NO.	DESCRIPCION
1	Definir los objetivos ingenieriles de la investigación, lo cual es, las interrogantes que se necesitan contestarse.
2	Recopilar y analizar los datos existentes en el sitio y de estos, desarrollar un "modelo geológico y geomecánico" tentativo del sitio.
3	Planear los trabajos de investigación requeridos para llenar los "Huecos" en los modelos tentativos, esto es, definir objetivos (tanto de naturaleza geológica como ingenieril) y preparar un esquema de actividades para alcanzar esos objetivos.
4	Preparar una estimación de costos teniendo en mente la importancia y los costos totales del proyecto, y también que los costos actuales de la investigación del sitio dependeran en gran medida de las condiciones subterráneas encontradas.
5	Llevar a cabo las investigaciones para completar el modelo con datos semicuantitativos (geológicos e ingenieriles).
6	Realizar las pruebas de campo y/o laboratorio para cuantificar los parámetros críticos en el modelo geológico y geomecánico.
7	Análisis de todos los datos tomando en cuenta los efectos de interacción entre la estructura ingenieril y los materiales del sitio. De este análisis, se deben responder las interrogantes mencionadas en 1.

Si, al final del concepto 7, todas las preguntas están contestadas con suficiente grado de confiabilidad, la investigación está completa. Si, no obstante, algunas interrogantes no están contestadas satisfactoriamente, los conceptos 3 a 7 deberán ser repetidos hasta obtener una respuesta satisfactoria.

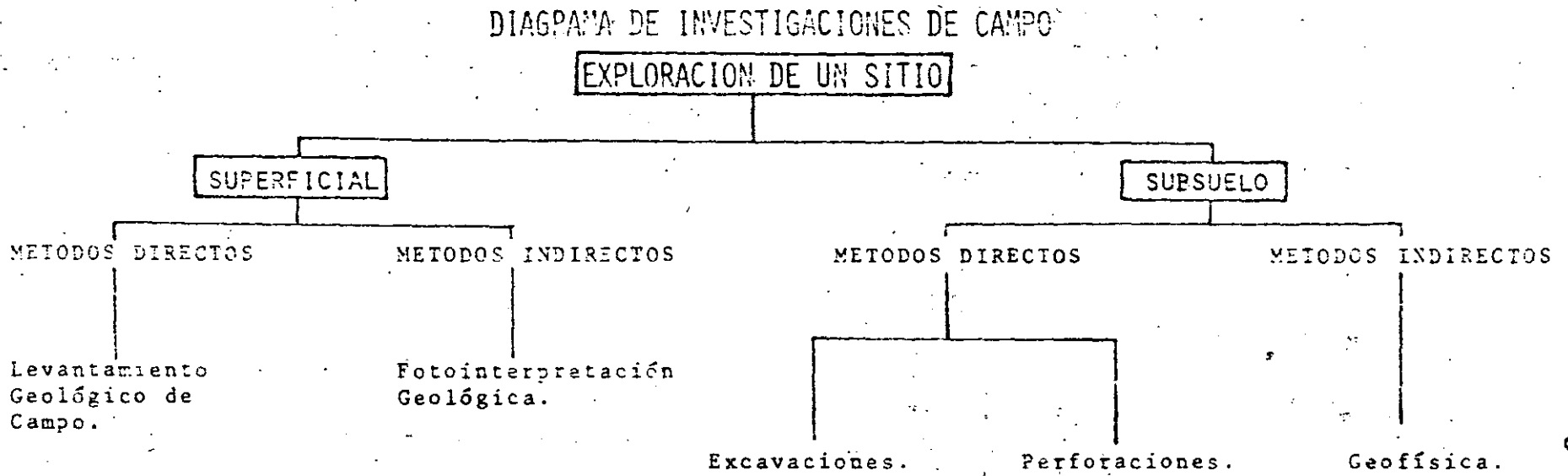
### 1.3. ETAPAS DE INVESTIGACION.

Una vez mencionada la secuencia general de actividades para una investigación del sitio, se procederá a analizar las etapas particulares para desarrollar un estudio geológico con fines de Mecánica de Rocas.

De una manera general, las investigaciones de campo pueden dividirse en dos grandes grupos: exploración superficial y exploración subterránea, mostradas en el diagrama de organización de la figura 2. Estas exploraciones varían en su objetivo, número, espaciamiento, profundidad, etc., de acuerdo con la etapa de investigación, así como por el tipo de obra, localización y acceso al sitio, condiciones geológicas y topográficas, equipo disponible y otros factores.

Las tres principales etapas de investigación geológica para fines de Mecánica de Rocas son:

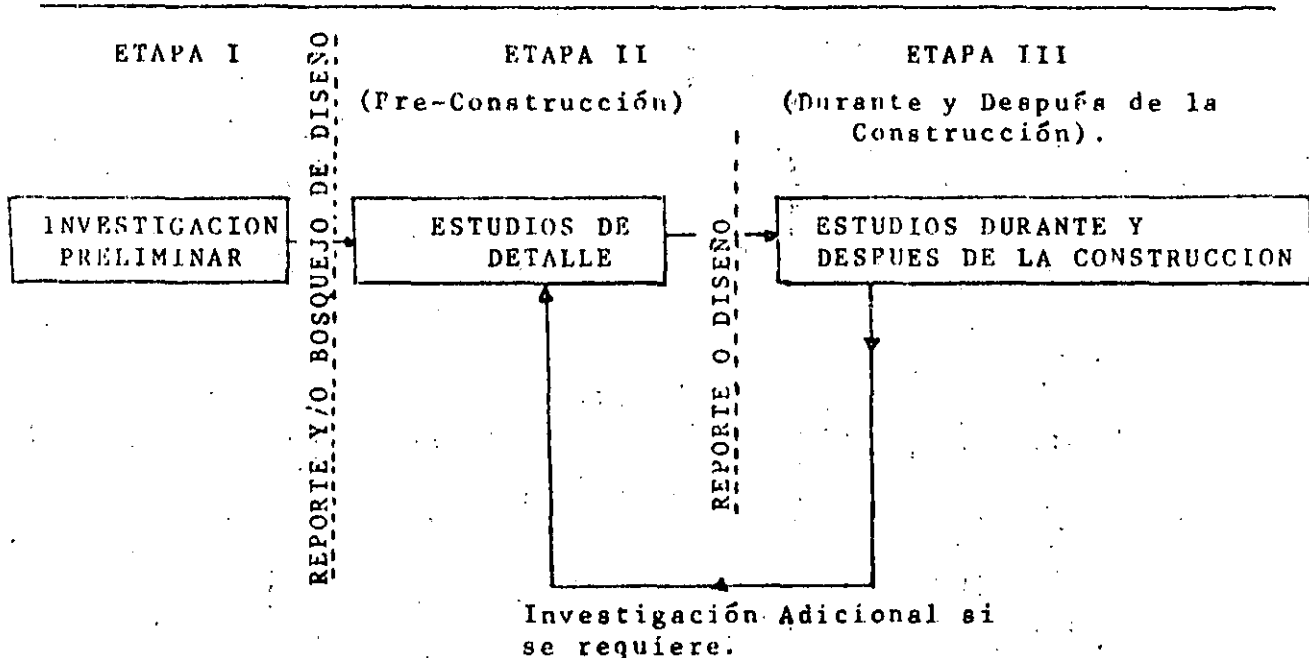
FIGURA 2



1. Investigación preliminar.
2. Estudios de detalle.
3. Estudios durante y después de la construcción.

La figura 2 muestra esquemáticamente las etapas básicas de investigación.

FIGURA 2  
FASES DE INVESTIGACION



En la práctica las etapas se fusionan cada una, pero deben ser mostradas independientemente para auxiliar a la siguiente presentación, y en la planeación y ejecución de trabajos.

Lo más conveniente es llevar a cabo las tres etapas en el orden mostrado; sin embargo, aquí influyen diversos aspectos, como el tipo de obra, su importancia, aspectos financieros o las condiciones geológicas, entre otros. Por ejemplo, si el sitio es muy pequeño, poco importante, o con la geología sencilla, para justificar los estudios detallados.

(etapa II), ocasionará que después de la etapa I se pasará a los estudios durante la construcción. Por lo tanto, cada obra requiere la planeación particular de sus etapas, con sus objetivos y actividades a realizar.

#### I. INVESTIGACION PRELIMINAR.

Los objetivos de la investigación geológica preliminar son reunir la mayor cantidad de información de una manera amplia, rápida y económica que permitan conocer las características generales del área de estudio, y así poder planear cuales son los datos adicionales que se requiere conocer, ampliar o detallar, y las técnicas más apropiadas para obtenerlos.

Es importante que en esta etapa colabore un geólogo con experiencia en geotécnica, ya que de estos trabajos serán la pauta para la planeación de estudios posteriores.

Las actividades que comunmente se realizan en esta etapa son las siguientes:

- Recopilación, procesamiento y análisis de la información existente; en donde se incluye estudios e informes geológicos del área de interés y sus alrededores; así como cartas topográficas, hidrológicas y geológicas de la región.
- Si es posible, se efectuarán vuelos de reconocimiento aéreo, con avioneta o helicóptero.



- Reconocimientos por caminamientos, de preferencia realizado por un cuerpo de ingenieros con experiencia, en donde debe llevarse a cabo una toma de muestras de roca y observaciones del marco geológico general.
- Cróquis geológico con brújula y cinta.
- Trabajos del subsuelo, como perforaciones, geofísica, etc, que se realizan si hay la necesidad de confirmar la información subterránea para el diseño, cuando no habrá etapa II, o para auxiliar a la planeación de un programa de estudios del subsuelo completo en la etapa II.
- Instrumentación preliminar de un sitio; por ejemplo, puede realizarse la instalación de simples piezómetros.

De los estudios preliminares debe resultar un informe en el que se indique la planeación de los estudios de detalle de la etapa siguiente.

## II. ESTUDIOS DETALLADOS.

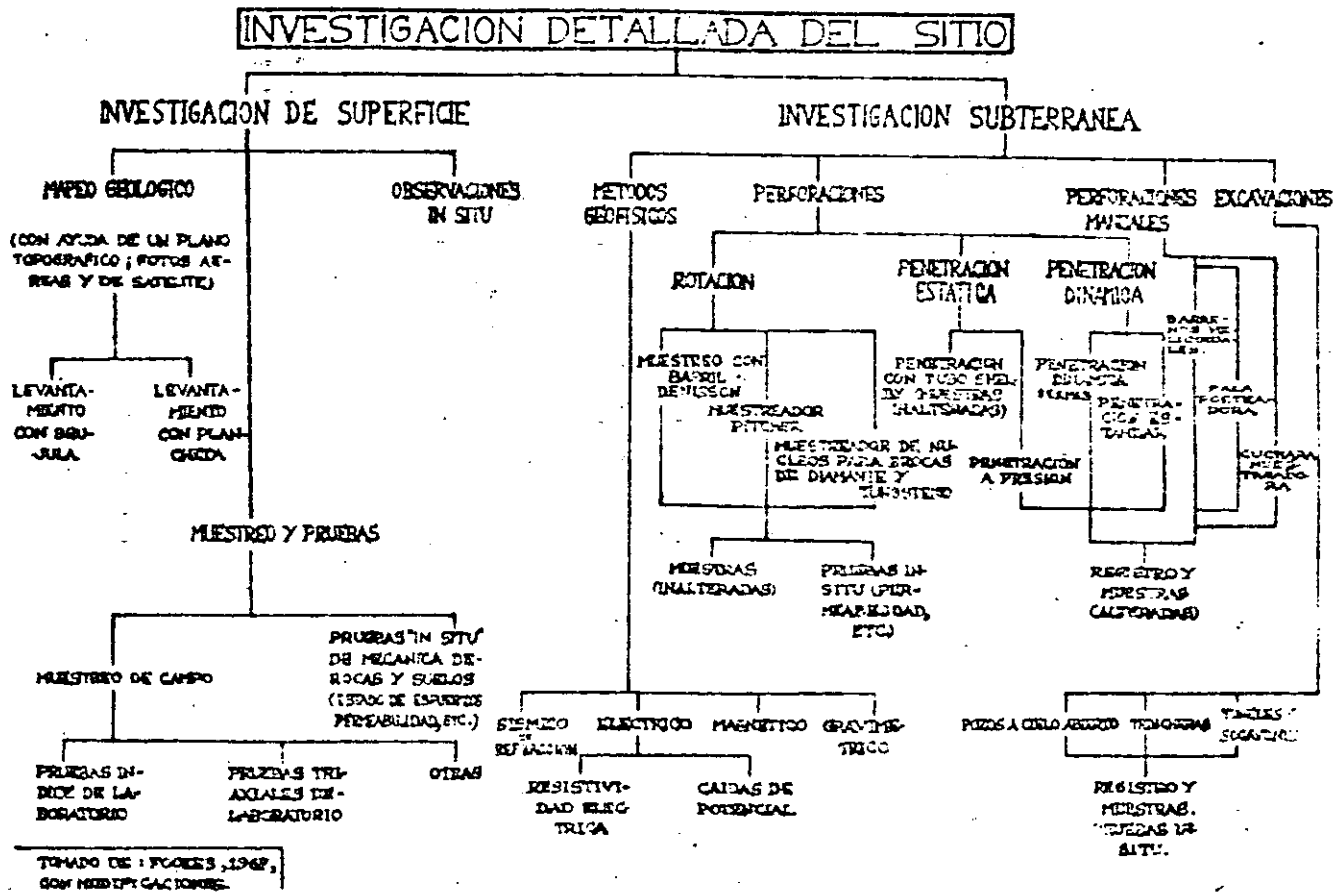
Siempre precedidos por una investigación preliminar, los estudios detallados tienen como finalidad el tratar de entender la geología completa del sitio y sus alrededores. Así mismo, en esta etapa deben obtenerse todos los datos necesarios para que el mecanista de rocas pueda diseñar satisfactoriamente los tratamientos o soportes necesarios según el tipo de obra.

La amplitud de los trabajos de esta etapa depende de la extensión e importancia de la obra a construir. Las actividades que se realizan durante un estudio detallado son:

- Mapeo geológico y/o geotécnico superficial a escala adecuada, auxiliado de una fotointerpretación detallada y un levantamiento de campo completo, con la finalidad de presentar la distribución de las formaciones geológicas y/o litológicas, así como los rasgos estructurales que afectan a las rocas.
- Mapeo geotécnico del subsuelo, el cual se lleva a cabo con el auxilio de técnicas directas e indirectas que permiten conocer la distribución de las unidades litológicas y sus características geológicas e ingenieriles.
- Obtención de muestras del subsuelo para estudios de laboratorio, y/o realización de pruebas "in situ" para conocer las propiedades índice y mecánicas de los macizos rocosos.
- La información obtenida de las actividades anteriores debe ser procesada e interpretada adecuadamente para que sea de máxima utilidad en el diseño.

Existen una gran variedad de técnicas que pueden ser usadas para un estudio detallado completo (Figura 4); pero debe llevarse a cabo una selección y coordinación adecuada de ellas para lograr obtener la información adecuada y mantener los costos bajos. Sin embargo, no deben escatimarse gas

FIGURA 4



tos de exploración, pues la falta de información o su mala calidad pueden provocar un diseño inadecuado que ocasione fallas peligrosas, o problemas constructivos y económicos, o bien un mal funcionamiento de la obra.

Las técnicas o métodos de exploración se tratarán con detalle en el siguiente capítulo de este curso.

### III. ESTUDIOS DURANTE Y DESPUES DE LA CONSTRUCCION.

Esta etapa de estudios es de suma importancia para la Mecánica de Rocas, ya que al construir una obra, en general se remueven las capas de materiales superficiales y se llegan a las zonas de desplante de estructuras, o bien en los túneles, se entra de lleno a la franja de materiales a excavar; esto significa que se puede confirmar los datos previstos en los estudios anteriores, o bien si es necesario, pueden obtenerse nuevos datos que modifiquen el diseño o el procedimiento constructivo.

Desgraciadamente no en todas las obras es posible realizar estudios durante la construcción; además es conveniente que el geólogo que realizó la etapa de estudios de detalle continúe durante los trabajos de construcción para que verifique y actualice la información geotécnica.

Las actividades que se desarrollan durante esta etapa incluyen:

- Levantamiento geológico y geotécnico de las obras durante

la excavación de túneles, desmonte de taludes, apertura de cortes y trincheras, explotación de bancos de material, etc. Deben realizarse en forma periódica.

- Mapeo Geotécnico Superficial y del Subsuelo; elaborando planos y secciones geotécnicas con información completa y actualizada.
- Muestreo para la realización de pruebas de laboratorio, así como pruebas "in situ" en zonas de interés o con problemas.
- Instrumentación directa.

Con esta información se procederá a ajustar o modificar en caso necesario el diseño de las obras.

Los métodos de investigación son en general, los mismos que se emplean en la etapa II (figura 4); sin embargo, existen algunas técnicas más adecuadas para esta etapa por realizarse en las zonas de interés, como los métodos geosísmicos, los socavones y las pruebas de campo.

#### 1.4. PLANEACION.

Las tres etapas descritas deben desarrollarse en una secuencia adecuada de técnicas para realizar un trabajo eficiente y a bajos costos. Esto puede lograrse estableciendo planes con rutas críticas que se basen en las condiciones geológicas del sitio y en las mejores técnicas que permitan evaluar

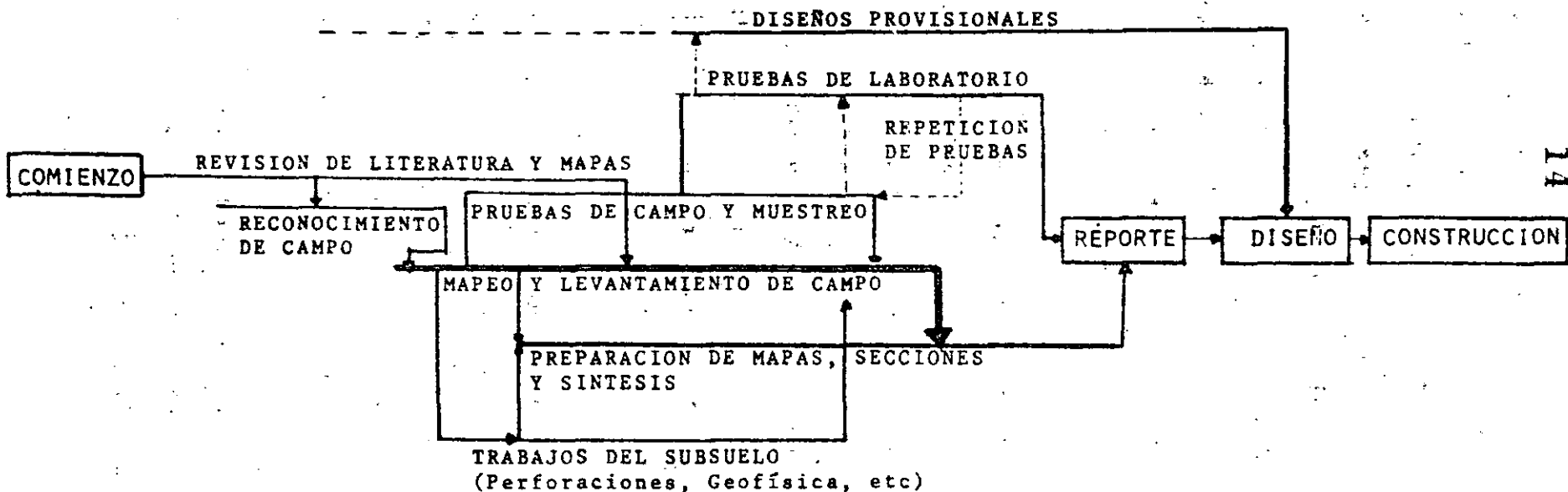
la información y predecir los problemas geotécnicos. Cada sitio requiere su propia ruta crítica, la cual debe ir diseñada para ella y modificada según los avances de trabajo y la información geológica. Por ejemplo, la figura 5 es una idealización generalizada de una ruta durante las etapas I y II para una presa media a grande, donde el aluvión o cubierta superficial no cubre totalmente a todo el sitio. En este caso la investigación se desarrolla principalmente durante el mapeo geológico ingenieril.

La investigación comienza con una revisión de literatura y mapas, seguida por reconocimientos de campo realizados por ingenieros geólogos, junto con mecanisistas de rocas y suelos. Los trabajos de campo propiamente dichos comienzan con un mapeo geológico y según se avance en el conocimiento geológico se irán programando las perforaciones o sondeos para comenzar los trabajos del subsuelo. Los pozos a cielo abierto y trincheras son realizadas para complementar el mapeo abajo de la cubierta superficial y para facilitar el muestreo; las muestras son enviadas al laboratorio para efectuarles pruebas, mientras se grafican los barrenos y se elaboran los planos; posteriormente se dibujan las secciones del subsuelo, y se evalúan y sintetizan los resultados de las pruebas de campo y laboratorio.

Los problemas geotécnicos específicos del sitio deben entonces estar claros y deben ser investigados de manera de obtener la mayor información sobre ellos. Finalmente, cuando toda la información esta completamente comprendida y cada aspecto ha sido provado, se procede a preparar el reporte final.

FIGURA 5. ORGANIZACION DE INVESTIGACIONES: EJEMPLO DE UN PLAN DE RUTA CRITICA PARA UNA PRESA DE TAMAÑO MEDIO.

### RUTA CRITICA GENERAL PARA INVESTIGACIONES





**DIVISION DE EDUCACION CONTINUA  
FACULTAD DE INGENIERIA U.N.A.M.**

MECANICA DE ROCAS APLICADA A LA MINERIA Y A LA CONSTRUCCION

SUGGESTED METHODS FOR THE QUANTITATIVE DESCRIPTION OF  
DISCONTINUITIES IN ROCK MASSES

MAYO, 1985



**INTERNATIONAL SOCIETY FOR ROCK MECHANICS  
COMMISSION ON  
STANDARDIZATION OF LABORATORY AND FIELD TESTS**

**SUGGESTED METHODS  
FOR THE QUANTITATIVE DESCRIPTION OF  
DISCONTINUITIES IN ROCK MASSES**

**CONTENTS:**

	<b>Page</b>
INTRODUCTION (Historical)	320
ACKNOWLEDGEMENTS	320
INTRODUCTION (TECHNICAL)	321
GLOSSARY	321
SAMPLING PHILOSOPHY	322
Suggested methods for the quantitative description of the following:	
1. ORIENTATION	322
(A) Compass and Clinometer-Method	322
(B) Photogrammetric Method	330
2. SPACING	333
3. PERSISTENCE	335
4. ROUGHNESS	338
5. WALL STRENGTH	346
6. APERTURE	351
7. FILLING	353
8. SEEPAGE	356
9. NUMBER OF SETS	359
10. BLOCK SIZE	360
11. DRILL CORE	363

The Commission on Standardization of Laboratory and Field Tests on Rock was appointed in 1967. Subsequent to its first meeting in Madrid in October 1968, the Commission circulated a questionnaire to all members of the International Society for Rock Mechanics, the answers received clearly showing a general desire for standardized testing procedures. At a further meeting in Oslo in September 1969, tests were categorized and a priority for their standardization was agreed upon.

Subsequent meetings were held in Belgrade in September 1970, in Nancy in October 1971, in Lucerne in September 1972, in Katowice in October 1973, in Denver in September 1974, in Minneapolis in September 1975, in Salzburg in October 1976 and in Stockholm in September 1977. At the Lucerne meeting the Commission was subdivided into two committees, one on standardization of laboratory tests and the second on the standardization of field tests.

The present document, which covers category I(9) in Table 1, has been produced through the efforts of an international Working Party consisting of a large number of individuals, including several members of the Committee on Field Tests. A list of contributors is given below. Most of the work has been through correspondence, coordinated by Tór Brekke (before 1974) and by Nick Burton (since 1974). Meetings of the Working Party were held in Denver in September 1974 and in Minneapolis in September 1975.

The purpose of these "Suggested Methods" is to achieve some degree of uniformity in the description of discontinuities in rock masses, as an aid to communication between the geologist and the engineer. However, the various suggested methods should not be treated as standard procedures, rather as a frame of reference. The description of rock masses and discontinuities is necessarily a subjective operation and it must not be expected that the same degree of standardisation can be achieved as in the testing of a rock specimen.

Any person interested in these recommendations and wishing to suggest additions or modifications should address his remarks to the Secretary General, International Society for Rock Mechanics, Laboratório Nacional de Engenharia Civil, Avenida do Brasil, Lisboa 5, Portugal.

**Acknowledgements:** The following persons contributed in the drafting of these "Suggested Methods": W. E. Bamford, C. M. Barton, B. MacMahon (Australia); M. A. Kaniji (Brazil); K. Babcock, J. M. Boyd, D. Cruden, J. A. Franklin, G. Herget, G. Mackoed and D. J. Piteau (Canada); D. Cawsey, W. Dearman, M. DeFreitas, J. M. Edmond, P. G. Fooks, and T. R. Harper (England); K. Saito, M. Fagundinho (Finland); K. John (Germany); G. Manfredini (Italy); A. Bello (Mexico); N. Rengers (Netherlands); N. Barton (Norway); H. Barkey, R. Lien, T. Loken, F. Loset, and A. Palmström (Norway); N. F. Grossman and R. Oliveira (Portugal); J. H. DeBeet, J. E. Jennings (South Africa); M. Bergman and I. Hansagi (Sweden); D. C. Banks, T. L. Brekke, D. U. Deere, H. H. Finsten, C. H. Miller, H. J. Pincus, D. Ross-Brown and J. Warriner (United States of America); J. Obrudovic (Yugoslavia). 44 individuals, 14 countries.

TABLE 1. TEST CATEGORIES FOR STANDARDIZATION

**Category I: Classification and Characterization****Rock material (laboratory tests)**

- (1) Density, water content, porosity, absorption.
- (2) Strength and deformability in uniaxial compression; point load strength.\*
- (3) Anisotropy indices.
- (4) Hardness, abrasiveness.\*
- (5) Permeability.
- (6) Swelling and slake-durability.\*
- (7) Sound velocity.\*
- (8) Micro-petrographic descriptions.\*

**Rock mass (field observations)**

- (9) Joint systems: orientation, spacing, openness, roughness, geometry, filling and alteration.\*
- (10) Core recovery, rock quality designation and fracture spacing.
- (11) Seismic tests for mapping and as a rock quality index.
- (12) Geophysical logging of boreholes.\*

**Category II: Engineering Design Tests****Laboratory**

- (1) Determination of strength envelope (triaxial and uniaxial compression and tensile tests).\*
- (2) Direct shear tests.\*
- (3) Time-dependent and plastic properties.

**In situ**

- (4) Deformability tests.\*
- (5) Direct shear tests.\*
- (6) Field permeability, ground-water pressure and flow monitoring; water sampling.
- (7) Rock stress determination.\*
- (8) Monitoring of rock movements, support pressures, anchor loads, rock noise and vibrations.
- (9) Uniaxial, biaxial and triaxial compressive strength.
- (10) Rock anchor testing.\*

\* Asterisks indicate that final drafts on these tests have been prepared.

## INTRODUCTION (TECHNICAL)

The majority of rock masses, in particular those within a few hundred meters from the surface, behave as discontinua, with the discontinuities largely determining the mechanical behaviour. It is therefore essential that both the structure of a rock mass and the nature of its discontinuities are carefully described in addition to the lithological description of the rock type. Those parameters that can be used in some type of stability analysis should be quantified whenever possible.

For example, in the case of rock slope stability certain quantitative descriptions can be used directly in a preliminary limit equilibrium analysis. The orientation, location, persistence, joint water pressure and shear strength of critical discontinuities will be direct data for use in analysis. For purposes of preliminary investigation the last two parameters can probably be estimated with acceptable accuracy from a careful description of the nature of the discontinuities. Features such as roughness, wall strength, degree of weathering, type of infilling material, and signs of water seepage will therefore be important indirect data for this engineering problem.

For the case of tunnel stability and estimation of support requirements, all the descriptions will tend to be indirect data since a direct analysis of stability has yet to be developed. However, a careful description of the structure of a rock mass and the nature of its discontinuities can be of inestimable value for extrapolating experience of support performance to new rock mass environments. Descriptions should be sufficiently detailed that they can form the basis for a functional classification of the rock mass.

In time, as descriptions of rock masses and discontinuities become more complete and unified, it may be possible to design engineering structures in rock with a minimum of expensive *in situ* testing. In any case careful field description will enhance the value of *in situ* tests that are performed, since the interpretation and extrapolation of results will be made more reliable.

## GLOSSARY

A selection of terms commonly used in these "Recommended Methods" are defined here. Contributors to the Working Party were divided in their recommendations for the best general term to represent all "breaks" in rock masses. However, a clear majority preferred *discontinuity* rather than *fracture*, as the collective term for all joints, bedding planes, contacts and faults.

*Joint*

A break of geological origin in the continuity of a body of rock along which there has been no visible displacement. A group of parallel joints is called a set and joint sets intersect to form a joint system. Joints can be open, filled or healed. Joints frequently form parallel to bedding planes, foliation and cleavage and may be termed bedding joints, foliation joints and cleavage joints accordingly.

*Fault*

A fracture or fracture zone along which there has been recognisable displacement, from a few centimeters to a few kilometres in scale. The walls are often striated and polished (slickensided) resulting from the shear displacement. Frequently rock on both sides of a fault is shattered and altered or weathered, resulting in fillings such as breccia and gouge. Fault widths may vary from millimetres to hundreds of metres.

*Discontinuity*

The general term for any mechanical discontinuity in a rock mass having zero or low tensile strength. It is the collective term for most types of joints, weak bedding planes, weak schistosity planes, weakness zones and faults. The ten parameters selected to describe discontinuities and rock masses are defined below:

1. *Orientation*—Attitude of discontinuity in space. Described by the *dip direction* (azimuth) and *dip* of the line of steepest declination in the plane of the discontinuity. Example: *dip direction/dip* (015°/35°).
2. *Spacing*—Perpendicular distance between adjacent discontinuities. Normally refers to the mean or modal spacing of a set of joints.
3. *Persistence*—Discontinuity trace length as observed in an exposure. May give a crude measure of the real extent or penetration length of a discontinuity. Termination in solid rock or against other discontinuities reduces the persistence.
4. *Roughness*—Inherent surface roughness and waviness relative to the mean plane of a discontinuity. Both roughness and waviness contribute to the shear strength. Large scale waviness may also alter the dip locally.
5. *Wall Strength*—Equivalent compression strength of the adjacent rock walls of a discontinuity. May be lower than rock block strength due to weathering or alteration of the walls. An important component of shear strength if rock walls are in contact.

6. *Aperture*--Perpendicular distance between adjacent rock walls of a discontinuity, in which the space is air or water filled.
7. *Filling*--Material that separates the adjacent rock walls of a discontinuity and that is usually weaker than the parent rock. Typical filling materials are sand, silt, clay, breccia, gouge, mylonite. Also includes thin mineral coatings and healed discontinuities, e.g. quartz and calcite veins.
8. *Seepage*--Water flow and free moisture visible in individual discontinuities or in the rock mass as a whole.
9. *Number of Sets*--The number of joint sets comprising the intersecting joint system. The rock mass may be further divided by individual discontinuities.
10. *Block Size*--Rock block dimensions resulting from the mutual orientation of intersecting joint sets and resulting from the spacing of the individual sets. Individual discontinuities may further influence the block size and shape.

### SAMPLING PHILOSOPHY

Geological engineering investigations are generally carried out in several stages, to provide information appropriate detail to the current state of the project:

- (i) feasibility
- (ii) detailed planning
- (iii) construction/operation

The degree of detail required for each stage will vary considerably from project to project.

There are two basic levels at which a rock mass survey may be carried out depending upon the amount of detail that is required. In a *subjective* (biased) survey, only those discontinuities which appear to be important are described. In an *objective* (random) survey all discontinuities intersecting a fixed line or area of rock exposure are described.

A prerequisite for both types of survey is the study of any available geological maps followed by a geological reconnaissance of rock types, major geological structures, faults, dykes, and lithological contacts. A study of air photographs will often be invaluable for planning this reconnaissance. At this preliminary stage, efforts should be made to recognise *domains*, where systematic features such as joints possess similar orientation or spacing. The fabric of the rock mass is statistically homogeneous in a domain.

The objective approach to sampling suffers from the major disadvantage that it is time consuming. Some form of automatic data processing may be required to analyse all the data. However, if structural domains cannot readily be delineated there may be no alternative. The subjective approach is best applied where structural domains are clearly recognised. This will save time and effort and will usually reveal all the discontinuity systems found in any subsequent line or area survey.

Rock masses and their component discontinuities can be described by the principal methods:

- (a) outcrop description
- (b) drillcore and drillhole description
- (c) terrestrial photogrammetry

### 1. ORIENTATION

#### (A) *Compass and Clinometer Method*

Scope

(a) The orientation of a discontinuity in space is described by the *dip* of the line of steepest declination measured from horizontal, and by the *dip direction* measured clockwise from true north. Example: *dip, direction/dip* (025°/45°).

(b) The orientation of discontinuities relative to an engineering structure largely controls the possibility of unstable conditions or excessive deformations developing. The importance of orientation increases when other conditions for deformation are present, such as low shear strength and a sufficient number of discontinuities or joint sets for slip to occur.

(c) The mutual orientation of discontinuities will determine the shape of the individual blocks, beds, or mosaics comprising the rock mass.

#### *Equipment*

(a) *Compass and clinometer*: Compasses which need to be levelled by means of a spherical bubble, before taking a dip reading with the lid parallel to the dip, have the advantage that the maximum declination (dip) is measured directly. Other types of clinometer need to be moved across the discontinuity wall until the maximum value is registered.

(b) When the rock is strongly magnetic a clinorule and 50 m tape, or a direct reading azimuth protractor can be used.

(c) When estimating the dip of inaccessible joints it

## Suggested Method for the Quantitative Description of Discontinuities

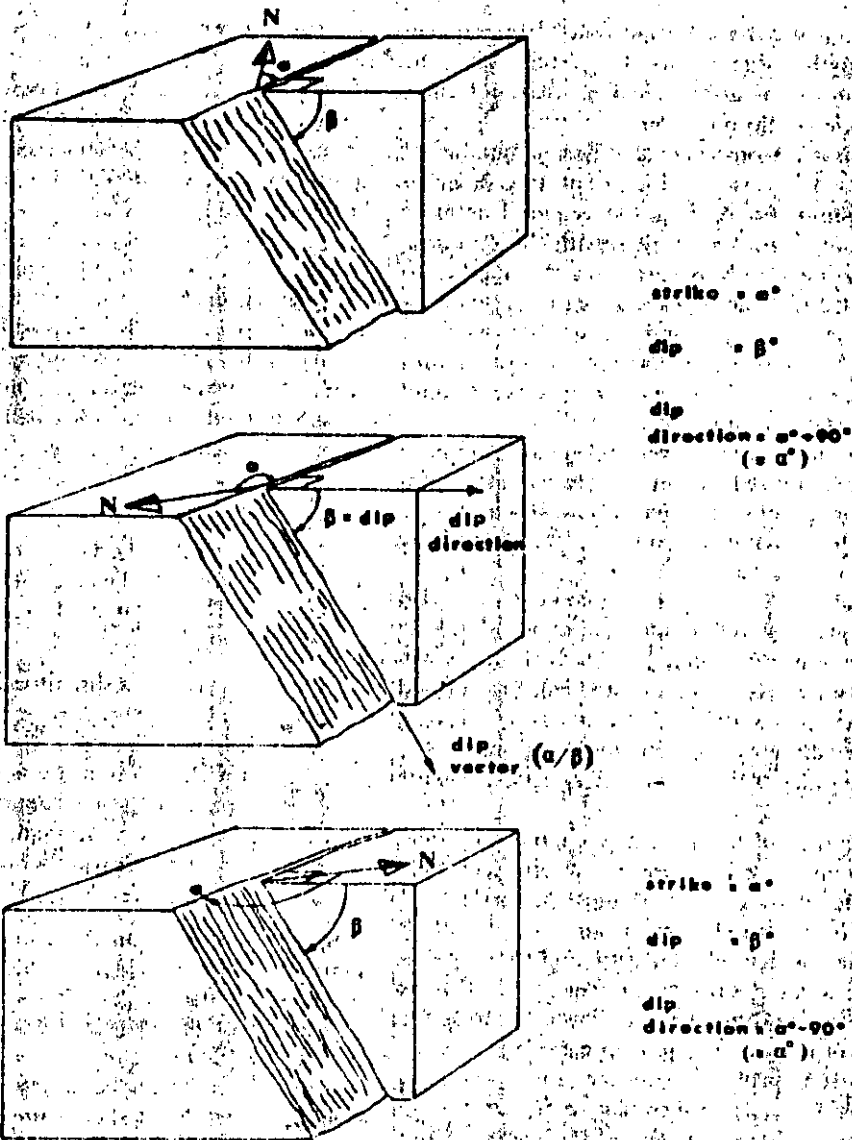


Fig. 1. Diagrams indicating the strike, dip and dip direction of three differently orientated planes.

convenient to use a clinometer with an inclinable sighting device; and incorporating a reflected image of a horizontal bubble.

#### Procedure

(a) The maximum declination (dip) of the mean plane of the discontinuity is measured with the clinometer, and should be expressed in degrees as a two digit number, e.g. 05° or 55° (00°-90°).

(b) The azimuth of the dip (dip direction) is measured in degrees counted clockwise from true north, and expressed as a three digit number, e.g. 010° or 105° (00°-360°).

(c) The dip direction and dip should be recorded in that order, with the three digit and two digit numbers separated by a line, e.g. 010°/05°. The pair of numbers represents the dip vector. See Fig. 1.

#### Notes

(a) Magnetic deflections caused by iron pipes or rails, or anomalies due to ore bodies will sometimes cause compass readings to be unreliable. In such cases a 50 m. long tape should be stretched parallel to the rock face or tunnel wall and orientated by means of plans and ground surveys. Dip direction can then be measured relative to this tape using a clino-rule, placing one leg parallel to the tape. The data should be corrected to true north before analysis of the field measurements is undertaken. Alternatively a direct reading azimuth protractor can be employed in place of the clino-rule and tape.

(b) The dip of discontinuities considered critical for stability should be measured using a down-dip base length exceeding the wave length of surface undulations. The local inclination of non-planar features rela-

tive to mean dip will be an important component in the shear strength of the surface in question. The estimated direction of potential movement may not coincide with the down-dip direction.

(c) It is desirable to measure a sufficient number of orientations to define the various joint sets of given domains. Opinions concerning the required number vary from about 80 to 300. A reasonable compromise would seem to be 150. It is clear that the number to be recommended will vary with the area to be mapped, with the randomness of the orientations, and with the detail required in subsequent analyses. If orientations are consistent, careful sampling will reduce the amount of orientation data considerably.

(d) Several countries on the European continent have for many years utilized survey equipment and compasses with horizontal scales divided into 400 parts (e.g. 0-400°). This has obvious advantages when measuring to decimal point accuracy.

The vertical circle of many clinometers is also expressed in quadrants of 100° instead of 90°. The particular system utilized should be clearly stated when orientation data is reported. For the purpose of soil and rock mechanics stability analyses it is most convenient to have dip measurements measured in, or converted to, the older 0-90° system. (Conversion factor: 9/10).

(e) The accuracy of compass and clinometer orientation measurements will depend on several factors of which the following are probably most important: accessibility of the plane of interest, areal extent of the exposed plane, degree of planarity and smoothness, occasional magnetic anomalies, human errors. Human errors can be reduced by using a clinometer to locate the direction of maximum dip, before taking the compass reading. It is probably sufficient for rock mechanics purposes to read *dip direction* to the nearest 5° and *dip* to the nearest even number of degrees. However, if poles are to be plotted it may in the end be more convenient to read to the nearest degree to reduce the occurrence of coincidental plotted points.

(f) The mean orientation of major discontinuities can be obtained by the *three point method*. The coordinates of three points lying in the plane of the discontinuity are all that is required. In the case of surface outcrops the coordinates may be determined by accurate location on a contoured relief map. The orientation of major features may also be estimated from three boreholes that intersect the plane. However less persistent features may not be intersected by all the holes.

(g) The orientation of minor discontinuities can be estimated from a single borehole, provided that the core can be orientated or that the borehole walls can be viewed. Core can sometimes be orientated using structural features such as bedding or foliation if these natural markers have consistent orientation. Several artificial orientation devices operated from the core barrel are also available, e.g. the Crælius core orientator. Alternatively, the orientation of minor discon-

tinuities can be estimated by down-the-hole visual techniques such as borehole television cameras, photographic cameras and borehole periscopes. Regardless of orientation, these methods also provide invaluable information concerning spacing, the thickness of the continuity fillings and the level of seepage paths. (See 11. Drill Core for details).

(h) A special core recovery method known as the integral sampling method [1] is recommended for obtaining orientation data in heavily fractured rock mass. The method essentially consists of recovering a core sample which has previously been reinforced with grouted bar whose azimuth is known from position rods. The reinforced bar is coaxially overcored with a larger diameter coring crown.

#### Presentation of results

(a) *Strike and dip symbols.* The simplest methods of data presentation are the strike and dip symbols drawn in the correct location on the geological map of the area. For example:

45° represents a discontinuity with a dip of 45° and strike as shown by the orientation of the line. The dip direction is indicated by the down-dip symbol.

— represents a horizontal discontinuity.

— represents a vertical discontinuity with strike as shown by the orientation of the line.

Space limitations on the geological map obviously limit the number of planes which can be represented in the above manner. Nevertheless, for giving a general impression of the principal discontinuity orientations they can be quite useful.

Further detail can be obtained by using different symbols to represent the various types of discontinuities. For example, the following symbols are often used to represent joints, bedding and foliation:

— joints      — bedding      — foliation

A clear key to symbol terminology should always be given.

The outcrop of major discontinuities should be drawn directly on geological maps. For example, thin continuous lines (—) can be used for major, persistent discontinuities that are visible, and thick broken lines (---) for major discontinuities whose persistence is implied, but which are locally covered.

(b) *Block diagrams.* At an early stage in the assessment and communication of raw field data it is helpful to present orientation measurements qualitatively using some visual technique. Perspective drawings such as that shown in Fig. 2(a) help to give an overall view of the relationship between the engineering structure and the rock mass structure. (If available, a stress ellipsoid giving the measured principal stress vectors might also be presented on such a diagram, to aid in the evaluation of the optimum orientation of the structure.)

Suggested Methods for the Quantitative Description of Discontinuities

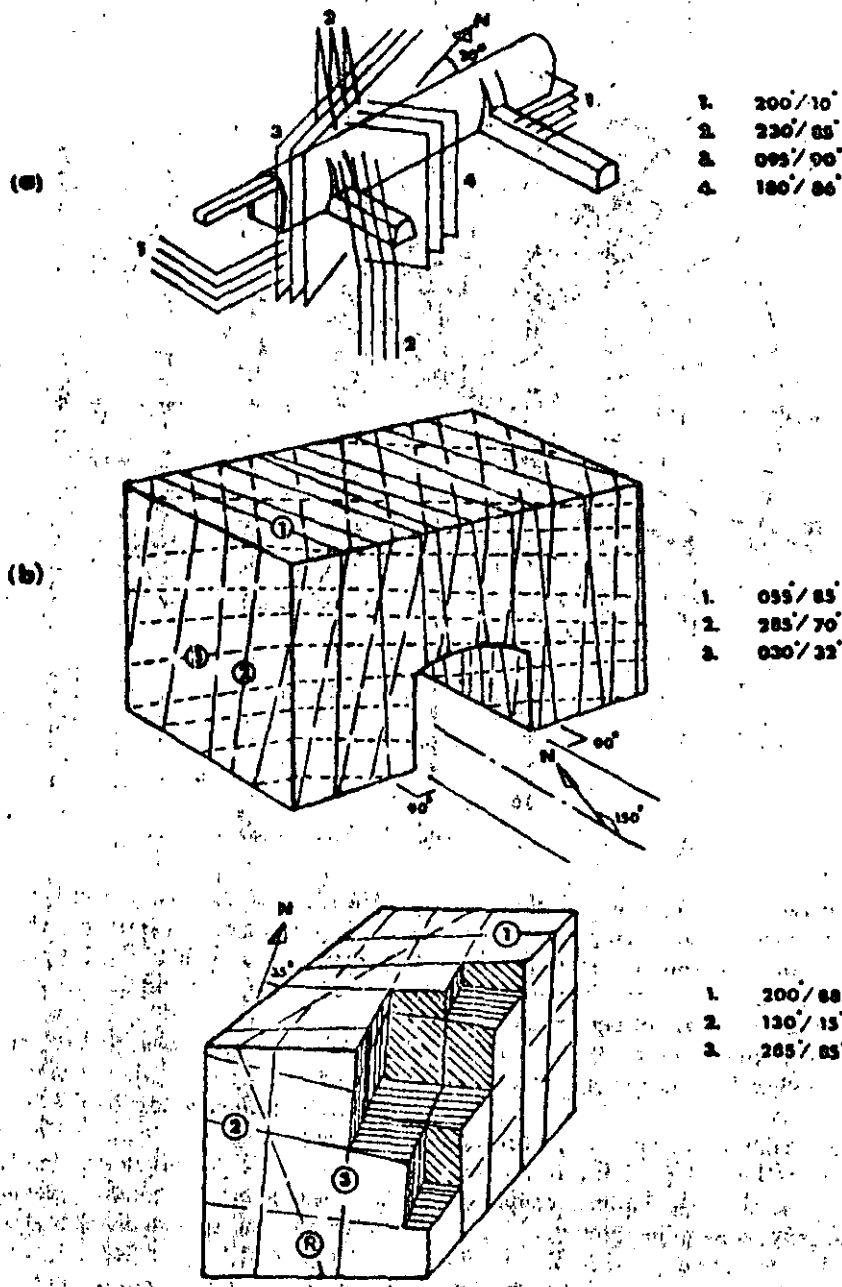


Fig. 2. Perspective views and block diagrams provide a qualitative picture of jointing and its relationship in engineering structures.

On a more detailed scale *block diagrams* can be used, such as that illustrated in Fig. 2(b). Many types of structure can be represented in this idealized manner, for example tunnel portals, cross-sections through tunnels or large rock caverns, rock slopes, dam abutments etc. (Depending upon the scale the discontinuity spacing and persistence may be represented in addition to the orientation.)

(Block diagrams showing "excavated" corners as in Fig. 2(c), give a visual impression of the rock structure. They are also a useful substitute for photographs where foliage or soil cover partly obscure the exposure.

In the examples shown in Fig. 2 it is helpful to

number the joint sets, show the orientation relative to true N, and list the dip direction and dip at the side of the diagram. (This is also helpful when presenting photographs of rock mass structures.)

(c) *Joint rosettes*. A common method of plotting and presenting a large number of orientation measurements in a more quantitative manner than the above is by means of joint rosettes.

In this instance measurements are represented on a simplified compass rose, marked from 0-360° (or 0-400°) with radial lines at 10° (or 10°) intervals. Observations are grouped in the nearest 10° sectors.

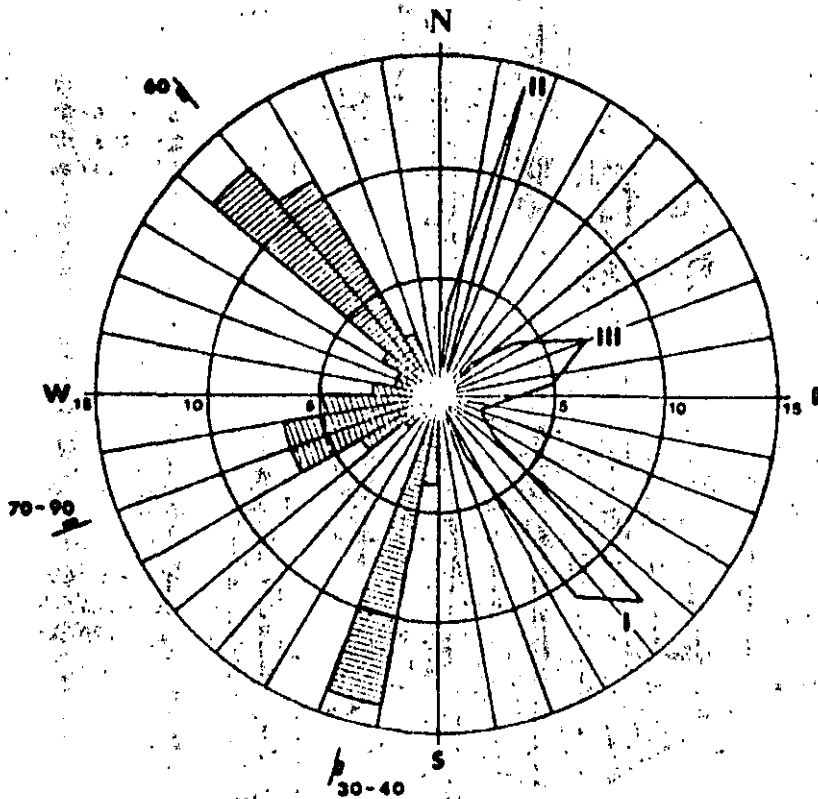


Fig. 3. Two methods of representing orientation data on a joint rosette.

The number of observations are represented along the radial axes, using numbered concentric circles representing 5, 10 and 15 observations, or as convenient. The resulting strike "petals" have mirror images about the centre of the rosette. The range of dip observations for each discontinuity set cannot be represented within the rosette and must therefore be shown outside the circumference.

Note that measurements of strike or dip direction of sub-horizontal discontinuities are inherently unreliable. Therefore in general, such features cannot be represented satisfactorily using joint rosettes.

It should be noted that although the joint rosette is a widely used polar diagram it misrepresents the data to some extent. Large concentrations are exaggerated and small concentrations are suppressed. This bias results from the fact that areas in each angle sector vary with the square of the radial coordinate, whereas in a true histogram the area of each bar or sector should vary with the frequency, not with the square of the frequency. (Accordingly the polar diagrams should ideally have a square-root radial scale, Pincus [2]).

Figure 3 shows two methods of representing orientation data on a joint rosette: The observations grouped in the nearest  $10^\circ$  (or  $10^\circ$ ) sectors can be represented either as solid radial sectors (left hand side), or their strike values averaged resulting in "petals" (right hand side). The latter method reduces the bias referred to above, but may not be satisfactory, if there is little dispersion of the data.

(The radius of the polar diagram can be used to good effect in plotting other parameters than the frequency of observation. A particularly useful parameter is the total observed length of discontinuities of given orientation.)

(d) *Spherical projection.* Several projection methods are used to represent the orientation of geological planes. The geological text books listed in the reference give comprehensive discussions of the various techniques available. In this short summary only one projection will be mentioned, the *equal area projection* (In this method the spatial distribution of data is accurately represented on a Schmidt, or Lambert net. In the case of *equal angle projection* the angular relationships between features are accurately represented by plotting data on a Wulff net.)

A discontinuity plane ( $\alpha/\beta$ ) can be uniquely represented as a great circle or as a pole on a reference hemisphere, when the centre of the sphere lies in the plane of the discontinuity. (See Fig. 4a.) For engineering purposes the lower reference hemisphere is used. A two dimensional representation is obtained by projecting this information onto an equal area net.

In Fig. 4(a) the pole P of the discontinuity K is the point of intersection of the normal to the plane with the lower hemisphere. To plot the pole on a polar equal area net (Fig. 4b), the dip  $\beta$  is counted from the centre of the net at right angles to the strike towards the periphery.

To plot the plane as a great circle on an equatorial equal area net (Fig. 4c), the strike ( $\alpha + 90^\circ$ ) is counted



## Suggested Methods for the Quantitative Description of Discontinuities

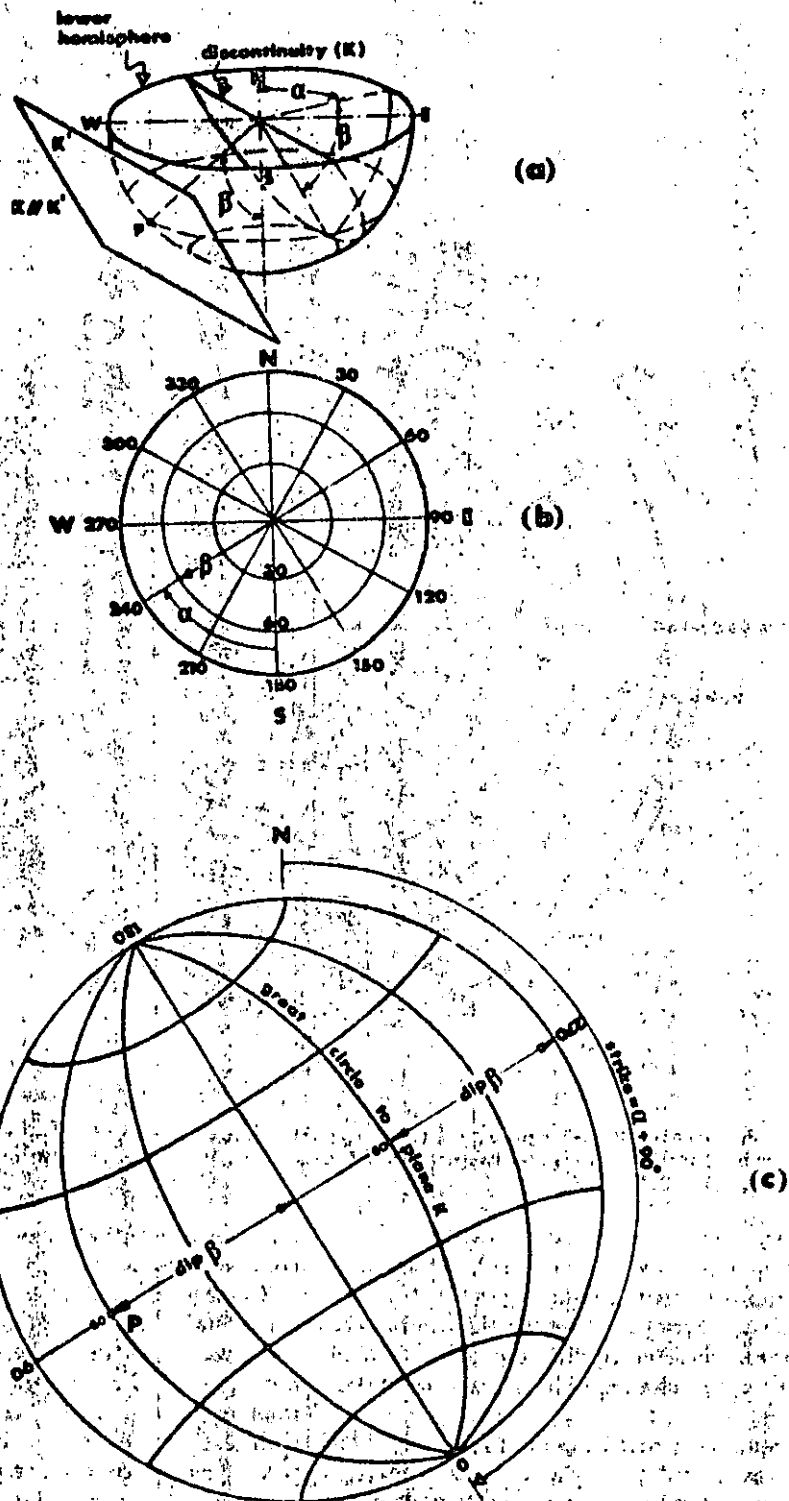


Fig. 4. Method of representing a discontinuity  $K$  as a pole  $P$  and as a great circle on a polar equal-area net (b) and on an equatorial equal-area net (c) using the lower reference hemisphere. A rotatable transparent overlay is used with the equatorial equal-area net.

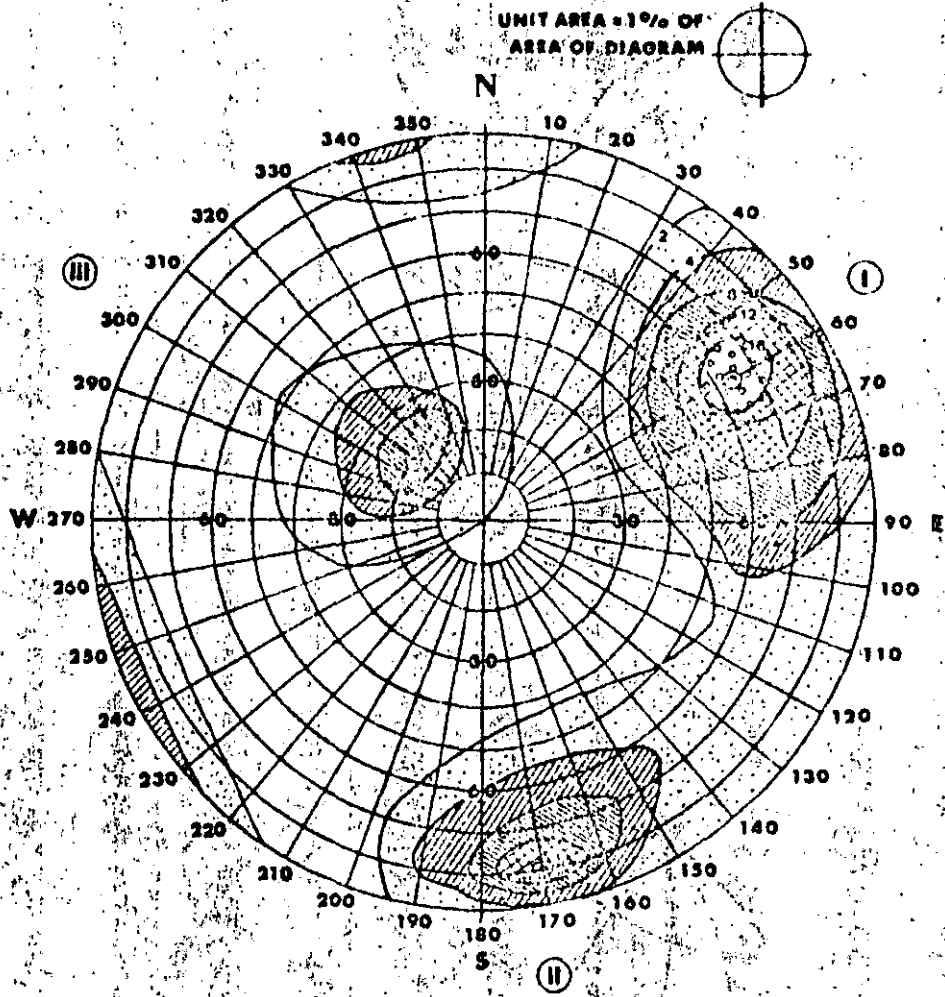


Fig. 5. Schmidt contour diagram representing the orientation of three sets of joints plotted on a polar equal-area net. The main sets I and II are approximately normal to each other, and the minor set III is nearly horizontal.

from north clockwise on the periphery, using a rotatable tracing or plastic overlay on which N has been marked. The dip is plotted at right angles to the strike, measured from the periphery towards the centre. The pole P can also be represented on the equatorial equal area net, both nets yielding the same geometrical distribution of poles.

The polar equal area net is the most convenient for plotting poles as no rotation of overlay is necessary. The first step in obtaining mean orientation data for the different discontinuity sets requires that clusters of poles can be visually recognised. The Schmidt contouring method is used to determine the pole densities, an example of which is shown in Fig. 5.

The contouring involves superimposing a square grid on the equal area net. A circle, shown in Fig. 5, which represents 1% of the total area of the equal area net, is placed with its centre at the grid intersections. The number of poles within the circle is counted and noted

on each grid intersection. Pole densities can then be contoured, using up to six contour intervals.

The central value of highest concentration of poles can be taken as representing the mean orientation of the given set of discontinuities. However, since they are variations from the mean, orientation is strictly a random variable with a certain dispersion associated with each mean value. Probability techniques are recommended for a more precise analysis. (It should be noted that density contours obtained by the Schmidt method violate probability theory since poles are counted more than once.)

Figure 6 illustrates the use of equatorial equal area nets for plotting both poles and great circles to represent typical rock mechanics problems, such as slope stability. Spherical projection methods are of greater value where stability depends on the relative three dimensional orientation of discontinuities and free surfaces.

## Suggested Methods for the Quantitative Description of Discontinuities

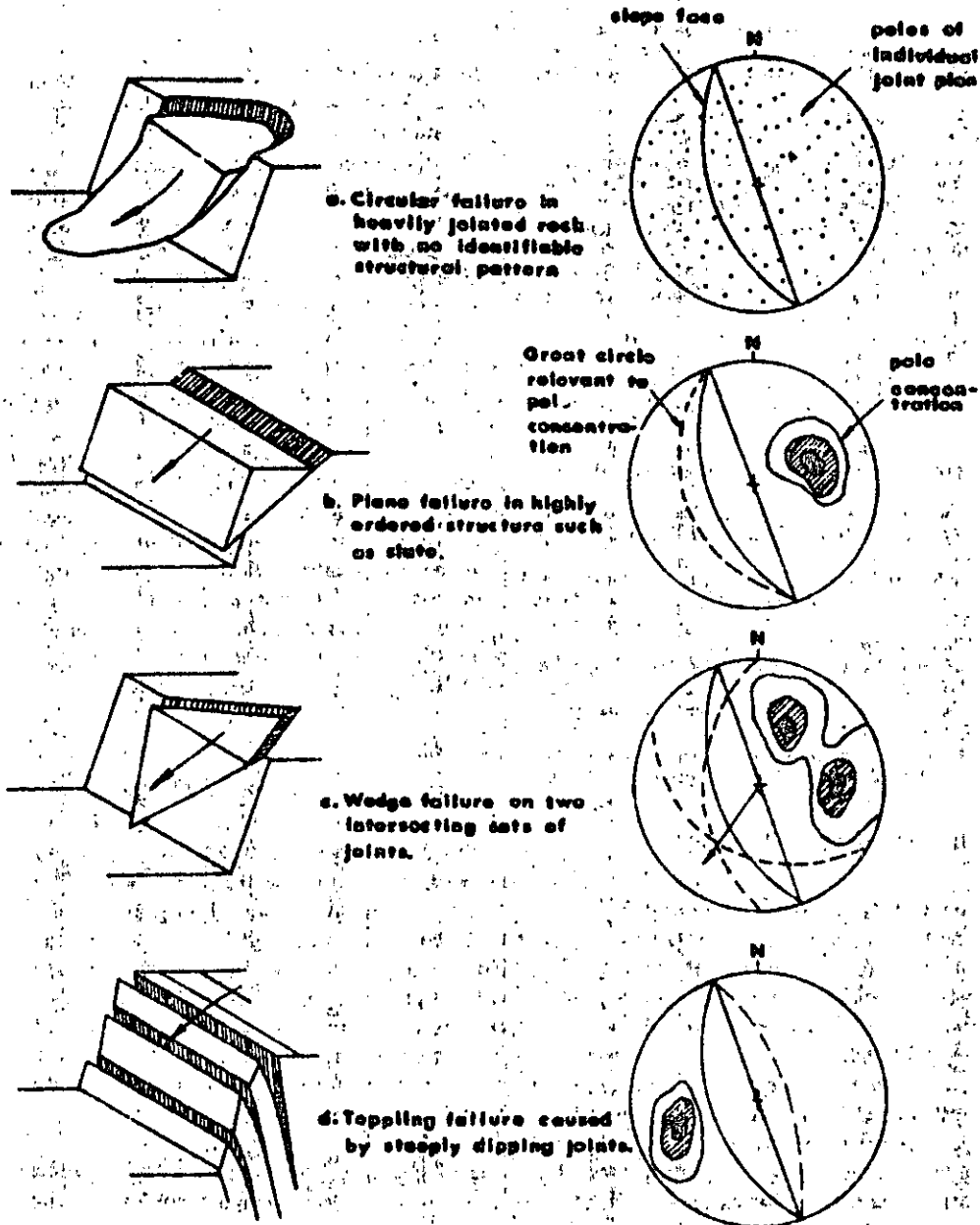


Fig. 6. Representation of structural data concerning four possible slope failure modes, plotted on equatorial equal-area nets as poles and great circles. [3].

## REFERENCES

1. Soga M. & Barrero M. Some applications of the new integral sampling method in rock masses. *Symposium of ISRM on Rock Fracture*, Nancy, Paper 1-21, 12 p. (1971).
2. Pincus H. J. The analysis of aggregates of orientation data in the earth sciences. *J. Geol.* 61, 482-509 (1953).
3. Hoek E. & Bray J. *Rock Slope Engineering*, The Institution of Mining and Metallurgy, London, 209 p. (1974).
4. Ingley P. C. *Structural Methods for Exploration Geologists*, Harper Brothers, New York, 280 p. (1959).
5. Hodgson R. A. Regional study of jointing in the Comb Ridge-Navajo Mountain area, Arizona and Utah. *Bull. Am. Ass. Petrol. Geol.* 45, 1-38 (1961).
6. John K. W. An approach to rock mechanics. *J. Soil Mech. Fdns Div. Am. Soc. civ. Engrs.* SM4, pp. 1-30 (1962).
7. Muller L. *Der Felshau*, Ferdinand Enke-Verlag, Stuttgart, 624 p. (1963).
8. Turner, F. J. & Weiss L. E. *Structural Analysis of Metamorphic Tectonites*, McGraw-Hill, New York, 545 p. (1963).
9. Pincus H. J. A procedure for rapid plotting of point diagrams. *J. Geol. Educ.* Vol. 13, 7-8 (1965).
10. Terzaghi R. D. Sources of error in joint surveys. *Geotechnique*, 15, 287-306 (1965).
11. Nickelsen R. P. & Hough V. N. D. Jointing in the Appalachian Plateau of Pennsylvania. *Bull. geol. Soc. Am.* 78, 609-630 (1967).
12. John K. W. Graphical stability of slopes in jointed rock. *J. Soil Mech. Fdns Div. Am. Soc. civ. Engrs.* 94, No SM2, 497-526, with discussion and closure in 95, SM6, 1969, 1541-1545 (1968).
13. Broadbent C. D. & Ripper K. H. Fracture studies at the Kimberley Pit. *Proc. Symposium on Planning Open Pit Mines*, Johannesburg, 1970. Balkema, Amsterdam, 1971, pp. 171-179 (1971).

14. Patton F. D. & Deere D. U. Significant geological factors in rock slope stability. *Symposium on Planning Open Pit Mines*, Johannesburg, 1970. Balkema, Amsterdam 1971, pp. 143-151 (1971).
15. Phillips F. C. *The Use of Stereographic Projections in Structural Geology*. Edwards Arnold, London, 3rd edn, 90 p. (1971).
16. Piteau D. R. Geological factors significant to the stability of slopes cut in rock. *Symposium on Planning Open Pit Mines*, Johannesburg, 1970. Balkema, Amsterdam 1971, pp. 33-53 (1971).
17. Robertson A. MacG. The interpretation of geological factors for use in slope theory. *Symposium on Planning Open Pit Mines*, Johannesburg, 1970. Balkema, Amsterdam 1971, pp. 55-71 (1971).
18. Kniff J. L. The engineering geology of the Crouhan underground power station. *Engng Geol.* 6, 289-312 (1972).
19. Babcock E. A. Regional jointing in Southern Alberta. *Can. J. Earth Sci.* 10, 1769-1781 (1973).
20. Pincus H. J. Note: A modified transit for measuring strike on the underside of surfaces. *Int. J. Rock Mech. Min. Sci.* 10, 83-84 (1973).
21. Piteau D. R. Characterizing and extrapolating rock properties in engineering practice. *Rock Mechanics* (Springer-Verlag), Suppl. 2, 5-31 (1973).
22. Bolstead D. D. & Mahtab M. A. A Bureau of Mines direct reading azimuth protractor. USBM, Information Circular 8617, 7 p. (1974).
23. Cording E. J. & Mahar J. W. The effect of natural geologic discontinuities on behaviour of rock in tunnels. *Proc. 2nd North American Rapid Excavation and Tunneling Conference*, San Francisco, Vol. I, Chap. 12, pp. 107-138 (1974).
24. Posch R. *Bermerkning* (Geoteknik, Ed. S. Hansho) Almqvist & Wiksell, Stockholm, 236 p. (1974).
25. Cruden D. M. A composite net for rock slope stability. *Q. J. Engng. Geol.* 9, 119-124 (1976).
26. Goodman R. F. *Methods of Geological Engineering in Discontinuous Rocks*, West Publishing N.Y., 472 p. (1976).

### (B) Photogrammetric Method

#### Scope

(a) This discontinuity mapping technique utilizes photogrammetry to determine the coordinates of at least four points on each visible discontinuity plane, thereby defining the orientation of the given planes. Large planes may often be mapped quite precisely by the photogrammetric technique, but the accuracy decreases rapidly as the area of the plane decreases.

(b) The method is usually only economic if the orientation of a large number of discontinuities is required. However, there are occasions when photogrammetry is the only practical alternative, for example if the relevant rock face is in the vicinity of magnetic anomalies, or if the rock face is unstable and/or inaccessible.

(c) The following summary of equipment and procedures is designed as an introduction to the technique. Potential users should consult the detailed papers listed in the references.

#### Equipment

(a) Reconnaissance survey equipment: square, Abney level, alidade, and reconnaissance grain mounted on a plane table.

(b) Phototheodolite and tripod. A phototheodolite is a theodolite with a survey camera located between the upper and lower circles. The survey camera includes fiducial marks and has a lense of negligible distortion characteristics. Six control targets are required in location on the rock face to be photographed. In order to be seen clearly in the stereoscopic model their minimum dimensions should be  $\frac{1}{200}$  of the distance to the rock face. Their colour should be chosen for maximum contrast with the rock when viewed in black and white photography. Photographic plates, photographic development facilities (on site if possible, to check for overexposures) and light meter are also required.

(c) Control survey equipment: tripods, tribrachs, tripod targets, plumbing devices, subtense bar.

(d) Stereoscopic plotting instrument or stereocomparator, with automatic recording equipment (on punched tape). This equipment will normally be operated by a trained photogrammetrist.

#### Procedure

(a) *Reconnaissance survey.* The purpose of a reconnaissance survey is to determine suitable positions for both the camera stations overlooking the face, and for control targets on the face. (See Figs 7 and 8) The height of the face being photographed, the accuracy required, the vertical and horizontal field angles of the camera and the available camera tilt must be considered prior to photography. In many cases there will be physical limitations imposed by the site itself, as illustrated in Fig. 9. Much better use of the available area is possible if the camera axes can be approximately normal to the face.

(b) *Photography.* The phototheodolite is set up on one of the base line tripods, with an interchangeable target on the other. The instrument is then levelled, the camera tilt, exposure time and counter are set, and the photographic plate is loaded. The camera is orientated at right angles to the theodolite, and the telescope is sighted on the other station. With the camera axes thus normal to the base, the photograph is taken. The phototheodolite and target are then interchanged at the

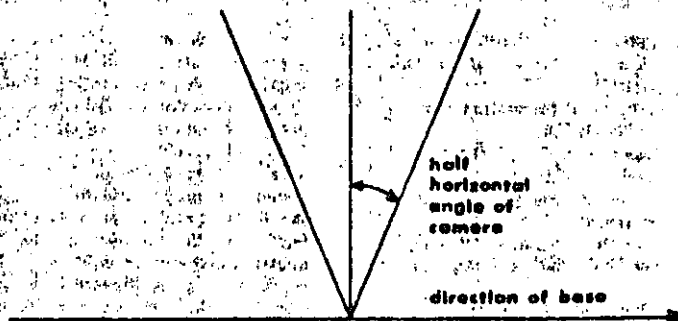


Fig. 7. Reconnaissance diagram mounted on plane table.

## Suggested Methods for the Quantitative Description of Discontinuities

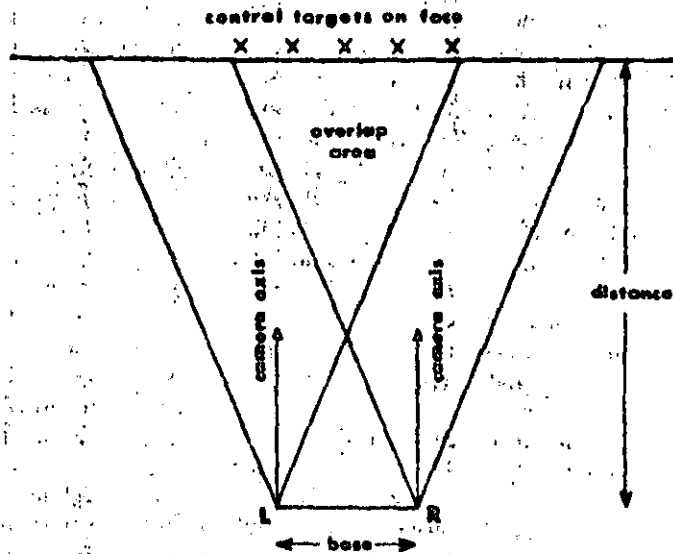


Fig. 8. Field set-up to obtain overlapping stereopair.

base-line stations and the procedure is repeated. It is recommended that the photographic plates are developed in a suitable site office dark room so that, if the plates are not up to the high standard required for photogrammetric analysis, the photography may be retaken before the camera station tripods and control targets are removed. It is desirable to complete all the photography as soon as possible in order to avoid differences caused by shadow on corresponding photographs of a stereopair.

(c) *Control survey.* After completion of the photography, a control survey has to be performed in order to determine the coordinates of at least four targets within the overlap area. The camera can be removed from the theodolite and the necessary angle measurements recorded from each end of the baseline. Generally two rounds of horizontal and vertical angles are made to the control targets and at least three other stations whose coordinates are known. From these latter observations the camera coordinates may be determined by resection.

The baseline is measured by setting an interchangeable subtense bar on one station tribrach, and observing it from the other. The distance is calculated from the mean subtended angle. This procedure is performed from both ends of the baseline as a check.

A minimum of one day should normally be allowed for the field work associated with each stereopair. The baseline may subsequently be extended to a series of consecutive camera stations if the overlap area obtained with one stereopair is insufficient to cover the whole rock face.

(d) *Survey information.* The exact form of the survey information required depends on the program being used to analyse the results. Generally, if the theodolite observations have been made from the same tribrach positions as used for the photography, the survey information required consists of the theodolite coordinates in the ground system, and the vertical and horizontal theodolite observation to the targets, reduced and meaned as appropriate.

(e) *Instructions to photogrammetrist.* It is convenient

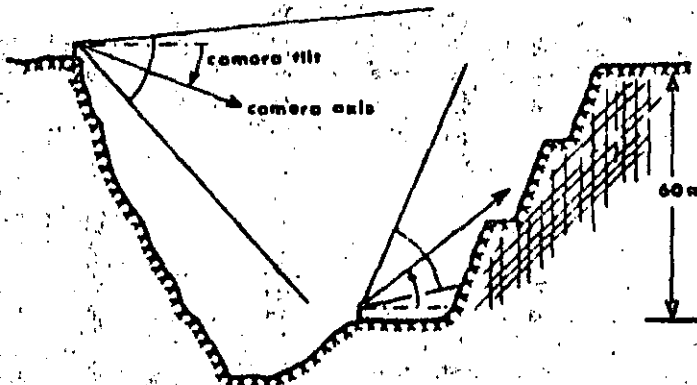


Fig. 9. Two alternative base line locations at a difficult site.

to work in a routine manner in order that the information may subsequently be handled by a computer. The work is best specified by making detailed notes for the photogrammetrist and by making an enlarged photograph of the overlap area. The following information may be requested:

Joint areas—areas indicated on the enlarged photograph from which a specified number of orientations are required for statistical analysis (e.g. plotting on an equal area net).

Special discontinuities—particular planes, individually identified on the enlarged photograph, for which the location, orientation and extent are required more precisely, as for example for use in a stability analysis. Generally up to ten pointings per plane are sufficient for defining these features.

(f) *Observational procedure.* Usually the negative plates are observed directly but if preferred by the operator diapositives can be made. An operator unaccustomed with the technique of observing discontinuities usually requires a few hours observing practice. The coordinates of at least four points are required for each visible plane. Each pointing is punched onto tape in an identical format and consists of an identifier followed by X, Y and Z coordinates of the pointing. Normally all the pointings referring to a particular discontinuity have the same identifier. The operator thus proceeds from pointing to pointing, discontinuity to discontinuity and area to area. About 10% of the larger discontinuities are identified on the large photographic print for the convenience of the engineering geologist doing the interpretation. It is important that the operator makes a number of independent checks on the accuracy of his observations at field scale. This will give all concerned a feel for the likely errors.

(g) *Computations.* The basic information required consists of the control survey data (e) and the photogrammetric punched tape (f). In summary, computer calculations comprise transformation of the target coordinates to the ground system and setting up the transformation matrix.

Planes are fitted to the sets of pointings by the method of least squares, and direction cosines are determined from a symmetric coefficient matrix and subsequently transformed by the transformation matrix. The planes may then be described in terms of *dip direction* and *dip*. The last part of the computational phase involves the calculation of probable errors. Special techniques are used to estimate the maximum probable errors in dip and dip direction for each joint [1].

#### Notes

(a) In any photogrammetric system the following sources of error have to be considered: film, camera, plotting instrument, recording method, control survey, earth's curvature, atmospheric refraction, instrument operator. Compared to the other sources of error, the operating errors caused by the instrument operator are

very significant. These are mainly due to the error in the operator's stereoscopic perception and to misinterpretation. The operator must make decisions as to the positioning of the float on the instrument if discontinuity images are not defined. These operating errors can usually be kept to tolerable levels by using large base/distance ratios.

(b) In highly altered or weathered rocks it is difficult to distinguish discontinuities and planar features even by close inspection. In such cases photogrammetry is clearly of little help. Sometimes rough or very curved discontinuities are encountered and the validity of fitting a plane to such surfaces may be questioned. The error in plane fitting may be negligible for discontinuities defining near-perfect planes with any orientation, and for planes normal to the camera axis of any roughness. However, the error may be significant for very rough planes approaching an edge-on position when viewed on the photographic plates. This is especially true of discontinuities that strike within 5° of the direction of the camera axis. If photogrammetry is the main mapping technique being used, then more than one stereo-pair taken from different directions may be required to pick up all discontinuities exposed on a face. Alternatively, edge-on discontinuities may be mapped conventionally in order to make the equal area net complete.

(c) There is a great deal of useful information that can be obtained from the photogrammetric mapping technique in addition to orientation data. For example, rock surface profiles can be plotted for use in estimating overall volumes involved in the stability analysis. If the camera to object distance is reasonable, *profile* profiles of individual joints may be obtained. They may be used to estimate shear strength. The *spacing* distribution of joint spacing can be measured and *joint persistence* may also be assessed. In addition, stereo-pairs exposed at different stages during the life of a project (e.g. an open pit), provide a permanent visual record, which can be especially useful when extrapolating major features.

#### Presentation of results

Suggested methods for presenting orientation data will be found under (A) *Compass and Clinometer Method*.

The large amount of orientation data likely to be produced by systematic photogrammetric work is suitable for statistical treatment. A first step in the presentation of results will be the plotting of poles on equal area nets.

#### REFERENCES

1. Ross-Brown D. M., Wickens E. H. & Markland J. T. Use of photogrammetry in open pits: 2: an aid to geological mapping. *Trans. Inst. Min. Metall. (Section, A, Min. Industry)*, 82, Pt. 1, A115-A130 (1973).
2. Linkwitz K. Terrestrisch-photogrammetrische Klüftungsmessung. *Rock Mech. Engng Geol.* 1, 152-159 (1963).
3. Terzaghi R. D. Sources of error in joint surveys. *Geotechnique* 15, 287-304 (1965).

4. Savage J. F. *Terrestrial Photogrammetry for Geological Purposes*. International Training Centre for Aerial Survey publication, Series B, No. 33, pp. 41-53 (1965).
5. Thompson M. M. (Ed.). *Manual of Photogrammetry* 3rd edn. American Soc. of Photogramm. Falls Church, Virginia (1966).
6. Rengers N. *Terrestrial photogrammetry: a valuable tool for engineering geological purposes*. *Rock Mech. Engng Geol.* 5, 150-154 (1967).
7. Calder P. N., Bauer A. & Macdougall A. R. *Stereophotography and open pit mine design*. 72nd Annual Meeting Can. Inst. Min. Metall. April 1970. Preprint (1970).
8. Wickens E. H. & Barton N. R. The application of photogrammetry to the stability of excavated rock slopes. *Photogram. Rec.* 7(37), April, 46-54 (1971).
9. Ross-Brown D. M. & Atkinson K. B. *Terrestrial photogrammetry in open pits: I—description and use of the phototheodolite in mine surveying*. *Trans. Inst. Min. Metall. (Sect. A: Min. Industry)*, 81, pp. A205-A213 (1972).
10. Ross-Brown D. M. *Aspects of slope design in open pit mining*. Ph.D. Thesis, University of London (1973).

## 2. SPACING

### Scope

(a) The spacing of adjacent discontinuities largely controls the size of individual blocks of intact rock. Several closely spaced sets tend to give conditions of low mass cohesion whereas those that are widely spaced are much more likely to yield interlocking conditions. These effects depend upon the persistence of the individual discontinuities.

(b) In exceptional cases a close spacing may change the mode of failure of a rock mass from translational to circular or even to flow (e.g. a "sugar cube" shear zone in quartzite). With exceptionally close spacing the orientation is of little consequence as failure may occur through rotation or rolling of the small rock pieces.

(c) As in the case of orientation, the importance of spacing increases when other conditions for deforma-

tion are present, i.e. low shear strength and a sufficient number of discontinuities or joint sets for slip to occur.

(d) The spacing of individual discontinuities and associated sets has a strong influence on the mass permeability and seepage characteristics. In general the hydraulic conductivity of any given set will be inversely proportional to the spacing, if individual joint apertures are comparable.

### Equipment

(a) Measuring tape of at least 3 m length, calibrated in mm divisions.

(b) Compass and clinometer.

### Procedure

(a) Whenever possible, the measuring tape should be held along the exposure such that the surface trace of the discontinuity set being measured is approximately perpendicular to the tape. If the tape is not perpendicular, directional bias corrections are required to obtain the true spacing.

(b) All distances ( $d$ ) between adjacent discontinuities are measured and recorded over a sampling length not less than 3 m (or the thickness of the rock unit being observed if this is less than 3 m). The sampling length should preferably be greater than ten times the estimated spacing. The distances ( $d$ ) should be measured to within 5% of their absolute values.

(c) The smallest angle ( $\alpha$ ) between the measuring tape and the observed joint set is measured with a compass to the nearest 5°.

(d) The most common (modal) spacing is calculated from the equation:

$$S = d_m \sin \alpha$$

where  $d_m$  is the most common (modal) distance

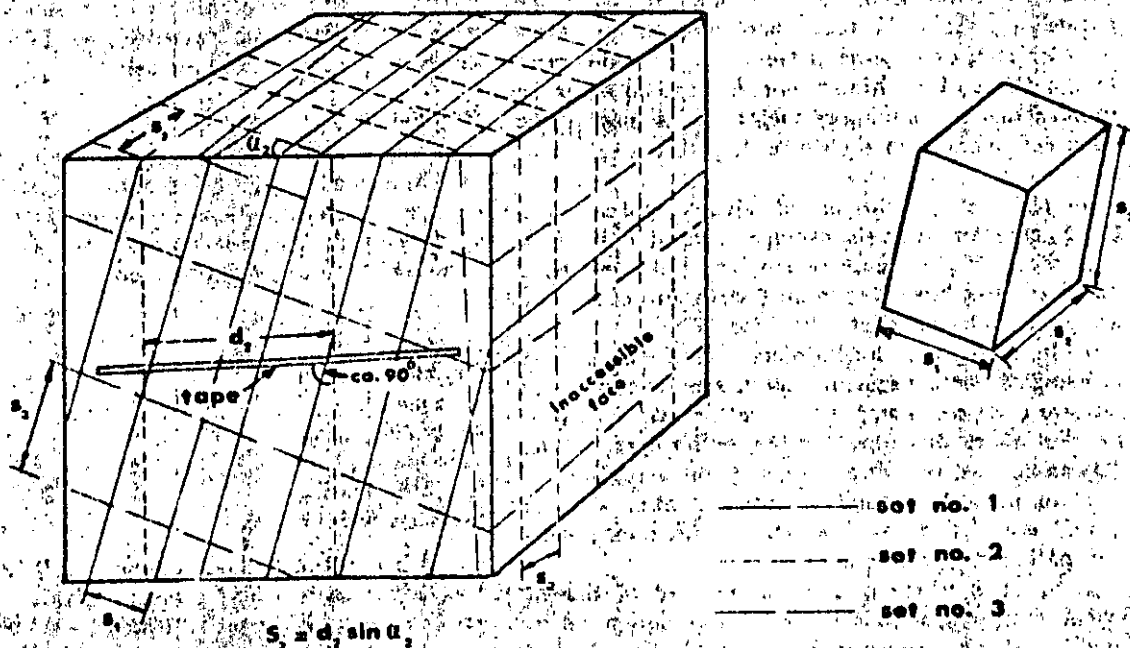


Fig. 10. Measurement of joint spacing from observation of a rock exposure.

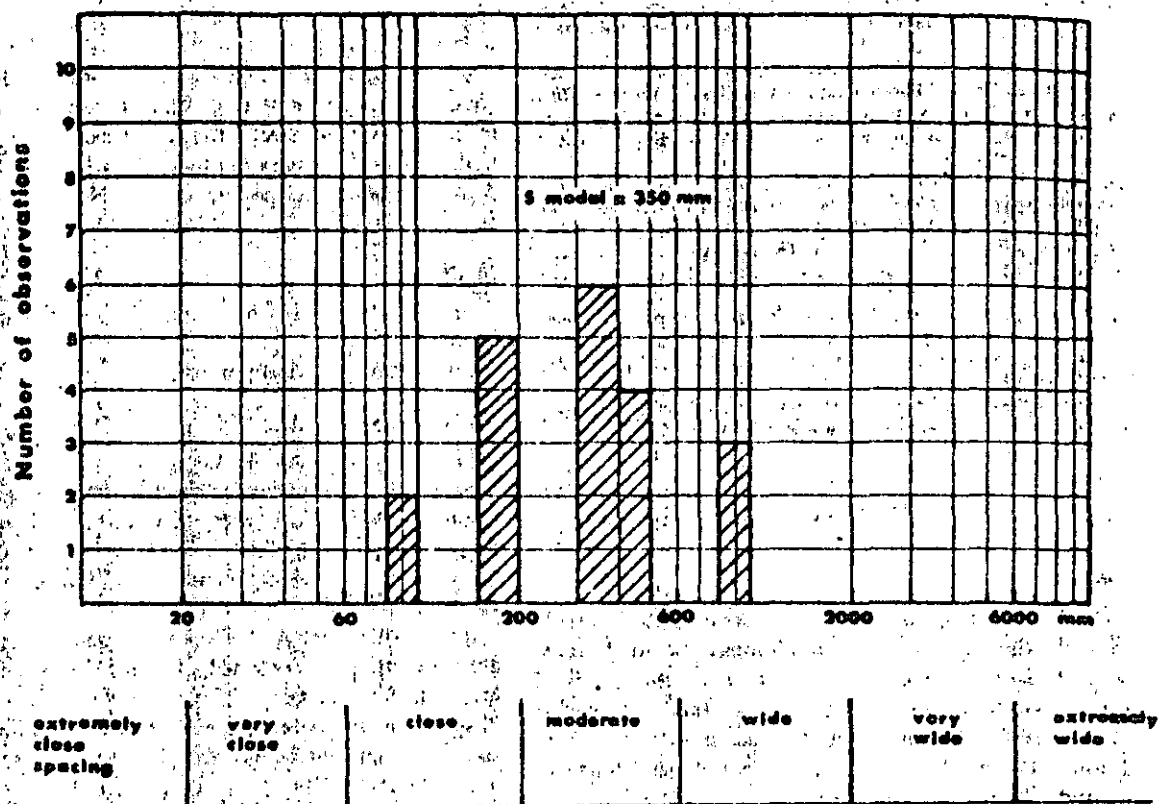


Fig. 11. Histogram showing modal, minimum and maximum spacings obtained from observations of the spacing of one set. Suggested descriptions given at base of histogram.

measured. It is helpful to present the variation in spacing by means of a histogram, as illustrated in Fig. 11.

#### Notes

(a) The use of a measuring tape and compass is strongly recommended, but it is not essential if the engineering geologist is experienced in taking these measurements using visual judgement. This will depend on the degree of precision required. It should be borne in mind that discontinuities such as joints may not be sufficiently parallel in a given set to justify great precision.

(b) The average value of individual modal spacings ( $S_1$ ,  $S_2$  etc.) represents the average dimension of typical rock blocks if persistence is assumed. Other methods of representing block size from observations of spacing are given under parameter 10, Block Size.

(c) In any given discontinuity set, domains with recognizably similar spacing may be separated by more massive rock containing a few widely spaced discontinuities. Block diagrams (Fig. 2b) or histograms (Fig. 11) can be used to indicate this type of variability.

(d) In general, fractures caused by blast damage should be excluded from consideration when measuring the spacing of discontinuities.

(e) In cases where rock exposures are of limited extent, or absent, seismic refraction techniques can be used to estimate spacing in the upper 20-30 m. Several investigators have found a fairly reliable relationship

between frequency, i.e. number of discontinuities per metre, and the longitudinal or compression (P) wave velocity  $V_p$ .

(f) The spacing or frequency of discontinuities can also be determined from analysis of drill core and from borehole viewing techniques such as borehole television cameras, photographic cameras and borehole periscopes (see 11, Drill Core for details).

#### Presentation of results

(a) The minimum, modal and maximum spacing,  $S$  (min),  $S$  (max) should be recorded for each discontinuity set. The distributions can conveniently be presented as histograms, one for each set (Fig. 11). The following terminology can be used:

Description	Spacing
Extremely close spacing	< 20 mm
Very close spacing	20-60 mm
Close spacing	60-200 mm
Moderate spacing	200-600 mm
Wide spacing	600-2000 mm
Very wide spacing	2000-6000 mm
Extremely wide spacing	> 6000 mm

(b) A convenient method of presenting large numbers of spacing measurements for which statistical treatment may be required, is the use of histograms, one for each set of discontinuities. Frequency curves for each set can be drawn on the same diagram, giving an immediate



## Suggested Methods for the Quantitative Description of Discontinuities

impression of the respective modal values and dispersions. (Note: using mean in place of modal spacings may help to eliminate difficulties with samples having multiple, poorly-defined modes, and with samples with modes at very small spacings, i.e. from negative exponential distributions.)

(c) Spacing may also be expressed as the inverse i.e. number of discontinuities per metre. This is termed frequency.

## REFERENCES

1. Terzaghi R. Sources of error in joint surveys. *Geotechnique*, 15, 287-304 (1965).
2. Weaver R. & Call R. D. Computer estimation of oriented fracture set intensity. Reprint *Symp. on Computers in Mining and Exploration*, Tuscon, Arizona, 17 p. (1965).
3. Da Silva A. F., Rodrigues F. P., Grossman N. F. & Mendes E. Qualitative characterization of the geometric parameters of jointing in rock masses. *Proc. 1st. Congress of the Int. Soc. Rock Mech.*, Lisbon, Vol. 1, pp. 225-233 (1966).
4. Halstead P. N., Call R. D. & Ripper K. H. Geological structural analysis for open pit slope design, Kimberley pit, Ely, Nevada. Reprint. Annual AIME meeting, New York, 25 p (1968).
5. Ward W. H., Burland J. B. & Gallois R. W. Geotechnical assessment of a site at Mundford, Norfolk, for a large proton accelerator. *Geotechnique*, 18, 399-431 (1968).
6. Broadbent C. D. & Ripper K. H. Fracture studies at the Kimberley pit. *Proc. Symp. on Planning Open Pit Mines*, Johannesburg, 1970. Balkema, Amsterdam, 1971, pp. 171-179 (1971).
7. Piteau D. R. Geological factors significant to the stability of slopes cut in rock. *Proc. Symp. on Planning Open Pit Mines*, Johannesburg, 1970. Balkema, Amsterdam, 1971, pp. 33-53 (1971).
8. Robertson A. MacG. The interpretation of geological factors for use in slope theory. *Proc. Symp. on Planning Open Pit Mines*, Johannesburg, 1970. Balkema, Amsterdam, 1971, pp. 55-71 (1971).
9. Grainger P., McCann D. M. & Gallois R. W. The application of the seismic refraction technique to the study of fracturing of the Middle Chalk at Mundford, Norfolk. *Geotechnique*, 23, 219-237 (1973).
10. Piteau D. R. Characterizing and extrapolating rock properties in engineering practice. *Rock Mechanics* (Springer-Verlag), Suppl. 2, pp. 5-31 (1973).
11. Priest S. D. & Hudson J. A. Discontinuity spacings in rock. *Int. J. Rock Mech. Min. Sci. & Geomech. Abstr.* 13, 135-148 (1976).

## 3. PERSISTENCE

## Scope

(a) Persistence implies the areal extent or size of a discontinuity within a plane. It can be crudely quantified by observing the discontinuity trace lengths on the surface of exposures. It is one of the most important rock mass parameters, but one of the most difficult to quantify in anything but crude terms.

(b) The discontinuities of one particular set will often be more continuous than those of the other sets. The minor sets will therefore tend to terminate against the primary features, or they may terminate in solid rock.

(c) In the case of rock slopes and dam foundations it is of the greatest importance to attempt to assess the degree of persistence of those discontinuities that are unfavourably orientated for stability. The degree to which discontinuities persist beneath adjacent rock blocks without terminating in solid rock or terminating

against other discontinuities determines the degree to which failure of intact rock would be involved in eventual failure. Perhaps more likely, it determines the degree to which "down-stepping" would have to occur between adjacent discontinuities for a failure surface to develop. Persistence is also of the greatest importance to tension crack development behind the crest of a slope.

(d) In the case of tunneling, failure in the first instance may be a rather local affair, and persistence across a limited number of blocks may be all that is required provided that other conditions are compatible with failure, i.e. the existence of smooth or clay filled discontinuities or at least three sets. Planar discontinuities that can be traced without offset for 5-10 m in a tunnel construction may be of major significance to stability, while being of minor importance in the case of a 100 m high rock slope or large dam abutment.

(e) Frequently, rock exposures are small compared to the area or length of persistent discontinuities, and the real persistence can only be guessed. Less frequently it may be possible to record the dip length and the strike length of exposed discontinuities and thereby estimate their persistence along a given plane, through the rock mass using probability theory. However, the difficulties and uncertainties involved in the field measurements will be considerable for most rock exposures encountered.

## Equipment

(a) Measuring tape of at least 10 m length.

## Procedure

(a) Individual rock exposures, or recognised domains, should first be described according to the relative persistence of the different discontinuity sets present. The sets of discontinuities can be distinguished by the terms *persistent*, *sub-persistent* and *non-persistent* respectively. Simple labelled field sketches such as those illustrated in Fig. 12, can be useful aids in subsequent interpretation.

(b) Efforts should then be made to measure the discontinuity lengths in the direction of dip and in the direction of strike. This may be impossible in the case of limited planar exposures. However, in the case of large three-dimensional exposures such as curved open pits with benches, or underground openings with intersecting tunnels, it may be possible to obtain useful size-frequency histograms for each of the discontinuity sets.

The modal trace lengths measured for each set can be described according to the following scheme:

Very low persistence	< 1 m
Low persistence	1-3 m
Medium persistence	3-10 m
High persistence	10-20 m
Very high persistence	> 20 m

(c) A useful procedure during the mapping of discontinuity lengths is to record the type of termination according to the following scheme. Discontinuities

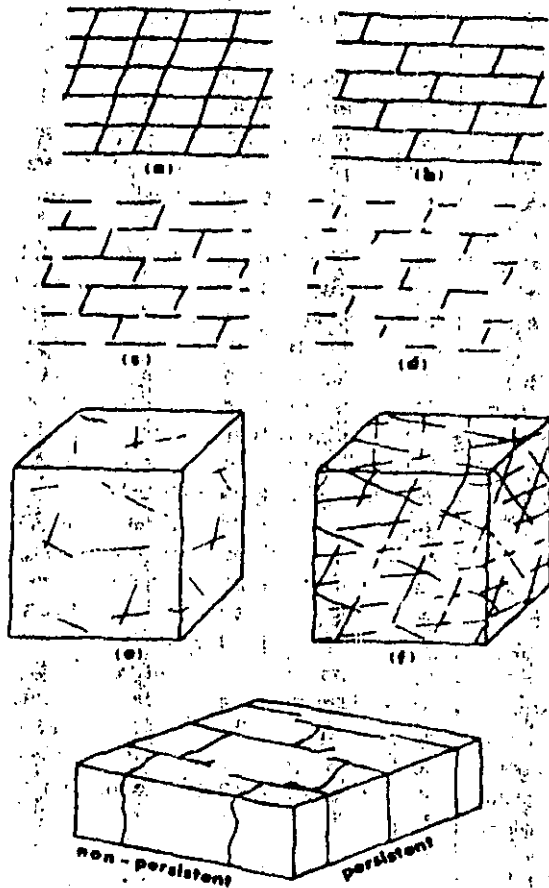


Fig. 12. Simple sketches and block diagrams help to indicate the relative persistence of the various sets of discontinuities. Examples adapted from [1] and [2].

which extend outside the exposure (x), should be differentiated from those that visibly terminate in rock in the exposure (r), and from those that terminate against other discontinuities in the exposure (d). A systematic set of discontinuities with a high score in (x), is obviously more persistent than a sub-systematic set with predominant scores in (d). Non-systematic discontinuities will tend to have highest scores in (r).

(d) Termination data (x, r or d) should be recorded for each end of the relevant discontinuities, together with the length in metres. (Example:  $2(dx) \Rightarrow$  discontinuity length of 8 m, one termination against another discontinuity other termination invisible because feature extends beyond the limits of the exposure). It is important to specify the dimensions of the exposure on which measurements were made since this will obviously influence both the number of (x) observations and the relevant lengths.

#### Notes

(1) Piteau [3] has demonstrated that discontinuities where both terminations can be seen are generally smaller than discontinuities where one or no terminations can be seen. In a sample of 3844 joints at the Nchanga Mine, 1394 (36%) with an average length of 1.4 m had both ends exposed, 1538 (40%) with an aver-

age length of 2.9 m had one end exposed, and 912 (24%) with an average length of 6.3 m had no ends exposed.

(b) Analyses of dip lengths and strike lengths performed by Robertson [4] have indicated that discontinuities tend to be of approximately isotropic dimensions. When terminating in solid rock they may therefore tend to be circular, and presumably rectangular when terminating against other discontinuities.

(c) Statistical tests simulating circular outline discontinuities with a normal distribution of diameters randomly spaced in the rock mass, indicate that the mean trace length can range from slightly smaller to slightly larger than the mean diameter [5]. This is the result of the greater probability of intersecting the larger discontinuities outweighing the fact that trace lengths (chords) are inherently shorter than diameters.

(d) Statistical methods can be used to analyse the maximum lengths of discontinuities. Using such techniques it is possible to estimate the expected recurrence interval for discontinuities of any specified length. Alternatively it is possible to estimate the mean probability of a discontinuity exceeding a specified length occurring in any portion of the rock mass. For example, if after analysis it is found that major discontinuities with strike lengths of 50 m or more are spaced on the average at 150 m, it is possible to estimate the probability of strike lengths of 50 m or more occurring in any 100 m interval measured normal to the strike. The probability is equal to  $100/150 = 0.66$ . If the complete distribution of sizes is known (Procedure (b)), the probability of occurrence of a discontinuity of a certain size can be evaluated on the basis of extreme value statistics. A useful example of its application to rock slope stability analysis is given by McMahon [6]. Note that the ill-defined lower bound to observations of trace length (inevitable if the shortest features are ignored) leads to underestimation of the frequency of discontinuities and overestimation of their size.

(e) The descriptive term persistence may in theory be quantified by defining it as the percentage of the total area of a plane through the rock mass which is formed by discontinuities coincident (co-planar) with this reference plane. In practice, waviness of most discontinuities frustrates strict interpretation. A practical alternative is to select a band width equal to the mean spacing of the discontinuities in the particular set, and to estimate the persistence within this reference band. Since, on a probability basis, only one discontinuity would be expected to occur within this band, a slightly more realistic estimate of persistence is obtained.

(f) When assessing the persistence of the various discontinuity sets it is important to investigate the possibility of a stepped failure surface forming, as illustrated by failure modes (2) and (3) in Fig. 13. This mode of failure may tend to occur when the set involved in shear has less than 100% persistence. Downstepping will tend to develop such that only a minimum percentage of the resulting shear surface passes through intact rock. The persistence of a potential failure surface will normally be higher than that along planes or bands

## Suggested Methods for the Quantitative Description of Discontinuities

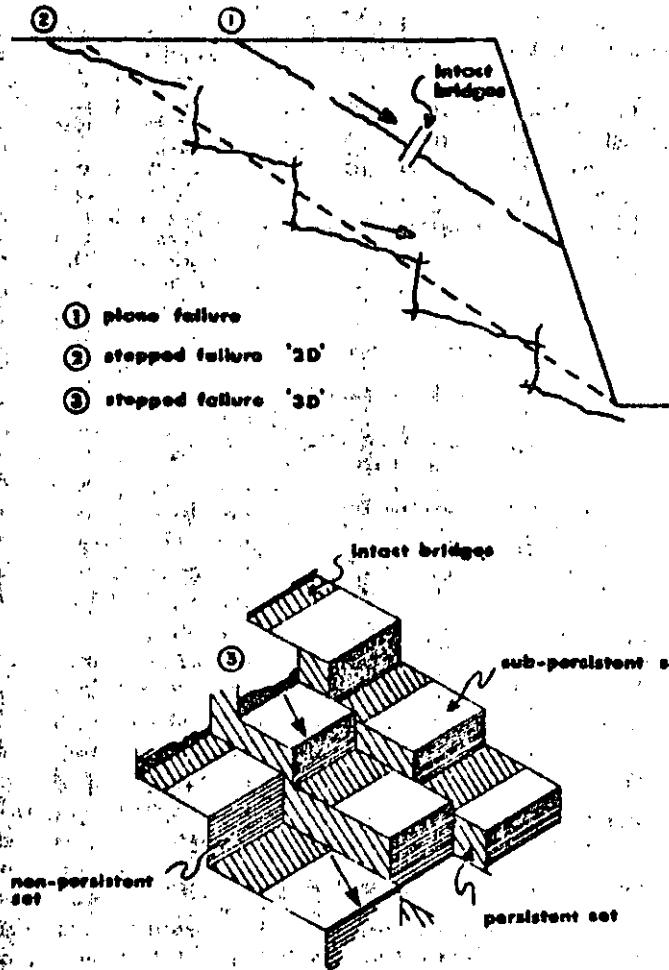


Fig. 13. Idealized examples of potential failure planes showing the importance of "intact bridges" and "down-stepping".  
Examples adapted from [4] and [7].

parallel to a single set, unless the latter have 100% persistence.

(g) Estimates of *persistence* for given planes, bands or specific failure surfaces have at present to be based on engineering judgement and should be purposely weighted in the direction of conservatism (i.e. closer to 100% persistence since the shear strength of the intact rock bridges will form a dangerously high percentage of the total shear strength of the compound failure surface. The shear strength (cohesion) due to any intact rock bridges can be crudely estimated from the following relationship which is derived from the Mohr diagram, assuming a linear shear strength envelope:

$$c = \frac{1}{6}(\sigma_c - \sigma_t)$$

where:

$\sigma_c$  = uniaxial compressive strength of the intact rock  
 $\sigma_t$  = tensile strength of the intact rock.

If it is assumed for simplicity that  $\sigma_c/\sigma_t \approx 9$ , then the cohesive strength is equal to one sixth of the unconfined compressive strength. It is safer to assume 100% persistence when in doubt, since the above cohesion is usually one to two orders of magnitude greater than the shear strength of the discontinuities.

#### Presentation of results

(a) The various sets of discontinuities should be described as *systematic*, *sub-systematic* or *non-systematic* according to their relative persistence. Block diagrams or photographs should be labelled accordingly.

(b) Where exposures are of suitable dimensions, size-frequency histograms of trace lengths observed for each set of discontinuities should be given. (This is necessary if probability theory is to be applied subsequently). Mean trace lengths (in both strike and dip directions) should be quoted.

(c) Termination data which has been recorded for each discontinuity summed (e.g. 8dx), should be presented in the form of a *termination index* ( $T_r$ ) for the rock mass as a whole, or for chosen domains.  $T_r$  is defined as the percentage of the discontinuity ends terminating in rock ( $\Sigma r$ ) compared to the total number of terminations ( $\Sigma r + \Sigma d + \Sigma x$ ). The latter is equal to twice the total sample since each trace has two ends.

$$T_r = \frac{(\Sigma r) \times 100}{2(\text{no. of discontinuities observed})} \%$$

(It is to be hoped that systematic collection of data

concerning  $T$ , through application of these ISRM Suggested Methods will eventually improve the estimation of persistence).

(d) The persistence of potential failure surfaces (including stepped surfaces) should be estimated, if this is appropriate to the project being investigated. The estimate should perhaps be rounded upwards, to the next multiple of 10% (i.e. 92% is assumed to be 100%).

## REFERENCES

- Müller L. *Der Felsbau*. Ferdinand-Enke-Verlag, Stuttgart, 624 p. (1963).
- Price N. J. *Fault and Joint Development in Brittle and Semibrittle Rock*. Pergamon, Oxford, 176 p. (1966).
- Piteau D. R. Characterizing and extrapolating rock joint properties in engineering practice. *Rock Mechanics* (Springer-Verlag), Suppl. 2, pp. 5-31 (1973).
- Robertson A. MacG. The interpretation of geological factors for use in slope theory. *Symp. on Planning Open Pit Mines*, Johannesburg, 1970, Balkema, Amsterdam 1971, pp. 55-71 (1971).
- Barton C. M. An analysis of rock structure and fabric in the CSA Mine, Gobur, NSW. CSIRO Division of Applied Geomechanics, Tech. Paper No. 24 (1976).
- McMahon B. K. Design of rock slopes against sliding on pre-existing fractures. *Proc. of 3rd. Cong. of Int. Soc. Rock Mech.* Denver, *Advances in Rock Mechanics*, Vol. II, pp. 803-808 (1974).
- Jennings J. E. A mathematical theory for the calculation of the stability of slopes in open cast mines. *Symp. on Planning Open Pit Mines*, Johannesburg, 1970, Balkema, Amsterdam 1971, pp. 87-102 (1971).
- Hodgson R. A. Regional study of jointing in the Comb. Ridge-Navajo Mountain area, Arizona and Utah. *Bull. Am. Ass. Petrol. Geol.* 45, 1-38 (1961).
- John K. W. An approach to rock mechanics. *J. Soil Mech. Fdn. Div. Am. Soc. Civ. Engrs* SM4, 1-30 (1962).
- McMahon B. K. Indices related to the mechanical properties of jointed rock. *Proc. of 9th. Symp. on Rock Mech., Status of Practical Rock Mech.*, Ch. 6, pp. 117-133 (1967).
- Nickelsen R. P. & Hough V. N. D. Jointing in the Appalachian Plateau of Pennsylvania. *Bull. Geol. Soc. Am.* 78, 609-630 (1967).
- Hulstead P. N., Call R. D. & Ripper K. H. Geophysical stress analysis for open pit slope design. *Kimberly Ppt. Etc.*, AIME, Preprint No. 68-Am 85 (1968).
- Piteau D. R. Geological factors significant to the stability of slopes cut in rock. *Symp. on Planning Open Pit Mines*, Johannesburg, 1970, Balkema, Amsterdam 1971, pp. 33-53 (1971).
- Babcock E. A. Regional jointing in Southern Alberta. *Can. J. Earth Sci.* 10, 1769-1781 (1973).
- Bernais J. Properties of rock and rock masses. (General). *Proc. 3rd. Cong. Int. Soc. Rock Mech.* Denver, *Advances in Rock Mechanics*, Vol. IA, pp. 9-38 (1973).
- Cruden D. M. Describing the size of discontinuities. *Int. J. Rock Mech. Min. Sci. & Geomech. Abstr.* (Pergamon) 14, 131-132 (1977).

## 4. ROUGHNESS

### Scope

(a) The wall roughness of a discontinuity is a potentially important component of its shear strength, especially in the case of undisplaced and interlocked features (e.g. unfilled joints). The importance of wall roughness declines as aperture, or filling thickness, or the degree of any previous displacement increases.

(b) In general terms the roughness of discontinuity walls can be characterized by a waveness (large scale undulations which, if interlocked and in contact, cause dilation during shear displacement since they are too large to be sheared off) and by an unevenness (small scale roughness that tends to be damaged during shear displacement unless the discontinuity walls are of high strength and/or the stress levels are low, so that dilation can also occur on these small scale features).

(c) In practice waveness affects the initial direction of shear displacement relative to the mean discontinuity plane, while unevenness affects the shear strength that would normally be sampled in a laboratory or medium scale *in situ* direct shear test (see Fig. 14).

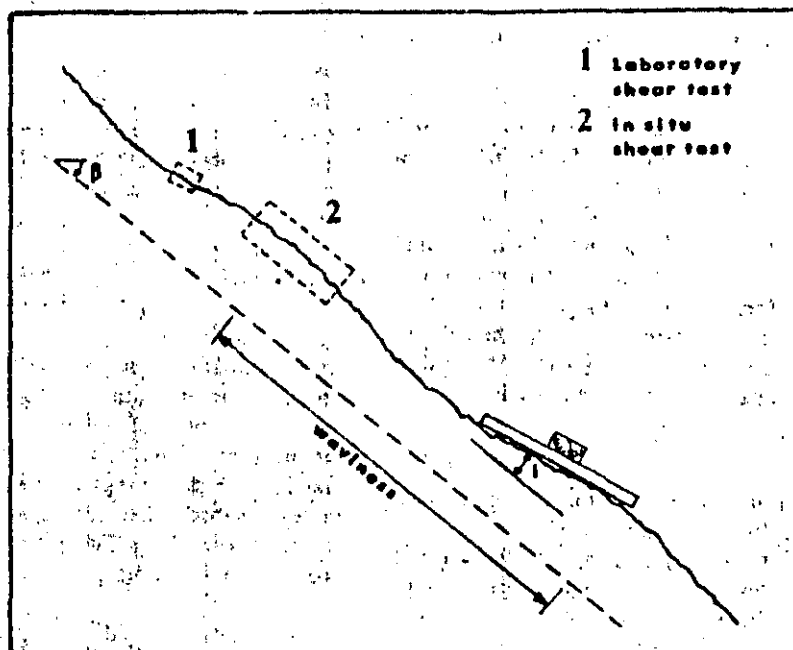


Fig. 14. Different scales of discontinuity roughness are sampled by different scales of tests. Waveness can be characterised by the angle  $\theta$ .

## Suggested Methods for the Quantitative Description of Discontinuities

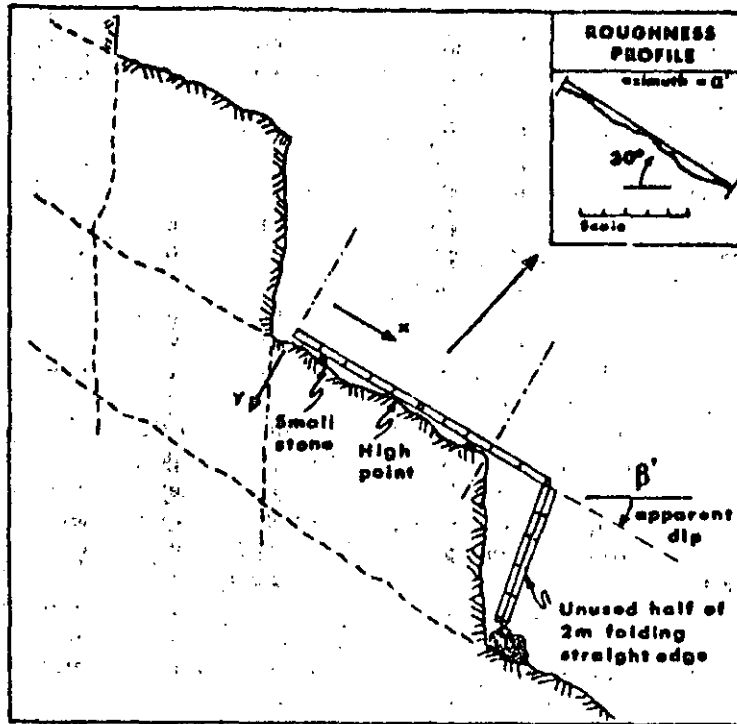


Fig. 15. A method of recording discontinuity roughness in two dimensions, along the estimated direction of potential sliding.

(d) If the direction of potential sliding is known, roughness can be sampled by linear profiles taken parallel to this direction. In many cases the relevant direction is parallel to the dip (dip vector). In cases where sliding is controlled by two intersecting discontinuity planes, the direction of potential sliding is parallel to the line of intersection of the planes. In the case of arch dam abutment stability, the direction of potential sliding may have a marked horizontal component.

(e) If the direction of potential sliding is unknown, but nevertheless of importance, roughness must be sampled in three dimensions instead of two. This can be done with a *compass and disc-clinometer*. Dip and dip direction readings can be plotted as poles on equal-area nets. Alternatively, discontinuity surfaces can be contoured relative to their mean planes using *photogrammetric* methods. This can be a useful technique if the critical surfaces are inaccessible.

(f) The purpose of all roughness sampling methods is for the eventual estimation or calculation of shear strength and dilation. Presently available methods of interpreting roughness profiles and estimating shear strength are summarised under the section *Presentation of results*.

#### Equipment

(a) The *linear profiling* method of sampling roughness requires the following equipment: (i) folding straight edge of at least 2 m length graduated in mm, (ii) compass and clinometer, (iii) 10 m of light wire or nylon with paint markings at 1 m intervals (red) and 10 cm intervals (blue). The line should be attached to small wooden blocks or similar at each end, so that

it can be tensioned to form a straight reference line above the plane of large undulating discontinuities.

(b) The *compass and disc-clinometer* method of sampling roughness requires the following equipment: (i) Clar (Breithaupt) geological compass which incorporates a horizontal levelling bubble and a rotatable lid which is connected to the main body of the compass through a graduated hinge for recording dip; (ii) four thin circular plates made of light alloy of various diameters (i.e. 5, 10, 20 and 40 cm) which can be fixed in turn to the lid of the compass [1].

The photogrammetric method of sampling roughness requires assorted equipment described under *Photogrammetric Method* (page 330).

#### Procedure

(a) *Linear profiling*. Discontinuities are selected that are accessible and typical of the surface presumed to be involved if shear failure was to occur.

Depending upon the relevant dimensions of each plane either the 2 m straight edge or the 10 m wire (or sections of either) are placed or stretched above the plane of the discontinuity parallel to the *mean direction* of potential sliding. For convenience they should be in contact with the highest point or points of the discontinuity and they should be as straight as possible. (A small lump of "plasticene" can be helpful in preventing the straight edge from sliding down steeply dipping joints. It can be placed between the straight edge and the high spots.) The perpendicular distances (y) from the straight edge (or wire) to the surface of the discontinuity are recorded to the nearest mm, for given tangential distances (x) (see Fig. 15). It is advisable to be flex-

ible in the choice of (x) since a regular interval (for example 5 cm) might result in missing a small step or similar feature of potential importance to the shear strength. On average, (x) intervals equal to approximately 2% of the total measuring length are sufficient to give a good overall impression of roughness.

The (x) and (y) readings are recorded in parallel, together with the azimuth and dip of the measuring direction. This may be different from the orientation  $\alpha/\beta$  of the discontinuity.

Profiles typical of the minimum, most common and maximum roughness are recorded using the above procedures. These profiles may apply to a whole discontinuity set, to one critical discontinuity, or to each surface measured, depending upon the detail required.

The waviness angle ( $\theta$ ) illustrated in Fig. 14, should be recorded using the straight edge and clinometer, if the profile was so short that waviness was not automatically sampled during profiling.

The approximate wave length and amplitude of waviness too large to be sampled by profiling should be estimated, or measured where accessibility is no problem.

Photographs representing the surfaces of minimum, modal and maximum roughness should be taken, with a 1 m rule placed against the surface in question clearly visible.

(b) *Compass and disc-clinometer.* Discontinuities are selected that are accessible, and typical of the surface presumed to be involved if shear failure was to occur.

The small scale roughness angles ( $\theta$ ) (Fig. 16) are measured by placing the largest circular plate (e.g. 40 cm dia) against the surface of the discontinuity in at least 25 different positions, and recording dip direction and dip for each position. (A surface area at least ten times as large as the area of the largest plate is assumed).

This procedure is repeated in turn for the other plate diameters. The overall sensitivity of the measurements is improved if a large number of positions are recorded with the smaller plate diameters, for example 50 positions with a 20 cm plate, 75 positions with a 10 cm plate, and 100 positions with a 5 cm plate.

Each set of dip direction and dip data is plotted on a separate equal area net in terms of poles. Contours are drawn for each set of poles.

Photographs representing surfaces of minimum, modal and maximum roughness should be taken, with a 1 m rule placed against the surfaces in question clearly visible.

(c) *Photogrammetric method.* In special cases, terrestrial photogrammetry can be used to obtain the coordinates of numerous points on the surface of inaccessible discontinuities using the procedures outlined under *Photogrammetric Method* (page 27). From this data it is possible to compute contour maps or profiles of the surface roughness. The minimum contour intervals will depend on the distance of the camera base from the surface in question. In some instances 1 mm intervals might be achieved, though 1 cm or 5 cm would

be more likely. Profiles should be computed for the direction of potential sliding, if this is known.

#### Notes

(a) *Linear profiling.* The mm graduated ruler used to measure the perpendicular distances (y) should be tapered to a point so that the fine details of roughness can be recorded if desired.

Several automatic recording profilographs are described in the literature [1, 3]. Most of these are suitable for describing the finest details of roughness. They obviously give a much more accurate picture of roughness than that obtained by the present suggested method. Normally this accuracy is unnecessary for rock mechanics purposes.

Offsets or steps dividing a discontinuity surface into several parallel planes are indicative of lack of persistence, and should be carefully profiled.

There are many other methods of recording roughness in addition to the profiling method. For example the wave length and amplitude of surface features could be measured and recorded for several different scale intervals, i.e. <1 cm, 1-10 cm, 10-100 cm, >1 m. Alternatively a very large undulating joint exposure could be rapidly recorded by laying a straight edge (for example 1 m length) against the surface at 1 m intervals in the down-dip direction and recording the dip of each position by means of a clinometer fixed to the straight edge. The length of straight edge could be varied in the same manner as with the compass method, if desired.

(b) *Compass and disc-clinometer.* The smallest base plates give the greatest scatter of readings and also the largest roughness angles. The largest base plates give the least scatter of readings and also the smallest roughness angles.

The large number of dip direction and dip readings (from approximately 200 plate positions) represents at least one hour's work per sampled plane. This will only be justified in special circumstances. If a large number of discontinuities need to be measured, the *photogrammetric* method is recommended. Alternatively if the potential sliding direction is known, the *profiling* method is recommended, thereby reducing the amount of data collection to the single direction of potential sliding.

The maximum roughness angles for the given disc sizes can be plotted for any direction of potential sliding. (See Fig. 16). The tangent of these maximum roughness angles multiplied by the appropriate base length (disc diameter) gives the displacement (dilatation) that will occur perpendicular to the discontinuity for a shear displacement equal to the given base length. Several base lengths (disc diameters) are analysed in this way, so that a dilation curve can be obtained. This will give a realistic picture of the shearing process when there is minimal damage to asperities. The method is therefore most appropriate to shearing of joints in hard rocks at low effective normal stress levels. (Asperities smaller than the minimum plate diameter are assumed

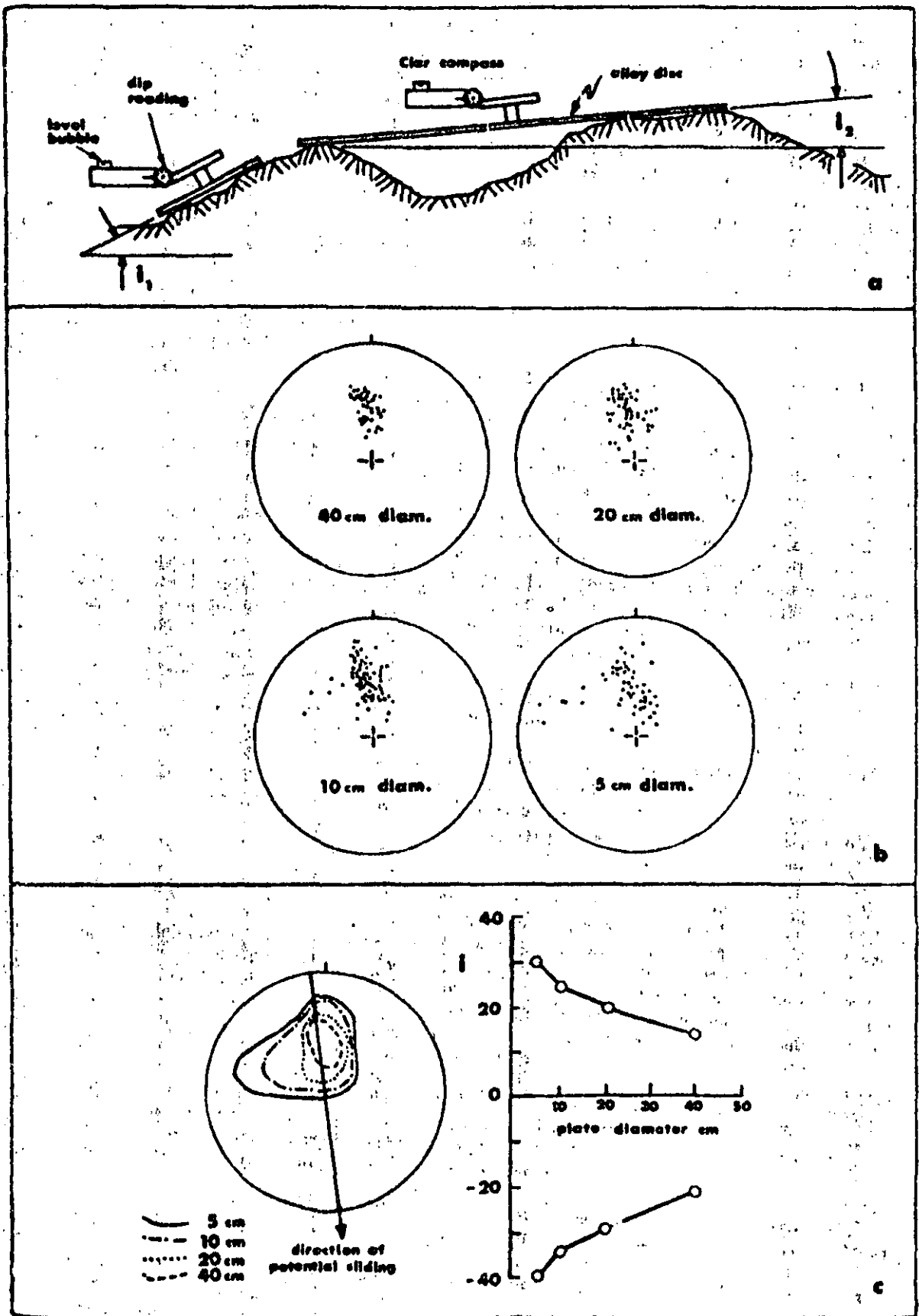


Fig. 16. A method of recording discontinuity roughness in three dimensions, for cases where the potential direction of sliding is not yet known. Circular discs of different dimensions (e.g. 5, 10, 20 and 40 cm) are fixed in turn to a Clar compass and clinometer. The dip direction and dip readings are plotted as poles on equal-area nets. Adapted from: (1) and (2).

not to influence the process of dilation). See Fecker and Rengers [1] for further details.

(c) *Photogrammetric method.* The coordinates representing points on the surface of the given discontinuity are recorded using a stereoscopic plotting instrument or a stereo comparator, with automatic recording equipment (i.e. punched tape). Roughness profiles can be drawn by computer.

Methods are available for estimating the shear strength and dilation characteristics of discontinuities (specifically unfilled joints), based on statistical analysis of these surface coordinates [4, 5].

#### Presentation of Results

(a) *Linear profiling.* The (x) and (y) readings should be plotted to the same scale (not distorted), and inclined correctly, as shown diagrammatically in the inset to Fig. 15. Profiles representing the minimum, most common, and maximum roughness should be drawn on the same page to make comparison easier. The three profiles may represent a discontinuity set, a single critical discontinuity, or each surface sampled. This will depend on the amount of detail required. A scale should be included in all the drawings. Profiles should be identified clearly, and the azimuth and dip of the measuring direction should be stated, in case this differs from the previously recorded orientation  $\alpha/\beta$  of the discontinuity.

Photographs of the relevant surfaces showing minimum, modal and maximum roughness should be presented together with the profiles.

(b) *Compass and disc-clinometer.* The field measurements of dip direction and dip obtained with the various diameters of discs should be plotted as poles on equal area nets, one for each disc. These can be combined and presented on a single contoured plot, as shown in Fig. 16.

Measurements from several discontinuities of a given set, may be grouped on the same equal area net if desired, to show the range of roughness (and the overall variation in orientation caused by any waviness).

Photographs of the relevant surfaces showing minimum, modal and maximum roughness should be presented together with the pole diagrams.

(c) *Photogrammetric method.* For purposes of visual presentation in a report, the most useful figures will be profiles rather than contour diagrams of surface roughness. The profiles, which will normally be plotted by computer, should be presented with 1:1 vertical:horizontal scales, in preference to exaggerated vertical scales.

If the direction of potential sliding is unknown, the profiles should be computed and presented to represent the roughness in the line of dip (dip vector direction). Correctly orientated profiles can be produced at a later stage.

Photographs of the relevant surfaces showing minimum, modal and maximum roughness should be presented together with the profiles.

(d) *Descriptive terms.* In the preliminary field mapping (i.e. during feasibility studies) time constraints may prevent the use of the above measuring techniques. The description of roughness will be limited to descriptive terms which should be based on two scales of observation:

Small scale (several centimetres)

Intermediate scale (several metres)

- I Rough (or irregular), stepped
- II Smooth, stepped
- III Slickensided, stepped
- IV Rough (or irregular), undulating
- V Smooth, undulating
- VI Slickensided, undulating
- VII Rough (or irregular), planar
- VIII Smooth, planar
- IX Slickensided, planar

The term "slickensided" should only be used if there is clear evidence of previous shear displacement along the discontinuity.

The intermediate scale of roughness is divided into three degrees: stepped, undulating and planar, and the small scale of roughness superimposed on the intermediate scale is also divided into three degrees: rough (or irregular), smooth, slickensided. The direction of striations or slickensides should be noted as shear strength may vary with direction. Roughness profiles typical of the nine classes are illustrated in Fig. 17.

(The effective roughness angles ( $\theta$ ) displayed by the categories of profile mean that in terms of shear strength, I > II > III, IV > V > VI and VII > VIII > IX assuming that mineral coatings are entirely absent or present in equal amounts. It is also evident that I > IV > VII; II > V > VIII, III > IX and VI > IX. Some of the inequalities are less certain. For example VII might be stronger than III. This would depend on whether or not dilation was inhibited. Around underground excavation dilation is usually inhibited by the stiffness of the surrounding rock mass. Beneath a rock slope it may not be).

There may also be a large scale waviness superimposed on the above small and intermediate scale observation. In such cases these characteristics should also be noted i.e. smooth, undulating (class VI) or large scale waviness (10 m wave length, 50 m amplitude).

The descriptions associated with persistence, i.e. systematic, sub-systematic, non systematic will obviously be of the greatest importance in determining the relative importance of the above descriptions of roughness.

#### Estimation of shear strength

The main purpose in describing the roughness of the walls of discontinuities is to facilitate the estimation of shear strength, in particular in the case of unfilled discontinuities where estimates may be quite uncertain.

In crude terms, shear strength will consist of a minimum (peak) or minimum (residual) friction angle, plus some intermediate angle (depending upon the degree



Suggested Methods for the Quantitative Description of Discontinuities

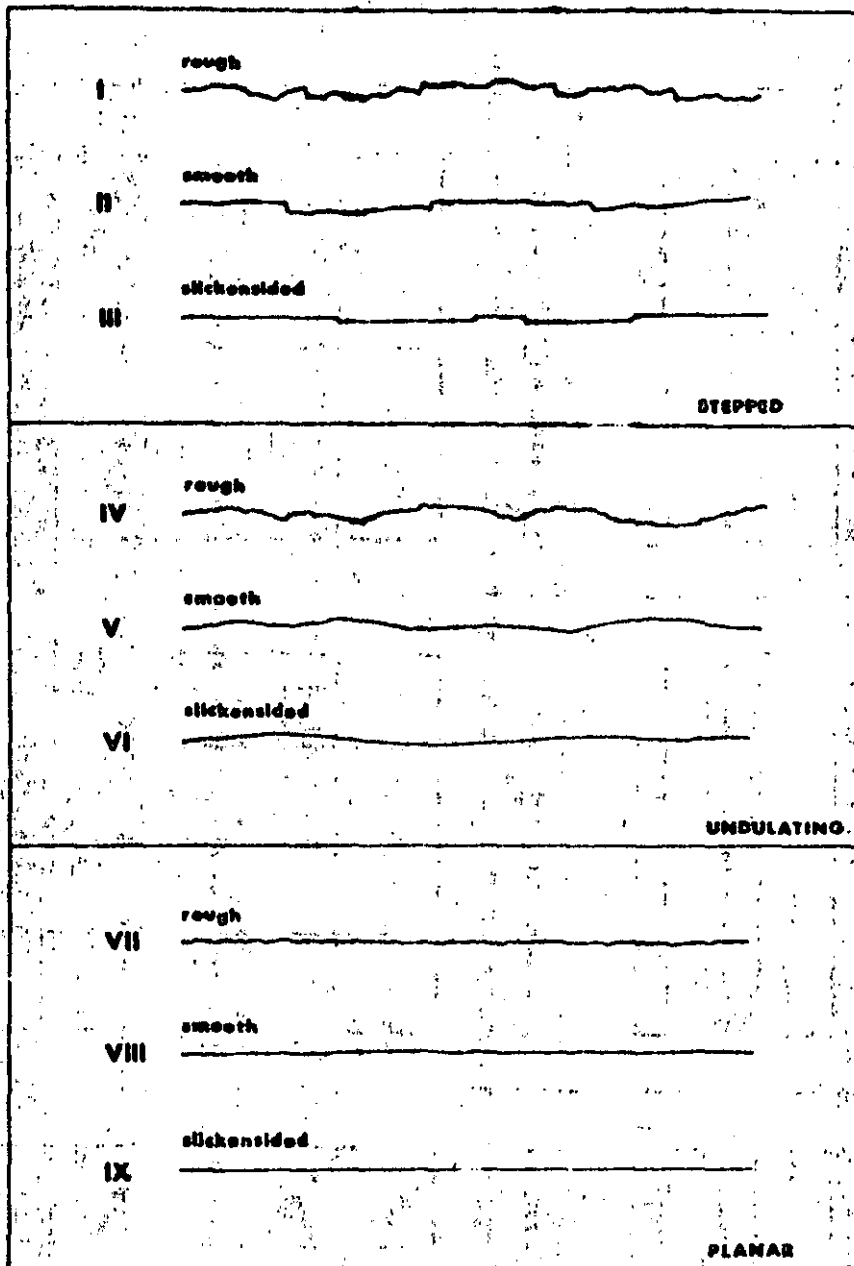


Fig. 17 Typical roughness profiles and suggested nomenclature. The length of each profile is in the range: 1 to 10 metres. The vertical and horizontal scales are equal.

of previous shear displacement) plus a contribution (i) due to large scale waviness, if this exists.

- Thus:
- $\tau = \sigma_n \tan(\phi + i)$
  - $\tau$  = shear strength (peak or residual)
  - $\phi$  = friction angle (peak or residual)
  - $\sigma_n$  = effective normal stress
  - $i$  = waviness (if present)

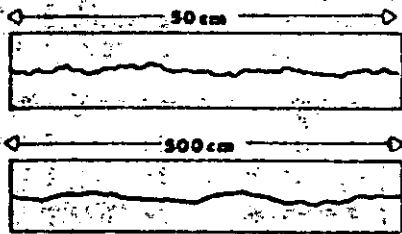
The value of  $\tau_{(peak)}$  will depend on the value of  $\sigma_n$  and on the degree of roughness. In the case of unfilled joints  $\phi_{(peak)}$  values generally range from about 30 to 70° and commonly average about 45°. In the case of joints having vertical or very steep steps, or less than 100% persistence, there will also be a cohesion (c) to

add to the above value of  $\tau$ . (e.g. profiles I, II, and III, Fig. 17).

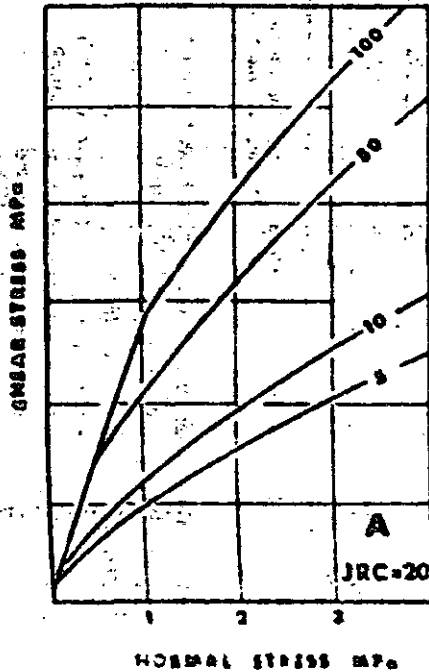
The value of  $\phi_{(residual)}$  will depend on the degree of weathering of the discontinuity walls and on the rock type. In the absence of weathering,  $\phi_{(residual)}$  usually varies from about 25 to 35°, most commonly around 30°. In the case of strongly weathered walls, the value may fall to around 15°, even in the absence of actual clay fillings. A method of estimating  $\phi_{(residual)}$  is described by Barton and Choubey [6]. The estimate is based on the ratio between the Schmidt hammer rebound (r) obtained on the weathered joint wall and the rebound (R) obtained on the unweathered rock.

Values of  $\phi_{peak}$  can be estimated using the following

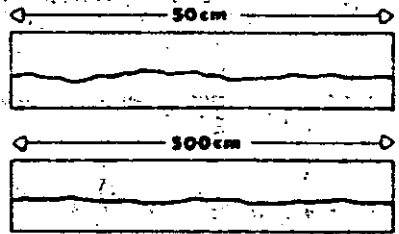
**A. ROUGH UNDULATING** - tension joints, rough sheeting, rough bedding.



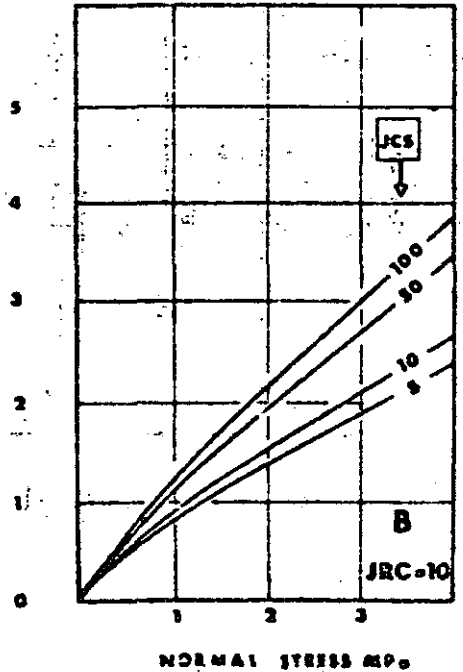
$$\tau_{\sigma_n} = \tan(20 \cdot \log_{10} \left( \frac{JCS}{\sigma_n} \right) + 30^\circ) \quad (A)$$



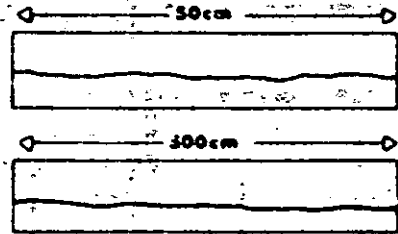
**B. SMOOTH UNDULATING** - smooth sheeting, non-planar, foliation and bedding.



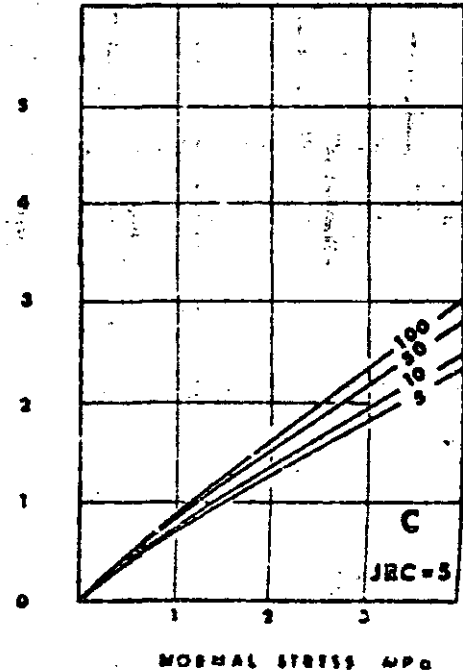
$$\tau_{\sigma_n} = \tan(10 \cdot \log_{10} \left( \frac{JCS}{\sigma_n} \right) + 30^\circ) \quad (B)$$



**C. SMOOTH NEARLY PLANAR** - planar shear joints, planar foliation, bedding.



$$\tau_{\sigma_n} = \tan(5 \cdot \log_{10} \left( \frac{JCS}{\sigma_n} \right) + 30^\circ) \quad (C)$$



## Suggested Methods for the Quantitative Description of Discontinuities

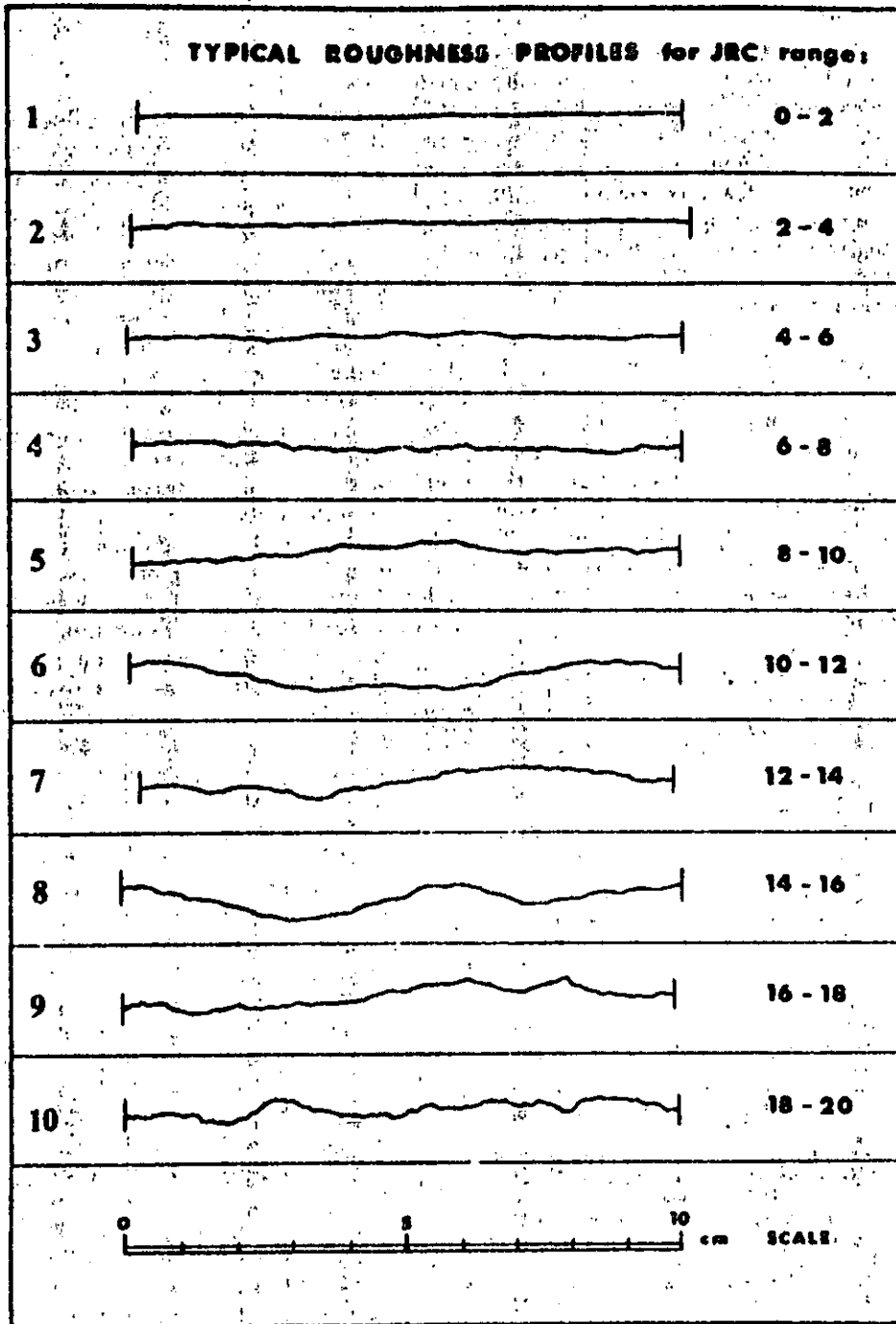


Fig. 19. Roughness profiles and corresponding range of JRC values associated with each one [6].

formula:

$$\phi_{\text{peak}} = \text{JRC} \log_{10} \left( \frac{\text{JCS}}{\sigma_n} \right) + \phi_r$$

where

JRC = joint roughness coefficient

JCS = joint wall compression strength

$\phi_r = \phi_{\text{residual}}$

The method of application is illustrated in Fig. 18. Firstly, the measured roughness profiles are matched with the three sets given at the top of Fig. 18, to obtain an estimate of the appropriate JRC value. (More

detailed profiles are given in Fig. 19 to facilitate this quantification). Secondly, the discontinuity walls are tested with a Schmidt hammer to estimate JCS and  $\phi_r$ . Note that in Fig. 18,  $\phi_r$  has been assumed as  $30^\circ$  in every case. The above method is a surprisingly accurate and cheap method of estimating  $\phi_{\text{peak}}$ . Further details are given by Barton and Choubey [6].

Since peak shear strength is mobilized after relatively small displacements it may not be realistic to add the large scale waviness angle (i) to this estimate of  $\phi_{\text{peak}}$ . For most practical purposes  $\phi_{\text{peak}}$  can be regarded

maximum value for a joint of 100% persistence. However,  $\phi_{\text{residual}}$  is not mobilized until relatively large displacements have occurred; which generally makes the large scale waviness angle (i) a realistic addition to shear strength. In the case of completely planar discontinuities or discontinuities that have sheared to the extent that no further dilation is possible, then  $\phi_{\text{residual}}$  will be the only shear strength component left; and will represent the absolute minimum shear strength for that discontinuity.

The above method for estimating the JRC value of a measured roughness profile is obviously subjective. Objective methods of analysing profiles are described in the literature by Fecker and Rengers [1] (compass and disc-clinometer method) and by Barton [5] (photogrammetric method). As described under Note (b), the method of analysing compass and disc-clinometer readings results in a dilation curve which is a plot of roughness (i) angles versus shear displacement. These (i) angles are added to  $\phi_p$  to estimate the shear strength for displacements intermediate between peak and residual strength.

#### REFERENCES

1. Fecker E. & Rengers N. Measurement of large scale roughnesses of rock planes by means of profilograph and geological compass. *Rock Fracture, Proc. of Int. Symp. Rock Mech. Nancy*, Paper 113 (1971).
2. Hoek E. & Bray J. *Rock slope engineering*. The Institution of Mining and Metallurgy, London, 309 p (1974).
3. Fecker E. Geologische Kartierung des Gebietes nordwestlich von Neustadt Weinstrasse sowie Bau und Anwendung eines Profilographen. Diplomarbeit, Universität Karlsruhe (1970).
4. Rengers N. Influence of the surface roughness on the friction properties of rock planes. *Proc. of 2nd Cong. of Int. Soc. Rock Mech.*, Belgrade, Vol. I, pp. 229-234 (1970).
5. Barton N. A relationship between joint roughness and joint shear strength. *Proc. Int. Symp. Rock Mech. Nancy, Rock Fracture*, Paper 1, 8 (1971).
6. Barton N. & Choubey V. The shear strength of rock joints in theory and practice. *Rock Mechanics* (Springer-Verlag), 10, 1-54 (1977).
7. Barton N. Review of a new shear strength criterion for rock joints. *Engng Geol.* 7, 287-332 (1973). (Also NGI Publ. No. 105, Oslo, 1974).
8. Patton F. D. Multiple modes of shear failure in rock and related materials. Ph.D. Thesis, Univ. of Illinois, 282 p (1966).
9. Patton F. D. & Deere D. U. Significant geologic factors in rock slope stability. *Proc. Symp. on Planning Open Pit Mines*, Johannesburg 1970, Balkema, Amsterdam, 1971, pp. 143-151 (1970).
10. Piteau D. R. Geological factors significant to the stability of slopes cut in rock. *Symp. on Planning Open Pit Mines*, Johannesburg, 1970, Balkema, Amsterdam, 1971, pp. 33-53 (1971).
11. Rengers N. Unebenheit und Reibungswiderstand von Gesteinsflächen. Dr. Ing. Dissertation, Fakultät für Bauingenieur- und Vermessungswesen, Universität Karlsruhe, 129 p (1971).
12. Wickens E. H. & Barton N. R. The application of photogrammetry to the stability of excavated rock slopes. *Photogram. Rec.* 7(37), April, 46-54 (1971).
13. Ross-Brown D. M., Wickens E. H. & Markland J. Y. Terrestrial photogrammetry in open pits: 2. An aid to the geological mapping. *Trans. Inst. Min. Metall. (Sect. A, Mining Industry)* 82, pp. A115-A130 (1973).
14. Schneider H. J. Rock friction—a laboratory investigation. *Proc. 1st Cong. of Int. Soc. Rock Mech. Denver, Advances in Rock Mechanics*, Vol. II, A, pp. 311-315 (1974).
15. Richards L. R. The shear strength of joints in weathered rock. Ph.D. Thesis, Univ. of London, 427 p (1975).
16. Goodman R. E. *Methods of Geological Engineering in Discontinuously Rocks*. West Publishing, N.Y., 422 p (1976).
17. Schneider H. J. The friction and deformation behaviour of rock joints. *Rock Mechanics* (Springer-Verlag) 8, 169-184 (1976).

#### 5. WALL STRENGTH

##### Scope

(a) The compressive strength of the rock comprising the walls of a discontinuity is a very important component of shear strength and deformability, especially if the walls are in direct rock to rock contact as in the case of unfilled joints. Slight shear displacement of individual joints caused by shear stresses within the rockmass often results in very small asperity contact areas and actual stresses locally approaching or exceeding the compression strength of the rock wall material, hence the asperity damage.

(b) Rock masses are frequently weathered near the surface, and are sometimes altered by hydrothermal processes. The weathering (and alteration) generally affects the walls of discontinuities more than the interior of rock blocks. This results in a wall strength some fraction of what would be measured on the fresher rock found in the interior of the rock blocks, for example that sampled by drill core. A description of the state of weathering or alteration both for the rock material and for the rock mass is therefore an essential part of the description of wall strength.

(c) There are two main results of weathering: one dominated by *mechanical disintegration*, the other by *chemical decomposition* including solution. Generally, both mechanical and chemical effects act together, but, depending on climatic regime, one or other of these aspects may be dominant. Mechanical weathering results in opening of discontinuities, the formation of new discontinuities by rock fracture, the opening of grain boundaries, and the fracture or cleavage of individual mineral grains. Chemical weathering results in discolouration of the rock and leads to the eventual decomposition of silicate minerals to clay minerals; some minerals, notably quartz, resist this action and may survive unchanged. Solution is an aspect of chemical weathering which is particularly important in the case of carbonate and saline minerals.

(d) The relatively thin "skin" of wall rock that affects shear strength and deformability can be tested by means of simple index tests. The apparent uniaxial compression strength can be estimated both from Schmidt hammer tests and from scratch and geological hammer tests, since the latter have been roughly calibrated against a large body of test data.

(e) Mineral coatings will affect the shear strength of discontinuities, to a marked degree if the walls are planar and smooth. The type of mineral coatings should be described where possible. Samples should be taken when in doubt.

(f) Procedures (a) and (b) concerning the weathering grade of the rock mass and the rock material are descriptive only. Procedures (c) *manual index tests* and (d) *Schmidt hammer tests* are increasingly quantitative. The latter is recommended for obtaining estimates of wall strength for subsequent calculation of shear strength, when utilizing the wall roughness coefficient (JRC) described under Roughness.

## Suggested Methods for the Quantitative Description of Discontinuities

Term	Description	Grade
Fresh	No visible sign of rock material weathering; perhaps slight discolouration on major discontinuity surfaces.	I
Slightly weathered	Discolouration indicates weathering of rock material and discontinuity surfaces. All the rock material may be discoloured by weathering and may be somewhat weaker externally than in its fresh condition.	II
Moderately weathered	Less than half of the rock material is decomposed and/or disintegrated to a soil. Fresh or discoloured rock is present either as a continuous framework or as corestones.	III
Highly weathered	More than half of the rock material is decomposed and/or disintegrated to a soil. Fresh or discoloured rock is present either as a discontinuous framework or as corestones.	IV
Completely weathered	All rock material is decomposed and/or disintegrated to soil. The original mass structure is still largely intact.	V
Residual soil	All rock material is converted to soil. The mass structure and material fabric are destroyed. There is a large change in volume, but the soil has not been significantly transported.	VI

**Equipment**

- (a) Geological hammer with one tapered point.
- (b) Strong pen knife or similar.
- (c) Schmidt hammer (L type) with conversion table and graph:
  - (i) to correct for orientation of hammer (supplied by the manufacturer)
  - (ii) to convert corrected rebound number to an estimate of uniaxial strength (Fig. 20)
- (d) Facilities for measuring the dry density of small rock samples, e.g. oven, balance, beaker, water.

**Procedure**

(a) *Weathering grade of rock mass.* The grade of weathering (or alteration) of the rock mass as a whole should be described first. The terms above are general and may be modified to suit particular situations.

(b) *Weathering grade of rock material.* The grade of weathering (or alteration) of the rock material comprising the walls of individual discontinuities or of the walls of a particular set of discontinuities (e.g. an unfavourably orientated set of joint(s)) should be described according to the following scheme:

(c) *Manual index tests.* The manual index tests detailed in the table on page 348 should be performed on the walls of discontinuities or on material representative of the walls. The choice and number of test locations will depend on the detail required. The approximate range of strength for the walls of a critical set of joints may be sufficient. Alternatively a single critical discontinuity may need to be characterised in detail.

The manual index tests can be performed on hand-sized pieces of freshly broken rock if the strength of intact rock bridges is of interest. Alternatively, the results of point load tests, if available, can be used to estimate the strength of the intact portions of any potential failure surface (see Persistence).

(d) *Schmidt hammer test.* The Schmidt hammer is applied in a direction perpendicular to the discontinuity wall of interest. The rock surface should be tested under saturated conditions to give the most conservative result. If the surfaces are unavoidably dry, this fact should be reported in the results. The surface should be free of loose particles, at least under the hammer position.

If the impulse from the spring-loaded projectile of the Schmidt hammer is sufficient to move the surface being tested, the resulting rebound will be artificially

Term	Description
Fresh	No visible sign of weathering of the rock material.
Discoloured	The colour of the original fresh rock material is changed. The degree of change from the original colour should be indicated. If the colour change is confined to particular mineral constituents this should be mentioned.
Decomposed	The rock is weathered to the condition of a soil in which the original material fabric is still intact, but some or all of the mineral grains are decomposed.
Disintegrated	The rock is weathered to the condition of a soil in which the original fabric is still intact. The rock is friable, but the mineral grains are not decomposed.

The stages of weathering described above may be subdivided using qualifying terms, for example "slightly discoloured", "moderately discoloured", "highly discoloured".

Grade	Description	Field Identification	Approx. range of uniaxial compressive strength (MPa)
S1	Very soft clay	Easily penetrated several inches by fist	<0.025
S2	Soft clay	Easily penetrated several inches by thumb	0.025-0.05
S3	Firm clay	Can be penetrated several inches by thumb with moderate effort	0.05-0.10
S4	Stiff clay	Readily indented by thumb but penetrated only with great effort	0.10-0.25
S5	Very stiff clay	Readily indented by thumbnail	0.25-0.50
S6	Hard clay	Indented with difficulty by thumbnail	>0.50
R0	Extremely weak rock	Indented by thumbnail	0.25-1.0
R1	Very weak rock	Crumbles under firm blows with point of geological hammer, can be pried by a pocket knife	1.0-5.0
R2	Weak rock	Can be pried by a pocket knife with difficulty, shallow indentations made by firm blow with point of geological hammer	5.0-25
R3	Medium strong rock	Cannot be scraped or pried with a pocket knife, specimen can be fractured with single firm blow of geological hammer	25-50
R4	Strong rock	Specimen requires more than one blow of geological hammer to fracture it	50-100
R5	Very strong rock	Specimen requires many blows of geological hammer to fracture it	100-250
R6	Extremely strong rock	Specimen can only be chipped with geological hammer	>250

Note: Grades S1 to S6 apply to cohesive soils, for example clays, silty clays, and combinations of silts and clays with sand, generally slow draining. Discontinuity wall strength will generally be characterized by grades R0-P6 (rock) while S1-S6 (clay) will generally apply to filled discontinuities (see Filling).  
Some rounding of strength values has been made when converting to SI units.

low. Such test results can normally be heard, since there is a "drummy" sound. These results should be ignored. For the above reason this field index test is unsuitable in a loose rock mass containing very closely spaced discontinuities. (In such cases small block samples can be removed and tested when clamped rigidly to a heavy base.)

Each surface of interest should be tested a number of times to ensure a representative set of results. It is suggested that tests are performed in groups of 10 (i.e. 10 tests per discontinuity, or 10 tests per unit area of a large critical discontinuity, applying the hammer to a new part of the surface before each impact. The five lowest readings of each group of 10 are discounted and the mean value ( $\bar{r}$ ) of the five highest readings is quoted.

The mean values of the Schmidt rebound ( $\bar{r}$ ) and rock density ( $\rho$ ) (see individual ISRM "Suggested Method") for a given discontinuity are used to estimate the value of the joint wall compressive strength (JCS) using Fig. 20 (see Note (c)).

The Schmidt hammer test can be performed on the surfaces of, or on material obtained from freshly broken rock when the strength of the intact rock bridges ( $\sigma_c$ )

is of interest. Alternatively the results of point load tests, if available, can be used to estimate the strength of the intact portions of any potential failure surfaces (see Persistence).

Discontinuities with thin mineral coatings that appear quite persistent over a given surface, and which would probably prevent initial rock to rock contact should be tested with the Schmidt hammer as above, applying the hammer to the surface of the mineral coating. Depending upon the thickness of the mineral coating and its hardness, the estimate of JCS may or may not be relevant for estimation of shear strength. In such cases of mineral coatings, the mineralogy should be described i.e. calcite, chlorite, talc, pyrite, gypsum, kaolinite, etc. Samples should be taken when in doubt. An estimate of the areal extent of the coating (e.g. 10%) and the range of the thickness of the coating (mm) should be included.

#### Notes

(a) Weathering grades of rock mass and rock material. Distribution of weathering grades in a rock mass

## Suggested Methods for the Quantitative Description of Discontinuities

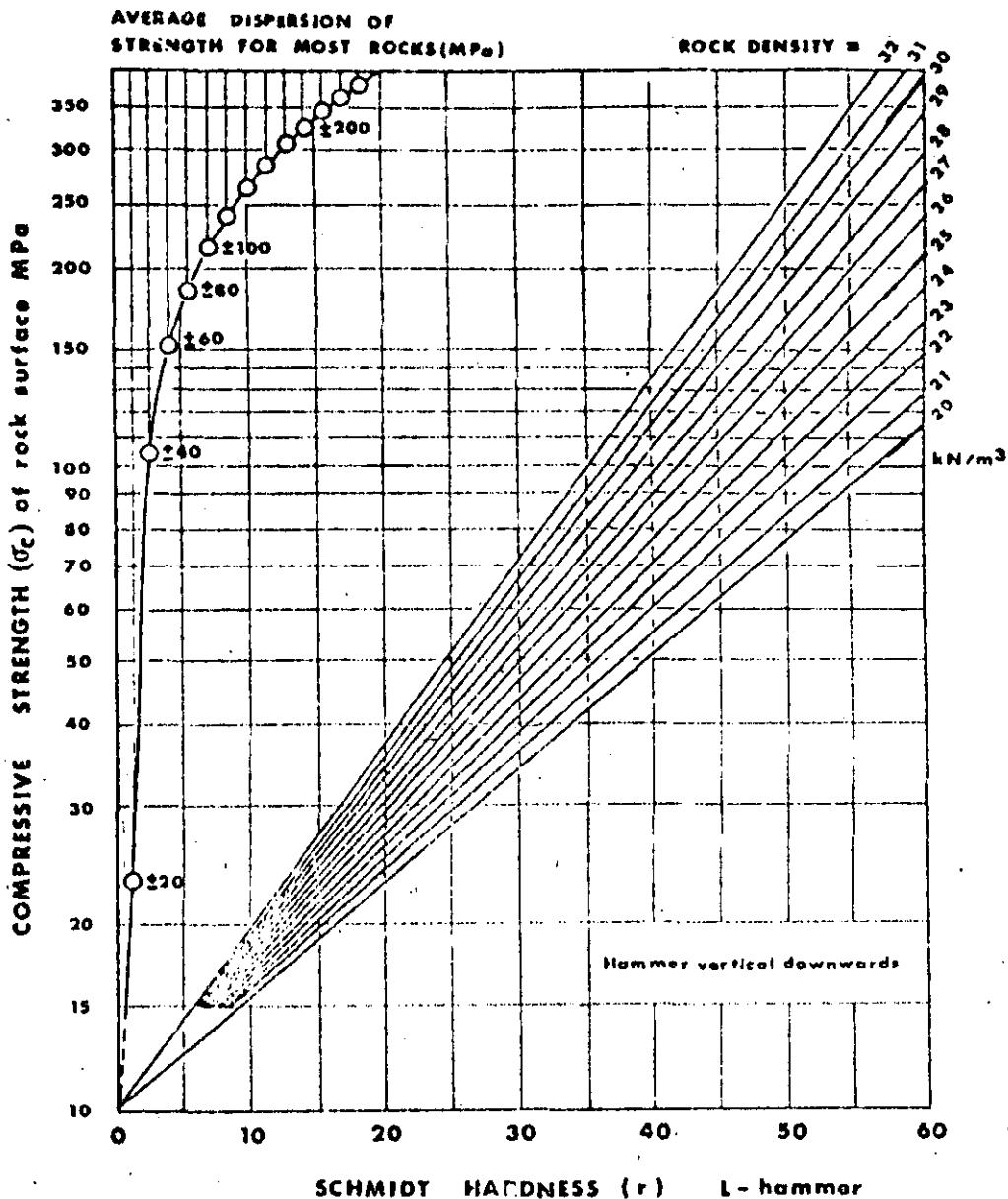


Fig. 20. Correlation chart for Schmidt (L) hammer, relating rock density, compressive strength and rebound number, after Miller [1]

be determined by mapping natural and artificial exposures. However, it should be borne in mind that isolated natural exposures of rock and excavations of limited extent are not necessarily representative of the whole rock mass, since weathering can be extremely variable.

Furthermore, all grades of weathering may not be seen in a given rock mass, and in some cases a particular grade may be present to a very small extent. Distribution of the various weathering grades of the rock material may be related to the porosity of the rock material and the presence of open discontinuities. In logging cores the distribution of weathering grades of the rock material may be recorded, but the distribution of weathering grades of the rock mass from which the cores were obtained can only be inferred.

Rock masses which are weathered due to exposure to, or infiltration from surface agents should be distinguished where possible from those that are altered as a result of infiltration of hydrothermal solutions. However, in many instances the effects of alteration are not easily distinguished from those brought about by weathering.

An abundant class of rock materials, notably those with high clay content, are prone to swelling, weakening or disintegration when exposed to short term weathering processes of a wetting and drying nature. Special tests are necessary to predict this aspect of mechanical performance. (See ISRM Suggested Methods for determination of swelling and slake-durability index properties.)

(b) Manual index tests. The manual index tests are

Corrections for reducing measured Schmidt hammer rebound ( $r$ ) when the hammer is not used vertically downwards

Rebound $r$	Downwards		Upwards		Horizontal $\alpha = 0^\circ$
	$\alpha = -90^\circ$	$\alpha = -45^\circ$	$\alpha = +90^\circ$	$\alpha = +45^\circ$	
10	0	-0.8	---	---	-3.2
20	0	-0.9	-8.8	-6.9	-3.4
30	0	-0.8	-7.8	-6.2	-3.1
40	0	-0.7	-6.6	-5.3	-2.7
50	0	-0.6	-5.3	-4.3	-2.2
60	0	-0.4	-4.0	-3.3	-1.7

preferred to conventional tests on carefully prepared rock cylinders because a very large number of discontinuities can be sampled, thereby giving a more representative picture of the condition of the walls. Furthermore conventional tests cannot be applied to the thin skin of wall rock or mineral coatings that dominate the shear strength and deformability of the rock mass.

The manual index tests for determining grades S1-S6 (clay, see Filling) can be replaced by more accurate assessment using a standard soil mechanics pocket penetrometer. This contains a stylus which is pressed into the sample at a constant rate. The maximum resistance can be read off a scale which is calibrated to show the maximum compressive strength of the sample. (This value is equal to twice the undrained shear strength =  $\frac{1}{2}(\sigma_1 - \sigma_3)$ .)

(c) *Schmidt hammer tests.* The Schmidt hammer rebound number ranges in practice from about 10 to 60. The lowest number applies to "weak" rocks (uniaxial compressive strength  $\sigma_c < 20$  MPa), while the highest number applies to "very strong" and "extremely strong" rocks ( $\sigma_c > 150$  MPa). "Very weak" rocks and "extremely weak" rocks cannot be tested with the L-hammer. *Manual index tests* must therefore be resorted to for rock weaker than 15-20 MPa.

For a given strength of surface the rebound number is minimum when the hammer is used vertically downwards (rebound against gravity) and maximum when used vertically upwards. The correlation given in Fig. 20 applies to vertical downwards tests only. The corrections given in the following table should be applied when the hammer is used in other directions.

Block movement (drumminess) in closely jointed rock, or crushing of loose grains are some of the reasons for unexpectedly low rebound numbers in a given set of results. Unexpectedly high readings are seldom obtained. The following two sets of actual results illustrate the suggested method of obtaining a realistic mean value:

(a) rough, planar iron-stained joints in granite

44, 36, 38, 44, 32, 44, 44, 40, 34, 42

mean of highest 5:  $r = 44$

(mean of 8 sets of 10 tests:  $r = 43$ )

(b) rough, undulating calcite-coated joints in hornfels

28, 28, 30, 30, 28, 24, 24, 28, 30, 20

mean of highest 5:  $r = 29$

(mean of 3 sets of 10 tests:  $r = 30$ )

The Schmidt test is one of the few tests, (with the exception of scratching tests) which takes into account the mechanical strength of the thin band of weathered wall material close to a discontinuity surface. Since it is this wall material which (in combination with roughness) controls the shear strength, it is of considerable importance as an index of rock quality. The joint rock compressive strength (JCS) is often as low as 25% of the adjacent intact rock strength ( $\sigma_c$ ) due to weathering effects. (See section *Estimation of Shear Strength* pp. 342-346.)

#### Presentation of results

(a) *Weathering grades of rock mass and rock material.* The weathering grades of recognizable weathering domains in the rock mass should be recorded on simplified sketches and/or vertical sections, with a clear key indicating the different weathering grades I, II, III etc.

The weathering grade of the rock material of individual discontinuities or of specific discontinuity sets should be described, i.e. "joint set no. 1: majority walls moderately discoloured, approx. 20% fresh".

(b) *Manual index tests.* The strength of the wall rock material of individual discontinuities or of specific discontinuity sets should be noted together with the assumed range of uniaxial compressive strength, i.e. "joint set no. 1: majority medium strong (R<sub>4</sub> 25-50 MPa), approx. 20% strong (R<sub>4</sub> 50-100 MPa)".

Values that are pertinent to the discontinuity sets should be carefully distinguished from any values that might have been recorded for the material representing the fresher rock within the rock blocks.

(c) *Schmidt hammer tests.* The mean rebound ( $r$ ) for the wall rock material of individual discontinuities or of specific discontinuity sets should be noted, together with the mean rock density ( $\gamma$ ), and the estimate of wall strength (JCS) in MPa. One set of 10 results should be selected to show the typical range of rebound values.

Values that are pertinent to the discontinuity sets should be carefully distinguished from any values that might have been recorded for the material representing the fresher rock within the rock blocks

#### REFERENCES

1. Miller R. P. Engineering classification and index properties of intact rock. Ph.D. Thesis. Univ. of Illinois (1965)



## Suggested Methods for the Quantitative Description of Discontinuities

2. Hucks V. A rapid method of determining the strength of rocks *in situ*. *Int. J. Rock Mech. Min. Sci.* 2, 127-134 (1965).
3. Terzaghi K. & Peck R. B. *Soil Mechanics in Engineering Practice*. 2nd edn. 729 p Wiley, New York, (1967).
4. Jennings J. E. & Robertson A. MacG. The stability of slopes cut into natural rock. *Proc. of VIIth. Int. Conf. on Soil Mechanics and Foundation Engineering*, Mexico, Vol. II, pp. 585-590 (1969).
5. Fookes P. G., Dearman W. R. & Franklin J. A. Some engineering aspects of rock weathering with field examples from Dartmoor and elsewhere. *Q. Jl. Engng Geol.* 4, 139-185 (1971).
6. Patton F. D. & Deere D. U. Significant geologic factors in rock slope stability. *Proc. Symp. on Planning Open Pit Mines*, Johannesburg 1970, Balkema, Amsterdam, pp. 143-151 (1971).
7. Piteau D. R. Geological factors significant to the stability of slopes cut in rock. *Planning Open Pit Mines*, Johannesburg, Symp. 1970, Balkema Amsterdam 1971, pp. 33-53 (1971).
8. Robertson A. MacG. The interpretation of geological factors for use in slope theory *Symp. Planning Open Pit Mines*, Johannesburg, 1970, Balkema Amsterdam 1971, pp. 55-71 (1971).
9. Geological Society Engineering Group Working Party Report on "The preparation of maps and plans in terms of engineering geology". *Q. Jl. Engng Geol.* 5, 295-382 (1972).
10. International Society For Rock Mechanics. Suggested methods for determining water content, porosity, density, absorption and related properties and swelling and slake-durability index properties. ISRM Commission on Standardization of Laboratory and Field Tests, 36 p (1972).
11. Barton N. Review of a new shear-strength criterion for rock joints: *Engng Geol.* Amsterdam, 7, 278-332 (1973) (also N-GI Publication No. 105, 1974, Oslo.)
12. Dearman W. R. The characterization of rock for civil engineering practice in Britain: *La Géologie de l'Ingénieur*, Société Géologique de Belgique, Liège, pp. 1-75 (1974).
13. Franklin J. A. Rock quality in relation to the quarrying and performance of rock construction materials. *Proc. of 2nd. Int. Cong. of the Int. Assoc. of Engng Geology*, São Paulo, Brazil, Vol. 1, IV-PC-2, 11 p (1974).
14. Martin G. R. & Millar P. J. Joint strength characteristics of a weathered rock. *Proc. of 3rd. Cong. of Int. Soc. Rock Mech.*, Denver. *Advances in Rock Mechanics*, Vol. II A, pp. 263-270 (1974).
15. Richards L. R. The shear strength of joints in weathered rock. Ph.D. Thesis, Univ. of London, 427 p (1975).
16. Barton N. & Choubey V. The shear strength of rock joints in theory and practice. *Rock Mechanics* (Springer-Verlag), 10, 1-54 (1977).

## 6. APERTURE

## Scope

(a) Aperture is the perpendicular distance separating the adjacent rock walls of an open discontinuity, in which the intervening space is air or water filled. Aperture is thereby distinguished from the width of a filled discontinuity. (see Fig. 21) Discontinuities that have been filled (e.g. with clay) also come under this category if filling material has been washed out locally.

(b) Large apertures can result from shear displacement of discontinuities having appreciable roughness and waviness, from tensile opening, from outwash, and from solution. Steep or vertical discontinuities that have opened in tension as a result of valley erosion or glacial retreat may have very large apertures.

(c) In most sub-surface rock masses apertures are small and will probably be less than half a millimeter, compared to the tens, hundreds or even thousands of millimetres width of some of the outwash or extension varieties. Unless discontinuities are exceptionally smooth and planar it will not be of great significance to the shear strength that a "closed" feature is 0.1 mm wide or 1.0 mm wide. However, indirectly as a result

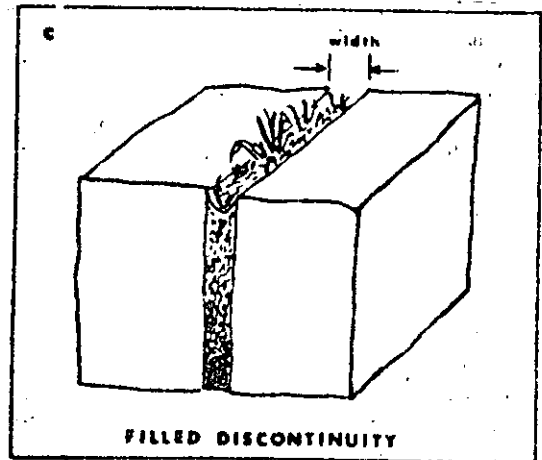
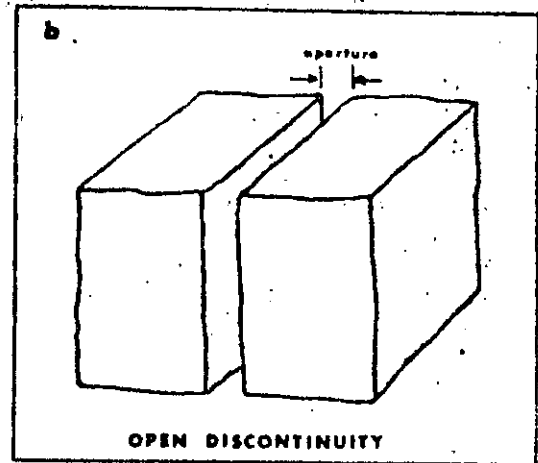
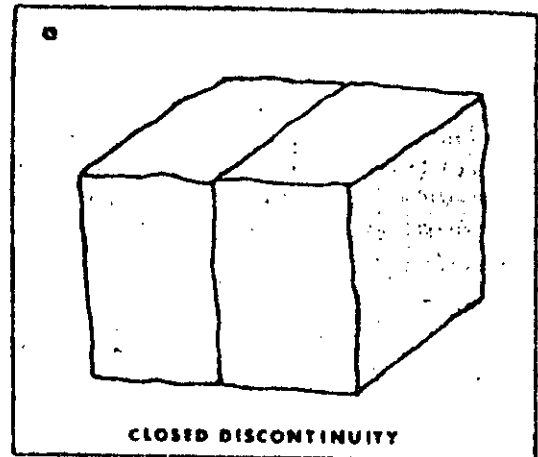


Fig. 21. Diagrams showing the suggested definitions of the aperture of open discontinuities and the width of filled discontinuities.

of hydraulic conductivity, even the finest may be significant in changing the effective normal stress and therefore also the shear strength.

(d) Unfortunately, visual observation of small apertures is inherently unreliable since, with the possible exceptions of drilled holes and bored tunnels, visible apertures are bound to be disturbed apertures, either

due to disturbance by blasting, or due to surface weathering effects. The influence of apertures is best assessed by water permeability testing. (This is the subject of an individual ISRM document.)

(e) Apertures are recorded from the point of view of both their loosening and conducting capacity. Joint water pressure, inflow of water and outflow of storage products (both liquid and gas) will all be affected by aperture.

#### Equipment

(a) Measuring tape of at least 3 m length, calibrated in mm.

(b) Feeler gauge (for estimating the width of fine apertures.)

(c) White-spray paint.

(d) Equipment for washing the rock exposure.

#### Procedure

(a) Dirty underground exposures should be washed clean. It is helpful to spray white paint along the desired lines of survey, so that the finest discontinuities are more easily visible. Good lighting is essential.

(b) Fine apertures can be measured approximately with feeler gauges, while the larger apertures can be measured with a rule graduated in mm. The apertures of all discontinuities intersecting the survey line will be recorded. Alternatively the variation in aperture of a major discontinuity can be measured along the trace of the discontinuity.

#### Notes

(a) The apertures visible in a rock exposure are inherently disturbed apertures, due either to localized surface weathering or to the mode of excavation. For these reasons measured apertures are likely to be larger than those existing within the rock mass. Tunnels that are machine bored (and borehole walls) should give a much more reliable indication of the undisturbed apertures. Borehole walls can be surveyed by means of periscopes, borehole cameras, and TV equipment, and by means of pressure sensitive packers, as described by Fairhurst and Roegiers [1].

(b) The borehole periscope is recommended when the depth from the surface does not exceed 30 metres. Greater depths result in distortion of the optical path which consists of a series of rigid tubes supporting a system of lenses and prisms. A mm calibrated scale, differently coloured from the rock, should be located on the outside of the periscope in such a position that the apparent apertures can be recorded. These readings must be corrected for orientation if the borehole does not intersect the discontinuities approximately at right angles.

(c) The core recovery method known as the *integral sampling method* [2] is recommended for obtaining aperture data in special circumstances. The method essentially consists of recovering a core sample which has previously been reinforced with a grouted bar. The reinforcing bar is co-axially overcovered with a larger diameter coring crown.

(d) Even undisturbed apertures give a poor indication of their water conducting potential. The surface roughness may reduce the actual conductivity to a fraction of its theoretical smooth-wall equivalent as a result of friction and tortuosity effects. In addition, there is much evidence that flow in joints may be tube-like rather than sheet-like [3]. *In situ* permeability testing will be a much more reliable indicator of the influence of apertures than direct measurement (*Field Permeability* forms the subject of an individual ISRM document).

(e) Apertures measured across discontinuities that are displaced by previous shearing (for example in an unstable slope) may vary widely from point to point. The "dead areas" caused by asperity contact and undetected debris will again make aperture measurements rather unreliable as a basis for conductivity estimation (e).

#### Presentation of results

(a) Apertures can be described by means of the following terms:

Aperture	Description	
< 0.1 mm	Very tight	
0.1-0.25 mm	Tight	"Closed" features
0.25-0.5 mm	Partly open	
0.5-2.5 mm	Open	
2.5-10 mm	Moderately wide	"Gapped" features
> 10 mm	Wide	
1-10 cm	Very wide	
10-100 cm	Extremely wide	"Open" features
> 1 m	Cavernous	

(b) Modal (most common) apertures should be recorded for each discontinuity set.

(c) Individual discontinuities having apertures noticeably wider or larger than the modal value should be carefully described, together with location and orientation data.

(d) Photographs of extremely wide (10-100 cm) or cavernous (> 1 m) apertures should be appended.

#### REFERENCES

1. Fairhurst C. & Roegiers J. C. Estimation of rock mass permeability by hydraulic fracturing—a suggestion. Discussion. *Ann. Int. Soc. Rock Mech. Symp.*, Stuttgart. *Percolation Through Fissured Rock*, D2, pp. 1-5 (1972).
2. Rocha M. & Barroso M. Some applications of the new integral sampling method in rock masses. *Proc. Int. Symp. on Rock Mech.* Nancy. *Rock Fracture*, Paper 1-21 (1971).
3. Wolters R., Reinhardt M. & Jäger B. Beobachtungen über die Anordnung und Ausdehnung von Klüffnungen. *Proc. Int. Soc. Rock Mech. Symp.*, Stuttgart. *Percolation Through Fissured Rock*, T1-1, 13 p (1972).
4. Sharp J. C. & Maini Y. N. T. Fundamental considerations on the hydraulic characteristics of joints in rock. *Proc. Int. Soc. Rock Mech. Symp.*, Stuttgart. *Percolation Through Fissured Rock*, T1-1, 15 p (1972).
5. Cecil O. S. Correlations of rockbolt—shotcrete support and rock quality parameters in Scandinavian tunnels. Ph.D. Thesis, University of Illinois, 414 p (1970).
6. Schneider T. R. Seelberg tunnel: Geologie des Bauprojektes Schweiz. Nationalstrasse, NZ, Zürich (1970).

## Suggested Methods for the Quantitative Description of Discontinuities

7. Neustadt L. Genesis und quantitative Charakteristik der Klüftigkeit (in Bezug auf den Wasserhaushalt). *Proc. Int. Symp. on Rock Mech.*, Nancy. *Rock Fracture*. Paper I-15 (1971).
8. Morfeldt C. O. Drainage problem in connection with tunnel construction in Precambrian granitic bedrock (in Sweden). *Proc. Int. Soc. Rock Mech. Symp.*, Stuttgart. *Percolation Through Fissured Rock*. Paper T4-G. 9 p (1972).
9. Rocha M. Discussion. *Proc. Int. Soc. Rock Mech. Symp.*, Stuttgart. *Percolation Through Fissured Rock*. D1. pp. 11-15 (1972).
10. Bieniawski Z. T. Geomechanics classification of rock masses and its application in tunneling. *Proc. 3rd. Cong. of Int. Soc. Rock Mech.*, Denver. *Advances in Rock Mechanics*. Vol. IIA. pp. 27-32 (1974).
11. Korhonen K-H., Gardemeister R., Jääskeläinen H., Niini H. & Vihäsarja P. Engineering geological rock classification (in Finnish) Geotechnical Laboratory, Report 12, Technical Research Centre of Finland, 78 p (1974).

## 7. FILLING

## Scope

(a) Filling is the term for material separating the adjacent rock walls of discontinuities, e.g. calcite, chlorite, clay, silt, fault gouge, breccia etc. The perpendicular distance between the adjacent rock walls is termed the *width* of the filled discontinuity, as opposed to the *aperture* of a gapped or open feature.

(b) Due to the enormous variety of occurrences, filled discontinuities display a wide range of physical behaviour, in particular as regards their shear strength deformability and permeability. Short-term and long-term behaviour may be quite different such that it is easy to be misled by favourable short term conditions.

(c) The wide range of physical behaviour depends on many factors of which the following are probably the most important.

- (i) Mineralogy of filling material
- (ii) Grading or particle size
- (iii) Over-consolidation ratio
- (iv) Water content and permeability
- (v) Previous shear displacement
- (vi) Wall roughness
- (vii) Width
- (viii) Fracturing or crushing of wall rock

(d) Every attempt should be made to record the above factors, using quantitative descriptions where possible, together with sketches and/or colour photographs of the most important occurrences. Certain index tests are suggested for a closer investigation of major discontinuities considered to be a threat to stability. In special cases the results of these field descriptions may warrant the recommendation for large scale *in situ* testing, at least in the case of dam foundations or major slopes.

## Equipment

- (a) Measuring tape of at least 3 m length, graduated in mm.
- (b) Folding straight-edge of at least 2 m in length.
- (c) Plastic bags for taking samples of the filling material of up to 1 or 2 kg in weight. In some cases undisturbed samples may be required for shear testing.

Various soil mechanics tube samplers can be used for this operation.

(d) Geological hammer with one tapered point.

(e) Strong pen knife or similar.

## Procedure

(a) *Width*. The minimum and maximum widths of simple filled discontinuities (e.g. clay filled joints) should be measured to the nearest 10%, and an estimate made of the most common (modal) width. Marked differences between the minimum and maximum widths may indicate that shear displacement has occurred if the walls are essentially unaltered or unweathered.

In cases where fillings are thin it may be helpful to try to measure the mean amplitude of wall roughness using the straight edge, and compare this with the mean width of the filling as illustrated in Fig. 22. This will be especially valuable when assessing shear strength and deformation characteristics in detailed studies.

The principal dimensions of complex filled discontinuities (e.g. shear zones, crushed zones, faults, fault zones, dykes and lithological contacts) should be estimated, or measured to the nearest 10%, when possible. In the case of important occurrences it is helpful to make field sketches such that the condition of the wall rock (i.e. degree of associated fracturing and/or alteration) is also communicated. See examples in Fig. 23.

(b) *Weathering grades*. Filled discontinuities that have originated as a result of preferential weathering along discontinuities may have fillings composed of *decomposed* rock, or *disintegrated* rock. The relevant type should be recorded.

**Decomposed:**— The rock is weathered to the condition of a soil in which the original material fabric is still intact, but some or all of the mineral grains are decomposed.

**Disintegrated:**— The rock is weathered to the condition of a soil, in which the original material fabric is still intact. The rock is friable, but the mineral grains are not decomposed.

(c) *Mineralogy*. For all types of filled discontinuities the finest fraction of the filling or gouge is of most interest since this usually controls the long term shear strength. The mineralogical composition of the finer filling material should therefore be determined, especially in cases where active clays or swelling clays are suspected. Samples should be taken when in doubt concerning the mineralogy.

In cases where swelling clay such as montmorillonite is identified or suspected, and where this condition might be critical for stability, samples should be taken for free swelling and swelling pressure tests. (It is of advantage to record the *in situ* water content of these samples where possible. Such samples should therefore be sealed.)

(d) *Particle size*. The method of describing the grad-

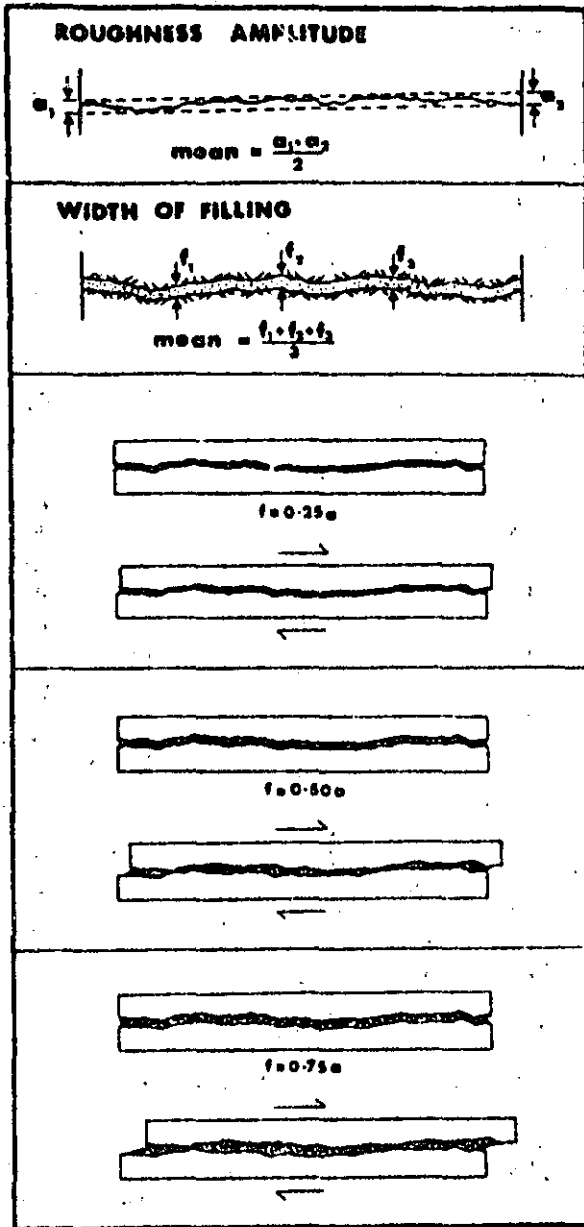


Fig. 22 In the case of simple filled discontinuities, the amplitude of the wall roughness and the thickness of the filling can help to indicate the amount of shear displacement required for rock contact (stiffening) to occur. (Zero volume change assumed during shear).

ing or particle size will depend on the type of occurrence. A rough quantitative description of the grading of discontinuity fillings can be given by estimating the percentages of clay, silt, sand and rock particles. ( $\pm 10\%$ ). Several kilos of filling material may need to be extracted and fingered before making these estimates.

Particle size can be classified according to the modified Wentworth scale below:

boulders	200-600 mm
cobbles	60-200 mm
coarse gravel	20-60 mm
medium gravel	6-20 mm
fine gravel	2-6 mm

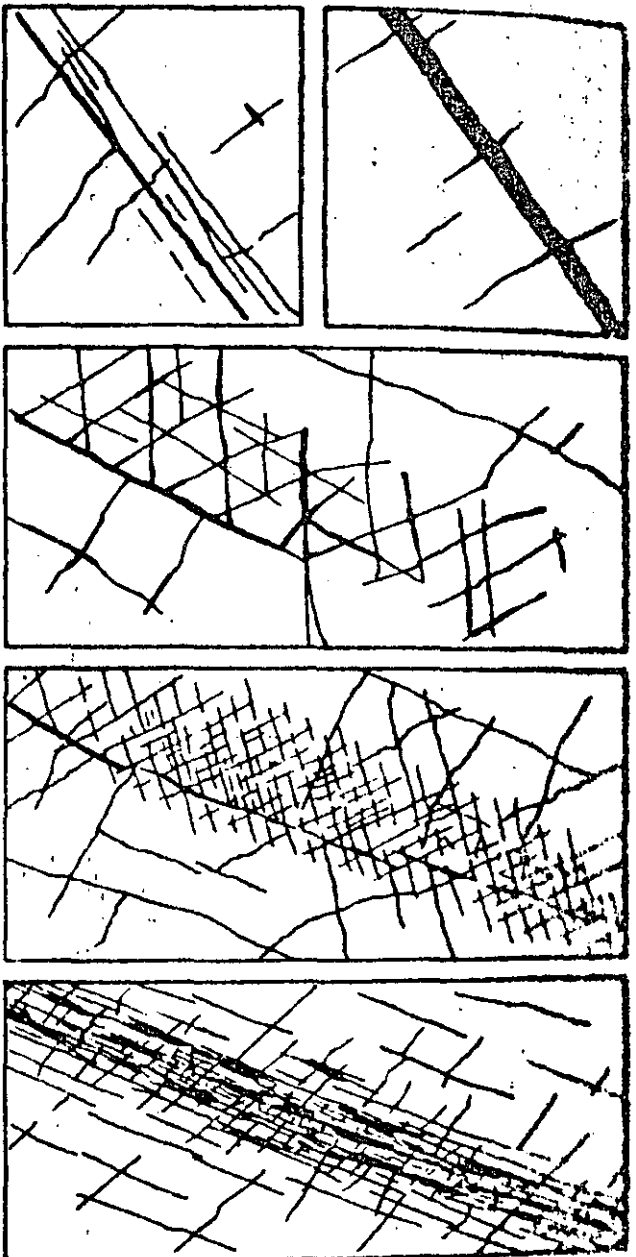


Fig. 23. Examples of field sketches of complex filled discontinuities [1].

coarse sand	0.6-2 mm
medium sand	0.2-0.6 mm
fine sand	0.06-0.2 mm
silt, clay	

## Suggested Methods for the Quantitative Description of Discontinuities

If a detailed soil mechanics investigation is warranted the finest fraction can be analysed in the laboratory to determine:

clay fraction (% < 2  $\mu$ )

% passing No. 200 sieve (74  $\mu$ )

Atterberg index tests to determine liquid limit and plasticity index:  $PI = (LL - PL) \%$

(e) *Filling strength.* Filling material, in particular the finer fraction which is usually weakest, can be assessed by means of the manual index tests tabulated below, as recommended under Wall Strength:

The undrained shear strengths of the soils represented in grades S1 to S6 are equal to one half of the given uniaxial compressive strengths (care should be taken in applying these estimates to fissured clays.)

If a detailed soil mechanics investigation is warranted (e.g. drained shear strength determination) due to the critical nature of an individual filled discontinuity, then undisturbed samples of the filling material may be required. Various tube samplers are available for this sampling operation.

(f) *Previous displacement.* Care should be taken to determine whether a given filled discontinuity has suffered previous shear displacement or not. (Stickensides,

shears, displaced cross joints, etc.) This should be recorded in conjunction with an estimate of the approximate over-consolidation ratio (OCR) of any clay filling.

(g) *Water content and permeability.* The water content and permeability of the filled discontinuity as a whole and of the clay filling in particular should be described as below (see also under Seepage). The decision to make actual measurements of these properties will depend on the importance of the occurrence to the project.

W1 The filling materials are heavily consolidated and dry, significant flow appears unlikely due to very low permeability.

W2 The filling materials are damp, but no free water is present.

W3 The filling materials are wet, occasional drops of water.

W4 The filling materials show signs of outwash, continuous flow of water (estimate litres/minute).

W5 The filling materials are washed out locally, considerable water flow along out-wash channels (estimate litres/minute and describe pressure i.e. low, medium, high).

Grade	Description	Field identification	Approx. range of uniaxial compressive strength (MPa)
S1	Very soft clay	Easily penetrated several inches by fist	< 0.025
S2	Soft clay	Easily penetrated several inches by thumb	0.025-0.05
S3	Firm clay	Can be penetrated several inches by thumb with moderate effort	0.05-0.10
S4	Stiff clay	Readily indented by thumb but penetrated only with great effort	0.10-0.25
S5	Very stiff clay	Readily indented by thumbnail	0.25-0.50
S6	Hard clay	Indented with difficulty by thumbnail	> 0.50
R0	Extremely weak rock	Indented by thumbnail	0.25-1.0
R1	Weak rock	Crumbles under firm blows with point of geological hammer, can be peeled by a pocket knife	1.0-5.0
R2	Weak rock	Can be peeled by a pocket knife with difficulty, shallow indentations made by firm blow with point of geological hammer	5.0-25
R3	Medium strong rock	Cannot be scraped or peeled with a pocket knife, specimen can be fractured with single firm blow of geological hammer	25-50
R4	Strong rock	Specimen requires more than one blow of geological hammer to fracture it	50-100
R5	Very strong rock	Specimen requires many blows of geological hammer to fracture it	100-250
R6	Extremely strong rock	Specimen can only be chipped with geological hammer	> 250

*Note.* Grades S1 to S6 apply to cohesive soils, for example, clays, silty clays and combinations of silts and clays with sand, generally slow draining. Some rounding of the strength values has been made when converting to SI units.

W6 The filling materials are washed out completely, very high water pressures experienced, especially on first exposure (estimate litres/minute and describe pressure).

#### Notes

(a) The manual index tests for determining grades S1 to S6 can be replaced by more accurate assessments using a standard soil mechanics penetrometer. This contains a stylus which is pressed into the sample at a constant rate. The maximum resistance can be read off a scale which is calibrated to show the maximum compressive strength of the sample. (This value is equal to twice the undrained shear strength =  $2(\sigma_1 - \sigma_3)$ .)

(b) Hydrothermal alteration of gouge material and/or the deposition of hydrothermal products will complicate the mineralogical identification of fillings since products not associated with the petrography of the crushed rock or the wall rock may be present.

(c) If previous displacement has occurred through the potential weakest layers, of a filled discontinuity, i.e. through the clay filling or clay gouge, as evidenced by slickensides and shears, then the over-consolidation ratio (OCR) of the clay will not be important since the discontinuity will be close to residual strength. However, if previous displacement through these weak layers is not suspected then the over-consolidation ratio will be important since the peak drained shear strength of the intact clay may be much higher than the residual strength. Short term stability will be deceptively high, especially in the case of unloading, due to the reduced or negative pore pressures. However, in time swelling and softening may occur due to increased pore pressure and water content and possibly also due to strain softening caused by engineering loading, for example by excavation of an overlying rock slope. This potential for reduction in strength with time should not be underestimated during field assessment.

(d) Faults frequently contain highly permeable brecciated gouge adjacent to highly impermeable clay gouge. The water conducting capacity will therefore be strongly anisotropic, and may even be confined to flow parallel to the plane of the fault. It may be premature to describe a fault zone as "dry" or "impermeable" if the tunnel or exploratory adit has not completely penetrated the feature.

#### Presentation of results

The detail of presentation will be dependent on the importance of the individual filled discontinuity (or set) to the project as a whole. In general the description should be arranged as below, so as to include a description of those factors of particular relevance to the project in hand.

- (a) Geometry: width  
wall roughness  
field sketch
- (b) Filling type: mineralogy  
particle size  
weathering grade

- (c) Filling strength: soil index parameters  
swelling potential  
manual index (S1-S6)  
shear strength  
over-consolidation ratio  
displaced/undisplaced  
water content (rating as  
W1-W6) permeability  
quantitative data
- (d) Seepage:

#### REFERENCES

1. Korhonen K.-H., Gardemeister R., Jääskeläinen H., Niemi H. & Vahäsarja P. Engineering geological rock classification (in Finnish). Geotechnical Laboratory, Report 12, Technical Research Centre of Finland, 78 p (1974).
2. Müller L. *Der Felsbau*. Ferdinand Enke-Verlag, Stuttgart, 624 p (1963).
3. Brekke T. L. & Selmer-Olsen R. Stability problems in underground construction caused by montmorillonite-carrying seams and faults. *Engng. Geol.* 1, 3-19 (1965).
4. Skempton A. W. Some observations on tectonic shear zones. *Proc. 1st. Cong. of Int. Soc. Rock Mech.* Lisbon, Vol. 1, pp. 329-335 (1966).
5. Skempton A. W. & Peckley D. J. The strength along structural discontinuities in stiff clays. *Geotech. Conf. on Shear Strength Properties of Natural Soils and Rocks*, Oslo 1967, Proc. Vol. 2, pp. 29-46 (1968).
6. Cecil D. S. Correlations of rock bolt-shotcrete support and rock quality parameters in Scandinavian tunnels. Ph.D. Thesis, Univ. of Illinois 414 p (1970).
7. Selmer-Olsen R. *Ingeniørgeologi* (part II, Tapir, Trondheim), 207 p (1971).
8. Brekke T. L. & Howard T. R. Stability problems caused by seams and faults. *Proc. 1st. North American Rapid Excavation and Tunneling Conference*, Chicago, Vol. 1, pp. 24-41 (1973).
9. Brekke T. L. & Howard T. R. Functional classification of poor quality materials from seams and faults in relation to stability problems in underground openings. Dept. of Civ. Eng., Univ. of California Berkeley, 153 p (1973).
10. Deere D. U. The foliation shear zone - an adverse engineering geologic feature of metamorphic rocks. *J. Boston Soc. of Civ. Engrs.* 60, 163-176 (1973).
11. Barton N. A review of the shear strength of filled discontinuities in rock. *Fjellsprengningsteknikk, Bergmekanikk. Conf. Oslo*, Tapir, Trondheim, pp. 19-19.38 (1973). (Also NGU Publ. No. 195, Oslo 1974).
12. Barton N., Lien R. & Lunde J. Engineering classification of rock masses for the design of tunnel support. *Rock Mechanics* (Springer-Verlag), 6, 189-236 (1974).
13. Cording E. J. & Mahar J. W. The effect of natural geologic discontinuities on behaviour of rock in tunnels. *Proc. 2nd North American Rapid Excavation and Tunneling Conference*, San Francisco, Vol. 1, Chap. 12, pp. 107-138 (1974).
14. Dearman W. R. The characterization of rock for civil engineering practice in Britain. *La Géologie de l'Ingénieur, Société Géologique de Belgique*, Liège, pp. 1-75 (1974).
15. International Society for Rock Mechanics. Suggested methods for determining shear strength. *ISRM Commission on Standardization of Laboratory and Field Tests*, 23 p (1974).
16. Norwegian Rock Mechanics Group. Suggested terminology, definitions and map symbols for rock mechanics and engineering geology (in Norwegian). Tapir, Trondheim (1974).
17. Selmer-Olsen R. & Rokoengen K. About swelling tests and stability of clay zones in hard rock. *Proceedings of 3rd. Cong. of Int. Soc. Rock Mech.*, Denver, *Advances in Rock Mechanics*, Vol. 2-3, pp. 1061-1068 (1974).

#### 8. SEEPAGE

##### Scope

(a) Water seepage through rock masses results mainly from flow through water conducting discontinuities

## Suggested Methods for the Quantitative Description of Discontinuities

inities ("secondary" permeability). In the case of certain sedimentary rocks the "primary" permeability of the rock material may be significant such that a proportion of the total seepage occurs through the pores. The rate of seepage is roughly proportional to the local hydraulic gradient and to the relevant directional permeability, proportionality being dependent on laminar flow. High-velocity flow through open discontinuities may result in increased head losses due to turbulence.

(b) The prediction of groundwater levels, likely seepage paths, and approximate water pressures may often give advance warning of stability or construction difficulties. The field description of rock masses must inevitably precede any recommendation for field permeability tests so these factors should be carefully assessed at this early stage.

(c) Irregular groundwater levels and perched water tables may be encountered in rock masses that are partitioned by persistent impermeable features such as dykes, clay filled discontinuities or permeable beds. The prediction of these potential flow-barriers and associated irregular water tables is of considerable importance, especially for engineering projects where such barriers might be penetrated at depth by tunneling, resulting in high pressure inflows.

(d) Seepage of water caused by drainage into an engineering excavation may have far reaching consequences in cases where a sinking ground water level would cause settlement of structures founded on overlying clay deposits.

(e) The approximate description of the local hydrogeology should be supplemented with detailed observations of seepage from individual discontinuities or particular sets, according to their relative importance to stability. A short comment concerning recent precipitation in the area, if known, will be helpful in the interpretation of these observations. Additional data concerning groundwater trends and rainfall and temperature records will be useful supplementary information.

(f) In the case of rock slopes, the preliminary design estimates will be based on assumed values of effective normal stress. If, as a result of field observations one has to conclude that pessimistic assumptions of water pressure are justified (i.e. a tension crack full of water with zero exit pressure at the toe of the unfavourable discontinuity) then this will clearly have the greatest consequences for design. So also will the field observation that ice formation is possible or probable. Deterioration of rock slopes and tunnel portals through ice wedging and/or increased water pressure caused by iceblocked drainage paths are serious seasonal problems in many countries.

#### Equipment

(a) Visual observation (in the case of tunnels good lighting is essential).

(b) Air photographs, rainfall and temperature records as appropriate and depending upon avail-

#### Procedure

(a) Available air photographs should be studied to obtain an overall view of the local drainage pattern and likely groundwater levels. (Groundwater may be indicated by growth of vegetation along faults and basic dykes.) Information on seasonal variations of groundwater levels, and on rainfall and temperature records should be obtained where possible.

(b) Description of the local hydrogeology will usually be limited in the preliminary stages of field mapping. There will probably be no boreholes for pumping tests, no wells for water level determination and drawdown tests, no tracer tests, and no piezometer installations. The hydrogeology will therefore have to be assessed from geological predictions of the likely locations of aquifers, from predictions of the likely orientation and location of impermeable flow barriers, and from predictions of the likely resultant seepage directions and ground water levels. The need for exploratory boreholes for water level determination, tracer testing, piezometer installation and pumping or drawdown tests should be assessed, and their optimum location indicated on appropriate plans.

(c) The mutual interaction of the planned engineering project and the assumed groundwater flow regime should be assessed and important consequences summarized. The effect of seepage towards or into a planned excavation such as a tunnel or slope should be described with a view to preliminary analysis. The predicted effect of any resultant drawdown of groundwater levels on existing installations, and on the settlement of clay foundations should be summarized.

(d) Seepage from individual unfilled and filled discontinuities or from specific sets exposed in a tunnel or in a surface exposure, can be assessed according to the following descriptive scheme:

#### Unfilled discontinuities

Seepage rating	Description
I	The discontinuity is very tight and dry, water flow along it does not appear possible.
II	The discontinuity is dry with no evidence of water flow.
III	The discontinuity is dry but shows evidence of water flow, i.e. rust staining, etc.
IV	The discontinuity is damp but no free water is present.
V	The discontinuity shows seepage, occasional drops of water, but no continuous flow.
VI	The discontinuity shows a continuous flow of water. (Estimate $k_{min}$ and describe pressure i.e. low, medium, high).

#### Filled discontinuities

Seepage rating	Description
I	The filling materials are heavily consoli-

ated and dry, significant flow appears unlikely due to very low permeability.

- II The filling materials are damp, but no free water is present.
- III The filling materials are wet, occasional drops of water.
- IV The filling materials show signs of outwash, continuous flow of water (estimate l/min).
- V The filling materials are washed out locally, considerable water flow along out-wash channels (estimate l/min and describe pressure i.e. low, medium, high).
- VI The filling materials are washed out completely, very high water pressures experienced, especially on first exposure (estimate l/min and describe pressure).

(e) In the case of a rock engineering construction which acts as a drain for the rock mass, for example a tunnel, it is helpful if the overall flow into individual sections of the structure are described. This should ideally be performed immediately after excavation, since groundwater levels, or the rock mass storage, may be depleted rapidly. Descriptions may be based on the following scheme:

#### Rock mass (e.g. tunnel wall)

Seepage rating	Description
I	Dry walls and roof, no detectable seepage.
II	Minor seepage, specify dripping discontinuities.
III	Medium inflow, specify discontinuities with continuous flow (estimate l/min/10 m. length of excavation).
IV	Major inflow, specify discontinuities with strong flows (estimate l/min/10 m. length of excavation).
V	Exceptionally high inflow, specify source of exceptional flows (estimate l/min/10 m. length of excavation).

(f) A field assessment of the likely effectiveness of surface drains, inclined drill holes, or drainage galleries should be made in the case of major rock slopes. This assessment will depend on the orientation, spacing and apertures of the relevant discontinuities.

(g) The potential influence of frost and ice on the seepage paths through the rock mass should be assessed. Observations of seepage from the surface trace of discontinuities may be misleading in freezing temperatures. The possibility of iceblocked drainage paths should be assessed from the point of view of surface deterioration of a rock excavation, and from the point of view of overall stability.

#### Notes

(a) Local rainfall records should be obtained where possible, to help in the interpretation of seepage observations. This is especially important in the case of

observation of surface outcrops, slopes, and tunnels at shallow depth.

(b) In the case of open pit mines, boreholes are drilled for mineral exploration and rock mechanics, commonly entertained only at a subsequent stage, if mineral evaluation is encouraging. The pre-existence of boreholes will allow a comprehensive hydrogeological study to be performed, including tracer tests, piezometer installation, falling-head and pumping tests. Borehole walls can be surveyed for seepage horizons by means of periscopes, borehole cameras and T.V. equipment.

(c) Testing performed in drill holes (e.g. falling head and Lugeon tests) for estimating rock mass permeability forms the subject of a separate ISRM "suggested method". The description of any available Lugeon values is obviously an important supplement to the present suggested methods for description of rock masses and discontinuities. (See also Drill Core.)

(d) Bedding joints and beds of sedimentary rocks having high "primary" permeability tend to be persistent features with the potential for hydraulically connecting large areas of sedimentary rock masses. Such efficient hydraulic connection will be inherently less marked in igneous and metamorphic environments if major regional joints and faults are absent.

(e) Faults sometimes contain highly permeable breccia adjacent to highly impermeable clay gouge. The hydraulic conductivity may therefore be strongly anisotropic, and may even be confined to flow parallel to the plane of the fault. It may be premature to describe a fault zone as dry if a tunnel or exploratory adit has not completely penetrated the feature.

(f) The highest location of seeping joints on a rock slope may be important indirect input for a preliminary stability analysis. Likewise the depth of a tunnel or its location relative to major weakness zones will be important, since this may imply potentially serious inflows.

#### Presentation of results

(a) Air photos, geological maps, or plans of suitable scale should be marked with arrows to indicate the general groundwater flow pattern that has been interpreted as a result of available hydrogeological data. If appropriate, rainfall and temperature records can be appended.

(b) Anticipated impermeable flow barriers, such as dykes, major clay-filled discontinuities and impermeable beds, should be drawn on simplified geological maps and vertical cross-sections, together with anticipated groundwater levels. Optimum locations for investigatory boreholes (and any existing boreholes) should be indicated as appropriate.

(c) The anticipated mutual interaction of the planned engineering project and the assumed groundwater flow regime should be described where possible. If sufficient data is available for reliable predictions, anticipated pre-construction and post-construction phreatic surfaces should be sketched. The likely effect of extreme



weather conditions should be indicated if possible. Possible effects of frost and of artificial drainage measures should be appended.

(d) Local seepage observations for individual discontinuities, for specific sets, or for the rock mass as a whole can be presented as seepage ratings I-VI. If enough observations are available, sketches showing the distributions of ratings can be contoured, drawn as histograms, or, in the case of tunnels, presented on longitudinal sections in parallel with structural data, in the same way that Lugeon values are presented parallel with borehole geology.

## REFERENCES

1. Casagrande A. Control of seepage through foundations and abutments of dams. *Geotechnique*, 11, 159-182 (1961).
2. Terraghi K. Stability of steep slopes on hard unweathered rock. *Geotechnique*, 12, 251-270 (1962).
3. Müller L. The rock slide in the Vajont Valley. *Felsmechanik und Ing. Geol.* 2, 148-212 (1964).
4. Londe P. La stabilité des massifs rocheux: application aux barrages. *Annls. Inst. tech. Batiment Trav. publ.* pp. 1617-1637 (1968).
5. Snow D. T. Rock fracture spacing, opening, and porosities. *ASCE, Proc. Vol. 94, No. SM1*, pp. 73-91 (1968).
6. Sharp J. C. Drainage characteristics of sub-surface galleries. *Proc. of 2nd. Cong. of Int. Soc. Rock Mech.* Belgrade, Vol. 3, Paper 6-10 (1970).
7. Sabarly-F., Pautre A. & Londe P. Quelques réflexions sur la drainabilité des massifs rocheux. *Proc. of 2nd. Cong. of Int. Soc. Rock Mech.* Belgrade, Vol. 3, Paper 6-12 (1970).
8. Cecil O. S. Correlations of rock bolt-shotcrete support and rock quality parameters in Scandinavian tunnels. Ph.D. Thesis, Univ. of Illinois, 414 p (1970).
9. Morfeldt C. O. Significance of groundwater at rock constructions of different types. *Proc. Int. Symp. on Large Permanent Underground Openings*, Oslo, 1969, pp. 305-317 (1969).
10. Sharp J. C., Maini Y. N. T. & Harper T. R. Influence of groundwater on the stability of rock masses: 1-hydraulics within rock masses. *Inst. of Min. and Metall. Trans.* Vol. 81, Sect. A, pp. A13-A20 (1972).
11. Wolters P., Reinhardt M. & Jäger B. Beobachtungen über Art, Anordnung und Ausdehnung von Klüftöffnungen. *Proc. of Int. Soc. Rock Mech. Symp.* Stuttgart. *Percolation Through Fissured Rock*, T1-1, 13 p (1972).
12. Morfeldt C. O. Drainage problem in connection with tunnel construction in Precambrian granitic bedrock (in Sweden). *Proc. of Int. Soc. Rock Mech. Symp.* Stuttgart. *Percolation Through Fissured Rock*, T4-G, 9 p (1972).
13. Louis C. Reconnaissance des massifs rocheux par sondages et classifications géotechniques de roches Sols et Fondations, No. 319, July-August, pp. 97-122 (1974).
14. Brawner C. O. Rock mechanics in open pit mining. *Proc. 3rd. Cong. of Int. Soc. Rock Mech.* Denver, Vol. 1A, pp. 755-773 (1974).
15. Hoek E. & Bray J. *Rock Slope Engineering*. The Institution of Mining and Metallurgy, London, 309 p (1974).
16. Harper T. R. The transient groundwater pressure response to rainfall and the prediction of rock slope instability. *Int. J. Rock Mech. Min. Sci. & Geomech. Abstr.* Vol. 12, pp. 175-179 (1975).

## 9. NUMBER OF SETS

### Scope

(a) Both the mechanical behaviour and the appearance of a rock mass will be dominated by the number of sets of discontinuities that intersect one another. The mechanical behaviour is especially affected since the number of sets determines the extent to which the rock mass can deform without involving failure of the intact rock. The appearance of the rock mass is affected since

the number of sets determines the degree of overbreak that tends to occur with excavation by blasting. (See Fig. 24.)

(b) The number of sets of discontinuities may be a dominant feature of rock slope stability, though traditionally the orientation of discontinuities relative to the face is considered of primary importance. However, if insufficient sets exist the probability of instability may be reduced almost to zero. On the other hand a large number of sets having close spacing may change the potential mode of slope failure from translational or toppling to rotational/circular.

(c) In the case of tunnel stability three or more sets will generally constitute a three-dimensional block structure having considerably more "degrees of freedom" for deformation than a rock mass with less than three sets. For example a strongly foliated phyllite with just one closely spaced joint set may give equally good tunneling conditions as a massive granite with three widely spaced joint sets. The amount of overbreak in a tunnel will usually be strongly dependent on the number of sets.

### Equipment

(a) Geological compass and clinometer.

(b) Visual recognition and/or photographic recording.

### Procedure

(a) The number of sets will often be a function of the size of area mapped. In a preliminary investigation it is important to record all sets present. The recognition of individual sets will usually proceed simultaneously with the orientation measurements. Up to 150 joints may need to be measured, and the number of sets can usually be determined by contouring joint poles plotted on polar equal area nets (see Orientation).

(b) If orientations are consistent, careful sampling may reduce the number of joints that have to be measured to define the number of sets.

(c) In the detailed stages of field investigations, the number of sets present locally should be recorded as a supplement to procedure (a). The stability of a given section of tunnel or rock slope, or the deformability of a given foundation will be a function of the relevant number of sets found locally, rather than of the total number mapped under procedure (a).

(d) Visual recognition of the number of sets should be accompanied by some system of numbering for identification purposes. For example the most systematic and persistent set can be labelled "set No. 1" and so on. (See Fig. 24). Alternatively sets can be numbered in the order of their importance to stability.

### Notes

(a) Systematic joint sets should be distinguished from non-systematic joints when recording the number of sets. In general systematic joints will be persistent features, with individual joints parallel or sub-parallel in plan, while non-systematic joints display random rather

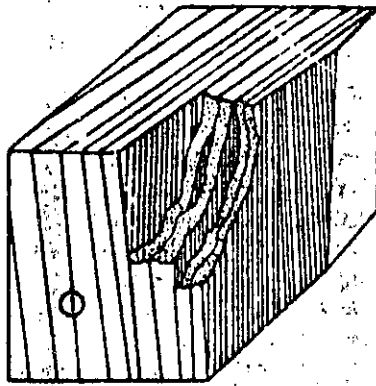
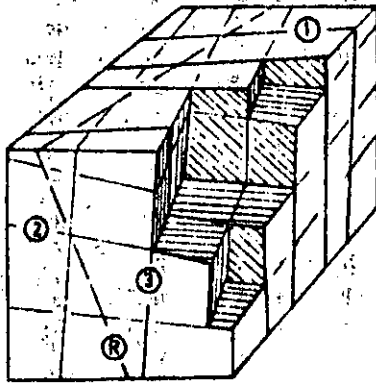
one  
joint  
setthree  
joint  
sets

Fig. 24. Examples that demonstrate the effect of the number of joint sets on the mechanical behaviour and appearance of a rock mass.

than oriented patterns in plan and section. Problems of set identification when sets cannot readily be distinguished in the field may be reduced by utilizing statistical tests for identifying trends in the distribution of poles plotted on polar equal area nets. (See Fig. 5, under Orientation.)

(b) Incipient discontinuities such as those that may develop parallel to bedding, or parallel to foliation or cleavage, should be included in the local estimate of the number of sets, if it is considered that the method of excavation employed will sufficiently disturb the rock mass to cause development of these features into equivalent bedding joints, foliation joints, etc.

(c) As noted under procedures (a) and (c), the number of sets recorded will tend to be a function of the size of area mapped, and should be interpreted accordingly. The spacing of individual sets will play an important role in this interpretation. For example, four sets recognised following a "conventional" survey of an area (using the pole contouring method) may include some sets with such wide spacing that these would be of little relevance to the stability of a short length of tunnel, though possibly of considerable importance to the stability of a major slope.

#### Presentation of results

(c) The number of joint sets present can be represented visually as part of the presentation of orientation

data. (See Fig. 2: block diagram, Fig. 3: joint rosettes, Fig. 5: Schmidt pole contour diagram.)

(b) The number of joint sets occurring locally (for example along the length of a tunnel) can be described according to the following scheme:

I	massive, occasional random joints
II	one joint set
III	one joint set plus random
IV	two joint sets
V	two joint sets plus random
VI	three joint sets
VII	three joint sets plus random
VIII	four or more joint sets
IX	crushed rock, earth-like

Major individual discontinuities should be recorded on an individual basis.

#### REFERENCES

- Hodgson R. A. Regional study of jointing in the Comb Ridge Navajo Mountain area, Arizona and Utah. *Bull. Am. Ass. Petrol. Geol.* 45, 1-38 (1961).
- John K. W. An approach to rock mechanics. *J. Soil Mech. Fdn. Div. civ. Engrs. SMA*, pp. 1-30 (1962).
- Müller L. *Der Felsbau*, Ferdinand Enke-Verlag, Stuttgart, 624 p (1963).
- Price N. J. *Fault and Joint Development in Brittle and Semi-Brittle Rock*, Pergamon, Oxford, 176 p (1966).
- Nickelsen R. P. & Hough V. N. D. Jointing in the Appalachian Plateau of Pennsylvania. *Bull. Geol. Soc. Am.* 78, 609-630 (1967).
- Cecil O. S. Correlations of rock bolt-shotcrete support and rock quality parameters in Scandinavian tunnels. Ph.D. Thesis, Univ. of Illinois. (also Swedish Geotechnical Institute, Proceedings No 27, Stockholm 1975, 275 p.) (1970).
- Piteau D. R. Geological factors significant to the stability of slopes cut in rock. *Symp. on Planning Open Pit Mines*, Johannesburg, 1970. Balkema, Amsterdam, 1971, pp. 33-53 (1971).
- Robertson A. MacG. The interpretation of geological factors for use in slope theory. *Symp. on Planning Open Pit Mines*, Johannesburg, 1970. Balkema, Amsterdam, 1971, pp. 55-71 (1971).
- Baicoeck I. A. Regional jointing in Southern Alberta. *Canadian J. Earth Sci.* 10, 1769-1781 (1973).
- Barton N., Lien R. & Lunde J. Engineering classification of rock masses for the design of tunnel support. *Rock Mechanics*, 6, 189-236 (1974).
- Hoek E. & Bray J. *Rock Slope Engineering*. The Institution of Mining and Metallurgy, London, 309 p (1974).
- Goodman R. E. *Methods of Geological Engineering in Discontinuous Rocks*. West Publishing, N.Y. 472 p (1976).

#### 10. BLOCK SIZE

##### Scope

(a) Block size is an extremely important indicator of rock mass behaviour. Block dimensions are determined by discontinuity spacing, by the number of sets, and by the persistence of the discontinuities delineating potential blocks.

(b) The number of sets and the orientation determine the shape of the resulting blocks, which can take the approximate form of cubes, rhombohedrons, tetrahedrons, sheets, etc. However, regular geometric shapes are the exception rather than the rule since the joints in any one set are seldom consistently parallel. Jointing

## Suggested Methods for the Quantitative Description of Discontinuities

in sedimentary rocks usually produces the most regular block shapes.

(c) The combined properties of block size and inter-block shear strength determine the mechanical behaviour of the rock mass under given stress conditions. Rock masses composed of large blocks tend to be less deformable, and in the case of underground construction, develop favourable arching and interlocking. In the case of slopes, a small block size may cause the potential mode of failure to resemble that of soil, (i.e. circular/rotational) instead of the translational or toppling modes of failure usually associated with discontinuous rock masses. In exceptional cases "block" size may be so small that flow occurs, as with a "sugar-cube" shear zone in quartzite.

(d) Rock quarrying and blasting efficiency are likely to be largely a function of the natural *in situ* block-size. It may be helpful to think in terms of a block size distribution for the rock mass, in much the same way that soils are categorized by a distribution of particle sizes.

(e) Block size can be described either by means of the average dimension of typical blocks (block size index  $I_b$ ), or by the total number of joints intersecting a unit volume of the rock mass (volumetric joint count  $J_v$ ).

#### Equipment

(a) Measuring tape of at least 3 m length, calibrated in mm divisions.

#### Procedure

(a) *Block size index ( $I_b$ )*. The index can be estimated by selecting by eye several typical block sizes and taking their average dimensions. Since the index may range from millimetres to several metres, a measuring accuracy of 10% should be sufficient.

Each domain should be characterized by a modal  $I_b$ , together with the range, i.e. typical largest and smallest block size indices.

The number of sets should always be recorded in parallel with  $I_b$ , since if there are only one or two sets, any subsequent attempt to convert  $I_b$  to typical block volumes may be unrealistic.

(b) *Volumetric joint count ( $J_v$ )*. The volumetric joint count is defined as the sum of the number of joints per metre for each joint set present. Random discontinuities can be included, but will generally have little effect on the results.

The number of joints of each set should be counted along the relevant joint set perpendicular. A sampling length of 5 or 10 m is suggested. Each joint count will then be divided by 5 or 10 to express the results as number of joints per metre.

A typical result for three joint sets and a random discontinuity counted along 5 or 10 m perpendicular sampling lines might appear as below:

$$J_v = 6/10 + 24/10 + 5/5 + 1/10$$

$$J_v = 0.6 + 2.4 + 1.0 + 0.1 = 4.1/\text{m}^3 \text{ (medium-size blocks)}$$

The following descriptive terms give an impression of the corresponding block size:

Description	$J_v$ (joints/m <sup>3</sup> )
Very large blocks	< 1.0
Large blocks	1-3
Medium-sized blocks	3-10
Small blocks	10-30
Very small blocks	> 30

Values of  $J_v > 60$  would represent crushed rock, typical of a clay-free crushed zone.

(c) *Rock masses*. Rock masses can be described by the following adjectives, to give an impression of block size and shape:

- (i) *massive* = few joints or very wide spacing
- (ii) *blocky* = approximately equidimensional
- (iii) *tabular* = one dimension considerably smaller than the other two
- (iv) *columnar* = one dimension considerably larger than the other two
- (v) *irregular* = wide variations of block size and shape
- (vi) *crushed* = heavily jointed to "sugar cube"

See Fig. 25 for examples of the above.

#### Notes

(a) *Block size index ( $I_b$ )*. The purpose of the block size index is to represent the average dimensions of typical rock blocks. The average value of individual modal spacings ( $S_1, S_2$ , etc., see Spacing) may not give a realistic value of  $I_b$  if there are more than three sets, since the fourth set, if widely spaced, will artificially increase  $I_b$ , but may have little influence on actual block sizes as observed in the field.

In the case of sedimentary rocks, two mutually perpendicular sets of cross joints plus bedding constitute an extremely common cubic or prismatic block shape. In such cases  $I_b$  is correctly described by:

$$I_b = \frac{S_1 + S_2 + S_3}{3}$$

(b) *Volumetric joint count ( $J_v$ )*. Field mapping can be performed very rapidly as a measuring tape can be dispensed with when individual joint spacings are not of interest. 5 or 10 m can be paced out or estimated with reasonable accuracy by most observers (i.e. to within  $\pm 10\%$  of the correct length). The observer should face in the direction of strike for each joint set that is to be counted and count perpendicular to the strike, thereby removing the angular correction factor.

It should be noted that

$$J_v \text{ is not equal to } \frac{1}{S_1} + \frac{1}{S_2} + \frac{1}{S_n}$$

The calculation of  $J_v$  is based on the mean spacings, not modal spacings. Generally the results will be similar, but spacing tends to be log-normally distributed.

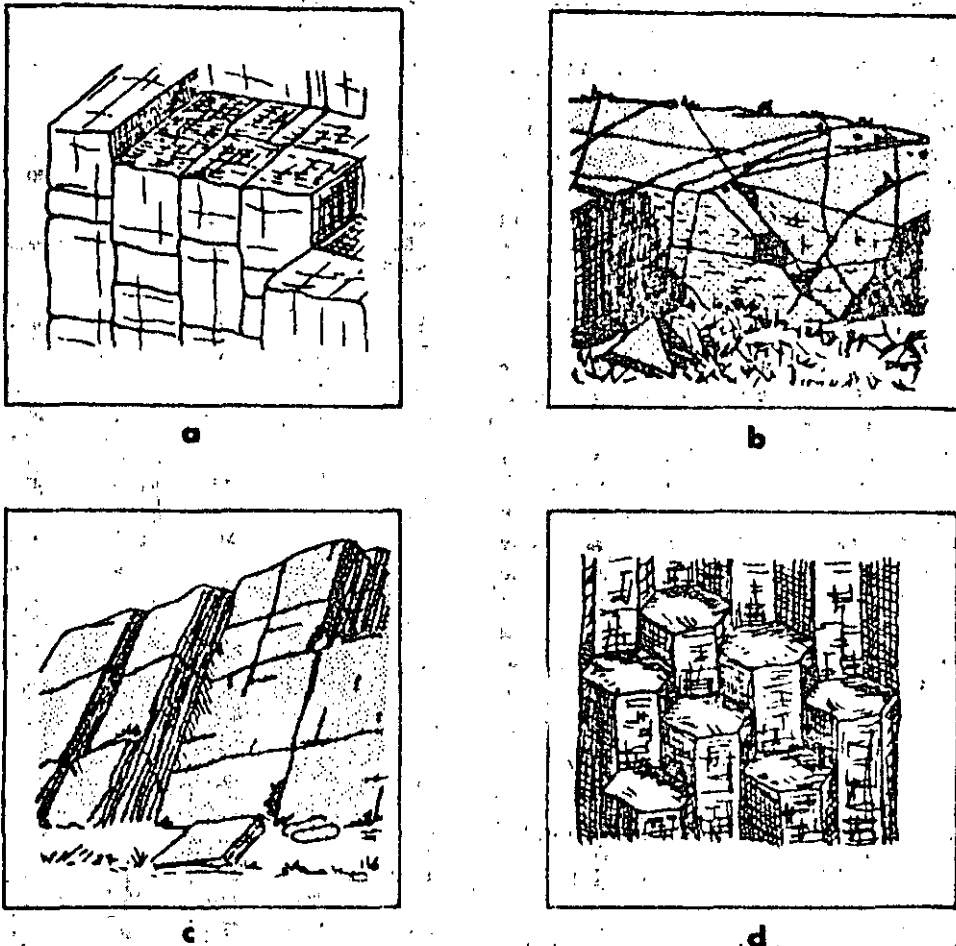


Fig. 25. Sketches of rock masses illustrating (a) blocky, (b) irregular, (c) tubular, and (d) columnar block shapes.

The occasional random discontinuities will not noticeably affect the value of  $J_v$  unless the spacing of the systematic joints is wide or very wide (i.e. 1–10 m). In such cases they should be included with appropriately wide spacing, for example 10 m.

In view of the widespread use of RQD in various rock mass classification methods it is of value to present an approximate correlation between  $J_v$  and RQD.

$$\text{RQD} = 115 - 3.3 J_v \text{ (approx.)}$$

$$(\text{RQD} = 100 \text{ for } J_v < 4.5)$$

This relationship can be used for estimating the order of magnitude of RQD when borecore is unavailable.

(c) *Orientation data.* Orientation data will provide additional descriptive data for a clearer expression of the form of an anisotropic block structure if present, i.e. "steeply dipping sheets, slabs, beds" etc. or "vertical columnar blocks" etc. When block dimensions are reasonably isotropic only the block shape need be described, i.e. cubic, rhombohedral, prismatic, tetrahedral, irregular, etc. as appropriate.

#### Presentation of results

(a) Record the modal block size index ( $I_b$ ), and  $I_s$ ,

values typical for the largest and smallest block sizes for the domain or domains of interest. (Also record the number of sets and describe the persistence).

(b) Record the volumetric joint count ( $J_v$ ) for the domain or domains of interest. (Also record the number of sets and describe the persistence).

(c) Describe the rock mass and its "blockiness" in general terms as: massive, blocky, tabular, columnar, crushed or as appropriate.

Where possible, block size and shape should also be communicated by means of photographs and/or field sketches of typical exposures (see Fig. 25).

#### REFERENCES

1. John K. W. An approach to rock mechanics. *J. Soil Mech. Fdn. Div. Am. Soc. Civ. Engrs.* SM4, pp. 1–30 (1962).
2. Müller L. *Der Fe'bau*. Ferdinand Enke-Verlag, Stuttgart, 624 p (1963).
3. Price N. J. *Fault and Joint Development in Brittle and Semi-brittle Rock*. Pergamon, Oxford, 176 p (1966).
4. Piteau D. R. Characterizing and extrapolating rock joint properties in engineering practice. *Rock Mechanics* (Springer-Verlag) Suppl. 2, pp. 5–31 (1973).
5. Franklin J. A. Rock quality in relation to the quarrying and performance of rock construction materials. *Proc. of 2nd. Int. Cong. of the Int. Ass of Eng. Geology*, São Paulo, Brazil, Vol. 1, IV-PC-2, 11 p (1974).

## Suggested Methods for the Quantitative Description of Discontinuities

6. Korhonen K.-H., Girdemeister R., Jääskeläinen H., Niini H. & Vähäsarja P. Engineering geological rock classification (in Finnish). Geotechnical Laboratory, Report 12, Technical Research Centre of Finland, 78 p (1974).
7. Palmström A. Characterizing the degree of jointing and rock mass quality (in Norwegian) (Internal Report, Ing. A.B. Berdal, Mariesvej 20, 1322 Hevik, Oslo, 26 p (1975).
8. Barton N. Unsupported underground openings. *Proc. Rock Mechanics Meeting*, BoFo, Stockholm, pp. 61-94 (1976).

### 11. DRILL CORE

#### Scope

(a) Drill core description is here intended primarily to provide information on the discontinuities.

(b) In the preliminary stages of field mapping, drill core is unlikely to be available. However, the need for drilling, and the optimum locations and orientations of holes should be described, based on existing information concerning the likely orientation of discontinuities.

(c) If drill core is available it can first be described by means of the following parameters: *total core recovery* (R), *discontinuity frequency* (F), and *rock quality designation* (RQD). However, these parameters alone do not usually provide sufficient information for design purposes.

(d) Drill cores (and drill holes) represent line samples of the rock mass. Structural features such as discontinuity orientation, spacing and the number of sets cannot normally be adequately sampled by one hole without prior knowledge of the orientation and the number of sets.

(e) Carefully planned and executed core drilling followed by detailed core description and hole inspection can provide approximate information about many of the ten specific rock mass parameters described under the preceding "suggested methods" i.e. 1. Orientation, 2. Spacing, 3. Persistence, 4. Roughness, 5. Wall strength, 6. Aperture, 7. Filling, 8. Seepage, 9. Number of sets, 10. Block size.

#### Equipment

(a) Measuring tape of at least 3 m length, calibrated in mm divisions. Protractor or similar scale for measuring the angles between the core axis and the discontinuities.

(b) Materials for washing the core.

(d) Subsequent measurements in the drill holes may require the use of at least one of the following: borehole periscope, camera, TV camera, water level indicator (electrical contact type), together with the associated cables and winding gear appropriate for the length of hole and the equipment selected.

#### Procedure

(a) Dirty rock core should in general be washed clean prior to making observations. However, this procedure should be avoided in the case of filled discontinuities and argillaceous rocks likely to be sensitive to wetting and drying.

(b) Before making detailed observations the core as a whole should be examined to determine the structural

boundaries (discontinuities) and geological features to be measured. The markers indicating depths of geological horizons and the start and end of each run should be carefully checked for errors.

(c) *Total core recovery* (R) defined as the summed length of all pieces of recovered core expressed as a percentage of length drilled should be measured and recorded to the nearest 2% if possible. When the core is highly fragmented the length of such portions is estimated by assembling the fragments and estimating the length of core that the fragments appear to represent.

Core recovery is normally used to describe individual core runs or whole boreholes, and not specific structurally defined rock units. The results obtained in a rock mass of poor quality will be strongly dependent on the drilling equipment and on the skill of the drilling crew. Core grinding may result in excessive lost core. Core that is damaged in this way should always be recorded.

*Total core recovery* (R) is in the first instance usually obtained directly from the drillers log, and is therefore based on individual lengths of uptake. These unit lengths will vary with the rate of drilling and the quantities of the rock drilled through.

Instructions should always be given to the drilling crew so that the depth drilled at the start and end of zones of core loss are carefully recorded. The relevant lengths lost can then be replaced by wooden blocks with markings on both ends.

(d) *Frequency* (F) defined as the number of natural discontinuities intersecting a unit length of recovered core, should be counted for each metre of core.

Since the orientation of the discontinuities is not considered at this stage, it is clear that differently orientated holes will usually produce different results.

Artificial fractures resulting from rough handling or from the drilling process should be discounted only when they can be clearly distinguished from natural discontinuities.

(e) *Rock quality designation* (RQD) is a modified core recovery percentage in which all the pieces of sound core over 10 cm long are counted as recovery, and are expressed as a percentage of the length drilled. The smaller pieces resulting from closer jointing, faulting, or weathering are discounted.

If the core is broken by handling or by the drilling process (i.e. if the fractures are fresh breaks rather than natural surfaces) the fresh broken pieces should be fitted together and counted as one piece, provided they form the requisite length of 10 cm.

Material that is obviously weaker than the surrounding rock such as over-consolidated gouge is discounted, even if it appears as intact pieces that are 10 cm or more in length. (This type of material will normally only be recovered when using the most advanced drilling equipment and experienced or carefully supervised drilling crews.)

The length of individual core pieces should be assessed along the centre line of the core, so that discontinuities that happen to parallel the drill-hole will

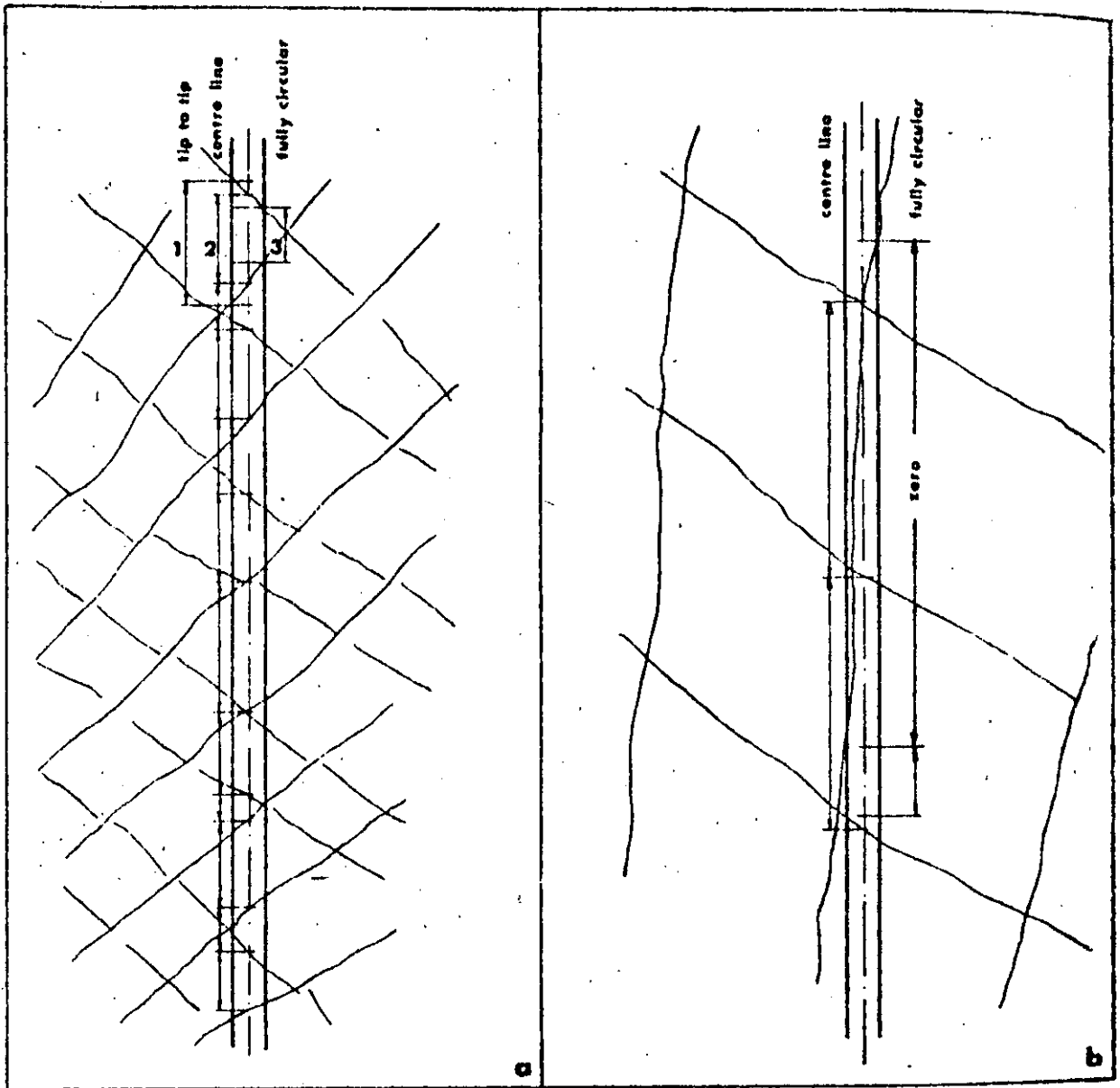


Fig. 26. Examples of three possible interpretations of the length of core pieces. The centre line length is suggested as the most realistic measurement and is recommended.

not unduly penalize the RQD values of an otherwise massive rock mass. (See Fig. 26).

It is suggested that RQD values are determined for variable rather than fixed lengths of core run. Values of individual beds, structural domains, weakness zones etc. should therefore be logged separately, so as to indicate any inherent variability, and provide a more accurate picture of the location and width of zones with low or zero RQD values.

#### Supplementary data

Subsequent to the general procedure for logging *total core recovery (R)*, *frequency (F)*, and *rock quality designation (RQD)*, the following supplementary procedures are suggested for determining as much quantitative

data as possible concerning the ten parameters:

1. Orientation
2. Spacing
3. Persistence
4. Roughness
5. Wall strength
6. Aperture
7. Filling
8. Seepage
9. Number of
10. Block size

A combination of core logging, *drift hole view*, (borehole periscope, TV camera) and/or water injection tests are suggested for assessing those parameters that

## Suggested Methods for the Quantitative Description of Discontinuities

are more or less disturbed in the recovered core, for example, *aperture, filling, seepage*.

#### Orientation

Efforts should be made to log the apparent orientation of discontinuities intersecting the core, using a protractor to measure the acute angles of intersection ( $\theta$ ) relative to the core axis ( $\pm 5^\circ$ ). If the relevant hole is vertical, the angles ( $90^\circ - \theta$ ) will represent the true dip of the discontinuities, but without orientated core the dip direction will remain unknown.

If two or more non-parallel drillholes have been drilled in a rock mass where there are recognisable markers such as bedding or foliation, the dip direction and dip of these features can be deduced using graphical techniques [1].

If existing surface mapping has already indicated the approximate orientation of certain joint sets, then carefully orientated drill holes can be used to check the orientation of these features at depth. In the case of anticipated vertical and horizontal jointing it is helpful to drill steeply inclined holes (i.e.  $60^\circ$ ) in preference to  $45^\circ$ , so that the differently orientated sets can be recognised during core logging by their different core intersection angles.

The true orientation of discontinuities (dip direction and dip) can be obtained from a single drill core if orientation devices are employed during the drilling process. Several methods are available:

(a) Orientation of the core based on the measured orientation in each run (Craelius method). This method works well if adjacent pieces of core can be matched. Zones of core loss and perpendicularly intersected discontinuities reduce the effectiveness of the method locally.

(b) Orientation of the core by means of a hardened steel groove scriber and compass photo device (Christensen-Huegel method).

(c) *Integral sampling method* in which the cores that are recovered have previously been reinforced with a grouted bar whose azimuth is known from positioning rods. The reinforcing bar is co-axially overcored with a larger diameter coring crown.

The orientation of discontinuities (dip direction and dip) can be obtained by drill hole inspection using special television cameras, and periscopes. TV cameras can be orientated such that a discontinuity plane shows as a straight line on the CRT screen. The dip direction and dip can be readily determined. Cameras have been used to depths of 400 m, though generally 150 meters is seldom exceeded due in part to water pressure problems. Minimum hole size for the cameras is generally 76 mm.

The borehole periscope can be used in smaller holes, but due to distortion of the optical path the depth is usually limited to about 30 m.

#### 2. Spacing

In rock with marked foliation or bedding features

it should be possible to match the individual core pieces such that the actual spacing of obliquely intersected foliation joints, bedding joints or other regular intersecting joint sets can be estimated. The spacing ( $S$ ) will depend on the length ( $L$ ) measured along the core axis between adjacent natural discontinuities of one set, and the acute angle ( $\theta$ ) that these features subtend with the core axis. Thus:

$$S = L \sin \theta$$

The angles ( $\theta$ ) between the core axis and the individual joints of a given set will be inherently less reliable than those recorded from observations of rock exposures due to the possibility of joint undulation and roughness.

When a joint set is intersected perpendicularly by the drill hole, spacing can obviously be measured directly since ( $S$ ) is equal to ( $L$ ).

When the rock has no consistent or clear marker features such as foliation or bedding, the estimation of spacing for any given set of joints will depend on the degree to which the core pieces can be matched. Zones of core loss will clearly frustrate this objective. However, if the joints that intersect the core have markedly different core intersection angles ( $\theta$ ) and/or markedly different surface features (i.e. mineral coatings, roughness) it may be possible to estimate the relevant spacings in a sufficient number of places along the core to make the exercise worthwhile.

Borehole viewing devices that can be orientated (periscope, TV camera) will clearly increase the reliability of spacing measurements.

#### 3. Persistence

Unless holes are drilled in a very closely spaced pattern, as may be the case for operations such as grout curtain injection, it will usually not be possible to assess the *persistence* from drill core or drill hole observations.

If closely spaced holes are available, very careful correlation of discontinuities will be required before any reliable conclusions can be drawn concerning the persistence of a given discontinuity or set.

#### 4. Roughness

Gross features of discontinuity wall roughness and corresponding full scale shear strength cannot obviously be assessed by means of drill core alone. However, it is usually possible to assign to a surface some degree of *planarity* (*planar, curved, irregular*) and some degree of *smoothness* (*slick, smooth, rough*). This suggested procedure is broadly consistent with the roughness description shown in Fig. 17, but with dimensions reduced to the scale of centimeters and millimeters respectively.

Drill hole inspection with periscopes or TV cameras will not generally provide an improved picture of roughness unless the rock type is so weak and/or the drilling so poorly performed that grinding of the core pieces has occurred.

### 5. Wall strength

The individual suggested methods for describing *wall strength* ((a) weathering grade of rock mass, (b) weathering grade of rock material, (c) manual index tests, (d) Schmidt hammer test) can also be applied to the description of drill core.

Since the drill core provides a ready-made line sample of the rock mass, such features as the depth of penetration of weathering into the discontinuity walls can be directly observed and therefore described quite accurately. Furthermore the drill core provides ready-made samples for mechanical testing (i.e. Schmidt hammer testing of rigidly clamped core pieces for describing *wall strength* or point load testing across the core diameter for describing *material strength*). Franklin *et al.* [2] strongly advocate logging the point load strength index ( $I_p$ ) simultaneously with recovery of the core from the core barrels.

When assessing wall strength, care should be taken to check if the relevant core pieces fit together. Lack of fit may indicate lost filling material, shear displacement, or partial grinding away of strongly weathered walls during the drilling process.

### 6. Aperture

The aperture of discontinuities intersected by drill holes can only be guessed unless the integral sampling method is used. If the core pieces on either side of a discontinuity can be fitted together by hand so that no visible void spaces remain, it is likely that the discontinuity is a *tight* feature *in situ* (i.e. very tight  $< 0.1$  mm, or *tight* 0.1-0.5 mm). However it is not certain that the feature is *tight*, it could also be "gapped" *in situ* (i.e. moderately wide 0.5-2.5 mm, or wide 2.5-10 mm, etc.) Alignment of the walls of the relevant core pieces should be checked in this respect.

If two pieces of adjacent core cannot be mated tightly across a discontinuity and if voids are visible, the term *open* can be used in describing the discontinuities. It is recognised that what appears to be an open or partially open discontinuity in the drill core actually may have been *tight in situ*, if softer filling materials have not been recovered, or if some wear of weathered material has occurred during the drilling operation.

Drill hole inspection using TV cameras or periscopes should be successful in distinguishing between the above *tight* and *open* categories, although it is unlikely that the apertures of the finest joints can be measured accurately. From the point of view of seepage potential the open discontinuities are most important, so this limitation should not be important where highly permeable rock masses are concerned. Methods are available for estimating the theoretical smooth wall apertures of water conducting discontinuities by statistical analysis of water injection tests [3]. However, the real apertures may be several times the theoretical smooth wall apertures due to wall roughness and tortuosity effects.

### 7. Filling

Unless the integral sampling method or best quality drilling equipment is used (i.e. double or triple tube core barrels, split inner tubes, and controlled flushing) the softer filling materials are unlikely to be recovered in significant amounts. Possibly only traces of clay minerals will be visible on the discontinuity wall, sampled by conventional drill core. Both traces and larger amounts of recovered filling should be described as to width, mineralogy and strength. The interpretative nature of these descriptions should be made clear.

Where *total core recovery* is less than 100% and it is suspected that significant amounts of filling or weathered material has been lost in the drilling process, attempts should be made to assess the thickness, location and orientation of the suspected filled zones. The drillers log describing the rate of advance and water loss, type of cuttings and colour of flushing fluid, may be invaluable here.

The uncertainties surrounding the parameter *filling*, and its extreme importance where deformation, stability and water seepage are concerned, strongly justify the use of special recovery techniques and the use of borehole viewing techniques.

### 8. Seepage

Observations of drill core may provide indirect evidence of water seepage levels. Reddish-brown iron ( $Fe^{++}$ ) staining usually indicates the zone of rock mass that lies above the mean ground water level. Oxidation in discontinuity walls lying beneath the ground water level may also occur, but at a greatly reduced rate. Frequently the strongest iron staining is found in the zone where the ground water level commonly fluctuates.

Drill holes obviously provide the means of checking ground water levels directly using simple battery operated electrical contact devices which are lowered into the holes. Additional information on standing water levels should be obtained from the drillers log for each drill hole. Drill hole walls can be surveyed for seepage horizons using periscopes and TV cameras.

Testing performed in drill holes (i.e. falling head tests, Lugeon packer tests, tracer tests, piezometer measurements) for estimating rock mass permeability, and for estimating the hydraulic conductivity of individual discontinuities and sets of discontinuities, forms the subject of a separate ISRM suggested method. The logging and presentation of any available Lugeon values gives important supplementary data, which can conveniently be presented as a log, parallel with that for *total core recovery*, *frequency* and *RQD*, etc.

### 9. Number of sets

The amount of information obtainable from drill core and drill hole observation will obviously depend on the orientation of the holes relative to existing sets, and on their length relative to the joint spacings. If existing surface mapping has already indicated the approximate orientation of certain discontinuity sets, then



## Suggested Methods for the Quantitative Description of Discontinuities

carefully orientated holes can be used to check the number of sets at depth. Drill core observation will be easier if holes are drilled to intersect the different sets at recognisably different angles. Usually at least two non-parallel holes will be required.

The number of sets observed at the surface is likely to be more than the number observed at depth. Comparison of surface observations with tunnel excavations suggests that this is not just due to the limitations of drill hole sampling.

10. *Block size*

The term *block size* is a composite description of the rock mass which is influenced by *spacing, number of sets, persistence and orientation*. A log of block size produced from observations of rock core can clearly only give an approximate picture of the true block size.

A rapid method of estimating the approximate block size from drill core is to select by eye several typical pieces of core and take their average dimensions ( $\pm 10\%$ ). Each rock unit or domain may be assessed in this way. If the relevant hole is orientated such that all sets present are intersected (i.e. a diagonal hole in the case of a cubic joint system) then these average core pieces will roughly represent the *block size index* ( $I_b$ ) defined under the relevant suggested method. A depth log showing the variation of this index can be a very useful supplement to drill core description.

## Notes

(a) When estimating *frequency* or *RQD* from drillcore it is necessary to discount fresh artificial breaks (fractures) clearly caused by the drilling process, and also those made deliberately when fitting core into the core boxes. The following criteria are suggested:

- (i) A rough brittle surface with fresh cleavage planes in individual rock minerals indicates an artificial fracture.
- (ii) A generally smooth or somewhat weathered surface with soft coating or infilling materials such as talc, gypsum, chlorite, mica or calcite obviously indicates a natural discontinuity.
- (iii) In rocks showing foliation, cleavage or bedding it may be difficult to distinguish between natural discontinuities and artificial fractures when these are parallel with the incipient weakness planes. If drilling has been carried out carefully then the questionable breaks should be counted as natural features, to be on the conservative side.
- (iv) Depending upon the drilling equipment part of the length of core being drilled may occasionally rotate with the inner barrels in such a way that grinding of the surfaces of discontinuities and fractures occurs. In weak rock types it may be very difficult to decide if the resulting rounded surfaces represent natural or artificial features. When in doubt the conservative assumption should be made, i.e. assume that they are natural.
- (v) It may be useful to keep a separate record of the frequency of artificial fractures (and associated

lower RQD) for assessing the possible influence of blasting on the weaker sedimentary and foliated or schistose metamorphic rocks.

(b) The degree of fracturing of the core during the drilling process may be partly a function of core diameter in the weaker rock types. Since some artificial fracturing is very difficult to distinguish from natural discontinuities (e.g. in the case of weak fissile, cleaved, or foliated rock) it is preferable that the core is not less than NS diameter (55 mm) where rock strength is in question. Use of smaller core diameters (i.e. 32 or 42 mm) puts an increasing responsibility on the drilling crew for the results obtained. A method of correcting RQD to the standard NX size has been suggested by Heuzé [4].

(c) Several possible interpretations of the length of core pieces are possible i.e. tip to tip (maximum) length, centre line length or fully circular length. These are illustrated in Fig. 26. Tip to tip measurement involves double-counting at each end of a core piece, while fully circular measurement ignores core pieces that happen to have been drilled with a small subtended angle to one discontinuity in otherwise massive rock. Centre line measurement is therefore strongly recommended.

(d) The results of core logging (frequency and RQD) can be strongly time dependent and moisture content dependent in the case of certain varieties of shales and mudstones having relatively weakly developed diagenetic bonds. A not infrequent problem is "discing", in which an initially intact core separates into discs on incipient planes, the process becoming noticeable perhaps within minutes of core recovery. The phenomena are experienced in several different forms:

- (i) Stress relief cracking (and swelling) by the initially rapid release of strain energy in cores recovered from areas of high stress, especially in the case of shaly rocks.
- (ii) dehydration cracking experienced in the weaker mudstones and shales which may reduce RQD from 100% to 0% in a matter of minutes, the initial integrity possibly being due to negative pore pressure.
- (iii) slaking cracking experienced by some of the weaker mudstones and shales when subjected to wetting.

All these phenomena make core logging of *frequency* and *RQD* unreliable. Whenever such conditions are anticipated core should be logged by an engineering geologist as it is recovered and at subsequent intervals until the phenomenon is predictable. An added advantage is that the engineering geologist can perform mechanical index tests such as the point load or Schmidt hammer test, while the core is still in a saturated state.

(e) In certain cases it may be helpful to log the *solid core recovery* in addition to the *total core recovery* (R) defined earlier. The *solid core recovery* includes as recovery only those pieces of core that have a complete

circumference. Total and solid core recovery will only be equivalent when no fragmental material is recovered, i.e. when the rock is massive, or when loss of sample is represented wholly by material carried away in the flushing system.

(f) Colour photographs provide a useful and convenient method of recording the appearance of cores and are of considerable value as a permanent record and means of rapid reference. The photograph of each core box should incorporate a suitable metric scale along the entire length of the box. Zones of core loss should be replaced by wooden blocks with legible depth markings. Wetting of the core before photography produces excellent contrast between different rock types and any form of mineralogical banding, but does not help in the observation of discontinuities, due to the general darkening that occurs with wetting.

#### Presentation of results

In view of the different requirements in rock engineering projects, no attempt will be made to suggest a standardized core log format. If a standard format was employed it would be certain that for one given project, much irrelevant information would be presented, while for another, unusual features of great significance would be missed out, because the format did not allow for their inclusion. Since it is impractical to include all the parameters given below, the following should only be used as a check list, so that relevant information is included, but irrelevant data excluded.

(a) *General information.* (i) Drill hole number. (ii) Site, project name. (iii) Grid reference. (iv) Elevation at drill hole collar. (v) Orientation of hole: dip direction and dip ( $\alpha/\beta$ ). (vi) Make of machine, type of feed, type of core barrel and bit, flush system.

(b) *Depth logs of relevant parameters selected from the following.* (i) Symbolic log showing rock type (with geological key). (ii) Point load strength index ( $I_p$ ). (iii) Total core recovery (R). (iv) Solid core recovery. (v) Lugeon packer tests (units of Lugeons) and ground water levels. (vi) Frequency (F). (vii) Rock quality designation (RQD). (viii) Block size index ( $I_b$ ). (ix) Symbolic log showing dip of main discontinuities.

(c) *Supplementary data.* Parameters from the following list are probably best presented in writing in a broad column at the side of the above depth logs, unless sufficient data is available to justify separate logs of the relevant data, for specific sets of discontinuities.

- (i) Spacing (estimate number of sets).
- (ii) Roughness.
- (iii) Weathering grades.
- (iv) Schmidt hammer tests (wall strength JCS).
- (v) Aperture.
- (vi) Filling and iron staining.

#### REFERENCES

1. Phillips F. C. *The Use of Stereographic Projections in Structural Geology*. Edward Arnold, London, 3rd edn, 90 p (1971).
2. Franklin J. A., Birch E. & Walton G. Logging the mechanical character of rock. *Trans Inst. Min. Metall. Section A*, 80, 21-27 (1971).
3. Snow D. T. Rock fracture, spacing, opening, and porosity. *ASCE, Proceedings*, Vol. 94, No. SM1, pp. 73-91 (1968).
4. Heuzé E. F. Sources of error in rock mechanics field measurements and related solutions. *Int. J. Rock Mech. Min. Sci. R.*, 297-310 (1971).
5. Deere D. U. Technical description of rock cores for engineering purposes. *Felsmechanik und Ingenieurgeologie*, 1, 16-22 (1963).
6. Knill J. L. & Jones K. S. The recording and interpretation of geological conditions in the foundations of the Roseires, Kariba and Latiyan dams. *Geotechnique*, 15, 94-124 (1965).
7. Terzaghi R. Sources of error in joint surveys. *Geotechnique*, 15, 287-304 (1965).
8. Deere D. U., Hendron A. J., Patton F. D. & Cording E. J. Design of surface and near-surface construction in rock. *Proc. 8th Symp. on Rock Mech.*, Minnesota, pp. 237-302 (1967).
9. Moye G. D. Diamond drilling for foundation exploration. *J. Inst. Engrs Aust.*, CE 9, 95-100 (1967).
10. Ege J. R. Stability index for underground structures in granite rock. In Nevada Test Site. *Mem. Geol. Soc. Am.* No. 110, pp. 185-198 (1968).
11. Ward W. H., Burland J. B. & Gallois R. W. Geotechnical assessment of a site at Mundford, Norfolk, for a large proton accelerator. *Geotechnique*, 18, 399-431 (1968).
12. Deere D. U., Meritt A. H. & Coon R. F. Engineering classification of *in situ* rock. Tech. Rept. no. AFWL-67-144, Air Force System Command, Kirtland Air Force Base, New Mexico (1967).
13. Geological Society, Engineering Group, Working Party Report on 'The logging of rock cores for engineering purposes'. *Q. J. Engng Geol.* 3, 1-24 (1970).
14. Rocha M. & Barrero M. Some applications of the new integral sampling method in rock mechanics. *Proc. of Symp. of ISRM, Rock Fracture*, Nancy, Paper 1-21 (1971).
15. Bergman M. Rock mass investigation in depth: reliability of different methods for drillhole investigations. *Proc. of 3rd Cong. of ISRM, Denver, Advances in Rock Mechanics*, Vol. II A, pp. 15-20 (1974).
16. Dearman W. R. The characterization of rock for civil engineering practice in Britain. *Colloquio Géologie de l'Ingenieur, Liège*, pp. 1-75 (1974).
17. Franklin J. A. Rock quality in relation to the quarrying and performance of rock construction materials. *Proc. of 2nd. Int. Cong. of the Int. Assoc. of Engng. Geology*, São Paulo, Vol. I, paper IV-PC-2, 11 p (1974).
18. Hansagi I. A method for determining the degree of fracturation of rock. *Int. J. Rock Mech. Min. Sci. & Geomech. Abstr.* 11, 379-388 (1974).
19. Hoek E. & Bray J. *Rock Slope Engineering*. The Institution of Mining and Metallurgy, London, 309 p (1974).
20. Louis C. Reconnaissance de massifs rocheux par sondages et classifications géotechniques de roches. *Soils et Foundations*, No. 31 July-August, pp. 97-122 (1974).
21. Rankilor P. R. A suggested field system for logging rock cores for engineering purposes. *Bull. Ass. Engng. Geol.* 11, 247-259 (1974).
22. Van Schalkwyk A. The application of computer techniques for the manipulation and storage of exploratory borehole data. *Proc. of 2nd. Int. Cong. of the Int. Assoc. Engng. Geology*, São Paulo, VI-22 (1974).
23. Priesti S. D. & Hudson J. A. Discontinuity spacings in rock. *Int. J. Rock Mech. Min. Sci. & Geomech. Abstr.* 13, 135-148 (1976).
24. Van Schalkwyk A. Rock engineering testing in exploratory boreholes. *Proc. of Symp. on Exploration for Rock Engineering*, Johannesburg, Vol. I, pp. 37-55 (1976).
25. South African Core Logging Committee. A guide to core logging for rock engineering. *Proc. of Symp. on Exploration for Rock Engineering*, Johannesburg, Vol. I, pp. 71-86 (1976).



**DIVISION DE EDUCACION CONTINUA  
FACULTAD DE INGENIERIA U.N.A.M.**

MECANICA DE ROCAS APLICADA A LA MINERIA Y A LA CONSTRUCCION

PROPIEDADES MECANICAS DE LAS ROCAS

MAYO, 1985

## Propiedades mecánicas de las rocas

### INTRODUCCIÓN

El comportamiento de una presa de tierra y enrocamiento depende, en muchos aspectos, de las propiedades mecánicas de su roca de cimentación. En efecto, la inestabilidad o permeabilidad de las formaciones geológicas del sitio pueden ocasionar problemas serios durante la vida de la obra y aun reducir su utilidad en conjunto. Además, aunque en casos especiales la compresibilidad y capacidad de carga de las masas rocosas no son motivo de preocupación al proyectar la cimentación de una cortina de tierra y enrocamiento, revisten importancia al analizar la estabilidad de las obras auxiliares. El estudio de las propiedades mecánicas de las rocas es, por tanto, fundamental.

La característica principal de una masa rocosa es su fisuración, su carácter discontinuo. Ciertas discontinuidades de la masa son visibles directamente (diachasas, fisuras, fallas), dando al macizo rocoso la apariencia de un amontonamiento de bloques más o menos regulares y de aspecto monolítico (fig 11.1). Un análisis más detallado muestra que los propios bloques están afectados por discontinuidades matriciales. De hecho, la existencia de fisuras de este tipo queda demostrada mediante la observación directa en láminas delgadas, con inyección de resinas. La generación de ruidos internos en una probeta sometida a una prueba de carga es, además, una manifestación cualitativa del crecimiento de dichas fisuras.

San numerosas las propiedades mecánicas de las rocas que pueden ser interpretadas con base en la existencia de discontinuidades microscópicas o macroscópicas. En el laboratorio, la anisotropía, la influencia del agua en la resistencia, la compresibilidad, la variación de la permeabilidad hidráulica al aire y de la velocidad de transmisión de ondas, en función del estado de esfuerzos aplicados, son ejemplos de la afirmación anterior. En el campo basta con mencionar la

compresibilidad, permeabilidad y anisotropía de los macizos rocosos, esencialmente regidas por las juntas de estratificación, fracturas o fallas, para percatarse de la importancia de estas superficies de discontinuidad. Por tanto, no resulta excesivo afirmar que la propiedad fundamental de las rocas es su carácter discontinuo.

### 11.1 MUESTRAS DE ROCA

Una roca está formada por un conjunto de minerales sustrado por discontinuidades. Se estudiará primero la estructura de la matriz rocosa, con objeto de definir las propiedades índice de las muestras de roca.

**11.1.1 Estructura y propiedades índice de las rocas.** Porosidad. Las rocas son materiales porosos. Ciertas rocas sedimentarias o ígneas extrusivos alcanzan valores de la porosidad de 20 por ciento, mientras que en las rocas ígneas intrusivas resultan del orden de 0.1 por ciento. La porosidad de la mayoría de las rocas queda comprendida entre esos límites.

La forma de las discontinuidades de la matriz rocosa es variable. Las rocas muy porosas tienen oquedades equidimensionales, aproximadamente esféricas, que provienen de desprendimientos de gases durante el enfriamiento de la roca ígnea extrusiva o de disoluciones por agua meteórica. Opuestamente, las rocas de porosidad reducida están sustradas por discontinuidades alargadas, en forma de grietas, producto de los esfuerzos internos generados en la matriz rocosa por efecto de la dilatación térmica diferencial de los minerales y, también, por efecto de los esfuerzos tectónicos. Los granitos, por ejemplo, formados por minerales de cuarzo y feldespato de coeficientes de dilatación volumétrica y de compresibilidad muy diferentes entre sí, son particularmente sensibles a los cambios de temperatura o del esfuerzo aplicado. Por tanto, no es sorprendente que tratando con granitos se haya podido

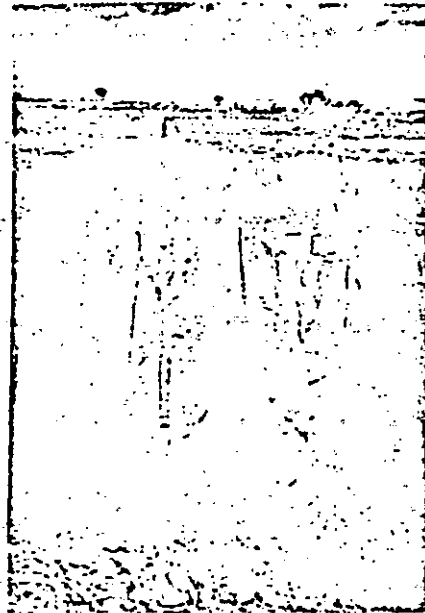


Fig 11.1 Los macizos rocosos son mejor discontinuos

demostrar (Isnard y Leymarie, 1963) que las direcciones de fisuramiento de los minerales de cuarzo coinciden con las direcciones de las fracturas macroscópicas de la masa rocosa estudiada. En consecuencia, existe la posibilidad de que se puedan determinar las direcciones preferentes de las discontinuidades macroscópicas de un macizo rocoso (diachasas, fallas, fracturas) a partir del estudio de las discontinuidades matriciales de la roca, lo que ha promovido el estudio detallado de la estructura matricial de las rocas en el laboratorio.

Con base en la distinción entre la porosidad ocasionada por las inclusiones y la debida a la presencia de grietas, se han definido la porosidad absoluta y la de fisuración. La primera se determina a partir de la medición del peso volumétrico de la muestra y de la densidad de sólidos. Este procedimiento, cuya precisión es del orden de 10 por ciento, arroja resultados variables, de acuerdo con el grado de combinación logrado en la roca. Para determinar la porosidad de fisuración se utiliza un porosímetro (Farran y Thevoz, 1965) que permite medir el volumen de aire que llena las grietas matriciales interconectadas. En forma indirecta, Walsh (1968) ha evaluado la porosidad de fisuración  $n_f$  mediante la obten-

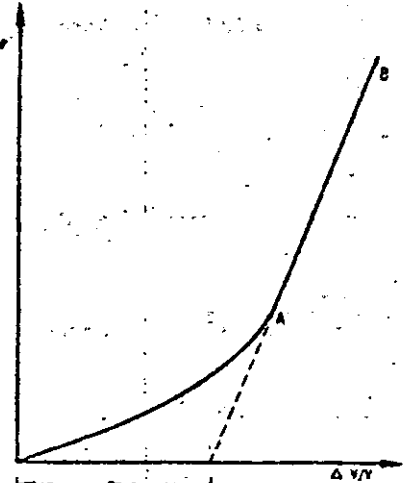


Fig 11.2 Variación del volumen de la muestra en función de la presión hidrostática aplicada

ción del módulo de compresibilidad volumétrica de una muestra de roca sometida a presión hi-

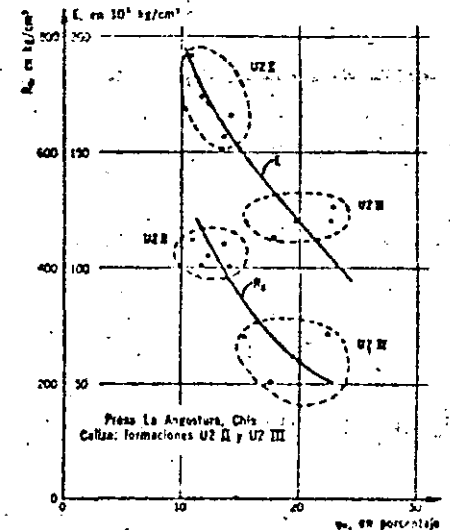


Fig 11.3 Porosidad de fisuración  $n_f$  vs resistencia a la compresión,  $R_c$ , y módulo de deformabilidad,  $E$

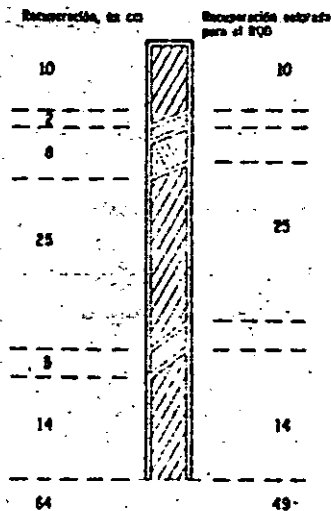


Fig. 11.4 Recuperación total e índice de calidad de la roca

destruictiva. En la fig. 11.2 se presenta un diagrama de variación del volumen de la muestra en función de la presión aplicada  $\sigma$ . Para niveles reducidos de  $\sigma$ , las fisuras se cierran progresivamente hasta alcanzar el punto A. La recta AB representa el comportamiento de la matriz no fisurada. En la misma grafica se presenta la forma de valorar  $\alpha$ .

La porosidad de fisuración está directamente ligada con la resistencia a la compresión simple de la roca y al modulo de deformabilidad inicial tangente (fig. 11.3). También se ha establecido una correlación experimental entre la velocidad de las ondas longitudinales y transversales y la porosidad de fisuración (Morbier, 1969).

En ingeniería se ha definido (Deere, 1963) un índice de calidad de la roca,  $RQD$ , basado indirectamente en el número de fracturas observadas en los corazones provenientes de un muestreo. En lugar de determinar el número de fracturas de las muestras, se procede a valorar el cociente de la longitud que resulta de sumar únicamente los trozos de roca mayores de 10 cm (fig. 11.4) y la longitud de avance del sondeo. La roca se clasifica de acuerdo con los valores del  $RQD$  (tabla 11.1).

Este índice se utiliza para establecer comparaciones entre muestras provenientes de diversos sondeos o zonas de un sitio estudiado.

Tabla 11.1. Descripción de la calidad de la roca

RQD, en porcentaje	Calidad
0-25	Muy pobre
25-50	Pobre
50-75	Aceptable
75-90	Buena
90-100	Excelente

**Contenido de agua.** Al aumentar el contenido de agua de una muestra de roca, disminuye su resistencia a la compresión simple. Dicha reducción de resistencia puede ser notoria, ya sea por la disminución de los esfuerzos efectivos o por efecto de cambios estructurales, particularmente en aquellos materiales ligeramente cementados y que no han estado sometidos previamente a saturación. En ciertas tobas muestreadas en el sitio de la presa Santa Rosa, Jal., la saturación produjo una disminución de la resistencia a la compresión simple de 210 a 30  $kg/cm^2$  en condiciones no drenadas (Instituto de Ingeniería, 1965). Mas notorio es el caso mencionado por Colback y Wiid (1965). Al variar el contenido de agua de una cuarcita de 0.015 a 0.09 por ciento, pasando del estado seco al saturado, la resistencia a la compresión simple varió de 1900 a 900  $kg/cm^2$  (fig. 11.5).

La presencia de agua en las fisuras de las rocas provoca la reducción de la energía superficial de sus minerales, o sea, la cohesión de la

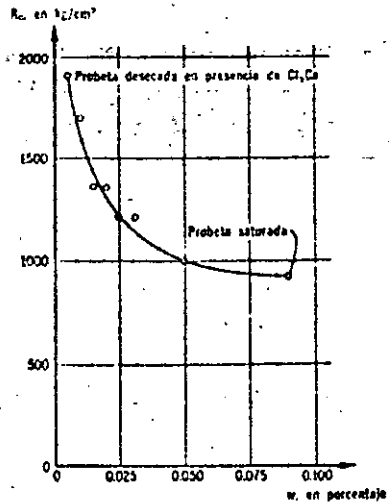


Fig. 11.5 Relación entre la resistencia a la compresión simple,  $R_c$ , y el contenido de agua,  $w$ , de una cuarcita (Colback y Wiid, 1965)

roca disminuye por la simple presencia de agua en los poros; en consecuencia, al saturarse la muestra, su deformabilidad aumenta y su resistencia a la compresión simple disminuye (Boozar *et al.*, 1962). Asimismo, las laderas del embalse de una presa, al saturarse, pueden sufrir una reducción drástica de su resistencia al cortante, por lo que pueden generarse movimientos notables de la masa rocosa y aun fallas de talud.

**Alteración y alterabilidad.** Las rocas, al ser sometidas a la acción agresiva del ambiente, sufren modificaciones en su estructura y composición mineralógica o, en otros términos, se alteran. En relación con este fenómeno, se estudian dos características de la roca: su alteración y su alterabilidad. El grado de alteración de una roca es un parámetro con el que se trata de definir el estado presente de la roca; la alterabilidad es la capacidad de una roca para alterarse en el futuro, bajo las condiciones ambientales reinantes en el sitio.

Cuando se altera una roca aumenta su porosidad. Las clasificaciones de las muestras provenientes de una formación rocosa dada, adoptando como criterios el grado de alteración o la porosidad serán, por tanto, idénticas. Sin embargo, resulta delicado determinar en forma precisa la porosidad de una roca. Por esta razón, tomando en cuenta la existencia de una relación entre esta magnitud y el peso de agua absorbida por la muestra previamente secada, al sumergirla (Krynine y Judd, 1957) se ha optado (Hamrol, 1962) por definir el grado de alteración como

$$I \text{ por ciento} = \frac{P_2 - P_1}{P_1} \times 100 \quad (11.1)$$

donde:

- $P_2$  peso de la muestra al finalizar la prueba de absorción
- $P_1$  peso de la muestra secada en horno a 105°C

La prueba de absorción se realiza manteniendo la muestra sumergida en agua durante un lapso constante de hora y media.

El grado de alteración se relaciona con la resistencia y deformabilidad de la roca: a mayor grado de alteración, menor resistencia y mayor deformabilidad del material. También el efecto de escala (inciso 11.1.2) disminuye al crecer el grado de alteración. Esto implica que la alteración, al aumentar, opaca el carácter discontinuo de la matriz rocosa y que, para valores grandes del índice de alteración, el comportamiento de la roca tiende al de un suelo en que el efecto de escala es reducido.

Al estudiar la alterabilidad de una roca es necesario subrayar nuevamente la importancia de

su microfisuración. De hecho, las discontinuidades de la matriz rocosa juegan un papel fundamental en el proceso de alteración; las fisuras abiertas permiten el acceso del agua hacia la matriz rocosa, agua que actúa entonces sobre áreas importantes de los minerales. Sin fisuras, la alteración de la masa rocosa sería prácticamente nula; sin embargo, resulta difícil valorar la influencia de la fisuración sobre la alterabilidad de una roca, pues su importancia está condicionada por otro factor: la alterabilidad específica de los minerales en las condiciones ambientales del sitio, o sea que la alterabilidad de una roca es consecuencia de la fisuración y la alterabilidad específica de sus minerales.

Se ha comprobado experimentalmente que la circulación de agua en las rocas compactas es posible solo a partir de un valor de la permeabilidad al aire igual a  $10^{-7}$  cm/seg, aproximadamente (Farran y Theno, 1955). De acuerdo con este criterio, que refleja la influencia de la fisuración de la roca en su alterabilidad, se pueden distinguir dos grandes familias de rocas. La primera es la integrada por las muy compactas, en las que el agua no circula y, por tanto, son inalterables sea cual fuere la alterabilidad específica de sus minerales. Las rocas de la segunda familia son permeables al agua y por tanto alterables, en caso de que sus minerales sean de elevada alterabilidad específica. Con objeto de valorar la alterabilidad específica de los minerales de una roca, se procede a una prueba de percolación con agua del sitio investigado a través de una muestra de la roca (Farran y Theno, 1955). La disminución o aumento del coeficiente de permeabilidad de la roca en función del tiempo indica la existencia de una reacción química entre el agua y los minerales constitutivos, o sea una alterabilidad específica diferente de cero. También es significativa la comparación entre la composición química del agua inyectada y la filtrada.

Al tratar de aplicar en la obra los resultados obtenidos en el laboratorio, es necesario tener en cuenta los daños ocasionados a la roca por los métodos de ataque, principalmente los explosivos. Una roca que es inalterable *in situ* por ser su permeabilidad al aire inferior a  $10^{-7}$  cm/seg, puede tornarse alterable si los procedimientos de excavación utilizados aumentan en forma notable su fisuración.

En conclusión, la alterabilidad de una roca depende de su grado de fisuración, inherente o proveniente, y de la alterabilidad específica de sus minerales.

**Sensitividad.** El concepto de sensibilidad de una muestra de roca se establece analizando la variación de su permeabilidad al agua, en función del estado de esfuerzos aplicado (Bernis, 1967).

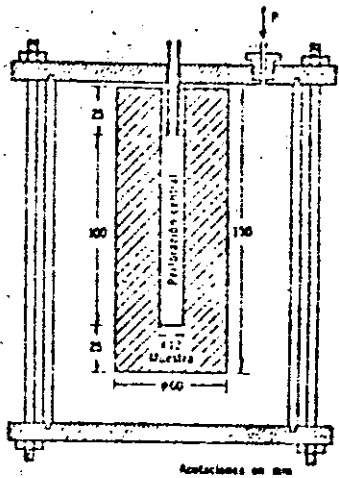


Fig. 11.6 Prueba de permeabilidad. Flujo radial convergente

La muestra probada (fig. 11.6) está formada por un corazón de 60 mm de diámetro y 150 mm de longitud, perforado en la parte central. En el extremo superior del conducto central, de 12 mm de diámetro y 100 mm de largo, se adapta un tubo metálico pegado a la roca con araldita. Las pruebas de permeabilidad se efectúan provocando un flujo radial de agua a través de la muestra, flujo que puede ser convergente o divergente. En el primer caso (fig. 11.6), la muestra se introduce en un recipiente hermético alimentado con agua a presión,  $p$ . El conducto central, que comunica con el exterior del recipiente, colecta el agua de filtración. En el segundo caso el agua a presión se inyecta en el conducto central de la muestra y se mide el gasto de filtración que fluye a través de la superficie lateral de la muestra.

Las redes de flujo, en las muestras probadas con flujo convergente o divergente, son idénticas. En consecuencia, la magnitud de las fuerzas de volumen debidas al gradiente hidráulico son iguales en ambas pruebas, pero ocasionan esfuerzos efectivos de compresión en el caso de flujo convergente y de tensión en el de flujo divergente. Si las rocas son fisuradas, las permeabilidades medidas con flujo divergente o convergente resultan diferentes, debido a la apertura o cierre de las fisuras por efecto de los esfuerzos de tensión o de compresión inducidos en las respectivas pruebas. Se denomina sensibilidad  $S$  de la roca a la magnitud

$$S = \frac{k_{z_1}}{k_{z_2}} \quad (11.2)$$

cociente de las permeabilidades medidas en condiciones de flujo radial divergente a presión de  $1 \text{ kg/cm}^2$  y flujo radial convergente a una presión de  $50 \text{ kg/cm}^2$ .

En numerosos casos de roca de diversas características se ha podido establecer una correlación entre el valor de la sensibilidad  $S$  y la intensidad de su fisuración (Hajib y Bernais, 1970). La sensibilidad de las rocas porosas no fisuradas es igual a 1 y alcanza valores de 10 000 para las masas fisuradas, como por ejemplo el gneis de Malpasset en Francia.

La variación de la permeabilidad en función del estado de esfuerzos aplicado, que constituye la base del concepto de sensibilidad, no solo permite valorar la intensidad de la fisuración de una muestra de roca, sino interpretar los resultados de las pruebas de permeabilidad Lugeon efectuadas en el campo (Sabary, 1953). El gasto  $Q$  de inyección de agua con presión  $p$  en una masa de roca fisurada que se comporta elásticamente, sigue la ley

$$Q = Ap^s \quad (11.3)$$

siendo  $A$  una constante.

En otros términos, la permeabilidad de la masa rocosa depende de la magnitud de la presión aplicada, pues provoca la apertura de las fisuras preexistentes en el medio. Esta ley se ha verificado en ciertos casos (fig. 11.7), como los presentados por Sabary (1968).

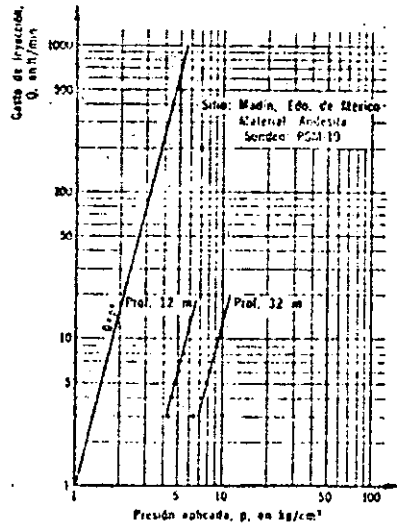


Fig. 11.7 Resultados de las pruebas Lugeon

En conclusión, la permeabilidad de la roca, a pequeña o gran escala, es variable en función del estado de esfuerzos aplicados por su efecto en el ancho de las fisuras tanto microscópicas como macroscópicas. La falla de la presa Malpasset en Francia, así como la variación del gasto de filtración en la cimentación en función del nivel de agua en el embalse, son manifestaciones a gran escala de este fenómeno (Sabary, 1968); asimismo, en la presa Santa Rosa, Jal. (fig. 11.8a) se observaron filtraciones en la galería de drenaje del arco de concreto que aumentan conforme al nivel del embalse de acuerdo con la ley presentada en la fig. 11.8b, según la cual

$$\frac{Q}{Q_1} = \left( \frac{Z - Z_0}{Z_1 - Z_0} \right)^{10} \quad (11.4)$$

donde  $Q$  y  $Q_1$  son los gastos de filtración correspondientes a los niveles  $Z$  y  $Z_1$  del embalse. Esta ley de variación corresponde a la siguiente idealización del fenómeno de apertura y cierre de las fisuras: puede suponerse que el gasto de filtra-

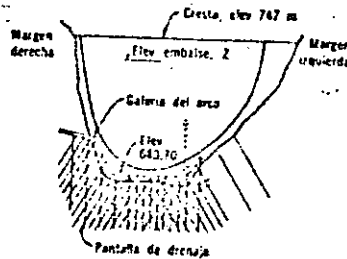


Fig. 11.8a Presa Sta. Rosa, Jal. Vista desde aguas abajo

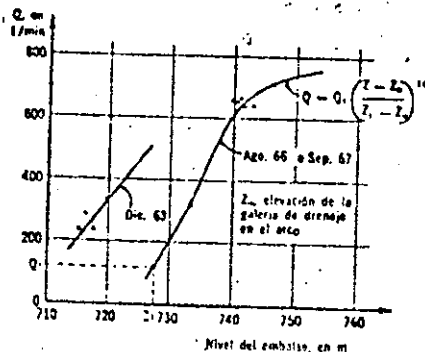


Fig. 11.8b Variación de los gastos de filtración en la galería del arco en función de la elevación del agua en el embalse

ción en la cimentación de la presa es proporcional al cubo del ancho  $e$  de las fisuras y a la carga de agua  $H$ . A su vez, el ancho de las fisuras varía con el estado de esfuerzos en la cimentación de la presa, que se modifica de acuerdo con el nivel  $H$  del agua en el embalse. Suponiendo que el ancho  $e$  de las fisuras en la cimentación aguas arriba de la presa varía proporcionalmente al momento de empotramiento del arco en su base, resulta que

$$e = H^3$$

por lo cual

$$q = H^6 = H^{10}$$

**11.1.2 Resistencia y deformabilidad.** La resistencia y la deformabilidad de la matriz rocosa, ocasionalmente pueden ser de utilidad directa para el diseño de las obras (pilares de excavaciones subterráneas, por ejemplo). Sin embargo, en la mayoría de los problemas planteados en una obra, la resistencia y deformabilidad de la matriz rocosa es de poco interés; en efecto, tratando con masas rocosas, la resistencia de las discontinuidades microscópicas, como fallas o juntas, es la que tiene el problema. Por tanto, los estudios de laboratorio se han utilizado fundamentalmente para aclarar en el comportamiento básico de las rocas, consideradas como medios discontinuos, utilizando un enfoque estadístico. Se ha logrado determinar en el laboratorio la influencia de la forma y dimensiones de las probetas, velocidad de carga y presión del fluido intersticial. La dispersión de los resultados obtenidos con muestras probadas en iguales condiciones, es también un parámetro fundamental.

**Efecto de escala.** Los resultados numéricos de las pruebas de resistencia realizadas con muestras cilíndricas de igual relación de esbeltez, varían con el volumen de las probetas ensayadas. Esta propiedad es característica de los medios fracturados o discontinuos.

La interpretación teórica de la disminución de resistencia en compresión simple al aumentar el volumen se basa en conceptos probabilísticos expuestos por Weibull (Javier y Cook, 1969), como el del *eslabón más débil* de una cadena. Según este concepto, la resistencia de un material sujeción por discontinuidades queda condicionada por la resistencia del elemento de volumen que contiene la zona más débil, o sea la más fracturada. Si para una densidad de fisuración dada el volumen de la probeta crece, el número total de discontinuidades aumenta, así como la probabilidad de incluir una fisura grande en la muestra.

Suponiendo una función de densidad probabilística de la resistencia, se puede establecer una

relación entre el volumen de la muestra y su resistencia. De acuerdo con la función exponencial para la densidad probabilística de la resistencia, propuesta por Weibull, la relación entre la resistencia media en compresión simple,  $\bar{R}_c$ , de una probeta y su volumen,  $V$ , está dada por

$$\bar{R}_c = (\pi V)^{-1/m} \left\{ \frac{1}{m} \Gamma\left(\frac{1}{m}\right) \right\} \quad (11.5)$$

en que  $\pi$  y  $m$  son constantes características del material y  $\Gamma$  es la función gamma. También se puede establecer que la variancia de la resistencia es igual, en esas condiciones, a

$$s^2 = (\pi V)^{-2/m} \left\{ \frac{2}{m} \Gamma\left(\frac{2}{m}\right) - \frac{1}{m^2} \Gamma\left(\frac{1}{m}\right)^2 \right\} \quad (11.6)$$

Con base en las relaciones anteriores se obtiene que el coeficiente de variación de la resistencia a la compresión simple de un lote de muestras de una misma roca es

$$\frac{s}{\bar{R}_c} = \sqrt{\frac{2/m}{(1/m)^2} - 1} \quad (11.7)$$

Este resultado es interesante, pues indica que el coeficiente de variación de la resistencia a la compresión simple de un lote de muestras es, de acuerdo con la teoría de Weibull, independiente del volumen de la probeta. La experiencia muestra que, por lo menos en ciertos casos (Bernaix, 1967), este coeficiente de variación es efectivamente independiente del volumen de los especímenes probados y, por tanto, constituye un parámetro característico de la roca ensayada en el sentido de que depende únicamente de  $m$ , que es una constante para cada material.

Tomando entonces como valor índice del efecto de escala el cociente de las resistencias a la compresión simple de probetas de relación de esbeltez 2 y diámetros 1 cm y 6 cm, resulta, de acuerdo con la ec 11.5:

$$\frac{\bar{R}_c \phi_{10}}{\bar{R}_c \phi_{60}} = (216)^{1/m} \quad (11.8)$$

$$\frac{s}{\bar{R}_c} = \sqrt{\frac{2/m}{(1/m)^2} - 1} \quad (11.9)$$

Ambas ecuaciones dependen únicamente del parámetro  $m$  y, en consecuencia, no son independientes. En la fig 11.9 se presentan las variaciones de los parámetros  $\bar{R}_c \phi_{10}/\bar{R}_c \phi_{60}$  y  $s/\bar{R}_c$  en función de  $m$ .

De acuerdo con la ley de Weibull (fig 11.9), a mayor valor de  $m$  menor efecto de escala y menor coeficiente de variación de los resultados.

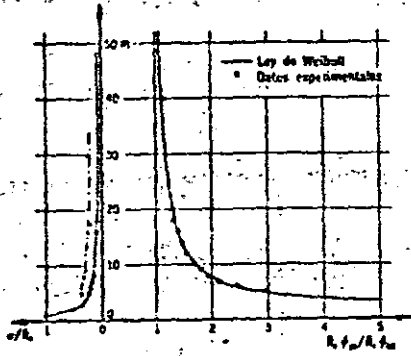


Fig 11.9 Efecto de escala vs dispersión de los resultados de resistencia a la compresión simple

En otros términos, a mayor grado de fisuración de la roca, mayor efecto de escala y mayor dispersión.

La tendencia mostrada por los resultados experimentales es la misma (fig 11.9). Con estos mismos datos reportados por Bernaix (1967) y Jaeger y Cook (1969), que se obtuvieron ensayando un número grande de probetas, se formó la tabla 11.2.

Aunque la aplicación de la ley de Weibull al caso de las rocas sea conceptualmente discutible (Bernaix, 1967; Hudson, 1968), los resultados obtenidos en pruebas de compresión simple verifican satisfactoriamente esta ley.

El efecto de escala es un factor fundamental para el diseño de los pilares de excavaciones subterráneas. La resistencia a la compresión simple de un pilar de una mina puede ser notablemente inferior a la de corozones de tamaño reducido, si la roca se encuentra muy fisurada. La dispersión de los resultados experimentales de pruebas de compresión simple permite orientar la elección del parámetro  $m$  que rige la magnitud del factor de escala.

El factor de escala disminuye al aumentar la presión confinante que actúa sobre la muestra, pues induce el cierre de las fisuras preexistentes y, por tanto, pierde importancia el carácter discontinuo de la roca (Habib y Youille, 1966). Correlativamente, cuando aumenta la presión de confinamiento, disminuye el coeficiente de variación de la resistencia al corte.

La comparación de las resistencias al esfuerzo cortante determinada en el laboratorio con probetas de dimensiones reducidas, e *in situ* en áreas grandes, muestra también que el efecto de escala es tanto más pronunciado cuanto más acentuado es el carácter discontinuo de la roca. Por

Tabla 11.2. Efecto de escala

Roca	Fisuración	m	$\frac{s}{\bar{R}_c}$	$\frac{\bar{R}_c \phi_{10}}{\bar{R}_c \phi_{60}}$	Referencia
Gneis de Malpasset, margen de roca	Microfisuración y macrofisuración muy intensa	5	0.37	2.9	Bernaix (1967)
Gneis de Malpasset, margen interior	Microfisuración y macrofisuración medias	8	0.30	1.9	Bernaix (1967)
Carbón de Duffryn	Surrado de fisuras y debilidades visibles	9.4	0.29	1.8	Jaeger y Cook (1969)
Caliza fisurada	Microfisuración débil, Macrofisuración intensa	16	0.25	1.4	Bernaix (1967)
Gneis con biotita y moscovita	Microfisuración media	30	0.22	1.2	Bernaix (1967)
Carbón de Barnsley Hard	Macrofisuración nula	17.5	0.24	1.35	Jaeger y Cook (1969)
Caliza de Saint Vaast	Fisuras preexistentes	∞	0.25	1.00	Bernaix (1967)

ejemplo, Rocha (1964) muestra que al aumentar el grado de alteración de un granito, o sea, al disminuir su carácter de material fisurado, el efecto de escala disminuye (fig 11.10).

En conclusión, y de acuerdo con lo expresado en el inciso 11.1.1, la sensibilidad de una roca, así como el factor de escala o la dispersión de su resistencia a la compresión simple, son manifestaciones de una misma realidad: su fisuramiento. En consecuencia, no es raro que estos parámetros no sean independientes. De hecho, se ha establecido (Bernaix, 1967; Habib y Bernaix,

1970), una correlación entre la sensibilidad  $S$ , el coeficiente de variación  $s/\bar{R}_c$ , y el factor de escala  $\bar{R}_c \phi_{10}/\bar{R}_c \phi_{60}$ : a mayor sensibilidad, mayor dispersión de la resistencia a compresión simple y mayor factor de escala.

**Efecto de la forma.** Son numerosos los estudios relativos a la influencia de la forma de las probetas sobre la resistencia a la compresión simple; así como las fórmulas propuestas para representar la reducción de resistencia observada al aumentar la relación de esbeltez de los especímenes. Parece ilusoria, en realidad, la búsqueda de una fórmula general aplicable cualesquiera que sean los materiales probados, la forma de las muestras y los procedimientos de ensayo utilizados; sin embargo, los estudios efectuados por Bertin y Tournay (1965) y Grosvenor (1963) han establecido que la resistencia disminuye apreciablemente al aumentar la relación de esbeltez hasta 2. Para valores superiores a 2, la variación de resistencia es reducida. En la fig 11.11 se presenta la variación de la resistencia a la compresión simple de muestras de andalita alterada en función de su relación de esbeltez.

En consecuencia, la práctica común consiste en efectuar las pruebas de resistencia con especímenes que tienen relación de esbeltez igual a 2.

**Anisotropía.** Las rocas metamórficas presentan a menudo textura foliada en la cual los minerales laminares, como mica y clorita, están alineados paralelamente unos con otros (gneis, pizarras, esquistos, por ejemplo). Se supone que en estos casos el comportamiento de las rocas es anisotrópico. En efecto, el módulo de deformabilidad en el sentido normal a la foliación es inferior al módulo paralelamente a la foliación hasta en 40 por ciento para los esquistos (Daye y Sibbys, 1965), 25 por ciento para las pizarras y las filitas, y 10 por ciento para las corozitas (Bruce, 1970). Para estas últimas, en el plano

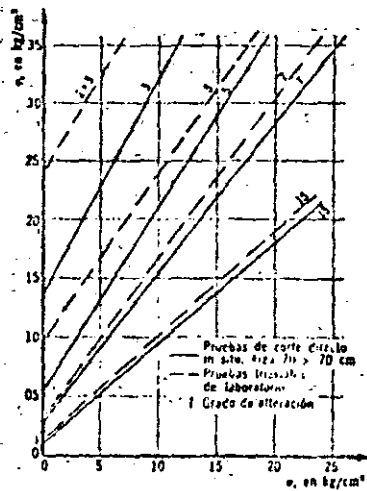
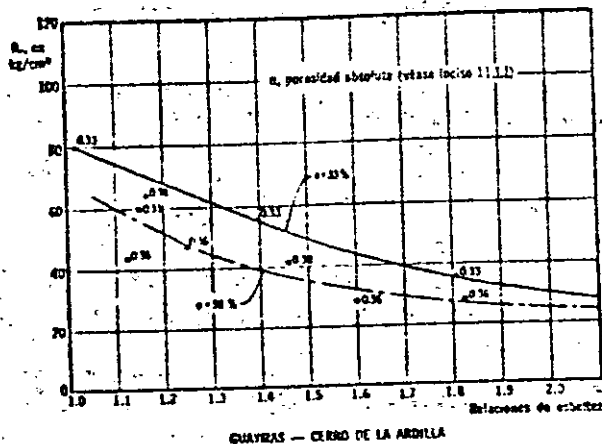


Fig 11.10 Disminución del efecto de escala con el aumento del grado de alteración, I (véase 11.1.1)



QUARRAS - CUERPO DE LA ARDILLA

de roca sometida a una prueba triaxial es función del esfuerzo confinante efectivo, o sea del esfuerzo confinante total aplicado menos la presión de poro desarrollada (Baron et al, 1963; Handin et al, 1963).

Es importante señalar que, en los experimentos diseñados con el fin de determinar la resistencia de una roca en términos de esfuerzos efectivos, resulta fundamental la consideración de la velocidad de carga o de deformación aplicada. En efecto, la permeabilidad de las probetas de rocas compactas es muy pequeña (del orden de  $10^{-20}$  o  $10^{-21}$  cm/seg), y en consecuencia el lapso de la presión de poro de la muestra es grande. Si el intervalo de tiempo a la falla impuesto no es mayor que el lapso de uniformación de la presión de poro, la medición de esta en la base de la probeta carece de sentido, pues no

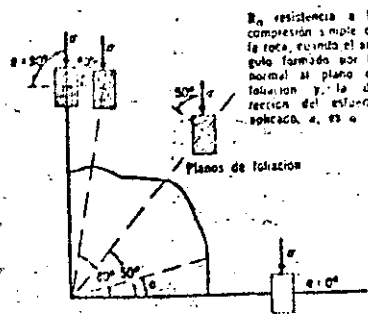


Fig. 11.12 Diagrama polar de la resistencia a la compresión simple de una roca foliada

es representativa de la presión de poro media actuante en la muestra. Por tanto, la resistencia en términos de esfuerzos efectivos de un material dilatante y saturado, probado en forma rápida, resulta superior a la del mismo material en estado seco, porque las presiones de poro negativas que se desarrollan no son medidas correctamente en la base de la muestra (Brace, 1970).

La generación y disipación de estas presiones de poro negativas bajo el efecto de una carga rápida ocasiona, por tanto, un incremento transitorio de resistencia de la roca, en términos de esfuerzos totales. Este fenómeno puede explicar el retraso que se presenta en ciertas minas profundas entre la apertura del túnel y la falla violenta de las paredes (popping).

También en el caso de taludes se ha observado que el proceso de falla ocurre en forma discontinua, a saltos, y una de las causas de este mecanismo podría ser la mencionada antes.

Estas evidencias experimentales subrayan la importancia del factor tiempo en la resistencia y deformabilidad de las rocas, que además muestran a largo plazo un comportamiento viscoso.

**Comportamiento viscoso.** La reducción en el diámetro de lumbreras de las antiguas minas romanas en el norte del Adriático, del antiguo "Toro de Abraham", cerca de Jerusalén, y de las lumbreras de acceso a túneles de riego de Irán, son ejemplos del comportamiento viscoso de las rocas a largo plazo (Westergaard, 1952).

En la fig. 11.13 se presenta la variación con el tiempo de las deformaciones de muestras de una misma roca sometidas a esfuerzos desviadores  $\sigma$  crecientes. Cuando  $\sigma$  es menor que el esfuerzo  $s$ , llamado resistencia última, las deformaciones alcanzan un máximo siguiendo una ley asintótica. En cambio, si  $\sigma$  es mayor que  $s$ , el flujo viscoso de la roca presenta tres fases:

a) Transitoria (fase I), con velocidad decreciente de deformación.

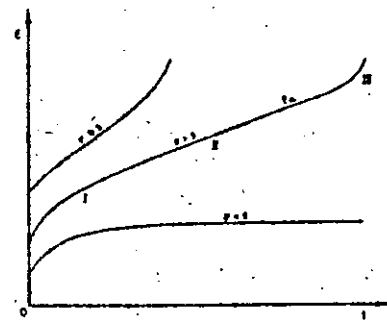


Fig. 11.13 Variación de la deformación en función del tiempo

b) Estacionaria (fase II), con velocidad constante de deformación  $\dot{\epsilon}_m$ .

c) De falla (fase III), en que la velocidad de deformación aumenta.

Las leyes experimentales utilizadas para describir cada una de estas fases son muy numerosas (Jaeger y Cook, 1969; Morlier, 1966).

Generalmente, la ley empírica utilizada para representar el comportamiento de flujo transitorio es la propuesta por Lonitz (1956):

$$\epsilon(t) = \epsilon_0 + A \ln(1 + t) \quad (11.10)$$

donde  $\epsilon_0$  es la deformación instantánea, y  $A$  y  $\sigma$  son constantes del material que dependen de la temperatura y de la presión confinante aplicada.

La velocidad de deformación  $\dot{\epsilon}_m$  durante la etapa de flujo estacionario es, de acuerdo con Griggs

$$\dot{\epsilon}_m = \dot{\epsilon}_0 \operatorname{senh} \left( \frac{\sigma - s}{\sigma_0} \right) \quad (11.11)$$

en que  $\dot{\epsilon}_0$  y  $\sigma_0$  son constantes del material y  $s$  es su resistencia última.

Al comparar esta relación con la propuesta por Morlier (1966) para calcular el tiempo a la falla,  $t_f$  de una muestra:

$$\dot{\epsilon}_m t = c t_0 \quad (11.12)$$

resulta que

$$t_0 \operatorname{senh} \left( \frac{\sigma - s}{\sigma_0} \right) = c t_0 \quad (11.13)$$

En otras palabras, el tiempo a la falla de una muestra sometida a un esfuerzo desviador  $\sigma$  es inversamente proporcional al seno hiperbólico de la diferencia  $(\sigma - s)$ . Este resultado es importante, pues coincide con numerosos datos experimentales (Morlier, 1966; Saito y Uesawa, 1961) y permite calcular el tiempo a la falla de una masa de roca a partir del momento en que su velocidad de deformación es constante.

Con base en su comportamiento reológico, las rocas pueden clasificarse en tres familias: densas-duras, porosas y plásticas blandas. En la tabla 11.3 se presentan los valores de la resistencia última para distintas rocas sometidas a pruebas de creep bajo esfuerzo axial constante y esfuerzo confinante nulo, a la temperatura ambiente.

El comportamiento reológico de las rocas varía también en función del esfuerzo confinante y la temperatura; al aumentar el esfuerzo confinante aplicado o la temperatura ambiente, predomina el componente plástico. En consecuencia, aumen-



Tabla 11.3. Resistencia última de varias rocas

Familia	Roca	Resistencia última, en porcentaje de $R_c$	Referencia
I. Rocas densas-duras	Granito	80	Mörler (1966)
	Gneis	80	
	Caliza	80	
	Caliza	80	
II. Rocas porosas	Dolomita	50	Price (1966)
	Arenisca Wolfstanoo	60	
	Arenisca Darley	50	
	Caliza	35	
	Granodiorita	27	
	Alabastro	37	
Arenisca Pennant	20		
III. Rocas plásticas blandas	Plutasa	25	Mörler (1966)

$R_c$ : resistencia a la compresión simple

tan sus deformaciones diferidas y disminuye la relación de la resistencia última a la resistencia medida con velocidad de carga convencional.

Esos datos experimentales han sido integrados, mediante el uso de modelos reológicos tipo Kelvin o Burgers, en el análisis de las deformaciones a largo plazo medidas en pruebas de placa u observadas en excavaciones subterráneas.

Finalmente, es digno de mención el hecho de que al tratar de representar, mediante modelos, los fenómenos tectónicos que ocurren en la corteza terrestre, haya sido necesario el girar materiales tan viscosos como la parafina para representar el comportamiento de las rocas.

**11.1.3 Criterios de falla.** El comportamiento de las rocas sometidas a pruebas de compresión triaxial varía en función del tipo de roca y del nivel de esfuerzos confinantes aplicados.

Al probar una serie de muestras provenientes de un mismo macizo rocoso a presiones confinantes  $\sigma_2$  crecientes, se observa una variación en las relaciones esfuerzo-deformación (fig 11.14). En efecto, para presiones  $\sigma_2$  reducidas, la muestra se comporta en forma elástica hasta niveles altos del esfuerzo desviador y falla repentinamente en forma frágil, produciéndose fisuras paralelas a la dirección del esfuerzo principal mayor  $\sigma_1$ . Cuando las presiones  $\sigma_2$  aumentan, la curva esfuerzo-deformación presenta un máximo seguido de una disminución de resistencia y la muestra falla a lo largo de planos inclinados con respecto a la dirección del esfuerzo  $\sigma_1$ . Finalmente, para presiones  $\sigma_2$  muy elevadas, el comportamiento de la muestra se asemeja al de un material elasto-plástico perfecto u con endurecimiento por deformación.

El valor del esfuerzo confinante  $\sigma_2$  para el cual el material se torna plástico o dúctil a la temperatura del ambiente, depende del tipo de roca. Las rocas densas duras (granitos máficos, cuarcitas y calizas competentes) se tornan plásticas

para valores del esfuerzo confinante superiores a 1 000 kg/cm<sup>2</sup> (Baron et al. 1963), que evidentemente no se presentan en ingeniería civil. Sin embargo, al tratar con problemas de vulcanología puede ser útil considerar esfuerzos confinantes de esta magnitud asociados a elevadas temperaturas (Atouser, 1969). Las rocas que se tornan dúctiles a niveles de esfuerzos confinantes comunes en obras de ingeniería son las más blandas y porosas (calizas recientes, margas, silvinitas, etc). Puede decirse, sin embargo, que en general la mayoría de las rocas se comportan en forma frágil en los problemas de ingeniería civil.

En vista de la complejidad del comportamiento de una roca, es evidente que no se puede definir un criterio de falla único. Por tanto, en el intervalo de comportamiento frágil, el criterio comúnmente utilizado es el propuesto por Griffith (1925); para niveles intermedios de la presión confinante se emplea el criterio de falla de Mohr-Coulomb, y, para valores elevados de la presión confinante se aplican los criterios clásicos de Tresca o de Von Mises.

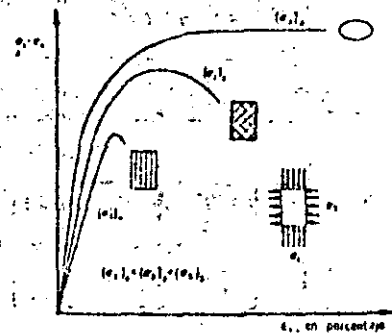


Fig 11.14 Variación del comportamiento de una roca en función del esfuerzo confinante aplicado

**Criterio de falla frágil de Griffith.** El esfuerzo  $T$  teóricamente necesario para fallar a tensión un material frágil y perfectamente homogéneo es:

$$T = \frac{E}{10} \quad (11.14)$$

siendo  $E$  su módulo de elasticidad (Freudenthal, 1950). Sin embargo, este material ideal dista mucho de ser representativo de las rocas, que fallan a tensión bajo esfuerzos mucho menores. Por tanto, es preciso admitir que esta discrepancia se debe a las concentraciones de esfuerzos que se presentan en la cercanía de las fisuras que surcan la matriz rocosa. Griffith (1925) analizó estas concentraciones de esfuerzos y supuso que las discontinuidades de la matriz son de forma elíptica.

Consideremos el caso de una muestra de roca sometida a una prueba triaxial (fig 11.15). La discontinuidad sujeta se asemeja a una elipse de ejes  $Ox$  y  $Oy$  inclinados según el ángulo  $\beta$  con respecto a la dirección del esfuerzo principal mayor. En tales condiciones y suponiendo que el material es elástico, se demuestra que en la cercanía de la cúspide de la discontinuidad:

$$\sigma_x = \frac{2(\sigma_1 m - \sigma_2 a)}{m^2 + a^2} \quad (11.15)$$

siendo  $m$  la excentricidad de la elipse, o sea el cociente de la longitud  $b$  de su eje menor y la de su eje mayor,  $a$ ;  $\alpha$  es el ángulo polar correspon-

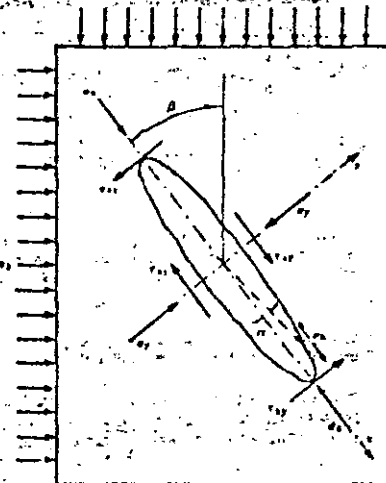


Fig 11.15 Criterio de Griffith. Nomenclatura

diente al punto de intersección de la elipse con el plano normal a esta en que actúa  $\sigma_1$  (fig 11.15).

Para  $\alpha = 0$ ,  $\sigma_x = \sigma_1$  y  $\tau_{xy} = 0$ , la ec. 11.15 se reduce a la propuesta por Griffith para la resistencia a tensión del material,  $\sigma_t$ :

$$\sigma_t = \frac{2\sigma_1}{m} = 2\sigma_1 \sqrt{\frac{a}{r_0}} \quad (11.16)$$

siendo  $r_0$  el radio de curvatura de la elipse, en su cúspide.

El máximo valor de  $\sigma_x$  se obtiene para

$$\sigma_x = \frac{m \sigma_1}{\sigma_1 - (\sigma_1^2 + \sigma_2^2)^{1/2}}$$

y vale

$$\sigma_x = \frac{1}{m} \left[ \sigma_1 - (\sigma_1^2 + \sigma_2^2)^{1/2} \right] \quad (11.17)$$

Remplazando en esta última expresión la magnitud  $m \sigma_t$  obtenida mediante la ec. 11.16, resulta:

$$2\sigma_t = \left[ \sigma_1 - (\sigma_1^2 + \sigma_2^2)^{1/2} \right]$$

o sea

$$\sigma_2 = 4\sigma_t(\sigma_1 - \sigma_t) \quad (11.18)$$

La ecuación parabólica 11.18 representa el envolvente de Mohr correspondiente al criterio de Griffith.

Si en lugar de haber una sola discontinuidad en la masa la fisuración fuera isotrópica, la falla ocurriría a lo largo de las fisuras para las que el esfuerzo de tensión generado fuera máximo. Dichas fisuras están orientadas según el ángulo  $\beta$ , tal que

$$\cos 2\beta = \frac{\sigma_1 - \sigma_2}{2(\sigma_1 + \sigma_2)} \quad (11.19)$$

En ese caso, los esfuerzos principales correspondientes a la falla se relacionan mediante la ecuación

$$(\sigma_1 - \sigma_2)^2 + 8\sigma_t(\sigma_1 + \sigma_2) = 0 \quad (11.20)$$

La resistencia a la compresión simple resulta, por tanto, igual a ocho veces la resistencia a la tensión del material, lo cual coincide satisfactoriamente con los datos experimentales.

La teoría de Griffith aquí propuesta define las relaciones entre esfuerzos principales que determinan el inicio de la propagación de las fisuras.

pero no abarca su desarrollo subsecuente. Esta relación entre esfuerzos principales no siempre coincide con un criterio de falla. En efecto, si para una prueba de tensión es de esperarse que la propagación de la fisura normal al esfuerzo aplicado lleve de inmediato a la falla del espécimen, no ocurre lo mismo en una prueba de compresión triaxial. En este caso, la fisura se propaga siguiendo un camino curvo hasta que se torna paralela a la dirección del esfuerzo principal mayor de compresión; en ese momento la fisura deja de propagarse (Brace y Dombulakis, 1963). Este fenómeno se correlaciona con las observaciones de los microrruídos que se generan durante la prueba a partir de esfuerzos de 25 y 60 por ciento de la resistencia a compresión simple para granitos porosos y densos, respectivamente (Pezami y Thevoz, 1969).

En conclusión, el criterio de falla de Griffith representa adecuadamente el comportamiento de las muestras de roca sometidas a esfuerzos de tensión. En el caso de pruebas de compresión, la relación entre esfuerzos principales que resulta de la teoría de Griffith corresponde, más bien, al inicio de la fase de microfisuración de la roca; en cuanto a la falla, esta ocurre por generación de esfuerzos cortantes excesivos a lo largo de las discontinuidades así creadas (fig. 11.16). En consecuencia, el criterio de falla comúnmente utilizado para el caso de compresiones triaxiales es el de Mohr-Coulomb.

**Criterio de Mohr-Coulomb.** Este criterio que matemáticamente puede expresarse

$$\tau = c + \mu \sigma \quad (11.21)$$

implica la falla por cortante a lo largo de planos. La teoría de Griffith despreciaba el hecho de que las fisuras pueden cerrarse cuando los esfuerzos de compresión son suficientemente grandes. En tal caso, es de esperarse que se generen fuerzas de fricción entre las caras de la fisura, y para tomar en cuenta este efecto Mc. Clintock y Walsh (1962) modificaron la teoría de Griffith. El resultado más importante de esta proposición es que para presiones normales elevadas, el criterio modificado de Griffith coincide estrictamente con el de Mohr-Coulomb. Por tanto, para fines prácticos y para presiones confinantes suficientemente grandes, puede considerarse válido el criterio de Mohr. Sin embargo, para presiones confinantes superiores a 1000 kg/cm<sup>2</sup> y en el caso de rocas duras y densas, el material deja de comportarse como friccionante y se torna dúctil, siendo aplicables los criterios de falla de Tresca o Von Mises.

**Criterios de Tresca y Von Mises.** Se ha estudiado detenidamente el comportamiento dúctil

de las rocas debido a sus implicaciones en problemas de geofísica y geología. En el campo de la mecánica de rocas su importancia es mucho menor, pues son pocas las circunstancias en que las temperaturas y presiones aplicadas a las rocas las tornan dúctiles.

Los criterios clásicos utilizados son los de Tresca y Von Mises, que suponen que la falla ocurre cuando el máximo esfuerzo cortante o la energía de distorsión, respectivamente, alcanzan un valor prefijado. Las expresiones correspondientes son, para el criterio de Tresca

$$\sigma_1 - \sigma_3 = \sigma_c \quad (11.22)$$

y para el criterio de Von Mises

$$(\sigma_1 - \sigma_2)^2 + (\sigma_1 - \sigma_3)^2 + (\sigma_2 - \sigma_3)^2 = cte \quad (11.23)$$

siendo  $\sigma_1$ ,  $\sigma_2$  y  $\sigma_3$  los esfuerzos principales.

## 11.2 MASAS ROCOSAS

El comportamiento mecánico e hidráulico de una masa de roca depende primordialmente de la configuración de sus discontinuidades. Estas se agrupan en familias de juntas, planos de estratificación, superficies de foliación y fallas. El primer paso al estudiar un sitio ha de ser, por tanto, la clasificación y levantamiento de las superficies de discontinuidad de la masa rocosa.

**11.2.1 Clasificación y levantamiento de discontinuidades.** La característica que permite diferenciar las fallas de las juntas es su corrimiento; las juntas son fracturas sin corrimiento y transversales a la estratificación o esquistosidad, mientras que las fallas constituyen superficies de discontinuidad con un corrimiento relativo entre ambos bloques de roca.

Las fallas se clasifican como normales, inversas, o transversas según las direcciones de los

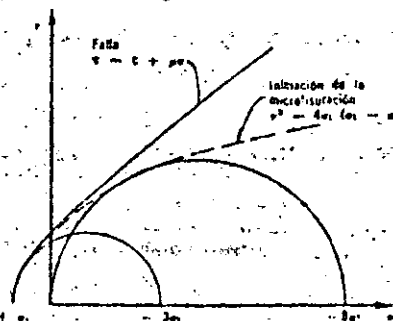


Fig. 11.16. Envolvente de falla de las rocas

## Capítulo 2

# Propiedades mecánicas de las rocas

A. J. Hendron, Jr.

### 2.1 Introducción

En muchos problemas de Mecánica de las Rocas son de importancia fundamental las propiedades de la sustancia rocosa. En otros, como se indicó en el capítulo anterior, debe considerarse el comportamiento de la roca *in situ* con las discontinuidades geológicas inherentes. En la primera parte de este capítulo se comentan las propiedades mecánicas de la sustancia rocosa. Entre ellas se incluyen la resistencia a tracción y a compresión simple, las características tensión-deformación en compresión simple, la resistencia y las características tensión-deformación de las rocas sometidas a tensiones combinadas y la dureza. En la segunda parte del capítulo se analiza la resistencia y compresibilidad de los macizos rocosos diaclasados.

### 2.2 Propiedades de la sustancia rocosa

#### 2.2.1 Resistencia a tracción

Resulta difícil la determinación de la resistencia a tracción mediante el ensayo directo de una probeta cilíndrica, ya que aún no se ha conseguido un método satisfactorio para sujetar la probeta sin introducir tensiones de flexión. Brace<sup>1</sup> ha utilizado muestras de forma especial que reducen el problema anterior, pero el método operatorio es costoso y quizá demasiado complicado para su empleo rutinario. El método más práctico para determinar la resistencia a tracción directa se consigue pegando, con resina epoxy, cañales de metal a muestras cilíndricas de roca que se ponen en tensión mediante cables o cadenas.

Como no suele ser necesaria una determinación exacta de la resistencia a tracción del material rocoso, ésta se suele medir generalmente por métodos rápidos indirectos. El «ensayo brasileño»<sup>2</sup> es un método indirecto muy usado para determinar la resistencia a tracción de la roca. En este ensayo, una probeta cilíndrica de longitud  $L$  y diámetro  $D$  se carga diametralmente con una carga  $P$ . La muestra se suele romper separándose en dos mitades según el eje de carga diametral. Se calcula entonces la resistencia a tracción  $\sigma_t$  en rotura mediante la Ec. (2.1) que da la tracción uniforme que actúa sobre la mayor parte del diámetro, normalmente a la línea que une los puntos de carga de acuerdo con la teoría elástica.

$$\sigma_t = \frac{2P}{\pi DL} \quad (2.1)$$

Un segundo método indirecto es el ensayo de tracción con carga puntual descrito por Reichnuth<sup>3</sup>. La resistencia a tracción para carga puntual se determina aplicando cargas de compresión puntuales a la superficie lateral de un testigo cilíndrico con el eje en posición horizontal. Las cargas puntuales se aplican mediante una prensa a través de rodillos de acero endurecido de pequeño diámetro, normales al eje del testigo. Esta carga produce tracciones perpendiculares al eje de carga; la resistencia a tracción  $\sigma_t$  viene dada por la expresión empírica:

$$\sigma_t = 0,0675 P/D^2 \quad (2.2)$$

donde  $P$  es la carga de rotura en kg y  $D$  el diámetro del testigo en centímetros. Miller<sup>4</sup> ensayó veintiocho tipos diferentes de roca, según este método encontrando que la resistencia a tracción media  $\sigma_t$  estaba relacionada con la resistencia a compresión simple  $\sigma_c$  por la Ec. (2.3).

$$\sigma_c = 21\sigma_t + 280 \text{ kg/cm}^2 \quad (2.3)$$

Para fines prácticos, probablemente es suficientemente exacto en la mayoría de los casos el suponer una resistencia a tracción del 5 al 10 % de la resistencia a compresión simple. Una determinación más exacta puede no estar justificada debido a la amplia variación de resistencias a tracción observadas en cualquier serie de muestras de roca. Además, por otro lado, las variaciones direccionales son muy grandes en rocas metamórficas y en rocas sedimentarias de estratificación fina<sup>5</sup>.

#### 2.2.2 Comportamiento a compresión simple

El comportamiento de la sustancia rocosa a compresión simple viene afectado en cierta extensión por las condiciones de ensayo. Las variables de ensayo más importantes son la relación longitud/diámetro de la muestra,  $L/D$ , la velocidad de carga y las condiciones de borde de la muestra.

Si se ensayan testigos de roca con valores  $L/D$  pequeños, es probable que no se puedan formar los planos de corte en la muestra sin atravesar el plano formado por la base de la muestra y el plato de la prensa. Así pues, el rozamiento entre la muestra y la prensa produce un efecto de confinamiento o triaxial que aumenta la resistencia obtenida. Una relación empírica debida a Obert y Duvall<sup>6</sup> relaciona la resistencia a compresión medida  $\sigma_c$  con la esbeltez  $L/D$ :

$$\sigma_c = \sigma_{c1} \left( 0,778 + \frac{0,222}{L/D} \right) \quad (2.4)$$

donde  $\sigma_c$  es la resistencia a compresión para  $L/D \neq 1$ , y  $\sigma_{c1}$  es la resistencia a compresión para  $L/D = 1$ . Se recomienda una relación  $L/D$  de 2,5 para asegurar una distribución de tensiones bastante uniforme en la muestra y aumentar la posibilidad de que el plano de rotura se pueda formar libremente sin interferir con el plato de la prensa.

La velocidad de carga es una variable de ensayo que influye sobre la resistencia a compresión y el módulo de elasticidad. La tabla 2.1 compara las resistencias medidas en la arenisca de Berea y en gabra con dos velocidades

∞

Tabla 2.1 Influencia de la velocidad de carga \*

Roca	Resistencia a compresión simple (kg/cm <sup>2</sup> )		
	Tiempo hasta rotura = 30 s	Tiempo hasta rotura = 0,030 s	Incremento de resistencia (%)
Arenisca de Peres	560	840	50
Giabro	2.170	2.800	30

de carga diferentes?. La figura 2.1 muestra el efecto de la velocidad de carga sobre el comportamiento del hormigón en masa. Al aumentar la velocidad, la resistencia y el módulo de elasticidad aumentan, disminuyendo la deformación de rotura. Resultados semejantes se han obtenido con sal gema; en un cierto grado puede esperarse que otras rocas se comporten de manera similar.

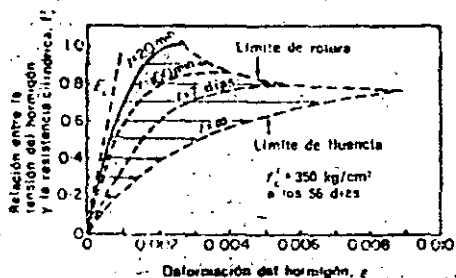


Figura 2.1 Influencia de la velocidad de carga sobre la resistencia y el módulo de elasticidad \*

Para velocidades comprendidas entre 0,70 y 7 kg/cm<sup>2</sup> s, sin embargo, Wuerker<sup>9</sup> y Watstein<sup>10</sup> han indicado que la influencia de la velocidad de carga sobre la resistencia de las rocas y el hormigón es despreciable. Normalmente se utilizan velocidades comprendidas entre esos límites en los ensayos monoaxiales en rocas<sup>4</sup>.

Las condiciones de borde de la muestra influyen sobre la forma de rotura y sobre la resistencia de las rocas. Obert y otros<sup>11</sup> recomiendan el empleo de muestras sin refrentar, ya que el material de refrentado suele ser más blando que la mayoría de las rocas. La tendencia de este material a romperse escapando radialmente produce una rotura por tracción que da lugar a una menor resistencia que en las muestras sin refrentar. Por esta razón las muestras de roca deben ensayarse sin refrentado, bastando con dejar bien pulidas sus caras extremas.

Como resultado de una amplia serie de ensayos con veintiocho tipos de rocas, Miller<sup>4</sup> clasifica las curvas de tensión-deformación en los seis tipos que aparecen en la figura 2.2. El tipo I presenta una forma prácticamente lineal hasta que se produce una rotura repentina. Este comportamiento es típico de los basaltos, cuarcitas, diabasa, dolomía y calizas extraordinaria-

mente duras, como la de Solenhofen. Las calizas más blandas, argilitas y tobas presentan una fluencia anelástica, continuamente creciente, al aproximarse a la carga de rotura, la cual puede caracterizarse por la curva del tipo II de la figura 2.2.

La curva tipo III es típica de la arenisca, granito, esquistos cortados paralelamente a la estratificación y algunas diabasas. Las rocas metamórficas,

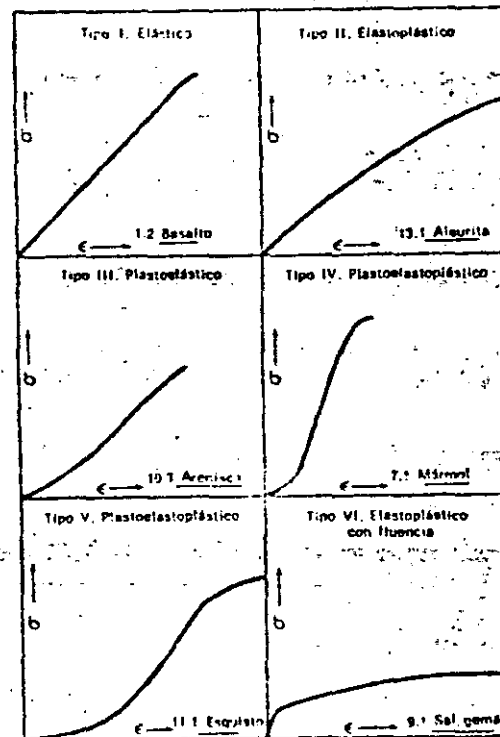
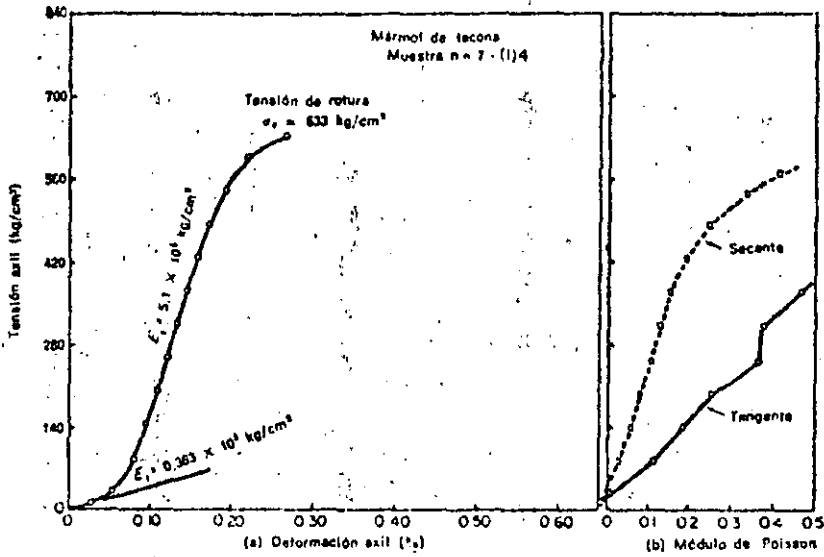


Figura 2.2 Curvas típicas tensión-deformación para rocas a compresión simple cargadas hasta rotura<sup>4</sup>

como los mármoles y gneis, están representadas por una curva en S con una parte central muy escarpada, de acuerdo con el tipo IV. Únicamente las muestras de esquistos cortados perpendicularmente a la estratificación presentan la elevada compresibilidad que señala la curva en S del tipo V. Las curvas de los tipos III, IV y V se caracterizan por una parte inicial cóncava hacia arriba que se hace más pendiente al cerrarse las superficies de microfisuras o exfoliación. La parte inicial se continúa por otra claramente lineal que va mostrando gradualmente diversos grados de fluencia anelástica al acercarse a la rotura. Las rocas del tipo III no presentan fluencia apreciable y se rompen de una forma frágil semejante a las del tipo I.

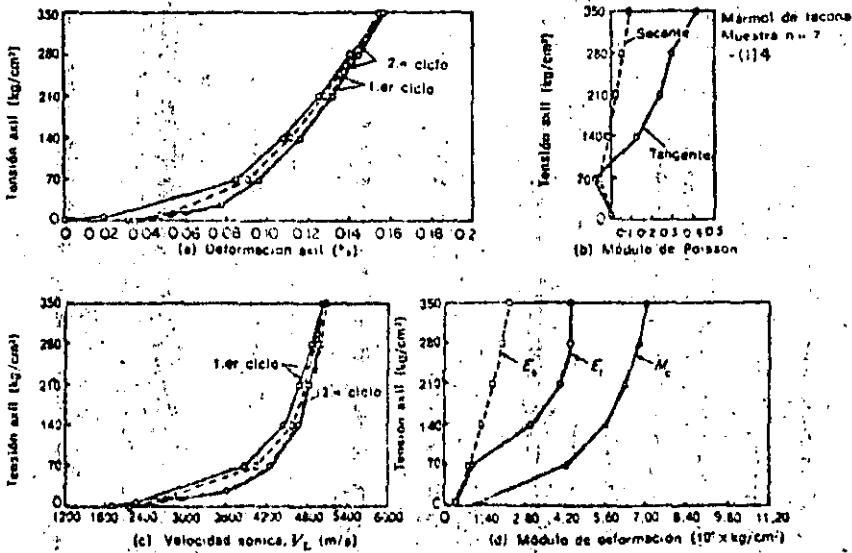


Tipo de roca	Mármol blanco (Tacona)
Muestra n.º	7,1-(1)4
L/D	2,006
$\gamma_s$	2,71 t/m <sup>3</sup>
$S_s$	36,9
$V_L$	2260 m/s
Textura	Compacta

Nota

$\gamma_s$  = Densidad seca  
 $S_s$  = Dureza Schmidt  
 $V_L$  = Velocidad sónica

Figura 2.3 Curva tensión-deformación y módulo de Poisson de una roca a compresión simple\*



Tipo de roca	Mármol blanco (Tacona)
Muestra n.º	7,1-(1)4
L/D	2,006
$\gamma_s$	2,71 t/m <sup>3</sup>
$S_s$	36,9
$\sigma_r$	633 kg/cm <sup>2</sup>
Textura	Compacta

Nota

$E_s$  = Módulo tangente (estático)  
 $E_t$  = Módulo secante (estático)  
 $M_c$  = Módulo con constricción lateral  
 $\sigma_{V_L}$  =  $\sigma_{V_L}$  (dinámico)  
 $V_L$  = Velocidad sónica

Figura 2.4 Comportamiento de tensión-deformación y velocidad sónica en compresión simple\*

La curva tipo VI es característica de la sal-gema y tiene una pequeña parte recta inicial seguida por una deformación anelástica creciente y una fluencia continua. Esta curva es también típica del comportamiento de la sal potásica y otras evaporitas.

En las figuras 2.3 y 2.4 se representan datos detallados de compresión simple del mármol de Taconá\*. Con tensiones bajas la curva tensión-deformación es cóncava hacia arriba, habiéndose medido un valor del módulo de Poisson ligeramente negativo. Las grandes deformaciones verticales se deben muy probablemente al cierre de las microfisuras y no a la compresión lateral. Los valores ligeramente negativos de la deformación circunferencial se deben probablemente a la sensibilidad transversal de los extensómetros. Al aumentar el nivel de tensiones, la curva tensión-deformación se vuelve lineal con un módulo tangente  $E$  de  $5,1 \times 10^3$  kg/cm<sup>2</sup> para el 50% de la carga de rotura. Los valores del módulo de Poisson, calculados a partir de las deformaciones axiales y circunferenciales medidas, aumentan gradualmente a lo largo del ensayo y superan el valor 0,5 con tensiones elevadas debido a que la muestra presenta dilatación al acercarse a la rotura. En la figura 2.4 aparecen las variaciones de las propiedades estáticas de tensión-deformación y de la velocidad sónica con las tensiones axiales para el mármol de Taconá. En la figura 2.4 c puede advertirse que la velocidad sónica  $V_L$  (medida en la dirección de la tensión axial) aumenta de 1.800 a 4.800 m/s cuando la tensión axial pasa de 0 a 175 kg/cm<sup>2</sup>. Por encima de 175 kg/cm<sup>2</sup> el aumento de la velocidad sónica con la tensión axial es pequeña, habiéndose medido una velocidad de 5.100 m/s para 350 kg/cm<sup>2</sup>. La curva estática de tensión-deformación (fig. 2.4 a) también se vuelve aproximadamente lineal para 175 kg/cm<sup>2</sup>. Así pues, la velocidad

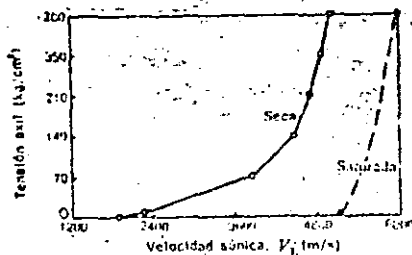


Figura 2.5 Variación de la velocidad sónica con la tensión axial en muestras secas y saturadas de mármol de Taconá

sónica, prácticamente constante por encima de 175 kg/cm<sup>2</sup>, indica probablemente que las discontinuidades de la muestra perpendiculares al eje de carga se han cerrado al alcanzar ese nivel de tensiones. Todos los ensayos con muestras inalteradas de rocas con curvas tensión-deformación de los tipos III, IV y V, muestran que la velocidad sónica depende mucho del nivel de tensión en la parte de estas curvas con concavidad hacia arriba\*. Una vez que la tensión axial alcanza la parte lineal de las mismas, la velocidad sónica tiende a un valor constante.

\* En realidad se trata de una caliza a la que se ha dado comercialmente el nombre de mármol (N. del T.).

La variación de la velocidad sónica con la compresión axial para muestras de mármol de Taconá secas o saturadas se muestra en la figura 2.5. La velocidad sónica en la muestra seca es sensible a cambios en la tensión axial, como se ha comentado anteriormente, mientras que la muestra saturada sufre pequeñas variaciones en la velocidad sónica al variar la tensión axial. Este comportamiento indica que el agua consigue transmitir el impulso a través de las microfisuras con niveles de tensiones bajos; por tanto, la velocidad sónica no es un indicador claro de la presencia de fracturas en muestras saturadas. Debido a que un comportamiento similar, a gran escala, puede preverse en un macizo rocoso natural, la velocidad sísmica no parece resultar adecuada para detectar las discontinuidades existentes en un medio rocoso saturado.

### 2.2.3 Comportamiento bajo cargas combinadas

El estado tensional influye sobre las propiedades de resistencia, rigidez, ductilidad y fluencia de la sustancia rocosa. La figura 2.6 a muestra la variación del desviador de tensiones ( $\sigma_1 - \sigma_3$ ) en función de la deformación axial

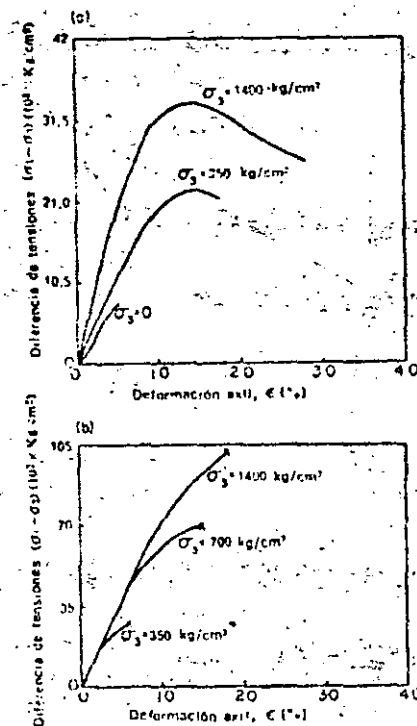


Figura 2.6 Variación de las propiedades tensión-deformación y de la resistencia de (a) arenisca de Ileren y (b) gabra con la presión de confinamiento.

en muestras cilíndricas de arenisca de Berea sometidas a presiones de confinamiento de 350 y 1.400 kg/cm<sup>2</sup> en el ensayo triaxial. El aumento de la presión de confinamiento da lugar a un aumento de la resistencia de pico y residual así como a una mayor deformación para la carga de rotura. Además, las deformaciones anelásticas antes de llegar a rotura aumentan con la presión de confinamiento. En las rocas más blandas, el módulo inicial tangente a la curva tensión-deformación también aumenta con la presión de confinamiento; este comportamiento es evidente en las curvas tensión-deformación que aparecen en la figura 2.6 a correspondientes a la arenisca de Berea.

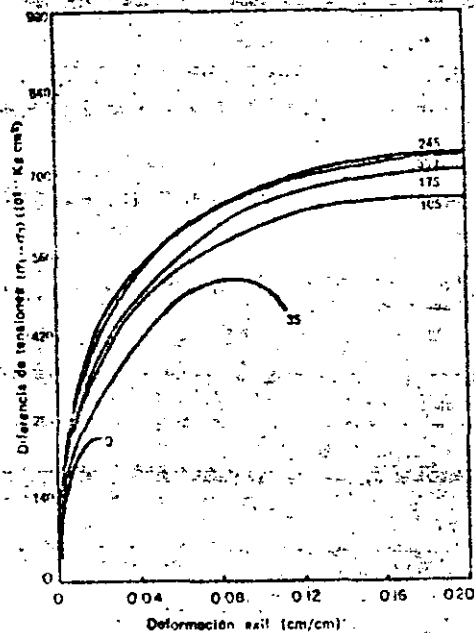


Figura 2.7 Variación de las propiedades tensión-deformación y de resistencia de la sal gema con la presión de confinamiento (indicada en kg/cm<sup>2</sup> en cada curva)

Las rocas muy duras también muestran un aumento de resistencia con la presión de confinamiento, pero frecuentemente los valores de los módulos resultan poco afectados por las variaciones de la misma. La figura 2.6 (b) reproduce los resultados de un ensayo triaxial con un gabbro, donde el aumento de resistencia y las propiedades elásticas iniciales no vienen afectadas por la presión de confinamiento. Debe también advertirse que el aumento de esta presión no produce en el gabbro el grado de deformación anelástica y comportamiento dúctil antes de llegar a rotura que se observa en la arenisca de Berea, más blanda.

En la figura 2.7 se muestran curvas típicas tensión-deformación de los ensayos triaxiales realizados con sal gema por el U. S. Bureau of Reclama-

tion<sup>12</sup>. Puede advertirse que la resistencia a compresión ( $\sigma_1 = \sigma_3$ ) se duplica prácticamente cuando la presión de confinamiento  $\sigma_3$  aumenta de 0 a 35 kg/cm<sup>2</sup>, pero el aumento no es proporcional a la variación de la presión de confinamiento. Con presiones de confinamiento más elevadas (175, 250 y 350 kg/cm<sup>2</sup>) la resistencia sólo aumenta ligeramente. En la sal gema las deformaciones de rotura aumentan mucho con la presión de confinamiento. Para la muestra en compresión de la figura 2.7 la deformación en rotura es del 2% y la curva tensión-deformación indica una rotura frágil. La deformación en rotura con una presión de confinamiento de 35 kg/cm<sup>2</sup> es aproximadamente del 11% y la curva tensión-deformación muestra una rotura más dúctil. Con presiones de confinamiento más elevadas se han observado deformaciones axiales del 20% o mayores, generalmente sin una clara evidencia de rotura.

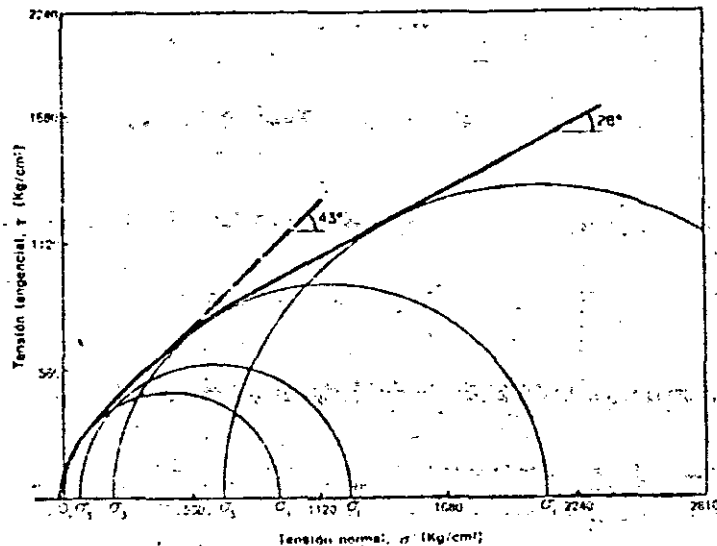


Figura 2.8 Curva de resistencia intrínseca de un gneis esquistoso intacto<sup>12</sup>

Los resultados de los ensayos triaxiales pueden resumirse en un diagrama de Mohr como el que aparece en la figura 2.8<sup>12</sup>. En este diagrama cada ensayo triaxial está representado por un círculo de Mohr, función de las tensiones principales mayor y menor en rotura, ignorándose la influencia de la tensión principal intermedia. Normalmente la rotura se define por el punto del diagrama tensión-deformación (fig. 2.6), donde la diferencia de tensiones es máxima. La curva tangente a la familia de círculos de Mohr correspondientes a ensayos realizados con diferentes presiones de confinamiento es la denominada *curva de resistencia intrínseca* de la roca ensayada. Mediante ensayos realizados con una amplia gama de presiones, suele ser posible aproximar la curva de resistencia intrínseca mediante una línea recta. En este caso, el ángulo que la envolvente forma con el eje de abscisas se denomina ángulo

de rozamiento interno  $\phi$ , y la ordenada en el origen es la llamada cohesión  $c$ . La relación entre las tensiones principales mayor y menor en rotura puede expresarse en función de los parámetros de Mohr-Coulomb por:

$$\sigma_1 = \sigma_3 N_\phi + 2c\sqrt{N_\phi} \quad (2.5)$$

siendo  $N_\phi = (1 + \text{sen } \phi)/(1 - \text{sen } \phi)$ . Los valores representados en la figura 2.8 para un gneis esquistoso tienen la particularidad de que, con tensiones

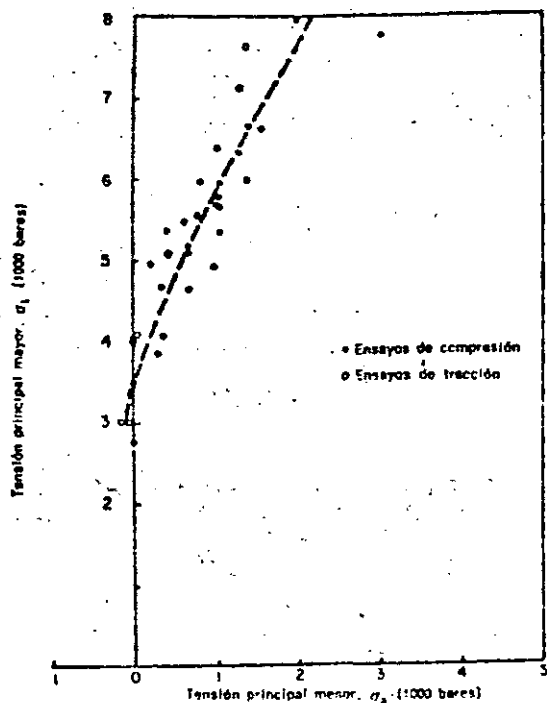


Figura 2.9. Relación entre las tensiones principales máxima y mínima en ensayos de tracción y compresión triaxial en la caliza de Solenhofen<sup>11</sup>

bajas, el ángulo de rozamiento interno es elevado (43°) y la curva de resistencia intrínseca va variando de forma que el ángulo de rozamiento interno disminuye con niveles de tensiones más altos. Debe advertirse que los parámetros de resistencia al corte de Mohr-Coulomb  $c$  y  $\phi$  varían en las rocas con la presión y sólo representan una aproximación de la curva de resistencia intrínseca dentro de una cierta gama de tensiones normales al plano de rotura potencial.

Muchos investigadores también representan los datos de los ensayos triaxiales en función de las tensiones principales mayor y menor en rotura,

como se indica en la figura 2.9 para la caliza de Solenhofen<sup>11</sup>. Aunque en este diagrama no se muestran los valores de la tensión principal intermedia, los puntos correspondientes a ensayos triaxiales de compresión o tracción muestran la misma tendencia, dentro de la dispersión de los datos experimentales. Por tanto, el efecto de la tensión principal intermedia carece aparentemente de importancia, ya que los ensayos triaxiales de compresión o tracción dan valores extremos de la misma ten los ensayos de compresión  $\sigma_3 = \sigma_2$  y en los de tracción  $\sigma_2 = \sigma_1$ . Los datos de resistencia triaxial representados en la forma de la figura 2.9 presentan una pendiente decreciente al aumentar la presión y, para materiales dúctiles como la sal o el mármol tienden

Tabla 2.2 Parámetros típicos de resistencia al corte de rocas intactas

Tipo de roca		$\sigma_c$ (kg/cm <sup>2</sup> )	$c$ , cohesión (kg/cm <sup>2</sup> )	$\phi$ (°)	$N_\phi - K$
Granito	Variación	700-2.800	98-405	51-58	8-17
	Media	1.750	250	55	11
Caliza	Variación	210-2.100	35-350	37-58	4-13
	Media	1.050-1.400	175-232	50	8
Arenisca	Variación	210-2.100	42-420	48-50	6-7
	Media	560-1.400	112-290	48	6

Relación entre las tensiones principales en rotura:

$$\sigma_1 = \sigma_3 N_\phi + 2c\sqrt{N_\phi}$$

$$\sigma_1 = K\sigma_3 + \sigma_c$$

asintóticamente a 45° para presiones elevadas. En general, si se aproxima la curva de resistencia intrínseca por una línea recta, como se indica en la figura 2.9, las tensiones principales en rotura vienen dadas por:

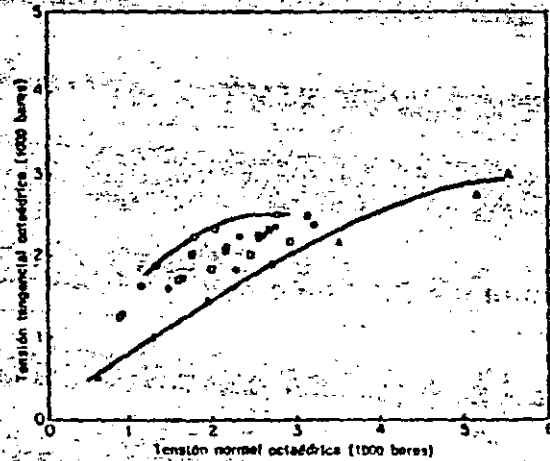
$$\sigma_1 = K\sigma_3 + \sigma_c \quad (2.6)$$

donde  $K$  tiene el mismo valor que  $N_\phi$  y  $\sigma_c$  es la resistencia a compresión simple. En la tabla 2.2 se resumen las propiedades resistentes típicas de diversos tipos de rocas en función de los parámetros de resistencia al corte de Mohr, que son los más empleados en la práctica.

Existe una tendencia entre los investigadores actuales a representar los datos de resistencia en un gráfico que expresa la tensión tangencial octaédrica en función de la tensión normal octaédrica. Este diagrama tiene de común con el de Mohr que la tensión tangencial y la tensión normal octaédricas actúan sobre el mismo plano. Sin embargo, el diagrama presenta la ventaja adicional de considerar el efecto de la tensión intermedia  $\sigma_2$  sobre la curva de resistencia intrínseca. En la figura 2.10 se dan los datos de tracción y compresión triaxial de la caliza de Solenhofen<sup>11</sup> representados de esta manera. Se deduce de este diagrama que la tensión principal intermedia tiene importancia y que la resistencia al corte octaédrica es mayor a compresión que a tracción. Esta conclusión es en cierta forma contradictoria con los mismos datos recogidos en la figura 2.9 que muestra resultados semejantes para los ensayos de tracción y compresión. Un estudio más detallado de los gráficos tensión tangencial-tensión normal octaédricas ha revelado que, incluso aunque la resistencia del



materiales fuera totalmente independiente de la tensión principal intermedia, la curva de resistencia intrínseca en compresión triaxial estaría por encima de la correspondiente a la tracción triaxial. Por tanto, las posiciones relativas de



- |                                |                          |
|--------------------------------|--------------------------|
| Ensayos de compresión          | Ensayos de tracción      |
| ○ Bloque 5                     | ▲ Bloque 5               |
| ⊗ Bloque 1, 2, 4               | ▲ Bloque 3 (Heard, 1960) |
| ● Bloque 3 (Heard, 1960)       |                          |
| ● Bloque 6 (Robertson, 1965)   |                          |
| □ Bloque 7 (Serdengecti, 1961) |                          |

$$\gamma_{oct} = \sqrt{(\sigma_1 - \sigma_2)}$$

$$\sigma_{oct} = \frac{1}{3}(\sigma_1 + \sigma_2 + 3\sigma_3)$$

$$\gamma_{oct} = \sqrt{(\sigma_1 - \sigma_2)}$$

$$\sigma_{oct} = \frac{1}{3}(3\sigma_3 - (\sigma_1 - \sigma_2))$$

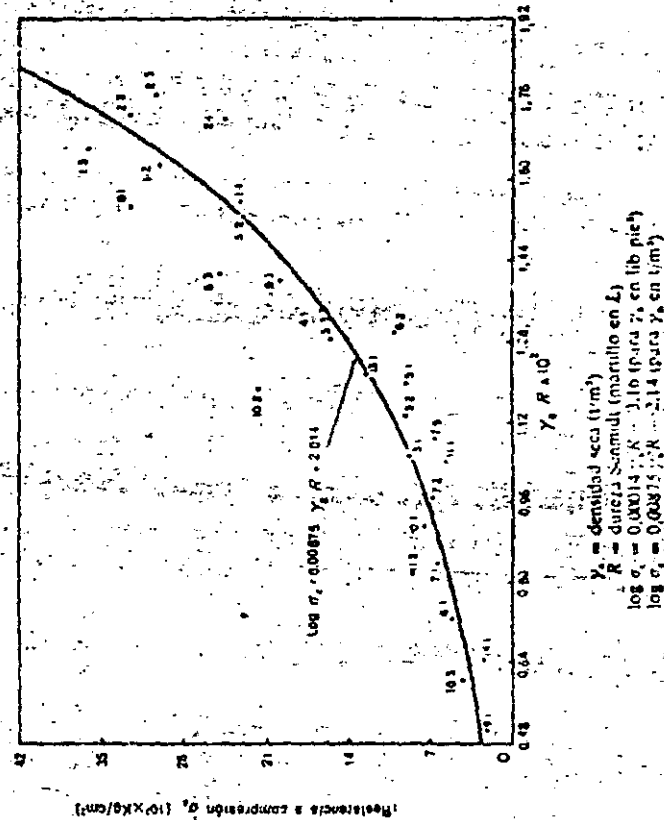
Figura 2.10 Relación entre las tensiones octaédricas normal y tangencial para la caliza de Solenhöfen en ensayos de tracción y compresión triaxial\*

los puntos de tracción o compresión en la figura 2.10 son función del método de representación y no puede deducirse la influencia de  $\sigma_3$  a partir de este diagrama.\*

### 2.2.4 Dureza

Diversos estudios han mostrado que la dureza de las rocas medida por el ensayo de indentación de Rockwell, el esclerómetro Shore o el aparato de impacto de Schmidt (energía del martillo en  $L = 0,74 \text{ m} \cdot \text{kg}$ ) está relacionada con la resistencia a compresión simple y el módulo de elasticidad (módulo tangente para el 50% de la resistencia a compresión) para un gran número de rocas.<sup>4,16</sup> La resistencia a compresión simple y el módulo de elasticidad se

\* El significado físico del término tensión octaédrica se puede interpretar más fácilmente mediante el empleo de los invariantes de tensiones. La tensión tangencial octaédrica es proporcional al segundo invariante y la tensión normal octaédrica es proporcional al primer invariante. Ambos términos se emplean ampliamente en la literatura (N. de E.).



$\gamma_o$  = densidad seca ( $\text{t/m}^3$ )

$R$  = dureza Schmidt (martillo en L)

$\log \sigma_o = 0,0015 \cdot R - 3,16$  (para  $\gamma_o$  en  $\text{lib/pie}^2$ )

$\log \sigma_o = 0,0015 \cdot R - 2,14$  (para  $\gamma_o$  en  $\text{t/m}^2$ )

Figura 2.11 Relación entre los valores medios de  $\gamma_o R$  y la resistencia a compresión simple

relacionan mejor con el producto de la dureza (valor Shore o Schmidt) por la densidad seca de la roca. La figura 2.11 muestra una correlación de este tipo determinada por Miller<sup>4</sup>. Se puede utilizar esta combinación de dureza y densidad seca para prever la resistencia a compresión simple o el módulo de elasticidad de un material, con un intervalo de confianza del 75%. Esto se ilustra en la figura 2.12 que es un ábaco para determinar la resistencia a com-

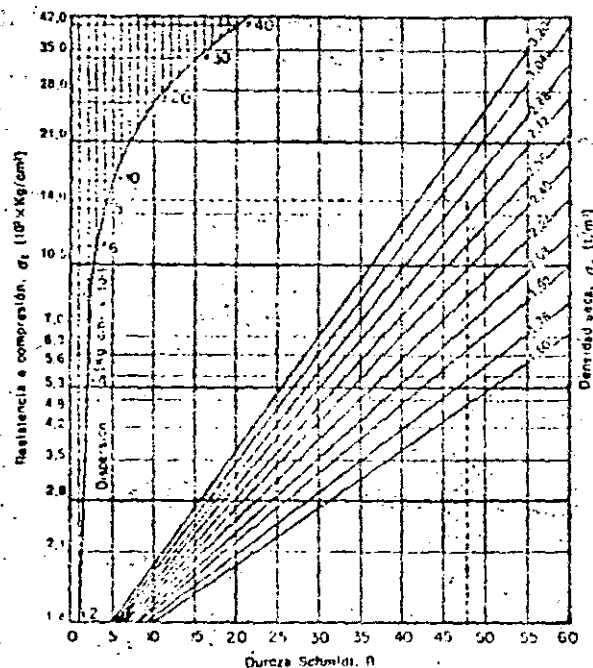


Figura 2.12 Diagrama de clasificación de las rocas basado en la dureza Schmidt<sup>4</sup>

Martillo L, de caída vertical

Límites de dispersión correspondientes a un intervalo de confianza del 75%

presión simple a partir de la dureza Schmidt y la densidad seca. Las líneas de trazos muestran que, para un gneis de Dworshak con una dureza Schmidt  $R = 48$  y una densidad seca  $\gamma_s = 2.80 \text{ t/m}^3$ , puede preverse una resistencia a compresión simple de  $1.510 \text{ kg/cm}^2$ . La resistencia realmente medida fue de  $1.650 \text{ kg/cm}^2$ .

Pueden ser necesarias otras medidas de dureza para estudiar las operaciones de ingeniería y construcción referentes a la perforación, excavación mecánica de túneles, etc. Los ensayos «microbit» y de abrasión propuestos por Miller<sup>4</sup> han resultado bastante útiles a este fin.

### 2.2.5 Fluencia de la sal gema bajo cargas combinadas

La fluencia de las rocas constituye un tema que aún requiere considerable investigación. Algunas rocas, como los gabros, granitos, etc., muestran una deformación casi independiente del tiempo incluso sometidas a compresión simple. En otras rocas las deformaciones de fluencia pueden superar en mucho a las deformaciones elásticas instantáneas. Un ejemplo límite de cierto significado práctico es el de las excavaciones en sal gema y otras evaporitas.

Con objeto de estimar la magnitud y velocidad de cierre de las cavidades previstas en depósitos salinos es necesario determinar las propiedades de fluencia del material. Suponiendo un estado hidrostático de tensiones en la roca salina a profundidad, la distribución de tensiones en torno a una cavidad esférica es tal que la tensión radial es la tensión principal menor, si tanto la tensión principal intermedia como la máxima son iguales a la tensión orientada tangencialmente a la cavidad. Los movimientos radiales en función del tiempo dependen, por tanto, de las características de fluencia de la sal gema en tracción triaxial, es decir ensayos donde  $\sigma_1 = \sigma_2 = \sigma_3$ . Así pues, las características de fluencia bajo carga combinada son más interesantes para el proyecto que los ensayos de fluencia monoaxial que se suelen realizar en diversos materiales.

En la figura 2.13 se dan los resultados de cinco ensayos de fluencia realizados por tracción triaxial<sup>18</sup>. En cada curva se ha indicado el desviador ( $\sigma_1 - \sigma_2$ ) con el que se ha realizado cada ensayo. La tabla 2.3 da los valores de las tensiones principales máxima y mínima, así como la temperatura ambiente en todos los ensayos. En las curvas de la figura 2.13 pueden verse las distintas partes de la curva clásica de fluencia: la parte elástica instantánea, la parte curva que representa la fluencia transitoria, la parte recta que indica la fluencia permanente, y la fluencia acelerada hasta rotura (sólo para desviadores de 264 y 220  $\text{kg/cm}^2$ ); las muestras sometidas a desviadores de 264 y 220  $\text{kg/cm}^2$  se rompieron 29 y 214 horas después de aplicar la carga. Las muestras sometidas a desviadores más pequeños mostraron una velocidad de

Tabla 2.3 Ensayos de fluencia en sal gema

Muestra	$(\sigma_1 - \sigma_2) (\text{kg/cm}^2)$	$\sigma_1 (\text{kg/cm}^2)$	$\sigma_2 (\text{kg/cm}^2)$	Temperatura (°C)
Ensayos de tracción triaxial				
1	70	140	70	23
2	105	175	70	23
3	175	210	35	23
4	220	240	20	23
5	263	270	7	23
Ensayos de compresión simple				
1	34	34	0	23
2	53	53	0	65
3	123	123	0	23
4	123	123	0	65
5	158	158	0	23
6	158	158	0	65
7	210	210	0	23
8	210	210	0	65

15

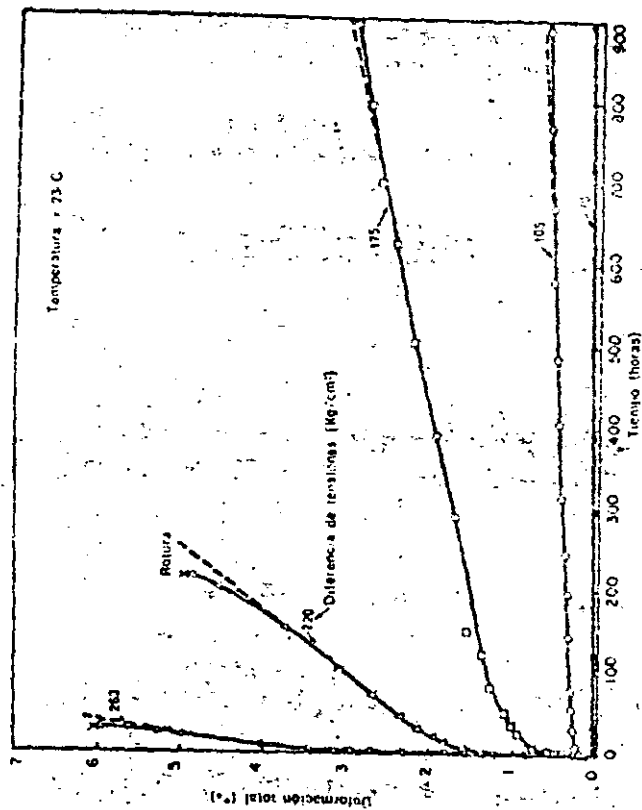


Figura 2.13 Curvas de fluencia en tracción triaxial de la sal gema \*\*

fluencia decreciente por encima de la fase de deformación permanente, indicando la aproximación a un estado de equilibrio. La velocidad de fluencia permanente fue mayor para las muestras cargadas con mayores diferencias de tensiones.

En la figura 2.14 se muestran las curvas de fluencia de 8 ensayos de compresión simple. Los símbolos en blanco representan ensayos realizados a 23 °C y los negros a 65 °C. Si se comparan las dos muestras cargadas a 123 kg/cm<sup>2</sup> se ve que, para la temperatura más alta, la deformación total es aproximadamente

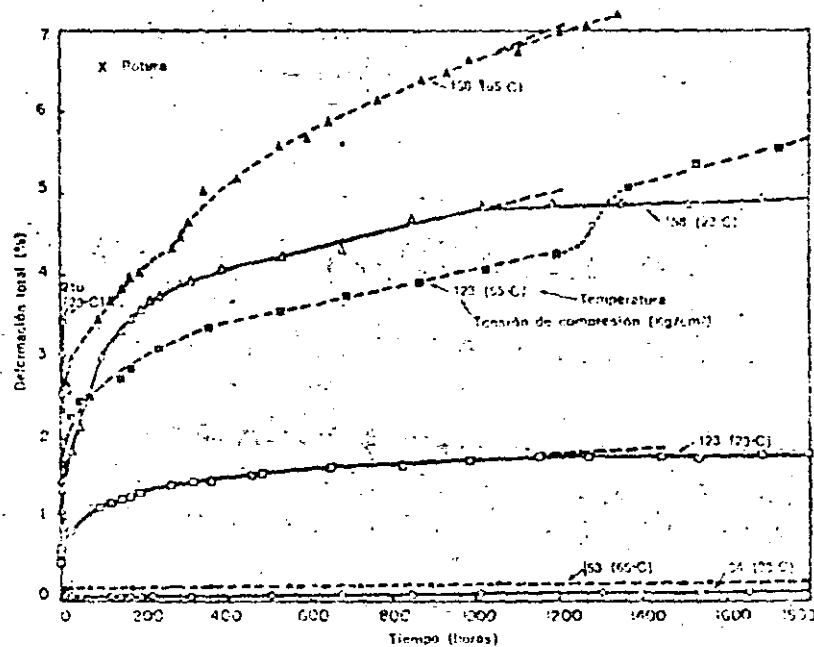


Figura 2.14 Curvas de fluencia en compresión simple de la sal gema \*\*

doble a la del ensayo a 23 °C y la velocidad de fluencia permanente es también mayor. Es evidente una tendencia similar, aunque en menor grado, para los ensayos realizados a 158 kg/cm<sup>2</sup>.

Se comparan en la figura 2.15 las velocidades de fluencia permanente en ensayos de tracción simple y triaxial. Hasta una diferencia de tensiones de 162 kg/cm<sup>2</sup> existe poca diferencia en las velocidades de fluencia y por debajo de 70 kg/cm<sup>2</sup> la velocidad de fluencia es despreciable en ambos ensayos. Por encima de 162 kg/cm<sup>2</sup> existe una considerable divergencia en los resultados. La curva de tracción triaxial muestra una velocidad de fluencia gradual creciente hasta 183 kg/cm<sup>2</sup>, continuando con un rápido incremento hasta y por encima de los 210 kg/cm<sup>2</sup>. Las curvas de compresión simple (a 23 y 65 °C) se confluyen en una y tienden asintóticamente al valor de 210 kg/cm<sup>2</sup>.

Estos resultados muestran que las velocidades de fluencia en tracción triaxial son menores que las de compresión simple para la misma diferencia de tensiones. Por esta razón, el ensayo de fluencia por tracción simple es demasiado riguroso para su empleo en la previsión de los corrimientos de fluencia en cavidades subterráneas. La mejor ecuación para describir la deformación en los ensayos de fluencia por tracción triaxial es:

$$\epsilon_a = K\sigma^n t^m \quad (2.7)$$

donde  $\epsilon_a$  es la deformación axial de una probeta cilíndrica,  $\sigma$  es la diferencia de tensiones en  $\text{kg/cm}^2$ ,  $t$  es el tiempo en horas y  $K, m, n$  son constantes. Para la

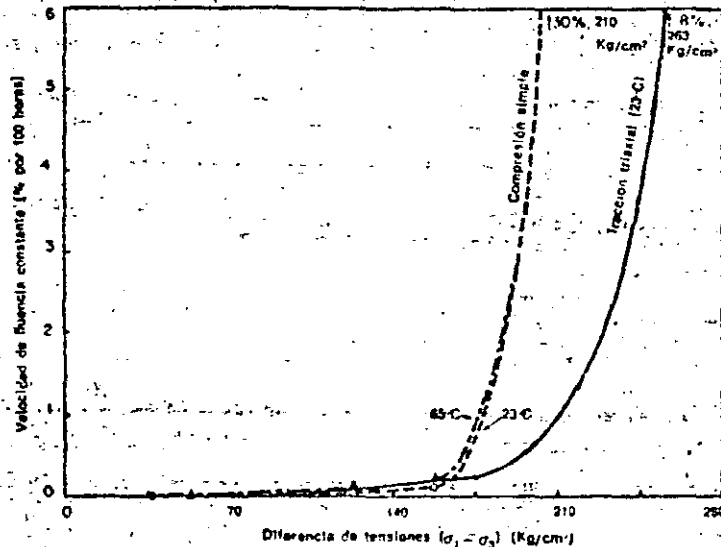


Figura 2.15 Velocidad de fluencia en función de la tensión para sal gema 1\*

sal gema aquí ensayada se encontró un valor de  $K$  de  $1,87 \times 10^{-13}$ ;  $m$ , 0,36 y  $n$ , 2,98. La Ec. (2.7) puede emplearse para calcular las deformaciones de fluencia en cavidades subterráneas si  $\epsilon_a$  se toma igual a la deformación radial  $\epsilon_r$ .

## 2.3 Propiedades mecánicas de las rocas «in situ»

### 2.3.1 Módulo de deformación

Las variaciones de tensión impuestas por la construcción de obras de ingeniería hace que se deforme un volumen de roca relativamente grande. La frecuencia y naturaleza de las discontinuidades geológicas dentro de la zona

\* Para  $\sigma$  expresada en lib/pulg<sup>2</sup> el valor de  $K$  es de  $5,6 \times 10^{-13}$  (N. del T.).

afectada constituyen factores importantes que determinan en gran parte la comprensibilidad del macizo rocoso. El único método que puede emplearse para conseguir una estimación razonable del efecto de estas discontinuidades —así como del valor numérico del módulo de deformación— es un ensayo de carga a escala real. La zona cargada debe ser suficientemente grande para abarcar un volumen de roca que contenga discontinuidades suficientes para ser representativo del macizo rocoso. Los ensayos de carga con placa y los de presión en galerías se emplean para medir el módulo de deformación *in situ*. Estos ensayos se describen con detalle en el capítulo 5.

Los resultados de los ensayos de carga con placa y de presión en galería muestran que el módulo del macizo rocoso es siempre inferior al módulo estático determinado a partir de testigos de roca. El módulo de elasticidad de los testigos inalterados, sin embargo, proporciona un límite superior del módulo del macizo en el caso en que las diaclasas estén muy separadas y muy cerradas. Al aumentar el grado de diaclasado de la roca, el módulo de deformación del macizo se reduce a una pequeña fracción del módulo de elasticidad determinado a partir de muestras en laboratorio.

### 2.3.2 Factor de reducción del módulo determinado a partir de testigos en laboratorio

Los ensayos de laboratorio sobre muestras inalteradas tomadas en la proximidad de ensayos de carga o de cámaras de presión permiten al ingeniero calcular la relación entre el módulo de deformación medido en el terreno y el determinado en laboratorio con muestras inalteradas. Esta relación es el *factor de reducción* que expresa la magnitud en que disminuye el módulo del macizo respecto al de la sustancia rocosa debido a la frecuencia y abertura de las diaclasas (calidad del macizo rocoso). Si se calcula este factor de reducción a partir de ensayos a escala natural realizados en varios puntos de una zona determinada donde la calidad del macizo sea diferente, el ingeniero puede conocer la forma en que el factor de reducción varía con la calidad de la roca. Aplicando esta interpretación podrá estimarse el módulo de deformación en otros puntos de la zona a partir del conocimiento de las propiedades de muestras inalteradas, valorando la calidad del macizo rocoso. Este método puede ser muy útil cuando el número de ensayos *in situ* está muy limitado por razones económicas.

El paso más difícil en la aplicación de este método es el establecimiento de una medida cuantitativa de la «calidad del macizo rocoso» de forma que dos ingenieros al juzgar un mismo emplazamiento obtengan el mismo valor. Los métodos más prometedores para describir cuantitativamente este concepto son el índice de calidad (RQD) y la velocidad relativa, comentados en el capítulo 1.

### 2.3.3 Factor de reducción del módulo por métodos sísmicos

La velocidad sísmica se suele emplear para estimar el módulo del macizo rocoso *in situ*. La ventaja principal del método sísmico es que la medida se hace en el lugar requerido, estando afectado el impulso sísmico, en cierta extensión, por el número y características de las discontinuidades existentes. Así pues, una roca muy fracturada o meteorizada presentará una velocidad inferior a la de una roca sana. Sin embargo, el módulo calculado directamente

a partir de esta velocidad,  $E_{1a}$ , es siempre superior al módulo de deformación estático determinado por ensayos de placa o en cámara de presión ya que el impulso sísmico es de muy corta duración y, lo que es más importante, con un nivel de tensiones muy bajo, de forma que el fenómeno observado es totalmente elástico. La relación entre el módulo de deformación estático y el módulo sísmico suele descender normalmente cuando baja la calidad del macizo rocoso. Más adelante daremos una correlación entre ambas magnitudes, o factor de reducción, con una valoración numérica de la calidad de la roca de acuerdo con el RQD o la velocidad relativa (Cap. 1).

### 2.3.4. Empleo de los índices de calidad en un estudio determinado

Se ha hecho una comparación entre el índice de calidad (RQD) y el módulo de deformación con placa a partir de datos correspondientes a la presa de Dworshak. Esta está situada en un gneis granítico de elevada resistencia y calidad en las proximidades de Orofino, Idaho. El RQD permitió explicar las variaciones obtenidas en el módulo de deformación con los ensayos de placa y sirvió para estimar el módulo de deformación de la cimentación de la presa.

Se realizaron un total de 24 ensayos de placa en posición vertical u horizontal en galerías sin revestir abiertas en los estratos rocosos, bajo la dirección de Shannon y Wilson<sup>18</sup> del Corps of Engineers. Los ensayos se hicieron utilizando gatos Freyssinet de 34 pulgadas de diámetro para transmitir una presión uniforme a la superficie rocosa. Se registraron tanto las deflexiones superficiales como las de extensómetros enterrados a profundidades de 0,30-0,60 y 5,40 m bajo la superficie. Se empleó la teoría elástica para determinar el módulo de deformación a partir de las curvas presión-asiento correspondientes tanto a los medidores superficiales como a los enterrados. Se sacó un testigo de diámetro NX a una profundidad de 6 m en el punto de emplazamiento de cada ensayo. Se realizaron ensayos de compresión simple con muestras intactas tomadas del testigo, valorando la calidad de la roca en función del RQD. Las fracturas próximas a la superficie estaban mucho más cargadas y tenían un efecto mucho mayor sobre la deformación de la placa que las fracturas más profundas. Por tanto, con objeto de comparar el índice de calidad de la roca (RQD) con el correspondiente módulo de deformación del ensayo de placa fue necesario ponderar los valores RQD de acuerdo con la teoría de distribución de tensiones de Boussinesq bajo las placas. Los detalles del método se han descrito en la referencia 18.

En la figura 2.16 se han representado los módulos de deformación en función de los índices de calidad determinados en los puntos de ensayo con placa. Los módulos de deformación están referidos al módulo estático obtenido en laboratorio con las muestras extraídas en cada punto de ensayo. Las variaciones en la relación de módulos,  $E_1/E_{1a}$ , eran por tanto función de las discontinuidades del macizo rocoso y no dependían de las propiedades determinadas en las muestras intactas. (El módulo de las muestras,  $E_{1a}$ , era aproximadamente de  $6,3 \times 10^9$  kg/cm<sup>2</sup> y no variaba mucho de un punto a otro del lugar.)

Se deduce de la figura 2.16 que el módulo de deformación determinado a partir de las células enterradas era considerablemente superior al obtenido con las superficiales. La mayoría de los extensómetros enterrados tenían un índice de calidad (RQD) superior al 80% y una relación de módulos de deformación mayor de 0,50, mientras que la mayor parte de los medidores

superficiales tenían un índice de calidad inferior al 80% y una relación de módulos menor de 0,60.

Aunque el gneis granítico de Dworshak era de excelente calidad, se apreciaban las amplias variaciones que se producen en la determinación del módulo de deformación a partir de ensayos con placa. Hubiera sido bastante difícil estimar un módulo de deformación para la cimentación de la presa únicamente a partir de los resultados de estos ensayos, sin tener en cuenta el carácter de la roca y el sistema de fracturas en el lugar de ensayo. Los medidores superficiales resultaron muy influenciados por las fracturas próximas a la superficie, originadas por la excavación de las galerías. Por tanto, el módulo determinado a partir de estas células probablemente hubiera dado valores demasiado

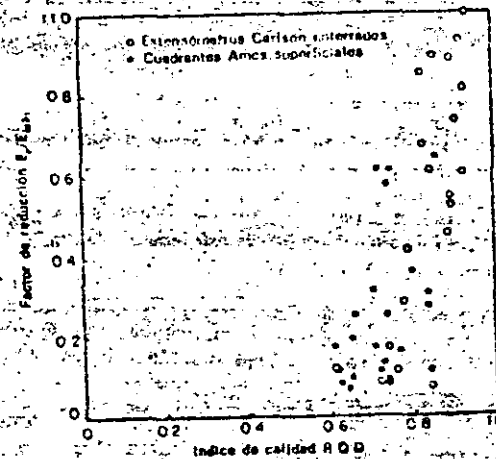


Figura 2.16 Variación del factor de reducción con la calidad de la roca en ensayos de carga con placa, presa de Dworshak<sup>18</sup>

bajos para aplicarlos a la cimentación de una presa que tenía una calidad general muy superior. La mejor estimación del módulo de la cimentación fue la obtenida a partir de los extensómetros enterrados. Los índices de calidad determinados a partir de ellos se correspondían de manera más adecuada con la calidad general de la cimentación. Entrando en el gráfico de la figura 2.16 con el RQD medio determinado a partir de los sondeos de reconocimiento realizados en el terreno de cimentación de la presa, puede obtenerse una estimación del módulo de deformación general de la cimentación.

### 2.3.5. Generalización de los resultados de los ensayos de deformación

Una interpretación general de los resultados de los ensayos utilizados para la determinación del módulo de deformación, que pueda emplearse eventualmente para relacionar los resultados obtenidos en diferentes lugares, requeriría el proceso descrito u continuación. Primeramente, deberían realizarse ensayos con placas o en cámaras de presión para determinar el módulo de deformación del macizo rocoso. En segundo lugar, habría que realizar

ensayos sísmicos en las proximidades de los ensayos anteriores. Por último, convendría realizar sondeos directamente bajo la superficie cargada, de forma que se pudieran realizar ensayos de laboratorio para determinar el módulo estático y la velocidad sísmica en muestras inalteradas. Una cuarta condición es la valoración cualitativa de la calidad de la roca RQD en la zona estudiada.

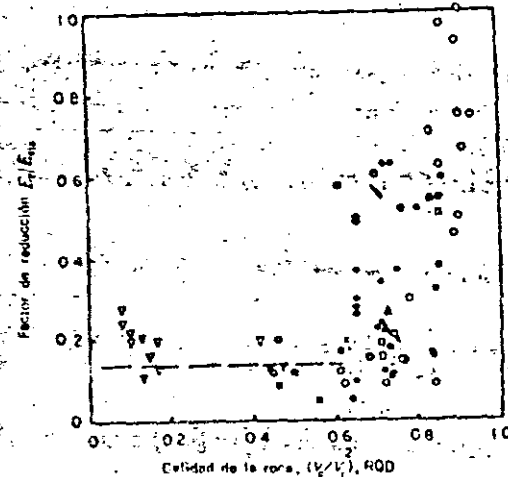
La disponibilidad de la anterior información en un emplazamiento determinado permite calcular la relación entre el módulo de deformación observado,  $E_s$ , y el módulo sísmico,  $E_{sm}$ , o el módulo de laboratorio sobre muestras inalteradas,  $E_L$ . Además, estas relaciones o factores de reducción pueden relacionarse con la variación de calidad de la roca. Se cree que gran parte de la variación y dispersión de los datos publicados en la literatura podría explicarse o definir una tendencia consistente si se hubiera investigado la calidad de la roca en cada punto de ensayo. Esta hipótesis viene confirmada por los ensayos de la presa de Dworshak que mostraron una gran variación en los valores medidos del módulo de deformación. Sin embargo, se consiguió definir la tendencia de estos resultados al considerar la calidad de la roca (fig. 2.16).

Si los factores de reducción  $E_s/E_{sm}$  y  $E_s/E_L$  son principalmente función de la calidad de la roca, se deduce la posibilidad de establecer una relación entre el factor de reducción y la calidad de la roca a partir de datos obtenidos en diferentes lugares o en una localidad determinada (fig. 2.16). Se han recogido datos descritos en la literatura sobre ensayos de carga con placa y en galería de presión para diferentes casos que satisficieron, en distinto grado, las cuatro condiciones antes expuestas. Un resumen de estos datos de ensayo aparece en la figura 2.17; el nombre de la obra y el lugar de publicación de los datos se indican en la misma figura. La ordenada es la relación entre el módulo de deformación obtenido en ensayos de carga con placa o en galerías de presión,  $E_s$ , y el módulo calculado por métodos sísmicos,  $E_{sm}$ . La abscisa es una medida de la calidad de la roca, expresada bien en función del RQD o del cuadrado de la velocidad relativa  $(V_s/V_p)^2$ . Los datos recogidos en esta figura muestran una tendencia bastante clara respecto al factor de reducción ( $E_s/E_{sm}$ ) bajando muy bruscamente cuando la calidad de la roca desciende del 100 al 65%. Un mayor descenso en la calidad de la roca no viene acompañado por una mayor reducción en la relación de módulos. Los datos correspondientes a una calidad inferior al 65% sugieren que el factor de reducción apropiado debe estar comprendido entre 0,1 y 0,2. En general, la interpretación de los datos sobre módulos de deformación en la forma indicada en la figura 2.17 constituye un método muy prometedor para combinar datos de diferentes lugares y de diferentes puntos en un mismo emplazamiento. Sin embargo, se requieren más datos para corroborar la tendencia apreciada en dicha figura.

### 2.3.6. Resistencia al corte

El sistema de diaclasas, zonas milonitizadas y fallas de un macizo rocoso reduce la resistencia al corte efectiva a un valor muy inferior al de la sustancia rocosa, al menos en direcciones paralelas a esas discontinuidades. La resistencia al corte de una roca *in situ* resulta por tanto muy anisótropa. Cuando las direcciones de carga son tales que las superficies potenciales de rotura deben atravesar las fracturas estructurales, la resistencia al corte será próxima a la de la sustancia rocosa. Cuando la dirección de carga sea paralela o subparalela a las singularidades estructurales, la resistencia al corte vendrá regida por la superficie de discontinuidad, siendo en general mucho menor.

Este último caso es el más crítico y es el que ha dado lugar a los roturas de Malpasset, Vaiont, Madison Canyon y otros lugares. Se está de acuerdo en general en que tal sollicitación es crítica, por lo que en los últimos años se ha dedicado un gran trabajo de investigación a las variables que rigen la resistencia al corte según las discontinuidades.



- Presa de Dworshak, ensayo de presión en galería (F), extensómetros enterrados<sup>11</sup>
- ◻ Presa de Dworshak, ensayo de presión en galería (F), extensómetros superficiales<sup>11</sup>
- ◼ Presa de Dworshak, ensayo de presión en galería (F), extensómetros enterrados<sup>11,12</sup>
- Presa de Dworshak, ensayo de presión en galería (F), extensómetros superficiales<sup>11</sup>
- Presa de Dworshak, ensayos de placa, extensómetros enterrados<sup>11</sup>
- ◻ Presa de Latiyan, Irán<sup>14</sup>
- ▲ Presa de Kariba, núcleo hiperamente meteorizado<sup>15</sup>
- ◻ Presa de Kariba, cuarcita muy diaclasada<sup>15</sup>
- × Zona de ensayos en Nevada, pórfido dacítico<sup>16</sup>
- Presa de Morrow Point<sup>17,18</sup>
- Presa de Amungweva<sup>19</sup>
- Río Agri, Italia<sup>20</sup>
- Presa de Koshiyū, ensayos de placa
- Presa de Koshiyū, ensayo de presión en galería
- El Novillo, México<sup>21</sup>
- Onidetu<sup>22</sup>
- ◻ Presa de Vaiont, Italia, talud superior, ensayo de presión en galería<sup>23,24</sup>

Figura 2.17 - Variación del factor de reducción con la calidad de la roca<sup>11</sup>

Observaciones de campo han mostrado que algunas características geológicas, como las zonas milonitizadas, las fallas y las vetas de material milonitizado, se han formado por desplazamientos tangenciales. Las irregularidades superficiales de la fractura o fracturas se han reducido en cierta extensión por efecto de los continuos desplazamientos. Cuanto mayor ha sido el desplazamiento inicial, más regular ha quedado la superficie y por tanto, menor será la resistencia al corte. Otros tipos de discontinuidades geológicas se han for-

mado por roturas de tracción. En tales casos, la superficie de rotura puede ser bastante irregular, ya que no se han producido desplazamientos tangenciales desde la formación de la fractura.

La figura 2.18 ilustra el primer caso donde la discontinuidad se debe a rotura por corte. En este proceso, la resistencia al corte a lo largo de la discontinuidad potencial alcanza un máximo para un pequeño desplazamiento, en el que

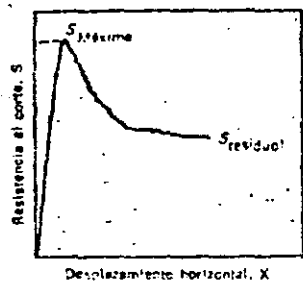


Figura 2.18 Resistencia al corte en función del desplazamiento (valores máximo y residual) <sup>19</sup>

se produce la fractura. La resistencia al corte disminuye gradualmente al continuar el desplazamiento. Por último, con grandes desplazamientos la resistencia al corte tiende asintóticamente a un valor mínimo que corresponde a la resistencia residual <sup>20-21</sup>.

En la figura 2.19 se muestran dos curvas de resistencia intrínseca trazadas a través de los valores máximo y mínimo de la resistencia al corte obtenida en muestras de roca bajo diferente carga normal  $N$ . La distancia vertical entre las dos curvas muestra la reducción de resistencia al corte bajo un desplazamiento continuo. Adviértase que la línea de resistencia residual no indica la existencia de cohesión y queda definida únicamente por el ángulo de resistencia residual al deslizamiento  $\phi_r$ . Así pues, la resistencia al corte según una discontinuidad, para un valor dado de la carga normal, depende de la magnitud de

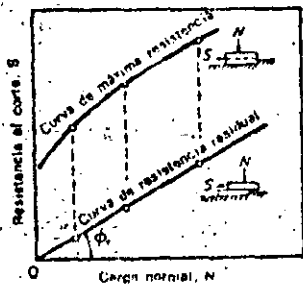


Figura 2.19 Curvas de resistencia intrínseca máxima y residual para muestras intactas <sup>19</sup>

los desplazamientos relativos previos que se hayan producido entre las superficies rócicas.

El mecanismo de la resistencia al corte según superficies irregulares ha sido explicado por ensayos analógicos realizados por Patton <sup>22,23</sup>. Este autor llevó a cabo ensayos de corte directo según planos horizontales, con muestras de yeso conteniendo un cierto número de «dientes» irregulares, como se indica en la figura 2.20. Se ensayaron muestras idénticas con diferentes cargas normales, pudiendo obtenerse una curva de resistencia intrínseca máxima OAB a través de los puntos de máxima resistencia al corte. Continuando los desplazamientos después de la rotura inicial y registrando para cada muestra

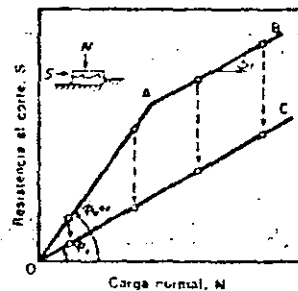


Figura 2.20 Curvas de resistencia intrínseca con superficies dentadas <sup>19</sup>

la resistencia al corte residual, se pudo dibujar la curva de resistencia intrínseca residual, línea OC, correspondiente a estos resultados. La línea OA se obtuvo para cargas normales bajas y se puede expresar por:

$$S = N \operatorname{tg}(\phi_o + i), \quad (2.8)$$

donde  $S$  es el ángulo que forman los dientes con la superficie de deslizamiento y  $\phi_o$  es el ángulo de rozamiento por deslizamiento de una superficie plana sin pulir de yeso intacto. A efectos prácticos,  $\phi_o$  es aproximadamente igual a  $\phi_r$ . Las roturas por corte correspondientes a la línea OA venían acompañadas por desplazamientos normales a la dirección de la fuerza tangencial. La línea AB se obtuvo con cargas normales mayores a las del caso en que la rotura se produjo por la base de los dientes, sin movimientos verticales de dilatación.

La distancia vertical entre las líneas OAB y OC indica la pérdida de resistencia al corte por desplazamiento. Puede verse que, aunque no haya cohesión, existe una contribución real de la resistencia «cohesiva» interna de los dientes para cualquier carga normal distinta de cero. Esta contribución alcanza un valor máximo cuando los dientes se rompen por su base y se mantiene constante para cargas normales elevadas. Para la curva OA, la cohesión movilizada es directamente proporcional a la carga normal. Para la curva AB, la cohesión es independiente de la carga normal. Las curvas de resistencia intrínseca máxima con dos pendientes diferentes, como OAB, pueden explicarse por dos modos de rotura diferentes.

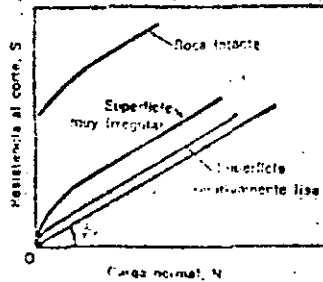


Figura 2.21 Posibles curvas de resistencia intrínseca de macizos rocosos<sup>18</sup>

La figura 2.21 muestra los tipos de curvas de resistencia intrínseca que pueden esperarse en macizos rocosos con la misma mineralogía y resistencia que la sustancia rocosa. La distancia vertical entre la curva de resistencia residual y la de resistencia máxima indica la resistencia correspondiente a las irregularidades naturales de la superficie de rotura para una carga normal dada.

La figura 2.22 muestra el diagrama de Mohr correspondiente a las resistencias al corte máximas obtenidas en muestras intactas, testigos de roca diaclasada y muestras serradas de monzonita cuarzosa<sup>22</sup>. Los resultados correspondientes a las superficies serradas muestran un ángulo de rozamiento que no varía dentro de las presiones utilizadas. Este ángulo es probablemente muy próximo a  $\phi_c$  para la monzonita cuarzosa. Con tensiones normales bajas (menores de 210 kg/cm<sup>2</sup>) la curva de resistencia intrínseca máxima para las

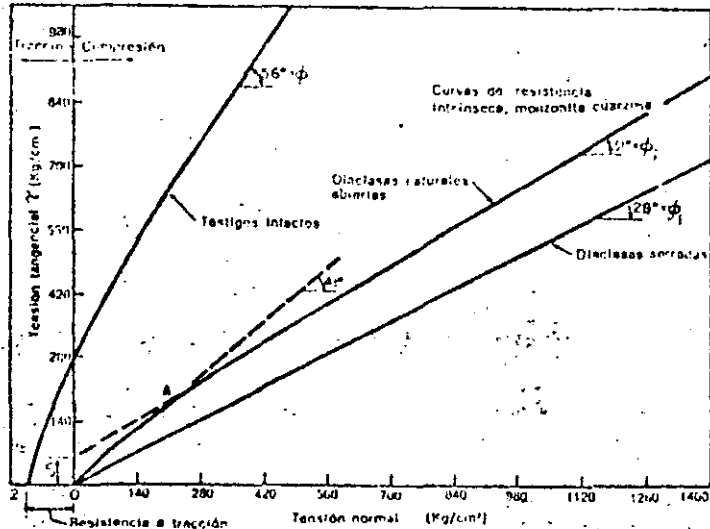


Figura 2.22 Resistencia de muestras intactas y diaclasadas de monzonita cuarzosa<sup>22</sup>

diaclasa naturales viene dada por la línea OA que corresponde a un ángulo de resistencia al corte aparente ( $\phi = \phi_c + i$ ) de 41°; así pues, las irregularidades parecen proporcionar un valor efectivo  $i$  de aproximadamente 13°. Para tensiones normales superiores a 210 kg/cm<sup>2</sup>, cambia la forma de rotura y probablemente algunas de las irregularidades de la superficie de las diaclasas resulten degolladas. El diagrama de resistencia al corte para las diaclasas naturales a partir del punto A puede expresarse en la forma:

$$\tau = c_1 + \sigma \operatorname{tg}(31^\circ), \quad (2.10)$$

donde  $c_1$ ,  $\tau$  y  $\sigma$  tienen los significados indicados en la figura 2.22. Como puede verse, estos ensayos con rocas naturales diaclasadas mostraron casi el mismo comportamiento que los ensayos idealizados de Patton<sup>20</sup>.

Aunque la ecuación

$$\tau = \sigma \operatorname{tg}(\phi_c + i) \quad (2.10)$$

sirve de base para interpretar los resultados de los ensayos de laboratorio o de campo con muestras diaclasadas, la aplicación práctica de este concepto

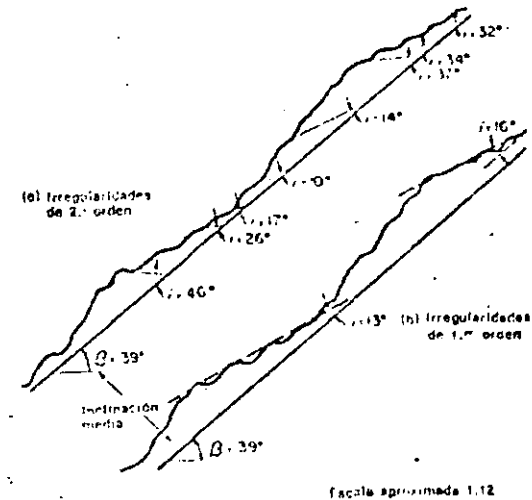


Figura 2.23 Ejemplo de una discontinuidad con irregularidades de 1.º y 2.º orden<sup>18</sup>

se apoya en la estimación *in situ* de  $i$ . La figura 2.23 muestra una superficie típica de diaclasa con valores de  $i$  de 14 a 36°. Puede advertirse que las irregularidades con mayores valores de  $i$  son también las más fácilmente degollables por tener la menor base. Por tanto, estas estrechas irregularidades son las más solicitadas bajo pequeños desplazamientos y, en cuanto algunas se rompen, la carga se transmite a las irregularidades más anchas y menos protuberantes. Por tanto, puede producirse en los taludes rocosos un mecanismo de rotura progresiva. Las medidas *in situ* realizadas por Patton<sup>20</sup> indican que un valor de  $i$  de 10-15° es razonable para la componente de resistencia debida a las irregularidades de las discontinuidades *in situ*.



## Referencias

1. W. F. Brace, «Brittle fracture of rocks», *State of Stress in the Earth's Crust* (Ed. W. R. Judd), Elsevier, Nueva York, 1964.
2. C. Fairhurst, «On the validity of the "Brazilian" test for brittle materials», *Intern. J. Rock Mech. Mining Sci.*, 1, núm. 4, 535-546 (1964).
3. D. R. Reichmuth, «Correlations of force-displacement data with physical properties of rock for percussive drilling systems», *Proc. Symp. Rock Mech., 8th, 1963*, Macmillan, Nueva York, pág. 33.
4. R. P. Miller, «Engineering classification and index properties for intact rock», *Ph. D. Thesis*, Univ. Illinois, 1965.
5. J. R. McWilliams, «The role of microstructure in the physical properties of rock», en *Testing Techniques for Rock Mechanics*, *Am. Soc. Testing Mater., Spec. Tech. Publ.*, 175-189 (1966).
6. L. Oberst y W. I. Duvall, *Rock Mechanics and the Design of Structures in Rock*, Wiley, Nueva York, 1967.
7. S. Seidenguetz y G. D. Boozar, «The effects of strain rate and temperature on the behavior of rocks subjected to triaxial compression», *Proc. Symp. Rock Mech., 4th, Bull. Mineral Ind. Expt. Sta., Penn. State Univ.*, núm. 76 (1961).
8. H. Rösch, «Researches toward a general flexural theory for structural concrete», *J. Am. Concrete Inst.*, 32, núm. 1, 1-28 (1960).
9. R. G. Wegerker, «Influence of stress rate and other factors on strength and elastic properties of rocks», *Quart. Colo. School Mines*, 54, núm. 3, 3 (1959).
10. D. Watson, «Effect of straining rate on the compressive strength and elastic properties of concrete», *J. Am. Concrete Inst.*, 24, núm. 8, 729 (1953).
11. L. Oberst, S. L. Whides y W. I. Duvall, «Standardized tests for determining the physical constants of mine rocks», *U. S. Bur. Mines, Rept. Invest.*, 3821 (1956).
12. U. S. Bur. Reclamation, «Triaxial compression tests of salt rock cores for the U. S. At. Energy Comm.», Project Dribble Concrete and Structural Br., Lab. Rept. núm. C-1043, Denver, Colo., 1962.
13. U. S. Corps Engrs., «Tests for strength characteristics of a schistose gneiss», MRD Lab. núm. 64126, U. S. Army Corps Engrs., Mo. River Div. Lab., Omaha, Nebraska, 1965.
14. J. Handin, H. G. Heard y J. N. Magouirk, «Effects of the intermediate principal stress on the failure of limestone, dolomite, and glass at different temperatures and strain rates», *J. Geophys. Res.*, 72, núm. 2, 611-640 (1967).
15. P. Kraatz, «Rockwell hardness as an index property of rocks», *M. S. Thesis*, Univ. Illinois, 1964.
16. U. S. Army W. E. S., «Project dribble, petrographic examination and physical tests of cores, Tatam Salt Dome, Mississippi», Tech. Rept. núm. 6-614, U. S. Army Waterways Exptl. Sta., Vicksburg, Mississippi, 1963.
17. Shannon y Wilson, Inc., Report on *in situ* rock tests, Dworshak Dam site, for U. S. Army Engineer District, Walla Walla, Corps Engrs., Seattle, Washington, 1964.
18. D. U. Deere, A. J. Hendron, Jr., F. D. Patton y E. J. Cording, «Design of surface and near-surface construction in rock», *Symp. Rock Mech., 8th, Minnesota, 1966* (AIME, 1967).
19. R. G. T. Lane, «Rock foundations: Diagnosis of mechanical properties and treatments», *Intern. Congr. Large Dams, 8th, Edinburgh, 1964*, I, R. 8.
20. W. R. Judd, «Some rock mechanics problems in correlating laboratory results with prototype reactions», *Intern. J. Rock Mech. Mining Sci.*, 2, núm. 2 (1965).
21. U. S. Bur. Reclamation, «Morrow Point Dam and powerplant foundation investigations», *Water Resources Tech. Publ.*, Denver, Colo., 1965.
22. L. O. Rice, «In-situ testing of foundation and abutment rock for dams», *Intern. Congr. Large Dams, 8th, Edinburgh, 1964*, I, R. 5.
23. K. Kawabuchi, «A study of strain characteristics of a rock foundation», *Intern. Congr. Large Dams, 8th, Edinburgh, 1964*, I, R. 11.
24. C. Lotti y M. Beaumont, «Execution and controls of consolidation works carried out in the foundation rock of an arch gravity dam», *Intern. Congr. Large Dams, 8th, Edinburgh, 1964*, I, R. 37.
25. D. U. Deere, comunicación privada.
26. T. F. Onoderá, «Dynamic investigation of foundation rocks *in situ*», *Proc. Symp. Rock Mech., 5th, Minnesota, 1963*, Pergamon, Nueva York, págs. 517-533.
27. H. Link, «Evaluation of elasticity moduli of dam foundation rock determined seismically in comparison of those arrived at statically», *Intern. Congr. Large Dams, 8th, Edinburgh, 1964*, I, R. 45.
28. C. Jaeger, «Rock mechanics for dam foundations», *Intern. Congr. Large Dams, 8th, Edinburgh, 1964, Suppl.*, 3-19.
29. W. C. Mauer, «Shear failure of rock under compression», *Soc. Petrol. Engrs. J.*, 5, núm. 2, 167-176 (1965).
30. F. D. Patton, «Multiple modes of shear failure in rock», *Proc. Intern. Congr. Rock Mech., 1st, Lisbon, 1966*, I, 509-514.
31. F. D. Patton, «Multiple modes of shear failure in rock and related materials», *Ph. D. Thesis*, Univ. Illinois, 1966.
32. U. S. Corps Engrs., «Strengthening of rock against shock effects, Piledriver Project», MRD Lab. núm. 64190, U. S. Army Corps Engrs., Mo. River Div. Lab., Omaha, Nebraska, 1964.

## Consideraciones geológicas\*

D. U. Deere

### 1.1 Introducción

La mecánica de Rocas es la ciencia teórica y aplicada que trata del comportamiento mecánico de las rocas; es la rama de la Mecánica que estudia la reacción de las rocas a los campos de fuerza de su entorno físico [1].

Esta definición, dada recientemente por un grupo de investigadores en Mecánica de Rocas, puede parecer a primera vista que realiza el papel de la mecánica, ignorando el de la geología. En realidad esta definición es de miras muy amplias. La frase «reacción de las rocas a los campos de fuerza de su entorno físico» es suficientemente general para que sea aplicable a problemas a cualquier escala. Por ejemplo, comprende los estudios del mecanismo de deformación de los cristales minerales sometidos a elevadas presiones y temperaturas, el comportamiento triaxial de una muestra de roca ensayada en laboratorio, la estabilidad del revestimiento de un túnel e incluso el mecanismo de los movimientos de la corteza terrestre.

El papel de la geología es evidente; todos los materiales estudiados son masas rocosas situadas en un entorno geológico o extraídas de él. Los materiales poseen ciertas características físicas que son función de su origen y de los procesos geológicos posteriores que han actuado sobre ellos. El conjunto de estos fenómenos en la historia geológica de una cierta zona conduce a una *litología* particular, a una determinada serie de *estructuras geológicas* y a un *estado tensional in situ* característico. Regionalmente se producen variaciones de estas condiciones y pueden también producirse localmente, aun con mayor importancia, dentro del emplazamiento de una obra determinada. Al realizar programas de reconocimiento, y al extrapolar los resultados de ensayo en un punto a las zonas adyacentes, es totalmente necesario considerar la distribución en el lugar de los diferentes elementos geológicos. La experiencia ha demostrado que quien mejor puede realizar este trabajo es un ingeniero-geólogo que no sólo tenga base suficiente en ciencias geológicas para apreciar los detalles de la geología del lugar, sino que también esté bien enterado de los métodos modernos de reconocimiento de las rocas y esté familiarizado con las exigencias de los técnicos en Mecánica de Rocas.

\* De una próxima publicación en dos volúmenes original de Donald U. Deere, títulos provisionalmente, *Engineering Geology* (Geología aplicada a la Ingeniería) y *Rock Mechanics* (Mecánica de las Rocas). Cita reproducida con la autorización de Prentice-Hall, Inc., Englewood Cliffs, New Jersey, E. U. U.

† Definición del Comité de Mecánica de Rocas de la Academia Nacional de Ciencias en «Rock-Mechanics Research», *Natl. Acad. Sci.-Natl. Res. Council*, Washington, D. C., 1966.

En la Mecánica de Rocas aplicada, en especial en los campos de Ingeniería civil y minera, el método de proyecto supone la selección de un anteproyecto y la predicción del comportamiento esperado. Se emplean las ecuaciones de la mecánica teórica y aplicada. Sin embargo, en la mayoría de los casos deben introducirse en las ecuaciones algunas propiedades mecánicas de la roca. La validez de la solución obtenida no es mayor que la validez de la propiedad mecánica empleada. Las propiedades mecánicas de una muestra inalterada ensayada en laboratorio pueden ser muy diferentes de las propiedades de un macizo rocoso del que se ha extraído la muestra. El reconocimiento de este hecho ha motivado en estos últimos años una gran atención hacia los ensayos *in situ*.

El comportamiento de un macizo rocoso sometido a una variación de tensiones viene determinado por las propiedades mecánicas del material rocoso y por el número y naturaleza de las discontinuidades geológicas existente en el mismo. La importancia relativa de cada uno de estos factores sobre el comportamiento de la roca depende principalmente de la relación entre las dimensiones de la obra de ingeniería a realizar y la separación entre las discontinuidades. Cuando la variación introducida en el estado tensional afecta a una zona grande respecto a la distancia entre diaclasas\*, por ejemplo, como es el caso de la cimentación de presas o grandes excavaciones subterráneas la influencia de las diaclasas puede ser muy pronunciada. Sin embargo, en aquellos casos en que la separación entre las mismas es muy grande respecto a las dimensiones de la obra, como en la perforación de un barreno o la construcción de un túnel a través de una roca masiva con una perforación mecánica el comportamiento de la roca depende más de las propiedades inherentes al material rocoso.

En muchos problemas de Mecánica de Rocas aplicada también se requiere conocer el estado tensional a una cierta profundidad en la zona estudiada. Como se señala en una sección posterior de este capítulo, el estado tensional es consecuencia directa de la historia geológica pasada de la zona. Sin embargo, el conocimiento de la historia geológica no basta por sí mismo para permitir una estimación razonable del estado de tensiones.

### 1.2 Importancia de la litología o tipo de roca

La litología de una roca hace referencia a su mineralogía, textura y fábrica. Junto con un nombre o término descriptivo de algún sistema de clasificación reconoce, por ejemplo, caliza oolítica, pizarra bituminosa, granito, clorita, biotita, esquistos, etc. Los nombres y la clasificación son geológicos. Los técnicos en Mecánica de Rocas han reconocido frecuentemente lo inadecuado de un sistema de clasificación de este tipo, advirtiendo al menos que rocas de una misma litología pueden presentar una gama extraordinariamente amplia de propiedades mecánicas. Se ha propuesto incluso abandonar tales nombres geológicos y adoptar un nuevo sistema de clasificación basado únicamente en propiedades mecánicas.

Esta propuesta puede resultar excesiva, ya que hay diversas razones para conservar los términos litológicos. En primer lugar, existe como mínimo

\* Para unificar hechos traduciendo, en todo el texto, *joints* por diaclasas, aunque se establezca diferencias entre éstas, las *litoclasas* y algunos otros tipos de discontinuidad fracturas (*N. del T.*).

razón de  $\frac{1}{2}$  para cualquier tipo de roca donde queda comprendido el valor de una cierta propiedad mecánica. Para algunas propiedades mecánicas y para algunos tipos de rocas este intervalo de variación puede ser desalentadoramente grande; para otras bastante más pequeño. Por ejemplo, la resistencia a compresión simple de una caliza puede variar de 350 a 2.500 kg/cm<sup>2</sup>; sin embargo, para la sal gema la variación es solamente de 200 a 350 kg/cm<sup>2</sup>, aproximadamente. La dureza de una cuarcita será elevada y prácticamente constante; mientras que la de una arenisca será muy baja o muy alta según el tipo y grado de cementación.

Otra razón importante para el empleo del nombre litológico es la relación entre la textura, fábrica y anisotropía estructural de las rocas de un determinado origen. Por ejemplo, la mayoría de las rocas ígneas tienen una estructura densa, bien encajada, con muy pequeñas diferencias de dirección en las propiedades mecánicas (con la excepción, por supuesto, de muchas rocas volcánicas superficiales, rocas intrusivas subsuperficiales, y algunas intrusivas profundas, como los granitos gneíscos, que presentan una estructura foliada en la periferia de la intrusión). Las rocas sedimentarias, como las pizarras arcillosas, las areniscas y algunas calizas, están estratificadas y por tanto muestran una anisotropía considerable en las propiedades mecánicas. Otras rocas sedimentarias, como la sal gema, el yeso y muchas calizas y dolomías, han recrystalizado en una textura compacta, presentando únicamente una ligera anisotropía. Las rocas metamórficas son quizá las más sorprendentes respecto a la anisotropía. La clorita, el talco y el micaquistito tienen superficies de exfoliación bien desarrolladas y se componen de minerales de estructura hojosa que dan lugar a grandes diferencias en la resistencia y el módulo de deformación según la dirección de ensayo. Los gneís \* muestran alguna anisotropía pero en menor grado. La pizarra es también muy anisotropa debido a su pronunciada estratificación. Otras rocas metamórficas, como el mármol y la cuarcita, han recrystalizado en una textura compacta, siendo bastante homogéneas.

Otra razón para conservar el nombre geológico es la asociación que puede hacerse entre ciertos tipos de rocas y otras características *in situ* que pueden presentarse. Por ejemplo, la presencia en el terreno de caliza, yeso y sal gema puede inclinar al investigador a la búsqueda de fenómenos de disolución como cavidades, torres y fisuras apuradas por la disolución. En otro caso, la presencia de una colada de lava basáltica puede indicar la posible presencia de un diaclasado columnar y llamar la atención sobre los problemas con él relacionados. Análogamente, algunos tipos de rocas presentan un comportamiento característico o problemas específicos. La existencia de sal gema u otras evaporitas puede dar lugar a problemas con deformaciones de fluencia. Debido a su contenido de arcilla, las pizarras arcillosas presentan frecuentemente hinchamiento y disgregación al aire por variaciones de presión y humedad. Resulta evidente que se da una información mucho más valiosa sobre las propiedades y el comportamiento de una roca cuando se indica su nombre geológico. Sin embargo, a efectos ingenieriles, el nombre geológico es insuficiente por sí solo y debe acompañarse de una clasificación de tipo mecánico según se indica en la sección siguiente.

\* Aunque últimamente se tiende a escribir *gneis* hemos preferido conservar la grafía tradicional (del T.).

### 1.3 Clasificación de las rocas en ingeniería

Se entiende por roca intacta aquella de la cual pueden tomarse muestras para su ensayo en laboratorio, no presentando características estructurales de gran escala, como diaclasas, planas, de estratificación, fracturas y zonas milonitizadas. Coates<sup>1</sup> ha empleado el término *massive rock*. Coates<sup>1</sup>, Coates y Parsons<sup>2</sup> y Miller<sup>3</sup> han realizado un trabajo acerca de la clasificación de la roca intacta a partir de las propiedades mecánicas determinadas en laboratorio. Deere y Miller<sup>4</sup> han dado una versión modificada del primer trabajo de Miller, siendo esta clasificación la que se describe a continuación.

La clasificación se basa en dos propiedades importantes de la roca: la resistencia a compresión simple y el módulo de elasticidad. El módulo empleado es el módulo tangente correspondiente a un nivel tensional igual a la mitad de la resistencia de la roca. La resistencia a compresión simple se determina con muestras de relación longitud/diámetro igual o superior a 2. La roca se clasifica en una de las cinco categorías de resistencia indicadas en la tabla 1.1.

Tabla 1.1 Clasificación de la roca intacta<sup>1</sup>

I. Basada en la resistencia ( $\sigma_c$ )		
Clase	Descripción	Resistencia a compresión simple (kg/cm <sup>2</sup> )
A	Resistencia muy alta	> 2.250
B	Resistencia alta	1.120-2.250
C	Resistencia media	560-1.120
D	Resistencia baja	280-560
E	Resistencia muy baja	< 280

Se advierte que las categorías de resistencia siguen una progresión geométrica. La línea divisoria entre las categorías A y B se ha fijado en 2.250 kg/cm<sup>2</sup> ya que éste constituye el límite superior de resistencia de las rocas más comunes.

Tabla 1.2 Clasificación\* de la roca intacta<sup>1</sup>

II. Basada en el módulo relativo ( $E_r/\sigma_c$ )		
Clase	Descripción	Módulo relativo <sup>b</sup>
H	Elevado módulo relativo	> 500
M	Módulo relativo medio	200-500
L	Módulo relativo bajo	< 200

\* Las rocas se clasifican según su resistencia y módulo relativo en AM, HL, BH, CM, etc.

<sup>b</sup> Módulo relativo =  $E_r/\sigma_c$

siendo  $E_r$  = módulo tangente para el 50 % de la carga de rotura,  $\sigma_c$  = resistencia a compresión simple.

Uniformemente unos pocos tipos de rocas entran en la categoría A, la cuarcita, la diábasa y los basaltos densos, entre ellos. La categoría B, 1.176-2.250 kg/cm<sup>2</sup>, comprende la mayoría de las rocas ígneas, las rocas metamórficas más duras y los areniscos bien cementados, las pizarras arenilosas duras y la mayoría de las calizas y dolomitas. En la categoría C, rocas de resistencia media en el intervalo 560-1.120 kg/cm<sup>2</sup>, se encuentran muchas pizarras arenilosas, areniscas y

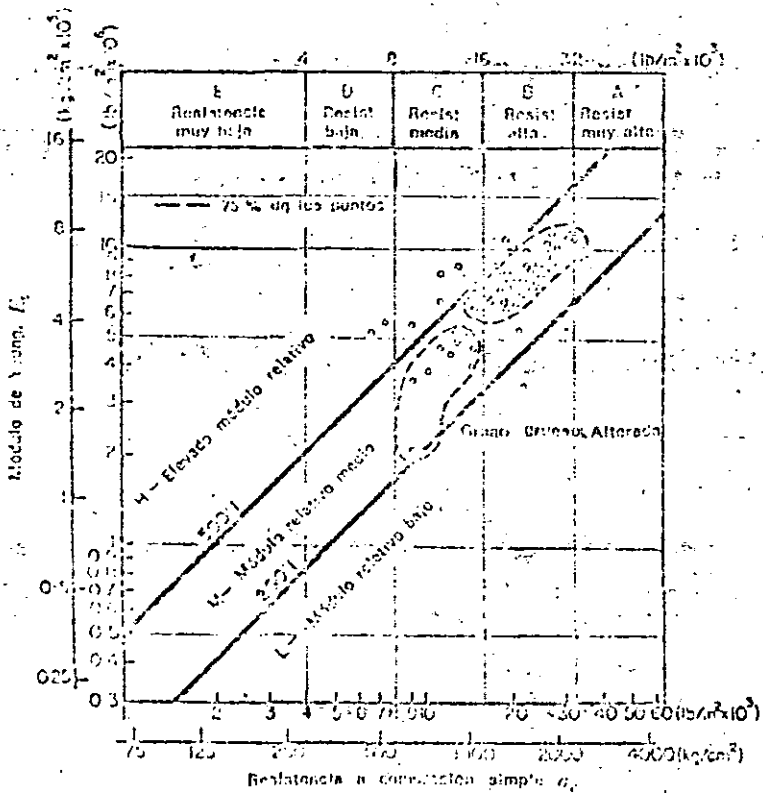


Figura 1.1. Clasificación de rocas ígneas de la familia del granito (80 muestras, 16 emplazamientos, varios investigadores).  
 $E_1$  = módulo tangente para el 50% de la carga de rotura.  
 La roca se clasifica como AM, BI, III, etc.

calizas porosas, las variedades más esquistosas, de las rocas metamórficas (por ejemplo la clorita, y los mica y talcoesquistos). Las categorías D y E, de resistencia baja a muy baja, comprenden rocas porosas o de baja densidad como la arenisca frías, la toba porosa, las pizarras muy arenilosas, la sal gema y las rocas meteorizadas o alteradas químicamente de cualquier litología.

El segundo elemento del sistema de clasificación es el módulo de elasticidad ( $E_1$ ). Sin embargo, en lugar de emplear el módulo propiamente dicho,

se utiliza la relación entre este módulo y la resistencia a presión simple el *módulo relativo*\*, según se indica en la tabla 1.2.

Puede emplearse un diagrama de clasificación como el de la figura 1.1. Los valores de la resistencia a compresión y del módulo de elasticidad se han representado en escala logarítmica para abarcar una amplia gama de valores. Las categorías de resistencia se indican en la parte superior de la figura. El *módulo relativo* se deduce de la posición respecto a las diagonales. La zona central viene limitada por una línea superior con un módulo relativo de 500:1 y una línea inferior correspondiente a un módulo de 200:1. Esta zona se designa con la letra M, o zona de módulo relativo *media*. Las rocas que poseen una estructura compacta y poca o ninguna anisotropía suelen entrar dentro de esta categoría. En ella están comprendidas la mayoría de las rocas ígneas. Los puntos marcados en la figura 1.1 representan 80 muestras de granito corres-

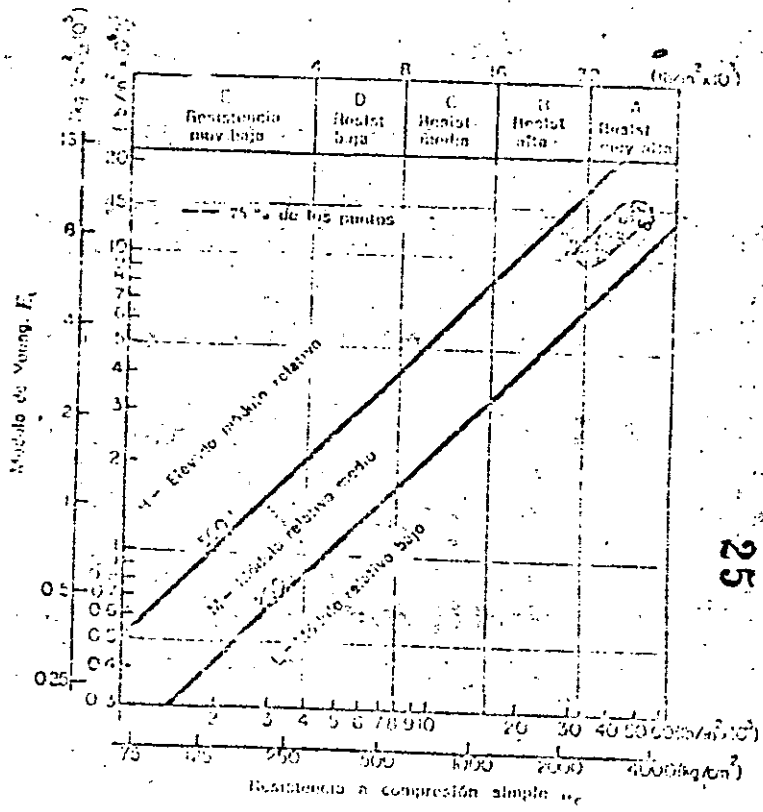


Figura 1.2. Clasificación de rocas ígneas-Diábasas (26 muestras, 8 emplazamientos, varios investigadores).  
 $E_1$  = módulo tangente para el 50% de la carga de rotura.  
 La roca se clasifica como AM, BI, III, etc.

pondencia arbitraria que proponemos para la *módulo relativo* del texto original. (N. del T.).

por cientos a 16 localidades. En la figura 1.2 muestran los resultados de 26 probetas de diabasa, roca ligera de masa y uniforme de grano fino a medio. Se advierte que los resultados son más uniformes y que la roca entra principalmente en la clasificación AM, roca de muy alta resistencia con un módulo relativo medio. En la figura 1.3 aparecen los resultados de 70 muestras de basalto y otras rocas volcánicas de grano fino. Como era de esperar, los resultados abarcan una

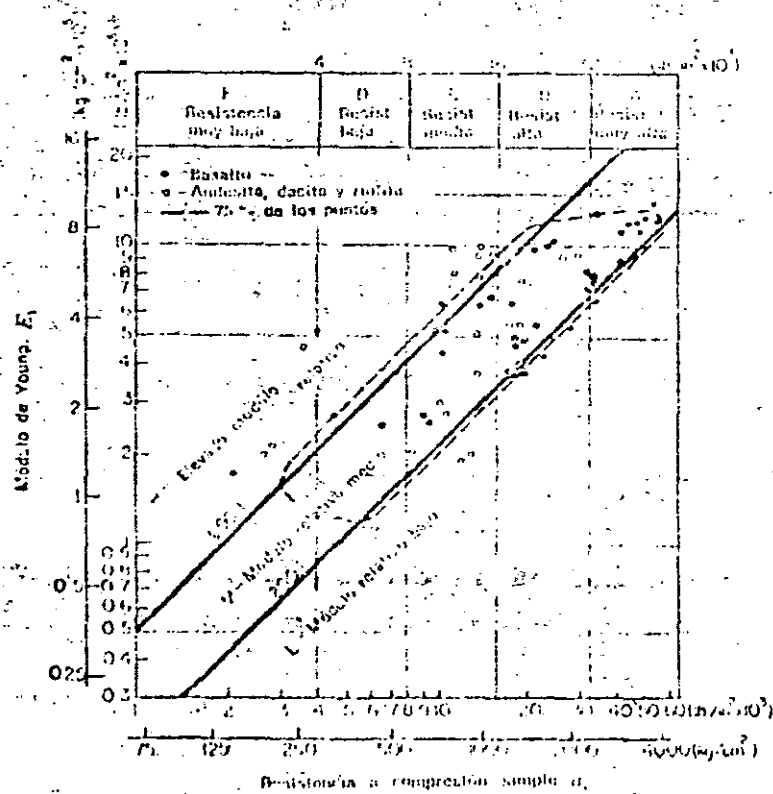


Figura 1.3 - Clasificación de rocas ígneas-Basalto y otras rocas volcánicas (70 muestras, 20 emplazamientos, varios investigadores)<sup>4</sup>  
 $E_t$  - módulo tangente para el 50% de la carga de rotura.  
 La roca se clasifica como AM, BH, BI, etc.

amplia gama de valores debido a la variación en la mineralogía, porosidad, tamaño del grano y estructura de cristalización. El diagrama resumen de las rocas ígneas se indica en la figura 1.4.

En la figura 1.5 aparece el diagrama resumen de las rocas sedimentarias. Se advierte que las calizas y dolomías entran principalmente en las categorías de resistencia B y C aunque algunas muestras son del tipo A, de muy elevada resistencia, o D, rocas muy débiles. Los detalles de estas calizas y dolomías se indican en la figura 1.6. Puede verse que muchos de los puntos caen próximos a la línea superior (módulo relativo, 500:1) o por encima de ella. Esta situación

parece deberse a la particular estructura (compacta) y microtextura (microfibrilada) de las calizas y dolomías. Los diagramas correspondientes a la arenisca y la pizarra, en la figura 1.7, aparecen abiertos por su extremo inferior debido a que diversos probetas se rompieron con presiones inferiores a 75 kg/cm². Se aprecia que tanto la envolvente de las areniscas como la de las pizarras entran en la zona de módulo relativo bajo. Esta situación es el resultado de la anisotropía creada

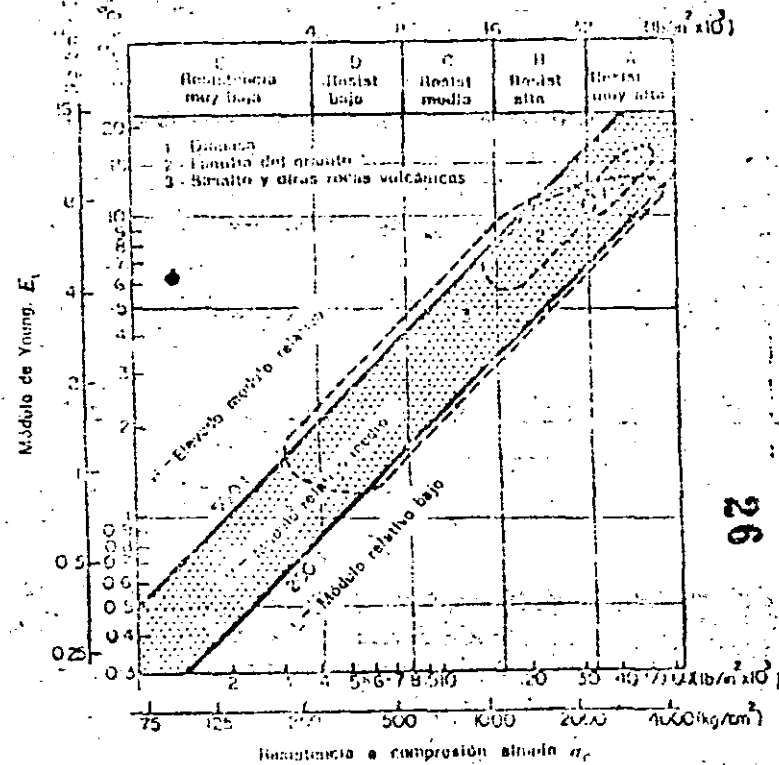


Figura 1.4 - Clasificación de rocas ígneas-Resumen de rocas ígneas (176 muestras, 75% de los puntos)<sup>4</sup>  
 $E_t$  - módulo tangente para el 50% de la carga de rotura.  
 La roca se clasifica como AM, BH, BI, etc.

por la estratificación o esquistosidad. Los módulos relativos son bajos ya que casi todas las muestras se ensayaron con el eje de carga normal al plano de estratificación. Esta orientación no modifica la resistencia pero da lugar a módulos bajos por efecto de la deformación originada por el cierre de los planos de estratificación incipientes y la alineación de los minerales, la mayoría de los cuales son aplanados, especialmente en las pizarras.

El diagrama resumen de las rocas metamórficas aparece en la figura 1.8. La dispersión de los resultados es superior a la de los otros tipos de rocas debido a la gran variación de mineralogía y grado de anisotropía. La mayoría de

rocas, cuando aparecen clasificadas como AM, en la misma posición que otros tipos de rocas densas, de granos ígneos y estructura compacta, como la diabasa y los basaltos densos. Los gneis vienen representados de forma semejante a los granitos pero con una resistencia media algo menor y una mayor dispersión en el módulo relativo. La dispersión adicional proviene de la mayor variación de mineralogía respecto al granito y a la anisotropía por efecto de

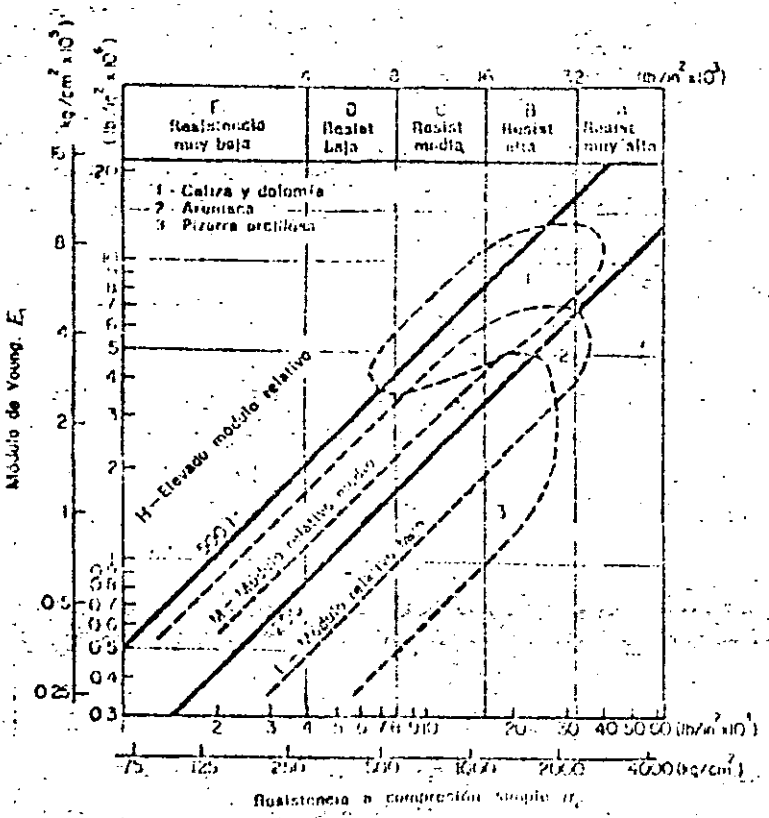


Figura 1.5 Clasificación de rocas ígneas-Resumen de rocas sedimentarias (193 muestras, 75% de los puntos) \*

\*  $E_1$  = módulo tangente para el 50% de la carga de rotura. La roca se clasifica como AM, BH, BI, etc.

tencia por efecto de roturas prematuras según los planos de esquistosidad con fuerte buzamiento. Por otro lado, la envolvente de las muestras con un pequeño ángulo de esquistosidad (45° o menos respecto a la horizontal) cae en la zona de módulos relativos bajos. En este caso, la resistencia no resulta muy afectada por la esquistosidad pero el módulo de elasticidad es bajo por efecto del cierre de las microfisuras paralelas a los planos de esquistosidad. La envolvente de

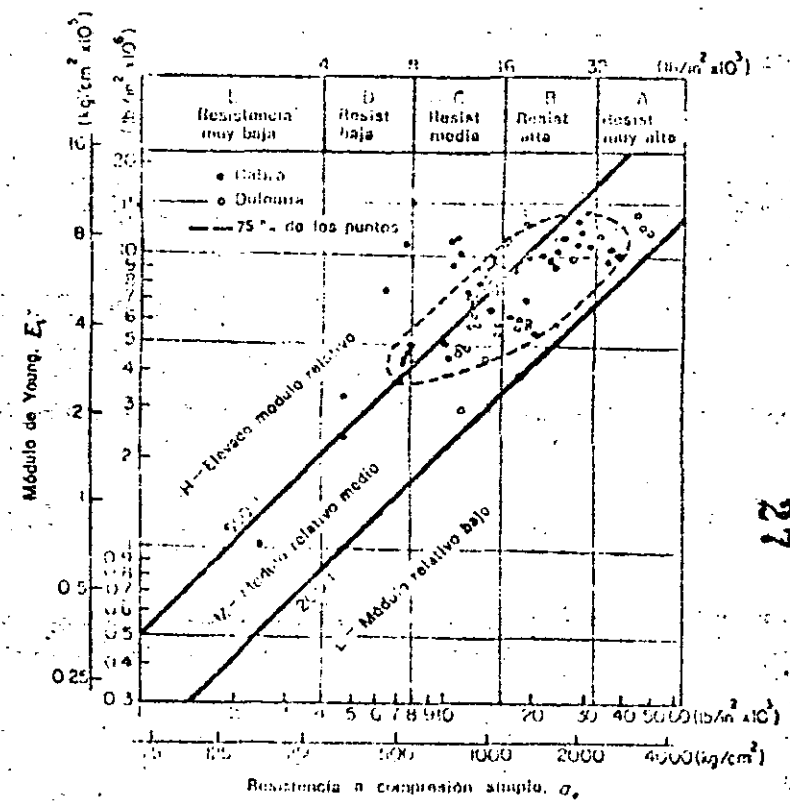


Figura 1.6 Clasificación de rocas ígneas-Caliza y dolomita (77 muestras, 22 ensayamientos, varios investigadores) \*

\*  $E_1$  = módulo tangente para el 50% de la carga de rotura. La roca se clasifica como AM, BH, BI, etc.

la esquistosidad. Muchos de los puntos que caen en la zona de elevado módulo relativo representan roturas según bandas esquistosas de muestras con una fuerte foliación.

Quizá el diagrama más interesante es el de los esquistos. La envolvente 4a (fig. 1.7) corresponde a muestras con una esquistosidad orientada hacia la vertical, es decir con un ángulo elevado (45° o superior) entre el plano de esquistosidad y la horizontal (testigos ensayados con el eje en posición vertical). El elevado módulo relativo de la mayoría de las muestras no corresponde tanto a un valor inherentemente alto sino más bien a un caso de baja resis-

mármol (fig. 1.7) corresponde a un pequeño número de muestras y, aunque 15 de las 22 muestras ensayadas quedaron comprendidas en esa envolvente se necesitan más resultados para poder generalizar. De hecho parece que el elevado módulo relativo se corresponde con la tendencia de las calizas y dolomías que contienen los mismos minerales.

En el diagrama resumen de las rocas metamórficas es significativo que la envolvente de los gneis se superponga con la de las cuarcitas y con las dolomías de los esquistos. Esta posición de transición indica una complejidad creciente de mineralogía y estructura, pasando de las cuarcitas a los gneis.

de éstos a los esquistos. Los diagramas resumen de las rocas ígneas y de las rocas sedimentarias muestran características semejantes en cuanto a las diferencias de mineralogía y estructura.

La clasificación propuesta se considera útil y manejable. Está basada en la resistencia a compresión simple y en el módulo de elasticidad —dos propiedades físicas importantes de la roca que intervienen en la mayoría de los

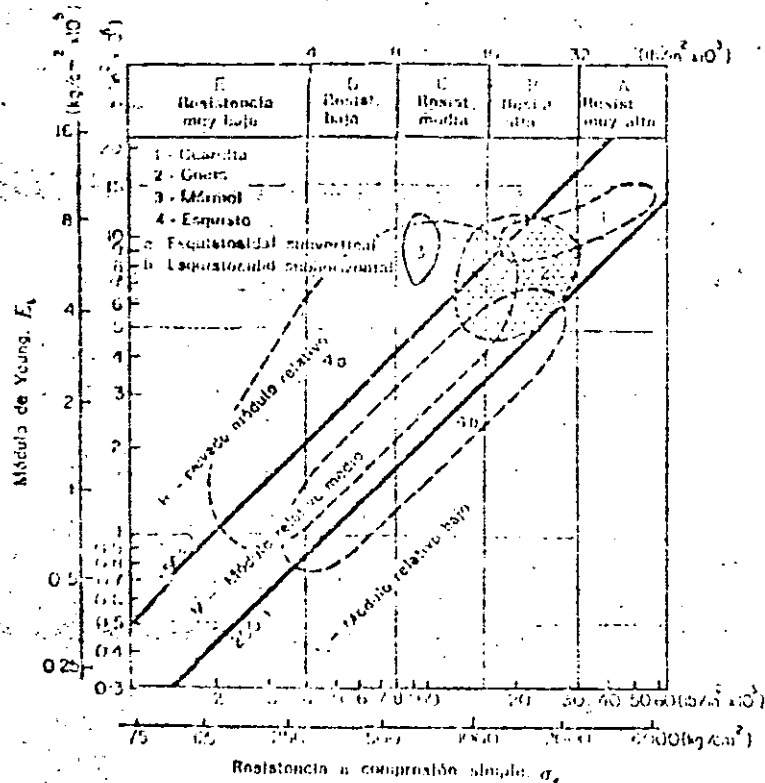


Fig. 1.7 Clasificación de rocas ígneas—Resumen de rocas metamórficas (157 muestras, 75 % de los puntos).

$E_s$  = módulo tangente para el 50 % de la carga de rotura.  
La roca se clasifica como AM, BII, BI., etc.

problemas de ingeniería. La clasificación también considera la mineralogía, textura, estructura y dirección de anisotropía de la roca, de forma que tipos específicos de roca caen dentro de áreas determinadas del diagrama de clasificación. La clasificación completa debería incluir también la descripción litológica, por ejemplo, Caliza: alta resistencia, elevado módulo relativo (BH); grano fino, densa, uniforme.

#### 1.4 Características estructurales de los macizos rocosos

Desde el punto de vista de la Mecánica de Rocas tiene una gran importancia cualquier estructura geológica que pueda influir sobre las propiedades de la roca *in situ*, como la resistencia, el módulo de deformación o la permeabilidad. Las singularidades estructurales más comunes son las diaclasas, los planos de estratificación y esquistosidad y las fallas. Debido a que constituyen discontinuidades planas o quasi-planas tienen un importante efecto anisótropo sobre las propiedades del macizo rocoso.

##### 1.4.1 Representación de las discontinuidades geológicas

Es importante representar cuidadosamente todas estas estructuras geológicas indicando su emplazamiento, orientación (dirección y buzamiento) y separación. Deben también describirse las características físicas. Se ha advertido que, incluso en los testigos rocosos obtenidos por perforación con diamante, puede observarse la abertura e irregularidad de las superficies de discontinuidad así como el tipo de material de relleno entre o a lo largo de superficies adyacentes, siendo conveniente registrar estos datos. Los términos *abierto* o *cerrado* pueden aplicarse para describir el grado de abertura; *plano*, *curvo* o *irregular* para señalar la homogeneidad del perfil; y *pulida*, *lisa* o *rugosa* para indicar la textura superficial. También deberían obtenerse valores numéricos siempre que fuera posible medirlos.

Los reconocimientos de campo pueden dar resultados muy útiles respecto a las características citadas. Sin embargo, debe tenerse cuidado en no sacar conclusiones erróneas de las medidas, por las razones siguientes: en primer lugar, los afloramientos pueden no ser lo suficientemente numerosos para proporcionar una muestra representativa estadísticamente; en segundo lugar, las discontinuidades principales, como fallas o zonas de fallas múltiples, pueden no ser visibles por efecto de la erosión o una meteorización profunda que las haya enmascarado; en tercer lugar, los afloramientos pueden no tener una exposición tridimensional suficiente para permitir determinar el número real y la separación de todas las discontinuidades (ver, por ejemplo, Terzaghi<sup>11</sup>) y, por último, las discontinuidades profundas pueden diferir considerablemente de las que aparecen superficialmente. Por estas razones, suele ser conveniente realizar los levantamientos no sólo en la superficie sino en pozos de reconocimiento, galerías y sondeos.

Se emplean dos métodos principales para realizar representaciones gráficas a partir de sondeos. Un método utiliza el testigo orientado<sup>12</sup>; el otro parte de la fotografía, bien por medio de la televisión<sup>13</sup> o con película en color<sup>14</sup>. La ventaja de los métodos fotográficos es que puede obtenerse cierta información sobre el ancho de las singularidades estructurales, permitiendo saber si están abiertas o rellenas de otro material.

##### 1.4.2 Presentación de los resultados

Los datos obtenidos por observación directa de las discontinuidades geológicas pueden representarse de dos formas básicamente diferentes: 1) como un plano de situación real, con las distintas singularidades estructurales identificadas en lo referente a su tipo, características físicas, orientación y emplaza-

alveolo, y 2) como diagramas estadísticos. En ambos los frecuencias relativas de las discontinuidades de diferente orientación, encontradas en el lugar. Ambos sistemas tienen sus ventajas y también sus limitaciones.

El primer tipo de representación es particularmente útil para un empleo general. Permite dibujar secciones transversales de cualquier zona especialmente crítica de una obra, como un estribo, un desmonte escarpado o las paredes de una gran excavación subterránea, permitiendo ver inmediatamente cualquier discontinuidad orientada peligrosamente. La ausencia de una estructura geológica de orientación crítica en tales secciones no significa necesariamente que no pueda existir; únicamente que se advierte que no fue advertida en el programa de reconocimiento. Deben examinarse los datos de las zonas circundantes para ver si, estadísticamente, puede tener alguna probabilidad de presentarse una discontinuidad crítica.

La situación real de las singularidades puede representarse en un plano; para los pozos y galerías de reconocimiento se recomiendan las secciones desarrolladas. La orientación se suele representar mediante un símbolo apropiado de dirección y buzamiento. El diagrama cuadrado de Müller constituye también una forma gráfica excelente para representar los datos.

Los diagramas estadísticos pueden ser de diversos tipos. Los dos más comunes son la roseta de dióclisis<sup>11</sup> y la proyección estereográfica<sup>12,13,14</sup>. La ventaja del diagrama estadístico es que permite reunir un gran número de observaciones dispersas en torno a un origen único, componiendo una figura de la que se pueden sacar conclusiones<sup>15</sup>. El diagrama estadístico es útil para obtener una indicación sobre las condiciones «medias». En algunos casos puede servir para definir las direcciones de excavación, etc., haciendo mínimos los problemas de estabilidad. Debe señalarse una vez más, sin embargo, que el factor más importante en un determinado emplazamiento suele no ser el estado «medio», sino la presencia de una estructura geológica de orientación crítica como una zona minorizada, una falla o una diaclasa principal.

### 1.5 Clasificación de las rocas «in situ» para obras de ingeniería

Además de la representación gráfica o estadística de las discontinuidades geológicas conviene disponer de alguna forma de clasificación que permita la caracterización del macizo rocoso. El objeto de esta clasificación es facilitar la comunicación entre los geólogos, técnicos de Mecánica de Rocas, ingenieros proyectistas y contratista. Para unificar la terminología en la descripción de las diaclasas, Deere<sup>6</sup> ha hecho la propuesta que figura en la tabla 1.3.

Tabla 1.3 Terminología descriptiva para la separación entre diaclasas<sup>6</sup>

Término descriptivo	Separación entre diaclasas
Muy juntas	Menor de 5 cm
Próximas	5 cm-30 cm
Bastante próximas	30 cm-1 m
Separadas	1 m-3 m
Muy separadas	Mayor de 3 m

A continuación se describen dos métodos generales para determinar calidad de la roca en un determinado emplazamiento a partir del porcentaje de fracturas y del grado de alteración. En un método, la clasificación se basa en el testigo recuperado de un sondeo. En el otro se emplea la velocidad sísmica.

#### 1.5.1 Índice de calidad de las rocas, RQD<sup>16</sup>

El índice de calidad (RQD) se basa en la recuperación modificada de testigo que a su vez depende indirectamente del número de fracturas y del grado de debilitamiento o alteración del macizo rocoso, según se puede observar por los testigos extraídos de un sondeo. En lugar de contar las fracturas, se obtiene una medida indirecta sumando la longitud total de testigo pero considerando únicamente aquellos trozos de testigo de longitud igual o superior a 10 cm, en estado sano y compacto.

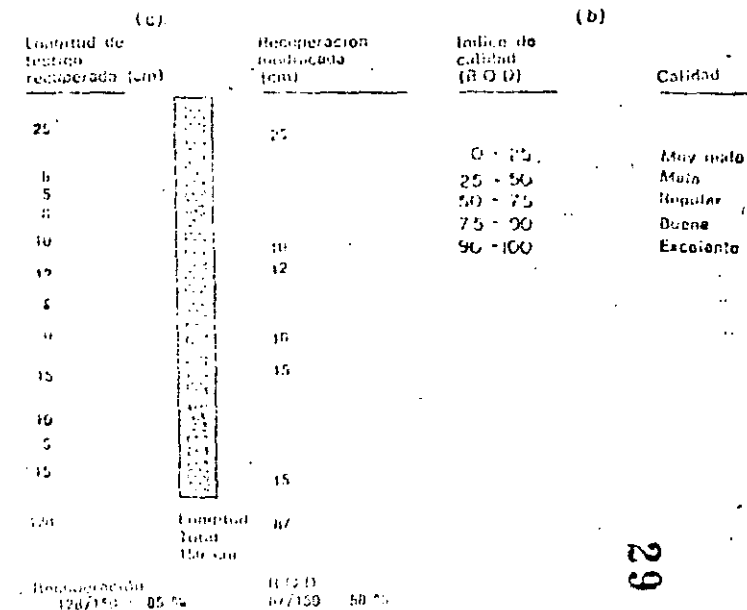


Figura 1.8 La recuperación modificada de testigo como índice de calidad de una roca<sup>16</sup>

En la figura 1.8 se muestra un ejemplo correspondiente a un sondeo de 150 cm. En este caso particular la recuperación total de testigo fue de 128 cm, con un porcentaje de testigo recuperado del 85%. Con la modificación, sólo se tienen en cuenta 87 cm, siendo el RQD del 58%. Se ha visto que el RQD es un índice más sensible y consistente de la calidad general de una roca que el porcentaje de recuperación total.

Si el testigo se ha roto por el manejo o por el proceso de perforación (por ejemplo, cuando se aprecian superficies de fractura recientes y regulares en lugar de diaclasas naturales), se juntan los trozos partidos y se cuentan

<sup>16</sup> Rock Quality Designation.



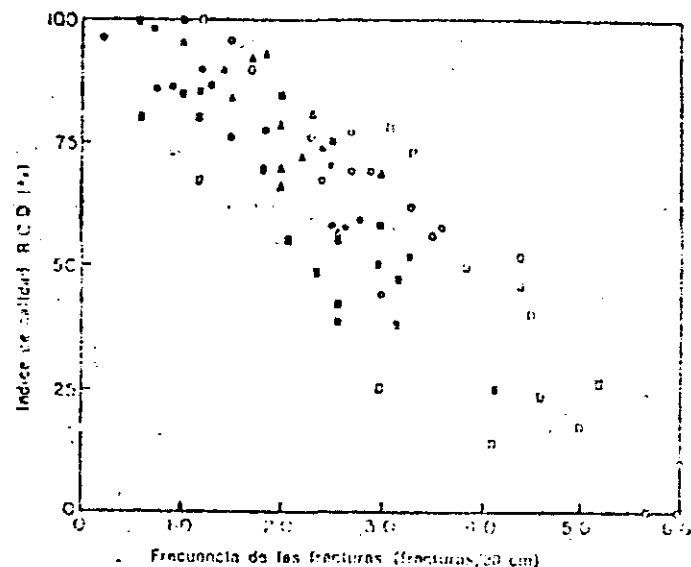
Tabla 1.4 Relación entre el RQD y la calidad de la roca

Índice de calidad (RQD) (%)	Calidad
0-25	Muy mala
25-50	Mala
50-75	Regular
75-90	Buena
90-100	Excelente

Algunos ingenieros prefieren emplear la frecuencia de las fracturas (por ejemplo, las discontinuidades naturales expresadas en fracturas por metro) como medida de la calidad de la roca. En la figura 1.9 se ve que existe una buena correlación entre la frecuencia de las fracturas y el RQD.

### 1.52 Velocidad relativa

El efecto de las discontinuidades del macizo rocoso puede estimarse comparando la velocidad *in situ* de ondas de compresión con la velocidad sónica determinada en laboratorio para un testigo inalterado extraído de la misma roca, como se indica en la figura 1.10. La diferencia entre ambas velocidades se debe a las discontinuidades estructurales que existen en el terreno. Ouedera <sup>19</sup> fue el primero en proponer como criterio de calidad el cociente de velocidades, o velocidad relativa ( $V_1/V_2$ ), donde  $V_1$  y  $V_2$  son las velocidades de la onda de compresión para el macizo rocoso *in situ* y para el testigo inalterado respectivamente. Para una roca masiva de excelente calidad, con sólo unas pocas diaclasas cerradas, la velocidad relativa debe ser próxima a la unidad. Al aumentar el grado de diaclasado y fracturación, la velocidad relativa disminuye a valores inferiores a la unidad.



- Granito del batolito Climax      Testigo NX
- Pared de túnel normalmente a las diaclasas
  - △ Pared de túnel paralelamente a las diaclasas
  - Testigo NX
  - Pesa de Dworshak, gncis granítico
  - △ Basalto de John Day
  - Aleutina de Hackensack

Figura 1.9 Correlación entre los índices de calidad de las rocas: frecuencia de las fracturas y RQD

Evidentemente este método es muy rígido para la roca cuando la recuperación es escasa, si bien una escasa recuperación suele indicar una pobre calidad de la roca. Pero esto no siempre es cierto, sin embargo, ya que un equipo de perforación o una técnica deficientes pueden también dar lugar a una recuperación escasa. Por esta razón, se requiere una batería de sondeo de doble tubo de diámetro mínimo NX (54 mm), siendo fundamental una adecuada vigilancia de la perforación.

Por simple que parezca el procedimiento, se ha encontrado que existe una correlación bastante buena entre los valores numéricos del RQD y la calidad general de la roca a efectos prácticos de ingeniería. Esta correlación se da en la figura 1.8 y en la tabla 1.4.

El RQD está siendo utilizado por diversas oficinas de proyectos, consultores en ingeniería y contratistas en los Estados Unidos para estimar la calidad de las rocas *in situ* y las variaciones en un mismo sondeo o de un sondeo a otro en una zona.

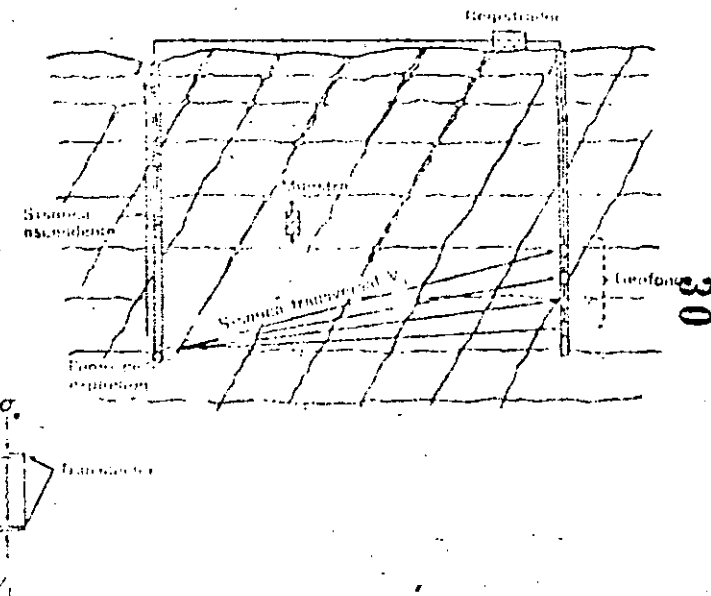


Figura 1.10 La velocidad relativa ( $V_1/V_2$ ) como índice de la calidad de una roca

La velocidad  $V_r$  se determina en laboratorio con un triángulo sometido a una tensión axial igual a la sobrecarga de peso propio calculada para la profundidad a la que se tomó la muestra, y con una humedad equivalente a la supuesta para la roca *in situ* (es decir roca o saturada). Preferentemente la velocidad sísmica en el terreno debe determinarse por la velocidad ascendente en un sondeo o la transversal entre sondeos o galerías de reconocimiento próximas, ya que con estas medidas se pueden reconocer zonas particulares homogéneas con más precisión que con la sísmica de refracción superficial.

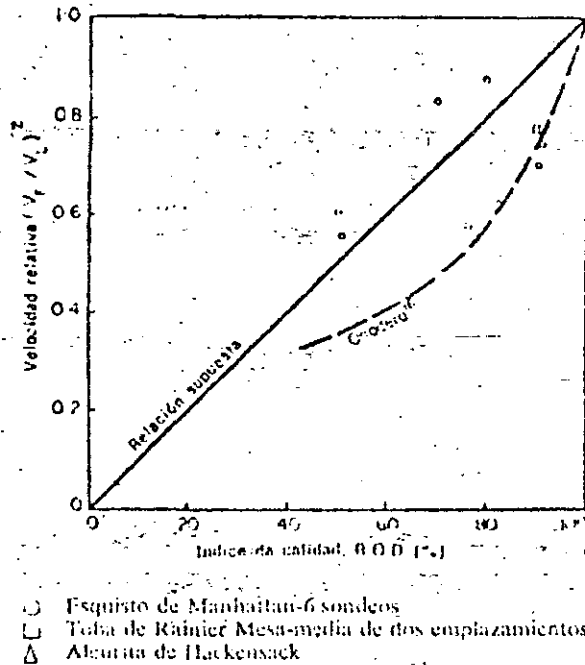


Figura 1.11 Correlación entre la velocidad relativa y el índice de calidad RQD<sup>12</sup>

En la figura 1.11 se muestra una correlación entre el cuadrado de la velocidad relativa  $(V_r/V_1)^2$  y el RQD. De los limitados datos recogidos se deduce que el cuadrado de la velocidad relativa puede utilizarse de forma equivalente al RQD en estudios de ingeniería. Sin embargo, se requiere un mayor número de datos para ampliar el conocimiento de la relación existente entre ambos índices de calidad. Se verá en los capítulos 2 y 7 que estas descripciones de la calidad de los macizos rocosos pueden relacionarse con las propiedades mecánicas *in situ*.

### 1.6 Estado tensional «in situ»

El estado de tensiones natural que existe en un punto en el interior de un macizo rocoso es función de todos los procesos geológicos anteriores que han actuado sobre éste. Por supuesto, es imposible conocer con un cierto grado de

precisión todo los acontecimientos ocurridos. Incluso con respecto a la historia geológica completa, no sería posible determinar el estado tensional por ignorar las propiedades características del material bajo ciertas condiciones de larga duración y el mecanismo real de deformación por efecto de la subspresión, erosión, etc.

No existe la menor justificación para suponer que la tensión horizontal, a una cierta profundidad bajo una superficie horizontal, está relacionada con la sobrecarga de peso propio, de acuerdo con la teoría elástica, por el factor  $\nu/(1-\nu)$  donde  $\nu$  es el módulo de Poisson. Cualquier fenómeno geológico ha podido hacer que la tensión horizontal difiera significativamente de este valor. Por ejemplo, en una zona de hundimiento regional activo, el centro de la misma habrá sufrido deformaciones de compresión, mientras que la periferia habrá estado sometida a tracciones. Evidentemente, las tensiones horizontales en el centro serán muy superiores a las de los bordes. Análogamente, los movimientos tectónicos profundos que producen plegamientos, formación de montañas, fallas de gravedad y empuje, darán lugar a ciertos estados tensionales, características estructurales y condiciones de contorno que diferirán grandemente de las consideradas por la teoría elástica. Además, la fluencia, la relajación y la reducción de tensiones por erosión o meteorización originarán tales modificaciones del estado tensional que localmente habrá grandes diferencias respecto a las tensiones inducidas inicialmente.

Como conclusión, es evidente que las tensiones *in situ* no pueden determinarse a partir de la geología de la zona ni, en el estado actual de conocimientos, mediante cálculos con las ecuaciones de la mecánica. El único método práctico para obtener una estimación del estado tensional consiste en medirlas en el propio terreno, un tema que se discutirá en los capítulos 5 y 6.

### Referencias

1. D. F. Coates, «Classification of rocks for rock mechanics», *Intern. J. Rock Mech. Mining Sci.*, 1, 421-429 (1964).
2. D. F. Coates y R. D. Parsons, «Experimental criteria for classification of rock substances», *Intern. J. Rock Mech. Mining Sci.*, 3, 181-189 (1966).
3. R. P. Miller, «Engineering classification and index properties for intact rock», *Ph. D. Thesis*, Univ. Illinois, 1965.
4. D. U. Deere y R. P. Miller, «Engineering classification and index properties for intact rock», Tech. Rept. No. AFWL-TR-65-116, Air Force Weapon Lab., Kirtland Air Force Base, Nuevo México, 1966.
5. D. U. Deere, «Technical description of rock cores for engineering purposes», *Rock Mech. Eng. Geol.*, 1, 18-22 (1963).
6. R. D. Terzaghi, «Sources of error in joint surveys», *Geotechnique*, 15, 287-30 (1965).
7. D. S. Rowley, C. A. Burk y T. Manuel, *Oriented Core*, Christensen Diamond Products Co., Salt Lake City, Utah.
8. L. Möller, *Der Felshut*, Ferdinand Enke, Stuttgart, 1963.
9. E. B. Burwell y R. H. Nesbitt, «The NX borehole camera», *Trans. AIME* 194, 805-808 (1954).
10. K. John, «An approach to rock mechanics», *Proc. Am. Soc. Civil Engrs.*, 88, (1962).
11. D. P. Krymne y W. R. Judd, *Principles of Engineering Geology and Geotechnic*, McGraw-Hill, Nueva York, 1957.
12. E. B. Knapp, «Petrofabrics in structural geology», en Behavior of Material in the Earth's Crust (2nd Ann. Symp. Rock Mech.), *Quart. Colo. School Mine* 52, 99-111 (1957).

13. P. C. Badgley, *Structural Methods for the Exploration Geologist*, Harper and Brothers, Nueva York, 1959.
14. P. C. Badgley, *Structural and Tectonic Principles*, Harper and Row, Nueva York, 1965.
15. D. U. Deere, A. J. Hendron, Jr., F. D. Patton y E. J. Cording, «Design of surface and near-surface construction in rock», *Symp. Rock Mech.*, 8th, *Minnesota*, 1966 (AIME, 1967).
16. T. F. Onodera, «Dynamic investigation of foundation rocks in situ», *Proc. Symp. Rock Mech.*, 5th, *Minnesota*, 1963, Pergamon, Nueva York, págs. 517-533.



**DIVISION DE EDUCACION CONTINUA  
FACULTAD DE INGENIERIA U.N.A.M.**

MECANICA DE ROCAS APLICADA A LA MINERIA Y A LA CONSTRUCCION

LA MECANICA DE ROCAS Y SU CAMPO DE APLICACION

Ing. José Luis Rosas López

MAYO, 1985

## LA MECANICA DE ROCAS Y SU CAMPO DE APLICACION

La Geología, Mecánica de Rocas y Mecánica de Suelos, se agrupan en una disciplina tecno-científica denominada GEOTECNIA. Cada una de estas ramas científicas se relacionan entre sí. La Geología debe proporcionar al ingeniero toda la información necesaria para comprender el futuro comportamiento mecánico de un macizo rocoso ó de un suelo. Debido a las cambiantes condiciones estructurales de la corteza terrestre, las fronteras entre suelos y rocas son algunas veces difíciles de precisar. Podemos encontrar grandes extensiones de masas rocosas, también grandes extensiones de suelos o bien estructuras geológicas donde se combinan suelos y rocas. Las discontinuidades contenidas en las masas rocosas frecuentemente están rellenas de materiales arcillosos o granulares o combinaciones de ambos; el comportamiento de estos materiales de relleno es, separadamente, muy diferente al de la masa rocosa; sin embargo, es el comportamiento del conjunto el que debe considerarse y para ello es necesario comprender y conocer el comportamiento mecánico de ambos materiales, suelos y rocas.

La Mecánica de Rocas estudia la reacción de las rocas a los campos de fuerza de su entorno físico y se define como: la ciencia que estudia el comportamiento mecánico de las masas rocosas que se encuentran bajo la acción de fuerzas producidas por fenómenos naturales (volcanismo, deriva de placas continentales, flujo o presencia de agua, etc), o impuestas por el hombre (cimentaciones, excavaciones, voladuras, etc).

La solución de problemas en este campo, así como sucede con el estudio del comportamiento estructural de diversos tipos de materiales

(entre ellos los suelos), implica el conocimiento de:

- a) La deformabilidad de los macizos rocosos, así como la relación entre fuerzas y deformación.
- b) La resistencia de los macizos, así como las condiciones que determinan su rotura.
- c) El estado de esfuerzos inicial o residual al que se encuentra sometido el macizo y, finalmente:
- d) Los estados de esfuerzo que se desarrollan en el macizo, en virtud de las sollicitaciones (estáticas y/o dinámicas) aplicadas, incluidas las debidas a flujo de agua.

El desarrollo de esta nueva rama de la mecánica es muy reciente y data del año 1951 en que se realiza el primer Coloquio de Mecánica de Rocas en Austria. Las primeras obras que tratan de agrupar los conocimientos existentes hasta el momento son las de Talobitz "Mecánica de Rocas Aplicada a los Trabajos Públicos" editada en 1957, y la del profesor Leopold Muller, editada en 1963 bajo el título de "Construcción en Roca".

A partir de 1924 se presentan los primeros trabajos o experiencias de Mecánica de Rocas en el "First Empire Mining and Metallurgical Congress", realizado en Inglaterra. En estas fechas (1925) se publica el libro "Erdbau Mechanick" (Mecánica de Suelos) de Karl Terzaghi que impulsa el desarrollo científico y técnico de la Mecánica de Suelos. En 1933 se realiza el Primer Congreso Internacional de Grandes Presas.

A principios de los años 60 se crea La Sociedad Internacional de Me

cánica de Rocas (ISRM) que impulsa vigorosamente la investigación en esta disciplina y se encauza a resolver los problemas más urgentes. En 1966 se realiza el Primer Congreso internacional de Mecánica de Rocas en Lisboa. Hasta el momento se han realizado cinco Congresos Internacionales (1966, Lisboa; 1970, Belgrado; 1974, Denver; 1979, Montreux; 1983 Melbourne) todos auspiciados por la ISRM.

En México el desarrollo de la Mecánica de Rocas ha estado asociado fundamentalmente a la construcción de presas para generación de energía eléctrica participando interdisciplinariamente con la geología aplicada; ha sido escasa su intervención en otros proyectos civiles, mineros, petroleros o geofísicos. Los primeros trabajos de Mecánica de Rocas los realiza la Comisión Federal de Electricidad (CFE) en 1958, durante la construcción de la presa La Soledad en el Río Apulco, Estado de Puebla.

En 1964 se crea el Laboratorio de Obras Civiles de CFE la sección de Mecánica de Rocas. Actualmente este laboratorio recibe el nombre de Subgerencia de Ingeniería Experimental y la Sección de Mecánica de Rocas se inserta como oficina del Departamento de Geotécnica. Hasta ahora, es la dependencia con mas recursos técnicos y humanos para resolver problemas de Mecánica de Rocas en el País.

En 1972 se funda la Sociedad Mexicana de Mecánica de Rocas que agrupa a los profesionistas especializados e interesados en esta rama científica.

Actualmente la Mecánica de Rocas tiene múltiples aplicaciones en el campo de la ingeniería, citaré solo algunas de ellas: excavaciones

subterráneas para diversos propósitos tales como: explotación de minerales, túneles para defensa, túneles para almacenamiento de petróleo, gas, armamento, desperdicios atómicos. Túneles para transporte de materiales diversos, túneles para conducción de agua (agua potable, aguas negras, residuos industriales, desvios, vertedores, para alojar tuberías de presión, etc.), túneles para fines de transporte (trenes, tranvías, automóviles, peatones, barcos, etc), cavidades en zonas urbanas (estacionamientos, centros comerciales, etc.).

Excavaciones a Cielo Abierto, para explotación de bancos de roca cuyo producto servirá para diversos fines tales como: escolleras, rellenos para soporte de estructuras, pedraplenes, balastro, agregados para concreto, enrocamientos, fachadas de casas e interiores, etc. Excavaciones para extracción de minerales, cortes para caminos, canales para conducción de agua y otros materiales, etc.

Cimentaciones de presas, torres de transmisión, edificios y casas, otras estructuras urbanas, reactores, radares, puentes, etc.

Otras aplicaciones: Uso de fracturamiento hidráulico para extracción de petróleo, fracturamiento hidráulico para activación de pozos geotérmicos, tratamiento de masas rocosas mediante inyecciones, etc.





**DIVISION DE EDUCACION CONTINUA  
FACULTAD DE INGENIERIA U.N.A.M.**

MECANICA DE ROCAS APLICADA A LA MINERIA Y A LA CONSTRUCCION

CARACTERIZACION DEL MACIZO ROCOSO

MAYO, 1985

## 1.- CARACTERIZACION DEL MACIZO ROCOSO

### 1.1 Ingeniería Geológica

#### 1.1.1 Estudios Geológicos

- a) Estratigrafía
- b) Petrografía
- c) Fotogeología y Sensores remotos
- d) Geomorfología

#### 1.1.2 Estudios Geofísicos

- a) Métodos de Exploración
- b) Propiedades elásticas dinámicas
- c) Zonificación de masas
- d) Intemperismo y Permeabilidad
- e) Limitaciones y Ventajas

#### 1.1.3 Estudios Geohidrológicos

- a) Niveles freáticos
- b) Regimen del Ciclo Hidrológico
- c) Permeabilidad Secundaria
- d) Carst

#### 1.1.4 Estudios Estructurales

- a) Cartografiado
- b) Descripción Geotécnica
- c) Dominios Estructurales
- d) Proyecciones Estereográficas
- e) Estadística y Probabilidad
- f) Aplicación

#### 1.1.5 Estudios Sismo-tectónicos

- a) Tectónica Regional
- b) Estado de esfuerzos
- c) Sismicidad Tectónica
- d) Sismicidad Volcánica
- e) Sismicidad Inducida
- f) Riesgo sísmico

#### 1.1.6 Métodos de Exploración Directa

- a) Perforación de diamante
- b) Zanjas y Trincheras
- c) Socavones y Lumbreras

#### 1.1.7 Estudios Para Bancos de Materiales

- a) Estratigrafía y Mineralogía
- b) Fracturamiento
- c) Intemperismo
- d) Técnicas de Muestreo
- e) Cubicación

## 1.2 Propiedades Geométrico-Mecánicas

1.2.1 Estudios de campo

1.2.2 Métodos fotográficos

1.2.3 Descripción básica de las discontinuidades

1.2.4 Determinación propiedades índice en roca intacta

1.2.5 Estudios in-situ

1.2.6 Técnicas de muestreo

1.2.7 Factores que regulan propiedades geomecánicas

1.2.8 Criterio empírico de fallamiento.

1.2.9 Propiedades elásticas de la roca

# BIBLIOGRAFIA

28

## GEOLOGIA

- Billings, M.P. (1972), Structural geology, Prentice Hall, Inc., Nueva York, 606 pp
- Birkeland, P.W. y Larson E.E., (1978), 3rd ed. Putnam's Geology, University Press, Nueva York
- Freeze, R.A. y Cherry A.J. (1979), Groundwater, Prentice-Hall, Englewood, Nueva Jersey
- Hobbs, B.E., Means, W.H. y Williams, P.F. (1976), An Outline of Structural Geology, John Wiley & Sons, Nueva York, 473 pp

## TECTONICA

- Bird, M.J. (1980), 2nd ed. Plate Tectonics, American Geophysical Union, Washington, D.C.
- Ramsey, J.G. (1967), Folding and Fracturing of Rocks, McGraw-Hill Book Co. Inc. Nueva York, 568 pp
- Uyeda, S. (1978), The New View of the Earth, W. H. Freeman, San Francisco, 217 pp
- Walters, R.C.S. (1971), Dam Geology, Butterworths, London
- Wilson, J.T. (1974), 2nd ed. Deriva Continental y Tectónica de Placas, H. Blume, Scientific American, España

## GEOFISICA

- Dobrin, M.B. (1960), Introduction to Geophysical Prospecting, McGraw-Hill Book Co., Nueva York, 435 pp
- Griffits, D.H. y King, R.F. (1965), Applied Geophysics for Engineers and Geologists, Pergamon Press
- Siegel, B.S. y Gillespie, A.R., eds (1980), Remote Sensing in Geology, John Wiley & Sons, Nueva York, 234 pp
- Telford, W.M., Geldart, L.P., Sheriff, E.R. y Keys, D.A. (1976), Applied Geophysics, University Press, Cambridge

Coor. M.C. L. ESPINOSA-GRAHAM  
Prof. M.C. T. LUGO-IBARRA  
Prof. M.C. J.I. MAYCOTTE

## INGENIERIA GEOLOGICA

- Attewell, P.B. y Farmer, I.W. (1976), Principles of Engineering Geology, Chapman y Hall, London, 1045 pp
- Bell, F.G. (1980), Engineering Geology and Geotechnics, Newnes Butterworth, 497 pp
- Blyth, F.G.H. y Freitas, M. (1974), A geology for engineers, 6th ed., Edward Arnold, London, 557 pp
- Farmer, I.W. (1968), Engineering properties of rocks, E & F.N. Spon. Ltd., London, 180 pp
- Goodman, R.E. (1976), Methods of Geological Engineering, West Publishing Co., St. Paul, 427 pp
- Krynine, D.P. y Judd, W.R. (1957), Principles of Engineering Geology and Geotechnics, McGraw-Hill Book Co. Inc., Nueva York, 730 pp
- Legget, R.F. (1983) 3rd ed., Geology and Engineering, McGraw Hill Book Co. Inc., Nueva York
- Mathewson, C. (1981), Engineering Geology, Charles E. Merrill
- Wiegel, R.L. ed (1970), Earthquake Engineering, Prentice Hall, Inc. Englewood Cliffs, Nueva Jersey, 505 pp
- Zaruba, Q. y Mencl, V. (1976), Engineering Geology, Elsevier, Nueva York

## GEOTECNIA

- Desai, C.S. (1976), Numerical Methods in Geomechanics, ASCE, Vols 1, 2 y 3, Nueva York, N.Y.
- Desai, C.S. y Cristian, J.T. (1977), Numerical Methods in Geotechnical Engineering, McGraw Hill Book Co.
- Elsevier Publishing Co. (1969-1982), Development in Geotechnical Engineering, Netherlands, Holland
- Golzé, R. A. (1977), Handbook of Dam Engineering, Van Nostrand Reinhold, Nueva York
- Marsal, R. J. (1960), Earth dams in Mexico, Procs. I Pan. Conf. on Soil Mech. and Found. Engng. Vol. 2, pp 67-98, Sao Paulo
- Marsal, R. J. y Reséndiz-Núñez, D. (1975), Presas de tierra y enrocamiento, Editorial Limusa, México, 535 pp
- Marsal, R. J. y Taméz, E. (1954), Earth dams in México: Design, Construction and Performance, Mem. V Cong. Inter. Grandes Presas, París
- McLean, A. C. y Gribble, C. D. (1979), Geology for Civil Engineers, London
- Roberts, A. (1977), Geotechnology, Pergamon Press, Nueva York
- Stagg, K. G. y Zielkewicz, O. C. (1968), Rock Mechanics in Engineering Practice, Wiley and Sons, Ltd. London, 422 pp
- Thomas, H. H. (1976), The Engineering of Large Dams, Parte 1 y 2, John Wiley & Sons, Nueva York, N.Y. 375 pp, 402 pp

## MECANICA DE ROCAS Y ESTABILIDAD DE TALUDES

- Canmet (1981), Pit Slope Manual, Canada Centre for Mineral and Energy Technology, Chapters 1-10, Minister of Supply and Services, Canada, Ottawa
- Goodman, R. E. (1980), Introduction to Rock Mechanics, John Wiley and Sons, Nueva York, N.Y. 478 pp
- Hoek, E. y Bray, J. W. (1977), 3rd ed. Rock Slope Engineering, Institution of Mining and Metallurgy, London
- Hoek, E. y Brown, T. (1980), Underground Excavations in Rocks Institution of Mining and Metallurgy, London
- Jaeger, J. C. (1972), Rock Mechanics and Engineering, Cambridge University Press
- Jaeger, J. C. y Cook, N.G.W. (1979), 3rd ed., Fundamentals of Rock Mechanics, John Wiley & Sons, Nueva York
- Obert, L. y Duvall, W. (1967), Rock Mechanics and the Design of Structures in Rock, John Wiley & Sons
- Royster, D. L. (1979), Landslide Remedial Measures, Assoc. Engng. Geol., Bull. Vol. 16, No. 2
- Schusters, R. L. y Krizek, R. J. Eds. (1978), Landslides, Analysis and Control, Special Report 176, Transp. Res. Board, NAS, Washington, D.F.
- Voight, B. ed. (1978), Rock slides and avalanches, 1, Elsevier, Nueva York
- Voight, B. ed. (1979), Rock slides and avalanches, 2, Elsevier, Nueva York

## REVISTAS ESPECIALIZADAS (JOURNALS)

Bulletin of the Association of Engineering Geologists, A.E.G.  
California, Sacramento, Cal.

Newsletter of the Association of Engineering Geologists, Quaterly  
Sacramento, Cal.

Canadian Geotechnical Journal, National Research Council of  
Canada, Ottawa

The Quaterly Journal of Engineering Geology, Geological Society  
of London, Inglaterra

Bulletin of the International Association of Engineering Geolo-  
gists, París, Francia

Journal of International Society of Rock Mechanics, Alemania  
Occidental (antes Rock Mechanics and Engineering Geology,  
Spinger-Verlag, Viena)

Journal of Engineering Geology, Elsevier, Netherlands

Géotechnique, Inst. of Civil Engineering, London

International Journal of Rock Mechanics and Mining Sciences,  
Pergamon Press

International Water Power and Dam Construction

Tunnels and Tunnelling

Earthquake Information Bulletin



# 8 The principal geological factors affecting certain engineering projects

P-104

## 8.1 THE STABILITY OF SLOPES AND CUTTINGS

### 8.1.1 Geological factors affecting the stability of a new excavation

The static conditions that control the initial, and also the later, stability of a steep face cut into soil or rock, and which may determine the need for support or remedial treatment are as follows.

The properties in bulk, particularly the shear strength, of the material forming the cutting: the stability of a cutting in rock is usually dependent on the occurrence of joints and other planes of weakness, and on the amount of cohesion and the friction across these planes.

The structure of the rocks and soils, and specifically how any planes of weakness are orientated relative to the newly exposed face: for example, horizontal bedding planes in poorly jointed sandstone often give near-vertical faces which are stable, whereas faults or joints striking parallel to the new face, and dipping steeply towards it, will probably be planes of movement or potential instability.

The groundwater conditions: saturation significantly lowers the strength of most soils compared with their values when dry. Certain soils weaken to a stage where they run like viscous liquids. High pore pressure of ground water in a layer, or in a plane of weakness, lowers frictional resistance to movement. (The mechanism is the same as that which allows a hovercraft to glide over water or land on a high-pressure cushion of air.) A dramatic example of instability triggered by high pore pressure within a body of soils was the Aberfan disaster in 1966, where a spoil heap of mine waste slid downwards onto a Welsh village.

Stresses produced by natural loads adjacent to the cutting: steep-sided valleys or mounds affect the state of stress in the ground near the surface, not only below themselves but also for some distance around. This lateral change in stress conditions may be

sufficient to cause instability of weak rocks and soils. For example, valley bulges (p. 76) are produced in this way, and they may be accompanied by instability of an adjacent slope.

### 8.1.2 Other geological factors causing instability of existing slopes

An initially stable slope may become unstable with the passage of time because of human disturbance. This may consist of adding a fresh load such as a spoil heap, removing support by excavating, or triggering movement by vibrations from nearby heavy machinery. The common geological causes are as follows.

Weathering of the soil or rock of the slope so that it becomes weaker: this may affect the bulk of the material (for example, boulder clay) or may be concentrated along planes in a rock. Chemical alteration of existing minerals is important under certain conditions, as is mechanical breakdown in others (pp. 50-3). Periglacial weathering in Pleistocene times also affects the stability of some present-day cliffs.

Erosion of the slope by a river or other natural agent, usually at its base but possibly along a weaker layer or plane, may cause undermining to take place.

Change in water content of the soil or rock: heavy rain, especially after a drought, saturates the material forming the slope, increasing its mass and the gravitational pull on a given volume, and also reducing the strength of soils and the friction along any discontinuities.

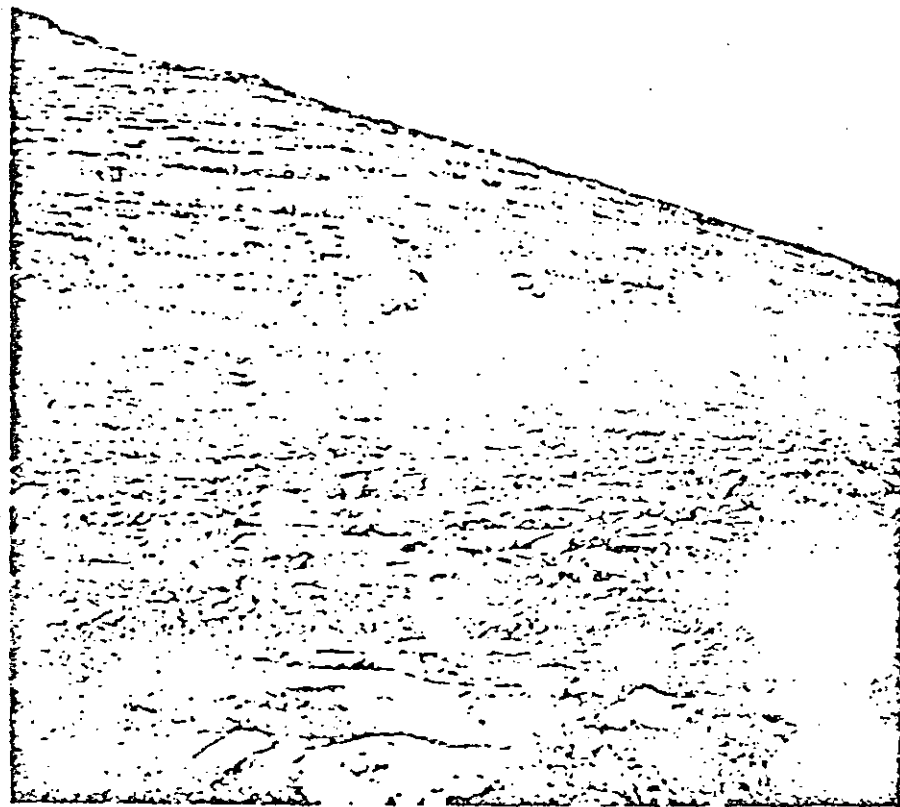
### 8.1.3 Types of failure of soil slopes

Instability of soils on a slope may take one of the following forms.

Creep occurs on steep slopes and produces a downhill movement at low rates (less than 10 mm per year) of the top few metres of soil (see Photo. 8.1). It is facilitated by the effects of frost, and by heavy rain washing out fines from the soil. Any excavation on a slope affected by creep is likely to increase movement. Creep may be recognisable from displacement of fencing, or of a cover of turf, or by drag effects of strata under the soil.

Flow is a rapid movement of waterlogged soil, broken rock and mud, downhill, usually after prolonged rain.

Scree or talus slide occurs where rock fragments spall off a fractured rock mass which has been subjected to mechanical



Photograph 8.1 Minor ridges on a hillside produced by soil creep. (Institute of Geological Sciences photograph, C1333, published by permission of the Director, NERC, copyright.)

weathering. They rest at a natural angle of repose at the foot of the slope. Excavation at the foot of a scree slope or inadequate drainage, which increase pore water pressure in the mass, will lead to instability of the slope.

Translational failure involves movement along a particular plane of weakness in the soils of the slope. For example, in a slope formed of a clay layer in sand layers, deterioration of the shear strength of the clay may lead to movement at the boundary of clay and sand. Failure of this type may occur with slope angles as low as 6 degrees.

Rotational slip affects clays or clay-rich rocks such as mudstones and shales. The surface of movement is curved, and is such that shear

resistance along it is given by the equation

$$S = C_c + (\sigma + u) \tan \phi_c$$

where  $\sigma$  is the stress normal to the surface,  $u$  is the pore water pressure,  $C_c$  is the cohesion of the clay,  $\phi_c$  is the angle of frictional resistance of the clay and  $S$  is the shearing resistance. Photograph 8.2 shows rotational slip failure in a slope in California.

Rotational slip is usually preceded by development of vertical tension cracks at the top of the slope. These cracks may reach a maximum depth of  $2C/\gamma$  where  $C$  is the cohesion of clay and  $\gamma$  is the density of clay. Typical laboratory values for marl (a clay-rich rock) are

$$C = 2.5 \text{ MN m}^{-2} \quad \text{and} \quad \phi = 42^\circ \quad (\text{under dry conditions})$$

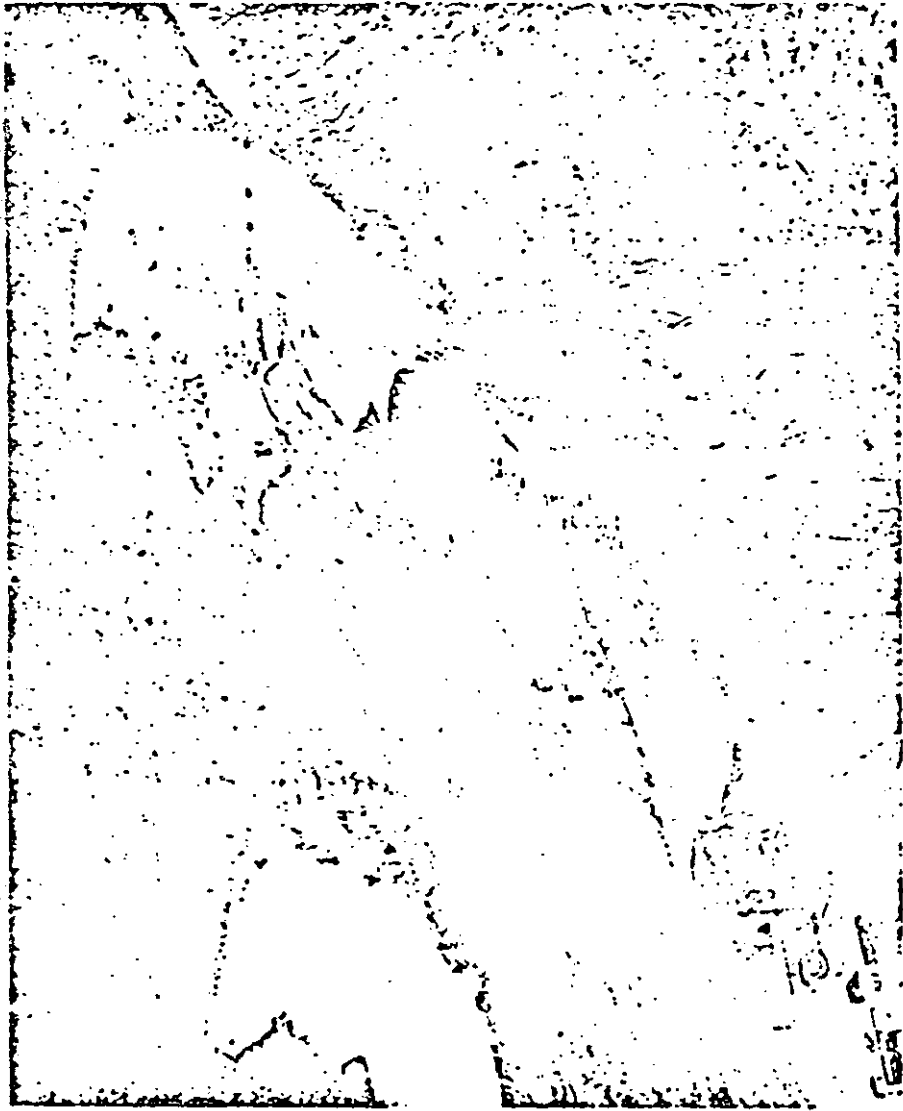
$$C = 2.0 \text{ MN m}^{-2} \quad \text{and} \quad \phi = 21^\circ \quad (\text{under saturated conditions}).$$

#### 8.1.4 Types of failure of natural rock slopes

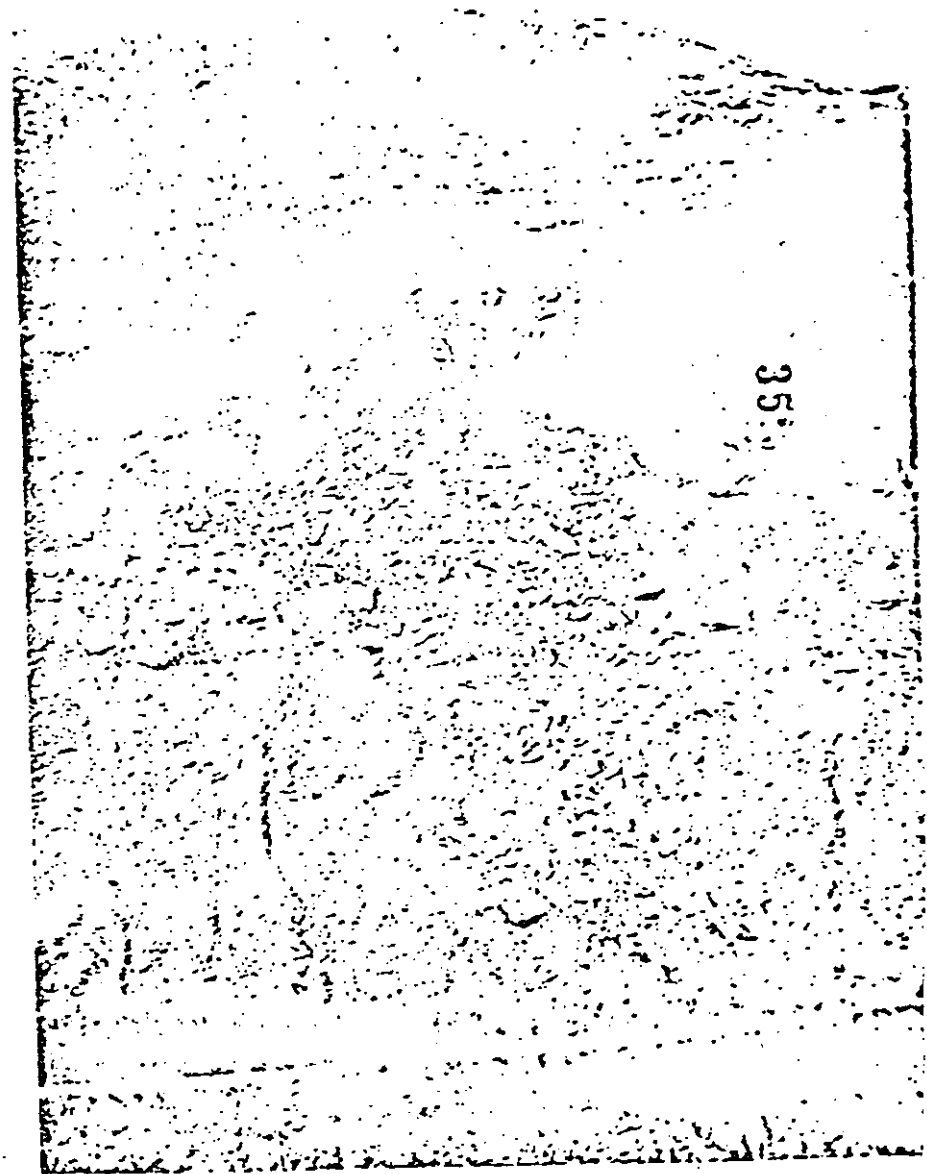
Minor rock falls are produced by weathering acting on unstable rock slopes. The susceptibility of a given rock to weathering processes can be estimated by determining its saturation moisture content ( $i_s$ ) and swelling coefficient ( $\epsilon_s$ ). Igneous and high-grade metamorphic rocks with  $i_s$  values of less than 1% are generally safe from weathering effects. Sedimentary rocks and low-grade metamorphic rocks are considered to be safe on slopes if their  $i_s$  values are less than 3%. If exposed rocks on a slope have high saturation moisture contents, then tests should be carried out over a period of time, under both freeze/thaw and wet/dry conditions, and their swelling behaviour noted. Ice action is important if joints are present. If the rock mass has a low block volume, that is, less than  $0.5 \text{ m}^3$ , minor rock falls may occur, even if the rock has a low saturation moisture content.

Major rock falls usually result from collapse caused by undermining of rocks above a weak layer (see Photo. 8.3) The agent may be weathering, erosion or mining. Common weaknesses in a rock mass which can lead to collapse after weathering and etching out by erosion are layers of clay rock, chlorite in joints and carbonate rocks, including calcareous sandstones.

Translational failure along a particular plane of weakness may occur in a rock mass cut by faults, master joints or steep bedding planes. Photograph 8.4 illustrates spectacular slope failure along San Andreas



Photograph 8.2 Slope failure at Sonoma County, California. (Reproduced by kind permission of California Division of Highways.)



Photograph 8.3 A major rock fall in the Scottish Highlands menacing the West Highland Railway. (Institute of Geological Sciences photograph, MNS1733(8) published by permission of the Director; NERC copyright.)

Table 8.1 Angles of frictional resistance ( $\phi$ ) and unconfined compressive strengths of some common rock types. The data are from Hoek (1970), Hoek and Bray (1974) and Attewell and Farmer (1976).

	$\phi_d$ (deg)	$\phi_{ult}$ (deg)	Unconfined compressive strengths (MN m <sup>-2</sup> )
<b>Igneous rocks</b>			
basalt	47	<45	150-300
dolerite	} similar to basalt		100-350
gabbro			250-300
andesite	31-35	28-30	
porphyry	40	30-34	
diorite	similar to granite		150-300
granite	>35	31-33	100-250
<b>Sedimentary rocks</b>			
sandstone/greywacke	27-38	25-34	20-170
siltstone	43	43	10-120
shale/mudstone	37	27-32	5-100
limestone	>40	33-37	30-250
<b>Metamorphic rocks</b>			
schist	variable, probably quite low		100-200
gneiss	variable, less than quartzite		50-200
quartzite	44	26-34	150-300
<b>Infill materials</b>			
	$\phi_{average}$ (deg)		
calcite	20-27		
breccia	22-30		
rock aggregate	40		
shaley material	14-22		
clay	10-20		



Photograph 8.4 Housing tract, Daly City, California, located on unstable ground in San Andreas Fault zone. Houses at end of tract (mid-right picture) removed after destruction by slide. (Reproduced by kind permission of US Geological Survey, Menlo Park, California.)

Fault Zone, California. The shear strength of the infill in these discontinuities determines the stability of any slope cut in the rock mass. As in soils, the shearing resistance along any plane is given by the equation

$$S = C_s + (\sigma - u) \tan \phi_s$$

where  $C_s$  is the cohesion between the two sides of the discontinuity,  $\sigma$  is the stress acting normal to the plane of discontinuity,  $u$  is the pore pressure in the discontinuity, and  $\phi_s$  is the angle of frictional resistance attributed to the plane of movement. In Table 8.1,

values of  $\phi$  are given: one ( $\phi_d$ ) assumes that there is some cohesion, the other ( $\phi_{ult}$ ) is for a cohesionless surface. Friction angles for materials commonly found infilling joints are given, as also are some representative values of unconfined compressive strength of rocks.

In rock masses with discontinuities which are not infilled, a slope will be stable only if the angle of dip of any discontinuities orientated towards the slope is less than the angle of friction,  $\phi$ , of the rock. Water pressure in the discontinuity may reduce the safe slope angle, and must be taken into account. If the angle of dip of a discontinuity is greater than the angle of friction, the slope will only be stable if there is some cohesion, that is, if  $C$  has a value greater than zero.

If the discontinuities are infilled with a weak mate such as clay,

stability of a slope in such a rock mass will depend on its shear strength. If a rock mass consists of alternating layers of strong and weak rocks, tests *in situ* and in the laboratory are necessary to determine whether failure is likely to occur because of shear failure in the weak bands, or because of sliding along the bedding planes, if they dip steeply.

Rotational failure occurs when the stresses generated by gravity on rocks near the slope exceed the inherent strength of the rock mass. It may be accompanied by translational failure. The extra load of a spoil heap may trigger failure of this type.

Creep failure takes place when certain rocks, such as clays, absorb water, swell, slowly deform and move downhill. If they are overlain by a more stable, stronger layer, translational failure may take place along the bedding plane between them. Cambering (p. 76) is produced in this way.

### 8.1.5 Stabilisation of slopes

Full accounts of slope stabilisation methods can be found in advanced texts such as Attewell and Farmer (1976). In brief, the three common measures taken to prevent slope failure are as follows:

- The slope is modified by removing material from the potentially active part of the slope and adding it to the 'toe' of the slope.
- The slope is drained to reduce load and increase strength or frictional forces by means of trenches filled with rubble.
- The slope is supported by a retaining wall or by embedded piles which are anchored to the rock mass. The soil and rock behind the wall must be drained.

### 8.1.6 Case history: the Kishorn Dock excavation, Wester Ross, Scotland

Some of the largest excavations of solid rocks made in the UK in the 1970s were in the course of preparation of sites at which oil production platforms could be constructed. Kishorn Dock is a site of this type excavated entirely in Torridonian sedimentary rocks (p. 104). The detailed section of these strata at the site is shown in Figure 8.1. The arkose (gritstone group) bands are unaltered, but the thin shaly layers contain some chlorite produced by very slight thermal metamorphism. These strata dip at angles ranging between 13° and

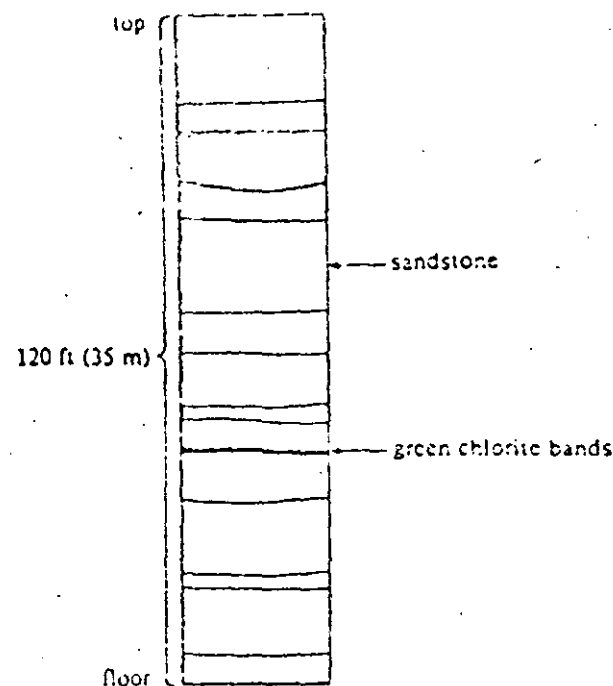


Figure 8.1 Section through Torridonian sediments at Kishorn Dock. Figure 8.2 gives precise location of section. The rocks include red coarse-grained arkoses (gritstone group) with intercalated green bands of chlorite. These bands comprise 5% of the total volume of the rock.

21° to the SW, and have strikes of between N315 and N330 (Fig. 8.2). The bedding plane discontinuities present little problem of instability in a vertical cut, but there is also a second important set of discontinuities which strike roughly parallel to the highest face of the excavation and dip steeply (at about 65°) in towards it. Table 8.2 gives data on all the discontinuities present. They are small reverse faults, which are secondary fractures related to the Kishorn Thrust plane. This is not present at Kishorn Dock, but crops out nearby. Before erosion to present land surface level, it lay a few hundred metres above the reverse faults seen in the Dock. The relationship of thrust and minor faults below it is a familiar model in structural geology, and the pattern could have been expected at the stage of preliminary investigation.

These discontinuities and the broken rock adjacent to them make the rock mass at Kishorn Dock inhomogeneous, potentially unstable in vertical cuts, and awkward to excavate. For example, a flat floor is an essential feature for a dock of this type, but one which was

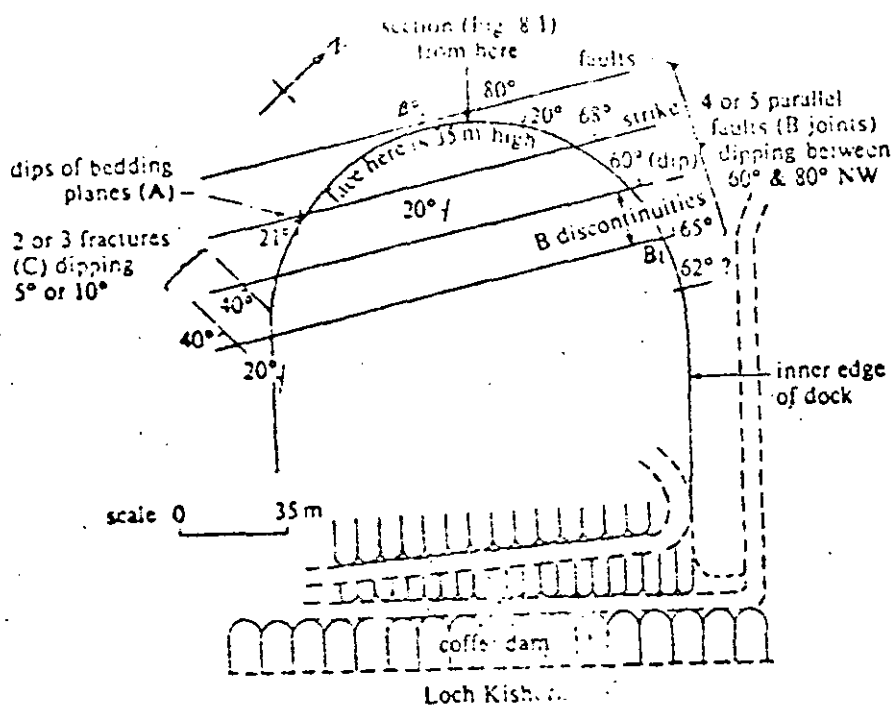


Figure 8.2 Map of the Kishorn Dock excavation showing the main discontinuities, and also the bedding planes of the rocks

Table 8.2 Discontinuity data (see Appendix H).

<b>A discontinuities (bedding planes)</b>	
(a)	spacing variable (see section)
(c)	tight discontinuity, rough irregular surface/no water flow
(d)	330°/20° SW (dip variable between 13° and 21°)
<b>B discontinuities (set of parallel faults - very rare)</b>	
(b)	very widely spaced 18 m
(c)	open discontinuity 10 mm, smooth with slickensides/no water flow
(d)	025° to 030°/60° to 80° NW
<b>C discontinuities (joint set) found in south excavation</b>	
(b)	very widely spaced 15 m
(c)	open discontinuity, smooth surface/no water flow
(d)	090°/40° S

difficult to achieve as mechanical shovels tended to gouge the fractured zones preferentially, and overexcavate locally. It also proved difficult to blast clean-angled benches on the excavated face, and raised the important question of what angle of slope was needed to make them safe? On the western side of the excavation, the strike of the reverse faults is tangential to the excavated face of the Dock, and their dip is away from the face at steep angles (more than 65°). When blasting took place there, the nearest fault plane to the face tended to open, and the wedge of rock between the plane and the face would spall off, leaving the Dock face with a dangerous overhang. The most stable Dock face there would be one with a low angle of slope (to the horizontal): theoretically a slope at right angles to the angle of dip of the reverse faults (i.e. an angle of about 30°). This angle would fit well with the friction angle data given in Table 8.2 (see sandstone).

In practice, it was not feasible because of cost, and because there was insufficient free ground at the edge of the excavation, to allow these shallower-angled benches to be dug. Instead, the slope angle of the main bench was reduced from vertical to 75°, and chain mesh was hung on the face to minimise the risk from any rock fall.

Stability of the face in the western part of the dock was confused and reduced by the presence of another important set of joints (the C joints in figure 8.2. The same considerations ruled out a slope of 35° but it was reduced from 80° to 45° and hung with chain mesh. These solutions proved to be adequate, and during the first two-year period after construction, no rockfall occurred.

## 8.2 IMPOUNDED SURFACE WATER: THE GEOLOGY OF RESERVOIR AND DAM SITES

### 8.2.1 Leakage and other considerations

A reservoir is meant to hold water, hence the principal geological criterion of the suitability of a reservoir site is that the rocks and soils around and below it form an impervious basin naturally, without need of excessive and expensive grouting of potential leakage paths. Other geological factors to consider are the consequence of a change in the position of the water table as the reservoir fills, and the rate at which sediment will accumulate in the reservoir.

The important sources of leakage from a reservoir are (a) rough

permeable soils, (b) through rock aquifers, and (c) along faults and master joints.

- (a) In regions which have escaped glacial erosion, there may be a thick mantle of weathered rock forming a permeable soil. In glaciated regions, however, soils (most notably boulder clay) may form a useful impervious skin on the reservoir, but other deposits (particularly sand and gravel) may offer paths for leakage. Buried channels, infilled with sand and gravel, are a possible hazard in both types of region. Superficial deposits can present other problems as well. Drift obscures the shape of the rock head surface. Peat may flavour and colour the water in the reservoir, and may need to be removed before filling it. A change in the water table as the reservoir fills may affect the stability of screes and other soils on the hillsides and cause landslides.
- (b) Leakage through rock aquifers is controlled by their structure, and its relationship to the hydraulic gradients produced by the head of water in the reservoir. For example, leakage along the sandstone layer (Fig. 8.3) would take place in structure b but not in a. The hydraulic gradient slopes down from the reservoir end of the aquifer to its outcrop in an adjacent valley. If, however, the water table in an aquifer, which forms one side of the reservoir (Fig. 8.3), were higher than the top water level of the impounded water, then flow would be towards the reservoir, and there would be replenishment rather than leakage. In general, dips of the aquifer towards the reservoir inhibit

leakage along it. Springs and seepages may be useful in indicating the position of the water table and the movement of ground water around the reservoir. Ideally, a reservoir should be sited on impervious rocks or, if only some layers are impervious, on a syncline plunging upstream. Limestone, and to a lesser extent sandstone with a calcareous cement, may present serious hazards. The calcite dissolves, especially if the water has been in contact with peat and is slightly acidic, and leakage paths progressively widen with time. The rock may become cavernous after several years.

- (c) Fault zones filled with pervious breccia and open joints may serve as paths for leakage. If the trend and location of a fracture offers a possible conduit then its outcrop in the reservoir valley should be sealed with grout. Fractures are particularly hazardous if they affect calcareous rocks and, if a reservoir must be sited on limestone, then extra effort and resources must be spent to locate and seal all faults and master joints. In glaciated valleys, incipient plucking of the rock surface by ice has opened fractures to produce lift joints. These may be present at depths up to 20 m.

The rocks below and at the sides of a dam should form part of the impervious basin together with the reservoir area, and the same geological considerations about avoiding leakage apply to it, plus some additional criteria. These include the strength of the foundations and the depth to rock-head.

Leakage under a dam leads not only to loss of impounded water but may also affect the foundations by the *uplift pressure* of the percolating water, and by erosion where seepage is discharged, on the downstream side of the dam. Progressive erosion of weak rocks or soils backwards along flow paths produces *pipng*, which can endanger the dam. The critical hydraulic gradient at which there is a danger of piping is approximately 1 in 1. To lower the gradient to at most 1 in 4, and also reduce leakage, the flow paths from the reservoir should be increased in length by constructing an impervious barrier before, below or behind the dam. This may be an apron of clay on the floor of the reservoir, a curtain of grout injected into the aquifer below the dam or a weir built on the downstream side. A filter of graded gravel at the outlet for the seepage may be added to prevent washing out of fine material.

Large dams are almost invariably founded on strong solid rock,

69

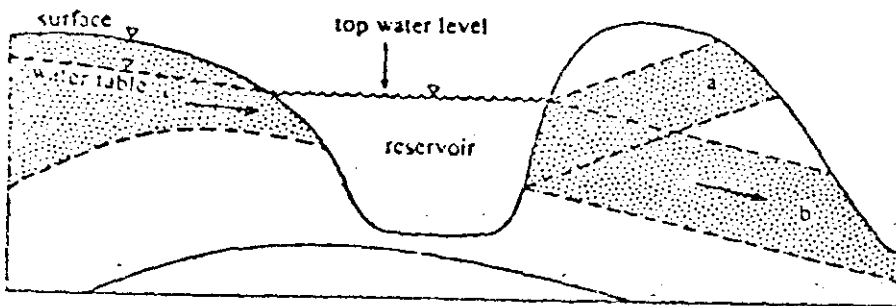


Figure 8.3 A sandstone aquifer (dotted) is a path of leakage from the reservoir if its structure is as represented by b, but not if it dips towards the reservoir as in a. On the left-hand side the water table in the aquifer slopes towards the reservoir and produces flow towards it.

and the thickness of any cover of soils and the strengths of the rocks, at the dam site are important factors in planning and costing the construction, and possibly in designing the dam. The additional excavation required at a site over a glacial rock basin, compared with one over a rock barrier which lies a few hundred metres away, may add significantly to the costs. It is important, therefore, to explore the position of rock head within the entire area of choice, and to make a contour map of rock head. The methods of systematic exploration are described in Chapter 6. Seismic-refraction surveys should be used, combined with borings, to define rock head, and may also be combined with laboratory measurements of specimens to delineate areas of badly fractured or rotten rock. At the later stages of exploration, rocks at the dam site should be inspected *in situ* for weathering and fracture, by digging pits or by boring large-diameter holes. Particular attention should be paid to mapping fractures which might behave as zones of seepage from the reservoir, and as zones of weakness under and at the sides of the dam.

### 8.2.2 Case history: leakage from Clubbiedean Dam, Midlothian, Scotland

An account of a major dam or of a spectacular disaster might be invoked to illustrate these basic geological points, but this can be done more simply by referring to a modestly scaled problem described by Sivasubramaniam and Carter (1969). Clubbiedean Dam is a small earth dam built in 1850 which impounds water for seasonal storage. Leakage had persisted over a long period, with eventually some local collapse, and visible free flow into the ground through cracks at the bottom and sides of the depressions. The succession of strata at the dam site (see Fig. 8.4) is as follows.

#### Carboniferous Old Red Sandstone

Calcareous shales and thin limestones  
 Top Sandstone – a soft grey limy sandstone  
 Top Marl – calcareous mudstone  
 Middle Sandstone – soft and permeable near rock head but otherwise well cemented  
 Middle Marl – calcareous mudstone  
 Bottom Sandstone – hard pink sandstone  
 Basal Beds – conglomerate with marl  
 Lavas – impermeable except where jointed

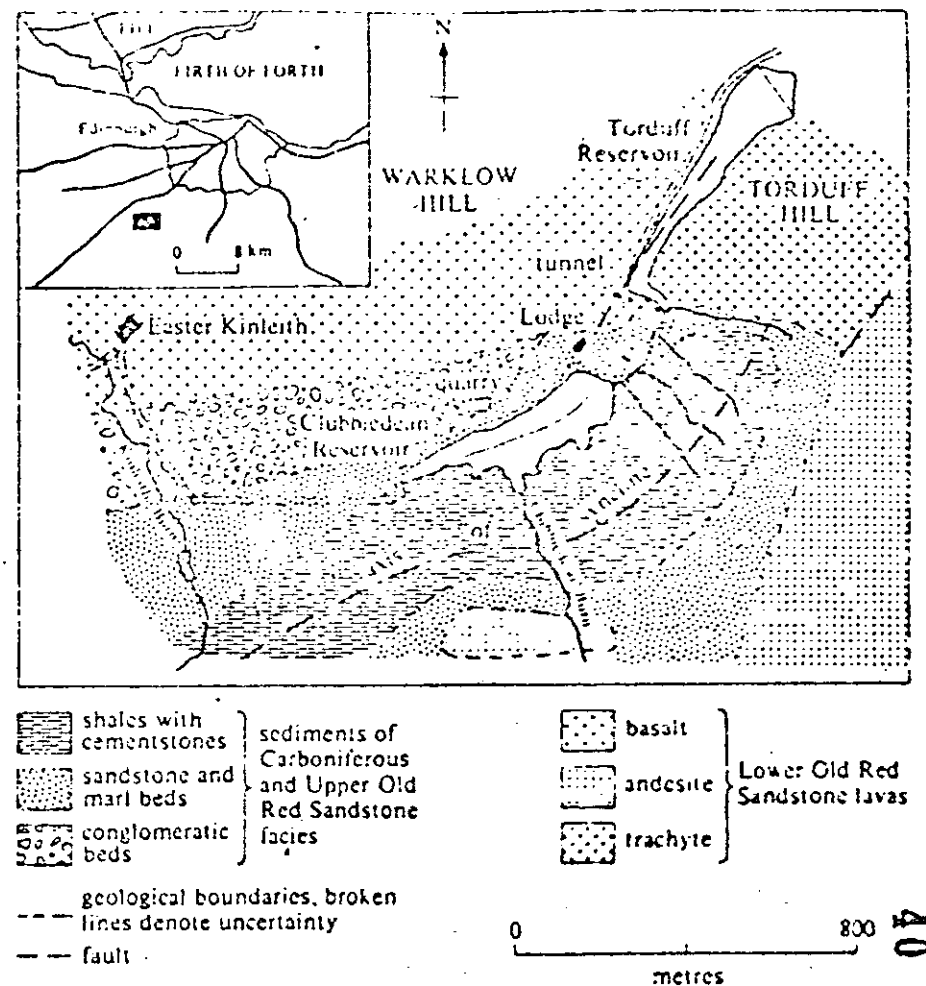


Figure 8.4 Geological map of the area around Clubbiedean Reservoir (from Sivasubramaniam and Carter 1969, by kind permission of the *Scottish Journal of Geology*).

The impermeable cover of boulder clay on the reservoir site, which might have afforded some protection against leakage, had been mostly stripped away either for use as fill in the dam, or as a result of erosion. The strata are folded into a shallow syncline, and the dam is founded on the northern flank of the syncline.

Leakage and subsidence were due to seepage through the sandstones, which had increased as solution cavities formed and quartz grains were washed away. The Top Sandstone is most



affected by cavities, and the Middle and Bottom Sandstones were similarly weakened where they are near the surface. The cavernous zone may have extended to a depth of about 10 m below rock head. During the site investigation by trial pits and bores, there was loss of circulation of drilling water, some sudden drops in drilling rods and poor core recovery.

The treatment used was to inject cement down a line of holes to form a grout curtain under that part of the dam where leakage was taking place. A total of 30 grout holes, some to a depth of 3 m, some to 6 m, and some to 10 m, were used. When the reservoir was refilled leakage was only 1% of the previous amount.

## 8.3 THE GEOLOGY OF TUNNELS

### 8.3.1 Geological considerations in tunnelling

In few engineering projects are the feasibility, the planning, the costing, the design, the techniques used and the risk of serious accidents during construction so dependent on the geology of the site as in tunnelling. The area in which a tunnel is built is determined by its purpose, but the decision to tunnel, rather than say build a bridge, is influenced by the relative geological difficulties, and the precise line of the tunnel may be determined by a choice of favourable or difficult local geological conditions. The relative ease of extraction of the rocks and the strength of the rock and face are prime factors in rates of progress, in planning costs, and also in determining whether a rock-boring machine can be used, whether the ground needs support and whether it is necessary to use compressed air. For example, if a buried channel or deep scour on the sea floor, infilled with saturated sand and gravel, were unexpectedly encountered, the resultant inrush of water at the tunnel face would result in a serious accident.

The geological factors considered in tunnelling projects are as given below:

- (a) the ease of extraction of the rocks and soils;
- (b) the strength of the rocks and the need to support them;
- (c) the amount inadvertently excavated beyond the perimeter of the tunnel outline (that is, overbreak), particularly where explosives are used;

- (d) the groundwater conditions and the need for drainage; and
- (e) the temperature in very deep tunnels and the need for ventilation.

The amount, or degree, of change in these conditions along the tunnel line can be as important in planning and costs as their average or maximum values. The change is related to structure, which not only controls what type of rock is present in a particular segment of the tunnel but also how its layering and other anisotropic properties are orientated relative to the tunnel face, and how weakened it is by fracture. Ideal geological conditions for excavation of a tunnel are to encounter only one type of rock, devoid of fault zones or intrusions, which is easily excavated but is stiff enough not to need immediate support near the face, which is impermeable and which is not adversely affected on exposure to air. By a fortunate chance, large areas of London are underlain by a layer (the London Clay) which approaches this ideal, and the most extensive system of tunnels in Britain (the London Underground and the London sewage tunnels) are excavated partly in it. Uniform geological conditions allow a uniform, if moderate, rate of progress without the troublesome and time-consuming need for changes of techniques, imbalances in the effort required from different work sections, and elaborate and vulnerable arrangements.

### 8.3.2 Methods of excavation

The main problem in constructing a tunnel through non-plastic soils or weak ('soft') rocks is to support the ground, rather than to excavate it. Excavation is usually done by a soft-ground tunnelling machine fitted with a rotary cutting head. This may have a full-face rotary breasting system which remains in contact with the soil face as the cutter head moves. Small slices of soil are fed through slots into the cutter head. The working face is supported by compressed fluid, which may be compressed air, either in the tunnel or, where a complex machine is used, restricted to the face area by a pressure bulkhead. The older method of having compressed air in the tunnel itself carries the risk of disabilities to workers, and requires time spent unproductively at the end of each shift on decompression. In recent, successful developments, a slurry of mud and water with thixotropic clay added is used at the face instead of air. The clay impedes settlement within the slurry, and tends to form a sealing

cake on the face. As the machine advances, supports are installed behind it. The type used depends on the particular geological conditions.

The principal factor controlling rate of progress and costs in constructing a tunnel in strong ('hard') rocks, is usually relative ease of excavation. The traditional method is to blast out successive sections of the tunnel by drilling a pattern of holes in the rock, charging them with explosives and firing. The need for any support and the type of support used are dependent on the relative stability of the roof and walls of the tunnel. For example, widely spaced rock bolts and wire mesh might be used as a shield for small loose fragments, and closely spaced ring beams might be employed where there was a danger of a rock fall. This approach is still used for the majority of modest projects of underground excavation, such as short, large-diameter rail or highway tunnels. Since the early 1950s, however, the use of explosives has been increasingly replaced by rock-boring machines for certain types of *major* tunnelling projects. The machines are heavy and expensive and may be designed specially for one major tunnel. Machines equipped with special cutters containing closely spaced tungsten carbide inserts seem to be capable of tackling rocks with compressive strengths in excess of  $300 \text{ MN m}^{-2}$ . The limiting factor in design is the strength of the cutter edge. The cutters usually wear out but, if they meet a hard block of rock during boring, they may smash on impact. Their rate of wear and replacement is an important economic factor in tunnel costs.

### 8.3.3 Complications arising from local geological conditions

In soft-rock tunnels, heterogeneous rock or variable conditions at the face can produce serious problems and add to costs. A boulder clay, or other soil containing large pebbles, creates a near-impossible problem for existing slurry-face machines. Hard-rock rolling cutters can cope with hard boulders, but have difficulty in other soft soils. A mixed face of hard rock and wet non-cohesive soil presents an even worse headache to the engineer. The variation of strength in the soils along the tunnel line should ideally be anticipated so that appropriate support can be used while the face is being excavated. Inability to do so can result in overexcavation. Apart from the obvious variations of strength among soil types (for example, between non-cohesive sand and partly consolidated clay), variation related to saturation and porosity may produce significant differences. A small

difference in water content can change an otherwise stable soil into running ground. Unstable soils can be consolidated by injecting chemicals or cement into them, or by freezing them.

In hard-rock tunnels, the relative difficulty of excavating particular rocks depends partly on whether explosives or a rock-boring machine is used. Nevertheless, both methods share some important factors. The rate of excavation in both cases is inversely related to the crushing strength of the rocks, and directly related to the amount of fracturing. When explosives are used, the relationship to strength is complicated by the way in which some weak non-brittle rocks, such as mica-schist, react to blast, and do not *pull* well for a given charge; and by the much greater role that fracturing plays. Fractures serve both as paths for expanding gases from the explosion, and as planes of weakness along which the rock will part. In tunnelling, the ease of drilling shot holes is dependent on the hardness and abrasiveness of the rock face (p. 235), and also of the variation of hardness within it, since, at a sharp boundary between hard and soft, the drill tends to be deflected. The hard mineral most likely to give any trouble is one of the varieties of silica, such as quartz, flint or chert, occurring as veins or nodular concretions. Shales containing ironstone nodules can also be an awkward mixture. Relatively hard minerals and strong rocks are often produced by thermal metamorphism. A weak, soft, calcareous schist may be altered to a strong, hard calc-hornfels. This proved to be a significant geological factor in certain hydroelectric projects, where the reservoir is sited on the high ground corresponding to the outcrop of a large granite intrusion. Tunnelling within the thermal aureole tends to become increasingly difficult as the granite is approached.

Excessive ease of extraction because of overhelpful planes of weakness can lead to overbreak (Fig. 8.5) and to potential rockfalls from the roof. A certain amount of excess excavation between the ideal outer surface of the lining and a pay line is usually covered by contract, but allowance for treating any overbreak beyond that is likely to be borne by the contractor and should be allowed for in his tender. Overbreak depends on the intensity of jointing and the presence of other planes of weakness, such as bedding and schistosity, and also on the orientation of the dominant planes relative to the tunnel face. In general, massive uniform rock, properly blasted, will give a clean section; well bedded, fractured rock will give overbreak. This is greatest in steeply dipping layers where the tunnel is parallel to their strike. For example, the overbreak in mica-schists

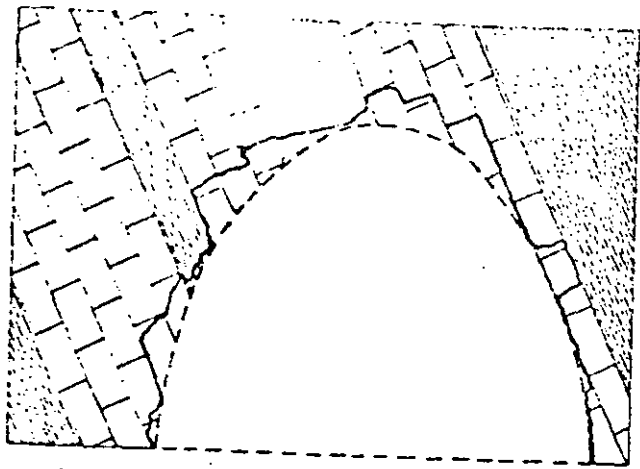


Figure 8.5 The ideal tunnel outline is shown by the broken line. The strata to be excavated are alternating shales and well jointed limestones, dipping steeply and striking parallel to the tunnel. The actual amount pulled out by explosives along the planes of weakness is indicated by the thick black line. This excess rock, excavated beyond the perfect section, is called overbreak.

was observed to vary in one tunnel from values of 16% across the foliation of 40% along it.

Predicting instability of the roof and the need to support and back-fill parts of a tunnel are problems common to both excavation by explosives and excavation by a rock-boring machine – as are seepage, water-filled soils in channels or fissures, swelling and popping rock, and high temperatures.

Excessive overbreak and the risk of rockfalls from the roof are most likely where the following conditions are met:

- (a) at fault zones, especially if they contain loosely cemented breccias;
- (b) at dykes, narrower than the tunnel, which have well developed horizontal cooling joints;
- (c) at synclinal axes, as the tensional joints developed at the hinge of the fold diverge towards the tunnel, and the blocks are not supported;
- (d) at layers of loosely compacted fragmental rocks, such as some volcanic breccias; and
- (e) where thin layers of strong and weak rocks (for example, alterations of limestone and shale) are present at the level of the roof, or strike along the tunnel and have a steep dip.

Where a tunnel is likely to follow such a zone of weakness for an appreciable distance, consideration should be given to re-aligning it. This may have to be done after excavation starts, if exploration has not revealed the structure. For example, the location of every minor dyke in a deep tunnel in a mountainous area cannot always be anticipated, but the trend of the dyke swarm is probably known, and may be used to assess the extent to which the dyke and tunnel line are likely to coincide.

The amount of seepage into a tunnel through pervious rocks and joints may be a significant factor in design. It must be assessed from a knowledge of groundwater conditions, bulk permeabilities of rocks and the geological structure. For example, crystalline rocks, such as granite, gneisses and schists, are typically dry except for flow along joints and faults, and perhaps at the margins of any dykes which cut them. In pervious rocks, the flow of ground water into the tunnel is likely to increase at fault zones, and at synclinal axes (which tend to channel flow towards the tunnel). Water-filled fissures, especially in limestones, present a more serious hazard, which must be insured against in certain projects by probing ahead of the working face with small horizontal boreholes. The consequences of driving the tunnel into the wet soils of a buried channel cut into the solid rock are so serious that exploration must be thorough enough to delineate rock head everywhere along most tunnel lines, particularly under the sea, under estuaries and under rivers. Depressions in the rock head surface may be pre-glacial channels or trenches scoured by strong tidal currents, or large fissures leached in limestone, which have subsequently been infilled with Pleistocene or Recent sediments. In areas which have not been glacially eroded, the bedrock near the surface may be altered by periglacial or other weathering, and consequently have a permeability and strength intermediate between its values when fresh, and those of any residual soils formed from it.

The temperatures in a tunnel, prior to ventilation, are related mainly to distance from the surface, the thermal conductivity of the rocks and the amount of water circulating through them. It is a significant factor only in very deep tunnels. Any sudden drop in temperature at the tunnel face is usually an indication that heat is being drawn from the rocks by circulation of water close to the face, and it may serve as a warning of a water-filled fissure and the threat of a sudden inrush. Inflow of warm water occurred in tunnels through the Alps.

At depths below about 150 m, the pressure of overburden is

augmented locally by appreciable secondary stresses in some parts of the excavation. The resultant strain in the rocks around the tunnel may take the form of swelling into the tunnel in shales, or some movement along bedding or other planes of weakness in brittle rocks. It may, however, produce explosive scaling from the surface of massive brittle rocks which cannot make such adjustments. This is called a rock-burst or popping rock and it can be hazardous. It is probably the cause of many of the minor tremors generated as mining subsidence takes place.

The prediction of ground conditions, and how they vary along the line of a tunnel, follows the general lines of site exploration described in Chapter 6, with appropriate emphases. Zones of weakness and permeability – particularly fault zones, buried channels, lenses of waterlogged running sand, and dykes – must be delineated with especial care. The rocks in many major tunnelling projects are covered by water, and continuous seismic-reflection profiling can be used to advantage. There is always need for a line of borings along the proposed tunnel, to prove the geology and provide samples for physical measurements. As a final check, test drilling may be done ahead of the working face by driving small holes outward from the face parallel to the tunnel axis to confirm the prognosis, and to ensure that no hazards are encountered unexpectedly. These points are illustrated in the case history in the next section.

Any need to change the method of excavation or support because of an unforeseen change of geological conditions can be a difficult and costly decision for a contractor. The accurate prediction of all such changes, before excavation starts, is more than can be provided by present exploratory methods. Some geological complications and hazards only become known as tunnelling proceeds. For these reasons, it is very important that the fullest possible appraisal of the geology is made, and that exploration is *not* thought to be finished once excavation has started.

#### 8.3.4 Case history: the proposed Channel Tunnel

The project to build a tunnel under the English Channel and link England to France by rail was shelved as one of the cuts made in British public expenditure in the mid-1970s. This was done, however, at a site where the geology of the site had been investigated and assessed by members of the Channel Tunnel Study Group, as part of a comprehensive study and estimate of costs (£454m at 1973 prices).

The project seems a reasonably sound one in terms of economic strategy, financial probity and technical feasibility. The prospects are encouraging and realistic enough to attract some private capital, and the technology already exists. The tunnel project may be revived as economic conditions are improved by oil revenues. The following account is drawn mainly from Destombes and Shephard-Thorn (1971), and from an account by Hanlon (*New Scientist* 60, no. 867, October 1973). The geological investigations and tests were carried out in 1964–5.

Where the Channel narrows, Cretaceous Chalk crops out on both coasts, and its low dips suggested that it might be continuous at the level of the tunnel from one end to the other. The geology below the Channel for some distance on both sides of the shortest route was reconnoitred using shallow seismic-reflection profiling (sparker). A pattern of lines, trending NE–SW at 0.5 km intervals, were linked by 12 tie lines to give several hundreds of kilometres of continuous profile. As a control on the interpretation of these lines, and to provide samples for testing, 73 boreholes were made in the sea floor and, in all 6 km of cores were recovered. Microfossils from them were used to recognise finer divisions within the Chalk, and so assist in delineating the detailed structure of the layering. Laboratory tests of permeability, water content, density and compressive strength were made, plus some others related to the problems of this particular tunnel: for example, ultrasonic velocity determinations for detailed sparker interpretation, variation in clay and calcite content, static strain modulus and slaking tests.

The investigations showed that the Chalk is folded gently into one major anticline and several lesser folds, all trending east–west. The maximum dips, up to 15°, are found on the French side. One fault with a throw of only 12 m was mapped, and the few others detected are even smaller. Tests in boreholes adjacent to some of them showed no significant increase of bulk permeability, and it is inferred that they are sealed by later mineralisation, or by clay. They do not represent a serious hazard. The sea floor is swept by tidal currents and superficial deposits are generally thin. Sand, migrating slowly in giant sand waves, is present near the French coast. There are also several deep hollows cut into the bedrock, which are filled with Pleistocene silt and sandy clay. The largest in mid-Channel extends to 140 m below sea level. Fortunately, the Chalk below them is unaffected by periglacial weathering and there is more than 25 m of sound rock above the tunnel along its entire route. This is considered

to be an adequate safety margin. The lack of weathering of the Chalk in the hollows indicates that the infill of drift was already present as a protective cover before the last glaciation (an alternative explanation, which is possible but less likely, is that some of the hollows are scours cut by strong tidal currents, which have been filled with recent sediment).

The lowered sea levels of Pleistocene times left the present sea bed of the Channel exposed to periglacial weathering, which has increased the permeability and lowered the strength of the Chalk by breakage and fissuring. The seismic velocity in the weathered Chalk is up to 30% less than in fresh rock. (This effect must be allowed for in interpretation of the sparker profiles.) The white Upper Chalk is the only layer seriously affected. The penetration of the weathering, particularly along joints, is controlled partly by the minor folds. The badly weathered zones can admit large amounts of water to lower levels to produce serious and unexpected water problems, but the tunnel line is sited safely below all known hazards of this type.

The permeability of chalk is inversely related to its clay content. A Channel Tunnel cut in chalk consisting of more than 80% calcite would probably suffer serious seepage, and this limit was a vital criterion in selecting which layer of the Chalk the tunnel should follow. The Chalk Marl, a layer up to 30 m thick within the Lower Chalk, has a suitable permeability combined with adequate strength to support the forward area until lining can be installed. It consists of a series of units, each 0.3–0.7 m thick, with clay-rich rock at the base grading upwards into purer, harder chalk. The ribs of chalk give strength and the clay acts as a sealant. The permeability of the matrix of the Chalk Marl is nearly zero across the bedding, and the effective bulk permeability *in situ* is entirely due to fissures. Assessments of strength are borne out by the fact that older trial tunnels excavated in the 1880s are still standing although they are unlined. The ease of excavation of the Chalk Marl by rotary cutting machines is shown by results of 30 m per day during trials.

It is possible to route the tunnel through Chalk Marl for most of its length, and the main geological complications are at the coasts. The low dips on the English side give considerable freedom of choice horizontally in siting terminal facilities, but the steep dips and narrower outcrops on the French side are more restrictive, unless a geological penalty is accepted. For example, the tunnel should preferably avoid the water-bearing sandstones that occur below the

Despite the careful preliminary investigation and its favourable results, there is still a possibility that some water-filled fissures – joints or bedding-planes – have not been delineated by the survey, and indeed cannot be recognised by present techniques with certainty. They present a potential hazard which must be insured against by stipulating that small-diameter holes should be bored ahead of the tunnel face to probe the rocks ahead. These holes would be fitted with valves so that they can be sealed and, if necessary, grout can be pumped into any pervious zone they penetrate to seal it. The cost of this procedure is largely determined by time delays when drilling of the main tunnels is halted.

The proposed design includes two main traffic tunnels and a central service tunnel. The main tunnels were costed on the basis of a diameter of 6.85 m, which would accommodate lorries at least 4 m high, loaded on rail transporters. The service tunnel would be advanced first, and borings could be made sideways from it to probe conditions along the sites of the two main tunnels. The net progress, including lining, was projected to 0.5 km per month for the service tunnel, and 0.75 km per month for the main tunnels. These estimates are based on an aimed excavation rate of 6 m per hour by the rotary boring machines.

The Study Group also reported on the geological factors relevant to an alternative 'immersed tube' scheme, in which an open trench would be excavated in the Channel floor, and special caissons, which would serve as segments of the tunnel, would be sunk into it. The topography of the sea bed is the most important factor in the choice of route, and feasibility, of this scheme. The principal geological consideration is ease of excavation of the trench. It was concluded that no particular difficulties would be likely where Chalk cropped out, but that the silt in the buried channels would be liable to collapse into the trench during construction. Mobile sand waves would also be a problem locally. Otherwise there appeared to be no serious problem of silting up of the trench by the movement of recent sediments.

## REFERENCES AND SELECTED READING

- 8.1 Attewell, P. B. and I. W. Farmer 1976. *Principles of engineering geology*. London: Chapman and Hall.  
 Bishop, A. W. 1973. The stability of tips and spoil heaps. *Q. J. Eng. Geol.*

- Fookes, P. G. and M. Sweney 1976. Stabilization and control of local rock falls and degrading rock slopes. *Q. J. Eng. Geol.* 9, 37-56.
- Geological Society Engineering Group Working Party 1977. The description of rock masses for engineering purposes. *Q. J. Eng. Geol.* 10, 335-88.
- Hoek, E. 1970. Estimating the stability of excavated slopes in opencast mines. *Trans Inst. Min. Metall.* 79A, 119-32.
- 1973. Method for the rapid assessment of the stability of three-dimensional rock slopes. *Q. J. Eng. Geol.* 6, 243-56.
- Hoek, E. and J. W. Bray 1974. *Rock slope engineering*. London: Inst. Min. Metall.
- Hutchinson, J. N. and D. Brunsden 1974. Mudflows: a review and classification. *Q. J. Eng. Geol.* 7, 327-8.
- Londe, P. 1973. Analysis of the stability of rock slopes. *Q. J. Eng. Geol.* 6, 93-124.
- Watkins, M. D. 1970. Terminology for describing the spacing of discontinuities of rock masses. *Q. J. Eng. Geol.* 3, 193-5.
- Weeks, A. G. 1969. The stability of natural slopes in south-east England as affected by periglacial activity. *Q. J. Eng. Geol.* 2, 49-62.
- Zaruba, Q. and V. Mencl 1969. *Landslides and their control*. Amsterdam: Elsevier.
- 1976. *Engineering geology*. Prague: Academia.
- 8.2 Little, A. L. 1977. Investigating old dams. *Q. J. Eng. Geol.* 10, 271-80.
- Sivasubramaniam, A. and A. V. F. Carter 1969. The investigation and treatment of leakage through Carboniferous rocks at Clabbiudean Dam, Midlothian. *Scott. J. Geol.* 5, 207-23.
- Stevenson, P. C. and W. R. Moore 1976. A logical loop for the geological investigation of dam sites. *Q. J. Eng. Geol.* 9, 65-72.
- Wahlstrom, E. E. 1974. *Dams, dam foundations, and reservoir sites*. Amsterdam: Elsevier.
- Walters, R. C. S. 1962. *Dam geology*. London: Butterworths.
- 8.3 Anderson, J. G. C. 1970. Geological factors in the design and construction of the Ffestiniog pumped storage scheme, Merioneth, Wales. *Q. J. Eng. Geol.* 2, 183-94.
- Carter, P. and D. Mills 1976. Engineering geological investigations for the Kielder tunnels. *Q. J. Eng. Geol.* 9, 125-42.
- Destombes, J. P. and E. R. Shephard-Thorn. 1971. *Geological results of the Channel tunnel site investigation 1964-65*. Rep. Inst. Geol. Sci. 71/11.
- Hanlon, J. 1973. Bore of the century? The Channel tunnel. *New Scientist* 60, 92-110.
- McGregor, K. 1968. *Drilling of rocks*. London: McLaren.
- Wahlstrom, E. E. 1973. *Tunnelling in rock*. Amsterdam: Elsevier.
- Wood, A. M. M. 1972. Tunnels for roads and motorways. *Q. J. Eng. Geol.* 5, 111-26.
- Robbins, R. J. 1976. Mechanised tunnelling - progress and expectations. *Trans Inst. Min. Metall.* 85A, 41-50.

FOUNDATIONS FOR DAMS  
ASILOMAR CONFERENCE GROUNDS  
INST. INGRA. E-9 U.N.A.M.  
ABRIL 1974

47

GEOTECHNICAL STUDIES FOR  
LA ANGOSTURA PROJECT

R. J. Marsal\*

SESSION:

ENGINEERS AND GEOLOGISTS

\* Research Professor, Instituto de Ingeniería, UNAM

INTRODUCTION	1
GEOLOGY	2
SEEPAGE INVESTIGATIONS	4
ROCK MECHANICS STUDIES	8
DAM CONSTRUCTION	11
COMMENTS	16
REFERENCES	17
TABLES AND FIGURES	19



The design, construction and even the operation of a dam, require the combined efforts of the geologist and the engineer in order to establish a thorough understanding of the geotechnical problems involved.

In the past, geologists commonly worked in isolation and produced thick reports containing general descriptions of the regional topography and geology, some information on the reservoir area and the account of explorations undertaken at the damsite. There was little interaction, if any, between geologist and engineer and the result usually was that the engineer failed to take into account important facts revealed by the geological survey. On the other hand, the geologist knew little of the bearing of these features on the project as a whole or on any particular structure. Therefore, no special studies were performed in time to avert a condition unfavourable either from the standpoint of economics or safety. Fortunately this state of affairs has improved as we travelled along a lengthy and sometimes arduous path, but much remains to be done to coordinate the joint interests of engineers and geologists.

To illustrate several aspects of the type of cooperative effort required, the geotechnical studies performed by the Comision Federal de Electricidad (CFE) and the Instituto de Ingenieria, UNAM, at the design stage and during the construction of La Angostura Project will be examined.

La Angostura Project is a hydroelectric power plant located in the upper Grijalva River, State of Chiapas (Fig 1). The dam is of rockfill type, 145 m high; it has a central, inclined clay core and pervious shoulders made of rockfill, sand and gravel. The total storage capacity of the reservoir is  $18 \times 10^9 \text{ m}^3$ , of which  $7 \times 10^9$  are needed for flood control. The spillways, two gated open channels with ski-jumps located in the left bank (Fig 2), are designed for a maximum discharge of  $6,000 \text{ m}^3/\text{sec}$ . The powerhouse was built in a cavern (right bank, Fig 2), approximately 22 m wide, 40 m high and 100 m long; it contains 3 x 150 MW units and four power transformers. The turbines are fed by lined tunnels 6.5 m in diameter, connected to the intake works through shafts where the emergency and service gates are installed. The river was diverted by means of two cofferdams, the upstream one being 60 m and the downstream 30 m high (Fig 3), and two concrete lined tunnels, 13 m in diameter.

#### GEOLOGY

The upper Grijalva River flows along the Chiapas Plateau through La Angostura Canyon, located 700 km South-East of Mexico City. For a schematic presentation of the structural geology and tectonics of this region see the N-S section of Fig 4. The plateau is divided in several blocks due to thrust faulting and the crystalline basement is underlain to the South by the Pacific basaltic crust.

In the reservoir area, the river cuts through stratified sedimentary formations of the Jurassic and Cretaceous ages composed of limestones and shales. These strata dip toward the North-East with an average inclination of 8 degrees.

Fig 5 presents the geology of the region bounded by the Grijalva and Santo Domingo rivers, both running in an almost parallel northerly direction. The map indicates the folding and the approximate boundaries of the different geological units that were identified in field inspections and by photogeological interpretation. The sequence of these units in a N-S section is attached to the above figure. The highly karstic stratum designated UD, underlies others of pure to clayey limestone; at La Angostura, the latter are covered by reefy formations and shales.

The structural geology and tectonics of this area is presented in Fig 6. The set of fractures was further traced and explored in the vicinity of the damsite, with the purpose of evaluating seepage losses through the abutments (see Fig 10).

Seismicity. Studies based on the location of epicenters and intensities of earthquakes in the upper Grijalva basin, indicate that this region is very active from the standpoint of seismicity. Since 1900 to date, 678 earthquakes of a magnitude exceeding 5 (Richter Scale) had the epicenters located in

the Chiapas area\*, six of them being of magnitude 7 or greater (Figueroa, 1973).

#### SEEPAGE INVESTIGATIONS

Reservoir. In view of the geological characteristics of La Angostura watershed, permeability investigations were undertaken at the early stages of the design. These studies consisted of topographical surveys, photogeological identification of prominent fractures and faults (Fig 6), and measurements of water table levels in the sedimentary formations, covering the area comprised by the Grijalva and Santo Domingo rivers. About 50 observation wells were drilled to depths of between 100 and 200 m, distributed over two areas, El Parral and La Angostura, as shown in Fig 7. Over a period of several years (since 1967), the water levels were determined and correlated with those of the Grijalva River. In general, the water table rises gently from the river to a distance of 2 km inwards, at which the elevation is higher than the intended pool level (N.W.S., 539.50). Thus, it was concluded that a seepage connection with the Santo Domingo River is unlikely.

Damsite. The selection of the damsite was influenced by the presence of a highly karstic limestone (unit UD) that outcrops in the reservoir (Fig 5). In preliminary studies, Sites I, II and III shown in Fig 6 were investigated. Site I, very at-

---

\*Region bounded by latitudes 14 and 19 degrees and longitudes 90 and 95 degrees (see Fig 4).

tractive from the topographical standpoint, was abandoned due to the poor conditions of the limestone in the left abutment (open fractures and solution conduits); furthermore, unit UD is only 20 m below the rock surface in the river. Site II was well suited for a concrete arch dam with tunnel spillways, but it is close to a conspicuous fault in the left bank (Fig 6). Finally, Site III was chosen for the rockfill dam as enjoying better geological conditions since it is 600 m downstream of the fault mentioned about and unit UD dips down 200 m below the river channel at this point.

The observation wells drilled at La Angostura (Fig 8) allowed the investigation of drainage conditions of the rock at the damsite area. Contour lines of the water table for two different dates (Oct. 1970 and Jan. 1972) are presented in the above figure. Neither sets of measurements reveal substantial differences with time. In the right bank, the water table rises from elevation 420 (river level) to 500, approximately, at a distance of 1 km; then, it decreases to elevation 460 at 1.5 km inwards from the river; finally, it climbs abruptly to elevation 595, the maximum observed at the farthest gage point. The zone of low water elevations reflects the influence of fractures on the drainage of this bank. The water table in the left side of the river varies from elevation 420 to maxima of 485 and 450 in October 1970 and January 1972, respectively; but, it falls to elevation 435 in the observation well located 1.5 km from the river. Further in-

side this bank, the water table rises again and attains elevations above the pool level (N.W.S., 539.50).

Water Absorption Tests (WA). Tests of this type were performed in most of the borings drilled at the damsite either for coring or piezometric observation. WA-values varied within a range depicted by the examples given in Fig 9. Water absorptions of 10 to 20 Lugeons were observed at some test sections, suggesting the presence of fractures or solution conduits in the limestone. However, a tendency of WA to diminish with depth was noted; with a few exceptions, WA was less than 2 Lugeons below river level. All the borings tested at this stage of the geological exploration were vertical.

The apparent inconsistency between water table measurements and the results of the water absorption tests commented above, promoted an additional study of the drainage conditions of the rock by means of inclined borings drilled in the vicinity of prominent fractures. Each of the selected fractures was intersected by three borings at different depths and water tested. The distribution and values of water absorption did not reveal much difference with those registered in vertical holes. It was confirmed that one has to expect greater permeability above the water table than in the deeper strata of both banks.

Based upon the above information, it was decided to 1) confine the grout treatment of the foundation and a-

butments to elevation 400; 2) drill holes inclined at 15 to 20 degrees to the vertical, and 3) distribute these borings in two lines using the split-spacing method.

Seepage Losses Through the Abutments. A problem posed by the presence of almost vertical fractures in both abutments, outside the zone to be grouted, was the evaluation of the potential seepage losses of water around the dam. This required a detailed mapping and inspection of the fractures together with hydraulic laboratory tests. Through the latter it was established that Dupuit's formula was acceptable for vertical open channels (fractures) of variable width with a horizontal bottom (Cruickshank, 1970).

The grid of fractures shown in Fig 10 was based on photogeological studies at the damsite, controlled by exploratory trenches and adits dug at several points. The width of the fractures and their probable variation with depth was the main unknown in the computations, because of the limited number of places where direct observation was possible. Therefore, ranges of width ( $\bar{w}$ ) and its coefficient of variation ( $V_w$ ) were chosen arbitrarily.

Expected values of the seepage losses  $E(Q)$  in  $m^3/sec$  for  $\bar{w}$  over the interval 1 to 20 mm and  $V_w = 0, 0.5$  and  $3$ , are presented in Fig 11 (Cruickshank, 1970). For  $\bar{w} = 5$  mm and  $0 < V_w < 3$ ,  $E(Q)$  varies from 1 to 10  $m^3/sec$ , approximately. Economic studies of the effect of water losses in the en-

ergy production of the power plant, showed that a maximum seepage value of  $20 \text{ m}^3/\text{sec}$ , about 7 per cent of the average rate of flow of the river, was admissible. Hence, the decision was taken 1) to limit the abutment treatment to about 100 m inside both banks in order to take care of tectonic fractures as well as those parallel to the canyon developed by stress relief, and 2) to find a feasible and economic way to seal, close to the slopes, the most prominent fractures connected to the reservoir. In this respect, a new series of exploratory trenches and galleries in the vicinity of several fractures was excavated upstream of the damsite. Only the fault located on the right bank (Fig 10) was grout treated, as described below.

#### ROCK MECHANICS STUDIES

For design purposes of the underground powerhouse and the stability investigation of spillway cuts, in situ and laboratory determinations as well as field measurements during the excavation of these structures were undertaken by CFE and analyzed by J. Alberro (1973).

Results of laboratory tests performed with specimens sampled in one of the three borings drilled around the powerhouse, are presented in Table 1. Standard deviations of the porosity, unconfined compressive and tensile strengths and moduli of deformation, show a rather high scattering in these characteristics for geological formations U2 and U3 (Fig 5), in which the cavern was to be excavated.



Table 2 presents average values of the static and dynamic moduli of deformation determined in two galleries dug in the right bank, 12 m about the vault and normal to the longitudinal axis of the cavern. These tests were made with rigid and flexible plates, the Goodman jack and the microseismic method, perpendicular and parallel to the stratification. Note the differences between the values of the static modulus parallel to the stratification for Galleries 2 and 3, which may be explained by the presence of fractures in the vicinity of the latter test gallery. Also, the Goodman jack values are low; this is attributed to fissuring around the test hole caused by horizontal tectonic stresses. Based on 1) the dynamic results; 2) the frequency of transversal waves, and 3) a known empirical correlation, the computed static moduli are 50,000 and 90,000 kg/cm<sup>2</sup> for the normal and parallel directions, respectively. These values agree with those obtained by means of static load tests.

Stress relaxation tests were carried out in the powerhouse area (Gallery 2), to investigate the magnitude and direction of tectonic stresses prior to excavation. The results of these measurements, combined with the computation of stresses due to the overburden, disclosed a horizontal tectonic stress parallel to the river of 80 kg/cm<sup>2</sup>.

An example of the effect of blasting on the slopes of the spillway channels is illustrated by Fig 12. The

displacements induced by the explosives (pre-split) during the excavation were measured with longitudinal extensometers and inclinometers. The horizontal deformations detected by Inclinometer 15 (Fig 12) was of 5 mm, about constant for a depth of 15 m, and nil for the underlying strata. On the direction of Extensometer 22, the displacements toward the hill increased from zero to 6 mm in the first five meters from the slope, and thereon decreased to zero over a length of 30 m.

Fig 13 shows measurements undertaken in Diversion Tunnel 1 during its excavation (performed in two stages) and afterwards. Displacements toward the tunnel in Points 1 and 3 registered with longitudinal extensometers were 8 and 5 mm, respectively, at the end of the first stage of excavation; they increased linearly with time and the effect of the second stage is not appreciable. Furthermore, the total vertical displacement of Point 3 was 13 mm over five months of observation, which means a deferred deformation 1.4 times greater than the initial deformation (5 mm).

Based on the mechanical characteristics of the rock and the evaluation of tectonic stresses, Alberro (1973) computed the deformations of the mass in the vicinity of the cavern for the powerhouse using the finite-element method. Fig 14 presents a comparison of computed and measured horizontal displacements at the end of excavation; the ratio between them is about two. As commented by Alberro, to account for

this difference one has to bear in mind 1) the effect of the blasting on the deformation of the mass, as disclosed by observations in the spillway (Fig 12); 2) the deferred deformations of the rock revealed by measurements in the Diversion Tunnel 1 (Fig 13), and 3) that the static moduli of deformation used in the analysis was determined in a loading process, whereas the stresses around the cavern are decreasing upon excavation. Had the dynamic moduli (Table 2) been used, the correlation between measured and computed deformations would have been almost perfect.

The above geotechnical studies helped in the planning of the excavation and reinforcement of the cavern, and also in the design of the gate structures of the spillway.

#### DAM CONSTRUCTION

Design. Feasibility studies which included several alternatives for the dam, powerhouse and spillway, showed that the most convenient scheme was that composed of a rockfill dam, two gated channels for the spillway and an underground powerhouse in the right bank (Figs 1 and 2).

The initially designed cross-section of the dam is shown in Fig 15. A rather thin core of compacted soil in the central portion supported by masses of rockfill, transitions zones and filters, are the main features of this section; the upstream outer slope is 2H:1V and the downstream,

1.8H:1V. The cofferdams are incorporated in the dam and removal of the alluvial deposits in the river channel was prescribed along the core and part of the pervious sections. About half the volume of the rockfill zones as well as the filters and transitions were to be compacted in layers by means of vibratory rollers.

The use of about 75 per cent of the rock to be excavated from the spillway area, was the economic concept of this design. The abovementioned percentage was based on the examination of cores obtained from borings drilled along the original location of the spillway and the experience gained in previous cuts along access roads. For reasons explained later, the estimation of useful rockfill was grossly in error and caused significant changes in the cross-section of the dam.

Foundation Treatment. As indicated above (Fig 15), the design called for the removal of the alluvial deposit prior to the placement of the core and part of the pervious zones. Exploratory borings showed that this deposit was essentially composed of sands and gravels, but there were doubts about the distribution of these soils and the possible existence of some layers or lenses of silty materials. Excavations in the river-bed (Fig 16) disclosed a mixture of sand and gravel interspersed with lenses of medium to fine sands; no silty or clayey soils were found.

Fig 17 shows the character of the rock upon

cleaning and trimming of the exposed surface. At the bottom, the rock was sound and presented small potholes, smoothed fractures and some karstic zones. On both sides of the canyon, the stratification of the limestone was clearly revealed by layers of hard clay or marl, which were eroded by the river to a depth varying from 10 to 50 cm. Weathered rock was removed and the important defects corrected by means of dental work. It is worthwhile noting that, upon finishing the excavation between cofferdams, the total seepage through the abutments and the cutoff walls was less than 20 l/sec for water heads of 40 m (Ramírez de Arellano and Moreno, 1972).

The transversal profile of the canyon shown in Fig 18 reveals pronounced overhangs on both sides and from elevation 520 to the crest (elev. 543) the limestone was fractured and weathered. These conditions of the abutments required 1) the excavation of a trench to place the core over sound rock, and 2) trimming and concrete fillings to improve the shape of the foundation surface. The profile of this surface along the core was recommended upon studies of tension zones by the finite-element method (Covarrubias, 1970).

The entire core-rock foundation was treated with water-cement grouts injected through 2 in. borings 8m deep, under a pressure of 1 kg/cm<sup>2</sup>. Grout takes of this blanket in different zones of the foundation are shown in Table 3.

Both the river channel and the abutments were

grout treated down to elevations 360 and 400, respectively. This work was done from galleries excavated at three elevations (Fig 19), one of them below the rock surface at the river channel (elev. 369). Mixtures with water-cement ratios of 1:1 to 10:1 by volume, were injected in 1.5 in. inclined holes drilled in at least two lines following the split-spacing method. A summary of this treatment is presented in Table 4. The total length of drilling was 48,840 m and the corresponding cement consumption of 3,216 ton; the average grout takes ranged from 0.03 to 1.73 m<sup>3</sup>/m. From the abovementioned galleries and upon finishing the grouting operations, a series of holes 3 in. in diameter at 10 m centers, were drilled to provide drainage.

After studies on seepage losses through fractures and subsequent exploration of the most important ones connected to the reservoir, it was decided to treat the fault located in the right bank 600 m upstream of the dam (Fig 10). The other fractures explored pinched a few meters inside the hill or had impervious fillings. The treatment of the abovementioned fault was performed from three galleries, using grout mixtures injected through a series of overlapping borings that extended from pool level to a few meters below the river deposit.

The effectiveness of the whole treatment described above is not known since the first filling of the reservoir will start on May 1974.

Rockfill Production. As mentioned previously, the original design of the dam called for the use of a large amount of the rock to be excavated at the spillway area. It should be mentioned that the first location of this structure was near the canyon and involved open cuts up to 100 m high. Since this was deemed undesirable in view of structural conditions of the rock mass, the discharge channels were moved inside the hill as shown in Fig 1 and the spillway works redesigned. The rock at the new location was explored with a limited number of borings; no substantial differences between this and the former exploration was detected.

As the excavation of the spillway channels progressed, the output of useful rock was low and its improvement with depth smaller than predicted. Both the useful and excavated volumes of rockfill as a function of time are plotted in Fig 20; by April 1972, the ratio of the above volumes was 0.41. In addition, the limestone was rather soft ( $q_u < 500 \text{ kg/cm}^2$ ) and it produced large quantities of fine particles. The breakage of rock fragments caused by four passes of a 13 ton vibratory roller was large, resulting in a mass of gravelly material with a high content of fines. At this stage of the construction it was decided to change the design of the dam by substituting an important amount of the compacted rockfill zone for sand and gravel, borrowed from alluvial deposits located from 4 to 7 km downstream of the site. Fig 21 presents the maximum cross-section of the dam as finally built; the to-

tal volume of the rockfill placed was  $1.96 \times 10^6 \text{ m}^3$ , 54 per cent of the material excavated at the spillway area. As a consequence, the actual cost of the dam compared with its bidding estimate increased 8 per cent.

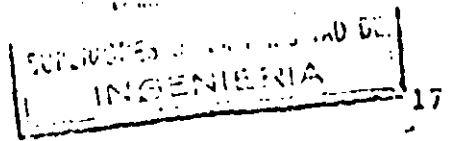
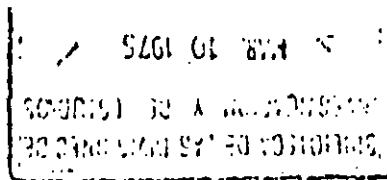
The use of the gravelly materials in lieu of the rockfill was beneficial. Due to the poor quality of the rock obtained from the reefy limestone, the deformation of the pervious mass induced by grain breakage would have been large, particularly during the first filling of the reservoir, and their effect upon the core almost unpredictable.

#### COMMENTS

a) Two problems in La Angostura Project remain uncertain, i.e., the permeability of the reservoir and the rate of seepage losses through the abutments. The first filling of the reservoir by the end of 1974 will allow us to confirm or rectify 1) the conclusion about the permeability based on the piezometric observations in the reservoir, and 2) the prediction about seepage losses through the fractures in both banks.

b) The reefy limestone in the spillway area, not detected until the excavation for the discharge channels was well advanced, brought substantial changes in the construction of the dam. Its original design contemplated the use of a large quantity of rock from the spillway. Due to the poor quality of the excavation product, the pervious zones of the dam were built with sand and gravel protected with the best rockfill





obtained from the abovementioned source. One has to admit that exploration was limited and that our experience of this type of sedimentary formation was scanty.

c) The geotechnical studies at the site not only contributed to the design of the underground powerhouse and other appurtenant structures, but also provided a better understanding of the tectonics and the behavior of the rock mass upon several types of excavation. Furthermore, the measurements in the spillway and Diversion Tunnel 1 suggested the possible causes for the differences between observed and computed displacements in the rock around the cavern for the powerhouse.

#### REFERENCES

1. Cruickshank C., 1970, "Flujo en un sistema de fracturas verticales", Publ. of the Instituto de Ingeniería, UNAM, N° 263
2. Covarrubias S., 1970, "Análisis de esfuerzos en la presa La Angostura", Report of the Instituto de Ingeniería, UNAM to CFE
3. Ramírez de Arellano L. and Moreno E., 1972, "Field Measurements at La Angostura Cofferdams", ASCE Specialty Conference, Purdue University, Vol. I, Part 1
4. Alberro J., 1973, "La Angostura Dam Underground Powerhouse: Prediction and Measurement of Displacements during Excavation", Third International Conference on Rock Mechanics, Denver, Col.
5. Figueroa J., 1973, "Sismicidad en Chiapas", Publ. of the Instituto de Ingeniería, UNAM, N° 316

TABLE 1. TEST RESULTS FOR SAMPLES OF BORING CM-1 AT THE POWERHOUSE AREA

Test parameter	Formation	Number of tests	$\bar{x}$	$\sigma$
Porosity (n), %	U2	44	14.1	9.1
	U3	38	22.8	5.0
Unconfined compressive strength ( $\sigma_c$ ), kg/cm <sup>2</sup>	U2	55	404	96
	U3	51	202	79
Tensile strength ( $\sigma_t$ ), kg/cm <sup>2</sup> (Brazilian test)	U2	23	32.4	46
	U3	20	22.9	11
Modulus of deformation (D), 10 <sup>3</sup> kg/cm <sup>2</sup>	U2	27	166.3	59.3
	U3	29	126.5	46.7

$\bar{x}$  = average value

$\sigma$  = standard deviation

TABLE 2. IN SITU MODULI OF DEFORMATION, GALLERIES 2 AND 3, LIMESTONE FORMATION U2 (Alberro, 1973)

Test site	Type of test	Direction	Number of tests	Mean value of D, in kg/cm <sup>2</sup>
Gallery 2 (in a zone of sound rock)	Rigid plate $\phi = 28$ cm	//	4	130 380
		⊥	6	43 740
	Flexible plate $\phi = 1$ m	//	4	126 830
		⊥	2	55 980
	Goodman jack	//	6	57 500
		⊥	2	49 000
	Micro-seismic	//	1	190 000
		⊥	1	150 000
Gallery 3 (close to a zone affected by vertical fractures)	Rigid plate $\phi = 28$ cm	//	3	17 520
		⊥	4	40 760
	Flexible plate $\phi = 1$ m	//	1	54 100
		⊥	2	44 840
	Microseismic	//	1	170 000

D = modulus of deformation

TABLE 3. DATA ON THE GROUT BLANKET

Section	Length of drilling (m)	Cement consumption (ton)	Grout takes (m <sup>3</sup> /m)			
			Stage I	II	III	IV
River channel	4 900	191	0.09	0.07	0.18	-
Right bank	5 690	611	0.32	0.21	0.28	0.24
Left bank	5 250	545	0.30	0.31	0.26	0.08

TABLE 4. DATA ON THE GROUT CURTAIN

Section	Length of drilling (m)	Cement consumption (ton)	Grout takes (m <sup>3</sup> /m)			
			Line A	B	C	D
River channel	2 030	64	0.14	0.05	-	-
Right abutment	2 260	190	0.26	0.13	0.24	0.34
Left abutment	1 970	102	0.16	0.14	0.23	0.05
Gallery No 1	6 910	74	0.06	0.03	0.02	-
Gallery No 1 bis	1 590	23	0.04	0.06	0.09	-
Gallery No 2	6 520	166	0.10	0.06	0.04	0.12
Gallery No 3	5 680	957	0.60	0.37	0.31	0.23
Connection No 3	2 800	732	1.72	0.61	0.17	0.10
Gallery No 4	7 880	701	0.31	0.20	0.11	0.18
Gallery No 5	9 300	205	0.10	0.06	0.06	0.04
Gallery No 6	1 900	2	0.02	0.04	-	-

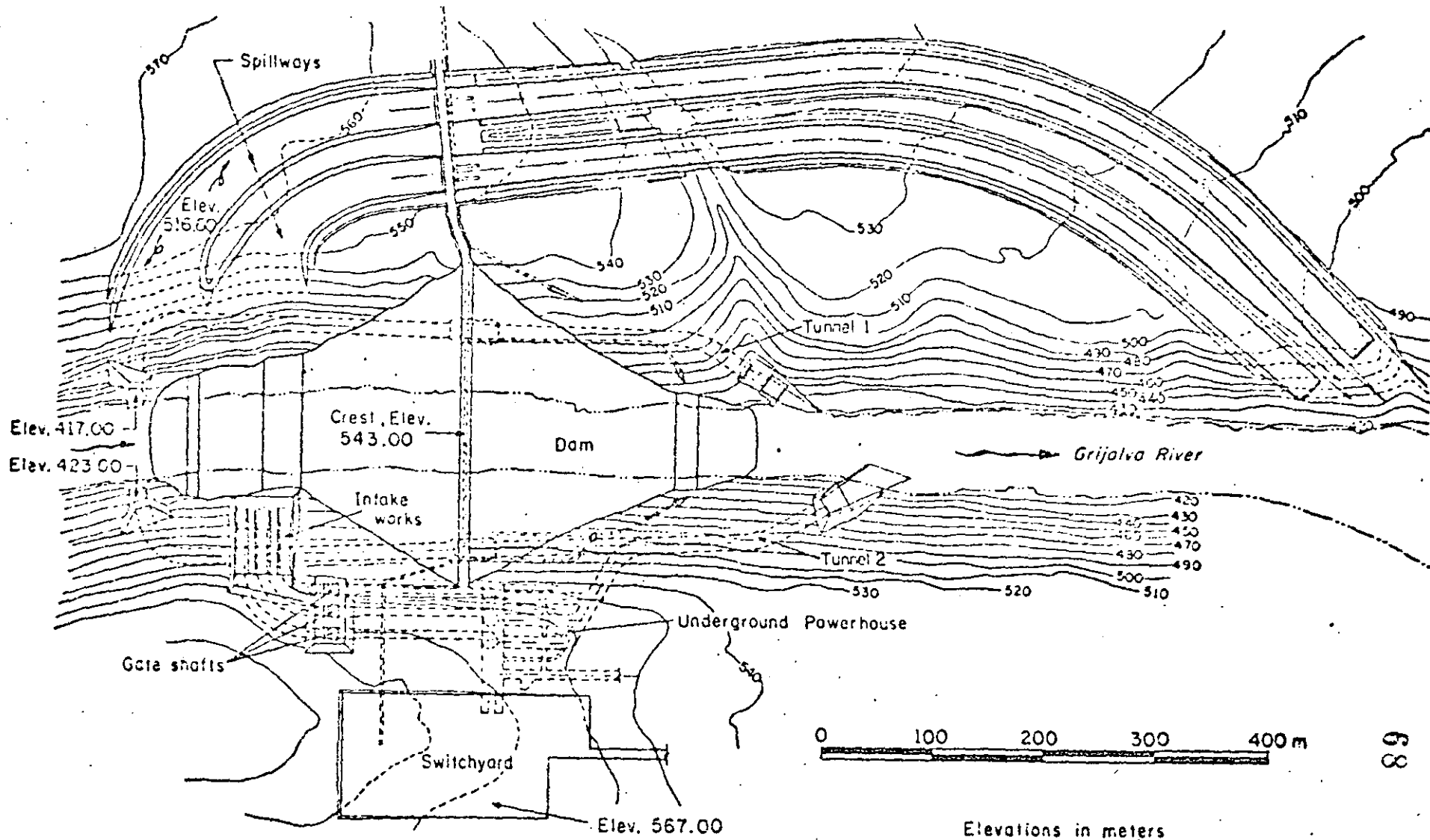


Fig 1. Plan view of La Angostura Project

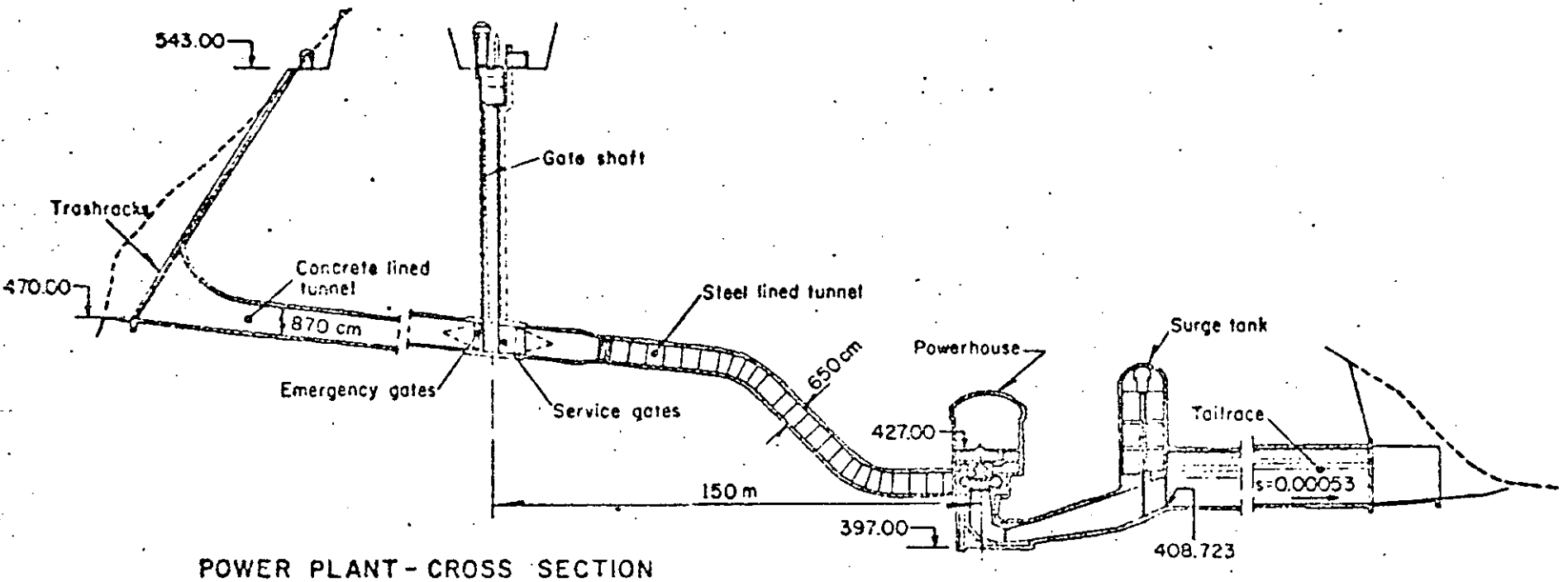
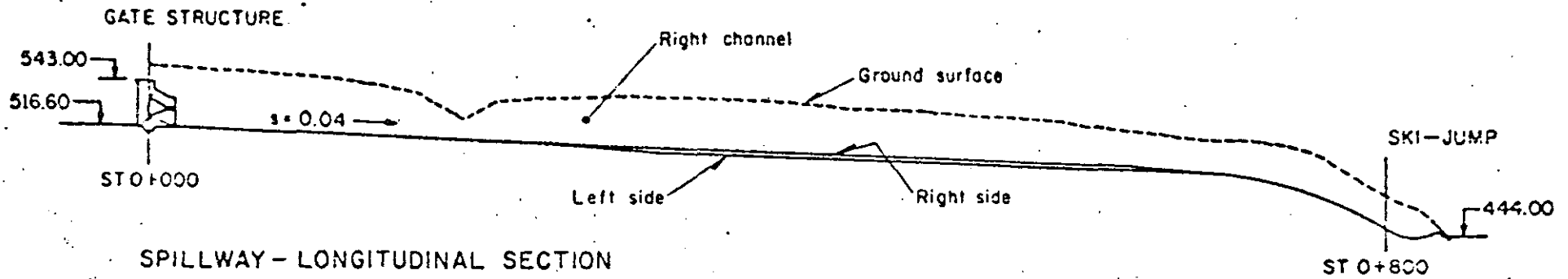


Fig 2. Spillway and Power plant

- ① River bed materials
- ② Dumped rock
- ③ Dumped clayey soil
- ④ Compacted clayey soil
- ⑤ Compacted sand and gravel
- ⑥ Rockfill

Total volume : Upstream cofferdam 490,300 m<sup>3</sup>  
Downstream cofferdam 101,000 m<sup>3</sup>

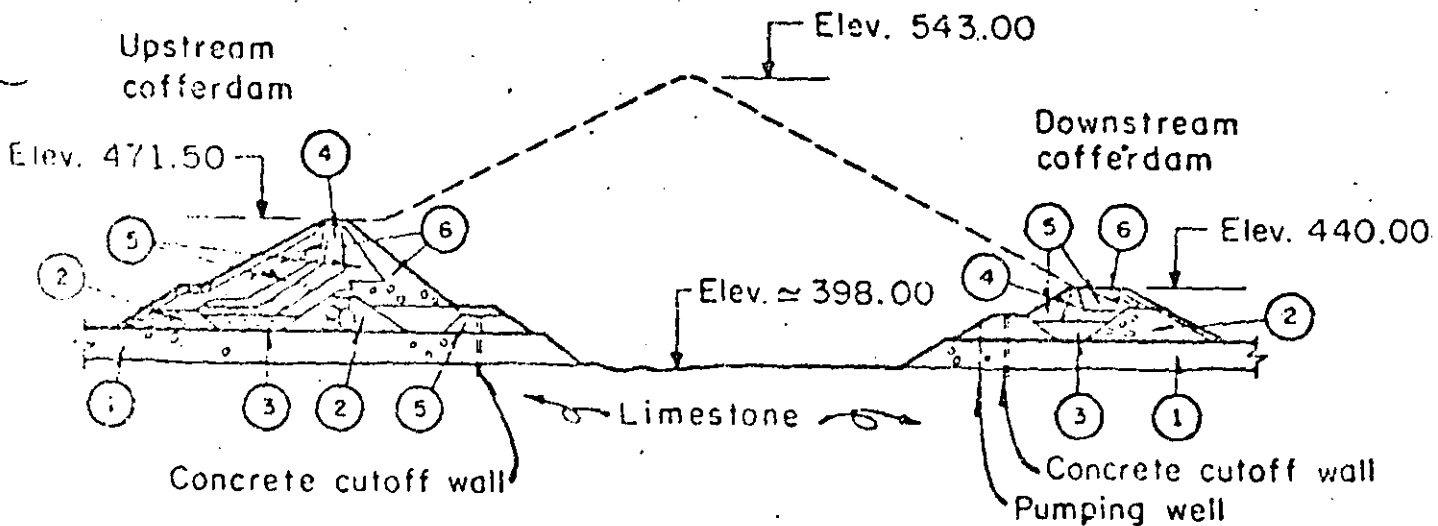
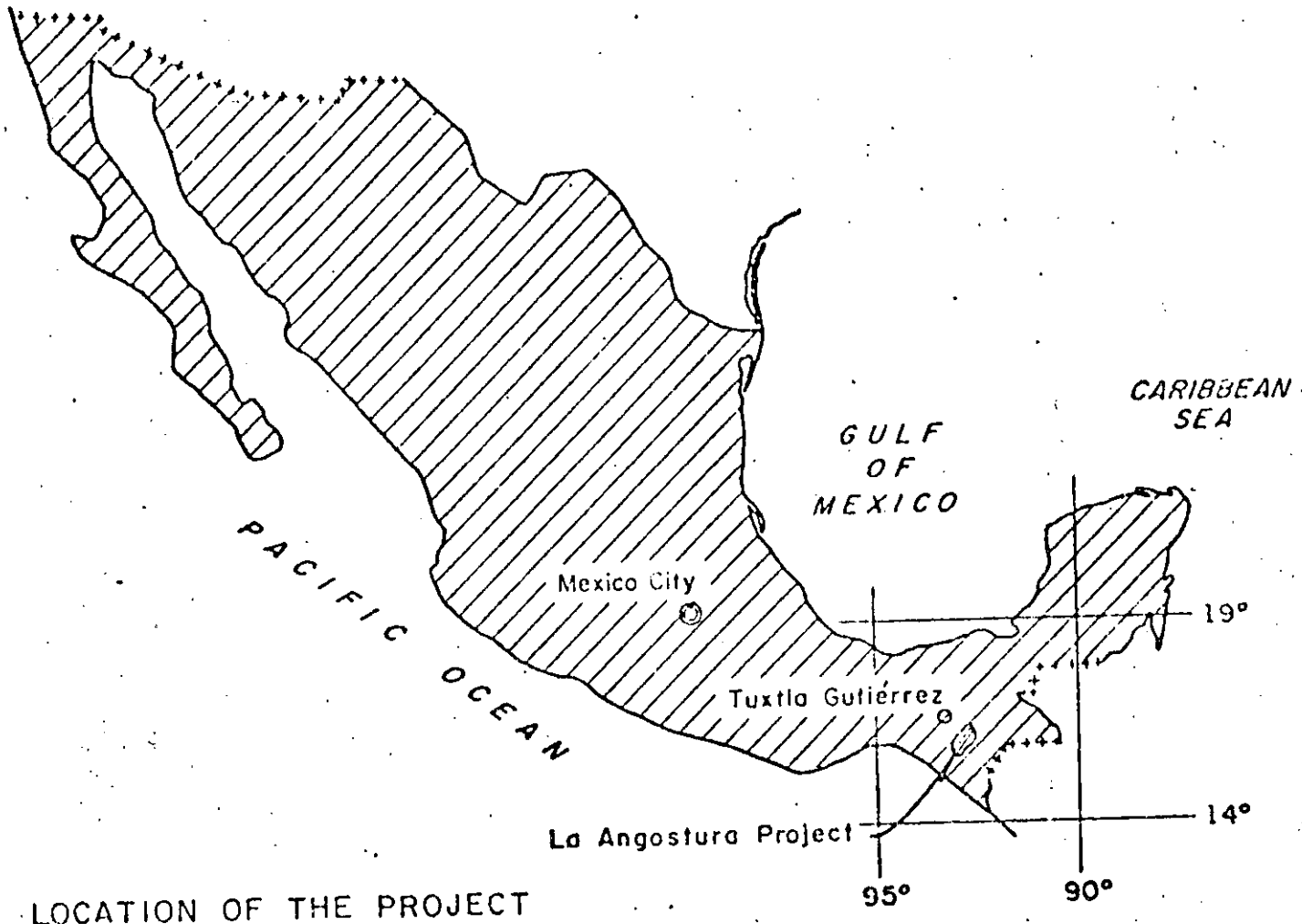
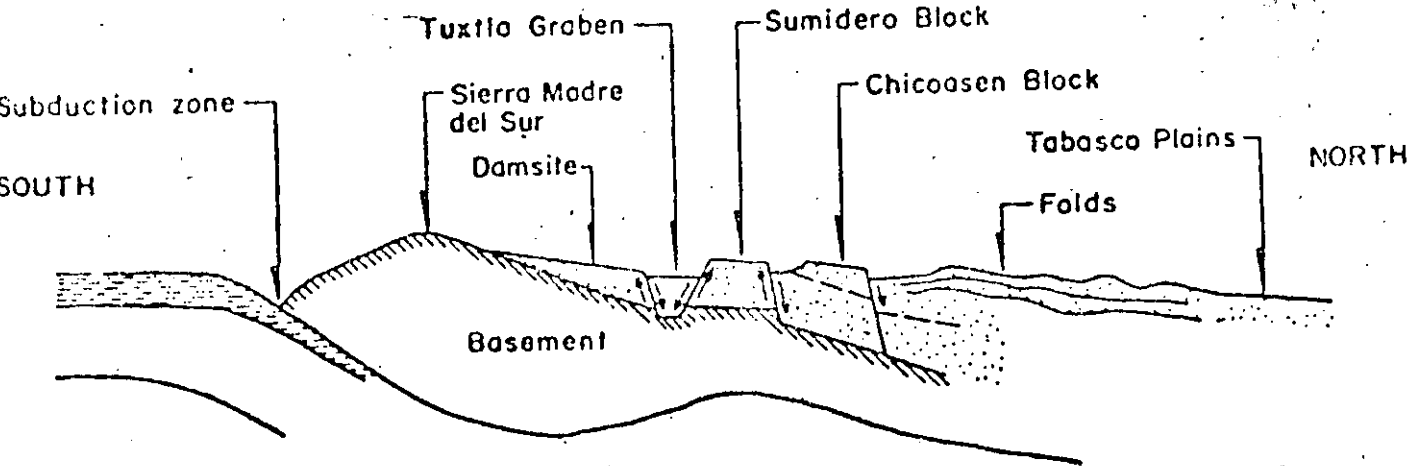


Fig 3 . Cofferdams for diversion of the river (Ramírez de Arellano and Moreno , 1971)

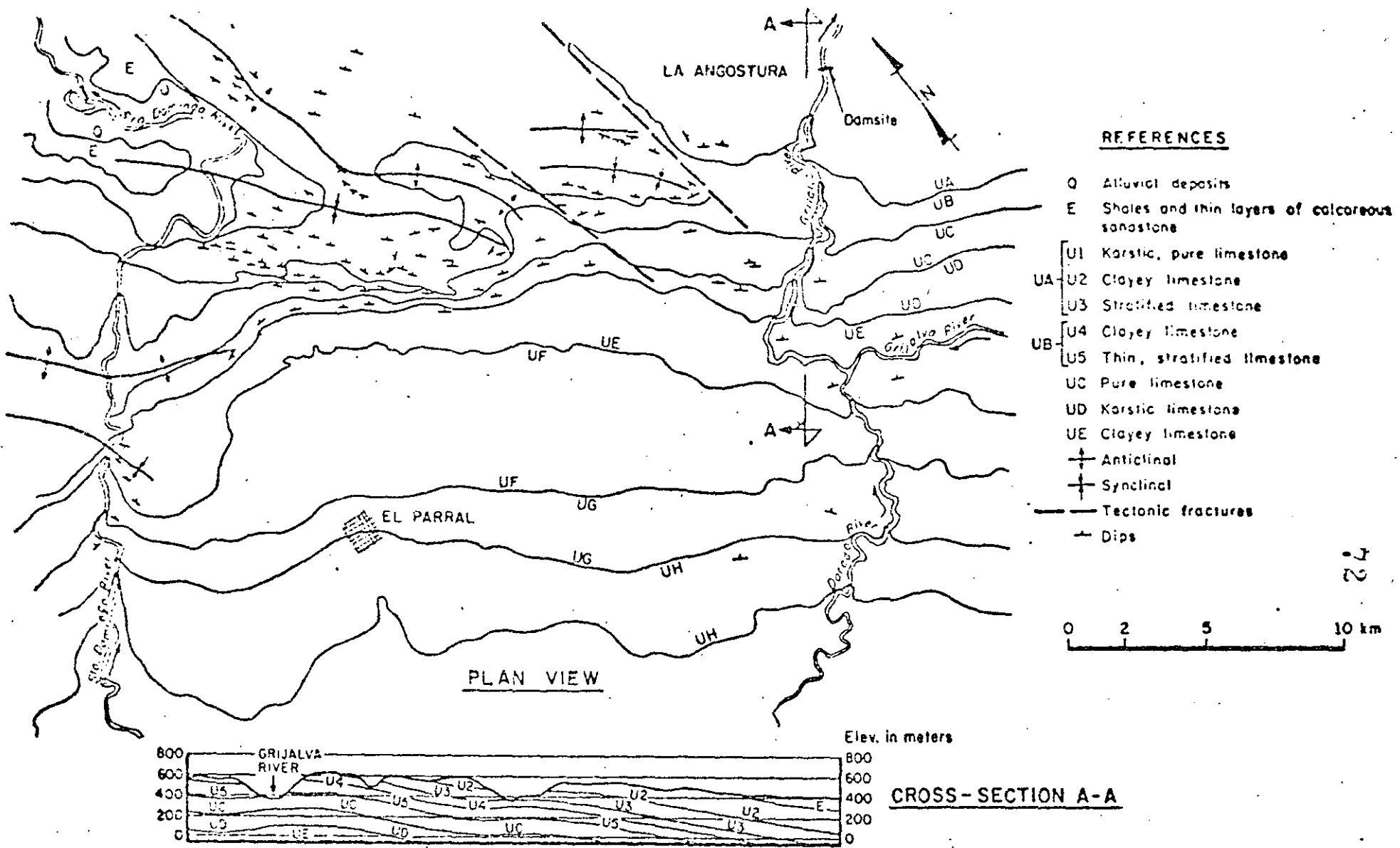


LOCATION OF THE PROJECT



N-S SECTION OF CHIAPAS (F. MOOSER)

Fig 4. Location of La Angostura Project and structural geology of Chiapas

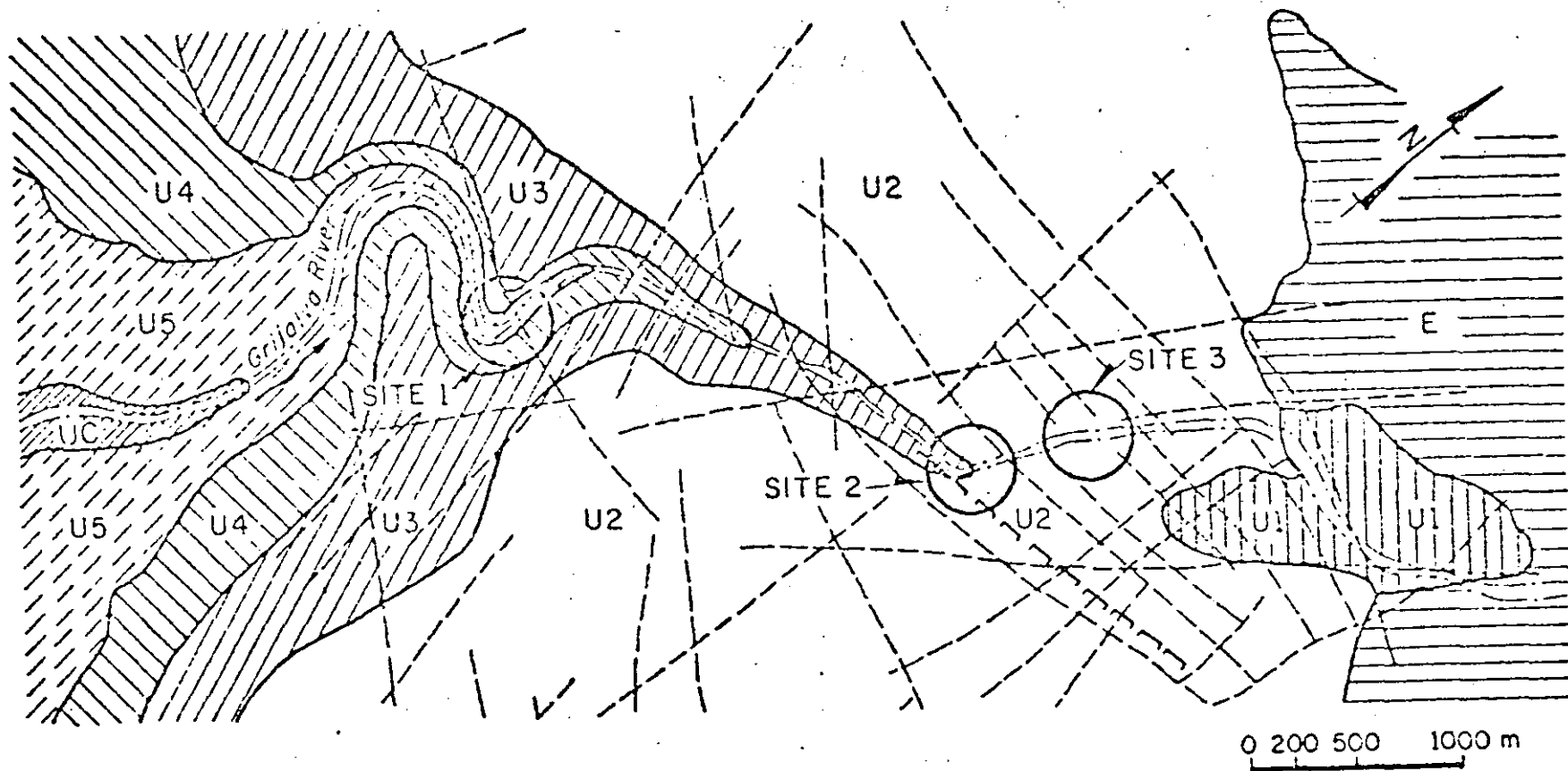


**REFERENCES**

- O Alluvial deposits
- E Shales and thin layers of calcareous sandstone
- U1 Karstic, pure limestone
- U2 Clayey limestone
- U3 Stratified limestone
- U4 Clayey limestone
- U5 Thin, stratified limestone
- UC Pure limestone
- UD Karstic limestone
- UE Clayey limestone
- Anticlinal
- Synclinal
- Tectonic fractures
- Dips

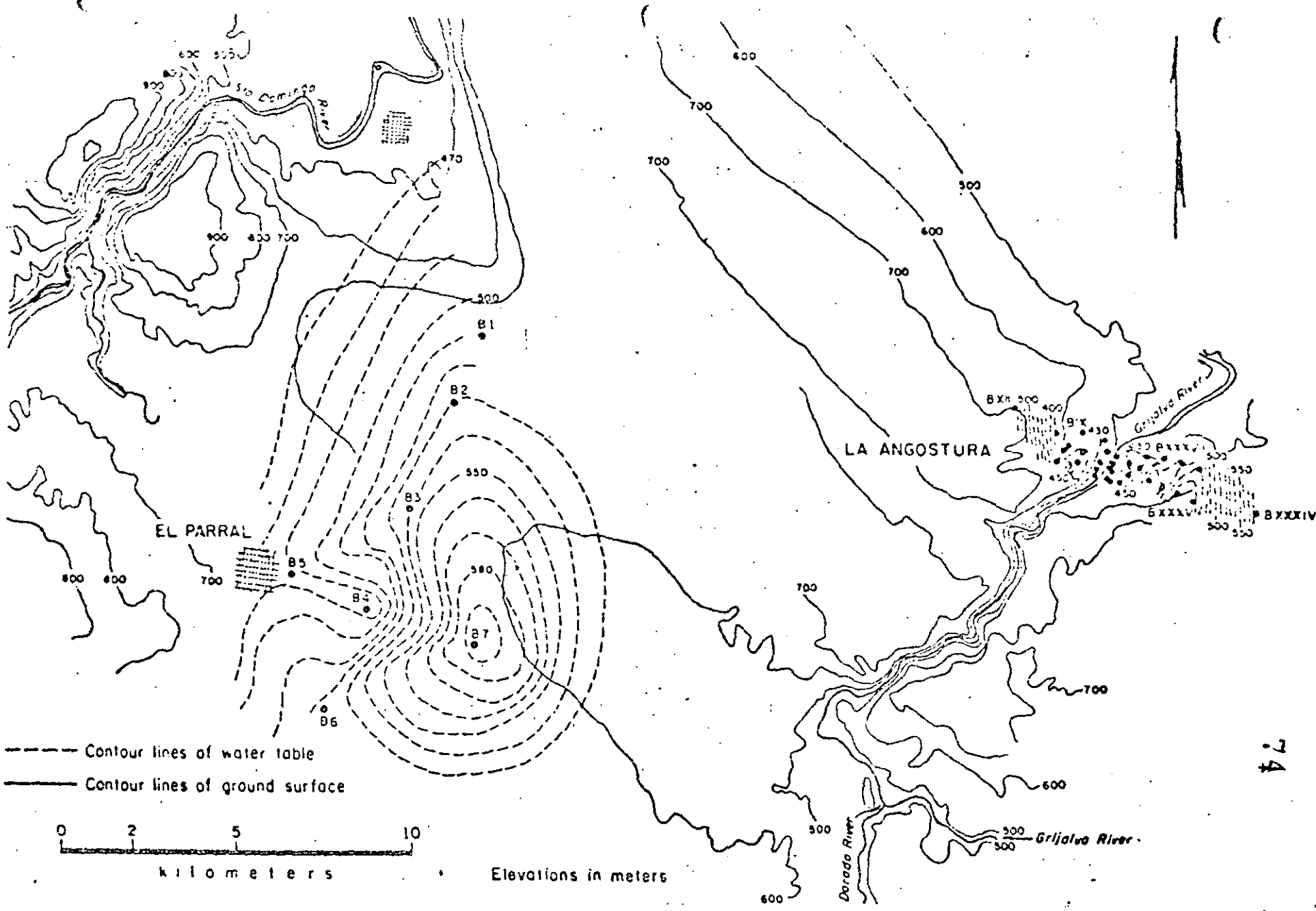
Fig 5. Geology of the region bounded by the Grijalva and Santo Domingo rivers





- |     |  |     |                               |
|-----|--|-----|-------------------------------|
| --- | Tectonic fractures                               | --- | Fault                         |
| UA  | U1 Karstic, pure limestone                       | UB  | U4 Clayey limestone           |
|     | U2 Clayey limestone                              |     | U5 Thin, stratified limestone |
|     | U3 Stratified limestone                          |     | UC Pure limestone             |
|     | E Shales and thin layers of calcareous sandstone |     |                               |

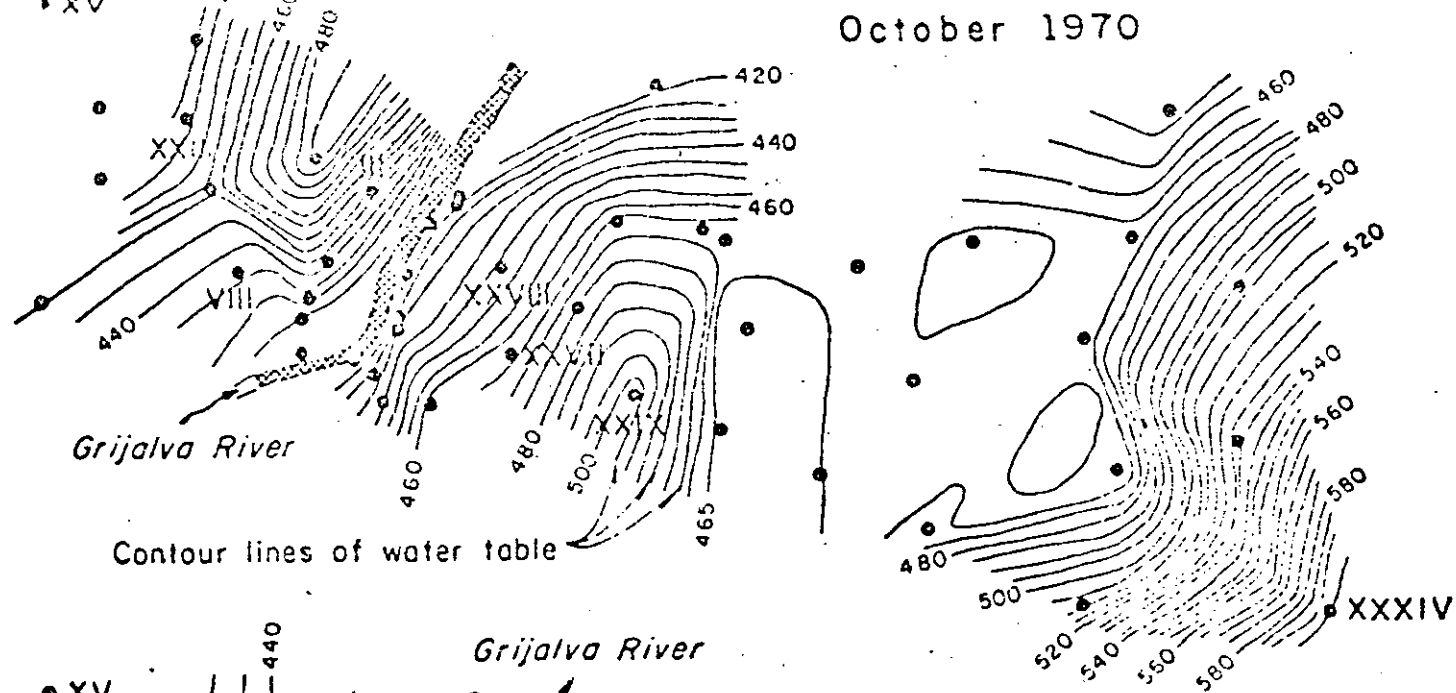
Fig 6. Geology and tectonics of La Angostura Canyon



74

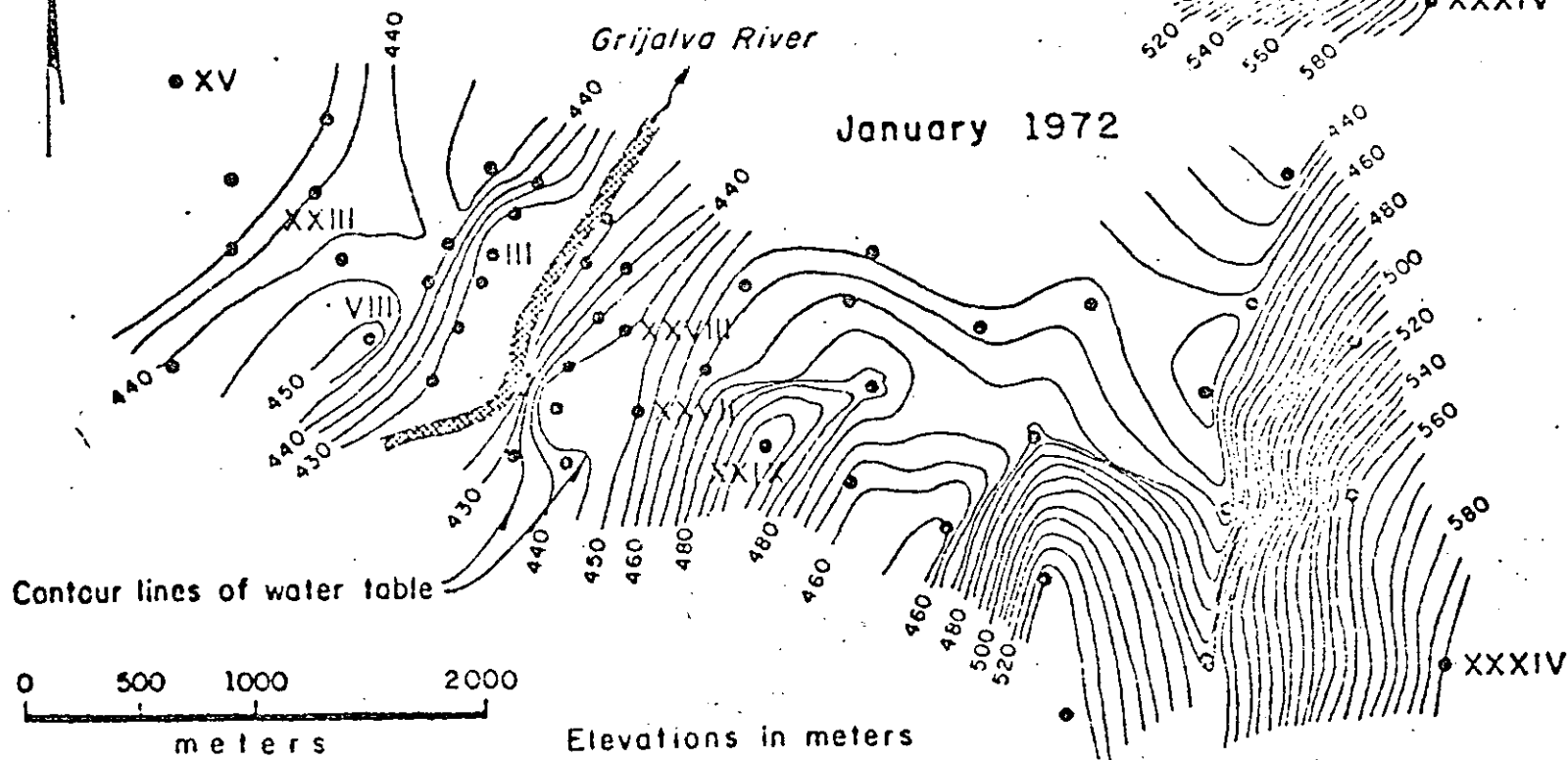
Fig 7. Water table observations in the Parral and La Angostura areas

October 1970



Contour lines of water table

January 1972



Contour lines of water table

Elevations in meters

Fig 8. Water table observations at La Angostura

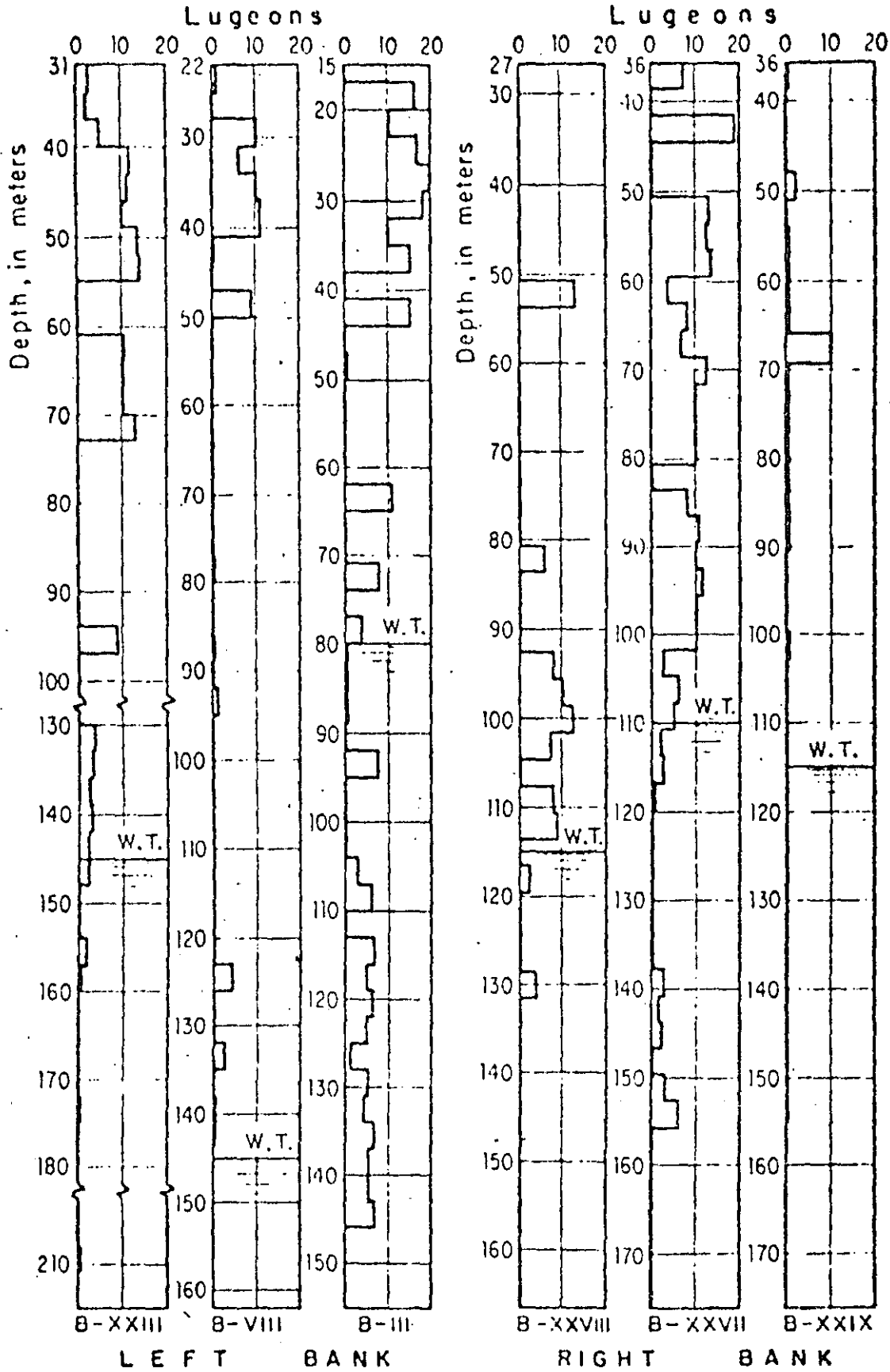


Fig 9. Water absorption tests at the damsite

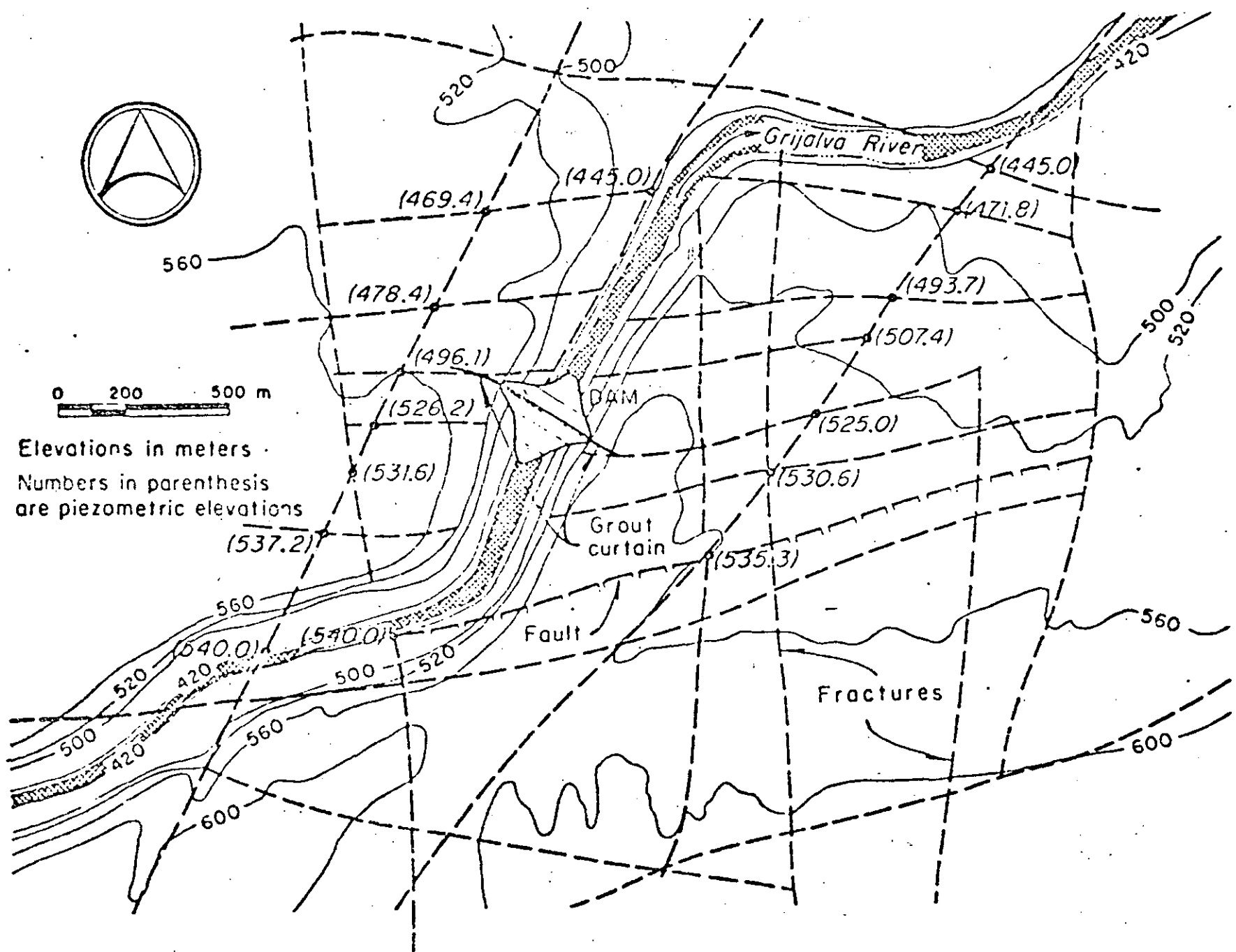


Fig10. Grid of fractures and some of the computed piezometric elevations at La Angostura damsite

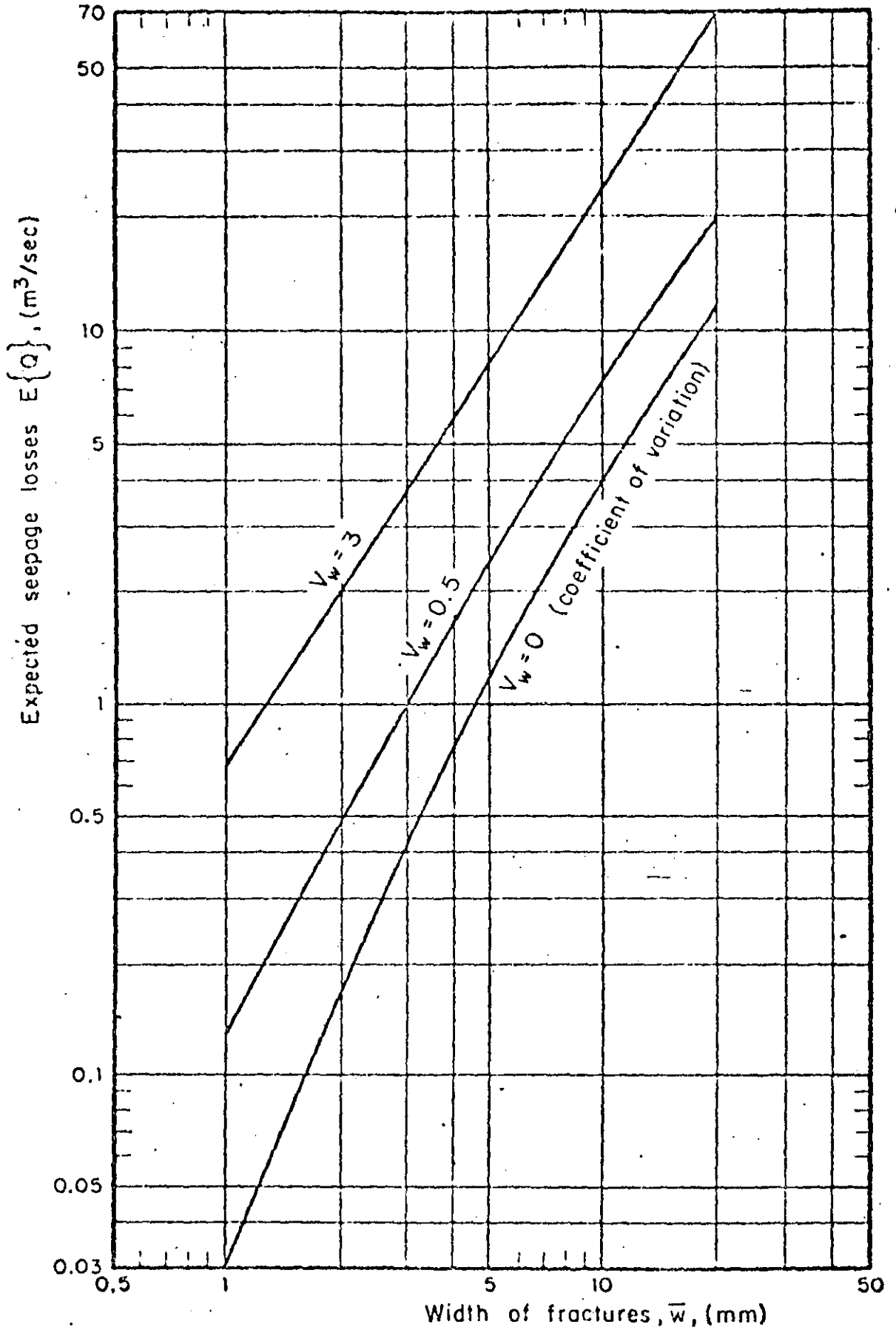


Fig 11. Seepage losses vs width of fractures (Cruckshank, 1970)

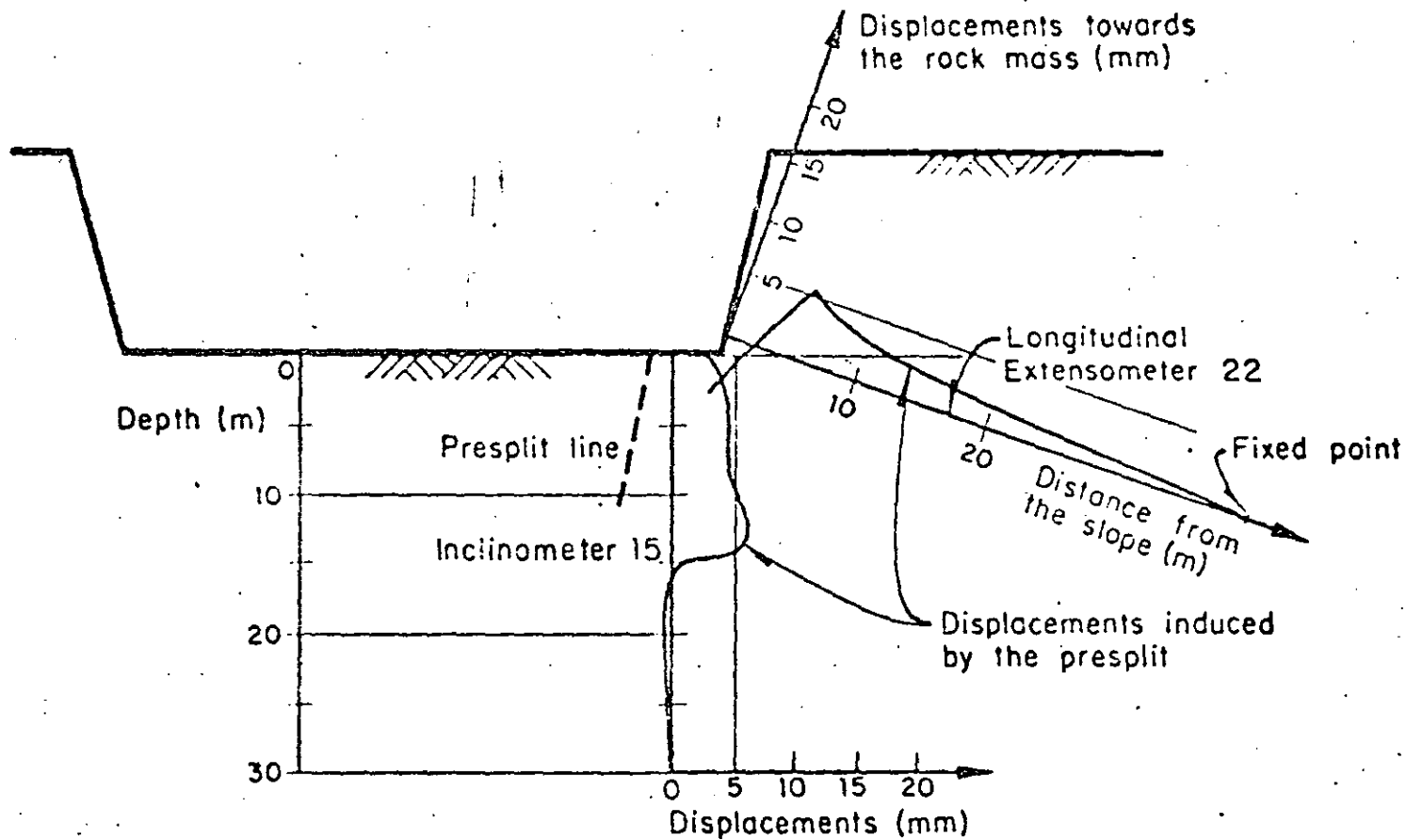


Fig 12. Displacements induced by presplit. Right spillway channel, St. 0+050 (Alberro, 1973)

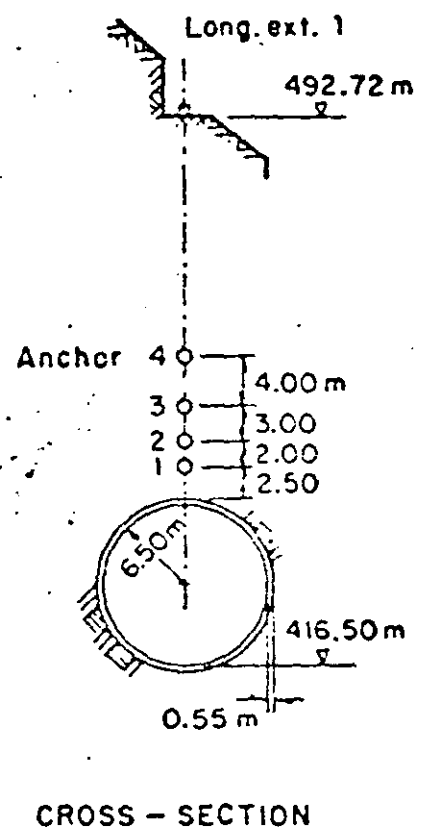
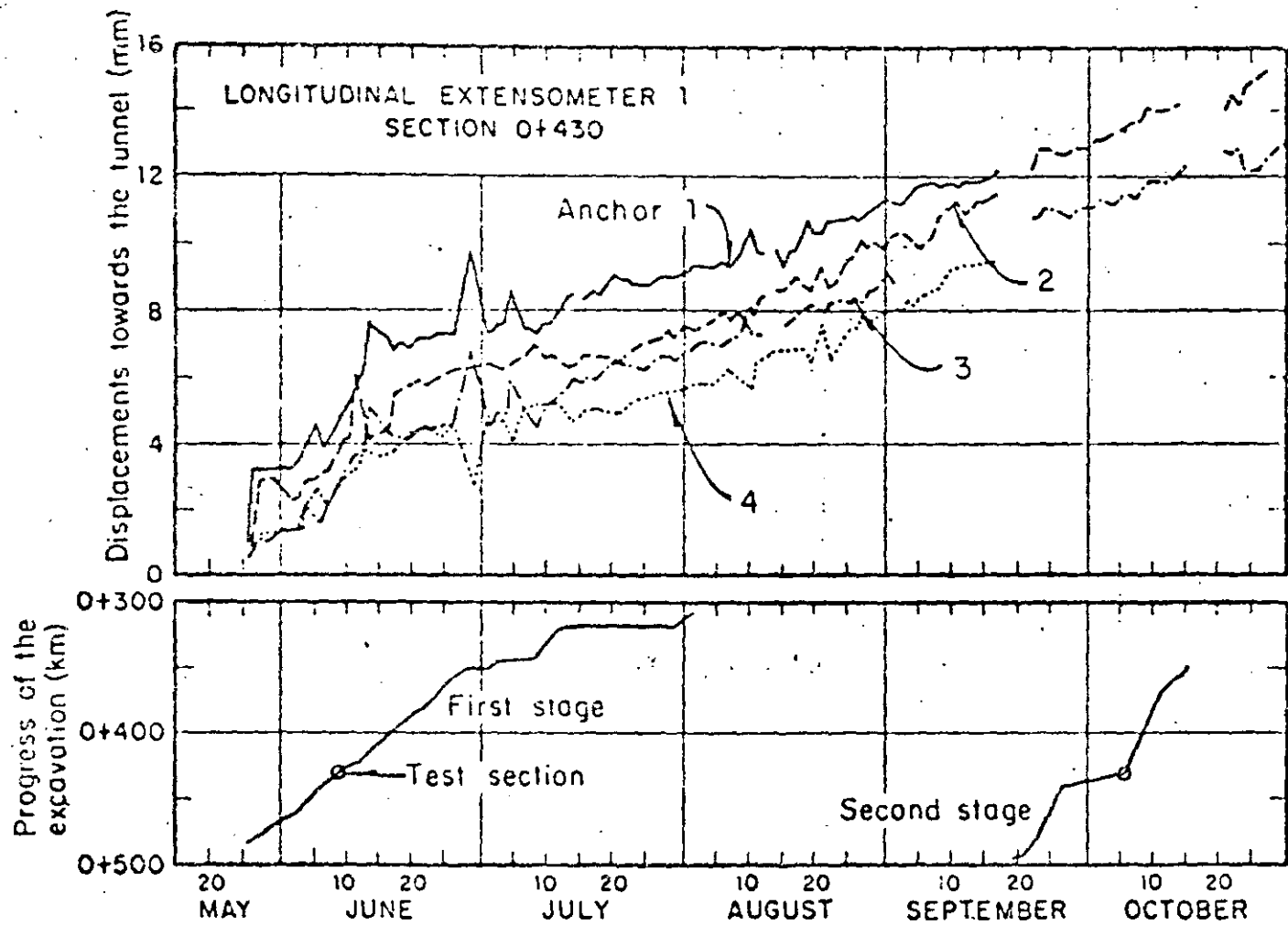


Fig 13. Vertical displacements in the rock upon excavation of Diversion Tunnel 1 (Alberro, 1973)



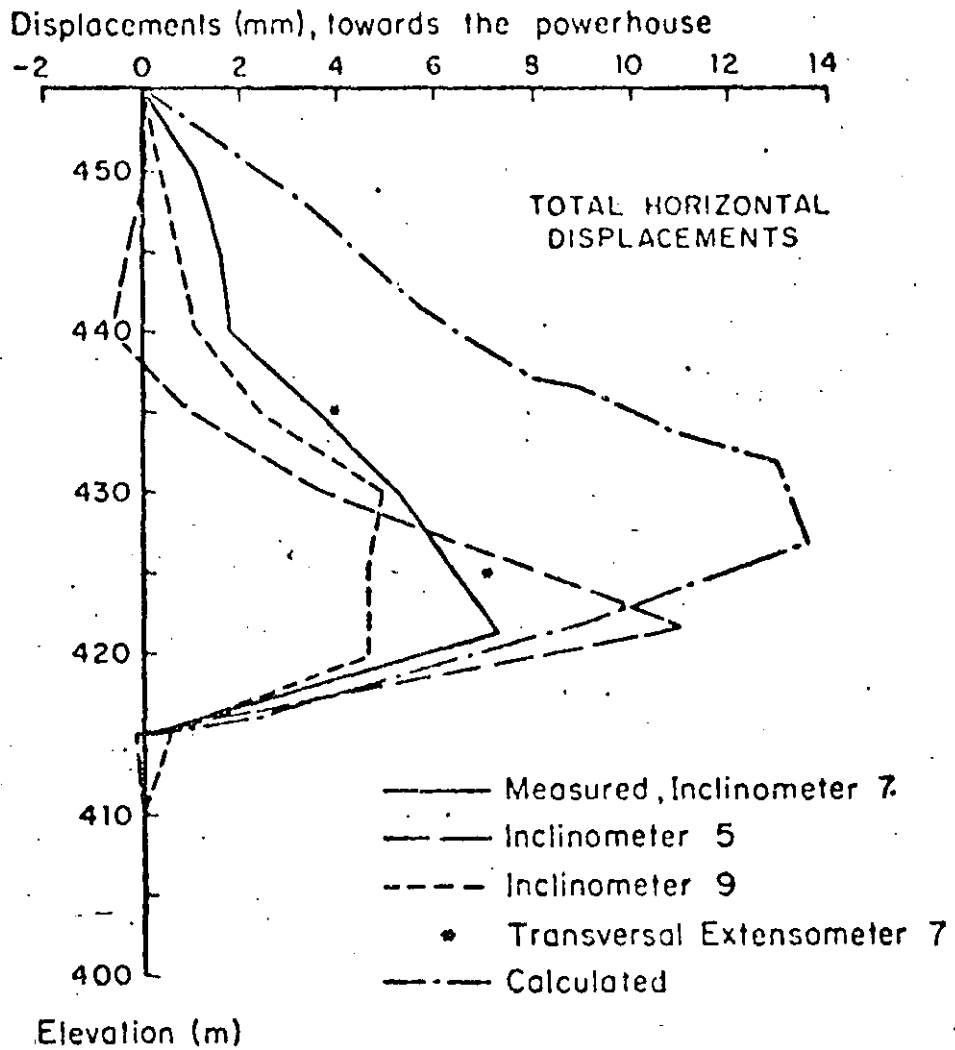


Fig 14. Total horizontal displacements at the end of the excavation, measured and calculated (linear elastic behavior) (Alberro, 1973)

Symbol

Item

Volume in m<sup>3</sup> \*

①	Compacted clayey soil	350,000
②	Filters	90,000
③	Compacted sand and gravel	400,000
④	Compacted rockfill	3,600,000
⑤	Dumped rockfill	
⑥	Rockfill (wave protection)	

\* Figures include materials for cofferdams

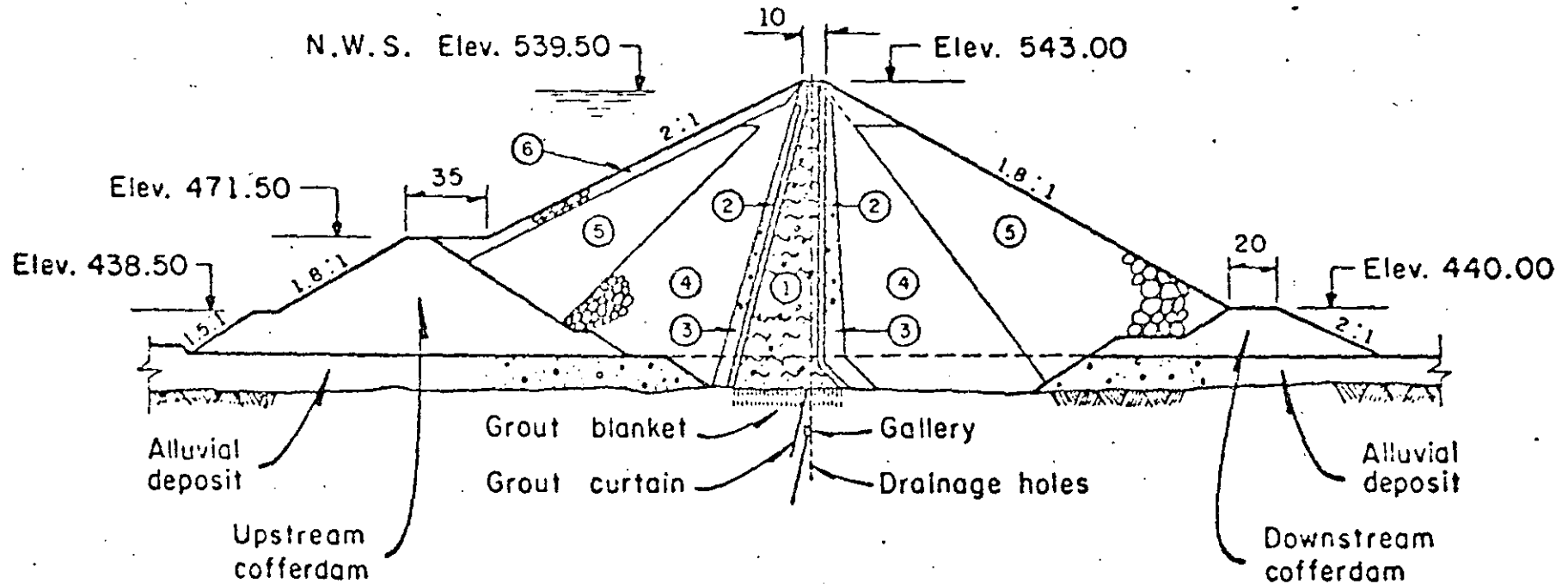


Fig 15. Maximum cross-section of the dam as originally designed

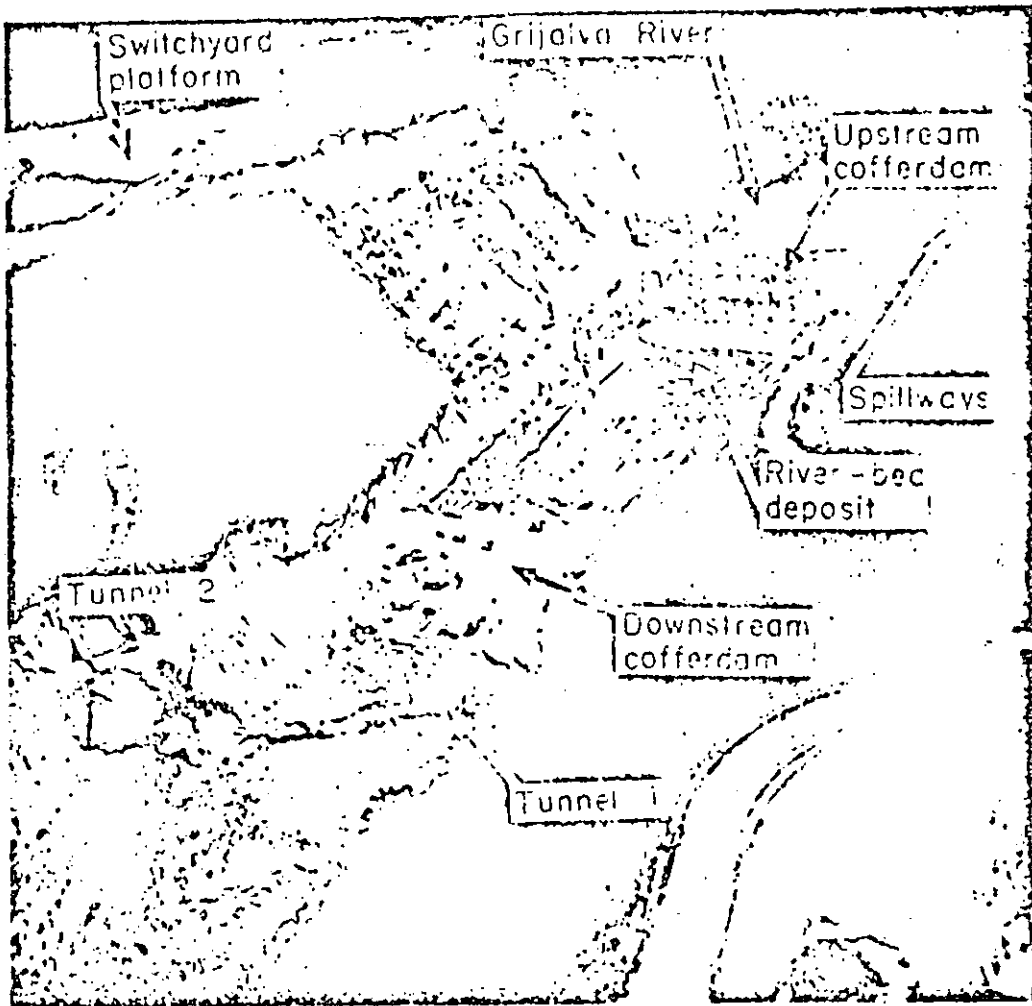


Fig 16. Excavation of river-bed deposit



Fig 17. Trimming and cleaning of the rock foundation

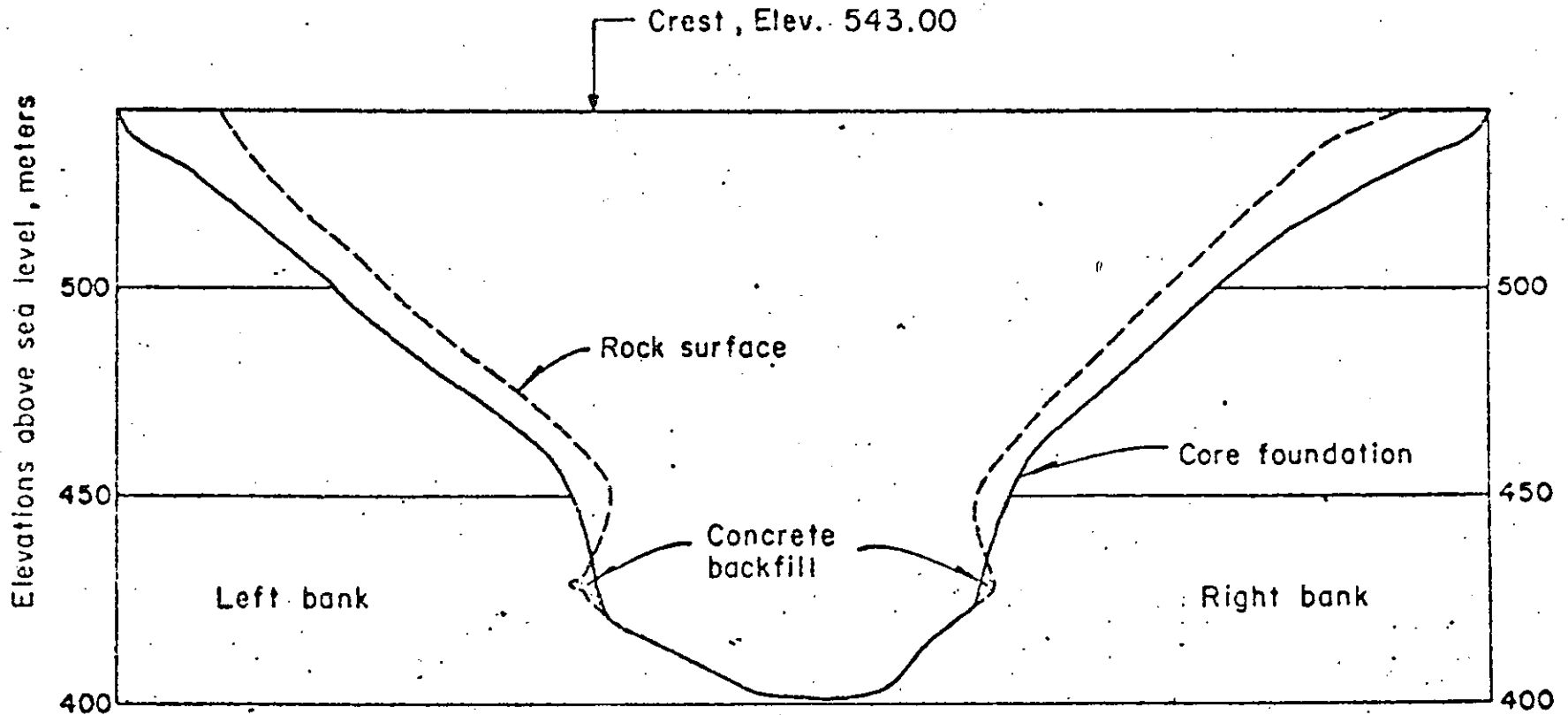


Fig 18. Cross-section of La Angostura Canyon and profile of core foundation

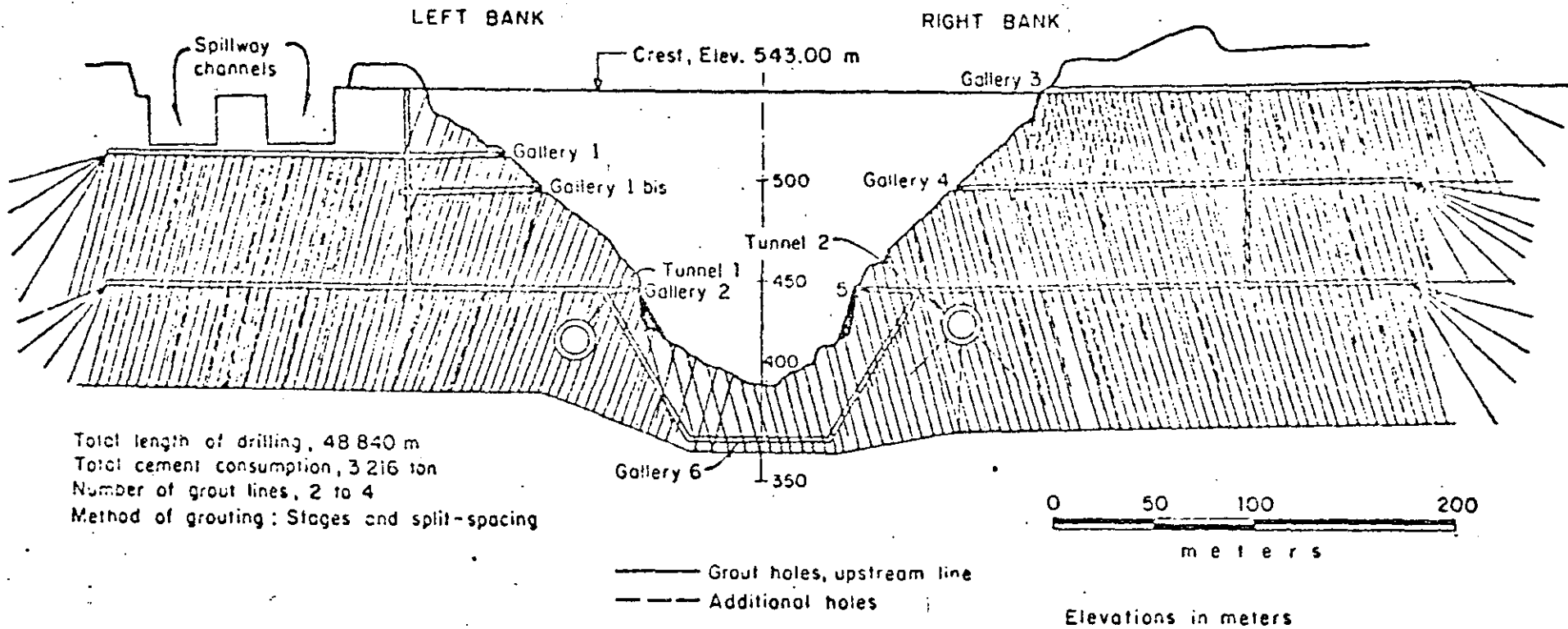


Fig 19. Grout curtain

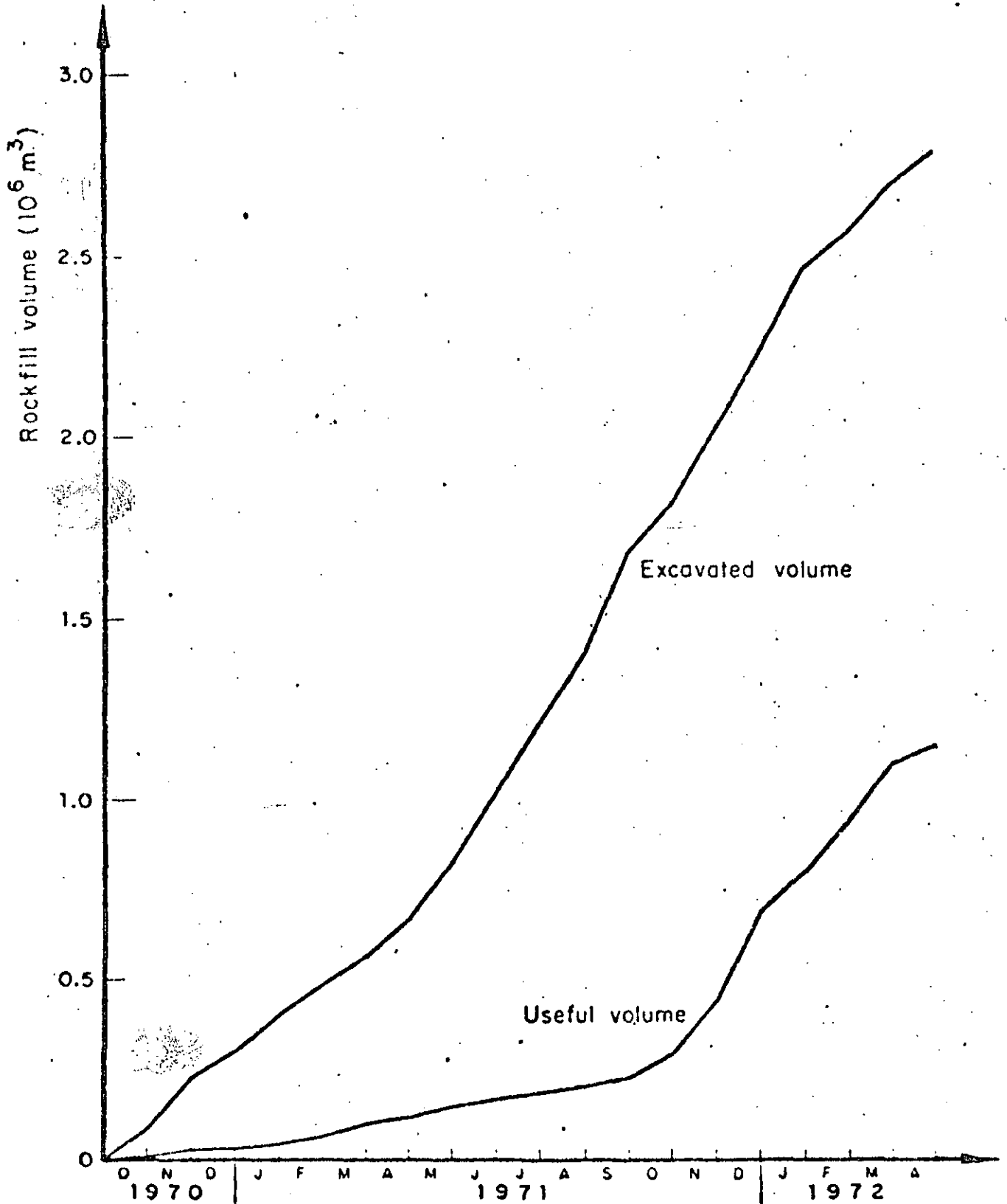


Fig 20. Useful and excavated volumes of rockfill obtained from the spillway

Symbol	Item	Volume in m <sup>3</sup> *
①	Compacted clayey soil	555,900
②	Compacted sand and gravel	1,641,700
③	Compacted rockfill	1,457,800
④	Dumped rockfill	315,200
⑤	Rockfill (wave protection)	185,100
		1,958,100
* Figures include materials for cofferdams		

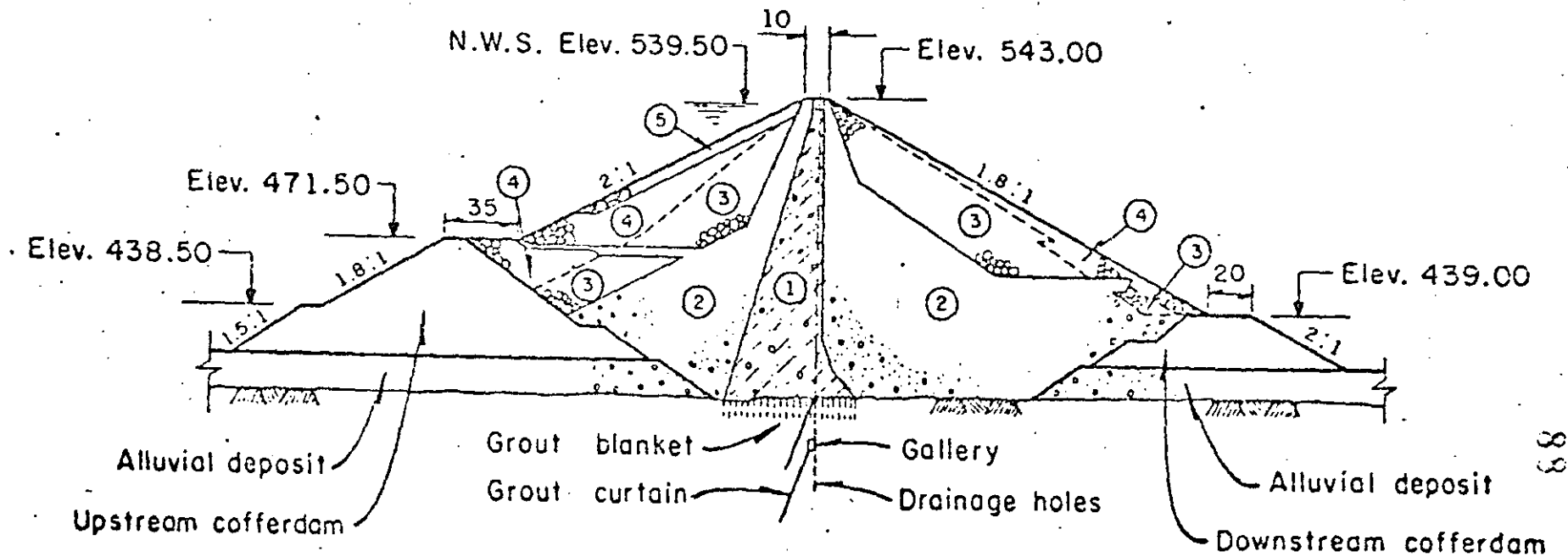


Fig 21. Maximum cross-section of the dam as built





**DIVISION DE EDUCACION CONTINUA  
FACULTAD DE INGENIERIA U.N.A.M.**

MECANICA DE ROCAS APLICADA A LA MIENRIA Y A LA CONSTURCCION

THE SEISMIC METHOD

MAYO, 1985

## CHAPTER IV

# The Seismic Method

## I. OUTLINE OF THE METHOD

In the seismic method an elastic pulse (or less commonly a continuous elastic wave) is generated near the surface of the ground, and the resulting motion of the ground at nearby points on the surface is detected by small seismometers or "geophones". Measurements of the time intervals between the generation of the pulse and its reception at geophones at various distances give the velocity of propagation of the pulse in the ground. The ground is generally not homogeneous in its elastic properties, and this velocity will therefore vary both with depth and laterally. Where the structure of the ground is simple the values of elastic wave velocity and the positions of boundaries between regions of differing velocity can be calculated from the measured time intervals. "Velocity" boundaries usually coincide with geological boundaries, and a cross-section on which velocity interfaces are plotted may therefore resemble the geological cross-section, although the two are not necessarily the same. The seismic method has been applied most extensively in the search for oil, although it cannot of course detect oil directly, but only the geological structures most favourable for its accumulation. In prospecting for other minerals the method is little used, mainly because they generally occur in a geological context which is too complicated for a ready interpretation of the measurements. This same factor, and the expense of a conventional seismic survey, has hitherto limited the extent to which civil engineers have been able

to use seismic methods in site exploration, but in recent years much experience has been gained in solving cheaply the class of problem in which low-velocity "soil" (using this word in the engineer's rather than in the geologist's sense) overlies a hard high-velocity "bedrock" at no great depth. In site exploration, and to a lesser extent in larger-scale seismic work, the values of seismic velocity which are measured are useful in themselves in that they can provide a basis for estimating other rock properties, such as porosity, elastic constants and fluid content, which are of direct interest to the engineer, even though velocity alone can never be exactly diagnostic of a particular rock type.

## 2. GENERATION AND PROPAGATION OF ELASTIC PULSES

The most usual way of generating an artificial seismic pulse is by firing a shot of high explosive in a hole tamped with water which may be as much as 100 ft deep. For shallow investigations smaller charges and shot-holes only a few feet deep can be used, and in such work it is often practicable to produce a pulse of adequate amplitude by striking with a hammer a steel plate lying on the surface or by dropping a weight. Continuous waves, as opposed to discrete pulses of very limited duration, can be produced by various types of mechanical and electromechanical vibrators which impart a periodic vertical or horizontal motion to a limited area of the surface.

However the pulse (or wave) is generated the ground motion recorded by a geophone is very complex, partly because different types of elastic wave, travelling with different velocities, are generated together, and partly because each of these wave types can, by reflection and refraction at interfaces, follow several different paths to the geophone. The *seismogram* or record of the ground motion produced by a short pulse will therefore extend over a much longer time than the pulse duration.

Wave Types

In an elastically homogeneous ground, stressed suddenly at a point *S* near its surface (Fig. 4.1), three elastic pulses travel

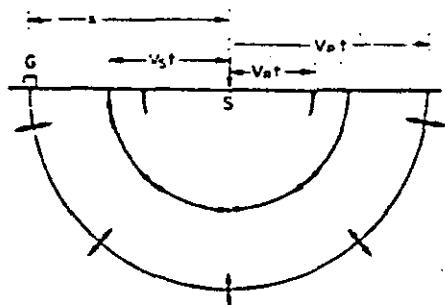


FIG. 4.1. Pulse fronts of the P, S and R wave types at a time *t* msec after their initiation at the point *S*.

outwards at different speeds. Two are *body waves*; that is, they are propagated as spherical fronts affected to only a minor extent by the free surface of the ground, and the third is a *surface wave* which is confined to the region near this free surface, its amplitude falling off rapidly with depth in the body of the medium.

The two body waves differ in that the ground motion within the pulse is in the direction of propagation (i.e. radial) in the faster or "P" (primary) wave, but normal to it (i.e. tangential to the pulse front) in the slower "S" (secondary) wave. The stresses in the *P* wave, which is a longitudinal wave like a sound-wave in air, are thus due to uniaxial compression, whilst during the passage of an *S* wave the medium is subject to shear stress. The velocities  $V_p$  and  $V_s$  of these two waves are related to the elastic constants and density of the medium by the equations

$$V_p = \sqrt{\left( \left( k + \frac{4}{3}n \right) / \rho \right)} \quad (4.1)$$

$$V_s = \sqrt{(n/\rho)} \quad (4.2)$$

where *k* is the bulk modulus (or "incompressibility"), *n* the shear modulus and  $\rho$  the density. The shear wave thus travels at little more than half the velocity of the *P* wave in most rocks: the actual value of  $V_s/V_p$  can be shown to depend only on Poisson's ratio  $\sigma$ . (See §4.3.)

The *surface wave* travels more slowly than either body wave, and is generally complex. In the special case of a homogeneous ground which we are now considering, the surface disturbance is caused entirely by the wave known as a *Rayleigh wave*, in which both vertical and horizontal components of ground motion are present. The horizontal ground motion is of rather smaller amplitude than the vertical, and is 90° out of phase with it, so that the resultant path of an element of the medium during the passage of a Rayleigh wave cycle follows an ellipse lying in the plane of propagation. The ground motion becomes negligibly small within a distance from the free surface of the same order as the wavelength of the disturbance. The velocity  $V_R$  of the Rayleigh wave is only about 10 per cent less than the body shear wave velocity, the ratio  $V_R/V_s$  again depending only on Poisson's ratio.

These three waves appear in order on the idealized seismogram of Fig. 4.2, which is a graph of ground motion against time at a particular geophone *G* a distance *x* from the "shot-point" *S*. The time zero is, of course, the time of the shot, and it is clear that the three velocities  $V_p, V_s, V_R$  could be found from this

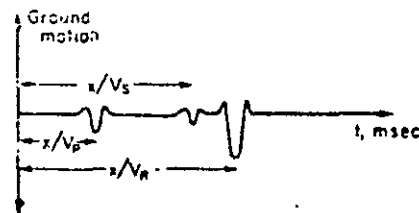


FIG. 4.2. Idealized seismogram of the ground motion at a distance *x* from a source in homogeneous ground.

record. A better determination is made by combining on a *time-distance graph* as in Fig. 4.3 the information from several geophones at various distances from the shot. Each seismogram will give three travel-times for a particular value of  $x$ , and the points should lie on three straight lines passing through the origin. It is usual to take the *distance axis* of the graph to be horizontal, and so the slopes of the graphs measured from this axis will be equal to  $1/V_p$ ,  $1/V_s$  and  $1/V_r$ . The velocities themselves can be quickly found by reading off from the graph the distance travelled in, say, 10, 50 or 100 msec. If distances are measured in feet and times in milliseconds it is convenient to measure seismic velocities in feet per millisecond, that is in thousands of feet per second. The range of velocities commonly encountered is 1-20 ft/msec, and conventional timing equipment is capable of an accuracy of  $\pm 1$  msec or better.

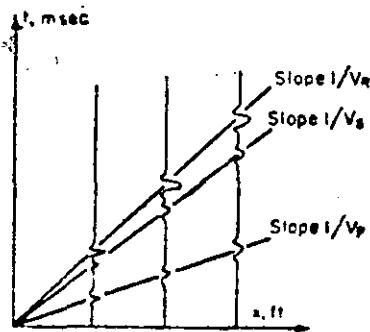


FIG. 4.3. Travel-time graph constructed from a set of seismograms such as that of Fig. 4.2 recorded at various ranges  $x$ .

If the seismograms from a set of geophones are arranged side by side with their time axes vertical, and separated by horizontal distances proportional to the actual geophone separation on the ground, the travel-time graph can be traced directly through the various pulses apparent on the seismograms. This has been done

in Fig. 4.4 for a set of real seismograms obtained on ice, which is one of the better natural approximations to a homogeneous solid medium. The slopes corresponding to the velocities of the three main wave types are clearly shown. A later event corresponding

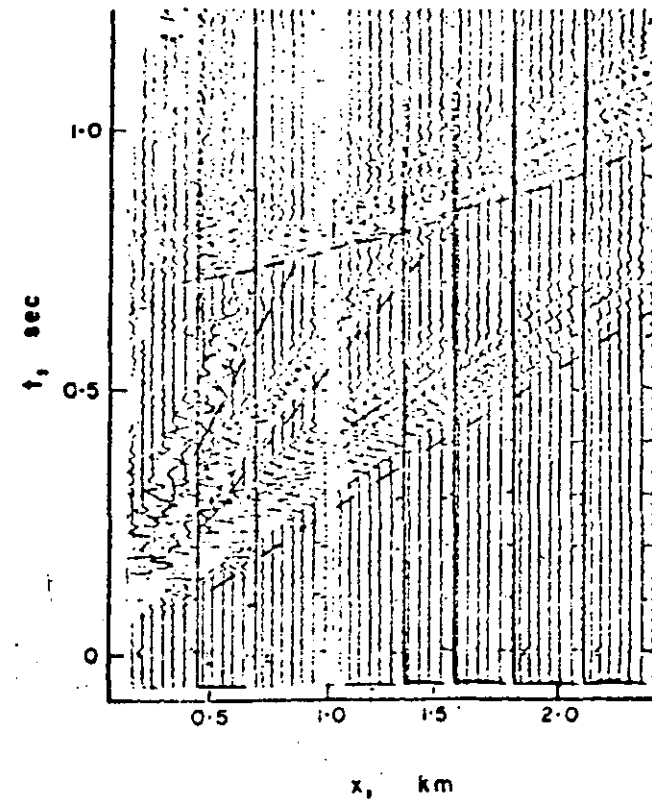


FIG. 4.4. A set of seismograms recorded on ice (from Holtzschler and Rebin, 1954). The broken lines have been drawn through the main events recorded, giving approximate travel-time graphs for the P, S and surface waves. The curved line is drawn through an event which can be identified as the P-wave reflected from the bed-rock below the ice (see Fig. 4.9).

to a reflection from the base of the ice (see below, p. 73) can also be seen.

In geophysical prospecting, as distinct from large-scale earthquake seismology, shear waves are not normally of great importance. The stress system near a shot is predominantly one of radial compression, and therefore preferentially generates a compressional pulse. When this is refracted and reflected at discontinuities in the ground some transformation into shear pulses occurs, but conventional geophones are sensitive only to the vertical component of ground motion, and this often results in further discrimination against shear motion, which is horizontal for pulses returned at steep angles to the surface. It is therefore generally assumed in the first place that the events on a seismogram are all either  $P$  waves or surface waves, although the possibility of the appearance of  $S$ -wave events cannot be entirely neglected. When the impact of a weight or hammer is used as a source,  $S$  waves may be of much greater importance, and in some cases it may be desirable to deliberately generate  $S$  waves so that  $V_S$  can be determined as well as  $V_P$  (see §3). In the following simplified treatment, only  $P$  waves will be considered.

#### Ray Paths in a Layered Medium

A diagram like Fig. 4.1 which shows the position of the pulse front at a single moment of time tells us nothing about its propagation over the rest of the path between shot-point and geophone. In seismology it is the travel-time over this path that is of interest, and so it is more convenient to represent the path by means of rays. A ray is a line which is drawn so as to be always perpendicular to successive portions of the pulse front (this is strictly true only for isotropic materials), and is therefore a path along which the energy of the pulse is propagated. To any one pulse front there corresponds an infinite number of rays, but only a selected few of these are drawn on any one diagram, which therefore gives an incomplete picture. More information is given

by a pulse-front diagram on which the positions of the front at fixed intervals of a few milliseconds are drawn. We shall use either ray or pulse-front diagrams as seems most appropriate, sometimes combining the two on one figure. The rays can always be distinguished as heavier lines with arrowheads.

#### One Horizontal Interface

Real inhomogeneous ground, which in fact often consists of stratified material, is usually best approximated by a layered medium, each layer having a constant velocity or one changing in a simple and regular way with depth. The interfaces between the layers may be inclined at any angle to the horizontal and to each other, but the model can be treated most simply when the layering is horizontal. We shall first consider the case of one horizontal interface at a depth  $h$  between media in which the  $P$  wave velocities are  $V_1$  and  $V_2$ ,  $V_2$  being the greater. Figures 4.5 and 4.6 are ray diagrams showing three possible paths for body waves between a shot  $S$  and a geophone  $G$ : we shall consider them in the order in which the rays are numbered.

The first path (Fig. 4.5) is of course the same as the path of the surface wave, but we are now discussing the  $P$  wave only, and this direct wave travels with the velocity  $V_P$ , which is much greater than the Rayleigh wave velocity  $V_R$ .

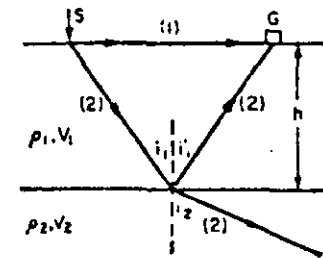


FIG. 4.5. The paths of a direct ray (1) and of a ray (2) of the same pulse which is reflected and refracted at an interface.

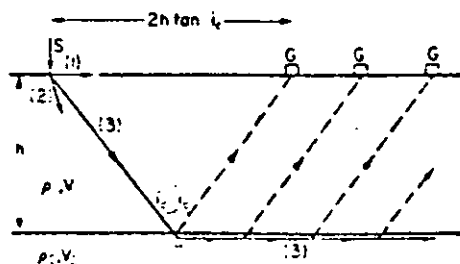


FIG. 4.6. Critically refracted ray path (full line) and a set of rays of the "head wave" pulse (broken lines).

Any wave meeting an interface between media of differing velocities\* is partly reflected and partly refracted. The laws of reflection and refraction are the same as those familiar in optics, so that for ray 2 in Fig. 4.5,  $i_1 = i_1'$  and

$$\sin i_1/V_1 = \sin i_2/V_2 \text{ (Snell's Law).} \quad (4.3)$$

The "refractive index" of the interfaces is thus  $\sin i_1/\sin i_2 = V_1/V_2$  and in the case under consideration the refraction is away from the normal.

The amplitudes  $A_r$  and  $A_t$  of the reflected and transmitted waves vary in a complicated way with the angle of incidence, but the reflection coefficient  $r = A_r/A_i$  for a normally incident wave of amplitude  $A_i$  depends only on the properties of the media and is given by

$$r = \frac{\rho_2 V_2 - \rho_1 V_1}{\rho_2 V_2 + \rho_1 V_1} = \frac{Z_2 - Z_1}{Z_2 + Z_1}. \quad (4.4)$$

It depends on the "acoustic impedances"  $Z_2$  and  $Z_1$  of the media rather than on their velocities alone, but density changes are in practice no more than about  $\pm 10$  per cent, while seismic velocity

\* The "velocity of a medium" is the conventional abbreviation for "velocity with which seismic waves are propagated through a medium".

may change by  $\pm 50$  per cent. It is clear that an interface with a good velocity contrast (strictly speaking, impedance contrast) will give rise to a strong reflection, and also that if  $Z_2$  is less than  $Z_1$ , i.e. if the reflection is at the surface of a slower medium, the reflection coefficient is *negative*. This simply means that such a reflection takes place with a complete reversal of phase: a compression is reflected as a rarefaction, and vice versa. Velocity, density, and therefore acoustic impedance generally increase with depth, so that most strong reflections encountered in applied geophysics are positive, that is, without phase change.

The ray 2 of Fig. 4.5 gives rise then to two rays: a reflected ray returning to the surface to be recorded at G, and a refracted ray in a direction more nearly parallel to the boundary than was the incident ray.

In Fig. 4.6 another ray 3 of the same pulse front is drawn: this meets the interface at a greater angle of incidence  $i_c$  which is in fact so great that the refracted ray path is parallel to the boundary, that is,  $\sin i_2 = 1$  and so

$$\sin i_c = V_1/V_2. \quad (4.5)$$

This is the condition of critical incidence and  $i_c$  is known as the *critical angle*: rays meeting the boundary with greater angles of incidence than this are totally reflected. If  $V_2$  is less than  $V_1$  so that the ray path is refracted away from the normal this critical refraction cannot occur.

The ray parallel to the boundary is in the lower medium and the ray treatment alone would lead us to suppose that no energy can be returned to the surface by this path. However, if the theory of wave propagation with these boundary conditions is fully worked out, it can be shown that the pulse, as it travels with velocity  $V_2$  along the lower side of the interface, will generate in the upper medium a pulse of rather small amplitude known as the "head wave" in which the ray paths are inclined at the same angle  $i_c$  to the normal as are the down-going rays which are critically refracted. A geophone on the surface at any distance greater

than  $2h \tan i$  from  $S$  will lie on one of these rays and will record the arrival of the head wave at the appropriate time.

The nature of the head wave can be qualitatively understood if we remember that the seismic pulse is a region of stress in the rock, and that a pulse in the lower medium will necessarily be accompanied by some stresses in the part of the upper medium immediately above the boundary. This elastically stressed region of the upper medium travels along the interface with the higher velocity  $V_2$  (Fig. 4.7(a)). Since elastic waves can travel in the upper medium only with the lower velocity  $V_1$  the situation is similar to that which exists when an aircraft or rifle bullet travelling at supersonic speed is stressing a region which moves at a higher speed than that of sound waves in air. This results in the generation of a "shock wave" as shown in Fig. 4.7(b), and the "head wave" can be thought of as its analogue.

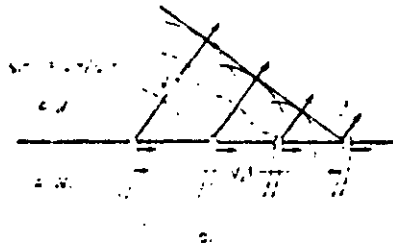


FIG. 4.7. (a) The generation of a head wave by the passage of a refracted pulse along a boundary.

Although in calculating the travel-time of the pulse by these three paths it is convenient to refer to the ray diagrams of Figs. 4.5 and 4.6, we can better understand the process of its propagation by visualizing the successive positions of the pulse fronts, to which the rays are normal. Pulse-front diagrams for the direct, reflected and refracted fronts, and of the head wave, are given in Fig. 4.8. The reflected front has been shown on a separate diagram merely for clarity; the two diagrams would have to be

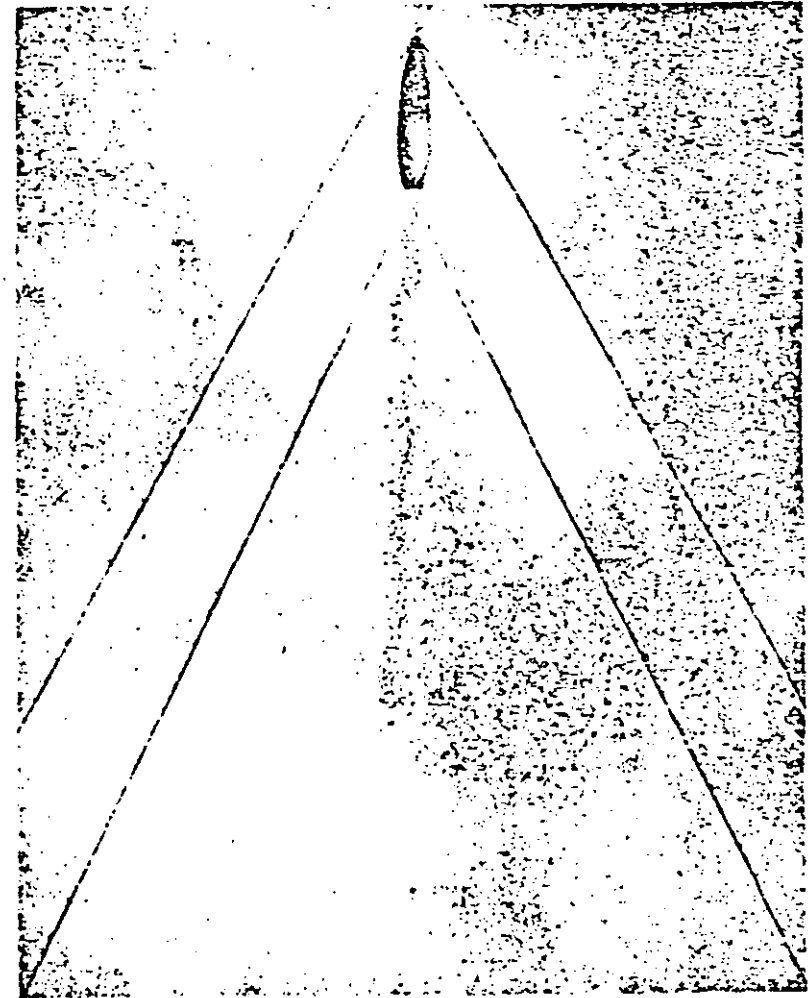


FIG. 4.7. (b) A photograph of the somewhat analogous generation of a shock wave in air by a rifle bullet (from *Sound Waves, Their Shape and Speed* by D. C. Miller, Macmillan, 1937).

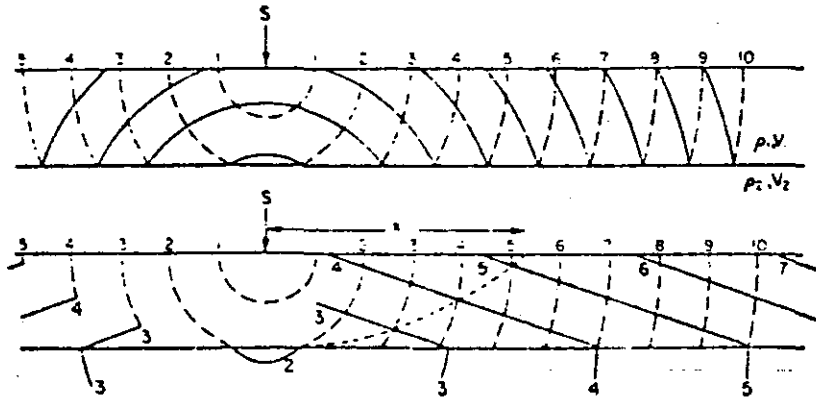


FIG. 4.8. Pulse front positions at equal intervals of time for (a) direct and reflected pulse; (b) direct pulse and refracted and head wave pulses. The dotted line joins points to which the travel-times of direct and head pulses are equal. It reaches the surface at the critical distance  $x_c$  from S. The left-hand part of the diagram has been further simplified by omitting those parts of the pulse fronts which do not produce "first arrivals" at the surface.

superposed to give a true picture of events. It is clear that at a geophone near the shot, the direct wave arrives before the head wave, but that at distances greater than a *critical distance*  $x_c$  the head wave, which now spends a greater proportion of its time in the high-velocity medium, is the first arrival. We shall now discuss these ideas in a more quantitative way.

*Travel-time Graphs for a Layered Medium*

*Single Horizontal Interface*

How will the travel-time along these three paths appear when they are plotted against distance measured along the surface? The graph for the direct P wave has already been given in Fig. 4.3, and Fig. 4.9 is the complete graph for the single horizontal interface of Figs. 4.5 and 4.6, ignoring the slower S and R waves.

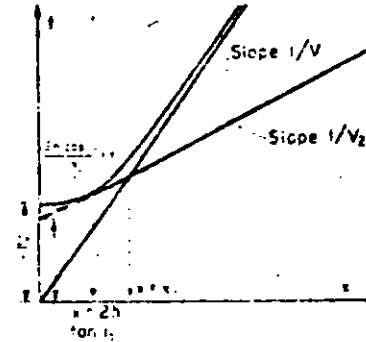


FIG. 4.9. Travel-time graphs for direct, reflected and head waves. A single horizontal interface at depth  $h$  divides an upper medium of velocity  $V_1$  from a lower of velocity  $V_2$ .

It is easy to see from the ray diagram that a geophone near the shot-point will record the arrival of the reflected pulse after a time  $2h/V_1$ , and also that at horizontal ranges much greater than the depth  $h$  the reflected path becomes practically the same as the direct one, so that the graphs for these two paths must come together asymptotically for large values of  $x$ . The actual length of the reflected path is, in fact

$$2\sqrt{((x/2)^2 + h^2)}$$

as may be seen from Fig. 4.5. and as this is traversed entirely at the velocity  $V_1$ , we see that the time-distance relationship for the reflected pulse must be

$$t = \frac{2\sqrt{((x/2)^2 + h^2)}}{V_1} \tag{4.6}$$

$$= \sqrt{(x^2 + 4h^2)}/V_1$$

giving a hyperbolic relationship between  $x$  and  $t$  with the limiting behaviour we have just described for very small and very large values of  $x$ .



The form of the graph for the head wave can also be qualitatively foreseen if we remember that this wave is generated by a disturbance travelling horizontally at the higher velocity  $V_2$  and will therefore have this apparent velocity when seen from the surface: this point is referred to again in the next section. The graph will not, of course, pass through the origin, as does that for the direct wave, since the wave is subject to a delay in travelling down to the high-velocity refractor and to another delay in returning to the surface. These two delays result in an intercept on the time axis if the graph is produced back to  $x = 0$ . One must realize that the graph has no *physical* reality for angles of incidence

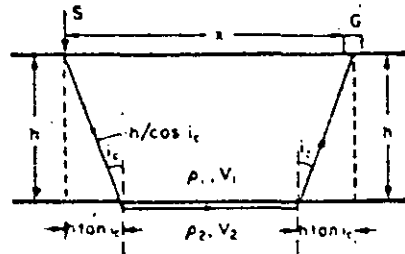


FIG. 4.10. Geometry of the path of the head wave.

less than the critical angle (that is, for values of  $x$  less than  $2h \tan i_c$ ) as the head wave does not exist at all for such short ranges. Even at slightly greater ranges, the head wave will be so delayed by the inclined parts of its path that it will arrive *after* the direct wave, and only beyond the critical distance  $x_c$  will the head wave be the first event recorded on the seismogram. Since the head wave is usually much smaller than the direct wave, the part of its travel-time graph before the critical distance can rarely be observed in practice.

The equation of the time-distance line for the head wave can be found quite readily by adding the times spent on each of the three sections of its path (Fig. 4.10).

Thus

$$t = \frac{1}{V_1} \cdot \frac{h}{\cos i_c} + \frac{1}{V_2} (x + 2h \tan i_c) + \frac{1}{V_1} \cdot \frac{h}{\cos i_c}$$

$$= \frac{x}{V_2} + 2h \left( \frac{1}{V_1 \cos i_c} - \frac{\tan i_c}{V_2} \right).$$

Remembering that

$$\sin i_c = V_1/V_2 \tag{4.5}$$

this becomes

$$t = \frac{x}{V_2} + \frac{2h \cos i_c}{V_1} \tag{4.7}$$

That is,

$$t = \frac{x}{V_2} + t_i \tag{4.8}$$

representing a line of slope  $1/V_2$  and "intercept time"  $t_i = 2h \cos i_c/V_1$ , the intercept of the line on the time axis. The critical distance  $x_c$  is the value of  $x$  which satisfies both this equation and that of the "direct wave" line  $t = x/V_1$ , so that

$$x_c/V_1 = x_c/V_2 + t_i \tag{4.9}$$

Hence

$$x_c = t_i / \left( \frac{1}{V_1} - \frac{1}{V_2} \right)$$

$$= 2h \sqrt{\frac{V_2 + V_1}{V_2 - V_1}} \tag{4.10}$$

The travel-time equations (4.6) and (4.8) form the bases of the seismic reflection and refraction methods for determining the depth to an interface. Their use is described in more detail in the next chapter; here we shall only draw attention to the fact

that the refraction method relies essentially on the measurement of travel-times of the earliest arrivals at the geophones, and is therefore technically a simpler matter than observing reflected waves which occur later in a complex record and which are of small amplitude compared with the direct wave. This is not to say that later arrivals (in particular the arrivals of the direct wave beyond the critical distance) are of no value in the refraction method: in fact it is always desirable to identify them if possible, and they may often be essential to an unambiguous interpretation.

#### Two Horizontal Interfaces

Figure 4.11 shows the reflected ray paths and travel-time graphs for a ground with two horizontal interfaces. Here two reflected waves are possible (we are neglecting for the moment "multiple" reflections between the interfaces, which are mentioned in Chap. 5) and the minimum travel-time for the second one is

$$t = \frac{2h_1}{V_1} + \frac{2h_2}{V_2} = \frac{2(h_1 + h_2)}{\bar{V}} \quad (4.11)$$

This equation is of the same form as equation (4.6) for  $x = 0$  if the appropriate average velocity  $\bar{V}$  is used. This is an average weighted in accordance with the thickness of the layers and is given by

$$\bar{V} = (h_1 + h_2) \left( \frac{h_1}{V_1} + \frac{h_2}{V_2} \right) \quad (4.12)$$

This result is easily generalized if many layers are present, and an average velocity  $\bar{V}$  may be used in equation (4.6) when  $x$  is small compared with the depth of investigation. This is almost always so in applied reflection seismology.

The graph representing the first arrivals (Fig. 4.12) now consists of three branches whose slopes give the reciprocals of the velocities  $V_1$ ,  $V_2$  and  $V_3$ . Using the method by which equation (4.8)

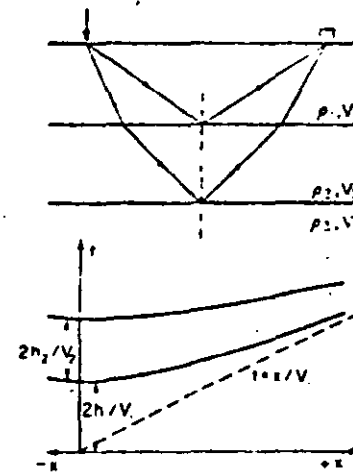


FIG. 4.11. Reflected ray paths and travel-time graphs when two horizontal interfaces are present.

was derived, it can be shown that the intercepts  $t_1$  and  $t_2$  are given by

$$\left. \begin{aligned} t_1 &= 2h_1 \cos i_{11}/V_1 \\ t_2 &= 2h_1 \cos i_{12}/V_1 + 2h_2 \cos i_{22}/V_2 \end{aligned} \right\} \quad (4.13)$$

In this notation an angle of incidence  $i_{mn}$  is that of a ray in the  $n$ th layer which is critically refracted at the base of the  $n$ th layer, i.e. travels horizontally in the  $(n + 1)$ th layer. This result can also be extended if more layers are present.

#### Apparent Velocity

Figures 4.11 and 4.12 also serve to illustrate an important concept which is of great use in discussing the interpretation of seismic records, that of *apparent velocity*, which is simply the velocity of a pulse measured by timing its passage between two closely spaced geophones on the ground surface. For the direct pulse or indeed for any horizontally travelling pulse, the apparent velocity

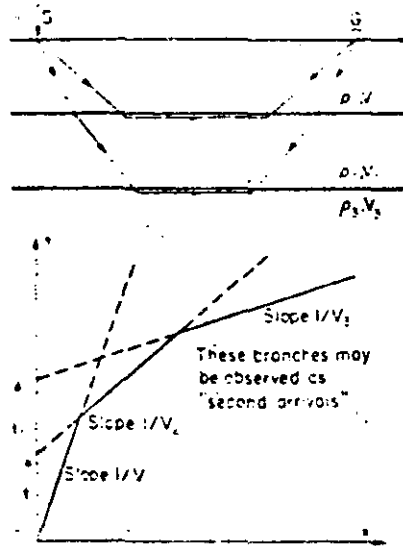


FIG. 4.12. Head wave ray paths and travel-time graphs for two horizontal interfaces.

measured along the ground surface is obviously equal to the true velocity  $V_1$ , but if the pulse front is inclined at an angle  $\theta$  to the surface, Fig. 4.13 shows that its intersection with the surface

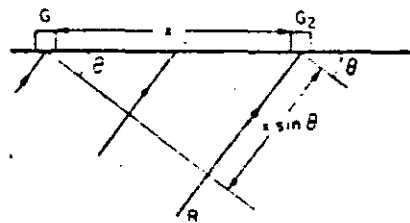


FIG. 4.13. Relationship of true and apparent velocities.

travels a distance  $G_1G_2 = x$  while the pulse moves only the smaller distance  $x \sin \theta$  along the ray path  $R$ . If the true velocity of the pulse is  $V_1$ , this will take a time  $t = x \sin \theta / V_1$ . The apparent

velocity measured between  $G_1$  and  $G_2$  will be  $V_a = x/t = V_1/\sin \theta$ . For the direct pulse,  $\theta = 90^\circ$  and, as we have already seen,  $V = V_1$ . For a vertically travelling pulse, such as the reflected pulse (taken to be plane over a small distance) returning to the surface near the shot-point,  $\theta = 0^\circ$  and therefore  $V_a$  is infinite. This simply expresses the fact that the pulse arrives almost simultaneously at any two closely spaced geophones. The apparent velocity of the reflected pulse becomes less and less as it is measured further away from the shot point and  $\theta$  increases to  $90^\circ$ , when  $V_a$  has the limiting value  $V_1$ .

The pulse front of the head wave from a horizontal boundary has the form of a truncated cone with a vertical axis, and in this special case is inclined at an angle  $i_c$  to the horizontal, since its ray makes an angle  $i_c$  with the normal to the interface. The apparent velocity of the head wave is therefore constant and equal to  $V_1/\sin i_c$ , and because  $\sin i_c = V_1/V_2$  it follows that  $V_a = V_2$ , the velocity of the lower medium, a result that might have been foreseen from the way in which the head wave is generated.

We should perhaps here anticipate the discussion of interpretation in the next chapter to the extent of pointing out that this last result is true only for a *horizontal* interface or for a series of such interfaces. If the interface is dipping downwards in the direction of propagation at an angle  $\alpha$ , the head wave will be inclined to the surface at an angle  $i_c + \alpha$ , and the apparent velocity will be

$$V_a = V_1/\sin(i_c + \alpha) \tag{4.14}$$

which is *less* than  $V_2$  by an amount depending on  $\alpha$ . A dip in the opposite direction will clearly lead to an apparent velocity *greater* than the true velocity of the lower medium.

### The Form of the Seismic Pulse

A seismogram is a record of the resultant ground velocity (generally of its vertical component), which is due to the sum of a large number of impulses from waves of different types travelling

by different paths. In attempting to analyse waves of a seismogram it is useful to know the form of the velocity impulse which is generated by an explosive source in homogeneous ground, since this is the principal unit from which a seismogram is constructed. The classical treatment of this problem is due to Ricker (1953), who showed that the "spike" impulse of velocity (Fig. 4.14(a))

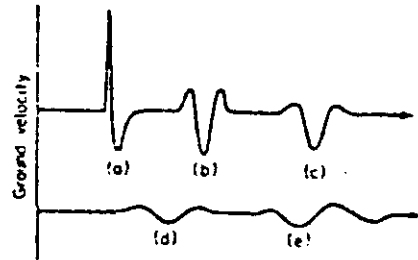


FIG. 4.14. The change in shape of the pulse. (a) Impulse of ground velocity near to the shot; (b) Transition shape; (c) and (d) The "Ricker" pulse, broadening and decreasing in amplitude with increasing range.

which must exist very near to the source is transformed in the early stages of its propagation to the symmetrical form of Fig. 4.14(b). This elementary impulse, which has become known as the "Ricker wavelet", becomes broader and smaller in amplitude at greater distances (Figs. 4.14(c) and (d)), but is essentially unaltered in form. In the analysis of seismograms it is necessary to remember that a Ricker wavelet of ground velocity is distorted by the recording apparatus (Anstey 1956), the most common form of distortion being the addition of extra "loops" to the wave form, as in Fig. 4.14(e).

Both the broadening of the pulse by further selective attenuation of high-frequency components and its general decrease in amplitude take place at a rate which is dependent on the mechanical properties of the ground. Hard compact rocks transmit the pulse with little attenuation, while loose soils attenuate it heavily

with accompanying rapid broadening. Attenuation and broadening are much less readily measured than pulse velocity, and so it is the velocity which has so far been used as an indicator of the mechanical properties of the medium. As we shall see in the next section, however, this indication is only of the truly *elastic* properties: if we are interested in the time-dependent elastic properties of the ground, and in its permanent deformations, the change in pulse shape is of great importance, and there are indications that advances in technique may make possible meaningful measurements of this effect.

### 3. RELATIONSHIPS BETWEEN SEISMIC VELOCITIES AND ELASTIC PROPERTIES OF ROCKS

Most seismic investigations are carried out with the object of finding the positions of interfaces between media of different velocities: the values of the velocities themselves are of course needed in the interpretation process, but they also tell us something about the nature of the rocks themselves. It is easy to take either of two extreme attitudes: either to say that the relationship between seismic velocity and lithology is so vague and unreliable as to be useless for predicting one from the other; or to suppose that a measurement of velocity is characteristic enough in itself to identify a formation in geological terms and to specify all its elastic constants. The truth, of course, lies between them, and in this section we shall show what other information can (and cannot) be reasonably inferred from a knowledge of seismic velocities.

The compressional wave velocity is

$$V_p = \sqrt{\left(k + \frac{4}{3}n\right) / \rho} \quad (4.1)$$

and as a granular medium of a given composition is compacted, it is found that the elastic moduli  $k$  and  $n$  increase more rapidly

than does the density, so that in sediments  $V_p$  increases with compaction. An empirical relationship between velocity and density (which is simply related to porosity for a given mineral density) is shown in the graph of Fig. 4.15. A group of experimental results for a particular rock type varying *only* in porosity

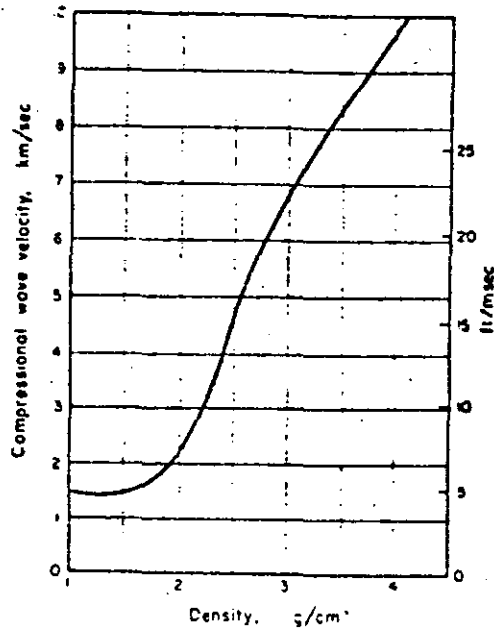


FIG. 4.15. Experimental relationship between P-wave velocity and density (Nafe and Drake, unpublished data, reproduced in Talwani, Worzel and Ewing, 1961).

may fit the form of this relationship well, but other variables (mineral composition, cementation, degree of fissuring) should be taken into account if the velocity of the material is to be estimated from its porosity. This means that if, on the contrary, the velocity has been *measured*, we need to have at least an estimate of these other variables if the velocity is to be used to make an accurate

estimate of porosity. For example, it is impossible from a measurement of velocity *alone* to say whether a rock formation consists of a permeable limestone or a more compact sandstone. However, as with most physical properties of rocks, it is possible to quote a range of velocities which covers (apart from exceptional values) each of the usual broad lithological divisions, and this is done in Table 4.1. This table also includes the corresponding ranges of values of density  $\rho$   $\text{g/cm}^3$

TABLE 4.1

	$V$ ft./msec	$V$ km./sec	$\rho$ $\text{g/cm}^3$
Clastic rocks, unconsolidated	1-6	0.3-1.8	1.5 (peat 1.0)-2.2
Clastic rocks, consolidated and/or cemented, but only gently folded	5-12	1.5-3.7	2.0-2.6
Clastic rocks in orogenic belts	10-20	3.1-6.2	2.5-2.8
Metamorphic rocks	15-20	4.6-6.2	2.7-3.0
Limestones	10-20	3.1-6.2	2.4-2.7
Igneous rocks	15-20	4.6-6.2	2.4-3.0

This table shows the general trend of increasing velocity with decreasing porosity (i.e. increasing density), and also to what extent rock types can be separated on the basis of seismic velocity. The regions of overlap are very apparent.

Both theoretical and experimental studies of material of very high porosity show that in the range of 50-70 per cent porosity, the seismic velocity may actually become *less* than that of the fluid filling the pore spaces, that is, less than 1.1 ft/msec for dry material and less than 4.5 ft/msec for soil saturated with water.

Materials of exceptionally low velocity are in fact encountered near the surface, and are of considerable importance in interpretation of seismic surveys, as we shall see in the next chapter.

The civil engineer is concerned less with giving a name to a rock than with estimating its elasticity, plasticity and strength. The strength of a rock is not uniquely related to its seismic velocity, but for unconsolidated materials there is a useful correlation of the two properties. "Soils" of velocity up to about 4 ft msec can generally be handled with ordinary earth-moving equipment, and a material of velocity above 8 ft msec would be classified as "rock" in the engineering sense. Elasticity is more directly related to seismic velocity, and a measure of elasticity can in fact be calculated from the velocity if the density  $\rho$  is known. The elastic properties of an isotropic material are completely specified by any two of the elastic constants.

Bulk modulus (incompressibility)  $k$

Shear modulus  $n$

Young's modulus  $E$

and Poisson's ratio  $\sigma$

because of the relationships that exist between them. The engineer commonly uses  $E$  and  $\sigma$ , and the equations (4.1) and (4.2) can be re-written in terms of these quantities

$$\rho V_p^2 = E(1 - \sigma)(1 + \sigma)(1 - 2\sigma) \quad (4.15)$$

$$\rho V_s^2 = E 2(1 + \sigma) \quad (4.16)$$

These equations show that Young's modulus can only be determined from a body wave velocity if both the density and Poisson's ratio are known. However, as  $\sigma$  and  $\rho$  do not vary widely for rock materials, experimentally determined values of  $V_p$  and  $E$  give points scattered about a parabolic graph (Fig. 4.16) from which  $E$  can be approximately estimated if a  $P$ -wave velocity measurement is made on unknown material. This method, due

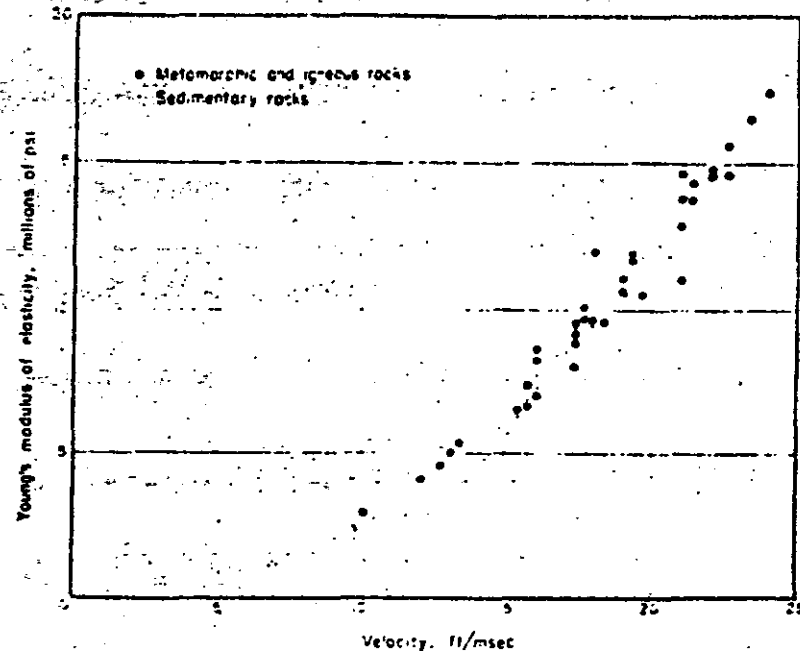


FIG. 4.16. Experimental relationship between  $P$ -wave velocity and Young's Modulus (from Brown and Robertshaw, 1953, reproduced by permission of the Institute of Civil Engineers).

to Brown and Robertshaw (1953), has been criticized by Evison (1956) who points out that variability of Poisson's ratio becomes of considerable importance when it takes larger values, as it does for just those unconsolidated materials of low ( $< 10$  ft/msec) seismic velocity to which the method is most likely to be applied. He devised a method using an electromechanical vibrator as a seismic source which produced shear waves of usable amplitude, so that both  $V_p$  and  $V_s$  could be measured. Now if the ratio  $V_s/V_p$  is denoted by  $r$ , it can be shown from equations (4.15) and (4.16) that

$$\sigma = (1 - 2r^2) / (2 - 2r^2) \quad (4.17)$$

so that  $\sigma$  can be found and  $E$  estimated with much greater precision than from a measurement of  $V_p$  alone. Szendrei (1959) gives a graph of this relationship (Fig. 4.17) together with that between  $\sigma$  and the ratio  $V_R/V_p$  of Rayleigh to compressional wave velocity, which may often be more easily measured than  $r$ .

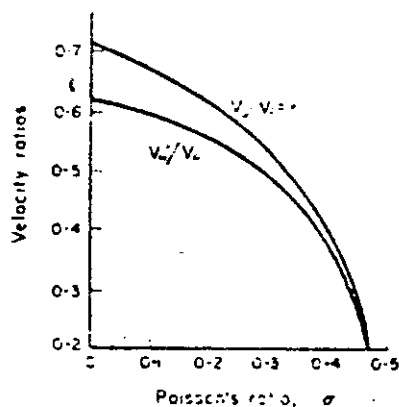


FIG. 4.17. Theoretical relationship between ratios of velocities of different wave types and Poisson's ratio (after Szendrei 1959).

The Rayleigh wave alone has been used by Jones (1962) in a technique for determining the thicknesses and elastic constants of the thin layers of different materials making up a road. In such a layered medium, the motion due to Rayleigh waves of longer wavelength will penetrate more deeply into the underlying media, and such waves will have a higher (or lower) velocity than those of short wavelength whose motion is essentially confined to the upper layer. The form of the variation of Rayleigh wave velocity with wavelength can be theoretically related to the nature of the layering, and this variation or "dispersion" is measured using a variable-frequency continuous oscillator as a source of vibrations.

Care is needed in using values of  $E$  determined seismically as a basis for structural design. In the first place, of course, the

modulus so measured is a true *elastic* modulus, and takes no account of plastic or other irreversible strains. Moreover, the method of measurement is equivalent to a loading experiment carried out in a time of the order of a hundredth of a second; it follows that visco-elastic strains with much longer time-constants than this cannot be recorded. Seismic determinations of  $E$  generally therefore give *higher* values than conventional methods in which the material is stressed for a much longer time. We must also remember that the velocity is measured (see §5.4) over a distance of the order of tens or even hundreds of feet, and that its value will be affected by fractures and other inhomogeneities found within this distance. A mass of badly fractured rock will, for example, show a seismic velocity considerably lower than will a small specimen of the same material (too small to contain any fractures) measured in the laboratory. The velocity measured *in situ* may therefore in this case give an estimate of  $E$  which is too *low*, but if it is also measured on a laboratory scale the discrepancy between the two results will suggest the presence of fissuring: a result of considerable importance in itself.

Clearly, "field" measurements of seismic velocity can give useful information about elastic properties, particularly if velocities can be measured for two wave types and compared with those resulting from laboratory tests. It is, however, unwise to rely on seismic estimations to the complete exclusion of static tests if a very accurate result is required. Static tests can give a result of high precision relating to a limited volume of material, just as a borehole *locally* determines structure very precisely, but the geophysical technique provides evidence about a much larger volume which may be more useful if the medium is inhomogeneous.

## CHAPTER V

Seismic Measurements  
and their Interpretation

## 1. INTRODUCTION

In the "reflection" method of applied seismology, a shot-to-geophone spacing small compared with the depth of investigation is used with the object of recording the pulses reflected at near normal incidence from horizons where the acoustic impedance (less strictly, the velocity) changes abruptly. The method is simple in principle (though not in practice), is able to record information from a large number of horizons down to depths of many thousands of feet, and requires shots no larger than a few tens of pounds of high explosive. It has considerable accuracy, particularly when only changes in the depth of a reflector, rather than absolute depths, are of interest. The resolution is also high, and is limited in principle mainly by the breadth of the pulse, which may be of the order of 200 ft. The method lends itself to routine techniques in which the ground is covered by a series of profiles, the rate of coverage usually being limited by the time required to drill shot-holes. A crew of about 15-20 men with nine vehicles, including two light drilling rigs each with two water-carrying trucks might cover two or three miles of profile in a day, but these figures will vary widely with the nature of the terrain, the difficulty of drilling, and the degree of elaboration of technique required in country where poor reflections are obtained. Line coverage can be much quicker over sheltered inland or coastal waters, when the process

can be made more truly continuous and an output of tens of miles per day may be common. All these features have commended the reflection method to those whose business it is to find structural domes of small relief, reefs, salt domes, small angular unconformities and other potentially oil-bearing features of sedimentary basins, and it is in the search for oil that the method is most widely used, so that we shall discuss it in this context.

In the problems of mining and civil engineering, on the other hand, one is generally trying to locate bodies or interfaces which are shallow, of small lateral extent, or both. Small bodies cannot give reflections of adequate amplitude, and the reflections from shallow bodies return to the recorder so soon that the amplifiers have not recovered from the severe overloading to which they are subjected by the direct wave. Special reflection equipment is now available which will record reflections as shallow as one or two hundred feet, but generally speaking this type of problem can be more readily solved by the refraction method, in which head waves are recorded, generally as first arrivals on the seismogram. These are plotted on a time-distance graph, and used to calculate the depth to the interface at which they originate by finding the "intercept time" defined in equation (4.3). The interpretation of refraction seismograms and time-distance curves will be discussed in this chapter mainly with application to mining and engineering problems in mind, but of course refraction methods are also used on a larger scale in prospecting for oil, either in the initial stages of the exploration of a sedimentary basin, in the location of salt domes, or in elucidating structure in areas where reflection methods give results of little or no value. If the "head wave" branch of the time-distance graph is to be properly defined, ranges of the order of five or six times the depth to the refractor will be normal, and this implies the use of very large charges in deep exploration, together with extra problems of communication along the profile. In investigations to depths of the order of a hundred feet, none of these difficulties arise, but they are replaced by others connected with the extreme inhomogeneity of near



surface earth materials and the consequent inadequacy of any simple layered model in interpretation.

In the mid-range of depths, over which either of the two main methods may be used, the refraction method suffers from the disadvantage that relatively few interfaces can be followed on one profile, and that all of these *must* be velocity increases: for example, the base of a thick bed of high-velocity limestone, which would probably give rise to a good reflection, cannot generate a head wave unless the underlying material is of even higher velocity. This fact, which is discussed more fully later in this chapter, gives rise to the possibility of serious misinterpretation. The chief advantage of the refraction method, on the other hand, is that it gives directly the velocities of the refracting beds, which may help to identify them and are in any case needed in the depth interpretation. The need to know velocity as a function of depth is as great in the reflection method, but has to be satisfied either indirectly by making measurements in boreholes or by special extensions of the technique.

## 2. THE INSTRUMENTS USED IN APPLIED SEISMOLOGY

An instrument for detecting and recording seismic waves is a *seismograph*: the detecting head itself is an electro-mechanical transducer called a *seismometer*.

Seismometers used on land are commonly known as *geophones*: most of these give an electrical output which is proportional to the vertical component of the ground velocity, though some types measure ground acceleration or (rarely in applied geophysics) ground displacement. Specially adapted geophones can be used on the sea-bed, but it is usually more convenient to suspend a pressure-sensitive seismometer or *hydrophone* freely in the water for marine work.

The most common type of geophone is shown in section in Fig. 5.1. The body is a permanent magnet with an annular gap

between the pole-pieces. In the radial magnetic field of this gap is a coil on a spring mounting which permits it to move vertically. Any vertical ground motion will cause the coil to move in the field and an e.m.f. proportional to the velocity of motion will be induced in the coil. This electrical output will also depend on the frequency of the ground motion relative to the natural frequency of the coil, but the damping of the system is so arranged that its response is approximately uniform over the range of frequencies (about 1 to 200 c/s) which is of interest. Where frequencies at the extreme ends of this range are present, (for example, long-range shots used in deep refraction work may give rise to frequencies of 5 c/s and below) a geophone of natural frequency lower or higher than the common values of 10–30 c/s may be used.

Any geophone with an output proportional to ground velocity must be directional: the geophone of Fig. 5.1 if laid on its side on the ground would not respond to the vertical component in, say, a Rayleigh wave, but only to the horizontal component. This is of importance if it is necessary to distinguish between waves

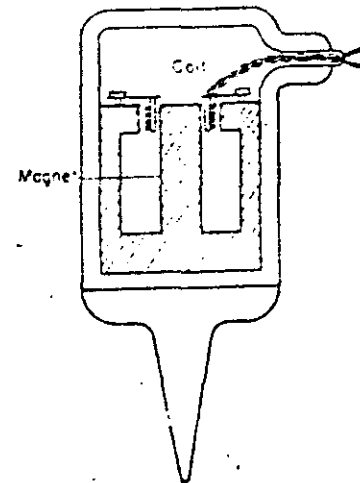


FIG. 5.1. Simplified sectional view of a typical moving-coil geophone.

of the different types described in §4.2. Since most hydrophones are *pressure-sensitive* devices their output is independent of the direction of water motion in a pulse.

The small signal from the seismometer must be amplified electronically before it can be recorded. The basic requirements for a seismic amplifier are reliability, portability and ease of servicing, and these are easily met with modern designs, often using transistors and printed circuits. The maximum gain of the amplifier should be enough for the normal background ground movement or "noise" to be detectable, and its response should cover a

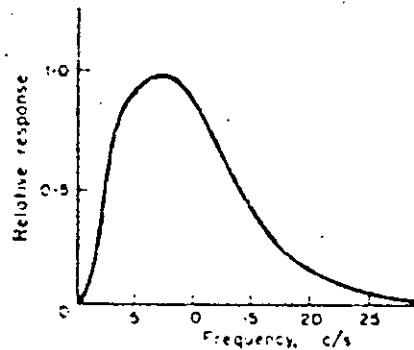


FIG. 5.2. Frequency response curve of a filter suitable for recording 5 c/s impulses in the presence of higher frequency noise.

frequency range of about 5 to 200 c/s. Electrical filters are incorporated in the amplifier so that this frequency response can be limited if required: for example, in long-range refraction work the predominant frequency of the head wave pulse may be of the order of 5 c/s, whilst the ground noise may cover a band from 20 c/s upwards. An improvement in useful sensitivity could obviously be obtained in this case by using a filter to give the frequency response of Fig. 5.2, which will practically eliminate the noise while leaving the signal unchanged. Filters are also used in this way in reflection equipment, but in this type of recording

the frequency difference between signal and noise is never so well marked as in the example just quoted. Amplifiers for reflection work must also be provided with an automatic gain control device which provides a low gain for the very strong signals of the direct wave and a much higher one for the weaker signals travelling by longer paths, so that the wide range of amplitudes of ground motion can be presented on a single record.

The recording itself may be by a galvanometer reflecting a light-spot on to moving photographic paper (the records of Fig. 4.4 were made in this way), but it is common practice now to record also on magnetic tape, so that the record can be played back with different amplifier characteristics, different time delays between the channels, and so on. A visual record is always needed, however, and this is made either in the "graphical" form of Fig. 4.4 or as a "variable-density" or "variable-area" record. These newer forms of presentation, which are shown in Fig. 5.3, are very helpful in making the reflected pulses which occur later in the record clear to the eye. The variable-area type has this advantage while retaining that of the graphical presentation that the waveform of the record can be studied in detail. All types are provided with timing lines at 10 msec intervals, derived from either a tuning fork or a crystal oscillator, and the shot impulse (derived from the firing of the electrical detonator) is also recorded on one of the traces.

A prospecting seismograph will consist of 12 or 24 complete channels of this kind (6 are shown in Fig. 5.4), usually mounted in a truck which also serves as a dark room. The complete equipment may, if transistorized, be so light and compact that it can readily be divided into units suitable for back-packing by 7 men on foot. Extra men and equipment are needed to drill shot-holes for investigations by the reflection method, but if the refraction method is being used over short ranges, shallow hand-augered shot-holes suffice, and since the seismograph may for this type of work be of only 6 channels, it is quite possible for 3 or 4 people to carry out the whole operation.

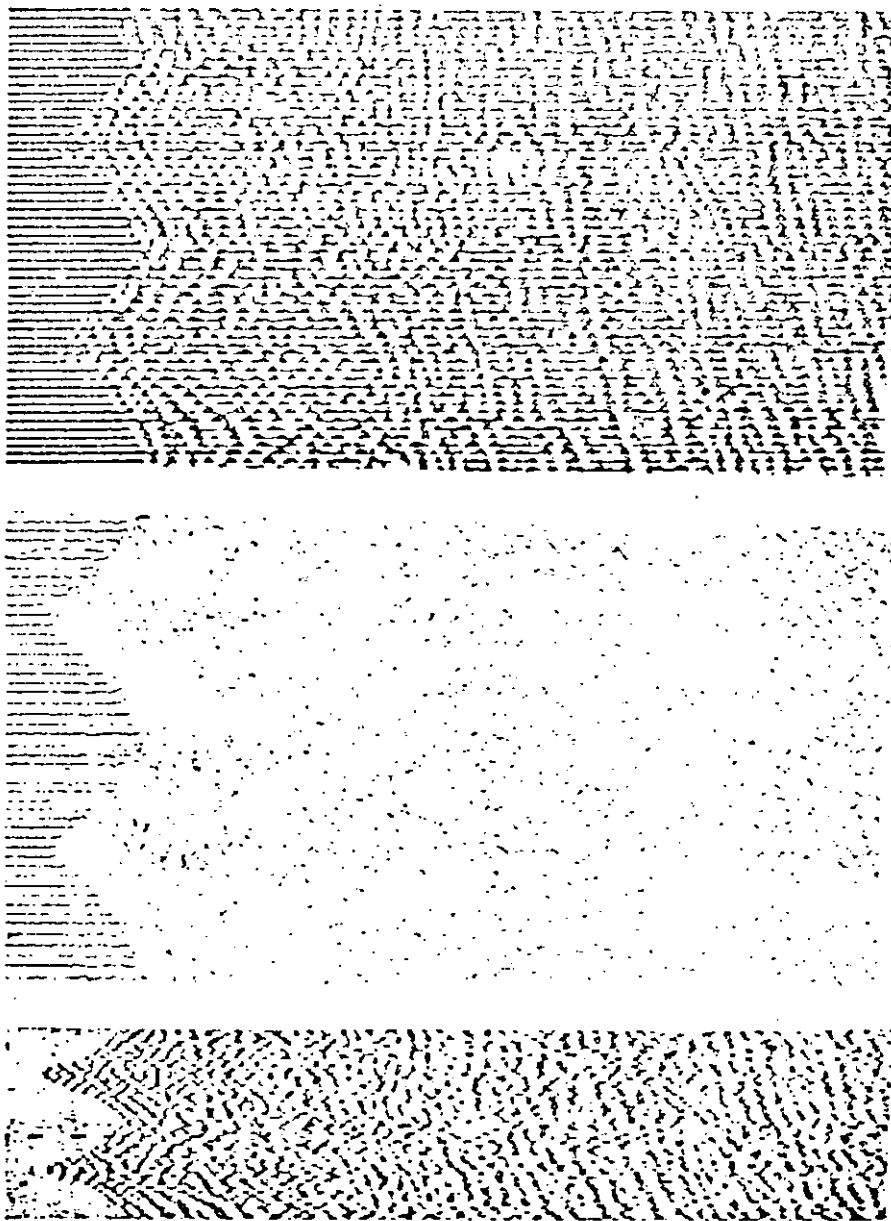


FIG. 5.3. A pair of reflection records from adjacent shot-points presented in different ways: (a) Variable density; (b) Graphical or "wiggle"; (c) Variable area.

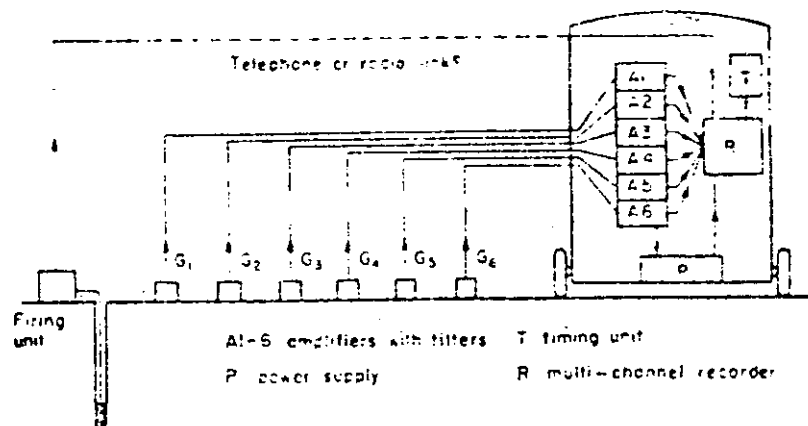


FIG. 5.4. Block diagram of a set of six seismic channels.

Formerly the source of the seismic pulse was always an explosive charge buried at a suitable depth in the ground: in reflection seismology investigating depths of the order of 5000–10,000 ft, a 20 lb charge in a 50 ft hole might be taken as typical. The depth of the shot-hole in this type of work is controlled by the necessity of placing the charge below the layer of surface low-velocity material to which the energy of the shot is otherwise largely confined (see §3).

In refraction seismology the size of the shot is controlled mainly by the maximum range from shot to geophone, which must be at least twice the critical distance  $x_c$  if the second branch of the time-distance graph is to be properly defined. The critical distance in turn depends on the depth to the refractor of interest. Thus for depths in the 5000–10,000 ft range, charges of up to a ton are likely to be needed, but on the scale of an engineering site investigation, a few pounds of gelignite will normally be ample.

At short ranges, in fact, a mechanical impact such as a sledgehammer blow has been used very successfully as a seismic source. The first description of a practical equipment using such a source was given by Gough (1952), and a simplified diagram of his

apparatus is given in Fig. 5.5(a). A simple impact switch closes as the hammer meets a steel plate on the ground, and so provides an electrical impulse which is used to start the time-base of a cathode-ray oscillograph. The amplified output of a single geophone deflects the oscillograph trace vertically so that a seismogram is displayed for a short time on the tube, which is of the "afterglow" type. The time interval between the hammer blow and any recognizable event on the trace can be measured by using calibrated controls to move a "marker" pulse along the time axis. The hammer blow can be repeated at any one range until satisfactory accuracy is obtained in this time measurement. The hammer and plate are then moved to a greater distance, and the process is repeated, so that a travel-time graph can be plotted. Gough claims a maximum range of 250 ft (which would give useful results from a refractor at a depth of 50 ft or so) using a 10 lb sledge-hammer. This range, however, would be expected to decrease inversely as the square root of the background noise level, which is very much greater in inhabited areas than in open country, where Gough's trials were carried out.

A variant on Gough's apparatus was developed by Mooney and Kaasa (1958) and is now commercially available in several forms (Fig. 5.5(b)). This makes use of counting circuits to time the passage of the impulse, which is not recorded visibly at all. The electrical impulse from the hammer-blow opens an electronic "gate" circuit which allows the output of a 10 kc crystal oscillator to pass to a set of decade counters. The seismic pulse which arrives first at the geophone is made to close the gate, so that the count of the oscillator cycles which is recorded on meters connected to the decade units is a measure of travel-time to the nearest one-tenth of a millisecond. This method has the obvious advantage over Gough's of extreme convenience in the actual time measurement, but this is offset to a considerable extent by the fact that the gate may be operated only by a strong second arrival in circumstances under which a visible record would have ensured the picking of a weaker, but earlier, event. It has also been found

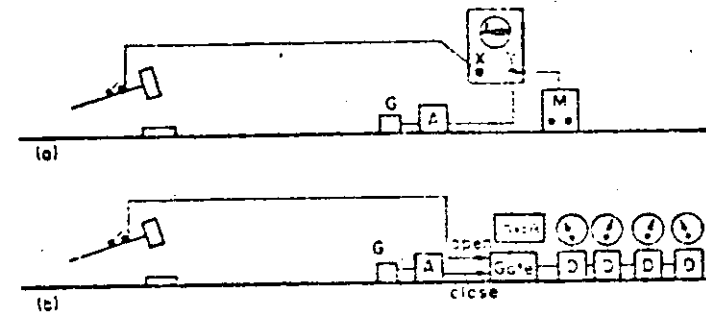


FIG. 5.5. (a) Short-range seismic equipment using oscillograph recording. G—geophone, A—amplifier, M—Marker pulse generator with calibrated time delay.

(b) Direct-reading equipment for measurement of "first-arrival" travel-time. D—decade counters

that the air wave, travelling at 1100 ft/sec, may cause considerable ground motion which will be registered as the first arrival if the overburden velocity is much less than this. If the arrival is not recognized as an air wave (its high frequency makes this easy on a seismogram), the overburden velocity will be taken to be 1100 ft/sec and the depth to a refracting interface therefore over-estimated.

More recent commercial instruments appear to combine the advantages of the two techniques to some extent, and incorporate improvements which are said to make it possible to detect reflections from shallow horizons. The different versions of this type of seismic equipment are all completely portable, and require only two operators, of whom one can be unskilled.

Impact sources have also come to be used on the much larger scale of prospecting for oil by the reflection method. A weight of 2 or 3 tons, mounted on a lorry, is dropped from a height of about 10 ft. The energy of the impact is adequate to give detectable reflections from considerable depth, but for a single impact these are normally masked by the very large amplitude surface waves which are generated. By compounding on magnetic tape

the records from a large number of drops, suitably spaced, cancellation of the surface waves can be produced, giving a record of quality comparable with that obtained by conventional shooting. The method is of particular value in areas where shot-hole drilling is difficult or impossible.

Truly continuous sources of elastic waves are of little value in prospecting because of the difficulty of timing their passage. Where essentially only one wave type and path is present, the problem is simply one of measuring the difference in phase between the signals at the source and the receiver. This is the method adopted by Jones in his work on the dispersion of Rayleigh waves which was mentioned at the end of Chap. 4. For a normal type of seismogram, however, a continuous signal would give an even more confusing picture than does a sharp pulse, and the only progress that is being made on these lines is by using a signal lasting perhaps a hundred complete cycles which changes its frequency continuously during this time (Crawford, Doty and Lee 1960). The method seems to be promising, but extra equipment is needed to convert the record obtained into one which can be directly interpreted.

### 3. THE REFLECTION METHOD

The reflection seismogram shown in Fig. 5.6 may be taken as typical of those obtained in routine work. The shot-hole is between the centre two geophones of the twenty-four, offset slightly from their line, and the shot instant is recorded as a break on the second trace from the edge of the record. The earliest arrivals are not normally due to the direct wave, but to critical refractions at the base of the *low-velocity layer*, commonly known as the "weathered layer". This layer, with a velocity usually in the range 1000–5000 ft/sec, is nearly always present, and extends from the surface downwards to a depth of perhaps 10–100 ft. Its base seems to be defined either by the water table or by a rather sharp decrease in porosity. The civil engineer's problems are often

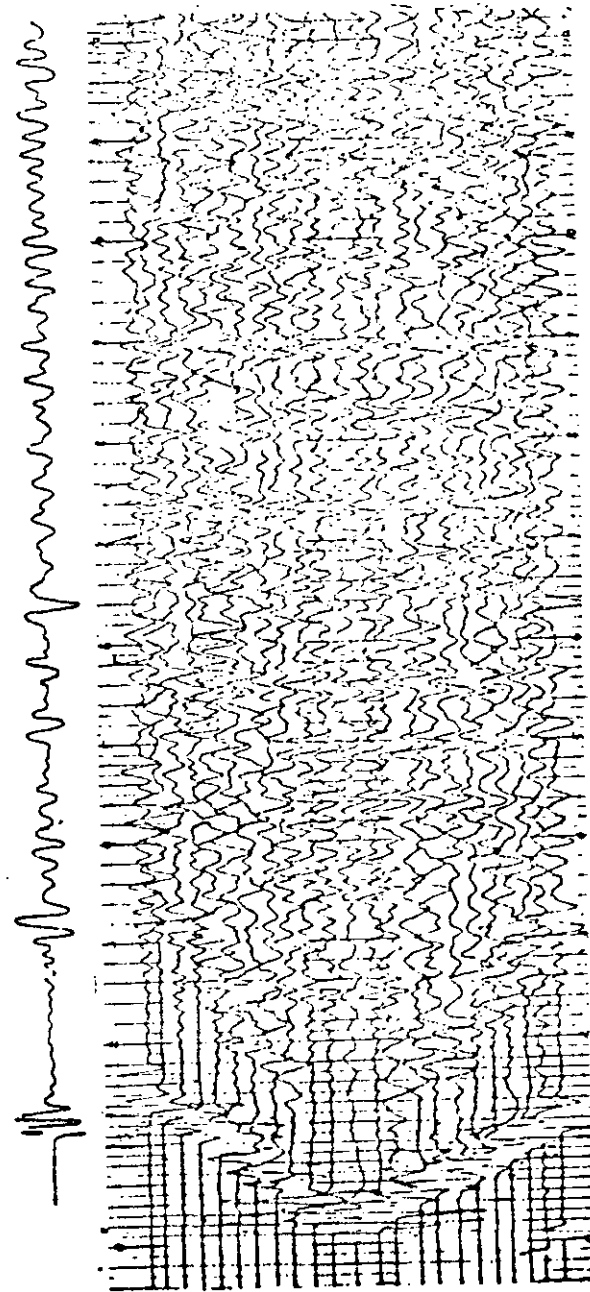


FIG. 5.6. A typical reflection seismogram. The geophones are spaced at 100 ft intervals up to about 1000 ft on each side of a central shot-point. If the end geophones coincide with the shot-points of adjoining geophone spreads, continuous coverage of the reflecting horizons is obtained.

directly concerned with the nature and thickness of the "weathered layer" in this sense, but in deeper investigations it is no more than a superficial nuisance, making an appreciable and very variable contribution to the measured reflection times.

The remainder of the seismogram is a complex of the wanted reflections (of which three are clearly visible), of body waves reaching the geophone by other paths, and of surface waves and other "noise". The isolated trace above Fig. 5.6 shows that it would be practically impossible to resolve this complex without a multi-channel record, on which events can be correlated from trace to trace and their time-distance relationships compared with theoretical ones for different pulse paths.

*First Arrivals; Datum Correction*

The variability of the weathered layer leads to a scatter of observed reflection times which must be eliminated if the possible accuracy of the method is to be realized. The usual practice is to correct for both weathered layer thickness and ground topography in one step known as the datum correction, in which all observed times are reduced to the values they would have if both shot and geophone were placed at  $S'$  and  $G'$  (Fig. 5.7) on a common surface; usually horizontal and a little below the deepest part of

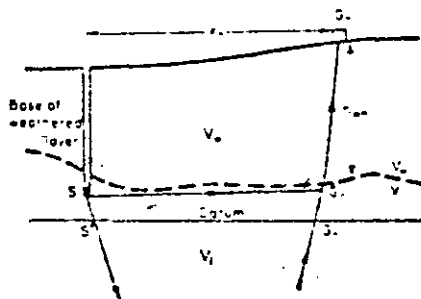


FIG. 5.7. The geometry of the datum correction

the base of the weathered layer. To apply this correction we need to know the velocities  $V_w$  and  $V_1$  and the distances  $SS'$ ,  $G_nG_n'$  and  $G_n'G_n$  to find the times spent by the reflected ray (assumed to be returned from a considerable depth) on each of these segments of its path. The time  $t_w$ ,  $V_w$  is the longest, most variable and therefore most important of these, and can be determined quite easily from the travel-time of the "first arrival" path  $SG_n'G_n$ , if the shot is supposed to be just below the base of the weathered layer, as is commonly the case. The time for this path is very nearly

$$t_n = x_n/V_1 + h_{wn}/V_w$$

$$= x_n/V_1 + t_w \tag{5.1}$$

for the  $n$ th geophone, since the velocity contrast between  $V_w$  and  $V_1$  is usually so great that the ray path in the weathered layer is nearly vertical, and the path  $SG_n'$  is close to the horizontal. A graph of first-arrival times  $t_n$  against geophone ranges  $x_n$  will therefore have the form shown in Fig. 5.8. Provided  $h_{wn}$  does not show a systematic increase or decrease over the spread, the best line through the points (the dotted line of the figure) will have a slope of  $1/V_1$ , and the departures of the points from a line parallel to this through the origin will be the required times  $t_w$ .

21

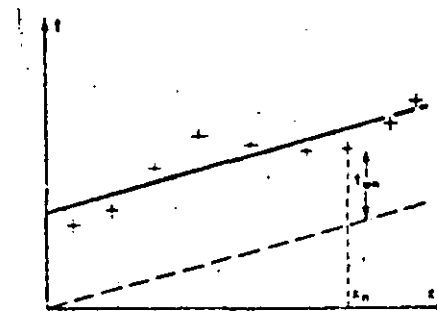


FIG. 5.8. Effect of delays in the weathered layer on first-arrival times.

The end geophone of the spread usually coincides with the shot-point of the next spread, and so for this geophone the value of  $t_u$  is determined as the "up-hole" time for the next shot, i.e., the travel-time recorded by a geophone a short distance from the shot-point.

Knowing  $V_1$  from the first-arrival times, and the elevations of the shot and the datum surface, it is a simple matter to determine the time spent on the path  $SS'$ . Similarly, if  $V_u$  is measured by short range shots either in a borehole or on the surface,  $h_{uu}$  and hence the elevation of  $G'$  can be found, and the remaining part  $t_{G'G}$  of the correction can be evaluated. Since  $V_u$  enters only into this term, it need be determined only relatively infrequently.

This datum correction, sometimes known as the "static" correction, since it has to be applied equally to all reflection times shown by a particular geophone, is of great importance and is also very tedious to make. When seismograms are recorded on magnetic tape it is possible to set the datum correction for each geophone as a displacement of the corresponding reproducing head, so that when the record is played back the correction is made automatically throughout its length.

#### *Identifying and "Picking" Reflections*

Figure 4.8(a) shows that, at ranges small compared with the depth to the reflector, the reflected pulse arrives nearly simultaneously at all geophones, and therefore appears on Fig. 5.6 as a series of peaks and troughs aligned almost directly across the seismogram. An alignment of this kind which can be followed across nearly all the traces of several records is likely to be a reflection, and is usually "picked" for measurement of the travel-time on the first peak or trough which can be so followed. Because of the increase in the length of the reflected path with range the alignment will in fact show a slight curvature or "move-out" which will be more pronounced for the early (shallow) reflections and which can of course be corrected for if necessary. The correction

may be done by the interpreter, but, as with the static correction, it is now more usual to apply it by shifts of the heads reproducing the magnetic records. In this case the correction is a "dynamic" one, that is, it varies down the length of the record, so that the reproducing heads have to be progressively shifted during playback.

The form of the reflected pulse is rarely that of the simple Ricker wavelet shown in Fig. 4.14. Real geological interfaces are generally complex, so that a number of Ricker pulses, erect and inverted, and with various small time delays, will be added to form the actual ground motion. The form of this is further distorted by the recording apparatus, which has the effect of adding extra "loops" to the pulse and of introducing other more complicated distortions. The net result of this is that the first peak or trough, to which the time measurement is made, has no *absolute* significance, so that the "seismic horizon" plotted from it may be a hundred feet or more from the lithological horizon with which it is correlated. Such an absolute error is not of great importance in prospecting for oil, provided that the seismic horizon accurately *parallels* the structures of the lithological horizon. Relative errors across a record or between one record and another are of course much more important, as they may mask a real structure or indicate the presence of a non-existent one. Such relative errors may be caused by a failure to follow the same "phase" (peak or trough) across the record, or by a lateral change of velocity which is not allowed for in the interpretation.

Besides the surface-wave "noise" which can be reduced by suitably combining the outputs of several geophones on one recording channel, a reflection seismogram also contains a large number of other events which were originally also classified as "noise". It is now recognized that many of these events are in fact multiple reflections travelling by some of the possible ray paths suggested in Fig. 5.9. These multiples may sometimes be identified by consideration of their travel-times, amplitudes and phases, or of the form of the reflector obtained by plotting them as though

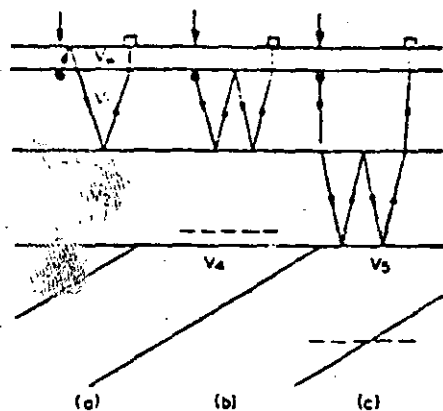


FIG. 5.9. Some possible ray paths giving rise to multiple reflections.

they were single reflections. For example, the multiple of Fig. 5.9(a) (a common event known as a "ghost") will always follow a strong single reflection after a time interval of  $2t_0$ , i.e. about twice the "up-hole" time: that of Fig. 5.9(b) will occur at almost exactly twice the travel-time of a single and will be inverted in phase by the reflection at the base of the low-velocity layer. The multiples of Fig. 5.9(b) and (c) will plot, if they are assumed to be single reflections, as horizontal reflectors in the positions of the broken lines: if it so happens that the reflecting horizons are here dipping very differently from those nearer the surface it will be apparent that the multiples cannot be singles from this depth.

If discontinuities such as faults are present in a reflector, they may show themselves not so much by a discontinuous change in the travel-time of the reflected pulse (which is often of small amplitude near a fault) as by generating a spherical or cylindrical diffracted pulse front, centred on the discontinuity as shown in Fig. 5.10. This may be distinguished from a reflection by the fact that the curvature of the front is twice as great as that normal for a reflection from that depth, and diffractions have proved to be very useful as indicators of minor faults which are otherwise not easy to detect by the reflection method.

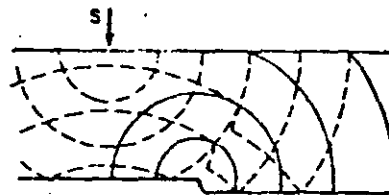


FIG. 5.10. The generation of a diffracted pulse front centred on a discontinuity in a plane reflector. The direct and reflected pulse fronts are shown as broken lines. Note that the diffracted front at the surface has about twice the curvature of the reflected front, and that its centre does not move with S.

*Plotting the position of reflectors*

After the spurious reflections are eliminated, time measurements are made on those remaining and are used to calculate the depth and dip of the reflector. We shall show how this is done for the simple case in which the velocity  $V_1$  down to the reflector is constant, and the dip is wholly in the line of the seismic profile. Clearly if dips perpendicular to this line are present they must be measured by cross-spreads and the plotting becomes more complicated.

The perpendicular depth  $h$  to the reflector is obviously given by

$$h = V_1 t_0 / 2 \tag{5.2}$$

where  $t_0$  is the measured reflection time for  $x = 0$ , i.e. for the centre trace of a conventional "split" spread.

If the reflector is dipping in the  $+x$  direction at an angle  $\theta$ , then it is clear from Fig. 5.11 that the reflected pulse, centred on the image point  $S'$ , will first reach the surface at the point  $P$ , at a distance  $2h \sin \theta$  from  $S$ , and it is at this point that the pulse front will be horizontal and the apparent velocity (see §4.2) infinite. At  $S$  the front will be inclined at the dip angle  $\theta$  to the horizontal, and if the total spread length  $2x$  is small enough compared with  $h$  for the curvature of the pulse front to be neglected, and  $t_{x_1}, t_{x_2}$  are the

23



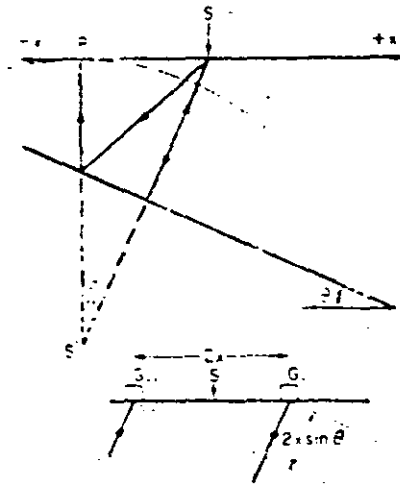


FIG. 5.11. Geometrical relationships for a shot spread over a dipping reflector. The inset diagram is an enlargement of the region near the shot-point, within which the reflected pulse front may be considered to be plane.

reflection times recorded by the end geophones of the spread, then

$$t_x - t_{-x} = 2x \sin \theta V_1 \quad (5.3)$$

Thus the reflection times (corrected to datum) for the two end traces will give the dip of the reflector provided that  $V_1$  is known, and from them and the centre-trace time  $t_0$  the position of a segment of the reflector can in principle be plotted on a cross-section. The length of the segment will be half that of the spread, or a little more if the dip is considerable, and its centre will of course be *up-dip* of the point vertically below  $S$ . The extra traces on a reflection seismogram are necessary, as we have seen in Fig. 5.6, to be sure that reflection events are correctly identified, and also so that random irregularities in the reflection times can be smoothed, giving better estimates of  $t_0$ ,  $t_x$  and  $t_{-x}$ .

If a seismic reflection record is placed with its time axis pointing vertically downwards, it can itself be regarded as a crude approximation to a geological section. The resemblance can be improved by making the surface corrections and "move-out" correction, and laying a number of records, covering adjacent segments of the reflectors, side by side, preferably then photographing them on a reduced scale. Profiles of this kind, usually using either the variable density or variable area methods of presentation, are becoming increasingly used, and it might be thought that they are in themselves a complete and final interpretation of the data. They are in fact not so, and it is important to appreciate their limitations. In the first place, reflection events appear vertically below the points on the surface at which they are recorded. This is correct only if the reflector is horizontal; if it is dipping, its "vertically plotted" position has to be "migrated" in the up-dip direction by an

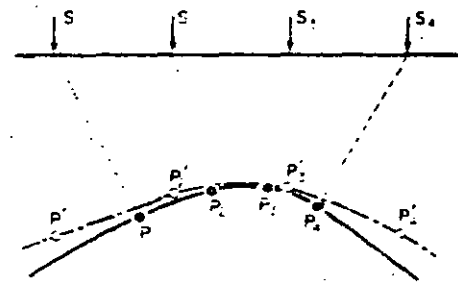


FIG. 5.12. True and "vertically plotted" positions of reflecting points.

amount depending on the angle of dip. This is made clear in Fig. 5.12, which shows normal ray paths from four shot-points, and the position of the corresponding vertically plotted points  $P_1'$ - $P_4'$ . Secondly, the profile prepared directly from the seismogram is of course a *time* section, and is of little practical value for most purposes until it is converted into a depth section: this conversion may change its appearance considerably, particularly if the velocity varies laterally, as is commonly the case. Moreover, the

multiple reflections and other "spurious" events present in the individual records may well be as prominent in the profile as the wanted reflections, again giving the possibility of misinterpretation. These warnings should not, of course, be read as a denial of the value of continuous profiles, which sometimes draw attention to important events whose correlation would not be apparent from the individual records, even when laid side by side.

#### 4. DETERMINATION OF VELOCITIES

We have seen in the previous section that the basic data required to plot the position of a seismic reflector (if its dip is entirely in the line of the profile) are the three times  $t_0$ ,  $t_x$  and  $t_{-x}$ , and the velocity  $V_1$ . This last quantity is the most difficult to determine with high precision, so that the final stage of seismic interpretation, in which travel-times are converted into depths, is often more subject to error than are the previous stages of identifying reflections and reading travel-times. The same consideration applies to the conversion of intercept times to depths in the refraction method. If the ground is uniformly and horizontally stratified, the velocity is likely to change with depth (generally increasing) so that  $V_1$  is not a simple quantity but an *average velocity* down to the depth of the reflector or refractor in question. An error in velocity determination under these conditions will of course lead to an *absolute error* in depth, but *relative* depths in gently dipping structures will not be greatly affected. If for any reason the average velocity varies laterally to any great extent, relative errors in depth can easily occur, of a size sufficient to mask minor structures in an horizon, or even to create structures where none exist.

##### *Velocities from Reflection Times*

The required average velocity, which is denoted by  $\bar{V}$  to distinguish it from the value  $V_1$  which we have used for the

homogeneous first layer, is related to the travel-time of the reflected pulse by

$$\bar{V}t_x = \sqrt{(x^2 + 4h^2)} \quad (5.4)$$

and on squaring this equation we see that if the square of the geophone distance is plotted against the square of the reflection travel-time to that geophone, we obtain a straight line whose slope gives the square of the average velocity. To use this method in practice, a set of records known as a "velocity profile" and covering a wider range of geophone distances than the usual "split-spread" of 2000 ft, is prepared by moving shot-point and geophone spread in such a way as to record reflections from the same part of the reflector at different ranges. A typical velocity profile and a ray diagram showing the way in which it was obtained appear as Fig. 5.13. A single "split-spread" record does not include large enough ranges for an  $x^2-t^2$  graph, in which the travel-times are subject to errors of a few milliseconds, to give an accurate determination of  $\bar{V}$ .

This method of measurement has the advantage that the quantity  $\bar{V}$  determined is the one which is directly used in interpretation, and that the measurement involves a fairly small addition to the routine work of shooting a reflection profile. However, it gives very little detailed information about the distribution in a vertical direction of the velocity, and it is very desirable that this distribution should be determined, in a borehole if possible.

##### *Measurements in Boreholes*

The interpretation of any geophysical survey is much less uncertain if it can be "tied" to at least one borehole, and surveys by reflection seismology are most frequently carried out in potential or known oilfields where drilling forms a large part of the exploration programme. Under these circumstances, the boreholes are invariably "logged" by some of the techniques now available for the determination of physical properties of rocks using various

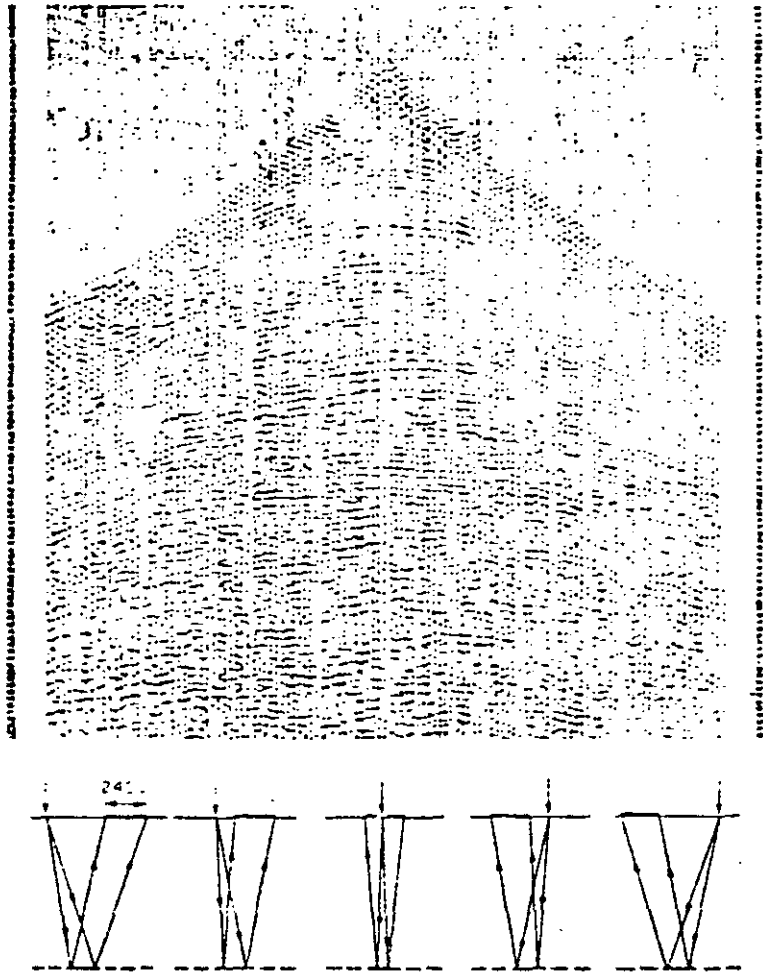


FIG. 5.13. A velocity profile. The diagram shows the successive positions of shot and geophone spread. Provided that the reflector is horizontal, the same part of it (the full line) is covered by each spread.

instruments mounted in "sondes" which can be lowered into the hole. These techniques are discussed in Ch. VIII, but it is appropriate to mention here that sondes have been developed to measure seismic velocity by timing the passage of an ultrasonic pulse through the rock over a distance of a few feet. This distance is so short that the instrument effectively measures velocity as a continuous function of depth, and so is known as the continuous velocity log or C.V.L. Measurements with the C.V.L. (a section of a typical record is shown in Fig. 5.14) show very well the detailed

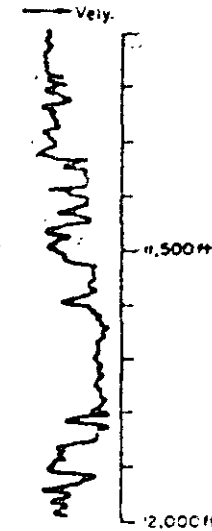


FIG. 5.14. Section of a continuous velocity log.

variation with depth of velocity, and can be used to pick out likely horizons of high reflection coefficient. Computation processes have in fact been devised by which the effect of all the reflecting horizons, major and minor, on an incident seismic pulse can be combined to give a "synthetic seismogram" which can be compared

in detail with the field results. To obtain a value of  $V$  for a particular reflection from a record like that of Fig. 5.14 will of course involve an averaging or integration of the actual times recorded in the sonde, and this may lead to a cumulative error. For this reason, the older technique of velocity measurement in boreholes, known as "well-shooting", is still important: shots are fired near the mouth of the well and recorded by hydrophones suspended in it at varying depths. The nature of this method is such that it cannot record detailed vertical variations of velocity as successfully as the C.V.L. (although its resolution is greater than that of the "velocity profile" method), but on the other hand, since it measures total travel-times to various depths, it measures directly the average velocity needed for interpretation. A combination of C.V.L. and well-shooting gives the most reliable determination of vertical velocity distribution at a point, but velocity profile measurements, or one of the other methods mentioned below, have to be used between boreholes unless these are closely spaced.

#### *Outcrop Shooting*

The most obvious way of measuring the velocity of a particular formation is to set up a spread of geophones on its outcrop, fire a shot into the spread, and time the passage of the direct wave across it. Since "outcrops" are almost invariably covered by appreciable thicknesses of low-velocity material, it is in fact the head wave from the base of this material that is timed, and this will be subject to varying delays in the varying thicknesses of overburden. It is therefore necessary to "reverse" the spread (see below, p. 122) to eliminate the effect of the overburden from the measurement. The "plus-minus" method, described in the next section (equation (5.12)), provides a convenient way of evaluating the required velocity. The distances from shot to spread must be great enough for the true direct wave through the overburden never to be the first arrival, and not so great that refracted arrivals are obtained from horizons below the one of interest. The method is of most

use in attempts to correlate velocities found in shallow refraction shooting with those of exposed formations in the same area. It is not a very satisfactory way of determining the velocity to use in the interpretation of reflection measurements.

#### *Laboratory Measurements*

Seismic velocity, like other physical properties of rocks, can be determined in the laboratory. A hand specimen is prepared with flat parallel faces, and an ultrasonic pulse transmitted across it. It is easy to time the pulse electronically, and so measure the velocity with a precision of 1 per cent or better, but measurements on a large number of representative specimens are necessary before the results can properly be used in seismic interpretation. Even if the sampling of the specimens is adequate there is the danger that they may consist of slightly weathered material, or that the formation in bulk is dissected by minor fractures which are too widely separated to be apparent on specimens a few inches across. For these reasons, laboratory measurements must be used with caution.

#### *Velocities from Refraction Measurements*

Finally, the more important changes of velocity in a section will give rise to separate branches of a time-distance graph of first arrivals in refraction seismology, and the slopes of these branches, as we have seen in Ch. IV, are the reciprocals of the velocities of the layers. It is thus an advantage of refraction seismology that the velocity information required in interpretation is a direct by-product of the exploration technique: if velocity measurements by refraction are to be used in interpretation of *reflection* surveys, a good deal of extra work is needed. However the measurements are used, it must be borne in mind that they are subject to two important limitations: firstly, that they give no information about layers of lower velocity than those immediately overlying them

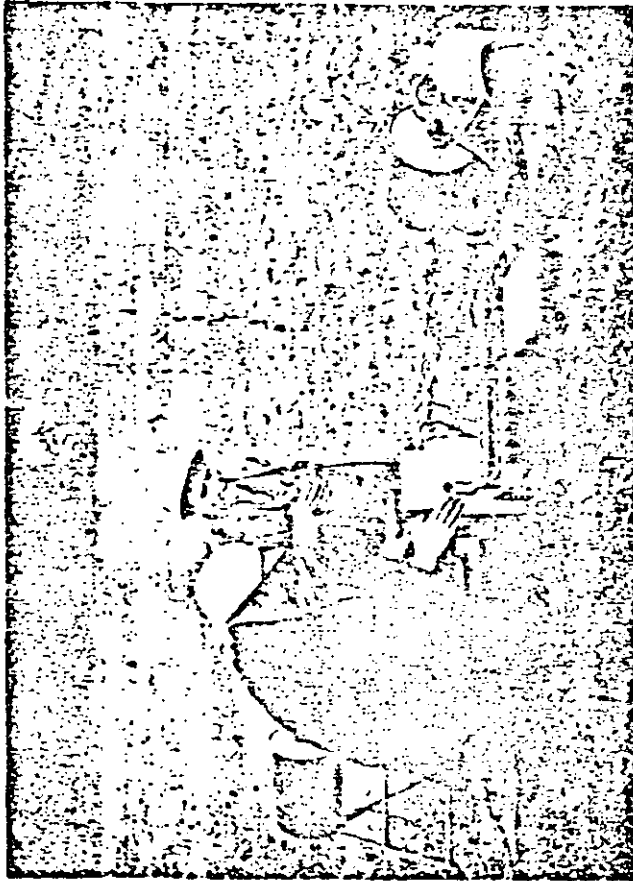


PLATE 1. A modern portable refraction seismograph (reproduced by permission of A.B.L.M., Stockholm).

(see the next section); and secondly, that the velocities obtained (as in outcrop shooting) are velocities in the *horizontal* direction, whereas in interpretation, of course, *vertical* velocities are required. In some rocks (massive sandstones and limestones, igneous rocks) this latter distinction is of little importance, but in shales and slates the velocity along the bedding or cleavage direction may be some 10–20 per cent higher than in the perpendicular direction.

The importance of full and accurate knowledge of velocities in seismic interpretation cannot be over-emphasized, and a considerable proportion of the effort of any seismic survey should go into obtaining this knowledge.

## 5. THE REFRACTION METHOD

In reflection seismology it is possible to use a standardized routine for obtaining records, from which only relatively small departures are made to take account of local variations in conditions. Thus the "split-spread", covering about 2000 ft of ground, with a central shot-point, the whole arrangement being moved about 1000 ft along the profile for the next shot to give continuous coverage of reflector, is very characteristic of a survey of this kind, and commercial reflection seismograph sets are designed with this routine in view.

In refraction work, on the other hand, the object is to build up a time-distance graph with an adequate number of points on the branches corresponding to all refractors of interest, and this obviously means that geophone spacing and total line length will have to be carefully chosen to suit each particular problem. It is therefore not possible to describe prospecting by the refraction method in terms of a standard routine, but only to indicate some of the ways in which such surveys may be carried out and interpreted.

*Time-Distance Graphs from Dipping Interfaces*

We have already seen in §4.2 that the apparent velocity recorded on the ground surface for a head wave from an interface dipping downwards in the positive  $x$  direction is not  $V_2$ , the true velocity of the lower medium, but

$$V_a = V_1 \sin(i_c + \alpha) = V_2 \sin i_c \sin(i_c + \alpha) \quad (5.5)$$

which is less than  $V_2$ . If the dip is upwards in the positive  $x$  direction, a high apparent velocity  $V_u$  is observed, given by

$$V_u = V_1 / \sin(i_c - \alpha) = V_2 \sin i_c / \sin(i_c - \alpha). \quad (5.6)$$

Since we normally have no knowledge of the value of the dip, it follows that a refraction profile shot in one direction gives only the apparent velocity  $V_a$  (or  $V_u$ ) which is related in an unknown way to the true velocity. It is clear that both the true velocity and the angle of dip can be found if the profile is "reversed", that is if a new travel-time graph is determined with its origin at the end-point of the first one. From then both  $V_a$  and  $V_u$  are known, and, if the refractor is plane under the profile

$$\left. \begin{aligned} i_c + \alpha &= \sin^{-1}(V_1/V_2) \\ \text{and } i_c - \alpha &= \sin^{-1}(V_1/V_u) \end{aligned} \right\} \quad (5.7)$$

from which  $\alpha$  and  $i_c$  (and hence  $V_2$ ) can be found. The meaning of "reversal" is illustrated in some detail in Figs. 5.15 to 5.17. Two ways of shooting a profile from  $A$  to  $B$  are shown in Fig. 5.15(a): they give the same information, since the origin of the time-distance graph (Fig. 5.16) remains at  $A$ , and the same ray paths are traversed, although the direction of travel of the seismic pulse is indeed "reversed" if the second arrangement is adopted. Normally, of course, it will be more convenient to use the first arrangement of simultaneous recording at several points of a single shot, though the alternative is useful if shots can be fired in water without the need for drilling. To reverse this profile in the

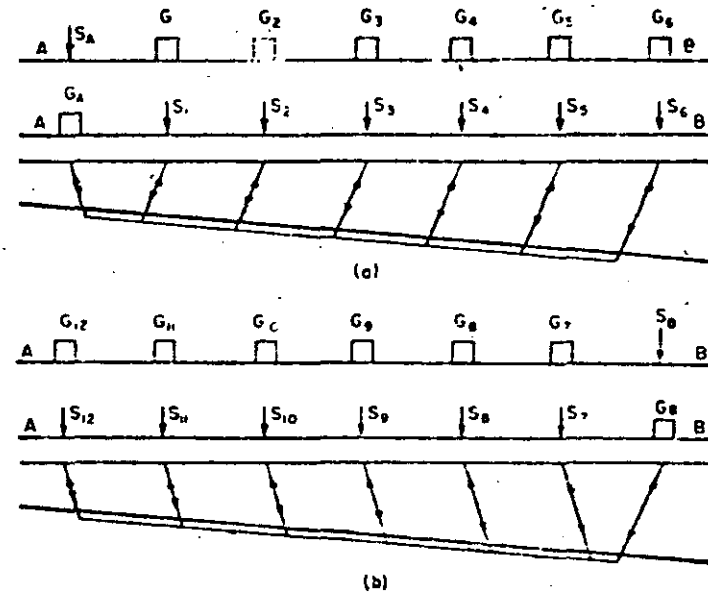


FIG. 5.15. The "reversal" of a refraction profile. (a) Two ways of shooting "from A to B." Note that no reversal is obtained. (b) Shooting in the reverse direction from B to A.

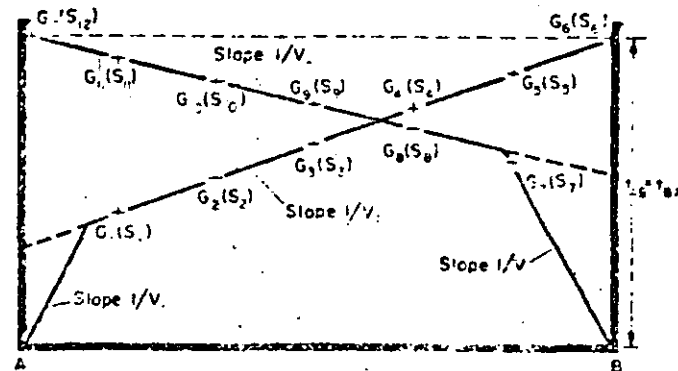


FIG. 5.16. The pair of travel-time graphs which would be given if a single refracting horizon were dipping uniformly from A to B.

29

seismological sense implies moving the origin of measurement to *B* (Fig. 5.15(b)) so that a different pattern of ray paths is produced. Again shots and geophones can be interchanged with no effect on the results. An important feature of a strict reversal of this kind is that the overall time from one end of the profile to the other (often called the "reciprocal time") is measured twice, so that a check on the internal consistency of the results is possible. Fig. 5.17 shows

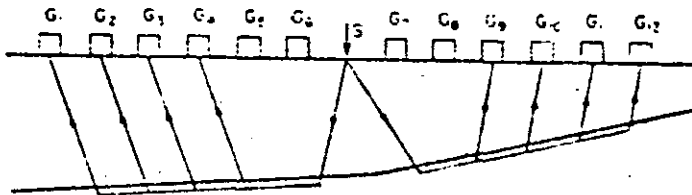


FIG. 5.17. Refraction ray paths for a split spread. The true refractor velocity could be obtained only if the dip were uniform from  $G_1$  to  $G_{12}$ .

that the standard split-spread of reflection work gives "reversal" of a kind for refraction arrivals: if the refractor were of uniform dip beneath the *whole spread*, then a single shot at *S* would give both up-dip and down-dip apparent velocities. As, however, the dip changes between  $G_4$  and  $G_6$ , where the head waves are first seen as first arrivals, it is clear that the two halves of the spread must be treated separately and both remain "unreversed". For strict "reversal" of a refraction line, the *same part* of the refractor must be covered by both time-distance graphs.

*Mapping of Irregular Interfaces*

The concept of apparent velocity helps us also to understand the form of the time-distance graph from an irregular refractor, such as the bed of an old river channel filled with alluvium. Clearly, as the interface dips downward in the direction of shooting, the time-distance graph will increase its slope (decrease in apparent velocity) and vice versa, so that the departures of the graph from a

line of slope  $1/V_1$  will qualitatively form a mirror image of the interface, as shown in Fig. 5.18. The features of the graph are displaced laterally in the direction of shooting from those of the refractor, since the head wave does not return vertically through the overburden.

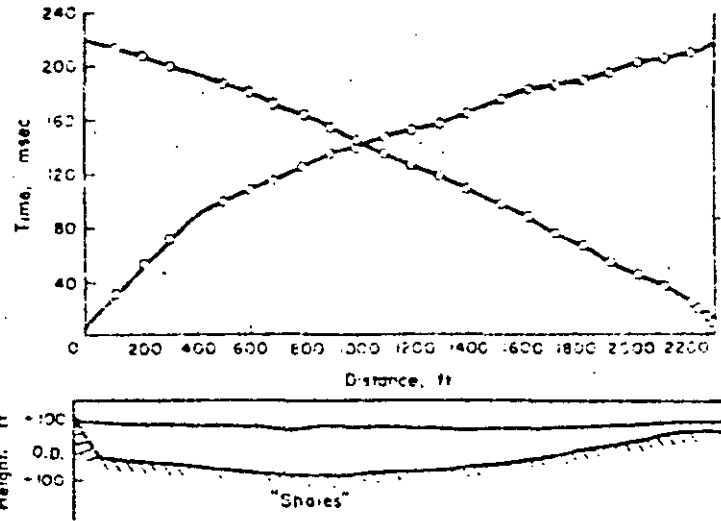


FIG. 5.18. A reversed profile across an irregular interface (Allen 1960).

Another way of appreciating the physical significance of the irregular time-distance graphs of Fig. 5.18 is to realize that the "intercept-time"  $2h \cos i_c / V_1$  for a horizontal refractor at depth may be regarded in the more general case of an irregular refractor as being composed of two "delay times"

$$t_s = h_s \cos i_c / V_1 \quad \text{and} \quad t_g = h_g \cos i_c / V_1$$

where  $h_s$  and  $h_g$  are the thicknesses (measured normal to the refractor) of the top layer at shot-point and geophone respectively. The delay time  $t_s$  can be defined (Fig. 5.19) as the difference

50

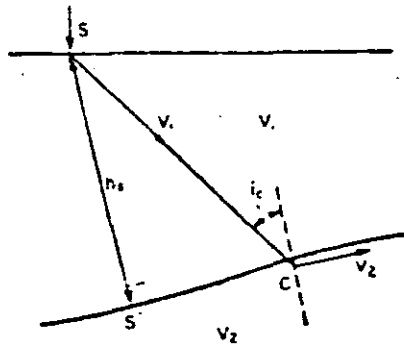


FIG. 5.19. The definition of the delay time

$$t_d = \frac{SC}{V_1} - \frac{S'C}{V_2} = h_1 \frac{1}{V_1 \cos i_c} - \frac{\tan i_c}{V_2} = h_1 \cos i_c \cdot V_1$$

A similar definition applies to  $t_d$ .

between the time actually spent by the pulse in the upper layer, and that which it would have spent in travelling in the refractor at velocity  $V_2$  from a point  $S'$  below the shot-point to the point of critical incidence  $C$ . In Fig. 5.18 the first of these delay times is constant, but the second increases and decreases with the local depth at the position of the geophone. The total travel-time is therefore increased above the value appropriate to a horizontal interface by an amount depending on the extra depth.

If  $V_2$  is known, together with the depth to the interface at the origin, the form of the interface can be calculated from an unreversed profile. If the profile is reversed (as is always desirable in case  $V_2$  should vary over its length), then the form of the refractor can be simply found by any one of a number of standard methods. For example, if in Fig. 5.18 the delay times at the two ends of the profile are  $t_{d1}$  and  $t_{d2}$ , and that at the geophone at a distance  $x$  from  $S_1$  is  $t_d$ , then

$$\begin{aligned} t_1 &= t_{d1} + t_d + x/V_2 \\ \text{and } t_2 &= t_{d2} + t_d + (X - x)/V_2 \end{aligned} \quad (5.8)$$

where  $X$  is the total length of the profile, and  $t_1, t_2$  are the travel-times of the head wave to the same geophone from the two shot-points. Adding these equations we have

$$t_1 + t_2 = t_{d1} + t_{d2} + X/V_2 + 2t_d \quad (5.9)$$

But the total travel-time from one shot-point to the other (in either direction) is the reciprocal time

$$T = t_{s1} + t_{s2} + X/V_2 \quad (5.10)$$

so that

$$t_d = \frac{1}{2}(t_1 + t_2 - T) = 2h \cos i_c / V_1 \quad (5.11)$$

and the depth  $h$  at this geophone can be found from the measured times and velocities. It is worth noting that

$$\begin{aligned} t_1 - t_2 &= t_{s1} - t_{s2} - X/V_2 + 2x/V_2 \\ &= \text{constant} + 2x/V_2 \end{aligned} \quad (5.12)$$

so that this time difference plotted against  $x$  gives a line whose reciprocal slope is half the refractor velocity. Changes in refractor velocity can be detected in this way. This method is described more fully by Hagedoorn (1959).

In the above discussion we have assumed that the geophones are set out in line with each other and with the shot-point. A basically different arrangement of shots and geophones is used in the "fan" or "broadside" shooting methods. Here the detectors are placed on an arc centred on the shot, or on a line at right angles to the line of shooting, so that the distance is approximately the same for all of them. This plan is particularly suitable for a preliminary location of bodies or structures which can then be explored in more detail by profiling. For example, if the "fan" contains a large steep-sided body of contrasting velocity, Fig. 5.20 makes it clear that the travel-times will show a minimum (if  $V_2 > V_1$ ) for those

31



paths which pass through the greatest thickness of the body. If the shot-to-geophone distances vary appreciably across the fan it will be necessary to prepare a "normal" time-distance graph for the area and to plot out the departures from it of observed travel-times across the anomalous body. A second "fan" approximately at right angles to the first, will enable the position and extent of the body to be roughly plotted. This method has been extensively

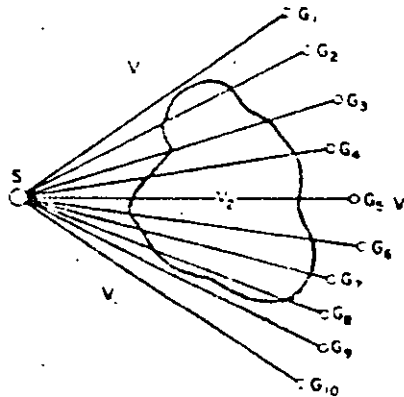


FIG. 5.20. Plan view of "fan" arrangement of geophones for locating a body (not necessarily outcropping at the surface) of high velocity  $V_2$  in homogeneous material of velocity  $V_1$ . The travel-times will be "normal" for geophones  $G_1$ ,  $G_9$  and  $G_{10}$  and anomalously low for the others.

used to locate salt domes, but could of course in principle locate ore-bodies of high seismic velocity, though the variations in travel-time become inconveniently small if the body has dimensions less than a few hundred feet.

With the same arrangement of shot and geophones, the course of a buried valley may be traced. In this case, the range  $x$  is chosen to be great enough for the head wave from the bedrock to be the first arrival at the geophones, so that the travel-time is given by

$$t = x/V_2 + t_s + t_g \quad (5.13)$$

where  $t_s$  and  $t_g$  are the delay times at shot-point and geophones. As  $x$  and  $t_s$  are the same for all geophones, variations in  $t$  are simply due to variations in  $t_g$ , i.e. to the thickness at the geophone of the alluvial layer, the velocity of which is supposed to be roughly constant. Fig. 5.21 shows how the method might be applied: the longer travel-times recorded on  $G_2$ ,  $G_3$  and  $G_4$  will show where the next detailed profile for investigation of the cross-

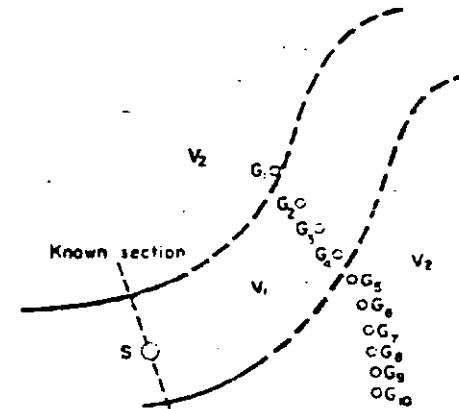


FIG. 5.21. Application of fan-shooting to tracing the course of a buried valley

section of the filled valley should be sited. If the two velocities are very uniform the range used can be as great as the likely course of the valley will allow. If  $V_2$  varies, as for example if there is an unsuspected anisotropy of 20 per cent so that in the direction of  $G_1$  it is 12 ft/msec but only 10 ft/msec in the direction of  $G_{10}$ , then at a range of little more than 1000 ft the time differences due to this become comparable with those to be expected from a valley 100 ft deep filled with material of velocity 5 ft/msec. Even in a preliminary exploration of this kind, then, the importance of velocity control is very great.

*Limitations on the Reliability and Accuracy of Interpretation of Refraction Surveys*

Even assuming that a refraction survey has been properly carried out, with adequate charges to give clear "first breaks", careful surveying of positions of shots and detectors, and so forth, there remain many uncertainties about the interpretation of even such an apparently straightforward pair of travel-time graphs as those of Fig. 5.18. In the first place, near surface irregularities of a low-velocity layer may introduce variable time delays, and a correction to datum should be made as with a reflection survey. The presence of a surface low-velocity layer may be shown by the first observed branch of the graph not passing through the origin, but it may be present only over a part of the profile well away from the origin and so not show itself in this way. For this reason, and because the value of  $V_1$  may well vary over the length of the profile, it is essential to shoot a series of short profiles within the main one, whose only object is to determine  $V_1$  and the time delay, if any, introduced by a layer of lower velocity.

If the control on velocity is good, and the branches of the time-distance graph represent the *only* layers present in the ground, there is no reason why a refractor at a depth of the order of 100 ft should not be plotted to within a few feet. Although this refractor is likely to coincide with a conventional geological horizon, this is not necessarily so, and it is really essential for a refraction profile to be "tied" to known geology either at outcrop or in a borehole, so that the refracting horizons can be identified with certainty.

There are two important circumstances in which the travel-time graph does *not* give the full information about the ground layering. If a layer overlies one of lower velocity, instead of each interface being one of a velocity increase downward, as we have so far supposed, Fig. 5.22 shows that since the refraction at this boundary will be *towards* the normal, there can be no ray travelling below the  $V_2$ - $V_3$  interface to generate a head wave and a corresponding

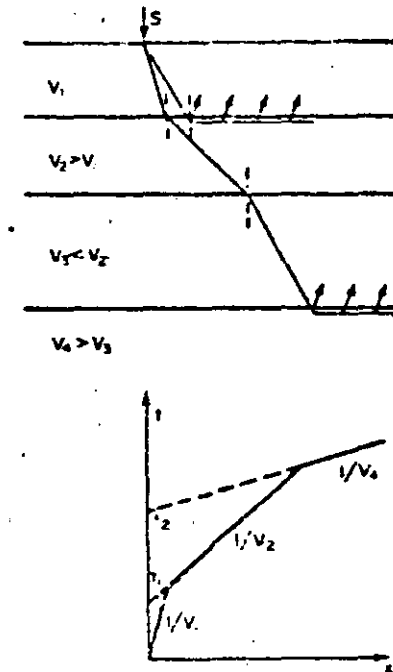


FIG. 5.22. *The effect of a downward decrease in velocity.*

" $V_3$ " branch of the graph. If the graph is the only evidence available, the intercept time  $t_2$  will be used to find the depth to the top of the  $V_4$  layer as though the  $V_3$  layer had the higher velocity  $V_2$ , and an over-estimate of depth will result. The over-estimate may be considerable, being determined by the thickness of the  $V_3$  layer and the amount by which its velocity falls short of  $V_2$ .

If one of a series of layers is thin in comparison with its depth, the head wave from it may never reach the surface as a first arrival, since the head wave from the layer below overtakes it at a range at which it still arrives later than the direct pulse. This situation can lead to a misinterpretation if *only* first arrivals are

plotted on the graph. A good example of this is shown in Fig. 5.23, taken from a paper by Soske (1959). The first interpretation as a two layer case (note that the velocity of 23 ft msec is improbably high to represent a third layer, and so is more plausibly interpreted as an "up-dip" apparent velocity of the head wave from the 16 ft msec refractor) is shown to be erroneous by a borehole near the shot-point, which passes through a relatively thin bed of basalt of intermediate velocity. With the addition of the borehole control, or by recording the "second arrivals" of the head wave from the basalt, a correct interpretation is possible. Another example, on a much larger scale, of the possibility of a "blind zone" is the fact that the layer of sediment, perhaps 2 km thick, on the bed of the oceans, does not contribute first arrivals to a refraction profile shot on the ocean surface: the depths and velocities involved in this case are in fact such that the sedimentary layer would have to be more than 10 km thick before it could be detected without making use of later arrivals. The greatest possible thickness of a blind zone can readily be calculated from apparently "two-layer" data if a velocity is assumed for the intermediate layer (Green 1962).

## 6. THE CHOICE BETWEEN THE SEISMIC AND RESISTIVITY METHODS IN GEOPHYSICAL PROSPECTING

Far more money is spent on applied seismology, and in particular on reflection seismology, than on any other geophysical method. This is partly because it is an inherently expensive method, and partly because it has been found to be more successful than any other in exploration for oil, which is the largest single field of geophysical effort. It does not, of course, follow that the seismic method should be applied automatically to every problem, even if economic considerations are not of over-riding importance. As an example of the way in which the choice may be made, let us consider the problem of delineating the bedrock

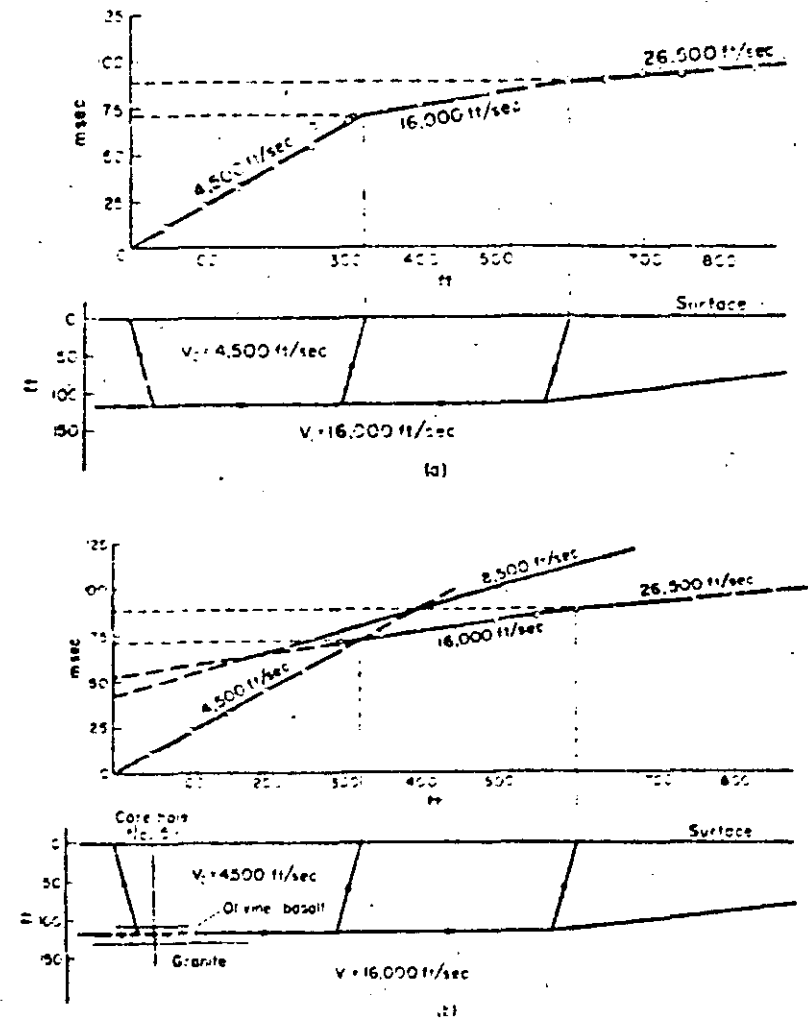


FIG. 5.23. The "blind zone" in refraction seismology. (From Soske, 1959). (a) Erroneous interpretation based on first arrivals only; (b) The structure shown by drilling; with calculated time-distance graph for head waves from second layer.

surface under cover of no more than a hundred feet of alluvium along a single line. It is physically possible to solve this problem by placing either a set of boreholes, or a set of resistivity depth-meters (see Ch. II and III), or a set of geophones, at intervals along the line. If cost is the only consideration the resistivity method will certainly be used, with the seismic method as second choice, as the cost of drilling a set of holes to give equally closely spaced values of the depth to bedrock will be very much greater than either of the geophysical methods, even allowing for the fact that they would need one or two boreholes as control points. When the quantity and quality of information obtained by the three methods is taken into account, however, a different decision may well be made. The resistivity method might still be chosen if rather large ( $\pm 20$  per cent) errors in the depth are tolerable, but often the nature of the work will be such that the greater accuracy (about  $\pm 10$  per cent in a typical case of this kind) of the seismic method might more than pay for its greater cost. Another point to be considered is whether the velocities determined in the one case are likely to be more diagnostic of the ground properties in which one is really interested than are electrical resistivities. A series of closely spaced boreholes will give greater accuracy still, but hardly a gain in keeping with the extra cost, particularly when it is remembered that any gain of accuracy in point measurements may be more apparent than real unless the points are very closely spaced indeed. The information (other than depth) obtained by boring is of course much more than that given by either geophysical method, but may be too definite if the bedrock or overburden are so variable that a knowledge of their average properties is of more use than a limited number of spot checks.

It is of some interest to speculate how the relative value of these three techniques is likely to change as a result of technological advances. Both the cost of drilling and the nature of the information it provides seem unlikely to change appreciably, and the same may be said of the electrical resistivity method. The equipment required for this is already cheap (about £200) and the cost of a

resistivity survey is mainly in the time taken to carry it out and interpret the results, which cannot be greatly reduced. The seismic method, however, with the advent of light, transistorized equipment and simple impact sources has come to compete in cost with resistivity measurements for shallow investigations, and it is now often possible to make the choice between them on scientific rather than on economic grounds.



**DIVISION DE EDUCACION CONTINUA  
FACULTAD DE INGENIERIA U.N.A.M.**

MECANICA DE ROCAS APLICADA A LA MINERIA Y A LA CONSTRUCCION

GEOPHYSICAL STUDIES OF ROCK MASSES

MAYO, 1985

5th ISRM

Melbourne 1983

S. H. Maycott

1

## GEOPHYSICAL STUDIES OF ROCK MASSES

Etudes géophysiques des massifs rocheux

Geophysikalische Untersuchungen von Fels

A. I. Savich

Dr.Sc.(Phys.-Math.), Chief of Geophysical Department

A. D. Mikhailov

Dipl.Eng., Chief Expert of Geophysical Department

V. I. Koptev

Cand.Sc.(Tech.), Chief Expert of Geophysical Department

M. M. Iljin

Cand.Sc. (Phys.-Math.), Senior Geophysicist of Geophysical Department  
"Hydroproject" Institute, Moscow, USSR

### SUMMARY

The paper presents the basic results and methods of geophysical studies of rock masses in the USSR. Three main objectives of studies are considered: studies of the structure, properties and the state of natural rock masses, studies of change of their properties as a result of mining and construction work and studies of the dynamics of deformation processes going on in the foundation rock of the structures in operation.

### RESUME

Le rapport traite de principaux résultats et de la méthodologie d'études géophysiques des massifs rocheux en URSS, effectuées dans les trois directions principales: étude de la constitution, des propriétés et de l'état naturel des massifs rocheux, étude de modifications de ces propriétés au cours des travaux d'excavation et de construction, étude de la dynamique des déformations dans les fondations d'ouvrages au cours de l'exploitation.

### ZUSAMMENFASSUNG

Im Beitrag werden Hauptergebnisse von geophysikalischen Untersuchungen sowie Felsuntersuchungstechnik in der UdSSR behandelt. Es sind drei Hauptrichtungen der Untersuchungen zu verzeichnen: Studien von Felsbeschaffenheit im natürlichen Zustand, Erfassung von Beschaffenheitsänderungen im Felsbau, Studien der Dynamik der Verformungsprozesse in Gründungen von Bauwerken beim Betrieb.

## 1. INTRODUCTION

The designing, construction and operation of modern structures founded on rocks or cut in rocks foregrounds the urgent problem of comprehensive studies of rock masses. Judging by the problems arising hereat and the methods of tackling the problems one can distinguish the following objectives:

- studies of the structure, properties and state of natural rock masses;
- assessment of changes in properties and state of rocks in the process of mining and construction work and of various kinds of treatment for improvement of rock masses in the zones of their interaction with structures;
- studies of deformation processes in rock masses and prediction of the resultant phenomena during the service life of the engineering structures.

The paper deals with the principles, methods and outcomes of the solution of some typical problems of the above studies using geophysical and, mainly, seismic methods. The report is based on the generalized data of geophysical survey conducted in the areas of large hydroelectric projects in the USSR, considering

the data of analogous studies obtained in other fields of the engineering geology, mining and exploration geophysics.

## 2. STUDIES OF THE STRUCTURE, PROPERTIES AND STATE OF NATURAL MASSES

The typical problems of this trend, as well as the main geophysical methods, used to solve them, are summed up in Table I. As a rule, to solve these problems the methods of engineering geophysics are used in close relation with traditional methods of engineering survey: engineering-geological, hydrogeological and geo-technical survey methods. As the engineering geophysics developed and improved, its role in solution of the problems in question is steadily increasing, while the volumes of laborious and expensive traditional surveys are going down.

Physical prerequisites for solution of the problems listed in Table I — the geophysical methods are the theoretical and experimental relations between the parameters of different geophysical fields (elastic waves fields, electric and magnetic fields and other physical fields in rocks) and characteristics of

Table 1. System of geophysical methods used in engineering-geological studies of rock masses.

Purpose of investigation	Methods and types of investigation									
	seismic methods	ultra-sonic and seismic methods	electrical profiling and vertical electrical sounding	methods of induced polarization and self-potential methods	magnetic bearing and micro magnetic survey	standard electrical logging	resistivity and double-solution method	nuclear methods	tele-and-photo logging	seismometric methods
<b>1. Investigation of rock mass structure.</b>										
1.1 Lithological zonation	+	+	+	+	+	+	-	+	+	-
1.2 Singling out of fault zones	+	+	+	+	+	+	+	+	+	+
1.3 Estimation of thickness and nature of weathering zone	+	+	+	-	-	+	-	+	+	-
<b>2. Determination of physical-mechanical properties of state of the rocks.</b>										
2.1 Studying of jointing intensity	+	+	+	-	+	+	-	-	+	-
2.2 Assessment of elastic and deformability indices	+	+	+	-	-	+	-	-	-	-
2.3 Determination of strength parameters	+	+	-	-	-	+	-	-	-	-
2.4 Studying of permeability properties	-	+	-	-	-	+	+	+	-	-
2.5 Assessment of water saturation, water content and porosity	-	+	-	+	-	+	+	+	-	-
2.6 Assessment of rock preservation "in situ"	+	+	+	-	-	+	-	-	-	+
2.7 Assessment of anisotropy and heterogeneity	+	+	+	-	-	-	+	-	-	-
2.8 Studying of state of stress	+	+	-	-	-	-	-	-	-	-

the media under study (Goryainov, Lyakhovitski, 1979; Nikitin, 1931; Ogilvi, 1962; Savich et al., 1969). The solutions sought are mainly based on the absolute quantities of measured geophysical parameters (time of wave run, propagation velocities and indices of elastic wave attenuation, electric resistance values, magnetic susceptibility etc.) and also on the regularities of their distribution in space. To obtain the data rather complicated schemes of measurements are applied, the observations conducted on the surface of rock masses and in the interior points of the medium being closely combined (Goryainov, Lyakhovitski, 1979; Savich et al., 1969) for interpreting the obtained data the machine processing methods based on the theoretical solutions developed in the areal and research geophysics and also in engineering geophysics, are finding ever increasing use (Lyakhovitski, Kapadenaki, 1976; Rydzanski et al., 1978).

#### 2.1 Rock masses mapping.

To do this the most promising systems are the areal and volumetric observation systems when several geophysical methods characterizing the medium by a combination of various geophysical parameters are used at a time. This ensures not only a greater degree of reliability in distinguishing the rocks with different physical properties in the rock mass, but also increases the trustworthiness of the engineering and geological interpretation of the geophysical survey data.

As an example to the above statement, on Fig. 1 is shown a geological-geophysical section obtained as a result of a complex of areal (over the mass surface) seismic prospecting and electrometric and magnetometer surveys conducted. The drilling that followed the surveys has proved that the errors in defining the main engineering-geological boundaries are not in excess of 5% at practically full agreement of the quantitative and qualitative characteristics of properties of rocks in the distinguished structural elements of the mass. These

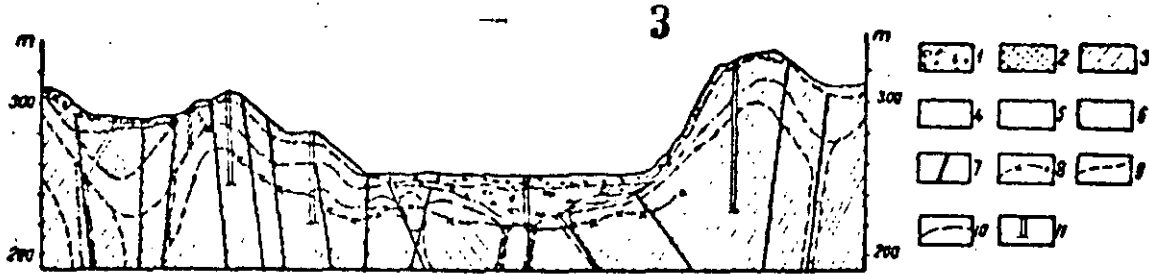


Fig. 1 Geological-geophysical section at the dam site

1 - talus-and-alluvial deposits; 2-6 - quartzites and quartzitic schists with interlayers of micaceous sandstones and clay-micaceous schists having respective values of  $V_p$ : 1.4-2.0; 2.0-2.8; 2.8-3.5; 3.5-4.7; 4.7-5.3 km/sec; 7 - zones of tectonic dislocations; 8 - footing of intensive weathering zone; 9 - lithologic boundaries; 10 - boundaries of rocks having various degrees of preservation; 11 - boreholes.

sections evidently contain a considerable amount of engineering-geological information and may serve a basis for elaboration of the respective engineering designs.

A more detailed differentiation of the rock mass and, especially, of its inner parts can be obtained using the volumetric observation systems and in particular, the multipoint sounding. The numerical methods of solution of primal and inverse problems of sounding (Yefimova, 1973; Karus et al., 1980), widely used in the USSR, make it possible to single out zones with anomalous values of geophysical parameters in the rock pillars between the mining excavations (Fig. 2) The combination of these data

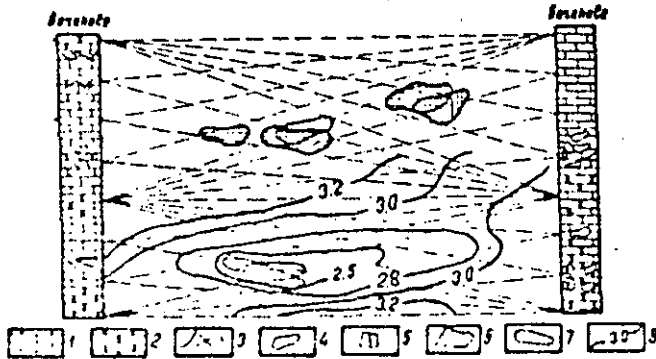


Fig. 2 Results of acoustic sounding of carbonate rock between coreholes (acc. to Karus, 1980)

1 - limestone; 2 - dolomite; 3 - fissures; 4 - inclusions; 5 - drop zone of drilling tools; 6 - zone of abnormal great intake values; 7 - zone of low velocities; 8 - isolines of velocities, km/s.

and the results of the profile geophysical measurements makes it possible to build free

volumetric engineering-geological models (see Fig. 3). Such models practically give a comprehensive characteristic of the mass structure and predetermine the authenticity of the results of subsequent studies of properties and state of rocks in situ.

## 2.2 Studies of properties and state of rocks

The last years are marked by certain achievements in the use of geophysical methods for studying the physical and mechanical properties of rocks and state of rock masses. It was promoted by the development of the required equipment and methods of measuring of the same geophysical parameters of the medium at different scale levels: from samples of some cm<sup>3</sup> in volume to large geostructural blocks of hundred meters and first kms in size. The mentioned possibility to use the engineering geophysics allowed one to realize the following principle of the technique of studying the rocks "in situ" conducting of measurements at different scale levels and an integrated interpretation of the data of different-scale measurements (Savich et al., 1969). Such studies resulted in more comprehensive analysis of the factors which govern the variability of physical-and-mechanical properties of rock masses and in the development of the methods of quantitative estimation of properties with the help of geophysical methods. Some of them are considered below.

### 2.2.1 Estimation of rock mass heterogeneity

Parallel with traditional statistical methods, the different-scale geophysical measurements allow using a radically new approach to the estimate of heterogeneity of rock masses, namely: to estimate the nature and degree of heterogeneity of the medium by the shape and slope of scale curves\*) for the geophysical parameters to be measured.

An alternative of this method, where the elastic wave velocities are used as initial parameters, has been in application for a number of years in the USSR for estimation of heterogeneity of rock foundations of hydroelectric structures (Savich et al., 1969; Lykoshin, 1971). In accordance with the data obtained, rock masses which are composed of different types of rocks and located in various natural conditions, feature particularly specific laws of variation of mean values of velocities of elastic waves  $\bar{V}$  depending on the scale of single

\*) i.e. curves which represent the variation of mean (or most probable) values of the parameter in question against the given scale of measurements  $W_1$ .



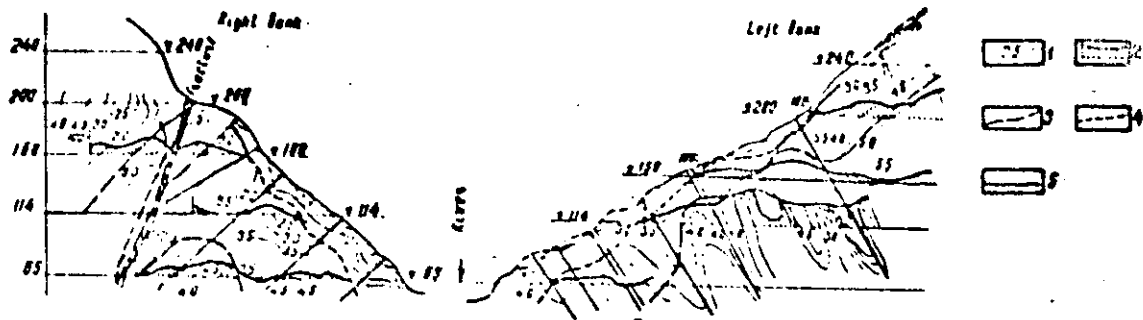


Fig. 3 Character of spatial distribution of geophysical waves velocities  $V_p$  and  $V_s$  in rock mass of the Inguri dam, high foundation (section along the line of granite galleries)

1 - isoline of velocity  $V_p$  km/sec; 2 - curves in mining openings; 3 - isoline of  $\gamma = 200 \cdot 10^5 \text{ N/m}^2$ ; 4 - isoline of  $\gamma = 100 \cdot 10^5 \text{ N/m}^2$ ; 5 - large tectonic fissure

measurements  $W_i$ , which is determined by the approximate expression (1).

$$W = \pi R (\alpha \lambda)^2 \quad (1)$$

where  $\lambda$  - length of elastic waves;  $\lambda = V/f$ ,  
 $f$  - frequency of elastic vibrations;  $\alpha = 0.25$ ;  
 $R$  - base (interval) of velocity measuring.

A series of such relationships is given in Fig. 4. It was found out that the slopes of

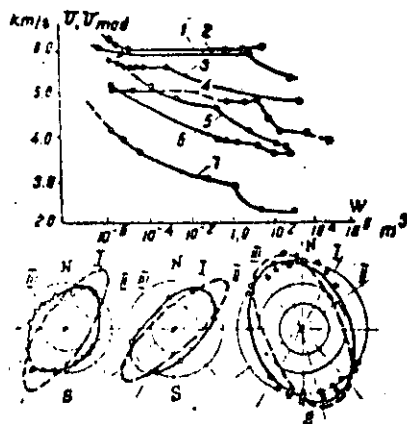


Fig. 4 Alteration of average values (a) and anisotropy (b) of elastic waves velocities depending on the scale of investigations

1 - diabbases; 2 - granites; 3 - porphyritic basalts; 4 - aleurolites; 5 - gneisses, crystalline schists; 6 - limestones; 7 - limestone; Volumes 1-3 respectively 1; 10;  $10^2 \text{ m}^3$ .

curves  $\bar{V} = f(W_i)$  indicate the degree of heterogeneity of rock masses in question, while the breakpoints show the prevailing degree of heterogeneity of different levels and orders (Savich et al., 1969). Judging from the data presented in Fig. 4 different rock masses have their own clearly defined heterogeneity charac-

teristics. The knowledge of these characteristics is necessary both for the choice of optimal technique of studying the properties of the rock mass, (in order to choose the measurement bases, frequencies of elastic vibrations etc), and for the estimation of the scale effect as applied to the moduli of elasticity and deformation, strength indices etc.

### 2.2.2 Studies of anisotropy

It is well known that anisotropy of rock masses is governed by various natural factors and each factor has a tangible influence on the media properties only at a certain scale level (Lykoshin et al., 1970). For practical purposes it is important to have an estimate of anisotropy of the mass at a level which corresponds to the scale of the structure under designing or its separate elements. The problem can be solved by means of azimuthal measurements of geophysical parameters provided there is a strong correlation between the technique and scale of studies. In Fig. 4 are given examples of such measurements for one and the same rock mass at three scale levels: the anisotropy of the carbonate rock mass in question, caused by the effect of diversely oriented tectonic fissures of various order, for rock blocks of about 1 m and 20-25 m in size, differs greatly both in its intensity and in its character. Such phenomena can be also caused by other factors: bedding, appearance of tectonic stresses etc (Lavrova, 1976; Savich, Yashchenko, 1979). Variations of anisotropy of properties of rocks at different scale levels can be most substantial and they must be taken into account when giving a general geomechanical characteristic of rock masses in question.

### 2.2.3 Determining of elastic and deformation properties

At present geophysical and, in particular, seismoacoustic methods have become the leading methods of quantitative studies of elastic and deformation properties of rock masses (Goryainov, Lyakhovitski, 1979; Mikitin, 1981; Savich, Yashchenko, 1979). The methods used in the USSR to solve the problems are the following:  
 - numerous measurements of the geophysical parameters in different parts of the given mass;  
 - schematic zonation of the rock mass on the basis of geophysical and engineering-geological studies;  
 - determination of reasons which govern the variation of measured geophysical parameters and singling out of the zones within which

the effect of one of factors is predominating;  
- establishment of correlation relations between the geophysical parameters and measured static modulus of elasticity  $E_s$  or modulus of formation  $D$ ;

conversion of geophysical parameters to moduli  $E_s$  and  $D$ ; statistical processing of the data and estimation of the generalized parameters of deformability (Savich, Yashchenko, 1979).

The seismoacoustic methods are used most successfully. The generalization of the obtained results made it possible to elicit clear defined regularities in relations between the elastic waves velocities  $U_p(U_s)$  and their usage for estimating the values of dynamic modulus of elasticity  $E_{dyn}$  and the sought values  $E_s$  and  $D$ . The interrelations between the given parameters are governed mainly by the type of rocks under study and by the conditions of estimation of the static moduli  $E_s$  and  $D$ : duration of application of static load  $\sigma$ , maximum value  $\sigma = \sigma_{max}$ , number of loading cycles (Savich, Yashchenko, 1979). Under fixed conditions of definition of static parameters the relations between moduli  $E_{dyn}$ ,  $D$  and  $E_s$  are very authentically given by expressions (2) - (3) (Savich, 1979).

$$\rho_g E_s - A E_s e^{-\alpha \sigma_{max}} \rho_g E_{dyn} - B E_s e^{-\beta \sigma_{max}} \quad (2)$$

$$\rho_g D - A D e^{-\alpha \sigma_{max}} \rho_g E_{dyn} - B D e^{-\beta \sigma_{max}} \quad (3)$$

Values  $A$ ,  $B$ ,  $\alpha$  and  $\beta$  for the rocks of the definite geological complexes are rather close. The statistical processing of the obtained data has indicated that rocks can be divided to four groups, each group having constant values of the above coefficients. The rock groups are the following: sedimentary carbonate rocks, sedimentary clastic and dust-like rocks, igneous and metamorphic rocks \*). The values of the  $A$ ,  $B$ ,  $\alpha$  and  $\beta$  coefficients for the mentioned groups according to Savich, (1979) are given in Table II. Using these data it is

Table II Summary table of coefficients for equations 2 and 3 for various types of rocks\*\*

Sl. Nos.	Rocks	static moduli $E_s, D$	A	$\alpha$	B	$\beta$
1.	I. Carbonate rocks	$D_z$	0.970	0.0119	6.153	0.0110
2.		$E_s$	0.344	0.0176	2.425	0.0149
3.	II. Igneous rocks	$D_z$	0.944	0.0188	5.730	0.0148
4.		$E_s$	0.462	0.0260	2.775	0.0200
5.	III. Crystal-line gneiss	$D_z$	0.723	0.0090	5.004	0.0076
6.		$E_s$	0.216	0.0160	1.614	0.0100
7.	IV. Sandstone, alurolite tuff	$D_z$	0.460	0.0140	3.000	0.0100
8.	breccia	$E_s$	0.180	0.0185	1.230	0.0100

\*) This gradation coincides with division of rocks by their properties, adopted in engineering geology (Sergeiev, 1976).

\*\*) The coefficients shown correspond to values  $D, E_s, E_{dyn}$  having the dimensions in  $10^9 \text{ N/m}^2$ .

very easy to obtain the relation between the values  $D$ ,  $E_s$  and  $D$  for any type of rock. For instance, for carbonate rocks, the relation between the modulus  $E_{dyn}$  and summary modulus of deformation  $D_z$ , corresponding to the value  $\sigma_{max} = 8 \text{ MPa}$ , is described by the following expression\*):

$$\rho_g D_z = 0.970 e^{-0.119 \cdot 8.0} \rho_g E_{dyn} - 0.193 e^{-0.110 \cdot 8.0} \quad (4)$$

$$- 1.515 \rho_g E_{dyn} - 3.427$$

The use of such correlating equations allows one to determine the sought values of the static parameters of deformability without conducting of labour-consuming and expensive geotechnical tests. With a probability 0.9 the error when calculating the moduli  $D$  and  $E_s$  is below 30 per cent, which is good enough for solution of most of practical problems.

#### 2.2.4 Determining of permeability properties

To give a quantitative characteristic of the permeability properties of rocks different electric radioactive and other borehole investigations are successfully used (Dakhnov, 1975; Melkovitski et al., 1982; Ogilvie, 1962).

The defining of the direction and velocity of the seepage flow is based both on the data of the inter-hole studies and the data of observations carried out in one borehole. The inter-hole studies are carried on with the help of thermometric, calorimetric and, most often, electrometric and radioisotope methods. The last ones have been known for a long time, however, the modern measuring devices and the methods of pulse excitation of the borehole allow obtaining far more reliable data. When conducting studies in one borehole the tracer method (Peronski, 1977) and electrometric and flowmetering methods (Grinbaum, 1975) are used.

The main factor which complicates the interpretation of the geophysical data is a non-uniform and complex nature of the seepage flow conditioned by the rocks jointing. That is why, it is necessary to define the permeability properties for particular quasi-homogeneous rock mass blocks, singled out during the engineering-geological zonation.

#### 2.2.5 Estimate of a degree of preservation of rocks in the mass

In the practice of hydroelectric resources development in the USSR the qualitative classification of rock masses by their preservation has found wide application. The term "preservation" covers the degree of variability of the indices of the main physical and mechanical properties of the rocks, such as parameters of jointing, strength and deformability under the action of natural and technogenic factors combination. Objective characteristic of the preservation degree can be obtained from the data of geophysical investigation and particularly on the basis of measuring the longitudinal wave velocities  $U_p$ . As the absolute  $U_p$  values are considerably dependent on the lithology of the rock masses under investigation, that is why the parameter  $q = U_p / U_{p_{max}}$  is used

\*) The dimensions of  $D$  and  $E_{dyn}$  are  $0.1 \text{ MPa}$ .

as the preservation degree characteristic; here  $V_{p\max}$  is the velocity of longitudinal waves in non-weathered monolithic rock varieties. This parameter serves as the objective characteristic of the degree of preservation if conditions of the  $V_p$  and  $V_{p\max}$  determination are standardized. For this reason, on assessing the parameter "q", the value of  $V_p$  is determined usually as the mean value of the velocities from the seismic data, characterizing the generalized indices of the properties of the rock blocks with linear sizes  $n$  (10 to 100)m,  $V_{p\max}$  being defined as the mean maximum value of the velocity for the given variety of the rocks by the results of ultrasonic logging. Further the parameter "q" is used for singling out zones and rock blocks considerably differing in the degree of their preservation.

To classify the rocks by the categories of their preservation, the generalized empirical relations between the velocities of longitudinal waves  $V_p$  and deformation modulus  $D$  (Savich Yarnozhko, 1979), compressive strength  $R_{\text{compr}}$ , rock mass (Shaumyan, 1972), joint void volume ratio  $Q_{jv}$  and other indices are employed. Boundaries of the rocks of differing categories are found from condition that indices of the strength and deformability properties for two neighbouring categories differ 1.5 to 2.5 times (see Fig.5). Table III shows the relative indices of the properties of the rocks of different categories. The set forth approach to the assessment of the rock mass preservation has been employed at the projects in the USSR and abroad.

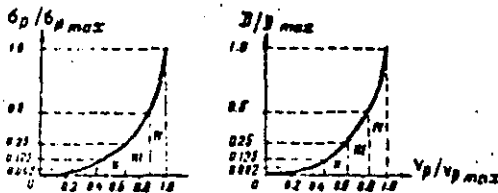


Fig.5 To estimation of limiting values of  $V_p$  for rocks of various degrees of preservation

a - "strength" criterion (the graph is taken from the paper by Shaumyan, 1972); b - deformation modulus criterion (according to the data taken from the paper by Savich et al., 1969); I-IV - degrees of preservation.

### 2.2.6 Study of rock jointing

Geophysical methods in engineering survey are used both when studying the general nature of rock mass jointing and when making the quantitative assessment of their jointing. Usually, the data of seismoacoustic methods and results of some types of logging are used for these purposes.

Relation between velocities of elastic waves and value and nature of joint void ratio for the rocks (Lykoshin et al., 1971; Salganik, 1973) serves as the physical basis for handling the mentioned problems. In the first approximation this relation can be described by

Table III. Relative indices of the properties of the rocks of different categories of preservation

Category of preservation	Ratio	Ratio	Ratio	$q^2$	Characteristics of rock condition
	$D/D_{\text{max}}$	$R_c/R_{c\text{max}}$	$q = V_p/V_{p\text{max}}$		
	%	%	%	%	
IV <sub>2</sub>	100-72	100-72	100-97	100-95	Superior
IV <sub>1</sub>	72-52	72-46	97-87	95-75	Good
III	52-25	46-19	87-65	75-44	Normal
II	25-11	19-8	65-50	44-25	Poor
I	11-4	8-24	50-35	25-12.5	Very poor
O <sub>2</sub>	4-1.5	2.4-0.5	35-25	12.5-6.2	Semi rocks
O <sub>1</sub>	1.5	0.5	25	6.2	Rock debris, alluvium, gruss.

the equations similar in form to that of "mean time", if in this case the parameter "a<sub>j</sub>" which means a certain effective velocity in void and joint filler is happily chosen:

$$\frac{1}{U} = \frac{Q_{jv}}{a_j} + \frac{1 - Q_{jv}}{U_{\text{max}}} \quad (5)$$

Here  $U$  is the velocity of elastic waves in a jointed medium.  $U_{\text{max}}$  is the velocity of waves in monolithic rocks. All things being equal, the "a<sub>j</sub>" value depends on the frequency of elastic vibrations used for determination of  $Q_{jv}$  values, thus the problem of  $Q_{jv}$  assessment is closely related to the problem of determining the parameter "a<sub>j</sub>" for the various conditions of measuring velocities of the elastic waves. As a rule, the value of parameter "a<sub>j</sub>" by seismic data is 1.3 to 2.0 times lower than those obtained by the ultrasonic investigation.

Criterion of correctness of assessing the joint void ratio is the direct correlation of the values  $Q_{jv}$ , determined by geophysical methods, with the results of geological documentation. Example of such correlation is shown in Fig.6, where the values  $Q_{jv}$  calculated by the data of ultrasonic logging are compared with the values of areal joint void ratio  $K$ , defined when examining the exploration pits by visual inspection of the mining openings. Proceeding from these data, the value  $Q_{jv}$  determined by geophysical investigation is 1.7 to 2 times more than the value  $K$  determined by geological tests. The latter finds its explanation in the fact that, firstly, the geophysical methods yield the value of joint voids volume, while the geologic methods allow, as a rule, for determination of the relative value of joints area; besides, the ultrasonic measurements take account of not only visible joints but also of microjoints which cannot be identified in boreholes visually. The diagram 2 shows the comparison of joints void volume data obtained

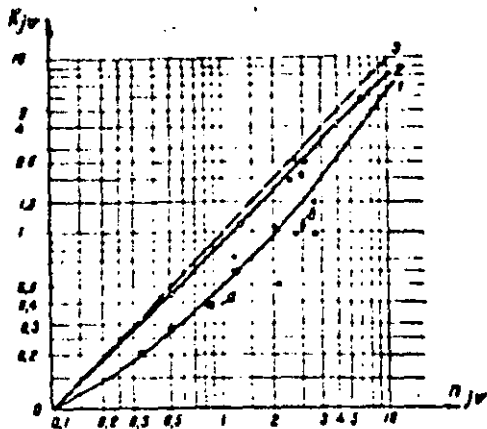


Fig. 6. Correlation between joint voids acc. to the data of geophysical survey (ratio of joint voids) and acc. to seismic data  $n_{jv}$ .

1 - ultrasonic logging, a - Ust-Ilim hydropower station, b - Inguri hydropower station; 2 - seismic survey (Ust-Ilim hydropower station); 3 - the line of equal values of  $n_{jv} = K_{jv}$ .

in seismic surveys and by visual documentation of boreholes. These data are evidencing that, provided the initial parameters are selected correctly, the ultrasonic methods and the logging give the values of the joints void volume fully agreeing with data of geologic documentation.

### 2.2.7 Estimation of rock mass state of stress

First applications of geophysical methods in studying rock mass state of stress were made in the USSR in the Institute of Geophysics, Academy of Sciences, USSR, in the 60-s under Rizinchenko guidance (Rizinchenko, 1956, 1967). By the present time enough experience of the similar investigation has been gained and the range of typical problems has been delineated. The main problems are as follows:

- 1 - determination of dimensions and nature of the relief zone and the stress concentration around the underground excavations, river valley slopes, construction pits, etc.;
- 2 - estimation of tensor and orientation of principal axis of stresses;
- 3 - determination of variability of behaviour of stress fields of variable levels and orders with time.

When handling the first problem, the nature of variation of geophysical parameters within the area of underground workings and slopes is studied. As usual, elastic wave velocities or electrical resistivities are used.

By variability of  $V_p(V_s)$  and  $\rho_k$  values the qualitative information on the structure of the stress field around underground workings (Fig. 7) and in the slopes can be gained and zones of stress concentration and relief can be singled out (Lavrov, 1981; Rizinchenko et al., 1956, 1967; Savich, Koptev, 1981).

quantitative solution of the problem is based on the relation between the elastic wave velo-

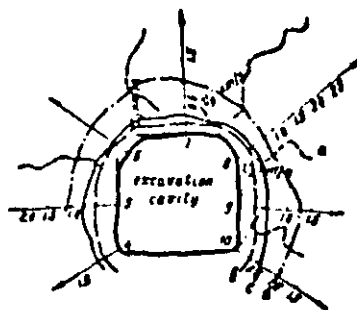


Fig. 7. Alteration of the longitudinal waves velocities in the rock mass around excavation

1, 2, 3, ... 10 - shot holes; a - graph of  $V_p$  alteration along the shot hole; b - boundaries of a zone of intensively relieved rocks; c - boundaries of a zone of weakened rocks; d - external boundary of zone of increased stresses.

cities and pressure applied to the rock. The relation is usually used as the "calibrating" one for determination of the stresses by elastic wave velocities. The methods of stress evaluation based on the similar relations are termed "correlating" ones.

Relatively widespread is the method by which the calibrating curves are obtained by mass measurements on rock samples and then used for assessment of the stress values in any point of the rock mass. Nevertheless, the calibrating curves obtained on the samples do not represent the process of the natural rock mass deformation development, either by the scale, or by the loading pattern. That is why there is a trend to change sample testing for field loading plate testing. In sufficiently homogenous rocks utilization of this procedure yields in satisfactory results (Miyachkin, 1978; Turchaninov, Panin, 1978).

The procedure of plotting the system of calibrating curves of the form  $\Delta V/V_0 = f(V_0, \sigma)$ , where  $V_0$  is the velocity under no-load condition, with heterogeneity of rocks and scale effects taken into account, has been recently developed in the "Hydroproject" Institute (Moscow, USSR) on the basis of empirical and experimental studies of velocity variation during the rock deformation process. The procedure and the results obtained are presented in detail (Salavadze, 1981; Savich, Koptev, 1981).

Alongside with correlating methods, a method, termed the "neisomacoustic version of stress relief method" is widely used. The method is based on the following main provisions: each underground working is considered as an original field test of the rock mass relief. On determining the radial deformations  $\epsilon_r$  developing in the case and with the  $E_{0.6}$  and  $D$  values known one can assess the stresses existing in the rock mass. On the basis of Khachikian's solution for the deformation of the walls of the cylindrical underground workings the equation was obtained which relates the indices of elastic and deformability properties of the rocks

around the underground workings to the radial stress  $\sigma_r$  value:

$$\sigma_r = \frac{D_m \cdot h_0}{(1 + \mu_m)(r_{ef} + h_0)} \left[ 1 + (1 + \mu_m) \frac{D_m}{D_0} \left[ n \left( 1 + \frac{h_0}{r_{ef}} \right) \right]^{-1} \right] \quad (6)$$

where  $D_m$  and  $D_0$  are the deformation modulus of the rocks undisturbed in the process of driving and the mean deformation modulus of the rocks in the weakened zone;  $h_0$  is the thickness of the weakened zone;  $\mu_m$  is the Poisson ratio for the rocks beyond the underground working influence zone;  $r_{ef}$  is the effective radius of the underground working. All the parameters in this equation can be defined from the seismic-acoustic survey data (Savich, Koptev, 1981). Fig. 3 contains the data of determining the horizontal component of stress  $\sigma_r$  (parallel to the river valley slope) in the area of the Inguri Dam using the above method (Balavadze et al., 1981)

### 3. STUDIES OF CHANGES IN PROPERTIES AND STATE OF ROCKS DURING CONSTRUCTION AND MINING WORK

With the help of geophysical methods, and mainly with the help of seismic-acoustic methods many problems which arise in the process of construction are being successfully solved. The following problems are the most widely encountered:

- study of rock properties and conditions in the vicinity of mine excavations (tunnels, shafts, underground machine rooms, etc.);
- estimation of overburden stripping work upon the rock mass properties and study of the surface zone of the construction pits;
- control of quality and estimation of efficiency of grout injection and, in particular, of consolidation grouting;
- estimation of variability of the physical and mechanical properties of the rock mass which is brought by mining and construction work.

Let us have a look upon some examples which confirm the efficiency of this trend in engineering geophysics.

#### 3.1 Study of the surface overburden stripping work in construction pits

Such study is carried out on the basis of detailed seismic researches at the network of the surface profiles and observations effected in construction excavations (Savich et al., 1974). As an example, in Fig. 8 are shown seismic-geological sections at geophysical profiles which have been used for drawing of maps of isolines of depths of rocks having various elastic properties, as well as the maps of rock properties below the weakening zone. As a result of such investigations at the Inguri Dam site it was found that after execution of stripping work and removal of the weathered layer in the foundation pit everywhere was formed the "secondary" weakening zone, 2 to 15 m deep. This zone can be divided into some subzones, and the rocks of those subzones significantly differ in their properties. The structure and thickness of the secondary weakening zone is being governed by the rock properties in the unchanged part of the rock mass, as well as by gypsometric position of the area under investigation and by the

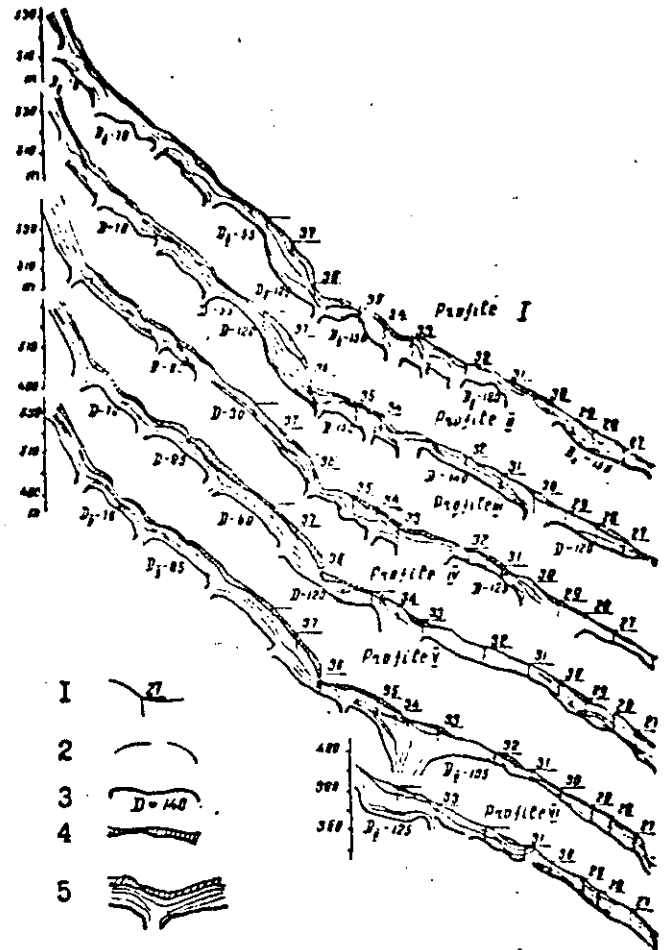


Fig. 8 Seismic-geological sections of the foundation pit of the Inguri arch dam

1 - earth surface, section boundary and its No.; 2 - isolines of longitudinal waves velocities; 3 - boundary of rocks unchanged by the relief and values of deformation moduli  $D \cdot 10^{22}/m^2$  and the velocities of longitudinal waves  $V_p$  km/s; 4 - zone of rocks broken by explosions, with velocities of longitudinal waves not less than 1,0 km/s.

steepness of the slope.

Similar work executed in the foundation pit of the Ust-Ilim hydropower station have allowed to find with great precision and details the thickness of the zone of rock to be removed (Mikhailov, et al., 1977). The control drilling and the recording documentation on the excavation have confirmed the results of the geophysical researches (Fig. 9).

The geophysical work carried on in the construction pits of the structures enabled to give the detailed properties of rocks in the top part of the section, which allows to specify the quantity of rock to be removed, to localize the most weak areas of the rock mass,

and finally, to make the rock foundation preparation work cheaper.

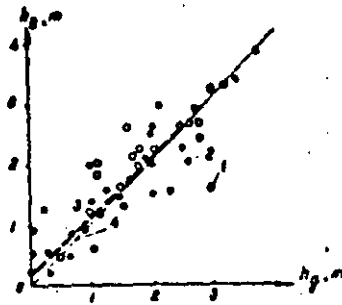


**Fig. 9** Comparison of data from seismic ( $h_g$ ) and geological ( $h_0$ ) methods on the slopes of construction pits at the Ust-Ilim hydropower station

1 - boreholes-pits ( $d=915$  mm); 2 - core drilling boreholes; 3 - empiric dependence between  $h_g$  and  $h_0$ ; 4 - line of equal values of  $h_g$  and  $h_0$ .

### 3.2 Study of slope relief zone

At the slopes of construction pits, at the slopes of deep navigation locks excavations and of water passage structures the same geophysical methods are being successfully used for controlling the dynamics of relief process, as well as for estimation of the slopes stability. The researches which have been carried out in the foundation pit of the Dnieper navigation lock can serve an example of such work (Andriev, Lavrov, 1976), excavated in granite. Under the combined influence of explosions and stress relief in the pit slopes, zones of technogeneous weakening were formed, characterized with various velocities of longitudinal waves  $V_p$  and with indices of relative preservation  $q$ . (Fig. 10) With the help of repeated observations the dynamics of the technogeneous relief in time has been studied. It turned out that during three years after completion of excavation the velocities of longitudinal waves in the rocks of the relieved slope gradually decreased. Total reduction of velocities in the relieved rock was equal to 200 to 300 per cent, the deformation modulus - by 4 to 6 times, and the ratio of jointing voids by 10 to 20 times.

### 3.3 Grouting quality control

The geophysical methods are being used as well also for quality control of consolidation and anti-seepage grouting of rock foundations. When doing so, as a rule, the consolidation grouting is controlled with seismic-acoustic methods, while the anti-seepage grouting is controlled with electrical logging (Savich et al., 1979).

Efficiency of grouting is estimated from the relative alteration of velocities of the longitudinal waves or of the specific electrical resistances. Usually, the following problems are to be solved: to find the possible efficiency of grouting in the given type of rocks and at the specified technology of grouting; to set the grouting quality degrees; to locate the zones and areas of poor quality grouting; gene-

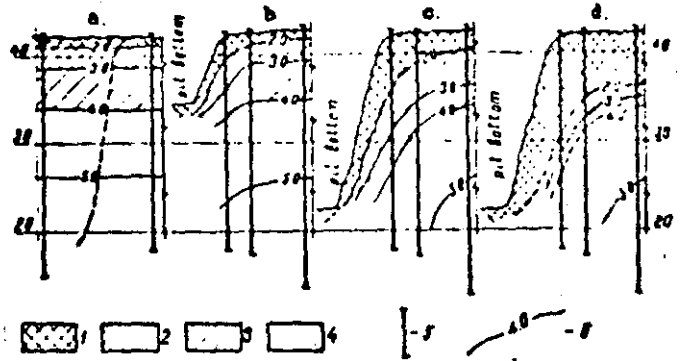


**Fig. 10** Generalized seismicological-geological cross-sections across the construction pit slopes for the cases of the pit still unexcavated (a), for the depth of the pit 7 m (b) and 15 m (c,d). Line interval between cases of a and d is one year (acc. to the paper by Andriev and Lavrova, 1976)

1 - intensively relieved rock mass,  $q=0.8$ ; 2 - strongly relieved rock mass,  $q=0.8-0.5$ ; 3 - relieved rock mass,  $q=0.5-0.3$ ; 4 - poorly relieved rock mass,  $q=0.3-0.1$ ; 5 - borehole; 6 - isoline of velocity, km/s.

ral and differentiated estimation of grouting efficiency.

The first out of the above mentioned problems is solved in the process of grouting at the experimental grounds, and as a result of this curves are drawn interrelating the quality of grouting and the values of corresponding changes of geophysical parameters. The graphs of relative change of the longitudinal waves velocities which are used for grouting quality estimation at the foundation of the Inguri arch dam (Fig. 11) can serve an example of this. Estimation of grouting quality is effected on the basis of repeated measurements of velocities of the longitudinal waves, prior and after grouting, with the help of seismic sounding of the rock between the boreholes.

Control over consolidation grouting quality is also effected behind the lining of pressure tunnels with the help of the geophysical methods. Work in the Inguri power station power tunnel (Lavrov, 1981) can serve an example of such researches where the control was effected with radial boreholes which have been drilled prior and after grouting.

### 4. INVESTIGATION OF ALTERATION OF ELASTIC WAVES VELOCITIES IN ROCKS AND DEVELOPMENT OF DEFORMATION PROCESS IN TIME

This problem has come into being in connection with construction of big engineering structures and, mainly, high dams with deep and vast storage reservoirs which brought with themselves active influence of man upon properties and conditions of environment. The cases of large landslides, downfalls, significant deformations of the foundations and powerful local earthquakes which have been provoked by technoge-

neous factors predetermined the arrangement of special complex of work to study dynamics of state of stress-and-strain of the subsurface parts of the earth shell in the regions of location of the most important engineering structures.

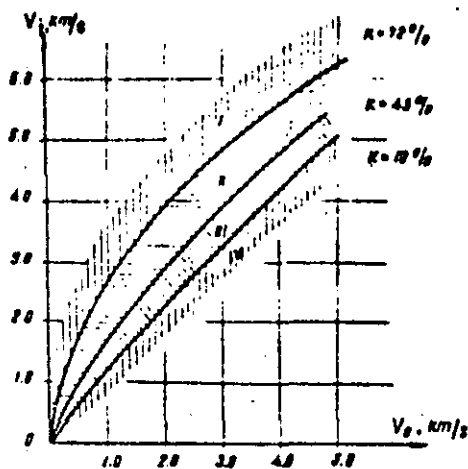


Fig. 11 Nomograph for estimation of grouting quality according to the velocity of longitudinal waves measured prior to grouting ( $V_p$ ) and after grouting ( $V_p$ )

I - "excellent" grouting zone; II - "good" grouting zone; III - "satisfactory" grouting zone; IV - "unsatisfactory" grouting zone.

A component part of this complex is longterm geophysical observations which allow on the basis of study of the alteration of the parameters of various geophysical fields with time to get some certain information on deformation processes which take place at different parts of the rock mass under study. The procedure of longterm geophysical investigations employed in the USSR provides for their use in combination with the traditional (geotechnical and geodetic) field studies. These studies are being effected in their full scope only in some individual (reference) parts of the rock mass and serve a basis for correct and reliable quantitative interpretation of geophysical data. The task of geophysical methods is to get information on the deformation processes which develop in time at various scales and in different (at the surface and inside) parts of the rock mass.

The most complete complex of alike longterm observations is being made in the USSR at present in the region of the Inguri arch dam, 271.5 m high, and deep Inguri storage reservoir which is located in Western Georgia in the zone of 8-points seismicity (Balavadze et al., 1981).

This complex of work consists of the following:  
1 - detailed seismic, electromagnetic and ultrasonic investigations at the different points of the arch dam foundation in the range of depths from 0 to 200-250 m, where the processes which take place in the structural blocks, 1.0-10.0 m<sup>3</sup> to 1000-10,000 m<sup>3</sup> in volume are studied;  
2 - seismic studies at the submerged profile in

the head part of the reservoir where the processes which take place in geostructural blocks having line sizes  $n=100$  m, at the depths down to 1.0 km, are studied;

3 - regional geophysical (electrometric, gravimetric and magnetic-metering) as well as the instrumental seismological observations which render information on the processes which take place in the blocks having linear sizes of  $n$ -km at the depths down to 5-10 km.

The above mentioned observations are combined with high accurate inclinometering and deformation studies, with field geotechnical observations as well as with the repeated detailed and regional geodetic measurements. The detailed description of this complex can be found in the published papers (Balavadze et al., 1981; Savich et al., 1979). The observations over changes of parameters of the geophysical fields in the region of the Inguri power station are being made during 6-8 years, and thanks to this work the most general regularities of deformation processes development were revealed.

The general trends of alteration of the media properties during construction of the dam prior to filling the reservoir are distinctly shown in the curves of the variation of the longitudinal waves velocities  $V_p$  against electric resistances  $R$  (Fig. 12). These data confirm that placing concrete in the dam body and creation of a surplus surcharge on the foundation have brought with themselves a significant growth of  $V_p$  and  $R$  values, and at the background of this growth there have taken place some relative variations of those parameters, connected with alterations of season temperatures, water content in the rock mass and with some occasional factors.

Judging by the results of the different-scale investigations the mentioned deformation processes in the larger blocks occur with a greater intensity. It means that the compaction of the rock mass which brings with itself the growth of  $V_p$  and  $R$  values happens, mainly, thanks to closure of large fissures. It is notable that, depending of the depth, the variations of  $V_p$  and  $R$  values attenuate, and deeper than 80 m those variations are practically not found. But, as far as those depths coincide with the boundary of significant settlement of rock, the above mentioned boundary can be interpreted as the boundary of zone which is an active deformed zone under the structure.

Filling of the reservoir has brought with itself a sharp change in the nature of deformation processes and the corresponding alterations in parameters of the various geophysical fields. In the area of the arch dam it has caused a reduction of the elastic waves (longitudinal and transverse) velocities as well as a reduction of electrical resistances (Fig. 13). The most intensive reduction of the  $V_p$  and  $R$  values took place in the periods of water level rise in the reservoir, and it was a little bit weaker during the periods when the water level was being kept constant. The analysis has shown that this phenomenon has been caused by entering of water inside the rock mass and by development of pressure inside the fissures. The last phenomenon, in particular, is con-

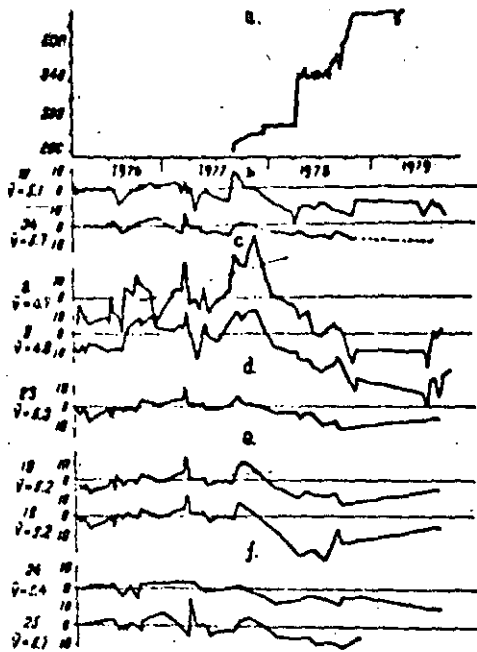


**Fig. 12** Variations of relative velocities of elastic waves in seismic range of frequencies  $U_0$  at the intermediate zone of the middle part of the left-bank slope in different directions in respect to the Inguri river valley

a - reservoir filling graph; b - variation of velocities along OX axis; c - variation of velocities along OY axis; d - variation of velocities along OZ axis; e - variation of velocities parallel to the slope; f - alteration of velocities normally to the slope; 16, 8.25 - Nos of observation points;  $V = 5120$  - average values of zero cycle velocities.

firmly by the shift in time of the reduction of the value  $U_0$  in different parts of the rock mass, this shift being governed by water filtration velocities inside the rocks under investigation.

The observed reduction of the velocities  $U_p$  and of electric resistances is accompanied with a sharp reduction of the foundation settlement; this phenomenon is interrelated with the process of a relative de-consolidation of rock mass which is caused by the hydrostatic pressure of water which has entered the rock mass. The boundary of the zone, where this process takes place under the dam, is at a depth of some 250 m, while at the head part of the reservoir it is at the depth of some 500 m.

The influence of the water storage reservoir upon the deformation processes has manifested itself distinctly in the peculiarities of alteration of the local seismicity of the region (Balavadze et al., 1981). The variations of the regional seismicity which accompanied the filling of the Inguri power station water storage reservoir, have reached their top one and a half year after beginning of water level rise,

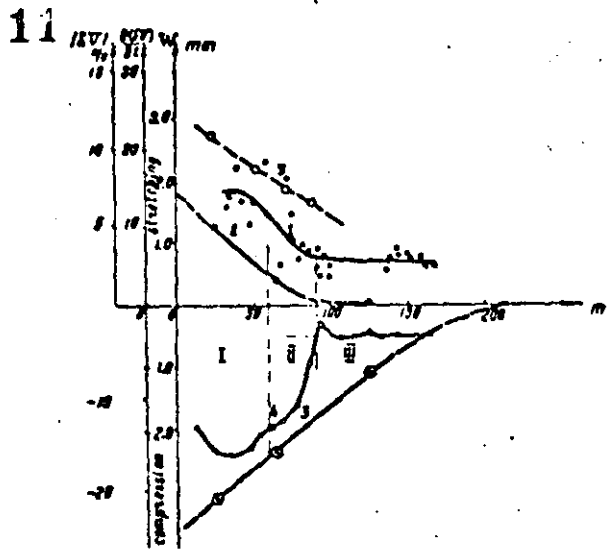


**Fig. 13** Alteration of variations intensity for velocities of seismic waves and rocks deformation in the middle part of the left-bank apartment of the area depending on the depth from the earth surface in the rock mass

1 -  $1 - \delta U / U = f(h) / \delta V / - \frac{U_p - U_0}{U_0}$ , where  $U_0$  is velocity  $U_p$  in the cycles which took place prior to filling the water storage reservoir; 2, 3 -  $\partial(\delta U) / \partial t = f(h)$ , where  $\partial(\delta U) / \partial t$  is a temporary gradient of value  $\delta U$  in  $(\text{m}) / (\text{year})^{-1}$ ; data prior to (2) and (3) in the period of reservoir filling; 4, 5 - graphs of deformations in the rock mass under investigation prior to (4) and in the period of (5) filling of reservoir (acc. to data provided by Kouznetsov); h - depth from the earth surface along the normal to the slope; I-III - zones of various intensity of  $U_p$  variations.

and one year since the relative stabilization of the water level at 130 m. However, the first (weak enough) stage of seismic activity began one month since the said filling of the reservoir. It has manifested itself in a series of seismic shocks with the magnitude  $M = 0.5$  to 1.7 under the head part of the reservoir. Later on the foci of earthquakes moved to south-west along tectonic structures which separate the water-bearing limestones of the lower body from the watertight strata of Jurassic deposits. This process was finalized with a powerful outbreak of seismic activity. Within the limited area at a distance of 10 to 30 km south-west from the dam, in a period of time since December of 1979 to March of 1980 there have happened more than 100 earthquakes with a magnitude  $M \sim 1.7-4.3$ , and the most powerful of them have caused local seismic effects of 6-7 points. It was found that one of the main factors which determines the said seismic activity within the region of the Inguri hydropower station is the inside pressure in joints. The above mentioned migration of the earthquake foci is a good illustration for spreading of water along the fissures to the periphery of the water reservoir.



Thus, widening of the zone of influence of the reservoir manifests itself in the variations of different geophysical fields, and it is characterized at various scale levels with some peculiarities.

#### CONCLUSION

The paper deals with some standard engineering-geological problems which are solved in the USSR with the help of geophysical methods. The examples shown here clearly illustrate the efficiency of those geophysical methods in solving various problems of geology and rock mechanics, as well as advantages of further development of the engineering geophysics for studying of rock masses.

#### REFERENCES

- Андреев В.Н., Лавров Л.Д. Геолого-геофизическое определение зон выветривания и разгрузки в гранитах Днепротэкс-П. Труды Гидропроекта, вып. 50, М., 1976.
- Балавадзе Б.А./ред./ Геолого-геофизические исследования в районе Ингурской ГЭС. Труды 1-го координационного совещания, май 1979 г. Изд-во "Мецниереба", Тбилиси, 1981.
- Горяинов Н.Е., Ляховицкий Э.М. Сейсмические методы в инженерной геологии. Изд-во "Недра", М., 1979.
- Гринбаум И.И. Геофизические методы определения фильтрационных свойств горных пород. "Недра", М., 1975, 271 с.
- Дахнов В.Н. Геофизические методы определения комплексных свойств и нефтегазонасыщенности горных пород. "Недра", М., 1975.
- Еримова Е.А. Решение прямой задачи сейсмического просвечивания численными методами. Вестник МГУ, вып. IV, № 5, 1973.
- Карус Е.В. /ред./ Методические указания по проведению междисциплинарного прозвучивания и интерпретации его результатов при решении инженерно-геологических задач. М., ВНИИГТ, 1980, 58 с.
- Лаврова Л.Д. Изучение анизотропии скального массива сейсмоакустическими методами. Изв. АН СССР, сер "Физика Земли", № II, М., 1976.
- Лавров В.Е. Применение сейсмоакустических методов для исследований в гидротехнических тоннелях в процессе строительства. Труды Гидропроекта, вып. 78, М., 1981.
- Лыкошин А.Г. /ред./ Труды Гидропроекта, сб. 21, Инженерная геофизика, М., 1971.
- Ляховицкий Э.М., Нападенский Г.Б. Опыт автоматической обработки данных малоуглубинной сейсморазведки МЭВ. В кн.: "Разведочная геофизика", М., "Недра", 1976, вып. 70.
- Мельковичский И.М., Ряполова В.А., Хордиакян Н.А. Методика геофизических исследований при поисках и разведке месторождений пресных вод. "Недра", М., 1962, 102-145 с.
- Михайлов А.Д., Яценко З.Г., Даниленко С.Д. Изменения под нагрузкой состояния скального массива в основании плотин Братской и Усть-Илимской ГЭС по данным геофизических исследований. Сб. "Отражение современных полей напряжений в свойствах пород в состоянии скальных массивов", Апатиты, 1977.
- Мячкин В.И. Процессы подготовки землетрясений. Изд-во "Наука", М., 1976.
- Никитин В.Н. Основы инженерной сейсмологии. Изд-во МГУ, М., 1961, 176 с.
- Огильви А.А. Геофизические методы исследования. Изд-во МГУ, М., 1962.
- Писецкий В.Б., Бондарев В.И., Крылатков С.У. Система программ для обработки данных инженерной сейсморазведки. Труды СТИ им. В.В. Выхрушева, Свердловск, 1978.
- Ризниченко Ю.В., Сялаева С.И. и др. Сейсмоакустические методы изучения напряженного состояния горных пород на образцах и в массиве. Труды Геоиз. ин-та АН СССР, № 34 (161), Изд-во АН СССР, 1956.
- Ризниченко Ю.В. и др. Исследование горного давления геофизическими методами. Изд-во "Наука", М., 1967, 215 с.
- Савич А.И., Коптев В.И., Никитин В.Н., Яценко З.Г. Сейсмоакустические методы изучения массивов скальных пород. Изд-во "Недра", М., 1969.
- Савич А.И., Кереселдзе С.Б. Обоснование параметров зоны сжима в котловане арочной плотины Ингуры ГЭС. Журнал "Гидротехническое строительство", № 6, М., 1974.
- Савич А.И., Яценко З.Г. Исследование уругов в деформационных свойствах горных пород сейсмоакустическими методами. Изд-во "Недра", М., 1979.
- Савич А.И., Коптев В.И. Изучение напряженного состояния массивов скальных пород сейсмоакустическими методами в связи со строительством подземных гидротехнических сооружений. Сб. Труды Гидропроекта, вып. 78, 1981, 47-65 с.
- Савич А.И., Коптев В.И., Михайлов А.Д. Применение геофизических методов для изучения свойств и состояния массивов горных пород. Сб. научных трудов Гидропроекта, вып. 76, М., 1981.
- Савич А.И., Яценко З.Г., Горбунов А.А. Опыт оценки качества укрепительной цементации скальных пород сейсмографическими методами на Ингуры ГЭС. Гидротехническое строительство, 1977, № 9.
- Салганик Р.Л. Механика тел с большим числом трещин. Изв. АН СССР, МТТ, 1973, № 4.
- Сергеев Е.М. Инженерная геология. Изд-во МГУ, М., 1978.
- Турчанинов И.А., Панян В.И. Инженерные геофизические методы определения и контроля напряженно-деформированного состояния массивов пород. Изд-во "Наука", Л., 1975, 112 с. с ил.
- Феровский В.И. Радиозонные методы исследования в инженерной геологии и гидрогеологии. Атмосфер, 1977, 130-291 с.
- Шаумян Л.В. Физико-механические свойства массивов скальных горных пород. Изд-во "Наука", М., 1972.
- Lykoshin A.G. et al. Studies of Properties and Conditions of rock Massifs by Seismic-Acoustic Methods. If. on the Second Congress of the IAGG, Zagrad, 1970.
- Savich A.I., Koptev V.I., Iljin M.K., Zakhraev A.M., Lipkayeva A.L. Geophysical methods for study of deformation processes in foundations of large hydraulic structures and storage reservoirs. Bull. of the Int. Ass. of Engineering Geology, № 20, 1979, pp. 58-61



**DIVISION DE EDUCACION CONTINUA  
FACULTAD DE INGENIERIA U.N.A.M.**

MECANICA DE ROCAS APLICADA A LA MINERIA Y A LA CONSTRUCCION

EVALUATION OF THE RISK OF INDUCED SEISMICITY AT THE ITZANTUN  
HYDROELECTRIC SITE, CHIAPAS, MEXICO

A. Uribe Carvajal  
and  
E. Nyland

MAYO, 1985

## EVALUATION OF THE RISK OF INDUCED SEISMICITY AT THE ITZANTUN HYDROELECTRIC SITE, CHIAPAS, MEXICO

A. URIBE-CARVAJAL and E. NYLAND

*Institute of Earth and Planetary Physics, Department of Physics, University of Alberta,  
Edmonton, Alta. T6G 2J1 (Canada)*

(Received September 20, 1982; revised version accepted July 1, 1983)

### ABSTRACT

Uribe-Carvajal, A. and Nyland, E., 1983. Evaluation of the risk of induced seismicity at the Itzantun hydroelectric site, Chiapas, Mexico. *Eng. Geol.*, 19: 247-259.

Consolidation theory and concepts of rock failure can be used to evaluate the probable risk of induced seismicity as a result of filling of reservoirs. This evaluation indicates the safest way to fill a reservoir, and depends only on the geometry of the load, the rate of filling and the geological structures in the area. The stability function is actually a measure of the risk of having failure, with time, for a particular loading history in respect to a plane of weakness.

The stability function is applied to the area of the Itzantun reservoir, which will be in southern Mexico. Drawdowns can increase the risk of triggering earthquakes in this area, which is prone to thrust faulting. It is possible to estimate the stresses after a period during which the water level is maintained and a decrease in stresses with the depth of the observation point.

The estimates of the probable induced seismicity are limited as the residual stress in the area prior to the impounding is unknown. With a measure of the residual tectonic stress it will be possible to determine an optimal filling rate to reduce the probability of induced seismicity.

### INTRODUCTION

During the last twenty years, it has been observed that large engineering projects may change the characteristics of the seismic events in the surrounding region. These changes are induced by changes in stress that are a result of man's activities. Among the activities and events that cause induced seismicity are fluid injection, fluid extraction, mining, underground detonations, flooding, and reservoir impoundment (Packer et al., 1977). Here we will deal only with reservoir impoundment.

There are many examples of where the filling of reservoirs has changed the characteristics of events in an area. These changes range from the induction of large magnitude events to changes in the micro-earthquake activity. The filling of large reservoirs, however, has not always resulted in induced seismicity. Attempts to relate induced seismicity to size or depth of a reservoir have had little success. The changes in seismic activity do not follow

a simple pattern (Gough, 1978). Excellent reviews of the observed changes have been prepared by Simpson (1976), and Gupta and Rastogi (1976).

Induced seismicity is difficult to prove. An increase in seismic activity in areas that were already active is difficult to attribute entirely due to the filling of the reservoir. In other areas the pattern of seismic events changes radically, and there seems to be an obvious association with the filling of the reservoir. In some areas, there appears to be an increase of seismic activity during the initial filling, whereas in others, the increase occurs some years after filling. There appears to be a correlation between the water depth and the number of earthquakes at some reservoirs (Withers and Nyland, 1978). And there also appears to be a relation to the rate of filling (Simpson and Negmatullaev, 1981).

The amount of data on reservoir-induced seismicity is limited. Up to 1977, there had been 55 reported cases of reservoir-induced seismicity (Packer et al., 1977). Of these, Packer et al. classify 16 as clear cases, 35 as questionable and 4 as probably not reservoir-related. They reach the following conclusions regarding induced seismicity due to reservoir loading.

- (1) The initial state of stress in the ground is of prime importance.
- (2) Failure of unfractured material as a result of reservoir filling is unlikely, but failure is likely to occur along pre-existing faults in fractured material.
- (3) "Instantaneous" stresses generated by rapid reservoir filling lead to shear stress along faults without increasing the effective stress.
- (4) Instability along faults could occur at great depths as shown by the curvature of the failure envelope. The shearing resistance of the material is reduced as the confining pressures increase.

There is by no means unanimous agreement about the existence of reservoir-induced seismicity. Other authorities claim that only 3 clear cases of reservoir-induced seismicity exist. The difficulty is to provide a viable mechanism for failure caused by reservoirs and to use a convincing stress-strain relation for crustal rock. We believe that the evidence from other reservoirs indicates convincingly that failure can be caused by relatively small external influences (i.e., Raleigh et al., 1976; Pomeroy et al., 1976; Cook, 1976; Gough, 1978; Wetmiller, 1981). The fact that statistically rigorous observations do not exist for reservoirs does not deny that reservoirs can induce seismicity; it merely means that seismic evidence by itself, from reservoirs alone, is not sufficient to resolve the matter.

Adding, however, the existence of faults on which seismicity is known to occur, the fact that stimulated seismicity has been observed for other kinds of processes, and the fact that a reasonable physical mechanism for reservoir-induced seismicity can be postulated, justifies modelling studies of this problem to determine the range of risk.

Any prediction of seismicity involves assumptions about the stress-strain relations of crustal rock and the conditions under which faults will fail. The largest stress increment due to large reservoirs is of the order of 10 bar. Under increment loads of 10 bar most crustal rocks deform elastically. Of course the incremental response of a rock confined under  $10^3$  bar at 10 km

depth may be different from that of a rock at the surface, but its elastic nature remains due to the small size of the stress increment. Therefore, the assumption of elastic behaviour is plausible.

The variation of elastic behaviour can be deduced from seismic data. Young's modulus deduced from seismic data for depths from 0 to 25 km varies from  $6 \cdot 10^5$  to  $8 \cdot 10^5$  kg cm<sup>-2</sup>. This variation is small compared with its magnitude. Hence, the assumption that the elastic properties are constant is reasonable albeit not entirely satisfactory. Other authorities (i.e., Turcotte, 1974; Kirby 1977) have considered the upper 25 km of the lithosphere to be elastic.

Obviously water pressure plays a crucial role in the dynamics near a reservoir. The simplest extension of elasticity theory that takes into account the presence of water is the Biot consolidation theory. It is normally applied to soils and is justified here only by the fact that it is a simple tractable extension which can deal with the presence of pore fluids in a plausible way. It may not be correct, but at these relatively low pressures it is a reasonable first approximation.

The general conclusion from the observation of induced seismicity is that reservoir volume is not always a reliable indicator of the risk of induced seismicity. The larger the volume, the greater the probable risk, but there is always the potential for surprises such as were encountered at Hydro-Quebec in Canada (Leblanc and Anglin, 1978). Manicougan 3 on the Canadian Shield caused seismicity changes while the nearby Manicougan 5, twice as deep and with a considerably larger volume, has not induced any seismicity. Manicougan 3 has a height of 108 m and its volume is  $1.04 \cdot 10^{10}$  m<sup>3</sup>.

In only a few cases have the depths of these seismic events been determined accurately. Local observations and the teleseismic data all indicate that the hypocentres are shallow. Gupta et al. (1972) have determined the depths and positions from the events at Koyna from a local array, and found that the majority of the events occurred at a depth of less than 10 km, but some occurred as deep as 30 km.

Migration of seismic events has also been observed in some reservoirs. Simpson (1976), Soboleva and Mamadaliev (1976) and Simpson and Negmatullaev (1981) indicate that the events at Nurek are migrating toward the reservoir.

The focal mechanisms (Bufe et al., 1976; Gough and Gough, 1976; and others) observed that different reservoirs are consistent with the types of preexisting faults in the neighbourhood. At Kariba, Kremasta and Oroville, dip-slip faulting was observed, while at Koyna, Hsinfenkiang and Hoover, the mechanism was strike-slip faulting. At Nurek the induced seismicity is occurring along a series of thrust faults connected by short segments that show strike-slip motion (Simpson and Negmatullaev, 1981). Simpson (1976), Bell and Nur (1978) and Withers and Nyland (1976) suggest that rapid lowering and raising of the water level may be an important factor in inducing seismicity in regions of thrust faulting.

The magnitudes of the main shocks near reservoirs have been as high as

6.5 at Koyna (Gupta et al., 1972), 6.3 at Kremasta (Comninakis et al., 1968), 6.1 at Hsienfengkiang (Wang et al., 1976). It is not possible to give an upper limit for the magnitude of induced earthquakes, as the filling of reservoirs acts only as a trigger of the preexisting stress.

### THE ITZANTUN SITE

The Itzantun site is in the state of Chiapas in the southern part of Mexico, 120 km NE of the city of Tuxtla Gutierrez (Fig.1). It is in a region with several rivers, the most important of which are the Tlacotalpa, the San Pedro and the Huitupan. The Tlacotalpa flows in the Itzantun gorge, and at this location the flow is  $2 \cdot 10^6$  m<sup>3</sup> of water per year. The geologic formations in the area are chiefly thick assemblages of mudstones and massive limestones.

The foundation of the Itzantun dam will be sandstone, mudstone, and limestone which appears reasonably homogeneous, at least at the surface. Many fractures in the formations near the dam have been filled with calcite but some are open and show evidence of recent movement of the order of centimetres.

The Itzantun fault crosses the reservoir just upstream from the dam and

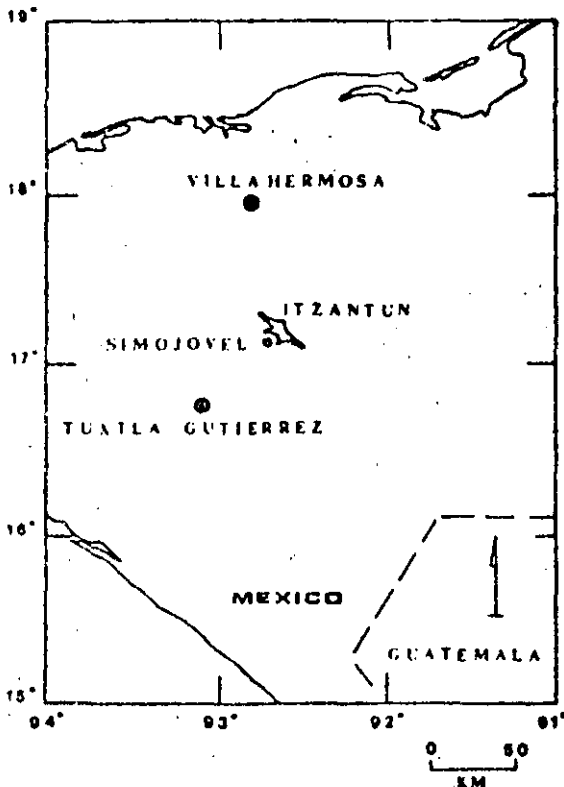


Fig.1. Location map of the study area.

is clearly the significant structural feature in an analysis of the risk of induced seismicity (Fig.2). The gorge itself was not developed along a fault zone. The irregular directional changes of the river, and the fact that no fault breccia was found in a borehole slanted to go under the gorge, indicate that the river has eroded along minor fractures and joints. Nevertheless the strike of the river is along a potential failure plane. (The known faults in the area are approximately at right angles to the strike of the river.)

#### MODEL STUDIES

As a first approximation it is possible to model the problem as consolidation of a water-logged half space. Our computer programs for two- and three-dimensional analysis treat the modelling problem by considering the earth to be a uniform, isotropic half-space consisting of an elastic matrix affected by fluid under pressure. This material is characterized by a single permeability, a relative fluid matrix compressibility, a coupling factor (or hydraulic transmissibility) for the bottom of the reservoir, and two elastic moduli. The reservoir load can be approximated as a "long" two-dimensional load or within limits treated as three-dimensional.

The major deficiency of this approach is that effects on the strength of faults must be judged qualitatively. Interpretive examples are given in

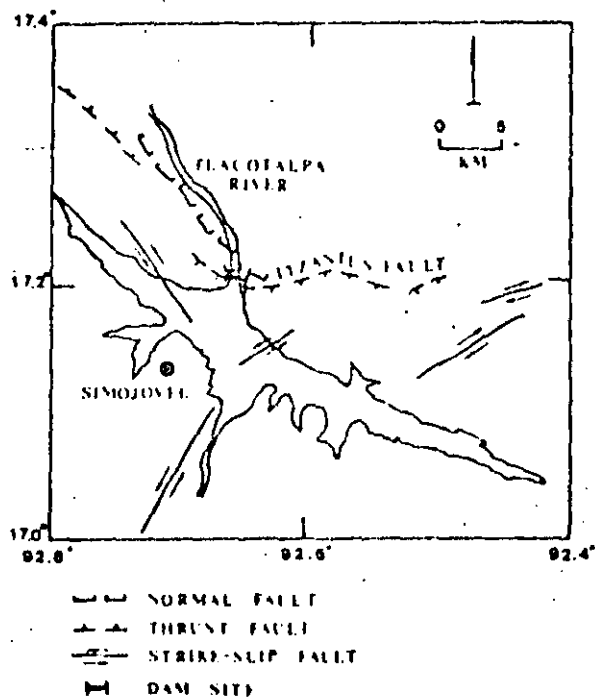


Fig. 2. Major geological features of the area of Itzantun and the location of the Itzantun fault with respect to the dam site.

Withers and Nyland (1978). They point out that the incremental stresses due to a reservoir are rarely large enough to cause failure by themselves. The potential for failure must exist and may be triggered by the reservoir.

### STRESSES IN POROUS MEDIA

The definition of stresses in porous media meets with certain difficulties, but some heuristic theory has been developed to deal with these stresses. Terzaghi (1951) proposed that stresses in porous media are a "neutral stress", the stress in the fluid, and an "effective stress", the difference between the total stress prevailing in the fluid-filled media and the neutral stress. It is the effective stress that causes deformation (Scheidegger, 1974).

Biot (1941) suggested that the compaction of soils is caused by a phenomenon called "soil consolidation". This means that the settlement is caused by the gradual adaptation of the soil to a load variation. Biot made the following assumptions: (1) isotropy of the material; (2) linear stress-strain relations; (3) the strains in the media are small; (4) the water contained in the pores is incompressible but may contain air bubbles; and (5) the water flows through the porous skeleton according to Darcy's law.

With these assumptions, Biot developed the theory for the consolidation of porous media; the basic relations that describe the phenomenon are given by Biot in a series of papers published since 1941. Little has changed in this theory since then (Rice and Cleary, 1976).

In order to approach the consolidation problem outlined earlier, we have followed the technique described by Withers and Nyland in their series of papers (Withers and Nyland, 1976, 1978; Withers, 1977). In order to solve the consolidation equations, use is made of the displacement functions of McNamee and Gibson (1960). This implies the development of a procedure to allow us to determine the double Fourier and Laplace transforms of the water load. The Fourier transforms are done by using the Advanced Mathematical Library of the array processor (AP-190L), which allows the whole computation to be overlapped with data-access time. This permits us to deal with the two-dimensional transforms of the load at a given time as a vector and determine the change of the stresses up to that time.

Once the values of the transforms of the stresses at the desired location corresponding to each of the times of the known load history are determined, we have the information necessary to construct a curve for which inverse Laplace transform will give the behaviour of one of the components of stress at any time. From these components, a failure criterion and an assumption about the orientation of a plane of weakness, we calculate estimates of stability of a point in the formation. The inclusion of several segments in the loading history curve is done by applying the superposition principle. Thus after the inverse Fourier transform is performed in the AP for a given component of stress, the resulting values at some  $X$ ,  $Y$ ,  $Z$ , are the Laplace transform in discrete form of the change in time of one component of stress. The result is a function of time, which defines the way a point in the formation moves towards, or away from, failure.



## FAILURE CRITERIA

In the Mohr's circle representation in three dimensions, the normal and shear stress across a plane of weakness whose normal has director cosines  $l$ ,  $m$ ,  $n$ , are given by Jaeger and Cook (1979, p.27). Fixing two of the direction cosines (say  $n$  and  $l$ ) two equations can be obtained. Each of them represents one family of Mohr's circles in two dimensions and for a fixed value of the corresponding direction cosine each represents a unique circle. Therefore, by fixing  $n$  and  $l$ , two circles can be drawn such that their intersection will lie at a point on the surface of a three-dimensions Mohr representation, and will be a unique location for these two circles whose centres are at  $(\sigma_1 + \sigma_2)/2$  and  $(\sigma_2 + \sigma_3)/2$  and whose ratios are  $AC$  and  $BD$ , respectively, as shown in Fig.3.

With the previous procedure it is possible to determine the values of  $\sigma$  and  $\tau$  for every combination of stresses. That is, the location of point  $P$  can be determined for any time. A simple failure criterion is that of Coulomb (Fig.3) which suggests that failure occurs when the shear on a failure plane exceeds

$$\tau = S_0 + \sigma_n \tan \alpha$$

where  $\tau$  is the shear strength of the rock,  $\alpha$  is the angle of shear resistance;  $\sigma_n$  is the normal effective stress on the plane of fracture;  $S_0$  is the apparent cohesion and is the shear strength of the material under zero normal pressures.  $S_0$  ranges considerably from zero in a fractured material to several hundreds of bars in an intact material (Withers, 1977). In Itzantun, fractures are present and  $S_0$  is probably small. If  $\alpha$  lies between  $25^\circ$  and  $45^\circ$ , then the coefficient of friction is between 0.47 and 1.0 but it is usually around 0.6 ( $\alpha = 30^\circ$ ).

As the value of  $S_0$  is unknown, we set it to zero. Now the variation of the minimum distance between the failure envelope and the point  $P$ , defines the changing stability of the system.

By fixing the angles  $\theta$  and  $\phi$ , the plane of weakness of the material is determined. The variation with time of the distance between the corresponding

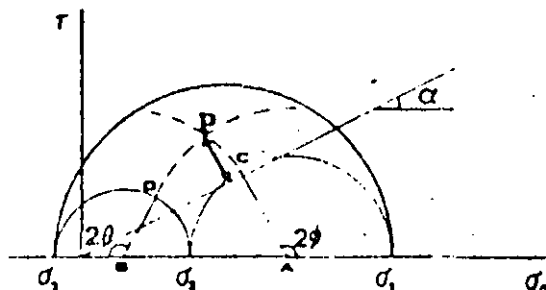


Fig.3. Definition of the STABILITY function as the distance between  $P$  and the failure envelope.

point  $P$  on the surface of the Mohr's circles and the failure envelope will result in a "STABILITY" history for a given location of coordinates  $X$ ,  $Y$ ,  $Z$ . This stability history can be represented as a curve in a stability value vs time diagram and we refer to this curve as the stability function.

The stability function depends only on the loading history, the known geological structures (that will determine the angles  $\theta$  and  $\phi$ ), and the geometry or the bathymetry of the lake. Stability has been defined as a function proportional to the minimum distance between the failure envelope and  $P$ .

The use of a Coulomb failure criterion implies that the rocks will behave in an elastic way and that fracture will occur in a brittle way. Although rocks behave in a more complicated way, the assumption of elastic materials is often made in geophysics; Solomon et al. (1980) and many others have suggested that the upper few tens of kilometres of the earth's crust can be treated as elastic materials. Turcotte (1974) determined that the upper bound for this pseudo-elastic behaviour is 300°C; this temperature is well above that expected at the depths we consider here.

Assuming Mohr-Coulomb failure is consistent with the assumption that the incremental stresses cause elastic deformation, particularly near failure. The assumption of brittle failure may not be true for all faults, but it is a reasonable, tractable hypothesis.

We acknowledge that the treatment of the earth as a porous half-space consisting of an elastic matrix saturated with water is a simplistic model. However, the stability functions are relative, and only serve as indicators of how the risk of inducing seismic activity is changing with respect to a reference initial value.

## DISCUSSION OF RESULTS

We attempt here to evaluate the risk of induced seismicity in a qualitative way. In order to do this we have made and justified as far as possible a number of assumptions.

(1) In the upper 25 km of the earth incremental stress changes cause an elastic response and failure occurs according to a Mohr-Coulomb failure criterion.

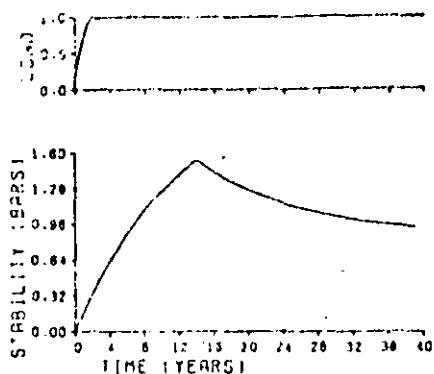
(2) The in-situ stresses are such that small increments can cause failure.

(3) The effect of water can be modelled by the Biot consolidation theory.

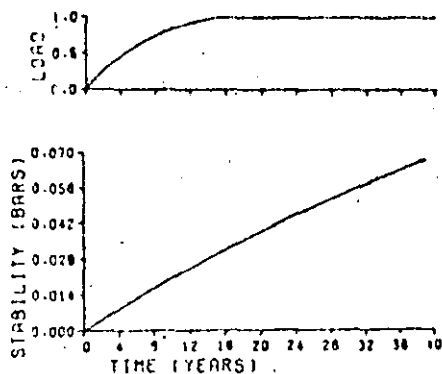
(4) A uniform half-space is a reasonable approximation to reality.

(5) The geologic estimates of fault orientation define the location and direction of expected failure. Intact rock will not fail under reservoir-induced loads.

With these assumptions the results shown in Figs.4-7 were obtained. Figs.4 and 5 represent the stability function for two loading histories consisting of monotone increasing loads, to a constant load. Both have been calculated for a point beneath the deepest part of the reservoir at a depth of 1 km and show the relation of the resulting stress to the rate of filling. For the curve where the complete load is reached 16 years after the beginning of



T=2, DEPTH=1 KM.



T=16, DEPTH=1 KM.

Fig.4. The upper graph shows a loading history consisting of a continuously increasing exponential, where the total load is reached after 2 years of loading. The bottom graph shows the stability function corresponding to a point below the deepest part of the reservoir at 1 km depth.

Fig.5. The upper graph shows a loading history consisting of a continuously increasing exponential, where the total load is reached after 16 years of loading. The bottom graph shows the stability function corresponding to a point below the deepest part of the reservoir at 1 km depth.

the impoundment, the increase in stress is much smaller than when the total load is reached after 2 years.

Fig.4 also illustrates that when the load is kept constant for a certain time period, the stresses begin to decrease to a limiting value. This means that the effect of the anomalous stress produces changes that lead to an equilibrium state that does not necessarily have to be the initial state of stress in the area. This can be thought of as related to the existence of residual stresses.

The non-linear dependence of the risk function on the rate of filling is shown in Table I. This table shows the value of the stability function 20 years

TABLE I

Variation of the stability function for different rates of filling of the reservoir, the time required to attain complete filling for each of the loading histories considered, and the maximum and final value observed for the stability curve during each of these cases

Duration of loading (years)	Stability function in bars		
	Max. value		Value after 20 years
	Attained	Time (years)	
2	1.54	15	1.21
3	0.95	20	0.95
4	0.51	20	0.51
8	0.15	20	0.15
16	0.04	20	0.04

after impounding was begun and the maximum value attained during that period. This is done for a location at 1 km beneath the deepest part of the Izantun reservoir. The loading histories used to obtain this table are as follows, where  $T$  is the time at which the lake was first completely filled, and  $D$  is the maximum depth of the reservoir. After  $.25 T$  the reservoir had water up to  $.45 D$ . After  $.5 T$  it had  $.75 D$ . At  $.75 T$  it was  $.9 D$  full. From the time  $T$  the reservoir remains filled. It is obvious that a peak in the stability function has been reached during this 20 years interval only for the first case of Table I. With a faster rate of filling the risk of reaching failure is higher; for the first case the risk increases sharply, it reaches its maximum value 2 years from the beginning of the filling of the reservoir and then it decreases to a value of about .9 bar and remains constant.

The rate of filling of the reservoir is not the only way in which artificial lakes could change the seismic activity of an area. Some changes have been observed after filling and draining the reservoir, like in the case of Oroville, CA, where an event of magnitude 5.9 occurred after this kind of loading history (Withers, 1977).

In order to see the effect of draining of a reservoir on the stability function, we applied the loading history shown in Fig.6. This example shows that the stability function for unloading tends to have a second minimum, in this case after 8 years. The effect of a fast decrease in the value of the stability function must generate sudden changes in the stresses that might trigger seismic events.

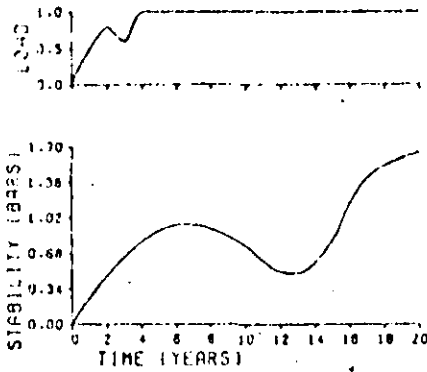
Other histories involving reduction of loads show that if lowering the water level is done rapidly, the negative slope of the stability function moves toward a horizontal position. This reduces the risk over a thrust fault but increases it for a normal fault, as the values in the latter part of the stability curve are much bigger.

Decrease in loads in the loading history result in a stability decrease that attenuates rapidly with the depth of the observation point. For a depth of 4 km the effect is not observed at all (Fig.7).

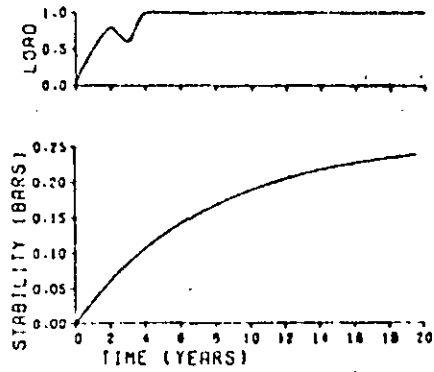
## CONCLUSIONS

Why the filling of some reservoirs causes seismic events is poorly understood. We give no firm predictions for Izantun. Studies indicate residual stresses, differences in permeability, and differences in physical properties of the formations under the reservoir may determine whether there is induced seismicity risk or not. None of these factors are known with precision at Izantun.

The changes in stability in a water reservoir due to the presence of the water can be predicted in a qualitative way by assuming: (a) a model of a porous half-space consisting of an elastic matrix saturated with water, (b) that brittle failure can occur in the upper 10 km of the lithosphere if small stress changes are made, and (c) that the effect of water in rocks can be approximated with Biot's consolidation theory.



$T=4$ . DEPTH=1 KM.



$T=4$ . DEPTH=4 KM.

Fig.6. The upper graph shows a loading history in which an unload takes place in the interval from the second year of loading until the third one, after which the increase in load is continued until the fourth year when the total load is attained. The bottom graph shows the stability function corresponding to a point below the deepest part of the reservoir at 1 km depth.

Fig.7. The upper graph shows the same loading history as that of Fig.6. The bottom graph shows the stability function corresponding to a point below the deepest part of the reservoir at 4 km depth.

We suggest that to diminish the risk of induced seismicity at Itzantun, the filling of the reservoir should be as slow as economics permits, with intervals at which the water level is held constant.

#### ACKNOWLEDGEMENTS

We are grateful to the Instituto de Ingenieria from the Universidad Nacional Autonoma de Mexico and to the Comision Federal de Electricidad of Mexico for the support given in the first stages of this work. We are particularly grateful to J. Havskov and S.K. Singh for many valuable discussions.

A. Uribe-Carvajal is supported at the University of Alberta by the Consejo Nacional de Ciencia y Tecnologia (CONACYT) of Mexico. This research was supported by the Natural Sciences and Engineering Research Council (NSERC) of Canada.

#### REFERENCES

- Bell, M.L. and Nur, A., 1978. Strength changes due reservoir pore pressure and stress and application to lake Oroville. *J. Geophys. Res.*, 83: 4469-4483.
- Biot, M.A., 1941. General theory for three dimensional consolidation. *J. Appl. Phys.*, 12: 578-581.
- Bufe, C.G., Lester, F.W., Lahr, K.M., Lahr, J.C., Seekins, L.S. and Hanks, T.C., 1976. Oroville earthquakes: Normal faulting in the Sierra Nevada foothills. *Science*, 192: 72-74.

- Comninakis, P., Drakopoulos, J., Moumoulidis, G. and Papazachos, B.C., 1968. Foreshock sequences at the kremasta earthquake and their relation to water loading of the Kremasta artificial lake. *Ann. Geol. (Rome)*, 21: 39-71.
- Cook, N.G.W., 1976. Seismicity associated with mining. *Eng. Geol.*, 10: 99-122.
- Gough, D.I., 1978. Induced seismicity. In: *The Assessment of Mitigation of Earthquake Risk*. UNESCO, 341 pp.
- Gough, D.I. and Gough, W.I., 1970a. Stresses and deflection in the lithosphere near lake Kariba-I. *Geophys. J.R. Astron. Soc.*, 21: 65-78.
- Gough, D.I. and Gough, W.I., 1970b. Load induced earthquakes at lake Kariba-II. *Geophys. J.R. Astron. Soc.*, 21: 79-101.
- Gough, D.I. and Gough, W.I., 1976. Incremental stresses near the Cabora Bassa Gorges. *Eng. Geol.*, 10: 211-218.
- Gupta, H.K. and Rastogi, B.K., 1976. *Dams and Earthquakes*. Elsevier, Amsterdam, 229 pp.
- Gupta, H.K., Rastogi, B.K. and Narain, 1972. Common features of the reservoir associated seismic activities. *Bull. Seismol. Soc. Am.*, 62: 481-492.
- Jaeger, J.C. and Cook, N.G.W., 1979. *Fundamentals of Rock Mechanics*. Wiley, New York, N.Y., 593 pp.
- Kirby, S.H., 1977. State of stress in the lithosphere: inferences from flow laws of olivine. *Pure Appl. Geophys.*, 115: 245-258.
- Leblanc, G. and Anglin, F., 1978. Induced seismicity at the Manic 3 reservoir, Quebec. *Bull. Seismol. Soc. Am.*, 68: 1469-1485.
- McNamee, J. and Gibson, R.E., 1960. Displacement functions and linear transforms applied to diffusion through porous media. *Q.J. Mech. Appl. Math.*, 13: 98-111.
- Nyland, E. and Withers, R.J., 1976. A fast method for computing load induced stresses in the earth. *Geophys. J.R. Astron. Soc.*, 44: 689-698.
- Packer, D.R., Lovegreen, J.R. and Born, J.L., 1977. *Reservoir Induced Seismicity*, Vol 6. Woodward-Clyde Consultants, San Francisco, Calif., 124 pp.
- Pomeroy, P.W., Simpson, D.W. and Sbar, M.L., 1976. Earthquakes Triggered by surface quarrying - Wappingers Falls, New York sequence of June, 1974. *Bull. Seismol. Soc. Am.*, 66.
- Raleigh, C.B., Healy, J.H. and Bredehoeft, J.D., 1976. An experiment in earthquake control at Rangely, Colorado. *Science*, 191: 1230-1237.
- Rice, J.R. and Cleary, M.P., 1976. Some basic stress diffusion solutions for fluid-saturated elastic porous media with compressible constituents. *Rev. Geophys. Space Phys.*, 14: 227-241.
- Rothe, J.F., 1973. Summary: geophysical report. In: *Man-made Lakes: Their Problems and Environmental Effects*. Am. Geophys. Union, *Geophys. Monogr.*, 17: 441-454.
- Scheidegger, A.E., 1974. *The Physics of Flow Through Porous Media*. University of Toronto Press, 353 pp.
- Simpson, D.W., 1976. Seismicity changes associated with reservoir loading. *Eng. Geol.*, 10: 123-150.
- Simpson, D.W. and Negmatullaev, S.K., 1981. Induced Seismicity at Nurek Reservoir Tadzhikistan, USSR. *Bull. Seismol. Soc. Am.*, 71: 1561-1586.
- Soboleva, O.V. and Mamadaliev, U.A., 1976. The influence of the Nurek reservoir on local earthquake activity. *Eng. Geol.*, 10: 293-306.
- Solomon, S.C., Richardson, R.M. and Bergman, E.A., 1980. Tectonic stress: models and magnitudes. *J. Geophys. Res.*, 85: 6086-6092.
- Terzaghi, K. Van, 1951. *Theoretical Soil Mechanics*. Wiley, New York, N.Y.
- Turcotte, D.L., 1974. Are transform faults thermal contraction cracks? *J. Geophys. Res.*, 79: 2573-2577.
- Wang, M., Hu, Y., Chen, Y., Yang, M., Li, T., Chin, Y. and Feng, J., 1976. Mechanism of the reservoir impounding earthquakes at Hsinfengkiang and a preliminary endeavour to discuss the case. *Eng. Geol.*, 10: 331-351.

- Wetmiller, R.J., 1981. Microseismicity in the Rocky Mountain House seismogenic zone, Western Canada. Abstract G.A.C./C.G.U. Meeting, Calgary.
- Withers, R.J., 1977. Seismicity and Stress Determination at Man made Lakes. Ph.D. Thesis, The University of Alberta, Edmonton, Alta., 241 pp.
- Withers, R.J. and Nyland, E., 1976. Theory for the rapid subsidence near reservoirs on layered and porous media. Eng. Geol., 10: 169-185.
- Withers, R.J. and Nyland, E., 1978. Time evolution under artificial lakes and its implication for induced seismicity. Can. J. Earth Sci., 15: 1526-1534.



**DIVISION DE EDUCACION CONTINUA  
FACULTAD DE INGENIERIA U.N.A.M.**

MECANICA DE ROCAS APLICADA A LA MINERIA Y A LA CONSTRUCCION

THE INFLUENCE AND CONTROL OF GROUNDWATER IN LARGE SLOPES

By Adrián Brown

MAYO, 1985



*L. Maycotte*

**Brown, A.** The influence and control of groundwater in large slopes. *Proc. 3rd Intl. Conf. on Stability in Surface Mining, Vancouver.* AIME., Vol. 3, 1981.

## THE INFLUENCE AND CONTROL OF GROUNDWATER IN LARGE SLOPES

By Adrian Brown

Principal  
Golder Associates  
Denver, Colorado

### INTRODUCTION

The primary tool which is available to improve the stability of an open pit mine at a given slope angle is control of groundwater pressure. This paper sets out the methods by which water pressure control can be achieved in large mines in different materials.

The emphasis of this paper is on large mine slopes because these slopes exhibit the greatest need for groundwater control, the greatest economic benefit from groundwater control, and the greatest technical challenge in achieving groundwater control.

### STABILIZATION USING WATER PRESSURE CONTROL

Groundwater pressures reduce the stability of slopes in two fundamental ways, as shown schematically in Figure 1. In the example, a horizontal failure surface intersects a vertical joint or weak zone. Water pressure acts:

- o On the base plane to reduce the normal force on the sliding surface and hence reduce frictional resistance to sliding, and
- o On the vertical back plane, to create a driving force for the system.

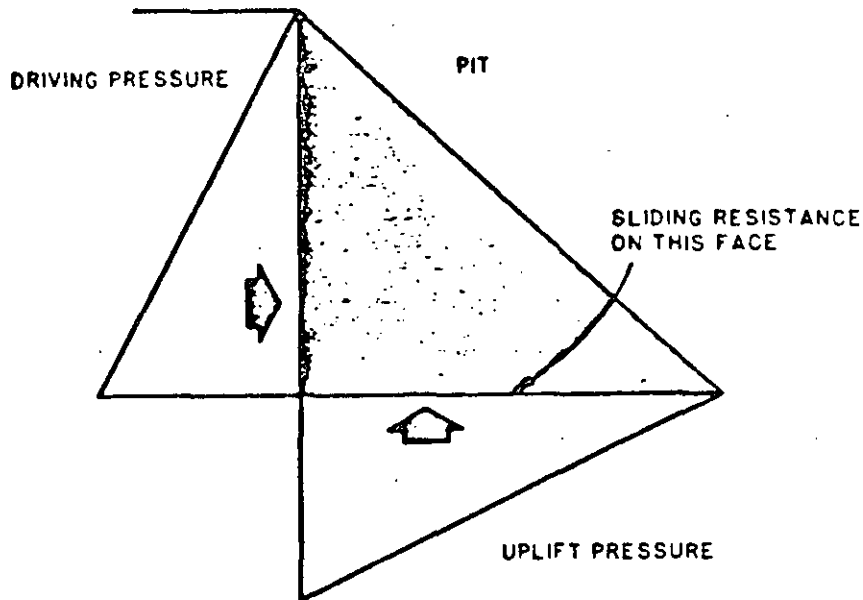


Fig. 1. Example of Effect of Groundwater Pressure on Slopes.

This particular slope stability example was chosen to have water as the only driving force, so that water pressure reduction clearly improves the stability of the system dramatically. It is of interest to note that in this example, about 70% of this increased stability comes from reduction of the driving pressure, and about 30% comes from increase of the frictional resistance on the base plane.

A powerful way to illustrate the need for groundwater pressure reduction is to contrast the extreme cases of fully saturated slopes and completely depressurized slopes. The relationship between slope angle and the primary factors which determine slope angle (height, friction, cohesion, and material unit weight) has been elegantly presented for five groundwater scenarios by Hoek and Bray (1977). Subtracting the slope angle for a completely depressurized slope from that for a completely saturated slope gives the increased slope angle available through water pressure control. The resulting diagram is presented as Figure 2.

The significance of the savings available for mine operators becomes clear when it is recognized that an increase of  $10^\circ$  in slope angle in most large mines halves the required stripping.

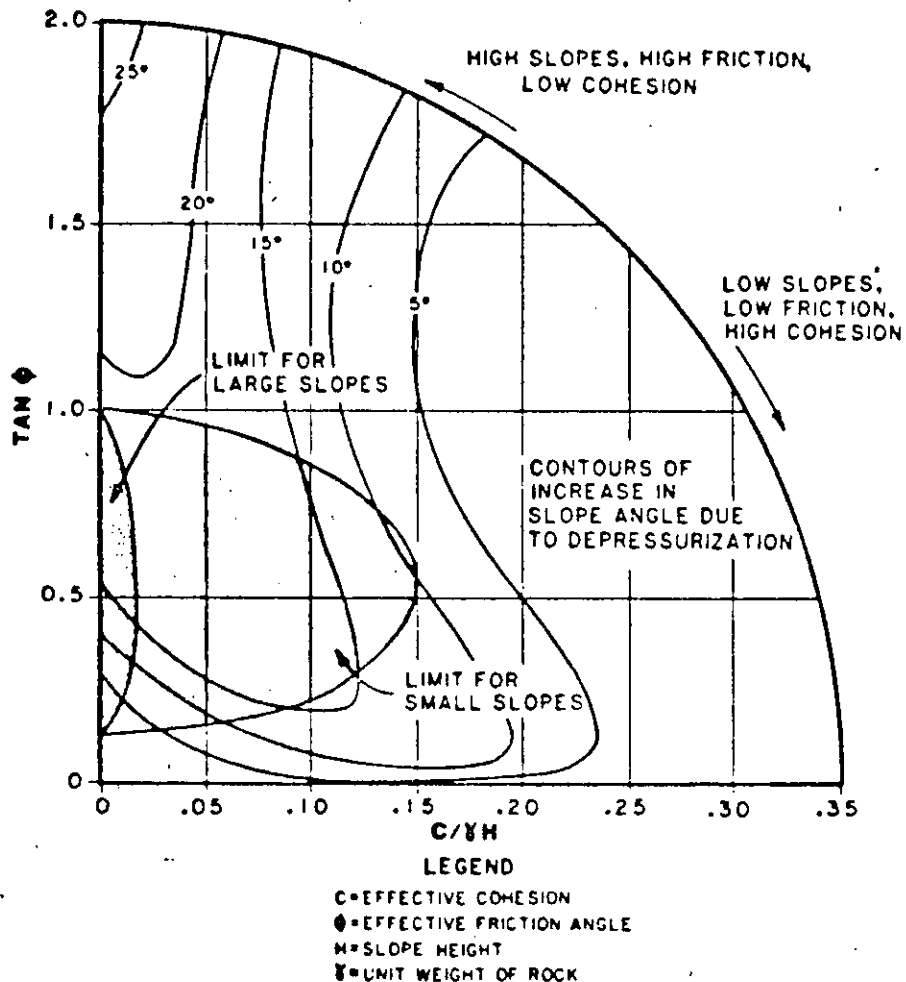


Fig. 2. Maximum Available Slope Angle Increase as a Result of Groundwater Pressure Control.

### THE NATURE OF LARGE SLOPE FAILURES

The nature of most large slope "failures" (using the term in the geomechanical sense that some materials in the slope have yielded) is usually more complex than the simple example above, or the model used by Hoek and Bray. Such failures are rarely rapid, except over a bench or two, and bench scale failures, while an operational and safety concern, are beyond the scope of the present discussion.

Large pit wall failures usually begin as slow movement of the surface of most of the wall. At first, the rates are in the order of a few millimeters per day. If mining continues, these movements gradually accelerate over a period of months or even years. Surface disturbance inside the pit become more marked, and bench access and

integrity becomes impossible to maintain. Cracking at or outside the crest is common. Movements are much more marked in wet periods (rain, snowmelt) and immediately following mining at or near the toe. If nothing is done about these failures, the movements become more and more rapid until finally a major translational failure of the wall occurs.

If the conditions within the slope are observed, it is seen that these failure mechanisms are deep seated. The movement zone often extends into most of the region beneath the slope to the total pit depth (i.e., the shaded zone in Figure 1). What is happening during failure is that the interlocking rock particles are being disturbed in this entire zone, and the initial cohesive strength is being reduced. At some point in this process, the strength of a continuous daylighting failure surface drops below that required for stability, and the wall fails in a translational manner.

Most big pit failures do not reach this stage. Water pressure control or slope flattening or both are usually used to reduce movements. However, some big pit slopes have failed without translational failure because the continual movements have become operationally intolerable.

For the purposes of this paper, the following points about failure are important:

- o Large pit failures are deep seated
- o Water pressure is an important driving force when it is present
- o Slope control can, in general, only be achieved by slope flattening or deep water pressure control

The remainder of the paper evaluates the ways in which deep water pressure control can be obtained.

#### PARAMETERS CONTROLLING WATER PRESSURE IN SLOPES

In slope stabilization using water pressure control, the focus is on reducing groundwater pressure. Typically, any stabilization involves installing pressure control devices at a number of locations and waiting for the water pressure to drop in the material around and between those devices. The process focuses on obtaining a major water pressure reduction in an acceptable length of time. There are two disciplines which have traditionally dealt with matters of transient groundwater pressure changes: groundwater hydrology and soil mechanics.

## Groundwater Hydrology Approach

Groundwater hydrology has its foundation in the provision of water supply from aquifers. Ever since the classic paper by Theis in 1935, groundwater hydrologists have used two major parameters to describe the characteristics of aquifers:

Transmissivity (T)--which is defined as the quantity of water which flows through a unit width of an aquifer under a unit hydraulic gradient. It has the units  $[L^2/T]$ .

Storage Coefficient (S)--which is defined as the quantity of water produced by a unit area of the aquifer when the aquifer is subjected to a unit head reduction. It has no units.

Both these parameters implicitly include the thickness of the aquifer, and so for mine hydrology work it has been usual to divide them by the material thickness to produce three corresponding parameters:

Hydraulic Conductivity (k)--which is defined as the quantity of water which flows through a unit area of a material under a unit head gradient. It has the units  $[L/T]$ .

Specific Storage ( $S_g$ )--which is defined as the volume of water which is produced from a unit volume of saturated material when it is subjected to a unit head reduction. It has the units  $[L^{-1}]$ .

Drainable Porosity ( $n_d$ )--which is defined as the volume of water produced per unit volume of material as the water table moves through the material. It has no units.

The basic general differential equation for heads in a groundwater system is as follows for a planar one-dimensional case:

$$\frac{\partial h}{\partial t} = \frac{T}{S} \frac{\partial^2 h}{\partial x^2} = \frac{k}{S_g} \frac{\partial^2 h}{\partial x^2}$$

where

h = head  
t = time  
x = distance

### Soil Mechanics Approach

By comparison, the soil mechanics approach to this particular problem comes from the study of the settlement of buildings, and is embodied in consolidation theory. The classic statement of this theory is in a book by Terzaghi and Peck, first published in 1948, and repeated in later editions (Terzaghi and Peck, 1967). There are three parameters which characterize this approach, as follows:

Hydraulic Conductivity ( $k$ )--as before.

Coefficient of Volume Compressibility ( $m_v$ )--which is defined as the change of pore volume per unit total volume per unit of pressure increase. It has the units inverse pressure [ $LT^2/M$ ].

Coefficient of Consolidation ( $c_v$ )--which is defined by the following equation:

$$c_v = \frac{k}{\rho_w g m_v}$$

where  $\rho_w$  = density of water

$g$  = acceleration due to gravity

The standard equation for consolidation in a one-dimensional case is:

$$\frac{\partial u}{\partial t} = c_v \frac{\partial^2 h}{\partial x^2}$$

where  $u = \rho_w g h$  = the pore-water pressure

Thus, by substitution, the differential equation can be converted to:

$$\frac{\partial h}{\partial t} = c_v \frac{\partial^2 h}{\partial x^2}$$

### Comparison Between Parameters

Clearly, from the two main differential equations,

$$\frac{T}{S} = \frac{k}{S_E} = c_v$$

and  $c_v$ , the coefficient of consolidation, controls the time rate of change of head at any point in a transient groundwater pressure system. This parameter will be used extensively in this paper.

## WATER PRESSURE CONTROL METHODS

There are four major water pressure control methods which appear economic today in the context of most large mines. They are:

- o Unaided drainage
- o Horizontal drainholes
- o Wells
- o Drainage adits

They are listed in order of increasing cost, increasing effectiveness, and increasing operational convenience.

In addition, for very low permeability materials, the physical unloading associated with mining can also lower pore water pressures enough to create a useful stabilizing effect.

Each of these five strategies is evaluated below in the context of their effectiveness in stabilizing slopes in large open pit mines.

### Unaided Drainage

Method. Unaided drainage uses the excavation itself as a collector drain. Water flows into the pit and is pumped out from there.

Theory. The effectiveness of the method as a function of coefficient of consolidation of the host rock is shown in Figure 3 for a typical mining case. Conditions selected were:

Pit depth = 500 meters  
 Time for material to depressurize = 1 year  
 Depth of critical zone = 500 meters

The 1 year depressurization time is appropriate as the critical areas are adjacent to the pit floor, which is usually continually deepening. Thus, relatively rapid pressure control in this area is important.

If we assume that 80% reduction in water pressure is required, then this method of pressure control will be effective in long pits with coefficients of consolidation of  $2 \times 10^{-2}$  meters squared per second or greater, and in radial pits with coefficients of consolidation of about 2 meters squared per second or greater.

Practice. These values are available in most relatively free draining rocks, with average horizontal hydraulic conductivities greater than  $10^{-6}$  meters per second. (Note that average specific storage of most rock materials is about  $10^{-6}$  meters<sup>-1</sup>.) However, even a few meters of clay in (say) faults



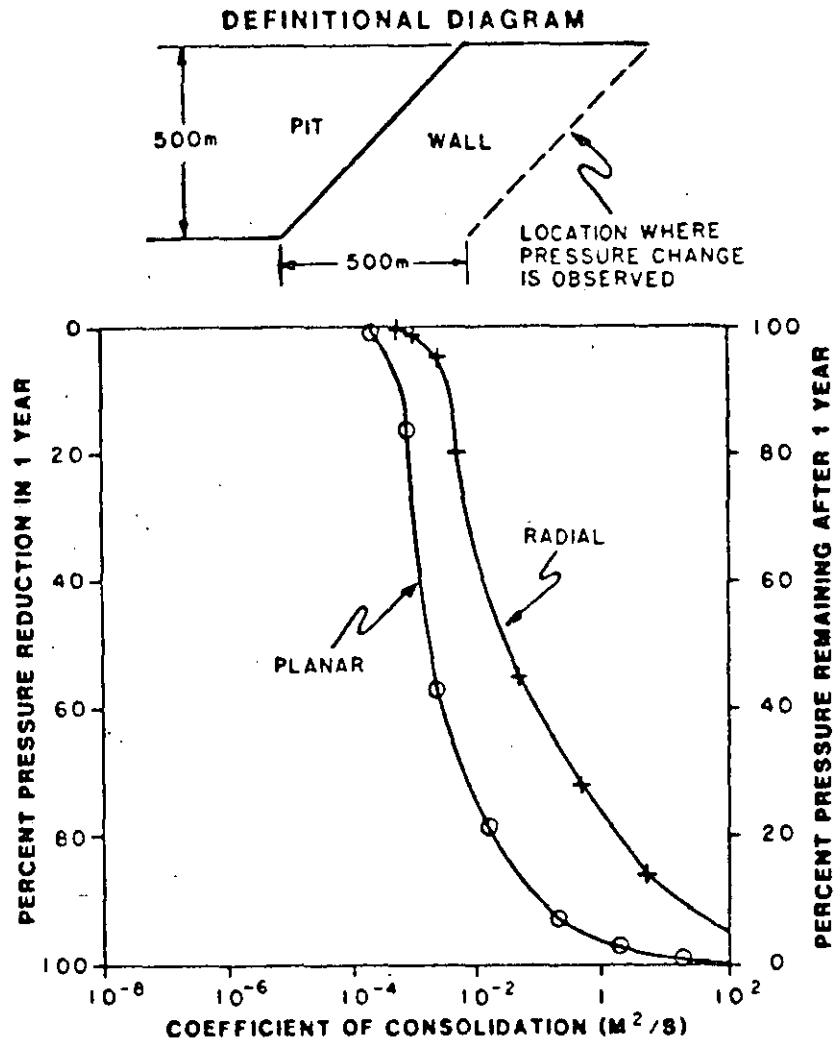


Fig. 3. Effectiveness of Unaided Drainage as a Function of Pit Shape and  $C_v$ .

parallel to the face will so reduce the effective hydraulic conductivity as to render this method of stabilization ineffective. In flat-bedded sedimentary systems it can work well, provided the egress of water at the face is not sufficiently concentrated to cause piping of any poorly cemented materials.

**Operational Aspects.** Operationally, the major disadvantage of unaided drainage is the uncontrolled flow into the pit, most of it coming to the pit floor and lower slope areas. This flow (often in excess of 0.1 cubic meters per second because of the relatively high hydraulic conductivity) makes operations difficult, and also must usually be treated before discharge, as it is degraded in quality when it flows onto the pit floor. Thus, most mines which could stabilize the walls by this method choose not to do so for other reasons.

### Horizontal Drainholes

**Method.** Horizontal drains are drilled into the wall from the pit floor as the pit deepens and provide a pressure relief conduit for the wall material. Typically, they penetrate the wall in a grid, with spacing both vertically and horizontally in the 25 to 100 meter range. Holes are usually in the 200 to 300 millimeter diameter range and are cased with slotted PVC or steel liner pipe.

**Theory.** The effectiveness of horizontal drains in parts of the wall which they penetrate is shown on Figure 4 as a function of the average coefficient of consolidation of the wall material. As can

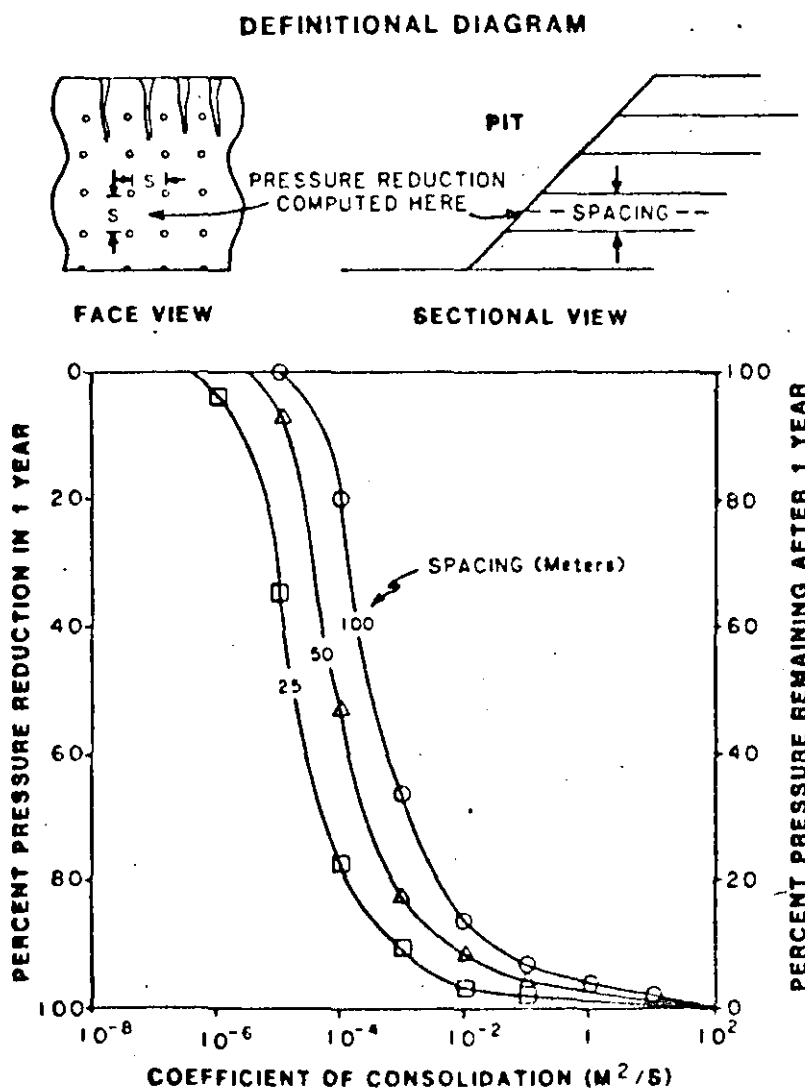


Fig. 4. Effectiveness of Horizontal Drains as a Function of Spacing and  $C_v$ .

be seen, 80% pressure reduction after 1 year can be achieved with coefficients of consolidation down to  $10^{-3}$  meters squared per second with a drain spacing of 25 meters or more. In rock mines this indicates that this strategy can be effective in wall material penetrated by drains down to an average hydraulic conductivity of  $10^{-9}$  meters per second.

Practice. The practical advantage of horizontal drains is that they penetrate structures in the wall and provide pressure relief behind them. As many large mines exhibit steeply dipping structures filled with low permeability material, this method of pressure relief is extraordinarily effective.

The primary disadvantage of horizontal drains is that they are very difficult to advance beyond 100 to 150 meters. Their effectiveness beyond this reach is typically modest, so that they are frequently inadequate for the total pressure control of deep mines. This effect is shown on Figure 5. However, they can be and often are used as a part of a total pressure relief strategy.

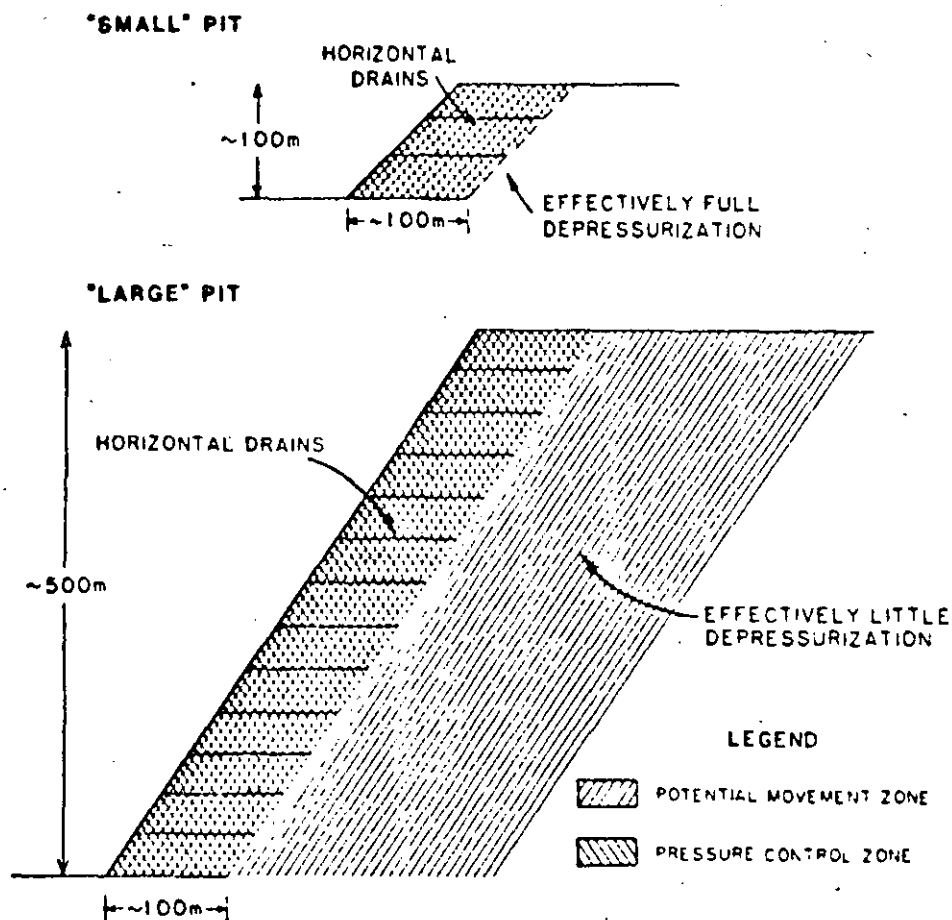


Fig. 5. Impact of Slope Size on Effectiveness of Horizontal Drains.

Operational Aspects. Horizontal drainhole systems are difficult to maintain in an operating mine. Ideally, water should be collected from each hole and piped to a point from which it can be pumped from the pit. This avoids resaturating the slope immediately below the drain, partially nullifying the effect of lower drains. The drains must also be maintained with annual cleaning and occasional replacement. Both of these aspects require maintaining access to the benches from which the holes were drilled, which is usually difficult and makes steep slopes difficult to achieve.

Finally, the drains are usually lost on each push back, and the network of holes, pipes, sumps, and pumps needed in an operating system creates obstacles for normal pit operations.

There are, however, many successfully operating horizontal drain systems in mines around the world, and they provide a low capital water pressure control strategy in relatively low permeability materials.

## Wells

Method. The classical dewatering strategy for mines is pumped wells, and there are many systems in use today. The usual installation involves wells around the periphery of the mine, augmented with some in pit wells in larger mines. Wells are typically screened over their entire length with an inexpensive screen, and gravel packed when installed in poorly cemented materials. Pumping is usually by submersible electric or shaft driven turbine pumps. Unlike water supply wells, dewatering wells are pumped until the drawdown approaches the bottom of the well in order to maximize the pressure reduction effect. Water from wells is typically piped directly to discharge without becoming contaminated. Treatment of discharge is occasionally needed.

Theory. In essence, most well systems seek to cut off water entry into the mine slope area by creating a low pressure line along the mine crest. The effectiveness of an infinite line of wells is shown in Figure 6, for various well spacings and coefficients of consolidation. Practical well spacings for large mines are in the 200 to 500 meter range, which indicates that they will be effective in depressurizing a mine slope when the average horizontal coefficient of consolidation exceeds about 1 meter squared per second. Note that this value is quite strongly dependent upon well spacing.

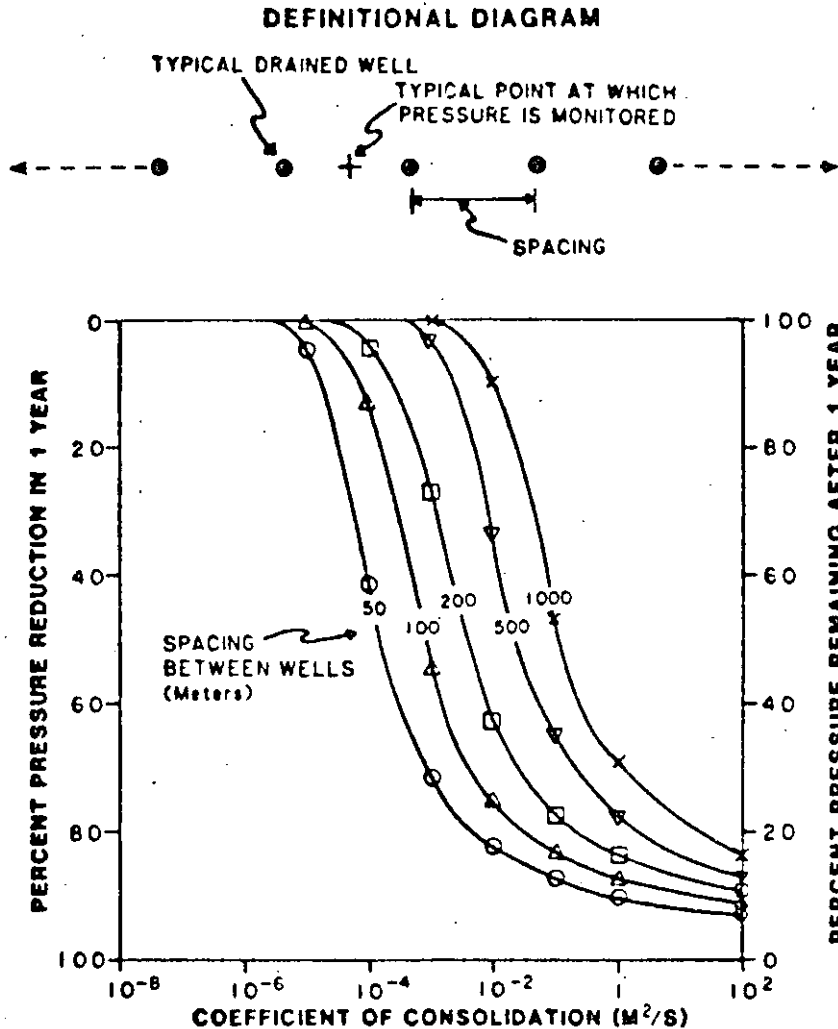


Fig. 6. Effectiveness of Vertical Wells as a Function of Spacing and  $C_v$ .

Practice. The practical limit to the ability of well dewatering systems is usually the nature of the wall materials between the line of wells and the toe of the slope. For large slopes, the wells may be some 1,000 meters from the toe, and any major, low permeability feature in this distance will reduce the effect of the system. For this reason, it is common for wells to be used in conjunction with horizontal drains. Also for this reason, wells do best in flat-bedded sedimentary materials.

The location of the wells is important. Wells are very sensitive to slope movement and should therefore be located outside the potential movement zone. If they are not, then they tend to fail at the very moment when they are most needed.

Operational Aspects. From an operating point of view, well systems have some good and some bad aspects.

On the positive side, the systems can usually be placed outside the active operating area, and are not an obstacle to mining. On the negative side, wells are an alien technology to most mine operations personnel, and require constant attention. This can cause difficulties in the overall operation of the mine.

### Drainage Adits

Method. The drainage adit or gallery has been a standard (if expensive) depressurization option for at least a century. The basic design of the gallery is shown on Figure 7. The adit is

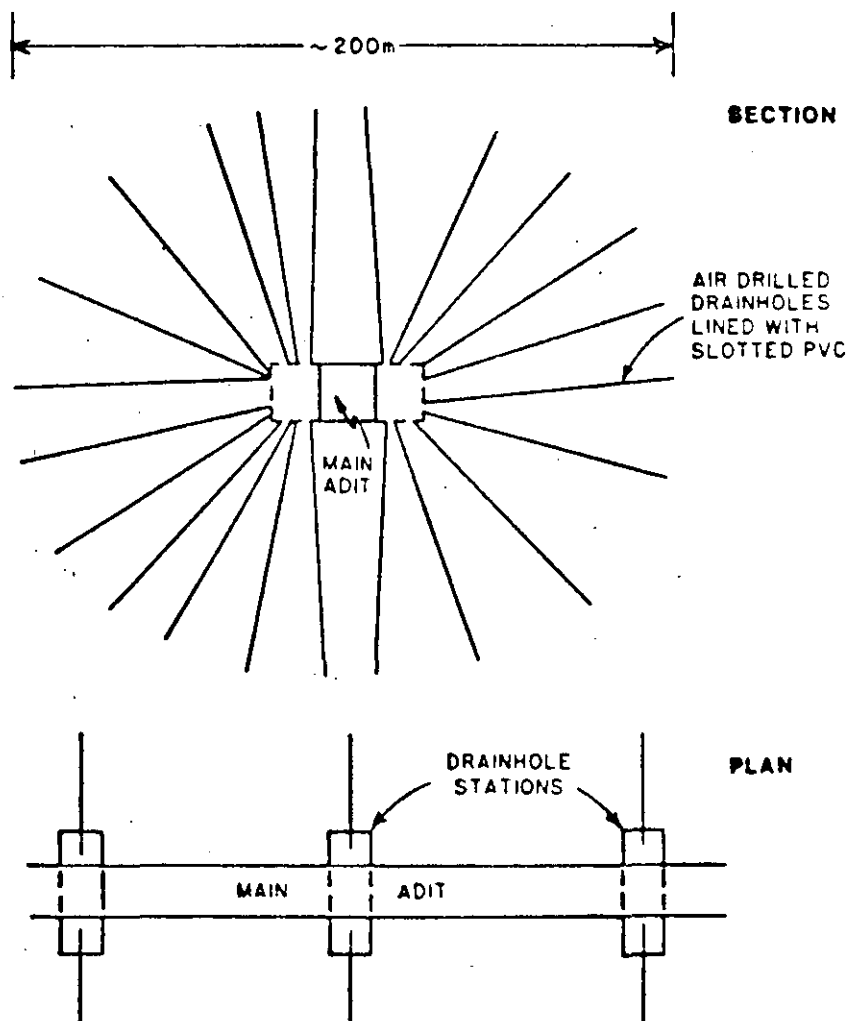


Fig. 7. Typical Drainage Adit Layout (Schematic).

usually advanced by conventional means, with stations slashed out every 50 to 100 meters for fan drilling of drainholes. Typical drainhole length is also 50 to 100 meters, at about 50 millimeter diameter. Slotted PVC pipe is usually inserted into the drains to keep them open.

Theory. The effectiveness of adits was investigated by first evaluating the effectiveness of a single adit, and then multiple adits for large mine slopes. The results of analysis for a single adit are shown on Figure 8. This is computed for an effective adit radius of 100 meters and indicates that for a mine 500 meters deep, a single adit will be effective for average coefficients of consolidation in excess of about 0.1 meters squared per second.

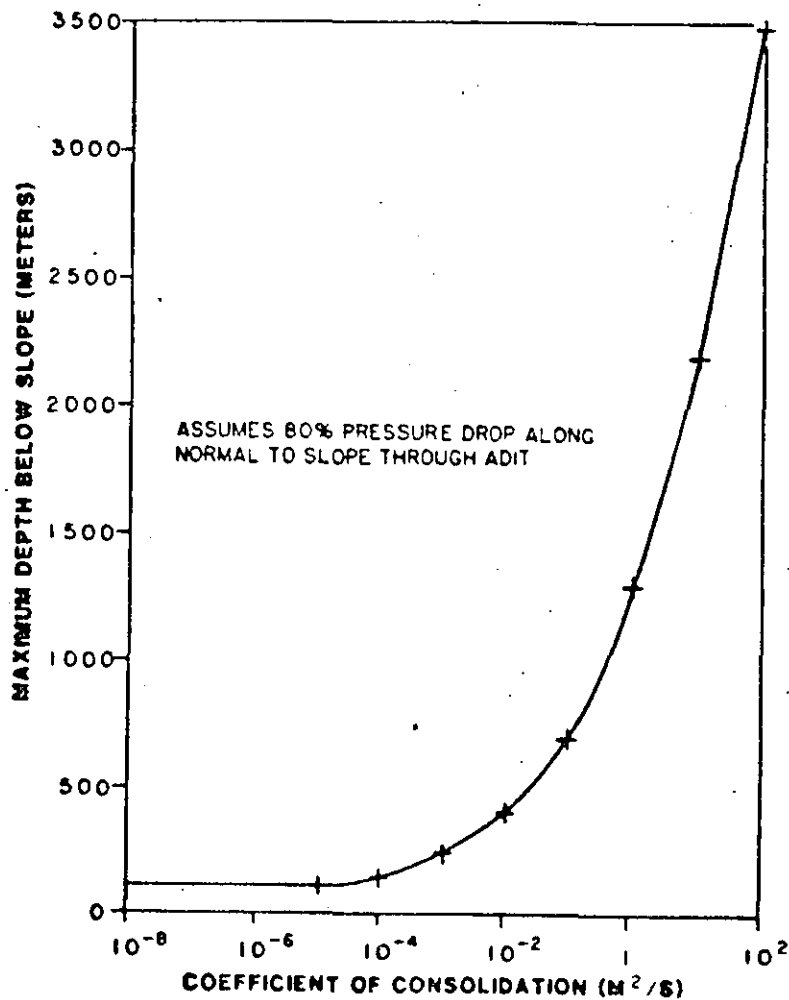


Fig. 8. Maximum Depth of Cover for Effective Adit Performance.

For materials with lower values of coefficient of consolidation, several adits may be needed. The analysis of adit spacing as a function of average coefficient of consolidation and depth of cover over the adit is given in Figure 9. The cutoff in adit effectiveness occurs when radial drains are no longer effective to drain the material between each drain.

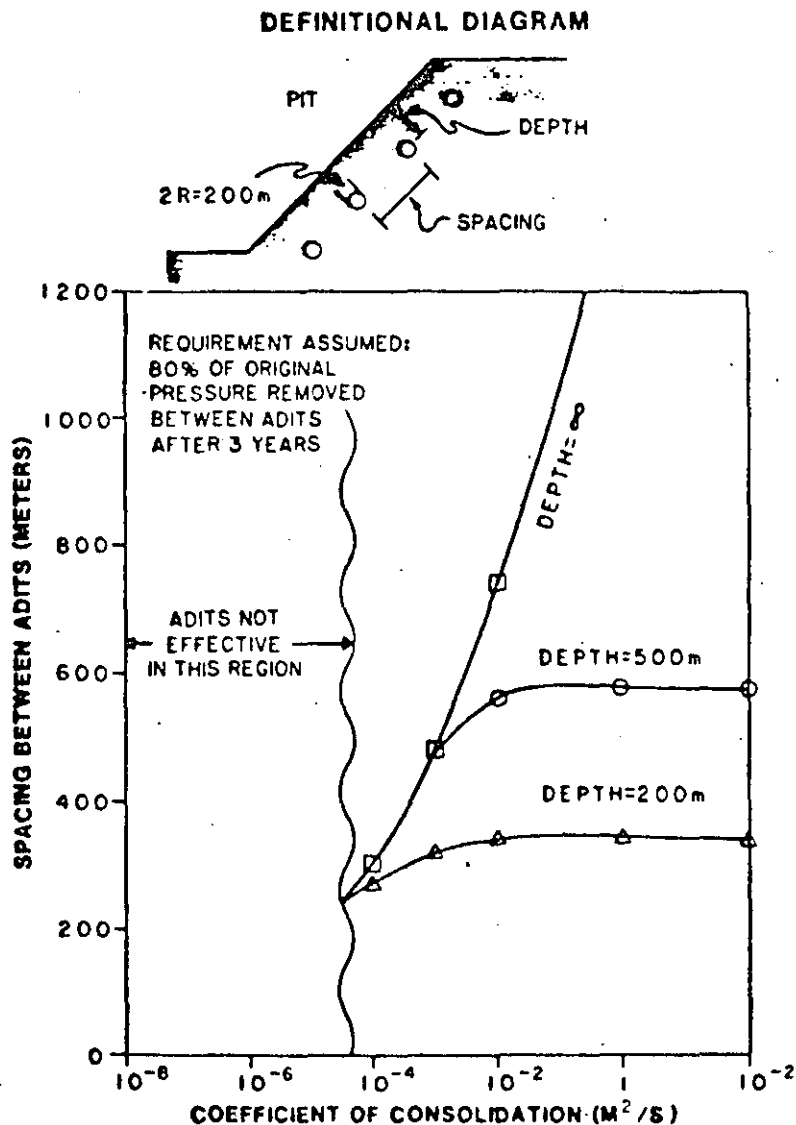


Fig. 9. Required Spacing Between Adits as a Function of Depth and  $C_v$ .



The conclusions of the study of the theory of adits is summarized below for pits in the 500 meter deep range.

<u><math>C_v</math>(m<sup>2</sup>/sec)</u>	<u>Adit Requirement</u>
Less than $10^{-4}$	Adits ineffective
$10^{-4}$ to $10^{-3}$	Multiple, close spaced adits close to pit surface
$10^{-3}$ to $10^{-2}$	Two adits, deeply buried one at toe and one mid-height
Greater than $10^{-2}$	One adit located beneath the crest, at about toe level. Expect high initial flows.

Practice. The practical application of drainage adits rests also on geologic conditions. While, in theory, one adit can depressurize very large volumes of rock, provided the coefficient of consolidation is reasonably high, in actual operation the effect may only spread as far as the nearest thick, gouge-filled discontinuity. Adits work best in relatively isotropic materials for similar reasons.

One of the major benefits of adits is that they can be installed well ahead of the mine development, to give the maximum time for pressure reduction to occur. They can also, of course, be established outside the movement zone of the mine for operational safety. In any case, they are not particularly sensitive to modest movements.

Operational Aspects. Drainage adits offer several operational advantages. First, they are outside pit operations and need not influence them. Second, they collect all drainage water in one location for easy handling and discharge.

The primary operational disadvantage of drainage adits is their inflexibility. If the pit is expanded or the slope location changed, the adit system is difficult and expensive to modify.

### Unloading

Method. Continual unloading of slopes is a normal procedure in most types of open pit mining. It occurs whenever a wall is pushed back.

Theory. When a load is removed from a column of material, it expands. If the material is porous and saturated with water, the load removal causes an instantaneous drop in the pressure of the pore fluid equal to the stress reduction due to the load removal. In time, the pressure returns to a new equilibrium as water is drawn in

from the boundaries. For materials with low coefficients of consolidation, this equilibrium may take many years; in these materials, unloading is the only practical method of groundwater control.

The theory has been approached in two ways: first, by looking at the pressure effect of unloading at shallow depths, and second, by looking at the entire unloading history of a large mine.

The shallow effects have been simulated by unloading a single 10 meter cut and checking the remaining head after 3 years at various depths. These results are shown on Figure 10. From this figure, it

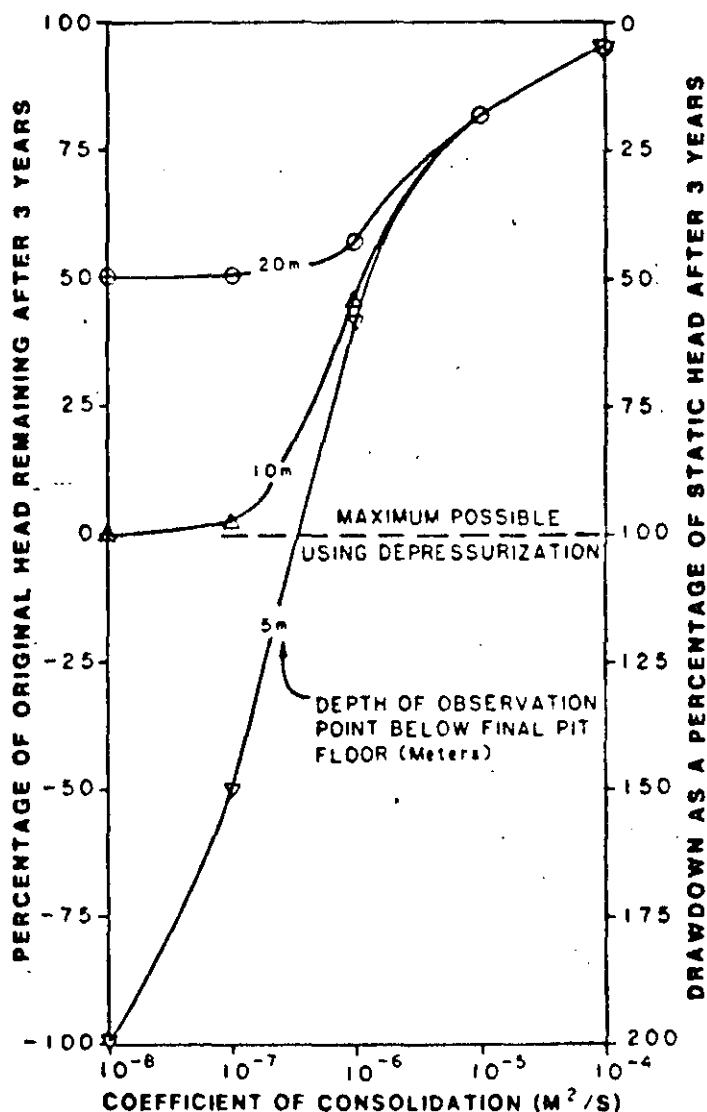


Fig. 10. Effectiveness of Unloading as a Strategy for Stabilization--Shallow Case Showing Effect of 10 Meter Cut After 3 Years.

can be seen that for coefficients of consolidation less than about  $10^{-6}$  meters squared per second, the surface of the mine would stay effectively depressurized.

The deep effects have been simulated by unloading a column of material sequentially as mining progresses, and evaluating the distance below the slope in which the groundwater pressure has been reduced below zero. This data is presented in Figure 11. As can be seen, it would appear that a mine in a material with a coefficient of consolidation less than about  $10^{-4}$  meters squared per second will develop useful unloading water pressure reduction in its life. It will, however, be necessary to accept considerably flatter angles for the slopes in the early part of the life of the mine.

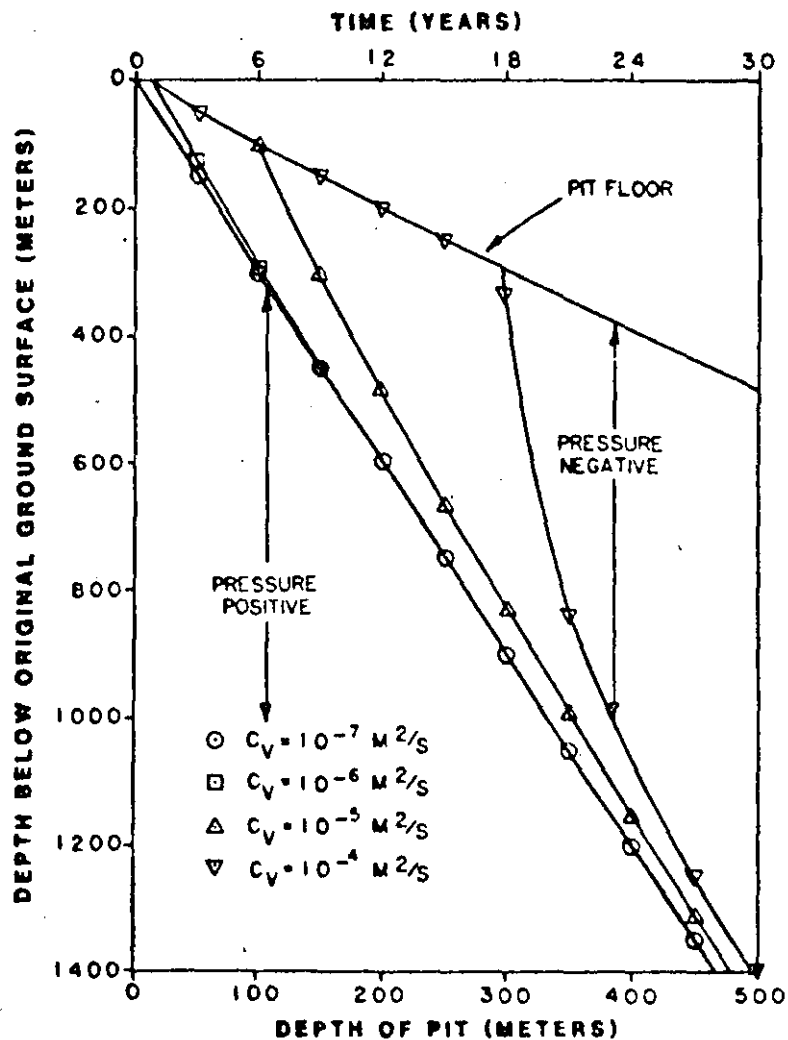


Fig. 11. Depth of Negative Pressure Zone as Pit Develops as a Function of  $C_V$ .

In summary, the unloading phenomenon can be described as follows:

<u><math>C_v</math> (m<sup>2</sup>/sec)</u>	<u>Unloading Effect</u>
More than $10^{-4}$	No useful depressurization
$10^{-4}$ to $10^{-6}$	Depressurization effect increases through life of mine
Less than $10^{-6}$	Depressurization effective even at early times

Practice. The phenomenon described above has actually been observed in a number of man-made cuts, most notably the Panama Canal (Banks, 1972) and railway cuttings in London Clay (Skempton, 1977). In this latter material, the coefficient of consolidation would appear to be in the order of  $10^{-8}$  meters squared per second, based on its liquid limit. The author is not aware of any mine where there has been a positive identification of pore water pressure being depressed by this method; however, it is suspected that a considerable number of mines are presently stable for this reason.

Clearly, the deep geology is of critical importance. There must be no major conduits into the mine area from depth to allow rapid pore pressure equilibration.

Operational Aspects. If mining is to take place in materials which exhibit this phenomenon, then the mining method should be modified to maximize the effect. Specifically, each part of the mine should be excavated at least annually, so that material is removed from over the entire mine area. Permanent slopes should be avoided until the end of the project. Upon cessation of operations, the pit would gradually begin to fail, with the failures continuing slowly until pore water pressure equilibrium was established. In the case of London Clay and the Panama Canal cuts, this process has taken more than 50 years.

#### Summary of Groundwater Pressure Control Options

Table 1 identifies the primary results of the above evaluation. The ranges of values of coefficient of consolidation for which each of the strategies outlined is valid are shown on Figure 12. In addition, an approximate material characterization has been presented to guide users in material types which might be expected to exhibit the nominated coefficients of consolidation.

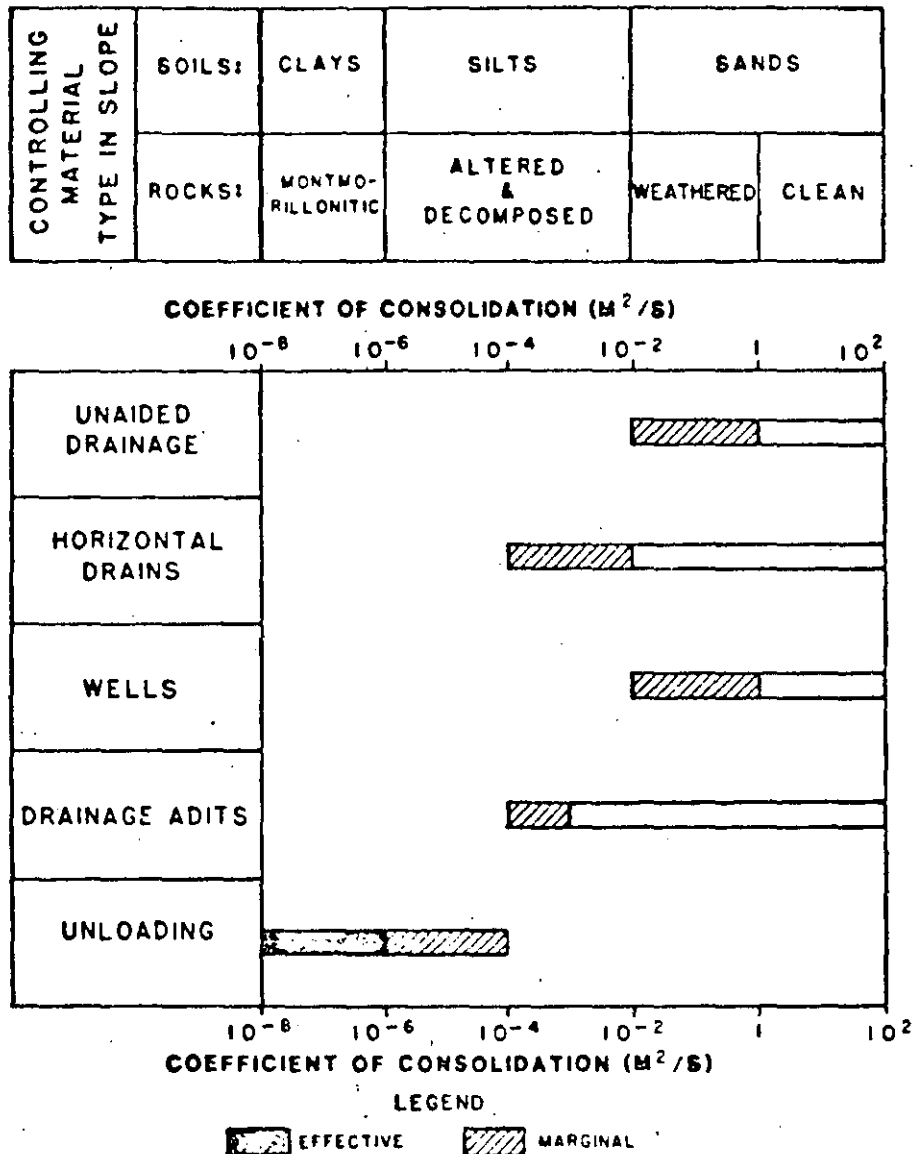


Fig. 12. Summary of Groundwater Pressure Control Strategies for Large Mine Slopes.

Several aspects become immediately obvious.

- o Materials exhibiting an effective coefficient of consolidation in excess of 1 meter squared per second can be readily depressurized. Flow control is more of an issue than pressure control in these materials.
- o Materials exhibiting an effective coefficient of consolidation of between 1 meter squared per second and 10<sup>-3</sup> meters squared per second can be depressurized using combinations of horizontal drains and wells, or by adits.

- o Materials exhibiting an effective coefficient of consolidation below  $10^{-6}$  meters squared per second will generally depressurize themselves if mining is designed to take advantage of the unloading phenomenon.
- o Materials exhibiting an effective coefficient of consolidation of between  $10^{-3}$  meters squared per second and  $10^{-6}$  meters squared per second are virtually impossible to economically depressurize. These materials include fine silts and highly altered rocks. Electro-osmosis may be the only available method, and this is prohibitively expensive on a large pit scale.

### CONCLUSIONS

This paper has sought to identify the benefits to be gained by groundwater control in large open pit mines, and the ways in which these benefits can be obtained in commonly encountered mining materials. The conclusions are as follows:

- o Up to 20° increase in slope angle is available as a result of groundwater pressure removal.
- o The parameter which allows a determination of the feasibility of groundwater pressure removal is the coefficient of consolidation ( $c_v$ ).

$$c_v = \frac{T}{S} = \frac{k}{S_s}$$

- o Materials with a  $c_v$  in excess of 1 meter squared per second can be readily depressurized using unaided drainage, horizontal drains, wells, or adits. These materials include sands and clean fractured rock.
- o Materials with a  $c_v$  between  $10^{-3}$  and 1 meter squared per second can be depressurized with more difficulty, using an adit system or a combination of wells and horizontal drains. These materials include fine sands, silts, and weathered, gouge-filled rocks.
- o Materials with an effective  $c_v$  lower than  $10^{-6}$  meters squared per second will depressurize themselves due to the effects of unloading. These materials include massive clays and montmorillonitic rocks.
- o Materials with a  $c_v$  between  $10^{-6}$  and  $10^{-3}$  meters squared per second are exceedingly difficult to depressurize economically on a mining scale. These materials include fine silts and highly altered or decomposed rocks.

## REFERENCES

- Banks, D.C., 1972, "Study of Clay Shale Slopes," 13th Symposium on Rock Mechanics, University of Illinois.
- Hoek, E., and Bray, J.W., 1977, Rock Slope Engineering, Revised Second Edition, Institution of Mining and Metallurgy, London.
- Morgenstern, N.R., 1971, "The Influence of Groundwater on Stability," Stability in Open Pit Mining, C.O. Brawner and V. Milligan, (eds), Society of Mining Engineers, New York.
- Skempton, A.W., 1977, "Slope Stability of Cuttings in Brown London Clay," Special Lecture, Proceedings Ninth International Conference on Soil Mechanics and Foundation Engineering, Tokyo, pp. 261-270.
- Theis, C.V., 1935, "The Relation Between the Lowering of the Piezometric Surface and the Rate and Duration of Discharge of a Well Using Groundwater Storage," Trans. Amer. Geophysical Union, Vol. 16, pp. 519-524.
- Terzaghi, K., and Peck, R.B., 1967, Soil Mechanics in Engineering Practice, Wiley, New York.



**DIVISION DE EDUCACION CONTINUA  
FACULTAD DE INGENIERIA U.N.A.M.**

MECANICA DE ROCAS APLICADA A LA MIENRIA Y A LA CONSTURCCION

WATER CONTROL IN TUNNELING USING GROUND FREEZING

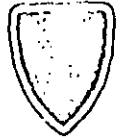
B. Braun and Wm. R. Nash

MAYO, 1985



*L. L. Maycotte*

PREPRINT 82-017



1

# WATER CONTROL IN TUNNELING USING GROUND FREEZING

B. Braun and Wm. R. Nash

ASCE

Las Vegas, Nevada

April 26-30, 1982

\$2.00



Bernd Araun<sup>1</sup>  
Member  
ASCE

William R. Nash<sup>2</sup>  
Member  
ASCE

Ground Freezing for Support of Tunnel Excavations

Many construction projects in urban areas require extensive subsurface work with minimal or no disturbance of the surface. Frequently, ground support and groundwater control within the excavation are major problems for completion of the subsurface work. Typical construction methods implemented for tunnels in soft waterbearing soils are: conventional mining and lining techniques, New Austrian Tunneling Method (shotcrete), pipe jacking, and various types of shields ranging from manual excavation to mechanized shields for full-face tunneling. With these excavation methods, groundwater is usually controlled by one of the following: Wellpoints or deep wells, slurry walls, sheet pile, compressed air or slurry for the full-face tunnel shields.

For almost a century, freezing has been used successfully as an art to stabilize ground and control groundwater. First employed by the mining industry in Europe, it has since been widely adopted throughout the world to (1) stabilize all types of excavations including shafts up to 915 m (3,000') in depth, (2) control groundwater, and (3) underpin structures. Recent improvements in the sciences of frozen ground engineering and refrigeration technology have opened up many new economical applications for freezing in construction and mining industries. Therefore, in the last decade ground freezing has become a viable and competitive construction alternative for providing temporary ground support and groundwater control for tunnel excavations in difficult soil conditions.

A wide variety of ground freezing projects in the United States have been inspected and accepted by OSHA, MSHA, EPA, and numerous other Federal, State and local agencies.

Principle and Advantages of Ground Freezing

The principle behind ground freezing is the use of refrigeration to convert in-situ pore-water to ice. The ice becomes a bonding agent, fusing together adjacent particles of soil or blocks of rock to increase their combined strength and make them impervious. The heat removal is accomplished through the use of a coolant, usually calcium chloride brine, circulating through refrigeration pipes embedded in the zone of soil to be frozen. Excavation and other required work can then proceed safely either within or adjacent to the barrier of strong, watertight frozen earth.

1. Special Projects & Operations Manager, Deilmann-Daniel GmbH  
Postfach 130220, Hamsterbeck 1, 4600 Dortmund 13, West Germany
2. Chief Mining Engineer, Frontier-Scoper Constructors  
P. O. Box 6548, Evansville, Indiana 47712

This preprint has been provided for the purpose of convenient distribution of information at the convention. To defray, in part, the cost of printing, a convention price of \$2.00 to all registrants has been established. The post-convention price, when ordered from ASCE headquarters will be \$2.00 while the supply lasts. For bulk orders (of not less than 200 copies of one preprint) please write for prices.

No acceptance or endorsement by the American Society of Civil Engineers is implied; the Society is not responsible for any statement made or opinion expressed in its publications.

Reprints may be made on condition that the full title, name of author, and date of preprinting by the Society are given.

Cover photo: View of Hoover Dam as seen looking upstream from Lookout Point, August 1934.

Frozen ground is normally employed to provide one or more temporary functions such as temporary support for an excavation, structural underpinning and/or groundwater control.

Ground freezing is adaptable to practically any size, shape or depth of either an excavation or a structure. Freezing can be implemented utilizing specialized portable plants regardless of the particular geometric site conditions.

The mechanical properties of ice, the critical ingredient, are much more dependent on time and temperature than on the geology of the strata. Therefore, ground freezing is less sensitive to advance geologic prediction than other alternative construction methods. Freezing may be used in any moist soil or rock formation, regardless of its structure, grain size or permeability.

Ground freezing creates no smoke, vibration, shock or undue noise; hence, it is well suited for use in areas where these environmental considerations are important.

The freezing process does not affect the existing water table or water quality. When the refrigeration of the soil or rock is discontinued, the ground thaws and the ice wall removes itself. Usually, the earth then returns to its original condition with no detriment to the soil, rock or groundwater regime of the site.

Because the frozen earth itself is the principal structural element in ground freezing, no bracing or sheeting is normally required. The excavation area can be kept unobstructed, and both the excavation and the installation of the final structure can be easily mechanized which is extremely important on tunneling projects.

It can be stated that freezing is well suited where minimal disturbance of the ground and groundwater during and after construction are important. It is due to these factors that ground freezing has seen increased application on difficult tunnel projects throughout the world.

#### Limitations of Ground Freezing

Despite its broad versatility, ground freezing does have limitations (as well as lesser considerations) which may limit its attractiveness for application to a tunneling project.

The soil must have sufficient moisture to allow stabilization by freezing. The complete saturation of the soil is not required, but a 10% saturation can be considered as a lower limit. To increase the moisture content, it is possible to entrain water into the soils prior to freezing to permit stabilization by the freezing method.

Extreme care must be exercised when freezing is attempted in ground where lateral groundwater flows are expected. If the energy carried away by the flowing water exceeds the energy input from the refrigeration plant, it is impossible to install a watertight frozen earth wall. Freezing, therefore, should not be used where lateral groundwater flows are expected to exceed 1.8 meters per day (6 lpd) unless special provisions are made to handle the excess heat and/or reduce the groundwater flow in the formation.

Measures to handle the excess heat are:

Reduction of refrigeration pipe spacing;

- Installation of several rows of refrigeration pipes;
- Installation of low-temperature refrigeration equipment;
- Use of expendable refrigerants such as liquid carbon dioxide or liquid nitrogen for ultra-low temperatures.

Measures to reduce the flow in pervious soils are:

- Grouting;
- Interception of a portion of the flow with wells to reduce the hydraulic gradient.

Depending on the groundwater regime and in situ confining pressures, the freezing process may cause ground movements to occur in some soils. Potential ground movements associated with ground freezing can be caused by three phenomena:

- Basic frost expansion due to conversion of the existing pore water to ice during phase change;
- Secondary frost expansion due to pore water migration and ice segregation with time at the freezing isotherm or in the frozen zone;
- Consolidation during the thawing period.

The first phenomenon is small and predictable. The other two phenomena are much more complicated and more difficult to predict. However, laboratory tests and analytic procedures exist to evaluate the potential for secondary frost expansion and/or thaw consolidation for any given soil.

#### Design Methodology

A thorough knowledge of the mechanics of the freezing process and the effects of the freezing on the soil are required to:

- Evaluate the feasibility of a ground freezing application for tunneling.
- Design a frozen earth system.

In contrast to most other alternatives which are constructed in a specific manner, there are several alternative ground freezing methods and basic philosophies of approach which may be employed on any given project. It is due to this versatility that a somewhat more involved design procedure is necessary to determine the technical feasibility of freezing for a given application, as well as the specific method, materials and equipment. In general, the design phase consists of six distinct steps which must be completed for every project.

They are:

1. Develop Design Criteria - applied loads and material properties for the soil, rock, water and structural surcharge, if any, at the site.
2. Determine technical feasibility of freezing based on design criteria, site and project constraints, and known characteristics of the freezing method.
3. Complete structural analysis of the frozen earth mass to determine the geometry required for overall stability and related internal stresses. For nonstructural cutoff wall applications this step unnecessary.
4. Thermal analysis to determine refrigeration method to be employed as well as the amount and duration of refrigeration necessary to

form and maintain the desired frozen earth mass.

5. Select specific construction approach and equipment to install the required freezing system.
6. Estimate the cost of the work as designed.

Each of the design steps mentioned above could be the subject of an extensive technical paper. Though a thorough treatment of these steps is beyond the scope of this paper, some comments are appropriate.

The subsurface site exploration should consist of a sufficient number of borings to adequately define the site stratigraphy and to collect representative samples of the soil types. It is important that the borings locate permeable zones in which high groundwater flow rates might occur.

The laboratory tests to be performed on the collected soil samples should consist of index property tests, such as gradation analyses, Atterberg limits, moisture contents and saturation. After defining these index data, more frequently than not, it is possible to refer to data obtained from previous projects to estimate the strength-deformation behavior of the frozen soils. However, for final design on critical and complicated projects, it is recommended to perform laboratory tests on the soils in the identical frozen states to that which the soil will experience in the field. The load deformation behavior of the frozen soil is determined by unconfined compression or triaxial creep tests.

If soft silts and clays are frozen, the potential for frost heave and thaw consolidation must be investigated by laboratory testing and geotechnical analysis for the particular application, e.g., underpinning of a building foundation.

Qualified test facilities which have performed such tests are located throughout the world (United States, Canada, Europe, Japan and Russia). Once the basic data have been obtained, a qualified engineer is able to rationally design a frozen earth system for a tunnel. Due to the complex ground structure interaction of frozen soil support systems for tunnels, the finite element method is now often used for structural analysis.

Both the shape and the required temperature of a frozen support system for a tunnel are characterized by the following criteria:

- The function of the freeze wall, i.e., structural support and/or water cutoff;
- The time freeze wall is exposed to load, i.e., the time from initial excavation of the tunnel until either a structural preliminary or final lining is installed;
- The mechanical behavior of the freeze wall, especially the deformation of the freeze wall under various stress levels versus time (creep);
- The mechanical behavior of the unfrozen soil surrounding the tunnel;
- The hydrological conditions as well as the soil and/or rock strata immediately above, within and below the tunnel;

- The geometry of the tunnel;
- The depth of overburden to tunnel crown;
- The surface constraints immediately above the tunnel.

Refrigeration pipes must be installed for the circulation of coolant in order to construct an "ice wall." The refrigeration pipes can be placed: 1) from the surface (Fig. 1), 2) from within small diameter construction galleries (Fig. 2), or 3) horizontally from within cofferdams or from within the tunnel itself (Fig. 3).

To better demonstrate how versatile ground freezing can be used as a support and/or ground water control system, a few case histories are described.

#### Railway Tunnel - Salerno, Italy

Construction of a 10.3 km (6.4 miles) two-track railway tunnel required the crossing under part of the city of Salerno. In this tunnel section the overburden, varying from 8 to 25 m (25' to 76'), consisted of sandy to clayey silt, alluvial sands and soft powdery dolomite. Tunneling in the dolomite would have posed no problems as long as the water could be isolated from this strata. However, the unavoidable stress relief during excavation resulted in fissures in the dolomite with water seeping through, turning this layer shortly into a "quick soil." The potential cave-ins could have caused settlements and a threat to the buildings above the tunnel.

The tunnel with a cross section of 85 m<sup>2</sup> (914 SF) was driven with conventional drilling and blasting techniques using steel beams and shotcrete as a preliminary lining followed by a final lining of reinforced concrete. To permit safe tunneling under this heavily-populated area, a specialized construction technique had to be used to meet the following requirements:

- Method should provide complete groundwater control;
- Method should provide structural support with no settlements until such time that a preliminary is installed;
- Excavation of tunnel should be kept free of obstructions;
- Tunneling to be continued with equipment already in use on site;

After a careful examination of a variety of solutions, the ground freezing method was chosen to be the safest and most economical system. The proposed solution was an umbrella or arch of frozen earth over the tunnel reaching approximately 1m (3.3') below the invert excavation to provide both a water cutoff and a structural support (Fig. 4).

Triaxial frozen soil tests were performed in a laboratory to verify that the anticipated stresses to be encountered would not result in creep of the frozen soil.

All of the refrigeration pipes were installed from the surface. The arrangement of the refrigeration pipes resulted in freezing more soil than structurally required, but this was cheaper than insulating them in the upper part. Four rows of refrigeration pipes were installed to form the structural freeze wall (Fig. 5). In order to keep the refrigeration load as a minimum, the total tunnel length of 71m (233') to be frozen was divided into three sections. Each section was separated from the adjoining by frozen bulkheads.

Two refrigeration plants with a capacity of  $1.01 \times 10^6$  kJ/h (80 TR) each at  $-25^\circ\text{C}$  ( $-13^\circ\text{F}$ ) brine temperature were installed. After a freezing time of approximately four weeks, rapid tunneling proceeded under the protection of the frozen earth wall and neither forepoling nor breasting was necessary.

A top heading and benching method was used with a preliminary lining for crown support. Immediately following the top heading excavation, the preliminary lining of arch rib segments, wire mesh and shotcrete were installed. The final lining of reinforced concrete followed as soon as possible. It was placed in 4.0m (13.1') sections. In a time period of less than three months, tunneling with an excavation exceeding  $6,000\text{m}^3$  (7,800 CY) was completed without any difficulties.

Settlement monuments above the tunnel showed no ground movements during the freezing and the subsequent thawing.

#### Subway Tunnel Essen, Section 17b - West Germany

Contract Section 17-b required the construction of 302m (990') of a twin-track subway tunnel with an excavation of  $62\text{m}^2$  (667 SF) in mixed-face conditions in downtown Essen. The cover over the tunnel crown consisting of unconsolidated silty soils varied from 5.7m to 9.5m (19' to 31'). The average groundwater level was 2.5m (8.2') above the tunnel crown.

The owner specified the driving of the first 180m (590') under the protection of a freeze wall for groundwater control and for the stabilization of the sensitive silty layers. The refrigeration pipes were to be installed in stages from within the tunnel (cavern or drill chamber method).

Because of the building density, buried utility lines and the intensive traffic, only underground construction methods could be tendered.

A joint venture was awarded the contract with an engineering value design for the ground freezing work. The planning called for the drilling of the refrigeration holes and execution of all freezing work from auxiliary construction galleries running parallel to and above the main tunnel (Fig. 6). The advantages were as follows:

- Ground freezing (as an auxiliary construction method) is completely separated from all work in the main tunnel;
- Driving of the tunnel could be done continuously without interruptions;
- Length of the refrigeration pipes placed from the galleries and to be tied 0.5m (1.6') into competent rock could easily be adjusted to the irregular surface of the bedrock;

Ground freezing process could be easily controlled. To minimize frost heaves in the silt layers, the freeze wall thickness was limited to 1.0m (3.3');

- Dewatering of the tunnel excavation could be done with filter wells placed from the gallery;
- Earlier completion date of the main tunnel.

An access shaft was sunk and the galleries were driven using the pipe-jacking method (Fig. 6). The galleries had an internal diameter of 1.96m (6.4') to allow drilling of the refrigeration holes. The refrigeration pipes were placed on 0.90m (3') centers. To check the frost penetration and to verify the required freeze wall thickness, several temperature monitoring pipes were installed in the ground.

Based on a weekly tunnel advance rate of 13.5m (44') two refrigeration plants with a total capacity of  $1.4 \times 10^6$  kJ/h (110TR) at a brine temperature of  $-20^\circ\text{C}$  ( $-4^\circ\text{F}$ ) were installed.

During tunneling the freeze wall was kept 30m (98.4') ahead of the tunnel face. Refrigeration pipes were connected to the brine system according to the actual achieved tunnel progress considering that 2.5 weeks were required to build the freeze wall. Once the freeze wall had its required thickness, heat removal was reduced by intermittent running of the brine in the refrigeration pipes.

Benching was used to drive the tunnel using a double-drum roadheader. A preliminary lining, designed for the full static load and extending into the bedrock, immediately followed the excavation. It consisted of:

- Steel ribs on 1.0m (3.3') centers (spacing was later increased to 1.6m (5.25') because of the stiffness of the freeze wall);
- 0.05m (2") shotcrete layer with wire mesh as seal to avoid thawing of the freeze wall;
- 0.27m (10-1/2") structural shotcrete layer with a double wire mesh.

Freezing was discontinued as soon as the preliminary lining was installed.

Surface surveys did not indicate frost heave. Ground subsidences of up to 60mm (2.4") were measured as a result of the pipe-jacking, as well as the subsequent tunnel driving.

#### Anacostia Sewer Tunnel - Washington, D. C.

A sewer line under a railroad crossing required the construction of a circular tunnel with a diameter of 3.66m (12') and 34.5 (113') in length, passing 2.7m (8.9') beneath four sets of railroad tracks. The subsurface conditions consisted of fill with cinders, interbedded sands, silts and clays underlain by coarse-to-fine sand and gravel, and an organic silt layer. The water table was 1.0m (3.3') below the ground surface.

After thorough investigations by the Engineers, considering the potential difficulties to be experienced when driving a tunnel under highly-trafficked railroad tracks, ground freezing was specified as the support and groundwater control system.

A frozen earth ring was required to completely surround the excavation to provide a watertight support system as the tunnel had to be driven under the water table. According to the specifications, the live load for the design was required to be a full Cooper E-80 trainload on any two adjacent tracks. Furthermore, design of the frozen earth ring had to be based on the ultimate strength of the frozen soil for a loading duration of 1,000 hours.

Laboratory tests of the frozen and unfrozen soil, including cyclic loading tests, were performed to determine the mechanical properties of the soil for this particular design. The long-term frozen strength and stress-strain data determined from these tests were used as input data to a finite element program to determine the probable stress levels to be anticipated in the frozen earth mass.

The structural design was done with a three-dimensional finite element analysis using both the linear elastic stress-strain moduli from the laboratory tests to model the behavior of the frozen soil and the ICES STAPOL II program. With a 1.0m (3.3') frozen earth ring, the maximum calculated shearing stress in the frozen zone was 377 kN/m<sup>2</sup> (54 psi) with principal stresses of 708 kN/m<sup>2</sup> (100 psi) and 33 kN/m<sup>2</sup> (4.7 psi) both in compression. The maximum tensile principal stress was 262 kN/m<sup>2</sup> (37 psi), occurring at the crown. The maximum calculated deflection was 17mm (.70").

As the surface was not accessible, refrigeration pipes had to be installed more or less horizontally, parallel to the tunnel bore from the shafts to be sunk on either side of the railroad embankment. The placing of refrigeration pipes parallel to the tunnel axis is the most efficient way to provide a frozen earth support system for tunnel, because the pipes can be placed around any shape of tunnel and the amount of frozen soil can easily be limited to that required for the structural freeze wall. However, this method is limited by the accuracy one can drill horizontal holes. With today's available technology and equipment, holes can be reliably and accurately drilled over a distance of 20m to 50m (65' to 164') depending on the soil conditions. However, methods are being developed worldwide to install horizontal pipes more accurately.

To create the structurally required frozen ring of 1.0m (3.3') thickness, it was intended to install 19 refrigeration pipes equally spaced around a 5.50m (18') diameter circle. A groundmat, an air-actuated, in-the-hole displacement hammer with a special cone and chisel was chosen to install the refrigeration pipes. Due to the difficult ground conditions, this method could not effectively be used and the refrigeration pipes had to be driven with a pile hammer from both access shafts. Deviations of the pipes were checked with a special deflectometer. To account for the unavoidable end of pipe deviations, the refrigeration pipes were overlapped at least 3.0m (9.8'). Nevertheless, several additional pipes had to be installed to satisfy the maximum spacing of the specifications.

A refrigeration plant with a capacity of  $1.4 \times 10^6$  kJ/h (110 TR) at -20°C (-4°F) brine temperature performed the freezing. Temperature sensors were installed in the ground at various locations to verify the extent of the freeze wall and to monitor the required design temperature.

Excavation was done with a backhoe and jackhammers to trim to neat line. Subsequently, when the entire excavation area was frozen solid, a backhoe with an impact hammer attachment was used to excavate the frozen soil. This was not the most expedient excavation method, but blasting was not permitted and a roadheader, which could have easily cut the frozen soil, was not available. The tunnel was lined with liner plates which were grouted in place immediately following the excavation.

This was not the first time horizontal freezing had been used in the

United States, but it was the first time for its implementation under railroad tracks. This method was used in Charleston, South Carolina for constructing a 2.44m (8') diameter tunnel under an Interstate. Meanwhile, this support method has been applied for another railroad crossing in Syracuse, New York, and for a tunnel in Louisville, Kentucky.

#### Milchbuck Tunnel - Zurich, Switzerland

The three-lane Milchbuck Tunnel is part of a new expressway system in the city of Zurich. This tunnel, crossing under a heavily built-up area, sometimes with a minimum cover of 6m (19.7') is 1,310m (4,297') long with an excavation area of 145m<sup>2</sup> (1,560 SF). At its southern end, the tunnel had to pass through a 350m (1,148') long moraine section, consisting mainly of silty material. Inclusions of extensive, sandy, gravelly lenses under artesian pressure as well as large boulders represented major difficulties to tunnel driving.

The ground freezing method was specified by the Engineers as the support and groundwater control system to be used during tunneling, not only because of economic reasons, but because of the following technical reasons:

- . The method is not sensitive to rapidly changing soil conditions.
- . The freeze wall would provide two functions--structural support and watertightness.
- . The settlements on the surface could be kept low because of the rigidity of the freeze wall.
- . Special underpinning of the buildings above or the vicinity of the tunnel was not necessary.
- . Minimal surface disturbance of the heavily built-up area.
- . Shortening of overall time schedule.

In order to provide the structural support during tunneling, an arch had to be frozen around the tunnel. The shape of the frozen arch depended on several factors such as geology, overburden pressure, and the location of buildings above the tunnel. In most areas along the tunnel, the frozen arch was carried to springline.

Extensive laboratory testing was performed to obtain the design parameters for the freeze wall. The finite element analyses showed that a frozen arch of 1.50m (4.9') thickness was sufficient with a mean temperature of -10°C (14°F) of the frozen wall.

The heaving tests revealed that dewatering would considerably reduce the potential heave on the surface and thus facilitate tunnel driving. Therefore, small diameter filter wells were installed on both sides of the tunnel. Furthermore, pressure-relief holes were installed from the tunnel itself 30m to 50m (98' to 164') ahead of the tunnel face.

All freezing and related work had to be executed from within the tunnel. Therefore, the 360m (1,181') section to be frozen was separated into eleven sections of 30m to 50m (111' to 164') lengths. The pipes were placed on a slightly upward batter in order to enlarge the excavation from 145m<sup>2</sup> (1,560 SF) up to 195m<sup>2</sup> (2,098 SF) over a length of approximately 6m (20') to allow drilling of the refrigeration holes.

for the 2nd section. The frozen arch always extended some 4m to 6m (13' to 19') beyond the end of each excavation section (Fig. 7).

The time the frozen arch had to carry the load was minimized to avoid creep of the frozen soil. Therefore, the preliminary lining consisted of 0.40m (1.3') of shotcrete with wire mesh and rib steel immediately following the excavation.

A benching method and a roadheader were used for the tunnel excavation. Both the walls and the invert excavation and concrete lining followed at a distance of 6m to 8m (20' to 26') behind the tunnel face in order to complete the preliminary lining as a structural support. Subsequently, the waterproofing and the inner final reinforced concrete lining were installed (Fig. 8).

An extensive instrumentation program was developed to monitor ground temperatures and ground movements:

- . Heave markers at approximately 300 stations;
- . Inclinometers installed from the surface;
- . Extensometers installed from the surface and from within tunnel;
- . Convergence measurements at 10m to 15m (33' to 49') intervals;
- . Various temperature measurements within the frozen arch from temperature-monitoring pipes.

From the obtained field data, prior calculations could be checked and design parameters verified. More importantly, from the actual field experience gained, modifications in the freezing procedure or ground support measures could be made in the following excavation sections.

Good examples were the heaving and settlement readings which were critical on this project. Heaving rates of up to 105mm (4") were measured in the first section. This was attributable to the extended time (161 days) that the freezing had to be maintained, due to initial start-up difficulties in tunneling and to the extensive overfreezing as freeze wall thicknesses of up to 4.0m (13') were monitored. Such heave could not be tolerated in the third freezing section with seven-story buildings above the tunnel.

Additional measures were taken to reduce those rates:

1. By changing the design parameters.
2. Better controlling the size of the freeze wall through intermittent freezing during the maintenance period.
3. Improving the tunnel advance rate. Only 61 days total freezing time were required in the second section and the maximum heave was reduced to 32mm (1.25"). In the critical third section, the total freezing time was further reduced to 41 days and maximum heave of only 15mm (.60") was observed.

The field measurements revealed that the moraine material was sensitive to thaw consolidation. Subsidence up to 61mm (2.40") were monitored in the first two sections. In the critical areas (buildings) these settlements were successfully reduced to 21mm (0.82") by performing cement grouting during the thawing of the freeze wall.

On this project it was impressively demonstrated that ground freezing can be used under the most difficult of conditions. By adjusting to the in-situ monitored field conditions, the subsidence were kept to a minimum.

#### Cost

The general "rule of thumb" in estimating cost is that "there are no rules of thumb." With the number of parameters and variables involved with ground freezing, the estimation of cost becomes site specific.

Major factors affecting the cost of a ground freezing project are:

- . Tunnel length;
- . Functions of freeze wall (structural and/or groundwater control);
- . Accessibility for drilline;
- . Excavation and lining method.

The cost data for the case histories follows:

<u>Project</u>	<u>Approximate Total Cost (1982 Dollars)</u>
Railway Tunnel, Salerno, Italy	\$ 700,000
Subway Tunnel, Essen, West Germany	1,100,000
Anacostia Sewer Tunnel, Washington, DC	450,000
Milchbuck Tunnel, Zurich, Switzerland	2,750,000

#### Conclusions

Construction ground freezing is an extremely versatile subsurface construction technique used to provide temporary ground support, groundwater control and structural underpinning for tunneling. With the recent improvements in the sciences of frozen ground engineering and refrigeration technology, ground freezing has matured to the point where it can be rationally designed, estimated, and executed for a wide variety of projects, thus providing another powerful tool for the foundation engineer to cope with the challenging underground problems posed by many modern projects.

#### Acknowledgments

For one of the case histories, slides were provided by Electrowatt Engineering Services, Ltd., Zurich, Switzerland.

#### References

- "Proceedings 1st International Symposium on Ground Freezing," Ruhr University, Bochum, GFR, March 1978.
- "Proceedings 2nd International Symposium on Ground Freezing," Norwegian Institute of Technology, Trondheim, Norway, June 1980.
- "Milchbuck Tunnel," Publication No. 100 of the Swiss Society of Soil and Rock Mechanics, Zurich, 1979 (in German).

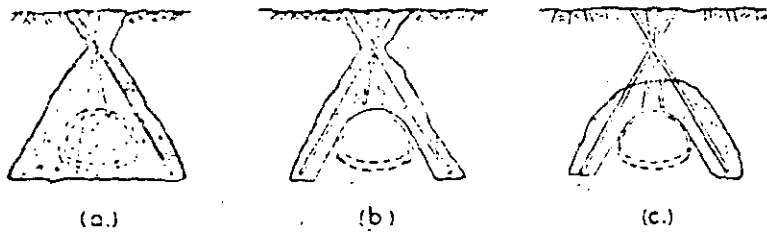


FIG. 1

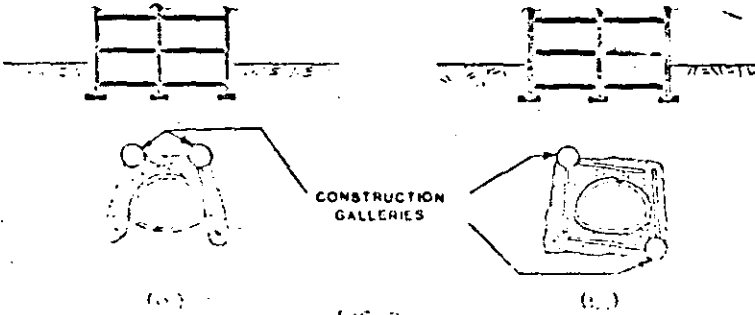


FIG. 2

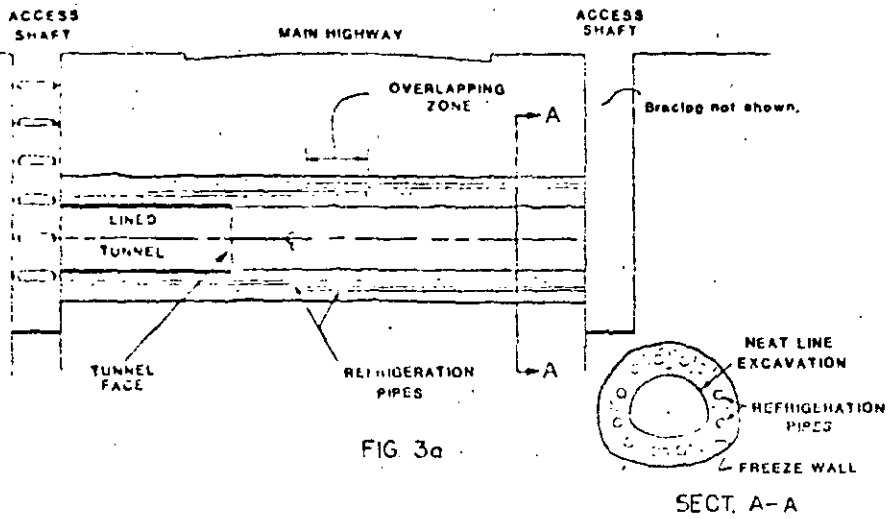


FIG. 3a

SECT. A-A

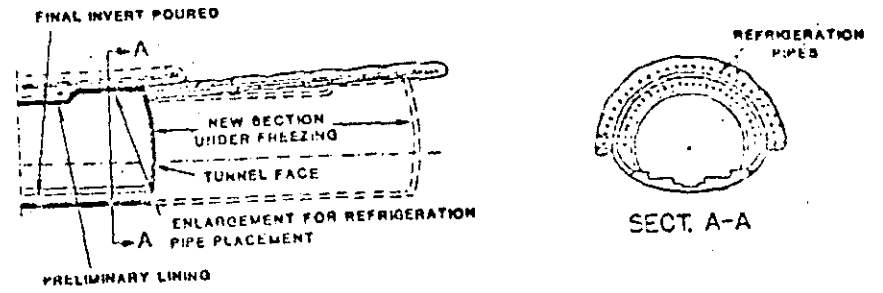


FIG. 3b

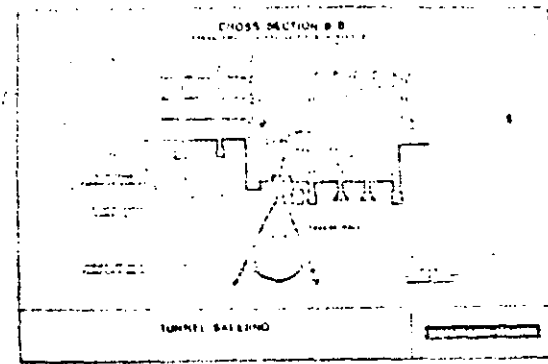


FIG. 4



FIG. 5



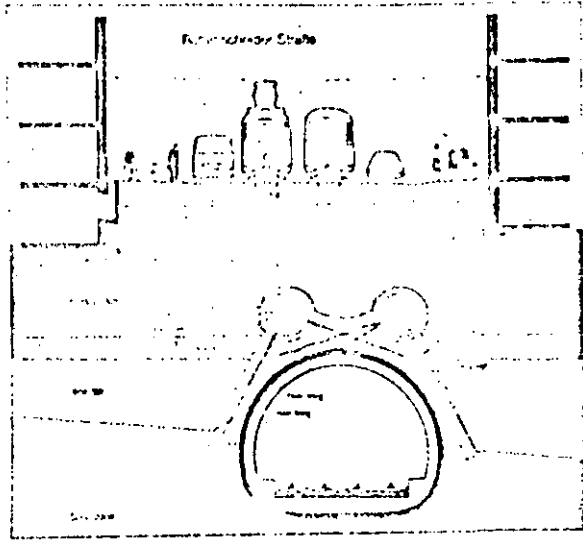


FIG. 6

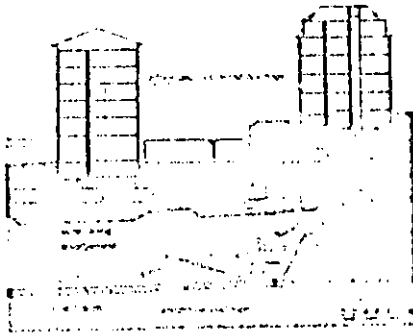


FIG. 7

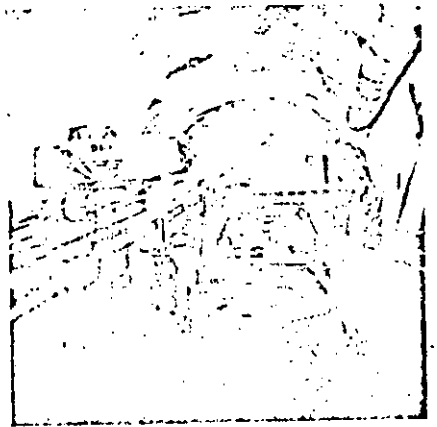


FIG. 8



**DIVISION DE EDUCACION CONTINUA  
FACULTAD DE INGENIERIA U.N.A.M.**

MECANICA DE ROCAS APLICADA A LA MINERIA Y A LA CONSTRUCCION

THE MEASUREMENT OF PORE PRESSURES WITH PIEZOMETERS

P. R. Vaughan

MAYO, 1985

FIELD INSTRUMENTATION  
IN GEOTECHNICAL ENGRNG.

SYMPOSIUM BY BRITISH  
GEOTECH. SOCIETY. - 1973

HALSTED PRESS BOOK  
JOHN WILEY & SONS

THE MEASUREMENT OF PORE PRESSURES WITH PIEZOMETERS

P.R. Vaughan

Lecturer in Civil Engineering, Imperial College, London

INTRODUCTION

The field measurement of pore pressures with piezometers has developed over some 40 years. Such measurements are used to check assumptions made in effective stress analyses and to monitor the effectiveness of drainage and de-watering works.

The pore fluid in soil may be water or a mixture of gas and water. A piezometer is a hollow filter element, embedded in the soil, sometimes within a sand pocket. The cavity within the filter is usually filled with water, the pressure of which is measured and presumed to be equal to the pore fluid pressure. A correct measurement involves equalization of the pore fluid pressure with the cavity pressure and the accurate measurement of the cavity pressure. In partly saturated soils equalization may be to either the water or the gas pressure.

Piezometers cannot be used to measure pore pressures below absolute zero, which may occur in partly saturated or unloaded saturated soils, as the free water in the cavity will not sustain tension. Indirect methods of measuring pore water tensions in partly saturated soils have been developed (Richards:1969a, Escario:1969). The author knows of no measurements of pore water tensions in saturated soils. Problems due to the formation of air bubbles in the piezometer cavity increase as the cavity pressure approaches absolute zero.

Pore pressure measurement with piezometers is considered in this paper in three sections: equalization between the cavity pressure and the pore pressure in saturated soils, equalization in partly saturated soils and measurement of the cavity pressure. Principles, sources of error and current uncertainties are reviewed. Equipment details are not discussed. Bishop *et al* (1969) reviewed recent practice and gave a more comprehensive bibliography than can be included here.

## EQUALIZATION IN SATURATED SOILS

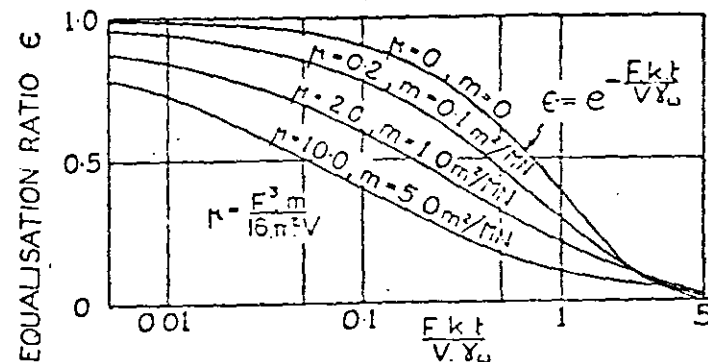
Richards (1969b) has pointed out that equalization may be inhibited by temporary osmotic effects in a fine grained soil. Bolt & Lagerwerffe (1965) examine these effects. They are usually ignored and the likely extent of errors in piezometer measurements due to them needs further study. Where they may be ignored, the pressure in the piezometer cavity will equalise to a steady uniform pore pressure by the processes of seepage and consolidation, provided that the installation of the piezometer does not influence this pore pressure. This requires that the connections to the piezometer do not form a preferential seepage path. Vaughan (1969) considered the influence on a steady pore pressure of a borehole backfilled with material of higher permeability than the surrounding soil and found that the backfill could be of the order of ten times more permeable than the soil before the influence on the pore pressure became significant.

Theory for the equalization of an out-of-balance cavity pressure with a steady pore pressure has been developed by Hvorslev (1951), for an incompressible soil, and by Gibson (1963) for a compressible elastic soil obeying the Terzaghi consolidation theory. Such theory may be used to estimate soil properties from the results of equalization tests or to estimate the time taken for sufficient equalization to enable a pore pressure measurement to be made. Gibson (1963) showed that the 'compressible' and the 'incompressible' theory give similar results at high degrees of equalization (which is illustrated in Fig.1) and at these high degrees of equalization a large error in estimated response time only implies a small error in pore pressure measurement. Thus the simple 'incompressible' theory is generally adequate for engineering purposes. It may be expressed as an equalization ratio,  $\epsilon$ , where

$$\epsilon = \frac{u_g - u_m}{u_g - u_{m0}} = \exp \left\{ - \frac{F \cdot k \cdot t}{V \cdot \gamma_w} \right\} \quad \dots (1)$$

where  $u_g$  is the pore pressure,  $u_m$  is the pressure in the cavity at time  $t$ ,  $u_{m0}$  is the initial pressure in the cavity  $F$  is the intake factor which depends on the size and geometry of the piezometer,  $k$  is the coeff. of permeability of the soil,  $V$  is the volume factor (or compressibility) of the piezometer system defined as the flow into the piezometer for unit pressure change in the cavity and  $\gamma_w$  is the unit weight of water.

The influence of the volume factor on response was examined by Penman (1960). Table 1 shows response times calculated from equation 1 for some typical piezometer installations. The influence of trapped air is significant if rapid response is required. A particular problem lies in ensuring that sand



Coefficient of volume compressibility,  $m$ , calculated assuming  $F = 180\text{cm}$ ,  $V = 1.76 \text{ cm}^3/\text{gm}$ .

Figure 1 Influence of soil compressibility on theoretical piezometer response (after Gibson : 1963)

pockets used with borehole piezometers are saturated. Response times are generally rapid enough for engineering purposes unless open stand pipes are used in clay soils.

There are four field situations in which piezometer response must be considered. These are :-

Measurement of a pore pressure varying due to drainage In these circumstances the pore pressure must be equalized locally and, provided the piezometer is small in relation to the pore pressure gradient, the theory previously described

Piezometer system	V cm <sup>3</sup> /gm	F cm	t hours
Borehole piezometer, sand pocket 60cm x 15cm dia. 1.5cm dia. standpipe	5	180	820
Ditto with 150cm 3mm bore nylon tube & 3mm Hg manometer	4	180	1.6
Ditto with electric transducer in the piezometer cavity	0.05	180	0.002
Ditto with transducer with 100 cm <sup>3</sup> air in the cavity	400	180	19
Fill piezometer 10cm x 4.5 cm dia, with 150cm nylon tubing & 3mm bore Hg manometer	35	40	7.3
Ditto with transducer in place of manometer	7	40	1.5

Coefficient of permeability of soil,  $k = 10^{-10} \text{ m/s}$

The cavity pressure behind the pore-pressure can be estimated by representing the changing pore pressure as a sequence of instantaneous changes and applying the principle of superposition. It should be noted that rate of change of the pore pressure and the response time of the piezometers are both controlled by the permeability and compressibility of the soil. Thus the lag depends only on the intake and volume factors of the piezometer. It can be shown that adequate measurements can be made even with a standpipe piezometer of slow response irrespective of the soil permeability, provided it is not close to a drainage boundary where rapid changes in pore pressure can occur. With piezometers installed in boreholes, remoulding and smear adjacent to the borehole may reduce the permeability locally. The response of the piezometer will then become slower in relation to the rate of change of pore pressure.

Pore pressure changes due to undrained loading The rate of such pore pressure changes is not controlled by the soil properties and they may be rapid. The deformability of the piezometer will be different from that of the surrounding soil and thus the total pressure and pore pressure changes near the piezometer will be atypical. The equalization of the cavity pressure to the true pore pressure will depend on the rate at which this perturbed pore pressure zone equalizes, as well as on the response time of the piezometer as defined in equation 1. No theoretical study of this problem is known to the author but it is probable that the changes in average total stress will be small compared to the changes in principal stresses. Therefore the perturbations of the pore pressure distribution are likely to be smaller than the perturbations of total stress which, for instance, cause difficulties when earth pressure cells are used.

Soderberg (1962) examined the equalization of a zone of perturbed pore pressure around an expanded, impermeable cylinder, using the Terzaghi-Rendulic consolidation theory. This is approximately equivalent to equalization of a perturbed pore pressure zone around a long cylindrical piezometer of zero volume factor. Depending on the amount of plastic yield of the soil, Soderberg found that 80% equalization at the cylinder surface ( $\epsilon=0.2$ ) occurred at a time equal to approximately  $10 \cdot r^2/c$  and 95% equalization at  $30 \cdot r^2/c$ .  $r$  is the radius of the cylinder and  $c$  the coefficient of consolidation. These figures should be conservative for typical piezometers of finite length, as three dimensional effects will accelerate equalization. Comparison of the above figures with equation 1 indicates that equalization of a typical standpipe piezometer will be, at a similar or slightly slower rate than equalization of the perturbed pore pressure zone. For all other types of piezometer equalization of the perturbed pore pressure zone will be much slower than response according to equation 1.

Equalisation of the perturbed pore pressure will be accelerated if the piezometer (or its sand pocket) is made as small as possible. Installation in a small diameter borehole may be facilitated if the tip is placed in a porous grout such as plaster of paris, which ensures an intimate contact with the soil and the exclusion of air. A rigid probe piezometer may be especially prone to error during rapid loading, as stress changes may be concentrated at the end of the probe where the pore pressure is measured.

Apparent undrained pore pressure changes observed after loading ceases may indicate the magnitude of lag during loading, although they may be due also to creep in the soil. A study of such changes, as recorded by piezometers subject to typical engineering rates of loading, suggests that errors due to non-equalization during loading are not of great significance. However, if measurements are made where loading is more rapid such as near driven piles, greater errors may result and further study of the problem would be desirable.

Initial equalization around a borehole piezometer This problem is similar to that described in the previous section. The perturbed pore pressure zone is due to the drilling of the borehole. The stress and pore pressure changes will be large and the pore pressures will be reduced. If the piezometer responds more rapidly than the zone of perturbed pore pressure can equalize and if the cavity pressure is initially higher than the pore pressure around the borehole (as may occur due to grout pressures or due to initial filling of a standpipe), the piezometer may appear to equalize to a pressure lower than the true pore pressure. This is illustrated in figure 2, in which the initial equalization of a rapidly responding pneumatic piezometer is shown. The equalization of an adjacent standpipe piezometer is shown for comparison. The slower overall equalization suggests that the response time of the piezometer is more important than the equalization of the perturbed pore pressure zone. Pore pressures around a driven piezometer will be increased and the process described above will be reversed. The overall rate of equalization can be accelerated by reducing the diameter of the borehole.

Equalization after in-situ tests or 'de-airing' Piezometers with hydraulic connecting tubes may be used for falling and constant pressure seepage tests, for hydraulic fracture tests to estimate the minor principal stress (Vaughan : 1972) and they may be de-aired by circulating water under a differential pressure. All these operations create a zone of perturbed pore pressure around the piezometer, the size of which is dependant on the time the disturbing pressure has been applied, or, in the case of hydraulic fracture tests, on the volume of water forced into the soil. The equalization of the perturbed pore pressure zone may control the overall equalization of the piezometer, as described previously. The equalization of a

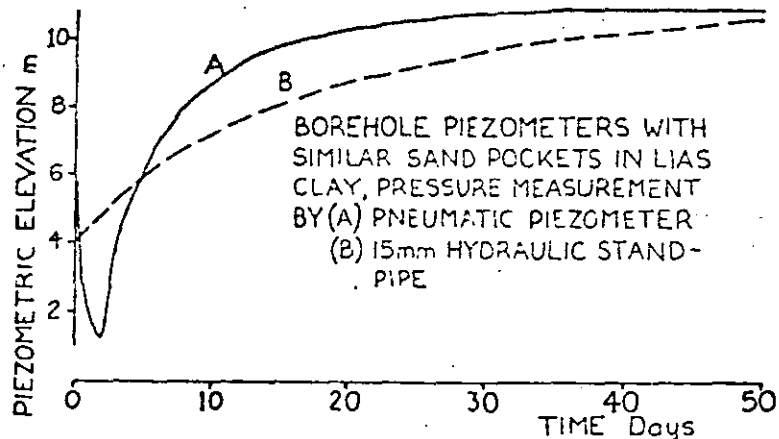
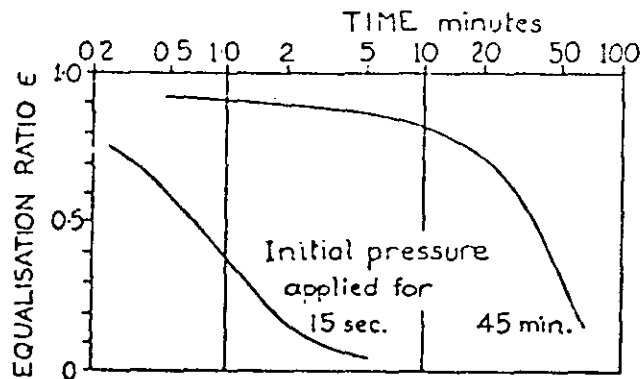


Figure 2 Initial equalization of borehole piezometers of varying response times (data from R.J Chandler)

piezometer to which an excess pore pressure has been applied for varying periods of time is shown in Figure 3. In the experience of the author, equalization after a hydraulic fracture test is comparable to that after a constant pressure seepage test (Vaughan : 1972).

#### EQUALIZATION IN PARTLY SATURATED SOILS

In partly saturated soils (fills, soils above the water table and soils in which gas is generated from organic matter) the pressure in the piezometer cavity may equalize to either the water or the gas pressure, the gas pressure being the higher due to capillarity. The gas or air may be continuous or it may exist in discrete bubbles, depending on the degree of



Disc piezometer,  $F = 13\text{cm}$ , in moraine fill ( $k = 2 \times 10^{-7}\text{m/s}$ )  
Pressure measurement by Hg manometer  $3\text{mm}$  dia.

Figure 3 Equalization of piezometer after the application of a constant pressure for varying times.

saturation. If the air is continuous, the air permeability is high, the pore air pressure will tend to equalize to atmospheric pressure and the pore water pressure will be sub-atmospheric. If the porewater pressure is greater than atmospheric the air will generally be discontinuous.

In partly saturated soils it is essential to know whether pore air or pore water pressure is being measured. It is much more useful to measure pore water pressure, as changes in this pressure usually control changes in effective stress and it is also the pressure which directly responds to drainage of water. The principles of measuring pore water pressure are discussed in detail by Bishop *et al* (1964). If the cavity pressure equalizes to the pore water pressure the rate of equalization will be controlled by processes similar to those described for saturated soils.

If pore water pressure is to be measured, the piezometer filter must be of sufficiently fine pore size for it to be able to resist by capillarity at its surface an air-water pressure difference (the air entry value or blow-through pressure) greater than the pressure difference in the soil; otherwise the water in the filter and the piezometer cavity will be replaced by air and, unless this air is continuously removed, the pore air pressure will be measured. Spontaneous and continuous removal of air may occur in standpipe piezometers as air bubbles rise in the standpipe.

If the piezometer cavity is enclosed, then, even with a high air entry value filter, air will still enter the cavity by diffusion. This process occurs according to the general diffusion equation and Henry's law of solubility. Thus air flows from bubbles at high pressure to bubbles at low pressure. Diffusion of air through water is very slow. If an air bubble forms within the piezometer cavity its pressure will tend to that of the water in the cavity, it will be less than that of the air in the surrounding soil and diffusion of air into the cavity will continue. While the cavity still contains free water the porewater pressure will be measured. Once the cavity has emptied of water, the air pressure, which is being measured, will slowly rise as more air diffuses into the cavity until it equalizes with the pressure of the air in the surrounding soil. If the air is flushed from the cavity the cavity pressure will again equalize to the pore water pressure.

If the air is continuous (which implies sub-atmospheric pore water pressure) diffusion is only required across the thickness of the filter, whereas if the air is discontinuous diffusion must also occur through the surrounding soil and it will be much slower. The mass of air required to fill the cavity will depend on the cavity pressure and the lower the pressure the more rapidly the cavity will empty. Thus break-

of pore water pressure measurement may be expected to be much more rapid when pore water pressures are sub-atmospheric than when they are above atmospheric. Practical experience (Bishop et al : 1969) confirms this prediction. Bishop et al (1964) quote the total flow of air into a high air entry value piezometer recording pore water pressures just above atmospheric in boulder clay fill. An inflow rate of  $3\text{cm}^3/\text{year}$  is given for the first four years of operation. Assuming that all this air was entering the piezometer cavity, breakdown of measurement should not have occurred for at least 5 years. Fig. 4, after Bishop et al (1964), shows the pressure recorded by a similar piezometer in rather dry shale fill with continuous air. Breakdown is indicated as de-airing restored the measurement of sub-atmospheric pressure. The measured pressure rises smoothly as if responding to water inflow and breakdown is not apparent unless de-airing is performed.

Torblaa (1966) discusses the use of a thick high air entry value filter with a sealed cavity electric piezometer to inhibit breakdown by lengthening the diffusion path. Such units may operate without breakdown for many years if pore water pressures above atmospheric are measured. If breakdown occurs when sub-atmospheric pressures occur initially, correct reading may be restored if pore water pressures rise sufficiently rapidly for the air in the cavity to be compressed and for free water to enter it again. Breakdown should also be inhibited if the volume of water within the filter is initially as large as possible. However, provision for de-airing is always an advantage, as breakdown cannot be detected directly and correct reading may not be restored naturally. If sub-atmospheric pressures are to exist for very long, current experience suggests that provision for de-airing is essential. The provision of tubes for de-airing does not preclude measurement of pressure in the cavity by electric or pneumatic transducers. Careful thought should be given to such a system before it is used. Cavitation within the tubes, with the resulting flow of water into the cavity, may inhibit equalization, as well as preventing breakdown by supplying free water to the cavity.

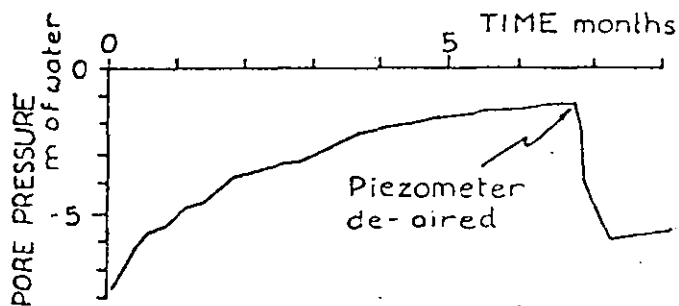


Figure 4 Breakdown of a sub-atmospheric pore water pressure measurement.

Two additional factors should be considered in providing piezometers for partly saturated soils. The seals at the piezometer tip must be capable of resisting the same 'blow-through' pressure as the filter. Where practicable, a blow through test should be performed on the assembled tip before it is installed. If the piezometer has de-airing tubes its internal shape should be 'clean' so that all air bubbles can be flushed out.

#### MEASUREMENT OF PRESSURE IN THE PIEZOMETER CAVITY

Pressure measurement may be via water-filled tubes connecting to an external measuring point, by an electric transducer in the piezometer cavity or by a variety of pneumatic pressure sensing systems in the cavity.

Hydraulic measurement The simplest form of hydraulic measurement is the open standpipe. The pressure to be measured must be above atmospheric. Provided that the standpipe is of sufficient diameter to allow air bubbles to rise freely (in the author's experience a 'clean' diameter of about 12mm is required) the system is self de-airing. Access to the top of the standpipe is generally required for plumbing the water level, although this can be determined remotely using an air bubbling system (Vaughan : 1965) which enables the top of the standpipe to be buried.

In twin-tube hydraulic piezometers, the cavity is connected to a remote measuring point by the two water-filled tubes, which are available for de-airing. The cavity pressure differs from the pressure at the measuring point by the head difference between them; the tubes must be air free for a true correction to be applied. The entry of air into the tubing is insignificant if the correct tubing is used. Nylon 11 tubing, sleeved with polythene, is impermeable to both air and water and such tubing will operate at positive pressures for many years without de-airing being required. A difference in measured pressure between the two measuring tubes will often indicate the presence of air in them. Air in the cavity will not cause such a difference. For trouble-free operation, pressures throughout the connecting tubes should be above atmospheric and the system will not operate at all if tension occurs in the tubes. This places a restriction on the relative levels of the piezometer, the tubes and the measuring point.

Other disadvantages of the system are : very fast response times are prevented by the compressibility of the tubing; exposed parts of the system may freeze and anti-freeze solutions can cause osmotic pressures; the tubing and the piezometer cavity must be filled initially with de-aired water, while this can be done off-site in part it complicates installation; joins in the tubing (which should be avoided if poss-

ible) and joins with the piezometer tip are potential causes of constrictions and blockages, they pull apart under tensile forces and small coils should be formed in the tubing on each side of couplings to reduce the tensile forces which can be applied to them ; tubes should be checked for continuity and leaks before installation ; dirty water can cause blockages and should not be used ; pressure measuring systems and de-airing units tend to be large and expensive and to require large and expensive gauge houses, although modern developments allow the use of small terminal valve units (which can be buried in small chambers to avoid freezing) together with portable measuring and de-airing systems.

Other advantages of hydraulic systems are : in-situ tests can be performed, both to determine soil properties and to check the piezometer ; automatic recording is possible ; pressure measuring systems are external and calibrations, etc., can be checked ; piezometer tips and connecting tubes are cheap ; there are no buried moving parts and long term reliability is very good.

A variety of de-airing systems have been developed for hydraulic piezometers, some automatic. From the author's experience, de-airing systems should allow the following: the maximum pressure applied should not be sufficient to fracture the ground at the piezometer ; a small outflow from the piezometer into the ground should occur during de-airing ; pressure changes in the tubing should be minimised. A back pressure on the return tube is generally necessary to meet these requirements. It is often forgotten that occasional de-airing can be performed from two portable water containers at the appropriate levels.

Electric measurement Electric piezometers usually have no provision for de-airing. The pressure in the cavity is measured by determining the deformation of a diaphragm between it and a second chamber. Usually, this chamber is sealed with a known pressure in it, although it can be vented to atmospheric pressure. Because the deflection of the diaphragm is small, very fast response times can be achieved (see Table 1). Where the piezometers are permanently buried and where the signal must be transmitted long distances, vibrating wire strain gauges are usually used to sense the diaphragm displacement. Such strain gauges are very stable and the signal is suitable for long distance transmission as it is uninfluenced by the resistance of the cables. For short term observations where transmission is over short distances, there is a growing tendency towards the use of mass produced transducers with resistance strain gauges.

Advantages of electric measurement include : convenient installation, as only a single cable needs to be laid out ;

the equipment is not subject to freezing, small and convenient terminal units can be used, with portable reading units ; there are no restrictions on the relative levels of the equipment. Disadvantages include : the high cost of the piezometers, connecting cables and the reading units ; the piezometer requires a calibration which cannot be checked after installation unless special provision is made ; the buried and inaccessible part of the equipment is sophisticated and long-term reliability must always be in some doubt as no check tests can be performed.

Pneumatic measurement Pneumatic systems involve two air-filled tubes connecting the measuring point to the piezometer, which contains a valve operated by the difference between the applied pneumatic pressure and the pressure in the piezometer cavity. Either the valve shuts when the input air pressure equals the cavity pressure, in which case the maximum pressure built up in the return tube gives the cavity pressure, or the valve opens, in which case the maximum pressure sustained in the input tube gives the cavity pressure. In most systems, the operation of the valve involves a small calibration factor. Operation of the valve also requires a small volume change within the piezometer cavity. Potential errors may arise due to this volume change, their magnitude depending on the volume factor of the system. Such errors may be overcome, at least in part, if the valve has a 'snap' action triggered by the pressure operating before the valve moves. If there are no hydraulic tubes connecting to the cavity (as can be provided for de-airing) the response time will be very short. The connecting tubes must be kept free of water. They must be of suitable impermeable material and dry gas must be used to operate the system. Other problems with plastic connecting tubes are as described for hydraulic connections.

Advantages of pneumatic systems include : they should not freeze ; portable reading units can be used, with small and cheap terminal valve boards ; installation is more convenient than with hydraulic systems, as the connecting tubes do not require filling with water ; tubing is cheap ; there are no relative level problems (unless de-airing tubes are used) ; while the buried valve may have an uncheckable calibration the effect of this is usually small and the main pressure measurement is external and checkable. Disadvantages include : the usual absence of de-airing facilities ; operation is slow and time consuming ; if the connecting tubes are long head losses in them during operation may become significant ; dirt entering the system may prevent valve operation ; piezometer tips are relatively expensive.

Pneumatic systems are a comparatively recent development and there is little experience of long term operation. Malfunction of valves due to corrosion, sticking, perishing of plastic



parts and the like seems to be the most likely potential cause of failure. Until experience is obtained, the use of pneumatic systems for long term measurement requires caution. There is some possibility of checking the operation of pneumatic systems by in-situ tests on the circulating tubes.

#### REFERENCES

- Bishop, A.W., M.F. Kennard & P.R. Vaughan (1964) Developments in the Measurement and Interpretation of Pore Pressure in Earth Dams. Trans. 8th. Congress Large Dams, 1, 47.
- Bishop, A.W., P.R. Vaughan & G.E. Green (1969) Report on Speciality Session 'Pore Pressure Measurements in the Field and in the Laboratory'. Proc. 7th. Int. Conf. Soil Mech. & Found. Eng. 3, 427
- Bolt, G.H., & J.V. Lagerwerffe (1965) Consequences of Electrolyte Redistribution during Pressure Membrane Equilibration of Clays. Soil Science, 99, 3:147.
- Escario, V. (1969) Discussion. Proc. 7th. Int. Conf. Soil Mech. & Found. Eng. 3, 433.
- Gibson, R.E. (1963) An Analysis of System Flexibility and its Effect on Time-lag in Pore-water Pressure Measurement. Geotechnique, 13, 1:1
- Hvorslev, M.J. (1951) Time-lag and Soil Permeability in Ground Water Observations. Bull. No. 36, U.S. Waterways Experiment Station, Vicksburg.
- Penman, A.D.M. (1960) A Study of the Response Times of Various Types of Piezometer. Proc. Conf. Pore Pressure & Suction in Soils, Butterworths, London, 53.
- Richards, B.C. (1969a) Psychrometric Techniques for Measuring Soil Water Potential. C.S.I.R.O Div. Soil Mech. Australia, Tech. Report No. 9.
- Richards, B.C. (1969b) Discussion. Proc. 7th. Int. Conf. Soil Mech. & Found. Eng. 3, 433.
- Soderberg, L.O. (1962) Consolidation Theory applied to Foundation Pile Time Effects. Geotechnique, 12, 3;217.
- Torblaa, I. (1966) Poretrykksmåler Utført ved Dam Hyttejuvet med Fonskjellig Maleutstyr. Norwegian Geotech. Inst. Pub.68,25.
- Vaughan, P.R. (1965) Field Measurements in Earth Dams. Ph.D. Thesis, University of London, 1, 76.
- Vaughan, P.R. (1969) A Note on Sealing Piezometers in Boreholes. Geotechnique, 19, 3:405.
- Vaughan, P.R. (1972) Discussion. 5th. European Conf. on Soil Mech. & Found. Eng., Madrid, 2, 72.

SOME P  
APPLIE

A.

The Ma  
Kent C

INTRODU

The pre  
Wrothan  
bounda  
crop.  
carried  
decided  
factors

Two sit  
selecte  
Gault C  
investi

The pap  
details  
which w

PROGRAM

The pile  
ten and  
of nomin  
from 9.  
Kensing  
layout



**DIVISION DE EDUCACION CONTINUA  
FACULTAD DE INGENIERIA U.N.A.M.**

MECANICA DE ROCAS APLICADA A LA MIENRIA Y A LA CONSTRUCCION

UPLIFT PRESSURES IN HYDRAULIC STRUCTURES

By I. G. K. Soos

MAYO, 1985

*J.S. Maycotte*

**Soos, I.G.K.** Uplift pressures in hydraulic structures. *Water Power and Dam Construction*. May 1979.

# Uplift pressures in hydraulic structures

By I. G. K. Soos  
Consulting Engineer\*

Three methods of calculating the uplift forces on a structure subject to hydraulic pressure are described; by simple calculation, by elastic plate simulation, and by electrical analogue.

COMMON TO THE calculations which follow are four basic assumptions:

- the rock foundations are integral parts of the structures and their stratification is considered in the analysis;
- each individual rock formation, or strata, constituting the foundation is within itself homogeneous and uniformly permeable in the horizontal plane, with a possible different vertical permeability, satisfactorily predictable by field and laboratory measurements;
- the concrete is homogeneous and, for any practical purpose, impermeable; and,
- the permeability along the seepage-path no. 1, that is, along the contact planes is the same, as in the corresponding strata provided, that the normal forces are compressive.

The pressure-variation between two points, in a homogeneous ground, is rectilinear, ie. the hydraulic gradient is constant:

$$i = dP/l$$

The variation of the hydraulic gradient between two adjacent strata is proportional to the variation of the permeability of these strata.

The relative thickness of a stratum that is, the relative length of the seepage path in a stratum ( $l'_j$ ) is directly proportional to the actual length of the seepage path and inversely to the permeability of this stratum:

$$l'_j = (l/k_j)$$

$$\text{and } l'_1:l'_2:\dots:l'_n = l_1/k_1:l_2/k_2:\dots:l_n/k_n$$

As the total length of the seepage path

$$l = l_1 + l_2 + \dots + l_n,$$

to satisfy the condition of

$$l = l'_1 + l'_2 + \dots + l'_n,$$

the relative length of the seepage path in a stratum will be:

$$l'_j = l (l/k_j) / \sum_1^n (l/k_j)$$

and the hydraulic gradient in a stratum will be:

$$i_j = i_n (l'_j/l), \quad i_n \text{ being the global hydraulic gradient or, as } i_n = h_0/l, \quad h_0 \text{ being the differential head,}$$

$$i_j = (h_0/l) (l'_j/l) = (h_0/l) (l/k_j) / \sum_1^n (l/k_j) = h_0/k_j \sum_1^n (1/k_j)$$

Considering a horizontal contact-plane, the pressure-head at a point at  $l_j$  distance from the origin will be:

$$h_x = h_u - (h_0/l) x$$

$h_u$  being the upstream head and  $l'_j$  the relative distance. Applying this theory to pressure exerted over a contact-surface of various inclinations,  $l$  will become the developed length of the total contact surface,  $l_j$  will be measured along the inclined line and  $h_u$  will be the upstream head, related to the point of examination. (Fig. 1).

There are three design-elements which can strongly influence the intensity of the uplift forces:

- the upstream blanket, which increases the length of the seepage path;
- the grout-curtain, which consolidates part of the foundation rock and increases the length of the seepage path; and,
- the drainage curtain, which relieves water-pressure.

Upstream blankets are used in alluvial foundation material, where grouting is impracticable.

The grout-curtain forms an individual stratum with a

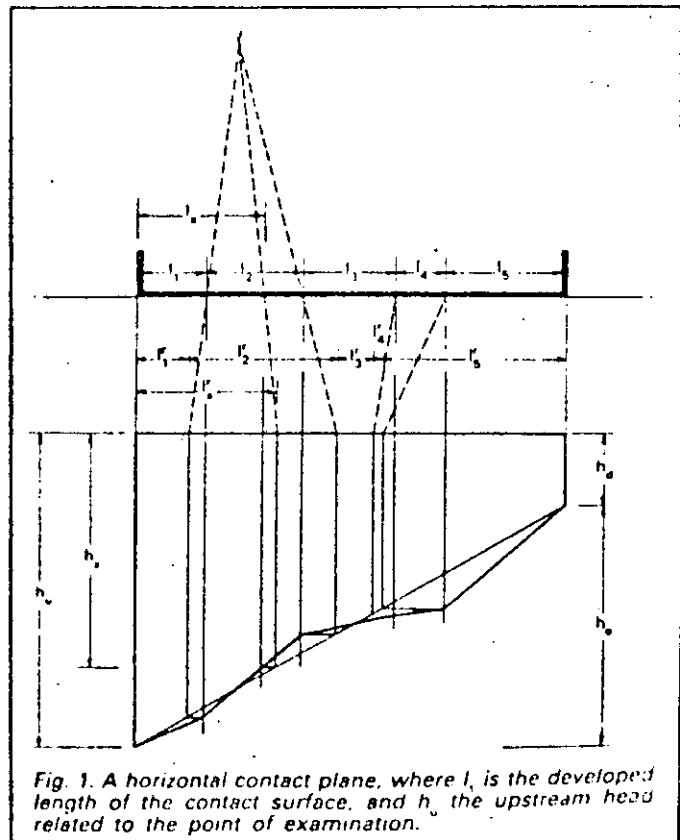


Fig. 1. A horizontal contact plane, where  $l$  is the developed length of the contact surface, and  $h_u$  the upstream head related to the point of examination.

\* Av. Paulista 810, Apto. 3, 01310 Sao Paulo, Brazil.

decreased permeability. As the practical value of decrease in permeability cannot exceed the value of the increasing length of the seepage path around the grouted rockmass, the permeability factor of this stratum will be taken as:

$$k_{gr} = k_0 d / (2d + l_0)$$

where  $k_0$  is the permeability factor of the ungrouted rock,  $l_0$  the contact-length of the grouted strata and  $d$  the depth of the grouting.

Two methods of installing grout-curtains are considered. In one, the injection is made before concreting of the foundation. It is inaccessible after the completion of the structure. In the other, the injection is made from the completed gallery, the grout material filling all contact surfaces. Reinjection can be made whenever necessary.

The second technique has the following advantages:

- The grouting is carried out from a covered area, on a straight ground, not delaying or interfering with any other operation.
- Higher grouting-pressures can be used, due to the weight of the structure.
- Grouting is carried out after a good part of the shrinkage of the concrete has finished, thus filling all fissures along the contact-surface.
- Regrouting can be done after the reservoir has reached full height and the foundation-rock readjusted itself, or any time during the lifetime of the structure.

The influence of the drainage curtain on the uplift forces depends upon its efficiency, its position in the seepage path, and the level of its discharge (gallery, collecting drain etc).

The efficiency of a drainage curtain is the factor expressing the proportion of a flow that it can capture, or, in other words, by what proportion it can reduce the charge. It depends on the relation between the spacing of the wells and the length of the seepage path and the ability of the wells to handle the flow. As a 1.5 in hole in a reasonable condition can handle large flows the second parameter can be neglected. If the spacing of the wells is reasonably close in relation to the length of the seepage path in both directions, the proportion of the flow captured will be very high. The efficiency factor will be then approximately:

$$k_e \cong 1 - 4(d/l);$$

$d$  being the distance between two wells and  $l$  the total length of the seepage path. A more exact figure can be obtained with the elastic plate simulation, or the electric analogy method.

The charge on a drainage curtain is the difference between the undrained head at the drainage line and its level of discharge. Two levels of discharge can be distinguished, normal and catastrophic. Normal operation takes place at the level of the discharge drain, from where the water is collected and pumped out. A catastrophic level is the head of discharge above maximum tailwater.

The drainage elements can be categorized as:

- Infallible under all conditions;
  - wells of more than 0.5 m<sup>2</sup> cross-sectional area.
  - straight ducts between two accessible wells, of more than 0.25 m<sup>2</sup> cross-sectional area.
- Infallible under reasonable maintenance conditions;
  - all straight wells and ducts directly accessible from a gallery or well. (Note that in most hydraulic structures, the control and maintenance of the equipment is continuous. An abandoned structure is much more likely to fail because of the failure of its

mechanical equipment, than its drainage system.)

- Fallible;
  - No drainage lines accessible for control and maintenance. (Note that this drainage is useless for most practical purposes, as the structure has to be dimensioned as if this drainage would be inoperative.

The following examples of uplift pressures under different ground, construction and drainage conditions, use a horizontal contact-surface, to which all pressures will be related for the sake of simplicity and clarity.

Fig. 2a shows the hydraulic gradient, or pressure gradient, in a homogeneous ground, while Fig. 2b and 2c its possible decrease or increase, respectively, in a heterogeneous, stratified ground depending on the relative permeability of the consequent strata. It demonstrates also the importance of an exact geological survey.

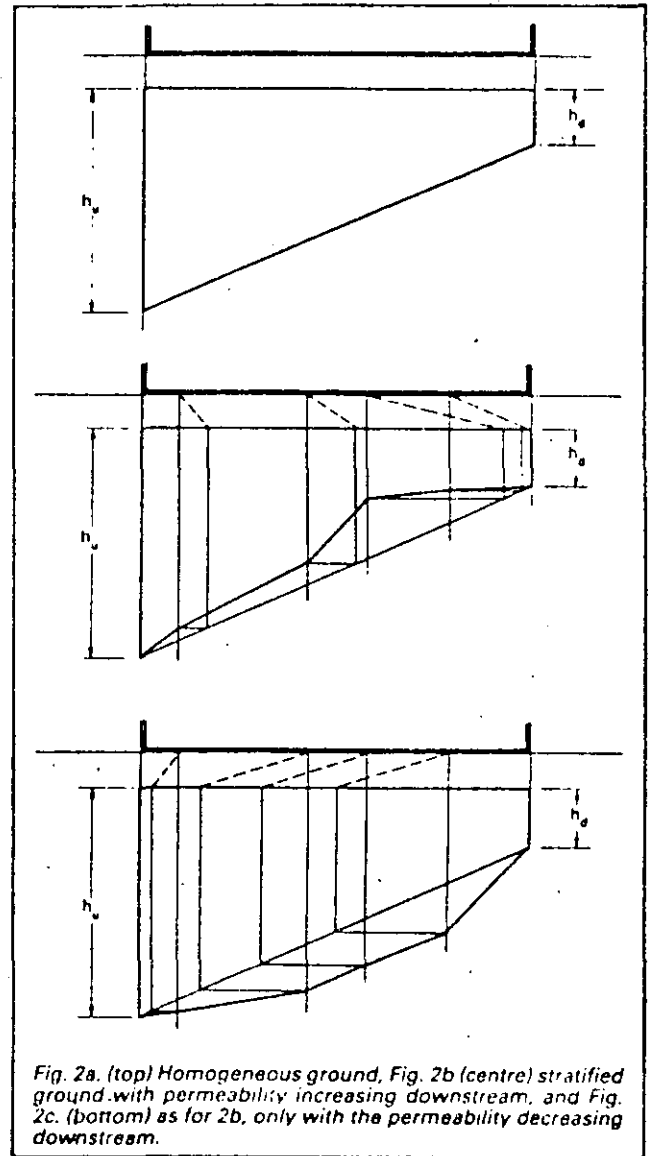


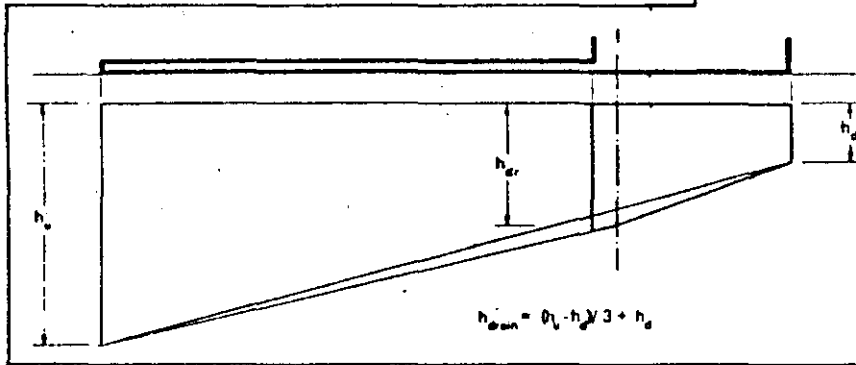
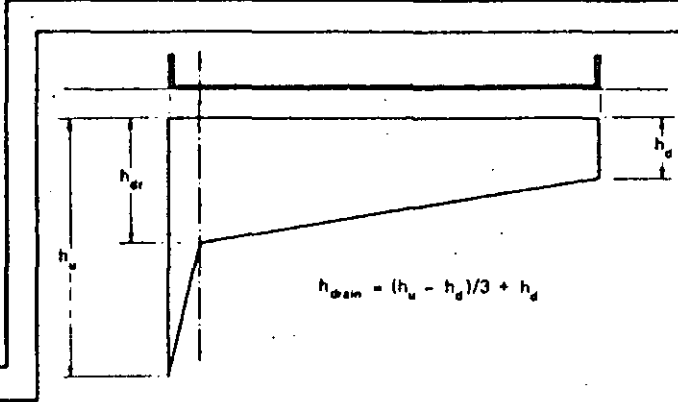
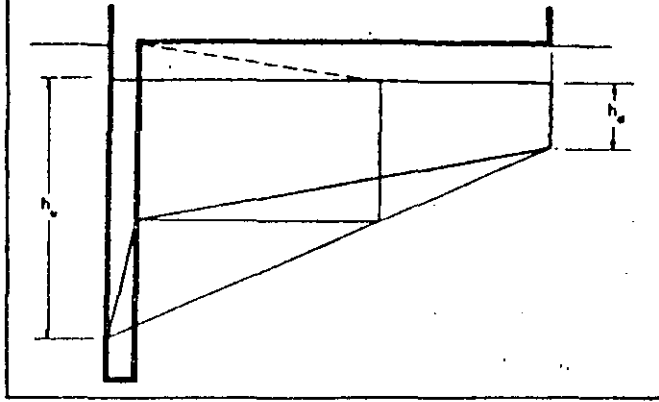
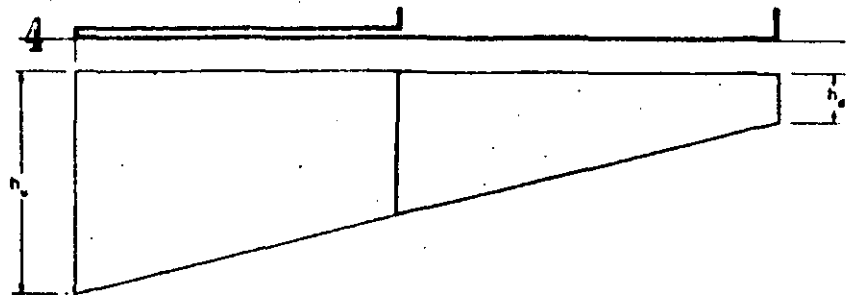
Fig. 2a. (top) Homogeneous ground, Fig. 2b (centre) stratified ground with permeability increasing downstream, and Fig. 2c. (bottom) as for 2b, only with the permeability decreasing downstream.

Fig. 3a shows a structure with an upstream blanket and Fig. 3b with an upstream grout-curtain, demonstrating how form can influence the uplift pressures.

The uplift pressure in Fig. 4a is calculated with the familiar  $h_{drain} = [(h_u - h_d)\sqrt{3}] + h_d$  formula, which relates to the joint influence of grout and drainage curtains. Piezometric measurements have shown that this formula is very conservative. It also neglects the influence of the position and level of discharge of the drainage curtain.

Fig. 3a. Homogeneous ground; upstream blanket  $\triangleright$

$\nabla$  Fig. 3b. Homogeneous ground; upstream grout curtain.



$\Delta$  Fig. 4a. Homogeneous ground; upstream grout and drain curtain

$\triangleleft$  Fig. 4b. Homogeneous ground; upstream blanket and drainage curtain.

This leads to an anomalous situation shown in Fig. 4b, where the calculated uplift is larger with, than without drainage.

Figs. 5 and 6 show three basic conditions where the position and discharge level of the drainage curtain is taken into consideration with 100 per cent (Figs. 5a, 5b,

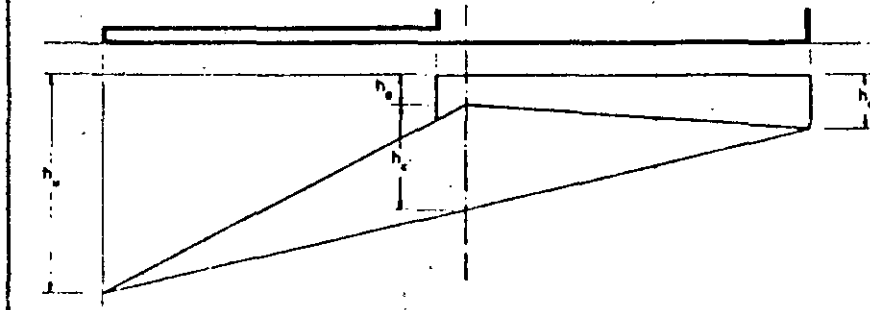
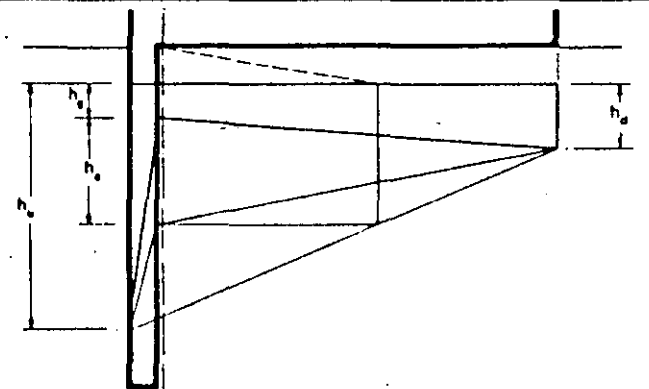
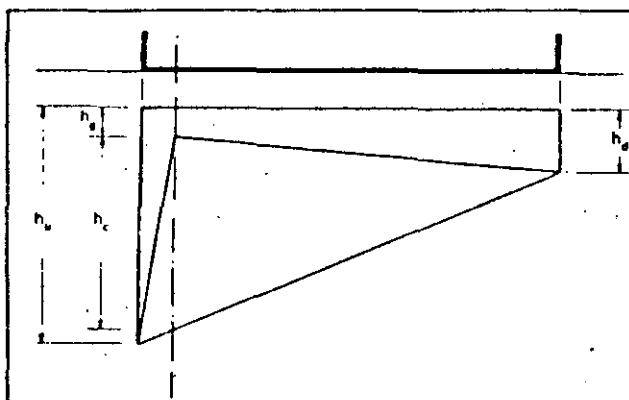
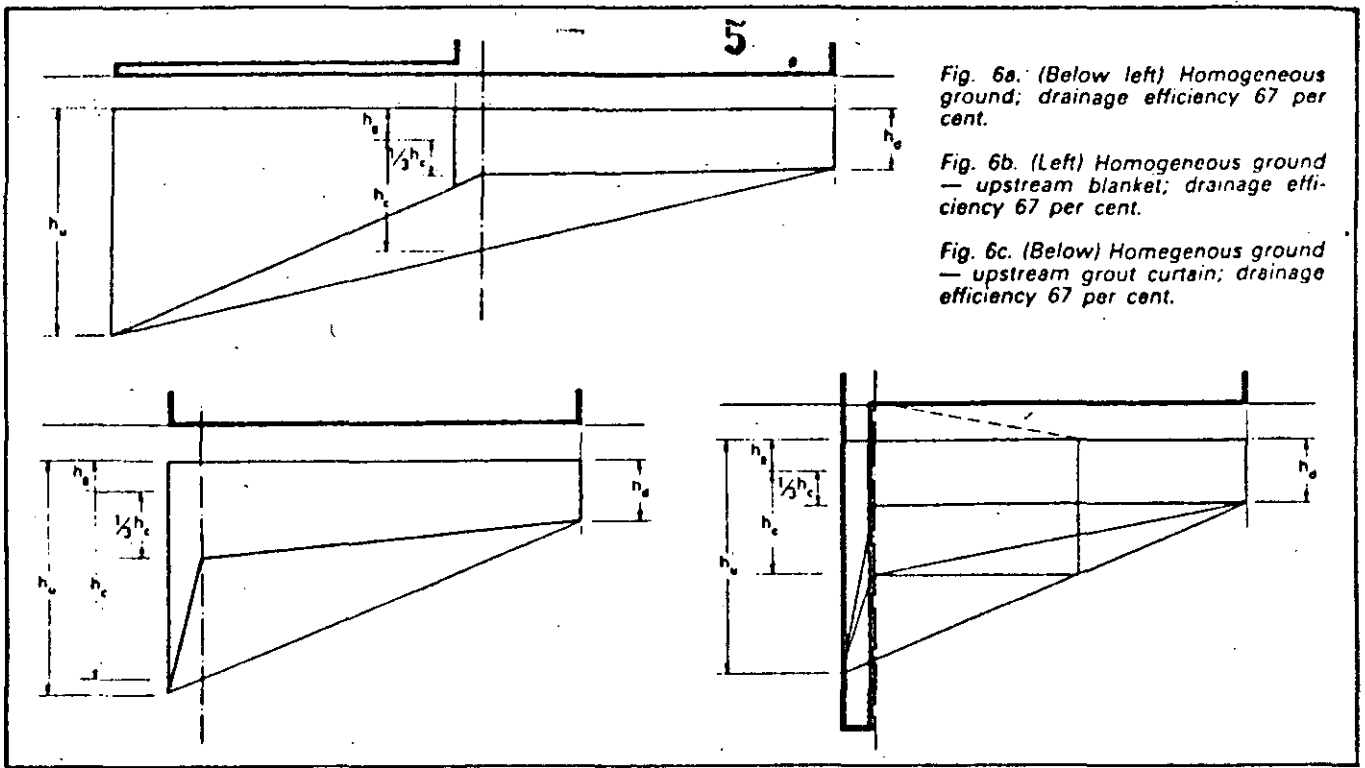


Fig. 5a. (Above left) Homogeneous ground; drainage efficiency 100 per cent.

$\triangleleft$  Fig. 5b. Homogeneous ground — upstream blanket; drainage efficiency 100 per cent.

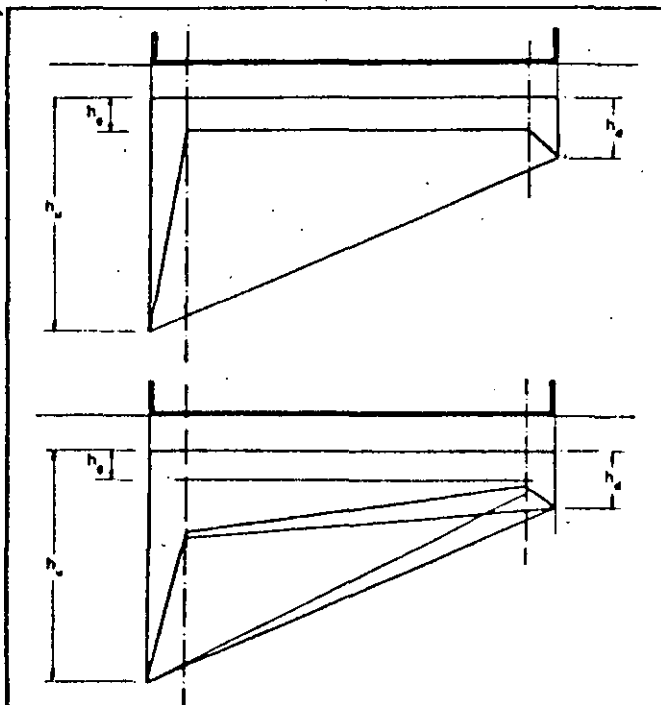
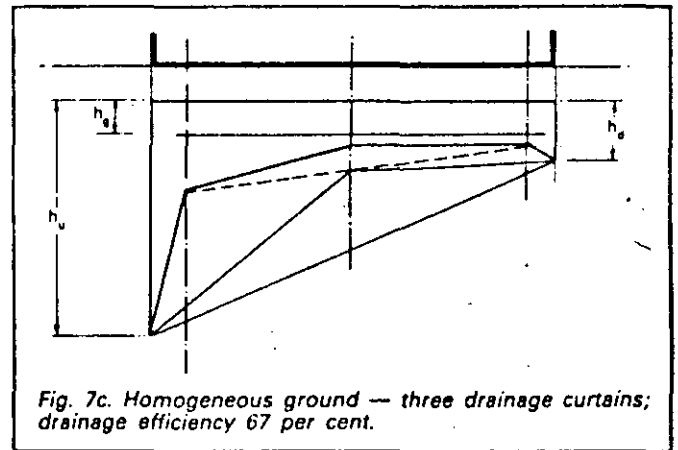
Fig. 5c. (Above right) Homogeneous ground — upstream grout curtain; drainage efficiency 100 per cent.



5c) and with 67 per cent (Figs. 6a, 6b, 6c) efficiency.

In Fig. 7 there are structures with two and three drainage curtains, represented, for simplicity's sake, without grout curtains. In Fig. 7a the drainage-curtain's efficiency is 100 per cent; consequently the pressure gradient drops from the upstream face, full reservoir head, to the upstream drainage curtain line, drainage head, down further to the downstream drainage curtain line, drainage head and continues to the downstream face, downstream head.

In Fig. 7b a similar layout (to Fig. 7a) with 67 per cent



well-efficiency is shown. The two wells' influence on each other is considered by constructing an auxiliary basic pressure-gradient from the upstream face, full head, to the downstream well line (in this case) 67 per cent efficiency point, disregarding the upstream drainage curtain and then doing the same between the first drainage curtain line 67 per cent efficiency point and the downstream face, downstream head. These lines mark the adjusted basic charge at the wells, which is then reduced by the drainage curtains efficiency factor. Fig. 7c shows a pressure diagram with three drainage curtains, constructed with this method.

In the elastic plate simulation method an elastic plate is placed having the dimensions of the contract area, and consisting of rigidly jointed elements, representing the different strata (inclusive of grout-curtains), each with a rigidity inversely proportional to the permeability of the respective strata. Alternatively, the plate can have uniform thickness and module of elasticity, with adjusted relative lengths ( $l'_j$ ). This plate is then forced between indeformable, articulated supports, representing the upstream and downstream faces (continuous) and the wells (points) on the XY plane and their respective pressure-heads with the Z coordinates. The displacement (Z coordinates) at each point will be proportional to the uplift pressure at that point.



**DIVISION DE EDUCACION CONTINUA  
FACULTAD DE INGENIERIA U.N.A.M.**

MECANICA DE ROCAS APLICADA A LA MINERIA Y A LA CONSTRUCCION

DETERMINATION OF BULK ROCK PROPERTIES FROM  
GROUND-WATER LEVEL FLUCTUATIONS

P.A. DOMENICO

MAYO, 1985



Local copy



P-235

# Determination of Bulk Rock Properties From Ground-water Level Fluctuations

P. A. DOMENICO

*Department of Geology, Texas A&M University, College Station, TX 77843*

## ABSTRACT

The response of ground-water levels to tides and changes in barometric pressure provides an in-situ measure of the response of the rock-water system to changes in stress. Tidal and barometric efficiencies can thus be expressed in terms of drained and undrained moduli. In addition, if the various moduli are known from laboratory measurements, the laboratory equivalents of both tidal and barometric efficiency can provide an estimate of the specific storage. The method is demonstrated to provide reasonable and consistent results when applied to various rock types of differing rigidity.

## INTRODUCTION

Numerous cases of water level fluctuations in wells in response to atmospheric pressure, ocean and earth tides, earthquakes, and passing trains have been reported (Jacob, 1939; Robinson, 1939; and Parker and Stringfield, 1950). An extensive bibliography is provided by Todd (1980). These fluctuations are generally accepted as evidence that confined aquifers are not rigid bodies, but are elastically compressible, an idea fostered by Meinzer (1928) and advanced by Jacob (1940). Currently, it is a matter of simple routine to compare the water level response to the loads which cause them in order to calculate certain hydraulic properties of the medium, namely specific storage. The purpose of this paper is to redevelop these ideas from stress-strain theory in order to relate water level fluctuations to the bulk elastic properties of the host rock. In certain cases, it would appear that these bulk properties may be determined directly from such fluctuations.

## BACKGROUND INFORMATION

The detailed constitutive relations for isothermal porous mediums have been presented by Biot (1941) and will be briefly restated here. These expressions

include stress-strain relationships in a saturated porous medium as well as corresponding equations for changes in fluid mass content:

$$\epsilon = (\sigma/K) + (P/H) \quad \text{Eq. 1}$$

where  $\epsilon$  is volumetric strain,  $\sigma$  is mean stress (negative in compression),  $K$  is the bulk modulus,  $P$  is fluid pressure, and  $H$  is an elastic constant. Corresponding equations for changes in fluid mass content are:

$$m/\rho = (P/R) + (\sigma/H) \quad \text{Eq. 2}$$

and

$$m/\rho = \xi\epsilon + (P/Q) \quad \text{Eq. 3}$$

where  $m$  is the mass of pore fluid per unit volume of porous medium,  $\rho$  is the density of the water, and  $R$ ,  $Q$ , and  $\xi$  are elastic constants. The relationship between these constants is given by:

$$1/Q = (1/R) - (\xi/H) \quad \text{Eq. 4}$$

The elastic constants cited above have been discussed at length by Palciauskas and Domenico (1982). Briefly,  $K^{-1}$  equal to the compressibility  $\beta$  reflects the bulk volume response to changes in stress

at constant pressure, i.e., the condition where the water is free to drain during loading. According to Biot (1941):

$$K = \xi H \quad \text{Eq. 5}$$

where  $\xi$  is the ratio of the water volume squeezed out to the volume change of the material if the latter is compressed at constant fluid pressure. If the volume of water so removed is equal to the volume change of the material, a common assumption in consolidation theory,  $\xi = 1$  and  $H = K$ . If this condition is not satisfied,  $\xi \neq 1$ , but is slightly less than 1. Thus,  $\xi$  is a proportionality constant between the pore and bulk volume changes at constant fluid pressure and can be described (Biot and Willis, 1957):

$$\xi = 1 - (K/K_s) = 1 - (\beta_s/\beta) \quad \text{Eq. 6}$$

where the subscript *s* stands for the polycrystalline grain structure. From Equations 5 and 6:

$$1/H = 1/K - 1/K_s = \beta - \beta_s = \beta_p \quad \text{Eq. 7}$$

where  $\beta_p$  is taken as the compressibility of the pores. Hence,  $1/H$  is a measure of the pore compressibility as the medium is compressed under the condition of constant fluid pressure.

The coefficients *R* and *Q* are formulated in a similar fashion. Biot (1941) has described  $1/R$  as a measure of the change in water content for a given change in fluid pressure, and  $1/Q$  as a measure of the amount of water which can be forced into a material under pressure while the volume of the material is kept constant. These coefficients can be expressed in terms of the compressibilities of the various components as well as in terms of drained and undrained moduli (Palciauskas and Domenico, 1982):

$$\begin{aligned} 1/R &= \beta_p + \psi(\beta_f - \beta_s) \\ &= \xi^2 K_u / K(K_u - K) \end{aligned} \quad \text{Eq. 8}$$

and

$$\begin{aligned} 1/Q &= \psi(\beta_f - \beta_s) + \beta_s \beta_p / \beta \\ &= \xi^2 / (K_u - K) \end{aligned} \quad \text{Eq. 9}$$

where  $\psi$  is porosity,  $\beta_f$  is the isothermal fluid compressibility, and  $K_u$  is an undrained bulk modulus, i.e., the modulus determined under constant fluid mass. It follows that the undrained response will be elastically stiffer than the drained response.

As the stated purpose of this paper is to express some of the routine calculations in ground-water hydrology in terms of the formulations cited above, a few words seem to be appropriate here on the nature of these calculations. Reference here is spe-

2 cifically to what has been termed the barometric and tidal efficiencies as described by Jacob (1940). First, we recognize that both calculations assume a condition of constant fluid mass so that the condition  $m = 0$  in Eq. 2 or Eq. 3 is appropriate. Tidal efficiency (T.E.) is defined as the ratio of the piezometric level amplitude as measured in a well to the tidal amplitude or, in terms of pressures:

$$\text{T.E.} = \rho gh / \rho g A \quad \text{Eq. 10}$$

where *h* is head, *g* is the gravitational constant, and *A* is the amplitude of the tide. That is to say, as the ocean level deviates from its mean by plus or minus *A*, the hydraulic head in confined aquifers extending under the ocean fluctuates accordingly. As the tidal fluctuation represents nothing more than a fluid pressure response to a variation in load at constant fluid mass, the appropriate expression becomes, from Equation 2.

$$\text{T.E.} = (\partial P / \partial \sigma)_m = -R/H. \quad \text{Eq. 11}$$

It may be noted that this expression also describes Skempton's (1954) pore pressure coefficient *B*.

Barometric pressure has an inverse relationship with water levels. The barometric efficiency (B.E.) is used to describe how faithfully a water level responds to changes in atmospheric pressure, and is defined:

$$\text{B.E.} = \rho gh / P_a \quad \text{Eq. 12}$$

where  $P_a$  is atmospheric pressure. As B.E. plus T.E. equals one (Jacob, 1940), the barometric efficiency is obtained from Equation 4 and Equation 12:

$$\text{B.E.} = 1 - (1/\xi)(1 - R/Q). \quad \text{Eq. 13}$$

It is clear from Equation 13 that if  $\xi$  equals one for incompressible grains, B.E. =  $R/Q$ . As a final word, it may be noted that a "specific storage" *S*, may be incorporated in some of these statements as a volume of water released from a unit volume of porous medium when the pressure in the unit volume is reduced a unit amount. This relationship is expressed exactly by  $\rho g'R$ . However, this expression differs somewhat from the one presented by Jacob (1940) in that it includes compressible grains and is not restricted to vertical compression only. These same conditions hold also in the cited relationships for the various efficiencies. A closer but not yet exact correspondence to Jacob's (1940) definitions can be obtained by considering the grains to be incompressible. In any case, the approximate order of magnitude of the specific storage so obtained should

not differ appreciably from that obtained in strict accordance with Jacob's (1940) definition. All further reference to a "specific storage" and both "tidal and barometric efficiencies" in this paper incorporates these additional conditions.

### SAMPLE CALCULATIONS

#### Incompressible Grains

The case of incompressible grains is the most straightforward and the one generally employed in ground-water hydrology. For this assumption,  $\xi = 1$ ,  $H = K$ ,  $1/Q = \psi\beta_1$ , which is merely a reflection of the compressibility of the water in the pores, and  $1/R = 1/K + \psi\beta_1$  so that  $\rho g/R$  is equivalent to a specific storage. The specific storage, however, is described in terms of the bulk modulus  $K$  instead of a constrained modulus  $K_c$ , where the two moduli are related by  $K = K_c - 4\mu/3$  where  $\mu$  is the shear constant. From Equation 3 for constant fluid mass:

$$\partial c/\partial P = -1/Q \quad \text{Eq. 14}$$

and, from Equations 14 and 11

$$\partial c/\partial \sigma = (1/Q)(R/K) \quad \text{Eq. 15}$$

which is obviously of the form of an undrained modulus. Thus, from Equation 4:

$$(1/Q)(R/K) = (1/K) - (1/K)(R/K) \quad \text{Eq. 16}$$

or

$$1/K_c = (1/K)(1 - R/K) \quad \text{Eq. 17}$$

where  $R/K$  is the tidal efficiency and  $1 - R/K$  is the barometric efficiency. It is interesting to note that  $B.E. = K/K_c$  whereas  $T.E. = 1 - K/K_c$ .

Some data from Long Island will be used to illustrate the nature of the calculations, where Jacob (1941) has reported a porosity of 0.35 and a tidal efficiency of 0.42. For the Lloyd sand, this translates into a specific storage of  $8.66 \times 10^{-4}$ . For a 200 foot aquifer, this gives a storativity of  $1.73 \times 10^{-4}$ , quite reasonable for a sandstone and comparable to Jacob's (1941) measurement of  $3 \times 10^{-4}$ . It is noted, however, from Jacob's 1940 and 1941 papers, there is considerable uncertainty as to the value of the storativity. In addition,  $1/K_c$  is calculated to be  $0.00715 \text{ kbar}^{-1}$  and  $1/K$  is  $0.012 \text{ kbar}^{-1}$ , both of which are of the expected orders of magnitude for a sandstone. For example, measured laboratory values for  $1/K_c$  and  $1/K$  for the Kayenta sandstone are  $0.0052$  and  $0.0105 \text{ kbar}^{-1}$ , respectively (Dropek et al., 1978).

Further support for the method described above

3 can be obtained by employing some calculations from earth tide studies. Bredehoeft (1967) has provided computations of porosity and specific storage from an analysis of earth tide fluctuations for three different areas. For a limestone aquifer in Iowa City, the barometric efficiency has been reported as 0.75. Bredehoeft's (1967) calculations indicate an average porosity of 0.178 and an average specific storage of  $2.8 \times 10^{-4} \text{ ft}^{-1}$ . Utilizing this value for porosity, specific storage is calculated to be  $3.3 \times 10^{-4}$ , which is quite close to the figure cited above. The moduli are calculated to be  $0.0022 \text{ kbar}^{-1}$  for  $1/K_c$  and  $0.0029$  for  $1/K$ . For this limestone, it appears that the undrained response is only slightly stiffer than the drained response.

An interesting application for a composite rock section is possible from data reported by Carr and Van Der Kamp (1969). These authors measured several values of both barometric and tidal efficiencies in sediments consisting of mostly sandstone and siltstone, with smaller amounts of claystone and conglomerate. The barometric efficiency averaged about 0.37 and the tidal efficiency averaged about 0.57. The difference of 0.06 between the sum of these values and unity is reported to be within the range of experimental error. Forty rock samples provided a mean value for porosity of 0.177. Specific storage was determined by both the tidal method and from pumping tests, giving mean values of  $6.3 \times 10^{-4} \text{ ft}^{-1}$  and  $9 \times 10^{-4} \text{ ft}^{-1}$ , respectively. Calculations based on the methods described above gives a specific storage of  $6.48 \times 10^{-4} \text{ ft}^{-1}$ ,  $1/K$  of  $0.0145 \text{ kbar}^{-1}$ , and  $1/K_c$  of  $0.00536 \text{ kbar}^{-1}$ . These obviously represent averages over the geologic section.

#### Compressible Grains

When  $\xi$  is not equal to one, it is clear that we have more unknowns than equations so that some estimates have to be made. For this case, the pertinent equations become, from Eq. 4:

$$T.E. = R/H = (1/\xi)(1 - R/Q) \quad \text{Eq. 18}$$

or, substituting  $R$  and  $Q$  (Eqs. 8 and 9)

$$T.E. = R/H = (1/\xi)(1 - K/K_c) \quad \text{Eq. 19}$$

In addition we have

$$B.E. = 1 - (1/\xi)(1 - R/Q) \quad \text{Eq. 13}$$

or

$$B.E. = 1 - (1/\xi)(1 - K/K_c) \quad \text{Eq. 20}$$

where  $B.E. + T.E. = 1$ .

Table 1. Calculations and measurements for various rock types.

Factors	Units	Clay	Sandstone	Limestone	Basalt
$\xi$		1	0.756	0.69	0.23
1/H	kbar <sup>-1</sup>	1.6	0.00794	0.00237	0.00052
1/R	kbar <sup>-1</sup>	1.7	0.0119	0.00948	0.00438
1/Q	kbar <sup>-1</sup>	0.017	0.0059	0.00784	0.00426
R/H		0.99	0.67	0.25	0.12
1/K	kbar <sup>-1</sup>	1.6	0.0105	0.003	0.00222
1/K <sub>u</sub>	kbar <sup>-1</sup>	0.016	0.0052	0.00237	0.00216
S <sub>v</sub>	ft <sup>-1</sup>	$5 \times 10^{-7}$	$3.5 \times 10^{-7}$	$2.78 \times 10^{-7}$	$1.29 \times 10^{-7}$
$\downarrow$		0.35	0.20	0.178	0.08

As an illustration of the nature of the required approximations, the limestone aquifer discussed above will be used as an example. It is assumed that the calculation of specific storage includes both compressible fluids and grains, i.e.,  $S_v = \rho g R$  where  $R$  is defined by Equation 8. For  $S_v = 2.8 \times 10^{-7}$  ft<sup>-1</sup>, 1/R is calculated to be 0.00948 kbar<sup>-1</sup>. For a measured barometric efficiency of 0.75, 1/H is calculated to be 0.00237 kbar<sup>-1</sup>. At this point, an assumption is required for 1/K<sub>u</sub>, which for calcite can be taken on the order of 0.001 kbar<sup>-1</sup>. For this assumption,  $\xi$  is determined to be 0.69 and 1/K and 1/K<sub>u</sub> are readily calculated to be 0.003 and 0.0024 kbar<sup>-1</sup>, respectively. In this illustration, as in the previously cited incompressible grains base, the undrained response is only slightly stiffer than the drained response. This, however, does not seem out of line for these rocks, as well be demonstrated below. Further, these calculations do not differ appreciably from those given for the case of incompressible grains, but, as expected, indicate a slight increase in compressibility.

The methods described above can be extended to incorporate laboratory determinations to demonstrate the kinds of calculations that are possible. Table 1 is such a demonstration for several rock types. Laboratory data for both the Kayenta sandstone and the Hanford basalts are rather complete. At the other extreme, no data whatsoever are presented for the clay entry but, for comparative purposes, a porosity of 35 percent is assumed, along with the reasonable assumption that  $\xi$  equals 1. As R/H is a measure of the percentage of the load that is carried by the pore water under undrained loading, this value is set at 0.99 for highly compressive clays (see Lambe and Whitman, 1969, p. 395).

For the Kayenta sandstone, the only measured values are porosity and both  $K$  and  $K_u$  (Dropek et al., 1978). All other entries for the sandstone in Table

1 are calculations. These calculations required an assumption for 1/K<sub>u</sub> of 0.00256 kbar<sup>-1</sup>, which is reasonable for the compressibility of quartz. The limestone cited in Table 1 has been previously discussed, with the reported information including a barometric efficiency of 0.75, an assumed porosity of 0.178, and a calculated specific storage of  $2.8 \times 10^{-7}$  ft<sup>-1</sup> (Bredehoeft, 1967). All other entries for limestone in Table 1 are calculations, requiring an assumption for 1/K<sub>u</sub> of 0.001 kbar<sup>-1</sup> for calcite. For the basalt, the reported information includes the bulk modulus and the porosity (Rockwell International, 1980). The calculations required an estimate for 1/K<sub>u</sub> of 0.0017 kbar<sup>-1</sup> for a rock containing well in excess of 50 percent plagioclase and pyroxene. The basalts are further complicated by the fact that three porosities are reported, a total porosity, an apparent porosity, and an unconnected porosity, which is the difference between the total and apparent. A more exact calculation of specific storage is possible if we consider the apparent or connected porosity of 0.018 in conjunction with the constrained modulus,  $K_c = 811$  kbar, which is known from other measurements. For these measurements, the specific storage in strict accordance with Jacob's (1940) definition is calculated to be  $6.2 \times 10^{-8}$  ft<sup>-1</sup>, which differs appreciably from the value cited in Table 1. The lower porosity value employed is largely responsible for this difference.

In spite of the assumptions required, the consistency displayed in Table 1 is quite good. The rock types are arranged from left to right in order of what we would expect to be decreasing compressibility. Hence, unsurprisingly,  $\xi$  decreases from unity to something considerably less than unity as rock rigidity increases. This same statement holds for the coefficients 1/H, 1/R, and 1/Q, all of which are compressibilities of some sort. These values all decrease in the direction of increasing rigidity, except for 1/Q for the limestone. The index of rigidity, however, is best expressed by R/H, which gives the percentage of the load carried by the pore water under undrained loading. As the degree of rigidity increases, this percentage consistently decreases; or, stated another way, the percentage of the incremental stress carried by the grain structure ( $1 - R/H$ ) increases. This is further reflected by the specific storage, which, as expected, decreases in the direction of increasing rock rigidity. The calculations for 1/K and 1/K<sub>u</sub> likewise reflect what we would expect for the rock types cited. That is, with increasing rigidity, the difference between 1/K and 1/K<sub>u</sub> becomes impercep-

tibly small. The overall consistency exhibited by Table I thus suggests that the methods outlined in this paper may provide reasonable approximations for the pertinent parameters.

## REFERENCES

- BIOT, M. A., 1941. General theory of three dimensional consolidation: *Journal of Applied Physics*, Vol. 12, pp. 155-164.
- BIOT, M. A. AND WILLIS, D. G., 1957. The elastic coefficients of the theory of consolidation: *Journal of Applied Mechanics*, Vol. 24, pp. 594-601.
- BREIDHOFF, J. D., 1967. Response to well-aquifer systems to earth tides: *Journal of Geophysical Research*, Vol. 72, pp. 3075-3087.
- CARR, P. A. AND VAN DER KAMF, G. S., 1969. Determining aquifer characteristics by the tidal method: *Water Resources Research*, Vol. 5, pp. 1023-1031.
- DROPEK, R. K., JOHNSON, J. N., AND WALSH, J. B., 1978. The influence of pore pressure on the mechanical properties of the Kayenta sandstone: *Journal of Geophysical Research*, Vol. 83, pp. 2817-2824.
- JACOB, C. E., 1939. Fluctuations in artesian pressure produced by passing railroad trains as shown in a well on Long Island. New York: *Transactions of the American Geophysical Union*, Vol. 20, pp. 666-674.
- JACOB, C. E., 1940. On the flow of water in an elastic artesian aquifer: *Transactions of the American Geophysical Union*, Vol. 21, pp. 574-586.
- JACOB, C. E., 1941. Notes on the elasticity of the Lloyd Sand on Long Island. *Transactions of the American Geophysical Union*, Vol. 22, pp. 783-787.
- LAMB, T. W. AND WILLIAMS, R. V., 1969. *Soil Mechanics*. John Wiley and Sons, Inc., New York, NY, 553 p.
- MINZIE, O., 1928. Compressibility and elasticity of artesian aquifers: *Economic Geology*, Vol. 23, pp. 263-291.
- PALCIAUSKAN, V. V. AND DOMENICO, P. A., 1982. Characterization of drained and undrained response of thermally loaded repository rocks: *Water Resources Research*, Vol. 18, pp. 281-290.
- PARKER, G. G. AND STRINGFIELD, V. T., 1950. Effects of earthquakes, trains, winds, and atmospheric pressure changes on water in the geologic formations of Southern Florida: *Economic Geology*, Vol. 45, pp. 441-460.
- ROBINSON, T. W., 1939. Earth tides shown by fluctuations of water levels in wells in New Mexico and Iowa: *Transactions of the American Geophysical Union*, Vol. 20, pp. 656-666.
- ROCKWELL INTERNATIONAL, 1980. Thermal and mechanical properties of Hanford basalts. *Publication R110-BW1-C-50*. Rockwell International, Richland, WA.
- SKEMPTON, A. W., 1954. The pore pressure coefficients A and B: *Geotechnique*, Vol. 4, pp. 143-147.
- TODD, D. K., 1980. *Groundwater Hydrology*. John Wiley and Sons, Inc., New York, NY, 535 p.



**DIVISION DE EDUCACION CONTINUA  
FACULTAD DE INGENIERIA U.N.A.M.**

MECANICA DE ROCAS APLICADA A LA MIENRIA Y A LA CONSTRUCCION

CONTROLS OF SUBDUCTION GEOMETRY, LOCATION OF MAGMATIC ARCS,  
AND TECTONICS OF ARC AND BACK-ARC REGIONS

MAYO, 1985

# Controls of subduction geometry, location of magmatic arcs, and tectonics of arc and back-arc regions

GOOD

Book review

LITHOSPHERIC DEFORMATION

TIMOTHY A. CROSS *Exxon Production Research Company, P.O. Box 2189, Houston, Texas 77001*  
REX H. PILGER, JR. *Department of Geology, Louisiana State University, Baton Rouge, Louisiana 70803*

## ABSTRACT

Most variation in geometry and angle of inclination of subducted oceanic lithosphere is caused by four interdependent factors. Combinations of (1) rapid absolute upper-plate motion toward the trench and active overriding of the subducted plate, (2) rapid relative plate convergence, and (3) subduction of intraplate island-seamount chains, aseismic ridges, and oceanic plateaus (anomalously low-density oceanic lithosphere) cause low-angle subduction. Under conditions of low-angle subduction, the upper surface of the subducted plate is in contact with the base of the overlying plate, wedge of low-density asthenosphere is displaced by subducted lithosphere, and the width of the arc-trench gap either is significantly increased or a magmatic arc is not developed within the overlying plate. The fourth factor is age of the subducting lithosphere. Subduction of young lithosphere produces two opposing tendencies: (1) low-angle subduction and increased arc-trench distance, owing to its low density; and (2) decreased arc-trench distance, owing to its higher temperature.

Two factors of secondary importance contribute to variation in subduction-zone geometry and arc-trench distance. Accretion of sediment in trenches depresses the upper portion of the subducting oceanic plate and causes the trench axis to migrate seaward. Prolonged subduction thickens the upper plate, depresses the isotherms in the subducted plate, and may create a broader arc. Both factors increase the arc-trench gap.

The four primary factors also control development of other tectonic elements, such as regional subsidence (for example, the Amazon basin and a portion of the Cretaceous Interior Seaway of western United

States), intra-arc extension (for example, the Basin and Range province), foreland fold and thrust belts, and Laramide-style tectonics.

## INTRODUCTION

Since Luyendyk's (1970) pioneer attempt to relate subduction-zone geometry to some fundamental aspect(s) of plate kinematics and dynamics, subsequent investigations have suggested an increasing variety and complexity among possible controls and resultant configurations of subduction zones. Most of these investigations have examined cause and effect relations of bivariate systems. For example, attractive but imperfect correlations have been reported between convergence rates and dip of the inclined seismic zone (Luyendyk, 1970; Tovish and Schubert, 1978), between the volume of sediment accreted along trenches and the width of the arc-trench gap (Dickinson, 1973; Karig and Sharman, 1975; Karig and others, 1976; Jacob and others, 1977), between the direction and rate of absolute upper-plate motion and presence or absence of back-arc spreading (Morgan, 1972; Chase, 1978a; Uyeda and Kanamori, 1979), and between dip of the inclined seismic zone and curvature of island-arc and trench systems (Frank, 1968; Tovish and Schubert, 1978).

This report describes the major factors which control the geometry of subducted oceanic lithosphere and analyzes the consequent variations in space-time distribution of magmatic arcs. We recognize four principal factors or variables which control the geometry of subduction zones, and we believe that most of the observed variations in subduction-zone geometry can be explained by the interaction among these variables. The major variables are relative

convergence rate, direction and rate of absolute upper-plate motion, age of the descending plate, and subduction of aseismic ridges, oceanic plateaus, or intraplate island-seamount chains. It is crucial to recognize that, in the natural system of the Earth, the major factors may interact and, therefore, are interdependent variables. Depending on the associations among them, in a historical and spatial context, their effects on the geometry of subducted lithosphere can be additive, or by contrast, one variable can act in opposition to another variable and result in total or partial cancellation of the normal effects of each variable acting independently.

The interaction of these variables produces observed variations in geometry of subduction zones, principally with respect to angle of subduction and the depth to which oceanic lithosphere has been subducted. In turn, subduction-zone geometry and its evolution through time is a principal control on the space-time distribution of magmatic arcs, as well as other major tectonic features, such as the elevation of the upper plate above subducted lithosphere, regional subsidence and consequent accommodation of sediment within continental interiors, the occurrence of Laramide-style tectonics and foreland fold-and-thrust-belt deformation, variations in the petrochemistry of subduction-related magma, and extension in back-arc and intra-arc regions.

## CONTROLS OF SUBDUCTION-ZONE GEOMETRY

To isolate the principal factors controlling subduction-zone geometry and to determine their interactive effects, we have examined the characteristics of contemporary subduction systems in which two or more of the possible variables are constant

This article is included in a set of papers presented at a symposium on "Subduction of oceanic plates," held in November 1979.

and only one or two are changing. We present selected examples of subduction systems which empirically demonstrate the major controls of subduction geometry, how those controls interact, and some of the consequences of those interactions. Although this approach has not yielded quantitative measures of the various effects related to isolated or combined controlling factors, it does provide estimates of the relative importance among the factors of each subduction system. Further, it provides a means of understanding departure of par-

ticular subduction systems from otherwise systematic relations observed in bivariate plots. For example, bivariate plots of convergence rates against inclination of the Benioff zone show a systematic trend for most subduction systems, but others plot well off the trend (for example, Tovish and Schubert, 1978). Often, the source of these discrepant values is related to other major factor(s), such as subduction of an aseismic ridge, modifying the effect of relative convergence rates.

The factors which control subduction-

zone geometry and the principal effects of each, acting independently, are summarized in Table I and shown schematically in Figure 1. The first four factors are regarded as primary controls, whereas the last two are subordinate in importance with respect to their influence on the geometry of the entire subduction system and on other geologic and tectonic responses to subduction processes. We propose that the four major controls and their effects constitute a general empirical model for understanding and interpreting the geometries, kinematics, and

TABLE I. FACTORS AFFECTING THE GEOMETRY OF SUBDUCTION ZONES

Factor	Possible effects	Contemporary examples	Associated phenomena
A. Convergence rate	Increased rate decreases angle of subduction, depresses isotherms, and increases width of arc-trench gap (1-4)	Trans-Mexican volcanic belt (COCO-NOAM). (3-5)	Increased rate increases down-dip length of clined seismic zone. (6, 7)
B. Absolute motion of upper plate	Increased motion toward the trench decreases angle of subduction. Arc-trench separation either increases or the arc is extinguished and a new arc develops 600 to 1,000 km inland from the trench. Slow or retrograde motion permits steeper subduction and seaward migration of the trench. (3, 4, 8, 9)	Trans-Mexican volcanic belt (COCO-NOAM) versus Central American arc (COCO-CARB). (3, 4, 5, 10)	Rapid overriding and low-angle subduction creates compressional stress regime in upper plate; crustal shortening (Cordilleran or Laramide style) results. Retrograde motion creates extensional stress regime in upper plate; back-arc and/or intra-arc extension results. (3, 4, 11-15)
C. Subduction of aseismic ridges, intraplate island-seamount chains, or oceanic plateaus	Reduced average density and consequent relative buoyancy of lithosphere reduces subduction angle. Very low-angle subduction is common. Volcanic arc is extinguished, but a new one may form 600 to 1,000 km inland from the trench. (4, 16-18)	Aseismic ridges: Nazca and Cocos Ridges. (4)  Intraplate seamount chains: Juan Fernandez Ridge, Louisville Ridge, and Kodiak-Bowie seamount chain. (4)	Buoyant lithosphere resists subduction. Increased area of interface increases coupling between upper and lower plates. Compressional stress regime usually is produced in upper plate, and basement-rooted thrusting (Laramide style) may result. Isostatic subsidence above subducted ridge creates pericratonal basins. (19) If absolute upper-plate motion is retrograde, back-arc spreading rate is retarded.
D. Age of descending plate	Young lithosphere is relatively buoyant and subducts at reduced angle. In various combinations with other factors, subduction of young lithosphere will cause volcanism to migrate trenchward, landward, or cease entirely. (4, 20-24)	Trans-Mexican volcanic belt (COCO-NOAM). (3-5, 24)  Andean arc (NAZC-SOAM and ANTA-SOAM). (4)  Sandwich arc (SOAM-SCOT).	Subduction of young lithosphere generally results in back arc and intra-arc compression. Subduction of old lithosphere generally results in back-arc and intra-arc extension. Down-dip length of inclined seismic zone decreases with decreasing age. (4, 7, 20, 21)
E. Accretion of sediment in trenches	Flattens the inclined seismic zone at shallow levels only. Arc-trench separation is increased by seaward migration of the trench (25-28)	Circum-Pacific and northern Indian Ocean arcs. (25, 26, 28)	Weight of accretionary prism depresses oceanic plate prior to subduction. (27)
F. Duration of subduction and age of arc(?)	Additive effects of accretion (E.) and depression of isotherms due to prolonged subduction of old lithosphere increases the arc-trench separation. (29, 30)	Circum-Pacific arcs. (3)	Thickens upper plate? (29)

References: (1) Luyendyk, 1970; (2) Tovish and Schubert, 1978; (3) Cross and Pilger, 1978a; (4) this report; (5) Molnar and Sykes, 1969; (6) Isacks and others, 1968; (7) W. J. Morgan, cited in Deffeyes, 1972; (8) Hyndman, 1972; (9) Moberly, 1972; (10) Jordan, 1975; (11) Burchfiel and Davis, 1975; (12) Brewer and others, 1980; (13) Morgan, 1972; (14) Chase, 1978a; (15) Uyeda and Kanamori, 1979; (16) Kelleher and McCann, 1976, 1977; (17) Pilger, 1977, 1981; (18) Isacks and Barazangi, 1977; (19) Cross and Pilger, 1978b; (20) Molnar and Atwater, 1978; (21) England and Wortel, 1980; (22) DeLong and Fox, 1977; (23) Pilger and Henyey, 1979; (24) Truchan and Larson, 1973; (25) Karig and others, 1976; (26) Karig and Sharman, 1975; (27) Worzel, 1976; (28) Jacob and others, 1977; (29) James, 1972; (30) Dickinson, 1973.



MEXICAN TECTONIC? SLICES MADE ORIENTAL

dynamics of modern and ancient subduction systems and their associated magmatic arcs. Thus, low-angle subduction results from combinations of: (1) rapid absolute upper-plate motion toward the trench, (2) rapid relative plate convergence, (3) subduction of anomalously low-density oceanic lithosphere, and (4) subduction of young oceanic crust. Ancillary effects of low-angle subduction include landward displacement of the magmatic arc or cessation of subduction-related magmatism, compressional tectonics within and behind the arc, and widespread subsidence in pericratonic regions. Normal or steeper subduction results from combinations of: (1) slow or retrograde absolute upper-plate motion, (2) slow relative plate convergence, and (3) subduction of normal-density and old oceanic lithosphere. Ancillary effects of steeper subduction include development of a magmatic arc close to the trench and extensional tectonics within and behind the arc.

The two factors, load of an accretionary prism and prolonged subduction, that we regard as subordinate to the other four have been suggested by others and are reviewed briefly here.

In a review of arc-trench systems, Karig and Sharman (1975) noted an empirical correlation between the width of the arc-trench gap and the volume (width) of accreted sediment and slices of oceanic crust along the inner margin of the trench. This correlation corresponds to a flattening of the inclined seismic zone at shallow depths between the trench axis and the front of the volcanic arc. Karig and others (1976) demonstrated that the width of this flattened portion of the inclined seismic zone is proportional to the arc-trench separation for most subduction systems. Several investigators have suggested or inferred that accretion of sediment and slices of oceanic crust along the inner trench slope loads and depresses the subducting plate, reduces the angle of subduction in the shallow section of the Benioff zone, and causes the trench axis to migrate seaward; the direct result is an increase in the arc-trench separation (for example, Karig and Mammerickx, 1972; Burk, 1972; Dickinson, 1973; Hamilton, 1973; Seely and others, 1974; Karig and Sharman, 1975; Jacob and others, 1977; Hamilton, 1978). Expanding upon these suggestions, Worzel (1976) showed that the weight of the accretionary prism was sufficient to depress the subjacent lithosphere isostatically. From observed geological and geophysical data and from mathematical

modeling of the load applied by accreted material, Karig and others (1976) concluded that the geometry of the upper, shallow segment of the inclined seismic zone is controlled by the load of the accretionary prism on the subducting plate. Accretionary processes are dependent on the relative balance between rates of convergence and sediment supply. Under rapid-convergence situations, which independently induce flattening of the Benioff zone, accretion is rapid and is principally tectonic in origin. Under slow-convergence situations, tectonic accretion is slow, but sedimentary filling or accretion is variable and depends on the rate of sediment supply. Hamilton (1978, 1979) observed that large accretionary

prisms are formed only when voluminous sediments are carried to or are otherwise available on the subducting ocean floor. Inasmuch as accretionary loading affects the subducting plate only in the region between the inner slope of the trench and the upper-slope discontinuity (Karig and others, 1976), the geometry and dip of the remainder of the subducting plate are independent of the effects of loading. Through this reasoning, we regard accretionary loading as subordinate to the other four factors in controlling the geometry of the entire subduction zone.

The second factor which may act as a subordinate control of subduction-zone geometry is that of prolonged subduction of

PRINCIPAL CONTROLS ON GEOMETRY OF SUBDUCTED LITHOSPHERE

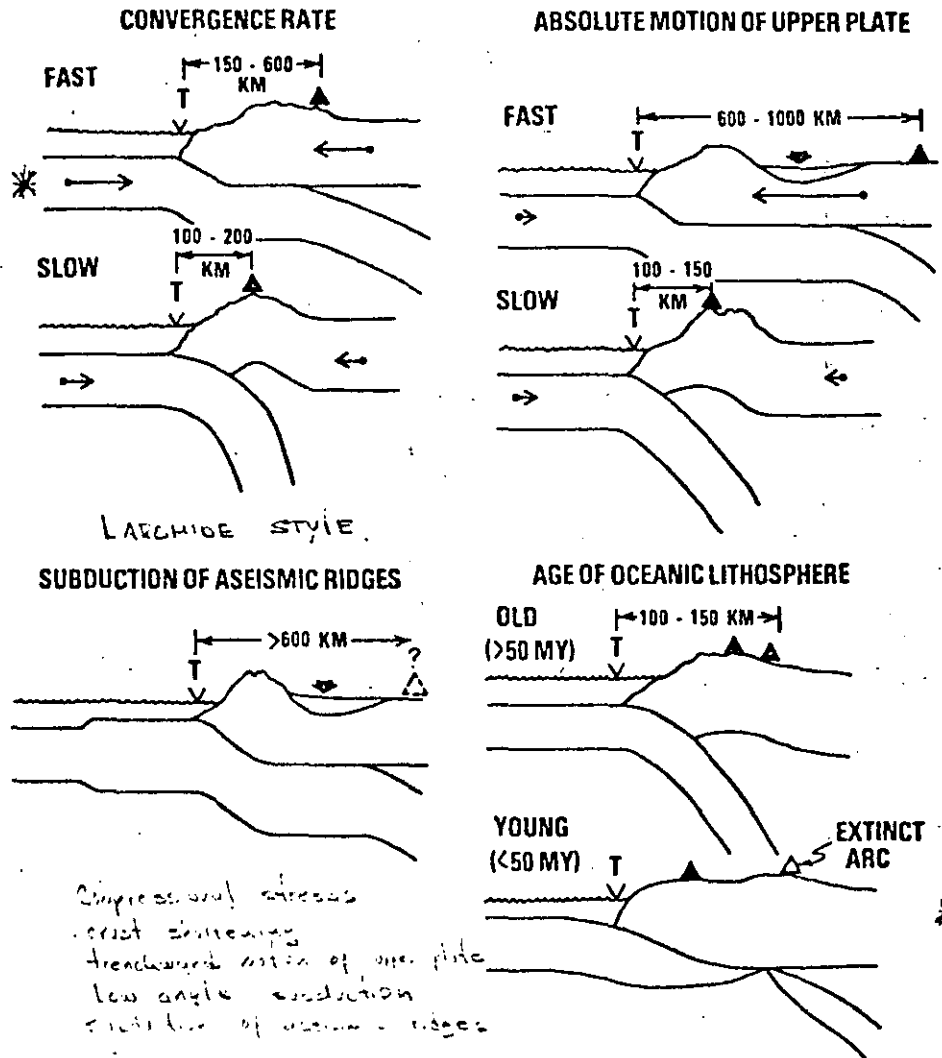


Figure 1. Schematic illustration of the subduction model, showing the effects of each major control acting independently. Drawn approximately to scale. Only subduction of oceanic lithosphere beneath continental lithosphere is considered. Solid triangles indicate positions of volcanic arcs. "T" indicates position of trench axis. Lengths of arrows are proportional to velocities of plates in a direction normal to strikes of trenches.

oceanic lithosphere. James (1971) suggested that prolonged subduction of cold oceanic lithosphere depresses isotherms within the subducting plate and the overlying mantle. Consequently, the zone of magma generation is displaced downward and laterally away from the trench, such that it underlies portions of the overlying plate at progressively greater distances from the trench and a broader arc is created. James also inferred, and Dickinson (1973) suggested, that this effect may be augmented by gradual thickening of the overlying plate through accretion of subduction-related volcanic and plutonic rocks. A crude, empirical correlation between crustal thickness and separation of the arc and trench, as well as duration of subduction and arc-trench separation, was shown by Dickinson (1973). We have not been able to extend these observations beyond an empirical level nor to incorporate the possible effects of prolonged subduction into the subduction model for two principal reasons. First, as Dickinson (1973) noted, it is usually difficult to determine whether increased arc-trench separation is the result of accretion (seaward trench motion), prolonged subduction (continentward arc motion), or of a combination of the two. Second, and more importantly, these empirical correlations are necessarily derived from study of older and often inactive subduction systems. In these instances, it is not possible to unequivocally demonstrate that the arc-trench separation is the product of prolonged subduction plus accretion, or of another cause, such as angle of subduction, which is controlled by the other four principal factors.

#### Relative Convergence Rates

Luyendyk (1970) first proposed an inverse correlation between convergence rate and angle of subduction. This relation was based on examination of four arc-trench systems in the western Pacific. More recently, Tovish and Schubert (1978) demonstrated that, when more arc-trench systems were included in such an analysis, the inverse relation between convergence rate and inclination of the subducting plate was exhibited by some arc-trench systems, but other systems did not conform to the anticipated relation. In addition, they observed that dips were constant throughout the length of each of five subduction zones, although the convergence rates varied by as much as 2.7 cm/yr along a single system. These exceptions to the general relation observed by Luyendyk (1970) are important in that they

ing controls on subduction-zone geometry. Acting independently, convergence-rate variation is presumed to control the dip of the inclined seismic zone and, consequently, the arc-trench separation in the following manner. Oceanic lithosphere is metastable because it is denser than the underlying asthenosphere. Under constant conditions of slow relative convergence, gravitational force predominates, the plate descends at a steep angle, and the separation of the volcanic arc and trench is small. By contrast, fast relative convergence results in a lesser component of gravitational sinking, smaller angle of subduction, wider spacing and depression of isotherms, and wider arc-trench separation.

One region that exhibits the effects of variation in relative convergence rates is along the Middle American trench where the Cocos plate is subducting beneath the North American plate (Fig. 2). Relative convergence rates increase from ~5.5 cm/yr in the north to ~7.0 cm/yr in the south along the trench, a consequence of close proximity to the relative-motion pole (Minster and others, 1974). Absolute motions of the North American and Cocos plates are almost invariant along the subduction boundary. The age of the Cocos plate increases from north to south along the trench. As predicted by the subduction model, the arc-trench distance increases progressively from north to south, corresponding to increasing relative convergence rates. The influence of age variation of the Cocos plate on subduction-zone geometry and arc-trench distance is discussed subsequently. At this stage, it is sufficient to note that increased arc-trench distance associated with subduction of progressively younger and relatively more buoyant oceanic lithosphere is not observed along the Middle American trench.

#### Absolute Plate Motion

Absolute plate motion, particularly that of the upper plate, is a second major control of subduction-zone geometry. It is not readily apparent that absolute motion of one or more plates can be treated or expressed differently than relative motions of the same plates. Nor is it readily apparent that absolute motions of two plates along a convergence boundary produce physical changes in the configuration of the subduction zone that are conceptually independent of the configuration induced by relative motions, that is, by relative convergence rates. Because motions of lithospheric plates along

lute and relative components, the two controls are always interdependent and only rarely can their independent effects on subduction-zone geometry be ascertained.

In contrast to relative plate motions, which are described by angular rotations about geometrically constructed poles of relative motion, absolute plate motions are described relative to some external (independent) reference, such as the Earth's center or axis of rotation, which is presumed fixed or which is stationary compared to relatively rapid motions of lithospheric plates. A common way of determining vectors (or angular rotations) of absolute plate motion is with respect to the hot-spot reference frame, assuming it is stationary over tens of millions of years, relative to rapid motions of lithospheric plates (for example, Minster and others, 1974; Molnar and Francheteau, 1975). One can also regard material in the asthenosphere as moving diffusely and more slowly than the overlying lithosphere (Jacoby, 1970; Elsasser, 1971). In this case, the deep mantle is nearly stationary, and motion of lithosphere relative to the deep mantle may be defined as absolute plate motion.

Along a convergence boundary, absolute motions of the adjacent plates may augment, leave unchanged, or oppose the physical effects on subduction-zone geometry induced by relative convergence rates. In order that the absolute motion of a plate may influence or control subduction-zone geometry independently of relative plate motion, the lithosphere must not be coupled directly to asthenosphere flow, at least along a wide margin parallel to the convergence boundary. This assumption is implicit in our analysis. The relative influence or dominance of the two controls is most directly related to the absolute motion of the upper plate. As noted by Solomon and others (1975), all subducting plates advance toward the trench in an absolute-motion frame, whereas upper plates move at varying rates and directions toward and away from convergence boundaries in the absolute-motion frame. On the basis of this difference, we argue that the absolute motion of the upper plate dominates over relative convergence rates in controlling the geometry of subduction zones.

Absolute upper-plate motion controls the geometry of subduction zones dynamically by modifying the effects induced by gravitational sinking of subducting lithosphere. Rapid absolute upper-plate motion toward the trench causes active overriding of the trench and the subduction zone, reduced

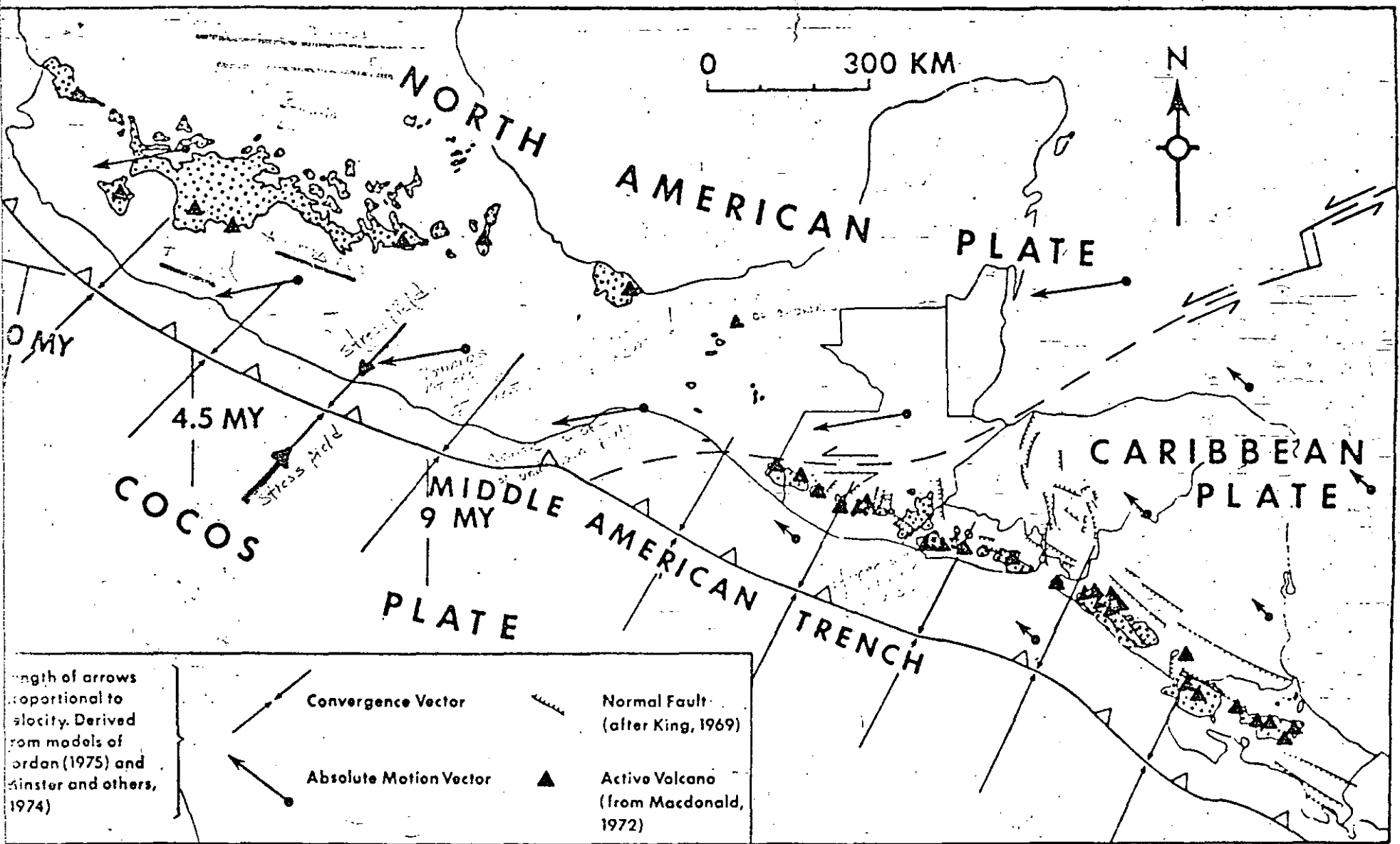


Figure 2. Plate-tectonic setting of Middle America, showing absolute motion of the North American and Caribbean plates and the relative motion of the North American, Caribbean, and Cocos plates, as determined by Minster and others (1974) and Jordan (1975). Plate boundaries modified from Molnar and Sykes (1969). Area of normal

faulting, positions of active volcanoes (▲), and Quaternary volcanic rocks (stippled pattern) are indicated. Age of Cocos plate in millions of years, as interpreted from magnetic anomalies, also shown.

subducting lithosphere, and consequent formation of a shallowly inclined subduction zone (Hyndman, 1972; Moberly, 1972). The major consequences are landward displacement of the volcanic arc or, in some cases, cessation of magmatism along the former arc and development of a new arc several hundred kilometres away from the trench (Cross and Pilger, 1978a). With slow absolute upper-plate motion toward the trench, gravitational sinking of the subducting lithosphere predominates and results in a more steeply inclined subduction zone, oceanward migration of the trench relative to the upper plate, and a narrow arc-trench separation (Moberly, 1972). Retrograde (away from the trench) absolute motion of the upper plate exerts little or no control on the geometry of the subduction zone, and the angle of descent is determined by the interaction of the other major controls and gravitational sinking of the subducted lithosphere. The contrast between generally steeply dipping, westward-verging subduction zones of the western Pacific and moderately dipping, eastward-verging subduction zones of the eastern Pacific (for example, Isacks and Barazangi, 1977) may reflect control by differences in absolute upper-plate motions. In the western Pacific, upper-plate absolute motion is retrograde or highly oblique with respect to strikes of trenches. By contrast, in the eastern Pacific, the North and South American plates are overriding the trenches in the absolute-motion frame (Morgan, 1972; Minster and others, 1974; Chase, 1978b).

The convergence boundary along Mexico and Central America provides a rare example where the effects of upper-plate absolute motion are distinguishable from the other major controls on the geometry of subduction zones. Along the Middle American trench, the Cocos plate subducts beneath two plates, the North American and the Caribbean (Fig. 2). In the vicinity of the three-plate boundary, the age of the Cocos plate is essentially constant (Herron, 1972) and the rates of relative convergence between the Cocos-North American and Cocos-Caribbean plate pairs are comparable. Of the four major controls on subduction-zone geometry, only the absolute motions of the upper plates are radically different. Whereas, in an absolute-motion frame, North America is overriding the Middle American trench (for example, Minster and others, 1974), the Caribbean plate is moving slowly subparallel to and slightly away from the trench (Jordan, 1975;

Chase, 1978b). As discussed previously, the arc-trench distance increases progressively from north to south in Mexico. A minor gap in active arc volcanism and a substantial offset of the volcanic arc toward the trench occur at the boundary between the North American and Caribbean plates (Fig. 2). Southward from that boundary, the volcanic arc in Central America is parallel to the trench, and the arc-trench separation is narrow and constant. The sudden narrowing of the arc-trench gap reflects contrasting absolute motions of the North American and Caribbean plates. The subduction model predicts shallow subduction of the Cocos plate beneath North America where the North American plate is overriding the trench. Conversely, the Cocos plate should descend at a steeper angle beneath the Caribbean plate where the upper plate is nearly stationary in the absolute-motion frame. Observations of earthquake foci distributions in this region support these predictions; the inclination of the seismic zone is steeper beneath the Caribbean plate than beneath the North American plate (Molnar and Sykes, 1969, Figs. 10 and 11).

#### Subduction of Aseismic Ridges, Oceanic Plateaus, and Island-Seamount Chains

Aseismic ridges, oceanic plateaus, and intraplate island-seamount chains of various origins stand as topographic prominences or as broad, topographically positive areas relative to surrounding oceanic crust. By virtue of the anomalous crust and mantle which underlie them, they are likely to produce anomalous effects on the configuration of subduction zones when subducted.

Aseismic ridges apparently form synchronously with adjacent oceanic crust, as indicated by DSDP data (Sclater and Fisher, 1974), subsidence curves (Detrick and others, 1977), isostatic gravity anomalies (Kogan, 1979; Detrick and Watts, 1979; Watts and others, 1980), and plate reconstructions (Pilger and Handschumacher, 1981). Kelleher and McCann (1976, 1977) reviewed evidence supporting the presence of anomalously thick crust or "structural roots" beneath aseismic ridges. Subsequent studies, based on gravity, seismic refraction, and isostatic modeling, have recognized that anomalously thick crust is characteristic of aseismic ridges and oceanic plateaus (Kogan, 1979; Detrick and Watts, 1979). Kelleher and McCann (1976, 1977) suggested that the increased thickness of oceanic

crust beneath aseismic ridges reduces the average density of the lithosphere such that lithosphere bearing an aseismic ridge is no longer gravitationally unstable. Consequently, as oceanic lithosphere bearing an aseismic ridge or oceanic plateau encounters a convergence boundary, it is buoyed up in the subduction zone, and low-angle subduction ensues. Alternatively, the ridge may accrete to the upper plate and a new subduction zone may develop outboard of the ridge. Because aseismic ridges are the same age as surrounding oceanic crust, little or no thermal contrast exists between the ridges and adjacent oceanic crust, and the buoyancy of ridges relative to adjacent crust is unlikely to be age-dependent. It is the *difference* in average density of lithosphere bearing aseismic ridges versus that of normal lithosphere that is critical in assessing the relative buoyancy of the ridge.

It is difficult to predict how deeply the buoyancy effect should persist. Experimental evidence, summarized by Ahrens and Schubert (1975), suggests that oceanic crust should transform to much denser eclogite in the depth interval of 40 to 80 km. Such a transformation of anomalously thick crust should increase the density contrast between oceanic lithosphere and asthenosphere and should reinforce the gravitational instability of the descending plate. Assuming that this transformation occurs, the experimental work predicts that aseismic ridges and oceanic plateaus should subduct at steeper angles than normal oceanic plates, owing to their greater average density. This prediction differs from observed relations; we consider possible resolutions of this discrepancy subsequently.

In contrast with aseismic ridges, island-seamount chains form in an intraplate position subsequent to formation of surrounding lithosphere and in association with a thermal anomaly of uncertain origin (for example, Morgan, 1972; Jarrard and Clague, 1977; Watts and others, 1980). As a consequence of their intraplate origin, island-seamount chains lack a substantially thickened crustal root; any increase in crustal thickness of such chains is confined to the volcanic edifice built on the sea floor. The thermal anomaly responsible for the chains also produces a decrease in density, thickness, or both, of the lithosphere beneath young chains. This response is manifested in a distinctive thermal swell of lithosphere adjacent to individual edifices (Crough, 1978; Detrick and Crough, 1978).

Consequently, lithosphere containing an island-seamount chain has an average density lower than that of normal oceanic lithosphere and is relatively more buoyant. The thermal anomaly associated with the formation of an island-seamount chain decays with age of formation of the chain (Detrick and Crough, 1978). Thus, lithosphere bearing island-seamount chains increases in thickness, average density, and gravitational instability as a function of age from the time of chain formation in a manner similar to that observed for lithosphere generated at spreading ridges (Parker and Oldenburg, 1973).

Despite their different origins, both aseismic ridges and intraplate island-seamount chains represent density anomalies in oceanic plates, and both are relatively

more buoyant than normal lithosphere. However, all aseismic ridges and intraplate island-seamount chains are not equally buoyant. Differences in relative buoyancy arise from differences in absolute age, contrast in age with respect to adjacent lithosphere, size, and crustal thickness. Upon subduction, the buoyancy effect for both normal oceanic lithosphere and lithosphere which includes an island-seamount chain is likely to be age dependent. That is, old lithosphere and old island-seamount chains have a less pronounced buoyancy effect than young lithosphere and young island-seamount chains. This relation conforms with tentative conclusions that young oceanic lithosphere subducts at lower angles than old lithosphere (DeLong and Fox, 1977; Molnar and Atwater, 1978).

Subduction of aseismic ridges produces the most dramatic effects on the configuration of subduction zones in the eastern Pacific, where lithosphere generally is young, where aseismic ridges are continuous and well developed, and where upper plates are overriding the subduction zone in the subduction zone in the absolute-motion frame. By contrast, in the western Pacific, where lithosphere generally is old, where aseismic ridges are thinner and discontinuous, and where upper plates are retreating from trenches in the absolute-motion frame, the effects of aseismic-ridge subduction are limited to retarded back-arc spreading and to slight decrease in the inclination of the subducting plate (Vogt and others, 1976; Isacks and Barazangi, 1977). These relationships are considered in the following analyses of four subduction systems.

**Nazca and Juan Fernandez Ridges.** Studies of earthquake-hypocenter distribution have demonstrated that the Nazca plate is subducting beneath South America at angles of  $25^{\circ}$  to  $30^{\circ}$  in the intermediate to deep zone along most of the convergence boundary (Isacks and Molnar, 1971; Stauder, 1973, 1975; Barazangi and Isacks, 1976, 1979; Isacks and Barazangi, 1977). Except for two conspicuous breaks, Quaternary stratovolcanoes form a continuous volcanic chain along the western margin of the Andes above what Barazangi and Isacks (1976) interpreted as the line of contact between the upper surface of the descending Nazca plate and the overlying wedge of partially molten asthenosphere. The gaps in recently active volcanism occur in northern and central Peru and central Chile and coincide with positions of very low-angle ( $<10^{\circ}$ ) subduction of the Nazca plate in the intermediate depth interval (Fig. 3; Barazangi and Isacks, 1976). Barazangi and Isacks (1976) attributed the absence of vol-

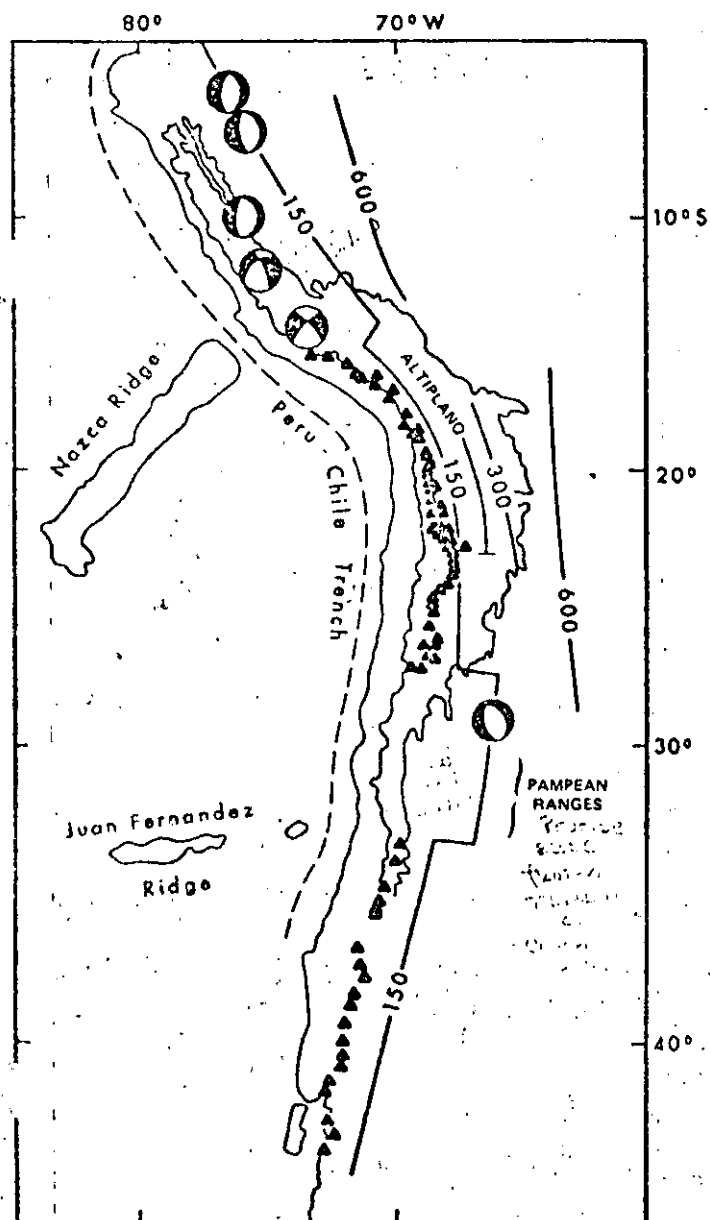


**Figure 3.** Peru-Chile subduction zone. Contours (in kilometres) on top of inclined seismic zone and location of active volcanoes from Barazangi and Isacks (1976) and Isacks and Barazangi (1977). Focal-mechanism solutions of shallow earthquakes within the South American plate from Stauder (1973, 1975). All indicate horizontal, east-west compression. Centers of shaded quadrants are the P axes; centers of unshaded quadrants are T axes. Thin solid line is 3-km topographic contour; note inverse correlation between width of Andes and dip of the inclined seismic zone.

canism in these two regions to displacement of the wedge of partially melted asthenosphere by the very low-angle subducting lithosphere and consequent direct superposition of two lithospheric plates. At the sites of very low-angle subduction, the Andes form a narrow, near-coastal mountain range instead of a broad, high plateau (for example, the Altiplano of the central Andes). Earthquakes with compressional focal mechanisms within the western South American plate are restricted to the sites of very low-angle subduction and are absent or undetected in segments of steeper ( $\sim 30^\circ$ ) subduction (Fig. 3; Stauder, 1973, 1975). Additional evidence for compressional stress in continental crust overlying a low-angle subduction segment occurs 500 km east of the Peru-Chile trench where the Argentine Pampean ranges comprise a reverse-block-faulted terrane of late Cenozoic age (Fig. 3; Stoll, 1964).

It is possible to qualitatively resolve the relative contributions of those factors which control the geometry of the subducted lithosphere beneath western South America, particularly the configuration of the two anomalous, very low-angle subduction segments. Relative convergence rate is essentially constant at  $\sim 11$  cm/yr along the South American-Nazca plate boundary (Minster and others, 1974), as is the age of the Nazca plate (about 41 to 46 m.y. B.P. at the Peru-Chile trench between  $35^\circ\text{S}$  and  $15^\circ\text{S}$  latitudes; Pitman and others, 1974). Absolute motion of each plate is constant, with South America moving toward the trench at about 2.2 cm/yr and the Nazca plate advancing toward the trench at about 9.3 cm/yr (Minster and others, 1974; Chase, 1978a, 1978b). Moderate-angle ( $\sim 30^\circ$ ) subduction characteristic of most of the convergence boundary, in all probability, is attributable to the effects of rapid convergence, overriding of the trench by the South American plate, and the relative youth of the subducting Nazca plate. Other factors which may affect subduction-zone geometry on a global scale also may contribute to moderate-angle subduction along South America in comparison to generally steeper inclinations of subduction zones having westward vergence. These include hydrodynamic forces (Jischke, 1975), and tidal drag (Bostrom, 1971; Nelson and Temple, 1972; Bostrom and others, 1974), although Jordan (1974) has argued that tidal forces are inadequate to significantly influence plate motions.

The major factors responsible for the two very low-angle subduction segments along the Peru-Chile trench, as well as the associated gaps in Quaternary volcanism along the Andean chain, are subduction of the Nazca Ridge opposite southern Peru and the Juan Fernandez seamount chain opposite central Chile. Barazangi and Isacks (1976) and Isacks and Barazangi (1977) noted the correspondence between subduction of the Nazca ridge and the anomalous low-angle subduction segment beneath Peru. Pilger (1977, 1981) expanded upon and documented this observation and suggested that this correspondence reflected a fundamental genetic relationship. He suggested that the Nazca and Tuamotu Ridges were generated contemporaneously by a single source, such as a "hot spot" (Easter Island mantle plume of Morgan, 1972) or other fundamental process, centered on or near the symmetrically spreading Nazca-Pacific Ridge. Pilger concluded that the geometry of the subducted portion of the Nazca Ridge could be reconstructed by assuming it was initially a mirror image of the Tuamotu Ridge. Using plate reconstructions and the assumption of initial mirror imagery, Pilger mapped the successive posi-

tions of the Nazca ridge beneath South America and demonstrated that the very low-angle subduction segment and other geologic features in Peru correspond in time and space to progressive subduction of the Nazca Ridge (Fig. 4). Thus, we conclude that thickened oceanic crust beneath the Nazca Ridge and consequent reduction in average lithospheric density has caused low-angle subduction beneath Peru.

In addition, Pilger (1981) showed that if an off-ridge "hot-spot" origin for the Juan Fernandez seamount chain is assumed, the plate reconstructions place the subducted portion of that chain in the zone of very low-angle subduction beneath central Chile. Buoyancy of the lithosphere beneath the Juan Fernandez Ridge, owing to its relative youth, is proposed as the mechanism producing the central Chilean low-angle subduction segment.

There is an apparent difficulty with the buoyancy hypothesis for aseismic ridge subduction that requires resolution. In the case of the Nazca Ridge, we observe that low-angle subduction extends to a depth of 150 km, well in excess of the 40- to 80-km depth at which the transformation of crust to eclogite is expected from experimental

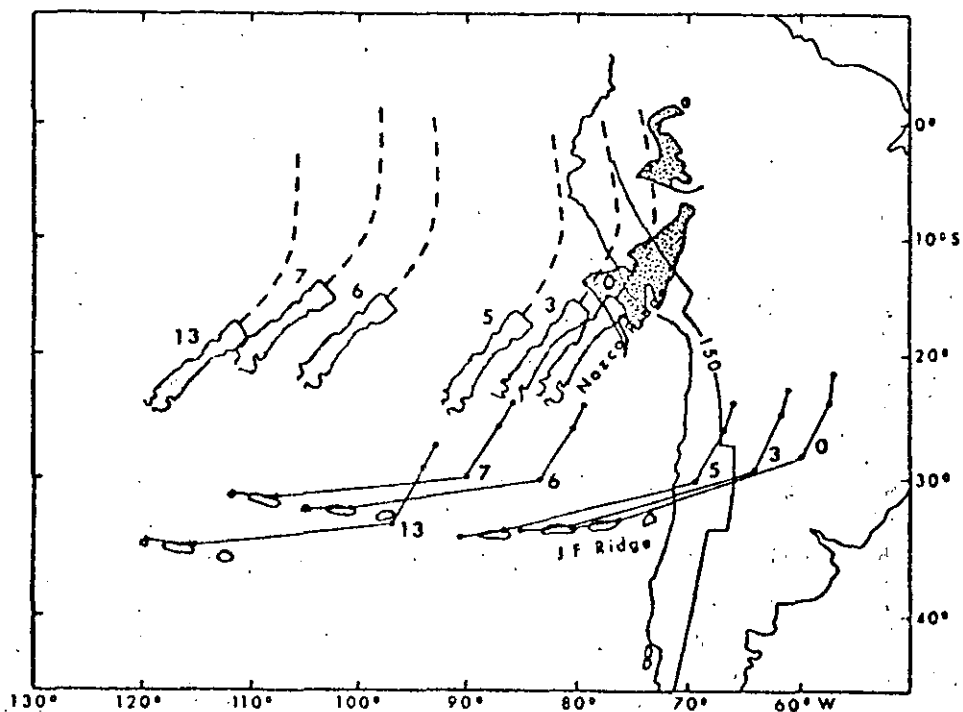


Figure 4. Reconstruction of the relative positions of the Nazca and South American plates at 0, 4.2, 9, 19.5, 25.5, and 35.6 m.y. B.P. (corresponding magnetic-anomaly numbers shown by numerals in parentheses). Outline of subducted portion of Nazca Ridge is shown by stippled pattern, assuming mirror-image symmetry with the Tuamotu Ridge. Modified from Pilger (1981).

ta (Ahrens and Schubert, 1975). The absence of steeper subduction in the vicinity of the Nazca Ridge projection indicates, by contrast, that either the transformation to eclogite has not occurred or that the basaltic component, which presumably would transform to eclogite, is absent from the subducted segment. The first postulation might be explained by low initial abundance of volatiles within the oceanic crust which are necessary to catalyze the transformation. Alternatively, the crust of the aseismic ridge may be sheared away from the mantle portion of the descending plate at shallow depths. Such an event was suggested by Nur and Ben-Avraham (1981) in another context. If phase transformation of basaltic crust to eclogite is the norm and is responsible for the increase in angle of dip typically observed in subduction zones involving "normal" oceanic lithosphere, then absence of transformed oceanic crust (that is, subducted lithosphere consisting only of peridotitic mantle) could result in reduced average density and low-angle subduction.

Both of these alternative hypotheses are speculative. Direct evidence is lacking for possible existence of sheared-off aseismic-ridge crust along the Peruvian segment of low-angle subduction. However, there is indirect evidence that such events may occur (see also Nur and Ben-Avraham, 1981). In the Oregon Coast Range, an apparent aseismic-ridge terrane was identified by Simpson and Cox (1977). They cited the evidence indicating that this tectonically anomalous element formed as oceanic crust and seamounts and postulated that an aseismic ridge or island-seamount chain was sheared off the subducting Farallon plate and was accreted to North America.

Physical separation, by shearing or other mechanism, of subducted aseismic-ridge crust from the subjacent mantle provides an explanation, alternative to that of Barazangi and Isacks (1976), for the corresponding absence of arc volcanism. Anderson and others (1976) suggested that dehydration of subducted oceanic crust may provide the water necessary to partially melt asthenosphere or the peridotitic mantle at the base of the upper plate. However, subducted lithosphere consisting only of peridotite mantle would be depleted in free water relative to normal oceanic lithosphere and would be relatively stable at shallow depths ( $\leq 150$  km). Consequently, dehydration of subducted mantle lithosphere would not occur and water would not be released. Altern-

tively, the absence of subducted oceanic crust would preclude partial melting of amphibolitic or eclogitic material, a mechanism that Green and Ringwood (1968) and Marsh (1976) have proposed for generation of andesitic magma along "normal" subduction zones.

**Cocos Ridge.** The subduction boundary separating the Caribbean and Cocos plates provides another example of the influence of a young aseismic ridge on the configuration of the subducting plate. Absolute motions of the two plates were discussed previously; relative convergence rate along the boundary is approximately constant at about 7.5 cm/yr (Jordan, 1975). The age of the Cocos plate as it enters the trench is

approximately constant from about 15 m.y. B.P. in the northwest to about 20 m.y. B.P. in the southeast, the region of principal concern (Fig. 5; Hey and others, 1977). Hey (1977) and Hey and others (1977) described the evolution of the Cocos-Nazca spreading ridge and of the Cocos plate. They concluded that the Cocos Ridge was generated by a "hot-spot" or other fundamental process centered on the Cocos-Nazca spreading center. Thus, the Cocos Ridge is the same age as the relatively young Cocos plate. The subduction model predicts that the Cocos plate should be relatively buoyant where the Cocos Ridge intersects the Central American trench and that it should subduct at a much reduced angle; magmatism should

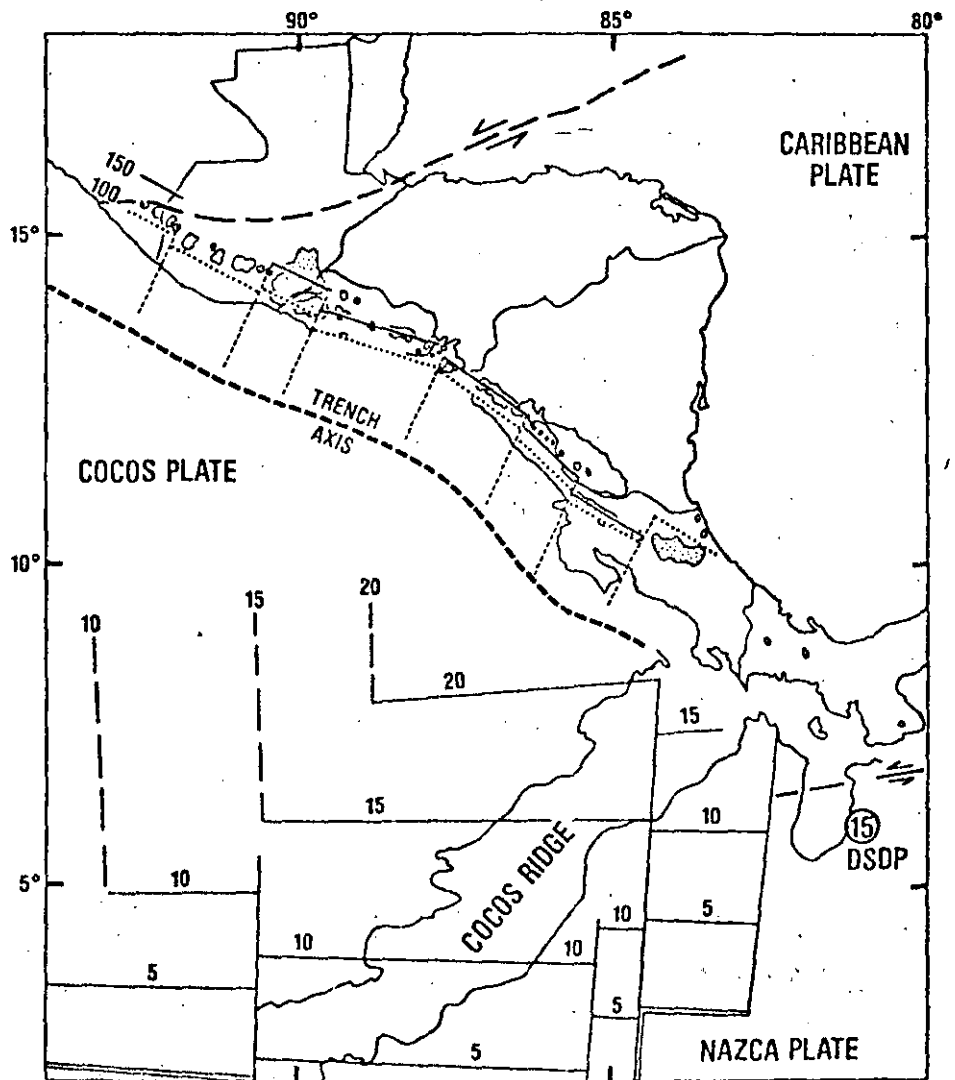


Figure 5. Plate-tectonic setting of the Central American volcanic arc. Active and Quaternary volcanoes (stippled pattern) from Macdonald (1971). Age of Cocos plate (in m.y. B.P.) from Hey and others (1977). 150-km (solid line) and 100-km (dotted line) contours on top of inclined seismic zone and segments of subducted lithosphere (dashed lines) from Carr and others (1979).

either cease or be displaced significantly from the trench axis. Carr and others (1979) summarized the observed relations between Quaternary volcanism and dip of the inclined seismic zone in Central America and documented the segmented nature of the subducting plate. From the triple-plate boundary at the northwest to the point of intersection of the Cocos Ridge and the trench, the subducted plate dips between  $45^\circ$  and  $60^\circ$  within the intermediate depth interval (Figs. 5, 6). Within the same region, the axis of the continuous Quaternary volcanic chain is parallel to and situated 150 to 200 km away from the trench. In central Costa Rica, immediately north of the intersection of the Cocos Ridge and Central American trench, the dip of the Benioff zone in the intermediate depth interval is abruptly and substantially reduced and the volcanic axis is displaced landward (Figs. 5, 6). Farther to the southeast, opposite the Cocos Ridge, historically active volcanoes are absent. In summary, moderate-angle subduction in the intermediate depth interval from Guatemala to Costa Rica is a product of relatively low convergence rate, absence of an actively overriding upper plate, and subduction of young lithosphere. The notable decrease in dip of the Benioff zone and the abrupt cessation of volcanism occur in the region where the aseismic Cocos Ridge intersects the trench, while all other factors presumed to control the geometry of the subducted lithosphere remain constant. A complicating factor in the analysis of the Cocos Ridge requires mention. Lonsdale and Klitgord (1978) suggested that the ridge has only recently ( $< 1$  m.y. B.P.) encountered the Middle America trench, so that the observed seismic effects may not be representative of prolonged subduction of an aseismic ridge.

**Kodiak-Bowie Seamount Chain.** Subduction of intraplate island-seamount chains affects the geometry of the subducted plate in a manner similar to that of subduction of aseismic ridges. However, for the reasons discussed previously, the changes are not always as dramatic. One region suitable for observing the effects of subduction of seamount chains is the Pacific-North American plate boundary along the Aleutian trench. Convergence rates are nearly uniform over the length of the Aleutian trench, from about 7 cm/yr on the west to about 6 cm/yr on the east (Fig. 7; Minster and others, 1974). In the absolute-motion frame, North America is moving to the southwest at about 2.3 cm/yr (Minster and others,

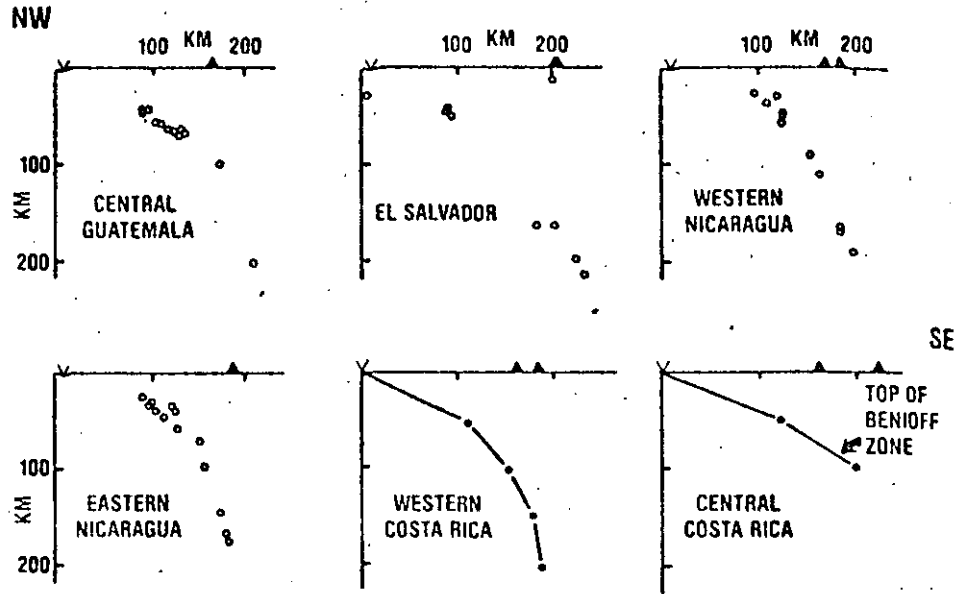


Figure 6. Cross sections normal to the trench axis of segments along the Central American subduction zone. Compiled from Carr (1976), Carr and others (1979), Stoiber and Carr (1973), and Molnar and Sykes (1969).

1974); Chase, 1978a, 1978b Uyeda and Kanamori, 1979), thus contributing a slow, strongly oblique (with respect to the strike of the trench) component to the relative motion. The age of the Pacific plate as it

enters the trench also is remarkably uniform at about 45 m.y. B.P. (Pitman and others, 1974).

The Aleutian Islands and the Alaskan Peninsula comprise a continuous volcanic

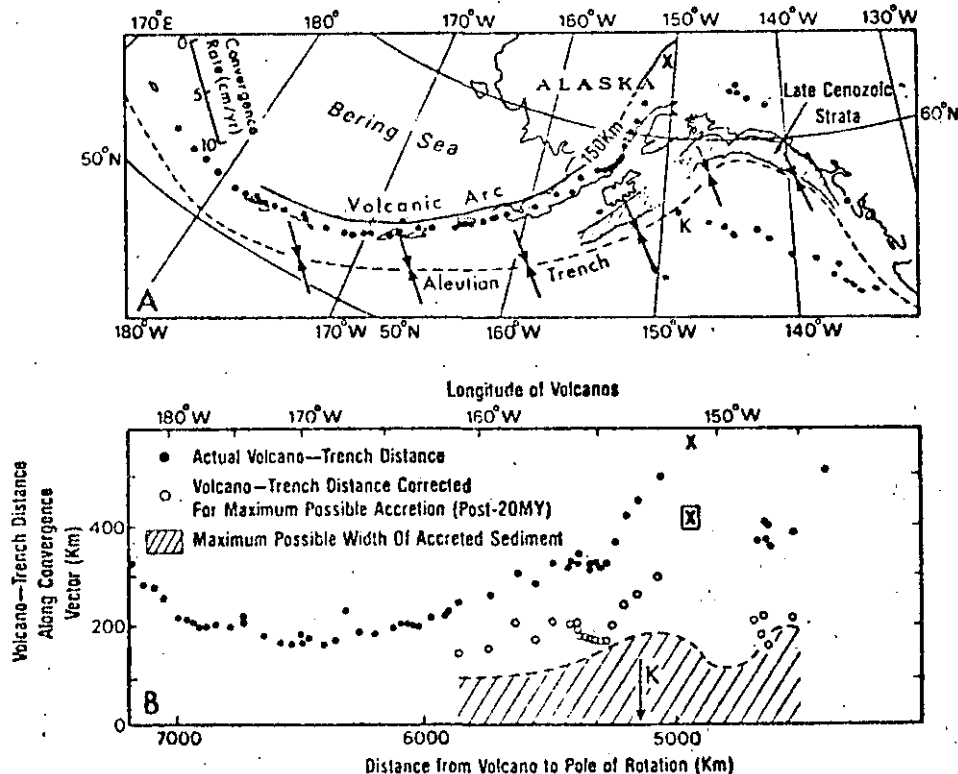


Figure 7. Plate-tectonic setting of Aleutian and Alaskan volcanic arc. 150-km contour on top of inclined seismic zone, locations of volcanoes (solid circles), and maximum width of accreted sedimentary prism since the Miocene (diagonal-lined pattern), from Jacob, Nakamura, and Davies (1977). Positions of the Kodiak seamount and Mount McKinley are indicated by "K" and "X" respectively.



in north of the Aleutian trench. The arc-trench separation increases progressively from west to east, from a minimum of about 170 km to a maximum of about 570 km in the Gulf of Alaska region (Fig. 7). The horizontal separation between the trench and the 150-km contour of the top of the inclined seismic zone (as projected to the surface) also increases from west to east, reflecting the gradual decrease in dip of the subducting plate. Jacob and others (1977) showed a correlation between the increase of the arc-trench distance and the width of the accreted sedimentary prism on the leading margin of the North American plate. They attributed much of the increase in arc-trench distance and the gradual decrease in dip of the subducting plate at shallow levels (<100 km) to accretion of the sedimentary prism since the mid-Miocene. The maximum estimated widths of the accretionary prism vary from 100 to 200 km in the Gulf of Alaska region. Removal of these values, equivalent to correcting for the maximum amount of increase in arc-trench distance attributable to post-mid-Miocene accretion, makes the arc-trench distance uniform along most of the subduction boundary (Fig. 7; Jacob and others, 1977).

Even with this correction, a major anomaly, in the form of an abrupt increase in the arc-trench separation and a decrease in the dip of the subducting plate, occurs in the region of intersection of the Kodiak-Bowie seamount chain and the trench. This anomaly also corresponds with a conspicuous gap in the volcanic chain centered about the Mt. McKinley region. Despite the absence of Quaternary volcanism, a well-developed inclined seismic zone lies beneath this region to depths greater than 150 km. The strike of the Kodiak-Bowie seamount chain is oblique to the magnetic-anomaly patterns of the northeastern Pacific. Isotopic ages of samples collected from several seamounts show an age progression from ~23 m.y. B.P. at Kodiak seamount to Recent at Bowie seamount in the southeast (Turner and others, 1973; Jarrard and Clague, 1977). These ages are considerably younger than the ages of the surrounding sea floor (Pitman and others, 1974) and indicate that the seamount chain was generated by an off-ridge "hot spot" or other process unrelated to crustal formation along spreading ridges.

We attribute this anomalous region of shallow subduction and absence of volcanism to subduction of an intraplate island-

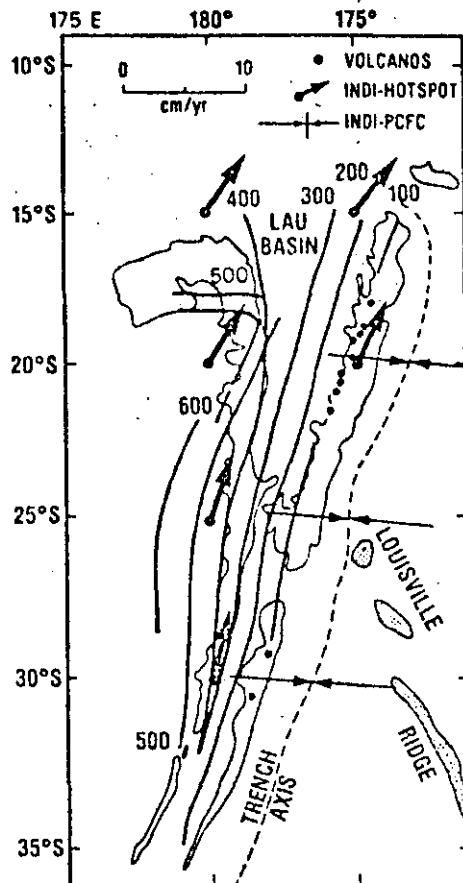


Figure 8. Plate-tectonic setting of Tonga-Kermadec subduction zone. Contours on top of inclined seismic zone (in kilometres), from Isacks and Barazangi (1977). Absolute-motion (INDI-hotspot) and relative-convergence (INDI-PCFC) vectors calculated from Minster and others' (1974) model; lengths of arrows are scaled to calculated rates. Thin contours show positions of Coalville, Lau, Tonga, and Kermadec subsea ridges.

seamount chain, the northern extension of the Kodiak-Bowie seamount chain. As the Pacific plate passed over the Bowie "hot spot," the lithosphere thinned by melting of the base of the lithosphere. Replacement of the base of the lithosphere by lower-density asthenosphere and concomitant thinning of mantle caused that portion of the plate to be more buoyant than surrounding "normal" lithosphere (Detrick and Crough, 1978). Low-angle subduction in the Gulf of Alaska region was a result of subduction of this relatively buoyant lithosphere. Absence of volcanism in the Mt. McKinley region may reflect the direct contact of the subducted plate with the base of the North American plate and consequent displacement of asthenosphere, as suggested by Barazangi and

Isacks (1976) for the Peru-Chile trench region.

**Louisville Ridge.** As age of an intraplate seamount chain increases, the buoyancy effect of the chain as it enters a subduction zone should be reduced. The intersection of the Louisville Ridge with the Tonga-Kermadec trench in the western Pacific illustrates this prediction. In contrast to the other areas cited in this review, the lithosphere in this part of the Pacific is old, although poorly determined at >80 m.y. B.P., and its gravitational instability, owing to its greater average density, approaches the maximum for oceanic lithosphere. The Louisville Ridge is probably no younger than 36 m.y. B.P., on the basis of isotopic ages of samples collected from the ridge, and it may be older (Jarrard and Clague, 1977). Watts and others (1980) determined that the Louisville Ridge was generated on old (>35 m.y. B.P.) lithosphere in an off-spreading-ridge position. Convergence rates between the Pacific and Indian plates along the Tonga-Kermadec trench change uniformly from ~7.5 cm/yr in the south to ~9.9 cm/yr in the north (Fig. 8; Minster and others, 1974; Chase, 1978a).

With such a configuration, but in the absence of an intraplate seamount chain, the subduction model predicts a fairly simple, uniform subduction zone with a steep inclination (possibly progressively shallower to the north) and a well-developed continuous volcanic arc on the upper plate. Figure 8 illustrates the generalized bathymetry of the seafloor, the positions of Quaternary volcanoes, and contours on the top of the inclined seismic zone. It is clear that the geometry of the subduction zone is not simple, as predicted, and therefore that subducted portions of the Louisville Ridge have modified its character.

The subduction zone to the south of the Louisville Ridge, opposite the Kermadec trench, dips about 72° in the intermediate and deep levels (Isacks and Barazangi, 1977), as indicated by the spacing of hypocenter depth contours (Fig. 8). The dip progressively shallows to about 58° in the intermediate level to the north of the Louisville Ridge-trench intersection (Isacks and Barazangi, 1977). Moreover, the subducted lithosphere progressively flattens at deeper levels opposite the Tonga trench. Kelleher and McCann (1976) previously noted that Quaternary and active volcanoes and major earthquakes in the subducted lithosphere are clustered between 18°S and 23°S latitudes and between 28°S and 32°S latitudes.

In the intervening gap, approximately opposite the Louisville Ridge-trench intersection, Quaternary volcanoes are absent and major earthquakes are rare. The breadth of the volcanic and seismic gap and the modified geometry of the subduction zone to the north of the Louisville Ridge is explained by oblique subduction of the Louisville Ridge and its presumed continuation to the northwest beneath the Lau basin. Isacks and Barazangi (1977) summarized the results of plate reconstructions which place the initial intersection of the Louisville Ridge extension and the Tonga trench to the north of its present position. Since the Pliocene, the point of intersection has migrated southward as successive seamounts comprising the Louisville Ridge were subducted obliquely. Subduction of this anomalous oceanic lithosphere was concomitant with the opening of the Lau basin.

In summary, local modification of subduction-zone geometry and other ancillary effects occur as aseismic ridges, oceanic plateaus, and intraplate island-seamount chains are subducted. Despite the different origins of these ridges, the lithosphere which contains them has a reduced average density relative to surrounding lithosphere devoid of such anomalous elements. The modifications are a consequence of the reduced average density and consequent buoyancy relative to surrounding lithosphere. In contrast to lithosphere bearing aseismic ridges and oceanic plateaus, the average density of lithosphere carrying island-seamount chains is strongly dependent on ages of the crust and the island-seamount chains. As shown in the cited examples, with progressive increase in age, the buoyancy effect is progressively reduced. Nonetheless, even old chains on old lithosphere cause the Benioff zone to dip at shallower angles and may inhibit generation of arc magma. The relative buoyancy of aseismic ridges and some oceanic plateaus is related to anomalously thick crust created during the formation of the ridges. This thickness and, therefore, the buoyancy effect are not age dependent. Greater crustal thicknesses of aseismic ridges may be related to formation on slow spreading centers or to mantle sources contributing anomalous volumes of magma at isolated positions along spreading centers.

#### Age of Lithosphere

Elevation of the sea floor along and marginal to oceanic spreading ridges is ther-

mally induced, and the sea floor is in isostatic equilibrium (Sclater and others, 1971). Initially, the thin lithosphere consists predominantly of light oceanic crust which forms near the ridge crest. With time, the lithosphere thickens, cools, and becomes denser, and the sea-floor elevation is gradually reduced (Parker and Oldenburg, 1973). Most of this thickening occurs within the mantle, whereas the crustal thickness is produced early and increases only slightly through time. As lithosphere ages, it consists of progressively lower ratios of crust to mantle. Consequently, the average lithosphere density is a function of age, and young lithosphere is relatively more buoyant than older, denser lithosphere.

The anticipated effect of lithospheric age on subduction zone geometry is derived from these generalizations. As old, dense lithosphere enters a subduction zone, it sinks more rapidly than young lithosphere, because it is gravitationally unstable. Other factors being equal, old lithosphere tends to subduct at steeper angles than young lithosphere. Consequently, a magmatic arc with a narrow arc-trench separation develops approximately parallel to the trench. Under otherwise similar conditions, young lithosphere will subduct at shallower angles because it is thinner, hotter, and more buoyant. In contrast to subduction of old lithosphere, the relation between arc magmatism and subduction is not as simple when young lithosphere is subducted. Low-angle subduction caused by relative buoyancy of young lithosphere produces effects similar to those induced by rapid convergence and rapid upper-plate motion toward the trench. These effects are either increased arc-trench separation or cessation of volcanism by displacement of subcontinental asthenosphere (Barazangi and Isacks, 1976). However, because young lithosphere also is hotter than old lithosphere, partial melting of the oceanic crust and generation of arc magma may occur more quickly and closer to the trench. Moreover, young lithosphere may be absorbed into the asthenosphere before appreciable low-density magma is produced. In this case, arc magmatism ceases. Subduction of young lithosphere thus produces two opposing tendencies with respect to arc magmatism: (1) low-angle subduction and increased arc-trench distance, owing to its low density; and (2) decreased arc-trench distance, owing to its higher temperature.

This rationale prompts the following predictions regarding relations of arc magmatism to subduction kinematics through time and under conditions of constant conver-

gence rates and absolute upper-plate motion. As a spreading ridge approaches a trench and progressively younger lithosphere is subducted, we anticipate gradual decrease in dip of the Benioff zone and migration of the arc away from the trench. As the thermal effect becomes dominant over the buoyancy effect, partial melting occurs progressively closer to the trench and the arc migrates back toward the trench, even though low-angle subduction continues. Finally, at some critical point, arc magmatism ceases as warm, young lithosphere is absorbed prior to significant magma generation. This critical point is dependent not only on lithosphere age, but co-varies with convergence rate and absolute upper-plate motion. In cases where relative plate motions require subduction of a spreading ridge and recently formed lithosphere on its oceanward flank, there will be a delay before arc magmatism is renewed. Resurgent volcanism will occur near the trench, and as progressively older lithosphere is subducted, the arc will migrate away from the trench.

In the previous discussion of the Cocos-North American plate boundary (Fig. 2), we noted the correlation between increasing convergence rates and greater arc-trench separation from north to south along the Middle American trench. The age of the Cocos plate also increases from north to south. With respect to arc magmatism, it is clear that the age-related buoyancy effect is subordinate to the opposing effect of age-related temperature. Although recently formed, relatively buoyant lithosphere is subducting beneath South America in the north, magma generation occurs early, close to the trench. This reflects the dominance of the age-related temperature effect, slow convergence, and moderate-angle subduction. To the south, as progressively older lithosphere is subducted, the age-related tendency toward steeper subduction is offset by increasing convergence rates and decreasing temperatures of the oceanic plate.

Observed relations of subduction-zone geometry and arc magmatism along the Peru-Chile trench north of the Chile Rise (Fig. 9) are compatible with our predictions, but they do not provide an unambiguous test of them. Absolute motions of the Nazca and South American plates along the subduction boundary are essentially constant. Convergence rates also are essentially constant (<2% deviation from maximum value of ~11 cm/yr at 39°S latitude), and they are notably higher than along the Middle American trench. The age of the Nazca

increases uniformly northward from the Chile Rise to about 30°S latitude. Excluding that portion of the subduction zone influenced by the Juan Fernandez Ridge, from 20°S to 40°S latitudes the Nazca plate subducts at moderate (~30°) angles beneath South America (Stauder, 1973; Barazangi and Isacks, 1976). From about 40°S to the intersection of the Chile Rise with the Peru-Chile trench at 46°S latitude, seismicity is less intense and generally is restricted to shallow levels and the geometry of the subducted plate is less well defined. Corresponding to the southward decrease in age of the Nazca plate, the arc-trench separation gradually decreases slightly from 30°S to 43°S latitudes. To the south, active volcanism terminates opposite the position where young lithosphere (~14 m.y. B.P.; anomaly 5b) is subducted (Weissel and others, 1977; LaBrecque and others, 1977). Cessation of arc volcanism in this region is probably a result of high convergence rates, shallow subduction of the young, relatively buoyant Nazca plate, and vertical juxtaposition of continental and oceanic lithosphere. However, available seismic data are insufficient to resolve this suggestion.

South of the Chile Rise, the Antarctic-Nazca spreading ridge has been subducted and the Antarctic plate is subducting be-

neath South America. Thus, South America is overriding the western flank of the former Chile Rise, and progressively older lithosphere is being subducted. The lithosphere adjacent to the trench is younger than 19 m.y. B.P. (anomaly 6; Weissel and others, 1977); therefore, the subducted portion of the Antarctic plate is young, warm, and thin. Convergence rate is slow, about 2 cm/yr, and most of the convergence is attributable to westward motion of South America. No magmatic arc is present east of the trench. Under these conditions of slow convergence and subduction of young lithosphere, the warm oceanic crust is being assimilated into the asthenosphere without attendant magma generation. The subduction model predicts that, as progressively older lithosphere is subducted, diffuse volcanism will occur within a broad region of South America, and gradually a volcanic arc will develop close to the trench.

**CONTROLS ON THE TECTONIC ENVIRONMENT OF CONVERGENT-PLATE MARGINS**

Along contemporary convergent-plate margins, deformation within upper plates at varying distances from trenches may be assigned to three principal styles of deformation. These are compression, extension,

and combined intracrustal compression with supracrustal extension. These tectonic styles result from different stress regimes in the crust of the upper plate imposed upon pre-existing thermomechanical properties of the crust. The stress regime is related to the geometry of subducting lithosphere. The four factors inferred as the principal controls on the geometry of subducting lithosphere, therefore, also are inferred to control the stress regime along the convergent margin of the upper plate and the deformational style within and landward of the volcanic arc.

The degree of compressional stress transmission through the crust of the upper plate is related to the area of interface and degree of coupling between the upper and lower plates and, thus, to the subduction angle. Low-angle subduction and efficient transmission of compressional stress are induced by combinations of rapid absolute upper-plate motion toward the trench, rapid relative convergence, subduction of young lithosphere, and subduction of anomalously low-density lithosphere. Regional extensional stress regimes within the crust are induced by steeper subduction (reduced coupling between the upper and lower plates) and retrograde upper-plate absolute motion. Extensional stress regimes at supracrustal levels may occur above a region of compressional stress where isostatically uplifted crust has greater gravitational potential to expand in the absence of lateral confining stress.

Within these regional stress regimes, deformational behavior is also partially controlled by thermomechanical properties of the crust, which are a product of its geologic history. Crustal shortening at depth in relatively cold, elastic regions at great distances from the trench (Laramide style) is a response to very low-angle subduction, rapid trenchward absolute motion of the upper plate, and subduction of aseismic ridges. Cordilleran style crustal shortening by fold and thrust deformation is a response to moderate or low-angle subduction and these aseismic ridges are supposed to be low angle subduction curves.

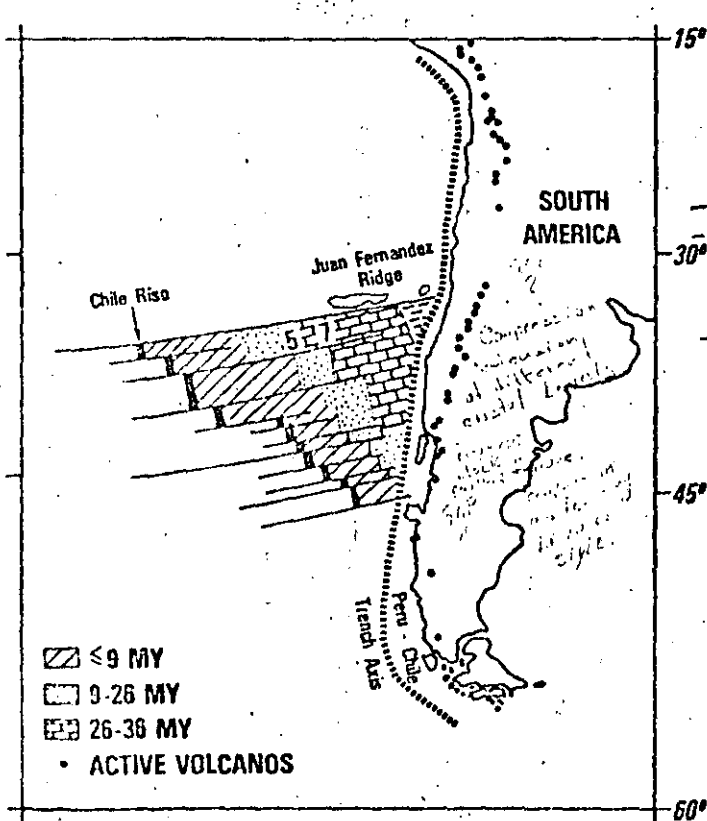


Figure 9. Plate-tectonic setting of southern Andean subduction zone. Age of the Nazca plate (shown by patterns) based on magnetic anomalies identified by Herron and Tucholke (1976), Weissel and others (1977), and Pitman and others (1974) and presented according to the time scale of LaBrecque and others (1977). Positions of identified magnetic anomalies shown by numerals.

underthrusting of the foreland beneath the ductile, isostatically uplifted back-arc. Usually, this compressional deformation is accompanied by extensional deformation at high crustal levels in the arc and back-arc regions, where the isostatically uplifted crustal mass expands in the absence of lateral confining stress. Extensional deformation within the crust of back-arc and intra-arc regions is related to steep subduction, but it requires retrograde absolute motion of the upper plate.

Contemporary back-arc extension is well documented behind the Izu-Bonin, Ryukyu, Mariana, and Tonga arcs in the western Pacific (for example, Karig, 1974; Herman and others, 1979), within the Andaman Sea in the Indian Ocean (Curry and others, 1979), and behind the Scotia arc in the South Atlantic (Barker, 1970; Barker and Griffiths, 1972). Intra-arc extension is present in the central part of the Middle American arc (Dewey and Algermissen, 1974) and occurred in the Basin-Range (Scholz and others, 1971; Cross and Pilger, 1979) and proto-Gulf of California (Karig and Jency, 1972) regions during the late Tertiary.

Megard and Philip (1976) concluded that the central Andes is a region of intra-arc extension. Other data suggest a coeval compressional stress regime within the same segment, but displaced to the east. Published cross-sections by Barth (in Zeil, 1979, p. 141-142) show thrust faults of late Cenozoic age along the eastern flank of the central Andes Altiplano. Shallow-focus (<70 km) earthquakes along the east flank of the Altiplano (for example, Barazangi and Isacks, 1976) may reflect contemporary movement along these faults. However, focal-mechanism solutions for these earthquakes have not been determined, and the state of stress and sense of faulting are not known. Few, if any, shallow-focus earthquakes have been detected within the Altiplano (Barazangi and Isacks, 1976).

Contemporary regional compression in back-arc and intra-arc regions, with the principal stress component oriented perpendicular to strikes of trenches, is documented along fewer subduction systems. The two segments of very low-angle subduction along the Peru-Chile trench, in northern Peru and central Chile, are characterized by east-west horizontal compressive stress within the shallow (<90 km) part of the upper plate (Stauder, 1973, 1975). These zones of compressive stress extend up to 700 km from the trench. As previously discussed, Quaternary volcanoes

are absent in the two segments, in contrast to the continuous chain of volcanoes of the central Andes. In addition, the Andes are markedly narrower along the two segments, by comparison with the Altiplano of the central Andes.

Regional intra-arc compression along the Aleutian and Alaskan volcanic chain is indicated by preferred orientations of dike swarms and distribution of volcanic cones and craters (Nakamura and others, 1977). Using this method, Nakamura and others (1977) determined that the maximum horizontal compressive stress is parallel with the direction of North America-Pacific convergence. By contrast, in the back-arc region of the Aleutian volcanic chain, maximum horizontal compressive-stress indicators are oriented approximately east-west, or parallel to the strike of the arc. Nakamura and others (1977) inferred a vertical maximum, an east-west intermediate, and a north-south minimum principal stress, thus placing the back-arc region in a dominantly extensional stress regime. In the back-arc of Alaska, coincident with the region of low-angle subduction, maximum horizontal compressive-stress indicators maintain an approximate parallelism with the direction of North America-Pacific convergence. Contemporary stress fields in back-arc and intra-arc regions of the Aleutian-Alaska and the Andean subduction systems are remarkably similar with respect to geometry of subducting lithosphere.

The state of stress and deformational style within and behind other volcanic arcs are less certain than the examples discussed above. The tectonic character of some of these was termed "simple" by Molnar and Atwater (1978), in the sense that neither extension nor compression ("Cordilleran" style) is dominant in back-arc or intra-arc regions. As they noted, the information base is not sufficient to definitively characterize the tectonic style of intra-arc and back-arc regions of Sumatra and Java, the Cascades, and the trans-Mexican volcanic arc.

Wilcox and others (1973) ascribed late Cenozoic compressional deformation in the back-arc region (foreland basin of Hamilton, 1979) of Sumatra to wrench-fault tectonics. Alternatively, we tentatively regard the region as a foreland fold and thrust belt analogous to the Canadian Rockies, on the basis of the dimension of the deformational zone, the anomalous moderate-angle dip (30°; Fitch, 1970) of the subducting plate, and the probability of moderate coupling

and stress transmission between the subducting and overriding plates.

Determination of crustal stress regime and deformational style in the Cascades volcanic arc is complicated by its proximity to two triple-plate junctions, a consequence of the small size of the subducting Juan de Fuca plate. However, east-west extension within the arc apparently is the principal deformational style, as indicated by numerous north-south trending normal faults and fissure zones that cut Pleistocene volcanics of the High Cascades Group (Hammond, 1979).

Volcanic centers of the trans-Mexican volcanic belt show a subtle northeast-southwest alignment on a regional scale (King, 1969). Through application of the techniques of Nakamura and others (1977), we infer a parallel maximum horizontal-stress orientation and note that this orientation is approximately parallel to the direction of North America-Cocos convergence (for example, Chase, 1978a). We suggest that the crust of the back-arc and intra-arc regions of Mexico is dominated by a regional compressive stress field, with the principal stress oriented northeast-southwest. Possible foreland fold and thrust belt development in the transitional crust beneath the Gulf of Mexico is marked by the northwest-southeast-trending Mexican Ridges fold belt (for example, Buffler and others, 1979).

This review of selected subduction systems shows clear correlations between the geometries of subduction zones and observed stress regimes and deformational styles within the leading margin of the upper plate. We infer that the four major factors that control the geometry of subduction zones also control the stress regime within the upper plate and influence the deformational style within and landward of the arc.

There is a direct correspondence between low-angle subduction and evidence of compressive stress and compressional tectonics. Barazangi and Isacks (1976) and Megard and Philip (1976) suggested that low-angle subduction results in mechanical or dynamic coupling and more efficient transmission of compressive stress between the descending and overriding plates than does steeper subduction. This general relation was applied successfully to explain several major Laramide events in western North America. These include basement-rooted thrusting in the central Rocky Mountains (Burchfiel and Davis, 1975; Brewer and

others, 1980) and a shift in locus and reduction in volume of magmatism from the Sierra Nevada to the Rocky Mountains (Cross and Pilger, 1978a). An ancillary effect of very low-angle subduction is regional isostatic subsidence of the upper plate due to subcrustal cooling and replacement of low-density asthenosphere by higher density oceanic lithosphere (Cross and Pilger, 1978b). This effect is reflected by the contrast in elevations between the broad Altiplano of the central Andes, which overlies a segment of moderate-angle subduction, and the lower elevations of the Amazon basin and by the narrow width of the Andes in central Peru. Cross and Pilger (1978b) also explained regional subsidence of the central Rocky Mountains area during the Late Cretaceous by this mechanism.

Another evident relation between the major controls on the geometry of subduction zones and tectonic style was observed by Morgan (1972) and discussed by Chase (1978a). All areas of back-arc extension overlie segments of steep subduction, and the absolute motion of the upper plate either is parallel to the trench or is retrograde with respect to the trench. In the Scotia Sea, back-arc spreading is observed (Laxer, 1970; Barker and Griffiths, 1972), but the absolute motion of the upper plate is uncertain. However, the analysis by Forsyth (1975) requires very slow upper-plate motion if the plate beneath the Scotia Sea is coupled to the Antarctic plate. To the extent that the descending plate tends to anchor the subduction zone, retrograde upper-plate motion requires crustal extension within the upper plate. The tendency for back-arc or intra-arc extension is increased by (1) the gravitational instability of the descending lithosphere and consequent seaward migration of the trench, and (2) the increased potential of the elevated crust in the arc region to expand in the absence of lateral confining stress.

Other subduction systems exhibit neither dominantly compressional nor dominantly extensional deformation. These are associated with moderate to steeply dipping subduction zones and absolute upper plate motion toward the trench. Evidence for contemporaneous compressional and extensional deformation often is found at differing structural levels or at varying distances from the trench along the same subduction segment. The central Andes provide an example of possible coexistence of extensional and compressional deformation. The Nazca plate is subducting at mod-

erate angles ( $\sim 30^\circ$ ) beneath the central Andes, and absolute-motion models indicate active overriding of the trench by South America (Minster and others, 1974; Chase, 1978a). This subduction configuration generates compressional stress across the base of the crust beneath the Altiplano. Compressional deformation occurs along the eastern margin of the Altiplano, where the South American foreland is underthrusting to the west beneath the Altiplano. Uplift of the Altiplano is the product of westward underthrusting of the foreland, elevated temperature and isostatic compensation above the wedge of partially molten, low-density asthenosphere, and addition of magma from depth. Uplift and addition of magma require expansion of the upper crust of the Altiplano. Thus, both crustal shortening and extension may occur concurrently along the same subduction segment, but at different structural levels or at different distances from the trench.

Molnar and Atwater (1978) argued that the major control on the tectonic environment of back-arc regions, whether extensional or compressional, is the age of the subducting lithosphere. They noted that subduction zones in the western Pacific are characterized by subduction of old, dense lithosphere and back-arc extension, whereas subduction zones in the eastern Pacific are characterized by subduction of young lithosphere and back-arc compressional tectonics (either Cordilleran style or "simple"). England and Wortel (1980) expanded and quantified the approach of Molnar and Atwater (1978) by combining convergence rate and dip of the inclined seismic zone to estimate sinking velocity. England and Wortel (1980) concluded that a combination of increasing lithospheric age and increasing descent velocity favors back-arc or intra-arc extension, while subduction of younger lithosphere at low rates of descent favors compressional (Cordilleran style) tectonics.

The analysis of England and Wortel (1980) shows attractive correlations between age of subducting lithosphere, descent velocity, and tectonic style within the upper plate. However, there are several areas which do not conform with these correlations. Major discrepancies include the Sandwich (Scotia Sea) and Central American arcs, in which relatively young lithosphere is subducting, but in which extensional tectonics appear dominant in back-arc and intra-arc regions. Similarly, compressional deformation in the Cascades

of Oregon and Washington would be predicted because of the slow subduction of the young Juan de Fuca plate, but existing evidence indicates regional extension. These discrepancies arise because the analysis neither includes an evaluation of the other controls on the dip of the subducting plate nor considers the effects of upper-plate absolute motion on the style of deformation within the upper plate.

Observed contrasts in tectonic style along the three segments of the Middle American arc are correlatable with combined variations in the four major controls of subduction-zone geometry. The subduction zone beneath the trans-Mexican volcanic belt is inclined at a moderate angle ( $\sim 20^\circ$ ), a consequence of relative youth of the Cocos plate, relatively rapid convergence, and southwestward absolute motion of the North American plate. On the basis of moderate-angle and shallow subduction (earthquake foci have maximum depths of about 150 km; Molnar and Sykes, 1969), we infer that the two plates are moderately coupled and that compressive stress is transmitted into the crust of Mexico in the back-arc and intra-arc regions. Intra-arc extension in Central America is, in all probability, primarily a response to slow, slightly retrograde absolute motion of the Caribbean plate. In the absence of upper-plate motion toward the trench, the older Cocos plate is gravitationally unstable, descends at steep angles, the trench migrates seaward, and the minimum principal stress within the Central American crust is oriented normal to the strike of the trench. Uplift of the arc above the wedge of partially molten asthenosphere provides additional gravitational potential for extension. This combination results in extension within the hot, ductile volcanic-arc region. The zone of extension within the central segment of the Middle American arc apparently ends in southern Costa Rica. In this area, back-arc thrusts are developed which continue offshore to the southeast along the base of the Caribbean continental margin of Panama (J. Case, 1980; oral commun.). The transition from intra-arc extension to back-arc shortening in Costa Rica corresponds with the intersection of the aseismic Cocos Ridge and the Middle American trench. We interpret back-arc thrusting as a direct consequence of enhanced coupling between the Cocos and Caribbean plates and transmission of compressive stress through the crust of the upper plate. This is a result of increased resistance to subduction of the

thicker crust and more-buoyant lithosphere beneath the Cocos Ridge, as suggested by Silver (1979), and in partial analogy with subduction of the Nazca Ridge beneath Peru.

In summary, the four major factors which control the geometry of subducting lithosphere also control or affect the state of stress and tectonic style in the upper plate. In general, the state of stress is most closely related to the inclination of the subducting plate and reflects the degree of coupling across the subduction interface and the effectiveness of stress transmission through the upper plate. Stress may be transmitted to the surface directly, by mechanical coupling over an interface of shear stress, or indirectly, by hydrodynamical coupling via the fluid asthenospheric wedge between the upper and lower plates.

Under moderate- or steep-angle subduction conditions, a regional extensional stress regime within the crust arises from isostatic uplift, consequent increased gravitational potential for extensional deformation, and thermal expansion (increased volume/mass ratio) of the crust. These are induced in two ways: (1) isostatic compensation and thermal expansion above the wedge of partially molten, low-density asthenosphere; and (2) uplift, thermal expansion, and increased volume by injection of magma from depth. Surficial uplift and near-surface extensional deformation within a dominantly compressional regime also may be induced by underthrusting of the foreland beneath the volcanic arc and immediate back-arc region (for example, the Altiplano). Extensional stresses are reinforced by seaward migration of the trench, a function of lithosphere density (age and presence or absence of anomalous crust), and absolute upper-plate motion. Slow or retrograde motion of the upper plate enhances the tensional stress regime and permits more-pronounced intra-arc or back-arc extension.

Extensional stress is reduced or replaced by compression under conditions of low-angle subduction. Low-angle subduction increases the interface of mechanical or dynamical coupling between the upper and lower plates, and shear stress is transmitted as compressive stress into the crust of the upper plate. In addition, the wedge of low-density asthenosphere may be displaced by oceanic lithosphere, resulting in lower surface elevations and reduced gravitational

potential for extensional deformation. Rapid upper-plate motion toward the trench tends to flatten the subducting plate, increases the area of interface and degree of coupling between the plates, and creates a compressional regime (or reduces the extensional stress) within the upper plate. Crustal shortening and extension may result at different structural levels within the same segment, as in the central Andes. Subduction of anomalously low-density lithosphere (for example, aseismic ridges, intraplate island-seamount chains, or very young lithosphere) augments the tendency toward low-angle subduction and causes compressive stress and crustal shortening to dominate in the upper plate. Displacement of the low-density asthenospheric wedge by anomalously low-density lithosphere, particularly aseismic ridges, may cause surficial subsidence and create a pericratonic sedimentary basin (for example, a portion of the Western Interior Seaway and the Amazon basin; Cross and Pilger, 1978b).

We regard both the extensional and compressional stresses as being broadly distributed within the crust. The actual location of deformation, whether intra-arc, back-arc, or both, is controlled by pre-existing thermomechanical properties of the crust.

#### ACKNOWLEDGMENTS

We are particularly indebted to Gordon Gastil for initially suggesting and encouraging preparation of this report. Helpful comments and criticisms were offered by Gordon Gastil, Dick Phillips, Kevin Biddle, and two anonymous reviewers. We thank them for their time and courtesy.

#### REFERENCES CITED

Ahrens, T. J., and Schubert, G., 1975, Gabbroeclogite reaction rate and its geophysical significance: *Reviews of Geophysics and Space Physics*, v. 13, p. 383-400.  
 Anderson, R. N., Uyeda, S., and Miyashiro, A., 1976, Geophysical and geochemical constraints at converging plate boundaries—Part I: Dehydration in the downgoing slab: *Royal Astronomical Society Geophysical Journal*, v. 44, p. 333-357.  
 Barazangi, M., and Isacks, B. L., 1976, Spatial distribution of earthquakes and subduction of the Nazca plate beneath South America: *Geology*, v. 4, p. 686-692.  
 ———, 1979, Subduction of the Nazca plate beneath Peru: Evidence from spatial distribution of earthquakes: *Royal Astronomical Society*

*Geophysical Journal*, v. 57, p. 537-555.  
 Barker, P. F., 1970, Plate tectonics of the Scotia Sea region: *Nature*, v. 228, p. 1293-1296.  
 Barker, P. F., and Griffiths, D. H., 1972, The evolution of the Scotia Ridge and Scotia Sea: *Royal Society of London Philosophical Transactions*, v. 271, p. 151-183.  
 Bostrom, R. C., 1971, Westward displacement of the lithosphere: *Nature*, v. 234, p. 536-538.  
 Bostrom, R. C., Sherif, M. A., and Stockman, R. H., 1974, Deformation of earth's lithosphere with reference to tidal couples: *American Association of Petroleum Geologists Memoir* 26, p. 463-485.  
 Brewer, J. A., Smithson, S. B., Oliver, J. E., and Brown, L. D., 1980, The Laramide orogeny: Evidence from COCORP deep crustal seismic profiles in the Wind River Mountains, Wyoming: *Tectonophysics*, v. 62, p. 165-189.  
 Buffler, R. R., Shaub, R. J., Watkins, J. S., and Worzel, J. L., 1979, Anatomy of the Mexican ridges, southwestern Gulf of Mexico, in Watkins, J. S., Montadert, L., and Dickerson, P. W., eds., *Geological and geophysical investigations of continental margins: American Association of Petroleum Geologists Memoir* 29, p. 319-328.  
 Burchfiel, B. C., and Davis, G. A., 1975, Nature and controls of Cordilleran orogenesis, western United States: Extensions of an earlier synthesis: *American Journal of Science*, v. 275-A, p. 363-396.  
 Burk, C. A., 1972, Uplifted eugeosynclines and continental margins: *Geological Society of America Memoir* 132, p. 75-85.  
 Carr, J. J., 1976, Underthrusting and active faulting in northern Central America: *Geological Society of America Bulletin*, v. 87, p. 825-829.  
 Carr, J. J., Rose, W. I., and Mayfield, D. G., 1979, Potassium content of lavas and depth to the seismic zone in Central America: *Journal of Volcanology and Geothermal Research*, v. 5, p. 387-401.  
 Chase, C. G., 1978a, Extension behind island arcs and motions relative to hot spots: *Journal of Geophysical Research*, v. 83, p. 5385-5387.  
 ———, 1978b, Plate kinematics: The Americas, east Africa, and the rest of the world: *Earth and Planetary Science Letters*, v. 37, p. 355-368.  
 Cross, T. A., and Pilger, R. H., Jr., 1978a, Constraints on absolute motion and plate interaction inferred from Cenozoic igneous activity in the western United States: *American Journal of Science*, v. 278, p. 865-902.  
 ———, 1978b, Tectonic controls of Late Cretaceous sedimentation, western interior, U.S.A.: *Nature*, v. 274, p. 653-657.  
 ———, 1979, Origin of Basin-Range extension: Back-arc spreading controlled by North American plate motion: *Geological Society of America Abstracts with Programs*, v. 11, p. 74.  
 Crough, S. T., 1978, Thermal origin of mid-plate hot-spot swells: *Royal Astronomical Society Geophysical Journal*, v. 55, p. 451-469.  
 Curray, J. R., Moore, D. G., Lawver, L. A., Emmel, F. J., Raitt, R. W., Henry, M., and Kieckhefer, R., 1979, Tectonics of the

- Andaman Sea and Burma, in Watkins, J. S., Montadert, L., and Dickerson, P. W., eds., Geological and geophysical investigations of continental margins: American Association of Petroleum Geologists Memoir 29, p. 189-198.
- Deffeyes, K. S., 1972, Plume convection with an upper-mantle temperature inversion: *Nature*, v. 240, p. 539-544.
- DeLong, S. E., and Fox, P. J., 1977, Geological consequences of ridge subduction, in Talwani, Manik, and Pitman, W. C., III, eds., Island arcs, deep sea trenches, and back-arc basins: American Geophysical Union, Maurice Ewing Series 1, p. 221-228.
- Detrick, R. S., and Crough, S. T., 1978, Island subsidence, hot spots, and lithospheric thinning: *Journal of Geophysical Research*, v. 83, p. 1236-1244.
- Detrick, R. S., and Watts, A. B., 1979, An analysis of isostasy in the world's oceans, 3. Aseismic ridges: *Journal of Geophysical Research*, v. 84, p. 3637-3653.
- Detrick, R. S., Sclater, J. G., and Thiede, J., 1977, The subsidence of aseismic ridges: *Earth and Planetary Science Letters*, v. 34, p. 185-196.
- Dewey, J. W., and Algermissen, S. T., 1974, Seismicity of the Middle America arc-trench system near Managua, Nicaragua: *Seismological Society of America Bulletin*, v. 64, p. 1033-1048.
- Dickinson, W. R., 1973, Widths of modern arc-trench gaps proportional to past duration of igneous activity in associated magmatic arcs: *Journal of Geophysical Research*, v. 78, p. 3376-3389.
- Elsässer, W. M., 1971, Sea-floor spreading as thermal convection: *Journal of Geophysical Research*, v. 76, p. 1101-1112.
- Fitch, T. J., 1970, Earthquake mechanisms and island arc tectonics in the Indonesian-Philippine region: *Seismological Society of America Bulletin*, v. 60, p. 565-591.
- Forsyth, D. W., 1975, Fault plane solutions and tectonics of the South Atlantic and Scotia Sea: *Journal of Geophysical Research*, v. 80, p. 1429-1443.
- Frank, F. C., 1968, Curvature of island arcs: *Nature*, v. 220, p. 363.
- Green, T. H., and Ringwood, A. E., 1968, Genesis of the calc-alkaline igneous rock suite: *Contributions to Mineralogy and Petrology*, v. 18, p. 105-162.
- Hamilton, W., 1973, Tectonics of the Indonesian region: *Geological Society of Malaysia Bulletin*, v. 6, p. 3-10.
- 1978, Mesozoic tectonics of the western United States, in Howell, D. G., and McDougall, K. A., eds., *Mesozoic Paleogeography of the Western United States*: Society of Economic Paleontologists and Mineralogists, Pacific Section, Paleogeography Symposium 2, p. 33-70.
- 1979, Tectonics of the Indonesian region: U.S. Geological Survey Professional Paper 1078, 345 p.
- Hammond, P. E., 1979, A tectonic model for the evolution of the Cascade Range: *Society of Economic Paleontologist and Mineralogists, Pacific Section, Paleogeography Symposium 3*, p. 219-237.
- Herman, B. M., Anderson, R. N., and Truchan, M., 1979, Extensional tectonics in the Okinawa trough, in Watkins, J. S., Montadert, L., and Dickerson, P. W., eds., *Geological and geophysical investigations of continental margins*: American Association of Petroleum Geologists Memoir 29, p. 199-208.
- Herron, E. M., 1972, Sea-floor spreading and the Cenozoic history of the east-central Pacific: *Geological Society of America Bulletin*, v. 83, p. 1671-1692.
- Herron, E. M., and Tucholke, B. E., 1976, Sea-floor magnetic patterns and basement structure in the southeastern Pacific: *Initial Reports of the Deep Sea Drilling Project*, v. 35, p. 263-278.
- Herron, E. M., Bruhn, R., Winslow, M., and Chaqui, L., 1977, Post Miocene tectonics of the margin of southern Chile, in Talwani, M., and Pitman, W. C., III, eds., *Island arcs, deep sea trenches, and back-arc basins*: American Geophysical Union, Maurice Ewing Series 1, p. 273-284.
- Hey, R., 1977, Tectonic evolution of the Cocos-Nazca spreading center: *Geological Society of America Bulletin*, v. 88, p. 1404-1420.
- Hey, R., Johnson, G. L., and Lowrie, A., 1977, Recent plate motions in the Galapagos area: *Geological Society of America Bulletin*, v. 88, p. 1385-1403.
- Hyndman, R. D., 1972, Plate motions relative to the deep mantle and the development of subduction zones: *Nature*, v. 238, p. 263-265.
- Isacks, B. L., and Barazangi, M., 1977, Geometry of Benioff zones: Lateral segmentation and downward bending of the subducted lithosphere, in Talwani, M., and Pitman, W. C., III, eds., *Island arcs, deep sea trenches, and back-arc basins*: American Geophysical Union, Maurice Ewing Series 1, p. 99-114.
- Isacks, B. L., and Molnar, P., 1971, Distribution of stresses in the descending lithosphere from a global survey of focal-mechanism solutions of mantle earthquakes: *Reviews of Geophysics and Space Physics*, v. 9, p. 103-174.
- Jacob, K. H., Nakamura, K., and Davies, J. N., 1977, Trench-volcano gap along the Alaska-Alutian arc: Facts and speculations on the role of terrigenous sediments, in Talwani, M., and Pitman, W. C., III, eds., *Island arcs, deep sea trenches, and back-arc basins*: American Geophysical Union, Maurice Ewing Series 1, p. 243-258.
- Jacoby, W. R., 1970, Instability in the upper mantle and global plate movement: *Journal of Geophysical Research*, v. 75, p. 5661-5680.
- James, D. E., 1971, Plate-tectonic model for the evolution of the central Andes: *Geological Society of America Bulletin*, v. 82, p. 3325-3346.
- Jarrard, R. D., and Clague, D. A., 1977, Implications of Pacific island and seamount ages for the origin of volcanic chains: *Reviews of Geophysics and Space Physics*, v. 15, p. 57-76.
- Jischke, M., 1975, On the dynamics of descending lithospheric plates and slip zones: *Journal of Geophysical Research*, v. 80, p. 4809-4813.
- Jordan, T. H., 1974, Some comments on tidal drag as a mechanism for driving plate motions: *Journal of Geophysical Research*, v. 79, p. 2141-2142.
- 1975, The present-day motions of the Caribbean plate: *Journal of Geophysical Research*, v. 80, p. 4433-4439.
- Karig, D. E., 1974, Evolution of arc systems in the western Pacific: *Annual Review of Earth and Planetary Science*, v. 2, p. 51-75.
- Karig, D. E., and Jansky, W., 1972, The proto-Gulf of California: *Earth and Planetary Science Letters*, v. 17, p. 169-174.
- Karig, D. E., and Mammerickx, J., 1972, Tectonic framework of the New Hebrides island arc: *Marine Geology*, v. 12, p. 187-205.
- Karig, D. E., and Sharman, G., 1975, Subduction and accretion in trenches: *Geological Society of America Bulletin*, v. 86, p. 377-389.
- Karig, D. E., Caldwell, J. G., and Parmentier, E. M., 1976, Effects of accretion on the geometry of the descending lithosphere: *Journal of Geophysical Research*, v. 81, p. 6281-6291.
- Kelleher, J., and McCann, W., 1976, Buoyant zones, great earthquakes, and unstable boundaries of subduction: *Journal of Geophysical Research*, v. 81, p. 4885-4896.
- 1977, Bathymetric highs and the development of convergent plate boundaries, in Talwani, M., and Pitman, W. C., III, eds., *Island arcs, deep sea trenches, and back-arc basins*: American Geophysical Union, Maurice Ewing Series 1, p. 115-122.
- King, P. B., compiler, 1969, *Tectonic map of North America*: U.S. Geological Survey map.
- Kogan, M. G., 1979, Gravity anomalies and origin of the Walvis Ridge: *Journal of Geophysical Research*, v. 84, p. 6019-6025.
- LaBrecque, J. L., Kent, D. V., and Cande, S. C., 1977, Revised magnetic polarity time scale for Late Cretaceous and Cenozoic time: *Geology*, v. 6, p. 330-335.
- Lonsdale, P., and Klitgord, K. D., 1978, Structure and tectonic history of the eastern Panama basin: *Geological Society of America Bulletin*, v. 89, p. 981-999.
- Luyendyk, B. P., 1970, Dips of downgoing lithospheric plates beneath island arcs: *Geological Society of America Bulletin*, v. 81, p. 3411-3416.
- Marsh, B. D., 1976, Mechanics of Benioff zone magmatism: *American Geophysical Union Monograph* 19, p. 337-350.
- Megard, F., and Philip, H., 1976, Plio-Quaternary tectono-magmatic zonation and plate tectonics in the central Andes: *Earth and Planetary Science Letters*, v. 33, p. 231-238.
- Minster, J. B., Jordan, T. H., Molnar, P., and Haines, E., 1974, Numerical modelling of instantaneous plate tectonics: *Royal Astronomical Society Geophysical Journal*, v. 36, p. 541-576.
- Moberly, R., 1972, Origin of lithosphere behind island arcs, with reference to the western Pacific: *Geological Society of America*

- Memoir 132, p. 35-55.
- Molnar, P., and Atwater, T., 1978, Interarc spreading and Cordilleran tectonics as alternates related to the age of subducted oceanic lithosphere: *Earth and Planetary Science Letters*, v. 41, p. 330-340.
- Molnar, P., and Francheteau, J., 1975, The relative motion of "hot spots" in the Atlantic and Indian Oceans during the Cenozoic: *Royal Astronomical Society Geophysical Journal*, v. 43, p. 763-774.
- Molnar, P., and Sykes, L. R., 1969, Tectonics of the Caribbean and Middle American regions from focal mechanisms and seismicity: *Geological Society of America Bulletin*, v. 80, p. 1639-1684.
- Morgan, W. J., 1972, Plate motions and deep mantle convection: *Geological Society of America Memoir 132*, p. 7-22.
- Nakamura, K., Jacob, K. H., and Davies, J. N., 1977, Volcanoes as possible indicators of tectonic stress orientation—Aleutians and Alaska: *Pure and Applied Geophysics*, v. 115, p. 87-112.
- Nelson, T. H., and Temple, P. G., 1972, Mainstream mantle convection: A geologic analysis of plate motion: *American Association of Petroleum Geologists Bulletin*, v. 56, p. 226-246.
- Nur, A., and Ben-Avraham, Z., 1981, Consumption of aseismic ridges and volcanic gaps in South America: *Geological Society of America Memoir 154*, p. 729-740.
- Parker, R. L., and Oldenburg, D. W., 1973, Thermal model of ocean ridges: *Nature Physical Science*, v. 242, p. 137-139.
- Pilger, R. H., Jr., 1977, Plate reconstructions, aseismic ridges, and low-angle subduction beneath the Andes [Abs.]: *EOS (American Geophysical Union Transactions)*, v. 58, p. 1232.
- 1981, Plate reconstructions, aseismic ridges, and low-angle subduction beneath the Andes: *Geological Society of America Bulletin*, Part 1, v. 92, p. 448-456.
- Pilger, R. H., Jr., and Handschumacher, D. W., 1981, The fixed hotspot hypothesis and origin of the Easter-Sala y Gomez-Nazca trace: *Geological Society of America Bulletin*, Part 1, v. 92, p. 437-446.
- Pilger, R. H., Jr., and Henyey, T. L., 1979, Pacific-North American plate interaction and Neogene volcanism in coastal California: *Tectonophysics*, v. 57, p. 189-209.
- Pitman, W. C., III, Larson, R. L., and Herron, E. M., compilers, 1974, The age of the ocean basins: *Geological Society of America Map MC-6*, scale 1:39,000,000.
- Scholz, C. H., Barazangi, M., and Sbar, M. L., 1971, Late Cenozoic evolution of the Great Basin, western United States, as an ensialic interarc basin: *Geological Society of America Bulletin*, v. 82, p. 2979-2990.
- Slater, J. G., and Fisher, R. L., 1974, Evolution of the east-central Indian Ocean, with emphasis on the tectonic setting of the Ninetyeast Ridge: *Geological Society of America Bulletin*, v. 85, p. 683-702.
- Slater, J. G., Anderson, R. H., and Bell, M. L., 1971, Elevation of ridges and evolution of the central eastern Pacific: *Journal of Geophysical Research*, v. 76, p. 7888-7915.
- Seely, D. R., Vail, P. R., and Walton, G. G., 1974, Trench slope model, in Burk, C. A., and Drake, C. L., eds., *The geology of continental margins*: New York, Springer-Verlag, p. 249-260.
- Silver, E. A., 1979, Back-arc thrusting: *EOS (American Geophysical Union Transactions)*, v. 60, p. 958.
- Simpson, R. W., and Cox, A., 1977, Paleomagnetic evidence for tectonic rotation of the Oregon Coast Range: *Geology*, v. 5, p. 585-589.
- Solomon, S. C., Sleep, N. H., and Richardson, R. M., 1975, On the forces driving plate tectonics: Inferences from absolute plate velocities and intraplate stress: *Geophysical Journal*, v. 42, p. 769-801.
- Stauder, W., 1973, Mechanism and spatial distribution of Chilean earthquakes with relation to subduction of the oceanic plate: *Journal of Geophysical Research*, v. 74, p. 5033-5061.
- 1975, Subduction of the Nazca plate under Peru as evidenced by focal mechanisms and by seismicity: *Journal of Geophysical Research*, v. 80, p. 1053-1064.
- Stoiber, R. E., and Carr, M. J., 1973, Quaternary volcanic and tectonic segmentation of Central America: *Bulletin of Volcanology*, v. 37, p. 304-325.
- Stoll, W. C., 1964, Metallogenic belts, centers and epochs in Argentina and Chile: *Economic Geology*, v. 59, p. 126-135.
- Tovish, A., and Schubert, G., 1978, Island arc curvature, velocity of convergence and angle of subduction: *Geophysical Research Letters*, v. 5, p. 329-332.
- Truchan, M., and Larson, R. L., 1973, Tectonic lineaments on the Cocos plate: *Earth and Planetary Science Letters*, v. 17, p. 426-432.
- Turner, D. L., Forbes, R. B., and Naeser, C. W., 1973, Radiometric ages of Kodiak seamount and Giacomini guyot, Gulf of Alaska: Implications for circum-Pacific tectonics: *Science*, v. 182, p. 579-581.
- Uyeda, S., and Kanamori, H., 1979, Back-Arc opening and the mode of subduction: *Journal of Geophysical Research*, v. 84, p. 1049-1061.
- Vogt, P. R., Lowrie, A., Bracey, D. R., and Hey, R. N., 1976, Subduction of aseismic oceanic ridges: Effects on shape, seismicity and other characteristics of consuming plate boundaries: *Geological Society of America Special Paper 172*, 59 p.
- Watts, A. B., Bodine, J. H., and Ribe, N. M., 1980, Observations of flexure and the geological evolution of the Pacific Ocean basin: *Nature*, v. 283, p. 532-537.
- Weissel, J. K., Hayes, D. E., and Herron, E. M., 1977, Plate tectonics synthesis: The displacements between Australia, New Zealand, and Antarctica since the Late Cretaceous: *Marine Geology*, v. 25, p. 231-277.
- Wilcox, R. E., Harding, T. P., and Seely, D. R., 1973, Basic wrench tectonics: *American Association of Petroleum Geologists Bulletin*, v. 57, p. 74-96.
- Worzel, J. L., 1976, Gravity investigations of the subduction zone, in Sutton, G. H., Manghni, M. H., and Moberly, R., eds., *The Geophysics of the Pacific Ocean basin and its margin*: *American Geophysical Union Geophysical Monograph 19*, p. 1-16.
- Zeil, W., 1979, The Andes, a geological review: *Beiträge zur Regionalen Geologie der Erde*, Band 13: Berlin, Gebrüder Borntraeger, p. 260.

MANUSCRIPT RECEIVED BY THE SOCIETY  
JUNE 25, 1981

MANUSCRIPT ACCEPTED JUNE 25, 1981





**DIVISION DE EDUCACION CONTINUA  
FACULTAD DE INGENIERIA U.N.A.M.**

MECANICA DE ROCAS APLICADA A LA MINERIA Y A LA CONSTRUCCION

SURFACE FAULTING AND RELATED EFFECTS

M. G. Bonilla

MAYO, 1985

## Chapter 3

# Surface Faulting and Related Effects

M. G. BONILLA

*Geologist, U.S. Geological Survey  
Menlo Park, California*

## 3.1 INTRODUCTION

Faults and faulting are important to engineers because (1) they can severely damage or destroy structures by shearing, compression, extension, and rotation caused by tilting or bending; (2) earthquakes may occur along them; and (3) past faulting may have greatly affected the physical properties of foundation materials by decreasing their strength, changing their permeability, or bringing together rock units with very different physical properties.

This chapter is based primarily on experience in North America and discusses only items 1 and 2 above, with emphasis on item 1. Item 2 is treated more fully in other chapters of this book, particularly the chapters by Bruce Bolt and G. W. Housner.

Fault rupture and the ground deformation closely associated with it can have extremely serious consequences even though the area directly affected is small compared to the area affected by shaking, landsliding,

compaction, and liquefaction. Buildings, bridges, dams, tunnels, canals, and pipelines have been severely damaged by fault rupture; damage of this kind is described in reports by Lawson and others (1908), Ambraseys (1960), Duke (1960), and the California Department of Water Resources (1967).

Not all faults are important to engineering. Some have displacements of only a few inches and lengths of a few to a few hundred feet. Their effects on the physical properties of the rock may have been minor; furthermore, many once-active faults are now healed and as sound as the surrounding rock. Most faults are not now the site of earthquakes. Many faults are very ancient, and the absence of movement for hundreds of millions of years can be demonstrated for some of them.

### 3.2 GLOSSARY

A short glossary defining selected geological terms used in this report is given below. The meanings apply to the terms as used in this chapter and are not intended as general definitions. Geological terms not in the glossary can be found in a standard dictionary or in the *Glossary of Geology and Related Sciences* (American Geological Institute, 1960).

*Dip*: The angle that a stratum, joint, fault, or other structural plane makes with a horizontal plane.

*Dip slip*: The component of the slip parallel with the dip of the fault.

*Fault*: A fracture or fracture zone along which the two sides have been displaced relative to one another parallel to the fracture. The displacement may range from a few inches to many miles.

*Fault creep*: Apparently continuous displacement along a fault at a low but varying rate, usually not accompanied by felt earthquakes (see also tectonic creep). As used in this chapter, fault creep is not necessarily tectonic in origin; it may result from artificial withdrawal of fluids or solids.

*Fault displacement*: Relative movement of the two sides of fault, measured in any specified direction.

*Fault sag*: A narrow tectonic depression common in strike-slip fault zones. Fault sags are generally closed depressions less than a few hundred feet wide and approximately parallel to the fault zone; those that contain water are called sag ponds.

*Fault scarp*: A cliff or steep slope formed by displacement of the ground surface.

*Fracture*: A general term for discontinuities in rock; includes faults, joints, and other breaks.

*Graben*: A fault block, generally long and narrow, that has been dropped down relative to the adjacent blocks by movement along the bounding faults. The

same form of the word is used for both the singular and plural.

*Landslide*: The downward and outward movement of slope-forming materials, such as rock, soil, artificial (or combinations of these materials (Varnes, 1958, p. 20); the topographic feature and the deposit resulting from such movement.

*Left slip*: Strike-slip displacement in which the block across the fault from an observer has moved to the left; also called sinistral strike slip.

*Normal fault*: A fault in which the block above an inclined fault surface has moved downward relative to the block below the fault surface; also includes vertical faults with vertical slip.

*Oblique slip*: A combination of strike slip and normal or reverse slip.

*Reverse fault*: A fault in which the block above an inclined fault surface has moved upward relative to the block below the fault surface.

*Right-normal slip*: Fault displacement consisting of nearly equal components of right slip and normal slip; also called dextral normal.

*Right slip*: Strike-slip displacement in which the block across the fault from an observer has moved to the right; also called dextral strike slip.

*Slip*: The relative displacement of points on opposite sides of a fault, measured on the fault surface.

*Strike*: The direction or bearing of a horizontal  $\mathcal{F}$  in the plane of an inclined or vertical stratum,  $j$  fault, or other structural plane.

*Strike slip*: The component of the slip parallel with the strike of the fault; the horizontal component of slip.

*Strike-slip fault*: A fault in which the slip is approximately in the direction of the strike of the fault; also called wrench or transcurrent fault. The historic displacements on strike-slip faults discussed in this chapter have, in places along those faults, included a vertical component that has generally been less than one-quarter of the horizontal component.

*Tectonic*: Of, pertaining to, or designating the rock structure and external forms resulting from deep-seated crustal and subcrustal forces in the earth.

*Tectonic creep*: Fault creep of tectonic origin; also called slippage.

### 3.3 SURFACE MANIFESTATIONS OF FAULTING

Surface manifestations of faulting and closely related processes include sudden rupture and displacement, creep, warping, tilting, and gross changes in land level. The first of these is of greatest importance for most engineering structures and consequently is treated fully than the others.

### 3.3.1 Sudden Rupture and Displacement

Sudden rupture and displacement occurs with normal, reverse, strike-slip, or oblique-slip faulting (see glossary). The historic record of surface faulting in the continental United States and adjacent parts of Mexico, as currently known, is summarized in chronological order in Table 3.1.

### 3.3.2 Length of Surface Ruptures

The length of surface ruptures given in column 3 of the table is the distance between the ends of continuous or nearly continuous breaks that formed at the surface in the listed earthquakes. This length can be substantially less than the length inferred from the distribution of aftershocks, from dislocation theory, or from other indirect means. The longest surface rupture (partly submarine) on record occurred along 270 mi of the San Andreas fault in 1906. The length of subsurface faulting that occurred in the 1964 Alaskan earthquake is estimated at about 370 mi by Savage and Hastie (1966, Table 1) and about 450 mi by Housner (Chapter 4, this volume).

### 3.3.3 Fault Displacements

Maximum recorded surface displacements accompanying earthquakes have ranged from 0.05 ft of strike slip in the Imperial, California, earthquake of 1966 (Brune and Allen, 1967) through 35 ft of vertical displacement in the Assam earthquake of 1897 (Oldham, 1899, p. 145) to possibly as much as 42 ft of vertical displacement in the Yakutat Bay, Alaska, earthquake of 1899 (Bonilla, 1967, pp. 9-10). The largest measured strike slip, 29 ft, occurred in the Gobi-Altai earthquake of 1957 (Florensov and Solonenko, 1965, p. 288). From measurements of offset stream channels, Wallace (1968) has suggested that strike slip on the San Andreas fault may have been 30 ft in 1857.

The vertical displacements for normal faults given in columns 4, 5, and 6 of Table 3.1 are the scarp heights except where otherwise specified. The scarp height generally is more critical for engineering purposes than the vertical component of fault displacement; furthermore, many published reports give only scarp heights. Scarps produced by normal faulting commonly are of greater height than the vertical component of fault displacement, chiefly because gravity graben form along the fault (Gilbert, 1890, p. 354; Slemmons, 1957, pp. 367-375). This is shown in Fig. 3.1, a diagrammatic cross section of a typical graben formed by gravity set-

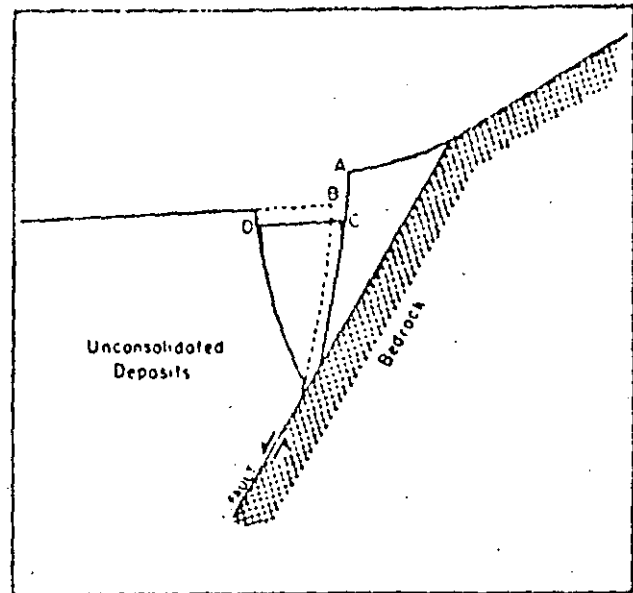


Fig. 3.1. Cross section of a gravity graben associated with a normal fault. The relative movement of the fault is shown by arrows.

ting of part of the hanging wall of a normal fault. The vertical component of fault displacement, equal to the vertical distance from A to B, is less than the scarp height AC. In order to avoid having to accommodate the full scarp height, a structure across the main fault would have to bridge the graben (Fig. 3.2). Because the width (Fig. 3.1, CD) of the graben is generally more than 10 ft and can be as much as 300 ft (Witkind, 1964, p. 45), structures may bear on the graben and have to accommodate the full scarp height.

In addition to the effects of graben formation, scarp heights may be increased by minor landsliding and other erosional processes that cause a gradual uphill retreat of the brow (Fig. 3.1, point A) of the scarp. Scarp heights are not given in the table for specific points where erosional processes are known to have substantially increased them as, e.g., parts of the Fairview Peak scarps formed in 1954 (Slemmons, 1957, pp. 373-375).

Although the scarp heights of normal faults are commonly greater than the vertical component of fault movement at the surface, they can be substantially less than inferred fault displacement at depth. The maximum scarp produced in the 1959 Montana earthquake, e.g., was 20 ft (Witkind, 1964, p. 37; Myers and Hamilton, 1964, p. 81), but the subsurface displacement based on dislocation theory was more than 40 ft (Brune and Allen, 1967, p. 510).

Small to moderate amounts of vertical movement have accompanied some strike-slip faulting. According to dislocation theory, a systematic quadrantal distribution of very small elevations and depressions is expected for strike-slip faulting that is not infinitely long (Chin-

Table 3.1. HISTORIC SURFACE FAULTING IN THE CONTINENTAL UNITED STATES AND ADJACENT PARTS OF MEXICO

Fault (name or location), date, and type of displacement* (See notes at end of table)	Magnitude (Richter) of associated earthquake	Length of surface rupture (miles)	Displacement (feet), main fault (maximum)	Displacements (feet) at indicated distances (miles) from center of main fault zone		Distances (maximum) from center of main zone to outer limits of			Remarks	Principal references	
				Branch faulting	Secondary faulting	Main zone	Branch faulting	Secondary faulting			
1	2	3	4	5	6	7	8	9	10	11	
1. New Madrid, Missouri; 1811-1812; N(?)			6(?) V							Fault whose scarp bounds Reelfoot Lake shows vertical separation of 40 ft in Eocene beds 160 ft below the surface. Uplift as well as subsidence occurred in this earthquake. See text.	Fuller, 1912; Fisk, 1944; U.S. Army Corps of Engineers, 1950
2. Hayward, California; 1836; R(?)		38(?)									Louderback, 1947
3. San Andreas, California; 1838; R(?)		55(?)									Louderback, 1947
4. San Andreas, California; 1857; R <sub>s</sub>		200 ±	Large, possibly 30								Lawson <i>et al.</i> , 1903; Wood, 1955; Allen <i>et al.</i> , 1965; Brown and Vedder, 1967; Wallace, 1968
5. Hayward, California; 1868; R(?)		30 ±	3R <sub>s</sub> (?), 1V	Displacement unknown	1.5V at 1.4		0.8 ± mi	1.8 mi		Given length includes a 21-mi southern segment and a probable segment 0.3 mi long, 7 mi to the north.	Lawson <i>et al.</i> , 1908; Radbruch, 1967
6. Owens Valley, California; 1872; RN and LN(?)	8.3 (estimated)	60+	23N; 16-20R <sub>s</sub>		18V at 1.6+; 4N at 8; 2.5N at 8; 15V at 1 1/2	0.5 mi		8 mi		Displacements given for secondary faults at 8 mi are scarp heights; net displacements were 1 1/2 and 1 ft.	Knopf and Kirk, 1918; Whitney, 1848; Hobbs, 1910; Bateman, 1961; Bonilla, 1967 and unpublished data
7. Mohawk Valley, California; 1875; N(?)										May have been landsliding rather than faulting.	Turner, 1891, 1876, 1897; Gianella, 1957; Bonilla, 1967
8. Sonora, Mexico; 1887; N		35+	26N			500 ± ft				Possible secondary faulting at maximum distance of 13 mi from main fault but contemporaneity is doubtful.	Aguilera, 1920; Goodfellow, 1888; Richter, 1958
9. San Jacinto, California; 1899; R(?)		2									Danes, 1907; Allen <i>et al.</i> , 1965
10. Yakutat Bay, Alaska; 1899; N(?) and L(?)	8.5-8.6	Unknown	29-42N (?)	See remarks	See remarks		See remarks	See remarks		Maximum uplift 47 ft. Inferred principal faults under water. Uplift, warping, and possible faulting in area at least 30 by 15 mi and probably much greater. Secondary (?) faulting produced scarps as much as 8 ft high, 21 mi from the inferred principal faults.	Tarr and Martin, 1906, 1912; Martin, 1907; Richter, 1958; Bonilla, 1967

Fault (name or location), date, and type of displacement* (See notes at end of table)	Magnitude (Richters) of associated earthquake	Length of surface rupture (miles)	Displacement (feet), main fault (maximum)	Displacements (feet) at indicated distances (miles) from center of main fault zone		Distances (maximum) from center of main zone to outer limits of			Remarks	Principal references	
				Branch faulting	Secondary faulting	Main zone	Branch faulting	Secondary faulting			
1	2	3	4	5	6	7	8	9	10	11	
11. Gold King, Nevada; 1903(?); N(?)		3+								Possibly 12 mi long. Fault marked by open crack 3 to 5 ft wide. No data available on vertical or horizontal components of displacement. Movement also occurred on this fault in 1954.	Siemmons <i>et al.</i> , 1959
12. San Andreas, California; 1906; Rs	8.3	270	20Rs; 3V		2V at 1.5; 0.5Rs at 1.3; 4Ls at 0.3; 1V at 0.2; 4Rs and 2.5V at 0.6	200 ft		1.5 mi		Small cracks in bedrock as much as 10 miles from fault. A tunnel perpendicular to the fault was offset and deformed along nearly a mile of its length; at 4000 ft from the fault the displacement was 14 in.	Lawson <i>et al.</i> , 1908; Bonilla, 1967
13. Shelter Cove (San Andreas?), California; 1906; Rs, RN(?)		2+	(?) Rs; 4(?)V	Displacement unknown	Displacement unknown					Right-slip movement indicated by appearance of trace. May be the San Andreas fault itself or a branch or secondary fault 1.5 to 7 mi east of the San Andreas.	Lawson <i>et al.</i> , 1908; Curray and Nason, 1967
14. Pleasant Valley, Nevada; 1915; N	7.6	*20 to 40	15N	None(?)	3V at 2.5	500 ft		2.5 mi		Northern 5 mi of fault is <i>en echelon</i> to principal segment, partly overlaps it, and is 2 mi perpendicular to it.	Jones, 1915; Page, 1935; Muller, Ferguson, and Roberts, 1931; Ferguson, Roberts, and Muller, 1952
15. Cedar Mountain, Nevada; 1932; RN	7.3	38	2.8Rs; 4V	See remarks	See remarks					Discontinuous traces scattered over a belt 4 to 9 mi wide and 38 mi long.	Gianella and Callaghan, 1934
16. Excelsior Mountains, Nevada; 1934; N	6.5	0.9	0.4N; slight Ls	None	None						Callaghan and Gianella, 1935
17. Hansel Valley (Kosmo), Utah; 1934; N	6.6	5+	1.7N								Neumann, 1936; Ryall <i>et al.</i> , 1966; Eppley, 1965
18. San Jacinto, Mexico; 1934; Rs(?)	7.1									Faulting inferred from aerial photos taken in 1935.	Kovach <i>et al.</i> , 1962; Bichter <i>et al.</i> , 1964
19. Imperial (El Centro), California; 1940; Rs	7.1	40+	19Rs; 4V	0.08Rs and 0.17V at 0.5	None	300 ft	0.5 mi				Ulrich, 1941; Richter, 1958; J. P. Buwalda, unpublished field notes
20. Vacherie, Louisiana; 1943; N		1	0.7N	None	None					In the Red River fault zone and on the flank of a salt dome. Evidence at surface of an earlier fracture; drilling indicates a vertical separation of 3 ft at depth. See text.	First, 1944, U. S. Army Corps of Engineers, 1950

Table 3.1. HISTORIC SURFACE FAULTING IN THE CONTINENTAL UNITED STATES AND ADJACENT PARTS OF MEXICO (cont.)

Fault (name or location), date, and type of displacement* (See notes at end of table)	Magnitude (Richter) of associated earthquake	Length of surface rupture (miles)	Displacement (feet), main fault (maximum)	Displacements (feet) at indicated distances (miles) from center of main fault zone		Distances (maximum) from center of main zone to outer limits of			Remarks	Principal references	
				Branch faulting	Secondary faulting	Main zone	Branch faulting	Secondary faulting			
1	2	3	4	5	6	7	8	9	10	11	
21. Manix, California; 1947; Ls	6.4	1	0.25Ls	None	None					Surface faulting may be secondary to concealed right-slip rupture.	Richter, 1958; Allen <i>et al.</i> , 1965
22. N. of Bakersfield, California; 1949; N(?)	No quake	2								May be related to subsidence.	Hill, 1954; Allen <i>et al.</i> , 1965
23. Fort Sage, California; 1950; N	5.6	5.5	0.6-2N	None	0.25V at 0.25	0.1 mi		0.25 mi		The given distance from the center of the main zone to its outer limits is one-half the perpendicular distance between overlapping <i>en echelon</i> segments.	Gianella, 1957
24. Superstition Hills, California; 1951; Rs	5.6	2±								Strike-slip indicated by <i>en echelon</i> fractures but amount of displacement unknown.	Dibblee, 1954; Allen <i>et al.</i> , 1965
25. White Wolf, California; 1952; LRv and N	7.7	33 (discontinuous)	2.5Ls; 4VRv; 4VN	1Ls at 1.1	0.3N at 8	0.5 mi	1.7 mi	8 mi		Ten feet of shortening measured across main fault zone at one locality. Shaking or regional readjustment of strain produced 0.5 ft vertical faulting for 400 ft along Garlock fault, 20 mi from White Wolf fault.	Buwalda and J. St. Amant, 1955; Dibblee, 1955; Kupfer <i>et al.</i> , 1955; Richter, 1958, pp. 83-84; Whitten, 1955
26. Rainbow Mountain, Nevada; 1954, July; N	6.6	11	1N	None	0.15V at 0.3	0.2 mi		0.3 mi			Tocher, 1956
27. Rainbow Mountain, Nevada; 1954, August; N	6.8	19	2.5N	None	?V at 0.3			0.3 mi		Partly overlaps the July 1954 Rainbow Mountain ruptures and increased the displacement on some of them.	Tocher, 1956
28. Fairview Peak, Nevada; 1954, December; RN	7.1	36	14Rs; 12N	?V at 1.6	3N at 2; 1.5Rs at 2.5; 1.7Rs at 0.6; 1.5N at 3±; 0.5N at 4±	0.5 mi	1.6 mi	4± mi		Produced scarps 16 to 23 ft high. Movement occurred along part of this zone of faulting in 1903 (Gold King fault). Maximum oblique slip was 16 ft.	Siemmons, 1957; Romney, 1957; Steinbrugge and Moran, 1957
29. Dixie Valley, Nevada; 1954, December; N	6.8	38	7± N (15' scarp)	None(?)	2N at 1.4; 0.5N at 2.4; 0.2N at 1.5; 0.2N at 2	3000 ft		2.5 mi			Same
30. San Miguel, Mexico; 1956; RN	6.8	12+	3N; 2.6Rs	None	0.75N at 0.4	450 ft		0.5 mi			Shor and Roberts, 1958
31. Fairweather, Alaska; 1958; Rs	8.0	115-124	21.5Rs; 6V		5N at 0.4			0.6 mi		Vertical displacement recorded along 0.25 mi of the fault. Vertical displacement was 3.5 ft where horizontal displacement was 21.5 ft, indicating oblique slip of 21.8 ft.	Tocher, 1960a; Tocher and Miller, 1959

Fault (name or location), date, and type of displacement* (See notes at end of table)	Magnitude (Richter) of associated earthquake	Length of surface rupture (miles)	Displacement (feet), main fault (maximum)	Displacements (feet) at indicated distances (miles) from center of main fault zone		Distances (maximum) from center of main zone to outer limits of			Remarks	Principal references
				Branch faulting	Secondary faulting	Main zone	Branch faulting	Secondary faulting		
1	2	3	4	5	6	7	8	9	10	11
32. Hebgen Lake, Montana; 1959; N	7.1	15±	20N	3N at 3	2.75N at 4.5±; 1N at 4; 1N at 7.5±; 1V at 8.5±; 0.7V at 8±; 3N at 8	500 ft	3 mi	8.5 mi		Myers and Hamilton, 1964; Witkind, 1964
33. Patton Bay, Alaska; 1964; Rv	8.4	39±	20-23 VRv; 1.41s(?); 26± dip slip	None	None	1500 ft			In addition to faulting of 8 ft at one place, distortion of 1 part vertical in 56 parts horizontal occurred within 800 ft of the fault. Magnitude given is for main shock, whose epicenter was more than 75 mi from the surface faulting. Four aftershocks within 50 mi of the faulting had magnitudes ranging from 6.2 to 6.6. Simultaneous faulting occurred 6 mi away (see Hanning Bay fault).	Plafker, 1965; Plafker, 1967
34. Hanning Bay, Alaska; 1964; Rv		4	16VRv	None	None	650 ft			For magnitude see Patton Bay fault, which occurred simultaneously 6 mi away.	Same
35. Imperial, California; 1966, March; Rs	3.6	6	0.05Rs	None	None					Brune and Allen, 1967
36. San Andreas, Parkfield, California; 1966, June; Rs	5.5	23	0.58Rs 0.16V		0.08Rs at 0.85	10 ft			Displacement given includes tectonic creep that occurred within 50 days following main shock. Initial strike-slip displacement unknown at this locality; at another locality strike-slip displacement totaled about 1.8 in. 10 hr after the shock and 4.7 in. 37 days later.	Brown and Vedder, 1967; Wallace and Roth, 1967
37. Buena Vista Hills, California; continuing fault creep; Rv	No quake								Fault creep has been occurring on this reverse fault, without felt earthquakes, for more than 30 years. Total dip-slip displacement 1.6 ft between 1933 and 1958. See text for other localities where creep has occurred.	Koch, 1933; Wilt, 1958

65

\* Abbreviations for type of displacement: Rs, right-slip; Ls, left-slip; N, normal slip (includes vertical faults); RN, right-normal slip; LN, left-normal slip; Rv, reverse (both high angle and low angle); LRv, left-reverse slip; V, vertical (either normal or reverse); VN, vertical displacement on normal fault; VRv, vertical displacement on reverse fault. Query (?) indicates uncertainty as to type, quantity, or identification. Blank spaces in table indicate no reliable data available.





Fig. 3.2. Ranch buildings astride a gravity graben that formed in the 1959 Montana earthquake. The view is from the top of the main scarp looking toward the opposing scarp about 2 ft high. *A* and *D* correspond to *A* and *D* on Fig. 3.1. Part of the collapsed concrete block wall can be seen under the building. Photo by J. R. Stacy, U.S. Geological Survey.

nery, 1961), but the observed vertical movements in strike-slip faulting in California and Alaska have not been described as systematic. The maximum vertical displacements reported were 3 ft for the 1906 faulting (Lawson *et al.*, 1908, p. 147), 4 ft for the 1940 faulting (Buwalda and Richter, 1941), and 6 ft for the 1958 faulting (Tocher, 1960a, p. 276).

The maximum horizontal and vertical movements given in Table 3.1 generally have not been at the same point on the fault.

### 3.3.4. Map Pattern of Faults

Fault ruptures may consist of a single narrow main break, but commonly they are much more complex

(Fig. 3.3) and are accompanied by subsidiary breaks. The following description of the 1906 California faulting (Lawson *et al.*, 1908, p. 53) makes this point:

The width of the zone of surface rupturing varied usually from a few feet up to 50 feet or more. Not uncommonly there were auxiliary cracks either branching from the main fault-trace obliquely for a few hundred feet or yards, or lying subparallel to it and not, so far as disturbance of the soil indicated, directly connected with it. Where these auxiliary cracks were features of the fault-trace, the zone of surface disturbance which included them frequently had a width of several hundred feet. The displacement appears thus not always to have been confined to a single line of rupture, but to have been distributed over a zone of varying width. Generally, however, the greater part of the dislocation within this zone was confined to the main line of rupture, usually marked by a narrow ridge of heaved and torn sod.

For descriptive purposes it is convenient to classify surface ruptures into three categories or zones. The subsidiary faults can be subdivided into branch faults and secondary faults, the main fault constituting the third category. This classification is illustrated in Fig. 3.4, which shows some of the surface faulting that accompanied the Fairview Peak, Nevada, earthquake of 19. The main fault and closely associated faults which, at a map scale of 1:250,000, form a band of varied width, constitute zone I. For this classification the fault with the greatest displacement, length, and continuity at the surface is considered the main fault for a particular episode of faulting. Some of the main surface faults (e.g., Patton Bay, Alaska, fault of 1964) actually may be subsidiary to a concealed principal fault that is more directly related to the earthquake-generating process. Zone II contains the branch faults; these diverge from and extend well beyond the main zone of faults. They either join the main fault at the surface or can reasonably



Fig. 3.3. Part of the main zone of faulting along the San Andreas fault in 1906. The main trace passes through the center of the photo, and another strand passes through the notch in the skyline to the right of the photo center. The dashed line is drawn to left of the fault traces; the dotted line indicates the inferred position of the traces. The maximum horizontal distance between the lines (on the ridge crest) is 5. Photo by G. K. Gilbert, U.S. Geological Survey.

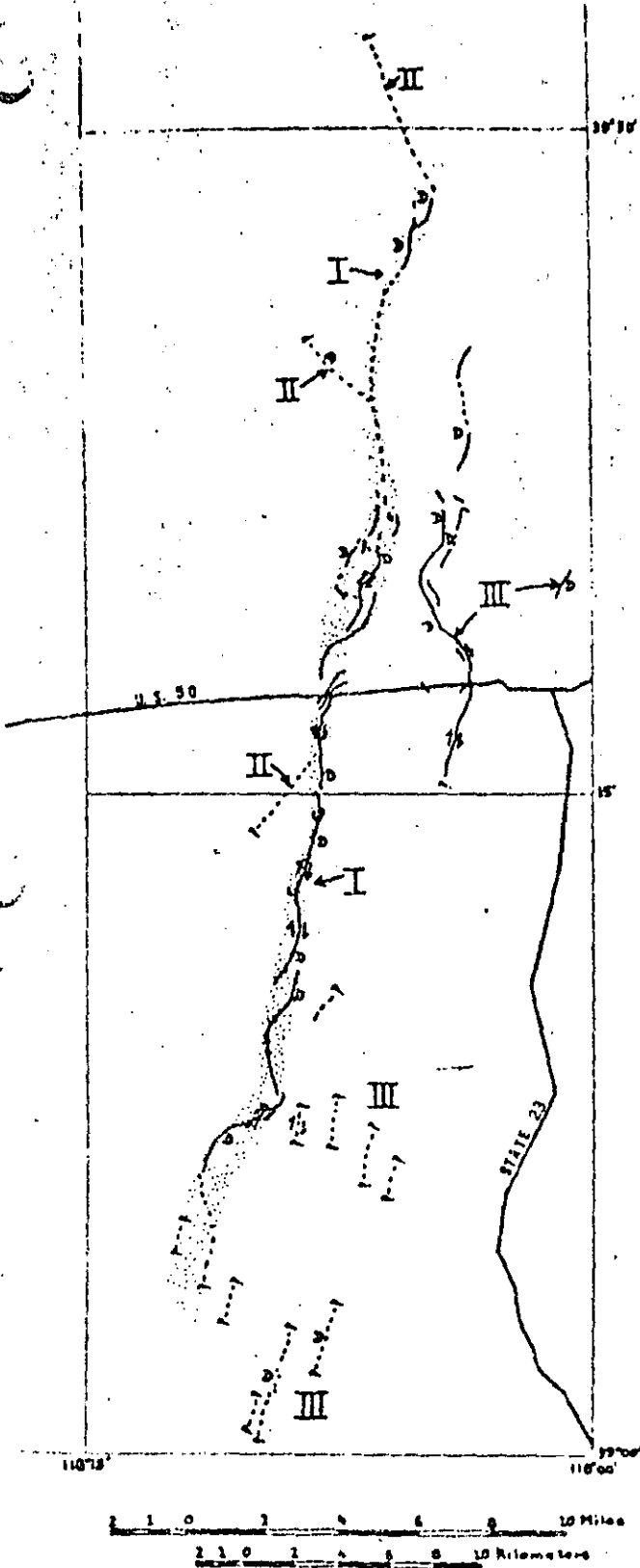


Fig. 3.4. Map of part of the Fairview Peak, Nevada, 1954, faulting, showing main fault zone (I), branch faults (II), and secondary faults (III). The dashed lines indicate faults seen from a distance or interpreted from aerial photographs; the query (?) indicates that the end of break was not determined; D indicates the downthrown side; the single-barbed arrow indicates the relative horizontal displacement. Modified after Stennons, 1957.

be inferred to do so underground. The distinction between the main fault and branch faults is, of necessity, somewhat arbitrary and often difficult to make. The secondary faults that make up zone III have no surface connection with the main fault.

Although the concept of zones is useful, it is not applicable to all historic surface faulting. In the Cedar Mountain, Nevada, faulting of 1932, e.g., the surface ruptures were widely scattered and there was no single, continuous main fault. Another example is the Yakutat Bay, Alaska, faulting of 1899 in which several large faults were postulated but no main fault has yet been identified.

### 3.3.5 Subsidiary Faults

At least half of the historic faulting events in North America have included subsidiary faulting, and the proportion is probably even greater because in only about one-sixth of these events is there good evidence that it did not occur. The importance of subsidiary faulting is indicated in Fig. 3.5, which shows the cumulative lengths of the main and subsidiary surface faults for 15 events. For some of these events the cumulative length of the subsidiary faulting was less than 5%, and for others more than 95%, of the length of the main fault.

The displacements on subsidiary faults can be substantial, even at some distance from the main fault, as shown in Fig. 3.6—a figure based on the data in Table 3.1. The occurrence of displacements of one to a few feet at distances as great as 8.5 mi from the main fault is worthy of note. The distances given in columns 5 through 9 of Table 3.1 were measured at right angles to the trend of the main fault from its approximate centerline. The distances given in columns 5 and 6 are to points where the displacement was actually measured or estimated by the investigator; the corresponding distances in columns 8 and 9 are generally greater, because they were measured to the most distant parts of the branch or secondary ruptures.

The data of Fig. 3.6 have been replotted on Fig. 3.7 with the displacements on the faults expressed as percentages of the displacements on the corresponding main fault. A curve that includes all but three of the data points below it has been sketched on the graph. The curve crosses the 20% line at a distance of 3 or 4 mi from the main fault and decreases at a low rate beyond that, but of course the curve could be drawn in other ways also. The part of the curve to the left of the 1-mi line represents an inference as to the maximum displacement that might occur. The three points above the sketched curve may not be in the correct positions with regard to the amount of displacement during the respective earthquakes. The upper pair were not measured until many years after the 1872 Owens Valley, California,

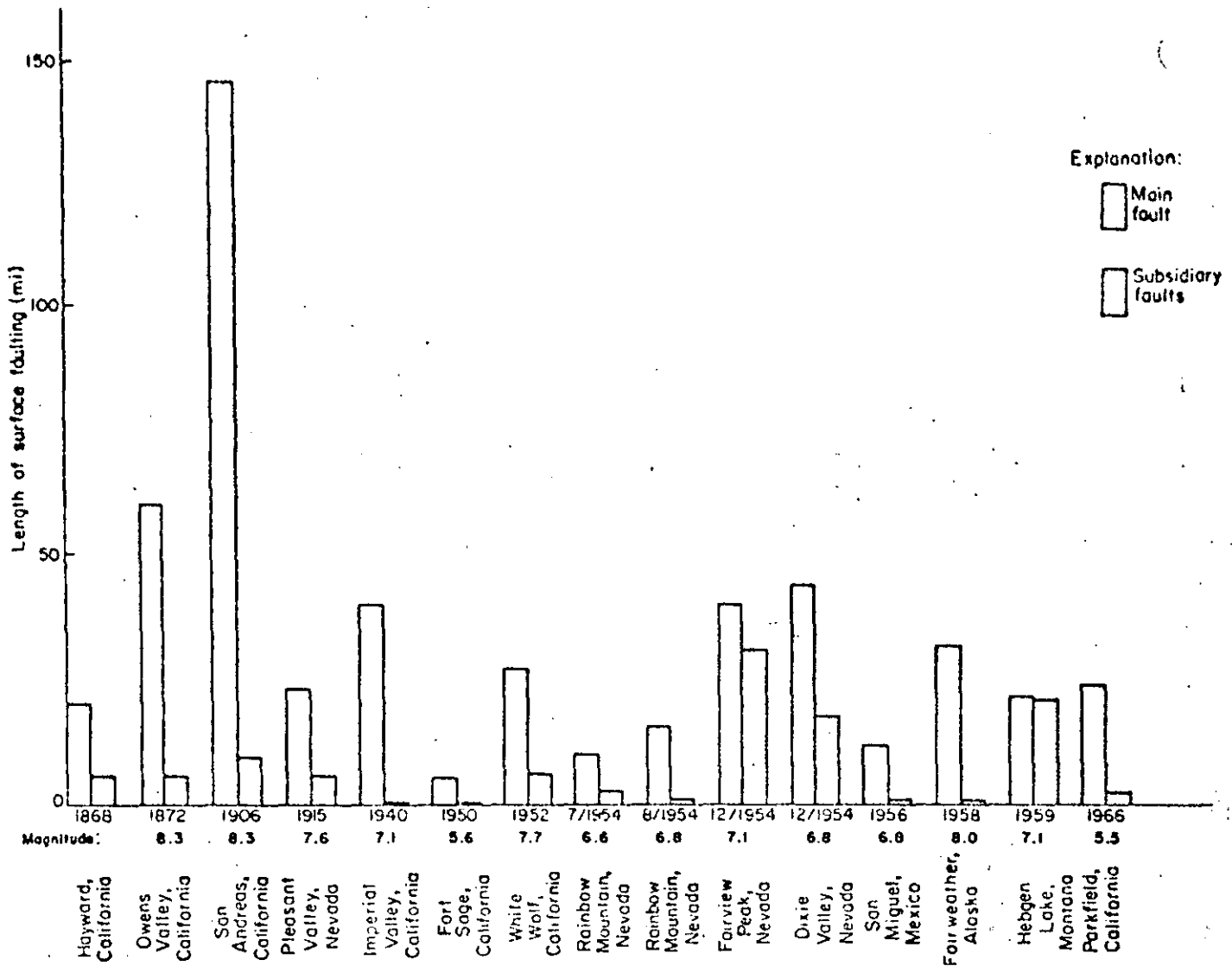


Fig. 3.5. Bar graph showing cumulative lengths of main fault and subsidiary faults for 15 events in North America. Lengths for San Andreas 1906 and Fairweather 1958 exclude parts covered by water or ice.

earthquake, and the lower one is based on the accounts of residents who experienced the 1868 Hayward, California, earthquake.

### 3.3.6 Width of Zones of Faulting

The maximum distances from the centerline of the main zone of faulting to the outer edges of the main, branch, and secondary zones of faulting are plotted against earthquake magnitude (Richter) in Fig. 3.8. The correlation between magnitude and distance to the outer edges of the zones is very poor. The figure serves to illustrate, however, that the maximum widths of the three zones differ among the four types of faults in this sample and that the zones of strike-slip faults are the narrowest. For each type of fault shown in the figure the

maximum distance to the outer edge of the three zones is indicated by roman numerals—I for the main zone, II for the zone of branch faults, and III for the zone of secondary faults. The maximum distance to the outer edge of zone I is less than 0.06 mi for strike-slip faults but between 0.5 and 0.6 mi for the other types; for zone II, 0.5 mi for strike-slip faults and 1.6 to 3 mi for the other types; for zone III, 1.5 mi for strike-slip faults and 8 to 8.5 mi for the other three types in the sample. Some of the zones may have been wider than indicated above. The faulting at Yakutat Bay, Alaska, in 1899 occurred over a broad area, but the main fault has not been identified. Secondary faulting is reported to have occurred 1.8 mi from the Hayward, California, strike-slip fault in 1868 (Lawson *et al.*, 1908, pp. 435 and 4; Radbruch, 1967) but is not shown on the figure because the magnitude is unknown.

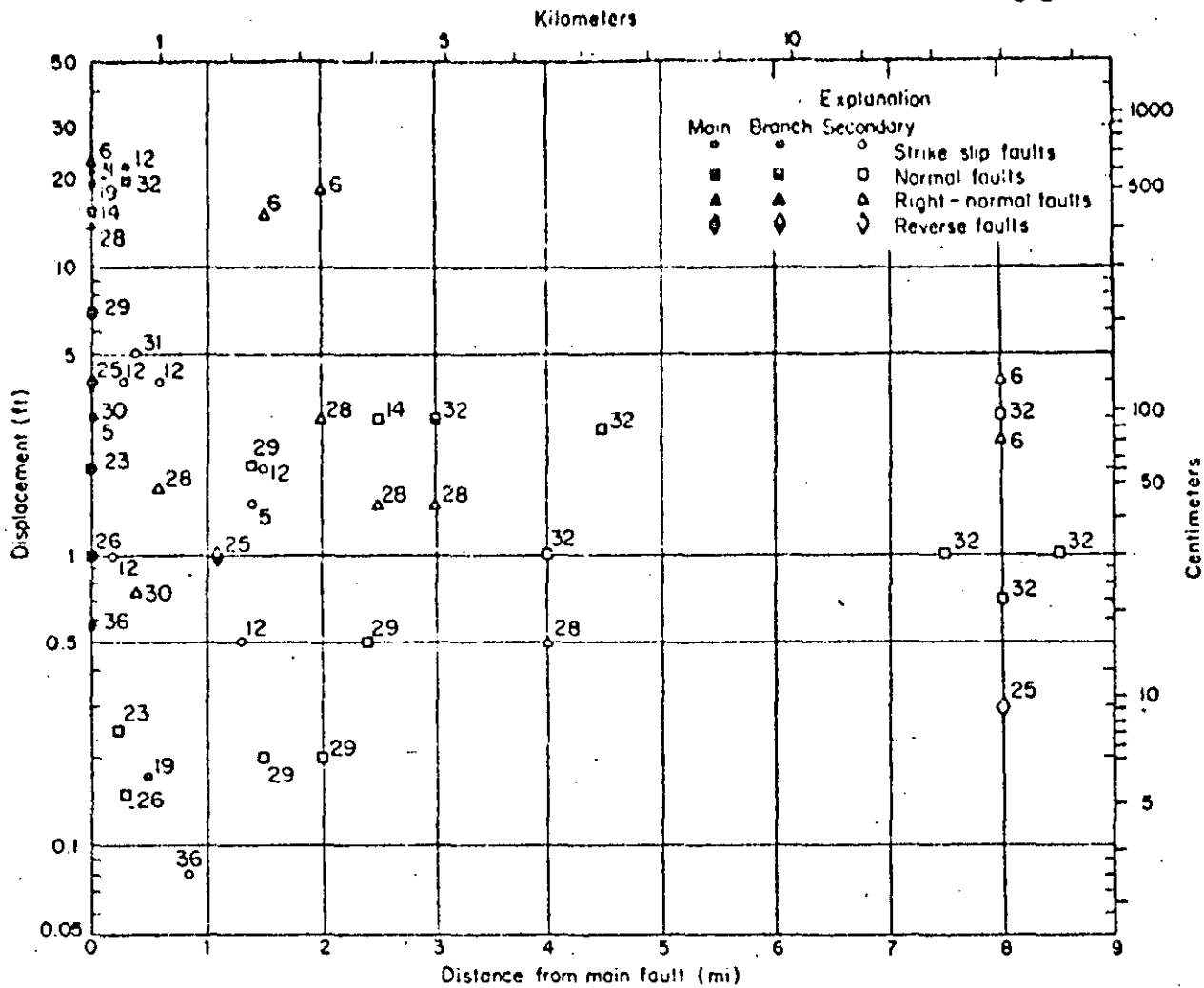
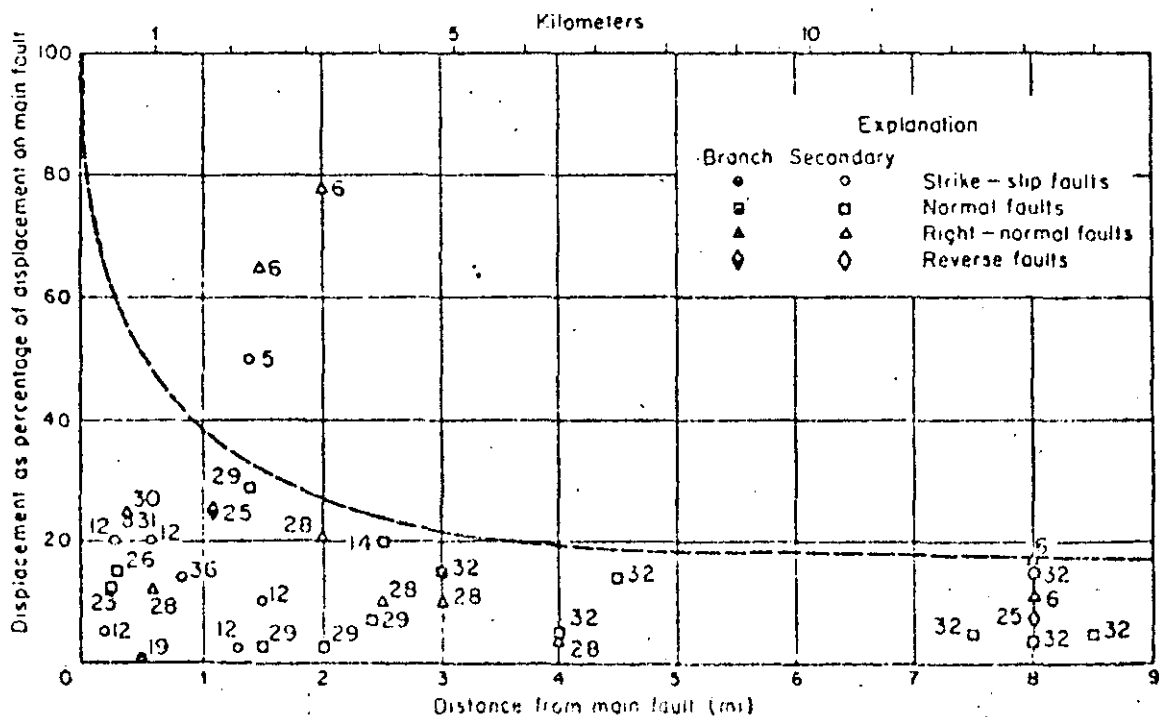


Fig. 3.6. Fault displacement as related to the distance from the main fault. The numbers beside the symbols refer to events listed in Table 3.1.

Fig. 3.7. Fault displacement (in percent of displacement on main fault) as related to distance from the main fault. The numbers beside the symbols refer to events listed in Table 3.1.



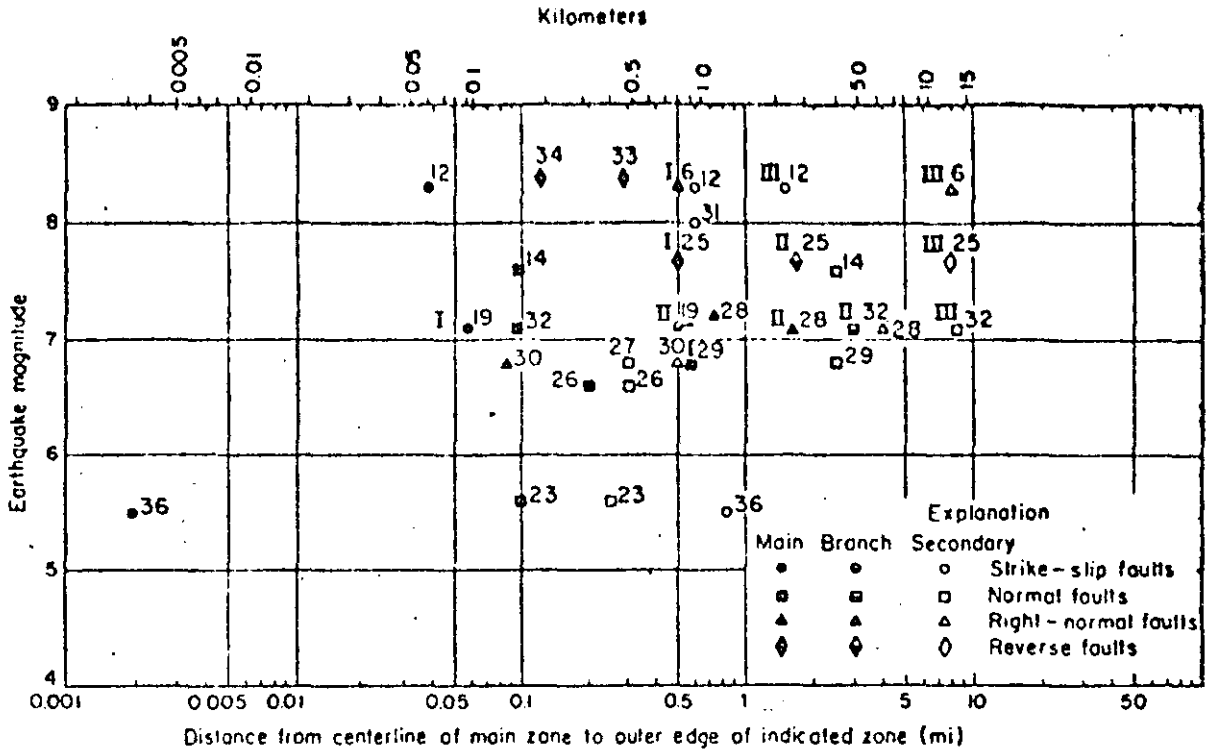


Fig. 3.8. Distances to outer edges of zones of faulting as related to the magnitude of associated earthquakes. The numbers beside the symbols refer to events listed in Table 3.1.

3.3.7 Absorption of Ruptures in Rock and Soil

Fault ruptures can be absorbed (i.e., die out or become indistinguishable) in short distances in rock or soil, but they also can be transmitted through thick deposits of unconsolidated sediments. For example, a part of the White Wolf, California, faulting of 1952 displaced railroad tunnels, but near the surface it seems to have been locally absorbed. Buwalda and St. Armand (1955, p. 48) state: "We have the dilemma that the faults indicated at the tunnels show displacements of at least several feet while the moletracks which are presumably their continuation on the hill above show relatively small offsets both horizontally and vertically." Kupfer and others (1955, p. 74) suggest that fractures conspicuous in rigid concrete might go unnoticed or be distributed and absorbed in the fractured and weathered bedrock and soil near the surface.

Similarly, strike-slip fault displacement of 8 ft in a tunnel diminished to less than 3 ft at the ground surface about 500 ft above during the Idu, Japan, earthquake of 1930 (Suyehiro, 1932, pp. 32-37; Richter, 1958, p. 580). The volcanic rock in which the tunnel was driven is overlain by at least 130 ft of sandy clay lake deposits (Nasu, 1931, p. 456).

The 1915 Pleasant Valley, Nevada, fault scarp does not cross a bedrock spur just north of Cottonwood Creek; this gap in the fault scarp is shown on the map by Page (1935, Fig. 3) and on the 1961 Mount Tobin 15-

min topographic map. Just north of the spur the scarp is about 10 ft high but dies out rapidly as it ascends the spur, then reappears to the south; possibly the displacement was taken up by bending rather than distinct faulting. The Red Canyon fault that accompanied the 1959 Montana earthquake accommodated the displacement locally by warping rather than by the usual high single scarp (Myers and Hamilton, 1964, p. 83).

One of the best examples of local absorption of faulting occurred on the Patton Bay, Alaska, fault in 1964 and is shown in Fig. 3.9. Reverse faulting produced a scarp 8½ ft high (A, Fig. 3.9) in the gravel-covered bedrock at beach level, but no comparable scarp could be found where the principal trace of the fault cut the top of the sea cliff (B, Fig. 3.9). Thus more than 8 ft of displacement was absorbed in rock between points A and B—a distance of about 700 ft. Scarps behind and parallel to the sea cliff suggest incipient landsliding (Plafker, 1967, p. G13), but only minor sloughing occurred during the earthquake; evidently the faulting was distributed and taken up along the numerous joints and minor faults in the rock.

From the foregoing, one might infer that fault ruptures would generally be absorbed by unconsolidated deposits; on the contrary, they have been transmitted through hundreds of feet of unconsolidated deposits, and in some places displacements have apparently been exaggerated in soft deposits. Much of the Owens Valley, California, faulting of 1872 was near

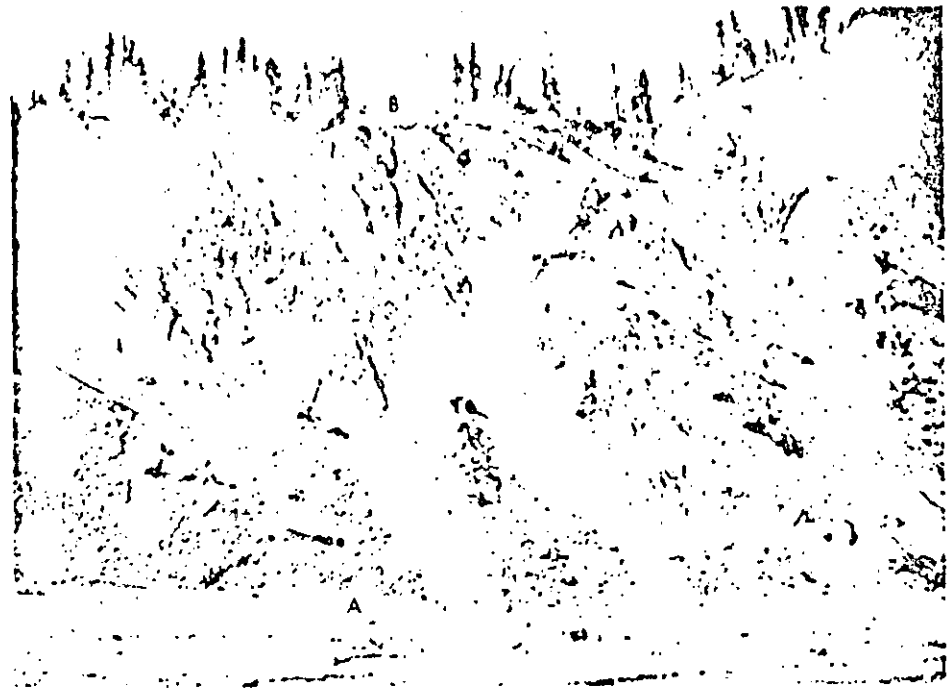


Fig. 3.9. Patton Bay, Alaska, faulting of 1964 produced a scarp 8½ ft high at *A* but no comparable scarp at *B*. The cliff is about 500 ft high, and points *A* and *B* are about 700 ft apart; note the helicopter in foreground.

the center of the valley—an area underlain by 500 ft or more of unconsolidated to semiconsolidated alluvium and lake deposits. The water table there was less than 10 ft below the surface in 1909 (Lee, 1912, p. 72-74) and probably just as shallow in 1872. Similarly, the Imperial Valley, California, faulting of 1940 that involved strike slip of more than 15 ft at the surface was propagated upward through many feet of poorly consolidated deposits. Logs of old water wells in Holtville and El Centro, about 5 mi east and west, respectively, of the 1940 fault, describe the sediments to depths in excess of 700 ft as clay, sand, and soil (Hutchins, 1914, pp. 213-222). A log of a boring in El Centro indicates a depth of 6 ft to groundwater in 1946. This log shows loam and clay to a depth of 100 ft (Duke and Leeds, 1962, Station Data Sheet 64). The sedimentary deposits through which the faulting was propagated are believed to be similar, in thickness and kind, to those described in the logs.

### 3.3.8 Extension and Compression

In addition to the shearing displacements that have been discussed above, surface faulting is often accompanied by extension or compression approximately perpendicular to the fault. An example of extension is shown by the fracture (Fig. 3.10) which formed 15 ft from the Patton Bay, Alaska, fault scarp. Numerous fractures of this kind formed in bedrock on the upthrown sides of the Patton Bay and Hanning Bay faults; they were as much as 0.4 ft wide and 200 ft long and were found as much as 1000 ft from the fault scarps (Pfläcker,

1967, pp. G7-G13 and G34-G35). Open fractures of much larger size commonly accompany normal faulting, because of a change in dip of the fault near the ground surface. An example is a fracture 9 ft wide on the Pleasant Valley, Nevada, fault (Jones, 1915, p. 203 and Fig. 10); another example is an open fracture about 10 ft wide on the Fairview Peak, Nevada, fault (Stemmons, 1957, Fig. 15). Open fractures are sometimes associated with strike-slip faulting, usually at or close to the main fault trace, and are arranged in an *en echelon* pattern. Some of the fractures close immediately, as was the case when a cow fell into a wide fracture along the San Andreas fault in 1906 and was entombed when the crack closed again (Lawson *et al.*, 1908, p. 72).

Fault sags, which are common along strike-slip faults, probably are caused in part by extension transverse to the fault, permitting the settlement of blocks bounded by faults. Many fault sags along the San Andreas fault were deepened in 1906, generally only a few inches but locally as much as 2 ft (Lawson *et al.*, 1908, pp. 32-33, 67, 69, 72-73). Fault sags are found 0.5 to 1 mi from the 1906 trace (Lawson *et al.*, 1908, pp. 33, 75; Higgins, 1961, p. 57).

Compression transverse to the fault occurred, at least locally, in the 1906 California earthquake. For example, at a place where a road perpendicular to the fault was severed and displaced 8 ft, board fences on each side of the road were broken, the boards overlapped, and the adjacent telephone wires sagged, indicating compression perpendicular to the fault (Lawson and others, 1908, p. 102).

Damage to structures by extension and compression can and has occurred on strike-slip faults without net

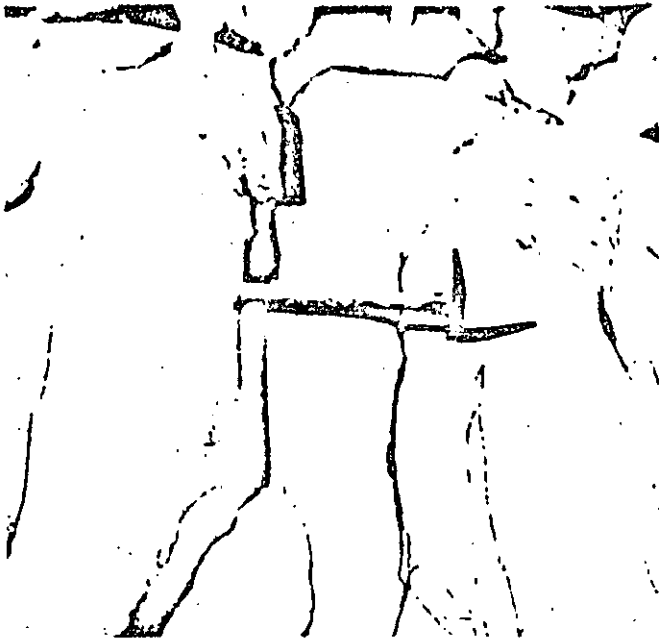


Fig. 3.10. Fracture produced in bedrock near the 1964 Patton Bay, Alaska, fault scarp. The fracture 1.6 in. wide follows a pre-existing tight mineralized joint.

extension or shortening normal to the fault. This occurs where a structure crosses the fault obliquely and the ends of the structure are brought closer together or pulled farther apart as the walls of the fault move. Structures crossing a right-slip fault obliquely from right to left (observer looking along the fault) will be lengthened, and structures crossing from left to right will be shortened; the reverse is true for left-slip faults (Reid, 1910, pp. 33-34). Many examples of this effect were noted in 1906 where the San Francisco aqueduct crossed the fault and was pulled apart or telescoped (Lawson and others, 1908).

### 3.3.9 Tilting, Warping, and Level Changes

Tilting, warping, and changes in elevation can seriously affect canals and shoreline facilities of various kinds by changing their relation to water level. The movements may be restricted to local areas adjacent to a fault or they may affect thousands of square miles. Figure 3.11 shows an example of a large shift in the shoreline as a result of tilting and subsidence of the Hebgen Lake basin in the 1959 Montana earthquake. The tilting extended 5 mi or more from the Hebgen fault scarp. In places the tilting ended not against a fault scarp but against a zone of warping in which 9 ft of vertical change occurred in a horizontal distance of about 650 ft (1 part in 72) without recognized faulting (Myers and Hamilton, 1964, pp. 81-82 Plate 2).

The Yakutat Bay, Alaska, earthquake of 1899 was

accompanied by both widespread elevation and local depression of the shoreline. The maximum uplift relative to sea level was more than 47 ft; in places substantial warping occurred, reaching 1 part vertically to 360 parts horizontally between points 2400 ft apart on the west shore of Disenchantment Bay (Tarr and Martin, 1912, Plate 14). Even steeper warping (1 in 56) occurred in the 1964 Alaskan earthquake within about 800 ft of the Patton Bay fault, and similar warping occurred near the Hanning Bay fault (Plafker, 1967, Fig. 2, pp. G7, G35, and Plate 1, Section A-A'), producing only the open fractures described in Section 3.3.8.

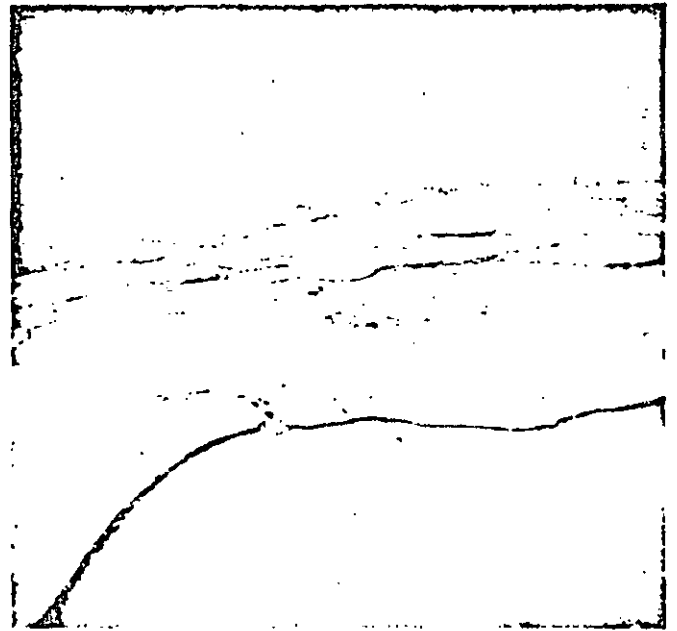


Fig. 3.11. Emergence of shoreline as a result of tilting of the Hebgen Lake basin in the 1959 Montana earthquake. Photo by J. R. Stacy, U.S. Geological Survey.

Regional tectonic movements accompanying large earthquakes have produced changes in level (uplift or depression) over very large areas. The 1899 Yakutat Bay uplift and subsidence has already been mentioned. Similar movements affected possibly 110,000 mi<sup>2</sup> in the 1964 Alaskan earthquake, producing uplifts of as much as 38 ft and downwarps of more than 7 ft (Plafker, 1967, pp. G2-G4). A somewhat lesser area was affected in the 1960 Chilean earthquake where uplift of 2½ m and subsidence of 2 m has been reported (Saint-Amand, 1963, p. 350); recent work by Plafker (written communication, 1968) shows that the maximum uplift and subsidence were 5.7 and 2.7 m, respectively and that more than 75,000 mi<sup>2</sup> were affected. The New Madrid, Missouri, earthquakes of 1811-1812 were accompanied by uplift and depression that produced Reelfoot Lake and lentils of St. Francis Lake; Reelfoot Lake is 8-10 mi long, 2-3 mi wide, and at least 20 ft deep (Fuller, 1912, p. 73).

### 3.3.10 Fault Creep

A description of the process of fault creep or slippage and some of its theoretical and practical consequences is given in Section 2.3, and only a few additional comments will be made here. As noted in the glossary, fault creep as used in this chapter is not necessarily limited to tectonic movements. Withdrawal of petroleum, water, sulfur, salt, or other substances can result in surface subsidence accompanied by extensional and compressional movements on faults. Where this occurs in an area that may be tectonically active it is sometimes extremely difficult to separate natural and artificial causes of fault creep. Examples of such areas are along the Casa Loma and San Jacinto faults, California (Fett, Hamilton, and Fleming, 1967); in parts of the city of Hollister, California, adjacent to the Calaveras fault (Rogers and Nason, 1967, p. 102); along the Buena Vista Hills, California, fault (Allen *et al.*, 1965, pp. 765-766; Whitten, 1961, pp. 313-319; Whitten, 1966, pp. 72-76); and near the Baldwin Hills Reservoir, California, faulting of 1963 (Kresse, 1966). Thus a general term such as fault creep is useful for those situations where the relative importance of tectonic creep and artificially induced creep is unknown.

In addition to the areas of fault creep cited in Chapter 2, several other areas can be mentioned. Tectonic creep has occurred on the San Andreas fault between the winery at Vineyard (Techer, 1960b) and the Parkfield-Cholame area, a distance of about 90 mi (Brown and Wallace, 1968), as well as north of the winery (Techer, 1966) and near San Juan Bautista (Rogers and Nason, 1967). Additional areas of fault creep or probable creep also have been found on the Hayward fault as far north as Richmond, the Calaveras fault near Gilroy, and the Pleasanton fault near Pleasanton, California (Radbruch, 1968; Gibson and Wollenberg, 1968).

Movements suggestive of tectonic creep occurred at least locally prior to the 1959 Montana earthquake. At the Madison Fork Ranch, 8.5 mi from the Red Canyon fault, several prequake scarps showed new movements ranging from a few inches to 1 ft. A lodge built across the projection of one of the scarps was being slowly deformed before the earthquake (Myers and Hamilton, 1964, p. 60), which strongly suggests that tectonic creep was active across this normal fault. In addition to discrete faulting, local warping in this vicinity affected a stream, ditch, and the local runoff pattern.

Fault creep also has occurred at various locations in Texas, where movements on faults have damaged roads, buildings, pipelines, and other structures (Bryan, 1933, p. 439; Sheets, 1947, p. 216; Bell and Brill, 1938; Weaver and Sheets, 1962; Wiggins, 1954, p. 308). Some of these movements are undoubtedly related to the withdrawal of fluids or to secondary effects related to the presence of

salt domes, but some probably are tectonic (Weaver and Sheets, 1962, p. 254; Russell, 1957, p. 69).

Tectonic creep at a rate probably greater than normal is known to have directly followed some faulting and is inferred in other instances. Postquake creep in the Parkfield-Cholame, California, area continued for many weeks after the June 27, 1966, earthquake. Measurements started shortly after the earthquake showed that in 2 weeks about 2 in. of creep occurred at a rapidly decreasing rate and then continued slowly (Wallace and Roth, 1967, Fig. 25). A similar pattern of postquake creep at a rapidly decreasing rate occurred on the Tanna, Japan, fault in 1930 and 1931. However the postquake creep there was less than 0.5 mm (0.02 in.) in the first 2 weeks after the earthquake (Takahasi, 1931, Fig. 10). Postquake creep probably accounts for the following: the fault movement noted after the 1962 Iran earthquake (Ambraseys, 1965a, pp. V-7, V-10); several inches of progressive overlapping of the boards of a broken fence on the Hayward, California, fault in 1868 (Lawson *et al.*, 1908, p. 442); small movements on the 1940 Imperial, California, fault (Richter, 1958, pp. 74-75); and movements at four locations on the White Wolf, California, fault in 1952 (Buwalda and Saint Amand, 1955, pp. 46, 48, 49; Kupfer *et al.*, 1955, p. 68). The postquake creep in the Parkfield-Cholame area exceeded the amount of the initial rupture, but in the other cases it was only a fraction of the initial rupture.

The foregoing examples show that fault creep is a widespread phenomenon that should be considered, along with the possibility of sudden rupture, in planning engineering structures on or near faults. Although not spectacular, it is persistent and capable of causing damage to some kinds of structures. Long-term rates of tectonic creep have ranged from about 0.1 in./year on the Hayward fault (see Chapter 2) to about 0.8 in./year for a long segment of the San Andreas fault (Brown and Wallace, 1968). Most reported fault creep has been concentrated in single narrow zones of a few tens of feet or less in width, but some seems to be distributed in zones as much as 500 ft wide (Brown and Wallace, 1968) or is in parallel overlapping *en echelon* zones more than 175 ft apart (Radbruch, 1968, p. 50; Nason, 1968, p. 87).

## 3.4 GEOGRAPHIC DISTRIBUTION OF HISTORIC SURFACE FAULTING

In North America nearly all of the historic faulting has been in the western part of the continent, as shown in Figs. 3.12 and 3.13 and in Fig. 2.2. The faults shown on Figs. 3.12 and 3.13 can be identified by the numbers, which are keyed to Table 3.1.

Faulting at the surface has not been unequivocally



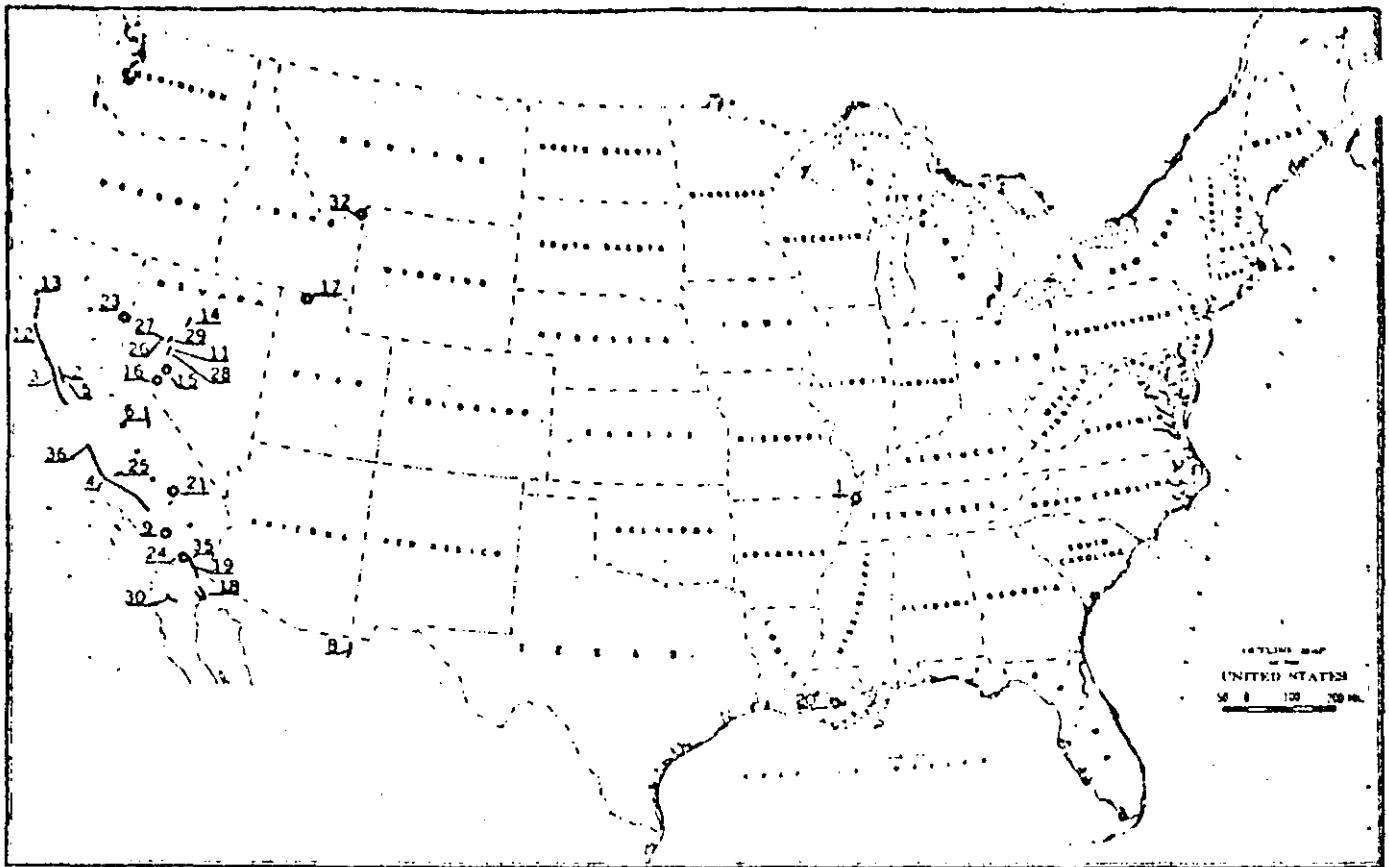


Fig. 3.12. Map of conterminous United States and part of Mexico showing location of historic surface faulting. Numbers identify faults (see Table 3.1).

established for the great New Madrid, Missouri, earthquakes of 1811-1812 (number 1 in table 3.1), but the available evidence strongly suggests that it did occur. Historic accounts mention the formation of both barriers and waterfalls across the Mississippi River near New Madrid; one of the waterfalls was estimated to be 6 ft high (Fuller, 1912, pp. 58, 59 and 62). Reelfoot Lake, which formed in the earthquake, is bounded on its southwest side by a fault, one side of which was uplifted while the other side subsided (Fuller, 1912, p. 75; Fisk, 1944, p. 25 and Fig. 33; U.S. Army Corps of Engineers, 1950, pp. 6-11). This fault extends below the surficial sediments, and borings show a vertical separation of 40 ft in Eocene beds 160 ft below the surface (U.S. Army Corps of Engineers, 1950, Fig. 4). Other areas that sank or rose during the earthquake also may be bounded by faults, but no definite information about them is available.

Faults that are expressed in the present topography are found in several parts of the lower Mississippi Valley (Fisk, 1944; U.S. Army Corps of Engineers, 1950; Veatch, 1906), and faulting of a Pleistocene terrace in the nearby southern part of Illinois has been reported by Ross (1963). This is a seismic region that experienced other great earthquakes prior to 1811 (Fuller, 1912, pp. 12-13) and has had many small to moderate earth-

quakes since then (Heinrich, 1941; U.S. Army Corps of Engineers, 1950, pp. A9-A17; Wollard, 1958; Heyl and Brock, 1961, p. D-4).

The tectonic origin of the Vacherie, Louisiana, faulting of 1943 (number 20 in Table 3.1) remains in doubt. This fault movement was accompanied by a small earthquake felt locally. The nearest seismograph, which was 50 mi away and designed to record large distant shocks, did not record the earthquake. The initial displacement was 3 in. but it increased to about 8 in. in the next 24 hr (U.S. Army Corps of Engineers, 1950, pp. A34-A37; Fisk, 1944, p. 33). The area is on the flank of a salt dome and is also in the Red River fault zone (Fisk, 1944, p. 33). A well being drilled nearby encountered a strong flow of water under 2000 lb of pressure at a depth of 8800 ft shortly before the surface faulting occurred. This flow suggested a possible cause-and-effect relation, but prior movement also had occurred on this fault. Drilling revealed 3.5 ft of vertical separation of upper Pleistocene sediments at a depth of 55 ft (Fisk, 1944, Plate 17).

Several other episodes of surface faulting or probable surface faulting are not shown on the map or table because little is known of them. Most of these have been on the San Andreas fault system in California and include episodes at Dos Palmas (near Salton) in 1868 (Townley and Allen, 1939, p. 50); near Clittenden, in

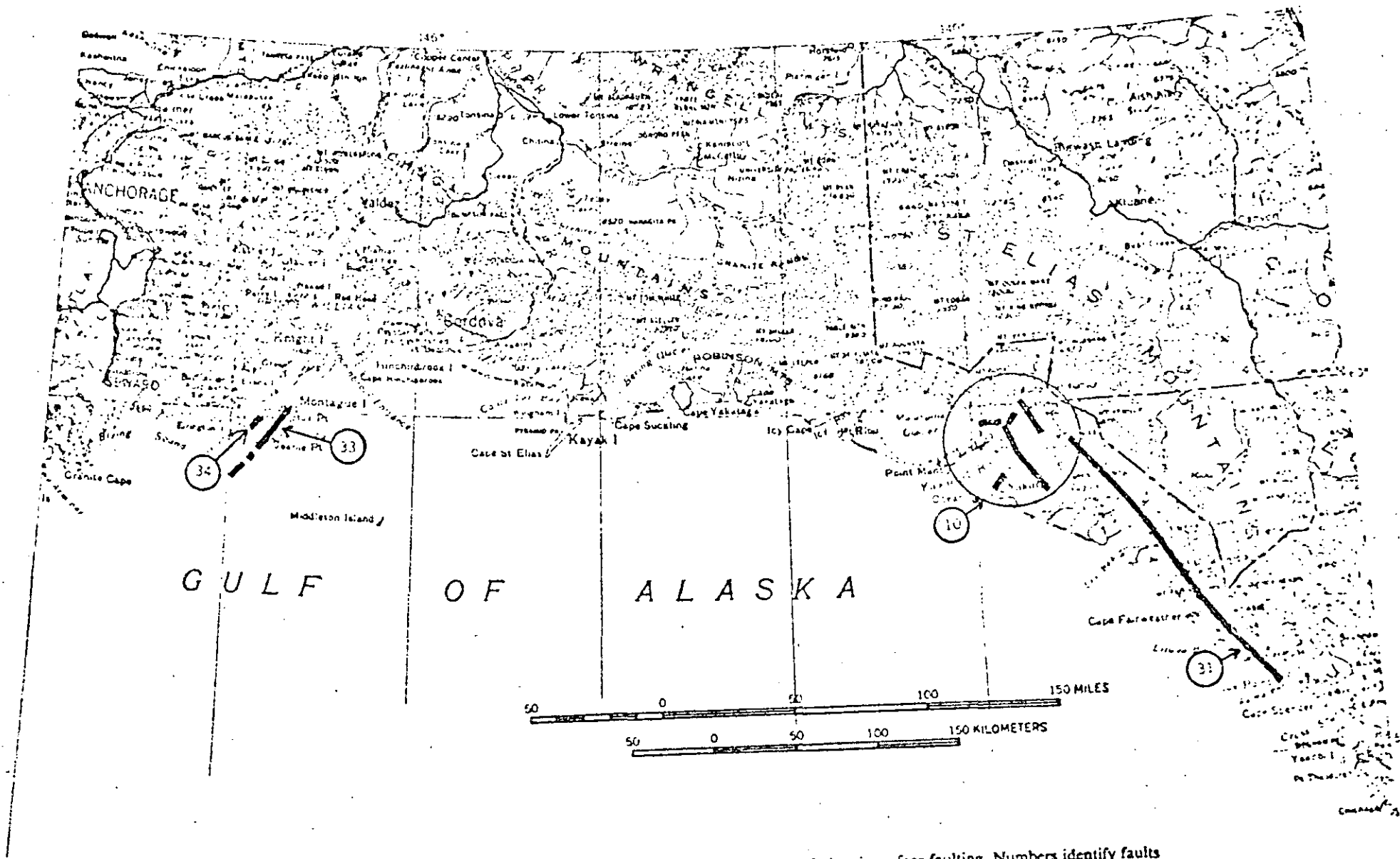


Fig. 3.13. Map of part of Alaska showing the location and approximate extent of historic surface faulting. Numbers identify faults (see Table 3.1).

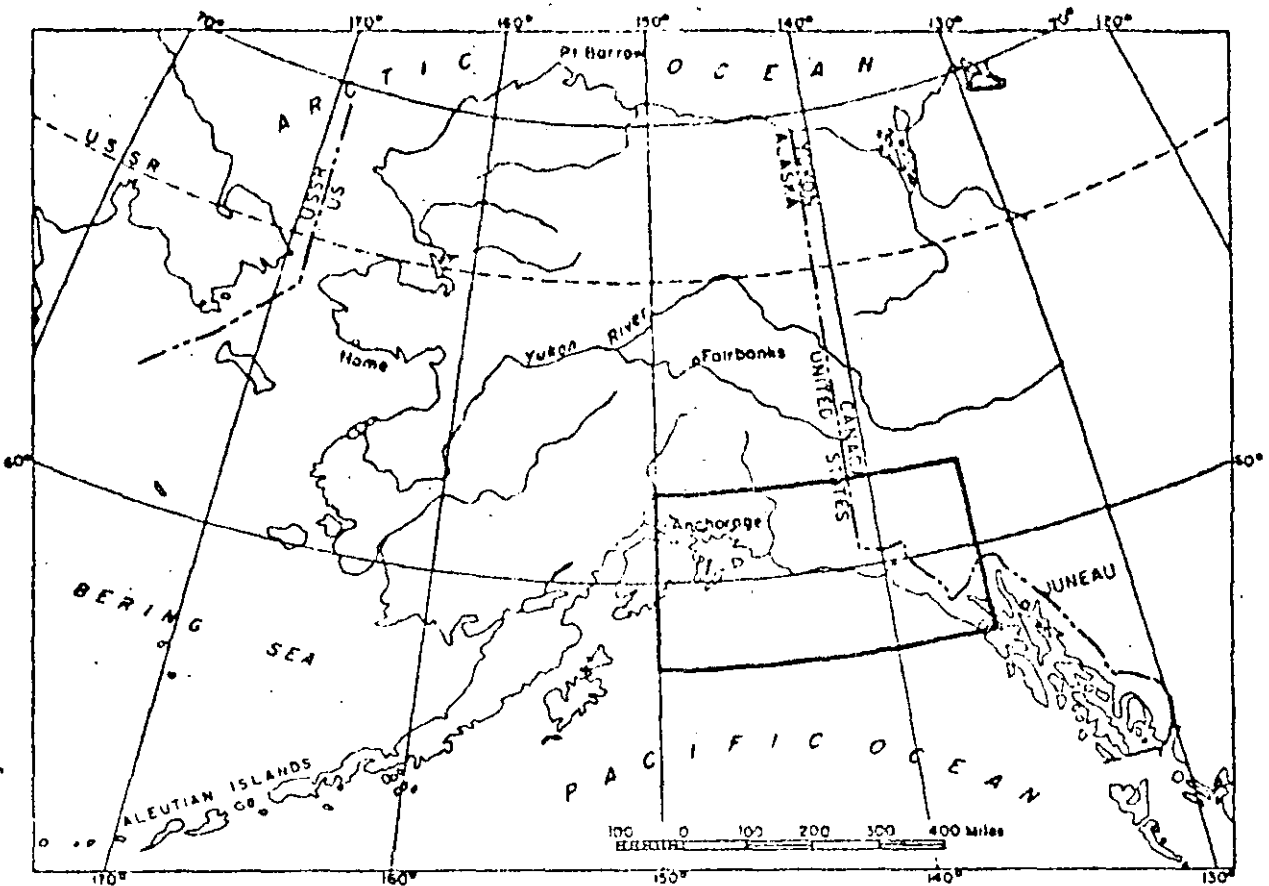


Fig. 3.13A. Index map for Fig. 3.13.

1890 (Lawson and others, 1908, p. 449); near Parkfield, in 1901, 1922, and 1934 (McEvilly, 1966, p. 970; Brown and Vedder, 1967, pp. 9-10); and possibly near Vineyard in 1961. Faulting or possible faulting also has been reported on the Calaveras fault in 1861 near Dublin, California (Radbruch, 1968, pp. 52-53); in 1852 on the Big Pine fault, California (Vedder and Brown, 1968, p. 256); in 1875 in the Mohawk Valley, California (Gianella, 1957, p. 177); and in 1869 on the Olinghouse fault zone, Nevada (Slemmons, 1967, Table I and Fig. 2).

Historic surface faulting has occurred in many places outside North America, but a detailed treatment of it is beyond the scope of this chapter. Faulting has occurred at least once in the following places: Argentina, Bulgaria, Greece, Hawaii, Japan, India, Iran, Kenya, Mongolia, New Zealand, Pakistan, Peru, Sudan, Sumatra, Taiwan, Turkey, and perhaps Yugoslavia. Nearly all of it occurred in the seismically active areas that are apparent in Fig. 2.1. A summary of most of this faulting is given by Richter (1958).

### 3.5 FAULTING AND EARTHQUAKES

#### 3.5.1 Earthquake Intensity Near the Fault

Most American geologists and seismologists believe that shallow earthquakes are caused by elastic rebound

(see Chapter 2) occurring at faults. This theory leads to the conclusion that shaking effects should be greatest at the fault and decrease away from it; experience shows this to be true in a general way. It does not necessarily follow, however, that the intensity of shaking rises to a high peak right at the fault. This idea was developed by Louderback (1942), who pointed out that the source of the earthquake waves, at least of strong earthquakes, was likely to be some miles beneath the surface and that the energy reaching the surface would be about the same in a moderately wide zone along the fault. Housner (Chapter 4) suggests that the accelerations decrease at a slow rate for about the same distance from the fault as the vertical dimension of the fault rupture. Accelerometer records for one earthquake (Parkfield, California, 1966) support this suggestion; they show very little diminution of maximum acceleration within 4 mi of the fault and rapid decrease beyond that. The records show 0.5 g at 270 ft from the fault, 0.46 g at 3.3 mi, 0.4 g at 4 mi, and 0.28 g at 5.7 mi (Cloud and Perez, 1967, Fig. 10). The vertical extent of the faulting has been inferred to be on the order of 6 mi or less (McEvilly, Bakun, and Casaday, 1967, p. 1240) for this earthquake. The lack of markedly greater shaking damage to structures adjacent to the surface trace of faults has been reported by several investigators (Jones, 1915, p. 195; Gianella and Callaghan, 1934, p. 367; Louderback, 1942, pp. 316-37; Steinbrugge and Cloud, 1962, p. 231; and Ambrascio, 1963, p. 735); note, however, the qualifications regarding

the Hebgen Lake, Montana, earthquake given by Steinbrügge (Chapter 9 of this volume).

The examples cited in the reports listed above indicate that neither multidirectional shaking nor "fling" were effective agents of destruction adjacent to the faults. Fling is the rapid displacement of rock masses to positions of no (or greatly reduced) elastic strain, as postulated in the elastic rebound theory. The displacement should be essentially parallel to the fault. Housner (1965, pp. 111-104) concluded from a theoretical analysis that a maximum acceleration on the order of 0.5 g would be produced near the fault, using a differential fault displacement equal to the 1906 San Andreas displacement (about 20 ft) in the analysis. The 0.5 g acceleration that was measured 270 ft from the 1966 Parkfield, California, rupture (fault displacement less than 1 ft at the surface) thus was unexpected; moreover, the displacement pulse was nearly perpendicular rather than parallel to the fault. Seismoscope records from three earthquakes in 1960 and 1961 on the San Andreas fault also show maximum motion at a high angle to the fault (Cloud, 1967, p. 1446). At least locally, displacement pulses directed at a high angle to the fault also occurred in 1906 (Lawson *et al.*, 1908, p. 192). Some short-duration but damaging earthquakes such as the ones at Port Hueneme, California (Housner and Hudson, 1958), Agadir, Morocco (American Iron and Steel Institute, 1962, pp. 81-82) and Skopje, Yugoslavia (Berg, 1964, p. 33; Ambraseys, 1965b, p. S23) have included unidirectional pulses possibly related to fling. Neither the importance nor even the existence of fling is universally accepted, and more facts are clearly needed about it. (See also Chapters 1 and 2 in this volume.)

### 3.5.2 Nonseismic Faults

Louderback (1942, p. 328) reasoned that some active faults, because of their small size or shallowness or because they cut incompetent rocks (even though long and deep), may produce only slight or unfelt earthquakes. Paterson (1958, p. 473), on the basis of laboratory work on marble, suggested that earthquakes would not be associated with faults that develop in calcite rocks. The discovery of fault creep at many places since publication of the reports by Louderback and Paterson leaves no doubt that fault displacement can occur at the surface without felt earthquakes. However, the Imperial, California, 1966 earthquake (magnitude 3.6, modified Mercalli intensity V) had its source "within the soft sedimentary section" (Brune and Allen, 1967, p. 512), and the Hebgen Lake, Montana, faults of 1959 cut through formations containing a large proportion of calcite rocks (Witkind, Hadley, and Nelson, 1964, Plate 5, p. 201). Furthermore, most of the fault segments affected

by tectonic creep have had moderate-to-strong earthquakes (e.g., the Hayward fault, 1868) along them in the historic past. Some historic fault movement has occurred on faults on which no historic earthquakes have been reported (see Section 3.3.10 and numbers 22 and 37 in Table 3.1), but the tectonic origin of those movements is uncertain. In the present state of knowledge, it does not seem prudent to conclude that a given active fault, because of the kinds of rocks it cuts near the surface or the occurrence of tectonic creep along it, will not produce damaging earthquakes.

### 3.5.3 Relation of Fault Displacement and Length at the Surface to Earthquake Magnitude

Figures 3.14 and 3.15 show the relation between the maximum displacement on the main fault at the ground surface and the magnitude of the associated earthquake. The displacement generally increases as the magnitude increases but with considerable scatter of individual points. A line of best fit (*A* in Fig. 3.14) for all the points has been obtained by the method of least squares, yielding the equation

$$\log D = 0.57 M - 3.39 \quad (3.1)$$

in which *D* is the maximum displacement in feet and *M* is the Richter magnitude. The line of best fit for strike-slip faults alone (not shown on graphs) is almost the same as the line for all the faults; the line for normal faults has a somewhat higher slope than the line for all faults. Inasmuch as only a small number of points are presently available for each of the various types of faults and the best-fit lines are not greatly different, all types have been combined in the calculations.

Another line (*B* in Fig. 3.14) that includes the largest displacements for all the faults has been drawn parallel to the line of best fit. Its equation is

$$\log D = 0.57 M - 2.67 \quad (3.2)$$

Still another line (*C* in Fig. 3.14) corresponding to line *B* has been drawn on the other side of line *A*, making the separation between lines *A* and *C* the same as between *A* and *B*. The equation for line *C* is

$$\log D = 0.57 M - 4.11 \quad (3.3)$$

Line *C* bounds all but one of the smallest displacements. The excluded point (number 21) represents the Manix, California, faulting of 1947. Richter has suggested that the surface faulting at Manix was secondary to a concealed main rupture (Richter, 1958, pp. 517-518; Allen *et al.*, 1965, p. 768). A larger displacement would shift point 21 closer to, or perhaps to the other side of, line *C*.

Lines *A*, *B*, and *C* on Figs. 3.14 and 3.15 and the corresponding Eqs. 3.1, 3.2, and 3.3 can be used to esti-

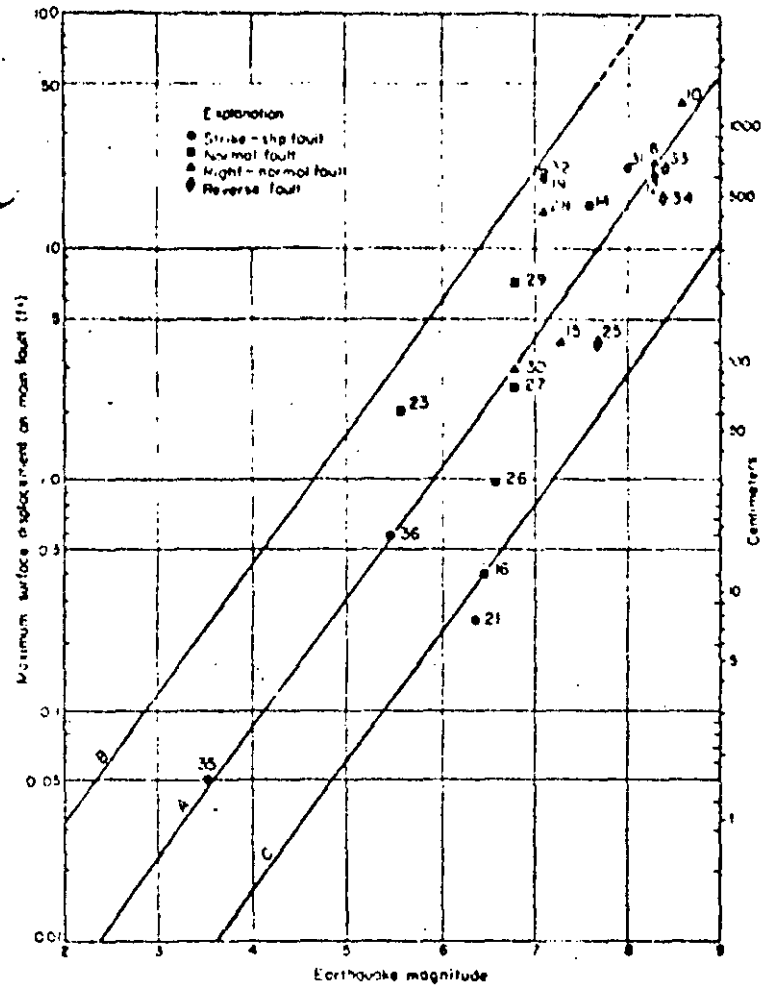


Fig. 3.14. Maximum displacement on main fault at the surface as related to earthquake magnitude (logarithmic plot).

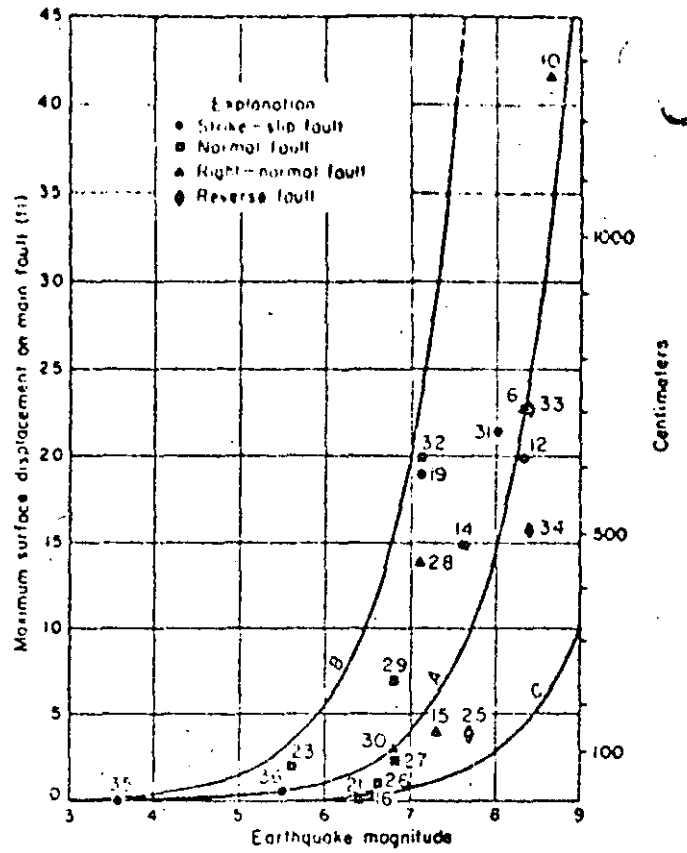
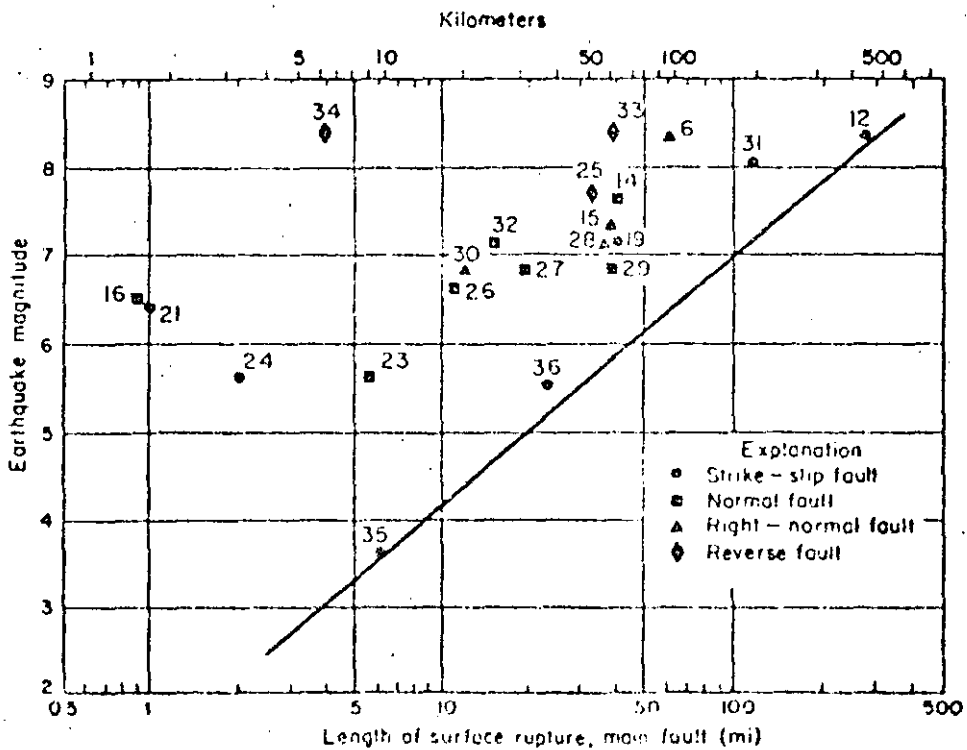


Fig. 3.15. Maximum displacement on main fault at the surface as related to earthquake magnitude (arithmetic plot).

Fig. 3.16. Length of surface rupture on main fault as related to earthquake magnitude.



imate fault displacement at the ground surface that may accompany an earthquake of a given magnitude in the continental United States. Whether line *A*, *B*, or *C* is used depends upon the degree of risk that can be tolerated. For high magnitudes, line *B* indicates displacements substantially larger than any that have been recorded to date, and therefore the line is dashed for magnitudes greater than 7.5. With this exception, the lines permit realistic estimates of fault displacement.

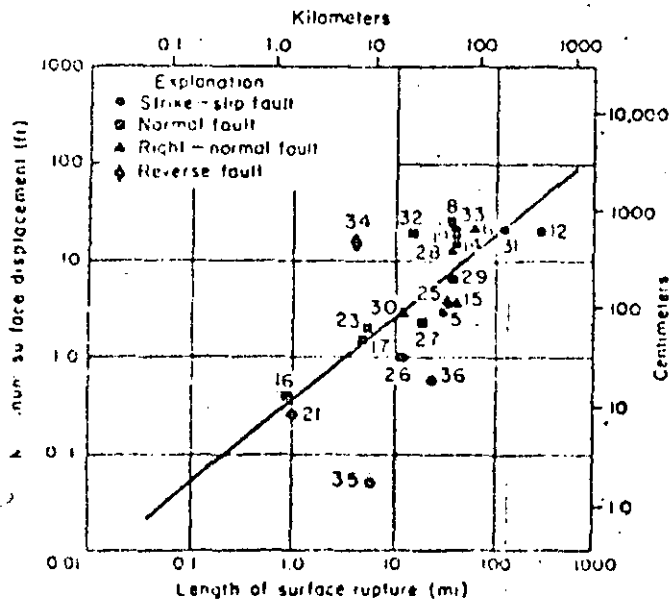
Figure 3.16 shows the relation between earthquake magnitude and the length of surface rupture on the main fault. The points show considerable scatter and a least-squares fit was not made, but a line has been drawn that bounds all of the data points on the graph. The line can be used as an aid in estimating the maximum length of faulting that may occur in an event of a given magnitude. The position of this line is strongly influenced by two small earthquakes accompanied by surface faulting (numbers 35 and 36) that occurred in 1966. Its position may have to be altered if future small earthquakes show even longer surface ruptures.

Figure 3.17 shows in a logarithmic plot the relation between the maximum surface displacement and the length of the surface rupture along the main fault in a given event. The general increase of maximum displacement with length of rupture is apparent. The line of best fit, obtained by the method of least squares, has the equation

$$\log D = 0.86 \log L - 0.46 \quad (3.4)$$

where *D* is maximum displacement in feet and *L* is length of surface rupture in miles. This graph can be used as an aid in roughly estimating the maximum displacement that may occur on a fault of known length.

Fig 3.17. Relation of maximum surface displacement to length of surface rupture on main fault. Numbers beside symbols refer to events listed in Table 3.1.



Surface faulting in a particular earthquake generally extends over just a part of the total length of the preexisting fault. The length of faulting accompanying historic earthquakes in southern California, according to Albee and Smith (1966, p. 20), has commonly been one-half to one-fifth the total length of the fault system on which it occurred, but there is a wide range in this ratio.

Numerous studies have been made relating earthquake magnitude to the product of the length and displacement on the fault. The earliest of these was by Tocher (1958), using California and Nevada faulting; followed by Iida (1959, 1965), using Japanese and worldwide faulting; and Slemmons (1966), using California and Basin-and-Range Province faulting. Slemmons' formula is

$$M = 3.68 + 0.41 \log LD \quad (3.5)$$

in which *L* is surface fault length and *D* is average surface displacement, both in centimeters. Slemmons (1966, p. 83) found that the average displacement in 15 examples ranged from 18 to 60% of the maximum displacement, and the median was 40%. The formulas of Tocher, Iida, and Slemmons are of the same form. King and Knopoff (1968, p. 253) have introduced the square of the displacement to give

$$\log LD^2 = 1.90 M - 2.65 \quad (3.6a)$$

which can be written as

$$M = 1.4 + \frac{\log LD^2}{1.9} \quad (3.6b)$$

in which *L* and *D* are in centimeters. The King-Knopoff formula given above is based on data from 42 worldwide events. The King-Knopoff form of the equation seems to best express the relation between magnitude, fault length, and displacement. However, the coefficients in their equations are based partly on fault dimensions that have been theoretically derived (e.g., 40 ft for Montana, 1959, whereas the maximum scarp height was only 20 ft; see Section 3.3.3 above).

The existing formulas and curves relating earthquake magnitude to fault length and fault displacement can serve as general guides, but without doubt all of them will need to be changed in the future as more data become available. All the formulas have some weaknesses. Among these are (1) the mixing of data from different kinds of faults, (2) the uncertain relation between fault displacement in unconsolidated materials and displacement in rock, (3) insufficient data to evaluate postquake fault creep as a component of fault displacement, (4) inferences regarding the relation between maximum and average fault displacement, both at the surface and at depth, and (5) inferences regarding length of faulting at depth. When the formulas and curves are used, the uncertainties in them need to be seriously considered.

### 3.6 FUTURE FAULTING

Anticipation of future surface faulting involves questions of whether, where, how much, what kind, and when. The answers currently available are not very satisfactory, but much research is underway. These questions are closely related to earthquake prediction, and a better understanding of the processes involved should progressively increase the quality of the answers. Some approaches to these answers are outlined below.

#### 3.6.1 Location of Future Faulting; the Active Fault

One of the best guides to the location of future faulting is the location of past faulting. Geologic evidence shows that most faults have had repeated movement on them, and some are known to have been active for millions of years. The San Andreas fault, e.g., has developed a zone of shearing that is a mile or more wide in some places because of repeated movement.

One would expect that once faults and fault zones were well established, the stresses would tend to be relieved along them rather than in the more sound rock nearby, and historic ruptures support this inference. All of the main faults listed in Table 3.1 (except possibly Sonora, 1887) followed preexisting faults for all or nearly all of their extent. Many of these faults were known prior to the rupturing, and all (except possibly Sonora) could have been identified beforehand; however, extensive investigation would have been necessary in some cases, and some would probably have been considered inactive. The White Wolf fault, which had surface displacements in 1952, had been classed as "dead" on the fault map of California (*Seism. Soc. Am.*, 1922); by 1930 it might have been classed as active, however, because Hoots (1930, p. 315) inferred that large post-Pliocene movement had occurred on it. At least one-third of the branch and secondary faulting listed in Table 3.1 also occurred on preexisting faults that could have been identified as faults by simple geologic investigations; whether the rest could have been identified is problematical. A possible instance of some new faulting occurred in 1959; inconclusive evidence suggests that part of the Hebgen Lake, Montana, faulting of 1959 may have advanced locally into previously unfaulted rock (Myers and Hamilton, 1964, p. 85).

Geologic and historic evidence suggests that most or all of the later movements along parts of some faults have been concentrated in narrow zones. For example, in most (but not all) segments of the San Andreas fault one or two narrower strands within the broad fault zone can be readily identified as being the locus of the more recent

movements. Wallace (1968, Fig. 8 and discussion) has presented evidence that 40 or more displacements have occurred in a strand less than 100 ft wide on one segment of the fault; however, he also notes that particular strand die out and the displacement is taken up by nearby *en echelon* strands. The 1906 ruptures were *en echelon* in at least two places, but unfortunately the width of the *en echelon* zone is not known (Lawson and others, 1908, p. 68; Taber, 1906, p. 307 and Fig. 2).

The 1966 Parkfield, California, faulting closely followed two strands within the fault zone that showed recent movement and had been identified prior to the earthquake; moreover, some of the 1966 ruptures were about 25 ft from ruptures formed in the 1934 earthquake (Brown and Vedder, 1967, pp. 4, 10). A similar example is provided by the 1966 Imperial faulting that occurred exactly where the 1940 ruptures had occurred (Brune and Allen, 1967, pp. 501, 502). The Borrego Mountain, California, faulting of April 9, 1968, closely followed earlier lines of faulting, but it also crossed areas that had no surface evidence of previous faulting (Allen *et al.*, 1968).

The examples given above were on strike-slip faults; repetition of breaks on two normal faults show more discordance between older and newer breaks. Most of the August 23, 1954, Rainbow Mountain, Nevada, faulting coincided with or extended the July 6, 1954, faulting, but some of the new ruptures were subparallel to the older ones (Tocher, 1956). Part of the December 1954 faulting north of Fairview Peak, Nevada, on the Gold King fault coincided with ruptures formed about 1903, but over most of its length it did not. Study of a somewhat generalized map of the 1903 breaks shows that the 1954 faulting crisscrossed the earlier faulting but was more than 200 ft from it in many places and more than 1000 ft in some places (Stemmons *et al.*, 1959, pp. 262-263, map).

Geologic evidence shows that some faults that were dormant for a long time have been reactivated. An example of this is the Hurricane fault in southwestern Utah, which has had several episodes of movement separated by periods of quiescence. Some of the quiescent periods were long enough to permit erosion of the faulted terrane and emplacement of lava flows. Its latest rejuvenation extends into the present and some earthquakes have occurred on the fault in historic time (Gardner, 1941; Averitt, 1964). Little is known of the rate at which faults, dormant for a long period (in geologic terms), have been reactivated.

The available evidence suggests that future faulting will occur on existing faults rather than on newly formed faults and that it probably will occur on those faults that are active. An active fault can be defined as one that has moved in the recent past and may move in the near future. The "recent past" as used here includes the current hour and extends back an indefinite time that many geologi-

ould take to include at least the Holocene Epoch (about 10,000 years). The "near future" as used above includes a length of time on the order of the useful life of engineering structures or the time span considered in long-range plans for the future. The determination of whether a fault is "active," as defined above, involves geology, geophysics, geodesy, and engineering. Some criteria currently in use are (1) the occurrence of earthquakes that can be related to the fault with reasonable assurance; (2) one or more episodes of surface rupture (including tectonic creep) or acute bending in the recent past as defined above; (3) instrumental evidence of elastic or inelastic strain; and (4) structural coupling to another fault (or other tectonic feature such as a monocline) that is active. At present some active faults may not be identifiable, but the ability to identify them should improve with time.

### 3.6.2 Amount of Future Faulting

At present, estimates of the type and amount of future faulting that may occur are based on the historic and geologic record. The type (i.e., normal, reverse, etc.) of faulting that has occurred in the past is generally assumed to be the type that will occur in the future. The length and displacement of prehistoric faulting sometimes can be estimated from the displacement of the ground surface—the height and length of scarps and the amount of offset of streams. The general rates of older displacements often can be estimated by measuring the displacement of formations of known age. With this geologic information as background, useful estimates of future displacement can be made by using various empirical curves and formulas (such as those in Section 3.5.3) that interrelate length, displacement, and earthquake magnitude. Conversely, estimates of magnitudes of prehistoric earthquakes can be made if the length and displacement of prehistoric ruptures can be determined by geologic investigations. Research currently underway may someday permit estimates of future displacement based on measurements of strain on the fault system.

### 3.6.3 Likelihood of Future Faulting

The most difficult question to answer regarding active faults is if and when surface faulting will occur. Surface faulting is more commonly associated with the larger-than the smaller-magnitude earthquakes, although this imbalance is probably much less than the present record indicates. The surface displacements that accompany small earthquakes are small, and the evidence is likely to be quickly obliterated, especially for strike-slip displace-

ments in areas that have few artificial structures; moreover, many earthquakes of moderate to small size in the western United States were never investigated in the field by geologists or seismologists. Furthermore, the recognition of the process of tectonic creep introduces the possibility that surface rupture on faults may accompany shallow-focus earthquakes of any magnitude.

The question of when surface faulting will occur cannot be satisfactorily answered at present on either a long-term or short-term basis. The problem is closely allied to earthquake prediction, and current research toward that goal probably will produce useful results. Various methods have been used to estimate the time between large earthquakes. By using strain rates, Reid estimated a return period of about 100 years after 1906 for the next great earthquake on the San Andreas fault in central California (see Chapter 2). By using rates of slip, Wallace (1968) has tentatively suggested a 700-year recurrence interval for another part of the San Andreas fault; he also suggested that the recurrence intervals on different parts of the fault may differ by several orders of magnitude. Another approach involves the use of the statistical relationship between the frequency of earthquakes and their magnitude. A study by Allen and others (1965) of the southern California region, using earthquake statistics for the 29-year period between 1934 and 1963, yielded a recurrence interval of 52 years for large earthquakes in that region; the historic record of large earthquakes since 1800 suggests that the calculated rate may be approximately correct. The same study, however, when applied to small areas within southern California yielded results that the authors believed were unrealistic. Recurrence curves for much of the western United States have been published by Ryall, Slemmons, and Gedney (1966). Other approaches involve measuring changes in various properties of the rock in the vicinity of the fault, but no practical method of estimating time of occurrence is yet available.

## ACKNOWLEDGMENTS

A review of historic surface faulting that forms much of the basis for this chapter was sponsored by the U.S. Atomic Energy Commission, Division of Reactor Development and Technology. The writer also acknowledges with thanks the ideas and information supplied by various colleagues, particularly E. H. Pampeyan, George Plafker, D. H. Radbruch, and Julius Schlocker—the sources of other ideas and data are cited in the text. Jane M. Buchanan compiled some of the data and prepared many of the illustrations. Publication of this chapter was authorized by the Director, U.S. Geological Survey.



## REFERENCES

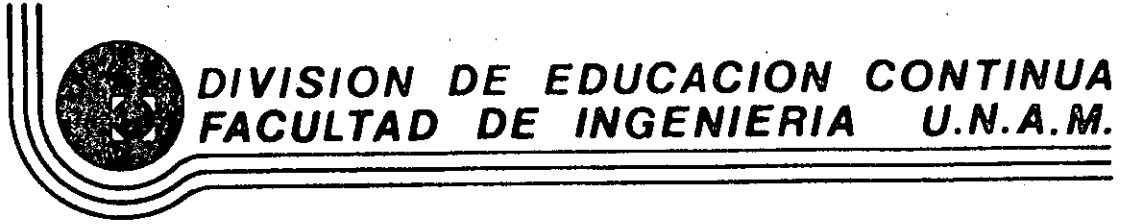
- Aguilera, J. G. (1920). "The Sonora Earthquake of 1887," *Seism. Soc. Am. Bull.*, 10(1), 31-44.
- Albee, A. L., and J. L. Smith (1966). "Earthquake Characteristics and Fault Activity in Southern California," in *Engineering Geology in Southern California*, pp. 9-34, Glendale, Los Angeles Section of Association of Engineering Geologists.
- Allen, C. R., A. Grantz, J. N. Brune, M. M. Clark, R. V. Sharp, T. G. Theodore, E. W. Wolfe, and M. Wyss (1968). "The Borrego Mountain, California, Earthquake of 9 April 1968—A Preliminary Report," *Seism. Soc. Am. Bull.*, 58(3), 1183-1186.
- Allen, C. R., P. St. Amand, C. F. Richter, and J. M. Nordquist (1965). "Relationship Between Seismicity and Geologic Structure in the Southern California Region," *Seism. Soc. Am. Bull.*, 55(4), 753-797.
- Ambroseys, N. N. (1960). *On the Seismic Behavior of Earth Dams, Proceedings of the Second World Conference on Earthquake Engineering*, Vol. 1, pp. 331-358, Tokyo and Kyoto, Japan.
- Ambroseys, N. N. (1963). "The Buyin-Zara (Iran) Earthquake of September 1962—A Field Report," *Seis. Soc. Am. Bull.*, 53(4), 705-740.
- Ambroseys, N. N. (1965a). *An Earthquake Engineering Study of the Buyin-Zahra Earthquake of September 1, 1962, in Iran, Proceedings of the Third World Conference on Earthquake Engineering*, Vol. 3, pp. V7-V26, New Zealand.
- Ambroseys, N. N. (1965b). *An Earthquake Engineering Viewpoint of the Skopje Earthquake, 26th July, 1963, Proceedings of the Third World Conference on Earthquake Engineering*, Vol. 3, pp. S22-S38, New Zealand.
- American Geological Institute (1960). *Glossary of Geology and Related Sciences*, 2nd ed., Washington, D.C.
- American Iron and Steel Institute (1962). *The Agadir, Morocco, Earthquake*, New York: American Iron and Steel Institute.
- Averitt, P. (1964). "Table of Post-Cretaceous Geologic Events Along the Hurricane Fault, Near Cedar City, Iron County, Utah," *Geol. Soc. Am. Bull.*, 75(9), 901-908.
- Bateman, P. C. (1961). "Willard D. Johnson and the Strike-Slip Component of Fault Movement in the Owens Valley, California, Earthquake of 1872," *Seism. Soc. Am. Bull.*, 51(4), 483-493.
- Bell, D. E., and V. A. Brill (1938). "Active Faulting in Lavaca County, Texas," *Am. Assoc. Petrol. Geol. Bull.*, 22(1), 104-106.
- Berg, G. V. (1964). *The Skopje, Yugoslavia, Earthquake July 26, 1963*, New York: American Iron and Steel Institute.
- Biehler, S., R. L. Kovach, and C. R. Allen (1964). "Geophysical Framework of Northern End of Gulf of California Structural Province," in T. H. van Andel and G. B. Shor, Jr. (eds.), *Marine Geology of the Gulf of California—A Symposium*, pp. 146-143, American Association of Petroleum Geologists.
- Bonilla, M. G. (1967). "Historic Surface Faulting in Continental United States and Adjacent Parts of Mexico," *U. S. Geological Survey Open-File Report*; also *U.S. Atomic Energy Commission Report TID-24124*.
- Brown, R. D., Jr., and J. G. Vedder (1967). "Surface Tectonic Fractures Along the San Andreas Fault, California," in R. D. Brown, Jr., et al., *The Parkfield-Cholame, California, Earthquakes of June-August 1966—Surface Geologic Effects, Water-Resources Aspects, and Preliminary Seismic Data*, U. S. Geological Survey Professional Paper 579, pp. 2-23.
- Brown, R. D., Jr., and R. E. Wallace (1968). "Current and Historic Fault Movement Along the San Andreas Fault Between Paicines and Camp Dix, California," in W. R. Dickinson and A. Grantz (eds.), *Proceedings of the Conference on Geologic Problems of the San Andreas Fault System, September 14-16, 1967, Stanford University*, pp. 22-41, Stanford, California: Stanford University Press.
- Brune, J. N., and C. R. Allen (1967). "A Low-Stress-Drop, Low-Magnitude Earthquake with Surface Faulting—The Imperial, California, Earthquake of March 4, 1966," *Seism. Soc. Am. Bull.*, 57(3), 501-514.
- Bryan, F. (1933). "Recent Movements on a Fault of the Balcones System, McLennan County, Texas," *Am. Assoc. Petrol. Geol. Bull.*, 17(4), 439-442.
- Buwalda, J. P., and C. F. Richter (1941). "Imperial Valley Earthquake of May 18, 1940," *Geol. Soc. Am. Bull.*, 52(12), 1944-1945.
- Buwalda, J. P., and P. St. Amand (1955). "Geological Effects of the Arvin-Tehachapi Earthquake," *Calif. Div. Mines Bull.*, 171, 41-56.
- California Department of Water Resources (1967). "Earthquake Damage to Hydraulic Structures in California," *California Department of Water Resources Bulletin 116-3*.
- Callaghan, E., and V. P. Gianella (1935). "The Earthquake of January 30, 1934, at Excelsior Mountains, Nevada," *Seism. Soc. Am. Bull.*, 25(2), 161-168.
- Chinnery, M. A. (1961). "The Deformation of the Ground Around Surface Faults," *Seism. Soc. Am. Bull.*, 51(3), 355-372.
- Cloud, W. K. (1967). "Seismoscope Results from Three Earthquakes in the Hollister, California, Area," *Seism. Soc. Am. Bull.*, 57(6), 1445-1448.
- Cloud, W. K., and V. Perez (1967). "Accelerograms—Parkfield Earthquake," *Seism. Soc. Am. Bull.*, 57(6), 1179-1192.
- Curry, J. R., and R. D. Nason (1967). "San Andreas Fault North of Point Arena, California," *Geol. Soc. Am. Bull.*, 78(3), 413-418.
- Danes, J. V. (1907). "Das Erdbeben von San Jacinto am 25 Dezember 1899," *Geog. Gesell. Wien Mitt.*, 50, 339-347.
- Dibblee, T. W., Jr. (1954). "Geology of the Imperial Valley Region, California," Chap. 2 in R. H. Jahns (ed.), *Geology of Southern California*, pp. 21-28, California Division of Mines Bulletin 170.
- Dibblee, T. W., Jr. (1955). *Geology of the Southeastern Margin*

- of the San Joaquin Valley, California, pp. 23-24, California Division of Mines Bulletin 171.
- Duke, C. M. (1960). *Foundations and Earth Structures in Earthquakes, Proceedings of the Second World Conference on Earthquake Engineering*, Vol. 1, pp. 435-455, Tokyo and Kyoto, Japan.
- Duke, C. M., and D. J. Leeds (1962). *Site Characteristics of Southern California Strong-Motion Earthquake Stations*, University of California at Los Angeles, Dept. Eng. Rept. No. 62-55.
- Eppley, R. A. (1965). "Stronger Earthquakes of the United States (Exclusive of California and Western Nevada)," Part I in *Earthquake History of the United States*, rev. ed. (through 1963): U.S. Coast and Geodetic Survey No. 41-1.
- Ferguson, H. G., R. J. Roberts, and S. W. Müller (1952) *Geologic Map of the Golconda Quadrangle, Nevada*, U.S. Geological Survey Geologic Quadrangle Map [GQ-15], scale 1:125,000.
- Fett, J. D., D. H. Hamilton, and F. A. Fleming (1967). "Continuing Surface Displacements Along the Casa Loma and San Jacinto Faults in San Jacinto Valley, Riverside County, California," *Engr. Geol.*, 4 (1), 22-32.
- Fisk, H. N. (1944). *Geological Investigation of the Alluvial Valley of the Lower Mississippi River*, U.S. Mississippi River Commission Report.
- Florensov, N. A., and V. P. Solonenko (eds.) (1963). "Gobi-Altayskoye Zemletryasenie," *Iz. Akad. Nauk SSSR*; also 1965, *The Gobi-Altai Earthquake*, U.S. Department of Commerce (Eng. trans.).
- Fuller, M. L. (1912). *The New Madrid Earthquake*, U. S. Geological Survey Bull. 494.
- Gardner, L. S. (1941). "The Hurricane Fault in Southwestern Utah and Northwestern Arizona," *Am. J. Sci.*, 239(4), 241-260.
- Gianella, V. P. (1957). "Earthquake and Faulting, Fort Sage Mountains, California, December 1950," *Seism. Soc. Am. Bull.*, 47(3), 173-177.
- Gianella, V. P., and E. Callaghan (1934). "The Cedar Mountain, Nevada, Earthquake of December 20, 1932," *Seism. Soc. Am. Bull.*, 24 (4), 345-384.
- Gibson, W. M., and H. A. Wollenberg (1968). "Investigations for Ground Stability in the Vicinity of the Calaveras Fault, Livermore and Amador Valleys, Alameda County, California," *Geol. Soc. Am. Bull.*, 79 (5), 627-638.
- Gilbert, G. K. (1890). *Lake Bonneville*. U.S. Geological Survey Monograph 1.
- Goodfellow, G. E. (1888). "The Sonora Earthquake," *Science*, 11, 162-166.
- Heinrich, R. R. (1941). "A Contribution to the Seismic History of Missouri," *Seism. Soc. Am. Bull.*, 31 (3), 187-224.
- Hetyl, A. V., Jr., and M. R. Brock (1961). "Structural Framework of the Illinois-Kentucky Mining District and Its Relation to Mineral Deposits," in *Geological Survey Research, 1961*, pp. D3-D6. U.S. Geological Survey Professional Paper 424-D.
- Higgins, C. G. (1961). "San Andreas Fault North of San Francisco, California," *Geol. Soc. Am. Bull.*, 72 (1), 51-68.
- Hill, M. L. (1954). "Tectonics of Faulting in Southern California" in R. H. Jahns (ed.), *Geology of Southern California*, pp. 5-13, California Division of Mines Bulletin 170.
- Hobbs, W. H. (1910). "The Earthquake of 1872 in the Owens Valley, California," *Beitr. Geophys.*, 10 (3), 352-385.
- Hoors, H. W. (1930). *Geology and Oil Resources Along the Southern Border of San Joaquin Valley, California*, pp. 243-338, U.S. Geological Survey Bulletin 812-D.
- Housner, G. W. (1965). *Intensity of Earthquake Ground Shaking Near the Causative Fault, Proceedings of the Third World Conference on Earthquake Engineering, New Zealand, 1965*, Vol. 3, pp. III 94-III 115.
- Housner, G. W., and D. E. Hudson (1958) "The Port Huene [California] Earthquake of March 18, 1957," *Seism. Soc. Am. Bull.*, 48 (2), 163-168.
- Hutchins, W. A. (1914). *Report on Investigation of Wells in Imperial Valley, 1914*, pp. 212-228, California Department of Engineering, Fourth Biennial Report.
- Iida, Kumizi (1959). "Earthquake Energy and Earthquake Fault," *Nagoya Univ., J. Earth Sci.*, 7 (2), 98-107.
- Iida, K. (1965). "Earthquake Magnitude, Earthquake Fault, and Source Dimensions," *Nagoya Univ., J. Earth Sci.*, 13 (2), 115-132.
- Jones, J. C. (1915). "The Pleasant Valley, Nevada, Earthquake of October 2, 1915," *Seism. Soc. Am. Bull.*, 5 (4), 190-205.
- King, Chi-Yu, and L. Knopoff (1968). "Stress Drop in Earthquakes," *Seism. Soc. Am. Bull.*, 58 (1), 249-257.
- Knopf, Adolph, and E. Kirk (1918). *A Geological Reconnaissance of the Inyo Range and the Eastern Slope of the Southern Sierra Nevada, California, with a Section on the Stratigraphy of the Inyo Range by Edwin Kirk*, U.S. Geological Survey Professional Paper 110.
- Koch, T. W. (1933). "Analysis and Effects of Current Movement on an Active Thrust Fault in Buena Vista Hills Oil Field, Kern County, California," *Am. Assoc. Petrol. Geol. Bull.*, 17 (6), 694-712.
- Kovach, R. L., C. R. Allen, and F. Press (1962). "Geophysical Investigations in the Colorado Delta Region," *J. Geophys. Res.*, 67 (7), 2845-2871.
- Kreese, F. C. (1966). "Baldwin Hills Reservoir Failure of 1963," in *Engineering Geology in Southern California*, pp. 93-103. Glendale, Los Angeles Section of Association of Engineering Geologists.
- Kupfer, D. H., S. Muessig, G. I. Smith, and G. N. White (1955). *Arvin-Tehachapi Earthquake Damage Along the Southern Pacific Railroad Near Bealville, California*, California Division of Mines Bulletin 171, pp. 67-74.
- Lawson, A. C., et al. (1908). *The California Earthquake of April 18, 1906—Report of the State Earthquake Investigation*

- Commission, Vol. 1, Part 1, pp. 1-254; Part 2, pp. 255-451. Carnegie Institution of Washington, Publication 87.
- Lee, C. H. (1912). *An Intensive Study of the Water Resources of a Part of Owens Valley, California*, U.S. Geological Survey, Water-Supply Paper 294.
- Louderback, G. D. (1942). "Faults and Earthquakes," *Seism. Soc. Am. Bull.*, 32 (4), 305-330.
- Louderback, G. D. (1947). "Central California Earthquakes of the 1830's," *Seism. Soc. Am. Bull.*, 37 (1), 33-74.
- Martin, L. (1907). "Possible Oblique Minor Faulting in Alaska," *Econ. Geol.*, 2, 576-579.
- McEvilly, T. V. (1966). "Preliminary Seismic Data, June-July, 1966," in "Parkfield Earthquakes of June 27-29, 1966, Monterey and San Luis Obispo Counties, California—Preliminary Report," *Seism. Soc. Am. Bull.*, 56 (4), 967-971.
- McEvilly, T. V., W. H. Bakun, and K. B. Casaday (1967). "The Parkfield, California, Earthquakes of 1966," *Seism. Soc. Am. Bull.*, 57 (6), 1221-1244.
- Muller, S. W., H. G. Ferguson, and R. J. Roberts (1951) *Geology of the Mount Tobin Quadrangle, Nevada*, U.S. Geological Survey Geologic Quadrangle Map [GQ-7], scale 1:125,000.
- Myers, W. B., and W. Hamilton (1964). "Deformation Accompanying the Hebgen Lake, Montana, Earthquake of August 17, 1959," in *The Hebgen Lake, Montana, Earthquake of August 17, 1959*, pp. 55-98. U.S. Geological Survey Professional Paper 435.
- Nason, R. D. (1968). *Fault Slippage at Hayward, California*, pp. 86-87, Geological Society of America, Cordilleran Section—Seismological Society of America—Paleontological Society, Pacific Coast Section, 64th Annual Meeting, Tucson, Arizona, 1968, Program.
- Nasu, N. (1931). *Comparative Studies of Earthquake Motions Above-Ground and in a Tunnel (Part I)*, Vol. 9, pp. 454-472. Tokyo University Earthquake Research Institute Bulletin.
- Neumann, F. (1936). "The Utah Earthquake of March 12, 1934," in *United States Earthquakes, 1934*, pp. 43-48. U.S. Coast and Geodetic Survey Serial 593.
- Oldham, R. D. (1899). "Report on the Great Earthquake of 12th June, 1897," *India Geol. Survey Mem.*, 29, 1-379.
- Page, B. M. (1935). "Basin-Range Faulting of 1915 in Pleasant Valley, Nevada," *J. Geol.*, 43 (7), 690-707.
- Paterson, M. S. (1958). "Experimental Deformation and Faulting in Wombeyan Marble," *Geol. Soc. Am. Bull.*, 69 (4), 465-475.
- Plafker, G. (1965). "Tectonic Deformation Associated with the 1964 Alaska Earthquake," *Science*, 148 (3678), 1675-1687.
- Plafker, G. (1967). *Surface Faults on Montague Island Associated with the 1964 Alaska Earthquake*, pp. G1-G42. U.S. Geological Survey Professional Paper 543-G.
- Radbruch, D. H. (1967). *Approximate Location of Fault Traces and Historic Surface Ruptures Within the Hayward Fault Zone Between San Pablo and Warm Springs, California*, U.S. Geological Survey Miscellaneous Geologic Investigation Map I-522, scale 1:62,500.
- Radbruch, D. H. (1968). "New Evidence of Historic Fault Activity in Alameda, Contra Costa and Santa Clara Counties, California," in W. R. Dickinson and A. Grantz (eds.), *Proceedings of the Conference on Geologic Problems of the San Andreas Fault System, September 14-16, 1967, Stanford University*, pp. 46-54, Stanford, California: Stanford University Press.
- Reid, H. F. (1910). "The Mechanics of the Earthquake," Vol. 2 in *The California Earthquake of April 18, 1906, Report of the State Earthquake Investigation Commission*, Carnegie Institution of Washington, Publication 87.
- Richter, C. F. (1958). *Elementary Seismology*, San Francisco: W. H. Freeman.
- Rogers, T. H., and R. D. Nason (1967). "Active Faulting in the Hollister Area" in *Guidebook, Gabilan Range and Adjacent San Andreas Fault*, pp. 102-104, American Association of Petroleum Geologists, Pacific Section, and Society of Economic Paleontologists, Pacific Section, Annual Field Trip.
- Romney, C. F. (1957). "Seismic Waves from the Dixie Valley-Fairview Peak Earthquakes [Nevada]," *Seism. Soc. Am. Bull.*, 47 (4), 301-319.
- Ross, C. A. (1963). *Faulting in Southernmost Illinois*, p. 229, Geological Society of America Special Paper 73.
- Russell, W. L. (1957). "Faulting and Superficial Structure in East-Central Texas," *Gulf Coast Assoc. Geol. Soc. Trans.*, 7, 65-72.
- Ryall, A., D. B. Stenmons, and L. D. Gedney (1966). "Seismicity, Tectonism, and Surface Faulting in the Western United States During Historic Time," *Seism. Soc. Am. Bull.*, 56 (5), 1105-1135.
- Saint-Amand, P. (1963). *The Great Earthquakes of May 1960 in Chile*, pp. 337-363, Smithsonian Institution, Washington Publication 4550.
- Savage, J. C., and L. M. Hastie (1966). "Surface Deformation Associated with Dip-Slip Faulting," *J. Geophys. Res.*, 71 (20), 4897-4904.
- Seismological Society of America (1922). *Fault Map of the State of California*, scale 1:506,880.
- Sheets, M. M. (1947). "Diastrophism During Historic Time in the Gulf Coastal Plain," *Am. Assoc. Petrol. Geol. Bull.*, 31 (2), 201-226.
- Shor, G. G., Jr., and E. E. Roberts (1958). "San Miguel, Baja California Norte [Mexico], Earthquakes of February, 1956—A Field Report," *Seism. Soc. Am. Bull.*, 48 (2), 101-116.
- Stenmons, D. B. (1957). "Geological Effects of the Dixie Valley-Fairview Peak, Nevada, Earthquakes of December 16, 1954," *Seism. Soc. Am. Bull.*, 47 (4), 353-375.
- Stenmons, D. B. (1966). *Long-Term Strain Release: An Earthquake History and Late Cenozoic Faulting in the Basin-and-Range Province*, pp. 82-84, *Proceedings of the*

- Second United States-Japan Conference on Research Related to Earthquake Prediction.*
- Stemmons, D. B. (1967). "Pliocene and Quaternary Crustal Movements of the Basin-and-Range Province, USA," *Osaka City Univ. J. Geosci.*, 10, 91-103.
- Stemmons, D. B., K. V. Steinbrugge, D. Tocher, G. B. Oakeshott, and V. P. Gianella (1959). "Wonder, Nevada, Earthquake of 1903," *Seism. Soc. Am. Bull.*, 49 (3), 251-265.
- Steinbrugge, K. V., and W. K. Cloud (1962). "Epicentral Intensities and Damage in the Hebgen Lake, Montana, Earthquake of August 17, 1959," *Seism. Soc. Am. Bull.*, 52 (2), 181-234.
- Steinbrugge, K. V., and D. F. Moran (1957). "Engineering Aspects of the Dixie Valley-Fairview Peak Earthquakes," *Seism. Soc. Am. Bull.*, 47 (4), 335-348.
- Suyehiro, K. (1932). "Engineering Seismology--Notes on American Lectures," *Am. Soc. Civil Engr. Proc.*, 58 (4), 1-43.
- Taber, S. (1906). "Some Local Effects of the San Francisco Earthquake," *J. Geology*, 14 (4), 303-315.
- Takahasi, R. (1931). "Results of the Precise Levellings Executed in the Tanna Railway Tunnel and the Movement Along the Slicken-Side that Appeared in the Tunnel," *Tokyo Univ., Earthquake Res. Inst. Bull.*, 9 (4), 435-453.
- Tarr, R. S., and L. Martin (1906). "Recent Changes of Level in the Yakutat Bay Region, Alaska," *Geol. Soc. Am. Bull.*, 17 (1), 29-64.
- Tarr, R. S., and L. Martin (1912). *The Earthquakes at Yakutat Bay, Alaska, in September 1899, with a Preface by G. K. Gilbert*, U. S. Geological Survey Professional Paper 69.
- Tocher, D. (1956). "Movement on the Rainbow Mountain Fault [Nevada]," in "The Fallon-Stillwater Earthquakes of July 6, 1954, and August 23, 1954," *Seism. Soc. Am. Bull.*, 46 (1), 10-14.
- Tocher, D. (1958). "Earthquake Energy and Ground Breakage," *Seism. Soc. Am. Bull.*, 48, 147-153.
- Tocher, D. (1960a). "The Alaska Earthquake of July 10, 1958, Movement on the Fairweather Fault and Field Investigation of Southern Epicentral Region," *Seism. Soc. Am. Bull.*, 50 (2), 267-292.
- Tocher, D. (1960b). *Movement on Faults, Proceedings of the Second World Conference on Earthquake Engineering*, Vol. I, pp. 551-564, Japan, 1960.
- Tocher, D. (1966). *Fault Creep in San Benito County, California*, p. 72, Geological Society of America, Cordilleran Section--Seismological Society of America--Paleontological Society, Pacific Coast Section, 62d Annual Meeting, Reno, Nevada. Program.
- Tocher, D. and D. J. Miller (1959). "Field Observations on Effects of Alaska Earthquake of 10 July 1958," *Science*, 129 (3346) 394-395.
- Townley, S. D., and M. W. Allen (1939). "Descriptive Catalog of Earthquakes of the Pacific Coast of the United States, 1769 to 1928," *Seism. Soc. Am. Bull.*, 29 (1), 1-297.
- Turner, H. W. (1891). "Mohawk Lake Beds [Plumas County, California]," *Philos. Soc. Wash. Bull.*, 11, 385-409.
- Turner, H. W. (1896). "Further Contributions to the Geology of the Sierra Nevada," *U.S. Geol. Survey Ann. Rept.*, 17 (1), 521-740.
- Turner, H. W. (1897). *Description of the Downieville Quadrangle, California*, U.S. Geological Survey Geological Atlas, Folio 37.
- Ulrich, F. P. (1941). "The Imperial Valley Earthquakes of 1940," *Seism. Soc. Am. Bull.*, 31 (2), 13-31.
- U.S. Army Corps of Engineers (1950). *Geological Investigation of Faulting in the Lower Mississippi Valley*, U.S. Army Corps of Engineers Waterways Experiment Station Technical Memorandum 3-311.
- Varnes, D. J. (1958). "Landslide Types and Processes," Chap. 3 in E. B. Eckel (ed.), *Landslides and Engineering Practice*, pp. 20-47, National Research Council, Highway Research Board Special Report 29, NAS-NRC Publication 544.
- Veatch, A. C. (1906). *Geology and Underground Water Resources of Northern Louisiana and Southern Arkansas*, U.S. Geological Survey Professional Paper 46.
- Vedder, J. G., and R. D. Brown, Jr. (1968). "Structural and Stratigraphic Relations Along the Nacimiento Fault in the Southern Santa Lucia Range and San Rafael Mountains, California," in W. R. Dickinson and A. Grantz (eds.), *Proceedings of the Conference on Geologic Problems of the San Andreas Fault System, September 14-16, 1967, Stanford University*, pp. 242-259, Stanford, California: Stanford University Press.
- Wallace, R. E. (1968). "Notes on Stream Channels Offset by the San Andreas Fault, Southern Coast Ranges, California," in W. R. Dickinson and A. Grantz (eds.), *Proceedings of the Conference on Geologic Problems of the San Andreas Fault System, September 14-16, 1967, Stanford University*, pp. 6-21, Stanford, California: Stanford University Press.
- Wallace, R. E., and E. F. Roth (1967). "Rates and Patterns of Progressive Deformations," in R. D. Brown, Jr., et al., *The Parkfield-Cholame, California, Earthquakes of June-August 1966--Surface Geologic Effects, Water-Resources Aspects, and Preliminary Seismic Data*, pp. 23-40, U.S. Geological Survey Professional Paper 579.
- Weaver, P., and M. M. Sheets (1962). "Active Faults, Subsidence, and Foundation Problems in the Houston, Texas, Area," in E. H. Rainwater, and R. P. Zingula, *Geology of the Gulf Coast and Central Texas and Guidebooks of Excursions*, pp. 254-265, Geological Society of America and Associated Societies, Annual Meeting, Houston, Texas.
- Whitney, J. D. (1888). "The Owens Valley Earthquake," in W. A. Goodyear, *Inyo County*, pp. 288-309, California Mining Bureau Eighth Annual Report State Mineralogist.
- Whitten, C. A. (1955). *Measurements of Earth Movements in California*, pp. 75-80, California Division of Mines Bulletin 171.

- Whitten, C. A. (1961). "Measurement of Small Movements in the Earth's Crust," *Acad. Sci. Fennicae Ann. Ser. A, Geol. Geograph. Suomalainen Tiedakatemia*, 3 (61), 315-320.
- Whitten, C. A. (1966). "Crustal Movements from Triangulation Measurements," in *ESSA Symposium on Earthquake Prediction, Rockville, Maryland, 1966*, pp. 72-76, U.S. Environmental Science Services Administration, Washington, U.S. Government Printing Office.
- Wiggins, P. N. (1954). "Geology of Ham Gossett Oil Field, Kaufman County, Texas," *Am. Assoc. Petrol. Geol. Bull.*, 38 (2), 306-318.
- Wilt, J. W. (1958). "Measured Movement Along the Surface Trace of an Active Thrust Fault in the Buena Vista Hills, Kern County, California," *Seism. Soc. Am. Bull.*, 48 (2), 169-176.
- Witkind, I. J. (1964). "Reactivated Faults North of Hebgen Lake," in *The Hebgen Lake, Montana, Earthquake of August 17, 1959*, pp. 37-50, U.S. Geological Survey Professional Paper 435.
- Witkind, I. J., J. B. Hadley, and W. H. Nelson (1964). "Pre-Tertiary Stratigraphy and Structure of the Hebgen Lake Area," in *The Hebgen Lake, Montana, Earthquake of August 17, 1959*, pp. 199-207, U.S. Geological Survey Professional Paper 435.
- Wollard, G. P. (1958). "Areas of Tectonic Activity in the United States as Indicated by Earthquake Epicenters," *Am. Geophys. Union Trans.*, 39 (6), 1135-1150.
- Wood, H. O. (1955). "The 1857 Earthquake in California," *Seism. Soc. Am. Bull.*, 45 (1), 47-67.



MECANICA DE ROCAS APLICADA A LA MINERIA Y A LA CONSTRUCCION

THE GEOMECHANICS CLASSIFICATION IN ROCK ENGINEERING APPLICATIONS

MAYO, 1985

# THE GEOMECHANICS CLASSIFICATION IN ROCK ENGINEERING APPLICATIONS

Classification géomécanique et son application pour l'ingénieur des roches

Geomechanische Gebirgsklassifizierung und ihre Anwendung in Felsbau

PROFESSOR Z. T. BIENIAWSKI, DSc(Eng)  
Professor of Mineral Engineering  
The Pennsylvania State University  
University Park, PA 16802, USA

140

## SUMMARY:

The Geomechanics Classification of rock masses was proposed in 1973 and has since been applied to such varied rock engineering projects as tunnels, caverns, slopes and foundations in civil engineering and to haulages and chambers in mines. The classification is based on six parameters: the uniaxial compressive strength of the rock material, drill core quality RQD, spacing, orientation and condition of discontinuities and groundwater conditions. Importance ratings are allocated to each parameter and total rock mass ratings (RMR) for five rock mass classes are specified. This paper summarizes the experience gained with this classification in the past five years.

## RESUME:

La Classification Géomécanique, une classification pour l'ingénieur des masses de roches fracturées, a été proposée en 1973 et a été appliquée en ingénierie civil et minière. Elle dépend de six paramètres: la résistance à la qualité des carottes de sondage obtenues (valeur RQD), espacement, orientation et état des fissures, et les venues d'eau souterraines. Un échelle des valeurs relatives pour chaque paramètre et des valeurs totales pour la masse rocheuse (RMR). Cette communication pourvoit un résumé de expérience avec cette classification pendant les derniers cinq ans.

## ZUSAMMENFASSUNG:

Die Geomechanische Gebirgsklassifizierung, eine für den Ingenieur bestimmte Klassifizierung für künftiges Gebirge wird vorgeschlagen in 1973 und in Bauingenieurwesen und Bergbau angewendet wird. Sie gründet sich auf sechs Parameter: die einachsige Gesteinsdruckfestigkeit, die Qualität der gewonnenen Bohrkörner (RQD - Wert), den Klufstabstand, die Kluffstellung und den Zustand der Klufte, sowie auf den Grundwasserzustand. Jeder Parameter wird nach seiner relativen Wichtigkeit bewertet und die Gesamtbewertung des Gesteines (RMR) wird definiert. Dieser Aufsatz zusammenfasst die Erfahrung mit dieser Klassifizierung während die vergangene fünf Jahre.

## 1. INTRODUCTION

Engineering classifications of rock masses are acknowledged today as a necessary adjunct for assessing rock mass conditions for engineering purposes. This subject has received considerable attention following the pioneering work by Fairbridge (1946), Lauffer (1958) and Deere (1964). More recently, three classification systems have been extensively employed particularly in the field of tunnelling. These were: the RSR Concept by Michas et al. (1972), the Geomechanics Classification by Bieniawski (1973) and the Q-System by Barton et al. (1974). A number of comparative studies have been conducted aiming at assessing these classification systems from the point of view of the ease of application, the accuracy of prediction and any possible correlation. Bouillon, 1975; Bieniawski, 1976; Barton, 1976 and Rutledge, 1978. In a study by the author (1975), a total of 111 case histories were analyzed involving tunnels and chambers in North America, Europe, South Africa and Australia and the following relationship was derived:

$$RMR = 9 \log_e Q + 44 \quad (1)$$

where RMR is the rock mass rating from the Geomechanics Classification and Q is the rock mass quality from the Q-System.

Recently, Rutledge (1978) correlated three classification systems on the basis of his tunnelling experience in New Zealand. He derived the following relationships:

$$RMR = 13.5 \log Q + 43 \quad (2)$$

$$RSR = 0.77 RMR + 12.4 \quad (3)$$

$$RMR = 13.3 \log Q + 45.3 \quad (4)$$

where RSR is the Rock Structure Rating after Michas et al., 1972.

## 2. RECENT DEVELOPMENTS

Notable developments in the last few years concerning rock mass classifications fall under seven items:

### 2.1 Extension of Applications

Although the main applications of rock mass classifications have traditionally been in tunnelling, the geomechanics classification is an exception having been also applied to other projects and not only to tunnels

and chambers. This included rock slopes (Steffen, 1976; A. W. John, 1978), dam foundations (Antonucci and Orr, 1976), foundation bearing pressure (Gibson, 1975), ground ripability (Lawver, 1976) as well as other applications: feasibility of ore (Koschek, 1976) and haulage stability (Gibson, 1977). Most recently, the Geomechanics Classification is being applied by the author to assess mine rock stability in a number of coal mines in the USA.

## 2.2 Use of borehole data

A trend has emerged to select engineering geological parameters on the basis of borehole data alone which would be sufficient for rock mass classification purposes without the need for tests in adits or pilot tunnels. As a result of the availability of more advanced coring techniques such as directional drilling and oriented core sampling as well as both borehole and core logging procedures, rock mass classifications can be conducted on the basis of core data alone.

## 2.3 Special rock conditions

The situations involving post rock conditions such as swelling and squeezing rock can now be handled by both the Geomechanics Classification and the Q-System. In the case of the former, Duvvuri (1977) has presented a rock durability system for use in conjunction with the Geomechanics Classification.

## 2.4 Monitoring during construction

Although some classification systems tend to rely exclusively on the accumulated case study experience, it is more appropriate to back support prediction based on rock mass classifications with a monitoring program during construction. The New Austrian Tunneling Method is a success story of the benefits that can be derived by combining rock classifications with monitoring.

## 2.5 Elimination of two-tier support for tunnels

The traditional concepts of primary (temporary) and secondary (permanent) support for rock tunnels are losing their meaning as the modern tendency is toward a single support system, that is rock reinforcement necessary to maintain tunnel stability for the life of the project. This raises the question as to the need for massive concrete linings which are featured on some tunneling projects.

## 2.6 Use of analytical procedures

The analytical techniques in the field of rock mechanics have experienced a tremendous growth and although analytical design cannot as yet replace empirical and observational designs (mainly due to the difficulty in providing reliable input data for the mathematical models), the value of the analytical techniques should not be overlooked. Progress can only be maintained if empirical approaches are backed by analytical studies.

## 2.7 Contractual aspects

While the project contracts in Austria, Germany and Switzerland have featured rock mass classifications as the basis of payment for many years, this matter is now receiving attention in a number of countries outside Europe.

## 3. THE GEOMECHANICS CLASSIFICATION

The main purpose of this paper is to demonstrate some rock engineering applications of the Geomechanics Classification in the last five years. The classification procedures are first summarized for the convenience of users.

### 3.1 Classification procedure

The Geomechanics Classification is presented in Table 1. In Section A five parameters are grouped into five ranges of values. Since the various parameters are not equally important for the overall classification of a rock mass, importance ratings are allocated to the different value ranges of the parameters, a higher rating indicating better rock mass conditions.

To apply the Geomechanics Classification, the rock mass is divided into a number of structural regions such that certain features are more or less uniform within each region. Although rock masses are

discontinuous in nature, they may, nevertheless, be uniform in regions when, for example, the type of rock or the joint spacings are the same throughout the region. In most cases, the boundaries of structural regions will coincide with major geological features such as faults, dykes, shear zones, etc.

After the structural regions have been identified the classification parameters for each structural region are determined from measurements in the field and entered onto the input data sheet given in the Appendix. Then, the importance ratings are assigned to each parameter according to Table 1, Section A. In this respect, the average conditions are evaluated. Furthermore, it should be noted that the importance ratings given for discontinuity spacings apply to rock masses having three sets of discontinuities. Thus when only two sets of discontinuities are present a conservative assessment is obtained.

Once the importance ratings of the classification parameters are established, the ratings for the five parameters listed in Section A of Table 1 are summed to yield the basic rock mass rating for the structural region under consideration.

The next step is to include the influence of strike and dip of discontinuities by adjusting the basic rock mass rating according to Section B of Table 1. This step is treated separately because the influence of discontinuity orientations depends upon the engineering applications, e.g. tunnel, slope or foundation. It will be noted that the "value" of the parameter "discontinuity orientation" is not given in quantitative terms but by qualitative descriptions such as "favorable". To facilitate a decision whether strike and dip orientations are favorable or not in tunneling, reference should be made to Table 2. For slopes and foundations, the reader is referred to a paper by Bieniawski and Orr, 1975. In the case of civil engineering projects an adjustment for discontinuity orientations will suffice. For mining applications, other adjustments may be called for, such as the stress at depth or a change in stress, and these were discussed by Laubscher, 1976.

After the adjustment for discontinuity orientations, the rock mass is classified according to Section C of Table 1 which groups the final (adjusted) rock mass ratings (RMR) into five rock mass classes. Note that the rock mass classes are in groups of twenty ratings each. Next, Section D of Table 1 gives the practical meaning of each rock mass class by relating it to specific engineering problems. In the case of tunnels and chambers, the output from the Geomechanics Classification is the stand-up time of an unsupported rock span for a given rock mass rating as shown in Figure 1. Longer stand-up time can be achieved by selecting rock reinforcement measures in accordance with Table 3. They depend on such factors as the depth below surface (in-situ stress), tunnel size and shape and the method of excavation.

It should be noted that Table 1 gives slightly different ranges of the classification parameters than those previously published, Bieniawski, 1976. The reason is that the ranges in Table 1 follow the latest recommendations of the International Society of Rock Mechanics (ISRM) Commission on Standardization and on Classification. The interested reader is referred to an ISRM document entitled: "Suggested Methods for Quantitative Description of Discontinuities in Rock Masses", Committee on Field Tests, 1978.

Since the ranges are slightly different, the ratings of the classification parameters are accordingly slightly modified.

## 4. APPLICATIONS

In the past five years the Geomechanics Classification found its applications in various types of engineering projects such as tunnels, slopes, foundations and mines.

### 4.1 Applications to tunneling

In the field of tunneling, the classification was applied to highway, railroad and water conveyance tunnels as well as to underground caverns for hydroelectric schemes. In total, 59 case histories were compiled which served as the basis for preparing the span versus stand-up time diagram given in Figure 1.



**GEOMECHANICS CLASSIFICATION OF JOINTED ROCK MASSES**

**A. CLASSIFICATION PARAMETERS AND THEIR RATINGS**

PARAMETER		RATING					
		1	2	3	4	5	
1	Strength of intact rock	1-2 MPa	3-10 MPa	20-40 MPa	50-80 MPa	100-150 MPa	
	Rating	1	2	3	4	5	
2	Discontinuity quality (RQD)	0% - 25%	25% - 50%	50% - 75%	75% - 90%	> 90%	
	Rating	1	2	3	4	5	
3	Spacing of discontinuities	2 m	1.0 - 2 m	200 - 600 mm	40 - 100 mm	< 40 mm	
	Rating	1	2	3	4	5	
4	Condition of discontinuity	Very rough surfaces, full of debris, highly weathered	Rough surfaces, some debris, some weathered	Slightly rough surfaces, some debris, some weathered	Smooth surfaces, no debris, no weathering	Very smooth surfaces, no debris, no weathering	
	Rating	1	2	3	4	5	
5	Gross water	Water table 10 m above	None	10-25 mm	25-50 mm	50-100 mm	> 100 mm
		Rating	1	2	3	4	5
	Cementation	Completely dry	Damp	Wet	Dripping	Flowing	
		Rating	1	2	3	4	5

**B. RATING ADJUSTMENT FOR JOINT ORIENTATIONS**

Range	Strike and dip orientations of joints	Very unfavourable	Unfavourable	Fair	Favourable	Very favourable
	Tunnels	0	1	2	3	4
Foundations	0	1	2	3	4	5
Skies	0	1	2	3	4	5

**C. ROCK MASS CLASSES OF TUNNELS FROM TOTAL RATINGS**

Rating	100-81	80-61	60-41	40-21	< 20
Class No.	I	II	III	IV	V
Description	Very good rock	Good rock	Fair rock	Poor rock	Very poor rock

**D. MEANING OF ROCK MASS CLASSES**

Class No.	I	II	III	IV	V
Average stand up time	12 years for 15 m span	8 months for 8 m span	1 year for 6 m span	10 hours for 2.5 m span	30 minutes for 1 m span
Compress of the rock mass	> 40 MPa	3.0 - 40 MPa	10 - 30 MPa	100 - 200 MPa	< 100 MPa
Friction angle of the rock mass	25-35°	15-25°	20-30°	15-20°	10°

Table 2.

The Effect of Discontinuity Strike and Dip Orientations in Tunneling.

Strike perpendicular to tunnel axis				Strike parallel to tunnel axis		Dip 0° - 20° irrespective of strike
Drive with dip		Drive against dip				
Dip 45°-90°	Dip 20°-45°	Dip 45°-90°	Dip 20°-45°	Dip 45°-90°	Dip 20°-45°	
Very favourable	Favourable	Fair	Unfavourable	Very unfavourable	Fair	Unfavourable

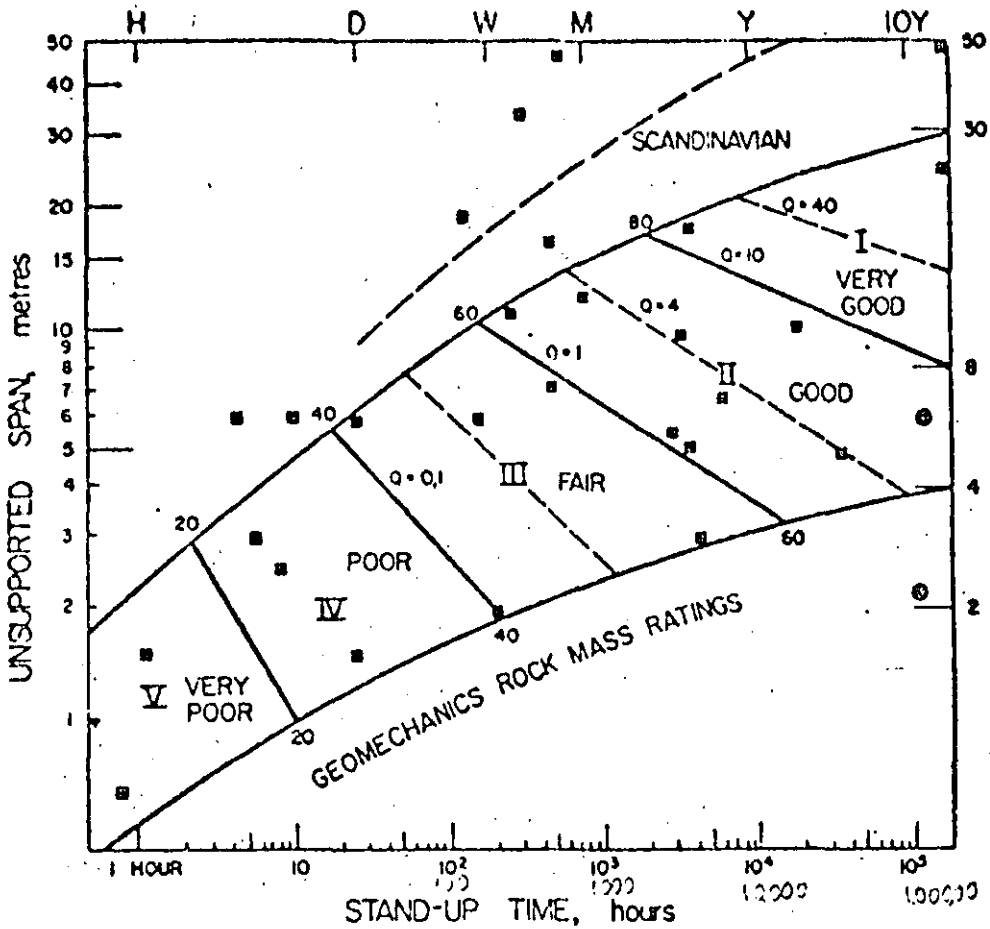


Figure 1. Geomechanics Classification of rock masses: output for tunneling. Plotted points represent case histories studied.

One railroad tunnel (5.5m diameter and 3.8km long) involved a year long tunnel monitoring program featuring sixteen measuring stations, the data from which was interpreted in conjunction with the Geomechanics Classification as recorded during construction (Bieniawski and Masarik, 1975). The classification ratings were correlated with such data as the amount of rock movement, the rate of face advance and the support used. In addition, as this tunnel was characterized by highly variable conditions - from very poor rock to very good rock - rock support requirements were estimated, for comparison purposes, by nine different classification systems (Bieniawski, 1976).

Another project involved the longest continuous tunnel in the world, a water conveyance tunnel 81km long and 6m diameter. The Geomechanics Classification was extensively applied and a doctoral dissertation reports the findings (Oltvier, 1977).

Applications to large underground caverns for hydro-electric schemes were particularly useful because a range of unsupported spans could be studied thus providing information on the influence of tunnel size on the stability of the surrounding rock mass (Bieniawski, 1978).

#### 4.2 Applications to rock slopes

The Geomechanics Classification was applied to rock slopes by Steffen, 1976, in South Africa and E. W. John, 1976, in Germany.

It should be noted that the Geomechanics Classification provides, as an output, the cohesion and friction data for the five rock mass classes. Steffen, 1976

classified 35 slopes, of which 20 had failed, using the Geomechanics Classification and based on the average values of cohesion and friction so obtained, he calculated the factors of safety using the design charts given by Hoek and Bray, 1977. The results were plotted in the form of a histogram showing the frequency of occurrence versus the factor of safety. A definite statistical trend was found. However, caution should be exercised when applying this classification to rock slopes since more case histories need to be analyzed. Research in this respect is currently conducted by K. W. John in Germany.

#### 4.3 Applications to rock foundations

For the design of rock foundations, knowledge of the modulus of deformability of rock masses is of prime importance. The Geomechanics Classification was found a useful method for estimating in situ deformability of rock masses (Bieniawski, 1978). This is demonstrated in Figure 2 and, as will be seen, the following correlation was obtained:

$$E_d = 2 \times RMR - 100 \quad (5)$$

where  $E_d$  is the in situ modulus of deformation in GPa and RMR is the rock mass rating from the Geomechanics Classification.

The above correlation was derived on the basis of 22 case histories involving wide range of in situ tests conducted in various parts of the world. The accuracy of the modulus prediction by the Geomechanics Classification is within 10% which is quite acceptable for rock engineering purposes.

On one major project (Bieniawski, 1973), the

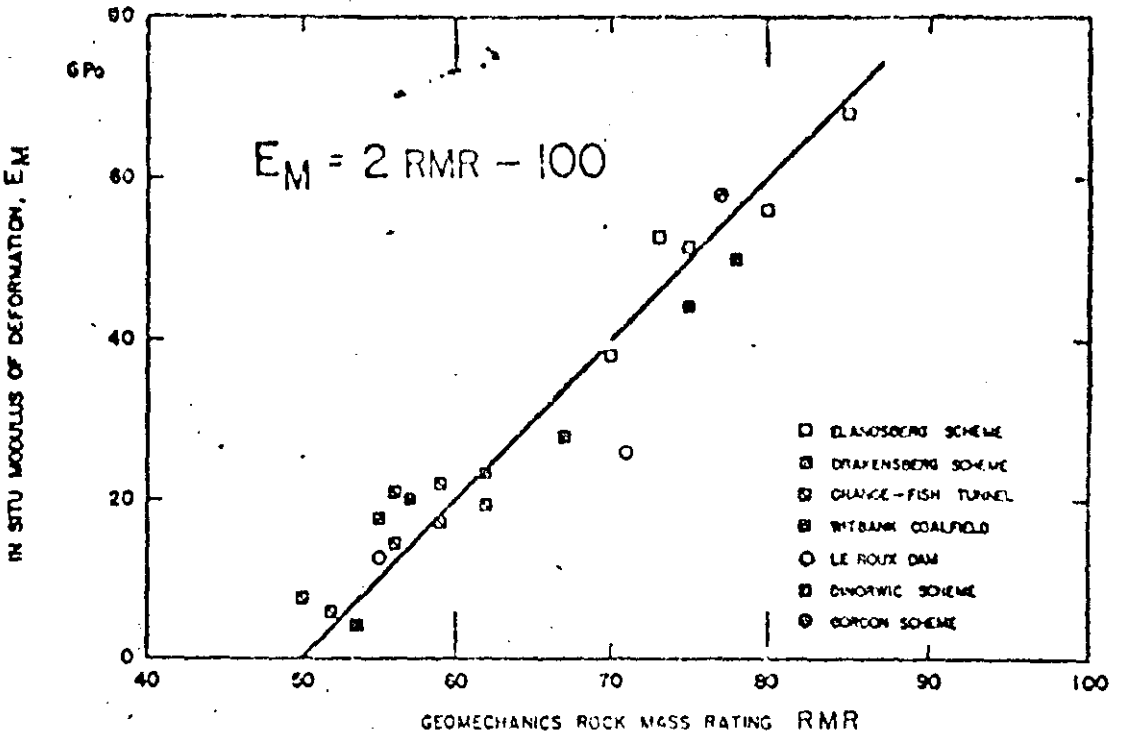


Figure 2. Correlation between the in situ modulus of deformation and the Geomechanics Classification rock mass rating (RMR) - Bieniawski, 1978.

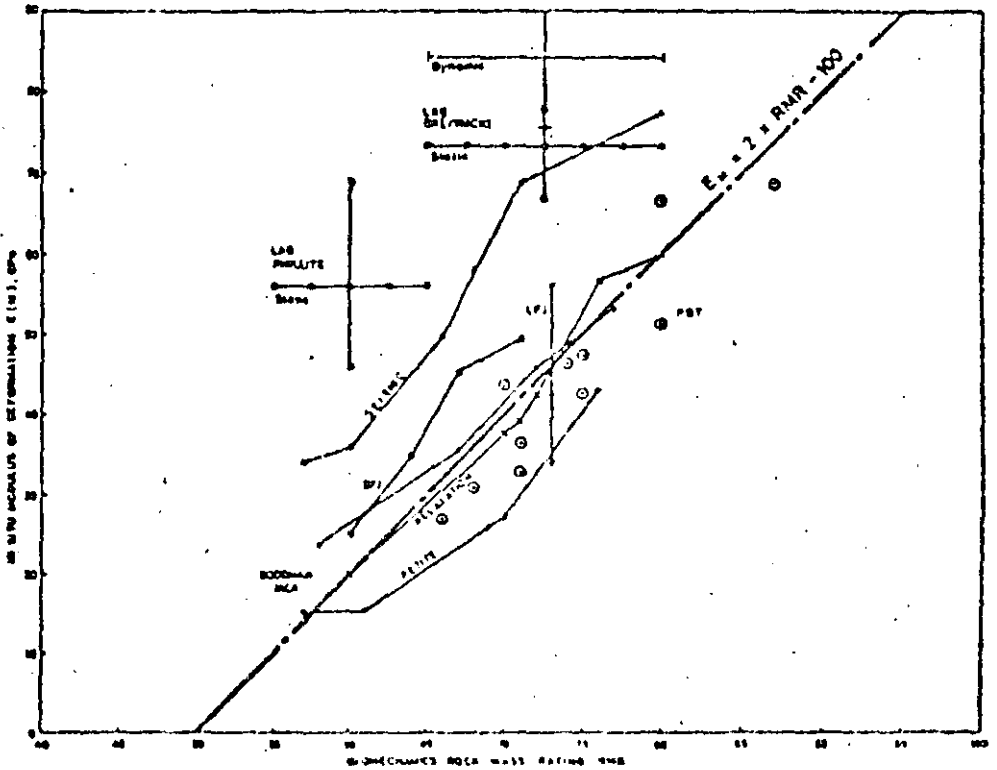


Figure 3. Comparison of in situ deformability data obtained by different test methods (Bieniawski, 1978): PBT - plate bearing tests; LFJ - large flat jacks; SFJ - small flat jacks; Goodman Jack - borehole jacking tests; Relaxation - tunnel relaxation convergence measurements; Petite - 'petite sismique' shear wave technique; seismic - seismic modulus.

classification was employed as a factor of comparison of the modulus of deformation results obtained by the different in situ test methods. These results are listed in Figure 1.

#### Applications in mining

Lubinski, 1976 has applied the Geomechanics Classification in mining specifically to assess feasibility of ore while a recent dissertation by Ferguson, 1978 extended this classification to mining tunnels and haulageways. Both were extensive studies involving over 50km of tunnels and borehole cores classified during three years. Slow mining in a dynamic process, additional adjustments to the classification parameters were introduced involving field and induced stresses, changes in stress and weatherability of rock.

Recently, the Geomechanics Classification is being applied by the author for assessing mine roof stability in a number of coal mines in the USA, Bieniawski and Stefanek, 1979.

### 3. CONCLUSION

The Geomechanics Classification has established itself as a useful and versatile technique for assessing rock mass conditions on engineering projects. Its application during the last five years demonstrated its reliability and ease of use. It is believed that greater effort should be made to apply this classification system in the field of mining.

### REFERENCES

- BARTON, M., LIEN, R. and LUNDE, J. Engineering classification of rock masses for the design of tunnel support. *Rock Mechanics*, vol. 6, no. 4, 1974, pp. 189-236.
- BARTON, M. Recent experiences with the Q-System of tunnel support. *Proc. Symp. Explor. Rock Engng.* Johannesburg, A. A. Balkema, vol. 1, 1976, pp. 107-117.
- BIENIAWSKI, Z. T. Engineering classification of jointed rock masses. *Trans. S. Afr. Instn. Civ. Engrs.* vol. 15, no. 12, 1973, pp. 335-344.
- BIENIAWSKI, Z. T. Rock mass classifications in rock engineering. *Proc. Symp. Exploration for Rock Engng.*, Johannesburg, A. A. Balkema, vol. 1, 1976, pp. 97-106.
- BIENIAWSKI, Z. T. Determining rock mass deformability: experience from case histories. *Int. J. Rock Mech. & Min. Sci.*, vol. 15, 1978, in press.
- BIENIAWSKI, Z. T. A critical assessment of selected in situ tests for rock mass deformability and stress measurements. *Proc. 19th US Symp. Rock Mechanics*, University of Nevada, Reno, 1978, pp. 323-335.
- BIENIAWSKI, Z. T. and MASCHKE, R. K. A. Monitoring the behavior of rock tunnels during construction. *Civ. Engr. S. Afr.* vol. 17, no. 10, October 1975, pp. 255-264.
- BIENIAWSKI, Z. T. and ORR, C. M. Rapid site appraisal for dam foundations by the Geomechanics Classification. *Proc. 12th Congress on Large Dams*, ICOLD, Mexico City, 1976, pp. 483-501.
- BIENIAWSKI, Z. T. and STEFANKO, R. A design approach to room and pillar coal mining. *Proc. 20th US Symp. Rock Mechanics*, Austin, Texas, June 1979, in press.
- BYRNE, D. U. Technical description of rock cores for engineering purposes. *Rock Mech. Engng. Geol.*, vol. 1, no. 1, 1964, pp. 17-22.
- FERGUSON, C. A. The design of support systems for excavations in sublevel mines. University of Rhodesia, M.Sc. thesis, Salisbury, 1977.
- HOEK, E. and SPAY, J. W. *Rock slope engineering*. Institution of Mining and Metallurgy, London, 1977, pp. 276-287.
- HUGHTON, D. A. The assessment of rock masses and the role of rock quality indices in engineering geology with reference to tunnelling in hard rock. M.Sc. Dissertation - Imperial College, London, 1975, 122 p.
- ISRM. Suggested methods for quantitative description of discontinuities in rock. *Committee on Field Tests*, 1978.
- JOHN, K. W. Personal communication, 1978.
- LAUBSCHER, D. H. Class distinction in rock masses. *Coal, Gold and Base Minerals of S. Afr.*, vol. 23, no. 6, August 1975, pp. 37-50.
- LAUFER, H. Gebirgsklassierung für den Stollenbau. *Geologie und Bauwesen*, vol. 24, 1959, pp. 46-51.
- NENTIN, J. Allowable bearing pressure estimation in rock masses for preliminary foundation design purposes. Natal Provincial Administration Roads Department, Ref. 2/1804, June 1975.
- OLIVIER, H. J. Importance of rock durability in the engineering classification of Karoo rock masses for tunneling. *Explor. Rock Engng. Symposium*, Johannesburg, 1976, vol. 1, pp. 137-144.
- OLIVIER, H. T. Engineering geological aspects of the Orange-Fish Tunnel. University of the Orange Free State, Ph.D. thesis, Bloemfontein, 1976.
- RUTLEDGE, T. C. and PRESTON, R. L. New Zealand experience with engineering classifications of rock for the prediction of tunnel support. *Proc. Int. Tunnel Symposium*, Tokyo, 1978, pp. A3-1-7.
- STEFFEN, D. K. H. Research and development needs in data collection for rock engineering. *Proc. Symp. Explor. for Rock Engng.*, Johannesburg, A. A. Balkema, vol. 2, pp. 93-104.
- TERZAGHI, K. Rock defects and loads on tunnel supports. *Rock tunneling with Steel Supports*, eds. Proctor, R. V. and White, T., Commercial Shearing Co., Youngstown, 1946, pp. 15-99.
- WEAVER, J. Geological factors significant in the assessment of ripability. *Civ. Engr. S. Afr.* vol. 17, no. 12, December 1975, pp. 313-316.
- WICKHAM, C. E., TILDEMAN, H. R. and SKINNER, E. B. Ground support prediction model (RSA concept). *Proc. 2nd Rapid Excavation & Tunneling Conference*, AIME, New York, 1974, pp. 691-707.

Table-3.

## Geomechanics Classification Guide for Excavation and Support in Rock Tunnels.

SHAPE: HORSESHOE; WIDTH: 10 m; VERTICAL STRESS: BELOW 25 MPa; CONSTRUCTION: DRILLING AND BLASTING

Rock mass class	Excavation	Support		
		Rockbolts (20 mm dia., fully bonded)	Shotcrete	Steel sets
Very good rock I RMR: 81-100	Full face. 3 m advance	Generally no support required except for occasional spot bolting		
Good rock II RMR: 61-80	Full face. 1.0-1.5 m advance Complete support 20 m from face	Locally bolts in crown 3 m long, spaced 2.5 m with occasional wire mesh.	50 mm in crown where required.	None
Fair rock III RMR: 41-60	Top heading and bench 1.5 - 3 m advance in top heading. Commence support after each blast. Complete support 10 m from face.	Systematic bolts 4 m long, spaced 1.5 m - 2 m in crown and walls with wire mesh in crown.	50 - 100 mm in crown and 30 mm in sides.	None
Poor rock IV RMR: 21-40	Top heading and bench 1.0 - 1.5 m advance in top heading. Install support concurrently with excavation-10m from face	Systematic bolts 4 - 5 m long, spaced 1 - 1.5 m in crown and walls with wire mesh.	100 - 150 mm in crown and 100 mm in sides.	Light to medium ribs spaced 1.5 m where required.
Very poor rock V RMR: <20	Multiple drifts. 0.5 - 1.5 m advance in top heading. Install support concurrently with excavation. Shotcrete as soon as possible after blasting.	Systematic bolts 5 - 6 m long, spaced 1 - 1.5 m in crown and walls with wire mesh. Bolt invert.	150 - 200 mm in crown, 150 mm in sides and 50 mm on face.	Medium to heavy ribs spaced 0.75 m with steel lagging and fore-poling if required. Close invert.



**DIVISION DE EDUCACION CONTINUA  
FACULTAD DE INGENIERIA U.N.A.M.**

MECANICA DE ROCAS APLICADA A LA MINERIA Y A LA CONSTRUCCION

RECENT EXPERIENCES WITH THE Q-SYSTEM OF TUNNEL SUPPORT DESIGN

MAYO, 1985

# Recent experiences with the Q-system of tunnel support design

NICK BARTON, PhD Norwegian Geotechnical Institute, P.O. Box 40 Laasen, Oslo 8 Norway.

## SUMMARY

The Q-system of rock mass classification and support design is based on a numerical assessment of the rock mass quality using six different parameters. The six parameters consist of: the RQD, the number of joint sets, the roughness of the most unfavourable joint or discontinuity, the degree of alteration or filling of the most unfavourable joint or discontinuity, the degree of water inflow, and the stress condition. Another classification system, the Geomechanics Classification (Bieniawski, 1973, 1974) is also based on six parameters. Qualitative differences between the two methods are discussed.

The 200 case records that were analysed when developing the Q-system, included more than 30 cases of permanently unsupported openings. An analysis of the rock mass characteristics involved has shown that certain characteristics are essential if an excavation is to be left permanently unsupported. If the maximum unsupported span for a given Q-value is exceeded, the safe life of the excavation may be shortened. A preliminary attempt is made to correlate stand-up time, rock mass quality Q, and span width.

The Q-system has been applied on several projects in Scandinavia and abroad since its development in 1973/1974. An example of a recent application is given in detail. The preliminary estimates of permanent support for a 19 metres span underground power house were obtained from an analysis of corelogs. In a subsequent site visit the Q-system was applied *in-situ*. The final estimates of permanent support were found to compare well with the preliminary estimates. Core logs, seismic profiles and surface mapping were used as a basis for preliminary design of permanent support for the 9 metres span tailrace tunnel, again using the Q-system. This tunnel is presently under construction so comparison of predicted and actual support is not yet possible.

## KEY WORDS

Rock mass, classification, tunnel, powerhouse, support, borecore, case record.

## INTRODUCTION

The six parameters chosen to describe the rock mass quality Q are as follows:

RQD = rock quality designation (Deere, 1963)

$J_n$  = joint set number

$J_r$  = joint roughness number

$J_a$  = joint alteration number

$J_w$  = joint water reduction factor

SRF = stress reduction factor

These parameters are combined in pairs and are found to be crude measures of:

1. relative block size ( $RQD/J_n$ )
2. inter-block shear strength ( $J_r/J_a$ ) ( $\approx \tan \phi$ )
3. active stress ( $J_w/SRF$ )

The overall quality Q is equal to the product of the three pairs:

$$Q = (RQD/J_n) \cdot (J_r/J_a) \cdot (J_w/SRF) \quad (1)$$

Thus, the following rock mass would be most favourable for tunnel stability: high RQD-value, small number of joint sets, appreciable joint roughness, minimal joint alteration or filling, minimal water inflow, and favourable stress levels.

Individual ratings of the six parameters have been published previously, together with detailed support tables from which estimates of appropriate permanent support can be obtained. In view of the fact that no changes have been found necessary, the support tables are not repeated in this paper, and readers should consult two earlier publications for such details (Barton, Lien and Lunde 1974, 1975). However the classification ratings are given here (see Appendix) so that the following examples of support prediction and classification philosophy may be more easily followed. These classification ratings are also unchanged from the original.

## COMPARISON WITH THE GEOMECHANICS

### CLASSIFICATION SYSTEM

It is not the intention here to make a quantitative comparison between the Q-system and Bieniawski's (1974) Geomechanics Classification since this is done in the general review paper in this symposium. However, certain qualitative differences can be mentioned which serve as a useful basis for discussion.

Bieniawski (1974) rates the following six parameters in his system:

1. Uniaxial compressive strength of rock material.
2. Drill core quality RQD.
3. Spacing of joints.
4. Condition of joints.
5. Groundwater conditions.
6. Orientation of joints.

It can be seen that stress is not used specifically as a parameter though it is apparently when selecting support measures. In the Q-system, the ratio ( $\sigma_1/\sigma_3$ ) (unconfined compression strength/major principal stress) is considered a more realistic method of treating this "rock burst" factor, and in fact the onset of rock bursting and slabbing problems can be quite accurately predicted (see Appendix, Table 6b). The Q-system also accounts for *loosening* caused by shear zones and faults, and *swelling* and *expanding* ground.

A common factor between the two systems is the use of Deere's (1963) RQD. However Bienawski also includes joint spacing and orientation, while the Q-system only considers the number of joint sets. The significance of the number of joint sets, particularly in the case of unsupported tunnels has been discussed at some length by Barton (1976).

The exclusion of orientation as a separate parameter in the Q-system has been criticised quite widely, but possibly the basic philosophy of the Q-system has not been fully appreciated by those concerned.

In all publications it has been emphasised that the parameters  $J_r$  joint roughness number, (Appendix: Table 3) and  $J_a$  joint alteration number, (Appendix: Table 4) should apply to the joint set or single discontinuity most likely to allow failure to initiate. The orientation of the feature relative to the excavation is implicit in these instructions. A practical example may be useful here. The Q-system was recently used for estimating the support requirements of a 19 meters span hydro power cavern and a parallel gate gallery of 3.5 meters span. A vertical narrow shear zone intersected the axis of both excavations, more or less perpendicularly. Besides other joint sets there was also a set of unfavourably orientated smooth, undulating joints dipping at about 50° from the downstream walls. The minimum value of  $J_r/J_a$  is obviously obtained from the shear zone. However, due to its favourable orientation this was ignored in the classification and the slightly higher value of  $J_r/J_a$  for the unfavourably orientated joints was considered more relevant. If the shear zone had been looser and clay bearing, then clearly it would re-establish itself as the potential source of failure, and a lower Q-value and heavier support would result.

Bieniawski (1974) appears to have favoured the rating-for spacing and orientation of the different joint sets according to the case record given in his paper.

The very detailed treatment of joint roughness and alteration which is perhaps the strongest feature of the Q-system is not particularly emphasised in the

Geomechanics Classification. In his original version Bienawski (1973) considered the condition of joints under three descriptive terms: *weathering* (5 ratings), *separation of joints* (5 ratings, <0.1 mm up to >5 mm) and *continuity of joints* (5 ratings, not continuous up to continuous with gouge). In his 1974 publication Bienawski condensed these three terms to *condition of joints* which again has five ratings; from *very light*, separation <0.1 mm, not continuous, up to *open* >5 mm, continuous gouge >5 mm. In his most recent publication (general review paper, this symposium) Bienawski also includes joint roughness in his fourth parameter *condition of joints*.

MAXIMUM SPANS FOR UNSUPPORTED EXCAVATIONS

A very interesting area of application for the Q-system is in the recognition of rock mass characteristics required for safe operation of permanently unsupported openings. A detailed analysis of all the available case records of unsupported excavations (Barton, 1976) revealed the following requirements. (The ratings of the various parameters should be checked against the descriptions given in the Appendix).

General requirements for permanently unsupported openings.

1.  $J_n \leq 9$ ,  $J_r \geq 1.0$ ,  $J_a \leq 1.0$ ,  $J_w = 1.0$ ,  $SRF \leq 2.5$

Conditional requirements.

2. If  $RQD \leq 40$ , should have  $J_n \leq 2$
3. If  $J_n = 9$ , should have  $J_r \geq 1.5$  and  $RQD \geq 90$
4. If  $J_r = 1$ , should have  $J_n < 4$
5. If  $SRF > 1$ , should have  $J_r \geq 1.5$
6. If  $SPAN > 10$  m, should have  $J_n < 9$
7. If  $SPAN > 20$  m, should have  $J_n \leq 4$  and  $SRF \leq 1$

Existing natural and man-made openings indicate that very large unsupported spans can be safely built and utilized if the rock mass is of sufficiently high quality. The case records that describe unsupported man-made excavations have spans ranging from 1.2 to 100 metres. If there are only a limited number of discontinuous joints and the rock mass quality Q is up to 500 or 1000 the maximum unsupported span may only be limited by the ratio of rock stress/rock strength. Naturally, if this ratio becomes unfavourable (see Appendix, Table 6b) the quality Q will not remain at this high value, and the maximum safe span will be reduced.

All the available case records of unsupported spans are plotted in Fig. 1. The tentative curved envelope is the assumed maximum design span for man-made openings based on these available cases. The five square data points plotting above this curve were obtained from the huge natural openings of the Carlsbad limestone caverns in New Mexico. If the data for man-made and natural openings is combined, it is seen that the limiting envelope is approximately linear.

It can be represented by the following simple equation:

$$SPAN = 2Q^{0.66} \tag{2}$$



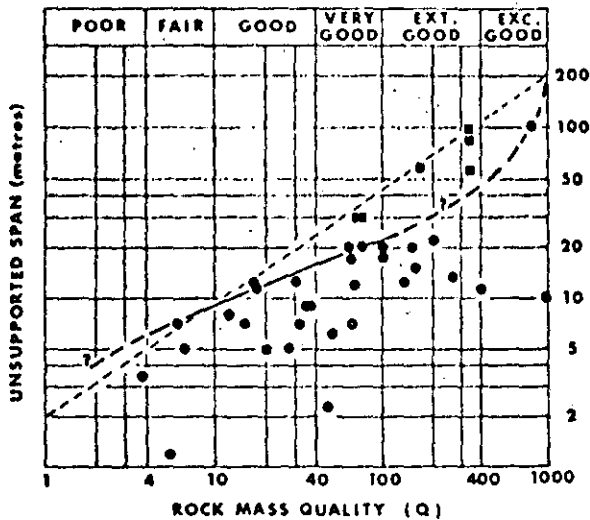


Fig. 1 Circles represent the man-made unsupported excavations reported in the literature. Squares represent some natural openings from Carlsbad, New Mexico. The curved envelope is an estimate of the maximum design span for permanently unsupported man-made openings.

For design purposes the evidence of the natural caverns is ignored. Suggested maximum design spans for different types of excavations are based on the curved envelope. Details are given by Barton (1976), and also in the last section of this paper.

#### STAND-UP TIMES FOR UNSUPPORTED EXCAVATIONS

The man-made openings which plot closest to the curved envelope in Fig. 1 were the following types of excavations; 7 m span major road tunnel (slow lane for lorries), 8 m span water collector tunnel for hydro scheme, 11.2 m span tailrace tunnel for hydro electric station, 12 m span waste water treatment plant, 12.5 m span head race tunnel for hydro scheme, 20 m span mine openings (two cases), 22 m span subway station, 100 m span mine opening.

In view of the type of excavations involved, and the fact that the mine openings in question have been perfectly stable for many years, it is certainly conservative to assume that the above excavations have a stand-up time in excess of 10 years. For practical purposes they can probably be regarded as permanent. Certainly the Carlsbad caverns must be considered as "permanent" unsupported openings. No appreciable rock fall has been observed in more than 50 years of public visits, and more than 1 million people pass through the caverns each year. Classification details and approximate dimensions of these caverns are given by Barton (1976).

The closeness with which an unsupported opening can be designed to the envelope of maximum design span will depend on the type of excavation, the degree of safety, and the stand-up time required. If the maximum design span is exceeded, or if some of the above conditional factors are not satisfied the stand-up time may be less than "permanent".

A group of excavations which are probably frequently designed with spans exceeding the maximum design envelope are temporary mine openings. As a group, they can be subdivided since the required stand-up times will depend on the time it takes to finish extracting ore in the vicinity of, or in the excavation in question. The stand-up time actually available with a given span will depend both on the shape of the roof, and on the rock mass quality  $Q$ , and it will also depend on the care with which blasting is carried out, although this effect should be automatically incorporated in the estimate of  $Q$ .

It has been assumed here that the excavations that plot closest to the curved envelope in Fig. 1 (the maximum design span) have stand-up times in excess of 10 years. In view of the type of excavations involved it is obviously expected that they will stand unsupported for at least a "life-time", in other words more than 50 years. This conservative range of 10 to 50 years to represent "permanency" is used to obtain Fig. 2, which is a preliminary attempt at correlating stand-up time,  $Q$ , and unsupported span.

The envelopes have been truncated at various time intervals as a concession to the approximate minimum construction periods of the various dimensions of excavation. The equivalent unsupported span at any one time can be considered as the length from the face to the supported zone, or as the span itself, whichever is the smaller. Except for the smallest spans there will be a significant stand-up period concurrent with the advance of the successive blasting rounds.

The actual inclination of the shaded zones drawn for various spans is unknown. In other words for a given span the relationship between stand-up time and rock mass quality is unknown. However, it seems quite likely that future case records will show that stand-up time reduces more abruptly and unexpectedly in the poorer qualities of rock. The shaded zones would then tend to bend down towards the vertical as suggested in Fig. 2.

The envelopes presented in Fig. 2 have been used by Bieniawski (general review paper, this symposium) to compare the Geomechanics Classification and the  $Q$ -system. The Geomechanics Classification was based initially on Lauffer (1958), which is now acknowledged to be excessively conservative. Despite later modification based on South African case records, Bieniawski's chart of stand-up time versus design span is still seen to be very conservative compared to the  $Q$ -system. In the best qualities of rock mass it is extremely conservative. This is clearly a reflection of the different tunneling practice in Scandinavia compared to South Africa. The greater confidence apparently exhibited in Scandinavian tunneling projects is clearly a function of the generally excellent rock, and the longer experience with excavations for civil engineering purposes.

The value of case records of tunnels that failed due to inadequate stand-up times cannot be overemphasized. The tunneling profession is constantly asked to assess the "factor-of-safety" of a given design. If we are honest we have to admit that our present state of knowledge is inadequate to allow us to come anywhere near the correct value. For this reason the analysis of a failed length of tunnel; the stand-up

STAND-UP TIME

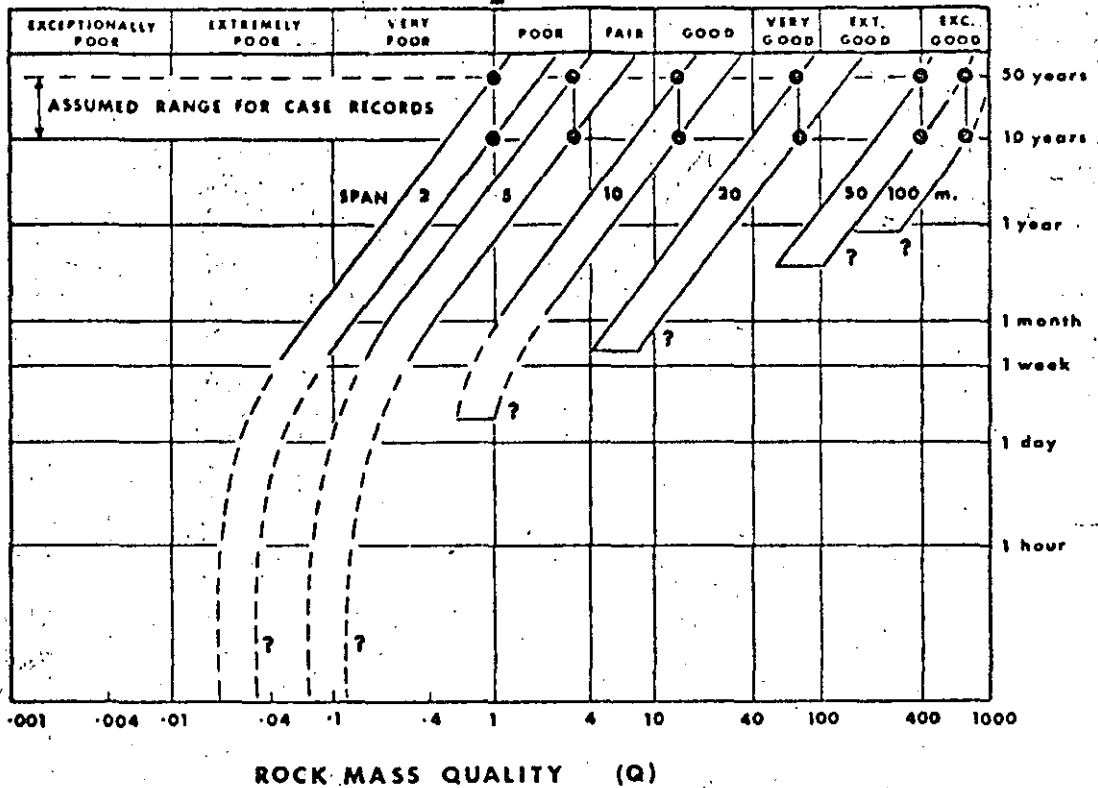


Fig. 2 The envelopes represent a preliminary attempt at predicting how much the stand-up time reduces when the span of an unsupported excavation is increased beyond the maximum design span (Fig. 1).

time, the Q-value and the span, can give us some indication of how conservative our present designs really are. We have to start on the "simple" case of unsupported openings, before attempting to assess the "factor-of-safety" of supported excavations, with all the associated complications of rock-support interaction.

When considering safety it should be remembered that the Q-system itself has a built in safety factor since it is firmly based on an engineering tradition that results in very few failures. Moreover, the majority of tunneling case records on which it was based were under construction or already built before 1970.

EXAMPLES OF APPLICATION OF Q-SYSTEM

The practical examples to be described here concern a power house and associated excavations and tunnels, which are presently being excavated at a depth of between 100 and 150 metres, mostly in quite massive biotite gneiss. The consultants claimed to have used the Q-system in their preliminary estimates of support requirements. However, the contractors, who were

widely experienced, doubted that the Q-system could have been used correctly, since the designed support was considered by them to be excessively conservative. This situation resulted in the contractor requesting an independent assessment of the rock mass conditions, and a re-assessment of the support requirements based on the Q-system.

1. Estimating support requirements from borehole logs.

The first re-assessment was based on geological reports and core logs made available by the contractor. No photographs were available, either of the core or of the existing excavations. Only later was the site visited and the Q-system applied in-situ in the existing tunnels and power house roof heading.

Five boreholes had been drilled in the neighbourhood of the power station. Four were vertical and one was inclined. The relevant core logs were studied, in particular the records of core recovered from between about 110 and 160 metres, which correspond to roughly ten metres above the roof down to the base of the excavation. "Best", "medium" and "poorest"

qualities were estimated from the relevant depths of each core. The following example shows the ratings estimated from the borehole that was most typical of the five holes. (The Appendix should be checked to obtain the appropriate verbal descriptions).

	Best	Medium	Poorest
RQD	100	90	70
$J_n$	3	4	9
$J_r$	2	2	1
$J_a$	1	2	4
$J_w$	1	1	0.66
SRF	1	1	2.5
Q	67	22	0.5

For the purpose of estimating the approximate overall support requirements, the average values obtained from the five lengths of borehole were used, equally weighted for each hole since there did not appear to be any hole with a particular advantage as regards location. The mean Q-values were 67, 20 and 1.2.

Geological engineering judgement was used to estimate the overall number of joint sets ( $J_n$ ). The geological report contained descriptions of up to three joint sets on individual surface outcrops, though several additional joint orientations were plotted in polar diagrams. It appears that this may have been one source or error in the consultant's estimates of  $J_n$  in other words the value of  $J_n$  was overestimated. The unbroken nature of most of the core made it unlikely that there were four or five joint sets in any one location. Therefore three sets were chosen to represent the "poorest" quality, since this corresponded to what was found at the surface in strongly weathered outcrops. The extrapolation to two sets for the "medium" quality, and one set plus random for the "best" was considered realistic in view of the excellent core recovery (mostly 100%) and the high RQD (mostly 100%) at the appropriate depths. (This assumption that the jointing was markedly less persistent at depth proved to be essentially correct on the subsequent site visit).

The joint roughness number ( $J_r$ ) was generally guessed to be 2 (smooth, undulating) in view of the foliated nature of the gneiss, while for the "poorest" quality it was assumed to be 1 (smooth, planar).

The joint alteration number ( $J_a$ ) was assumed to be 1 (unaltered joint walls) for the "best" quality, and down to 4 (chlorite coatings) for the "poorest" quality, since occasional chlorite and limonite coated joints were recorded in the corelog.

The joint water reduction factor ( $J_w$ ) was generally assumed to be 1 (dry excavations, or minor inflow) though for the "poorest" quality it was assumed to be 0.66 (medium inflow or pressure, occasional outwash of joint fillings). Many of the Lugeon pumping tests showed "zero" permeability, exceptions generally corresponding to zones where the RQD values were lower than 80 or thereabouts.

Finally, the stress reduction factor (SRF) was assumed to be 1 (medium stress,  $\sigma/\sigma_c$  between 10 and 200) for the "best" and "medium" qualities. The

assumed value of the maximum principal stress ( $\sigma_1$ ) was 50 kg/cm<sup>2</sup>, based on a depth of 150 m, a level topography and a geological history that suggested that high horizontal stresses would be absent. The assumed value of  $\sigma_c$  was 800 kg/cm<sup>2</sup> for the biotite gneiss. This value was actually measured, but an informed guess would probably have been in this region anyway. (According to Table 6b of the Appendix, mild rock burst problems would not be encountered unless the ratio  $\sigma/\sigma_c$  dropped to between 5 and 2.5). The value of SRF assumed to best represent the "poorest" zones was 2.5 (see Table 6a, description C, Appendix).

The three mean values of Q (67, 20 and 1.2) were used to obtain estimates of permanent roof and wall support for the 19 m span, 31 m high power house using the support tables given by Barton et al. (1974, 1975).

	roof arch	walls
"Best" (Q=67)	untensioned, grouted bolts, 5m long, c/c 2.0m	spot bolts
"Medium" (Q=20)	tensioned, grouted bolts, 5m long, c/c 1.7m	spot bolts
"Poorest" (Q=1.2)	tensioned, grouted bolts, 5m long, c/c 1.0m + shotcrete, mesh reinforced, 15cm thick	tensioned, grouted bolts, 7m long, c/c 1.4m + shotcrete, mesh reinforced, 12cm thick

The above estimates of support were apparently in line with those considered appropriate by the contractor.

Note: It is general practice to use alternating bolt lengths in caverns of this size (B=19 m). For example, 4 m and 6 m long bolts could be used in the roof arch on an intermeshed pattern, while 4 m and 8 m long bolts could be used in the walls. It is also general practice - though possibly of questionable value - to use long tensioned anchors when the rock mass quality is as low as the poorest value (Q=1.2). However, since these zones were likely to be relatively narrow, with quite massive rock surrounding them, there did not seem to be any necessity for anchors. Careful orientation ("stitching") of the bolts across the weakness zones was recommended.

### 2. Estimating support requirements from in situ classification.

The site in question was visited approximately one month after the above estimates were made. Nine locations were selected in and around the power station. The roof arch was shotcreted at this stage though some 3 to 6 metres of the walls were excavated and parts were not shotcreted. Both end walls were bare. Other unsupported locations were selected in the immediate vicinity of the power house in an attempt to predict conditions likely to be encountered when the cavern height was increased to the maximum 31 metres.

The six classification parameters were estimated at each location. In the case of the end wall of the power house three separate assessments were made, one for the localised silty-clay bearing fracture

zone (which had the worst quality of all), and the other two assessments for the medium and better rock also found in the end wall.

The separate assessments fell into three groups. For statistical purposes these were simply averaged:

	$RQD/J_n \times J_r/J_a \times J_w/SRF = Q$			
BEST	98/4.3	1.7/1.0	1/1	39
POORER ZONES	72/7	1.9/1.8	1/1	11
WORST	40/9	2/6	1/2.5	0.6

In terms of expected frequency of occurrence, it was estimated that more than 90% of the excavated surface in the power house (including roof and walls) would be of "best" quality, less than 10% of "poorer" quality, and probably only 1 or 2% of "worst" quality. A careful assessment of available borecore suggested that only the existing top part of the end wall would be affected by the "worst" quality zones. The remainder yet to be excavated could well be up to the "best" quality.

The mean ratings for the majority of the rock mass (BEST, Q=39) can be translated into the following descriptions:

1. RQD = 98 (excellent)
2.  $J_n = 4.3$  (approx. two joint sets)
3.  $J_r = 1.7$  (rough-planar to smooth-undulating)
4.  $J_a = 1.0$  (unaltered joints, surface staining)
5.  $J_w = 1.0$  (dry excavations)
6. SRF = 1.0 (medium stress; no rock bursting)

(A very favourable quality was the non-planarity of the joints. The slight displacement resulting from excavation allows joints to shear slightly thereby increasing the favourable interlock effect. A non-planar joint dilates strongly when sheared, especially if the normal stress level is not too high.

The three mean values of Q (39, 11, and 0.6) estimated from the  $J_n$  classification are each about half the value estimated from the earlier classification of bore core logs (Q=67, 20 and 1.2). However, due to the logarithmic arrangement of the Q rating (i.e. POOR=1-4, FAIR=4-10, GOOD=10-40 etc. see Figure 2) the two-fold discrepancy has a relatively small effect on the recommended permanent support. The support recommendations, which were again obtained from Barton et al. (1974, 1975), were as follows:

BEST	ca. 90% Q=39	Roof: B 1.7m c/c + c/m Walls: sb
POORER ZONES	ca. 10% Q=11	Roof: B 1.5m c/c + S(mr) 7cm Walls: B 1.6m c/c + c/m
WORST	1-2% Q=0.6	Roof: B 1.0m c/c + S(mr) 15cm Walls: B 1.2m c/c + S(mr) 12cm

KEY : B = systematic bolting with given c/c spacing  
sb = spot bolts  
S(mr) = mesh reinforced shotcrete  
c/m = chain link mesh or steel bands

The above recommendations for support, especially those for the majority of the rock mass (Q=39) will obviously appear grossly under-conservative in

6

countries where a concrete lining has been a common feature of final tunnel support. However, it should not be forgotten that the support recommendations obtained from the Q-system were based on the analysis of about 200 case records, and 79 of these were in the power house category. Underground excavations are supported with some confidence primarily because many others have been supported before them and they have performed satisfactorily.

The particular support method recommended by the Q-system depends on the rock mass quality Q, the span or wall height (whichever is relevant), and the type of excavation. Power houses are naturally amongst the most important excavations, where safety has to be permanently assured. The support recommendations are therefore inherently conservative, and the factor of safety against collapse is likely to be quite high.

If Figure 1 is examined, it will be seen that the Q value of 39 (BEST) and the span of 19m, lie some 3 to 4m above the maximum design span for permanently unsupported openings. The recommended systematic bolting (c/c 1.7m) and the steel banding (a single layer of shotcrete might be preferred for aesthetic reasons) do indeed seem to be overdesign considering that the joint spacing was 1 to 2m and the existing joints relatively discontinuous anyway. In addition it may be noted that the mean ratings of the six rock mass parameters for the BEST quality (Q=39) satisfy all the *practical* criteria apparently needed for an excavation to be left permanently unsupported. These were listed earlier.

#### 4. Estimating support requirements for tunnels

Estimating the support requirements for a tunnel that has yet to be excavated is obviously a difficult task, even if a large number of boreholes have been drilled. The problem is reduced somewhat if seismic measurements are available, although if the tunnel lies below the interface between the weathered zone and hard fresh rock, it is easy to underestimate the quality from seismic profiles. (In the present example the weathered zone extended down to a maximum depth of 40m.)

The problem of extrapolating the results of surface or near surface mapping to tunnel depth is clearly of considerable importance if cost estimates are to have any meaning. To take an example, one can consider a fault mapped at the surface. It might correctly be given the following classification:

$$RQD/J_n = 10/20, J_r/J_a = 1.0/8.0, J_w/SRF = 0.5/10$$

These ratings combine to give almost the worst possible quality Q=0.003 (EXCEPTIONALLY POOR), and correspondingly heavy support (cast concrete lining). The value of  $J_n = 20$  represents "crushed rock, earth like" which may be a good description of the surface condition of many faults and weakness zones. However, at the tunnel depth of say 100m, the same fault might only be a relatively narrow zone of weakness, and the classification and resulting support should then also reflect the quality of the surrounding rock.

In the present example a planned 5km long tailrace tunnel trace was investigated with 15 irregularly spaced boreholes. As a first attempt at support prediction, the corelogs were examined between the

appropriate depths, which in this case ranged from about 150-160m at the upstream (powerhouse) end, down to only 10-20m close to the downstream portal. Estimates of "best", "poorer zones", and "worst" qualities were made from examination of each corelog. The nearest 10m both above and below the planned 8.0m span tunnel were considered. The classification took into account the expected looser and more weathered state of the rock mass where the depth of cover was less than 30-40m, as was the case near the portal.

The average Q values for the 15 holes were as follows

BEST	Q=42
POORER ZONES	Q=12
WORST	Q=1.1

The variation from borehole to borehole was quite marked, as can be seen from the following maximum and minimum values :

BEST	max. Q=100	min. Q= 19
POORER ZONES	max. Q= 50	min. Q=4.1
WORST	max. Q=19	min. Q=0.03

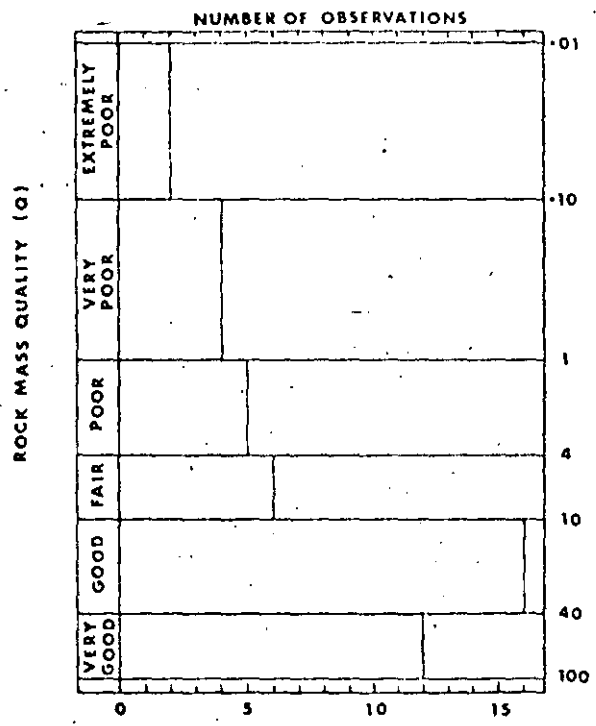


Fig. 5 The distribution of Q values from analysis of 15 corelogs for the long tailrace tunnel.

In view of the scatter the results were plotted as a histogram, as shown in Figure 3. The two minimum quality WORST zones had Q values of 0.07 and 0.03, and these were assumed to represent the quality of weakness zones at tunnel depth. Between 20 and 25 weakness zones were suspected from surface mapping and/or low seismic velocities.

The various estimates of permanent support are given below, based on a tunnel span and height of 8.2m and an ESR value equal to 1.3 appropriate to the relative importance of a tailrace tunnel. (ESR represents the type of excavation in terms of its relative safety requirement. The use of ESR values is described fully by Barton et al. 1974, 1975, and is summarised in the last section of this paper.)

BEST	Q=42	Roof : none	Wall : none
POORER ZONES	Q=12	Roof : B 1.5m c/c	Wall : none
WORST	Q=1.1	Roof : B 1.0m c/c + S(mr) 5cm	Wall : B 1.0m c/c + S 3cm, (or : S(mr) 5cm alone. depends on block size)
FAULTS or WEAKNESS ZONES	Q=0.05	Roof : S(mr) 20-25cm	Wall : S(mr) 20-25cm (include invert)

KEY : B = systematic bolting with given c/c spacing  
 S(mr) = mesh reinforced shotcrete  
 sb = spot bolts

(Note : There was no evidence of swelling clays, therefore the Q values and recommended support are not exceptional.)

Rock mass classification from an existing unsupported tunnel clearly gives a much more reliable estimate of support than the above extrapolation of surface mapping and borehole data. Experience with the Q-system in many kilometers of tunnels shows it to be a very rapid method both of mapping essential parameters and of estimating support requirements on site. The input data is listed on a simple form for each length of tunnel considered to require different support from the adjacent length.

If the engineering geologist prefers to consult the support tables (Barton et al. 1974, 1975) in the luxury of a site office, then a short verbal description of the different zones needing support is helpful. Alternatively, the number and letter coding appropriate to each of the six parameters can be recorded. From the appendix it will be seen that a rockmass with the following characteristics is extremely favourable for tunnel stability :

1.E/2.A, 3.A/4.A, 5.A/6.K

CRITICAL Q CONCEPT IN TUNNEL MAPPING

In this last section another problem of extrapolation is considered. The problem is one of extrapolating

observations from pilot tunnels or access tunnels to the full scale excavation. Apart from the great advantage of more reliable mapping that a pilot tunnel affords, the performance of the tunnel itself can provide useful pointers to full scale behaviour. If light support is just needed to maintain a section of the pilot opening, then the Q-value can be analysed and checked with the value estimated from the tunnel mapping. The reliability of the input data can then be assessed.

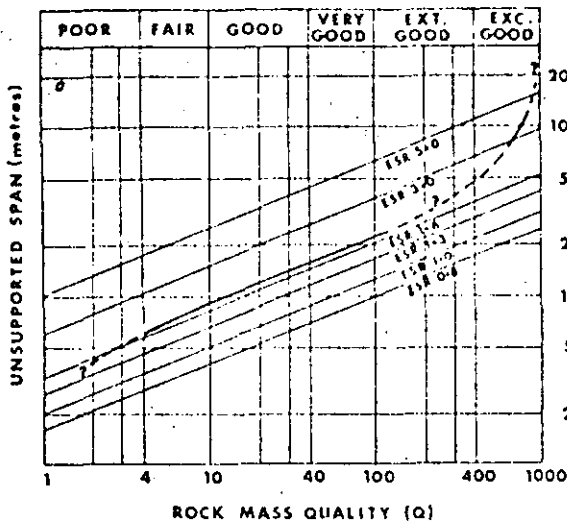


Fig. 4 Suggested design limits for the various types of excavation listed in the table opposite. ESR values greater than 1.0 apply to temporary openings, for which back analysis requirements concerning stand-up time are negligible. Support may be required if spans in excess of the relevant design limits are excavated.

The maximum span limit (curved envelope, Figure 1), has been redrawn in Figure 4, together with a set of parallel lines that represent the suggested span limits for unsupported excavations of various types. The table shows the suggested ESR classes of excavation and their corresponding ESR values. The span width divided by ESR (SPAN/ESR) and the rock mass quality Q give a combined measure of the degree of support that is required. The actual span limits for permanently unsupported openings can be expressed as follows:

$$\text{SPAN} = 2 \cdot \text{ESR} \cdot Q^{0.4} \quad (3)$$

The six parallel lines in Figure 4 correspond to this equation.

The vast majority of case records with spans exceeding these suggested design limits were supported in some way - for instance with various combinations of bolting, shotcrete and reinforcing mesh. Returning to the pilot tunneling station, it will be appreciated that a section that immediately requires support gives a spot check of the Q value, if this in situ evidence of support needs is evaluated according to Figure 4. Thus a 2m span pilot tunnel (ESR=1.6) will not require support unless Q lies in the VERY POOR

TYPE OF EXCAVATION	ESR	NO. CASES
A. Temporary mine openings	ca. 3-5 ?	(2)
B. Permanent mine openings, water tunnels for hydro power (exclude high pressure penstocks), pilot tunnels, drifts and headings for large excavations etc.	1.6	(83)
C. Storage rooms, watertreatment plants, minor road and railway tunnels, surge chambers, access tunnels, etc. (hemispherical caverns)	1.3	(25)
D. Power houses, major road and railway tunnels, civil defence chambers, portals, intersections etc.	1.0	(79)
E. Underground nuclear power stations, sports and public facilities, factories etc.	0.8	(2)

category (Q=0.1 to 1). The theoretical Q value according to equation 4 would be 0.3, based on the rearranged form of equation 3:

$$Q = \left( \frac{\text{SPAN}}{2 \cdot \text{ESR}} \right)^{2.5} \quad (4)$$

In routine mapping of tunnels, the theoretical Q value should be determined from Figure 4 (or equation 4) at the outset, so that sections requiring support can be more rapidly distinguished from the sections that can be left permanently unsupported.

In the case of a pilot tunnel the range of Q values obtained from mapping and back analysis provides an invaluable and specific range of values for estimating support for the full scale excavation. This would be selected from the support chart and support tables given by Barton et al. (1974, 1975), using the same range of Q values, but the value of SPAN/ESR relevant to the full scale excavation. Naturally, if geological mapping suggested different conditions in parts of the full scale excavation, perhaps due to the nearness of a fault zone, then the Q values obtained from the pilot tunnel would have to be modified accordingly.

The support recommendations for the large scale excavation would generally incorporate thicker shotcrete or cast concrete arches, and of course longer bolts. However, the increase in thickness of the shotcrete or concrete only goes up in approximate proportion to the span width. The bolt spacing and theoretical support pressure remain roughly the same. This appears to be in line with present practice in large excavations, and is justified because of the efficiency of modern temporary support methods (i.e. shotcrete and bolting). It is only under extremely difficult ground conditions, where even temporary support is "too late" that a large span excavation is likely to require a higher designed support pressure than a pilot tunnel through the same ground. A careful multiple heading technique can presumably reduce the discrepancy.

Tunnel mapping and support prediction have been performed at a rate of up to several kilometers per day using the Q system. While it is extremely unwise to rush this important task, it does illustrate that the method is certainly not "too complicated to be generally acceptable in practice", as has been claimed recently by Pells (1975). The method is in fact embarrassingly simple, once the user becomes experienced.

The Q system is essentially a *weighting process*, in which the positive and negative aspects of a rockmass are assessed. A store of experience (case records), which is itself based on earlier experience, is searched to try to find the most appropriate support measures for the given excavations and rock mass conditions. The whole procedure is probably not dissimilar to the mental process occurring when a very experienced tunneling consultant is asked for his support recommendations. While the assessment of most of the parameters is admittedly subjective, the process of support selection is organized and reasonably consistent.

#### ACKNOWLEDGEMENTS

The detailed descriptions of rock conditions in some Scandinavian tunneling projects given by Cecil (1970) provided an invaluable store of data for stage by stage improvement of the classification system during its development in 1973. The interest and practical advice given by Reidar Lien and Johnny Lunde of NGI is sincerely acknowledged.

#### REFERENCES

- Barton, N. (1976)  
Unsupported underground openings. *Rock Mechanics Discussion Meeting*, BeFo, Stockholm, February 1976.
- ✓ Barton, N., Lien, R. and Lunde, J. (1974)  
Engineering classification of rock masses for the design of tunnel support. *Rock Mechanics*, Springer Verlag, Vol. 6, pp. 189-236.
- ✓ Barton, N., Lien, R. and Lunde, J. (1975)  
Estimation of support requirements for underground excavations. *Design Methods in Rock Mechanics*, Proc. 16th. Symp. on Rock Mech., Univ. of Minnesota.
- Bieniawski, Z.T. (1973)  
Engineering classification of jointed rock masses. *The Civil Engineer in South Africa*, Dec. 1973, pp. 335-343.
- Bieniawski, Z.T. (1974)  
Geomechanics classification of rock masses and its application in tunneling. *Abstracts in Rock Mechanics*, Proc. of 3rd. Cong. of Int. Soc. Rock Mech., Denver, 1974, Vol. II.A, pp. 27-32.
- Cecil, O.S. (1970)  
Correlations of rock bolt - shotcrete support and rock quality parameters in Scandinavian tunnels. *Ph.D. Thesis*, Univ. of Illinois, Urbana, pp. 1-414. (Now published as Swedish Geotechnical Institute, Proceedings No. 27, Stockholm, 1975.)

Deere, D.U. (1963)  
Technical description of rock cores for engineering purposes. *Felersmeknik og Ingeniørvitenskap*, Vol. 1, No. 1, pp. 16-22.

Lauffer, H. (1958)  
Gebirgsklassifizierung für den Stollenbau. *Geologie und Bergbau*, Vol. 24, pp. 46-51.

Palmstrøm, A. (1975)  
Characterization of degree of jointing and rock mass quality. (In Norwegian) *Internal Report*, Ing. A.B. Berdal A/S, Oslo, pp. 1-26.

Pells, P.J.N. (1975)  
Discussion (of Barton, Lien, and Lunde, 1974). *Rock Mechanics*, Springer Verlag, Vol. 7, No. 4, pp. 246-248.

Table 1. Descriptions and ratings for the parameter RQD.

1. ROCK QUALITY DESIGNATION (RQD)

A. Very poor	0 - 25
B. Poor	25 - 50
C. Fair	50 - 75
D. Good	75 - 90
E. Excellent	90 - 100

Note: (i) Where RQD is reported or measured as  $\leq 10$ , (including 0) a nominal value of 10 is used to evaluate  $Q$  in equation (1).

(ii) RQD intervals of 5, i.e. 100, 95, 90, etc. are sufficiently accurate.

Table 2. Descriptions and ratings for the parameter  $J_n$

2. JOINT SET NUMBER ( $J_n$ )

A. Massive, no or few joints	0.5-1.0
B. One joint set	2
C. One joint set plus random	3
D. Two joint sets	4
E. Two joint sets plus random	6
F. Three joint sets	9
G. Three joint sets plus random	12
H. Four or more joint sets, random, heavily jointed, "sugar-cube" etc.	15
J. Crushed rock, earthlike	20

Note: (i) For intersections use  $(3.0 \times J_n)$

(ii) For portals use  $(2.0 \times J_n)$

Table 3. Descriptions and ratings for the parameter  $J_r$

3. JOINT ROUGHNESS NUMBER ( $J_r$ )

(a) *Rock will contact and*  
(b) *Rock will contact before 10 cm shear*

A. Discontinuous joints	4
B. Rough or irregular, undulating	3
C. Smooth, undulating	2
D. Slickensided, undulating	1.5
E. Rough or irregular, planar	1.5
F. Smooth, planar	1.0
G. Slickensided, planar	0.5

Note: (i) Descriptions refer to small scale features and intermediate scale features, in that order.

(c) *No rock wall contact when sheared*

H. Zone containing clay minerals thick enough to prevent rock wall contact	1.0
J. Sandy, gravelly or crushed zone thick enough to prevent rock wall contact	1.0

Note: (ii) Add 1.0 if the mean spacing of the relevant joint set is greater than 3 m.

(iii)  $J_r = 0.5$  can be used for planar slickensided joints having lineations, provided the lineations are orientated for minimum strength.

Table 4. Descriptions and ratings for the parameter  $J_a$

4. JOINT ALTERATION NUMBER ( $J_a$ ) ( $\phi_r$ ) (approx.)

(a) *Rock will contact*

A. Tightly healed, hard, non-softening, impermeable filling i.e. quartz or epidote	0.75	(-)
B. Unaltered joint walls, surface staining only	1.0	(25-35 <sup>o</sup> )
C. Slightly altered joint walls. Non-softening mineral coatings, sandy particles, clay-free disintegrated rock etc.	2.0	(25-30 <sup>o</sup> )
D. Silty-, or sandy-clay coatings, small clay fraction (non-soft.)	3.0	(20-25 <sup>o</sup> )
E. Softening or low friction clay mineral coatings, i.e. kaolinite or mica. Also chlorite, talc, gypsum, graphite etc., and small quantities of swelling clays	4.0	(8-16 <sup>o</sup> )

(b) *Rock will contact before 10 cm shear*

F. Sandy particles, clay-free disintegrated rock etc.	4.0	(25-30 <sup>o</sup> )
G. Strongly over-consolidated non-softening clay mineral fillings (continuous, but <5 mm thickness)	6.0	(16-24 <sup>o</sup> )
H. Medium or low over-consolidation, softening, clay mineral fillings (continuous but <5 mm thickness)	8.0	(12-16 <sup>o</sup> )
J. Swelling-clay fillings, i.e. montmorillonite (continuous, but <5 mm thickness). Value of $J_r$ depends on percent of swelling clay-size particles, and access to water etc.	8-12	(6-12 <sup>o</sup> )

(c) *No rock wall contact when sheared*

K. Zones or bands of disintegrated or crushed rock and clay (see M, G, H, J for description of clay condition)	6, 8, or 8-12	(6-24 <sup>o</sup> )
N. Zones or bands of silty- or sandy-clay, small clay fraction (non-softening)	5.0	(-)
O. Thick, continuous zones or		
P. bands of clay (see G, H, J for 10, 13, R. description of clay condition) or	13-20	(6-24 <sup>o</sup> )

Table 5. Descriptions and ratings for the parameter  $J_w$

5. JOINT WATER REDUCTION FACTOR ( $J_w$ ) Approx. water pres. (kg/cm<sup>2</sup>)

A. Dry excavations or minor inflow, i.e. <5 l/min. locally	1.0	<1
B. Medium inflow or pressure, occasional outwash of joint fillings	0.66	1-2.5
C. Large inflow or high pressure in competent rock with unfilled joints	0.5	2.5-10
D. Large inflow or high pressure, considerable outwash of joint fillings	0.33	2.5-10
E. Exceptionally high inflow or water pressure at blasting, decaying with time	0.2-0.1	>10



F. Exceptionally high inflow or water pressure continuing without noticeable decay .....  $(J_w)$  0.1-0.05 >10

Approx. water pres.

11

Note: (i) Factors C to F are crude estimates. Increase  $J_w$  if drainage measures are installed.

(ii) Special problems caused by ice formation are not considered.

(c) Squeezing rock plastic flow of incompetent rock under the influence of high rock pressure (SRF)  
 N. Mild squeezing rock pressure ..... 5-10  
 O. Heavy squeezing rock pressure ..... 10-20  
 (d) Swelling rock chemical swelling activity depending on presence of water  
 P. Mild swelling rock pressure ..... 5-10  
 R. Heavy swelling rock pressure ..... 10-15

Table 6. Description and ratings for parameter SRF

6. STRESS REDUCTION FACTOR

(a) Weakness zones intersecting excavation, which may cause loosening of rock mass when tunnel is excavated. (SRF)

A. Multiple occurrences of weakness zones containing clay or chemically disintegrated rock, very loose surrounding rock (any depth) .....	10
B. Single weakness zones containing clay or chemically disintegrated rock (depth of excavation $\leq 50$ m) .....	5
C. Single weakness zones containing clay or chemically disintegrated rock (depth of excavation $>50$ m) .....	2.5
D. Multiple shear zones in competent rock (clay-free); loose surrounding rock (any depth) .....	7.5
E. Single shear zones in competent rock (clay-free) (depth of excavation $\leq 50$ m) ..	5.0
F. Single shear zones in competent rock (clay-free) (depth of excavation $>50$ m) ..	2.5
G. Loose open joints, heavily jointed or "sugar cube" etc. (any depth) .....	5.0

Note: (i) Reduce these values of SRF by 25-50% if the relevant shear zones only influence but do not intersect the excavation.

(b) Competent rock, rock stress problems (SRF)

	$\sigma_c/\sigma_1$	$\sigma_t/\sigma_1$	(SRF)
H. Low stress, near surface	$>200$	$>13$	2.5
J. Medium stress .....	200-10	13-0.66	1.0
K. High stress, very tight structure (usually favourable to stability, may be unfavourable for wall stability) .....	10-5	0.66-.33	0.5-2
L. Mild rock burst (massive rock) .....	5-2.5	0.33-.16	5-10
M. Heavy rock burst (massive rock) .....	$<2.5$	$<0.16$	10-20

Note: (ii) For strongly anisotropic virgin stress field (if measured): when  $5 \leq \sigma_1/\sigma_3 \leq 10$ , reduce  $\sigma_c$  and  $\sigma_t$  to  $0.8 \sigma_c$  and  $0.8 \sigma_t$ . When  $\sigma_1/\sigma_3 > 10$ , reduce  $\sigma_c$  and  $\sigma_t$  to  $0.6 \sigma_c$  and  $0.6 \sigma_t$ , where:  $\sigma_c$  = unconfined compression strength, and  $\sigma_t$  = tensile strength (point load) and  $\sigma_1$  and  $\sigma_3$  are the major and minor principal stresses.

(iii) Few case records available where depth of crown below surface is less than span width. Suggest SRF increase from 2.5 to 5 for such cases (see H).

ADDITIONAL NOTES ON THE USE OF TABLES 1 TO 6.

When making estimates of the rock mass quality (Q) the following guidelines should be followed, in addition to the notes listed in Tables 1 to 6:

1. When borecore is unavailable, RQD can be estimated from the number of joints per unit volume, in which the number of joints per metre for each joint set are added. A simple relation can be used to convert this number to RQD for the case of clay-free rock masses (Palmstrom, 1975):

$$RQD = 115 - 3.3 J_v \text{ (approx.)}$$

where

$$J_v = \text{total number of joints per m}^3 \text{ (RQD = 100 for } J_v < 4.5)$$

2. The parameter  $J_n$  representing the number of joint sets will often be affected by foliation, schistosity, slaty cleavage or bedding etc. If strongly developed these parallel "joints" should obviously be counted as an complete joint set. However, if there are few "joints" visible, or only occasional breaks in bore core due to these features, then it will be more appropriate to count them as "random joints" when evaluating  $J_n$  in Table 2.

3. The parameters  $J_s$  and  $J_d$  (representing shear strength) should be relevant to the presence of significant joint set or clay filled discontinuity in the given zone. However, if the joint set or discontinuity with the minimum value of  $(J_s/J_d)$  is favourably oriented for stability, then a second, less favourably orientated joint set or discontinuity may sometimes be of more significance, and its higher value of  $J_s/J_d$  should be used when evaluating Q from equation 1. The value of  $J_s/J_d$  should in fact relate to the surface most likely to allow failure to initiate.

4. When a rock mass contains clay, the factor SRF appropriate to increasing loads should be evaluated (Table 6a). In such cases the strength of the intact rock is of little interest. However, when jointing is minimal and clay is completely absent the strength of the intact rock may become the weakest link, and the stability will then depend on the ratio rock-stress/rock-strength (Table 6b). A strongly anisotropic stress field is unfavourable for stability and is roughly accounted for as in Note (ii), Table 6b.

5. The compressive and tensile strengths ( $\sigma_c$  and  $\sigma_t$ ) of the intact rock should be evaluated in the saturated condition if this is appropriate to present or future in situ conditions. A very conservative estimate of strength should be made for those rocks that deteriorate when exposed to moist or saturated conditions.



**DIVISION DE EDUCACION CONTINUA  
FACULTAD DE INGENIERIA U.N.A.M.**

MECANICA DE ROCAS APLICADA A LA MINERIA Y A LA CONSTRUCCION

UNIFORM ROCK CLASSIFICATION FOR GEOTECHNICAL ENGINEERING PURPOSES

Douglas A. Williamson

MAYO, 1985

Analysis of the CSA Mine. Australian Geomechanics Journal, Vol. G6, No. 1, 1976, pp. 2-26.

27. T.C. Rutledge. New Zealand Experience with Engineering Classifications of Rock for Prediction of Tunnel Support. Proc., International Tunnel Symposium, Japan Tunneling Committee, Tokyo, 1978, pp. A3-1--A3-7.

18. K.A. Ikeda. Classification of Rock Conditions for Tunneling. Proc., 1st International Conference on Engineering Geology. International Association of Engineering Geologists, 1977.

29. Z.T. Bieniawski. The Geomechanics Classification in Rock Engineering Applications. Proc., 4th International Congress on Rock Mechanics, ISRM, Montreux, Switzerland, Vol. 2, 1979, pp. 51-58.

30. Z.T. Bieniawski, P. Rafia, and D.A. Newman. Ground Control Investigations for Assessment of Roof Conditions in Coal Mines. Proc., 21st U.S. Symposium on Rock Mechanics, Univ. of Missouri, Rolla, 1980, pp. 691-700.

NOTICE: This material may be protected by copyright law (Title 17, U.S. Code)

Description of Discontinuities in Rock Masses. International Journal of Rock Mechanics and Mining Sciences, Vol. 15, 1979.

27. D.U. Deere and R.P. Miller. Engineering Classification and Index Properties for Intact Rock. U.S. Air Force Weapons Laboratory, Kirtland Air Force Base, NM, Tech. Rept. AFNL-TR-65-116, 1966.

26. International Society for Rock Mechanics. Basic Geotechnical Classification of Rock Masses. In Report of Commission on Rock Classification, ISRM, Lisbon, 1977.

Engineering purposes. Proc., New Zealand Conference on Geomechanics, Australia Geomechanics Society, Melbourne, 1971, pp. 435-441.

39. W.R. Dearman. Weathering Classification in the Characterization of Rock. Bull., International Association of Engineering Geology, No. 13, 1976, pp. 123-127.

Publication of this paper sponsored by Committee on Exploration and Classification of Earth Materials.

# Uniform Rock Classification for Geotechnical Engineering Purposes

DOUGLAS A. WILLIAMSON (1980)

The Unified Rock Classification System (URCS) is used by a large organization, such as the Forest Service of the U.S. Department of Agriculture, to handle projects of all sizes that involve rock. Existing geologic classifications have not provided the necessary information. The usefulness of URCS is that the pertinent natural conditions related to design and strength are emphasized and can be read at a glance, which allows an immediate assessment. A decision is then made as to the appropriate level of detail and the extent of investigation needed to complete or evaluate the project. Efforts can be concentrated toward the rock conditions that are most critical to the project. The data base that covers rock

conditions is, in many instances, too detailed for collective analysis. URCS is a type of engineering shorthand to convey maximum design and construction information and omit specific details unrelated to a general evaluation.

The Unified Rock Classification System (URCS) was originally conceived in 1959 and used in simplified form to perform investigations and explorations for

the design and construction of major flood-control dams by the Portland District of the U.S. Army Corps of Engineers. The use of URCS materially increased efficiency and produced reliable rock information that resulted in successful design and construction as well as postconstruction evaluation. URCS in its present form dates from 1975 and is used by the Forest Service, U.S. Department of Agriculture (USDA), in Region 6 and parts of Regions 1 and 5. It has been found to be a reliable method of communicating rock conditions (including those in quarries, retaining walls, and extensive rock excavations) for the design of forest access roads. Information on URCS has been published by USDA (1).

#### PURPOSE AND NEED

The purpose of URCS is to establish a means of making rapid initial assessments of rock conditions related to design and construction by simple field tests that establish natural strength parameters. The purpose is threefold: (a) to present a rock classification for use in engineering geology and geotechnical investigations, (b) to outline field-identification procedures that require simple field apparatus, and (c) to establish the classification relationship to design and performance. Experienced professionals who deal with rock can, and often do, apply the principles of rock mechanics without any formally accepted rock classification. This is not the usual case, especially in an organization that has employees of many experience levels. URCS is not intended to supplant the existing geologic classifications but to implement and to eliminate the inherent confusion of subjective terminology when applied to civil engineering.

Classification is not the chief aim of geotechnical investigations; but a uniform working classification is necessary to effectively supply the needs of a large organization of differing professional disciplines. The assertion that there is no need for a new classification is easily discounted by the statement that a classification is always needed until one is found that meets general approval and acceptance. The statements that there are as many classifications as there are geologists and that no two geotechnical investigators will give the same name to the same rock are unfortunately still true. Because of the number of geotechnical personnel working in the field, it is vital that some uniformity of data exist. Even now, when one reads geotechnical reports, drilling logs, or contract documents, it is not possible to be sure that two different geotechnical specialists who are discussing the same rock are describing sufficiently identical design characteristics. A working classification requires uniform symbols, abbreviations, notations, and definitions that are established to be acceptable procedures (2).

#### BASIS OF URCS

URCS, as originally conceived, has the following basis:

1. The rock can be defined by simple field tests.
2. The information presented is in simple, understandable, nontechnical terms.
3. The conditions defined are related to design and construction.
4. The design notation is flexible to scale in that it applies to both a very small sample or section of rock or to a large rock excavation and is appropriate to evaluation.
5. The data collected are verifiable, reproducible, and consistent with the experience and training of the user.

6. The system is useful to all levels of experience.

7. The system allows immediate assessment, both directly and on notes or documents.

#### BASIC ELEMENTS

URCS uses the four basic elements, or major physical properties, related to design and construction evaluation: (a) degree of weathering, (b) strength, (c) discontinuity or directional weakness, and (d) gravity or unit weight. By establishing limiting values of these four basic elements by using uniform field tests and observations, terminology, notation, and abbreviations, URCS records and communicates a reliable indication of rock properties and performance. URCS permits a useful estimate of compressive strength, permeability, and shear strength--the three primary properties of a rock. When combined with other geotechnical information (stress history and water-table location), URCS permits a rough estimate of rock performance such as foundation suitability, excavation means, slope stability, material use, blasting character, and water transmittal.

The equipment used for the field tests and observations is simple and available: one's fingers, a 10-power hand lens, a 1-lb (2.2-kg) ball peen hammer, and a spring-loaded scale of the 10-lb (5-kg) range. The fingers determine the degree of weathering and the manual-strength estimate. The hand lens assists in defining the degree of weathering. The ball peen hammer is used to estimate the range of unconfined compressive strength from impact reaction. The spring-loaded scale determines the field-unit weight or apparent specific gravity.

URCS design notation consists of underlined groups of combinations of the letters A through E, which stand for the five categories or design-limiting conditions that define each of the four basic elements, or major physical properties of rock (weathering, strength, discontinuity, and weight). These five limiting conditions will be discussed for each basic element in the sections that follow.

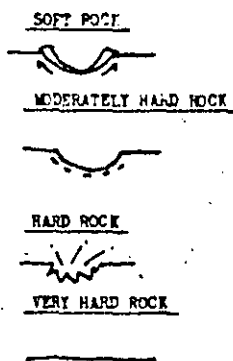
#### Degree of Weathering

In URCS the degree of weathering is restricted to chemical weathering. There are five design-limiting states or conditions that define the basic element degree of weathering: A, micro fresh state (MFS); B, visually fresh state (VFS); C, stained state (STS); D, partly decomposed state (PDS); and E, completely decomposed state (CDS). MFS is defined by examination by means of a hand lens; VFS is defined by examination by means of the naked eye; STS is weathered but not to the degree that it is remoldable by finger pressure; PDS remolds with the fingers to combinations of rock and soil due to weathering; and CDS remolds to soil.

1. MFS (A) is determined in the field by means of a 10-power hand lens. This condition exists when there is no oxidation alteration of any of the mineral components. It is desirable but not necessary to make this determination for ordinary rock-design evaluation, except for investigations of crushed rock and concrete aggregate.

2. VFS (B), the condition that is representative of the standard of quality for the site and the rock quality with respect to weathering, is not expected to change within the economic limits of the excavation. The mineral components are evaluated with the naked eye, and such an evaluation is usually accept-

Figure 1. Rock hardness related to impact.



Strength

A reasonable estimate of specimen strength can be made by striking the sample, rock core, or outcrop with the round end of a ball peen hammer (or with the rounded end of a 20-penny nail if the specimen is to be preserved). The resulting characteristic impact reaction indicates a range of unconfined compressive strength (5). The rock specimen or outcrop is struck several times to determine uniformity of response, and a quality is assigned based on the distinct reaction at the point of impact (Figure 1). There are five design-limiting conditions (A-E) in the URCS basic-element category of specimen strength: A, rebound quality (RQ); B, pit quality (PQ); C, dent quality (DQ); D, crater quality (CQ); and E, moldable quality (MBL).

able for all foundation and excavation designs. The rock material has a uniform color, usually shades of gray, green, blue, or black. The sample tested and classified is representative of maximum unit weight, maximum specimen strength, and least relative absorption for the site and from which comparisons to STS are made.

3. STS (C) denotes that the rock material is partly or completely discolored due to oxidation but cannot be remolded by means of finger pressure. The mineral components are usually shades of yellow or brown and have a reduced unit weight and a higher absorption of water than VFS. The specimen strength may or may not vary from that of VFS, and a comparison is made at a given site. Weight reduction is expressed as a percentage of the VFS unit weight.

4. PDS (D) is a condition that is defined by moldability and the size of the resulting aggregate. The rock material is remoldable by means of finger pressure to gravel-sized and large rock fragments with or without sand, silt, or clay mixtures. In other words, the material is solid when in place but becomes rock and soil mixtures when excavated. The relative percentage of rock fragments is estimated and the quality of individual fragments is assessed (by URCS), and fines are determined to be plastic or nonplastic. The in-place strength is estimated by manual consistency values or by size, shape, and gradation of the remolded aggregate. The remolded soil aggregate is tested for dilatency, dry strength, and toughness and classified according to field procedures of the Unified Soil Classification System (USCS) (3). Both URCS and USCS symbols are recorded (3,4).

5. CDS (E) is a condition of all remoldable mineral components to sand, silt, or clay, or mixtures of two or more sizes. In other words, the material is rock when in place and becomes soil when excavated. The remolded material is determined to be plastic or nonplastic, and dry-strength, dilatency, and toughness tests are performed. The in-place strength is estimated by manual consistency values. Both URCS and USCS symbols are recorded. Note that in URCS the boundary condition that defines rock and soil on a basis of size is the sieve size that divides gravel and sand (No. 4). It is generally accepted by most investigators, which includes laypersons, that gravel is composed of rock fragments but that sand is composed of minerals.

The degrees of weathering and their URCS symbols are summarized below:

Symbol	Condition	Definition
A	MFS	Fresh by using hand lens
B	VFS	Fresh by using naked eye
C	STS	Weathered but not moldable
D	PDS	Remolds to rock and soil
E	CDS	Remolds to soil

1. RQ (A) rock material shows no reaction under point of impact and is a true brittle-elastic substance in a mechanical sense. This classification quality has an estimated unconfined compressive strength greater than 15 000 lbf/in<sup>2</sup> (103 MPa). The exact unconfined compressive strength is seldom significant with respect to typical civil engineering design and construction once the strength reaches this value. RQ rock material produces free-draining fill that is suitable for road aggregate; however, it is often sharp and angular due to its brittleness and therefore produces a less desirable material. RQ rock material has a very high energy transfer in response to blasting and is difficult to drill and break in the absence of planar separations.

2. PQ (B) rock material produces an explosive departure of mineral grains under the point of impact, which results in a shallow, rough pit. This quality of specimen has an estimated range of unconfined compressive strength of 8000-15 000 lbf/in<sup>2</sup> (55-103 MPa) and is considered hard rock by the construction industry. PQ rock material produces free-draining fill and is suitable for road-surfacing material. It has a high energy transfer in response to blasting, which produces good fragmentation and satisfactory excavation slopes. No special blasting design procedure is necessary.

3. DQ (C) rock material produces a dent or depression under the point of impact. This indicates the presence of pore spaces between the mineral grains. This classification or quality has an estimated range of unconfined compressive strength of 3000-8000 lbf/in<sup>2</sup> (21-55 MPa) and is roughly equivalent to the strength range of concrete. DQ rock material usually does not meet absorption specifications and has a low energy transfer in response to blasting. Special blasting design is necessary to avoid boulders and sand as the end product. DQ material is usually not suitable for road fill or surfacing and is not free draining.

4. CQ (D) rock material has, as the term implies, a reaction under the point of impact that produces a shearing and upthrusting of adjacent mineral grains that is similar in shape to a moon crater. This category has an estimated range of unconfined compressive strength of 1000-3000 lbf/in<sup>2</sup> (7-21 MPa). CQ rock material can usually be recovered during diamond-core drilling operations, has high absorption, and will respond to freeze-thaw stresses by at least cracking and checking. It has a very low energy transfer when blasted and can be excavated by means of machinery, produces poorly drained embankments, and is not suitable for road fill or road-surfacing materials.

5. MBL (E) rock is in a condition in which otherwise visually similar and continuous rock

material can be remolded by means of finger pressure. This category has an unconfined compressive strength of less than 1000 lbf/in<sup>2</sup> (7 MPa). In all cases, the material is examined and tested as a soil and a dual classification is given. The material usually cannot be recovered by diamond-core drilling, can be excavated by machinery, and must be evaluated as a soil for design purposes.

The types of specimen strength and their URCS symbols are summarized below (1 lbf/in<sup>2</sup> = 0.007 MPa):

Symbol	Condition	Range of Unconfined Compressive Strength (lbf/in <sup>2</sup> )
<u>A</u>	RQ	15 000
<u>B</u>	PQ	8000-15 000
<u>C</u>	DQ	3000-8000
<u>D</u>	CQ	1000-3000
<u>E</u>	MQ	1000

### Discontinuity

Directional weaknesses of a rock mass or rock material are termed planar or linear features. Planar separations are open separations that already exist in the rock mass and are defined by relative capacity to transmit water. Linear features are directional weaknesses due to visual or nonvisual mineral alignment in an otherwise solid rock mass or material that usually requires blasting or mechanical crushing to produce a separation. For purposes of design evaluation, linear features are defined by breakage characteristics. Planar features or open planes of separation are defined by the scale dimension of the rock mass examined and by the geometric determination that defines a plane or a shape. The five design-limiting conditions discussed below are as follows: A, solid random breakage (SRB); B, solid preferred breakage (SPB); C, latent planar separations (LPS); D, two-dimensional open planar separations (2-D); and E, three-dimensional open planar separations (3-D).

1. SRB (A) represents ideal design conditions, in which there is no effect from planar and linear features within the dimension of the rock mass examined. The specimen strength equals the mass strength, so that the strength value of any individual sample tested is directly representative of the entire rock-mass strength. Needless to say, this is seldom the case, except in very limited foundation dimensions.

2. SPB (B) indicates that there is a nonvisual mineral alignment that results in a directional weakness in the rock mass or material. The rock breaks consistently along a constant angle or direction. SPB rock material may produce an undesirable shape or size for rock aggregate or may prevent the achievement of a designed slope in rock excavation. It is adverse in the production of dimension stone.

3. LPS (C) is a category that indicates visual mineral alignment, which may or may not affect the strength or breakage character of the rock mass or rock material during excavation or crushing. The latent planes may be stronger or weaker than the rock mass. The reaction of LPS material to impact defines the strength estimate. Latent planes occur in patterns or at random and are continuous or discontinuous; the plane may be of a measurable thickness. In all cases, the infilling of the material in the latent plane of separation is greater than 1000 lbf/in<sup>2</sup> (7 MPa). LPS material is usually not a foundation-design consideration,

because the material is, for practical purposes, a solid. In consideration of rock-slope design or road-aggregate source, blasting energy will, in most cases, be reflected by the latent plane and produce a separation and breakage 90° from the plane alignment.

4. The 2-D (D) category indicates the presence of one or more parallel open planes of separation that pass through the rock mass at the point of examination. The 2-D planar separations may vary in frequency and spacing but do not intersect. The attitude, relief, and continuity of the plane or planes are the fundamental elements of design analysis. Water transmission along the open planes can be determined by observation of the drilling operation or by water testing.

5. The 3-D (E) category indicates the presence of two or more intersecting planar discontinuities or open planes of separation that pass through the rock mass at the point of examination. The planar separation may form patterns or may be random in occurrence. Internal planar separations (IPS) terminate within the rock mass, and mass planar separations (MPS) pass entirely through the rock mass and are infinite in extent in terms of design. By geometric definition, three dimensions form a shape. This shape is often referred to as a joint block, which has an average size and weight that can be estimated. The degree of interlock between joint blocks defines the strength-of-foundation or the stability-of-excavation factor. If MPS occurs, the attitude of the plane or planes with respect to slope or excavation is the chief design factor. Whether or not the planes transmit water is estimated or measured as in category D.

The types of discontinuity and their URCS symbols are summarized below:

Symbol	Condition	Definition
<u>A</u>	SRB	No directional weakness
<u>B</u>	SPB	Nonvisual mineral alignment
<u>C</u>	LPS	Visual mineral alignment
<u>D</u>	2-D	Nonintersecting planes of weakness
<u>E</u>	3-D	Intersecting planes of weakness

### Gravity

Density or unit weight has been found to be one of the most useful and reliable means of communicating rock quality to the design engineers or contractors, due to their past experience with rock. The unit weight is determined in the field by using the spring-loaded scale. The apparent specific gravity is determined first; then it is converted to unit weight. Unit weight in pounds per cubic foot is used for a better individual appreciation of weight and changes in weight. Few persons understand the numerical differences of specific gravity without its conversion to unit weight. The URCS basic element related to gravity or weight has five categories or ranges of unit weight: 160 (A), greater than 160 lb/ft<sup>3</sup> (2667 kg/m<sup>3</sup>); 150 (B), 150-160 lb/ft<sup>3</sup> (2500-2667 kg/m<sup>3</sup>); 140 (C), 140-150 lb/ft<sup>3</sup> (2500-3333 kg/m<sup>3</sup>); 130 (D), 130-140 lb/ft<sup>3</sup> (2166-3333 kg/m<sup>3</sup>); and 130 (E), less than 130 lb/ft<sup>3</sup>. The unit-weight design evaluation establishes the driving force in problems of slope stability, the relative usefulness of the rock material as a surface course or concrete aggregate, or the weight-volume relationship for estimates of haul cost. Unit weight establishes the degree of change due to change of weathering state. As a general rule of thumb, rock material that has a unit

weight greater than 160 lb/ft<sup>3</sup> is suitable more than 50 percent of the time for use as road aggregate, concrete aggregate, riprap, or jetty stone without laboratory testing. Rock material that has a unit weight of 150-160 lb/ft<sup>3</sup> may be acceptable but will require laboratory testing for confirmation. Rock that has a unit weight of 150 lb/ft<sup>3</sup> is not usually acceptable for the above purposes, is not free-draining fill, and will degrade. Rock that has a unit weight of less than 130 lb/ft<sup>3</sup> can usually be excavated by machinery but will degrade during excavation under the abrasion of excavation equipment.

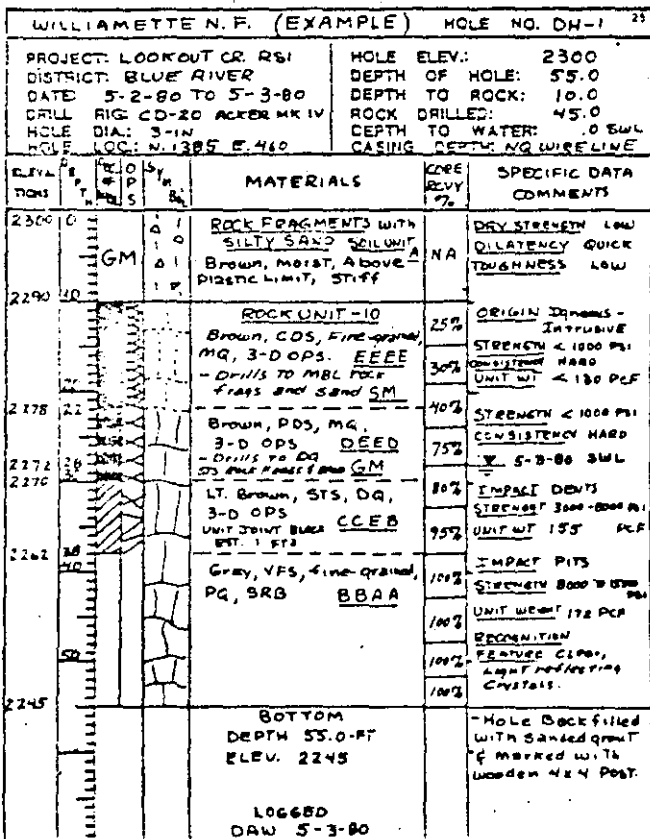
The categories of unit weight, their URCS symbols, and their specific gravity are given below:

Symbol	Unit Weight (lb/ft <sup>3</sup> )	Specific Gravity
A	160	>2.56
B	150	2.40-2.56
C	140	2.24-2.40
D	130	2.08-2.24
E	130	<2.08

CONTRACT SPECIFICATION OR DESIGN MEMORANDUM

Information that pertains to rock material or rock masses in current contract specifications or design memoranda is sketchy and ambiguous, to say the least, even when supported by laboratory testing. The terminology used in drilling logs and geologic sections usually fails to provide understandable information to the contractor for purposes of bid estimates. Here is an example of a rock description found in a typical contract specification or design

Figure 2. Logging example of URCS use.



memorandum: "Slightly weathered, moderately hard, highly fractured, lightweight, rhyolitic rock." This information is sincerely intended to portray the actual conditions existing at the site and will provide the basis of the design, the cost estimate, or the judgment of the construction method required. Descriptive terms such as these vary widely in meaning, depending on both the individual and the professional experience, and cannot be quantified with any degree of precision or uniformity. Design decisions, cost estimates, or construction methods based on this information vary widely when used by contractors, engineers, planners, or geologists.

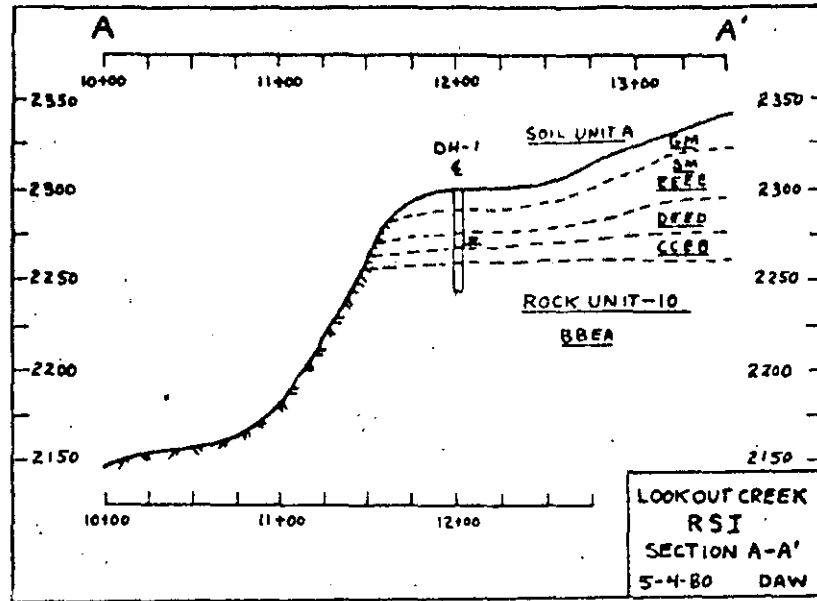
URCS ALTERNATIVE

URCS offers a suitable alternative to this ambiguous descriptive approach. The term "unified" refers to the necessary unification of geology and engineering for geotechnical purposes. The URCS equivalent of the typical rock description for contract specifications and design memoranda is **CCED**. This simple notation is based on uniform acceptable procedures that define design conditions. This notation indicates that the degree of weathering of the rock is the stained state (STS) or not representative of the standard design condition that exists at the site and that comparative data will have to be determined. The strength of the rock material is dent quality (DQ) and has a range of unconfined compressive strength of 3000-8000 lb/in<sup>2</sup>, which indicates that it is roughly comparable to concrete in strength when in a weathered state. The rock mass has three-dimensional planar separations (3-D), which will be the primary design and construction consideration with respect to stability, excavation, and material use. The size, shape, volume, and weight of the unit joint block have not been defined and will have to be determined as well as the continuity, attitude, and degree of interlock of the planes. Water transmission will have to be estimated or measured. The unit weight of the rock material is 130-140 lb/ft<sup>3</sup>, which indicates that there will be full loads for hauling equipment but that the material is probably not free draining nor can it be used in load-bearing fills or for surfacing. This simple but well-defined verifiable design notation is suitable for graphic abstracts, boring logs, plans and sections, and other documentation. Since it is based on basic design elements, the notation provides a reliable means for decision. The notation registers rapidly in the mind during scanning and allows rapid comparison with several rock conditions. Similarities and differences can be established immediately. The simple notation minimizes the drafting effort. The notation prevents subjective connotation and allows recording the significant information on a scale appropriate to the investigation. The information can be checked and verified. See Figures 2 and 3 for examples of how the notation looks in actual use.

CONCLUSIONS

URCS furnishes a means by which a relatively large number of persons from professional and technical disciplines who have different experience levels can work together in a successful team effort. The two government agencies involved were the Portland District Corps of Engineers from 1959 to 1975 and the Forest Service, Region 6, from 1975 to the present (6). URCS, although not universally accepted within these two agencies, did provide reliable information when used, which resulted in

Figure 3. Typical section that shows use of URCS.



effective planning, design, specification, and construction of projects that involved rock. Machiavelli wrote, in *The Prince* (1513),

It must be remembered that there is nothing more difficult to plan, more doubtful of success, nor more dangerous to manage than the creation of a new system. For the initiator has the enmity of all who would profit by the preservation of the old institution and merely lukewarm defenders in those who would gain by the new one.

#### REFERENCES

1. D.A. Williamson. Unified Rock Classification System. Field Notes (Forest Service, U.S. Department of Agriculture), Vol. 10, No. 11, Nov. 1978.
2. D.A. Williamson. The Unified Rock Classification. Presented at Regional Geotechnical Meeting, Forest Service, Region 6, U.S. Department of Agriculture, 1977.
3. A. Casagrande. Classification and Identification of Soils. Trans. ASCE, Vol. 113, 1948.
4. K. Terzaghi and R.B. Peck. Soil Mechanics in Engineering Practice. Wiley, New York, 1948.
5. D.A. Williamson. Rock Classification for Engineering Investigations. Presented at 20th Annual Meeting, Oregon Academy of Science, 1961.
6. D.A. Larson. Green Peter Dam Foundation Report. U.S. Army Corps of Engineers, Portland District, 1969.

*Publication of this paper sponsored by Committee on Exploration and Classification of Earth Materials.*





**DIVISION DE EDUCACION CONTINUA  
FACULTAD DE INGENIERIA U.N.A.M.**

MECANICA DE ROCAS APLICADA A LA MINERIA Y A LA CONSTRUCCION

THE RELATIONSHIP BETWEEN ROCK MASS QUALITY AND EASE OF EXCAVATION

MAYO, 1985

## THE RELATIONSHIP BETWEEN ROCK MASS QUALITY AND EASE OF EXCAVATION

## RELATION ENTRE LA QUALITE D'UN MASSIF ROCHEUX ET SA FACILITE D'EXCAVATION

ABDULLATIF O.M., CRUDEN D.M., Department of Geology, University of Alberta, Edmonton, Alberta, Canada. T6G 2E3

## Summary

Limestone, dolerite, granite, shale, ballclay and chinaclay from south west England have been classified in terms of rock mass quality by three different systems: point load strength and fracture spacing, the CSIR Rock Mass Rating and the NGI Quality Index system.

Comparison with excavation practice in quarries in these rock masses indicates that the CSIR Rock Mass Rating system may give better assessment of rock mass quality related to ease of excavation than the point load strength and fracture spacing and Quality Index systems.

## Résumé

Nous avons classé des massifs de calcaire, de dolérite, de granite, de schiste et d'argile dans le sud-ouest de l'Angleterre selon leur qualité et en utilisant trois systèmes différents. Ces systèmes sont ceux de Franklin (1972), Bieniawski (1976) et Barton *et al.* (1977).

Nous avons comparé la facilité d'excavation dans les carrières de ces massifs et les prédictions faites à partir des trois systèmes de classification. Le système de Bieniawski (1976) donne la meilleure indication de la facilité d'excavation.

## Introduction

No one feature of civil engineering work has been responsible for more dispute than the classification of rock to be excavated, and the consequent payment for this work. As unit prices for blasting may be considerably greater than the corresponding unit prices for ripping and digging the opportunity for dispute arising from questionable classification of rock masses will be obvious.

Therefore, not only is the collection of data to assess the rock mass quality essential, but also the selection of a suitable classification system is vital.

## Rock mass classification systems.

One of the first classification of rock masses was introduced by Terzaghi (1940) but this classification has been criticised on the ground that it is too general to permit an objective evaluation of rock mass quality. Subsequently Deere *et al.*, (1966) introduced the concept of Rock Quality Designation, RQD. Then, Franklin *et al.*, (1972) proposed a classification in which two parameters were used, the point load strength and the fracture spacing.

More recent classifications of rock masses include the CSIR Rock Mass Rating system introduced by Bieniawski, (1976) and the NGI Quality Index, Q, system (Barton *et al.*, 1977).

The Franklin, Bieniawski and Barton classification systems are discussed later in detail because they are the main systems used in this study.

There is good agreement between the various classi-

fications as regards the properties considered important, although the techniques of incorporating these properties are different. Features common to the classification systems as summarised by Just (1978) include:

- 1) They use clearly defined parameters which can be measured in the field.
- 2) Only those properties of rock mass judged to be most significant are included.
- 3) They all determine an index of the rock mass from various rock mass parameters weighted to account for their relative importance.

## Field investigation and data collection

The field work was designed to cover two aspects. First, to collect data related to the discontinuity characteristics of different rock masses. Such characteristics include intact strength, fracture spacing, joint orientation, joint condition and weathering. Second, to examine the excavation methods used for these rock masses.

All rock masses examined were exposed faces in quarries. A rapid mapping technique was used in the field. It involved mapping onto a polaroid photograph each rock mass examined, and then this mapping was transferred later to a normal black and white photograph taken from the same location (Abdullatif 1982). This mapping was supplemented by rock mass and discontinuity survey data sheets recommended by the Engineering Group Working Party (1977). The data sheets proved to be suitable for getting a quick and comprehensive description of a rock mass. The collected information is thought to be important for the assessment of rock mass quality.

of rock mass quality by the following classification systems:

- 1) Point load strength and fracture spacing
- 2) The NGI Quality Index
- 3) The CSIR Rock Mass Rating

#### Point load strength and fracture spacing system

Franklin *et al.* (1972) proposed a two parameter classification based on point load strength and the fracture spacing of the rock mass. These two parameters can be measured easily in the field.

In the point load test, the rock specimen is loaded between conical platens of standard dimension and the specimen fails by splitting between platen contact points. Then, the point load strength index,  $I_s$ , is obtained from the relation:

$$I_s = P/D^2$$

where, P = Force required to break the specimen

D = Distance between platen contact points

All point load measurements were taken for irregular lumps, and the average of several measurements was taken as the point load strength index,  $I_s$ , of the rock. For poor quality rock masses point load strengths were estimated.

Fracture spacing measurements were taken from exposed rock faces in quarries. Then, the fracture spacing index,  $I_f$ , was measured by counting the number of fractures which intersected a traverse line of known length. For each rock face, two or three traverses were taken and the average of these traverses was taken as the fracture spacing index of the rock mass.

Then, for the different rock masses examined, the point load strength index,  $I_s$ , and the fracture spacing index,  $I_f$ , rock mass quality classification are set out in Table 1.

Tab. 1: Point load strength and fracture spacing classification (Franklin *et al.*, 1972)

Tab. 1: La classification des massifs rocheux suivant la méthode de Franklin (1972).

Sample	Rock type	Point load strength $I_s$ (MN/m <sup>2</sup> )	Fracture spacing $I_f$ (m)
1	limestone	4.1	0.65
2	sandstone	0.83	0.46
3	sandstone	0.27	0.51
4	limestone	5.13	0.57
5	limestone	0.35 <sup>+</sup>	0.09
6	limestone	0.34 <sup>+</sup>	0.03
7	limestone	8.22	0.48
8	limestone	9.51	0.74
9	limestone	7.26	0.41
10	limestone	8.50	0.37
11	dolerite	20.17	0.47
12	granite	11.17	0.70
13	shale	4.27 <sup>*</sup>	0.07
14	shale	1.00	0.05
15	shale	0.65	0.03
16	shale	0.15 <sup>+</sup>	0.01
17	china clay	0.25 <sup>+</sup>	0.02
18	granite	3.51	0.56
19	gravel	0.26 <sup>+</sup>	0.06
20	ball clay	0.30 <sup>+</sup>	0.02
21	dolerite	12.59	0.45
22	granite	8.51	0.30
23	quartz veins	11.23	0.20

<sup>+</sup> assessed

\*  $I_s$  is measured perpendicular to bedding,  $I_s$  along bedding is 0.23 MN/m<sup>2</sup>

Barton *et al.* (1977) proposed the rock mass Quality Index, Q. The numerical value of this index is defined by:

$$Q = \frac{RQD}{J_n} \times \frac{J_r}{J_a} \times \frac{J_w}{SRF}$$

where, RQD = Rock Quality Designation  
 $J_n$  = Joint set number  
 $J_r$  = Joint roughness number  
 $J_a$  = Joint alteration number  
 $J_w$  = Joint water reduction factor  
 SRF = Stress Reduction Factor

Hock and Brown (1980) concluded that the Quality Index, Q, can be considered as a function of only three parameters, which are crude measures of the following:

- a) Block size (RQD/ $J_n$ )
- b) Intact block shear strength ( $J_r/J_a$ )
- c) Active stress ( $J_w/SRF$ )

For the calculation of the Quality Index, Q, the information collected in the rock mass and discontinuity survey data sheets was used to estimate all the parameters except the Rock Quality Designation, RQD, which was estimated from the average frequency of discontinuities likely to be encountered in a vertical drill hole, by Priest and Hudson's formula (1976). Thus, the Rock Quality Designation, RQD, is given by:

$$* \quad RQD = 100 e^{-0.1 \lambda} (0.1 \lambda + 1)$$

where,  $\lambda$  is the mean discontinuity frequency per metre.

Then, for the different rock masses examined, the calculation of the Quality Index, Q, is set out in Table 2.

#### The CSIR Rock Mass Rating classification system

This classification was proposed by Bieniawski (1976) Five basic parameters are involved:

- 1) Strength of intact rock
- 2) Rock Quality Designation
- 3) Spacing of joints
- 4) Condition of joints
- 5) Ground water condition

A number of points or rating is allocated to each range of values for each parameter, and the overall rating of the rock mass is made by adding the rating of the parameters. Then after the overall rating is adjusted for joint orientation, the rock mass is given a class representing the rock mass quality.

For all rock masses examined, the intact strength was estimated by using the point load strength measurements given in Table 1. Then, for Rock Quality Designation, RQD, the values estimated for the NGI Quality Index, Q, were used. The spacing of joints, condition of joints and ground water condition, were all estimated from the rock mass and discontinuity survey data sheets. Then, after every parameter is rated, the calculation of the Rock Mass Rating of all rock masses is set out in Table 3.

#### Excavation methods on sites

All excavation methods examined were carried out in quarries, where the excavated rocks are used either for concrete or road aggregate. The excavation methods include digging, ripping and blasting. Table 4 shows excavation methods used on sites, and description of these methods and rock masses is given by Abdullatif (1982).

Tab. 2: Calculation of NQI Tunnelling Quality Index (Barton *et al.*, 1977).

Tab. 2: La classification des massifs rocheux suivant la méthode de Barton *et al.* (1977).

Sample	Rock type	$\lambda$	RQD %	Jn	Jr	Ja	Jw	SRF	$\frac{RQD}{Jn}$	$\frac{Jr}{Ja}$	$\frac{Jw}{SRF}$	Q	Description
1	limestone	1.5	99.2	6	1.0	2	10	2.5	16.5	0.50	0.40	6.6	Fair
2	Sandstone	2.2	98.2	6	1.0	4	1.0	2.5	16.4	0.25	0.40	1.64	Poor
3	Sandstone	1.9	98.6	6	1.0	6	1.0	2.5	16.4	0.16	0.40	1.05	Poor
4	limestone	1.7	98.9	6	1.0	3	1.0	1	16.5	1.0	0.40	6.6	Fair
5	limestone	11.1	72.2	12	1.0	8	1.0	5	6.0	0.12	0.20	0.144	V. Poor
6	limestone	33.3	29.9	20	1.0	10	1.0	5	1.5	0.10	0.20	0.030	E. Poor
7	limestone	2.1	98.3	6	1.5	1	1.0	2.5	16.4	1.5	0.40	9.84	Fair/Good
8	limestone	1.4	99.3	6	1.5	1	1.0	2.5	16.6	1.5	0.40	9.96	Fair/Good
9	limestone	2.7	97.8	6	1.5	1	1.0	2.5	16.3	1.5	0.40	9.78	Fair/Good
10	limestone	2.7	97.8	6	1.5	1	1.0	2.5	16.2	1.5	0.40	9.72	Fair/Good
11	dolerite	2.1	98.3	4	3	2	1.0	2.5	24.6	1.50	0.40	14.76	Good
12	granite	1.4	99.3	4	4	1	0.66	2.5	24.8	3.0	0.26	19.30	Good
13	shale	14.3	62.5	6	1.0	2	1.0	2.5	15.6	0.50	0.40	3.120	Poor
14	shale	20.0	46.6	6	1.0	2	1.0	2.5	7.8	0.50	0.40	1.56	Poor
15	shale	33.3	29.7	9	1.0	4	1.0	5	3.3	0.16	0.20	0.106	V. Poor
16	shale	100	4.5	20	1.0	6	1.0	2.5	0.23	0.16	0.40	0.014	E. Poor
17	china clay	50	9.0	20	1.0	6	1.0	2.5	0.45	0.16	0.40	0.028	E. Poor
18	granite	1.8	98.7	6	1.0	2	1.0	2.5	16.45	0.50	0.40	3.29	Poor
19	gravel	16.7	56.6	15	1.0	6	1.0	5	3.77	0.16	0.10	0.060	E. Poor
21	dolerite	2.2	98.1	4	3	2	1.0	2.5	21.5	1.5	0.40	12.9	Good
22	granite	3.3	96.1	6	1.0	1	0.8	2.5	16.0	1.0	0.32	5.12	Fair
23	quartz veins	5.0	91.7	6	1.0	1	0.8	2.5	15.3	1.0	0.32	4.90	Poor/Fair

Tab. 3: Geomechanics classification of jointed rock masses (Bieniawski, 1976).

Tab. 3: La classification des massifs rocheux suivant la méthode de Bieniawski (1976).

Sample	Rock type	Strength MPa	Rating	RQD %	Rating	Joint Spacing m	Rating	Condition of Joints Rating	Ground water Rating	Joint Orientation Adjustment Rating	Total Rating
1	limestone	4.1	12	99.2	20	0.65	20	6	10	-10	63
2	Sandstone	0.83	2	98.2	20	0.46	20	6	10	-10	48
3	Sandstone	0.27	1	98.6	20	0.51	20	0	10	-10	41
4	limestone	5.13	12	98.9	20	0.57	20	10	10	-5	63
5	limestone	2.21	7	72.2	13	0.09	10	0	7	-12	30
6	limestone	0.34	1	29.9	8	0.03	5	0	7	0	21
7	limestone	8.22	15	98.3	20	0.48	20	20	10	0	85
8	limestone	9.51	15	99.3	20	0.74	20	12	10	0	77
9	limestone	7.26	12	97.8	20	0.41	20	9	10	-5	69
10	limestone	8.50	14	97.2	20	0.37	20	12	10	-5	72
11	dolerite	20.17	15	98.3	20	0.47	20	12	10	-5	72
12	granite	11.17	15	99.3	20	0.70	20	4	0	79	79
13	shale	4.27	12	62.5	13	0.07	10	12	7	-10	44
14	shale	1.00	4	46.6	8	0.05	10	10	10	-10	32
15	shale	0.65	2	29.7	8	0.03	5	0	7	-12	10
16	shale	0.15	1	4.5	3	0.01	5	0	7	-10	6
17	china clay	0.25	1	0.0	3	0.02	5	0	7	-10	6
18	granite	3.51	7	98.7	20	0.56	20	12	10	-5	64
19	gravel	0.26	1	56.6	13	0.06	10	0	7	-12	19
20	ball clay	0.30	1	9.0	3	0.02	5	6	7	-5	17
21	dolerite	12.59	15	98.2	20	0.45	20	12	10	-5	72
22	granite	8.51	15	91.7	20	0.30	10	12	7	-5	59
23	quartz veins	11.23	15	96.1	20	0.20	10	12	7	-5	59

Tab. 4: Excavation methods on sites.

Tab. 4: Les méthodes d'excavation.

Sample	Rock type	Excavation method	Machine
1	Limestone	Blasting	-
2	Sandstone	Ripping	Track loader
3	Sandstone	Ripping	Track loader
4	Limestone	Blasting	-
5	Limestone	Digging	Wheel loader
6	Limestone	Digging	Wheel loader
7	Limestone	Blasting	-
8	Limestone	Blasting	-
9	Limestone	Blasting	-
10	Limestone	Blasting	-
11	Dolerite	Blasting	-
12	Granite	Blasting	-
13	Shale	Ripping	Track loader 977L
14	Shale	Ripping	Track loader 977L
15	Shale	Digging	Track loader 977L
16	Shale	Digging	Track loader 977L
17	china clay	Digging	Bulldozer D9
18	Granite	Blasting	-
19	Gravel	Digging	Hydraulic face shovel
20	Balleclay	Digging	Hydraulic backhoe
21	Dolerite	Blasting	-
22	Granite	Ripping	Bulldozer D9L
23	Quartz veins	Ripping	Bulldozer D9L

Classification diagrams

All rock masses examined, have been classified in terms of rock mass quality, by the three classification systems mentioned previously. Then, two classification diagrams have been introduced.

Figure 1 shows a rock mass quality classification diagram based on point load strength index,  $I_s$ , and fracture spacing index,  $I_f$ . (Franklin *et al.*, 1972). The quality of a particular type rock mass is determined by plotting each rock mass as single point located in the diagram by means of its two indices given in Table 1. Similarly, Figure 2 shows a rock mass quality classification diagram of the same rock masses, based on Quality Index and Rock Mass Rating calculated in Table 2 and 3.

The two classification diagrams express the ease of excavation of the different rock masses, and define the location of digging, ripping and blasting in the classification diagrams. The ease of excavation shown in these classification diagrams is determined by the excavation methods given in Table 4.

Discussion of classification diagrams

Figure 1 shows that the fields containing rock mass suited to digging, ripping or blasting are distinct. However, there is not sufficient data to determine precisely the boundaries of the fields. The data do indicate that the boundaries are not parallel to one another.

Figure 2 also shows distinct fields for the different methods of excavation. The Rock Mass Rating indicates that rock mass can be dug up to RMR values of 30 and ripped up

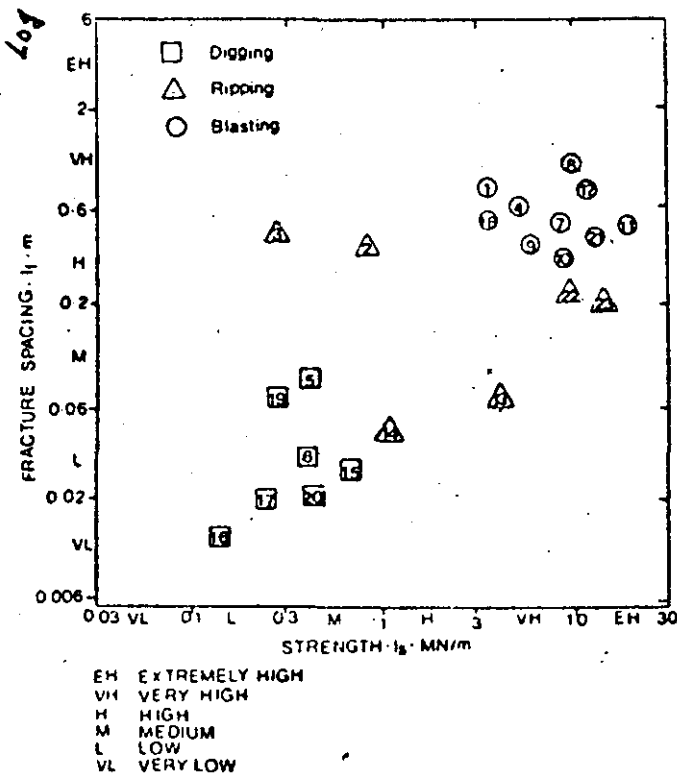


Fig. 1: Rock mass quality classification based on point load strength and fracture spacing indices. It shows excavation methods on sites.

Fig. 1: La classification des massifs rocheux suivant Franklin (1972) et les méthodes d'excavation.

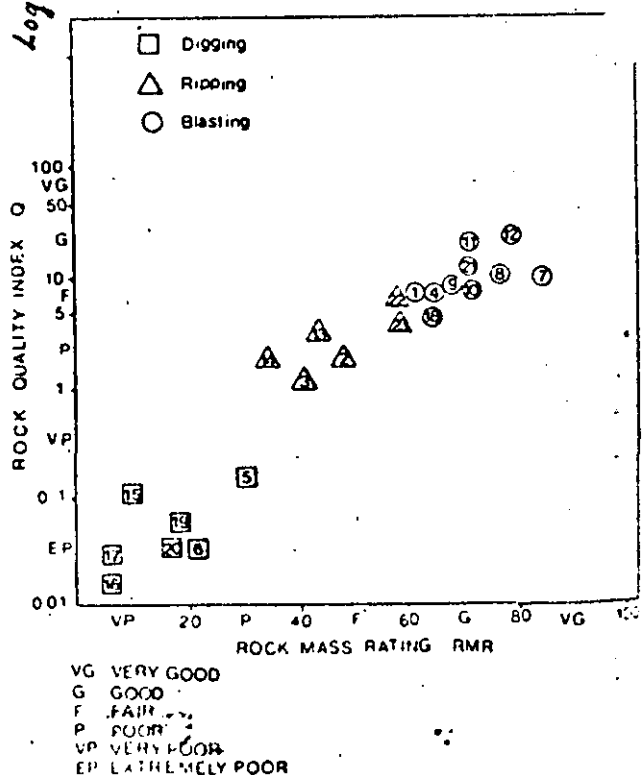


Fig. 2: Rock mass quality classification diagram based on rock mass rating and quality indices. It shows excavation methods on sites.

Fig. 2: La classification des massifs rocheux suivant Bieniawski (1976) et Barton *et al.* (1977). On voit aussi les méthodes d'excavation.

to RMR values of 60. Rock mass rated as "good" or better by Rock Mass Rating should be blasted.

There is a distinct gap between the Q values of rock masses that can be dug, Q values up to 0.14, and those that require blasting, Q values above 1.05. More data are required to determine whether few excavated rock masses have Q values in this range. There is overlap in Q values between 3.2 and 5.2 of rock masses which can be ripped and rock masses which require blasting. Thus, the use of Quality Index, Q, as a guide for excavation practice in rock mass appears then to present problems. The active stress parameter,  $J_w/SRF$ , important in considering the stability of underground openings shows little variation in our sample of rock masses at the ground surface. So Q is a product of only four variables, none of which explicitly consider the joint orientation, a contrast with the RMR.

## Conclusions

- 1) For excavation purposes, the Rock Mass Rating system gave a better assessment of rock mass quality than Quality Index and point load strength and fracture spacing system. This is because the Rock Mass Rating includes sufficient information to allow realistic assessment of rock mass quality.
- 2) Our preference for the Rock Mass Rating is based on limited experience from south west England. It would be interesting to see how relevant this experience is to areas with other climates and weathering and geological histories.

## Reference

N (1977): The description of rock masses for engineering purposes. *Q. J. Eng. Geol.* 10, 355-388.

- ABDULLATIF O.M. (1982): Correlation between strength and fracture spacing of rocks and ease of excavation. Msc. Thesis, Queen Mary college, University of London, pp. 61-53, 103-114.
- BARTON N., LIEN R. and LUNDE J. (1977): Estimation of support requirements for Underground Excavation. Proceedings, Fifth Symposium on Rock Mechanics, Minneapolis, American Society of Civil Engineers, New York, pp. 163-177.
- BIENIAWSKI Z.T. (1976): Rock mass classification in rock engineering. Proceeding Symposium on Exploration for Rock Engineering, Johannesburg, 1, 97-106.
- DEERE D.U., MILLER R.P. (1966): Engineering classification and index properties for intact rock. Report AWFL TR-65-116, Air Force Weapons Laboratory (WLDC) Kirtland Airforce base, New Mexico.
- FOOKES P.G., DEARMAN W.R. and FRANKLIN J.A. (1971): Some engineering aspects of rock weathering with field examples from Dartmoor and elsewhere. *Q. J. Eng. Geol.* 4, pp. 139-185.
- FRANKLIN J.A. (1970): Observation and Tests for Engineering description and Mapping of Rocks. Proc. 2nd Cong. ISRM, Belgrade, Vol. 1, paper 1-3.
- FRANKLIN J.A., BROCH E. and WALTON G. (1972): Logging the mechanical character of rock. *Trans. Inst. Min. Met. (GB)*, 80, pp. A1-A9.
- HOEK E., BROWN E. T. (1980): Underground Excavation in Rocks. *Min. Met.*, London, pp. 27-32.
- PRIEST S.D., HUDSON J.A. (1976): Discontinuity spacing in rock. *International Journal of Rock Mechanics and Mining Science*, 13, pp. 135-148.
- JUST G.D., WALTER G.W. (1978): Engineering potential of seismic methods of assessing rock breakage characteristics. *The Aus. Inst. Min. Met. Rock Breaking Symposium*, pp. 93-106.



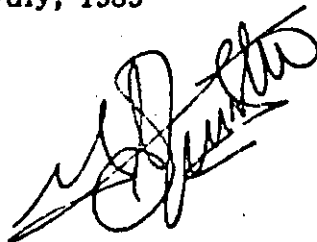
**DIVISION DE EDUCACION CONTINUA  
FACULTAD DE INGENIERIA U.N.A.M.**

MECANICA DE ROCAS APLICADA A LA MINERIA Y A LA CONSTRUCCION

AUTOMATION FOR MINERAL RESOURCE DEVELOPMENT

MAYO, 1985

Paper to be presented at the  
International Federation of Automatic Control  
Symposium on  
**AUTOMATION FOR MINERAL RESOURCE DEVELOPMENT**  
to be held in  
Brisbane, Australia  
9-11 July, 1985

A handwritten signature in black ink, appearing to be 'D. J. ...', written over a horizontal line.



# PREDICTION OF HAZARDS IN UNDERGROUND EXCAVATIONS

Evert Hoek

Golder Associates, 224 W 8 Ave., Vancouver, Canada

**Abstract.** Exceptionally weak ground, usually associated with faulting, unanticipated groundwater pressures or flows and exceptionally high stress concentrations are some of the hazards which confront the underground excavation engineer. One or more of these hazards can seriously delay or even halt a tunnel or mining project, and methods for predicting these hazards are urgently required, particularly for projects involving high speed drill and blast or tunnelling machine excavations.

This paper explores the current availability and the potential for the development of tools and techniques for the prediction of these hazards. It is concluded that systematic and automated geological data collection and interpretation represent the most promising avenue for development. It is suggested that there is room for the use of expert systems in which the computer is used to assemble and organize practical underground excavation experience into an interactive decision making system.

**Keywords.** Geological hazards; underground excavations; rock mechanics.

## INTRODUCTION

The cost per ton of ore recovered from the ground depends, to a significant degree, upon the ease with which this ore can be mined. Difficult mining conditions result in reduced rates of production and hence higher mining costs. As easy-to-find high grade deposits have been depleted and as the search for minerals has moved to more difficult terrain and/or to greater depths below surface, mining difficulties have tended to increase. These difficulties have been offset by technological advances which have resulted in more efficient mining equipment, blasting techniques and methods of rock support and hence mining costs have tended to remain reasonably stable.

In evaluating a new mine it is normal to consider a range of mining methods which are best suited to the type of orebody under consideration. The availability of suitable equipment and of skilled manpower need be considered together with the grade of the ore and the most suitable recovery processes. If, having considered all these factors, the mine is considered economically viable, detailed mine planning can commence and ultimately the mine will go into production.

Experience suggests that, however thorough the evaluation and planning of a mine, there will always be problems which were not or could not be anticipated and that these problems can have serious consequences upon the performance of the mine. Amongst the most serious of these problems are "bad ground" conditions caused by faulting, intense jointing, high groundwater pressures or flows, exceptionally high stress levels and other geologically related phenomena. These "bad ground" problems can be particularly serious if they are not anticipated and if a smoothly-running mining operation is brought to a halt by a large fall of ground, water inrush, rockburst or similar event.

### GEOLOGICAL HAZARDS IN UNDERGROUND MINING

While in no way wishing to diminish the importance of hazards in surface mining, this paper will concentrate upon the geological hazards which can have the most serious impact upon the safety and economic performance of underground mines. This choice has been made in order to limit the scope of the discussion and also because the prediction of these hazards is much more difficult in an underground environment than in the case of a surface mine.

One of the most obvious sources of "bad ground" problems in underground mining is the discontinuous nature of rock masses. In many cases the orebody is associated with major faulting and, in addition to concentrating the ore, these faults will also have caused a significant amount of fracturing in the surrounding rock mass. These fractures or joints reduce the strength of the rock mass by providing weak planes upon which movement is concentrated. Even in relatively massive rock, the presence of a few joints or bedding planes can reduce the strength of a pillar to about one quarter of that which is calculated on the basis of small scale laboratory tests on the intact rock material. In the case of heavily jointed rock masses, the rock mass strength may be one tenth or even one hundredth of the intact material strength.

The discontinuous nature of most rock masses is made worse by the presence of water. In near surface excavations, the downward migration of water carrying soil and clay will cause the deposition of weak infilling material in the discontinuities and this will reduce their strength even further. At greater depths, water under high pressure can move considerable distances along faults and joints and can be very dangerous if a water bearing discontinuity is intersected by the excavation.

As the depth below surface increases, so does the magnitude of the in situ stress level in the rock. Creation of excavations in highly stressed rock further increases the local stress levels and a point is reached at which these local stresses exceed the strength of the rock mass. In the case of weak rocks this will result in closure or squeezing of the excavations and, while this may be very inconvenient, it is not necessarily dangerous. On the other hand, when a strong brittle rock such as a granite or quartzite fails, it may do so with considerable violence and the energy released by the failure of a large volume of strong rock can generate a rockburst. These rockbursts, which are extremely difficult to predict, can have a serious impact upon the

operation of an underground mine, not only because of the physical danger associated with the event but also because of the uncertainty and fear generated by the phenomenon.

Other hazards in underground mining are associated with time-dependent deformation of evaporite rocks such as salt and potash, the presence of methane and other gases in rock associated with deposits of organic origin such as coal, high rock temperatures which occur in certain parts of the world with high thermal gradients and the danger of spontaneous combustion associated with oxidation of some sulphides .

## PREDICTION OF GEOLOGICAL HAZARDS

Ideally, during the exploration of a mineral deposit, all potential hazards should be defined so that, in planning the mining operation, appropriate steps can be taken to avoid or to minimize the impact of these hazards. Imagine some form of radar device or seismic exploration tool which could penetrate the earth to a depth of several thousand metres and which could define faults and zones of intense fracturing, sub-surface groundwater reservoirs, zones of exceptionally high stress and, of course, the detailed three-dimensional shape of the orebody. The availability of such a tool or tools would be of enormous value to the mining industry but they exist only in science fiction and are likely to remain there for many decades to come.

Even on a local level, where penetration is limited to tens of metres, these remote sensing tools have not lived up to expectations and the author's personal experience with these devices suggests that a great deal of development remains to be done before practical tools become available for general use.

In the absence of remote sensing tools, what techniques are available for the geologist, the geotechnical engineer or the mining engineer to use for the prediction of the geological hazards discussed earlier in this paper ? In the opinion of this author, the most promising techniques are to be found in the systematic collection and interpretation of geological data during site exploration and during the mining of underground excavations. In order to understand the use and the potential of these techniques, it is necessary to examine what geological data are important, how these data are collected and how this information is used for the prediction of hazards.

### *Relevant geological data*

The role of faults and joints in making the rock mass discontinuous has already been mentioned but it is not adequate to characterize a rock mass as faulted or jointed in order to understand its behaviour. The strength of the intact rock material, the nature of the infilling material in the faults or joints, the orientation and inclination of the discontinuities, the level of stress acting on the rock mass and the presence or absence of groundwater all have an influence upon the

behaviour of the rock mass. Consequently, any attempt to predict geological hazards must take all of this information into account.

Hook and Brown (1980) have discussed the question of interpretation of geological data for underground excavation design and have suggested that the rock mass classification systems developed by Bieniawski (1974) and by Barton, Lien and Lunde (1974) are currently the most logical vehicles for this interpretation.

Bieniawski's Rock Mass Rating is made up as follows:

$$RMR = A + B + C + D + E - F$$

where

- A = compressive strength of intact rock
- B = Rock Quality Designation (RQD) - an index determined from diamond drill core (Deere (1964))
- C = Spacing of joints
- D = Condition of joints
- E = Groundwater conditions
- F = Adjustment for joint orientation

Numerical ratings are given to each of these parameters on the basis of matching the field observations with standard descriptions published in Bieniawski's paper. Although qualitative, these descriptions provide a very practical and easy to use guide which permits rapid and systematic classification of rock masses on the basis of diamond drill core logging and/or mapping of surface outcrops or exploration adits.

Barton, Lien and Lunde's Tunnelling Quality Index (Q) is calculated as follows:

$$Q = RQD/J_n \times J_r/J_a \times J_w/SRF$$

where

- RQD = Rock Quality Designation as above
- J<sub>n</sub> = Joint set number
- J<sub>r</sub> = Joint roughness number
- J<sub>a</sub> = Joint alteration number
- J<sub>w</sub> = Joint water reduction factor
- SRF = Stress reduction factor

Barton, Lien and Lunde published a detailed set of tables to allow the user to establish the value of each of these parameters in the field and, although not quite as easy to use as Bieniawski's classification, the Tunnelling Quality Index is a very useful practical tool.

Both of these classifications include information which describes the strength of the intact rock, the size of average blocks within the rock mass, the surface characteristics (and hence the strength) of the discontinuity surfaces and the influence of water. The Rock Mass Rating system described by Bieniawski includes an allowance for joint orientation which makes it suitable for the classification of relatively shallow rock masses - say to depths of 200 metres. Barton, Lien and

Lunde's system allows for the influence of in situ stress and is more suited to the design of excavations at greater depth.

Once the geological data has been collected and assembled into one of these classification systems, the index obtained can be used to estimate rock mass strength or tunnelling conditions by means of empirical relationships derived from practical experience.

### *Systematic data collection*

In order to make use of rock mass classification systems for the prediction of geological hazards which could be encountered in the mining of underground excavations, it is important that sufficient data be collected to ensure that the site is adequately covered. Since diamond drilling and the mining of exploration adits are expensive, it is essential that the exploration programme be planned very carefully and that all meaningful information be collected systematically. Practical limitations imposed by the weather, by unrealistically tight budgets and by uncooperative contractors can make it very difficult to collect this information but these limitations must be allowed for in planning the exploration programme.

Because of the large amount of information which must be collected for rock mass classification, most users of these systems will have thought about automating the data collection process. Unfortunately, the descriptive nature of the information and the current lack of international or even national standards make this virtually impossible. In this author's opinion, the best which can be hoped for at present and for several years to come is to have a trained observer such as an engineering geologist or geotechnical engineer collect the information and input in into a central computer system by means of a portable computer or field terminal. The author is aware of one major civil engineering tunnelling contract where this is being done and where it is possible for the central computer to produce daily logs and drawings of the geological features mapped at the tunnel face.

It is relatively common when tunnelling into previously unmined ground to probe ahead of the tunnel face. Typically, a percussion drilled hole is extended several tunnel diameters ahead of the face to probe for high pressure water and to investigate the rock quality. During drilling, the rate of penetration, the thrust on the drill, the quality of the drill cuttings and of the cooling water return are monitored. When this information is compared with similar information obtained from previous probe holes, an indication can be obtained of possible changes in the rock ahead of the face. If major changes are indicated by the probe hole, the tunnel advance can be stopped while a horizontal hole is diamond drilled from the face. In addition to logging the core of such a hole, down-hole geophysics techniques can sometimes provide very useful supplementary information and, in extreme cases, borehole television cameras can be used to investigate potential trouble spots.

This probing ahead is particularly important when using a tunnelling machine or roadheader for excavation since these machines are far less flexible than drill and blast methods. Once a tunnelling machine has

been set in motion and its gripping system and cutting mechanisms chosen, it is very difficult to change these at short notice. Consequently, as much advance warning of changing ground conditions as possible should be available to the machine operator.

### ***Interpretation of geological data***

Imagine an ideal operation in which a very carefully planned exploration programme has been executed, borehole core has been carefully logged, exploration adits and existing excavations have been mapped and all of the information has been assembled by computer into rock mass classification systems. It is planned, once excavation commences, to have a full-time engineering geologist on site to continue the data gathering process and to assist the owner and the contractor in the interpretation of this information.

How is this information to be interpreted in order to predict excavation stability conditions, to design support systems, to predict excavation advance rates and, most important, to predict potential hazards which could seriously disrupt the operation? Unfortunately, at present, the interpretation of this information is based almost entirely upon judgement and experience. Fortunately, a great deal of this type of experience exists but very little of it has been formalized and presented in tables or charts which would permit someone other than a tunnelling specialist to draw meaningful conclusions. Bieniawski (1974) and Barton, Lien and Lunde (1974) attempted to use their rock mass classifications as a basis for drawing together experience on underground excavation support and they presented tables which gave recommended support designs for different rock mass classifications. These papers represent a good start but even the authors would not claim that their recommendations are adequate.

In the author's opinion, the interpretation of systematically collected and classified geological information presents one of the most exciting challenges for the application of computer based expert systems or, as it is sometimes called, artificial intelligence. In developing these systems for use in underground excavation engineering, a group of experienced mining and/or tunnel engineers would be asked a series of very carefully structured questions related to their interpretation of a number of sets of inter-related observations. For example, "What conditions would you anticipate when tunnelling in massive gneiss when the rock mass at the face exhibits intense jointing (four or five joint sets with spacings of 10 to 100mm), staining, water seepage from several of the joints, continuous raveling of small pieces of rock from the face?" The answers to many such questions would be stored and sorted by computer and would be organized into an interactive system in which, in addition to providing answers, the user would be asked questions which would narrow down or amplify the original input, thereby permitting progressive refinement of the interpretation.

This process is basically a means of collecting and recording the interpretations which would be made by a very experienced engineer or geologist when examining a large body of relevant data in search of a particular answer. The diagnostic techniques which are used are

peculiar to each individual and obviously depend upon the experience base from which that individual draws. Never-the-less, these interpretation techniques follow similar patterns and trends and it is these similarities which form the basis of the computer based expert systems. A parallel can be drawn with the medical profession where forms of expert systems have been used for many years in the diagnosis of illnesses.

Small expert systems have been successfully developed in some fields of geology, eg. Campbell *et al* (1982). As far as the author is aware, no serious attempt has yet been made to develop systems for the prediction of the types of hazards discussed in this paper. Since the entire science of artificial intelligence or expert systems is still in its infancy, it is probable that it will be many years before effective systems for the prediction of geological hazards become available and that many more years will pass before these systems are accepted by the conservative industries for which they are intended.

## CONTROL OF GEOLOGICAL HAZARDS

Suppose that a tunnel engineer or mine operator is lucky enough to have an experienced engineering geologist or geotechnical engineer on staff and that this individual can successfully predict most of the hazards which are likely to be encountered in underground excavations. What can be done, short of stopping the tunnelling or mining operation, to control these hazards ? The answer obviously depends upon the nature of the hazard and some of the more common problems which can be encountered underground are discussed below.

### *Rockfalls*

Rockfalls occur when blocks of rock are released from the roof or sidewalls of an underground excavation by intersecting discontinuities in the rock. These discontinuities can be naturally occurring bedding planes or joints or they can be fractures induced by blast damage or high stress concentrations. These latter types of discontinuities will be dealt with later in the paper and the present discussion will concentrate upon naturally occurring geological features.

Techniques for analyzing structurally controlled failures in underground excavations have been discussed by Hoek and Brown (1980) and new and improved techniques are being developed at several universities and research organizations. The lack of adequate analytical tools is not a problem but there are problems with the adequacy of the input data and with techniques for controlling structural failures. The data input problem is the same as that which plagues the entire subject of geotechnical engineering - there is never enough reliable information on which to base accurate predictions and analyses. This problem has already been discussed in this paper and, while improved exploration tools and systematic data collection techniques will help, the interpretation will still have to rely upon judgement and experience for the foreseeable future.

The question of control is much more dependent upon developments in practical support techniques. Once a potential structural failure has been identified, the miner has two choices - let it fall or support it. In the case of small wedges and blocks, the former choice is usually the most practical although it does have the potential of creating a progressive raveling problem if the block which falls is a key block which keeps the interlocking rock mass from falling apart. If the block is a key block or is of sufficient size that a fall could be dangerous, then support will be required.

The design of support to prevent structurally controlled failures is a relatively simple process since the driving force is the weight of the block and this driving force must be resisted by the installed support. The trick of good support for structurally controlled failures is to place it early. This is because, once a block or wedge is released, there is nothing to stop it falling and hence the principal aim of the support design is to prevent movement starting. There are many practical techniques for pre-supporting excavations in which structurally controlled failures are likely. One of the most effective is the pilot and slash method where a small pilot tunnel is driven ahead of the main tunnel to allow the installation of rockbolts before the full tunnel span is excavated. Others include spiling or forepoling where forward inclined bolts or grouted dowels are installed in such a way as to form an umbrella of pre-supported rock under which the tunnel face can be advanced. In the case of large fault controlled structural failures, the use of long grouted cables is usually required and the techniques for installing these are relatively well developed.

There is considerable potential for automating the equipment used to install the support in these cases and some equipment is already on the market. Ideally, a highly mobile rubber-tyred jumbo or similar unit, with an option for remote control, could drill holes in appropriate locations close to the face and then, without moving from a given location, install a mechanically anchored or resin grouted bolt or a friction anchored or expanded dowel. The advantages of such a unit in terms of safety and speed of operation are obvious and the need will become more urgent as mining conditions become more arduous and as it becomes more difficult to attract skilled miners to work under the crude conditions which are still common around the world.

### **Groundwater**

While the presence of groundwater in underground excavations can aggravate stability problems, the principal threat posed by groundwater is that of flooding or of a sudden, unanticipated inrush. Systematic data collection and careful probing ahead of the face are the main predictive tools available while drainage and grouting are the main methods of control.

In the case of isolated pockets of groundwater, drainage is the obvious remedy to subsurface groundwater problems. Where a large water reservoir is likely to be tapped by the excavation process, grouting followed by local drainage is the preferred route. This grouting may be carried out from holes drilled ahead of the face to form an impermeable



umbrella or it may be carried out from long holes aimed at specific water passages.

Currently, the practice of underground grouting is rather like shooting in the dark - there are very few techniques available to help the operator decide upon optimum location, grout viscosity, pressures and pumping rates during placing of the grout. The only successful test is that the water stops flowing but experience suggests that a great deal of grout is usually wasted before this test is passed.

The potential for the development of tools and automatic control systems for such grouting operations seems to be remote at present - mainly because it is very difficult to define the problem to be addressed. However, there is clearly a need for a better understanding of this process and this understanding will eventually lead to the development of suitable equipment for the control of underground grouting.

### *Stress induced fracturing*

The creation of any underground excavation results in a redistribution of the stresses in the rock mass and this generally leads to a concentration of stresses in the rock immediately surrounding the opening. When these local stresses exceed the strength of the rock, failure of the rock occurs and, if this failure is severe enough, complete collapse of the excavation can occur. In extreme cases, when mining in very hard, strong and brittle rock, these failures can occur as rockbursts in which significant amounts of energy are released with explosive violence.

The ingredients in the stress induced fracture problem are the direction and magnitudes of the in situ stresses in the rock, the shape and size of the excavations created and the strength characteristics of the rock mass. A full discussion on these problems exceeds the scope of this paper and the interested reader is referred to the general review published by Hoek and Brown (1980) and to the proceedings a recent conference on rockbursts published by the Institution of Mining and Metallurgy in London (1984).

In the context of this paper, the question of control of stress induced fracturing and rockbursts comes back to a full understanding of the in situ stresses and rock mass characteristics, based upon the systematic data collection and interpretation discussed earlier, and the incorporation of this information into the excavation design process. In choosing the shape of the excavations to be created and the percentage extraction, the mine designer has some control over the stresses which will be induced around the excavations and in pillars between excavations. The sequence of mining is also important in that remnants and island pillars which tend to attract high stress should be avoided.

Numerical models which can assist mine planners in avoiding the creation of high stress concentrations are becoming available and are being used in an increasing number of mines. A good example of one such application has been presented by von Kimmelman, Hyde and Madgwick (1984).

When conditions are such that it is not possible to avoid stress induced fracturing, a substantial amount of control is available by means of support using rockbolts, dowels, cablebolts, props, packs and backfill. In contrast to the support of structurally controlled failures, discussed earlier, some movement of the rock before the installation of support is desirable in order to allow a controlled amount of fracturing and the dissipation of some of the stored energy in the rock mass. In tunnelling, the time and deformation-dependent interaction between the rock mass and the installed support is reasonably well understood and goes under the names of the closure-confinement method, the rock-support interaction technique (Hoek and Brown (1980)) or the New Austrian Tunnelling Method (Rabcewicz (1964)). In the case of mining the problem is more complex because of the complex shape of most mine openings but practical techniques such as rockbolting and the use of rapid-yielding hydraulic props (Tyser and Wagner (1976)) have proved to be effective in controlling local problems of stress induced fracturing.

Rockbursts are a more serious problem and have many parallels to earthquakes. Not only are they extremely dangerous but their unpredictability gives rise to a fear of rockbursts which can be seriously disruptive in an operating mine or tunnel. Attempts to predict rockbursts have received a great deal of attention but have only been partially successful (Salamon (1984)). The monitoring of these events by means of microseismic techniques (Cook (1963)) has made an important contribution to our understanding of the location of rockbursts and refinements in microseismic monitoring techniques together with computer aided interpretation of the results offers some long term hope of further improvements in this understanding (Salamon (1984)).

### CONCLUSIONS

The purpose of presenting this paper at a conference on Automation for Mineral Resource Development has been to give a brief overview of the current state of our understanding and ability to predict geological hazards in the creation of underground excavations. Water inrushes, falls of ground and rockbursts are some of these hazards and the author has attempted to show that, while our understanding of the origins of these problems is reasonable, our ability to predict them is severely limited.

There are no magic tools which enable us to look into the earth and to detect the presence of trapped groundwater, zones of intense fracturing or areas of exceptionally high stress - some of the factors which contribute to the hazards encountered in underground mining. The most useful of the currently available techniques is the systematic collection and interpretation of relevant geological data during exploration or in advance of the tunnel or mining face. The wide availability of computers will be of great assistance in this data collection and interpretation system. There appears to be considerable merit in the use of expert systems in which the knowledge of experienced miners, engineering geologists and geotechnical engineers is gathered into an ordered computer based information system and developed into an inter-active design tool.

The control of geological hazards in underground excavations is an equally difficult task but significant practical progress has been made by trial and error development of mining equipment and support systems. There is certainly room for some automation of such equipment as drills, mucking machines and rockbolting equipment in order to increase the productivity and to give the operators a safer and more attractive working environment. However, it is considered unlikely that automation will contribute significantly to the control of geological hazards which will remain as inescapable part of the process of underground mining.

#### REFERENCES

Barton, N., Lien, R. and Lunde, J. (1974) Engineering classification of rock masses for the design of tunnel support. *Rock Mechanics*, Vol. 6, pp 189-236.

Bieniawski, Z.T. (1974) Geomechanics classification of rock masses and its application in tunnelling. In *Advances in Rock Mechanics, Vol. 2, part A: proc. 3rd congress International Society for Rock Mechanics*, Denver, 1974, pp 27-32.

Campbell, A.N., Hollister, V.F., Duda, R.O. and Hart, P.E. (1982). Recognition of a hidden mineral deposit by an artificial intelligence program. *Science*, Vol. 217, pp 927-929.

Cook, N.G.W. (1963) The seismic location of rockbursts. *Proc. 5th Rock Mechanics Symposium*, Oxford. Pergamon Press, pp 493-516.

Deere, D.U. (1964) Technical description of rock cores for engineering purposes. *Rock Mechanics and Engineering Geology*, Vol. 1, No. 1, pp 17-22.

Hoek, E. and Brown, E.T. (1980) *Underground Excavations in Rock*, Institution of Mining and Metallurgy, London.

Institution of Mining and Metallurgy, London. (1984) *Rockbursts: prediction and control*, IMM, London.

Rabcewicz, L.V. (1964) The new Austrian tunnelling method, *Water Power*, Vol. 16, 1964, pp 453-457 (part 1) and Vol. 17, 1965, pp 19-24 (part 2).

Salamon, M.D.G. (1984) Rockburst hazard and the fight for its alleviation in South African gold mines. *Proc. Symp. Rockbursts: prediction and control*, Institution of Mining and Metallurgy, London, pp 11-36.

Tyser, J.A. and Wagner, H. (1976) Review of six years of operations with the extended use of rapid yielding props at the East Rand Proprietary Mines, Limited and experience gained throughout the industry. *Association of Mine Managers of South Africa, Papers and Discussions*, 1976-1977, pp 321-347.

von Kimmelmann, M.R., Hyde, B. and Madgwick, R.J. (1984) The use of computer applications at BCL Limited in planning pillar extraction and the design of mining layouts. *Proc. ISRM Symp. Design and Performance of Underground Excavations*, Cambridge, UK, 1984, pp 53-63.



**DIVISION DE EDUCACION CONTINUA  
FACULTAD DE INGENIERIA U.N.A.M.**

MECANICA DE ROCAS APLICADA A LA MINERIA Y A LA CONSTRUCCION

ECONOMIC AND PLANNING CONSIDERATIONS

MAYO, 1985

*Young*

# Rock Slope Engineering

**Evert Hoek**

Professor of Rock Mechanics  
Imperial College of Science and  
Technology, London, England  
and

Principal, Colder, Hoek & Partners,  
Maidenhead, Berkshire, England

**John Bray**

Senior Lecturer in Rock Mechanics,  
Imperial College of Science and  
Technology, London, England

In designing the very large excavated slopes which are becoming increasingly common in both mining and civil engineering projects, the engineer is faced with two conflicting requirements. On the one hand, vast sums of money can be saved by steepening the slopes, thereby reducing the amount of material to be excavated. On the other hand, loss of life and serious damage to property can result from failures induced by excessive steepening of a particular slope. How does the engineer achieve an optimum design - a compromise between a slope which is steep enough to be economically acceptable and one which is flat enough to be safe?

Because the rock mass behind each slope is unique, there are no standard recipes or routine solutions which are guaranteed to produce the right answer each time they are applied. A practical solution is built up from the basic geological data, rock strength information, groundwater observations and a good measure of engineering common sense. These ingredients are blended in different proportions for each case and the only assistance available is a collection of tools and techniques which will help the engineer to collect the information quickly and efficiently and to process it in an orderly manner.

This book sets out to describe these tools and techniques and to illustrate their application to practical problems by means of a number of worked examples. As far as possible, the text has been kept free of mathematics and a number of simple design charts and graphical methods have been included to enable the non-specialist engineer rapidly to obtain approximate answers to his problem. These approximate answers are frequently adequate but there will be situations in which the engineer will wish to call upon a geotechnical specialist for assistance. Having attempted to solve the problem for himself, the engineer will be in a strong position to communicate his needs to the geotechnical specialist and to work out, with the specialist, the most practical engineering solution.

The authors make no apology for the fact that the book has been printed by offset lithography from typescript and that some of the drawings and photographs are not perfect. The intention has been to produce an engineering handbook at minimum cost rather than a fine example of the printer's art. Wide margins have been provided for the the reader's notes and the authors hope that each copy will wear out from hard use rather than decay in decorative inactivity.

This book is the outcome of a four year research project carried out at the Royal School of Mines\* between 1968 and 1972. The project was sponsored by the following mining companies:

---

\*Part of the Imperial College of Science and Technology which, in turn, is part of the University of London.

3

Anglo-American International (UK) Ltd. on behalf of six member companies:

Bougainville Copper (Pty) Ltd.  
Consolidated Gold Fields Ltd.  
English China Clays Ltd.  
Iranian Selection Trust Ltd.  
National Coal Board Opencast Executive  
Palabora Mining Company Ltd.  
Rio Tinto Espanola S.A.  
Rio Tinto Zinc Corporation Ltd.

Roan Selection Trust Ltd. on behalf of two member companies in Zambia and the following member companies of the Australian Mineral Industries Research Association Ltd.:

Broken Hill Proprietary Company Ltd.  
Cosinc Riotinto of Australia Ltd.  
Electrolytic Zinc Company of Australasia Ltd.  
Mount Isa Mines Ltd.  
New Broken Hill Consolidated Ltd.  
North Broken Hill Ltd.  
Western Mining Corporation Ltd.

Mr. M.J. Cahalan, of the Rio Tinto Zinc Corporation's Research Secretariat, acted as co-ordinator of the project.

The authors wish to acknowledge the generosity of these companies and also their willingness to provide information and practical assistance whenever it was requested.

The research was carried out by a team of staff members and research students at the Royal School of Mines and valuable criticism, advice and assistance was provided by a number of the authors' friends from all over the world. It would be impractical to name all of these persons but the authors gratefully acknowledge their contributions to the project and to the preparation of this book.

London  
November 1973.

E. Hoek  
J.W. Bray



## Introduction

This book is concerned with the stability of rock slopes, with methods for assessing this stability and with techniques for improving the stability of slopes which are potentially dangerous. Rock slope failures, or the remedial measures necessary to prevent them, cost money and it is appropriate that, before becoming involved in a detailed examination of slope behaviour, some of the economic implications of this behaviour should be considered.

A number of authors<sup>1-8\*</sup> have discussed the influence of slope angle upon the design and economics of open pit mining and the interested reader is referred to these publications which deal with the subject more fully than is possible in this introduction. One of the most obvious facts to emerge from these discussions is that, in order to reduce to a minimum the amount of waste rock which has to be excavated in recovering an ore body, the ultimate slopes of the mine are generally cut to the steepest possible angle. Since the economic benefits gained in this way can be negated by a major slope failure, evaluating the stability of the ultimate slopes is an important part of open pit mine planning.

Stewart and Kennedy<sup>1</sup> show that it is not only the steepness of the ultimate slopes in an open pit mine which has an influence upon the overall profitability of the operation. On the basis of cash flow calculations, they show that there is frequently considerable economic advantage to be gained from using steep slopes during the initial stripping programme. These authors also emphasise the fact that there are several factors, in addition to stability, which determine the steepness of the slopes in an open pit mine. Large mining equipment cannot be operated on narrow benches, haul road grades have to be kept within limits imposed by the optimum operating conditions of trucks or trains and this generally means flatter slopes and, in some cases, local mining regulations define maximum bench heights and widths.

While the overall slopes are clearly important in terms of the economics of the entire mining operation, the stability of individual benches is usually a matter of more immediate concern to the engineers responsible for the day-to-day mining operations. Slope failure in a bench, which carries a main haul road or which is adjacent to a property boundary or an important installation, can cause severe disruption to the mining programme. It is also in these relatively small failures, which can occur with very little warning, that lives can be lost and equipment damaged.

The stability of an individual bench is controlled by local geological conditions, the shape of the overall slope in that area, local groundwater conditions and also by the excavation technique used in creating the slope. These controlling factors will obviously vary so widely for different mining situations that it is impossible to give general rules on how high or how steep a bench should be

---

\* Numbers in parentheses refer to the list of references given to the end of each chapter.

to ensure that it will be stable. When the stability of a bench, which is important in a particular mining operation, is suspect, its stability must be assessed on the basis of the geological structures, groundwater conditions and other controlling factors which occur in that specific slope. This book is devoted to providing the engineer or geologist with techniques for carrying out such an evaluation.

### Economic consequences of instability

Possibly the best introduction to the subject can be given by an example which includes a consideration of the most important factors which control rock slope behaviour as well as the economic consequences of instability.

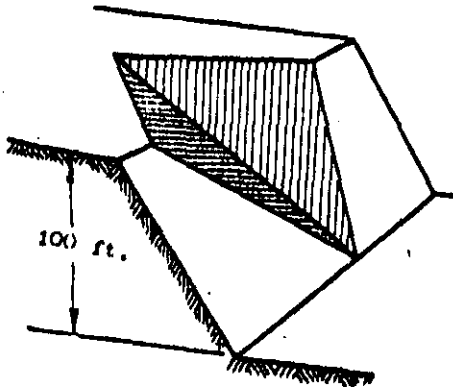


Figure 1 : Geometry of wedge failure in example of bench stability analysis.

Details of wedge geometry and material properties used in this analysis:

Discontinuity surfaces upon which wedge slides both dip at  $45^\circ$  and strike at  $45^\circ$  to the slope face, giving a symmetrical wedge. The surfaces both have friction angles of  $30^\circ$  and cohesive strength of  $1000 \text{ lb./ft}^2$ . The rock density is  $160 \text{ lb./ft}^3$ .

In the slope illustrated in Figure 1, two major discontinuities have been exposed during the early stages of excavation. Measurement of the orientation and inclination of these discontinuities and projection of these measurements into the rock mass shows that the line of intersection of the discontinuities will daylight in the slope face when the height of the slope reaches 100 feet. It is required to investigate the stability of this slope and to estimate the costs of the alternative methods of dealing with the problem which arises if the slope is found to be unstable.

The factor of safety\* of the slope, for a range of slope angles, is plotted in Figure 2 for the two extreme conditions of a dry slope and a slope excavated in a rock mass in which the groundwater level is very high. It will become clear, in the detailed discussions given later in this book, that the presence of groundwater in a slope can have a very important influence upon its stability and that drainage of this groundwater is one of the most effective means of improving the stability of the slope.

A slope will fail if the factor of safety falls below unity and, from Figure 2, it will be seen that the saturated slope will fail if it is excavated at an angle steeper than  $64^\circ$ . The dry slope is theoretically stable at any angle but the factor of safety of approximately 1.2 is not considered sufficiently high to ensure that the slope will remain stable. In most mining situations, where a slope is only required to remain stable for a relatively short period, a factor of safety of 1.3 is normally regarded as the minimum acceptable value. For more permanent slopes such as those which carry the haul road, a factor of safety of 1.5 is more appropriate.

In this example, a factor of safety of 1.3 is considered adequate and this means that, if no other steps are taken to stabilise the slope, it would have to be excavated at an angle of  $46^\circ$  for the saturated condition or  $55^\circ$  if it is dry in order to give this value.

An estimate of costs can only be obtained if the tonnages to be excavated or cleared-up, if failure occurs, are

---

\*The definition of this and of other terms used in the stability analysis is given later in the book. A detailed knowledge of the method of analysis is not necessary in order to follow this example.

Example of a wedge failure in a roadcut in Norway.

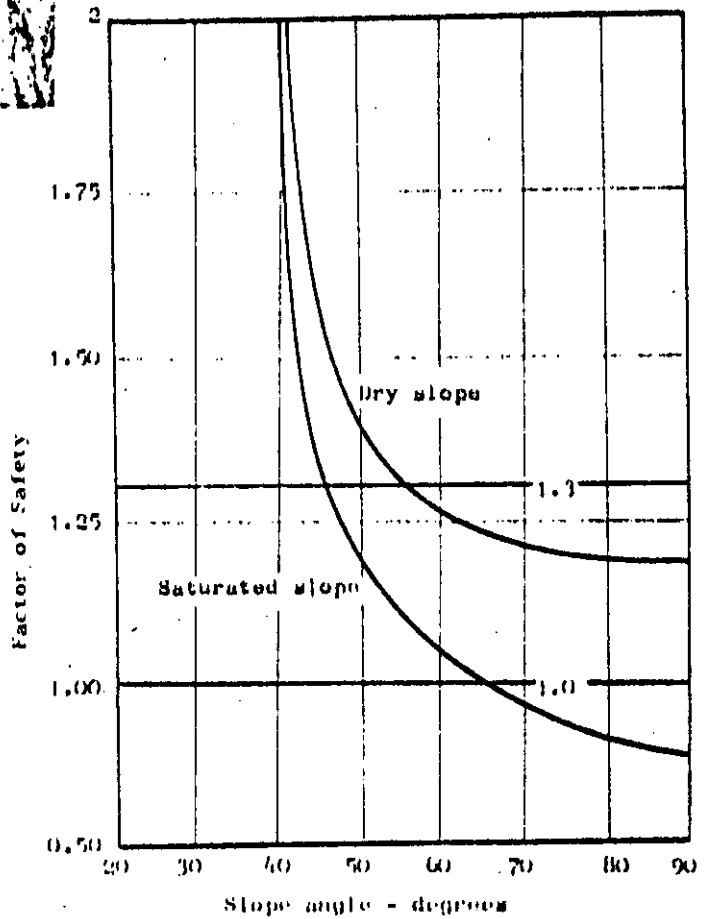


Figure 2: Variation in Factor of Safety with slope angle.

calculated. This has been done for a range of slope angles and the results are plotted in Figure 3. In calculating the tonnage involved in flattening the slope, it has been assumed that 300 feet of slope face has to be excavated. In many cases, flattening the slope would also influence benches above that under consideration and much larger tonnages than those given in Figure 3 would be involved.

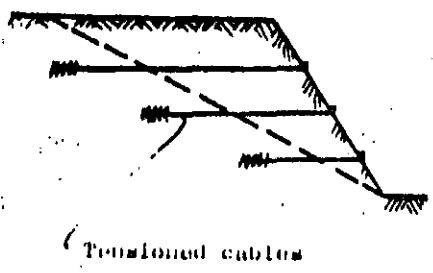
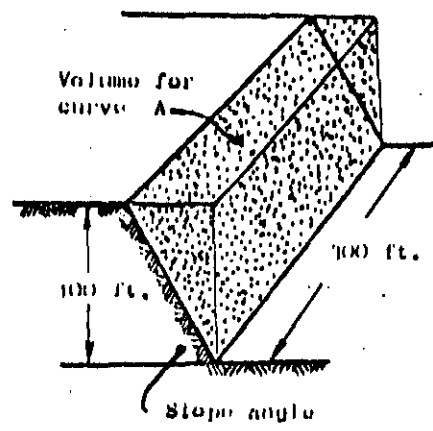
Also included in this figure are two curves giving the external load, applied by means of cables installed in horizontal holes drilled at right angles to the slope face and anchored in the rock behind the discontinuity planes, required to give a factor of safety of 1.3 for both dry and saturated slopes.

The cost of the various options which are now available to the engineer will depend upon the geographical location of the mine, availability of specialist services for installation of drainage or of tensioned cables and upon local labour costs. In deriving the costs presented in Figure 4, the following assumptions were made:

- a. The basic cost unit is taken as the cost per ton mined from the face. Hence, line A in Figure 4 is obtained directly from line A in Figure 3.
- b. The cost of clearing up a slope failure is assumed to be 2½ times the basic mining cost. This gives line B which starts from a slope angle of 64°, theoretically the flattest slope at which failure could occur.
- c. The design and installation of a drainage system involves a fixed cost of 75,000 units, irrespective of slope angle (line E).
- d. The cost of tensioned cables, installed by a specialist contractor, is assumed to be 10 units per ton of load. This gives lines C and D.

On the basis of a set of data such as that presented in Figure 4, the engineer is now in a position to consider the relative costs of the options available to him. Some of these options are listed hereunder.

- a. Flatten slope to 46° to give a factor of safety of 1.3 under saturated conditions. (Line A) Total cost: 116,000 units
- b. Flatten slope to 55° and install drainage system to give a factor of safety of 1.3 for a dry slope. (Lines A and E) Total cost: 159,000 units
- c. Cut slope to 64° to induce failure and clear up failed material. (Lines A and B) Total cost: 166,000 units
- d. Cut slope to 80° and install cables to give factor of safety for saturated slope of 1.3. (Lines A and C) Total cost: 137,000 units



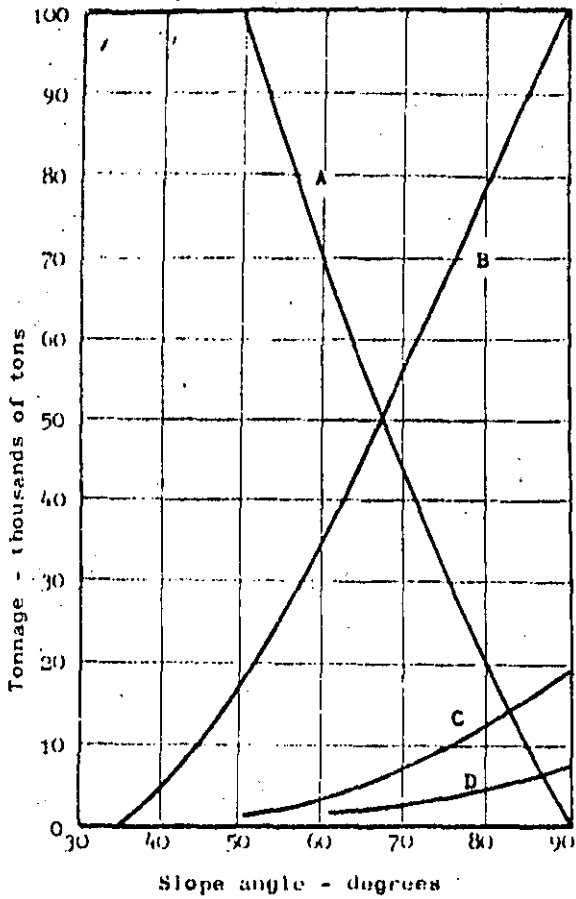
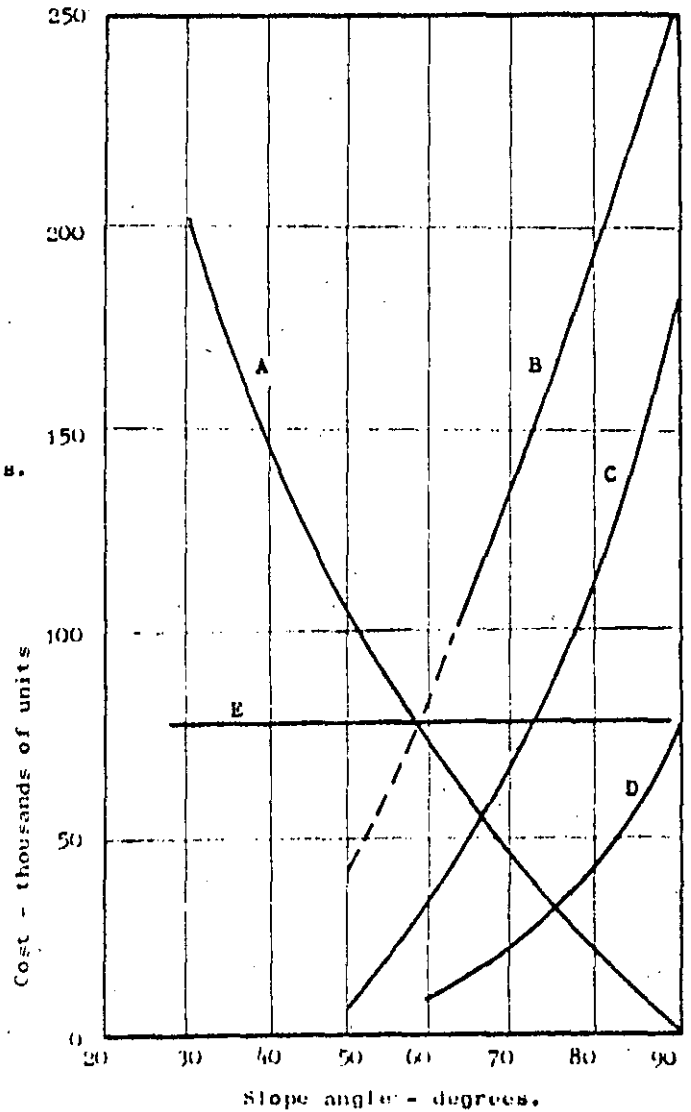


Figure 3 : Excavation tonnages and cable loads.  
 Line A - Tonnage excavated in flattening slope 100 ft. high x 300 ft. long.  
 Line B - Tonnage to be cleared up if wedge failure occurs.  
 Line C - Cable load required for factor of safety of 1.3 for saturated slope.  
 Line D - Cable load required for factor of safety of 1.3 for dry slope.

Figure 4 : Comparative costs of options.



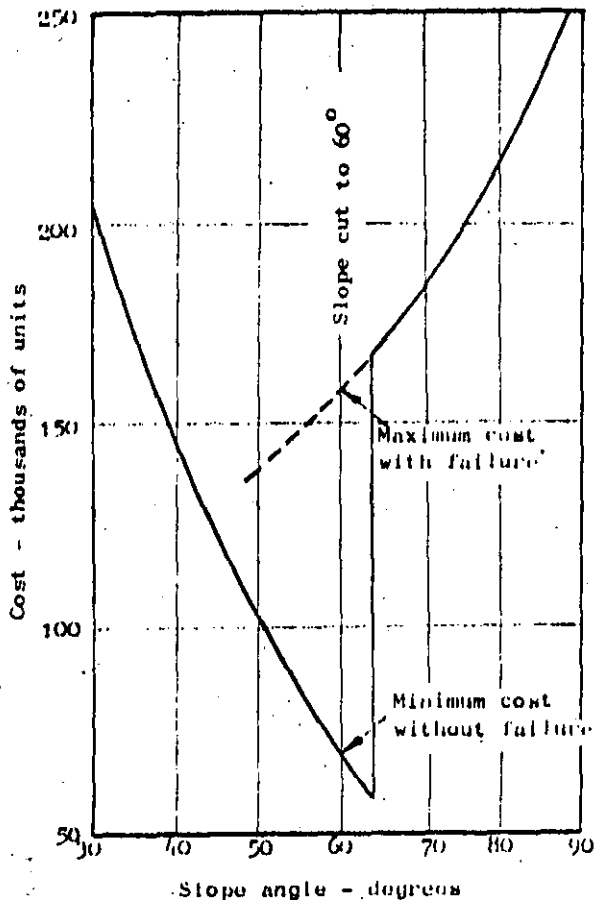


Figure 5 : Costs associated with mining the slope to a steep angle and accepting the risk of a failure.

- e. Leave slope vertical, install drainage system and cables to give factor of safety of 1.3 for dry slope. (Lines A,D and E)  
Total cost: 155,000 units
- f. Cut slope to 60° on the assumption that it may not fail and make provision for clearing up failure if it occurs. (Figure 5)  
Maximum total cost: 159,000 units  
Minimum total cost: 70,000 units

It must be emphasised that these estimates are hypothetical and apply to this particular slope only. The costs of these and other options will vary from slope to slope and no attempt should be made to derive general rules from the figures given.

On the basis of the estimates listed above, most open pit engineers would probably decide to flatten the slope to 46° and thereby to eliminate the problem. The cost of this option is lower than the others considered with the exception of the minimum cost of f. Flattening the slope to 46° has one important advantage over the other options in that it does not carry with it the possibility that, having spent a great deal of money on remedial measures, the slope could still fail as a result of some unforeseen combination of circumstances. The total cost, if this were to occur, would be very high.

required to give an adequate factor of safety under all conditions may not be possible. Under these circumstances, one of the other options would have to be considered.

In recognition of a decision which is frequently made in open-pit mining, although not often with the background of knowledge available in this example, the option listed as item f and illustrated in Figure 5 has been included. Figure 2 shows that failure of the slope is likely if it is cut steeper than  $64^{\circ}$  and if it is saturated. Assuming that this condition only arises during exceptionally heavy rains which may only occur once in the next 10 - 20 years, i.e. hopefully not during the anticipated life of the slope, the open pit engineer may decide to cut the slope to  $60^{\circ}$  and to accept the risk of failure as part of his mine planning. If he is lucky and failure does not occur, the total cost will have been kept to 70,000 units. On the other hand, if adequate provision has been made to accommodate and to deal with the failure, the total cost of 159,000 units incurred if failure occurs is still within the range of costs of the other options.

The publications of Kennedy et al<sup>9,10</sup>, dealing with the prediction and successful accommodation of a major slide at the Chuquicamata mine in Chile, have demonstrated that accepting a failure as part of a planned mining operation is feasible provided that the risk of loss of life and damage of equipment can be minimised. Knowledge of the likely behaviour of the slope, derived from a stability analysis such as that given above, is essential if any measure of control over the consequences of failure is to be achieved in this situation.

#### Planning stability investigations

A typical open pit mine may only suffer two or three slope failures during its operating life. How can the isolated slopes which are potentially dangerous be detected in the many miles of slopes created in a large mine?

The answer lies in the fact that certain combinations of geological discontinuities\*, slope geometry and groundwater conditions result in slopes in which the risk of failure is high. If these combinations can be recognised during the preliminary geological and pit layout studies, steps can be taken to deal with the slope problems which are likely to arise in these areas. Slopes in which these combinations do not occur require no further investigation. It must, however, be anticipated that undetected discontinuities will be exposed as the pit is excavated and provision must be made to deal with the resulting slope problems as they arise.

This approach to the planning of slope stability studies in open pit mines is outlined in the chart presented in Figure 6 and it will be seen that two distinct stages are proposed:

Stage 1 involves a preliminary evaluation of the geological data available from the prospecting or

---

\*The term discontinuity as used here covers faults, joints, bedding planes or any other surfaces upon which movement can take place.

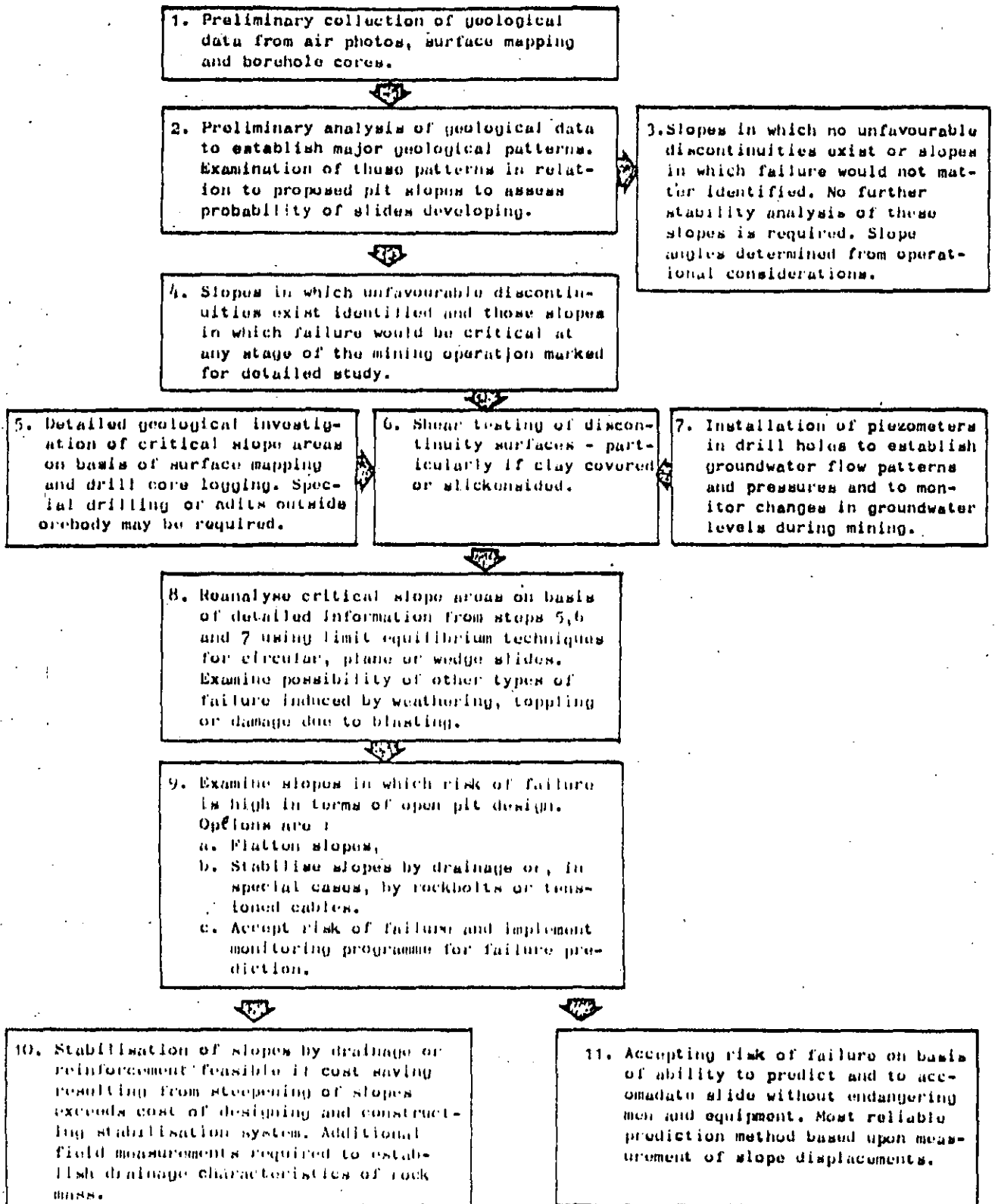


Figure 6 : Analysis of the stability of slopes in open pit mines.



exploration programme which normally includes air photo interpretation, surface mapping and diamond drilling.

Note that this data is collected for ore-reserve evaluation and it is usually necessary to re-examine it in terms of the factors which are important for stability.

The preliminary assessment of stability can be done using a number of simple techniques which will be described in the first part of this book. This preliminary study should identify those slopes in which no failure is likely, and which can therefore be designed on the basis of operational considerations, and those slopes in which the risk of failure appears to be high and which require more detailed analysis.

Stage 2, which applies only to those slopes in which potential instability could prove dangerous at some stage in the mining operation, involves a much more detailed study of the geology, the groundwater conditions and the mechanical properties of the rock mass. A detailed analysis of stability is then carried out on the basis of this information and this should provide the mine management with a set of quantitative data upon which rational decisions can be based.

The second part of this book will deal with the techniques which can be used for these detailed stability studies.

At this point the reader would probably wish to ask the questions: who should do this work and how much will it cost? The following comments on these questions are offered with the warning that they represent the personal opinions of the author and should not be regarded as general rules. Conditions will obviously vary widely from mine to mine and from country to country and the ultimate decision upon how to deal with stability problems in an open pit mine must be taken by the mine management after due consideration of the factors which are important to that particular mine.

The preliminary investigations listed above under Stage 1 should ideally be integrated into the evaluation and feasibility studies of the mine. Much of the information required for these preliminary slope studies can be obtained at minimal cost if provision is made for its collection during the exploration drilling programme. There is no reason why these preliminary studies should not be carried out by the geologists or engineers engaged in the feasibility studies on the mine. The techniques are not difficult and do not require any complex mathematical treatment. Outside assistance is only required at this stage if the company engineers or geologists feel that it is necessary to discuss their evaluation with someone with experience in slope analysis in order to check that no important points have been overlooked. There may be other situations in which the mine owners or management may consider it more efficient to contract this work out to consulting engineers or geologists and, under normal circumstances, a preliminary evaluation of slope problems would require between one and three man-months of work.

In existing open pit mines, a much more detailed knowledge of the geology and of areas of the pit which have shown signs of instability will already be available. Under these circumstances, the problems will have defined themselves and the preliminary investigations discussed above will probably not be necessary. However, some failures may already have developed to the extent that the remedial measures required to deal with them are more expensive than would have been the case if action had been taken earlier in the life of the mine.

Once the critical slopes in a mine have been defined, the more detailed studies which are then necessary will vary so much from mine to mine that general guide-lines are very difficult to define. It is unlikely that, with the exception of very large mining groups, there would be geologists or engineers in the company who would feel competent to deal with the more complex slope problems without some outside assistance. This does not mean that the techniques of slope analysis are particularly difficult but it does mean that these analyses provide only part of the answer to a slope problem. The rest of the answer comes from engineering judgement based upon experience from having dealt with a variety of slope problems.

Specialist geotechnical organisations which have dealt with a number of open pit mines studies are in a good position to provide sound advice in these cases and, because of their familiarity with similar problems, it is frequently cheaper and more efficient to use these services in preference to embarking upon a "do-it-yourself" study. If this course is adopted, it is useful if an engineer or geologist on the mine has a reasonable knowledge of techniques for stability analysis in order that an effective liaison between the management and the consultants should exist. It is hoped that this book will provide a comprehensive source of information on these techniques.

How much is a slope analysis by a specialist consultant likely to cost and what would be the cost of implementing the recommendations made as a result of this analysis? The answer to this question is subject to the same degree of uncertainty as is associated with a visit to the doctor and yet few of us would hesitate to visit the doctor if we suspected that something was wrong. Some mines can be involved in considerable expense in dealing with slope failures while others may spend virtually nothing on this problem. Experience suggests that a sum of 1% of the total mining cost may not be an unreasonable amount to spend on slope design and correction costs. Even if no positive action on designing optimum slopes is taken, the cost of dealing with unexpected failures during the life of the mine can easily exceed this figure.

Selected references on economic and planning considerations related to open pit mine slopes.

1. MOFFITT, R.B., YKIESH-GREENE, T.W. and LILLICO, T.M. Pit slopes - their influence on the design and economics of open pit mines. *Proc. 2nd Symposium on stability in Open Pit Mining*, Vancouver 1971. To be published by A.I.M.E., New York.
2. STEWART, R.M. and KENNEDY, B.A. The role of slope stability in the economics, design and operation of open pit mines. *Proc. 1st Symposium on stability in Open Pit Mining*, Vancouver 1970, A.I.M.E., New York 1971
3. STEFFEN, O.K.H., HOLT, W. and SYMONS, V.R. Optimising open pit geometry and operational procedure. *Planning Open Pit Mines*, Johannesburg Symposium 1970. Published by A.A. Balkema, Amsterdam 1971, pp.9-31.
4. HALLS, J.L. The basic economics of open pit mining. *Planning Open Pit Mines*, Johannesburg Symposium 1970, Published by A.A. Balkema, Amsterdam 1971, pp.125-131.
5. SODERBERG, A. and RAUSCH, D. Pit planning and layout. *Surface Mining*. Editor Eugene P. Pfleider. Publisher A.I.M.E., New York 1968. Chapter IV.
6. BLACK, R.A.L. Economic and engineering design problems in open pit mining. *Mine and Quarry Engineering*, Jan., Feb. and March 1964, 20p.
7. CROSZ, R.W. The changing economics of surface mining. *Proc. Intl. Symposium on Computer Applications in Mining Industry*. Publishers A.I.M.E., New York 1969, pp.401-419.
8. STEWART, R.M. and SEEGMILLER, B.L. Requirements for stability in open pit mining. *Proc. 2nd Symposium on Stability in Open Pit Mining*, Vancouver 1972. To be published by A.I.M.E., New York.
9. KENNEDY, B.A., NIERMEYER, K.E., FAHM, B.A. and BRATT, S.A. A case study of slope stability at the Chuquicamata Mine, Chile. Preprint No. 70-AM-81. *Society of Mining Engineers of A.I.M.E.*, February 1970.
10. KENNEDY, B.A. and NIERMEYER, K.E. Slope monitoring systems used in the prediction of a major slope failure at the Chuquicamata Mine, Chile. *Planning Open Pit Mines*, Johannesburg Symposium 1970. Published by A.A. Balkema, Amsterdam 1971, pp.215-225.

## Continuum mechanics approach to slope stability

A question which frequently arises in discussions on slope stability is how high and how steep can a rock slope be cut. One approach to this problem, which has been adopted by a number of investigators<sup>11-13</sup>, is to assume that the rock mass behaves as an elastic continuum. The success which has been achieved by the application of techniques such as photoelastic stress analysis or finite element methods in the design of underground excavations has tempted many research workers to apply the same techniques to slopes. Indeed, from the research point of view, the results have been very interesting but in terms of practical rock slope engineering, these methods have limited usefulness. These limitations arise because our knowledge of the mechanical properties of rock masses is so inadequate that the choice of material properties for use in the analysis becomes a matter of pure guesswork. For example, if one attempts to calculate the limiting vertical height of a slope in a very soft limestone on the basis of its intact strength, a value in excess of 3500 feet is obtained<sup>14</sup>. Clearly, this height bears very little relation to reality and one would have to reduce the strength properties by a factor of at least 10 in order to arrive at a reasonable slope height.

It is appropriate to quote from a paper by Terzaghi<sup>15</sup> where, in discussing the problem of foundation and slope stability, he said "...natural conditions may preclude the possibility of securing all the data required for predicting the performance of a real foundation material by analytical or any other methods. If a stability computation is required under these conditions, it is necessarily based on assumptions which have little in common with reality. Such computations do more harm than good because they divert the designer's attention from the inevitable but important gaps in his knowledge...".

Muller<sup>16</sup> and his co-workers in Europe have, for many years, emphasized the fact that a rock mass is not a continuum and that its behaviour is dominated by discontinuities such as faults, joints and bedding planes. Most practical rock slope designs are currently based upon this discontinuum approach and this will be the approach adopted in all the techniques presented in this book. However, before leaving the question of the continuum mechanics approach, the author wishes to emphasize that he is not opposed in principle to its application and indeed, when one is concerned with overall displacement or groundwater flow patterns, the results obtained from a numerical method such as the finite element technique can be very useful. Developments in numerical methods such as those reported by Goodman et al<sup>17</sup> and Cundall<sup>18</sup> show that the gap between the idealized elastic continuum and the real discontinuum is gradually being bridged and the author is optimistic that the techniques which are currently interesting research methods will eventually become useful engineering design tools.

Maximum slope height - slope angle relationship for excavated slopes

Even if one accepts that the stability of a rock mass is

situations where the orientation and inclination of these discontinuities is such that simple sliding of slabs, blocks or wedges is not possible. Failure in these slopes will involve a combination of movement on discontinuities and failure of intact rock material and one would anticipate that, in such cases, higher and steeper slopes than average could be excavated. What practical evidence is there that this is a reasonable assumption?

A very important collection of data on excavated slopes was compiled by Kley and Lutton<sup>21</sup> and this collection has recently been added to by Ross-Brown<sup>22</sup>. The information refers to slopes in opencast mines, quarries, dam foundation excavations and highway cuts. The slope heights and corresponding slope angles for the slopes in materials classified as hard rock have been plotted in Figure 7 which includes both stable and unstable slopes. Ignoring, for the moment, the unstable slopes, this plot shows that the highest and steepest slopes which have been successfully excavated, as far as is known from this collection of data, fall along a fairly clear line\* shown dashed in the figure. (One additional point at 42° and a height of 2200 feet from an opencast mine in Austria falls on the curve but has been omitted from the figure). This line gives a useful practical guide to the highest and steepest slopes which can be contemplated for normal open pit mine planning. In some exceptional circumstances, higher or steeper slopes may be feasible but these could only be justified if a very comprehensive stability study had shown that there was no risk of inducing a massive slope failure

#### Role of discontinuities in slope failure

Figure 7 shows that, while many slopes are stable at steep angles and at heights of several hundreds of feet, many flat slopes fail at heights of only tens of feet. This difference in stability results from the difference in inclination of the discontinuity surfaces upon which sliding can take place. This is strikingly illustrated in the simple example given in Figure 8 in which the critical height of a vertical slope containing an inclined weakness plane is given\*\* for both dry and saturated slopes<sup>16</sup>. This critical height decreases from more than 200 feet for a slope with discontinuities which are nearly horizontal and vertical to approximately 70 feet for slopes containing

\*The dashed curve corresponds to circular failure in a material with a friction angle  $\phi=30^\circ$  and a cohesive strength  $c = 6400 \text{ lb/ft}^2$ . Methods of analysing this type of failure are discussed later in this book.

\*\*The critical height of this vertical slope is given by

$$H = \frac{2c}{\gamma \cos \psi (\sin \psi - \cos \psi \tan \phi + \gamma_w / \gamma \cdot \tan \psi \tan \phi)}$$

where  $c$ , the cohesive strength of the surface =  $2000 \text{ lb/ft}^2$

$\phi$ , the friction angle of this surface =  $20^\circ$

$\gamma$ , the rock density =  $160 \text{ lb/ft}^3$

and  $\gamma_w$ , the density of water =  $62.5 \text{ lb/ft}^3$ .

$\gamma_w/\gamma = 0$  for dry slopes.

For discontinuity angles between  $0$  and  $30^\circ$  and  $80$  and  $90^\circ$ , the critical height is given by the dashed curve in Figure 7.



A planar discontinuity surface in an open pit bench.

691 2200

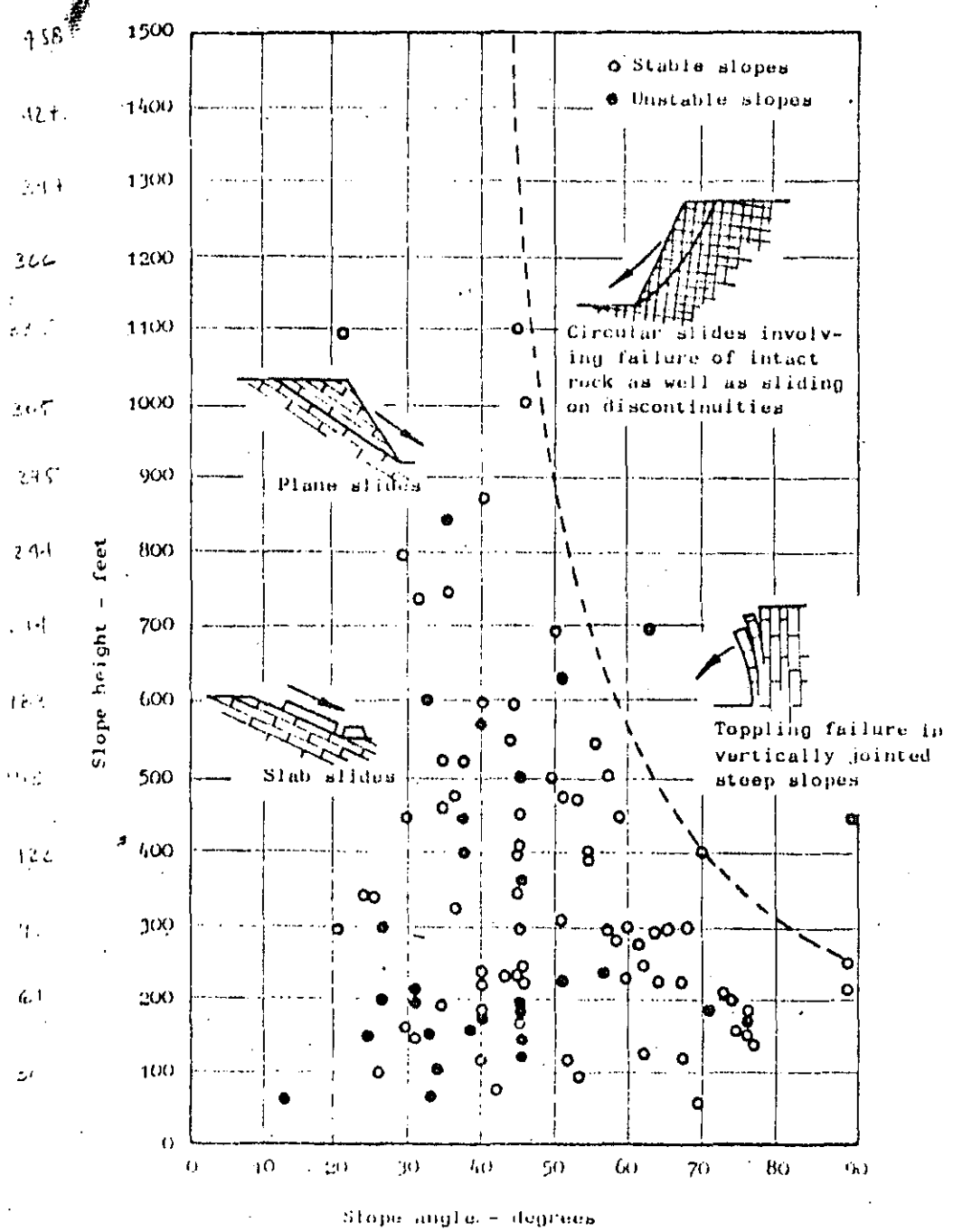
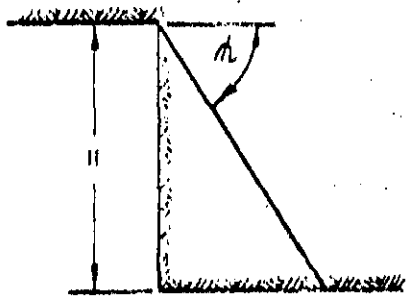
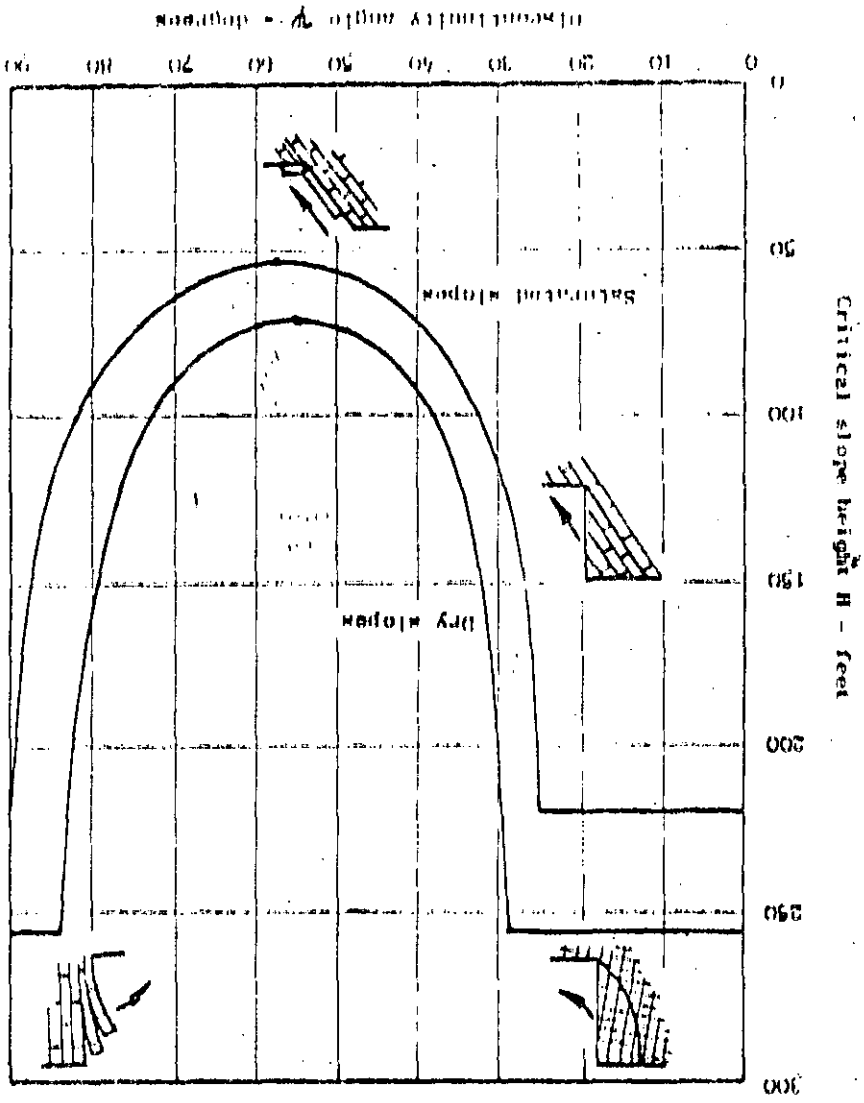


Figure 7 : Slope height versus slope angle relationships for hard rock slopes including data collected by Kley and Lutten<sup>21</sup> and by Ross-Brown<sup>22</sup>.

Figure 11 - Critical height of a vertical slope consisting of a plane of weakness dipping at an angle  $\alpha$ .



discontinuities inclined at 40 to 70°. Clearly the presence, or absence, of such discontinuities will have a very important influence upon the stability of rock slopes and the detection of these geological features is one of the most critical parts of a stability investigation. Techniques for dealing with this problem are discussed in the next chapter of this book.

### Friction, cohesion and density

The material properties which are most relevant to the discussion on slope stability presented in this book are the angle of friction, the cohesive strength and the density of rock and soil masses.

Friction and cohesion are best defined in terms of the plot of shear stress versus normal stress given in Figure 9. This plot is a simplified version of the results which would be obtained if a rock specimen containing a geological discontinuity such as a joint is subjected to a loading system which causes sliding along the discontinuity. The shear stress  $\tau$  required to cause sliding increases with increasing normal stress  $\sigma$ . The slope of the line relating shear to normal stress defines the angle of friction  $\phi$ . If the discontinuity surface is initially cemented or if it is rough, a finite value of shear stress  $\tau$  will be required to cause sliding when the normal stress level is zero. This initial value of shear strength defines the cohesive strength  $c$  of the surface.

The relationship between shear and normal stresses for a typical rock surface or for a soil sample can be expressed as:

$$\tau = c + \sigma \tan \phi \quad (1)$$

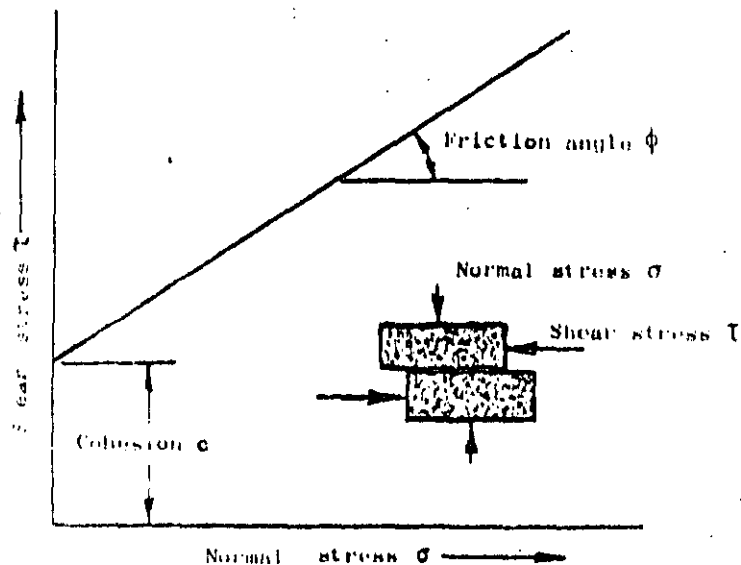


Figure 9 : Relationship between the shear stress  $\tau$  required to cause sliding along a discontinuity to the normal stress  $\sigma$  acting across it .



TABLE 1 - TYPICAL ROCK AND SOIL PROPERTIES

		Density $\gamma$		Friction angle $\phi$		Cohesion $c$			
Type	Material	Kg/m <sup>3</sup>	Lb/ft <sup>3</sup>	Material	Degs.	Material	Kg/m <sup>2</sup>	Lb/ft <sup>2</sup>	
COHESIONLESS	Sand	Dry coarse sand	1440	90	Compacted, well graded, uniform	40-45			
		Dry fine sand	1600	100	Uniform, coarse, medium fine or silty sand	35-40			
		Wet sand	1840	115					
		Very wet sand	1920	120	Loose, well graded sand	35-40			
					Fine dry sand	30-35			
	Gravel	Common mixed	1760	110	Common mixed	35-45			
		River gravel	2240	140	Shingle	40			
		Loose Shingle	1840	115	Sandy compact	40-45			
		Sandy gravel	1920	120	Sandy loose	35-40			
	Waste rock	Granite	1600-2000	100-125	Crushed or broken rock	35-45			
		Basalt and dolerite	1760-2240	110-140	Broken chalk	35-45			
		Limestone and sandstone	1280-1920	80-120	Broken shale	30-35			
Chalk		1000-1280	62-80						
Shale		1600-2000	100-125						
COHESIVE	Clay	Dry clay	1760	110	Dry boulder clay	30	Very stiff boulder clay	17600	3600
		Damp, drained clay	1840	115	Damp, drained boulder clay	40	Hard shaley clay	14600	3000
		Wet clay	1920	120	Stiff clay	10-20	Stiff clay	9800	2000
		Sandy loam	1600	100	Soft clay	5-7	Firm clay	4900	1000
		Marl	1760	110	Clay gouge	10-20	Soft clay	2400	500
		Gravelly clay	2000	125	Calcite shear zone material	20-27			
					Shale fault material	14-22			
	Overburden	Top soil	1360	85	Overburden soil	30-35	Overburden soil	490-	100-
		Dry soil	1440	90				4900	1000
		Moist soil	1600	100					
		Wet soil	1680	105					
	Rock mass	Granite	2614	164	Granite	30-50	Hard rock mass (granite, porphyry etc)	9800-30000	2000-6400
Quartzite		2614	164	Quartzite	30-45				
Sandstone		1950	122	Sandstone	30-45	Sandstone or limestone mass	4900-14600	1000-3000	
Limestone		3169	180	Limestone	30-50				
Porphyry		2580	160	Porphyry	30-40	Shale or soft rock mass	2400-9800	500-2000	
Shale		2400	150	Shale	27-45				
Chalk		1760	110	Chalk	30-40				

Typical values for the angle of friction and cohesion which are found in shear tests on a range of rocks and soils are listed in Table 1 together with densities for these materials. The values quoted in this table are intended to give the reader some idea of the magnitudes which can be expected and they should only be used for obtaining preliminary estimates of the stability of a slope.

There are many factors which cause the shear strength of a rock or soil to deviate from the simple linear dependence upon normal stress illustrated in Figure 9. These variations, together with methods of shear testing, are discussed in a later chapter.

### Sliding due to gravitational loading

Consider a block of weight  $W$  resting on a plane surface which is inclined at an angle  $\psi$  to the horizontal. The block is acted upon by gravity only and hence the weight  $W$  acts vertically downwards as shown in Figure 10. The resolved part of  $W$  which acts down the plane and which tends to cause the block to slide is  $W \sin \psi$ . The component of  $W$  which acts across the plane and which tends to stabilise the slope is  $W \cos \psi$ .

The normal stress  $\sigma$  which acts across the potential sliding surface is given by

$$\sigma = (W \cos \psi) / A \quad (2)$$

where  $A$  is the base area of the block.

Assuming that the shear strength of this surface is defined by equation (1) and substituting for the normal stress from equation (2)

$$r = c + \frac{W \cos \psi}{A} \cdot \tan \phi$$

$$\text{or } R = cA + W \cos \psi \cdot \tan \phi \quad (3)$$

where  $R = rA$  is the shear force which resists sliding down the plane.

The block will be just on the point of sliding or in a condition of *limiting equilibrium* when the disturbing force acting down the plane is exactly equal to the resisting force:

$$W \sin \psi = cA + W \cos \psi \cdot \tan \phi \quad (4)$$

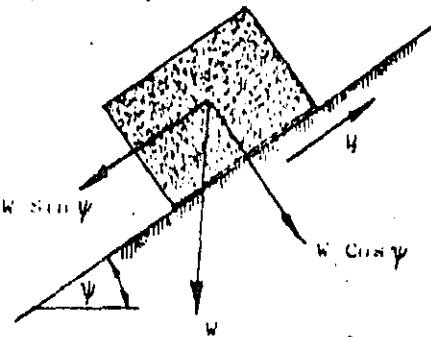
If the cohesion  $c = 0$ , the condition of limiting equilibrium defined by equation (4) simplifies to

$$\psi = \phi \quad (5)$$

### Influence of water pressure shear strength

The influence of water pressure upon the shear strength of two surfaces in contact can most effectively be demonstrated by the beer can experiment.

An opened beer can rests on an inclined piece of wood as shown in Figure 11a. (Drink the beer and refill the can with water if you wish to keep the cost of this experiment



to a minimum). The forces which act in this case are precisely the same as those acting on the block of rock in Figure 10 but, for simplicity, the cohesion between the beer can base and the wood is assumed to be zero. According to equation (5), the can with its contents of water will slide down the plank when  $\psi_1 = \phi$ .

The base of the can is now punctured so that water can enter the gap between the base and the plank, giving rise to a water pressure  $u$  or to an uplift force  $U = uA$ , where  $A$  is the base area of the can.

The normal force  $W \cos \psi_2$  is now reduced by this uplift force  $U$  and the resistance to sliding is now

$$R = (W \cos \psi_2 - U) \tan \phi \quad (6)$$

If the weight per unit volume of the can plus water is defined as  $\gamma_c$  while the weight per unit volume of the water is  $\gamma_w$ , then  $W = \gamma_c \cdot h \cdot A$  and  $U = \gamma_w \cdot h_w \cdot A$ , where  $h$  and  $h_w$  are the heights defined in the sketch opposite. From this sketch it will be seen that  $h_w = h \cdot \cos \psi_2$  and hence

$$U = \frac{\gamma_w}{\gamma_c} \cdot W \cos \psi_2 \quad (7)$$

Substituting in (6)

$$R = W \cdot \cos \psi_2 (1 - \gamma_w/\gamma_c) \tan \phi \quad (8)$$

and the condition for limiting equilibrium defined in equation (4) becomes

$$\tan \psi_2 = (1 - \gamma_w/\gamma_c) \tan \phi \quad (9)$$

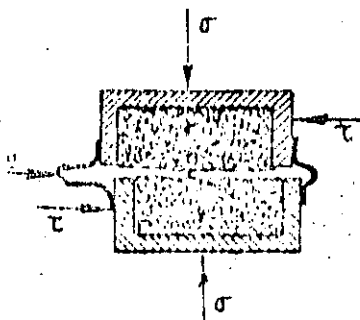
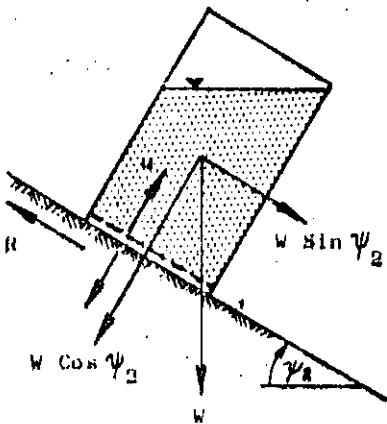
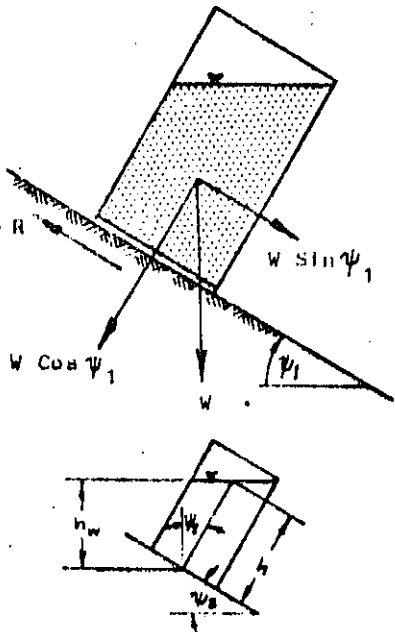
Assuming the friction angle of the can/wood interface is  $30^\circ$ , the unpunctured can will slide when the plane is inclined at  $\psi_1 = 30^\circ$  (from equation (5)). On the other hand, the punctured can will slide at a much smaller inclination because the uplift force  $U$  has reduced the normal force and hence reduced the frictional resistance to sliding. The total weight of the can plus water is only slightly greater than the weight of the water only. Assuming  $\gamma_w/\gamma_c = 0.9$  and  $\phi = 30^\circ$ , equation (9) shows that the punctured can will slide when the plane is inclined at  $\psi_2 = 3^\circ 18'$ .

### The effective stress law

The effect of water pressure on the base of the punctured beer can is the same as the influence of water pressure acting on the surfaces of a shear specimen as illustrated in the sketch opposite. The normal stress  $\sigma$  acting across the failure surface is reduced to the *effective stress* ( $\sigma - u$ ) by the water pressure  $u$ . The relationship between shear strength and normal strength defined by equation (1) now becomes

$$\tau = c + (\sigma - u) \tan \phi \quad (10)$$

In most hard rocks and in many sandy soils and gravels, the cohesive and frictional properties ( $c$  and  $\phi$ ) of the materials are not significantly altered by the presence of water and hence, reduction in shear strength of these

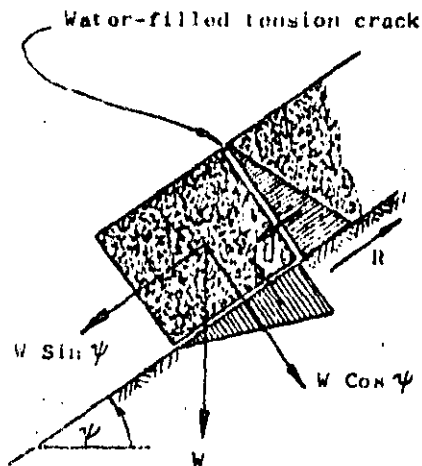


materials is due, almost entirely to the reduction of normal stress across failure surfaces. Consequently, it is *water pressure* rather than *moisture content* which is important in defining the strength characteristics of hard rocks, sands and gravels. In terms of the stability of slopes in these materials, the presence of a small volume of water at high pressure, trapped within the rock mass, is more important than a large volume of water discharging from a free draining aquifer.

In the case of soft rocks such as mudstones and shales and also in the case of clays, both cohesion and friction can change markedly with changes in moisture content and it is necessary, when testing these materials, to ensure that the moisture content of the material during test is as close as possible to that which operates in the field. Note that the effective stress law defined in equation (10) still applies to these materials but that, in addition,  $c$  and  $\phi$  change.

#### The effect of water pressure in a tension crack

Consider the case of the block resting on the inclined plane but, in this instance, assume that the block is split by a tension crack which is filled with water. The water pressure in the tension crack increases linearly with depth and a total force  $V$ , due to this water pressure acting on the rear face of the block, acts down the inclined plane. Assuming that the water pressure is transmitted across the intersection of the tension crack and the base of the block, the water pressure distribution illustrated in the sketch opposite occurs along the base of the block. This water pressure distribution results in an uplift force  $U$  which reduces the normal force acting across this surface.



The condition of limiting equilibrium for this case of a block acted upon by water forces  $V$  and  $U$  in addition to its own weight  $W$  is defined by

$$W \sin \psi + V = cA + (W \cos \psi - U) \tan \phi \quad (11)$$

From this equation it will be seen that the disturbing force tending to induce sliding down the plane is increased and the frictional force resisting sliding is decreased and hence, both  $V$  and  $U$  result in decreases in stability. Although the water pressures involved are relatively small, these pressures act over large areas and hence the water forces can be very large. In many of the practical examples considered in later chapters, the presence of water in the slope giving rise to uplift forces and water forces in tension cracks is found to be critical in controlling the stability of slopes.

#### Reinforcement to prevent sliding.

One of the most effective means of stabilising blocks or slabs of rock which are likely to slide down inclined discontinuity surfaces is to install tensioned rockbolts or cables. Consider the block resting on the inclined plane and acted upon by the uplift force  $U$  and the force  $V$  due to water pressure in the tension crack. A rockbolt, tensioned to a load  $T$  is installed at an angle  $\beta$  to the plane as shown. The resolved components of  $T$  are

T acting parallel to the plane is  $T \cos \beta$  while the component acting across the surface upon which the block rests is  $T \sin \beta$ . The condition of limiting equilibrium for this case is defined by

$$W \sin \psi + V - T \cos \beta = cA + (W \cos \psi - U + T \sin \beta) \tan \phi \quad (12)$$

This equation shows that the bolt tension reduces the disturbing force acting down the plane and increases the normal force and hence the frictional resistance between the base of the block and the plane.

The minimum bolt tension required to stabilise the block is obtained by differentiation of equation (12) with respect to the angle  $\beta$  and this shows that the optimum bolt inclination is given by

$$\beta = \phi \quad (13)$$

#### Factor of safety of a slope

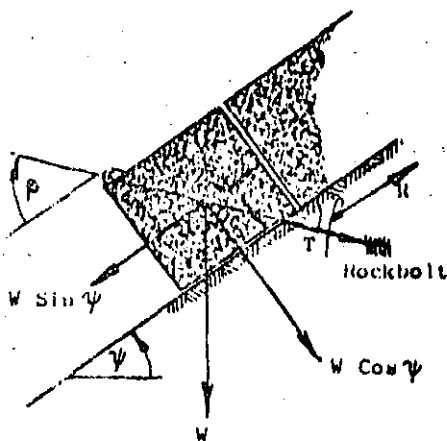
All the equations defining the stability of a block on an inclined plane have been presented for the condition of *limiting equilibrium*, i.e. the condition at which the forces tending to induce sliding are exactly balanced by those resisting sliding. In order to compare the stability of slopes under conditions other than those of limiting equilibrium, some form of index is required and the most commonly used index is the *Factor of Safety*. This can be defined as the ratio of the total force available to resist sliding to the total force tending to induce sliding. Considering the case of the block acted upon by water forces and stabilised by a tensioned rockbolt (equation 12), the factor of safety is given by

$$F = \frac{cA + (W \cos \psi - U + T \sin \beta) \tan \phi}{W \sin \psi + V - T \cos \beta} \quad (14)$$

Note that the condition of limiting equilibrium is represented by a factor of safety  $F = 1$ . Stable slopes must obviously have a factor of safety in excess of unity and a vital question for the slope engineer is - what value for the factor of safety should be used for design purposes?

This is one of the most controversial questions in rock engineering and many eminent engineers have argued that, because of the uncertainty associated with the input data for a factor of safety calculation, the value obtained is too unreliable to have relevance in engineering design.

Some authors have suggested that a *probabilistic* approach is more meaningful in that the safety of a slope can be assessed in terms of the variation of each of the factors which control its stability<sup>23,24,25</sup>. Although this approach has many attractive features, it has two drawbacks which have inhibited its development as a design tool. The first of these is the difficulty of obtaining adequate input data for a meaningful statistical analysis of all the parameters involved. The second drawback is associated with the average engineer's lack of understanding of statistical concepts and of the mathematical jargon which is so freely used in discussions on this subject. How does one relate the adequacy of a design to a probability of failure of 1 in 100,000? Indeed, to some clients, the



admission, by a consulting engineer, that there is a possibility of failure, however small, is totally unacceptable.

The author does not consider these drawbacks to be so serious that they will not be overcome in time and it is more than likely that the use of a factor of safety will eventually be replaced by some design index which has been determined by probabilistic methods. However, in the absence of acceptable statistical methods, the design engineer of today is still faced with the problem of how to compare a number of alternative slope designs or to assess the stability of an existing slope.

The most satisfactory solution to this problem is to carry out a *sensitivity analysis* of the influence of each variable upon the stability of the slope and to use the results of this analysis as a basis for engineering decisions. There are several ways in which such an analysis can be done and a simple example is given in Figure 2 on page 9 which shows the variation in factor of safety of a particular slope with changes in slope angle and groundwater conditions. Other types of sensitivity analysis will be illustrated in later chapters of this book in which detailed analyses of practical slope problems are presented.

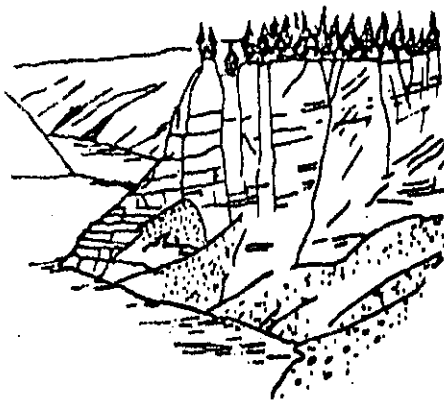
The merit of such a sensitivity analysis is that it does not place too much emphasis upon the *absolute* value of the factor of safety or of any other index which is used to measure the stability of a slope. The *relative* values of the index, for a range of different conditions, can usually be determined with reasonable accuracy and these relative values, together with sound engineering common sense, will usually provide an adequate basis for a practical slope design.

#### Slope failure due to toppling

One of the limitations of the factor of safety computed from equation (14) is that it is based upon sliding of the block and does not allow for rotational or toppling failure. The simplest conditions under which toppling can occur can be deduced by returning to the model of a block resting on an inclined plane. In this case, the shape of the block as well as its weight is important. This shape is defined by the height  $h$  and width  $b$  as illustrated in Figure 10a.

The condition for toppling is defined by the position of the weight vector in relation to the base of the block. If the weight vector, which passes through the centre of gravity of the block, falls outside the base of the block, toppling will occur.

In Figure 10b, the conditions for toppling and sliding are plotted. The criterion for sliding is based upon friction only (equation (5)) and a friction angle  $\phi = 35^\circ$  has been assumed. From this figure it will be seen that the danger of toppling increases with increasing discontinuity angle and steep slopes in vertically jointed rocks frequently exhibit signs of toppling failure<sup>26,27,28</sup>.



Suggested toppling failure mechanism of north face of Vajont slide. After Hofmann<sup>26</sup> and Muller<sup>27</sup>.

$c = 0$



Potential toppling condition

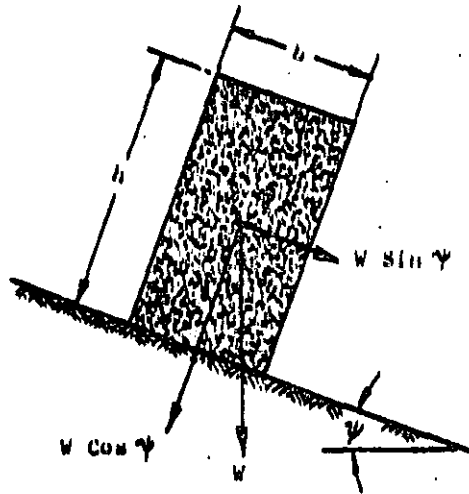


Figure 10a: Geometry of block on inclined plane

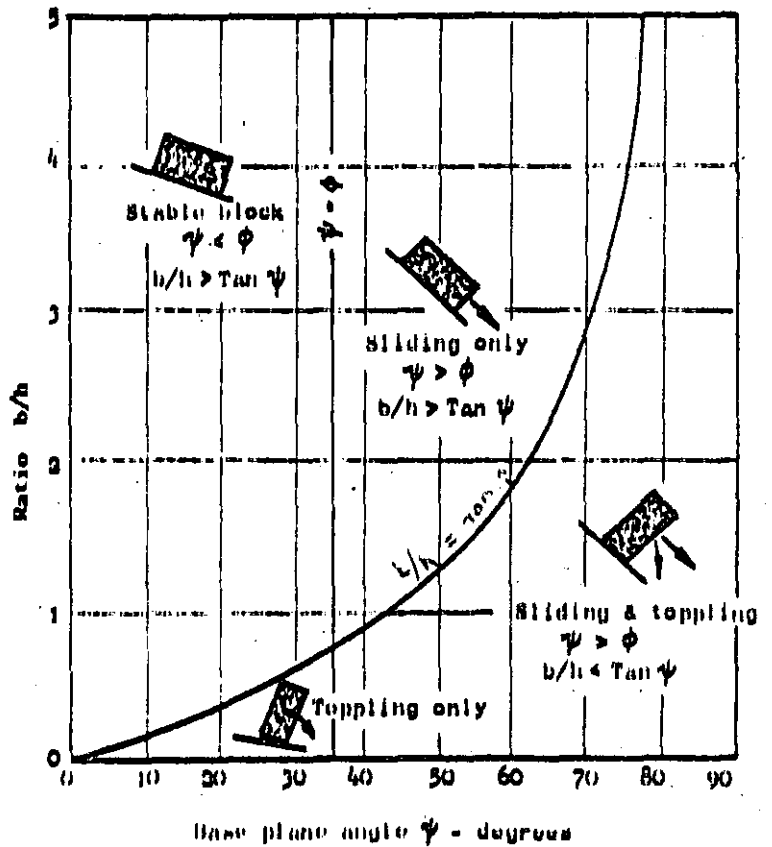
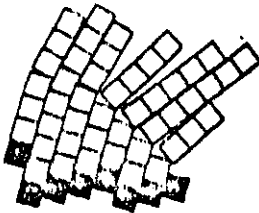
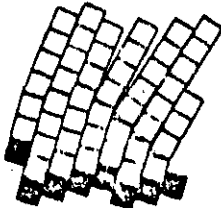
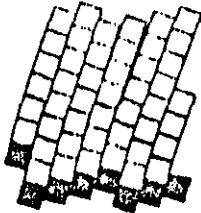
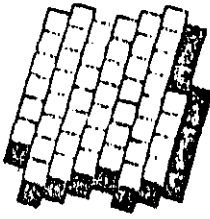
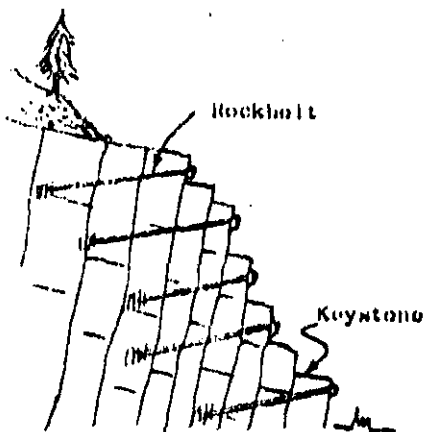


Figure 10b: Conditions for sliding and toppling of a block on an inclined plane.



Computer produced drawings  
of toppling failure. After  
Cundall<sup>20</sup>.

(Dark blocks are fixed)



Rock reinforcement to prevent  
toppling failure.

In an actual rock slope consisting of a large number of blocks of irregular shape, simple toppling such as that illustrated in Figure 10 will seldom occur. Failure will involve complex movement, both sliding and toppling, of blocks which will be in contact with surrounding blocks and will, therefore, be restricted in their movements. No satisfactory analytical techniques for dealing with this complex situation are currently available although a promising start on the development of such techniques has been made by Cundall<sup>20</sup>.

A useful qualitative technique for studying the possibility of toppling failure in a rock slope with steeply inclined discontinuities is illustrated in Figure 11. This method employs the same friction principle proposed by Goodman<sup>29</sup> and depends upon the simulation of gravitational loading by the frictional forces exerted on the base of a model when the paper on which it rests is pulled from under the model. The model can be constructed from any suitable material which happens to be available; the plastic blocks which make up children's toys such as "Lego" being ideal for simple models. In the example illustrated in Figure 11 a sheet of cork, such as that used for making gaskets for motor car engines, has been used as the model material. The geometry of the slope under consideration is traced onto the cork and the discontinuities are then cut by means of a modelling knife. A drawing board with a parallel movement system makes an ideal base for the model and the frictional load exerted on the base of the model as it is pushed over the surface of the board provides a remarkably accurate simulation of gravity loading<sup>30</sup>.

Although the results obtained from such a model are qualitative, they do provide the engineer or geologist with an understanding of the possible failure modes which are likely to occur in a particular slope and thereby enable him to arrive at a rational decision on how the problem should be tackled.

### Reinforcement to prevent toppling

The conditions for toppling defined in Figure 10 show that the danger of this type of failure occurring is greatest when tall slender rock columns are present in a slope. The principal aim of reinforcement, in the forms of rockbolts or cables, installed to prevent toppling should be to tie these columns together to form wider blocks. It is particularly important that the "keystone" which prevents the front face of the slope from moving should be identified and securely anchored since loss of the restraining action of this block will initiate a progressive failure process in the slope.

It is unlikely that attempts to stabilise a rock slope, in which toppling is the dominant failure mechanism, by drainage would be successful since the structure of the rock mass is disturbed to a much greater extent than in the case of failure by sliding and the slope is therefore self-draining.



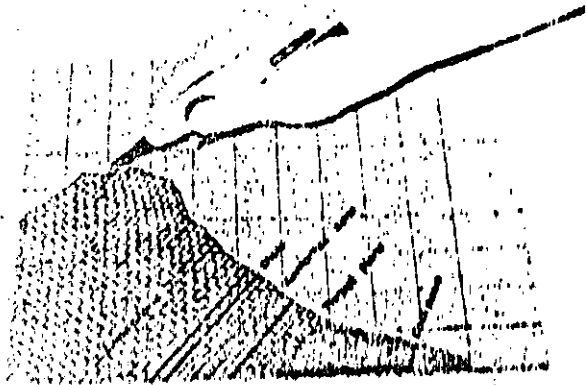


Figure 11a : Model is cut out from a sheet of cork with a modelling knife. The model in this case is of the Frank slide in Alberta, Canada which occurred in 1903 and which is discussed by Coates<sup>32</sup> and Terzaghi<sup>33</sup>.

Figure 11b : Model resting on a drawing board. Upward displacement of the parallel movement of the board results in the base of the model being subjected to frictional forces which simulate gravitational loading.

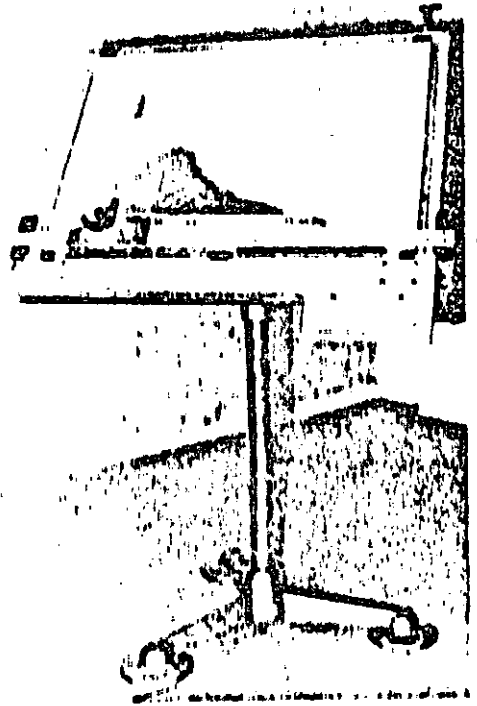


Figure 11c : The Frank slide as it is today. The slide involved approximately 30 million tons of rock and mining of a coal seam at the base of the mountain may have been partially responsible for this failure.

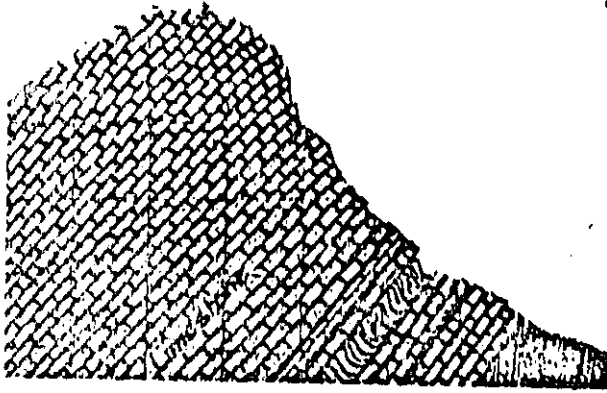


Figure 11d : Original profile of Turtle mountain on which the Frank slide occurred.

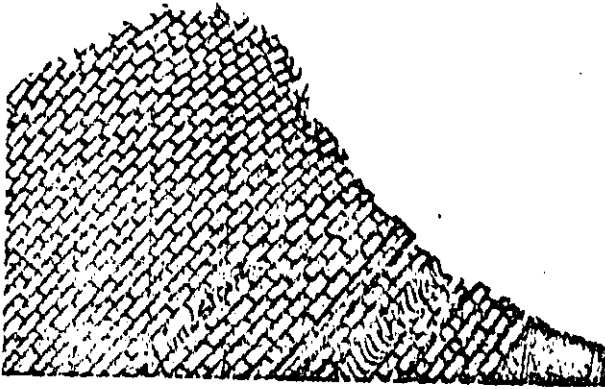


Figure 11e : Bending of strata on mountain top and start of block movement.

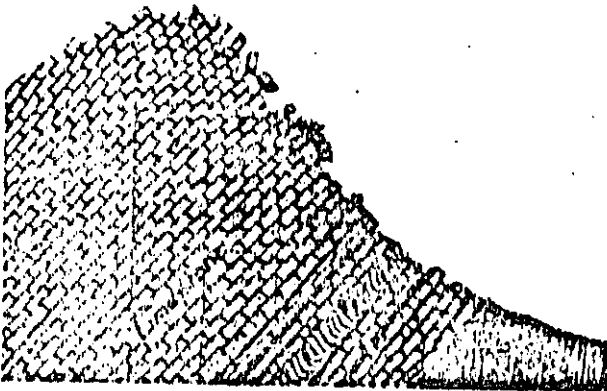


Figure 11f : Toppling and rolling of rock blocks

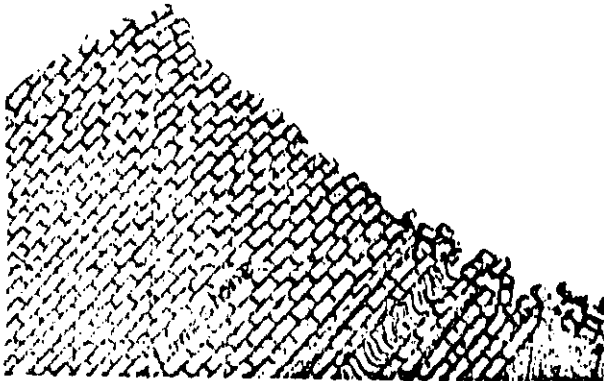
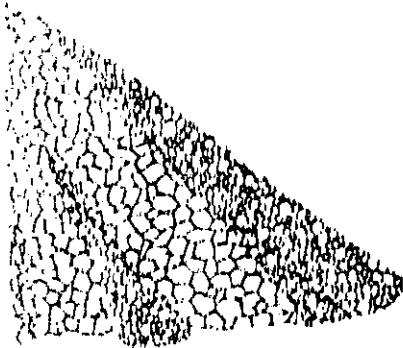
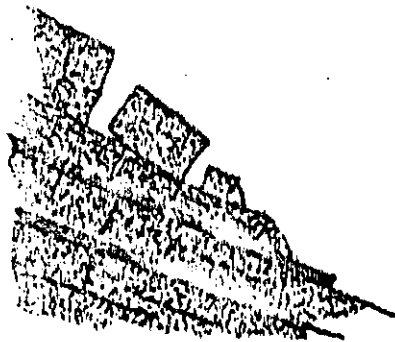


Figure 11g : Stable slope remaining after slide.

### Angle of repose of waste dumps



Waste rock dump



Stratified rock mass

A question which frequently arises in discussions on open cast mine slope design is whether the slope angle can be chosen on the basis of the angle of repose of waste dumps. The answer is a most emphatic no because the geometry of the rock mass is entirely different from that of the packing pattern in the waste rock. Although the rock mass may be heavily fractured, this fracturing generally follows systematic patterns and failure, when it occurs, usually follows a continuous feature such as a joint or a bedding plane. This is not the case in a waste rock pile in which no regular discontinuity pattern exists and in which failure involves a complex movement path for each individual piece of rock. The groundwater conditions in the rock slope and in the waste pile are also significantly different because of the differences in the drainage characteristics of the two systems.

Table I shows that the effective friction angle for waste rock generally lies between 35 and 45° and the angle of repose of waste rock dumps is frequently found to be approximately 38°. Failures in waste rock dumps can and do occur due to a variety of causes, most of which are associated with sliding on the surface upon which the dump has been placed or breakage of particles within the dump. These factors will be examined in more detail in a later chapter.

An interesting corollary to this difference between the behaviour of a waste rock dump and a rock mass is the proposal which is sometimes put forward to stabilise a slide by breaking up the plane on which sliding occurs by means of carefully placed blasts. This proposition is discussed by Zaruba and Mano<sup>20</sup> and they conclude that the technique is unreliable and that the risk of inducing a major slide by blasting probably outweighs the advantage of a slight increase in stability which may be achieved if the blast can be successfully carried out. The author is in complete agreement with this assessment and would not recommend this method of slope stabilisation except under very unusual conditions and subject to the control of a blasting specialist.

### Slope failure induced by weathering

Engineers are sometimes so concerned with the mechanics of slope failure that they forget that rock does not have the same predictable behaviour characteristics as man-made engineering materials such as steel and concrete. Weathering, which results in a progressive deterioration of the properties of the rock with time, is a factor which is sometimes not assigned sufficient importance by engineers.

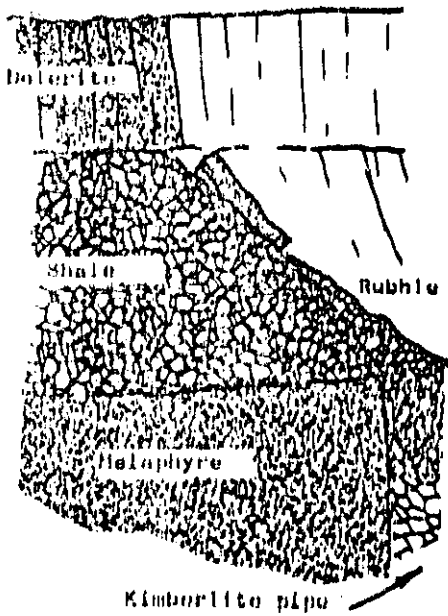
A complete discussion on weathering exceeds the scope of this handbook and the interested reader is referred to the extensive literature on the subject, recently reviewed by Saunders and Pookes<sup>21</sup>. One example will serve to warn the reader of the type of problem which may arise in rock slopes as a result of weathering.

The de Beer's diamond mine at Kimberley in South Africa is currently being re-opened, having ceased operations in 1908.



Slope in weathered surface material.

As shown in the sketch opposite, the vertically jointed dolerite which occurs on the surface rests on a thick bed of shale. This shale, which is a good medium/hard rock in its unweathered state, gradually weathers on exposure to a residual soil. This weathered material has a cohesive strength of zero and a friction angle of approximately  $32^{\circ}$  and progressive failure of the originally steep slopes in the shale has induced failure in the overlying dolerites as illustrated in the photograph reproduced below.



Approximate section through the de Boer's diamond mine.



Upper slopes on the de Boer's diamond mine at Kimberley in South Africa. Failure of the vertically jointed dolerite is induced by progressive weathering of the underlying shales.

## Selected reference on slope behaviour.

11. BLAKE, W. Stresses and displacements surrounding an open pit in a gravity loaded rock. *U.S. Bureau of Mines Report of Investigations* 7002, Aug. 1967, 20p.
12. BLAKE, W. Finite element model is excellent pit tool. *Mining Engineering, A.I.M.E.*, Vol. 21, No. 8, 1969, pp. 79-80.
13. YU, Y.H., GYENGE, M. and COATES, D.P. Comparison of stress and displacement in a gravity loaded slope by photoelasticity and finite element analysis. *Canadian Dept. Energy, Mines and Resources Report MR 6R-24 1D*, 1968.
14. WANG, F.D. and SUN, M.C. Slope stability analysis by finite element stress analysis and limiting equilibrium method. *U.S. Bureau of Mines Report of Investigations* 7341, January 1970, 16p.
15. STACKY, T.R. The stresses surrounding open-pit mine slopes. *Planning open pit mines*, Johannesburg Symposium 1970. Published by A.A. Balkema, Amsterdam, 1971. pp.199-207.
16. HOKK, K. The influence of structure upon the stability of rock slopes. *Proc. 1st Symposium on Stability in Open Pit Mining, Vancouver 1970*. A.I.M.E., New York, 1971, p49-63.
17. TERZAGHI, K. Stability of steep slopes on hard unweathered rock. *Geotechnique*. Vol. 12, 1962, pp.251-270.
18. MULLER, L. The European approach to slope stability problems in open-pit mines. *Proc. Third Symposium on Rock Mechanics, Colorado School of Mines Quarterly*. Vol. 54, No. 3, 1959, pp.116-133.
19. GOODMAN, R.E., TAYLOR, R.L. and BREKKE, T.L. A model for the mechanics of jointed rock. *J. Soil Mech. Foundation Div.* Vol. 94, No. SM6, 1968, p.637.
20. CUNDALL, P.A. A computer model for simulating progressive large-scale movements in blocky rock systems. *Proc. Symposium on Rock Fracture*. Nancy, France. October 1971. Section 2-8.
21. KIRBY, R.J. and LUTTON, R.J. Engineering properties of nuclear craters: a study of selected rock excavations as related to large nuclear craters. *Report U.S. Army Engineers*, No. PNL 5010 1967, 159p.
22. ROSS-BROWN, D.R. Slope design in opencast mines. *Ph.D. Thesis*, London University, in preparation.
23. MCMAHON, H.K. A statistical method for the design of rock slopes. *Proc. 1st Australia-New Zealand Conference of Geomechanics*, Melbourne, August 1971.

24. SHUK, T. Optimisation of slopes designed in rock. *Proc. 2nd Congress Intl. Society of Rock Mechanics, Belgrade, 1970, Vol. 2, Section 7-2.*
25. LANGEJAN, A. Some aspects of safety factors in soil mechanics considered as a problem of probability. *Proc. 6th Intl. Conference on Soil Mech. and Foundation Engineering, Montreal 1965, Vol. 2, pp.500-502.*
26. HOFMANN, H. The deformation process of regularly jointed discontinuum during the excavation of a cut (in German). *Proc. 2nd Congress Intl. Society of Rock Mechanics, Belgrade 1970, Vol. 2, Section 7-1.*
27. MÜLLER, L. The rock slide in the Valont Valley. *Rock Mechanics and Engineering Geology, Vol. 11/3-4, 1964.*
28. ZARUBA, Q. and MENCÍ, V. *Landslides and their control.* Academia press, Prague, 1969, 205 p. (available through Kluwer, London, New York and Amsterdam).
29. GOODMAN, R.W. Geological investigations to evaluate stability. *Proc. and Symposium on stability for Open Pit Mining, Vancouver, November 1971.* Publishers A.I.M.E., New York - in press.
30. ASHBY, J.P. Sliding and toppling modes of failure in models and jointed rock slopes. *M.Sc. Thesis, Univ. of London (Imperial College), 1971, 40 p.*
31. SAUNDERS, M.K. and POOKES, P.G. A review of the relationship of rock weathering and climate and its significance to foundation engineering. *Engineering Geology, Vol. 4, 1970, pp.289-325.*
32. COATES, D.F. *Rock Mechanics Principles.* Canadian Department of Energy, Mines and Resources, Mines Branch Monograph 874, 1965, 300 p.
33. TERZAGHI, K. *Mechanism of Landslides in Application of Geology to Engineering Practice (Berkey Volume).* Geological Society of America, 1950, p 84-127.

### Introduction

The dominant role of geological discontinuities in rock slope behaviour has already been emphasised and few engineers or geologists would question the need to base stability calculations upon an adequate set of geological data. But what is an adequate set of data? What type of data and how much detailed information should be collected for a stability analysis?

This question is rather like the question of which came first - the chicken or the egg? There is little point in collecting data for slopes which are not critical but critical slopes can only be defined if sufficient information is available for their stability to be evaluated. The data gathering must, therefore, be carried out in two stages as suggested in Figure 6.

The first stage involves an examination of existing regional geology maps, air photographs, easily accessible outcrops and the core recovered during exploration drilling. A preliminary analysis of this data will indicate slopes which are likely to prove critical and which require more detailed analysis.

The second stage involves a much more detailed examination of the geological features of these critical regions and may require the drilling of special holes outside the ore body, excavation of trial pits or adits and the detailed mapping and testing of discontinuities.

An important aspect of the geological investigations, in either the first or second stages, is the presentation of the data in a form which can be understood and interpreted by others who may be involved in the stability analysis or who may be brought in to check the results of such an analysis. This means that everyone concerned must be aware of precisely what is meant by the geological terms used and must understand the system of data presentation.

The following definitions and graphical techniques are offered for the guidance of the reader who may not already be familiar with them. There is no implication that these are the best definitions or techniques available and the reader who has become familiar with different methods should certainly continue to use those. What is important is that the techniques which are used in any study should be clearly defined in documents relating to that study so that errors arising out of confusion are avoided.

### Definition of geological terms

*Rock Material* or intact rock, in the context of this discussion, refers to the consolidated and cemented assemblage of mineral particles which form the intact blocks between discontinuities in the rock mass. In most hard igneous and metamorphic rocks, the strength of the intact rock is one or two orders of magnitude greater than that of the rock mass and failure of this intact material is not generally involved in the processes of slope failure. In softer sedimentary rocks, the intact material may be relatively weak and failure of this material may play an important part in slope failure.

*Rock mass* is the *in-situ* rock which has been rendered discontinuous by systems of structural features such as joints, faults and bedding planes. Slope failure in a rock mass is generally associated with movement on these discontinuity surfaces.



An ordered structural pattern in slate.

*Waste rock* or broken rock refers to a rock mass which has been disturbed by some mechanical agency such as blasting, ripping or crushing so that the interlocking nature of the *in-situ* rock has been destroyed. The behaviour of this waste or broken rock is similar to that of a clean sand or gravel, the major differences being due to the angularity of the rock fragments.

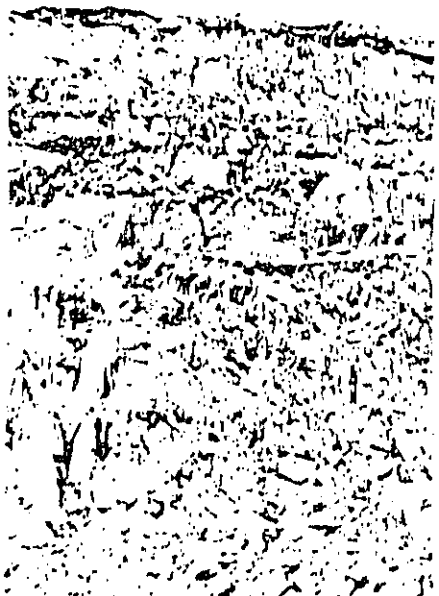
*Discontinuities* or weakness planes are those structural features which separate intact rock blocks within a rock mass. Many engineers describe these features collectively as *joints* but this is an over-simplification since the mechanical properties of these features will vary according to the process of their formation. Hence, faults, dykes, bedding planes, cleavage, tension joints and shear joints will all exhibit distinct characteristics and will respond in different ways to applied loads. A large body of literature dealing with this subject is available and the interested reader is referred to this for further information<sup>34, 35, 36</sup>. For the purposes of this discussion, the term *discontinuity* will generally be used to define the structural weakness plane upon which movement can take place. The type of discontinuity will be referred to when the description provides information which assists the slope designer in deciding upon the mechanical properties which will be associated with a particular discontinuity.

*Major discontinuities* are continuous planar structural features such as faults which may be so weak, as compared with any other discontinuity in the rock mass, that they dominate the behaviour of a particular slope. Many of the large failures which have occurred in open pit mines have been associated with faults and particular attention should be paid to tracing these features.

*Discontinuity sets* refers to systems of discontinuities which have approximately the same inclination and orientation. As a result of the processes involved in their formation<sup>34</sup>, most discontinuities occur in families which have preferred directions. In some cases, these sets are clearly defined and easy to distinguish while, in other cases, the structural pattern appears disordered.

*Continuity*. While major structural features such as faults may run for many tens of feet or even miles, smaller discontinuities such as joints may be very limited in their extent. Failure in a system where discontinuities terminate within the rock mass under consideration will involve failure of the intact rock bridges between these discontinuities. Continuity also has a major influence upon the permeability of a rock mass since this depends upon the extent to which discontinuities are hydraulically connected.

Continuity or persistence is the most difficult geological parameter to define and, as far as the author is aware, no satisfactory system for reliable evaluation of continuity is available. Jennings and his co-workers in South Africa<sup>37, 38, 39</sup> have attempted to measure continuity and to



An apparently disordered structural pattern in hard rock.



use these measurements to estimate the cohesive strength of potential failure planes. This author does not believe that continuity can be quantified in this way and prefers to err on the side of safety - if in doubt, assume that all discontinuities are continuous. Cohesive strength is estimated by other methods which will be described later.

*Gouge* or infilling is the material between two faces of a structural discontinuity such as a fault. This material may be the debris resulting from the sliding of one surface upon another or it may be material which has been precipitated from solution or caused by weathering. Whatever the origin of the infilling material in a discontinuity, its presence will have an important influence upon the shear strength of that discontinuity. If the thickness of the gouge is such that the faces of the discontinuity do not come into contact, the shear strength will be equal to the shear strength of the gouge. If the gouge layer is thin so that contact between asperities on the rock surfaces can occur, it will modify the shear strength of the discontinuity but will not control it<sup>40</sup>.

*Roughness*. Patton<sup>41,42</sup> emphasised the importance of surface roughness on the shear strength of structural discontinuities in rock. This roughness occurs on both a small scale, involving grain boundaries and failure surfaces, and on a large scale, involving folds and flexures in the discontinuity. The mechanics of movement on rough surfaces will be discussed in the chapter dealing with shear strength.

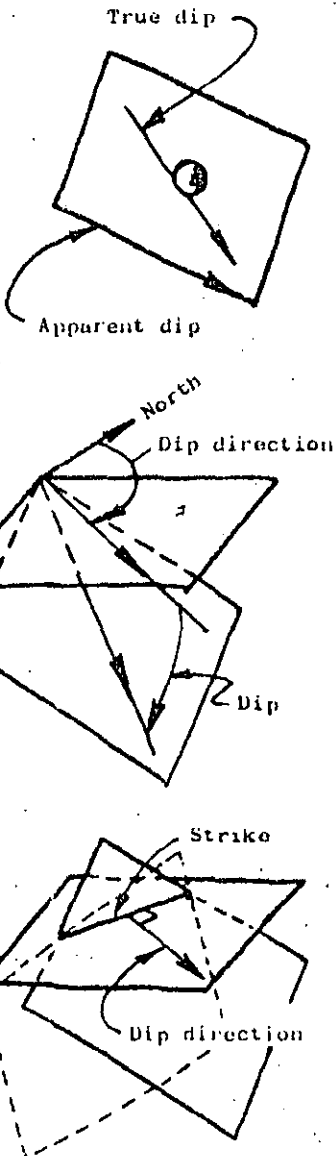
#### Definition of geometrical terms

*Dip* is the *maximum* inclination of a structural discontinuity plane to the horizontal. It is sometimes very difficult, when examining an exposed portion of an obliquely inclined plane, to visualise the *true dip* as opposed to the *apparent dip* which is the inclination of an arbitrary line on the plane. The apparent dip is always smaller than the true dip.

One of the simplest models which can be used in thinking about the definition of the dip of a plane is to consider a ball rolling down an obliquely inclined plane. The path of the ball will always lie along the line of maximum inclination which corresponds to the true dip of the plane.

*Dip direction* or dip azimuth is the direction measured clockwise from North, of the horizontal trace of the line of dip. In terms of the ball rolling down the oblique plane, it is the angle, measured clockwise in degrees on the compass dial, which the direction of rolling would take from true North.

*Strike* is the trace of the intersection of an obliquely inclined plane with a horizontal reference plane and it is at right angles to the dip and dip direction of the oblique plane. The practical importance of the strike of a plane is that it is the visible trace of a discontinuity which is seen on the horizontal surface of a rock mass. The disadvantage of using this term in slope analysis is that there are in fact *two* planes with the same dips and strikes as shown on the sketch opposite and, unless a strict convention is adopted in terms of the direction in which the strike is measured, confusion can easily arise.



For this reason, the term *strike* when it is used in this book, will always be defined as:

$$\text{Strike} = (\text{dip direction} - 90^\circ)$$

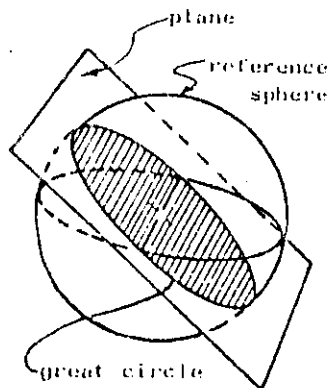
*Preferred terms.* In order to avoid the confusion which can arise from using *strike*, particularly when a number of engineers and geologists are involved in analysing the same set of data, many slope designers have turned to using dip and dip direction as the preferred terms for the presentation of all structural data. The same system has been adopted by the author and all the examples presented in this book are in terms of dip and dip direction.

### Graphical techniques for data presentation

One of the most important aspects of rock slope analysis is the systematic collection and presentation of geological data in such a way that it can easily be evaluated and incorporated into stability analyses. Experience has shown that spherical projections provide a convenient means for the presentation of geological data. The engineer or geologist, who is not familiar with this technique, is strongly advised to study the following pages carefully. A few hours invested in such a study can save many hours of frustration and confusion later when the reader becomes involved in studying designs and reading reports in which these methods have been used.

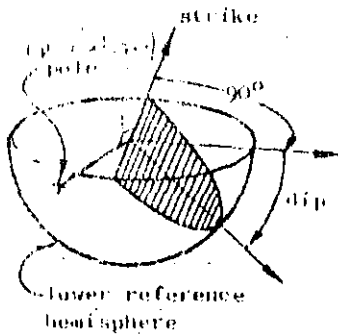
Many engineers shy away from spherical projection methods because they are unfamiliar and because they appear complex, bearing no recognisable relationship to more conventional engineering drawing methods. For many years the author regarded these graphical methods in the same light but, faced with the need to analyse three-dimensional rock slope problems, an effort was made, with the aid of a patient geologist colleague, and the mystery associated with these techniques was rapidly dispelled. This effort has since been repaid many times by the power and flexibility which these graphical methods provide for the rock engineer.

Several types of spherical projection can be used and a comprehensive discussions on these methods have been given by Phillips<sup>43</sup>, Turner and Weiss<sup>36</sup>, Badgley<sup>44</sup> and Friedman<sup>45</sup>. The projection which is used exclusively in this book is the *equal area projection*, sometimes called the Lambert projection or the Schmidt net.



### Equal-area projection

The Lambert equal area projection will be familiar to most readers as the system used by geographers to represent the spherical shape of the earth on a flat surface. In adapting this projection to structural geology, the traces of planes on the surface of a reference sphere are used to define the dips and dip directions of the planes. Imagine a reference sphere which is free to move in space but which is *not* free to rotate in any direction; hence any radial line joining a point on the surface to the centre of the sphere will have a fixed direction in space. If this sphere is now moved so that its centre lies on the plane under consideration, the great circle which is traced



out by the intersection of the plane and the sphere will uniquely define the inclination and orientation of the plane in space. Since the same information is given on both upper and lower parts of the sphere, only one of these need be used and, in engineering applications, the *lower reference hemisphere* is used for the presentation of data.

In addition to the great circle, the inclination and orientation of the plane can also be defined by the *pole* of the plane. The pole is the point at which the surface of the sphere is pierced by the radial line which is normal to the plane.

In order to communicate the information given by the great circle and the position of the pole on the surface of the lower reference hemisphere, a two dimensional representation is obtained by projecting this information onto the horizontal or equatorial reference plane. The method of projection is illustrated in Figure 12a and 12b illustrates the polar and equatorial projections of a sphere.

Polar and equatorial equal-area nets are presented in Figure 13 for use by the reader. Good undistorted copies or photographs of these nets will be useful in following the examples given in this chapter and later in the book.

The most practical method of using the stereonet for plotting structural information is to mount it on a base-board of  $\frac{1}{4}$  inch thick plywood as shown in Figure 14. A sheet of clear plastic film of the type used for drawing on for overhead projection, mounted over the net and fixed with *nellotape* around its edges, will keep the stereonet in place and will also protect the net markings from damage in use. The structural data is plotted on a piece of tracing paper or film which is fixed in position over the stereonet by means of a carefully centred pin as shown. The tracing paper must be free to rotate about this pin and it is essential that it is located accurately at the centre of the net otherwise significant errors will be introduced into the subsequent analysis.

Before starting any analysis, the North point must be marked on the tracing so that a reference position is available.

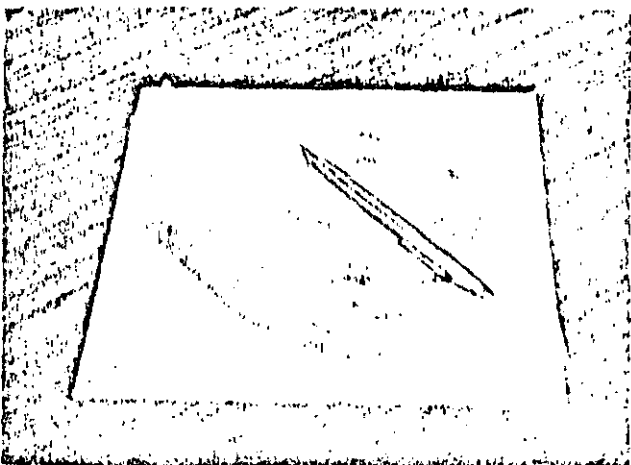


Figure 14:

Geological data is plotted and analysed on a piece of tracing paper which is located over the centre of the stereonet by means of a centre pin as shown. The net is mounted on a base-board of plywood or similar material.

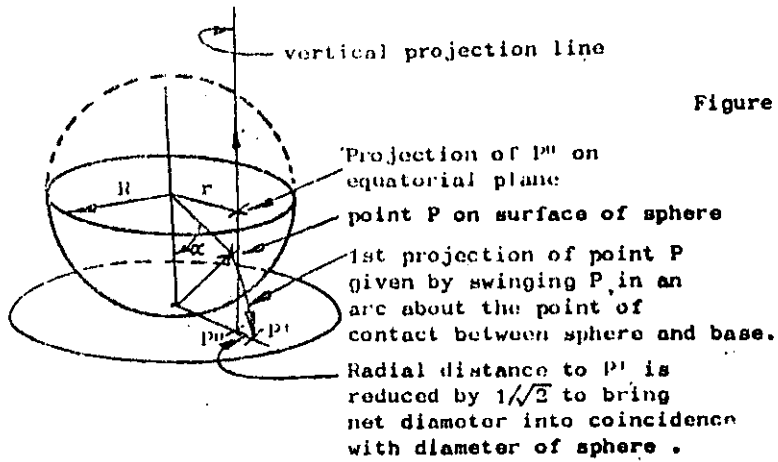


Figure 12a : Method of construction of an equal-area projection.

The radial distance  $r$  of the projected point  $P''$  on the stereonet is given by :

$$r = \sqrt{2} \cdot R \sin \frac{\alpha}{2}$$

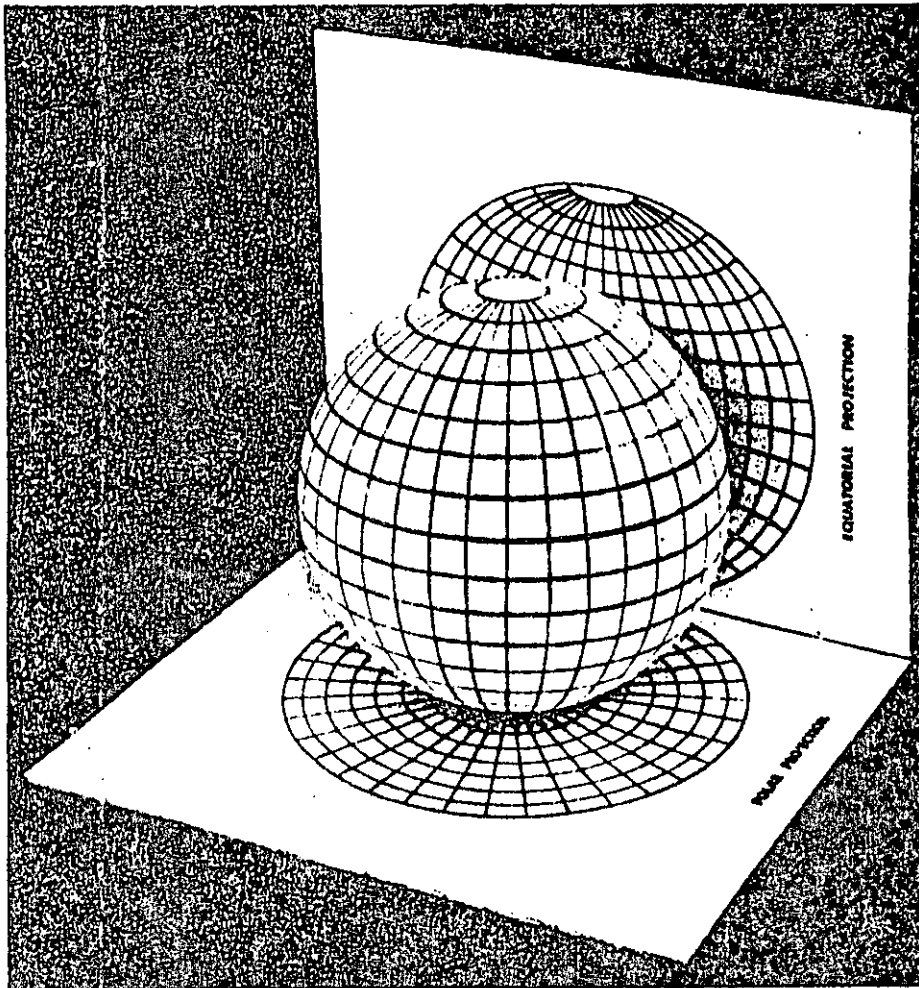


Figure 12b: Polar and equatorial projections of a sphere.

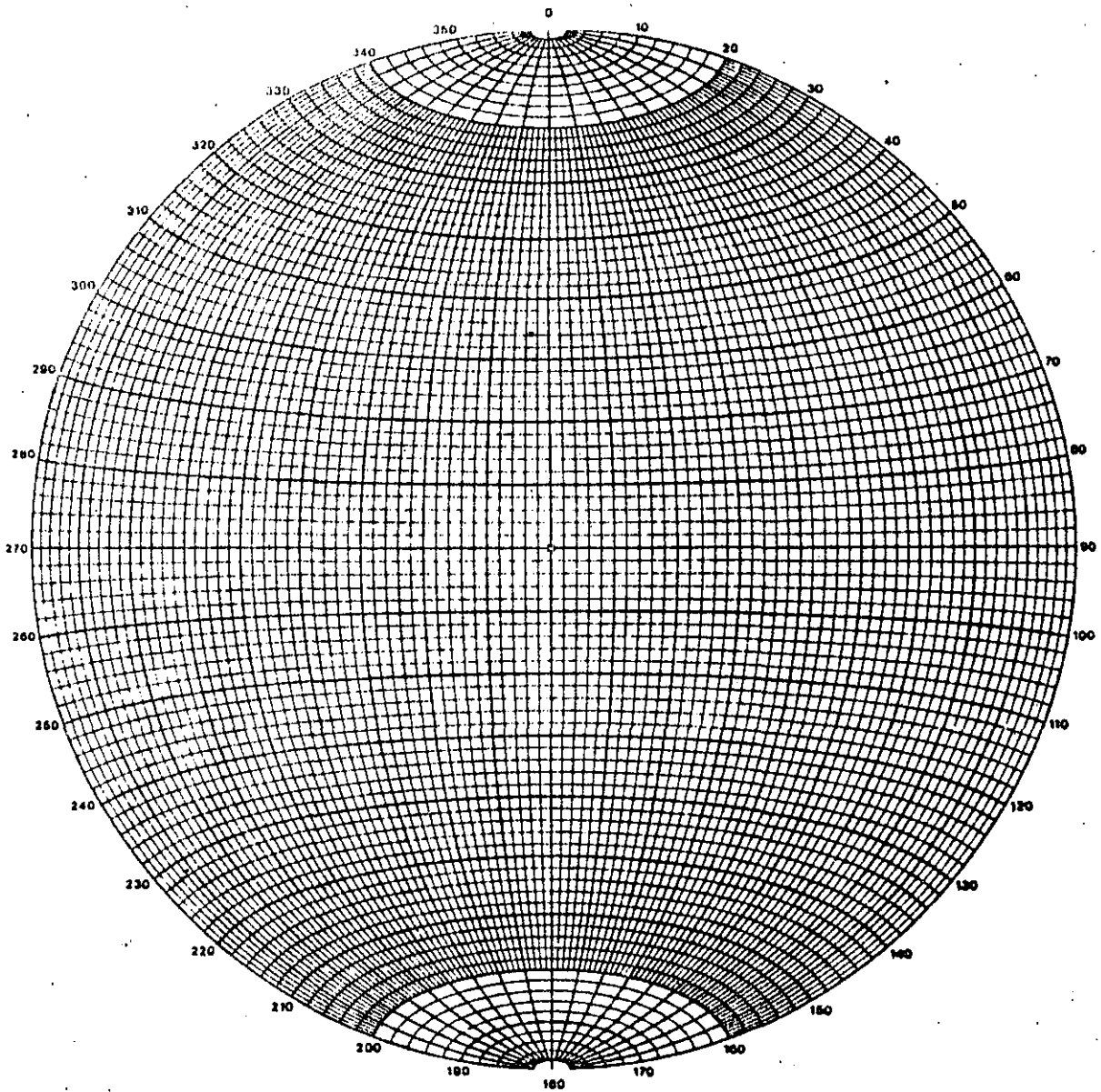


Figure 13a : Equatorial equal-area stereonet marked in 2° intervals. This net is most useful for the construction of great circles during the analysis of structural data.

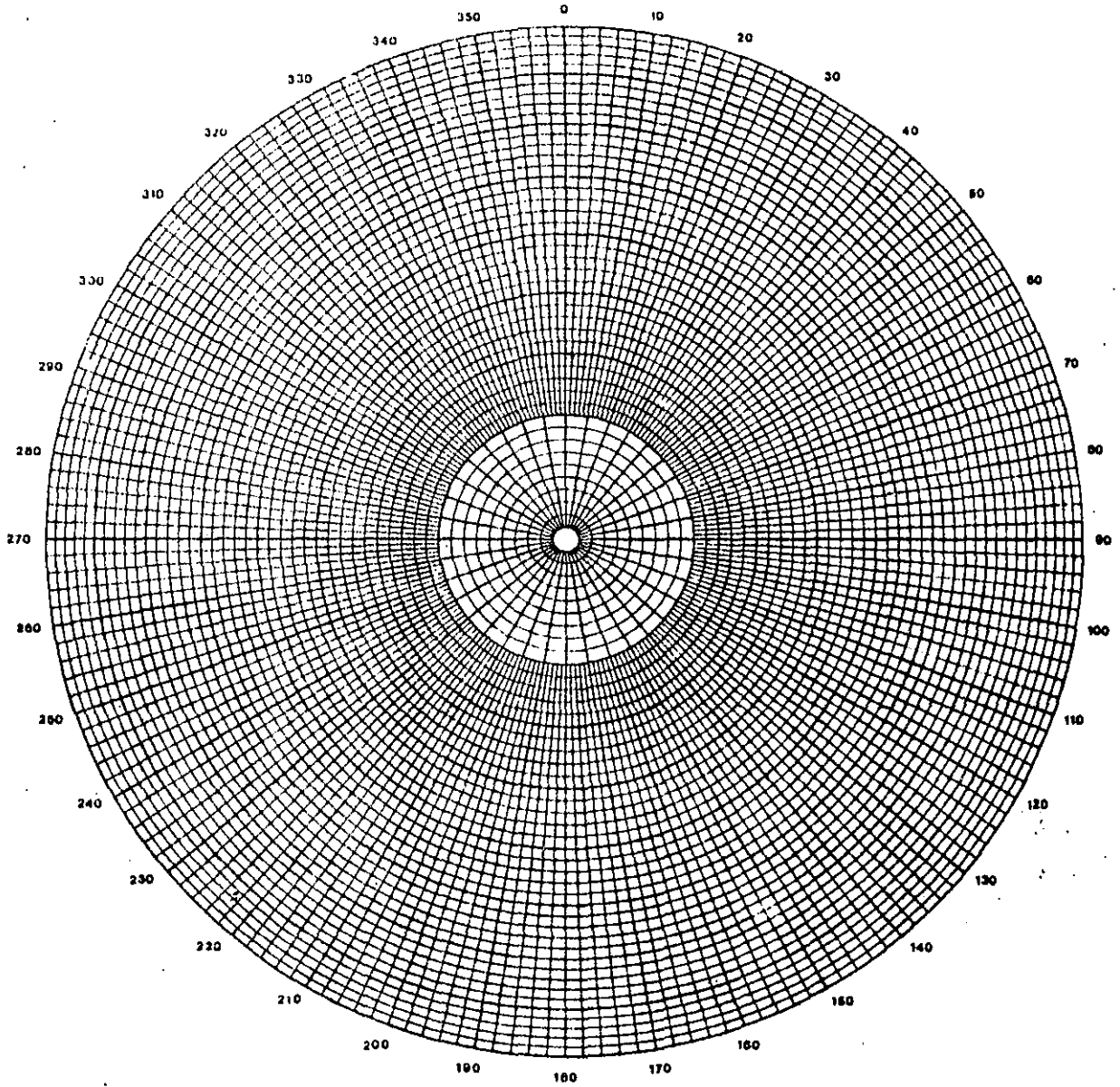
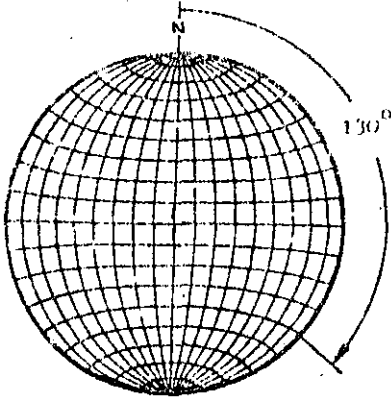


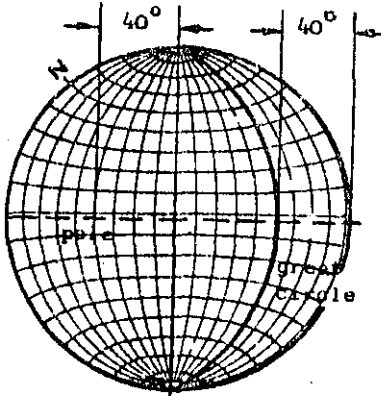
Figure 13b : Polar equal-area stereonet marked in 2° intervals.  
This net is used for plotting poles of planes during  
the analysis of structural data.

Construction of a great circle and a pole representating a plane.



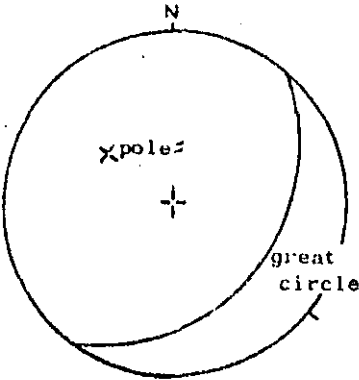
Consider a plane dipping at  $40^\circ$  in a dip direction of  $130^\circ$ . The great circle and the pole representing this plane are constructed as follows:

*Step 1:* With the tracing paper located over the stereonet by means of the centre pin, trace the circumference of the net and mark the north point. Measure off the dip direction of  $130^\circ$  clockwise from north and mark this position on the circumference of the net.

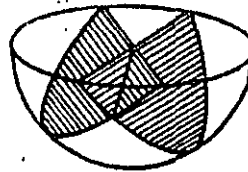


*Step 2:* Rotate the tracing about the centre pin until the dip direction mark lies on the W-E axis of the net, i.e. the tracing is rotated through  $40^\circ$ . Measure off  $40^\circ$  from the outer circle of the net and trace the great circle which corresponds to a plane dipping at this angle.

The position of the pole, which has a dip of  $(90^\circ - 40^\circ)$ , is found by measuring off  $40^\circ$  from the centre of the net as shown or, alternatively,  $50^\circ$  from the outside of the net. The pole lies on the projection of the dip direction line which, at this stage in the construction, is coincident with the W-E axis of the net.



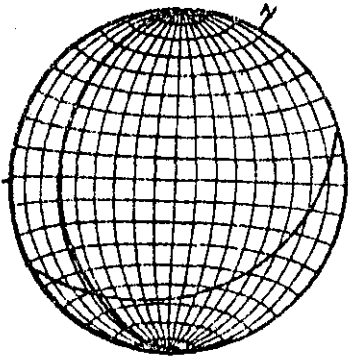
*Step 3:* The tracing is now rotated back to its original position so that the north mark on the tracing coincides with the north mark on the net. The final appearance of the great circle and the pole representing a plane dipping at  $40^\circ$  in a dip direction of  $130^\circ$  is as illustrated.

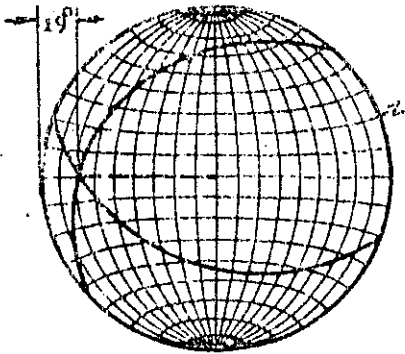


Determination of the line of intersection of two planes

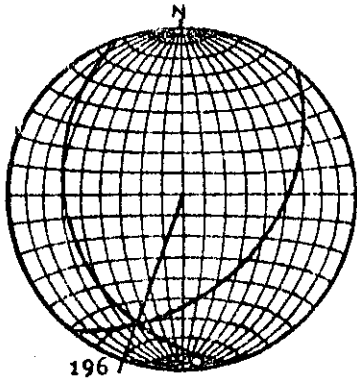
Two planes, having dips of  $40^\circ$  and  $30^\circ$  and dip directions of  $130^\circ$  and  $250^\circ$  respectively, intersect. It is required to find the dip and dip direction of the line of intersection.

*Step 1:* One of these planes has already been described above and the great circle defining the second plane is obtained by marking off the  $250^\circ$  dip direction on the circumference of the net, rotating the tracing until this mark lies on the W-E axis and tracing the great circle corresponding to a dip of  $30^\circ$ .

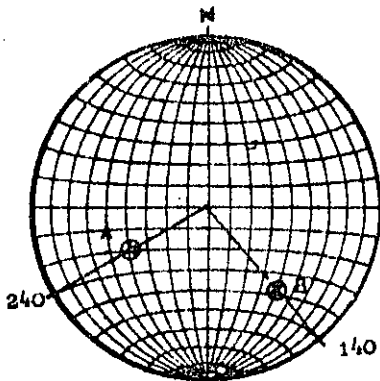




*Step 2:* The tracing is now rotated until the intersection of the two great circles lies along the W-E axis of the stereonet and the dip of the line of intersection is measured as  $19^\circ$ .



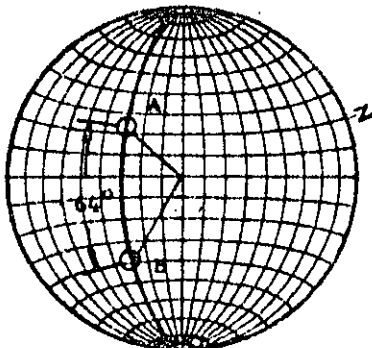
*Step 3:* The tracing is now rotated until the north mark coincides with the north point on the stereonet and the dip direction of the line of intersection is found to be  $196^\circ$ .



To determine the angle between two specified lines.

Two lines in space, e.g. lines of intersection or normals to planes, are specified by dips of  $54^\circ$  and  $40^\circ$  and dip directions of  $240^\circ$  and  $140^\circ$  respectively. It is required to find the angle between these lines.

*Step 1:* The points A and B which define these lines are marked on the stereonet as described under the procedure for locating the pole.



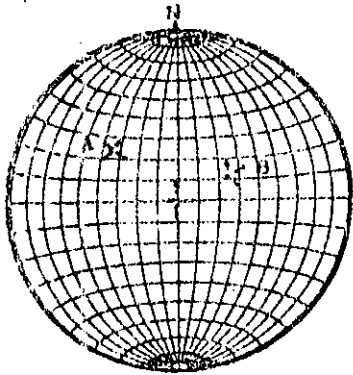
*Step 2:* The tracing is now rotated until these two points lie on the same great circle on the stereonet and the angle between the lines is determined by counting the small circle divisions between A and B, along the great circle. This angle is found to be  $64^\circ$ .

The great circle on which A and B lie defines the plane which contains these two lines and the dip and dip direction of this plane are found to be  $60^\circ$  and  $200^\circ$  respectively.

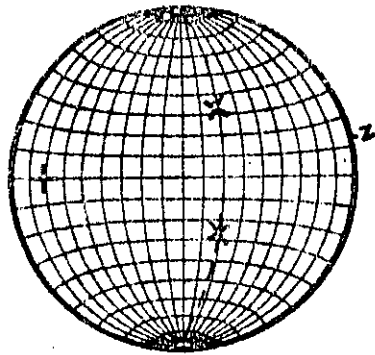


Alternative method for finding the line of intersection of two planes.

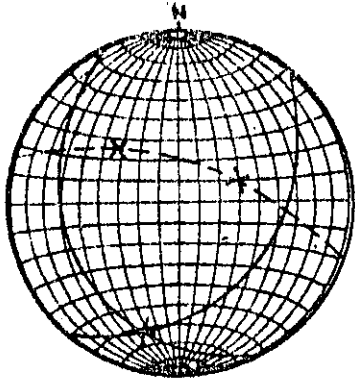
---



Two planes, dipping at  $40^\circ$  and  $30^\circ$  in dip directions of  $130^\circ$  and  $250^\circ$  respectively are defined by their poles A and B as shown. The line of intersection of these two planes is defined as follows:



*Step 1:* Rotate the tracing until both poles lie on the same great circle. This great circle defines the plane which contains the two normals to the planes.

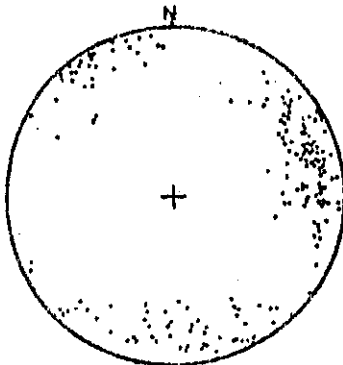


*Step 2:* Find the pole of this plane by measuring off the dip on the W-E axis of the stereonet. This pole P defines the normal to the plane containing A and B and, since this normal is common to both planes, it is, in fact, the line of intersection of the two planes.

Hence, the pole of a plane which passes through the poles of two other planes defines the line of intersection of those planes.

Determination of preferred orientations of discontinuity sets.

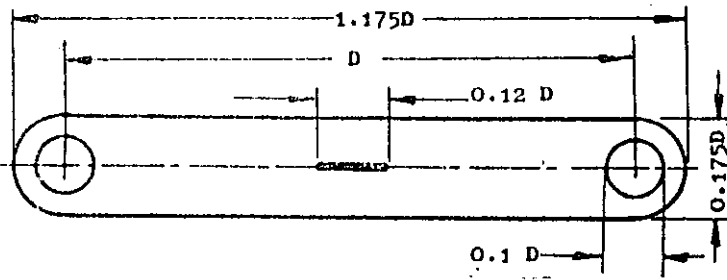
---



In plotting field observations of dip and dip direction, it is convenient to work in terms of poles rather than great circles since, when the number of observations exceeds about 10, the plot of great circles can be very confusing. Even when the information is plotted in terms of poles, using a polar stereonet, the overall picture, as shown opposite, can be confusing and requires additional interpretation.

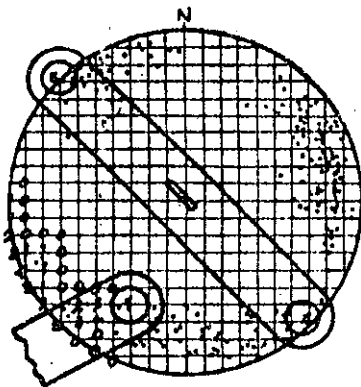
In order to identify the preferred orientations of systems of structural discontinuities from a pole plot such as that shown, a number of contouring techniques are available. One of these techniques will be described and the reader requiring further details on these methods is referred to texts such as that by Turner and Weiss<sup>36</sup>.

Schmidt or grid method

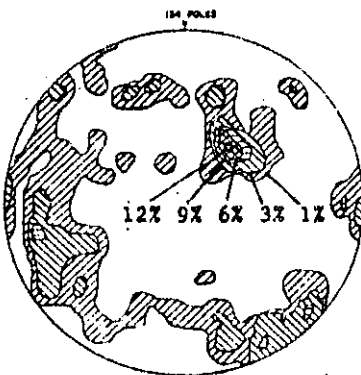


Schmidt point counter machined from 1.5 mm thick perspex sheet. Dimensions are given in multiples of D, the diameter of the stereonet.

The basic tool required for this contouring method is a transparent counter such as that illustrated above. These counters are not commercially available but can easily be machined from a sheet of perspex or similar material. The dimensions of the counter are given in terms of the stereonet diameter which, for this application, would normally be 15 to 20 cms. The centre slot is end-milled or cut with a fret-saw and should be approximately 1 mm wide.



The tracing, on which the poles have been plotted, is placed over a grid with lines spaced at one-twentieth of the grid diameter (i.e. a 1 cm grid for a 20 cm stereonet). With the centre of one of the circular holes at the end of the counter centred on a grid intersection, the number of poles falling within the circle is counted and this number is written on the grid intersection. The counting circle is moved to successive grid points and the count noted at each point. Where poles fall very close to the periphery of the stereonet, the counter is located with its centre slot over the centre pin of the stereonet and poles falling within both circles are counted as shown. The total number of poles in the two circles is noted at both intersection points.



Once the counting has been completed and all the counts noted at intersection points, contouring is carried out by joining intersection points having the same number written over them. The contour values are determined from the individual pole counts divided by the total number of poles on the stereonet. Hence, in the example given, the total number of poles is 134 and the line joining intersections with 8 poles represents the 6% contour. Similarly, 16 poles corresponds to 12% and 4 poles to 3%. The contour intervals are normally shaded as shown in order to assist the user in rapid identification of significant pole concentrations.

Evaluation of potential slope problems

Different types of slope failure are associated with different geological structures and it is important that the slope designer should be able to recognise potential stability problems during the early stages of a project. Some of the signs which should be watched for when examining stereoplots of the structural data are outlined on the following pages and a test for the possibility of sliding on one or more discontinuity is described.

Figure 15 shows the four main types of failure considered in this book and gives the appearance of typical stereoplots of geological conditions likely to lead to such failures. Note that in assessing stability, the cut face of the slope must be included in the stereoplot since sliding can only occur as a result of movement towards the free face created by the cut.

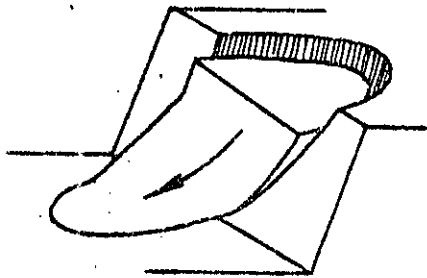
The diagrams given in Figure 15 have been simplified for the sake of clarity. In an actual rock slope, combinations of several types of geological structures may be present and this may give rise to additional types of failure. For example, presence of discontinuities which can lead to toppling as well as planes upon which wedge sliding can occur could lead to the sliding of a wedge which is separated from the rock mass by a "tension crack".

In a typical field study in which structural data has been plotted on stereonets, a number of significant pole concentrations may be present. It is useful to be able to identify those which represent potential failure planes and to eliminate those which represent structures which are unlikely to be involved in slope failures. John<sup>46</sup>, Panet<sup>47</sup> and McMahon<sup>23</sup> have discussed methods for identifying important pole concentration but the author prefers a method recently developed by Markland<sup>48</sup>.

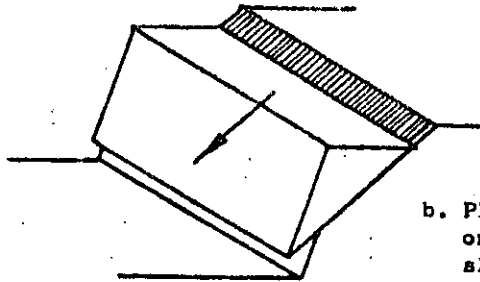
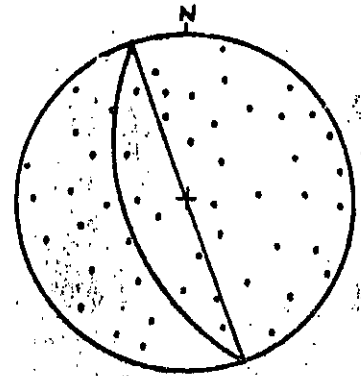
Markland's test, described hereunder, is to establish the possibility of a wedge failure in which sliding takes place along the line of intersection of two planar discontinuities as illustrated in Figure 15c. Plane failure, Figure 15b, is also covered by this test since it is a special case of wedge failure. If contact is maintained on both planes, sliding can only occur along the line of intersection and hence this line of intersection must "daylight" in the slope face. In other words, the dip of the line of intersection must be less than the dip of the slope face, measured in the direction of the line of intersection as shown in Figure 16a.

As will be shown in the chapter dealing with wedge failure, the factor of safety of the slope depends upon the dip of the line of intersection, the shear strength of the discontinuity surfaces and the geometry of the wedge. The limiting case occurs when the wedge degenerates to a plane, i.e. the dips and dip direction of the two planes are the same, and when the shear strength of this plane is due to friction only. As already discussed, sliding under these conditions occurs when the dip of the plane exceeds the angle of friction  $\phi$  and hence, a first approximation of wedge stability is obtained by considering whether the dip of the line of intersection exceeds the friction angle for the rock surfaces. Figure 16b shows that the slope is potentially unstable when the point defining the line of intersection of the two planes falls within the area included between the great circle defining the slope face and the circle defining an infinite series of planes (a cone) all dipping at the angle of friction  $\phi$ .

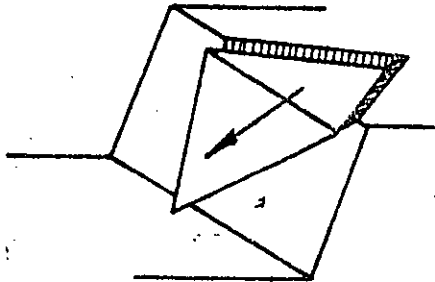
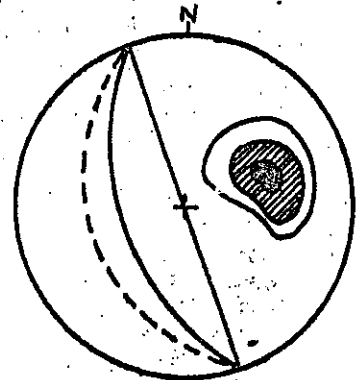
The reader who is familiar with wedge analysis will argue that this area can be further reduced by allowing for the influence of "wedging" between the two discontinuity planes. On the other hand, the stability may be decreased if water is present in the slope. Experience suggests that these



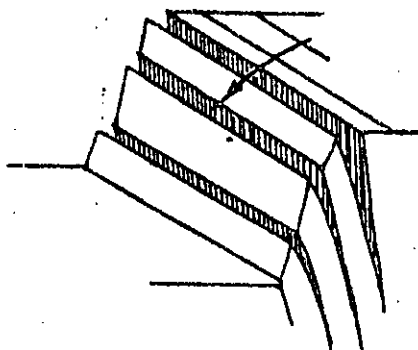
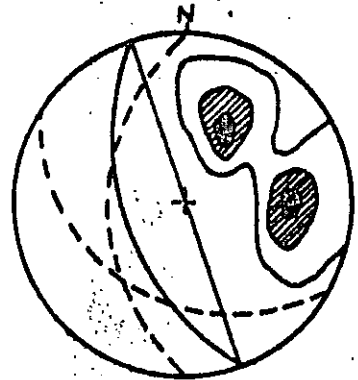
a. Circular failure in overburden soil, waste rock or heavily fractured rock with no identifiable structural pattern.



b. Plane failure in highly ordered structure such as slate.



c. Wedge failure on two intersecting discontinuities.



d. Toppling failure in hard rock which can form columnar structures separated by steeply dipping discontinuities.

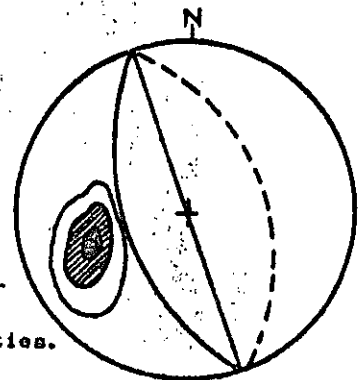


Figure 15 : Main types of slope failure and appearance of stereoplots of structural conditions likely to give rise to these failures.

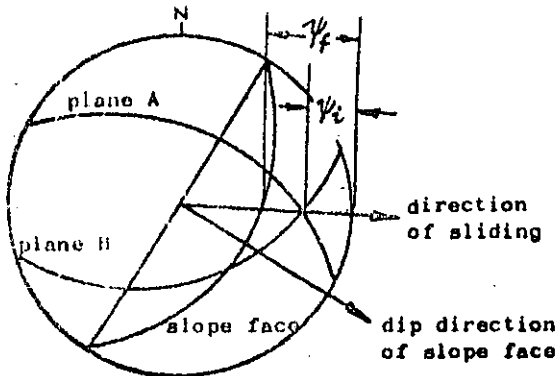
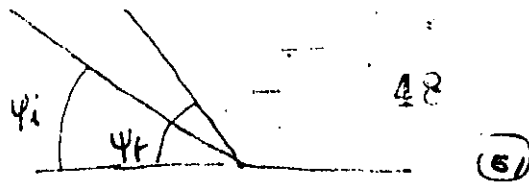


Figure 16a : Sliding along the line of intersection of planes A and B is possible when the dip of this line is less than the dip of the slope face, measured in the direction of sliding, i.e.  $\psi_f > \psi_i$ .

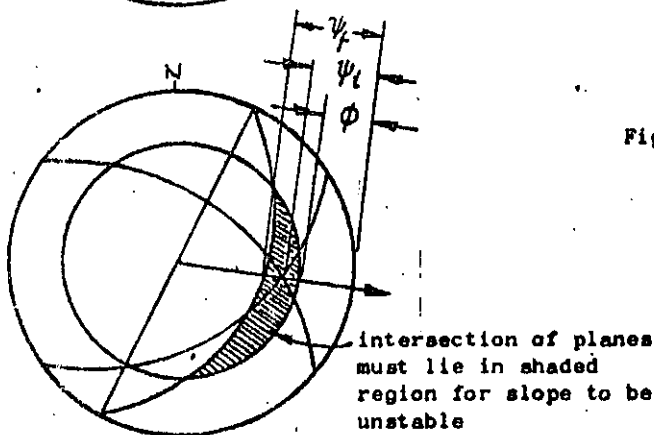


Figure 16b : Sliding is assumed to occur when the dip of the line of intersection exceeds the angle of friction, i.e. when  $\psi_f > \psi_i > \phi$ .

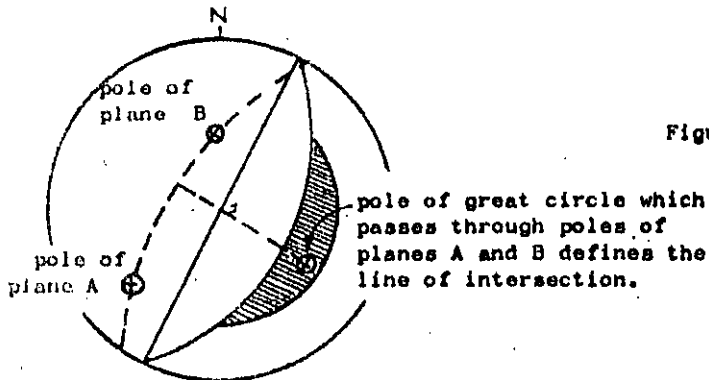


Figure 16c : Representation of planes by their poles and determination of the line of intersection by the pole of the great circle which passes through these poles.

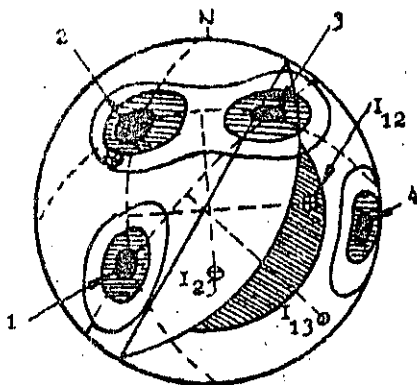


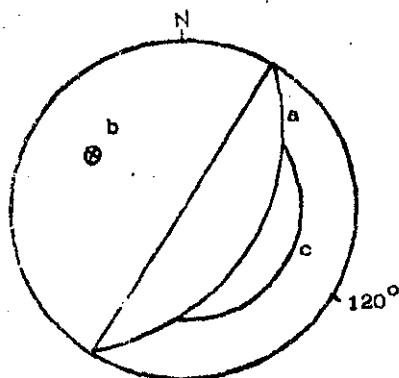
Figure 16d : Preliminary evaluation of the stability of a  $50^\circ$  slope in a rock mass with 4 sets of structural discontinuities.

two factors will tend to cancel one another in typical wedge problems and that the crude assumption used in deriving Figure 16b is adequate for most practical problems. It should be remembered that this test is designed to identify critical discontinuities and, having identified them, a more detailed analysis would normally be necessary in order to define the factor of safety of the slope.

Figures 16a and 16b show the discontinuity planes as great circles but, as has been discussed on the previous pages, field data on these structures is normally plotted in terms of poles. In Figure 16c the two discontinuity planes are represented by their poles and, in order to find the line of intersection of these planes, the method described on page 47 is used. The tracing on which the poles are plotted is rotated until both poles lie on the same great circle. The pole of this great circle defines the line of intersection of the two planes.

As an example of the use of this test consider the contoured stereonet of poles given in Figure 16d. It is required to examine the stability of a slope face with a dip of  $50^\circ$  and dip direction of  $120^\circ$ . A friction angle of  $30^\circ$  is assumed for this analysis. An overlay is prepared on which the following information is included:

- The great circle representing the slope face
- The pole representing the slope face
- The friction circle.



Overlay for checking possibility of wedge failures .

This overlay is placed over the contoured stereonet and the two are rotated together over the stereonet to find great circles passing through pole concentrations. The lines of intersection are defined by the poles of these great circles as shown in Figure 16d. From this figure it will be seen that the most dangerous combination of discontinuities is that represented by the pole concentrations numbered 1 and 2. The intersections  $I_{23}$  and  $I_{13}$  both fall outside the critical area and are not likely to give rise to instability. The pole concentration numbered 4 will not be involved in sliding but, as shown in Figure 15d, it could give rise to toppling or the opening of tension cracks.

In the example described above, it would be necessary to examine this slope, and particularly discontinuities 1 and 2, in more detail to establish whether the critical conditions suggested by this preliminary analysis do indeed exist or whether there are other factors which increase the stability of the slope.

In cases where only one major pole concentration occurs as in Figure 15b, plane failure is possible if this concentration lies close to the pole of the slope face. In the example given in Figure 16d, pole concentration 2 lies sufficiently close to the pole of the slope face for two dimensional sliding to be considered a possibility and to justify a more detailed examination of this possibility.

Suggested method of data presentation and analysis for open pit planning.

During the early feasibility studies on a proposed open pit mine, an estimate of safe slope angles is required for the calculation of ore to waste ratios and for the preliminary pit layout. The only structural data which is likely to be available at this stage is that which has been obtained by logging cores drilled for mineral evaluation purposes and by mapping surface outcrops. Scanty as this data is, it does provide a basis for a first estimate of potential slope problems and the author suggests that this data should be treated in the manner illustrated in Figure 17.

On an outline plan of the proposed open pit, contoured stereoplots of whatever structural data is available are drawn. These plots are drawn at the location of the field observations and should, where possible, be evenly spaced around the pit perimeter. It is particularly important that areas of major faulting or areas in which changes of rock type occur should be mapped.

An overlay is prepared as described earlier and, in Figure 17, it has been assumed that the stability of  $45^{\circ}$  slopes is to be checked. Where the geological mapping has indicated the presence of faults or clay seams, a friction angle of  $20^{\circ}$  should be used to define the friction circle. Where no such structures appear to be present, a friction angle of  $30^{\circ}$  is more realistic and this is the value used in Figure 17.

The eastern side of the hypothetical porphyry-copper pit illustrated in Figure 17 does not contain structures which are unfavourable to stability and, since porphyry is a good hard rock, steepening of these slopes can be considered. Figure 7 on page 20 can be used as a guide to the maximum permissible slope angle for a given pit depth.

Note that the structures which occur in the south-eastern part of the pit could give rise to toppling failure if steep slopes are created (see Figure 15d). This possibility should be kept in mind as the pit planning progresses and a further analysis carried out if required.

The structures in the south-western part of the pit are not critical but there are bound to be local discontinuities which will cause small wedge slides on individual benches. This would be particularly true for the porphyry/slate contact. Since flattening of the slate slopes is essential, it would be wise to start this flattening in the south-western corner of the pit.

The most critical area in this particular pit will be the western slopes where the slate dips into the pit at about the same angle as the slopes (note that the pole concentration coincides with the pole of the slope face - a critical limiting condition for two-dimensional sliding). It would be essential to carry out further investigations in this part of the pit. Additional drilling to check the extent of the slate, groundwater studies and shear testing of discontinuity planes would all be necessary. A detailed stability analysis, using methods described in later chapters, would have to be carried out to establish the safe slope angles for this part of the pit.

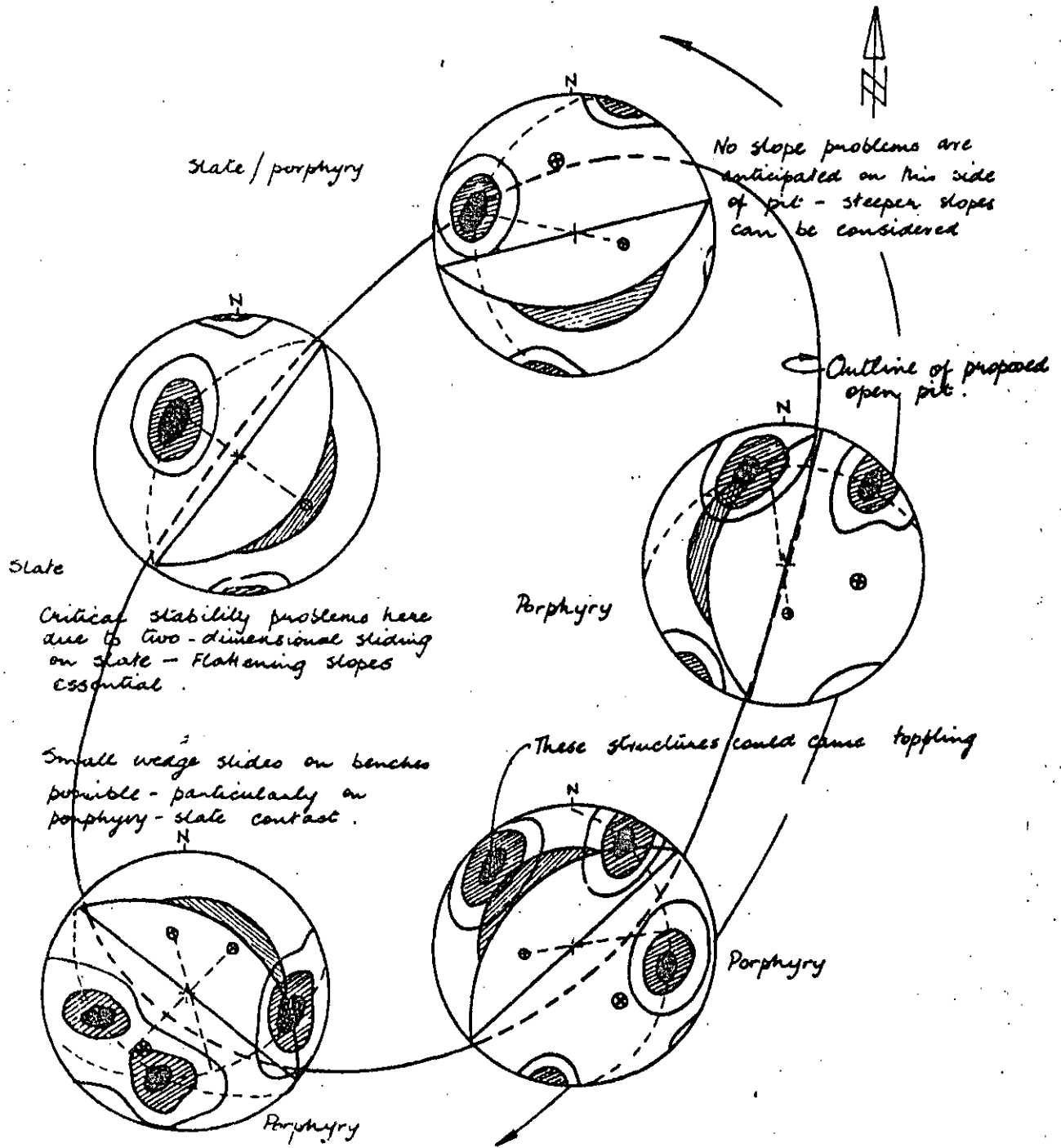


Figure 17 : Presentation of geological data and preliminary analysis of slope stability for feasibility study on hypothetical open pit mine.



Selected references on geological definitions and stereographic treatment of geological data.

34. PRICE, N.J. *Fault and joint development in brittle and semi-brittle rock*. Pergamon Press, London, 1966, 176 p.
35. LOUDERBACK, G.D. *Faults and engineering geology in Application of Geology to Engineering practices (Berkey volume)*. Geological Society of America, 1950, 327 p.
36. TURNER, F.J. and WEISS, L.E. *Structural analysis of metamorphic tectonites*. McGraw-Hill Book Co., New York, 1963, 545 p.
37. JENNINGS, J.E. A mathematical theory for the calculation of the stability of slopes in open cast mines. *Planning open pit mines*, Johannesburg Symposium 1970. Published by A.A. Balkema, Amsterdam, 1971, pp. 87-102.
38. PITEAU, D.R. Geological factors significant to the stability of slopes cut in rock. *Planning open pit mines*, Johannesburg Symposium 1970. Published by A.A. Balkema, Amsterdam 1971, pp. 33-53.
39. ROBERTSON, A. MacG. The interpretation of geological factors for use in slope theory. *Planning open pit mines*, Johannesburg Symposium 1970. Published by A.A. Balkema, Amsterdam 1971, pp.55-71.
40. GOODMAN, R.E. The deformability of joints in *Determination of the in-situ modulus of deformation of rock*. American Society for Testing and Materials Special Technical Publication, Number 477, 1970, pp.174-196.
41. PATTON, F.D. Multiple modes of shear failure in rock. *Proc. 1st International Congress on Rock Mechanics*. Lisbon 1966, Vol. 1, pp. 509-513.
42. PATTON, F.D. and DEERE, D.U. Significant geological factors in rock slope stability. *Planning open pit mines*, Johannesburg Symposium 1970. Published by A.A. Balkema, Amsterdam 1971, pp. 143-151.
43. PHILLIPS, F.C. *The use of stereographic projections in structural geology*. Edward Arnold, London. Third edition (paperback), 1971, 90 p.
44. BADGLEY, P.C. *Structural methods for the exploration geologist*. Harper Brothers, New York 1959, 280 p.
45. FRIEDMAN, M. Petrofabric techniques for the determination of principal stress directions in rocks. *Proc. Conference State of Stress in the Earth's crust*, Santa Monica 1963. Elsevier, New York 1964, pp. 451-550.
46. JOHN, K.W. Graphical stability analysis of slopes in jointed rock. *Journal Soil Mechanics and Foundation Div.* ASCE Vol. 94, No. SM2, 1968, pp. 497-526 with discussion and closure in Vol. 95, No. SM6, 1969, pp. 1541-1545.
47. PANET, M. Discussion on graphical stability analysis of slopes in jointed rock by K.W. John. *Journal Soil Mechanics and Foundation Div.* ASCE Vol. 95, No. SM6

1969, pp. 685-686.

48. MARKLAND, J.T. A useful technique for estimating the stability of rock slopes when the rigid wedge sliding type of failure is expected. *Imperial College Rock Mechanics Research Report*, No. 19, May 1972, 10 p.

### Introduction

The previous chapter was concerned with slope failure resulting from sliding on a single planar surface dipping into the excavation and striking parallel or nearly parallel to the slope face. It was stated that the plane failure analysis is valid provided that the strike of the failure plane is within  $\pm 20^\circ$  of the strike of the slope face. This chapter is concerned with the failure of slopes in which structural features upon which sliding can occur strike across the slope crest and where sliding takes place along the line of intersection of two such planes.

This problem has been extensively discussed in geotechnical literature and the authors have drawn heavily upon the work of Londe, John, Wittke, Goodman and others listed in references 152 to 162 at the end of this chapter. The reader who has examined this literature may have been confused by some of the mathematics which has been presented. It must, however, be appreciated that our understanding of the subject has grown rapidly over the past decade and that many of the simplifications which are now clear were not at all obvious when some of these papers were written. The basic mechanics of failure are very simple but, because of the large number of variables involved, the mathematical treatment of the mechanics can become very complex unless a very strict sequence is adhered to in the development of the equations.

In this chapter, the basic mechanics of failure involving the sliding of a wedge along the line of intersection of two planar discontinuities are presented in a form which the non-specialist reader should find easy to follow. Unfortunately, the very simple equations which are presented to illustrate the mechanics are of limited practical value because the variables used to define the wedge geometry cannot easily be measured in the field. Consequently, the second part of the chapter deals with the stability analysis in terms of the dips and dip directions of the planes and the slope face. In the transformation of the equations which is necessary in order to accommodate this information, the basic mechanics becomes obscure but it is hoped that the reader should be able to follow the logic involved in the development of these equations.

In the chapter itself, the discussion is limited to the case of the sliding of a simple wedge such as that illustrated in figure 91, acted upon by friction, cohesion and water pressure. The influence of a tension crack and of external forces due to bolts, cables or seismic accelerations results in a significant increase in the complexity of the equations and, since it would only be necessary to consider these influences on the fairly rare occasions when critical slopes are being examined, the complete solution to the problem has been presented in Appendix I at the end of the book. The analytical treatment of the problem presented in part III of the Appendix is particularly suitable for processing by computer and, once the reader has understood the basic mechanics of the problem, he should have no difficulty in having this general solution programmed for almost any type of computer, including the desk top machines which are now available.



Figure 91 : A typical wedge failure involving sliding along the line of intersection of two planar discontinuities.

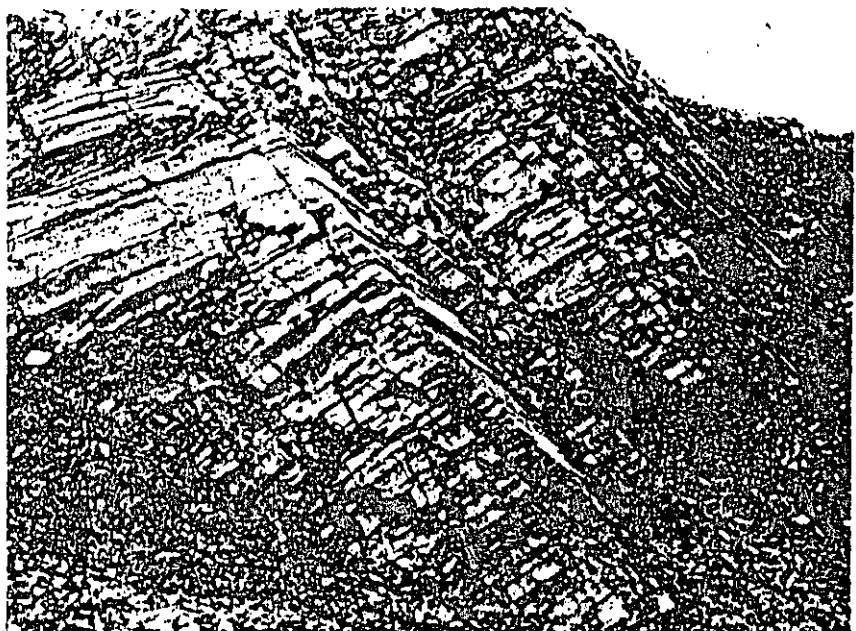
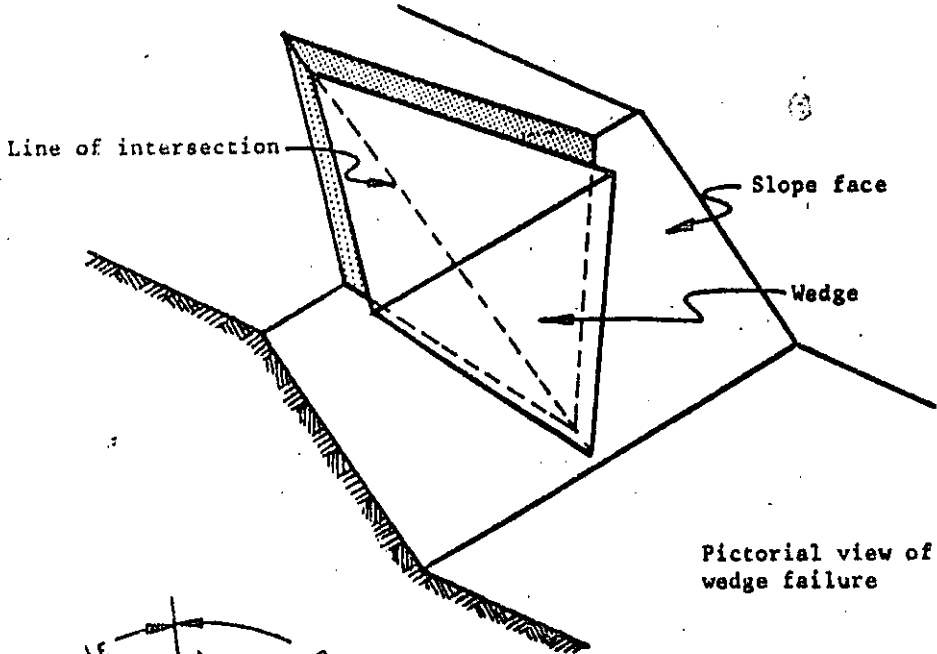
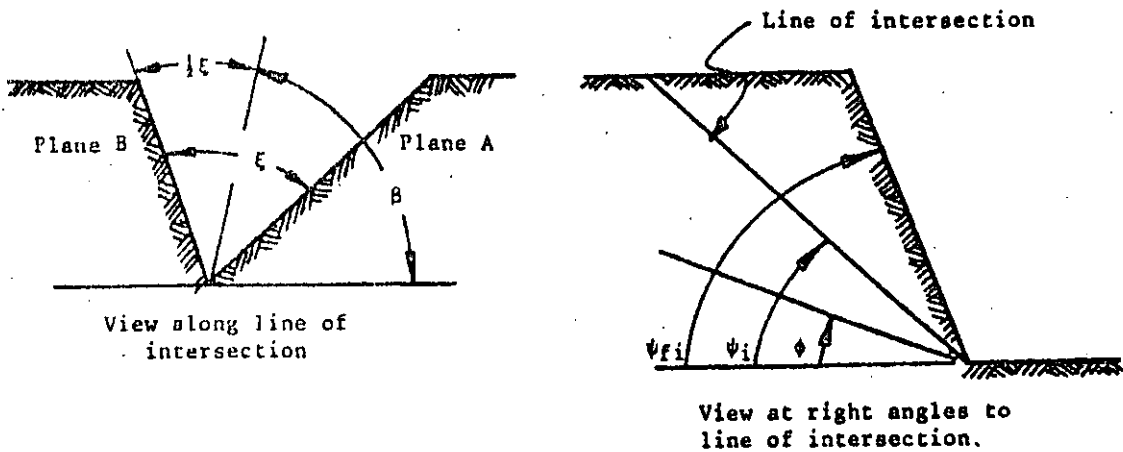


Figure 92 : Sets of intersecting discontinuities can sometimes give rise to the formation of families of wedge failures.

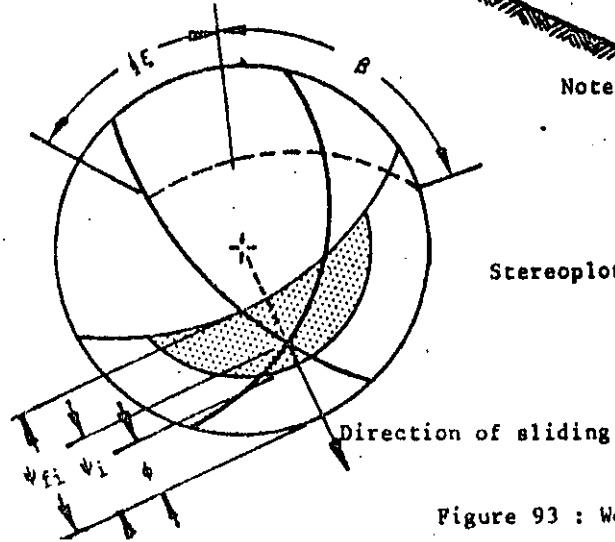
(Photograph reproduced with permission from Mr.K.M.Pare)



Pictorial view of wedge failure

Note : The convention adopted in this analysis is that the plane with the flatter of the two dips is always referred to as Plane A.

*of plane with gentler dip is referred to as Plane A.*



Stereonet of wedge failure geometry

Figure 93 : Wedge failure geometry.

Definition of wedge geometry

Typical wedge failures are illustrated in figures 91 and 92 which show, in the one case, the through-going planar discontinuities which are normally assumed for the analytical treatment of this problem and, in the other case, the wedge formed by sets of closely spaced structural features. In the latter case, the analytical treatment would still be based upon the assumption of through-going planar features although it would have to be realised that the definition of the dips and dip directions and the locations of these planes may present practical difficulties. The failure illustrated in figure 92 would probably have involved the fairly gradual ravelling of small loose blocks of rock and it is unlikely that this failure was associated with any violence. On the other hand, the failure illustrated in figure 91 probably involved a fairly sudden fall of a single wedge which would only have broken up on impact and which would, therefore, constitute a threat to anyone working at the toe of the slope.

The geometry of the wedge, for the purpose of analysing the basic mechanics of sliding, is defined in figure 93. Note that, throughout this book, the flatter of the two planes is called Plane A while the steeper plane is called Plane B.

*clines  
of same  
purpose*

As in the case of plane failure, a condition for sliding is defined by  $\psi_{fi} > \psi_i > \phi$ , where  $\psi_{fi}$  is the inclination of the slope face, measured in the view at right angles to the line of intersection, and  $\psi_i$  is the dip of the line of intersection. Note the  $\psi_{fi}$  would only be the same as  $\psi_f$ , the true dip of the slope face, if the dip direction of the line of intersection was the same as the dip direction of the slope face.

Analysis of wedge failure

The factor of safety of the wedge defined in figure 93, assuming that sliding is resisted by *friction only* and that the friction angle  $\phi$  is the same for both planes, is given by

$$F = \frac{(R_A + R_B) \tan \phi}{W \cdot \sin \psi_i} \tag{71}$$

where  $R_A$  and  $R_B$  are the normal reactions provided by planes A and B as illustrated in the sketch opposite.

In order to find  $R_A$  and  $R_B$ , resolve horizontally and vertically in the view along the line of intersection :

$$R_A \cdot \sin(\beta - \frac{1}{2}\epsilon) = R_B \cdot \sin(\beta + \frac{1}{2}\epsilon) \tag{72}$$

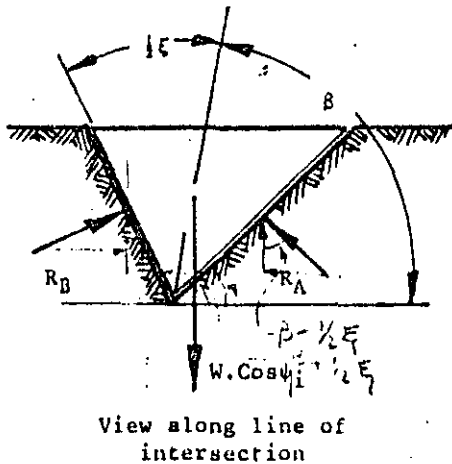
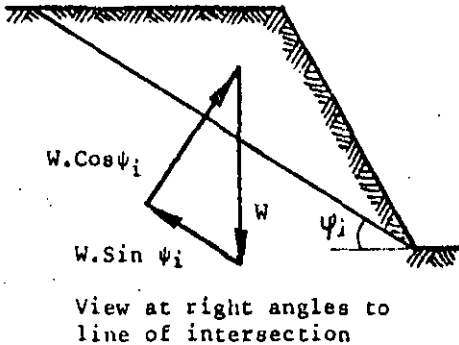
$$R_A \cdot \cos(\beta - \frac{1}{2}\epsilon) - R_B \cdot \cos(\beta + \frac{1}{2}\epsilon) = W \cdot \cos \psi_i \tag{73}$$

Solving for  $R_A$  and  $R_B$  and adding :

$$R_A + R_B = \frac{W \cdot \cos \psi_i \cdot \sin \beta}{\sin \frac{1}{2}\epsilon} \tag{74}$$

Hence

$$F = \frac{\sin \beta \cdot \tan \phi}{\cos \frac{1}{2}\epsilon \cdot \tan \psi_i} \tag{75}$$



In other words :

$$F_w = K.F_p \quad (76)$$

where  $F_w$  is the factor of safety of a wedge supported by friction only.  $F_p$  is the factor of safety of a plane failure in which the slope face is inclined at  $\psi_{fi}$  and the failure plane is inclined at  $\psi_i$ .

$K$  is a wedge factor which, as shown by equation 75, depends upon the included angle of the wedge and upon the angle of tilt of the wedge. Values for the wedge factor  $K$ , for a range of values of  $\beta$  and  $\xi$ , are plotted in figure 94.

As shown in the stereoplot given in figure 93, measurement of the angles  $\beta$  and  $\xi$  can be carried out on the great circle, the pole of which is the point representing the line of intersection of the two planes. Hence, a stereoplot of the features which define the slope and the wedge geometry can provide all the information required for the determination of the factor of safety. It should, however, be remembered that the case which has been dealt with is very simple and that, when different friction angles and the influence of cohesion and water pressure are allowed for, the equations become more complex. Rather than develop these equations in terms of the angles  $\beta$  and  $\xi$ , which cannot be measured directly in the field, the more complete analysis is presented in terms of directly measurable dips and dip directions.

Before leaving this simple analysis, the reader's attention is drawn to the important influence of the wedging action as the included angle of the wedge decreases below  $90^\circ$ . The increase by a factor of 2 or 3 on the factor of safety determined by plane failure analysis is of great practical importance. Some authors have suggested that a plane failure analysis is acceptable for *all* rock slopes because it provides a lower bound solution which has the merit of being conservative. Figure 94 shows that this solution is so conservative as to be totally uneconomic for most practical slope designs. It is therefore recommended that, where the structural features which are likely to control the stability of a rock slope do not strike parallel to the slope face, the stability analysis should be carried out by means of the three-dimensional methods presented in this book or published by the authors listed in references 152 to 162 at the end of this chapter.

#### Wedge analysis including cohesion and water pressure

Figure 95 shows the geometry of the wedge which will be considered in the following analysis. Note that the upper slope surface in this analysis can be obliquely inclined with respect to the slope face, thereby removing a restriction which has been present in all the stability analyses which have been discussed so far in this book. The total height of the slope, defined in figure 95b, is the total difference in vertical elevation between the upper and lower extremities of the line of intersection along which sliding is assumed to occur.

The water pressure distribution assumed for this analysis is based upon the hypothesis that the wedge itself is

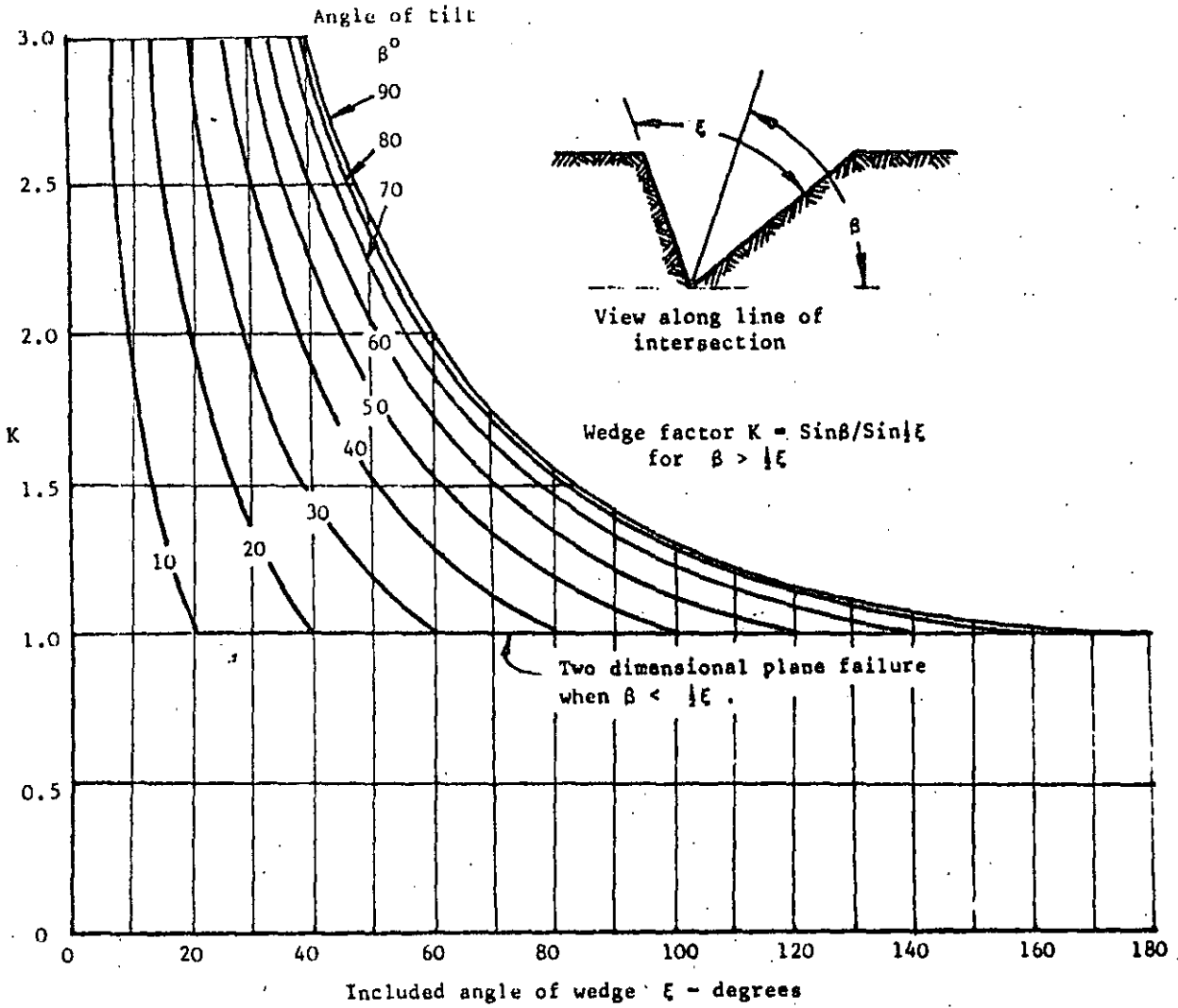
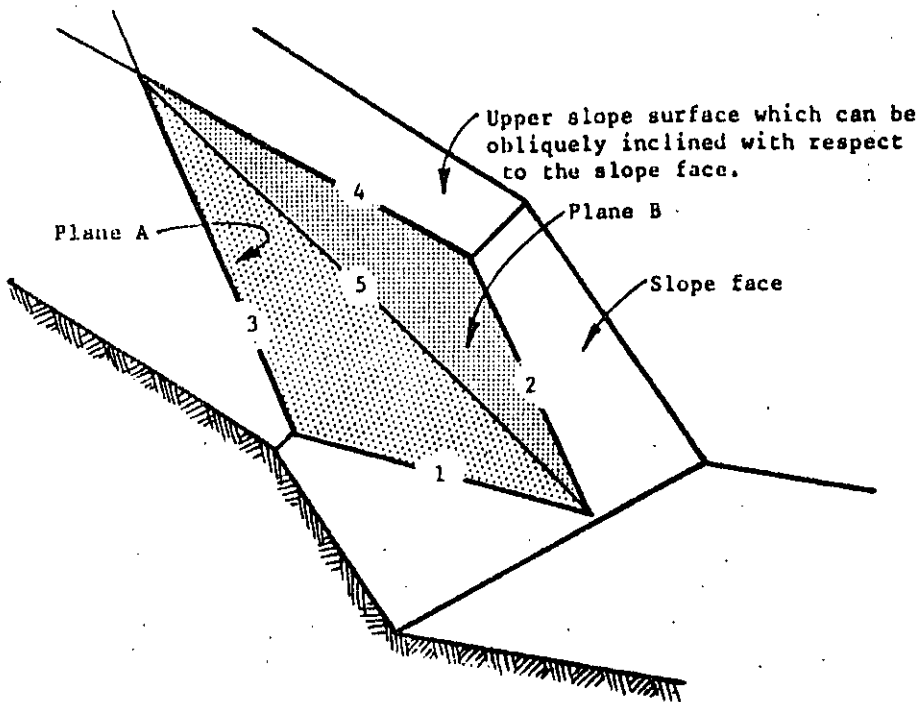
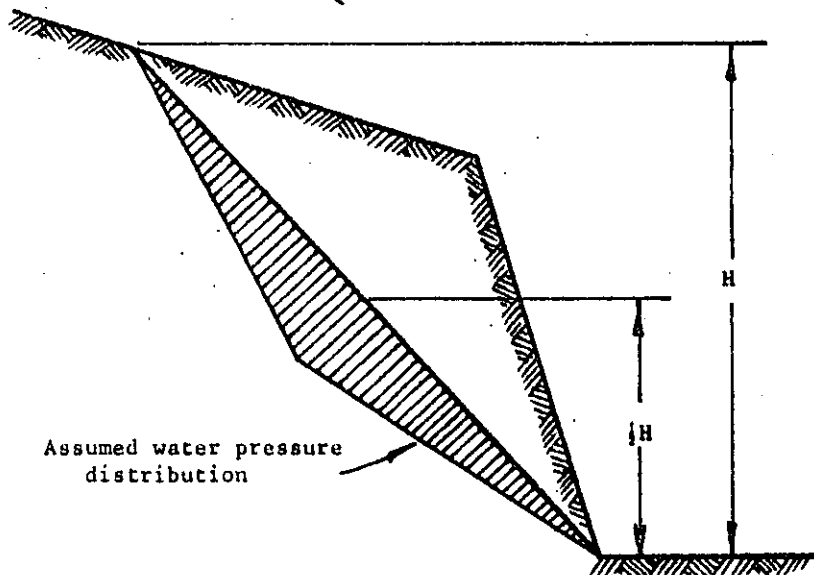


Figure 94 : Wedge factor K as a function of wedge geometry.





a. Pictorial view of wedge showing the numbering of intersection lines and planes.



b. View normal to the line of intersection 5 showing the total wedge height and the water pressure distribution.

Figure 95 : Geometry of wedge used for stability analysis including the influence of cohesion and of water pressure on the failure surfaces.

impermeable and that water enters the top of the wedge along lines of intersection 3 and 4 and leaks from the slope face along lines of intersection 1 and 2. The resulting pressure distribution is shown in figure 95b - the maximum pressure occurring along the line of intersection 5 and the pressure being zero along lines 1,2,3 and 4. This water pressure distribution is believed to be representative of the extreme conditions which could occur during very heavy rain.

The numbering of the lines of intersection of the various planes involved in this problem is of extreme importance since total confusion can arise in the analysis if these number are mixed-up. The numbering used throughout this book is as follows :

- 1 - intersection of plane A with the slope face
- 2 - intersection of plane B with the slope face
- 3 - intersection of plane A with upper slope surface
- 4 - intersection of plane B with upper slope surface
- 5 - intersection of planes A and B .

It is assumed that sliding of the wedge always takes place along the line of intersection numbered 5.

The factor of safety of this slope is derived from the detailed analysis presented in part III of Appendix I at the end of this book and is :

$$F = \frac{3}{\gamma H} (c_A \cdot X + c_B \cdot Y) + (A - \frac{\gamma_w}{2\gamma} \cdot X) \tan \phi_A + (B - \frac{\gamma_w}{2\gamma} \cdot Y) \tan \phi_B \quad (77)$$

Where

$c_A$  and  $c_B$  are the cohesive strengths of planes A and B

$\phi_A$  and  $\phi_B$  are the angles of friction on planes A and B

$\gamma$  is the density of the rock

$\gamma_w$  is the density of water

H is the total height of the wedge ( see figure 95)

X, Y, A and B are dimensionless factors which depend upon the geometry of the wedge.

$$X = \frac{\sin \theta_{24}}{\sin \theta_{45} \cdot \cos \theta_{2,na}} \quad (78)$$

$$Y = \frac{\sin \theta_{13}}{\sin \theta_{35} \cdot \cos \theta_{1,nb}} \quad (79)$$

$$A = \frac{\cos \psi_a - \cos \psi_b \cdot \cos \theta_{na,nb}}{\sin \psi_s \cdot \sin^2 \theta_{na,nb}} \quad (80)$$

$$B = \frac{\cos \psi_b - \cos \psi_a \cdot \cos \theta_{na,nb}}{\sin \psi_s \cdot \sin^2 \theta_{na,nb}} \quad (81)$$

where  $\psi_a$  and  $\psi_b$  are the dips of planes A and B respectively and  $\psi_s$  is the dip of the line of intersection 5.

The angles required for the solution of these equations can most conveniently be measured on a stereoplot of the

data which defines the geometry of the wedge and the slope.

Consider the following example :

Plane	dip <sup>o</sup>	dip direction <sup>o</sup>	Properties
A	45	105	$\phi_A=20^\circ, c_A= 500\text{lb}/\text{ft}^2$
B	70	235	$\phi_B=30^\circ, c_B= 1000\text{lb}/\text{ft}^2$
Slope face	65	185	$\gamma= 160\text{lb}/\text{ft}^3$
Upper surface	12	195	$\gamma_w= 62.5\text{lb}/\text{ft}^3$

The total height of the wedge H = 130 feet.

The stereoplot of the great circles representing the four planes involved in this problem is presented in figure 96 and all the angles required for the solution of equations 78 to 81 are marked in this figure.

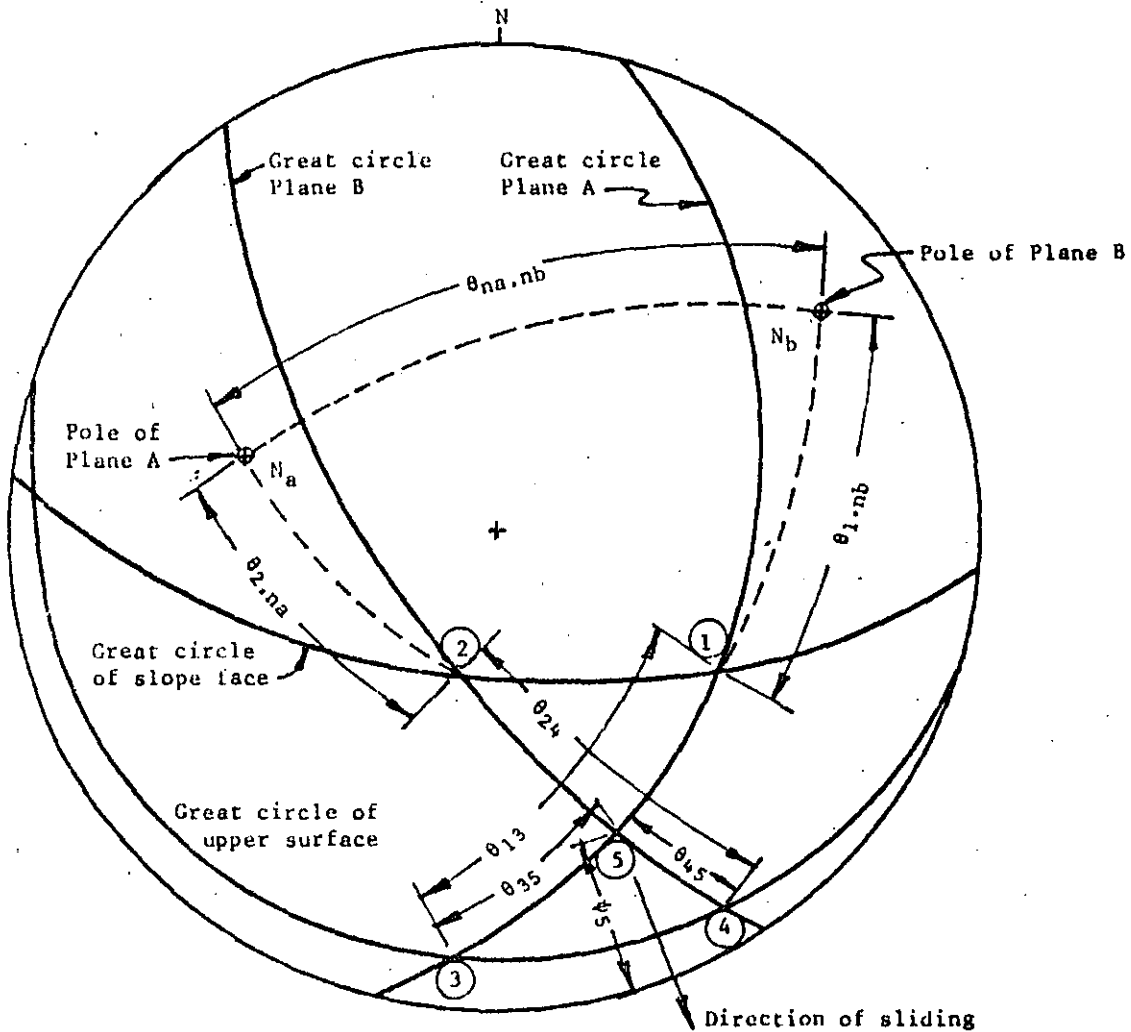


Figure 96 : Stereoplot of data required for wedge stability analysis.

WEDGE STABILITY CALCULATION SHEET

INPUT DATA	FUNCTION VALUE	CALCULATED ANSWER
$\psi_a = 45^\circ$ $\psi_b = 70^\circ$ $\psi_5 = 31.2^\circ$ $\theta_{na,nb} = 101^\circ$	$\text{Cos } \psi_a = 0.7071$ $\text{Cos } \psi_b = 0.3420$ $\text{Sin } \psi_5 = 0.5180$ $\text{Cos } \theta_{na,nb} = -0.191$ $\text{Sin } \theta_{na,nb} = 0.982$	$A = \frac{\text{Cos } \psi_a - \text{Cos } \psi_b \cdot \text{Cos } \theta_{na,nb}}{\text{Sin } \psi_5 \cdot \text{Sin }^2 \theta_{na,nb}} = \frac{0.7071 + 0.342 \times 0.191}{0.5180 \times 0.9636} = 1.5475$ $B = \frac{\text{Cos } \psi_b - \text{Cos } \psi_a \cdot \text{Cos } \theta_{na,nb}}{\text{Sin } \psi_5 \cdot \text{Sin }^2 \theta_{na,nb}} = \frac{0.3420 + 0.7071 \times 0.191}{0.5180 \times 0.9636} = 0.9557$
$\theta_{24} = 65^\circ$ $\theta_{45} = 25^\circ$ $\theta_{2,na} = 50^\circ$	$\text{Sin } \theta_{24} = 0.9063$ $\text{Sin } \theta_{45} = 0.4226$ $\text{Cos } \theta_{2,na} = 0.6428$	$X = \frac{\text{Sin } \theta_{24}}{\text{Sin } \theta_{45} \cdot \text{Cos } \theta_{2,na}} = \frac{0.9063}{0.4226 \times 0.6428} = 3.3363$
$\theta_{13} = 62^\circ$ $\theta_{35} = 31^\circ$ $\theta_{1,nb} = 60^\circ$	$\text{Sin } \theta_{13} = 0.8829$ $\text{Sin } \theta_{35} = 0.5150$ $\text{Cos } \theta_{1,nb} = 0.5000$	$Y = \frac{\text{Sin } \theta_{13}}{\text{Sin } \theta_{35} \cdot \text{Cos } \theta_{1,nb}} = \frac{0.8829}{0.5150 \times 0.500} = 3.4287$
$\phi_A = 30^\circ$ $\phi_B = 20^\circ$ $\gamma = 160 \text{ lb/ft}^3$ $\gamma_w = 62.5 \text{ lb/ft}^3$ $c_A = 500 \text{ lb/ft}^2$ $c_B = 1000 \text{ lb/ft}^2$ $H = 130 \text{ ft}$	$\text{Tan } \phi_A = 0.5773$ $\text{Tan } \phi_B = 0.3640$ $\gamma_w / 2\gamma = 0.1953$ $3c_A / \gamma H = 0.0721$ $3c_B / \gamma H = 0.1442$	$F = \frac{3c_A}{\gamma H} X + \frac{3c_B}{\gamma H} Y + (A - \frac{\gamma_w X}{2\gamma}) \text{Tan } \phi_A + (B - \frac{\gamma_w Y}{2\gamma}) \text{Tan } \phi_B$ $F = 0.2405 + 0.4944 + 0.8934 - 0.3762 + 0.3478 - 0.2437 = 1.3562$

63  
161

Determination of the factor of safety is most conveniently carried out on a calculation sheet such as that presented on page 191. Setting the calculations out in this manner not only enables the user to check all the data but it also shows how each variable contributes to the overall factor of safety. Hence, if it is required to check the influence of the cohesion on both planes falling to zero, this can be done by setting the two groups containing the cohesion values  $c_A$  and  $c_B$  to zero, giving a factor of safety of 0.62. Alternatively, the effect of drainage can be checked by putting the two water pressure terms (i.e. those containing  $Y_w$ ) to zero, giving  $F = 1.98$ .

As has been emphasised in previous chapters, this ability to check the sensitivity of the factor of safety to changes in material properties or in slope loading is probably as important as the ability to calculate the factor of safety itself. Hoek and Londe, in a general review of rock slope and foundation design methods<sup>165</sup>, have concluded that the information which is most useful to the design engineer is that which indicates the response of the structure to changes in significant parameters. Hence, decisions on remedial measures such as drainage can be based upon the rate of change of factor of safety, even if the absolute value of the factor of safety cannot be relied upon. To quote from this general review: "The function of the design engineer is not to compute accurately but to judge soundly".

#### Wedge stability charts for friction only

If the cohesive strength of the planes A and B is zero and the slope is fully drained, equation 77 reduces to

$$F = A.Tan\phi_A + B.Tan\phi_B \quad (82)$$

The dimensionless factors A and B are found to depend upon the dips and dip directions of the two planes and values of these two factors have been computed for a range of wedge geometries and the results are presented as a series of charts on the following pages.

In order to illustrate the use of these charts, consider the following example :

	dip <sup>o</sup>	dip direction <sup>o</sup>	friction angle <sup>o</sup>
Plane A	40	165	35
Plane B	70	285	20
Differences	30	120	

Hence, turning to the charts headed "Dip difference 30<sup>o</sup>" and reading off the values of A and B for a difference in dip direction of 120<sup>o</sup>, one finds that

$$A = 1.5 \text{ and } B = 0.7$$

Substitution in equation 82 gives the factor of safety as  $F = 1.30$ . The values of A and B give a direct indication of the contribution which each of the planes makes to the total factor of safety.

Note that the factor of safety calculated from equation 82 is independent of the slope height, the angle of the slope face and the inclination of the upper plane.

rather surprising result arises because the weight of the wedge occurs in both the numerator and denominator of the factor of safety equation and, for the friction only case, this term cancels out, leaving a dimensionless ratio which defines the factor of safety ( see equation 75 on page 185). This simplification is very useful in that it enables the user of these charts to carry out a very quick check on the stability of a slope on the basis of the dips and dip directions of the discontinuities in the rock mass into which the slope has been cut. An example of such an analysis is presented later in this chapter.

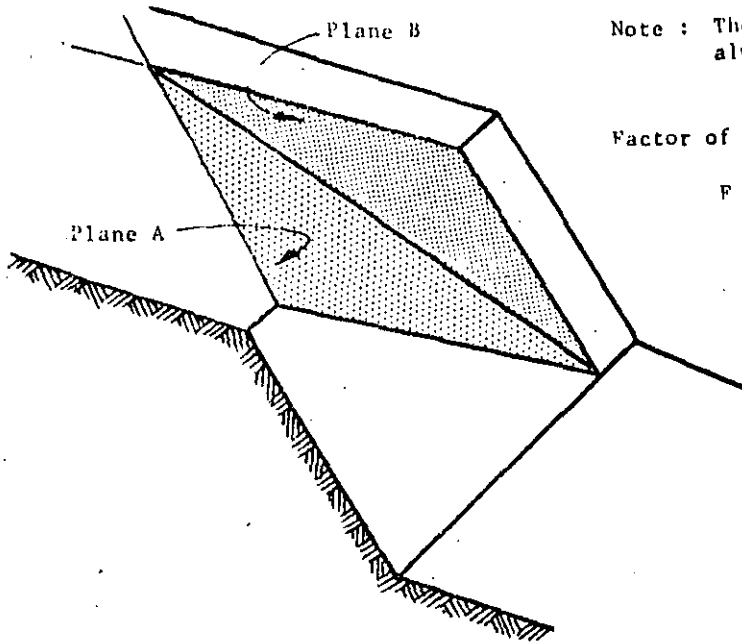
Many trial calculations have shown that a wedge having a factor of safety in excess of 2.0, as obtained from the friction only stability charts, is unlikely to fail under even the most severe combination of conditions to which the slope is likely to be subjected. Consider the example discussed on pages 190 to 192 in which the factor of safety for the worst conditions ( zero cohesion and maximum water pressure ) is 0.62. This is exactly 50% of the factor of safety of 1.24 for the friction only case. Hence, had the factor of safety for the friction only case been 2.0, the factor of safety for the worst conditions would have been 1.0, assuming that the ratio of the factors of safety for the two cases remains constant.

On the basis of such trial calculations, the authors suggest that the friction only stability charts can be used to define those slopes which are adequately stable and which can be ignored in subsequent analyses. Such slopes, having a factor of safety in excess of 2.0, pass into category 3 in the chart presented in figure 6 on page 14. Slopes with a factor of safety, based upon friction only, of less than 2.0 must be regarded as potentially unstable and pass into category 4 of figure 6, i.e. these slopes require further detailed examination.

In many practical problems involving the design of the overall slopes of an open pit mine or the cuttings for a highway, it will be found that these friction only stability charts provide all the information which is required. It is frequently possible, having identified a potentially dangerous slope, to eliminate the problem by a slight re-alignment of the pit benches or of the road cutting. Such a solution is clearly only feasible if the potential danger is recognised before excavation of the slope is started and the main use of the charts is during the site investigation and preliminary planning stage of a slope project.

Once a slope has been excavated, these charts will be of limited use since it will be fairly obvious if the slope is unstable. Under these conditions, a more detailed study of the slope will be required and use would then have to be made of the method described on pages 186 to 191 or of one of the methods described in Appendix I. In the authors' experience, relatively few slopes require this detailed analysis and the reader should beware of wasting time on such an analysis when the simpler methods presented in this chapter would be adequate. A full stability analysis may look very impressive in a report but, unless it has enabled the slope engineer to take positive remedial measures, it may not have served any useful purpose.

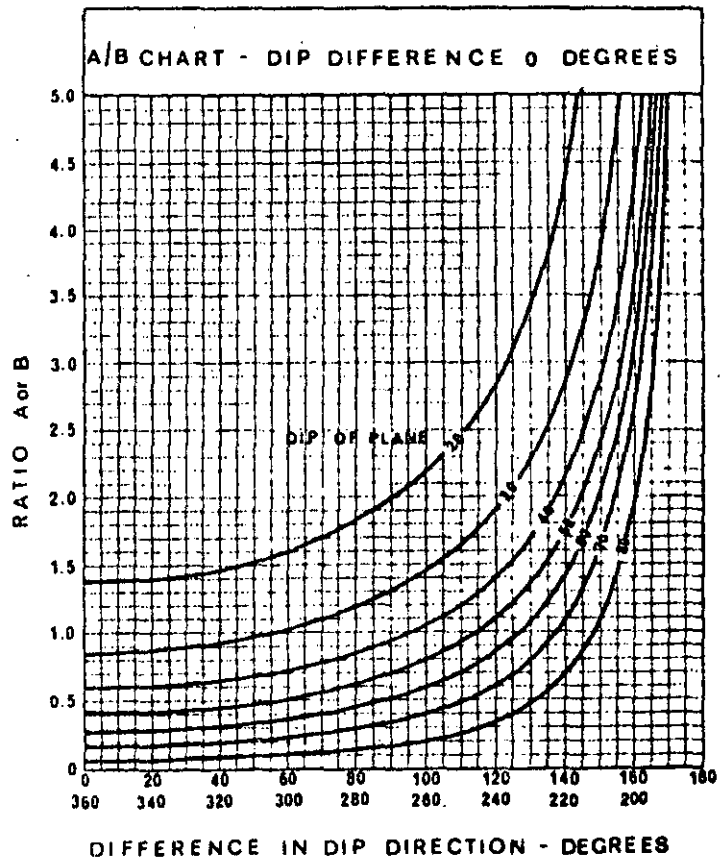
### WEDGE STABILITY CHARTS FOR FRICTION ONLY

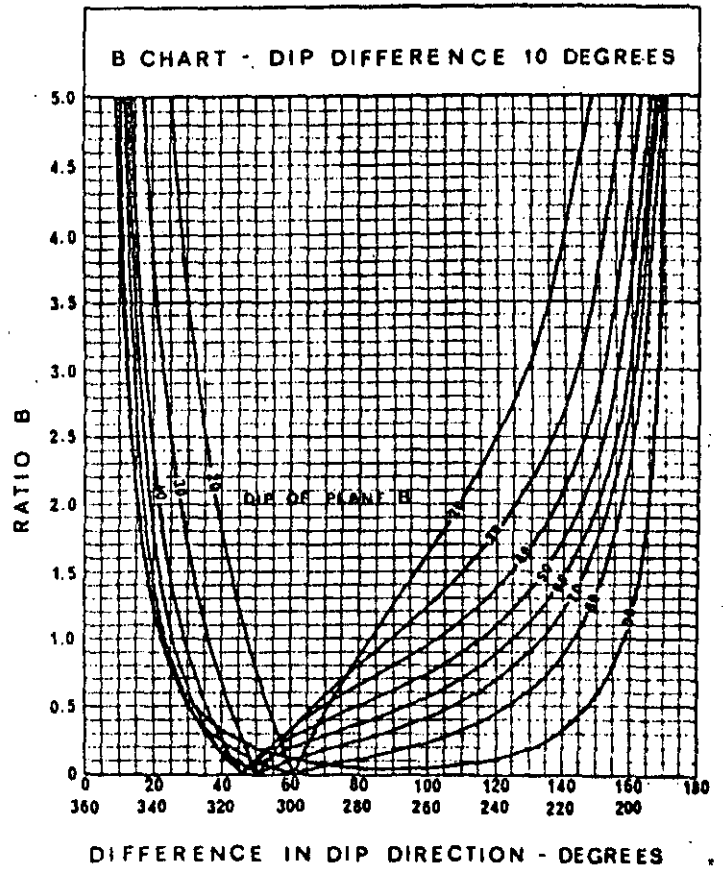
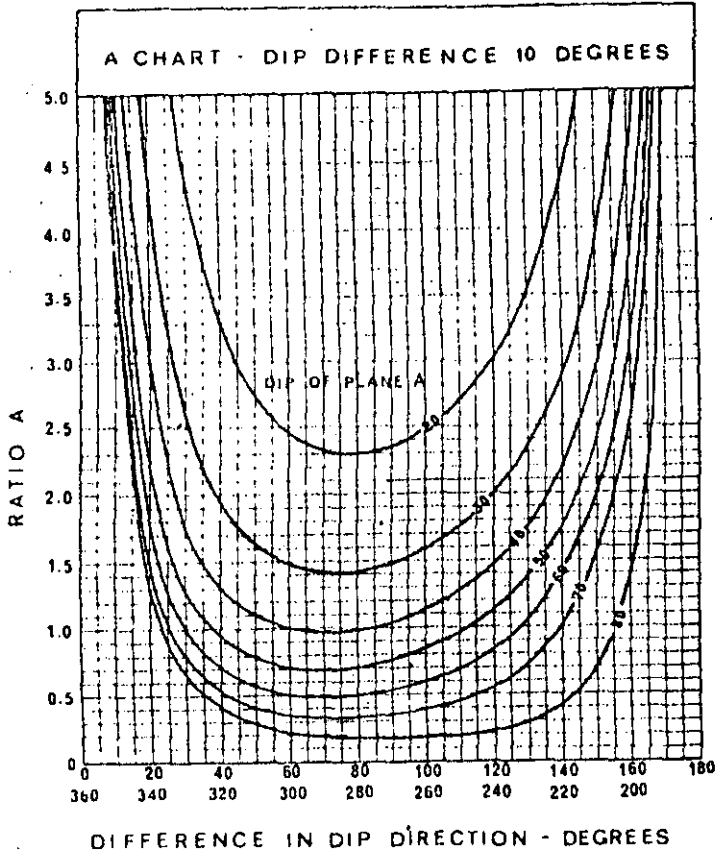


Note : The flatter of the two planes is always called Plane A .

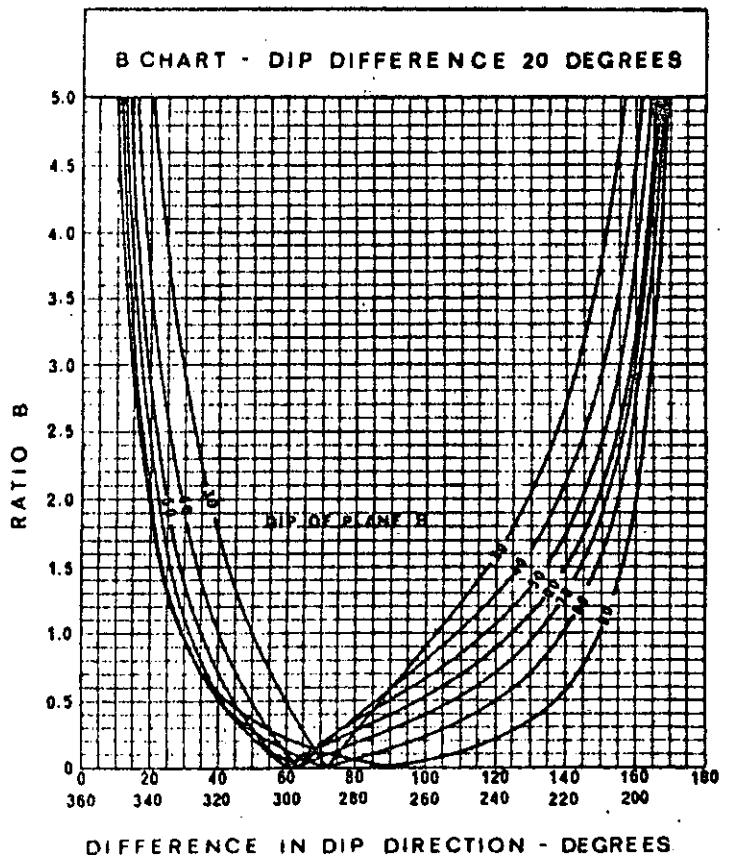
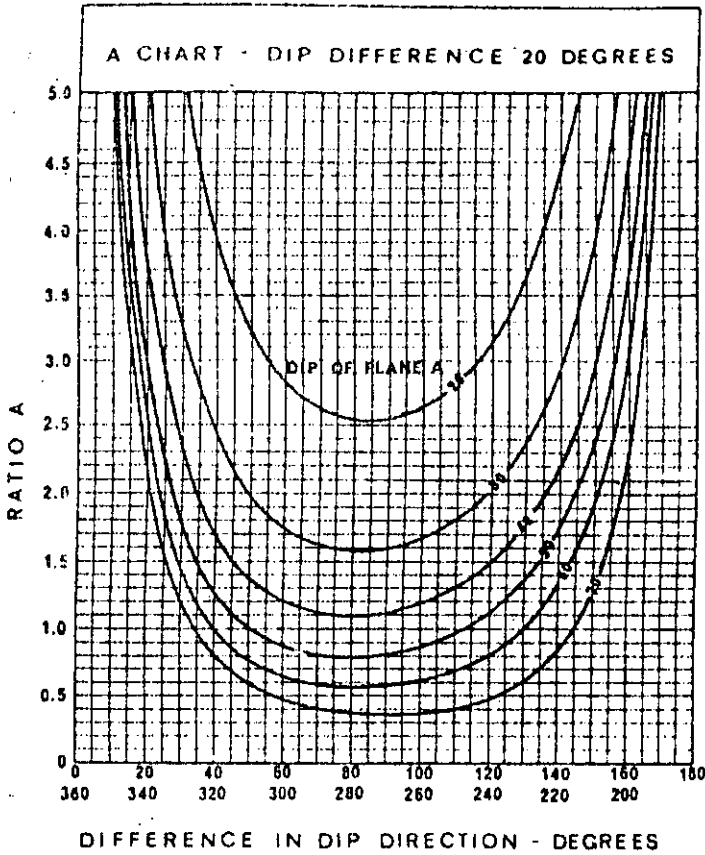
Factor of Safety

$$F = A.Tan\phi_A + B.Tan\phi_B$$

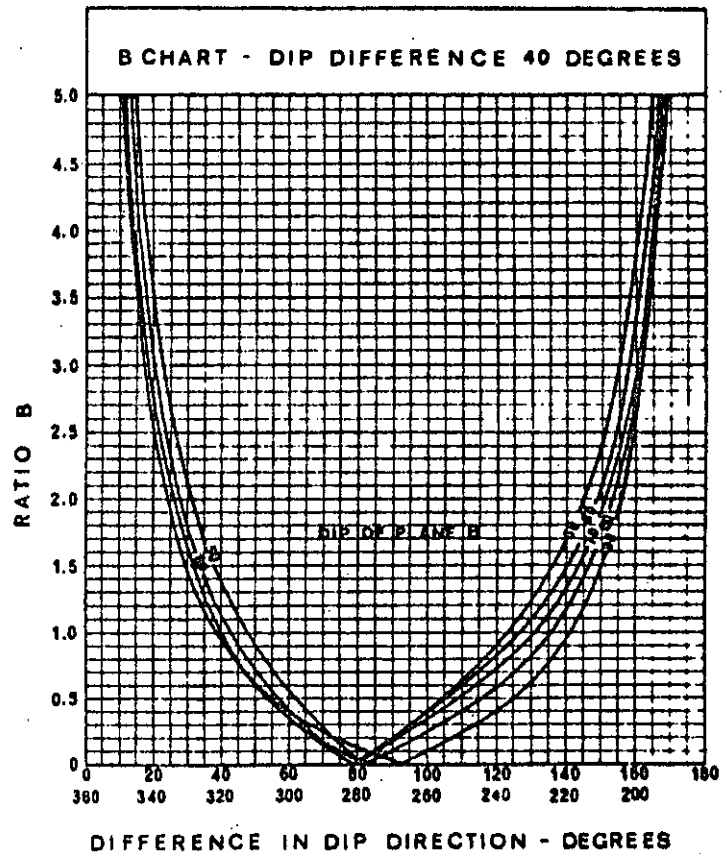
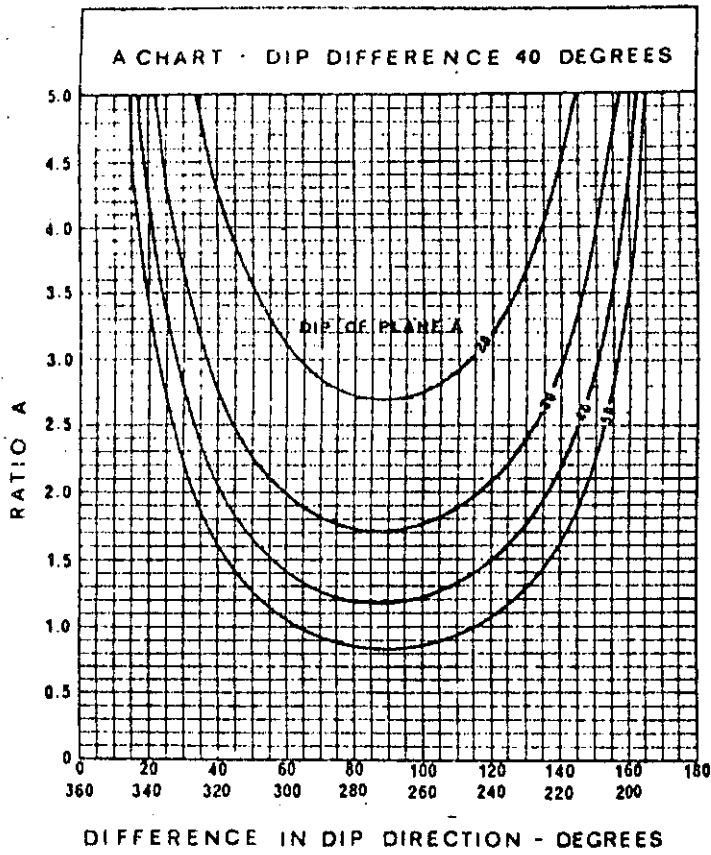


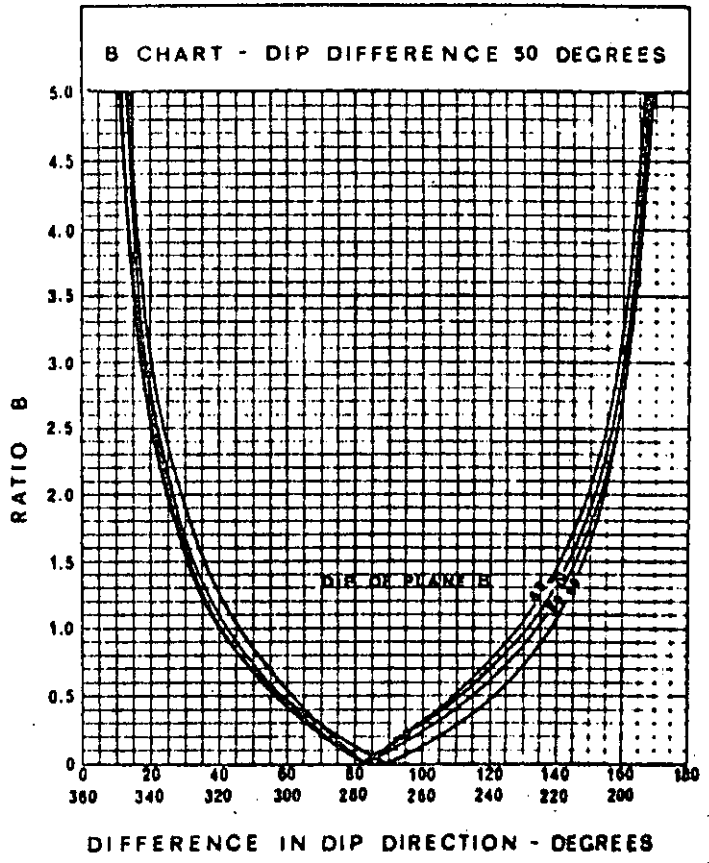
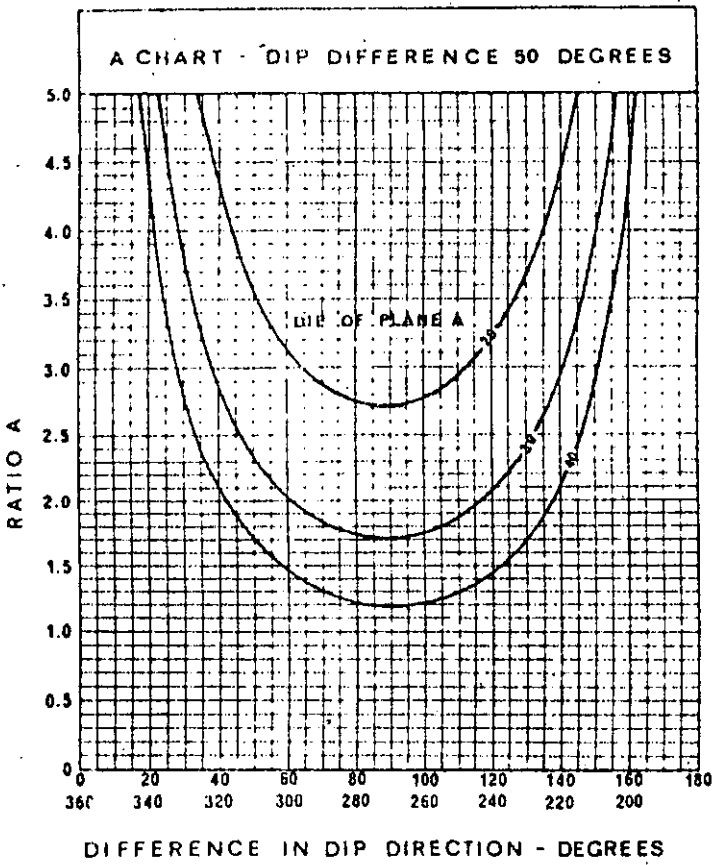


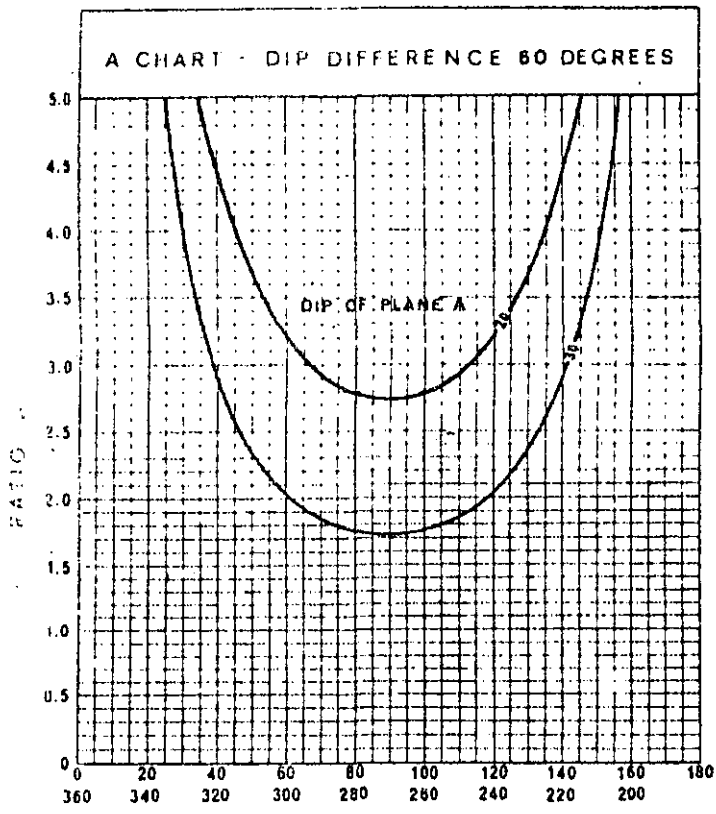




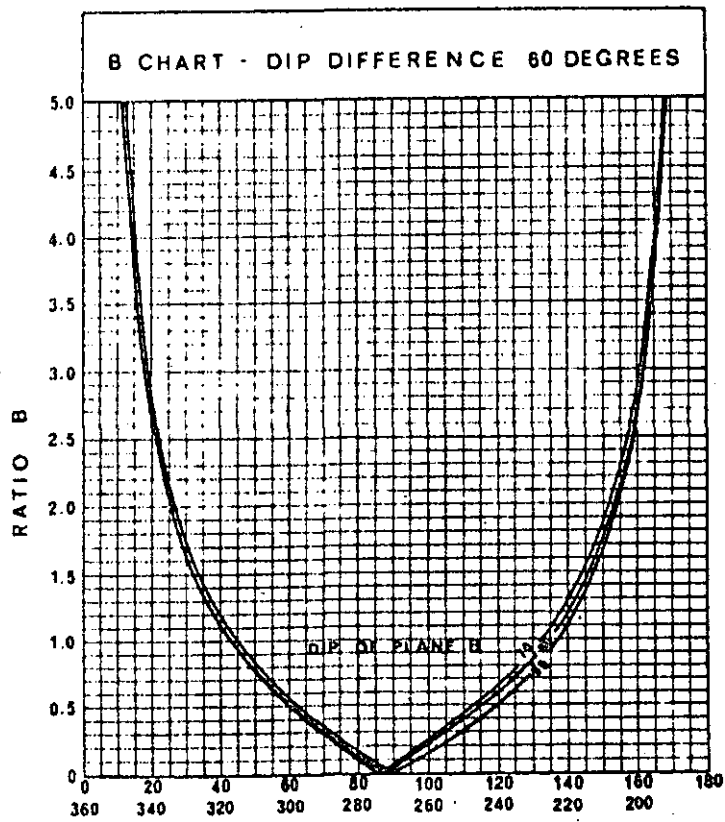




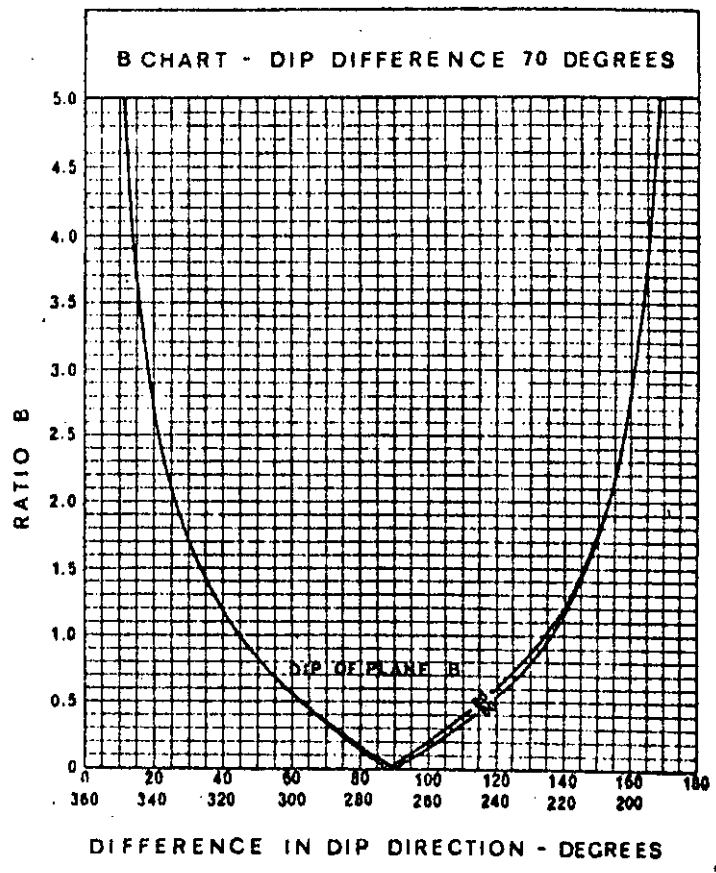
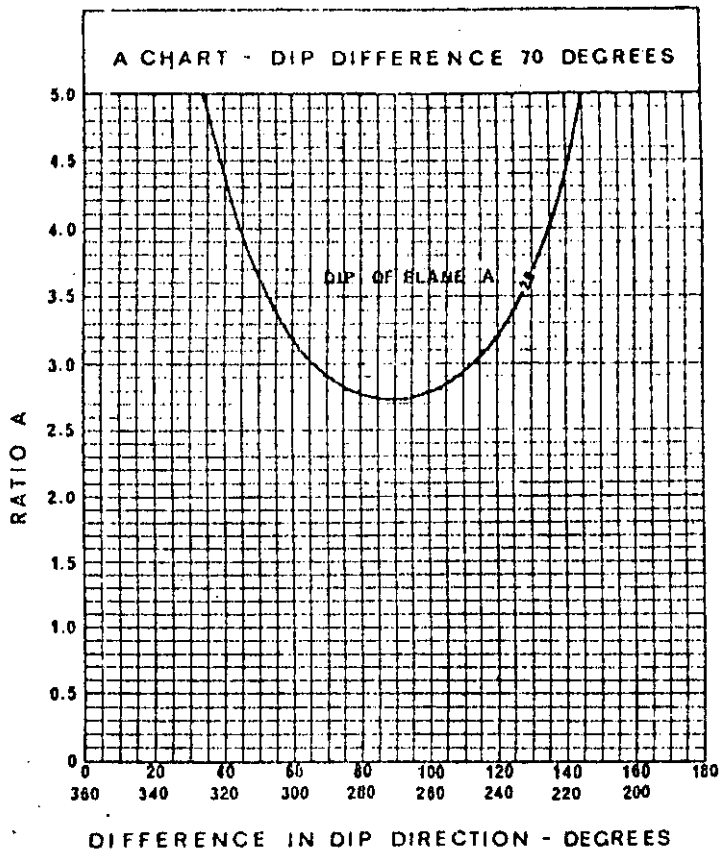




DIFFERENCE IN DIP DIRECTION - DEGREES



DIFFERENCE IN DIP DIRECTION - DEGREES



### Practical example of wedge analysis

During the feasibility study for a proposed open pit mine, the mine planning engineer responsible for the pit layout has requested guidance on the maximum safe angles which may be used for the design of the overall pit slopes. Extensive geological mapping of outcrops on the site together with a certain amount of core logging has established that there are five sets of geological discontinuities in the rock mass surrounding the ore body. The dips and dip directions of these discontinuities are as follows :

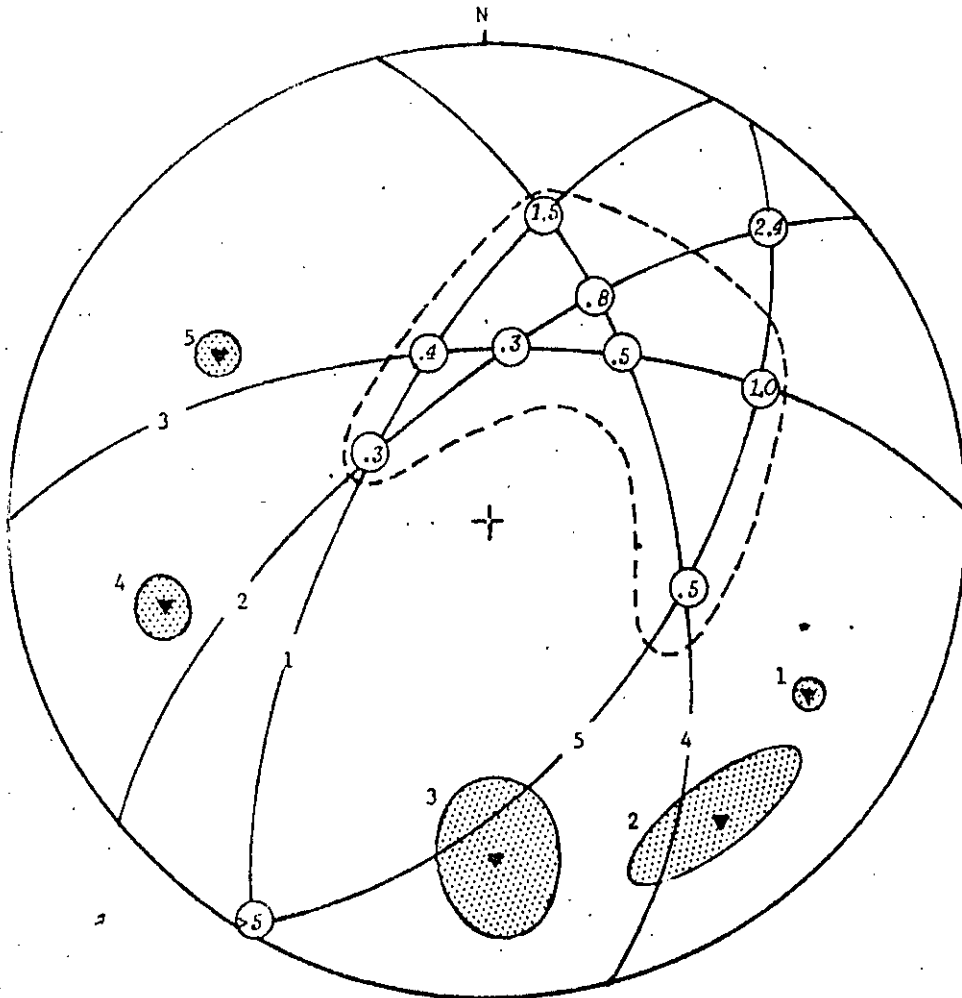
Discontinuity set	dip <sup>o</sup>	dip direction <sup>o</sup>
1	66 ± 2	298 ± 2
2	68 ± 6	320 ± 15
3	60 ± 16	360 ± 10
4	58 ± 6	76 ± 6
5	54 ± 4	118 ± 2

Note that, because this mapping covers the entire site which extends over several acres, the scatter in the dip and dip direction measurements is considerable and must be taken into account in the analysis. This scatter can be reduced by more detailed mapping in specific locations, e.g. figure 17 on page 54, but this may not be possible because of shortage of time or because suitable outcrops are not available.

Figure 97 shows the pole locations for these five sets of discontinuities. Also shown on this figure are the extent of the scatter in the pole measurements and the great circles corresponding to the most probable pole positions. The dashed figure surrounding the great circle intersections is obtained by rotating the stereoplot to find the extent to which the intersection point is influenced by the scatter around the pole points. The technique described on page 47 is used to define this dashed figure. The intersection of great circles 2 and 5 has been excluded from the dashed figure because it defines a line of intersection dipping at less than 20° and this is considered to be less than the angle of friction.

The factors of safety for each of the discontinuity intersections is determined from the wedge charts (some interpolation is necessary) and the values are given in the circles over the intersection points. Because all of the planes are relatively steep, some of the factors of safety are dangerously low (assuming a friction angle of 30°). Since it is unlikely that slopes with a factor of safety of less than 0.5 could be economically stabilised, the only practical solution is to cut the slopes in these regions to a flat enough overall angle to eliminate the problem.

The construction given in figure 98 is that which is used to find the maximum safe slope angle for different parts of the pit. This construction involves positioning the great circle representing the slope face for a particular dip direction in such a way that the unstable region (shaded) is avoided. The maximum safe slope angles are marked around the perimeter of this figure and their positions correspond to the position on the pit perimeter.

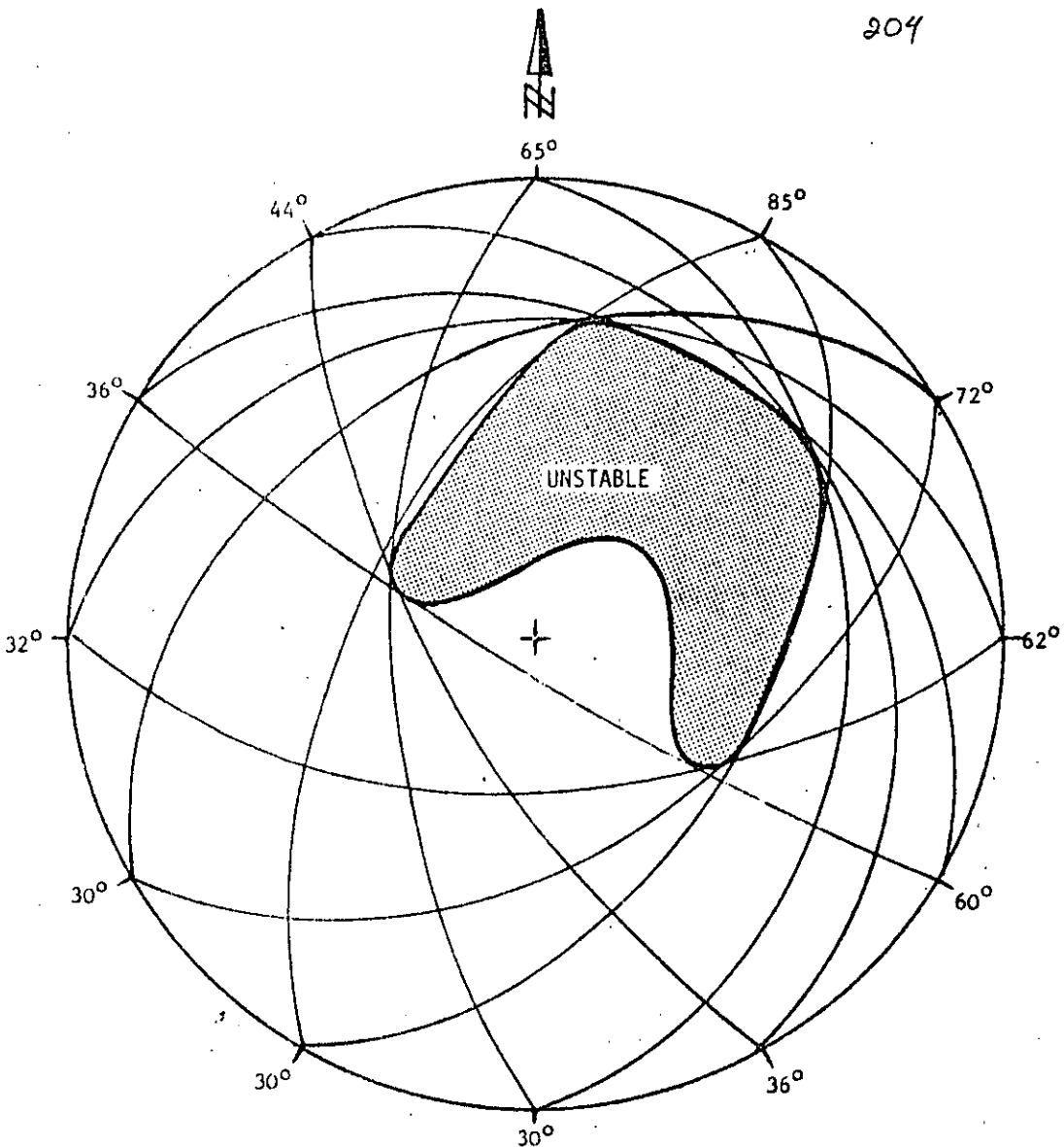


Notes :

- a. Black triangles mark most likely position of poles of five sets of discontinuities present in rock mass.
- b. Shaded area surrounding pole position defines extent of scatter in measurements.
- c. Factors of safety for each combination of discontinuities is given in *italics* in circle over corresponding intersection.
- d. Dashed line surrounds area of potential instability.

Figure 97 : Stereoplot of geological data for the preliminary design of an open pit





Note : Figures around the perimeter are the recommended stable slope angles for the corresponding position on the pit perimeter.

Figure 98 : Stereoplotted of great circles representing stable slopes around an open pit in a rock mass containing the five sets of discontinuities defined in figure 97.

Figure 99 shows the suggested pit layout as presented to the mine planning engineer by the rock slope engineer. The pit floor shape and elevation is that originally specified by the mine planning engineer on the basis of the shape of the ore body. This layout is for the overall slopes only, no benches or haul road have been included. It must also be pointed out that the slopes on the north-eastern side of the pit have been specified at  $70^\circ$  instead of the  $85^\circ$  suggested by figure 98. This laying back results from a consideration of the maximum slope height - slope angle relationship presented in figure 7 on page 20.

On no account should the layout suggested in figure 99 be regarded as the final pit plan. The next stage in the feasibility study would obviously be to consider the implications of this suggested pit shape on the overall stripping ratio and hence the economics of the operation. This could easily result in a re-definition of the economic ore body shape and the need for a new pit layout.

Once the general pit shape has been decided upon, the next step is to consider the layout of both production and final benches and to make provision for a haul road or for an alternative transportation system.

Wedge failures in the benches forming the south-western part of this pit would be unavoidable since any faces cut steeper than  $30^\circ$  would allow the wedge intersections to daylight and, considering the factors of safety shown in figure 97, stabilisation of these benches would not be economically feasible. It could, of course, happen that the assumption of friction only is grossly conservative and that the factors of safety are much too low. It may, therefore, be worth carrying out further stability studies on the south-western side of the pit to determine whether any cohesive strength could be relied upon. Back analysis of local quarry slopes, if such quarries exist in the area, would provide the most reliable source of cohesive strength data. Alternatively, shear strength testing would have to be carried out.

If further studies showed that the benches in the south-western part of the pit would be reasonably stable, this side of the pit would provide a good haul road route since this would permit the stripping ratio to be kept to a minimum by retaining the steep overall slopes on the north-eastern side of the pit.

On the other hand, many open pit operators dislike steep slopes and it may be decided, without further stability studies, to sacrifice on the stripping ratio and to place the haul road on the north-eastern side of the pit. While this would result in a considerable flattening of this side of the pit, it would ensure trouble-free benches since, with the reduced height of benches,  $80^\circ$  bench faces could be tolerated and, according to figure 98, such benches would be safe. This solution would probably be the most satisfactory from an operational point of view - provided that the ore body grade was high enough to stand the high stripping ratio.

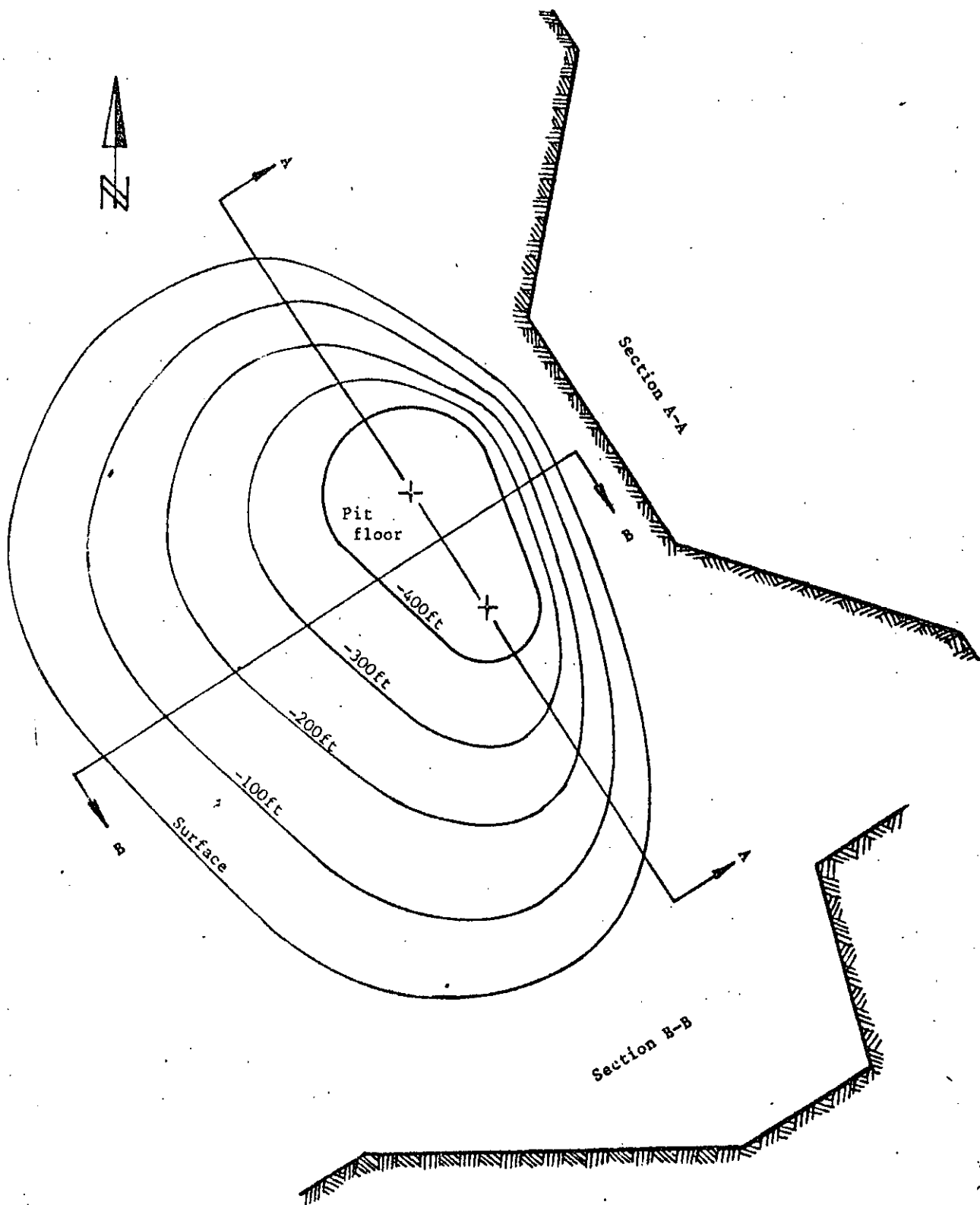


Figure 99 : Design of overall pit slopes according to safe angles defined in figure 98. Note that no benches or haul roads are included in this pit layout.

152. LONDE, P. Une méthode d'analyse a trois dimensions de la stabilité d'une rive rocheuse. *Annales des Ponts et Chaussées*. Paris. 1965. p 37-60.
153. LONDE, P., VICIER, G. and VORMERINGER, R. The stability of rock slopes, a three-dimensional study. *J. Soil Mech. and Foundation Div. ASCE*. Vol. 95, No. SM 1, 1969. p 235-262.
154. LONDE, P., VICIER, G. and VORMERINGER, R. Stability of slopes - graphical methods. *J. Soil Mech. and Foundation Div. ASCE*. Vol. 96, No. SM 4, 1970, p 1411-1434.
155. JOHN, K.W. Engineering analysis of three-dimensional stability problems utilising the reference hemisphere. *Proc. 2nd Congress. Intnl. Soc. Rock Mech.* Belgrade. 1970. Vol. 2, p 314-321.
156. WITKE, W.W. Method to analyse the stability of rock slopes with and without additional loading. (in German). *Felsmechanik und Ingenieurgeologie*. Supp. II. Vol. 30. 1965. p 52-79.  
(English translation in Imperial College Rock Mechanics Research Report No. 6, July 1971 )
157. GOODMAN, R.E. The resolution of stresses in rock using stereographic projection. *Intnl. J. Rock Mech. Mining Sci.* Vol. 1, 1964. p 93-103.
158. GOODMAN, R.E. and TAYLOR, R.L. Methods of analysis of rock slopes and abutments : a review of recent developments. in *Failure and Breakage of Rocks*. Edited by C.Fairhurst. AIME. 1967. p 303-320.
159. HEUZE, F.E. and GOODMAN, R.E. Three-dimensional approach for the design of cuts in jointed rock. *Proc. 13th Symp. Rock Mech.* Urbana, Illinois. 1971.
160. HENDRON, A.J., CORDING, E.J. and AIYER, A.K. Analytical and graphical methods for the analysis of slopes in rock masses. *U.S. Army Engineering Nuclear Cratering Group*. Tech. Rep. No. 36, 1971. 168p.
161. SRIVASTAVA, L.S. Stability of rock slopes and excavations. *J. Eng. Geology*. Indian Soc. Engineering Geology. Vol. 1/1, 1966. p 57-72.
162. SAVKOV, L.V. Considerations of fracture in the calculation of rock slope stabilities. *Soviet Mining Science* 1967, p 1 - 6.
163. HOEK, E., BRAY, J.W. and BOYD, J.M. The stability of a rock slope containing a wedge resting on two intersecting discontinuities. *Quarterly J. Engineering Geology*. Vol. 6, No. 1, 1973.
164. HOEK, E. Methods for the rapid assessment of the stability of three-dimensional rock slopes. *Quarterly J. Engineering Geology*. Vol.6, No. 3. 1973.
165. HOEK, E. and LONDE, P. General report on the design of rock slopes and foundations. *Proc. 3rd Congress Intnl. Soc. Rock Mech.* Denver, 1974 (in press ).

166. TAYLOR, C.L. Geometric analysis of geological separation for slope stability investigations. *Bull. Ass. Engineering Geologists*. Vol. VII, Nos 1 & 2, 1970. p 67-85.
167. TAYLOR, C.E. Geometric analysis of rock slopes. *Proc. 21st Annual Highway Geology Symposium*. Univ. Kansas, April. 1970.
168. WILSON, S.D. The application of soil mechanics to the stability of open pit mines. *Colorado School of Mines Quarterly*. Vol. 54 No.3. 1959. p 95-113.
169. MULLER, L. The European approach to slope stability problems in open-pit mines. *Colorado School of Mines Quarterly*. Vol. 54. No. 3. 1959. p 117-133
170. MULLER, L and JOHN, K.W. Recent developments of stability studies of steep rock slopes in Europe. *Trans. Soc. Min. Engineers, AIME*. Vol. 226, No.3 1963. p 326-332.
171. MULLER, L. Application of rock mechanics in the design of rock slopes. *Intl. Conf. State of Stress in the Earth's Crust*. Santa Monica. 1963. Elsevier, New York. 1964.
172. PETZNY, H. On the stability of rock slopes (in German) *Felsmechanik und Ingenieurgeologie*. Suppl. III. 1967.



**DIVISION DE EDUCACION CONTINUA  
FACULTAD DE INGENIERIA U.N.A.M.**

MECANICA DE ROCAS APLICADA A LA MINERIA Y A LA CONSTRUCCION

USO DEL STEREO NET PARA ESTUDIAR LA ESTABILIDAD DE ROCAS FRACTURADAS

Guillermo Krstulovic L.

MAYO, 1985

# USO DEL STERONEONET PARA ESTUDIAR LA ESTABILIDAD DE ROCAS FRACTURADAS

Guillermo Krstulovic L.\*

## 2. PROPIEDADES DE LAS PROYECCIONES ESFERICAS:

### 2.1. General.

La orientación de un plano en el espacio, definida por su rumbo y manteo, se representa mediante la intersección de dicho plano con una esfera de referencia a través de cuyo centro pasa el plano en cuestión. Para determinar esta línea de intersección en el espacio, es necesario proyectarla sobre el plano ecuatorial de la esfera. Diferentes métodos de proyección han sido ideados; sin embargo las distorsiones que se producen al proyectar variables tridimensionales en un plano bidimensional no han sido resueltas. Para obviar estos problemas dos tipos diferentes de proyecciones se usan en geología estructural. En cristalografía y estabilidad de taludes es deseable usar el método de proyecciones ideados por Wulff ya que en éste las medidas angulares no son distorsionadas. En otros casos, cuando se quiere conocer valores estadísticos de densidad y orientación de estructuras geológicas, es importante preservar una correcta representación de áreas y en consecuencia se emplean las proyecciones de Schmidt. La proyección equiangular (Wulff) es el método usado en este estudio.

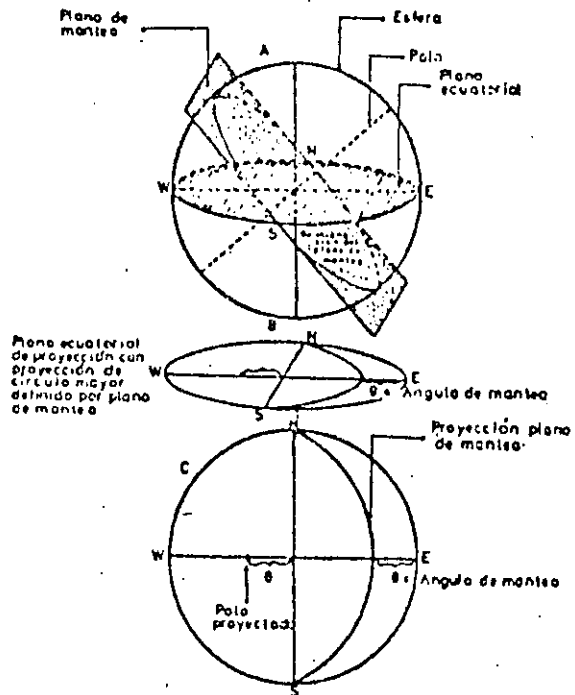


Fig. 1

### 2.2. Proyección equiangular.

El método de proyecciones Wulff ha sido extensamente explicado en la bibliografía (1,2) y no nos extenderemos en detalles. A modo ilustrativo la Fig. 1 muestra un plano tipo (representación de una falla o fractura geológica) interceptando la esfera imaginaria y su posterior proyección mediante un círculo mayor en el plano ecuatorial. La Figura 2 muestra un diagrama Stereonet obtenido de una proyección equiangular en el hemisferio inferior. En él se representa un plano con rumbo NS inclinado a  $40^\circ$  Oeste y también se indica la posición de un plano con rumbo N  $42^\circ$  E inclinado  $70^\circ$  SE, y la intersección de ambos. Se recomienda que una red de este tipo se dibuje en un plástico transparente tal que por superposición y rotación del transparente se puedan dibujar simultáneamente líneas con diferente manteo y rumbo.

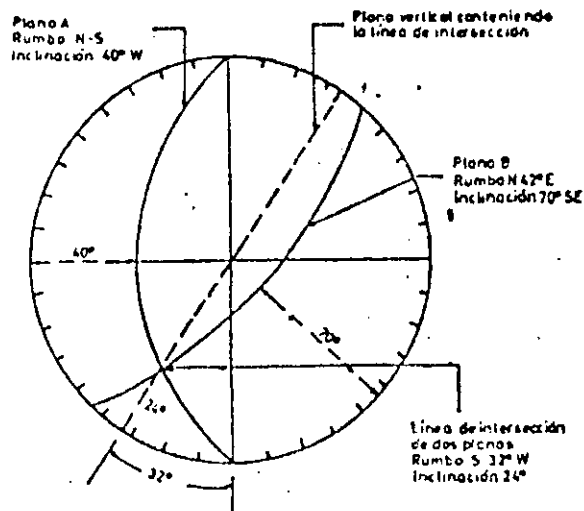


Fig. 2

\*Ing. Jefe del Laboratorio de Mecánica de Rocas, Departamento de Minas, Facultad de Ciencias Físicas y Matemáticas, Universidad de Chile.

II. USO DE STEREO NET PARA EVALUAR LAS FUERZAS DESLIZANTES Y RESISTENTES PARA UNA CUÑA DE ROCA EN DESLIZAMIENTO POTENCIAL.

El uso de Stereonet en el análisis de estabilidad para rocas fracturadas ha sido descrito por varios autores (3, 4, 5). El método puede ser utilizado para evaluar la estabilidad de una cuña de roca

tridimensional descansando sobre el plano con resistencia friccional. Su aplicación se asemeja al sistema poligonal para sumar fuerzas gráficamente, pero en ese caso sólo la orientación (y no la magnitud) de las fuerzas se determinan directamente con Stereonet.

En la Fig. 9 se muestra la orientación de las fuerzas de reacción en el plano de fallamiento

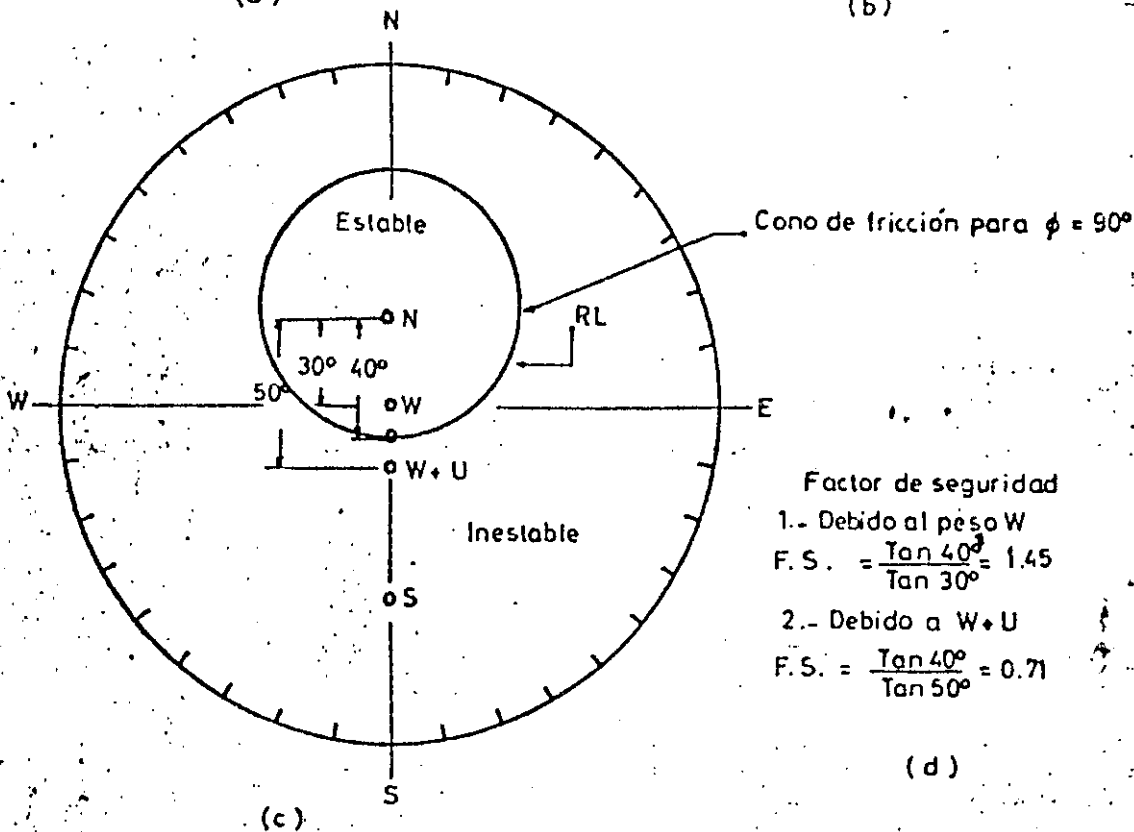
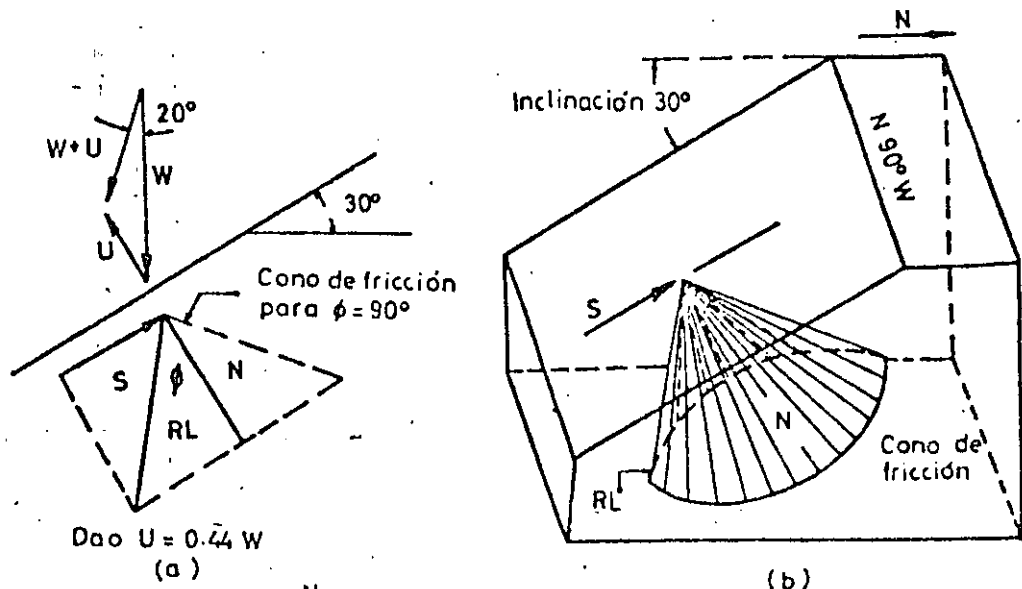


FIG. Nº 3. Deslizamiento en un plano. -



para el caso simple de deslizamiento en un plano. El análisis de estabilidad se divide en dos partes. Primero se dibuja en Stereonet la orientación de la reacción de resistencia máxima RL en el plano de fallamiento potencial. En este caso corresponde a la componente resistente definida por el ángulo de fricción interna  $\phi$ , el cual determina un "cono de fricción" ( $\phi$  grados con respecto a la normal al plano). La segunda parte corresponde a la determinación de la orientación de las fuerzas deslizantes actuando en la cuña. Estas fuerzas pueden incluir el peso del material, fuerzas de aceleración, presión de agua en los planos de falla y fuerzas pujantes que se presentan debido a estructuras de superficie (ejemplo apoyos de represas de agua).

La suma gráfica de vectores se usa con Stereonet para determinar la orientación de la resultante de fuerzas deslizantes, definiéndose con ello zonas de estabilidad e inestabilidad según el ángulo con que actúa la fuerza deslizante resultante. Por ejemplo, si esta fuerza actúa con un ángulo más alejado de la normal, con respecto al plano potencial de falla, que el ángulo de resistencia de reacción máxima  $\phi$  se produce el deslizamiento. Se destaca que la ubicación exacta de las fuerzas no es conocida y la suma de momentos no se efectúa.

En nuestro ejemplo el plano N 90° W ubica su polo sobre la línea NS en Stereonet. Para dibujar el cono de fricción  $\phi = 40^\circ$  es necesario usar el enmarcado de 40° desde N en la red Stereonet. Se observa que N no está en el centro del círculo formado por el cono de fricción.

En la Fig. 3 se han estudiado dos casos posibles. En el primero la cuña de roca está solicitada por su propio peso W que se representa en el centro de Stereonet y por lo tanto dentro de la zona estable delimitada por el cono de fricción. El factor de seguridad para este caso es 1,45. En el segundo, se ha supuesto una presión de poro U, equivalente a 0,44 W lo que ha desviado la resultante  $W + U$  en 20° fuera de la vertical. Esto en Stereonet significa quedar fuera de la zona estable con un factor de seguridad 0,71.

### III. ANALISIS DE ESTABILIDAD PARA MÚLTIPLES SISTEMAS DE FRACTURAS:

El ejemplo anterior ilustraba el caso más sencillo para una cuña de roca deslizante sobre un plano único. El método puede hacerse extensivo a una cuña formada por dos, tres o más planos de deslizamiento. Para múltiples planos Londe<sup>6</sup> y Hendron<sup>7</sup> han planteado varios posibles modos de fallamiento. Para el ejemplo mostrado en Fig. 4 podemos suponer los siguientes modos de fallamiento:

- Deslizamiento cuesta abajo en plano 1.
- Deslizamiento cuesta abajo en plano 2.
- Deslizamiento cuesta abajo en intersección de planos 1 y 2.

Además se presentan las posibilidades teóricas de "levantamiento de la cuña" desde los planos 1 ó 2.

#### III.1. Orientación de la línea de intersección de los planos y fuerza de reacción en el plano de fallamiento.

La orientación de la línea de intersección de los planos representados en la Fig. 4, se obtiene en Stereonet al dibujar los círculos mayores correspondientes a cada plano. Ver Fig. 5. En nuestro ejemplo la línea de intersección está orientada S 27°W con una inclinación 40° desde la horizontal.

Para el caso de deslizamientos solamente en el plano 1, la orientación de RL1 representada por el cono de fricción en el plano 1 define las zonas estables e inestables. Para deslizamientos en la intersección de planos 1 y 2, la orientación de  $RL1 + RL2$  separa las zonas estables e inestables. El límite entre deslizamientos en la línea de intersección y deslizamientos en plano 1 resulta ser el círculo mayor que pasa a través de N1 y S1, siendo estas las fuerzas normales y de cizalle actuando en el plano 1.

El estudio de estabilidad se inicia construyendo los conos de fricción para ambos planos. Ellos quedan determinados a partir de las normales N1 y N2 según se explicó en la Fig. 3c. Para el caso de deslizamientos en la intersección de ambos planos las fuerzas de cizalle  $S_1$  y  $S_2$  actúan en la dirección del deslizamiento siendo ésta paralela a la línea de intersección. Las fuerzas  $S_1$  y  $S_2$  se dibujan en el mismo punto en Stereonet. Conocidos N y S para cada plano, las fuerzas de reacción respectivas se deducen directamente y con la resultante RL en cada plano actuando en la misma sección que sus respectivas N y S. Por ejemplo, la dirección de las fuerzas de reacción RL1 puede localizarse dibujando un círculo mayor a través de N y S. RL1 se ubica donde este círculo intercepta el cono de fricción a través del plano 1. Conocidos RL1 y RL2 la resultante total del sistema  $RL1 + RL2$  debe actuar en un plano paralelo a RL1 y RL2. En Stereonet este dato se obtiene trazando un círculo mayor a través de RL1 y RL2, y la reacción total se ubicará en algún lugar de este círculo. Sin embargo se observa que su posición exacta dependerá de la orientación de las otras fuerzas deslizantes por considerar, ya que la orientación de estos vectores afecta la magnitud relativa de RL1 y RL2.

#### III.2. Fuerzas Mínimas requeridas para causar deslizamientos o estabilizar la cuña.

Para causar deslizamientos en la cuña, el vector deslizante resultante debe yacer fuera de las zonas estables y el factor de seguridad debe ser reducido al valor uno. Esquemáticamente ello se consigue

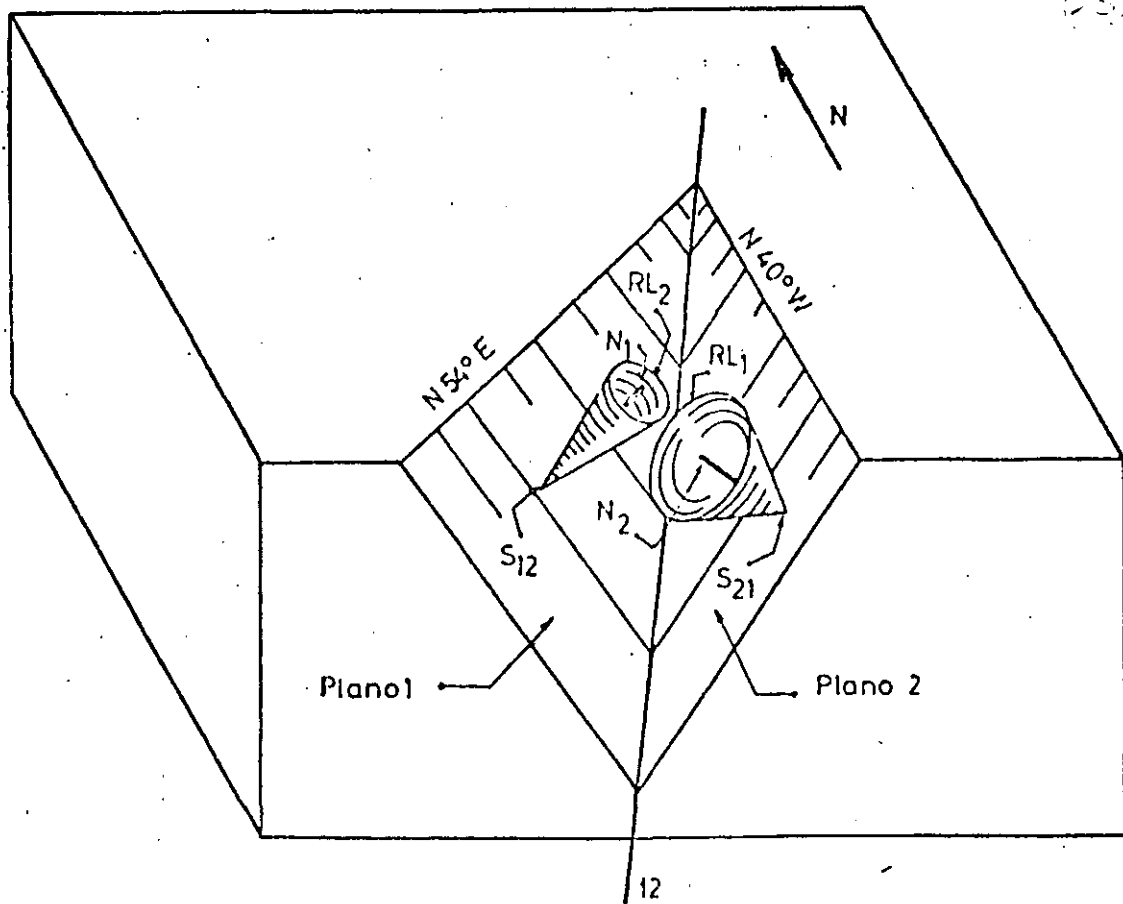


FIG. Nº4... Deslizamiento en dos planos...

mediante una fuerza NW que dibujada en un polígono de fuerza se ubicaría entre la punta del vector existente (vector peso  $W$  en este caso) y perpendicular al plano  $RL1 + RL2$ .

En la Fig. 6 el ángulo entre  $W$  y  $RL1 + RL2$  es cuatro grados. Se observa que el rumbo de la fuerza mínima NW ( $S 40^\circ W$ ) no es el mismo rumbo de la línea de intersección ( $S 27^\circ W$ ). De acuerdo al esquema de fuerza presentado en la Fig. 6 la magnitud de la fuerza mínima requerida para iniciar el deslizamiento es igual a  $0,07 W$  y se orienta al  $S 40^\circ W$  a  $4^\circ$  hacia arriba.

Una vez que se ha estimado la magnitud y dirección de la fuerza que podría causar el deslizamiento es necesario determinar la magnitud y dirección de las fuerzas necesarias para estabilizarla y establecer así el factor de seguridad. La característica de la fuerza estabilizadora dependerá del tipo de escurrimiento observado, por ejemplo:

CASO 1.

La cuña de Fig. 3 está solicitada por una fuerza

deslizante  $D$  y escurre potencialmente en el plano 1.

En este caso la orientación  $N1$  y  $D$  es conocida, siendo sólo necesario determinar las características de  $S1$  y  $RL1$ . Los vectores  $S1$  y  $RL1$  actúan dentro de los planos definidos por  $N1$  y  $D$ , su posición se obtiene dibujando un círculo mayor a través de  $N1$  y  $D$  (línea sólida en Fig. 7). Resulta así que  $S1$  se ubica a  $90^\circ$  de  $N1$  y  $RL1$  a  $\phi$  grados de  $N1$  a lo largo del círculo mayor. En el ejemplo, el ángulo entre  $N1$  y  $RL1$  es  $\phi = 20^\circ$ , el ángulo entre  $RL1$  y  $D$  es  $37^\circ$ . El factor de seguridad resultante es:

$$F.S. = \frac{\text{Fuerza de cizalle máxima}}{\text{Fuerza de cizalle movilizada}} =$$

$$\frac{\text{Tang } 20^\circ}{\text{Tang } (20^\circ + 37^\circ)} = 0,24$$

Para este caso el deslizamiento de la cuña será en dirección de las fuerzas de cizalle  $S$ , con incli-

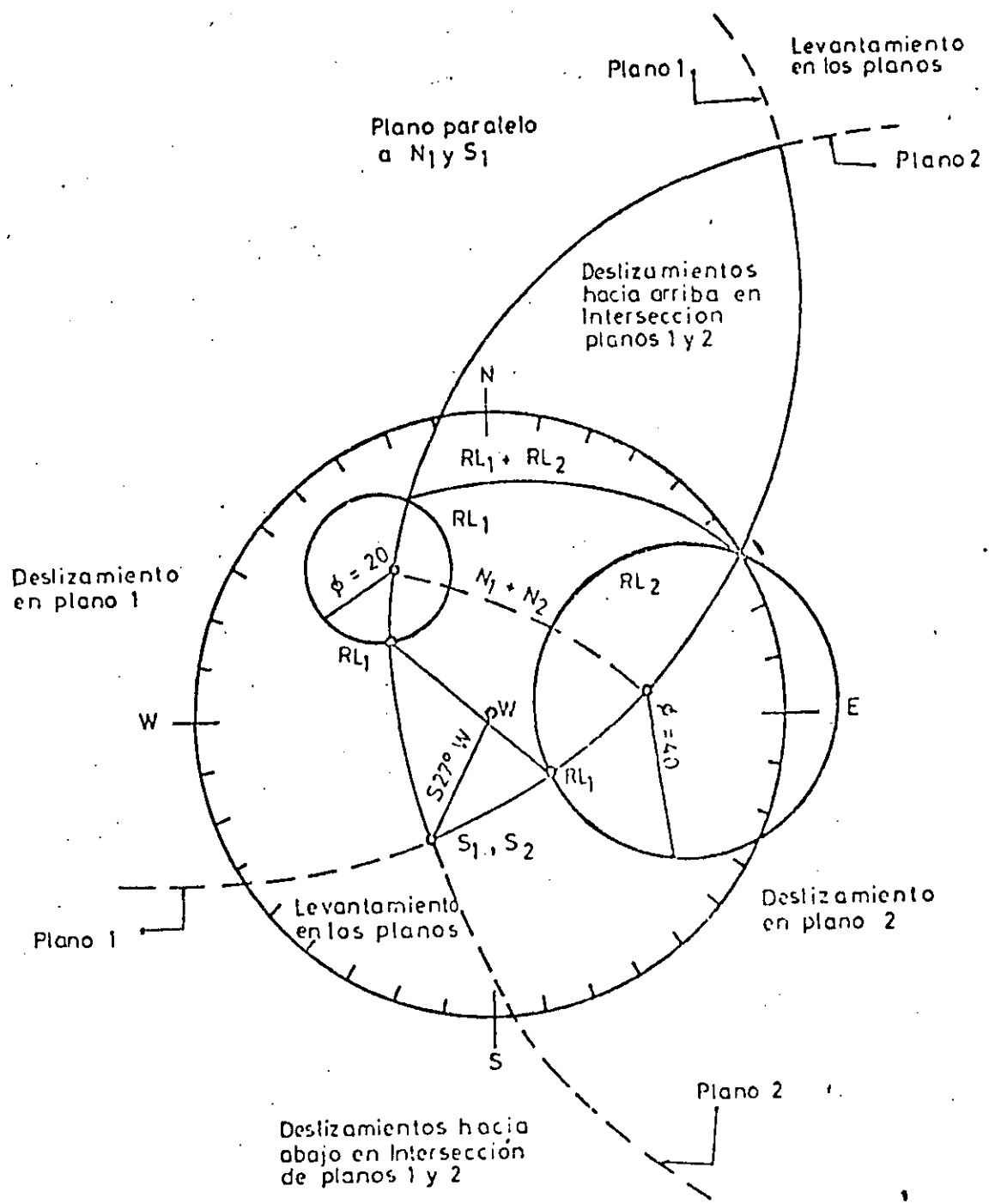


FIG. Nº 5.- Stereonet para deslizamientos en dos planos.-

nación de  $19^\circ$  y en la dirección S  $40^\circ$  W en el plano 1.

La magnitud de la fuerza mínima  $P$ , requerida para cerrar los  $37^\circ$  angulares existentes entre  $RL_1$  y  $D$  (y consecuentemente aumentar el factor de seguridad a uno), puede determinarse de la construcción gráfica en la Fig. 7. Si la magnitud  $D$  es conocida entonces la fuerza mínima es:

$$P_{min} = D \cdot \text{sen } 37^\circ$$

CASO 2.

La cuña es solicitada por el vector deslizante  $B$  y escurreá a lo largo de la línea de intersección de los planos 1 y 2,  $S_1$  y  $S_2$  actúan paralelos a la línea

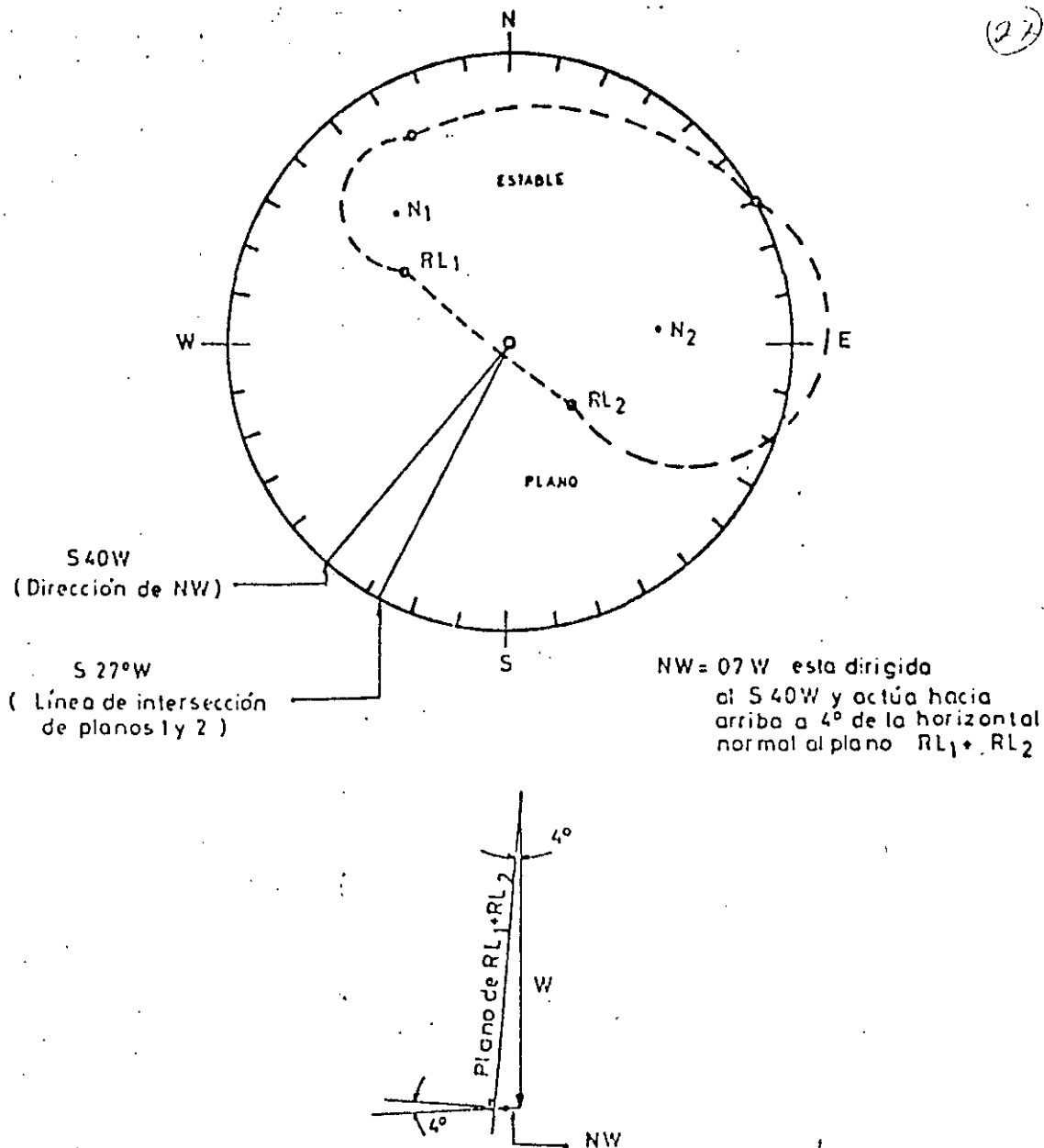


FIG. Nº 6.- Deslizamientos en dos planos  
Fuerza mínima requerida para causar deslizamiento..

de intersección de estos planos. La posición de N1 + N2 y RL1 + RL2 quedará definida al dibujar un círculo mayor (línea sólida en Fig. 7) a través de S1, S2 y B. El vector RL1 + RL2 se localiza en la intersección de este círculo mayor y otro círculo que pasa por RL1 y RL2. También el vector N1 + N2 se localiza en la intersección de los círculos mayores que pasan por S1 + S2, B y N1, N2 respectivamente.

El factor de seguridad queda definido por los ángulos 51° entre N1 + N2 y B, y el ángulo 33° entre N1 + N2 y RL1 + RL2.

$$F. S. = \frac{\text{Tang } 33^\circ}{\text{Tang } (33^\circ + 18^\circ)} = 0,53$$

La dirección del deslizamiento es a lo largo de la línea de intersección S 27° W con inclinación 40° hacia abajo.

#### IV. PROCEDIMIENTO COMPUTACIONAL

El método descrito resulta aparentemente complicado y tedioso en el dibujo manual, pudiendo

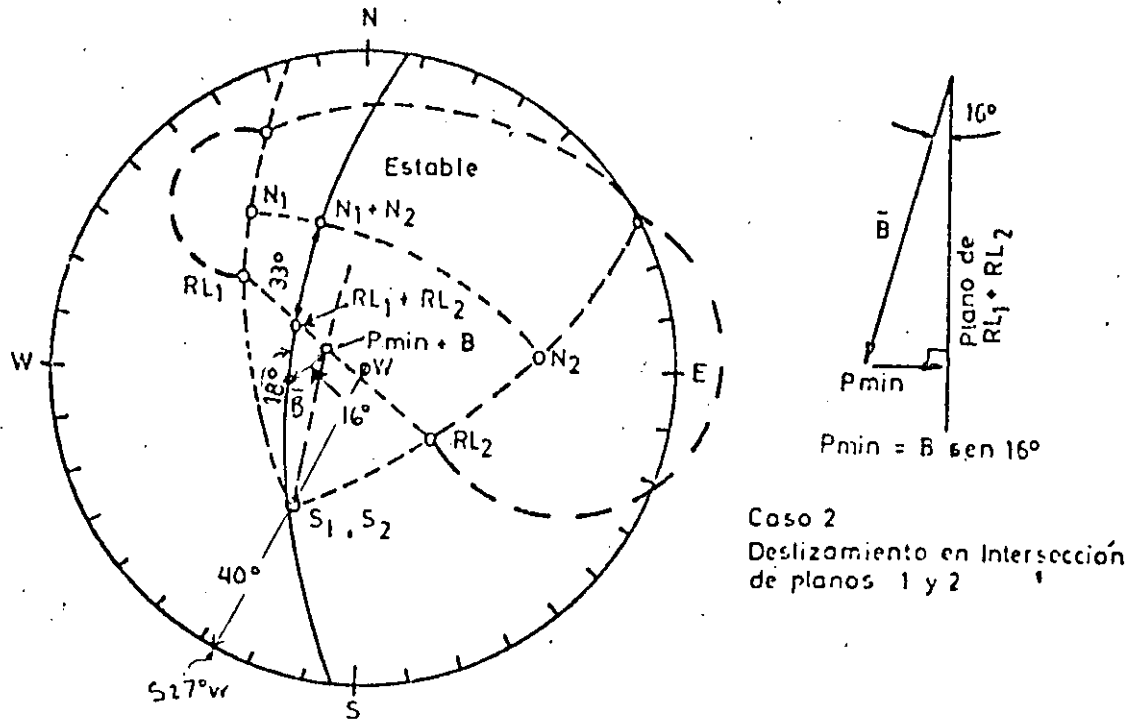
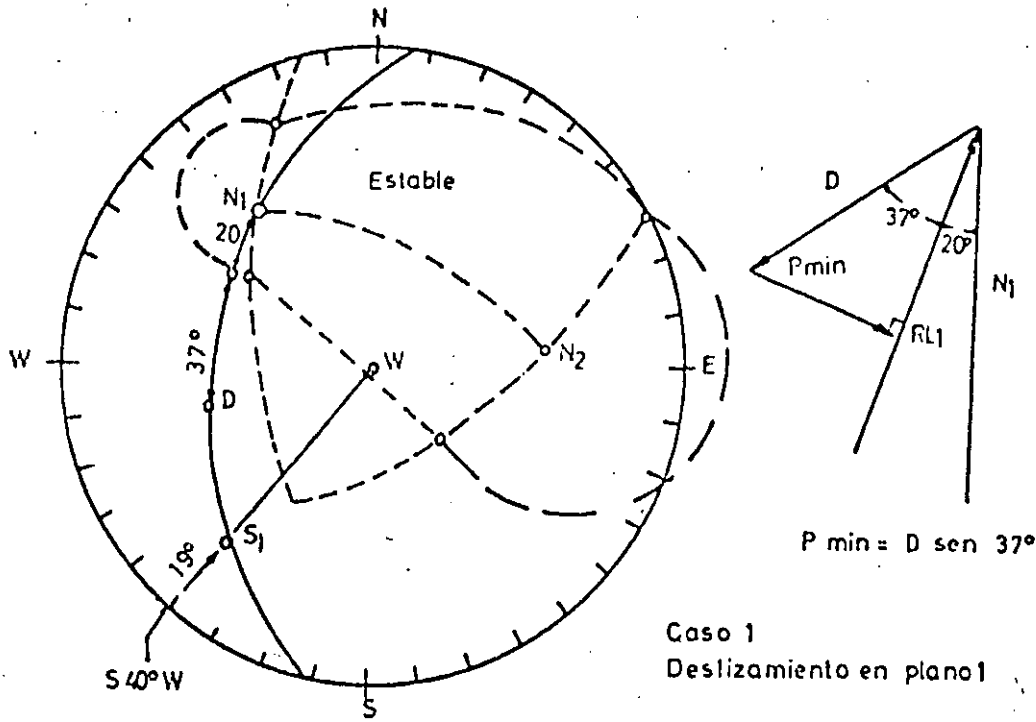


FIG. Nº 7.- Fuerza mínima requerida para establecer la cuña -

aumentar las dificultades al crecer el número de caras libres de la cuña de roca en estudio. Pues ésta muchas veces no se encuentra delimitada por una clara y delineada línea de falla sino por una serie de discontinuidades geológicas (vetas, diaclasas, etc.) que presentan planos de debilidad.

A objeto de obviar estos problemas se han diseñado una serie de programas de computación (8.9) para procesar toda la información por etapa. El ciclo se inicia con la recolección de información en terreno dividiendo la zona a estudiar en bloques (metros de galerías, minas subterráneas; super-

ficie de bancos, mina a tajo abierto). Los datos en forma de rumbo y manteo para cada discontinuidad geológica son procesados por STEREO NET I para dibujar concentración de palos en una Red de Wulff. STEREO NET II identifica formaciones de grupos de palos sacando su orientación media y desviación standard. Finalmente STEREO NET III obtiene las intersecciones de planos principales y analiza los factores de seguridad.

REFERENCIAS

1. Turner, F. J.; Weiss, L. E. (1963), Structural Analysis of Metamorphic Tectonites, Mc Graw-Hill.
2. Lowe, K. E.; Etrer, D. (1961), Petrofabric Counting by Digital Computer, Geol. Soc. Amer. Sp. Paper 68, p. 220.
3. Goodman, R. E. (1969), Discussion of Graphical Stability Analysis of Slopes in Jointed Rock by Klaus John. Proc. ASCE vol., 95 SM2. marzo.
4. John, K. W. (1968), Graphical Stability Analysis of Slopes in Jointed Rock. Proc. ASCE vol. 94 SM2. marzo.
5. Londe P. V. et al. (1960), Stability of Rock Slopes. Graphical Methods, Proc. ASCE vol. 96 SM4. julio.
6. Londe P. V., et al. (1969), Stability of Rock Slopes A three Dimensional Study. Proc. ASCE vol. 95 SM7. enero.
7. Hendron, A. J. (1971), Analytical and Graphical Methods for the Analysis of Slopes in Rock Masses. Department of Civil Engineering, University of Illinois.
8. Kristulovic, G. et al. (1974), Reporte Técnico RT-74-1 Stereonet. Programa de Computación para Cuantificar Discontinuidades Geológicas. Compañía de Cobre El Salvador, Colmesal.
9. Kristulovic, G. et al. (1975), Informe Técnico IN-75-1 Análisis Vectorial para el estudio de rocas fracturadas. Reporte Interno Sección Mecánica de Rocas, Depto. de Minas, Universidad de Chile.

MIEMBRO  
AMERICAN SOCIETY  
OF PHOTOGRAMMETRY



Y  
AMERICAN CONGRESS  
ON  
SURVEYING AND MAPPING

OFICINA TECNICA ANTONIO de GAVARDO

- LEVANTAMIENTOS AEROFOTOGRAMETRICOS     LEVANTAMIENTOS FOTOGEOLOGICOS CON CONTROL DE TERRENO     MENSURAS DE PROPIEDADES MINERAS POR FOTOGRAMETRIA     PROYECTOS DE CAMINOS Y FERROCARRILES     CUBICACION DE DESMONTES Y CONTROL DE TRANQUES POR FOTOGRAMETRIA TERRESTRE     CATASTRO DE PROPIEDADES MINERAS, ETC.

DISTRIBUIDOR EXCLUSIVO DE  
FILOTECNICA SALMOIRAGHI SPA

MILANO, ITALIA

REPRESENTANTES

MC. PHAR. GEOPHYSICS LTDA.

ONTARIO, CANADA

- TALLER REPARACION INSTRUMENTOS DE INGENIERIA Y OPTICA  
 TALLER COPIAS DE PLANOS

AV. ISIDORA GOYENECHEA 1162 - LAS CONDES

TELEFONOS: 551231 - 432191

CASILLA 107 - SANTIAGO 13



**DIVISION DE EDUCACION CONTINUA  
FACULTAD DE INGENIERIA U.N.A.M.**

MECANICA DE ROCAS APLICADA A LA MINERIA Y A LA CONSTRUCCION

SLOPE STABILITY WITH PLANE, WEDE AND POLYGONAL SLIDING SURFACES

MAYO, 1985

Reprint of the Proc. of Int. Symposium on  
"Rock Mechanics Related to Dam Foundations",  
Rio de Janeiro, 1978

SLOPE STABILITY WITH PLANE, WEDGE AND POLYGONAL SLIDING SURFACES

Prof. Dr. K. Kovari

Dipl. Ing. P. Fritz

Federal Institute of Technology Zurich, Switzerland



Summary - Résumé :

Slope stability for planar, polygonal and wedge-shaped sliding surfaces: A formula for the design of anchors in rock slopes is presented. Since several parameters can be lumped together in two factors and the cohesion appears in an explicit form the formula can be used to carry out parametric studies with little expenditure of time. Due to an analogy between plane failure and the sliding of a wedge on two planes the same formula can be used to describe the three dimensional problem. An extension of the work to problems involving polygonal sliding surfaces is presented, which is based upon the hypothesis that due to kinematic considerations a discrete number of internal slip surfaces must exist in the rock mass. These internal slips may take place on preferred surfaces, which arise from the actual geological situation. In the majority of cases, however, new ruptures are created, that depend only partially on existing planes of weakness. In the numerical procedure the rock mass is divided up into discrete elements governed by the assumed internal slip surfaces. The basic formula mentioned above is then applied to each element separately. The internal forces acting on the interfaces between elements are defined by an additional failure condition. In an example taken from rock engineering practice it is shown how great the influence of the rock mass in resisting the development of such internal slip surfaces is with respect to the stability of the slope.

Stabilité de talus rocheux sur des surfaces de glissement polygonales et spaciales: Pour dimensionner l'ancrage d'un talus rocheux, on présente une formule qui permet d'effectuer des analyses paramétriques avec un travail minimum du fait que plusieurs paramètres sont résumés dans deux facteurs et que la cohésion est prise en compte explicitement. Grâce à une analogie entre le problème plan des talus et le glissement d'un coin de roche sur deux plans, le problème spacial se laisse aussi traiter avec la même formule fondamentale. Un élargissement du domaine d'application à des problèmes à surfaces de glissement polygonales se base sur le fait que pour des raisons cinématiques il existe des glissements internes ou cisaillements dans la masse rocheuse. Ces surfaces de cisaillement sont parfois données par la nature, mais la plupart du temps il se forme des cassures nouvelles qui ne suivent que partiellement des zones faibles préexistantes. Les surfaces de cisaillement divisent la masse rocheuse en différentes parties où la formule fondamentale citée peut être appliquée séparément.

## 1. Introduction

Normally, for investigating numerically the stability of rock slopes, simplified deformation mechanisms are assumed. The computations are then carried out for various material properties and loading values. With the aid of the simple mathematical relationships presented here numerous behaviour hypotheses can be easily tested, so that a better understanding of the interplay of the forces in the rock structure is possible. Only on the basis of the knowledge thus gained and by considering influences not directly quantifiable can decisions be made regarding shape, drainage and safety measures in a rock slope. For a parameter analyses in rock engineering it is important that the extent of the mathematical formalism is kept to a minimum. The computational method given here meets this requirement in two respects. Firstly, a basic formula for the safety factor of rock slopes is presented, which is valid for both slip along a plane surface and of a three-dimensional rock wedge. This is possible thanks to the discovery of a formal analogy between the two problems. Secondly, the use of this formula is further simplified by means of charts or programming for a pocket calculator. The investigation of problems with polygonal slip surfaces gives a useful insight into the relationships holding for kinematically complex slides. Here, especially, the significance of potentially new failure surfaces, i.e. slip surfaces within the sliding rock mass, is evident.

## 2. Theoretical Foundations

The mathematical treatment of rock slides is based upon the hypothesis of limit equilibrium. The rock is idealized as a rigid body, and only sliding but no rotation or lifting-off of the potential sliding mass is considered.

### 2.1 Remarks on the definition of safety factor

In civil engineering safety factor is usually understood as the relationship between the applied stress and a strength. In this sense the safety factor with respect to sliding of a slope is formulated as

$$F_s = \left| \frac{\text{maximum shear resistance}}{\text{applied shear force}} \right| \quad (1)$$

Another definition that is frequently used is based upon a grouping of the forces acting on the sliding mass. This leads to the following definition of safety factor

$$F_s = \frac{\text{resisting forces}}{\text{driving forces}} \quad (2)$$

With the aid of a simple example it is shown that the two definitions can lead to completely different results (Kovari and Fritz, 1976). A body resting on an inclined plane is loaded by its self-weight  $W$  and an anchor force  $T$ . The corresponding components parallel and normal to the sliding surface,  $W_s$ ,  $T_s$  and  $W_n$ ,  $T_n$  respectively, are shown in Fig.1. If the maximum shear force at the moment of slip is designated by  $S_{max}$ , then according to definition (1)

$$F_s = \frac{S_{max}}{W_s - T_s}$$

so that the component of the anchor force  $T_s$  reduces the effective applied force in the denominator. The safety factor defined by (2), however, becomes

$$\bar{F}_s = \frac{S_{max} + T_s}{W_s}$$

i.e. the anchor force contributes to increase the resisting force in the numerator.

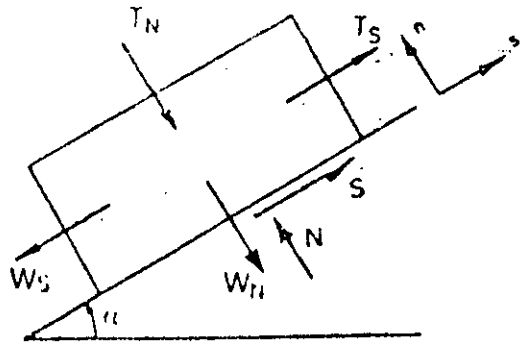


Fig. 1: Potential sliding mass with the components of self-weight  $W_s$ ,  $W_n$  and the anchor force  $T_s$ ,  $T_n$

It is evident that difficulties arise in applying the second definition. Whereas a loose anchor is considered as a passive resisting force in the numerator, if one is consistent, a prestressed anchor would be considered as an active force reducing the resultant driving force in the denominator.

A comparison of the two definitions of safety factor for a given case is shown in Fig. 2. The ratio  $T_s/W_s$  is plotted as abscissa, the ordinate representing the safety factor. Firstly, it is noticeable that the asymptotic value of  $F$  (Definition 1) at  $T_s = W_s$  is infinite, since the resultant force parallel to the sliding surface disappears at this value, which means that failure can never occur. For even higher values of  $T_s$  the rock mass will slide upwards and  $F_s$  decreases. The second definition, however, is not capable of taking into account these two phenomena. For  $T_s = W_s$  the value of  $F_s$  is finite. Furthermore upwards movement of the rock mass is not accounted for. Only for downwards sliding in the range of values of  $F_s$  around 1 is there agreement between the two definitions. It is clear that the second definition

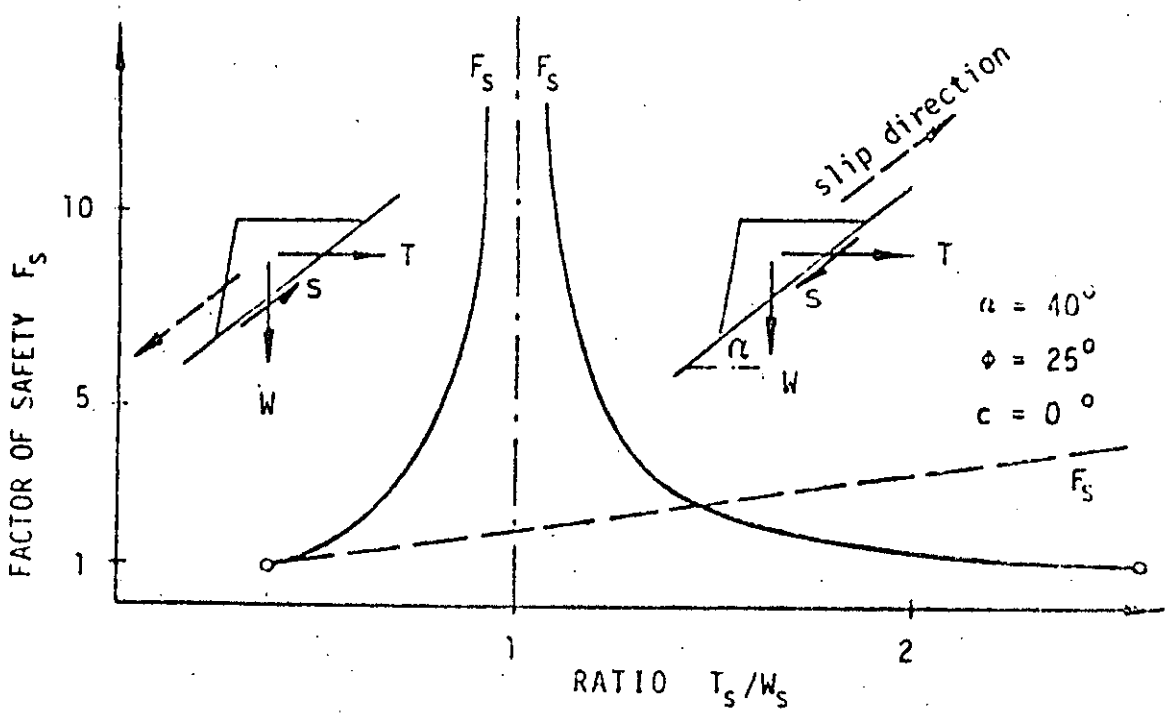


Fig. 2: Safety factor according to two different definitions

based on the consideration of driving and resisting forces should not be applied for the following reasons:

- upwards sliding is not accounted for,
- meaningless values are obtained for  $T_s = W_s$ .
- it infringes upon an elementary law of mechanics, according to which a group of forces acting on a rigid body is equivalent to its resultant. The determination of a resultant is not possible, because the external forces due to inadmissible grouping act partly as driving and partly as resisting.

## 2.2 Plane failure surface

A vertical section through a potentially unstable rock slope is shown in Fig.3. The weight of the rock mass is  $W$  and the contact area with the underlying rock on which it rests is  $A$ . The resultant  $R$  of all external forces acting (anchor force, water pressure, surcharge etc.) is directed at an angle  $\beta$  to the horizontal.

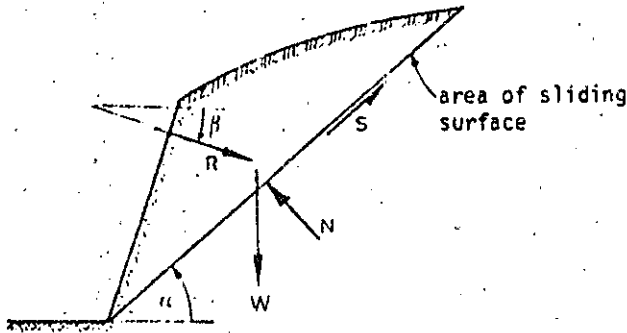


Fig. 3: Geometry of the slope and the forces acting on it

The geometry of the slope enters the calculation through the area  $A$ , the slope angle  $\alpha$  and indirectly through the self-weight  $W$ . The reaction on the failure surface is composed of a normal force  $N$  and a shear force  $S$ . Resolving the forces into components parallel and normal to the failure surface leads to the following equilibrium equations

$$S + R \cos (\alpha + \beta) - G \sin \alpha = 0.$$

$$N - R \sin (\alpha + \beta) - G \cos \alpha = 0.$$

The definition of safety factor according to (1) is

$$F_s = S_{\max} / S_{\text{acting}}$$

and Coulomb's failure condition for the contact surface is

$$S_{\max} = N \tan \phi + c A \quad (\text{where } c: \text{ cohesion, } \phi: \text{ friction angle}).$$

Thus the sought for basic formula (Kovari and Fritz, 1975), which represents the key to the simple treatment of slope stability problems, is obtained directly, namely

$$R = k_1 \left( 1 - \frac{cA}{W} k_2 \right) W$$

(3)

The coefficients  $k_1$  and  $k_2$  are given by the expressions below

$$k_1 = \frac{F_s \sin \alpha - c \cos \alpha \tan \phi}{F_s \cos(\alpha + \beta) + \sin(\alpha + \beta) \tan \phi}$$

$$k_2 = \frac{1}{F_s \sin \alpha - c \cos \alpha \tan \phi}$$

The following points are worthy of note with regard to the above formula:

- it, besides the anchor force, no other external forces are acting, it may be used directly as a design formula for the anchor force.
  - the cohesion  $c$  appears explicitly, which allows a very simple estimate of its influence to be made.
  - it is valid, as will be shown afterwards, also for the three dimensional problem of sliding of a wedge on two plane surfaces.
- The simple evaluation of this formula in practice is aided by the use either of a programmable pocket calculator or of design charts (Kovari and Fritz, 1976), whereby the factors  $k_1$  and  $k_2$  are a function of geometry, safety factor and friction angle only. An extension of this formula is described in appendix 4.1.

### 4.3 Sliding of a wedge on two planes

The three-dimensional problem is treated here of a wedge sliding on two planes with the contact areas  $A_1$  and  $A_2$ . It is shown (Fig.4a) how this case is analogous to the simple one previously handled. We define a cartesian coordinate system  $(s, n, h)$ . The  $s$ -axis lies in the direction of the line of intersection of the two planes, the  $n$ -axis is horizontal and the  $h$ -axis is in the vertical plane through the line of intersection. Fig.4b shows a section with a vertical plane through the intersection line, while Fig.4c shows a section normal to the intersection line.

The forces acting are divided into three groups:

- self-weight  $W$ .
- reaction (now two normal  $(N_1, N_2)$  and two shear forces  $(S_1, S_2)$  respectively).
- the resultant  $R$  of the external forces.

Analogous to the case of one sliding plane the basic relationships may be formulated for

- the three equations of equilibrium,
- the definition of safety factor  $(1)$ ,
- Coulomb's law of friction for shear resistance along the sliding surface.

To begin with, it will be assumed for the sake of simplicity, that the resultant  $R$  lies parallel to the vertical plane  $(s, n)$  through the intersection line, and further that the same friction angle applies to both planes. The combination of the five conditions with the help of elementary algebraic operations yields the following basic equation for wedge problems

$$R = k_1^* \left( 1 - \frac{c_1 A_1 + c_2 A_2}{W} k_2^* \right) W \quad (4)$$

where

$$k_1^* = \frac{F_s \sin \alpha_s - c \cos \alpha_s \tan \phi^*}{F_s \cos(\alpha_s + \beta) + \sin(\alpha_s + \beta) \tan \phi^*}$$

$$k_2^* = \frac{1}{F_s \sin \alpha_s - c \cos \alpha_s \tan \phi^*}$$

$$\tan \phi^* = \frac{\cos \omega_1 + \cos \omega_2}{\sin(\omega_1 \omega_2)} \tan \phi = \lambda \tan \phi$$

One immediately recognizes the correspondence of this formula with that for a single plane and the conditions of the analogy:

- instead of the slope angle  $\alpha$  of the single failure surface the slope angle  $\alpha_0$  of the line of intersection of the two failure surfaces is employed,
- instead of the friction angle  $\phi$  the angle  $\phi^*$  is used,
- instead of the product  $cA$  the sum  $c_1A_1 + c_2A_2$  must be considered.

The inclination  $\alpha_0$  of the intersection line and the factor  $\lambda$  for determining the angle  $\phi^*$  may be read directly from tables for various geometries (Kovári and Fritz, 1976). In the same work all the necessary derivations are given in detail, especially for the angles  $\alpha_1$  and  $\alpha_2$ .

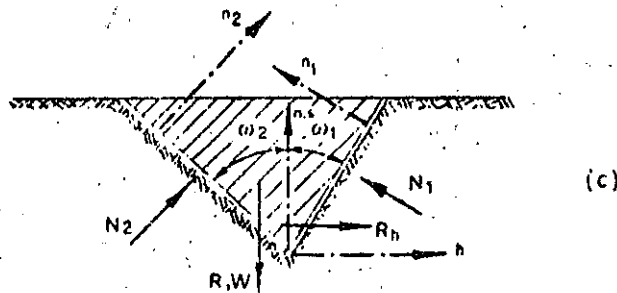
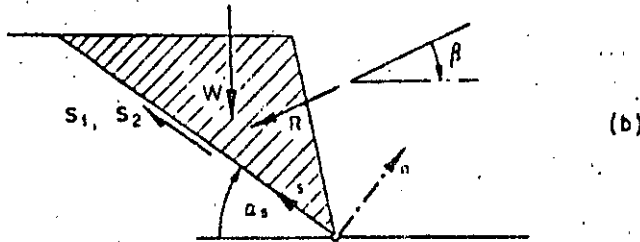
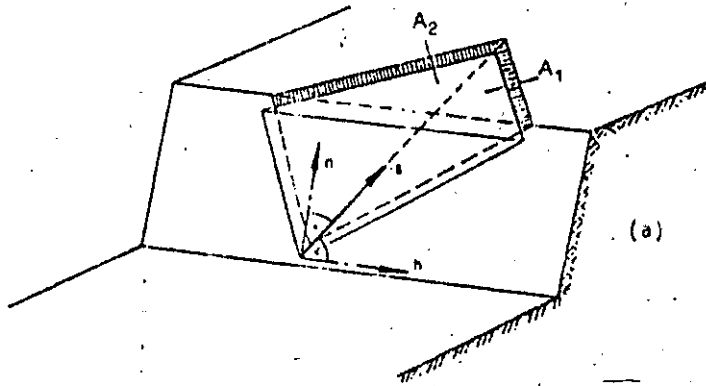


Fig. 4: Isometric view and sections of rock wedge

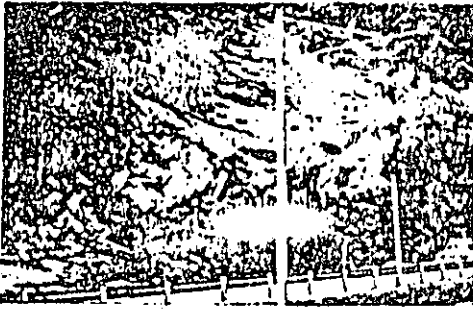


Fig. 5:  
Rock slope in Canton Grisons,  
Switzerland.

#### 2.4 Example from rock engineering practice

With the aid of a practical example it will be shown how a parametric study can be carried out using the basic formula presented here. In the course of the reconstruction of a mountain road in Switzerland a section, approximately 100 m long, of a steep rock slope slid down (Fig.5). Since sliding of the remaining part of the slope was feared the use of rock anchors as a possible remedial measure was to be investigated. Characteristic for the whole rock mass was intensive folding and shearing of the interchanging beds of limestone and argillaceous shale (Fig.5). The most important consideration regarding potential instability was the presence of shear surfaces in the plane of the axis of folding, inclined at an angle  $30^{\circ}$ - $40^{\circ}$  normal to the road. The rock mass could break free from one of a number of joint systems running through it. Based on this data the problem was reduced to one of sliding on a single plane, whereby strips 1 m wide were considered. The endangered rock mass was divided in cross-section (see Fig.6) more or less arbitrarily into three parts, with the idea that the safety factor was best considered, for either just the lower part breaking off or the whole rock mass coming down.

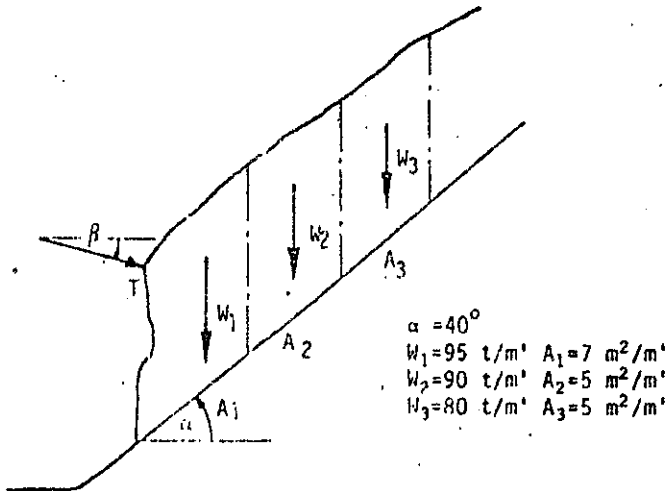


Fig. 6: Typical cross-section through the potential sliding mass

In a first computational step the material properties of the sliding surface were back-calculated from the stability of the whole rock mass with the help of the formula (3). Substituting a safety factor  $F_s = 1$  and various friction angles  $\phi$  the necessary cohesion  $c$  was calculated and plotted in Fig. 7 in function of  $\phi$ . Each point on this curve represents a possible combination of values of  $c$  and  $\phi$  satisfying the condition of limit equilibrium.

For typical pairs of values of  $c$  and  $\phi$  the required anchor force was determined for various values of safety factor. For example, in Fig. 8 the anchor force for three cases  $W = W_1$ ,  $W = W_1 + W_2$  and  $W = W_1 + W_2 + W_3$  is shown for a selected pair of values ( $c, \phi$ ). If a smaller probability of occurrence is attributed to the whole rock mass (i.e.  $W = W_1 + W_2 + W_3$ ), the safety factor  $F_s = 1.1$  may be regarded as adequate. The corresponding anchor force  $T = 25 \text{ t/m}$  means, however, that for sliding of the lower part

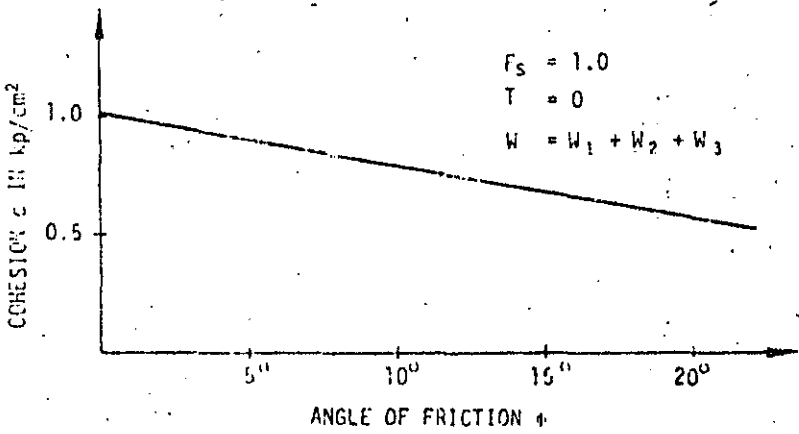


Fig. 7: Strength parameters for the limit equilibrium method (parameter back-calculation)

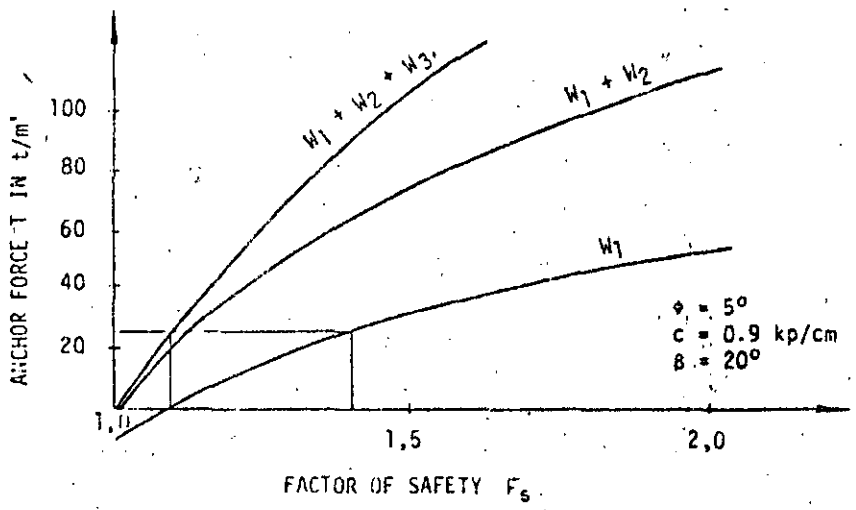


Fig. 8: Influence of the safety factor on the required anchor force



( $W = W_1$ ) alone the safety factor is  $F_s = 1.4$ . The increase of the safety factor compared with that for sliding of the whole rock mass is in agreement with the greater probability that was assigned to this case. 10

With the simple estimate for the anchoring costs  $P$  in dependence upon the number of borings  $n$ , the anchor lengths  $l$  and the price  $P$  per unit of the anchors and  $P_B$  of the borings, i.e.

$$P = (P_A + n P_B) l$$

an optimum anchor inclination  $\beta$  was finally determined. The anchor costs in percent of the minimum value are plotted as ordinate against the angle  $\beta$  as abscissa in Fig. 9. Depending upon the desired safety factor  $F_s$  there result, naturally, different anchor costs. However, the optimum inclination  $\beta$  for this example always lies between  $10^\circ$  and  $30^\circ$ .

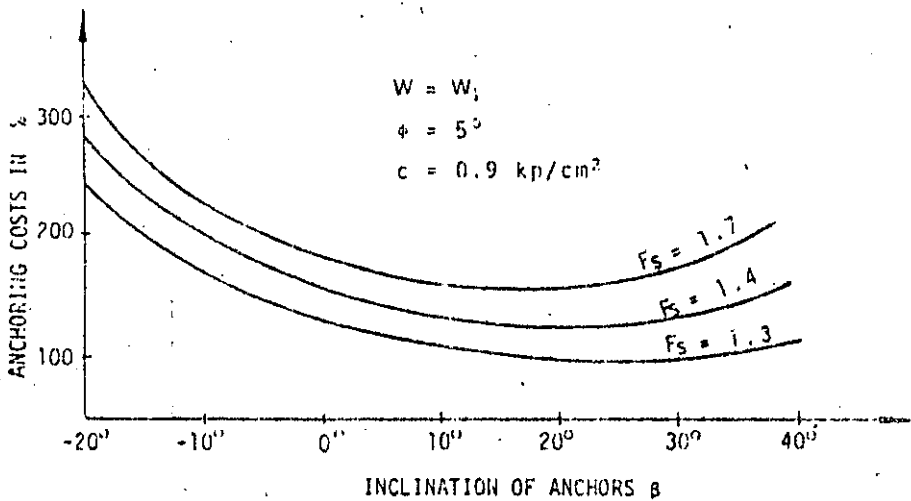


Fig. 9: Determination of the most economic anchor inclination

### 3. Sliding on polygonal sliding surfaces

From experience it is known that sliding, corresponding to the nature of rock, usually takes place on polygonally-shaped surfaces. For such cases Janbu (1954) and Morgenstern and Price (1965) have suggested practical methods of computation, whereby the endangered earth or rock mass is divided up into vertical strips or slices. The computational procedure is based on certain assumptions regarding the distribution and slope of internal contact forces, as well as the hypothesis of limit equilibrium. The method advocated here, however, is based upon the physical requirement that sliding on a polygonal surface is only possible kinematically if a sufficient number of internal shear surfaces can develop. For the sake of simplification, in the following only continuous plane shear surfaces starting from the intersection lines of the polygon sliding surface are assumed. Thus, as shown in Fig. 10, the slide of a mass on three planes must be accompanied by at least two internal shear surfaces. For  $n$  external sliding planes ( $n-1$ ) such interfaces are required. The method described here rests upon the following basic assumptions:

- a) The blocks comprising the rock mass are each considered to be rigid.
- b) The directions of the internal shear surfaces are known.
- c) On the internal and external sliding surfaces (at the condition of limit equilibrium) the Coulomb failure condition applies, and no tensile strength is permitted. The strength parameters may be allocated different values on each sliding surface.
- d) For the safety factor - according to definition (1) - the same value is assumed for all internal and external sliding surfaces.

17

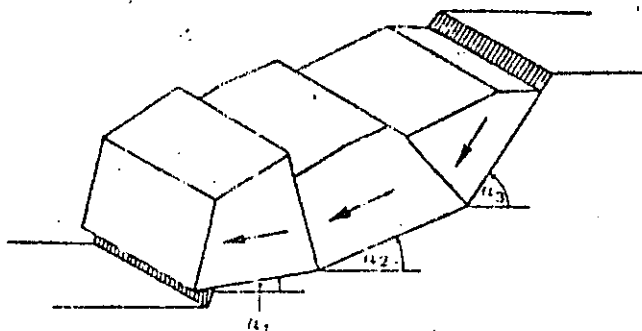


Fig. 10: Kinematics of a slope failure for a polygonal sliding surface

On the basis of these assumptions the safety factor and all external and internal reactions can be determined for a given geometry, loading and strength. The direction of the internal shear surfaces is chosen from case to case on the basis of a careful investigation of the structure of the potential sliding mass. However, for highly jointed rock the direction of the internal slip surfaces can be found by the condition of a minimum safety factor for the system. In an investigation of the stability of an earth dam Sultan and Seed (1967) used a similar criterium. It is readily seen that the resistance of a rock mass to splitting up into various parts plays an important role in stability calculations. The significance of interlocking effects in the joints and the strength of the rock are in this connection of great importance. Müller (1962, p.270) has already drawn attention to these aspects. With regard to the same safety factor being postulated for all slip surfaces the following remarks are offered. As will be shown in the next section, it would be formally possible to allocate a different safety factor to each slip surface. One limiting condition must be observed, i.e. that at the moment of slip the safety factor on all surfaces must be reduced to the value of unity. This refinement allowing for varying safety factors, however, seems to us, due to insufficient foundation and considering the many simplifications introduced to solve the problem, to be inappropriate. In any case, with considerations of this kind the contributions of the relative displacements along the interfaces, which are necessary to mobilize the shear resistance, must also be taken into account. One could quite easily imagine a situation, in which because of large deformations the external slip surface has reached a state of residual shear strength, whereas the internal slip surfaces (with smaller relative deformations) still exhibits the peak value of shear resistance. This consideration, which is related to the problem of progressive failure, exceeds the limits, however, of this present study. Indeed, the method of limit equilibrium, due to the assumption of rigid body behaviour, is not suitable to solve the problem of progressive failure. It is only possible to determine an admissible velocity field in the sense of the plasticity theory of Hill (1955).

The general case of a potential rock slide on a  $n$ -section polygonal slip surface is shown in Fig. 11. The geometry of the slope is fixed by the angles of inclination  $\alpha_i$  and  $\gamma_i$  and the corresponding areas  $A_i$  and  $\bar{A}_i$  of the respective slip planes. The forces acting are again divided into three groups:

- The weights  $W_i$  of the individual blocks,
- the external reactions  $N_i$ ,  $S_i$  and the inner reactions  $\bar{N}_i$ ,  $\bar{S}_i$  (contact forces),
- the resultant  $R_i$  (of slope  $\beta_i$ ) of the external forces (anchor force, water pressure in the external slip surfaces etc.). Water pressure, that may act in the joints normal to the internal slip surfaces, are taken care of by the forces  $Q_i$ .

If it is now assumed that there is a different safety factor in each slip plane, four unknowns are obtained for each plane, the safety factor, two reaction forces and one strength value ( $S_{\max}$ ). Thus for  $n$  external and  $(n-1)$  internal slip surfaces there are altogether  $(8n-4)$  unknowns to be determined. For this purpose, for each of the  $n$  blocks, two equilibrium conditions must be satisfied

$$\sum X_i = 0, \quad \sum Y_i = 0$$

as well as the  $[n + (n-1)]$  Coulomb conditions on the sliding planes and the corresponding expressions (1) for safety factor in the form

$$S_{i\max} = N_i \tan\phi + c_i A_i \quad (N_i \geq 0), \quad \bar{S}_{i\max} = \bar{N}_i \tan\bar{\phi} + c_i \bar{A}_i \quad (\bar{N}_i \geq 0)$$

$$F_{S_i} = \frac{S_{i\max}}{S_i}, \quad \bar{F}_{S_i} = \frac{\bar{S}_{i\max}}{\bar{S}_i}$$

In the above it was tacitly made use of the principle of action and reaction for the component forces  $\bar{N}, \bar{S}$  on the interface. Thus for the system as a whole with  $n$  blocks there are  $(6n-2)$  equations and  $(8n-4)$  unknowns, i.e. the problem is statically indeterminate to the  $(2n-2)$ th degree. This indeterminacy is a consequence of the working hypothesis of the method of limit equilibrium, as with the assumption of rigid behaviour the displacement and stress fields are unknown. The deficient equations, therefore, cannot be found using mechanical or physical laws. A possible hypothesis is to make the safety factors in the various slip planes dependent upon one another. Since the safety factor in the case of slip must be everywhere unity and here a simplified approach is sought, we assume that the safety factor is equal in all slip planes. The deficient equations are thus

$$F_{S_i} = F_{S_1} \quad (2 \leq i \leq n+n-1).$$

In solving the system of equations it should be noted, that most of the unknowns can be eliminated with the help of the basic formulas (3) and (7) respectively, leaving just  $n$  values. To solve the remaining equations, on account of their nonlinear character, an iterative method is used. The equations are best solved, therefore, by means of the computer program listed in appendix 4.2. For the special case of sliding on a two-degree polygonal surface it is shown in the next section that this problem can also be solved by hand with not too much effort. For the sake of completeness, a semigraphical procedure for the analysis of an  $n$ -degree polygonal sliding surface is also presented. Generally, this procedure would only find application if an electronic computer were not available.

Remark: If, with the exclusion of tensile strength of rock, negative contact (interaction) forces occur this points to a separation of the individual blocks. From the point of view of the stability analysis, the slide of the whole rock mass is no longer of interest, but only of a certain group of blocks.

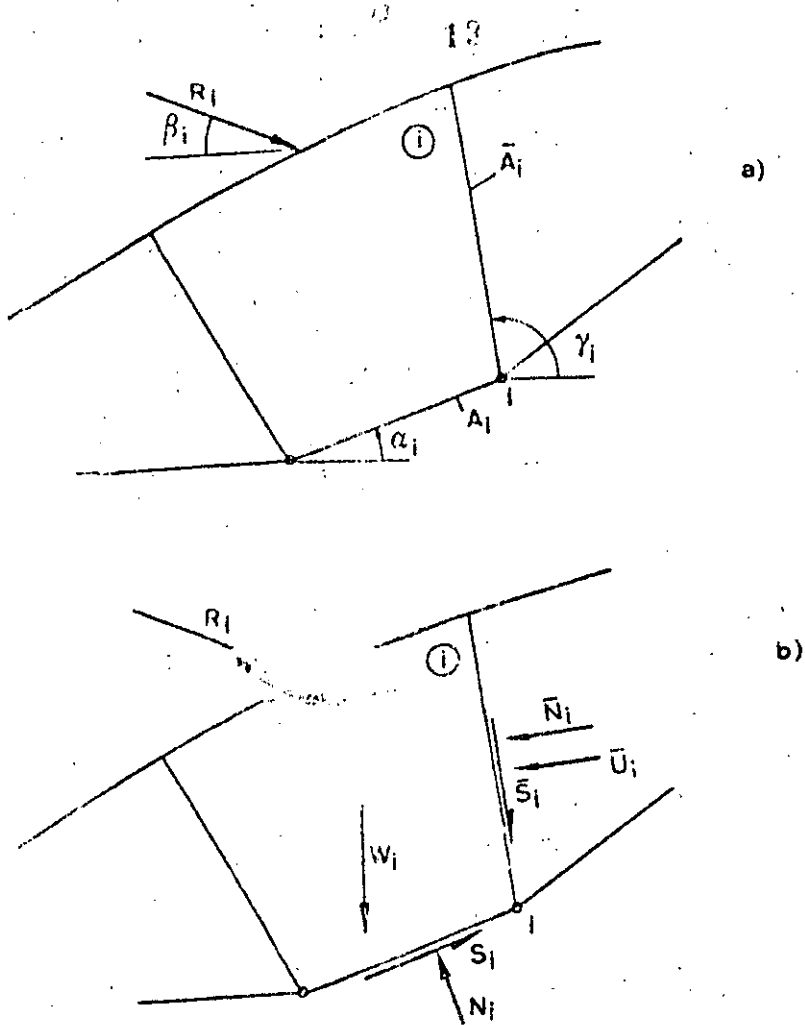


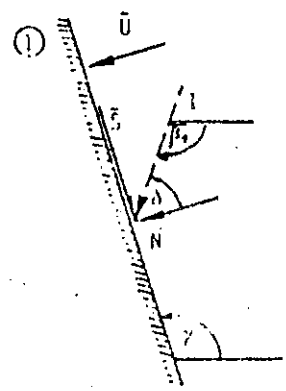
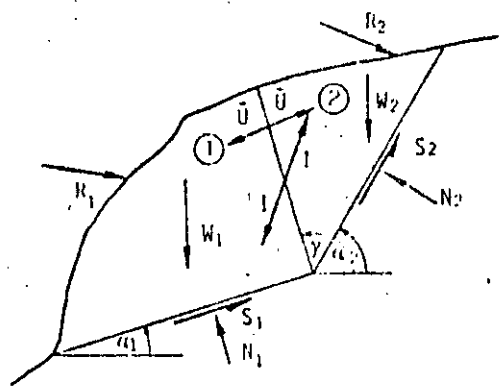
Fig. 11: Element  $i$  of a rock mass with a polygonal sliding surface  
 a) geometrical quantities  
 b) internal and external forces

### 3.2 Polygonal sliding surface composed of two planes

The rock mass shown in Fig. 12a rests on two potential sliding planes of angle of inclination  $\alpha_1$  and  $\alpha_2$ . Sliding is only possible if an internal slip surface with a certain inclination  $\gamma$  can develop, so that the mass is divided into two blocks of weight  $W_1$  and  $W_2$  respectively. Besides possible external forces  $R_1$  and  $R_2$  and a water pressure  $\bar{U}$  acting in the interface there are the reactions  $N_1$ ,  $S_1$  and  $N_2$  respectively on the external slip planes and an interaction force  $I$  on the internal slip surface. The components  $\bar{N}$ ,  $\bar{S}$  of  $I$  must fulfil the failure condition of Coulomb. With the parameters for the internal slip surface - cohesion  $\bar{c}$ , friction angle  $\bar{\phi}$  and contact area  $\bar{A}$  - the Coulomb condition is

$$\bar{N} = I \cos \delta$$

$$\bar{S} = I \sin \delta$$



DETAIL OF INTERNAL SHEAR SURFACE

a)

b)

Fig. 12: Rock mass with forces acting on it for a sliding surface consisting of two planes

$$\bar{S}_{max} = (\bar{N} - U) \tan \bar{\phi} + \bar{c} \bar{A}$$

Employing the definition (1) for safety factor, viz.

$$F_s = \frac{\bar{S}_{max}}{\bar{S}} = \frac{\bar{N} - U}{\bar{S}} \tan \bar{\phi} + \frac{\bar{c} \bar{A}}{\bar{S}}$$

one obtains the characteristic angle  $\delta$  (Fig.12b) between the interaction force  $U$  and the normal to the corresponding sliding surface:

$$\tan \delta = \frac{\bar{S}}{\bar{N}} = \frac{1}{F_s} \left( \tan \bar{\phi} + \frac{\bar{c} \bar{A}}{\bar{N}} \right) \tag{5a}$$

with the relationships

$$\bar{N} = I \cos \delta \text{ and } \bar{c}^* = \bar{c} - \frac{U}{\bar{A}} \tan \bar{\phi}$$

As a known special case one obtains, for cohesionless material, without water pressure in the interface and a safety factor  $F_s = 1$ , the value of  $\delta$  :

$$\delta^* = \bar{\phi} \tag{5b}$$

The angle of inclination  $\beta$  of the interaction force follows from considering Fig.12b for the lower block 1, i.e.

$$\beta_1 = \frac{3\pi}{2} - \gamma - \delta \tag{6a}$$

and for the upper block 2

$$\beta_2 = \beta_1 + \pi \tag{6b}$$

The safety factor for the whole rock mass is found from the condition that this value must be equal for both elements. In practice the necessary force  $I$  is found separately for each block with the aid of the basic formula (7) as a function of the safety factor. For the lower element 1 the following expression holds, for example:

$$I = k_1 \left( 1 - \frac{c^* A}{W_1 + R_{1W}} - k_2 \right) (W_1 + R_{1W}) - R_{1i}$$

The angle of inclination  $\beta$  of  $I$  is chosen, as a first approximation, with the help of eqns. (5b) and (6). The resultant force  $R_1$  or its components  $R_{1W}$  and  $R_{1i}$  in the directions of  $W$  and  $I$  respectively represent external forces acting on the block such as surcharge, anchor force, water pressure in the external slip surface (water pressure in the internal slip surface is accounted for by a reduced cohesion  $c^*$ ). For the angle  $\beta$  and the assumed value of safety factor  $F_s$  the coefficients  $k_1$  and  $k_2$  and thus the interaction force  $I$  are now determined. Fig. 13a shows the interaction force as a function of safety factor plotted separately for both blocks. The intersection of the two curves gives the required solution, because at this point both the interaction force and the safety factor are equal for the adjoining blocks. Since, however, the inclination  $\beta$  of the interaction force was only an initial trial value, it must be redetermined by substituting for  $F_{s\beta}$  and  $I$  in (5a) and then the calculation must be repeated iteratively with the new value of  $\beta$ . Usually the method converges very rapidly. A case of interest is shown in Fig. 13b, in which the equilibrium of the two blocks, i.e. the point of intersection of the two curves leads to a negative interaction force. This corresponds to the situation, where the safety factor of the lower element 1 is less than that of the upper element. Due to the requirement that the interforce cannot transmit tensile forces it follows that the lower element alone is decisive for stability consideration, with  $I = 0$  and not elements acting together. For example, if  $F_{s\beta} = 1$  sliding only of the lower element is to be expected, while the upper element may remain stable.

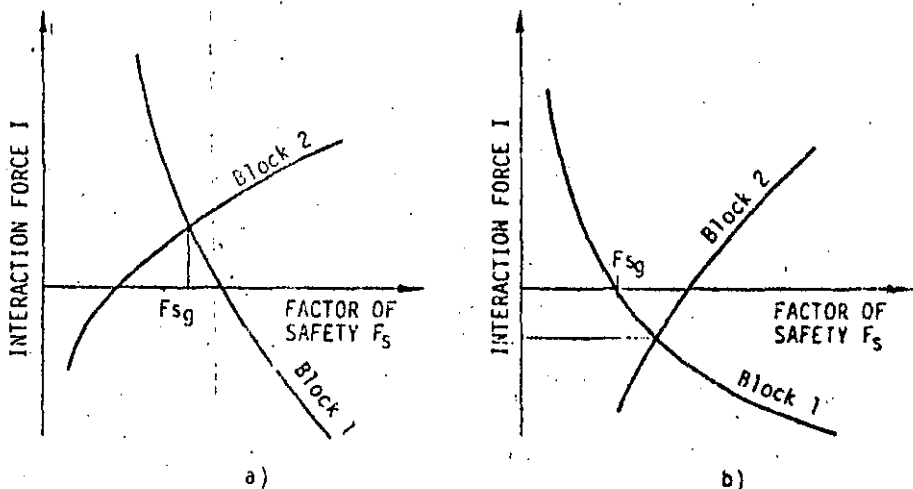


Fig. 13: Effective safety factor  $F_{s\beta}$  of a body on two planes of different inclinations

If an analysis has to be carried out for a multiple-plane slip surface and use is not made of the computer program given in the appendix, then it is also possible to obtain a solution by semi-graphical means. Essentially, this method is based upon a successive determination of the interaction forces  $I_i$  in the various blocks making use of the boundary condition  $I_n = 0$ . The following description should suffice to explain the detailed steps of the method: With the help of the basic formulae (3) or (7) the interaction force is found first for element 1 for various values of the safety factor  $F_s$ . Since the inclination  $\beta_1$  of the interaction force in eqns (5) and (6a) is dependent upon  $I_1$  this calculation is of an iterative nature. Using the graphical relationship for  $I_1 = f(F_s)$  in Fig. 14a one can find the interaction forces  $I_1 F_s^1, I_1 F_s^2, I_1 F_s^3$  corresponding to the three values of safety factor  $F_s^1, F_s^2, F_s^3$  respectively. The second block is now subjected to applied forces  $-I_1 F_s^i$  in a successive manner and for the corresponding values of the safety factor,  $F_s^i$ , the necessary interaction forces  $I_2 F_s^i$  are found (Fig. 14b). Due to the implicit representation of the inclination angle  $\beta_2$  this calculation must also be carried out iteratively. Afterwards, the third element is loaded with the forces  $-I_2 F_s^i$ , and so on. From the condition that for the n-th element  $I_n = 0$ , the sought-for factor of safety  $F_{sg}$  is obtained by means of interpolation in Fig. 14c.

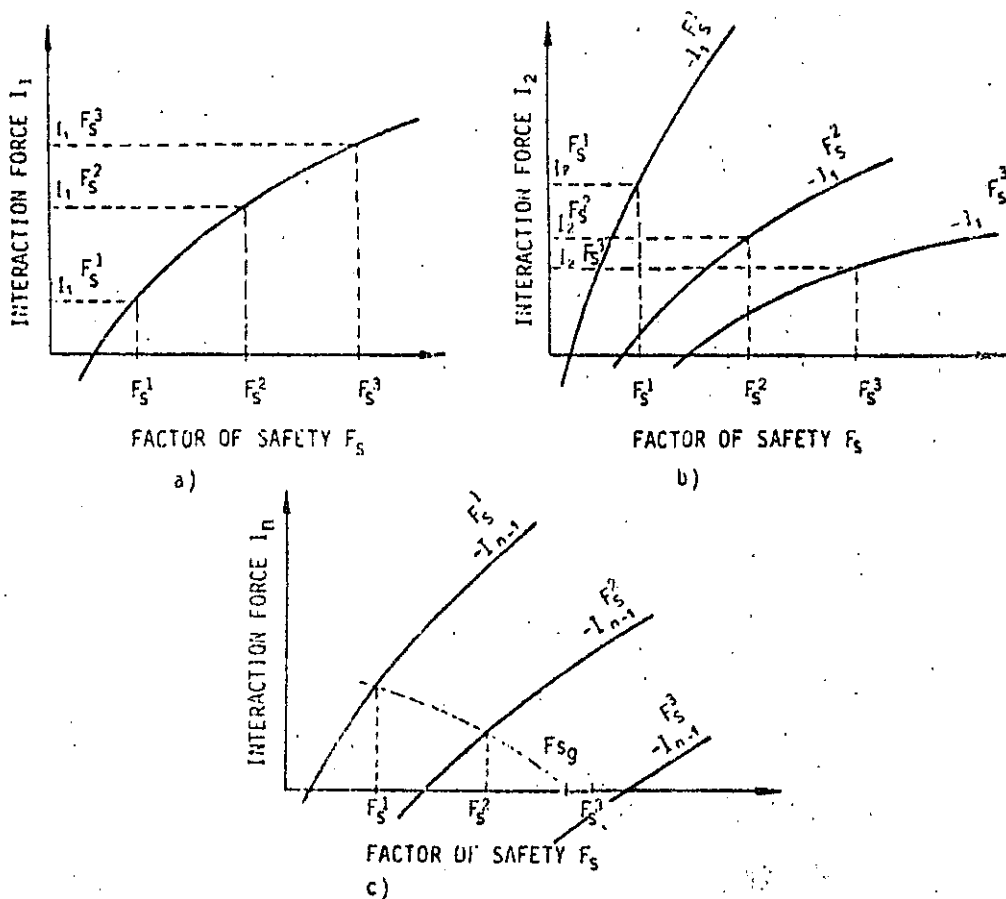


Fig. 14: Determination of the safety factor for a polygonal sliding surface

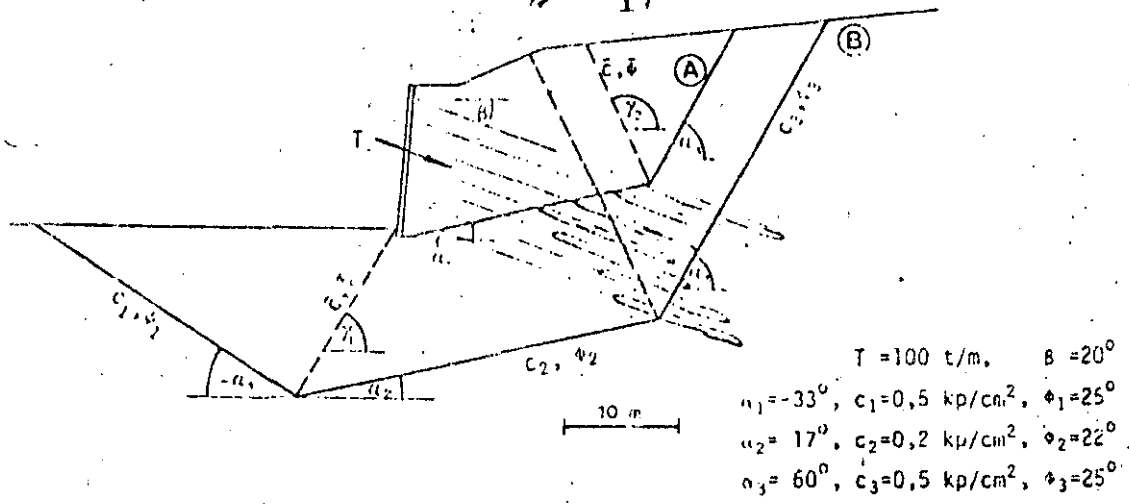


Fig. 15: Highway section with failure mechanisms (A) and (B)

3.4 Example of a stability check of a rock mass resting on an polygonal slip surface

As part of a national highway project in Switzerland it was proposed to use pre-stressed anchors to stabilize a section of highway cutting through rock. The rock mass, a chalky marl, was characterized in this area by pronounced bedding, dipping towards the road at a shallow angle. Due to the structure of the rock two different sliding mechanisms with polygonal slip planes were assumed (Fig.15). In case (A) the extent of the rock mass is such that the anchor forces are fully effective, whereas in case B the sliding surfaces were so deep that they were beyond the anchoring zones. For the upper sliding surface (case (A)) the influence of the inclination  $\gamma_2$  of the interface on the safety factor was investigated. The safety factor corresponding to various values of  $\gamma_2$  was evaluated (Fig.16), plotting  $\gamma_2$  as ordinate and safety factor as abscissa. The minimum safety factor leads to the critical value of  $\gamma_2$  for the safety factor  $F_{Sg}$  of the rock slope. The strength parameters for the internal slip surface were assumed to be  $\bar{c} = 1.0 \text{ kp/cm}^2$ , and  $\phi = 25^\circ$ . The second problem that had to be investigated in connection with this project was the stability with respect to a deep-seated failure surface (B). In a similar way to the previous case, the first step was to determine the critical inclinations of the internal slip surfaces. It was found that for the same strength parameters the same value of  $\gamma_2$  was obtained for the right interface (see Fig.15) as for case (A). The left slip surface with inclination  $\gamma_1$  was determined (practically independently of strength properties) due to the constraint that it passes through the foot of the retaining wall. The influence of strength in the shear surface on the stability of the potential sliding mass is evident from Fig.17. For constant material properties in the external slip surfaces an increase of the cohesion of  $2.0 \text{ kp/cm}^2$  in the internal slip surfaces effects an increase of safety factor  $\Delta F_s = 1.0$ . The influence of the friction angle  $\phi$  by contrast is much smaller. For the purpose of comparing these results with other methods of analysis, the safety factor based on Janbu's method was also computed for case (B). If, in Janbu's method, the interface forces are neglected, a safety factor  $v = 2.6$  results. This value holds per definition independent of the interface parameters  $\bar{c}$  and  $\phi$ . More "exact" computations using Janbu's method considering the interaction forces do not lead, for this example, to reasonable re-



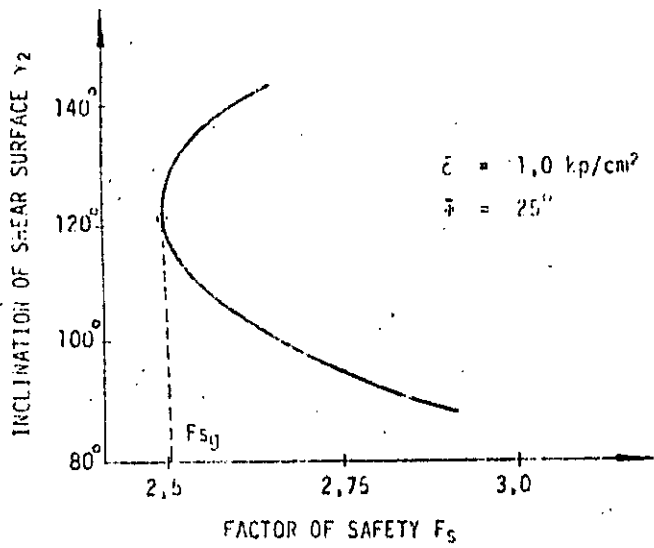


Fig. 16: Influence of the inclination of the internal shear surface on the safety factor (case (A))

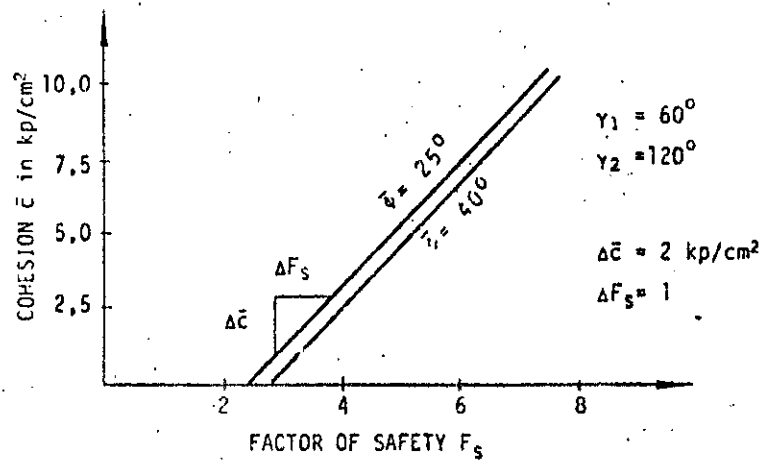
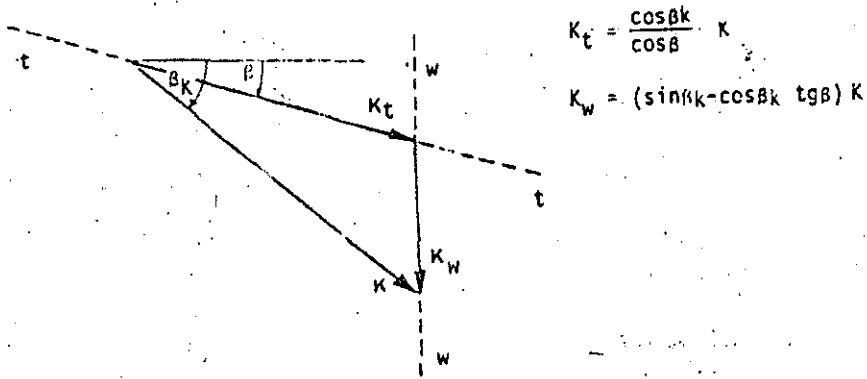


Fig. 17: Influence of the strength of the internal shear surfaces on the safety factor (case (B))

results, as a variation of the assumed slope of the pressure line or of the interaction forces by just a few degrees already has the effect of doubling the factor of safety.

4.1 Extension of the basic formula

Often the resultant  $R$  of all the external forces is composed of a force  $K$  whose magnitude and direction is known (e.g. water pressure) and of a force  $T$  whose direction  $\beta$  is known, but not its magnitude (e.g. anchor force, interaction force). In order to use the basic formulae (3) and (4) here also directly for design purposes (i.e. to find  $T$ ), the force  $K$  is resolved into its components  $K_t$  in the direction of  $T$  and  $K_w$  in the direction of gravity (Fig. 18).



$$K_t = \frac{\cos \beta_k}{\cos \beta} K$$

$$K_w = (\sin \beta_k - \cos \beta_k \operatorname{tg} \beta) K$$

Fig. 18: Resolution of a force  $K$  into the components  $K_t$  and  $K_w$

The resultant  $R$  is thus replaced in the basic formula by the value  $R = T + K_t$ . The effective weight increases to  $W' = W + K_w$ . Thus, in this instance, the modified form of equation (3) is

$$T = k_1 \left( 1 - \frac{cA}{W + K_w} k_2 \right) (W + K_w) - K_t \quad (7)$$

The coefficients  $k_1$  and  $k_2$  are the same as for eqn. (3).

4.2 Computer program for computation of polygonal sliding surfaces

The following simple program-subroutine, written in FORTRAN language, may be used to calculate the safety factor of a rock mass on a polygonal sliding surface. Geometry, material characteristics, and external forces are given as input data and the safety factor is calculated in function thereof, as well as the magnitude and direction of interaction forces. The input and output values are transferred by formal parameters. Their significance is explained at the head of the subroutine listing. The method of solution is based upon an extended form of eqn. (7). With the nomenclature of Fig. 11 one obtains the interaction force for the  $i$ -th element, viz.

$$I_i = k_1 \left( 1 - \frac{c_i A_i}{W_i + R_{iW}} k_2 \right) (W_i + R_{iW}) + R_{i1} + k_1 l_{i-1} - l_i - l_i' (1 \pm \operatorname{sign})$$

whereby  $l_0$  must equal zero ( $R_{i1}$  and  $R_{iW}$  designate the components of  $R_i$  in the directions of  $l_i$  and  $W_i$  respectively). The general form of this equation leads to a non-linear system of equations of the  $n$ -th degree, which, with the help of an iterative process, is solved in linear form. Since the number of equations  $n$  to be solved is normally quite small, the computer costs are also very small.

SUBROUTINE POLY(N, ALPHA, CFG, PHI, G, AR, BETAR, GAMA, CFS, PHIS, W,  
SNUE, AK, BETAK, MODE)

CC  
C  
C SLOPE STABILITY OF A ROCK MASS ON A  
C POLYGONAL SLIDING SURFACE  
C  
CC

C INPUT DATA (ALL ANGLES IN RADIAN)  
C  
C N NUMBER OF EXTERNAL SLIDING SURFACES  
C ALPHA(N) DIP ANGLE OF EXTERNAL SLIDING SURFACES  
C CFG(N) COHESION IN EXTERNAL SLIDING SURFACES MULTIPLIED  
C BY AREA OF SLIDING SURFACES  
C PHI(N) ANGLE OF FRICTION IN EXTERNAL SLIDING SURFACES  
C G(N) WEIGHT OF INDIVIDUAL BLOCKS  
C AR(N) EXTERNAL FORCES ACTING ON SLIDING BLOCKS  
C BETAR(N) ANGLE OF INCLINATION OF FORCES AR(N)  
C GAMA(N-1) DIP ANGLE OF INTERNAL SHEAR SURFACES  
C CFS(N-1) COHESION IN INTERNAL SHEAR SURFACES MULTIPLIED  
C BY AREA OF SHEAR SURFACES  
C PHIS(N-1) ANGLE OF FRICTION IN INTERNAL SHEAR SURFACES  
C W(N-1) WATER PRESSURE IN INTERNAL SHEAR SURFACES  
C (UNITS OF FORCE)

C OUTPUT DATA  
C  
C SNUE SAFETY FACTOR  
C AK(N) INTERACTION FORCES IN INTERNAL SHEAR SURFACES  
C BETAK(N) ANGLES OF INCLINATION OF FORCES AK(N) IN RADIAN  
C MODE = 0 COMPUTATION OK  
C > 0 INTERACTION FORCES < 0  
C = -1 ERROR: NO CONVERGENCE  
C CORRECTIVE MEASURE: DECREASE SFANT OR/AND  
C INCREASE TOLBELT, SPELNUE, SPEDEL  
C = -2 ERROR: DIVISION BY ZERO  
C = -3 ERROR: EQUATION SYSTEM NOT SOLVABLE

C R E M A R K S  
C  
C COMMON /MATRIX/ Z(N\*N) DIMENSIONING OF Z AND OF ALL  
C ACTUAL PARAMETERS HAS TO BE CARRIED  
C OUT IN THE CALLING PROGRAM  
C  
C P.FRITZ + K.KOVARI ETH ZUERICH  
C

CC

```
1 DIMENSION ALPHA(1), CFG(1), PHI(1), G(1), AR(1), BETAR(1),  
1 GAMA(1), CFS(1), PHIS(1), W(1), AK(1), BETAK(1)  
COMMON /MATRIX/ Z(1)  
DATA SPELNUE, SPEDEL/0.5,0.75/, TOLBELT/0.05/, TOLNUE/0.5/,  
1 TOL/0.0001/, LITERMAX/100/, SFANT, SMAX/1.5,50.0/  
  
IF(N.EQ.1) GOTO 35  
ATANI = ATAN(1.0)/45.0  
PHIS = 270.*ATANI
```

```

N1 = N - 1
DELTA(N) = 0.0
DO 2 I=1,N
2 PHIG(I) = TAN(PHIG(I))
DO 3 I=1,N1
PHIS(I) = TAN(PHIS(I))
3 CFS(I) = CFS(I) - W(I)*PHIS(I)
SNUEO = 1./SFARK
5 ITER = 0
SNUEO = SFARK*SNUEO
SNUE = SNUEO
IF(SNUEO.GT.SMAX) GOTO 40

```

CALCULATION OF THE DIRECTION OF CONTACT FORCES

```

10 NOW = -1
11 ITER = ITER + 1
IF(ITER.GT.ITERMAX) GOTO 41
IF(SNUE.EQ.0.0) GOTO 42
DO 19 I=1,N1
VORZ = 1.
IF(ALPHA(I+1).LT.ALPHA(I)) VORZ = -1.
IF(ITER.EQ.1) DELTA = ATAN(PHIS(I)/SNUE)
IF(ITER.GT.1) DELTA = PI15 - GAMA(I) - BETAK(I)
IF(ITER.GT.1.AND.CFS(I).NE.0.0) GOTO 13
TGDELTA = PHIS(I)/SNUE
GOTO 15
13 COSDELTA = COS(DELTA)
IF(COSDELTA.EQ.0.0) GOTO 42
TGDELTA = (PHIS(I)+CFS(I)/AK(I)/COSDELTA)/SNUE
15 DDDELTA = SFDELTA*(ATAN(TGDELTA)-DELTA)
DDARS = ABS(DDDELTA)
DMIN = AMIN1(DDARS,TGDELTA*DELTA)
DELTA = DELTA + SIGN(DMIN,DDDELTA)
BETAK(I) = PI15 - GAMA(I) - DELTA*VORZ
19 CONTINUE

```

LINEAR SYSTEM OF EQUATIONS SET UP WITH UNKNOWN CONTACT FORCES AK AND CHANGE OF SAFETY FACTOR USNUE

```

DO 29 J=1,N
NRZ = (J-1)*N
IE = J - 2
IF(J.LE.2) GOTO 22
DO 21 I=1,IE
21 Z(NRZ+I) = 0.
22 F1Z = SNUE*SIN(ALPHA(J)) - COS(ALPHA(J))*PHIG(J)
F1N = SNUE*COS(ALPHA(J)+BETAK(J)) + SIN(ALPHA(J)+BETAK(J))*PHIG(J)
IF(F1Z.EQ.0.0.OR.F1N.EQ.0.0) GOTO 42
F1 = F1Z/F1N
F2 = 1.0/F1Z
IF(J.EQ.1) GOTO 24
I = IE + 1
COSBKJ = COS(BETAK(J))
IF(COSBKJ.EQ.0.0) GOTO 42
Z(NRZ+I) = F1*(SIN(BETAK(J-1))-COS(BETAK(J-1))*TAN(BETAK(J)))
- COS(BETAK(J-1))/COSBKJ
24 CONTINUE
IF(J.EQ.N) GOTO 28
Z(NRZ+I) = 1.

```

22  
22

```

IF(J.EQ.N) GOTO 28
IA = J + 1
DO 25 I=1A,N
26 Z(NFZ(I)) = 0.
28 DF1 = (SIN(ALPHA(J))*F1N-COS(ALPHA(J)*BETAK(J))*F1Z)/F1N/F1N
DF2 = SIN(ALPHA(J))/F1Z/F1Z
ARG = (SIN(BETAK(J))-COS(BETAK(J))*TAN(BETAK(J)))*AR(J)
HILF = G(J) + ARG = F2*CFG(J)
Z(NKZ(N)) = -DF1*HILF + DF2*F1*G(J)
ARK = COS(BETAK(J))/ZCOS(BETAK(J))*AR(J)
29 AR(J) = F1*HILF - ARK

```

SOLUTION OF SYSTEM OF EQUATIONS, CONVERGENCE CHECK

```

CALL GAUSS(N,Z,AK,MODE)
IF(MODE.NE.0) GOTO 43
DO 33 I=1,N
IF(AK(I).LT.0.0) GOTO 5
33 CONTINUE
DSNUE = AK(N)
DSN1 = ABS(SPEINUE*DSNUE)
DSN2 = ABS(TOLNUE*SNUE)
DSN = SIGN(AMIN(DSN1,DSN2),DSNUE)
SNUE = SNUUE + DSN
IF(ITER.EQ.1.OR.ABS(DSNUE/SNUE).GT.TOL) GOTO 10
I = 0
IF(KONV.EQ.0) GOTO 40
KONV = KONV + 1
GOTO 11
35 SNUU = (AR(1)*SIN(ALPHA(1)+BETAK(1))+G(1)*COS(ALPHA(1)))
1 *TAN(PHIG(1)) + CFG(1)
SNUU = SNUUE/(G(1)*SIN(ALPHA(1))-AR(1)*COS(ALPHA(1)+BETAK(1)))
I = 0

```

TERMINATION

```

40 MODE = I
GOTO 46
41 MODE = -1
GOTO 46
42 MODE = -2
GOTO 46
43 MODE = -3
46 AK(N) = 0.0
IF(N.EQ.1) GOTO 49
DO 47 I=1,N
47 PHIG(I) = ATAN(PHIS(I))
DO 48 I=1,N1
CFS(I) = CFS(I) + W(I)*PHIS(I)
48 PHIS(I) = ATAN(PHIS(I))
49 CONTINUE
RETURN
END
SUBROUTINE GAUSS(N,Z,B,MODE)

```

SINGLE GAUSSIAN ALGORITHM (PIVOT ALWAYS DIAGONAL)

N NO. EQUATIONS  
Z(N\*N) COEFFICIENT MATRIX IN ROWS (IS OVERWRITTEN)

```

C      (N)      VECTOR OF CONSTANTS (R.H.S.), OVERWRITTEN BY
C      SOLUTION RESULTS
C      MOD.     PARAMETER IN GAUSS ROUTINE
C      = 0      SOLUTION ONLY
C      = 1      PIVOT = 0
C

```

```

DIMENSION Z(I),B(I)

```

```

N1  N - 1
DO 17 K=1,N1
NRZO = (K-1)*N
NRIV = NRZO + K
IA = K + 1
DO 19 J=IA,N
NRZ = (J-1)*N
NK = NRZ + K
IF(Z(NRIV).EQ.0.0) GOTO 41
S = Z(NK)/Z(NRIV)
DO 18 I=IA,N
NK = NRZ + I
NZ = NRZO + 1
18 Z(NK) = Z(NK) - S*Z(NZ)
19 B(I) = B(J) - S*B(K)

DO 29 I=1,N
I = N - I + 1
NRZ = (I-1)*N
S = B(I)
IF(I.EQ.N) GOTO 25
IA = I + 1
DO 22 IZ=IA,N
NZ = NRZ + IZ
22 S = S - Z(NZ)*B(IZ)
25 NZ = NRZ + I
29 B(I) = S/Z(NZ)
MODE = 0
GOTO 46
41 MODE = 1
46 CONTINUE
RETURN
END

```

References

Bill, R., 1955, The mathematical theory of plasticity. Oxford University Press.

Janbu, N., 1954, Application of Composite Slip Surfaces for Stability Analysis. Proc. Europ. Conf. Stability of Earth Slopes, V.3.

Kovári, K., Fritz, P., 1975, Stability Analysis of Rock Slopes for Plane and Wedge Failure with the Aid of a programmable Pocket Calculator. 16th Symp. Rock. Mech., Minneapolis, USA.

Kovári, K., Fritz, P., 1976, Stabilitätsberechnung ebener und räumlicher Felsböschungen, Rock Mechanics B. Int. Journal of ISRM, Springer.

Horgenstern, N.R., Price, V.E., 1965, The Analysis of the Stability of General Slip Surfaces. Geotechnique, V.15.

Miller, L., 1963, Der Felsbau. Verlag F. Enke, Stuttgart.

Sultan, H.A., Seed, H.H., 1967, Stability of sloping core earth dams. Journal Soil Mech. Found. Div., Proc. ASCE.



**DIVISION DE EDUCACION CONTINUA  
FACULTAD DE INGENIERIA U.N.A.M.**

MECANICA DE ROCAS APLICADA A LA MINERIA Y A LA CONSTRUCCION

TRATAMIENTO DE MACIZOS ROCOSOS

Ing. Raúl Cuéllar Borja

MAYO, 1985

## TRATAMIENTO DE MACIZOS ROCOSOS

ING. RAÚL CUÉLLAR BORJA ,  
AUXILIAR TÉCNICO  
COMISIÓN FEDERAL DE ELEC-  
TRICIDAD.  
MAYO, 1981.

### 1.- ANTECEDENTES.-

EL TEMA SE DESARROLLA EN UNA SERIE DE CUADROS EN LOS QUE SE IN-  
DICAN EN FORMA CONDENSADA LOS CRITERIOS BÁSICOS QUE SE UTILI-  
ZAN ACTUALMENTE EN EL TRATAMIENTO DE MACIZOS ROCOSOS EN RELA-  
CIÓN AL TRATAMIENTO DE CIMENTACIONES DE PRESAS. ALGUNOS CON-  
CEPTOS SON VÁLIDOS PARA LA ESTABILIZACIÓN DE TALUDES.

A MODO DE COMPLEMENTAR LA INFORMACIÓN CONTENIDA EN ESOS CUA-  
DROS A CONTINUACIÓN HAREMOS UNA BREVE EXPLICACIÓN DE LOS PRIN-  
CIPALES CONCEPTOS.

### 2.- COMPETENCIA DE LA ROCA.-

SE REFIERE AL COMPORTAMIENTO ESTRUCTURAL DEL MACIZO ROCOSO BA-  
JO EL EFECTO DE LAS NUEVAS SOLICITACIONES DE CARGA ( EMPUJES -  
HIDROSTÁTICOS Y EMPUJES DE LAS ESTRUCTURAS DE CONTENCIÓN ), --  
TANTO DURANTE LA ETAPA DE CONSTRUCCIÓN COMO DURANTE LA VIDA --  
ÚTIL DE LA PRESA, PREDICHAS, DESPUÉS DE HABER ESTUDIADO Y ANA-  
LIZADO EL ESTADO ACTUAL.

( EN FUNCIÓN DE LAS SOLICITACIONES DE CARGA OCURRIDAS EN EL --  
PASADO ).

LO ANTERIOR IMPLICA LA ESTABILIDAD TOTAL DEL MACIZO ROCOSO EN  
TODA SU EXTENSIÓN, ASÍ COMO, LA PRESERVACIÓN DE SUS PROPIEDA-  
DES GEOMECÁNICAS DE MANERA QUE NO SE PRESENTE EROSIÓN FUNDA---  
MENTALMENTE EN EL CONTACTO CORAZÓN-ROCA PARA EL CASO DE PRESAS  
DE MATERIALES GRADUADOS, ASÍ COMO, EROSIÓN O DEGRADACIÓN DE LA  
ROCA POR EFECTO DE SATURACIÓN EN LAS PAREDES DE EXCAVACIONES -  
DE ESTRUCTURAS AUXILIARES.

ADICIONAL A LOS EFECTOS DE EMPUJES HIDROSTÁTICOS Y DE LAS ES-  
TRUCTURAS DE CONTENCIÓN, DEBERÁN TOMARSE EN CUENTA LOS EFECTOS  
DINÁMICOS POR LA SISMICIDAD INDUCIDA. ( LLENADO DEL EMBALSE -  
QUE A VECES ROMPE EL EQUILIBRIO DE LA CORTEZA ).



### 3.- PREVENCIÓN CONTRA LA EROSIÓN.-

#### 3.1.- CONTACTO CORAZÓN-ROCA

LA PREVENCIÓN CONTRA LA EROSIÓN DEL CORAZÓN DE ARCILLA - EN EL CONTACTO CON LA ROCA SE REALIZA MEDIANTE TRATAMIENTO SUPERFICIAL SELLANDO LOS PASOS DE FILTRACIÓN DEL AGUA A TRAVÉS DE LAS DISCONTINUIDADES DE LA ROCA; FRACTURAS, FALLAS, OQUEDADES, ESTRATIFICACIÓN, UTILIZANDO:

A.- INYECCIONES DE CONSOLIDACIÓN E IMPERMEABILIZACIÓN -- (TAPETE), EN LAS CUALES LOS BARRENOS DEBERÁN TENER -- DIRECCIÓN E INCLINACIÓN PREFERENCIAL PARA ATRAVEZAR LOS PLANOS DE DISCONTINUIDAD MÁS IMPORTANTES EN LO -- REFERENTE A CIRCULACIÓN DE AGUA.

B.- RELLENO SUPERFICIAL DE LAS DISCONTINUIDADES DE LA ROCA MEDIANTE :

B.1.- CONCRETO DENTAL ( RELLENO DE PEQUEÑAS CAVIDADES ).

B.2.- CONCRETO DE REGULARIZACIÓN DEL TALUD

B.3.- MORTERO COLOCADO A MANO

B.4.- MORTERO O CONCRETO LANZADO, SIMPLE O ARMADO.

C.- ANCLAJE

D.- DRENAJE

### 4.- REGULARIZACIÓN DEL TALUD.-

SE REFIERE A LA CONFORMACIÓN DE UNA SUPERFICIE CONTÍNUA, MEDIANTE CORTES DE ROCA Y/O RELLENOS DE CONCRETO. AL EVITAR -- CAMBIOS BRUSCOS EN LA SUPERFICIE DE APOYO DEL CORAZÓN, SE EVITARÁ LA GENERACIÓN DE FRACTURAS DE TENSIÓN POR LA CONCENTRACIÓN DE ESFUERZOS DE COMPRESIÓN ( EFECTO DE ARQUEO ) FACILITAN DOSE EL FENÓMENO DE FRACTURAMIENTO HIDRAÚLICO.

### 5.- ACERO DE REFUERZO EN TALUDES.-

EN ESTE CASO EL USO DE ACERO DE REFUERZO EN LA ESTABILIZACIÓN DE TALUDES SE REFIERE A CUALQUIER TALUD.

SE PRESENTA LA DISTINCIÓN ENTRE ACERO ACTIVO Y ACERO PASIVO.

EL ACERO ACTIVO CORRESPONDE AL ANCLAJE DE TENSIÓN EN EL CUAL - LA FUERZA DE ESTABILIZACIÓN PUEDE CONOCERSE POR MEDICIONES YA

SEAN DE RETENSADO O DE CELDAS DE CARGA Y EL ACERO PASIVO CO-RESPONDE A ANCLAS DE FRICCIÓN EN LAS CUALES NO SE CONOCE LA FUERZA DE ESTABILIZACIÓN.

SE RECOMIENDA EL USO DE ACERO ACTIVO EN ROCA MUY FRACTURADA Y ACERO PASIVO EN ROCA SANA.

LA PROTECCIÓN ANTICORROSIVA DE LAS ANCLAS ES FUNDAMENTAL PARA GARANTIZAR UNA LARGA VIDA ÚTIL DE ESTOS ELEMENTOS.

## 6.- INYECCIONES DE CONSOLIDACION.-

ESTAS INYECCIONES DE CONSOLIDACIÓN SE REFIEREN AL TRATAMIENTO DE LA ROCA EN EL CONTACTO CORAZÓN-ROCA, CONOCIDAS COMO TAPETE DE CONSOLIDACIÓN E IMPERMEABILIZACIÓN, CON ESTE TRATAMIENTO SE OBTENDRÁ:

- A.- UN AUMENTO EN LA RESISTENCIA DE LA ROCA Y CONSECUENTEMENTE
- B.- UNA DISMINUCIÓN DE LA DEFORMACIÓN, AUNADA A,
- C.- UNA DISMINUCIÓN DE LA PERMEABILIDAD Y
- D.- UNA CIMENTACIÓN HOMOGÉNEA

LA TENDENCIA ACTUAL CONTEMPLA EL USO DE MEZCLAS GRUESAS O ESTABLES INYECTADAS A ALTAS PRESIONES.

AL HABLAR DE MEZCLAS ESTABLES NOS REFERIMOS A MEZCLAS AGUA-CEMENTO-BENTONITA Y EN ALGUNOS CASOS CUANDO HAY FLUJO DE AGUA EN LAS DISCONTINUIDADES SE AGREGARÁ SILICATO DE SODIO PARA AUMENTAR LA RESISTENCIA AL CORTANTE DE LA MEZCLA EN EL MOMENTO QUE ADQUIERE LA CONSISTENCIA DE UN GEL.

LA APLICACIÓN DE ALTAS PRESIONES EN ESTE TRATAMIENTO, QUE POR CONVENIENCIA DEBE SER LO MÁS SUPERFICIAL POSIBLE ( 4M A 6M ) - TOMANDO EN CUENTA QUE LA FINALIDAD ES LA PROTECCIÓN DEL MATERIAL DEL CORAZÓN, ES DE UN ESPECIAL GRADO DE DIFICULTAD POR LA FALTA DE CONFINAMIENTO DE LA ROCA.

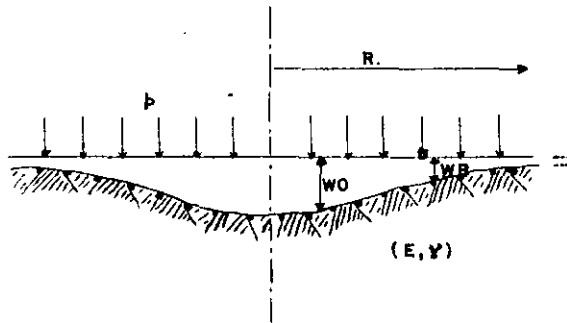
SIEMPRE SERÁ CONVENIENTE REALIZAR PRUEBAS DE INYECTADO PARA DEFINIR LA PRESIÓN MÁXIMA DE INYECCIÓN CONOCIDA COMO PRESIÓN DE RECHAZO, TENIENDO SIEMPRE CUIDADO DE NO PRODUCIR DISLOCACIONES EN LA ESTRUCTURA DEL MACIZO ROCOSO QUE PODRÍAN OCASIONAR SERIOS PERJUICIOS. EL FENÓMENO DE DISLOCACIÓN DE LA ESTRUCTURA POR EFECTO DE LA PRESIÓN HIDROSTÁTICA APLICADA EN ÁREAS RELATIVAMENTE GRANDES SE CONOCE COMO EFECTO DE " GATO HIDRÁULICO "

LA VERIFICACIÓN SOBRE LA EFICACIA DE ESTE TRATAMIENTO SIEMPRE SERÁ CONVENIENTE PARA LA TOMA DE MEDIDAS CORRECTIVAS. LOS MÉTODOS MÁS EFICACES SON EL MONITOREO DE DRENAJE Y LA PIEZOMETRÍA. TAMBIÉN SON RECOMENDABLES LOS MÉTODOS GEOFÍSICOS.

### 6.1.- PRESIÓN DE INYECCIÓN.

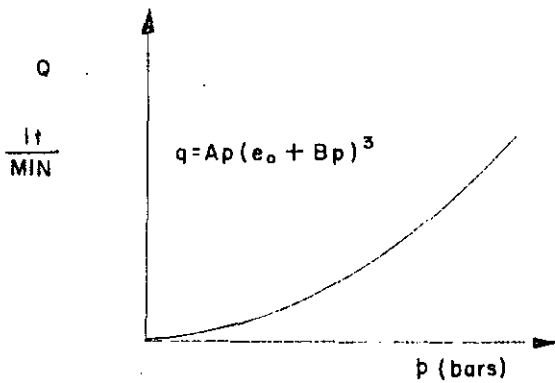
LA PRESIÓN DE INYECCIÓN JUEGA UN PAPEL PREPONDERANTE EN LA PENETRABILIDAD DE LA MEZCLA OBTENIENDO CON ELLO UNA DISMINUCIÓN EN LA BARRENACIÓN QUE REPRESENTA UNA ACTIVIDAD COSTOSA.

UNA MAYOR PENETRABILIDAD DE LAS MEZCLAS SE OBTIENE CUANDO LAS FRACTURAS SE ABREN ELÁSTICAMENTE SIN PRODUCIR ROTURA DEL MACIZO ROCOSO.



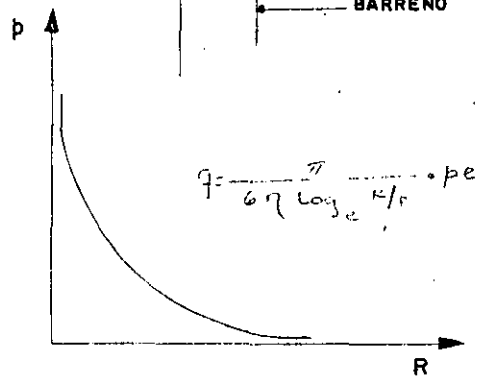
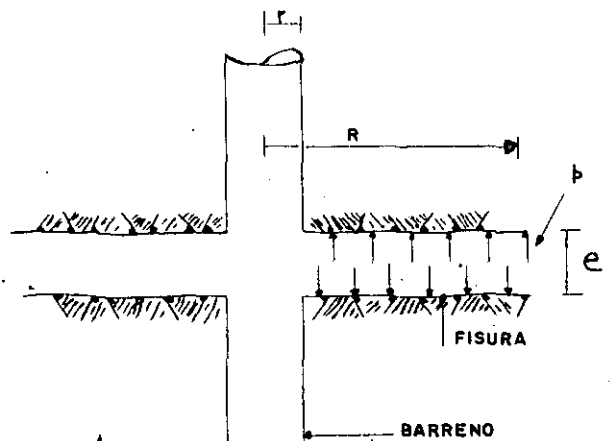
$$w_0 = \frac{2(1-\nu^2)R \cdot p}{E}$$

$$w_R = \frac{4(1-\nu^2)R \cdot p}{\pi \cdot E}$$



$$(1) \quad q = Ap(e_0 + Bp)^3$$

$$\therefore q = Ap^4$$



$\eta$ : viscosidad del agua

$$Ae = \alpha \frac{p}{E}$$

$$e_0 + \Delta e = e_0 + \alpha \frac{p}{E}$$

$$q = \frac{\pi}{6\eta \log_e R/r} \cdot p \left( e_0 + \frac{\alpha p}{E} \right)^3$$

EL GASTO VARÍA CON LA CUARTA POTENCIA DE LA PRESIÓN Y SE EXPLICA PORQUE SI SE GRAFICA EL GASTO CONTRA LA PRESIÓN EN ESCALA ARITMÉTICA SE OBSERVA QUE A UNA CIERTA PRESIÓN EL GASTO ABSORBIDO POR LA ROCA AUMENTA MUY RÁPIDO Y SE PIENSA QUE SE HA ALCANZADO EL FRACTURAMIENTO HIDRÁULICO, EN REALIDAD, SI SE REPRESENTA CON LA EXPRESIÓN (1) SE OBSERVARÁ QUE EL FENÓMENO ES PERFECTAMENTE CONTÍNUO. VER " LAS INYECCIONES Y LOS DRENAJES DE CIMENTACIÓN DE PRESAS EN ROCAS POCO PERMEABLES " POR FRANCIS SABARLY. A ESA PRESIÓN EN LA CUAL EL GASTO AUMENTA EN FORMA NOTABLE SE CONOCE COMO " PRESIÓN CRÍTICA " Y SE UTILIZA COMO VALOR LÍMITE DE LA PRESIÓN DE RECHAZO. ES NECESARIO DISTINGUIR PRESIÓN DE RECHAZO Y PRESIÓN DE INYECCIÓN.

- PRESIÓN DE RECHAZO.

ES LA PRESIÓN MÁXIMA O LÍMITE QUE SE ALCANZA EN LA OPERACIÓN DE INYECTADO Y UNA VEZ QUE SE ALCANZA SOLO DEBE APLICARSE MOMENTÁNEAMENTE PARA EVITAR UNA ALTA PRESIÓN SOSTENIDA Y NO DAR LUGAR A QUE SE PRESENTE EL EFECTO DE GATO HIDRÁULICO. LA PRESIÓN DE RECHAZO DEBE SER UN

POCO MENOR QUE LA PRESIÓN CRÍTICA.

- PRESIÓN DE INYECCIÓN

ES LA PRESIÓN QUE SE DESARROLLA DURANTE LA OPERACIÓN DE INYECTADO, CON LA DURACIÓN QUE SE JUZGUE CONVENIENTE PARA RELLENAR LAS OQUEDADES DEL MACIZO ROCOSO, SIN LLEGAR A LA PRESIÓN DE RECHAZO.

PENETRABILIDAD

ES LA DISTANCIA QUE SE ALCANZA DESDE EL BARRENO HASTA EL EXTREMO DE LA MEZCLA INYECTADA.

HAY QUE TENER MUCHO CUIDADO CON LOS GRANDES RECORRIDOS DE LAS MEZCLAS ( QUE A VECES LLEGAN A DISTANCIAS DEL ORDEN DE 100 M ) PUES NO SE LOGRARÁ LA EFECTIVIDAD DESEADA Y SE TENDRÁ UN AUMENTO IMPORTANTE DEL COSTO DEL INYECTADO.

6.2.- COMPOSICIÓN DE LAS MEZCLAS

TIPOS DE MEZCLAS MÁS USUALES:

A).- MEZCLAS AGUA-CEMENTO

B).- MEZCLAS AGUA-CEMENTO-BENTONITA

C).- MEZCLAS AGUA-CEMENTO-BENTONITA-SILICATO DE SODIO

D).- MEZCLAS AGUA-BENTONITA

E).- MEZCLAS AGUA-BENTONITA-SILICATO DE SODIO

F).- MEZCLAS AGUA-SILICATO DE SODIO

LA MEZCLA A) SE CONOCE COMO MEZCLA INESTABLE SON MEZCLAS QUE SE SEDIMENTAN RELATIVAMENTE RÁPIDO CON LO CUAL SE DISMINUYE SU PENETRACIÓN.

LAS MEZCLAS B) Y C) SE CONOCEN COMO MEZCLAS ESTABLES, TIENEN MENOR SEDIMENTACIÓN POR EL EFECTO DE MOVIMIENTO BROWNIANO DE LA BENTONITA AL FORMAR UN COLOIDE, EVITANDO LA SEDIMENTACIÓN DE LOS GRANOS DEL CEMENTO. TIENEN MAYOR PENETRACIÓN.

LA MEZCLA C) QUE ADQUIERE MAYOR RESISTENCIA AL ESFUERZO CORTANTE YA QUE TIENDE A PRODUCIRSE UN GEL EN CORTO TIEMPO DESPUÉS DE SU FABRICACIÓN SE USA CUANDO SE PRESENTA ESCURRIMIENTO DE AGUA EN LAS DISCONTINUIDADES DE LA ROCA EVITANDO EL DESLAVE DE LA MEZCLA. A ESA MAYOR RESISTENCIA SE CONOCE TAMBIÉN COMO RIGIDEZ.

LAS MEZCLAS F) SE UTILIZAN A VECES PREVIAMENTE AL INYECTADO DE LAS MEZCLAS A), B) Y C) OBTENIENDO LO QUE SE CONOCE COMO UNA SILICATIZACIÓN, ESTA SILICATIZACIÓN PRODUCE UNA DISMINUCIÓN DE LA RUGOSIDAD DE LOS PLANOS DE LAS DISCONTINUIDADES OBTENIÉNDOSE MENORES PERDIDAS DE PRESIÓN POR FRICCIÓN Y POR LO TANTO SE OBTENDRÁ UNA MAYOR PENETRACIÓN DE LA MEZCLA FINAL.

LAS MEZCLAS D) Y E) SE UTILIZAN EN LA INYECCIÓN DE SUELOS.

A LAS MEZCLAS ESTABILIZADAS CON BENTONITA Y/O SILICATO DE SODIO, AL TENER MAYOR RESISTENCIA AL ESFUERZO CORTANTE QUE EL AGUA, SE LES CONOCE COMO CUERPOS DE BINGHAM Y USUALMENTE SE DICE QUE SE TRATA DE MEZCLAS " BINGAMIAS ". A LOS FLUIDOS QUE NO TIENEN RESISTENCIA AL ESFUERZO CORTANTE SE LES CONOCE COMO FLUIDOS NEWTONIANOS Y EL AGUA SE APROXIMA A ESTE TIPO DE FLUIDOS.

NOTA : ES MUY IMPORTANTE EL ORDEN DE AGREGADO DE LOS COMPONENTES PARA FORMAR LA MEZCLA, PUES SUS PROPIEDADES FÍSICAS CAMBIAN EN FORMA NOTABLE HACIENDO QUE SU COMPORTAMIENTO REOLÓGICO ( CON EL TIEMPO ) VARRÍE DE MANERA IMPORTANTE Y SE TRANSFORMEN EN MEZCLAS QUE NO SE PUEDAN MANEJAR.

### 6.3.- PROPIEDADES DE LAS MEZCLAS.

LA PROPIEDAD FÍSICA O MECÁNICA MÁS IMPORTANTE DE LAS MEZCLAS PARA EL CASO DE TRATAMIENTO DE MACIZOS ROCOSOS ES LA RESISTENCIA EN COMPRESIÓN, QUE A LA VEZ SIGNIFICA RESISTENCIA A LA EROSIÓN Y BAJA PERMEABILIDAD.

ESTA PROPIEDAD FÍSICA DE RESISTENCIA DEPENDE DIRECTAMENTE DE LA DENSIDAD DE LA MEZCLA UNA VEZ ENDURECIDA.

POR LO TANTO, EN EL CONTROL DE CAMPO, UNO DE LOS PARÁMETROS BÁSICOS SERÁ EL PESO VOLUMÉTRICO DE LA MEZCLA, PARA FINES DE SU ELIMINACIÓN.

LA RESISTENCIA EN COMPRESIÓN MÍNIMA PARA EVITAR EROSIÓN POR FLUJO DEL AGUA ES DE 15 KG/CM<sup>2</sup>.

OTRO PARÁMETRO IMPORTANTE DE CONTROL ES LA " FLUIDEZ " DE LA MEZCLA. EN GENERAL, SE DEBE DE MANTENER UNA FLUIDEZ CONSTANTE EN CUALQUIER TIPO DE MEZCLA, DE MANERA QUE

SEA BOMBEABLE, UNA FLUIDEZ ENTRE 36 SEG Y 38 SEG EN CONO MARSH DÁ BUENOS RESULTADOS PARA SU MANEJO, DE TAL MANERA QUE DEBE VARIARSE EL CONTENIDO DE BENTONITA HASTA LOGRAR ESA FLUIDEZ.

LA "FLUIDEZ" ES FUNCIÓN DE LA VISCOSIDAD DE LA MEZCLA PERO NO ES PRECISAMENTE UNA MEDICIÓN DE LA VISCOSIDAD, - LA CUAL TIENE OTROS PARÁMETROS DE MEDICIÓN COMO EL POISE O EL POISEUILLE.

CUANDO SE PRESENTA DISPERSIÓN IMPORTANTE DE LA FLUIDEZ, DIGAMOS UNA VARIANCIA DE 10%, LA MEZCLA DEBE ELIMINARSE PUES HABRÁ UNA VARIACIÓN IMPORTANTE EN LA RESISTENCIA EN MAYOR O MENOR VALOR DE LA RESISTENCIA DE PROYECTO.

- TEMPERATURA DE LA MEZCLA.- ES UN PARÁMETRO IMPORTANTE - DE CONTROLAR PUES A TEMPERATURAS ALTAS DIGAMOS  $45^{\circ}\text{C}$  LA - MEZCLA CAMBIA SUS PROPIEDADES MECÁNICAS EN DETRIMENTO DE SU RESISTENCIA EN COMPRESIÓN. CUANDO LA MEZCLA EXCEDA - UNA TEMPERATURA  $> 45^{\circ}\text{C}$  DEBERÁ ELIMINARSE.
- TIEMPO DE LA MEZCLA.- CUANDO LA MEZCLA TENGA MÁS DE 2 HS. DE HABERSE FABRICADO TAMBIÉN CAMBIARÁ SUS PROPIEDADES FÍSICAS EN DETRIMENTO DE SU RESISTENCIA A CAUSA DE LA FORMACIÓN DE GRUMOS POR INICIO DE FRAGUADO, DANDO LUGAR A - QUE POSTERIORMENTE ESOS GRUMOS NO TENGAN BUENA ADHEREN-- CIA Y POR LO TANTO SE PIERDE RESISTENCIA. DEBERÁN TOMAR SE 2 HORAS COMO LÍMITE DE TIEMPO PARA USAR UNA MEZCLA -- DESPUÉS DE SU FABRICACIÓN. ( ESTE DATO CONVIENE VERIFI-- CARLO PARA CADA CASO PARTICULAR ).
- TIPO DE CEMENTO.- EN TODOS LOS CASOS CONVENDRÁ UTILIZAR CEMENTOS FINOS P.EJ. TIPO III, CON SUPERFICIE ESPECÍFICA O FINURA BLAINE  $\geq 4200 \text{ cm}^2/\text{GR}$ .  
LA RAZÓN ES QUE ENTRE MÁS PEQUEÑO SEA EL GRANO DE CEMENTO PODRÁ SER TRANSPORTADO POR LA MEZCLA A UNA DISTANCIA MAYOR, Y POR OTRO LADO, SE PODRÁN RELLENAR DISCONTINUIDADES MÁS CERRADAS, TOMANDO EN CUENTA QUE EL DIÁMETRO DE - LA PARTÍCULA DEBERÁ SER 15 VECES MENOR QUE EL ANCHO DE - LA DISCONTINUIDAD PARA EVITAR EL EFECTO DE "ARQUEO" Y SUBSECUENTEMENTE EL TAPONAMIENTO DE LA DISCONTINUIDAD.
- EXPRIMIDO.- ES EL FENÓMENO DE SEPARACIÓN DEL AGUA DE LA

MEZCLA AL PENETRAR EN DISCONTINUIDADES CADA VEZ MÁS CERRADAS. EL AGUA ES " EXTRUIDA " DE LA MEZCLA JUNTO CON EL AGUA QUE EXISTA EN LA DISCONTINUIDAD POR EFECTO DE LA PRESIÓN, POR LO TANTO, SU RELACIÓN AGUA-CEMENTO DISMINUIRÁ OBTENIÉNDOSE UNA RESISTENCIA MAYOR.

- AGUA LIBRE. - ES EL AGUA QUE QUEDA EN LA PARTE SUPERIOR DE LA MEZCLA POR EFECTO DE LA SEDIMENTACIÓN, TAMBIÉN SE LE CONOCE COMO SANGRADO.

A MAYOR PORCENTAJE DE AGUA LIBRE ES MAYOR LA SEDIMENTACIÓN.

ESTE PARÁMETRO SE UTILIZA PARA CLASIFICAR EL TIPO DE MEZCLA.

SI EL AGUA LIBRE ES  $\leq 5\%$  LA MEZCLA ES ESTABLE.

SI EL AGUA LIBRE ES  $\geq 5\%$  LA MEZCLA ES INESTABLE.

VER CUADRO CON RESUMEN DE PROPIEDADES DE LAS MEZCLAS ESTABLES.

- 7.- CRITERIOS PARA EL DISEÑO DE UNA PANTALLA DE INYECCION Y DRENAJE COMO EL OBJETIVO PRINCIPAL ES EVITAR EL FLUJO DE AGUA A TRAVÉS DE LA MASA DE ROCA, SERÁ NECESARIO DEFINIR SU ESTRUCTURA PARA SELLAR LAS DISCONTINUIDADES MÁS ABIERTAS QUE SE CONSIDERE ESTARÁN CONECTADAS CON EL EMBALSE. POR LO TANTO, LA DIRECCIÓN DE BARRENOS SERÁ PREFERENCIAL PARA INTERSECTAR LOS PLANOS DE ESAS DISCONTINUIDADES, TOMANDO EN CUENTA QUE EL FLUJO DE AGUA A TRAVÉS DE LA ROCA MISMA ES DESPRECIABLE, COMPARADO CON EL FLUJO DE AGUA A TRAVÉS DE LAS FRACTURAS.

LA PERMEABILIDAD A TRAVÉS DE LA ROCA SE CONOCE COMO PERMEABILIDAD PRIMARIA Y NO TIENE IMPORTANCIA PARA EL CASO QUE NOS OCUPA, SINO SOLO EN AQUELLOS CASOS EN QUE LA ROCA SEA EXPANSIVA Y SE DEGRADARÁ O DESINTEGRE POR SATURACIÓN, ESTO TENDRÁ OTRA SOLUCIÓN DE PROTECCIÓN MEDIANTE DRENAJE Y/O CONCRETO LANZADO.

LA PERMEABILIDAD SECUNDARIA, A TRAVÉS DE DISCONTINUIDADES SERÁ POR TANTO LA MÁS IMPORTANTE.

#### 7.1.- NÚMERO DE LÍNEAS DE INYECCIÓN.

SI HEMOS VISTO LA CONVENIENCIA DEL USO DE ALTAS PRESIONES Y MEZCLAS ESTABLES PARA OBTENER UNA MAYOR PENETRACIÓN DE LA MEZCLA, BASTARÁ UNA SOLA LÍNEA DE BARRENOS DE INYECCIÓN.



## 7.2.- CLASIFICACIÓN DE PANTALLAS

PANTALLAS SIMÉTRICAS.- CUANDO SE INTERNAN EN EL MACIZO ROCOSO Y SE PROTEGE TANTO LOS BLOQUES INESTABLES DE ROCA AGUAS ABAJO DE LA PRESA, COMO TODAS LAS EXCAVACIONES SUBTERRÁNEAS, INDEPENDIEMENTE DE LA ESTRUCTURA DE LA ROCA.

PANTALLAS SUSPENDIDAS.- CUANDO LA ESTRUCTURA DE ROCA ES HOMOGÉNEA Y NO EXISTE POSIBILIDAD DE EFECTUAR CIERRE HIDRÁULICO NATURAL EMPOTRANDO LA PANTALLA EN ESTRUCTURAS DE ROCA CON PERMEABILIDAD MENOR.

CIERRE HIDRÁULICO.- SE OBTIENE CUANDO LA PANTALLA DE INYECCIÓN Y DRENAJE SE EMPOTRA EN UNA ESTRUCTURA DE ROCA DE BAJA PERMEABILIDAD, FORMANDO LO QUE SE CONOCE COMO -- UNA " CAJA " O ENCAJONAMIENTO DEL AGUA, HACIA AGUAS ARRIBA LA LA PANTALLA.

## 7.3.- PANTALLA DE DRENAJE.- EN GENERAL BASTARÁ UNA LÍNEA DE DRENAJE TOMANDO EN CUENTA LAS SIGUIENTES CONSIDERACIONES:

- A).- DIRECCIÓN PREFERENCIAL PARA ATRAVEZAR EL MAYOR NÚMERO DE PLANOS DE DISCONTINUIDAD.
- B).- SE USARÁ EL MAYOR DIÁMETRO POSIBLE DE BARRENOS DENTRO DE LOS LÍMITES ECONÓMICOS.
- C).- VIGILANCIA POSTERIOR DURANTE SU FUNCIONAMIENTO, -- OBSERVANDO EL REQUERIMIENTO DE REPERFORACIÓN SI LLEGAN A TAPONARSE.
- D).- HACERLOS TRABAJAR COMO PIEZÓMETROS EN FORMA SELECTIVA, COLOCANDO VÁLVULAS Y MANÓMETROS, PARA OBSERVAR SU EFICACIA Y/O PELIGRO POTENCIAL DE INESTABILIDAD DE BLOQUES DE ROCA O EXCESO DE PRESIÓN CONTRA LAS ESTRUCTURAS SUBTERRÁNEAS.

## 7.4.- GALERÍA POR DEBAJO DEL CAUCE.- PARA EL CASO DE PRESAS DE MATERIALES GRADUADOS, SOLO SE JUSTIFICA CUANDO :

- A).- EL GASTO QUE SE ESPERA A TRAVÉS DE LA ROCA EN FUNCIÓN DE LA EXPLORACIÓN SEA RELATIVAMENTE ALTO Y CONVENGA INVERTIR DINERO PARA CONSERVAR ESA AGUA, MEDIANTE INYECCIONES DESDE LA GALERÍA.
- B).- COMO UNA MEDIDA DE PREVENCIÓN PARA REALIZAR TRATAMIENTO DEL CORAZÓN, PARA EL CASO DE LA EXISTENCIA

DE FALLAS QUE POTENCIALMENTE PUEDAN DESPLAZARSE Y -  
DAÑAR EL CORAZÓN,

- c).- EN CASO DE INCERTIDUMBRE SOBRE LA ESTRUCTURA DE RO-  
CA, POR DEBAJO DEL CAUCE. SERVIRÁ PARA EXPLORACIÓN  
GEOLÓGICA Y POSTERIORMENTE PARA TRATAMIENTO DE IN--  
YECCIÓN Y/O DRENAJE.

ING. RAUL CUELLAR BORJA

## PROBLEMAS CONSTRUCTIVOS EN UNA PRESA

- 1.. Competencia de la roca bajo nuevos esfuerzos
- 2.. Estabilidad total bajo nuevas condiciones
- 3.. Erosión
- 4.. Sismicidad inducida durante el llenado

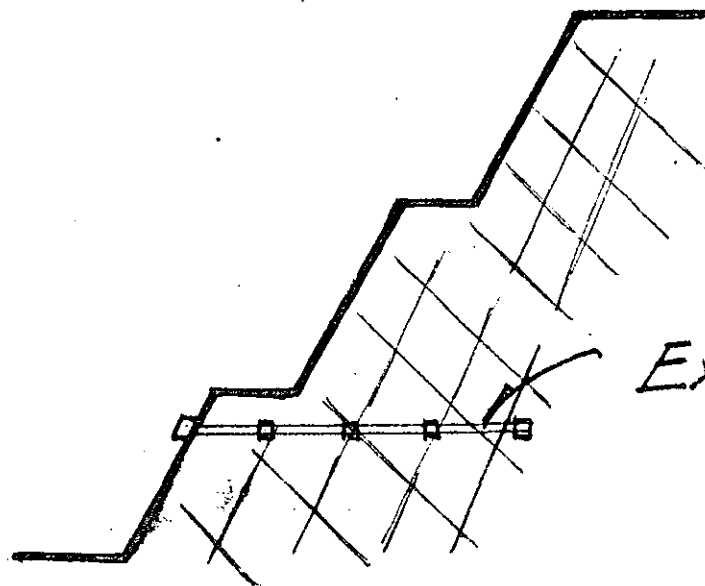
## PREVENCIÓN CONTRA LA EROSIÓN

- 1.. Tratamiento de las excavaciones
- 2.. Tratamiento del contacto roca-corazón
- 3.. Uso de acero de refuerzo

# TRATAMIENTO SUPERFICIAL

1. MUROS, ARMADURAS, CONSOLIDACION, TRATAMIENTO DISCONTINUIDADES (BUTRESS + RIGIDEZ + GAPS)
2. CONCRETO LANZADO (SHOTCRETE) • Simple • Armado
3. ANCLAJE SUPERFICIAL
4. REGULARIZACION DEL TALUD

Verificar el tratamiento de taludes con extensómetros



Usar sistemas de control remoto (radio)

Extensómetro

## REFORZAMIENTO CON ACERO

ACERO PASIVO \$ ACERO ACTIVO

ACERO ACTIVO.. TENSION.. Fuerza de estabilización conocida

ACERO PASIVO.. FRICCION.. La fuerza es conocida solo después de la deformación.

- en roca suave (o muy fracturada).. Usar acero activo (Postensado)
- en roca sana.. Usar acero pasivo

NOTA: El refuerzo postensado debe inyectarse para prevenir grandes movimientos

## INYECCIONES DE CONSOLIDACION

TENDENCIA : Uso de mezclas gruesas y altas presiones

- 1.- Aumento de resistencia
- 2.- Disminución de la deformabilidad  
(Sobre todo Cimentación homogénea)

VERIFICACION DE RESULTADOS (Muy pocos intentos)

- 1.- Drenaje
- 2.- Piezometría (en rocas suaves)
- 3.- Geofísica (el mejor método) Práctica Rusa

## CRITERIOS PARA EL DISEÑO CORRECTO DE UNA PANTALLA DE INYECCION Y DRENAJE

- 1.. Comprender el comportamiento de la roca
- 2.. Cubrir todos los posibles patrones de filtración
- 3.. Monitoreo mediante drenaje y piezometría

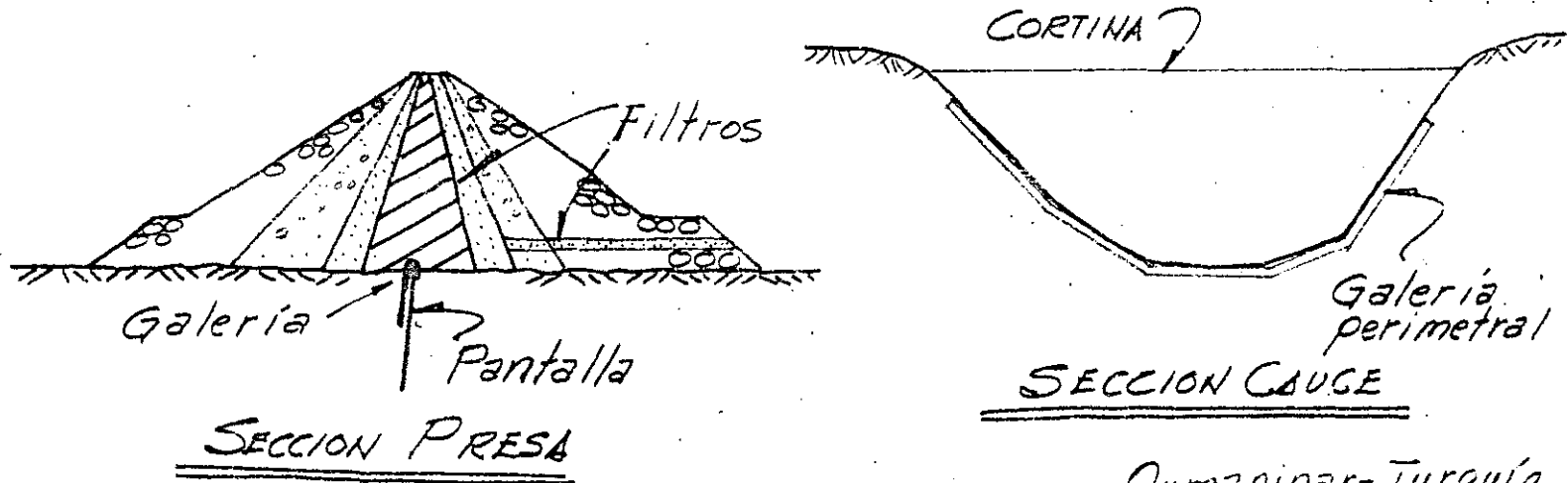


## OTROS ASPECTOS DEL DISEÑO :

- Número de líneas de inyección : Principalmente 1
- Numero de líneas de drenaje : 1 + Separación  $\leq 5$  m
- Monitoreo con piezometría - Vital
- Mantenimiento de drenaje
- Galería por debajo de la presa
  - + Para ejecución de pantalla
  - + Aumento en la eficacia del drenaje
  - + Monitoreo
  - + Acción correctiva

# PROBLEMAS DEL CONTACTO CORAZON-ROCA FISURADA

- 1.. Estanqueidad del agua
- 2.. Erosión de arcilla ( Filtros )
- 3.. Galería debajo del corazón



R. Cuéllar

Oymapinar-Turquía  
Caracol - México  
= 3.5 m

# PROPIEDADES DE LAS MEZCLAS ESTABLES

MEZCLA	A/C	FLUIDEZ MARSH	AGUA LIBRE	PESO VOL.	$f_c'$
	Peso	seg	%	Kg/m <sup>3</sup>	Kg/cm <sup>2</sup>
CRUZ AZUL II	1.66	38.2	6.5	1300	33
	1.25	39.4	6.0	1400	61
	0.83	<b>38.3</b>	4.5	1500	123
APASCO Y ANAHUAC III	1.66	37.3	7.0	1300	22
	1.25	36-38	4.0	1400	38
	0.83	33-35	3.0	1500	86

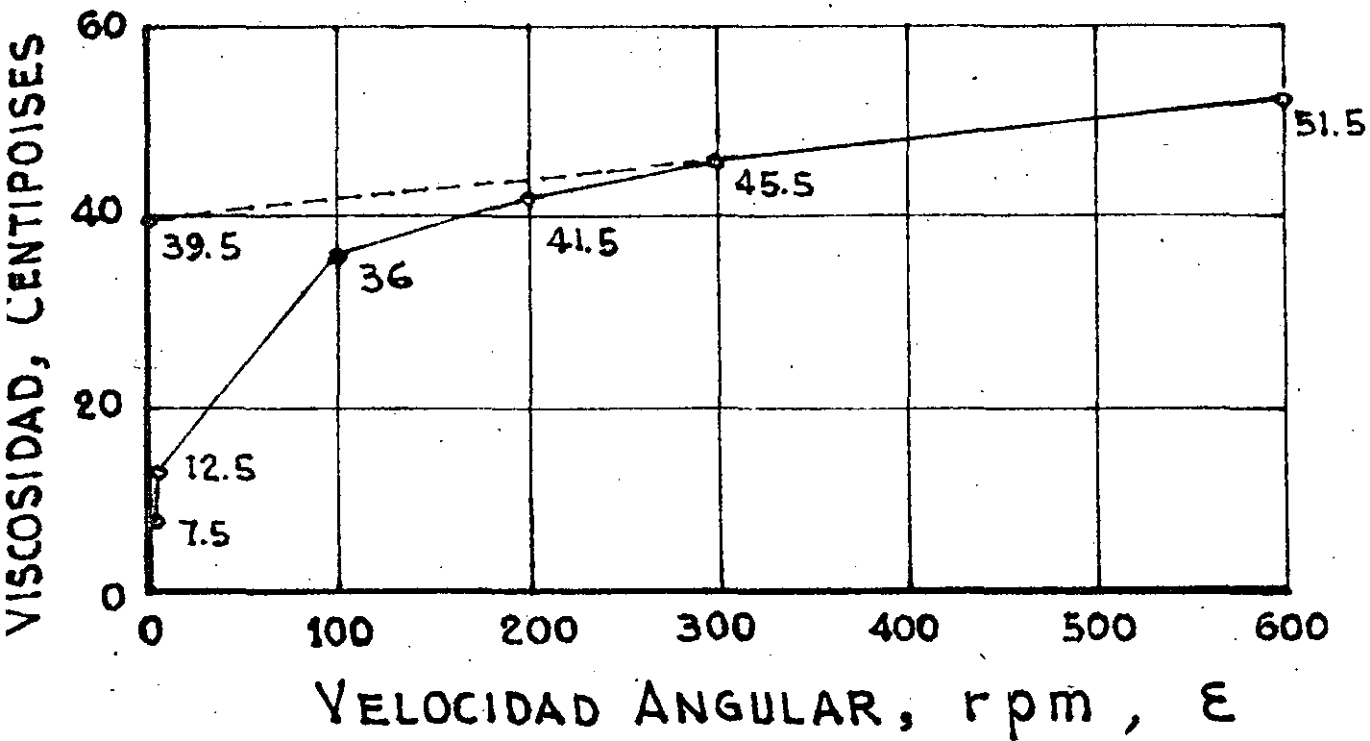
LODO BENT.

A/B = 12 (pesc)

FLUIDEZ : 42 seg

DENS : 1.025

RESISTENCIA MINIMA CONTRA EROSION O DESLAVE : 15 Kg/cm<sup>2</sup>



MEZCLA N° 1

$$\tau = \tau_f + \eta \epsilon$$

$$\rho_{\text{VISE}} = 10^{-1} \text{ Kg} \cdot \text{m}^{-3} \text{ s}^{\text{H}}$$

MEZCLA	REL A/c (peso)	BENTONITA % (Cemento)	$\tau_f$ , ep	$\eta$ ep/rpm
1 (B)	2	6	39.5	0.02
2 (B)	1.33	4	59.0	0.02
3 (B)	1	2	57.5	0.0267
4 (B)	0.8	1	50.0	0.0267
5 (B)	0.67	0.5	35.5	0.0383
6 (N)	0.57	0	24.0	0.0517

(B) BINGHAM (N) NEWTON

P.H. CHICOASEN, CHIS. VISCOSIDAD MEZCLAS

VISCOSIMETRO DE CIL. COAXIALES: FANN

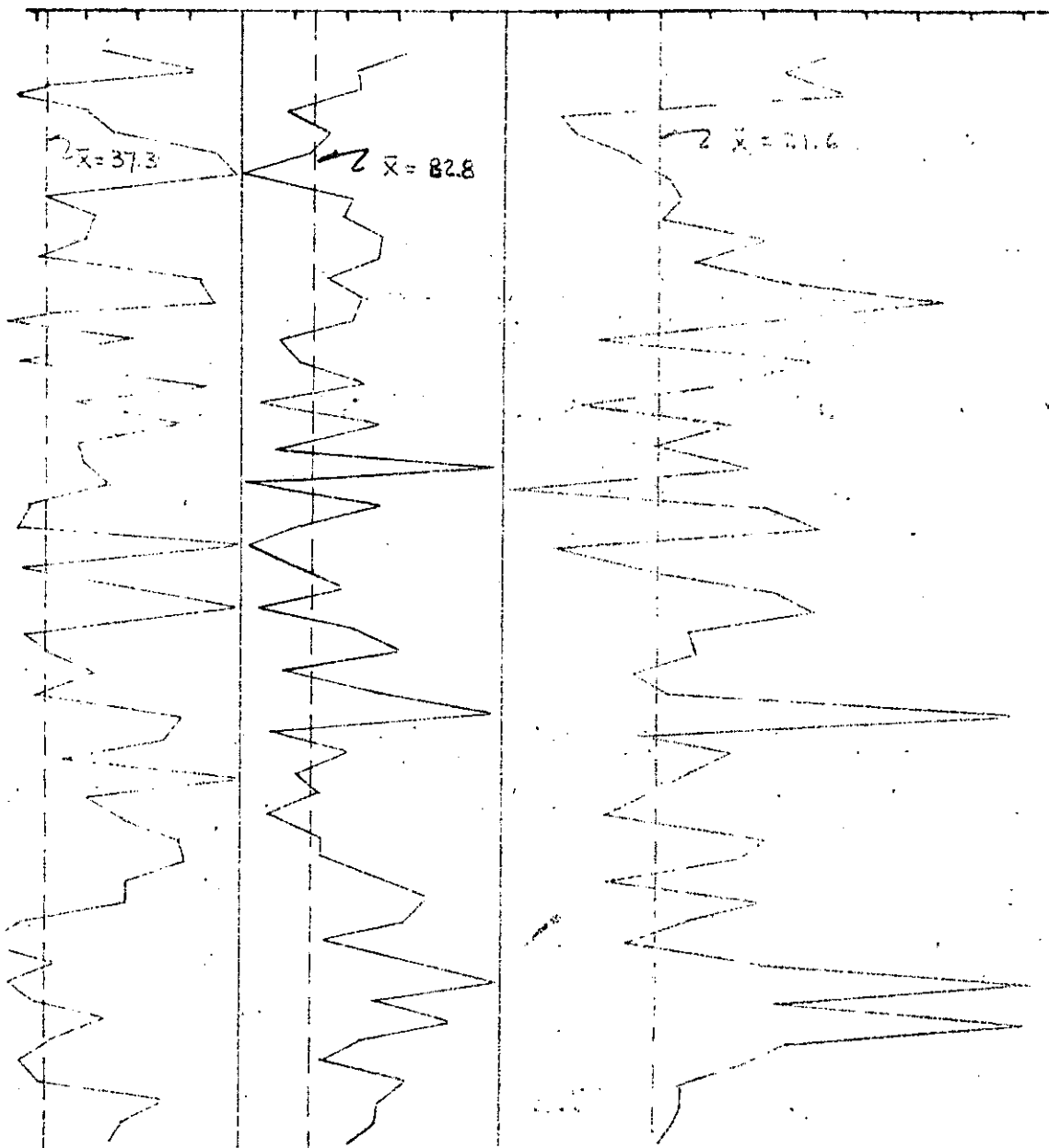
CEMENTO: PICO DE ORIZABA, TIPO II Fig. 10

$\tau_f$  = Punto de Fluencia ;  $\eta$  = Viscosidad plástica.

CEMENTO ANAHUAC TIPO III , MEZCLA : A

CORRELACION ENTRE PROPIEDADES DURANTE JUNIO 1979

FLUIDEZ\* Seg  $\gamma$ , lb/pic<sup>3</sup> COMPRESION SIMPLE Kg/cm<sup>2</sup>  
 36 38 40 42 82 84 86 88 14 18 22 26 30 34 38 42 46 50

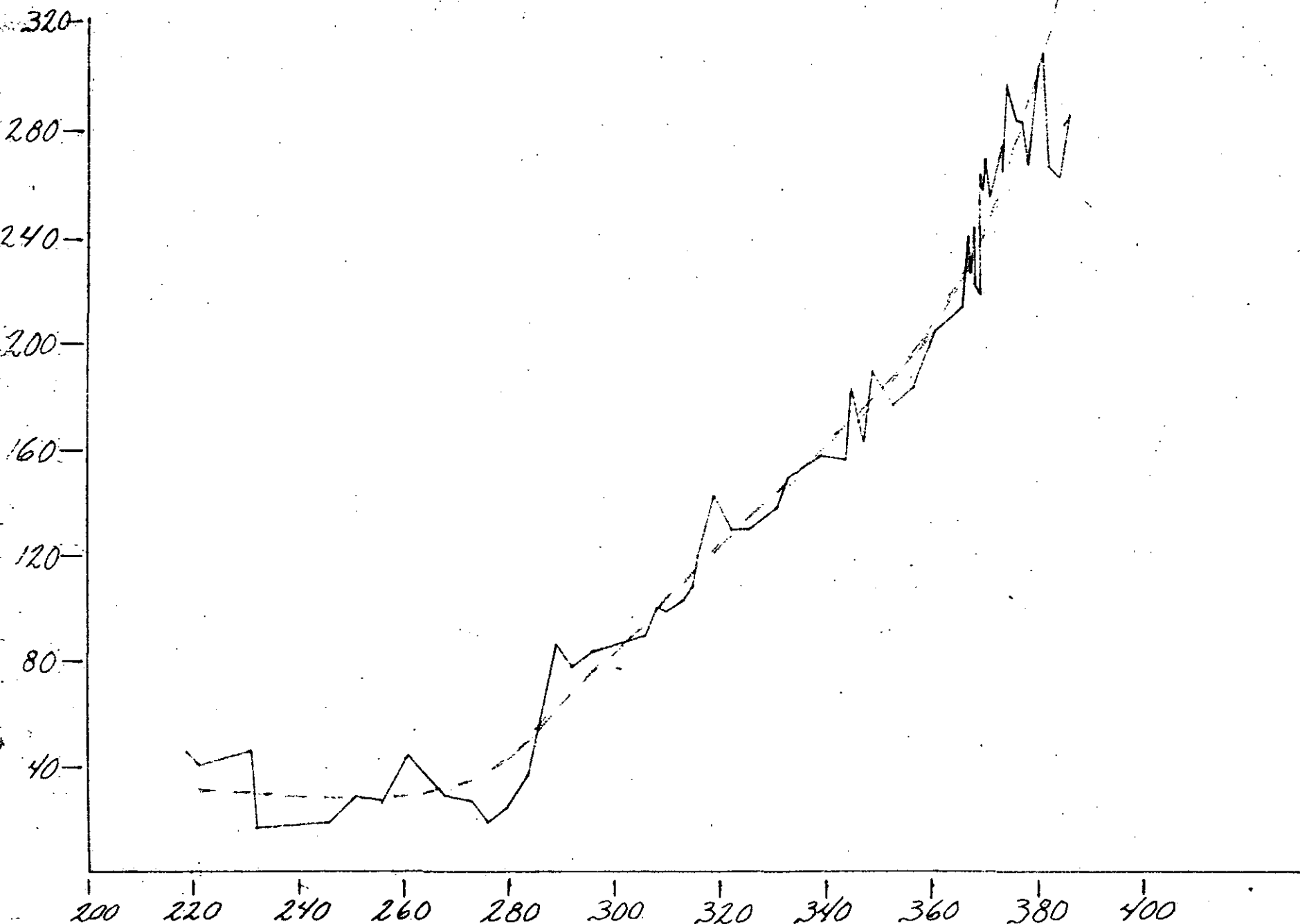


\* MARSH

R. Cuéllar

FIG. 11

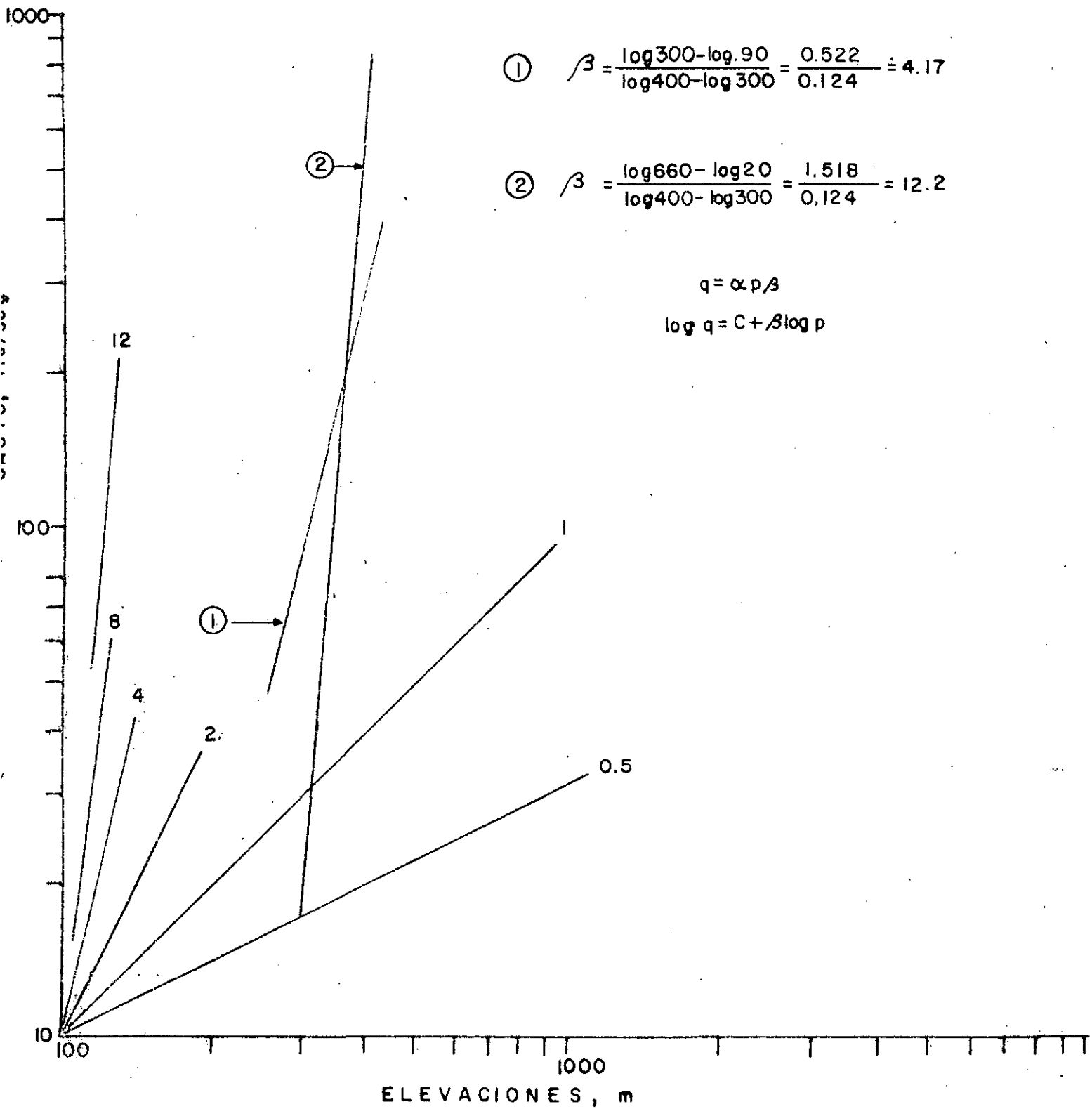
P.H. CHICLASEN CHIS.



R. Cuellar

ELEVACIONES EMBALSE (M.)

Fig. 1



# PRESION DE CONTACTO PERMISIBLE

## SOBRE ROCAS CON DISCONTINUIDADES

(FRÁCTURAS Y/O ESTRATIFICACION)

R.Q.D %	PRESION PERMISIBLE	
	Ton/m <sup>2</sup>	Kg/cm <sup>2</sup>
100	3000	300
90	2000	200
75	1200	120
50	650	65
25	300	30
0	100	10

NOTA: • Si los valores tabulados exceden la resistencia en compresión simple de roca intacta, se utilizará este valor como presión permisible

• Información de Ralph B. Peck



# TORQUES PARA ANCLAS DE TENSION

## CRITERIO EUROPEO

$$M = 300 d P$$

en donde: M está en  $\text{kg} \cdot \text{m}$

d está en m

P está en ton

## CRITERIO AMERICANO

1 TORQUE DE 1 lb-pie = 40 lb de carga

## EJEMPLO:

Si tenemos una barra  $\phi = 1"$  y queremos aplicar una carga  $P = 10 \text{ ton}$ , se tiene:

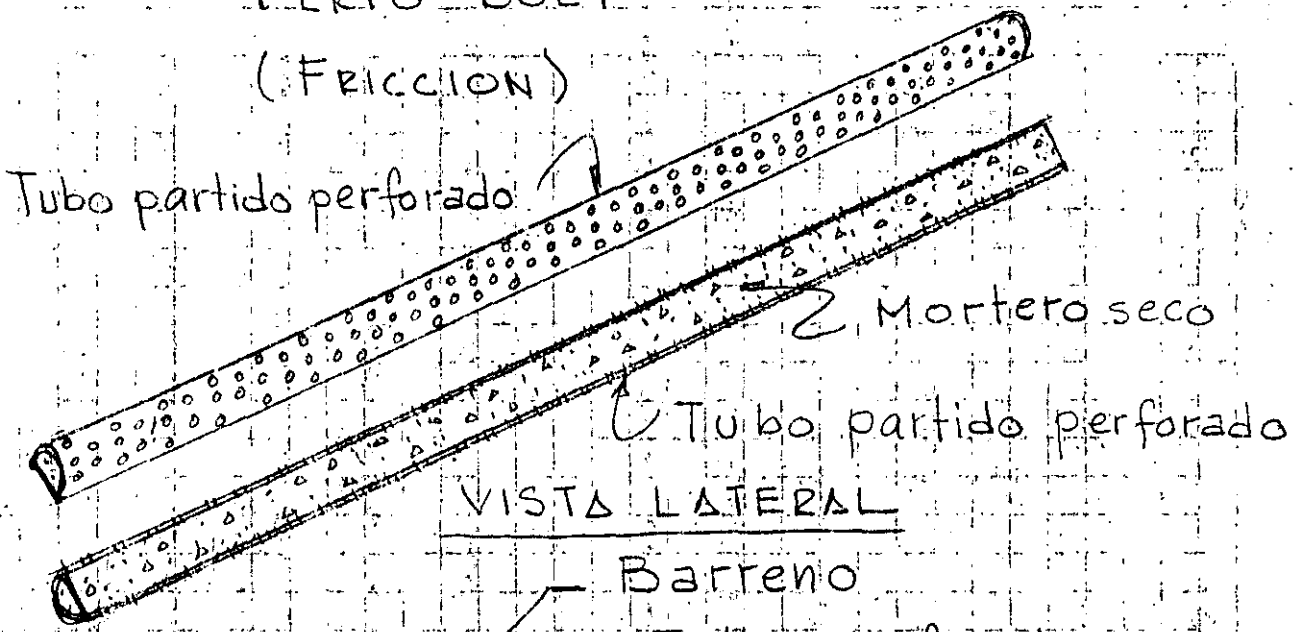
$$1) M = 300 \times 0,025 \times 10 = 75 \text{ kg} \cdot \text{m}$$

$$2) P = \frac{10\,000 \text{ kg}}{0,454} \cdot \frac{\text{lb}}{\text{kg}} = 22\,026 \text{ lb}$$

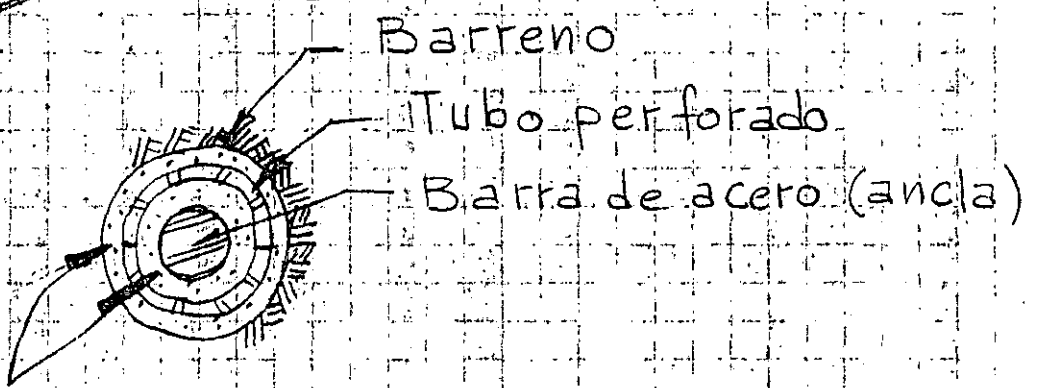
$$\text{Torque} = \frac{22\,026}{40} = 551 \text{ lb} \cdot \text{pie} = 76 \text{ kg} \cdot \text{m}$$

# ANCLAS

## PERFO-BOLT (FRICCION)



VISTA LATERAL



SECCION TRANSVERSAL

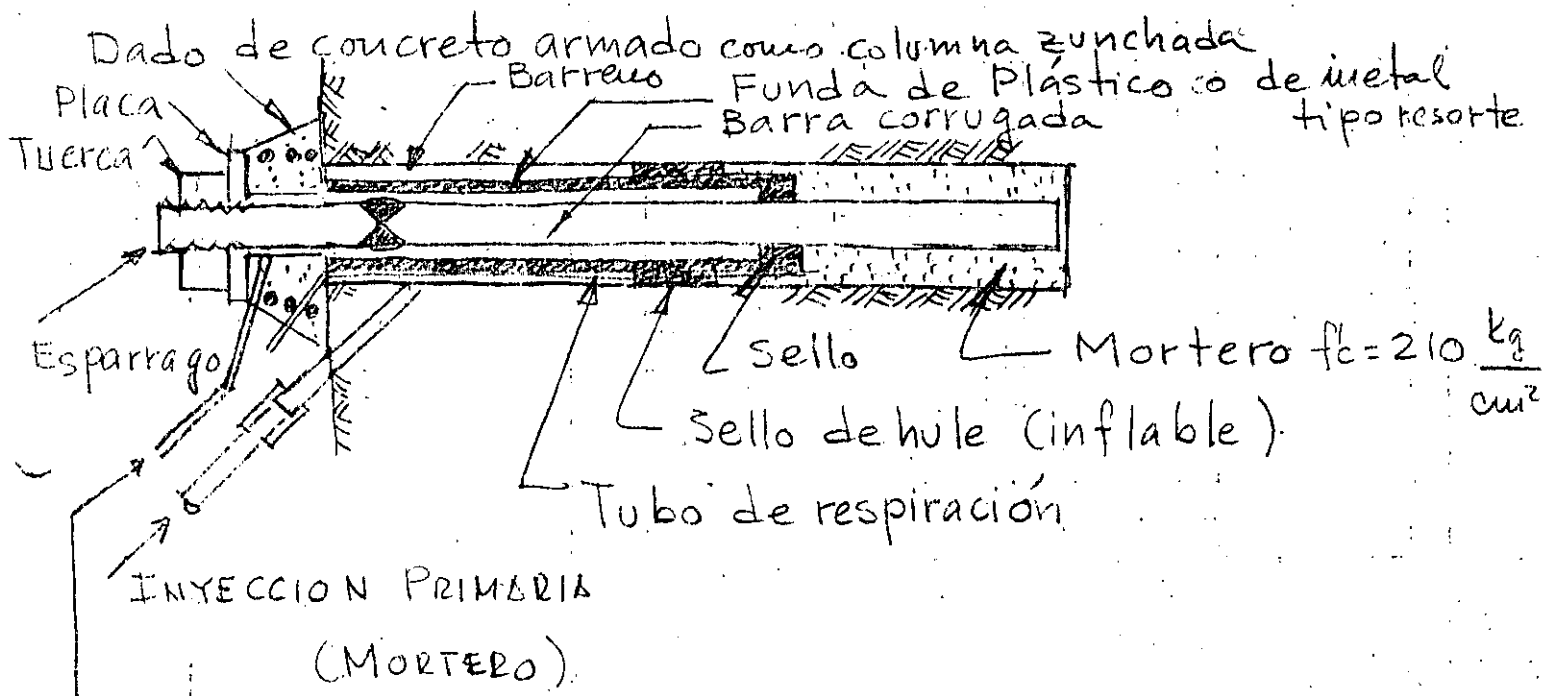
Mortero  
(extruido)

## ANCLAS SPLIT-SET

## DE FRICCION DE TUBO PARTIDO

# ANCLAS POSTENSADAS

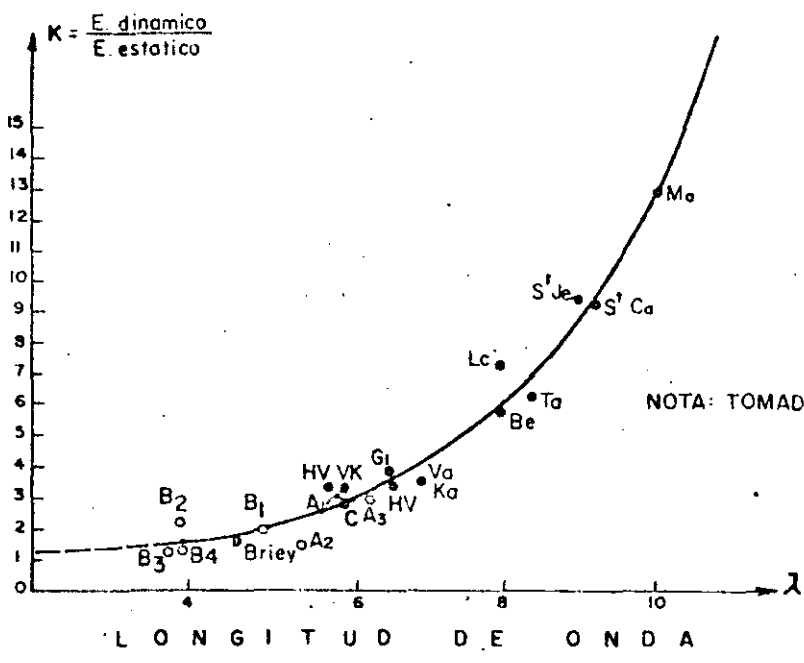
- DE BARRAS GRUESA - NORMAL - DIWYDAG
- DE BARRAS DELGADAS - DIWYDAG
- DE ALAMBRES
- DE CABLES



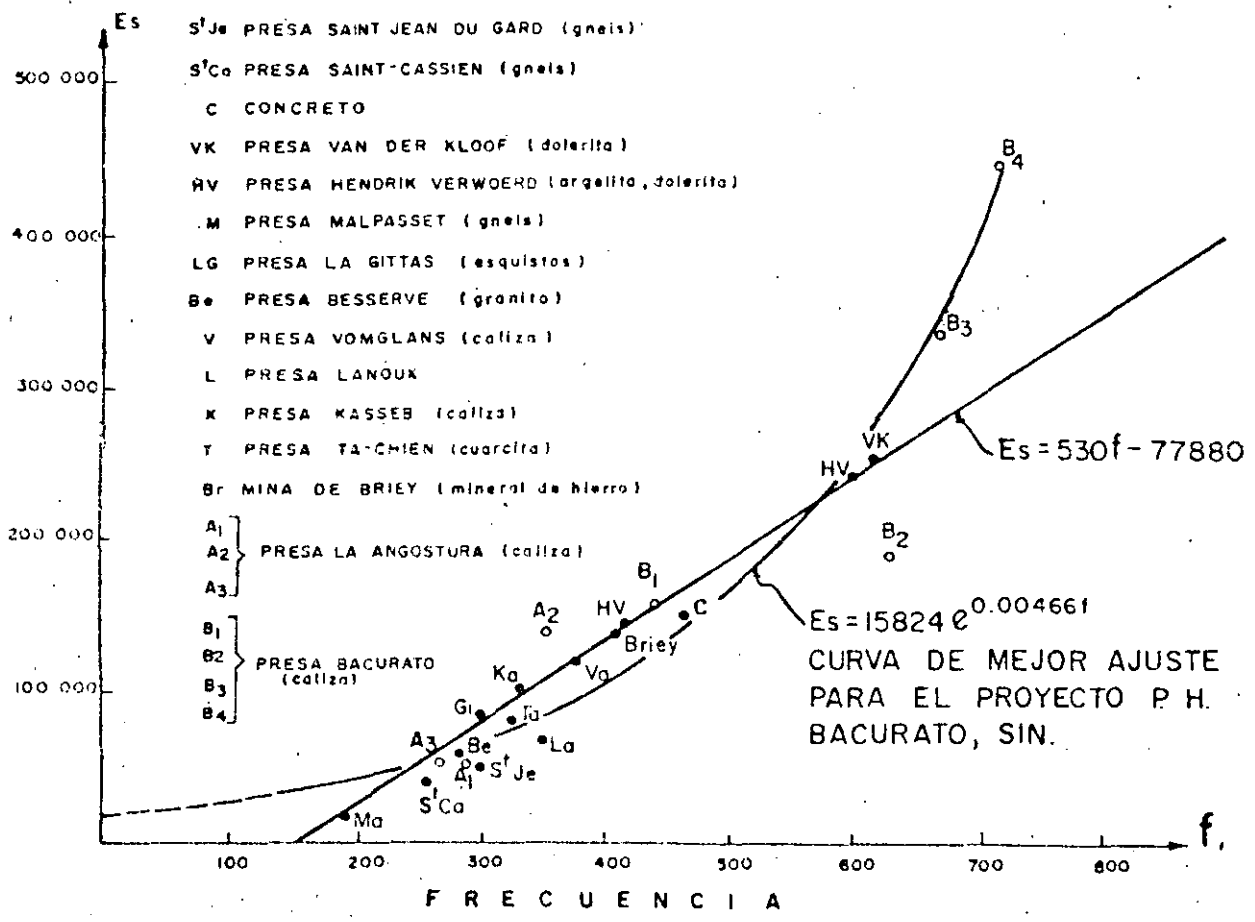
INYECCION SECUNDARIA DE PROTECCION

(MORTERO, GRASA, ACEITE, COMPOUND, ETC.)

FIG. 4 CORRELACIONES EXPERIMENTALES ENTRE PARAMETROS ESTATICOS Y DINAMICOS DE MODULOS ELASTICOS



NOTA: TOMADO DE ROUSSEL J. 1968



EXPERIENCIAS SOBRE EL USO DE ANCLAS DE FRICCIÓN CON RESINAS EPOXICAS EN TUNELES DE LA MINA DE CARBON DE RIO ESCONDIDO, COAH.

Por: Jorge E. Castilla Camacho\*

1. INTRODUCCION

Como parte integrante de los programas de expansión de la Comisión Federal de Electricidad se planea la construcción de la Planta Termoeléctrica de Río Escondido en el Estado de Coahuila, aproximadamente a 35 km al Sur de la Ciudad de Piedras Negras, Coah.

La planta tendrá una potencia instalada total de 1200 MW y en ella se utilizará como combustible el carbón mineral que será explotado de una mina construida ex profeso en la misma zona.

La ubicación de la planta obedece a que en el sitio se encuentra la mayor cuenca carbonífera explorada en el país, cuya explotación permitirá suministrar a la planta un máximo de 16,000 toneladas diarias de carbón. Las reservas detectadas permiten estimar la vida útil de la planta en 26 años.

El programa de la mina, cuya producción será mayor que la producción anual total en el país en los últimos años, ha propiciado numerosos estudios siendo uno de ellos el relacionado con el soporte de las bóvedas de los túneles en la forma más eficiente desde los puntos de vista de seguridad, economía y maniobrabilidad en el interior de la mina.

---

\* Oficina de Mecánica de Rocas, Departamento de Estudios Experimentales.

A principio de 1977 las autoridades encargadas del proyecto de la mina invitaron a la Oficina de Mecánica de Rocas del Departamento de Estudios Experimentales de C.F.E. y al Instituto de Ingeniería de la U.N.A.M. a colaborar en los programas de estudio para el diseño de un sistema de soporte adecuado para las características de la mina.

El presente trabajo describe las actividades desarrolladas por la Oficina de Mecánica de Rocas de C.F.E. en tramos experimentales de túneles, cuyas bóvedas se soportaron mediante anclas de fricción con resinas epóxicas, la instrumentación colocada en dichos tramos, los resultados obtenidos en las mediciones y las conclusiones derivadas de los mismos.

## 2. PRACTICA USUAL EN EL SOPORTE DE MINAS DE CARBON

Generalmente las minas de carbón se explotan mediante sistemas de túneles a partir de los cuales se extrae el mineral hasta provocar la falla del techo, por lo que en estos la estabilidad de la bóveda sólo es necesaria por un cierto tiempo. Sin embargo, existen túneles principales que deben ser estables durante toda la vida productiva de la mina y que por lo tanto deben contar con sistemas permanentes de soporte.

En México el sistema de soporte para bóvedas en minas de carbón se ha desarrollado por métodos empíricos y ha consistido principalmente en el uso de marcos de madera constituidos por dos troncos verticales de madera rolliza que soportan libremente a un tercero horizontal, el cual sostiene al techo.

Los troncos son generalmente de 6" u 8" de diámetro, con longitud variable. Ocasionalmente el tronco horizontal es substituído por una vigueta de acero de 4" ó 6" de peralte en túneles en los que la carga de roca es excesiva. La separación de los marcos es usualmente de un metro, en el sentido del túnel, pero llega a ser menor cuando por observación del comportamiento se juzga necesario.

En los túneles que funcionarán permanentes se acostumbra construir muros de mampostería paralelos al eje del túnel y próximos a las paredes a través de los cuales se transmite la carga del techo al piso. Transversalmente a ellos se colocan viguetas de acero con espaciamientos variables, generalmente de un metro.

En los frentes de explotación, sea esta por medio de pequeños túneles ó por el método de pared larga, en donde la carga aumenta por falta de apoyo al extraer el carbón, y el techo está en franco proceso de falla, se colocan, para seguridad de los mineros y del equipo de ataque, "huacales" formados por pares de troncos superpuestos hasta llegar al techo, tratando de formar una columna.

En países de Europa (Francia, Bélgica, Alemania, Inglaterra, etc.) y en los Estados Unidos, es práctica común el uso de anclas como soporte en túneles de duración temporal. El tipo de ancla más utilizado es el de fricción y de entre estos lo es el de resinas epóxicas que ofrecen un fraguado rápido y por lo tanto su trabajo es prácticamente in

mediato. Las anclas del tipo de expansión 6 de cuña son menos utilizadas debido a que en la mayoría de los casos la roca se encuentra junto con los depósitos de carbón no tiene la dureza necesaria para propiciar un buen trabajo de este tipo de ancla.

El sistema de soporte mediante anclas ofrece algunas ventajas con respecto al sistema tradicional del uso de marcos de madera como son un aumento en la maniobrabilidad dentro de los túneles al evitarse la presencia de postes verticales, que aunque próximos a las paredes ocupan un área dentro del túnel; la disminución del riesgo de derrumbes por deterioro del sistema de soporte al golpear los elementos verticales por los movimientos propios en el interior del túnel; el menor volúmen de material que constituye el soporte lo que frecuentemente puede representar también disminución en su costo; la facilidad de colocación sistemática, así como la rapidez en lograr el trabajo de los elementos de soporte.

No obstante lo anterior, existen desventajas del sistema de soporte con anclas como pueden serlo el que se requieren condiciones especiales de la roca sobre el techo de la mina para lograr un buen trabajo de las anclas, y el efecto psicológico que causa en el personal que trabaja en la mina al no observar los elementos de soporte por estar estos ocultos en perforaciones.



### 3. LA MINA DE CARBÓN DE RIO ESCONDIDO, COAH.

#### 3.1 Aspectos generales del proyecto

La breve descripción que a continuación se incluye, corresponde con el proyecto elaborado por la compañía polaca que asesoró a la C.F.E. en el año de 1976. No obstante que el proyecto ha sufrido modificaciones a la fecha, se efectúa esta descripción general debido a que los programas de ensayos en los tramos experimentales se realizaron con base en las características del proyecto mencionado. Sin embargo, las experiencias obtenidas pueden ser aplicadas a otros proyectos pues las características de los túneles serán similares.

Como se mencionó anteriormente la mina se proyectó para una producción máxima de 16,000 toneladas diarias. La explotación será por medio del sistema de pared larga con derrumbre de techo. El acceso a la mina se hará por tiros inclinados hasta la profundidad del manto. La mina se dividirá en dos secciones.

En cada sección de la mina existirán tres túneles ó cañones principales que deberán funcionar durante toda su vida productiva. Un cañón será el de arrestre, para extracción de material; otro el de transporte de personal y equipo y un tercero de ventilación. Consistirán en túneles de 4.0 m de ancho por 2.2 m de altura, y serán paralelos dejando entre ellos un espesor de 25 m de carbón. La longitud de los túneles permanentes será en total del orden de 20 km.

(15)

Transversalmente a estos túneles existirán los cañones de acceso a los frentes de pared larga. Estos consistirán en pares de túneles de 4.5 m de ancho por 2.5 m. de alto separados por un espesor de 15 m de carbón. Cada par de túneles quedará separado del siguiente por 180 m de carbón, que corresponde con el largo del frente de explotación.

Las medidas anteriores corresponden con las mínimas necesarias para la maniobrabilidad del equipo para explotación de los túneles, lo que se hará con mineros continuos, y para el movimiento de los escudos de protección de la frente de pared larga al trasladarlos de una frente a otra.

Los túneles ó cañones de acceso a los frentes de pared larga, deberán ser estables durante la explotación del frente al que dan acceso, lo que de acuerdo a los programas es del orden de un año. El soporte de estos túneles, los cuales en conjunto tendrán una longitud total del orden de 180 km, es el objeto de los trabajos que se incluyen en el presente reporte.

### 3.2 Descripción de la geología

La geología en la zona de la mina se ha determinado con ayuda de más de 200 barrenos con recuperación de núcleos.

La secuencia litológica en el área es muy uniforme existiendo en la superficie, con espesor variable entre 15 y 22 m, una capa de caliza de origen continental, de color blanco lechoso a café claro. Su dureza es muy variable.

Subyaciendo a este depósito existe un manto de lutita co-

lor pardo en el que se encuentran lentes de conglomerado e interestratificaciones de arenisca de grano fino a medio, - constituida por fragmentos de diferentes tipos de roca y - por feldespatos y cuarzo. Su matriz es arcillosa. En la zona de la mina la parte inferior de este manto se encuentra entre 42 m y 172 m de profundidad.

Bajo este manto y con espesor promedio de 2.0 m y máximo - de 2.8 m se encuentra el estrato de carbón explotable. Presenta una inclinación hacia el este de 1 a 2 grados y se - alarga en dirección Norte-Sur.

A continuación del manto de carbón existen areniscas de - grano fino a medio, de matriz arcillosa.

El nivel freático se define entre 5 y 10 m abajo de la superficie del terreno. Sin embargo, es probable que corresponda con mantos colgados confinados en los acuíferos constituidos por el conglomerado.

### 3.3 Propiedades de la roca

De ensayos efectuados en laboratorio en núcleos de roca extraídos de profundidades próximas al manto de carbón se determinaron las siguientes propiedades.

Propiedad	Valor medio	Coefficiente de variacion
a) Lutita:		
peso volumétrico seco	2.15 ton/m <sup>3</sup>	4%
resistencia a la compresión	137 kg/cm <sup>2</sup>	17"
resistencia a la tensión	11 "	65"
resistencia al corte simple	4 "	25"

Propiedad	Valor medio	Coefficiente de variación
b) Carbón:		
peso volumétrico seco	1.37 ton/m <sup>3</sup>	11%
resistencia a la compresión	175 kg/cm <sup>2</sup>	33"
resistencia a la tensión	9.5 "	38"
resistencia al corte simple	10.5 "	50"
c) Arenisca:		
peso volumétrico seco	2.20 ton/m <sup>3</sup>	6%
resistencia a la compresión	323 kg/cm <sup>2</sup>	59"
resistencia a la tensión	38 "	55"
resistencia al corte simple	19 "	38"
índice de alteración	10 "	7"

#### 4. TRAMOS EXPERIMENTALES DE TUNEL

La falta de experiencia en el uso de los sistemas de anclaje como soporte de la bóveda en minas de carbón, originaron la necesidad de efectuar ensayos en tramos de túnel y observar el comportamiento de los mismos:

Para la ejecución de los ensayos se eligió una pequeña mina, propiedad de C.F.E., próxima al sitio, de la que se extrae carbón para abastecer a la Planta Termoeléctrica de Nave, Coah. Esta mina se explota por métodos manuales, a base de túneles de 3 m de ancho y 2 m de alto, para obtener una producción de 400 ton diarias de mineral. El soporte en los túneles temporales de esta mina es el usual, a base de marcos de madera, dejándose además in situ los 10 ó 15 cm superiores del manto de carbón para proteger del intemperismo a la lutita que lo superyace.

Las características de los tramos de prueba se fijaron con la asesoría de los ingenieros A.G. Douthwaite y C. Rudge - del National Coal Board de Inglaterra quienes visitaron la mina antes mencionada y conocieron el proyecto de la nueva mina.

En un principio se pensó en ejecutar cinco tramos de prueba, de 50 m cada uno, en los que se soportaría el techo de la siguiente forma:

Tramo 1: anclas de 2.4 m de longitud espaciadas 1.20 m en dos direcciones ortogonales. Entre las hileras de anclas se colocaría malla de 3 x 3 pulgadas de alambre calibre 20, sujetándolo con las placas de las anclas.

Tramo 2: anclas de 2.4 m de longitud espaciadas 1.20 m en dos direcciones ortogonales. En cada hilera de anclas transversales al túnel se colocaría en tablón de 14 pies de largo, 8 pulgadas de ancho y dos pulgadas de grueso que estaría sujeto por las placas de las anclas y atravezado por estas últimas.

Tramo 3: igual al tramo 2 pero con anclas de 1.80 m de longitud.

Tramo 4: igual al tramo 2 pero con anclas de 1.80 m de longitud.

Tramo 5: sistema de anclaje "truso" patentado por la Torque Tensión, Ltd. de Inglaterra, consistente en un par de anclas colocadas con una inclinación de 45° en

el techo, junto a las paredes, unidas por un tensor horizontal que troquela al techo con polines de madera.

Las anclas deberían de ser del tipo de fricción colocadas con resina. Los tramos de prueba deberían tener 4.8 m de ancho y la altura sería igual a la del manto de carbón menos 15 cm que se dejarían para proteger a la lutita del intemperismo. Deberían escogerse tramos recién excavados de túnel para colocar las anclas, evitando así tramos en que el techo hubiera sufrido deformaciones anteriores. Los sistemas de soporte experimental deberían colocarse junto con el soporte de uso convencional en la mina y sólo cuando en los túneles se suspendiera la circulación de personal se procedería a retirar el soporte convencional y a observar el comportamiento de los tramos.

Una vez establecidas las características que deberían reunir los tramos experimentales y con el fin de no alterar los planes de explotación de la mina, se eligieron los cañones de regreso de ventilación números 3 y 4 para localizar los tramos de prueba. La elección se hizo también considerando que estos cañones irían a permanecer abiertos un período de un año y medio, tiempo en que se realizarían las observaciones.

##### 5. INSTALACIONES DEL SISTEMA DE SOPORTE

Los tramos elegidos para la ejecución de las pruebas se ampliaron de 3 a 5 m como se aprecia en las Figs. 1 y 3. Para soportar el techo se colocaron dos marcos colineales cada metro.

El sistema experimental de soporte se colocó intermedio a los marcos.

5.1 En este cañón la longitud del tramo de prueba fue de 41 m, como se ve en el recuadro de la Fig. 2. Se colocó también malla ciclón de 2 1/2 pulgadas por 2 1/2 pulgadas cubriendo el ancho del techo del túnel. En un tramo de 20 m de longitud, indicado en las figuras 1 y 2, se colocó un ancla adicional de 2.40 m de longitud, inclinada 45° y a una distancia del orden de un metro de la pared derecha del cañón, como refuerzo adicional, pues en esta parte, en el resto del tramo de prueba, se venía abriendo una grieta inclinada hacia el centro del techo del túnel.

Las anclas instaladas en el tramo fueron de dos tipos. Hasta la línea de anclas número 26 se colocaron anclas constituidas por varilla corrugada de acero grado duro ( $f_{yp}=4200\text{kg/cm}^2$ ) de 1 pulgada de diámetro con una tuerca soldada en su extremo exterior; el resto de las anclas consistió en varillas corrugadas de 7/8 de pulgada de diámetro con cabeza en forma de tuerca preparada en fragua.

Las anclas se instalaron en perforaciones de 1 3/8 de pulgada de diámetro en las que se introdujeron dos o tres cartuchos de resina epóxica de 20 pulgadas de longitud y 32 mm de diámetro. Se experimentó con diferentes cantidades de resina tratando de que se rellenara completamente el espacio entre las paredes de la perforación y el ancla. Se optó por utilizar 3 cartuchos pues el uso de más impedía la entrada del ancla hasta el fondo.

Las perforaciones se efectuaron con "stooper" y con este mismo se introdujo el ancla previa colocación de los cartuchos en el interior de la perforación. El stooper permitió introducir el ancla en la perforación con una velocidad de rotación de 200 revoluciones por minuto aproximadamente, lo que provocó el batido del catalizador y el endurecedor de la resina. La instalación de cada ancla desde el inicio de la perforación hasta su introducción total en la misma tomó entre 3 y 4 minutos. Para lograr un fraguado inicial suficiente se sostuvo el ancla, posteriormente a su colocación por un lapso de 5 minutos.

La resina utilizada fue la Celtite cuyas características son siguientes:

peso volumetrico:	1.85 gr/cm <sup>3</sup>
resistencia a la compresión:	1125 kg/cm <sup>2</sup>
resistencia a la tensión:	170 kg/cm <sup>2</sup>
resistencia al corte:	527 kg/cm <sup>2</sup>
tiempo de fraguado	1 minuto
tiempo de mezclado	15 segundos

### 5.2 Cañón 3

En este cañón el tramo de prueba fue de 50 m de longitud, dividido en tres zonas. Conforme se aprecia en la figura 3, en la zona A se colocó un ancla central de 1.80 m de longitud - completamente vertical, dos anclas con 60° de inclinación --



hacia las paredes del túnel y 2.40 m de longitud y dos anclas a 45° también de 2.40 m de longitud. Estas cinco anclas se colocaron atravesando una pieza de madera rolliza de 14 pies de longitud y 8 pulgadas de diámetro que sostenía a la malla ciclón. Además se colocó un ancla adicional, de 2.4 m de longitud y con 45° de inclinación separada entre 60 cm y un metro de la pared izquierda del cañón.

En la zona B no se colocó anclaje para poder contar con un tramo de referencia con el sistema convencional de soporte.

En la zona C el anclaje colocado consistió en anclas verticales de 1.80 m de longitud, espaciadas como se ve en la figura 3, colocadas sujetando un tablón de 16 pies de largo, 8 pulgadas de ancho y dos de espesor, el cual sostenía una malla ciclón.

Las anclas utilizadas en este cañón fueron todas varillas corrugadas de acero grado duro, de 7/8 de pulgada de diámetro con cabeza formada en fragua.

Por lo que respecta al procedimiento de instalación tipo de resina, etc. fueron los mismos utilizados en el cañón 4.

Durante la instalación de los sistemas de soporte experimental en ambos cañones, se procuró estar siempre lo más próximo posible al frente de explotación. Se llevaron registros del avance del frente, de la colocación de los marcos de madera y del anclaje en el techo. Con los datos reunidos se

formaron las gráficas de las figuras 2 y 4. Se observó que el hecho de no colocar el anclaje inmediatamente después de abierto el frente, permite la deformación del techo, aunque estén colocados los marcos. Cuando el anclaje se se paró del frente del orden de 3 m, se produjo una grieta pa ralela al eje del túnel en cada lado del techo. No se pudo determinar la profundidad de la grieta pero su dirección tenía tendencia a ir hacia el centro del túnel con aproximadamente 60° de inclinación con la horizontal.

6. INSTRUMENTACION

Para observar el comportamiento de las paredes, piso y techo del túnel, se fijaron secciones instrumentadas cada cinco metros de distancia en los tramos experimentales.

La instrumentación de las secciones consistió en la colocación de extensómetros de barra cuyo dispositivo de medición fue un potenciómetro eléctrico de presión. En el techo y paredes se utilizaron potenciómetros Helipot de 10 ohms, 0.5 de linealidad y 1.5 cm de radio. En el piso se utilizaron potenciómetros Spectrol también de 10 Ohms y 0.5 de linealidad pero de 3.5 cm de radio y sellados para protegerlos contra el agua.

La distribución de extensómetros en las secciones instrumentadas puede apreciarse en las figuras 7 a 17, junto con la profundidad a la que fueron fijados dentro de la roca. En algunas secciones se colocó, además de los extensómetros, un dispositivo para medir la convergencia del piso y

el techo.

En la figura 5 se incluye un croquis de la colocación de los extensómetros y del dispositivo para medir convergencia.

A los lados de la sección instrumentada 7 se colocaron dos extensómetros de 2 m de longitud y 2 de 3 m para conocer la distribución de los movimientos de la roca sobre el techo.

Todos los cables de los potenciómetros se llevaron a una consola fuera del área de prueba para evitar riesgos del personal que efectuaba las mediciones. Estas se realizaron con un Puente de Wheatstone.

Se colocó además un sistema de niveles hidráulicos para seguir las deformaciones del techo, pero este presentó problemas por la evaporación que ocurría en el interior de los túneles.

## 7. PRUEBAS EFECTUADAS

Como primer paso del programa de pruebas se extrajeron tres anclas de 1.80 m de longitud y 1 pulgada de diámetro, instaladas en perforaciones de 1 1/2 pulgada de diámetro. La figura 6 muestra las gráficas carga-deformación determinadas en los ensayos.

Una vez que los tramos experimentales dejaron de funcionar para la circulación en la mina, se procedió a la ejecución de las pruebas programadas.

Para retirar el soporte convencional se construyeron cerca de 100 gatos mecánicos de tornillo que se utilizaron para substituir los troncos verticales de los marcos de madera,

colocándose con una distribución de 1 m x 1 m bajo los troncos horizontales.

Al ir aflojando los gatos mecánicos el techo comenzó a deformarse y las anclas comenzaron a trabajar. Las deformaciones que se fueron presentando se detectaron con los instrumentos colocados. Algunas de las gráficas elaboradas se incluyen en las figuras 7 a 17.

La deformación máxima permisible en el techo se fijó en 12-cm correspondiente a 2% de expansión del techo entre el punto de medición y la cara libre (profundidad del extensómetro igual a 6 m).

A continuación se detallan las pruebas y resultados obtenidos en cada cañón.

7.1 Cañón 4

La prueba en este cañón se verificó en dos etapas. En la primera etapa, iniciada el 26 de septiembre de 1977 se movieron seis marcos, tres a cada lado de la sección instrumentada número 8 (ver fig. 1). La segunda etapa se inició el 17 de octubre siguiente moviendo 8 marcos más, hasta llegar a la sección instrumentada 6.

Al inicio de la primera etapa se aflojaron los tornillos de los gatos mecánicos hasta dejarlos prácticamente sin cargar. Se observaron las deformaciones en forma continua principalmente en la sección 8 llegándose a tener una deformación de 2 cm en el extensómetro central del techo después de 2 hrs. de iniciada la prueba, y 3.4 cm después de 24 hrs. Se prosiguió de esta forma, aflojando los gatos que se notaban cargando, diariamente, registrándose las deformaciones que

se iban produciendo.

Al comenzar la segunda etapa, ampliando el tramo con marcos apoyados en gatos mecánicos, las deformaciones sufrieron un aumento brusco llegando a ser del orden de 12 cm en el extensómetro central del techo de las secciones 7 y 8, el día 24 de octubre. En este momento se decidió suspender la prueba para no poner en peligro la estabilidad del túnel, por lo que se colocaron nuevamente los postes verticales de los marcos de madera y se retiraron definitivamente los gatos mecánicos. Las lecturas de deformaciones continuaron tomándose por un tiempo.

Las figuras 7 y 12 muestran gráficas de deformación de algunas de las secciones instrumentadas, de los extensómetros cortos (2 y 3 m) y de las mediciones de convergencia.

## 7.2 Cañón 3

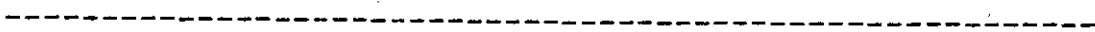
En este tramo sólo fue posible efectuar pruebas en la zona A, iniciándose ésta el 18 de enero del presente año. Se removieron todos los marcos de la zona (ver figura 3), en total 8 marcos, teniéndose lecturas de las deformaciones que ocurrían. El día 26 de enero en la sección 2 la deformación acumulada en el extensómetro central del techo alcanzó 12 cm por lo que se decidió suspender la prueba colocando nuevamente los postes verticales de madera y retirando los gatos mecánicos.

No fue posible efectuar la prueba en la zona C de este cañón

debido a que la mina fue cerrada al dejarse de operar la Planta Termoeléctrica de Nava, Coah.

8. CONCLUSIONES

- a) Los instrumentos colocados proporcionaron mediciones congruentes con el comportamiento estructural del túnel y consistencia durante su operación por lo que los datos obtenidos se juzgan confiables.
- b) Las deformaciones que ocurrieron en el techo en los tramos experimentales (secciones 7 y 8 del cañón 4 y sección 2 del cañón 3) fueron excesivas para la estabilidad del túnel de acuerdo a experiencias publicadas\*. Se alcanzaron deformaciones de 12 cm, correspondientes a una expansión del 2% entre el punto de medición y la cara libre de la roca, en un tiempo corto para lo que deben estar abiertos los túneles temporales de la mina.
- c) Las deformaciones del techo ocurridas en secciones en las que no se removieron los postes verticales de madera fueron entre 1 y 2 cm en el tiempo que duraron las pruebas (ver figuras 7, 13, 15, 16).
- d) De acuerdo a las mediciones de extensómetros colocados a diferentes profundidades en el techo, entre 2 y 3 m hay una deformación importante, posiblemente una grieta.
- e) Las anclas de 1.80 m de longitud parecen ser reducidas para el ancho de túnel ensayado. Anclas de mayor longitud.



RAFFOUX, J.F., P.SINOU y E.TENCELIN "Le boulonnage des voies - et des galeries minieres" Revue de L'industrie minerale, Julio 71.

podrían conducir a resultados más prometedores.

- f) La deformación de las paredes de los túneles fue muy reducida con valores máximos de 2 ó 3 mm.
- g) El piso del túnel manifestó expansión con valores del orden - de 2 cm como máximo.
- h) Los dispositivos para medición de convergencia proporcionaron datos congruentes con los obtenidos por medio de los extensómetros de piso y techo combinados.
- i) El tramo en el que se colocaron anclas con madera rolliza como trabes (zona A del cañón 3) presentó un comportamiento más uniforme que el tramo con anclas solas (cañón 4). Además hubo menos agrietamiento en el techo. Sin embargo, la longitud de anclaje y separación del mismo, no representó un soporte adecuado por la rapidez con que se llegó a la deformación máxima permisible.
- j) Se pudo observar que es muy importante para el buen funcionamiento del anclaje colocarlo inmediatamente atrás del frenteabierto para evitar deformaciones entre ambas operaciones se formaron grietas en el techo, próximas a las paredes y paralelas a ellas.

## 9. RECONOCIMIENTOS

Los trabajos descritos en el presente reporte fueron posibles gracias al patrocinio de la Coordinadora de Río Escondido, Coah. La colaboración del personal de la Mina de Río Escondido, Coah.

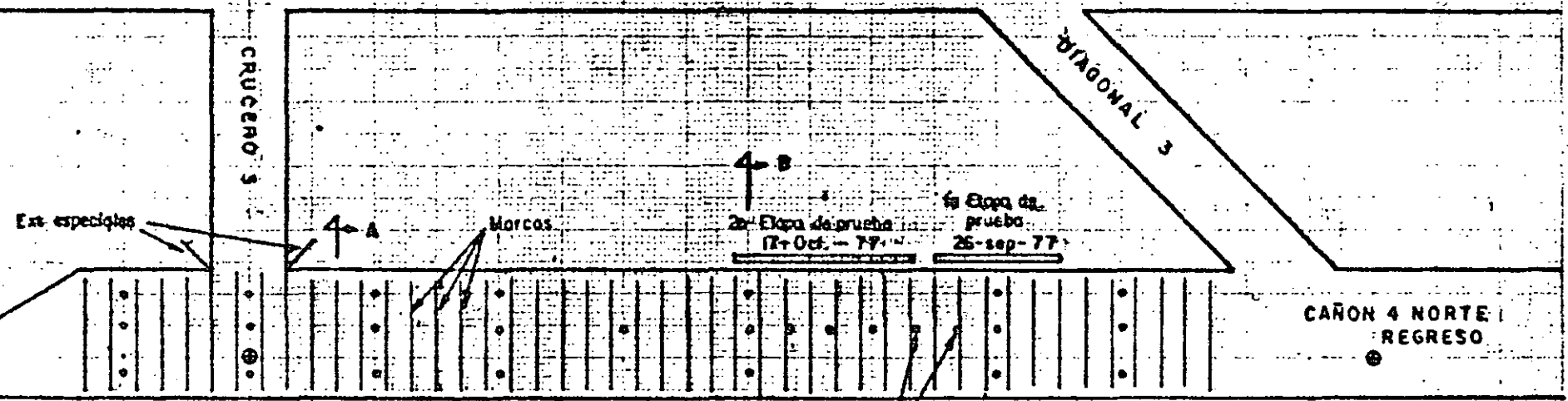
y especialmente del Ing. Salvador Uribe V., Superintendente de la Mina, permitieron el desarrollo de los programas de ensaye. La colocación del anclaje estuvo a cargo del Sr. Mario Urquijo B. En la coordinación de los trabajos de campo-participaron los Ings. Raúl Ramírez Aranda, Sergio Ochoa y Alfonso Rodríguez García. La colocación de instrumentos y ejecuciones de mediciones fue hecha por los Sres. Filadelfo Ayanegui U., y Humberto León M. Los trabajos de laboratorio fueron ejecutados por los Sres. Efraín Esperón Q., y Francisco Vallejo C. La fabricación de instrumentos fue hecha por personal del taller del Departamento de Estudios Experimentales, a cargo del Ing. Jorge Borbón.

NOTA: La suspensión imprevista de la operación de la mina - al cerrarse la Planta Termoeléctrica de Nava, Coah. - impidieron llevar a cabo la totalidad de las pruebas programadas. Se pretende continuar con los ensayos - una vez se cuente con la mina nueva.



30.00 m

CAÑON 4 NORTE ENTRADA



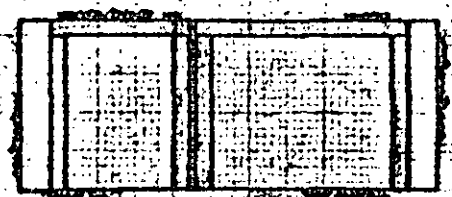
Sección de instrumentación

1 2 3 4 5 6 7 8 9 100m

45.00 m

Tramo con azida adicional a 45° en el lado derecho del techo

5.00m



CORTE A-A

Soporte con 2 marcos de madera



CORTE B-B

Sección de instrumentación

C.F.E. DEPTO. EST. EXP.  
MNA RIO ESCONDIDO, COAH.  
CAÑON 4 NORTE REGRESO  
TRAMO DE INSTRUMENTACION I

FIG. 1

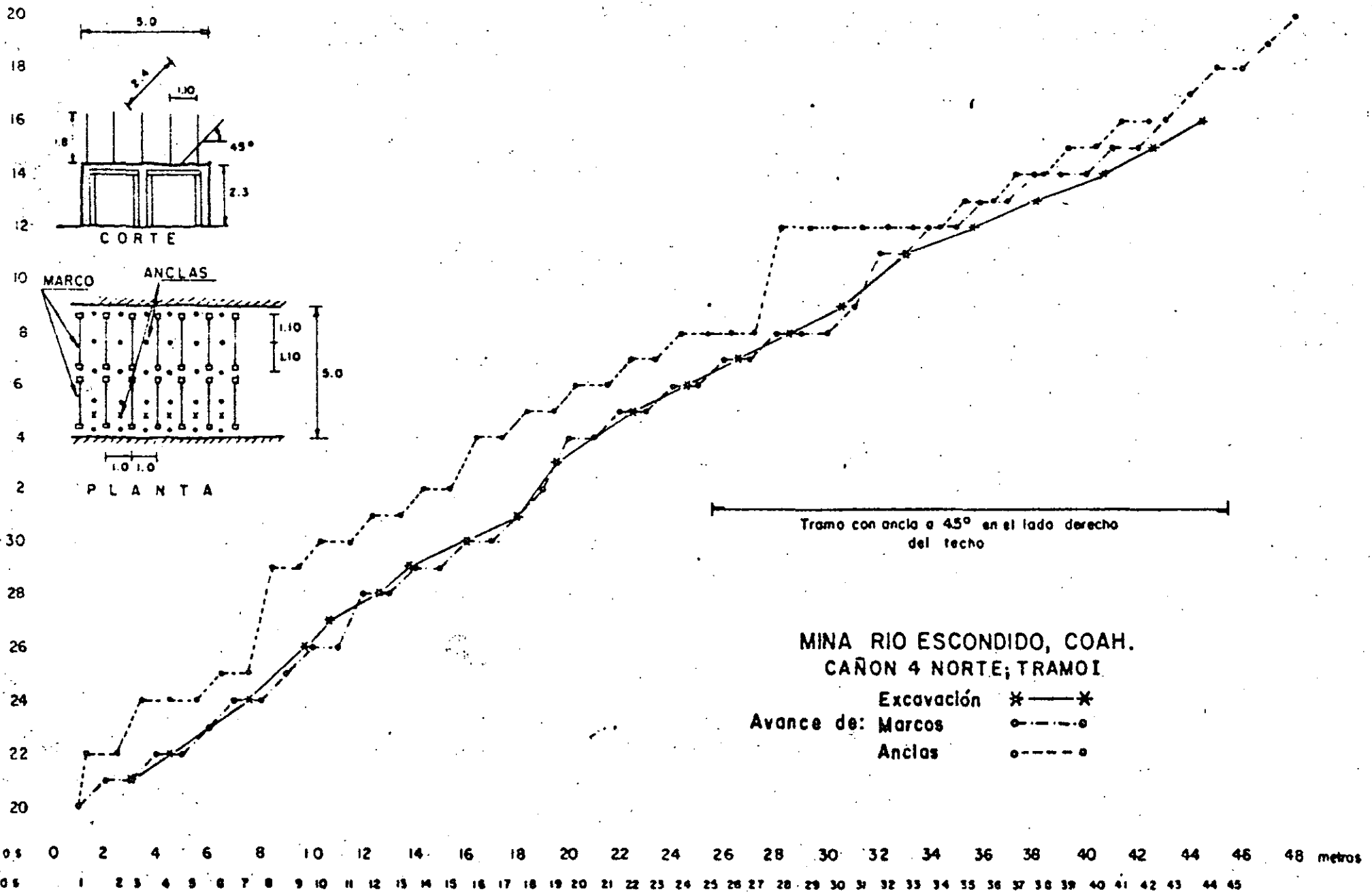
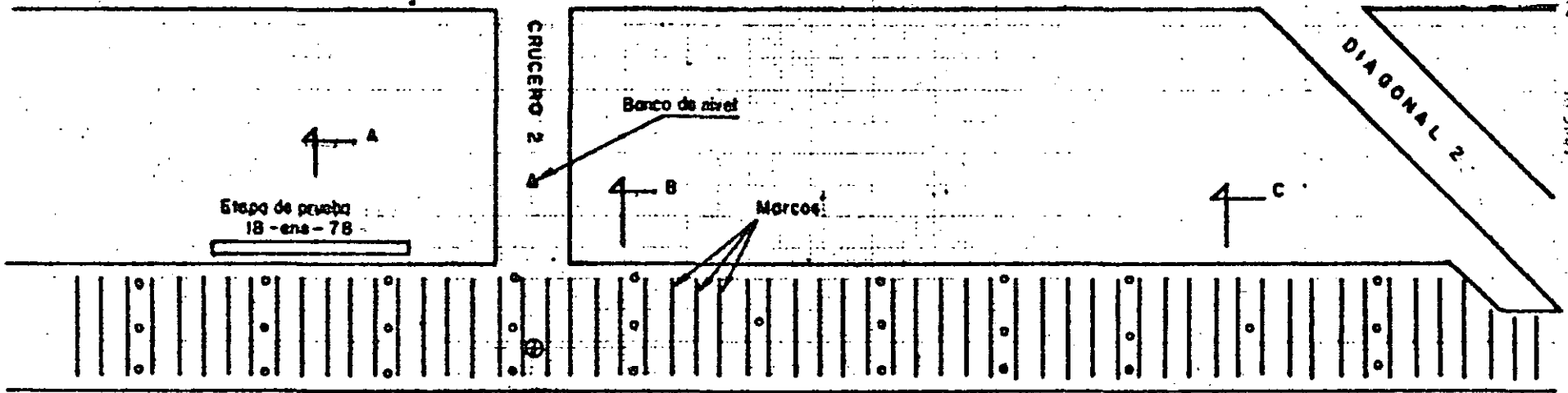


FIG. 2

250

30.00

CAÑON 3 NORTE ENTRADA



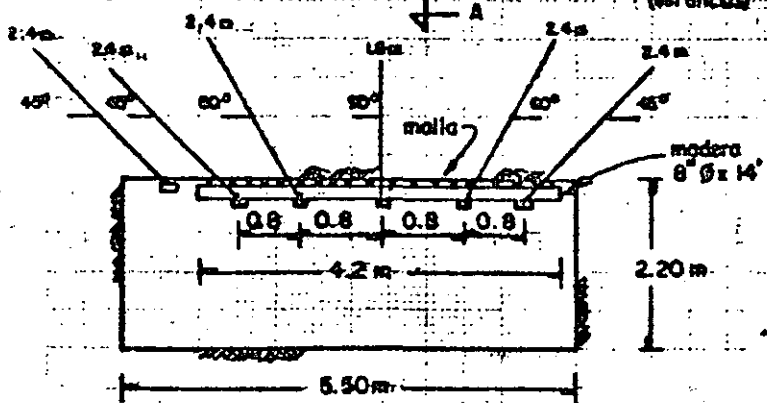
Secciones de los tramos de 1 2 3 4 5 6 7 8 9 10 H

8.0 m 11.0 m 31.0 m

ZONA A

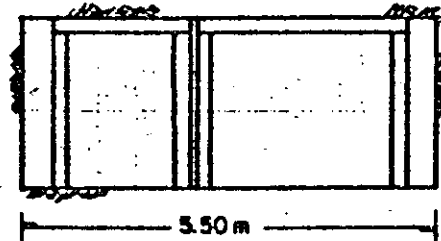
ZONA B (sin anclas)

ZONA C



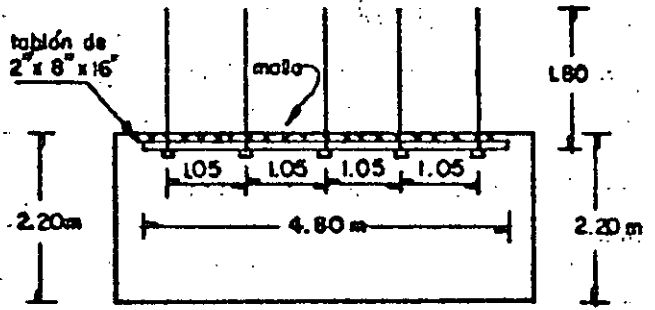
CORTE A - A

Anclaje en zona de prueba A



CORTE B - B

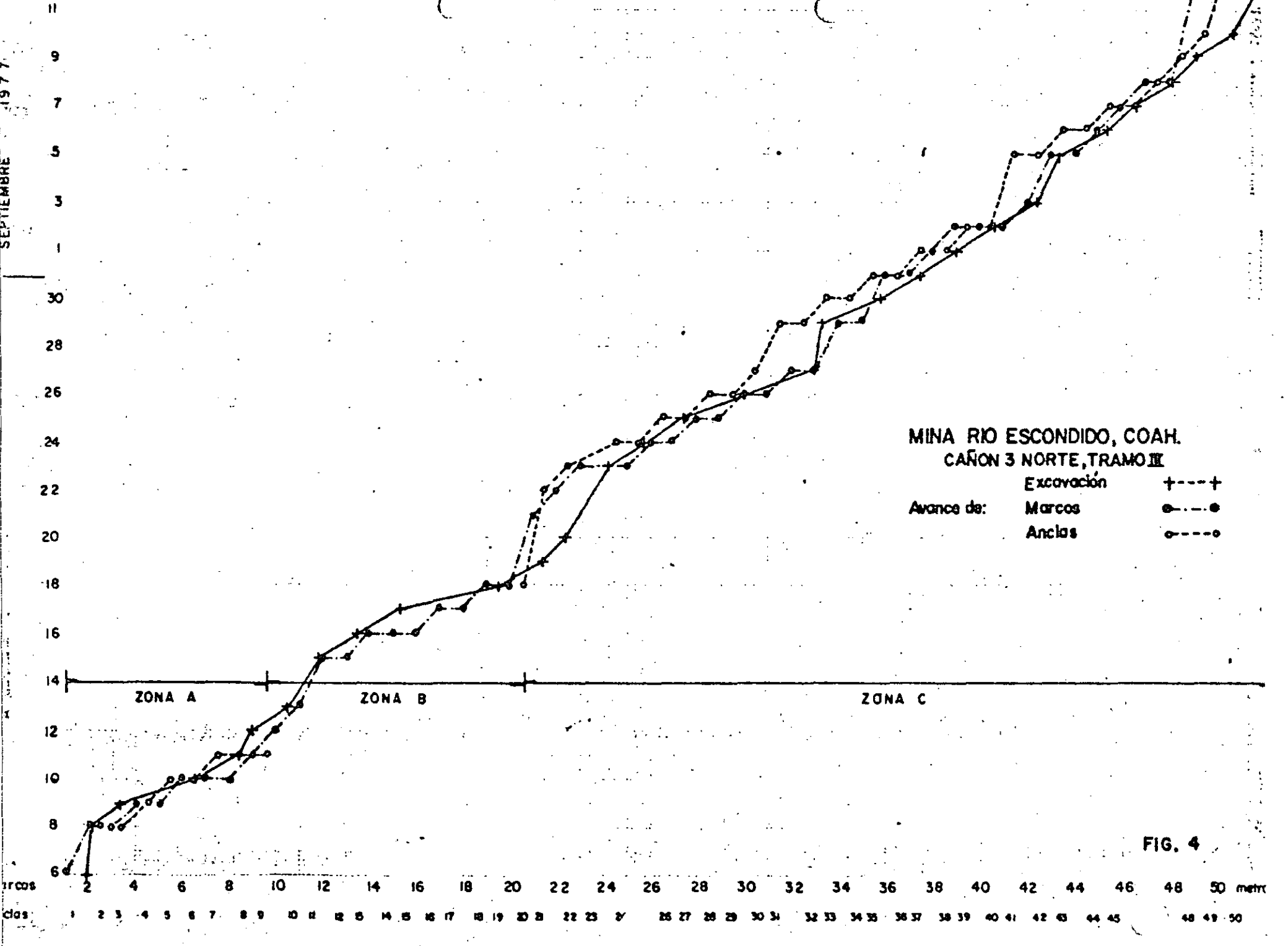
Soporte en zona B, sin anclas

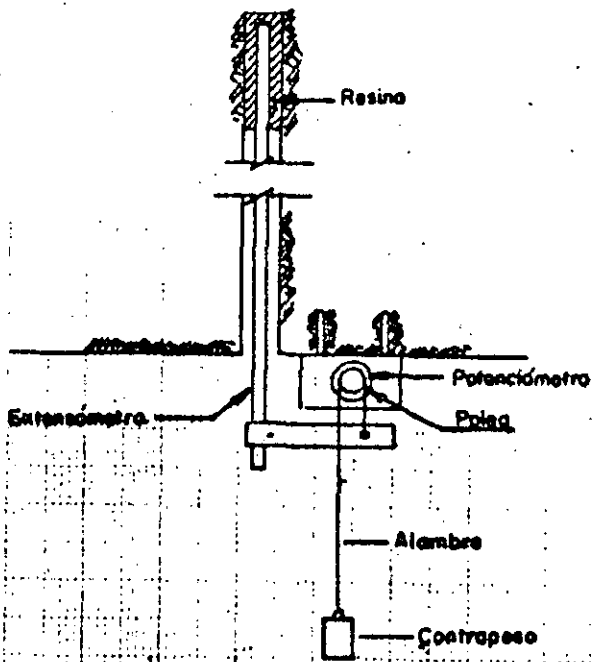


CORTE C - C

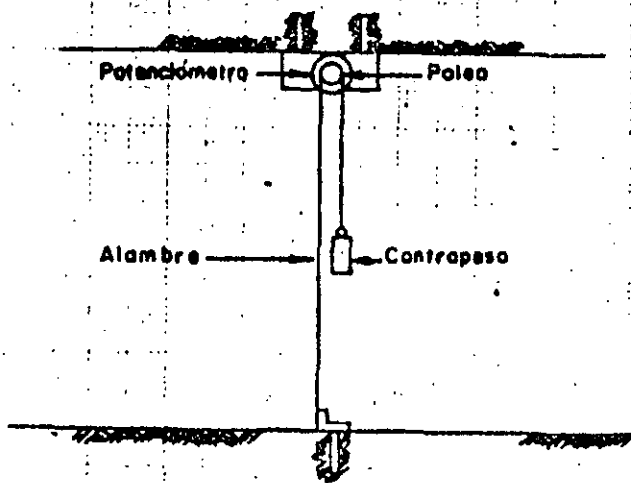
Anclaje en zona de prueba C

FIG. 3





EXTENSOMETRO DE PISO, PARED Y TECHO

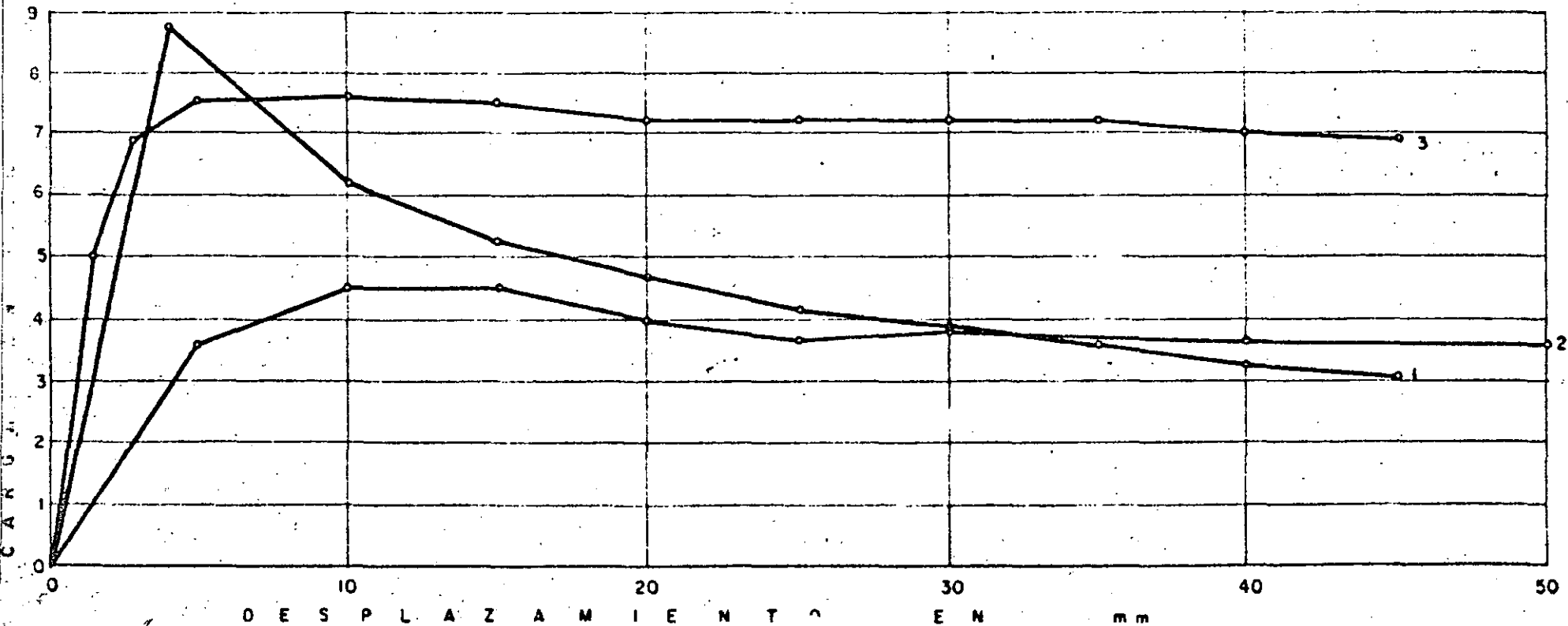


EXTENSOMETRO PARA MEDIR CONVERGENCIA

MINA RIO ESCONDIDO, COAH.  
PRUEBA DE TENSADO DE ANCLAS  
CAÑON 4 NORTE, REGRESO

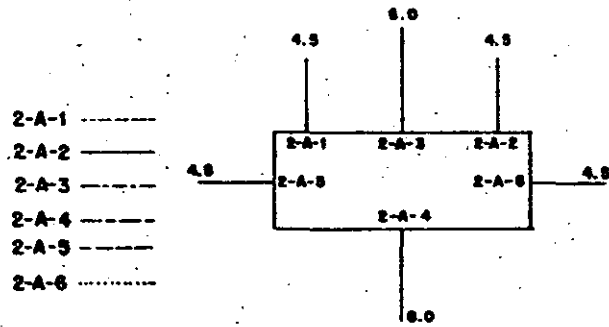
FIG. 6

Las anclas consistieron en varillas corrugadas de acero grado duro de 1" de diámetro y 1.80 m de longitud. Se instalaron en perforaciones de 1 1/2" de diámetro. La falla ocurrió siempre en el contacto resina-roca. El ancla No. 2 quedó con 38 cm sin resina en la proximidad de la boca del barreno. Las otras anclas quedaron totalmente cubiertas de resina.



254

C. F. E. DEPTO. EST. EXP.  
 Oficina de Mecánica de Roca  
 Mina Río Escendido, Coah.  
 Cañon No. 3 Norte, regreso  
 Tramo No. III, Sección 2, Tipo A

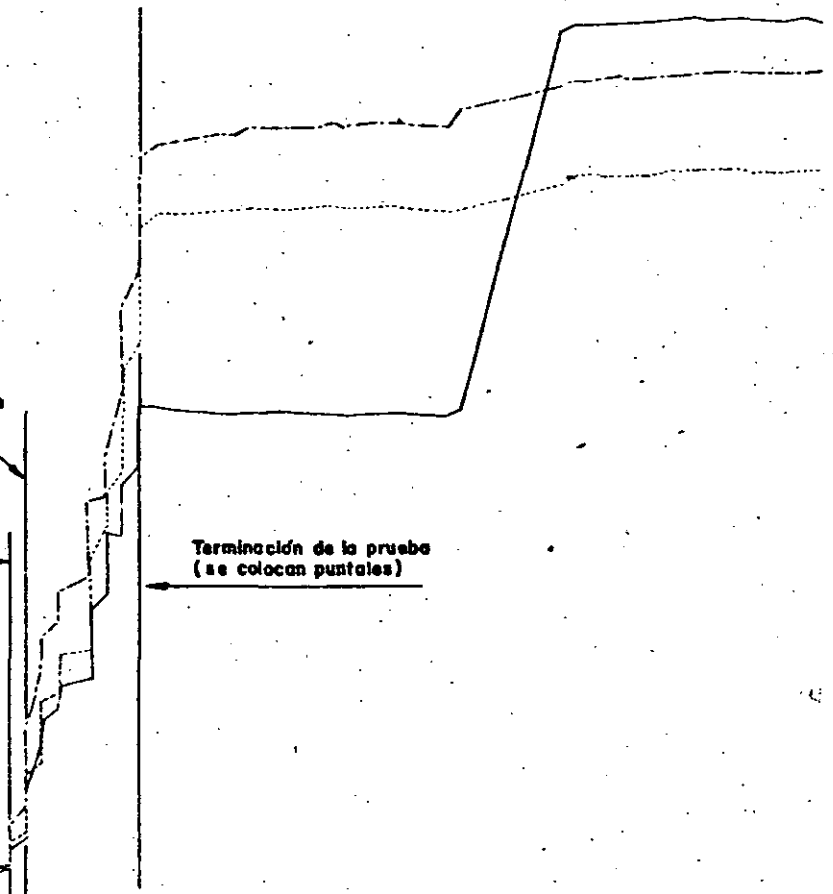


CROQUIS SECCION 2

Se aflojan tornillos en los gatos mecánicos

Inicio de la prueba.  
 (retiro de puntales en 10 m.)

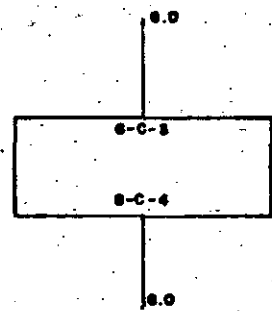
Terminación de la prueba  
 (se colocan puntales)



7 11 15 19 23 27 | 1 5 9 13 17 21 25 29 | 2 6 10 14 18 22 26 30 | 3 7 11 15 19 23 27 | 3 7 11  
 Noviembre | Diciembre 77 | 78 | Enero | Febrero | Marzo

C. F. E. DEPTO. EST. EXP.  
 Oficina de Mecánica de Rocas.  
 Mina Río Escondido, Coah.  
 Cañón N.º 3 Norte, regreso.  
 Tramo N.º III, Sección 6, Tipo C

6-C-3 ———  
 6-O-4 - - - -

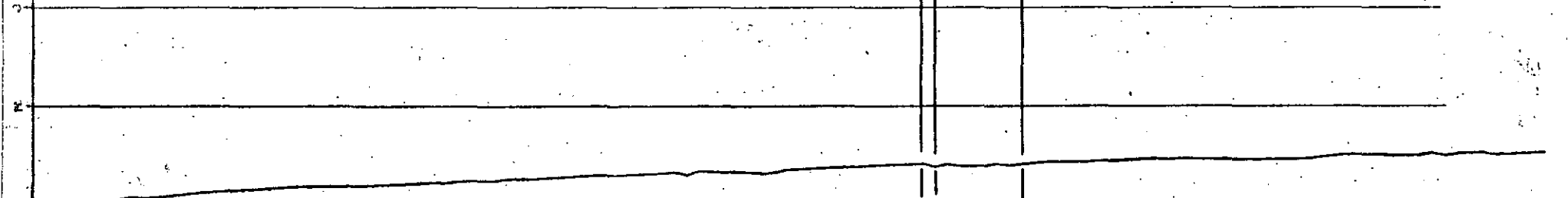


CROQUIS SECCION 6

Se aflojan tornillos en los  
 gatos mecánicos.

Inicio de la prueba  
 (retiro de puntales en 10m)

Terminación de la prueba  
 (se colocan puntales)



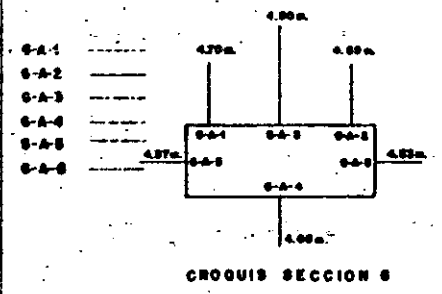
7	11	15	19	23	27	1	5	9	13	17	21	25	29	2	6	10	14	18	22	26	30	3	7	11	15	19	23	27	3	7	11
Noviembre						Diciembre								Enero						Febrero						Marzo					



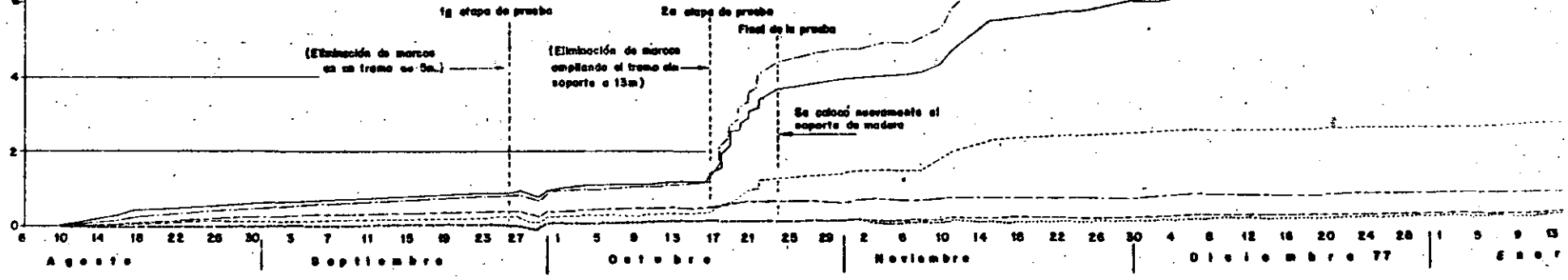
DESPLAZAMIENTOS EN CM.

C.F.E. DEPTO. ES. LXP.  
 Oficina de Mecánica de Rocas.  
 Mina Río Escondido, Coah.  
 Cañón No. 4 Norte, regreso.  
 Tramo No. I, Sección 6, Tipo A

FIG. 8



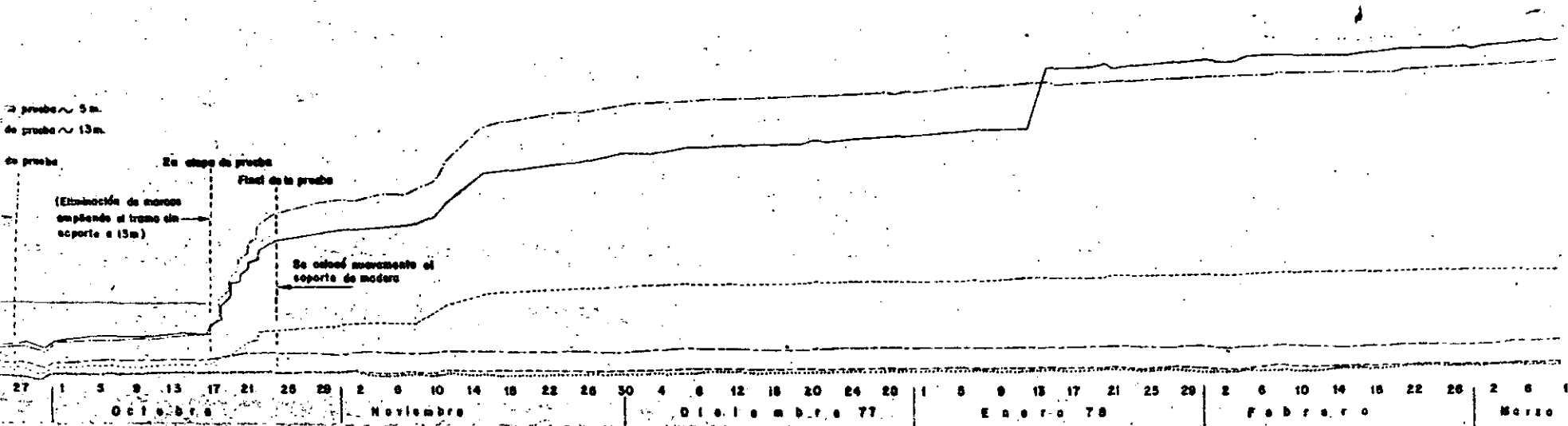
1a Etapa de prueba Se quitaron 6 marcas (entre secciones 9 y 7), long. de prueba ~ 9 m.  
 2a Etapa de prueba Se quitaron 6 marcas (entre secciones 8 y 5), long. de prueba ~ 13 m.



254

C. F. E. DEPTO. EST. EXP.  
 Oficina de Mecánica de Rocas.  
 Mina Río Escondido, Coah.  
 Cañón No. 4 Norte, regreso.  
 Tramo No. 1, Sección 6, Tipo A

FIG. 8



252

CUATRO METODOS PRINCIPALES

DE

VOLADURAS

CONTROLADAS

Un análisis de los principios... aplicaciones...  
ventajas... y limitaciones.

La información en esta publicación ha sido desarrollada  
por Du Pont para proporcionar a los consumidores de explosi-  
vos el conocimiento práctico relativo al arte de las Voladu-  
ras Controladas, para reducir el exceso de rompimiento.

A D V E R T E N C I A

La presente información comprende un análisis de los prin  
cipios, ventajas, aplicaciones y limitaciones de cuatro -  
métodos de voladuras controladas, basada en la informa---  
ción elaborada por DU PONT para proporcionar el conocimien  
to práctico sobre el uso de explosivos a fin de reducir -  
el exceso de rompimiento o sobreexcavación.

Los consumidores de explosivos han buscado y ensayado muchas maneras para reducir el exceso de rompimiento o sobreexcavación de las voladuras. Por razones de seguridad, el rompimiento excesivo es inconveniente tratándose de taludes, bancos, frentes o pendientes inestables y es también económicamente inconveniente cuando la excavación excede la "línea de pago" (implica concreto extra y los taludes fracturados requieren un mantenimiento costoso).

En voladuras controladas se utilizan varios métodos para reducir el exceso de rompimiento; sin embargo, todas tienen un objetivo común: Disminuir y distribuir mejor las cargas explosivas para reducir al mínimo los esfuerzos y la fractura de la roca más allá de la línea misma de excavación.

Los nombres descriptivos asociados con los métodos para las Voladuras Controladas son muy numerosos y en algunos casos, hasta -- confusos. Este informe ha sido preparado por Du Pont para aclarar -- estos términos y para establecer los principios básicos de los diversos procedimientos usados.

Desde que se empezaron a utilizar los explosivos en las industrias minera y de la construcción, se ha intentado desarrollar fórmulas que proporcionen métodos más seguros para controlar el exceso de rompimiento. En años recientes, los métodos se han vuelto más complicados; sin embargo, son todavía proposiciones esencialmente a base de ensayo y ajuste en lo que se refiere a su aplicación en el campo. Esto no es realmente sorprendente si se consideran las variantes geológicas involucradas en las voladuras. Es ilusorio creer que el mismo método de voladura pueda ser igualmente eficaz en formaciones ígneas compactas que en depósitos sedimentarios altamente estratificados.

Por muchos años la barrenación en Línea fue el único procedimiento utilizado para controlar el rompimiento excesivo. La Barrenación en Línea o de límite simplemente consiste de una serie de barrenos en línea, vacíos, a corta distancia unos de otros y a lo largo de la línea misma de excavación, proporcionando así un plano de debilidad que la voladura puede romper con facilidad.

A través de los años, las modificaciones al Barrenado en Línea han provocado la introducción de otros términos tales como: Voladuras Amortiguadas (Cushion Blasting), Voladuras Prefracturadas (Pre-Shearing), Voladuras Precortadas (Pre-Splitting), Voladuras Perfiladas (Smooth Blasting), Voladuras Esculturales (Sculpture Blasting), Voladuras Perimétrales (Perimeter Blasting) y Voladuras de Contorno (Contour Blasting). Estos procedimientos difieren del principio de la Barrenación en Línea, esencialmente, en que algunos o todos los barrenos se disparan con cargas explosivas relativamente pequeñas y debidamente distribuidas. La detonación de estas pequeñas cargas --

tiende a fracturar la roca entre los barrenos y permite mayores espaciamientos que en el caso de la Barrenación en Línea. Por lo tanto, los costos de barrenación se reducen y en muchos casos se logra un mejor control del exceso de rompimiento.

Los procedimientos de voladuras controladas descritas en este informe se agrupan en cuatro categorías:

- 1) Barrenación en Línea, de límite o de costura.
- 2) Voladuras Amortiguadas.
- 3) Voladuras Perfiladas o de afine.
- 4) Voladuras Prefracturadas.

Algunos de los procedimientos antes mencionados tienen aplicación tanto en trabajos subterráneos como a cielo abierto. Este informe enumera sus aplicaciones, ventajas y limitaciones bajo varias condiciones.

BARRENACION EN LINEA, DE LIMITE O DE COSTURA.

Principio.

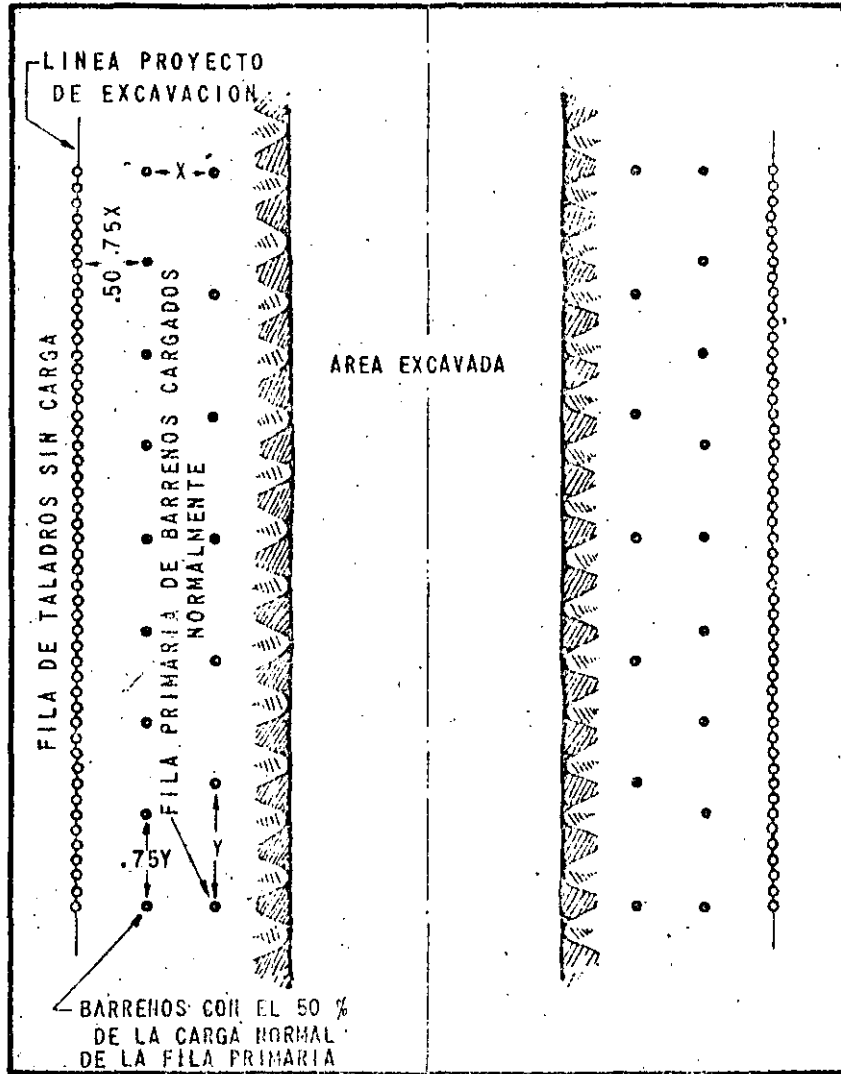
La Voladura con Barrenación en Línea involucra una sola hilera de barrenos de diámetro pequeño, poco espaciados, sin cargar y a lo largo de la línea misma de excavación. Esto proporciona un plano de menor resistencia, que la voladura primaria pueda romper con mayor facilidad. También origina que parte de las ondas de choque creadas por la voladura sean reflejadas, lo que reduce la trituration y las tensiones en la pared terminada.

Aplicación.

Las perforaciones de la Barrenación en Línea generalmente son de 2" a 3" de diámetro y se separan de 2 ó 4 veces de su diámetro a lo largo de la línea de excavación. Los barrenos mayores de 3" se usan poco con este sistema pues los altos costos de barrenación no pueden compensarse suficientemente con mayores espaciamientos.

La profundidad de los barrenos depende de su buena alineación. Para obtener buenos resultados, los barrenos deben quedar en el mismo plano. Cualquier desviación en ellos, al tratar de barrenar más profundamente, tendrá un efecto desfavorable en los resultados. Para barrenos de 2" a 3" de diámetro las profundidades mayores a 9 metros son raramente satisfactorias.

Figura 1



PLANTILLA TÍPICA DEL PROCEDIMIENTO DE BARRENACION EN LINEA

(41)

Los barrenos de la voladura directamente adyacentes a los de la Barrenación en Línea, se cargan generalmente con menos explosivos y también a menor espaciamento que los otros barrenos. La distancia entre las perforaciones de la Barrenación en Línea y los más próximos, cargados, es usualmente del 50 al 75% de la berma o línea de menor resistencia usual. Es práctica común reducir los espaciamentos laterales entre barrenos adyacentes cargados en el mismo orden con un 50% de reducción en la carga explosiva. Los explosivos deberán quedar bien distribuidos en el barreno, utilizando para ello separadores y Primacord.

Los mejores resultados con la Barrenación en Línea se obtienen en formaciones homogéneas en donde los planos de estratificación, juntas y hendiduras son mínimas. Estas irregularidades constituyen planos naturales de debilidad que tienden a provocar y prolongar el corte a través de los barrenos en Línea, y del paramento del corte. Por lo tanto, las formaciones sedimentarias de capas delgadas y las metamórficas menos consolidadas, son poco adecuadas para la Barrenación en Línea como control de rompimiento excesivo, a menos que la barrenación pueda hacerse perpendicularmente al sentido de la formación. Sin embargo esto es poco práctico en la mayoría de los trabajos de excavación.

Trabajos a cielo abierto.— La Fig. 1 muestra un patrón típico y un procedimiento para la Barrenación en Línea para trabajo a cielo abierto. Los mejores resultados se obtienen cuando la excavación primaria se mantiene retirada de una a tres filas de barrenos de la línea precisa de excavación. La última fila o filas de barrenos se separan entonces de la Barrenación en Línea utilizando estopines de retardo o conectores MS de Primacord. Este procedimiento permite la salida más fácil hacia el frente, pudiendo moverse la roca hacia éste y creando así menos presión hacia atrás que pudiera causar un exceso de rompimiento más allá de la Barrenación en Línea

En formaciones metamórficas no bien consolidadas y en formaciones sedimentarias de capas delgadas, los resultados con la Barrenación en Línea pueden mejorarse cargando ligeramente algunos de esos barrenos en línea. Este procedimiento condujo al desarrollo de los sistemas de Voladuras Amortiguadas y de Voladuras Perfiladas. También se encontró que los resultados de la Barrenación en Línea podían mejorarse en algunas formaciones, cargando ligeramente y disparando los barrenos en línea antes de la voladura principal. Esto condujo a la introducción del método conocido como Precortado o Prefracturado. Todas estas modificaciones a la Barrenación en Línea provocan mayor debilidad a lo largo de la línea proyecto de la excavación utilizando la fuerza del explosivo para cortar la roca entre los barrenos.



(42)

Trabajos subterráneos.- La aplicación de la teoría básica del sistema de Barrenado en Línea, esto es, utilizando solamente barrenos vacíos, es muy limitada en trabajos subterráneos. Generalmente se usan barrenaciones cerradas, pero siempre cargadas -- aunque ligeramente. A este procedimiento hemos preferido llamarle Voladura Perfilada y será descrita posteriormente.

Ventajas.- La Barrenación en Línea es aplicable en lugares donde aún con cargas explosivas ligeras, en combinación con otras técnicas de voladuras controladas, pueden causar fracturas -- más allá del límite de la excavación.

Cuando se utiliza con otros procedimientos de voladuras controladas, la Barrenación en Línea entre barrenos cargados -- ocasiona fracturas que mejora los resultados.

Limitaciones.- El Barrenado en Línea tiene ciertas limitaciones que deben conocerse:

Los resultados de la Barrenación en Línea no siempre son previsibles, excepto con formaciones muy homogéneas.

Debido a que la separación entre barreno y barreno es muy pequeña, los costos de barrenación son altos.

Debido a que la Barrenación en Línea requiere un gran -- número de barrenos a espacios muy cortos, la perforación llega a presentar dificultades por lo que los resultados a menudo no son satisfactorios debido al defectuoso alineamiento de los barrenos.

VOLADURAS AMORTIGUADAS.

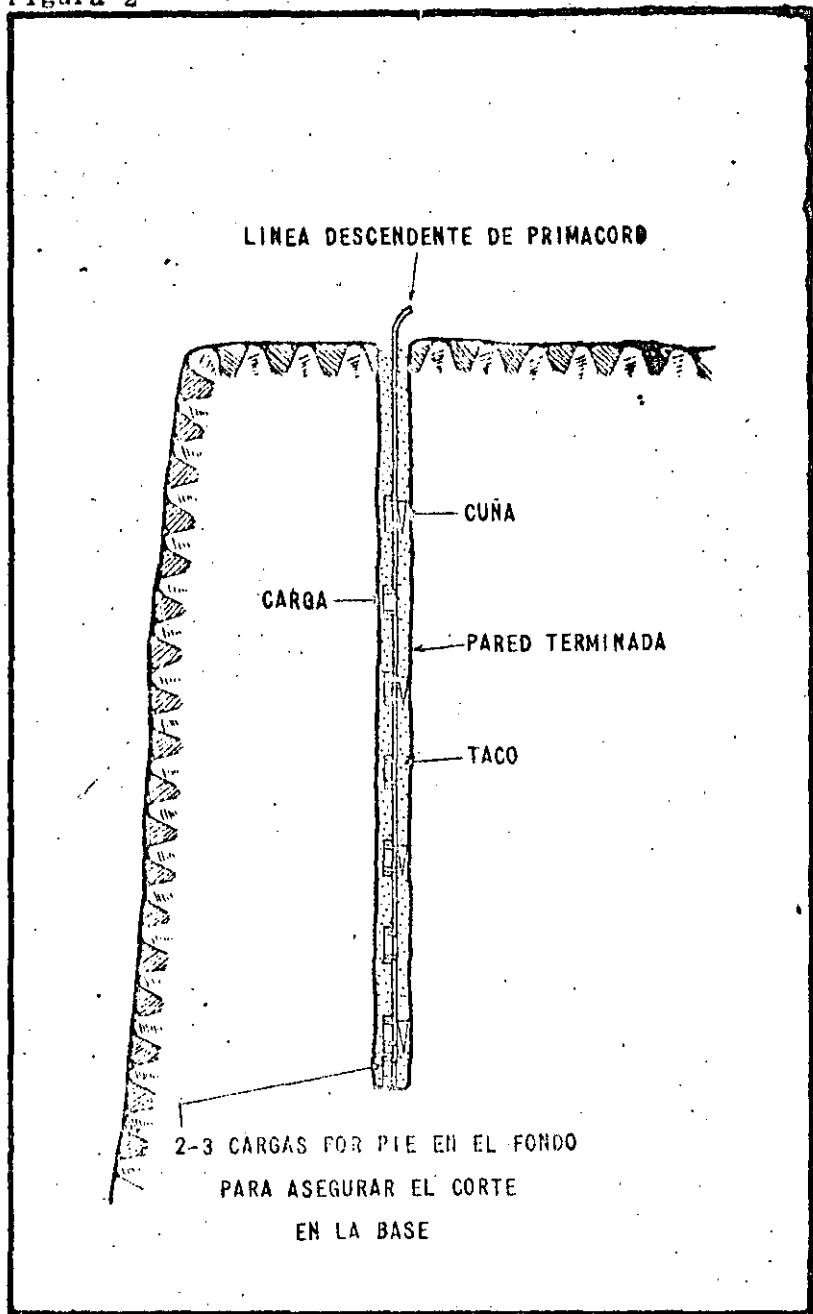
PRINCIPIO.

La Voladura Amortiguada a veces denominada como voladura para recortar, lejear o desbastar, se introdujo en el Canadá hace varios años. Al igual que la Barrenación en Línea, la Voladura -- Amortiguada implica una sola fila de barrenos a lo largo de la -- línea proyecto de excavación.

Aunque en esta voladura, como se practicó originalmente -- se hacían barrenos de 4" a 6 1/2" de diámetro, también ha utilizado barrenos pequeños hasta de 2" y 3 1/2" de diámetro. Las cargas para las voladuras amortiguadas deben ser pequeñas, bien distribuidas, perfectamente retacadas y se harán explotar después de -- que la excavación principal ha sido despejada. Al ser volada la -- berma, el taco amortigua la vibración dirigida hacia la pared ter

(43)

Figura 2



COLOCACION DE LAS CARGAS DE EXPLOSIVO  
PARA VOLADURAS AMORTIGUADAS

TABLA I

CARGAS Y PLANTILLAS PROPUESTAS PARA VOLADURAS  
AMORTIGUADAS

DIAMETRO DEL BARRENO EN PULGADAS	ESPACIAMIENTO EN (1) PIES	BORDO EN PIES (1)	CARGA EXPLOSIVA EN LIBRAS/PIE (1)
2-2 1/2	3	4	0.08 - 0.25
3-3 1/2	4	5	0.13 - 0.50
4-4 1/2	5	6	0.75 - 0.75
5-5 1/2	6	7	0.75 - 1.00
6-6 1/2	7	9	1.00 - 1.59

(1). - Dependen de la naturaleza de la roca.  
Las cifras anotadas son promedios.

(2). - El diámetro del cartucho deberá ser igual o menor que la mitad del diámetro del barreno.

minada, reduciendo así al mínimo la fractura y las tensiones en esta pared. Disparando los barrenos de amortiguamiento a pequeños intervalos, la detonación tiende a cortar la roca entre ellos dejando una superficie uniforme y con un mínimo de sobreexcavación.

Obviamente, a mayor diámetro de barreno, se obtiene mayor amortiguamiento.

APLICACION.

En la Voladura Amortiguada, se desaloja el área principal de excavación dejando un mínimo de banco frente a la línea final de excavación. Los barrenos de amortiguamiento pueden perforarse ya sea antes de la voladura primaria o justamente antes de remover el banco final.

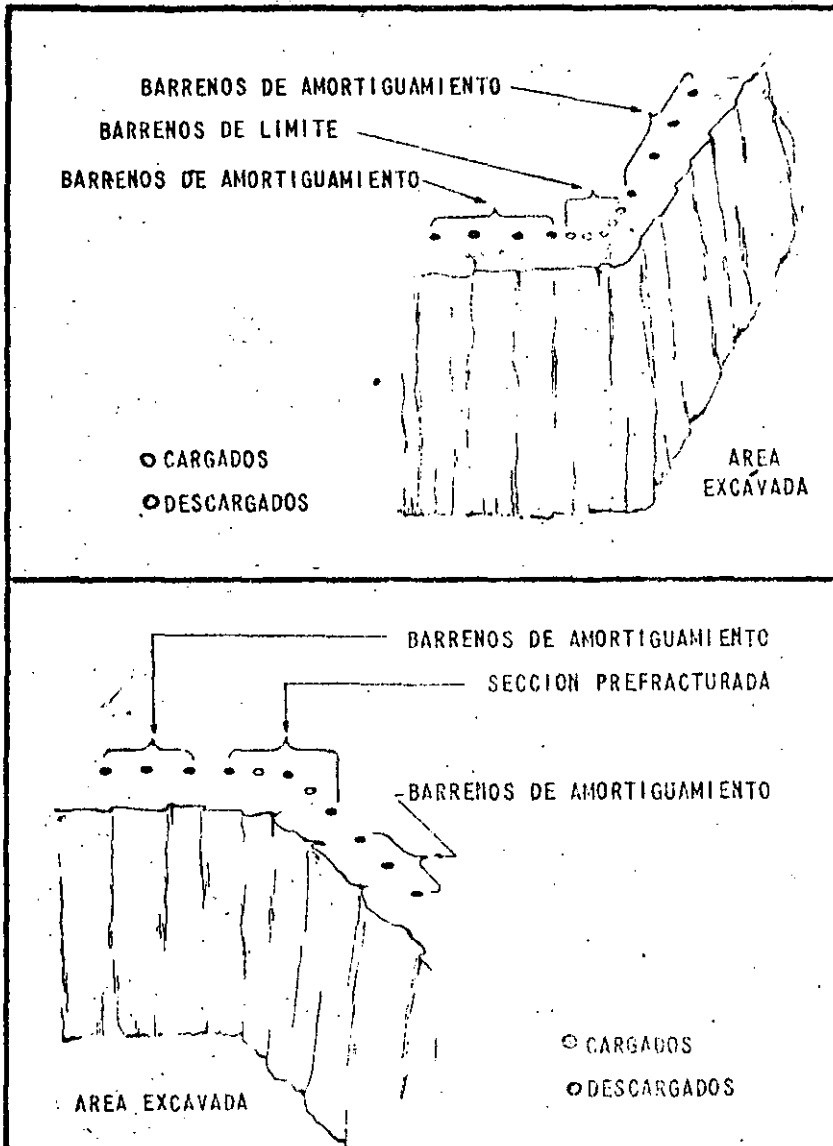
Trabajos a cielo abierto.— El banco o berma y el espaciamiento variarán de acuerdo con el diámetro de los barrenos que se hagan. La Tabla I muestra una guía de patrones y cargas para diferentes diámetros de barrenos. Nótese que los números mostrados cubren un campo promedio debido a las variaciones que resultan del tipo de formación por volarse. Con este procedimiento los barrenos se cargan con cartuchos enteros o fraccionados atados a líneas de Primacord a manera de rosario, usándose generalmente cartuchos de 1 1/2" de diámetro por 8" de largo y colocándose a 1 ó 2 pies de separación.

Para provocar el corte en el fondo del barreno, se utiliza una carga 2 ó 3 veces mayor que la utilizada en la parte superior del barreno. Para efectos de un amortiguamiento máximo, las cargas deben colocarse dentro del barreno tan próximas como sea posible a la pared correspondiente al lado de la excavación. Para lograr esto, puede rotacarse la parte posterior del barreno, pudiendo también colocarse cuñas o blocks dentro del mismo (Ver fig. 2).

Los cartuchos se fijan con cinta adhesiva a las líneas de Primacord, o cuando están provistos de tubos deslizantes para Primacord, pueden cargarse dejándoles resbalar a los intervalos deseados. Pueden utilizarse tubos espaciadores para obtener las distancias deseadas entre cartuchos. Si no se usan espaciadores, se puede colocar taco entre cada cartucho que se deje caer.

Cuando la carga entera para un barreno se arma previamente fijando a una línea de Primacord los cartuchos, el taco debe colocarse ya que la carga completa haya quedado colocada en el interior del barreno. En este caso, pueden servir como taco materiales como arena, piedra triturada o grava, siempre y cuando tengan su-

Figura 3.



VOLADURAS AMORTIGUADAS  
EN FRENTES, EN ESQUINA O EN RINCON

ficiente fluidez como parallenar el espacio entre los cartuchos.-- Subiendo y bajando continuamente la línea de Primacord a medida - que se va vaciando el taco, se ayuda al relleno entre cartuchos Los últimos 2 ó 3 pies del barrenos se atacan completamente y no se cargan. La cantidad de taco en la parte superior varía de -- acuerdo con la formación por volarse.

El retardo mínimo entre la explosión de los barrenos amortiguadores proporciona la mejor acción de corte entre barrenos y barrenos; por lo tanto, normalmente se emplean líneas troncales de Primacord. En donde el ruido y la vibración resulten críticos, se pueden obtener buenos resultados con estopines de retardo MS.

La relación berma o línea de menor resistencia/espacia -- miento, variará en algunas formaciones, pero para obtener un me -- jor corte entre barrenos, el espaciamento debe ser menor que el ancho del banco que deba ser volado. (Ver Tabla I)

La Voladura Amortiguada puede practicarse por métodos de -- banqueo o perforado previamente los barrenos de amortiguamiento -- hasta la profundidad completa de la excavación. Cuando es usado -- el banqueo, se deja usualmente un escalón mínimo de un pié por -- banco, ya que es imposible colocar el taladro al ras de la pared -- del banco superior.

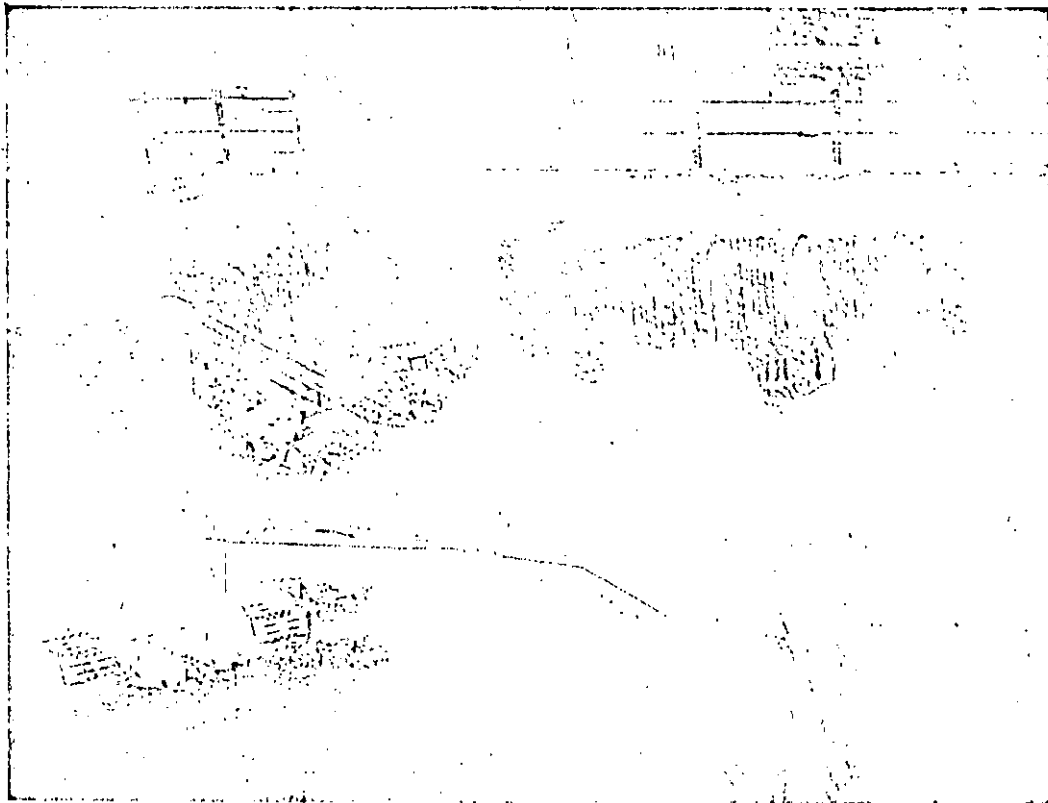
La profundidad máxima que puede volarse con éxito por es -- te método, depende de la precisión del alineamiento de los barre -- nos. Con barrenos de diámetros mayores puede mantenerse un mejor -- alineamiento a mayor profundidad. Las desviaciones de más de -- 6" del plano de los barrenos dan generalmente malos resultados. -- Se han hecho voladuras con éxito usando barrenos de amortiguamien -- to hasta de 90 piés de profundidad.

La velocidad de penetración del taladro debe también ser -- considerada al determinar la profundidad de los barrenos. Si por -- ejemplo, la penetración a una profundidad determinada resulta de -- masiado lenta, pueda resultar más económico banquar y así obte -- ner avances más reales para dar un costo global bajo de perfora -- ción.

Cuando se realizan voladuras por amortiguamiento en áreas -- curvas o en esquinas, se requiere menores espaciamientos que -- cuando se vuela una sección recta. Pueden también utilizarse ven -- tajosamente taladros-guía cuando se vuelan caras no lineales. En -- esquinas a 90°, una combinación de varios procedimientos para vo -- laduras controladas, dará mejores resultados que la voladura amor -- tiguada simple (Veáse la Fig. 3)

48

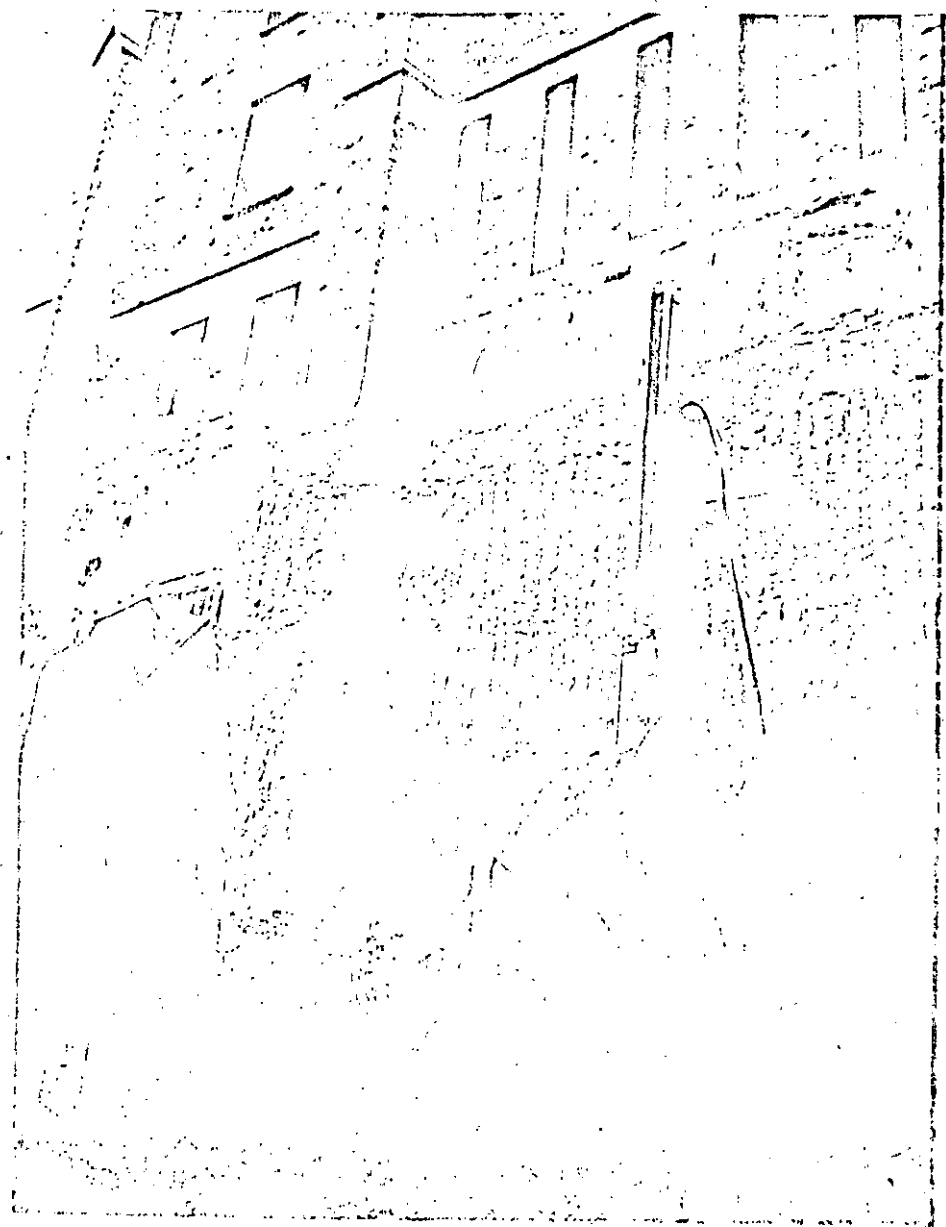
Figura No. 4



RESULTADO DE UNA VOLADURA AMORTIGUADA USANDO BARRENOS DE  
AMORTIGUAMIENTO DE GRAN DIAMETRO Y BARRENOS GUIA DE  
PEQUEÑO DIAMETRO.

Figura No. 5

(19)

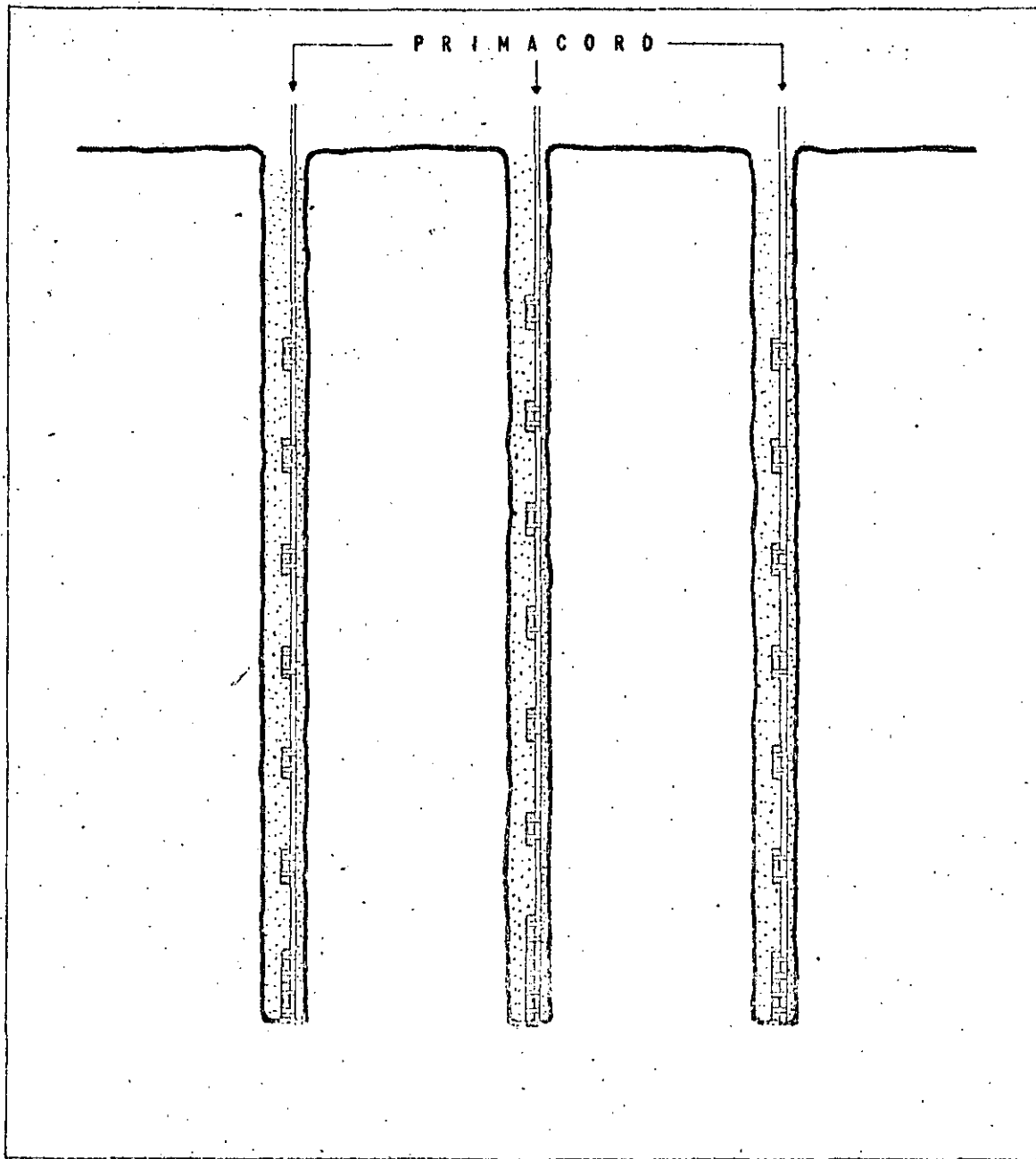


RESULTADO DE UNA VOLADURA AMORTIGUADA USANDO BARRENOS  
GUÍA Y BARRENOS AMORTIGUADOS DE PEQUEÑO DIAMETRO



Figura 6

(50)



CARGAS SALTEADAS PARA LA MEJOR DISTRIBUCIÓN DEL EXPLOSIVO

En formaciones sedimentarias sin consolidar, donde es difícil obtener una pared lisa, se recomienda intercalar taladros -- guía sin cargar entre los taladros de amortiguamiento. Generalmente se emplean taladros-guía de pequeño diámetro para reducir los costos de barrenación.

Donde sólo la parte superior de la formación está intemperizada, los taladros-guía se perforan solamente hasta esa profundidad y no hasta la profundidad total de los barrenos de amortiguamiento. Este procedimiento es común en el primer banco, puesto que el rompimiento hacia atrás es allí más probable que en los bancos inferiores. La Fig. 4 muestra los resultados de una combinación de voladura amortiguada con barrenos-guía en donde los últimos fueron perforados a la profundidad total. La Fig. 5 muestra los resultados de una voladura amortiguada utilizando taladros de pequeño diámetro y taladros-guía sin cargar.

Se han obtenido resultados satisfactorios en formaciones homogéneas retacando sólo los últimos 2 ó 3 piés del barreno y, no haciéndolo entre las cargas. En este caso, el aire entre las cargas y la pared del barreno sirve como colchón amortiguador de protección. Cuando no se utiliza taco entre las cargas, los gases formados por la explosión pueden encontrar una zona débil en la formación y fugarse antes de que se obtenga el efecto de corte deseado entre los barrenos. De igual manera, estos gases pueden encontrar superficies de debilidad atrás de la pared terminada y producir un exceso de rompimiento. A menos que la formación sea muy homogénea y dura, se recomienda introducir el taco completamente entre y alrededor de las cargas individuales. También, aunque no se practica generalmente en el campo, la colocación al tresbolillo (alternada) de las cargas en los barrenos, como se muestra en la Fig. 6, mejora la distribución del explosivo y proporciona mejores resultados.

La Voladura Amortiguada en trabajos a cielo abierto, encuentra aplicaciones tanto en barrenos verticales, como en inclinados. En ambos casos, es esencial el buen alineamiento de los barrenos.

Trabajos subterráneos. - Puesto que la más efectiva Voladura Amortiguada resulta de la colocación de material para atacadura entre y alrededor de las cargas, ésta tiene muy poca aplicación en trabajos subterráneos, donde se utilizan barrenos horizontales de diámetro pequeño. Obviamente, colocar tacos en tales barrenos no es práctico, aunque se puede obtener alguna ventaja-

con el espaciamiento de aire. En tiros o en cualquiera operación subterránea en la que intervengan barrenos verticales o inclinados, se aplican los mismos procedimientos que para los trabajos a cielo abierto.

Prácticamente, el control de la sobreexcavación en galerías subterráneas debe involucrar exclusivamente el uso del taco en el cuello del barreno. Este tema será tratado en las Voladuras-Perfiladas.

VENTAJAS.

La Voladura Amortiguada ofrece ciertas ventajas, tales como:

Mayores espaciamientos entre barrenos para reducir los costos de perforación.

Mejores resultados en formaciones no consolidadas.

Posibilidad de aprovechar ventajosamente la información geológica obtenida al vular los mantos principales cuando se cargan los barrenos amortiguadores. Resultado, menos ensayos en el trabajo.

Los resultados pueden ser observados desde el primer disparo, lo que permite el ajuste de las cargas, si es necesario, antes de proceder.

El mejor alineamiento obtenido con barrenos de gran diámetro permite perforar barrenos más profundos.

LIMITACIONES.

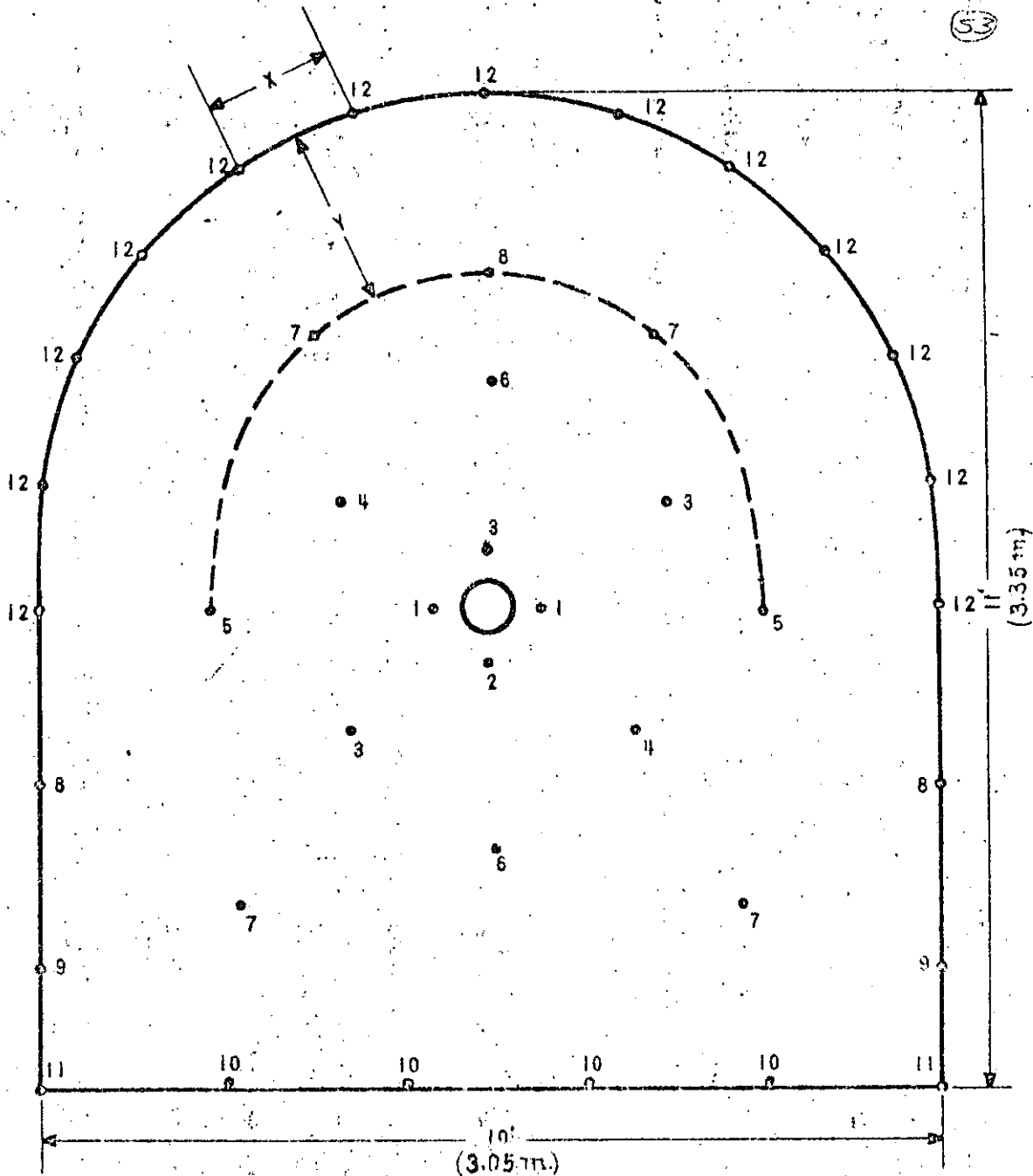
Hay ciertas limitaciones para las Voladuras Amortiguadas que deben tomarse en consideración. Entre éstas están:

La necesidad de despejar el área excavada antes de iniciar las voladuras amortiguadas.

No son prácticas para cortar esquinas a 90°, sin utilizar a la vez la Barrenación en Línea o el Prefracturado.

A veces, el exceso de rompimiento originado por las voladuras principales elimina completa o parcialmente el banco por volarse por amortiguamiento. Requiere así, varios ajustes a las cargas de diferentes barrenos.

Figura 7



PLANTILLA TIPICA PARA EXPLOSIONES RETARDADAS,  
EN  
GALERIAS DE AVANCE.

TABLA II.

VOLADURA PERFILADA.

DIAMETRO DEL BARRENO EN PULGADAS	ESPACIAMIENTO EN (1) PIES	BORDO EN PIES (1)	CARGA EXPLOSIVA LIBRAS/PIE (1)
1 1/2 - 1 3/4	2	3	0.12 - 0.25
2	2 1/2	3 1/2	0.12 - 0.25

(1).- Dependen de la naturaleza de la roca.

Las cifras anotadas son promedios.

VOLADURAS PERFILADAS O DE AFINE.

(55)

PRINCIPIO.

La Voladura de Afine, conocida también como de Contorno, - Perimetral o de Escultura, fué introducida en Suecia y es el método más ampliamente aceptado para controlar el exceso de rompimiento en galerías de avance o excavaciones escalonadas en trabajos -- subterráneos.

Los métodos de la Voladura de Afine; tal y como son descritos por Ulf Langefors y Björn Kihlström en su reciente libro: "La-técnica Moderna de Voladuras en Rocas", tienen aplicación tanto en trabajos subterráneos como a cielo abierto. Sin embargo, puesto -- que el uso de estos métodos en trabajos a descubierto es prácticamente idéntico a los de la Voladura Amortiguada, en este informe -- se tratará sobre su aplicación solamente en trabajos subterráneos.

El principio básico de la Voladura de Afine es el mismo -- que el de la Voladura Amortiguada: Se hacen barrenos a lo largo de los límites de la excavación y se cargan con poco explosivo para -- eliminar el banco final. Disparando con un mínimo de retardo entre los barrenos, obtiene un efecto cortante que proporciona paredes -- lisas con un mínimo de sobreexcavación.

APLICACION.

Trabajos subterráneos. - En frentes subterráneos, en donde -- la roca del techo y de los contrafuertes se derrumba y desmorona -- por la falta de consolidación del material, el exceso de rompimiento es común debido a la acción triturante de las voladuras.

Empleando el método de la Voladura Perfilada o de Afine -- con cargas ligeras y bien distribuidas en los barrenos perimetra- -- les, se requieren menos soportes y resulta una menor sobre-excavación. Aún en formaciones homogéneas más duras, este método proporciona techos y paredes más lisos y más firmes.

La Voladura Perfilada en trabajos subterráneos utiliza barrenos perimetrales en una relación de aproximadamente 1 1/2 a 1, -- entre el ancho de la berma y el espaciamento usando cargas lige- -- ras, bien distribuidas y disparadas en el último período de retar- -- do de la voladura. (Ver Fig. 7). Estos barrenos se disparan des- -- pués de los barrenos de pata o pié para asegurar que la roca frag- -- mentada se desplace lo suficiente para ofrecer el máximo desahogo -- a los barrenos de la Voladura Perfilada. Este franqueo permite la-

libre remoción del banco final y produce menos fractura más allá del límite de la excavación.

Para asegurar un máximo de desahogo se utiliza a veces -- una galería de avance o túnel piloto. Después de que esta galería ha sido totalmente excavada, se barra el banco final y se dispara. En este caso y con este procedimiento pueden perforarse y volarse a profundidades mayores que con una barrenación simple. El método de galería de avance permite el uso de las Voladuras Perfiladas alrededor de una parte mayor del frente de una galería.

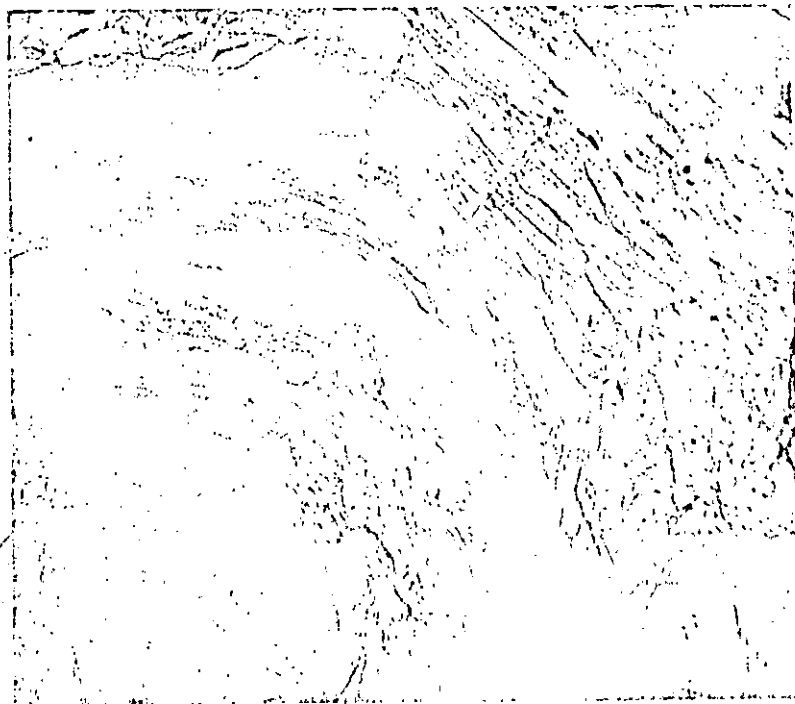
Al disparar barrenaciones preparadas con este método como aparece en la Fig. 7, el espacio de la parte volada se limita al arco y en parte, hacia la parte inferior de los costados pero debido al abundamiento de la rezaga, no debe esperarse que este sistema dé buenos resultados en la parte más baja de las paredes.

Aunque la relación de la berma al espaciamento de 1 1/2- a 1, se recomienda solamente como punto de partida; sin embargo, -- en la práctica puede necesitarse hacer modificaciones en la forma de la voladura. También disparar los barrenos de las Voladuras -- Perfiladas con un mínimo de retardo entre ellos, no es siempre necesario. Las cargas pequeñas bien distribuidas en los barrenos perimetrales usando plantillas y retardos convencionales, han producido regularmente resultados satisfactorios. La Tabla II propone las plantillas recomendadas y las cargas en libras por pié, para la Voladura Perfilada.

Puesto que no es conveniente ni práctico atar cargas a -- las líneas de Primacord en barrenos horizontales, la Voladura Perfilada se realiza cargando a carril cartuchos de dinamita de baja densidad de pequeños diámetros para obtener, tanto cargas pequeñas, como su buena distribución a lo largo del barrenos. Es necesario taponar estos barrenos con tarugos, arcilla o aún con un cartucho de dinamita de tamaño normal bien atacado. Si los barrenos para la Voladura Perfilada no se taponan, los cartuchos cargados a carril serán succionados por los barrenos del retardo anterior. -- El tapón evita también los escopetazos y permite el uso de cargas más ligeras.

Los cartuchos largos, de pequeño diámetro y con explosivos de baja densidad, mejoran su distribución a lo largo del barrenos. Sin embargo, se han utilizado con éxito cartuchos de 8" de largo y de diámetro standard en este tipo de voladuras subterráneas empleando espaciadores entre cartuchos para dar una concentración total más baja de carga (lbs./pié). Con este procedimiento, sin embargo, pueden producirse puntos de relativamente alta concentración, pero con resultados inferiores cuando se trata de --

Figura No. 8



RESULTADO DE UNA VOLADURA PERFILADA  
EN UNA GALERIA DE AVANCE.



Figura No 9

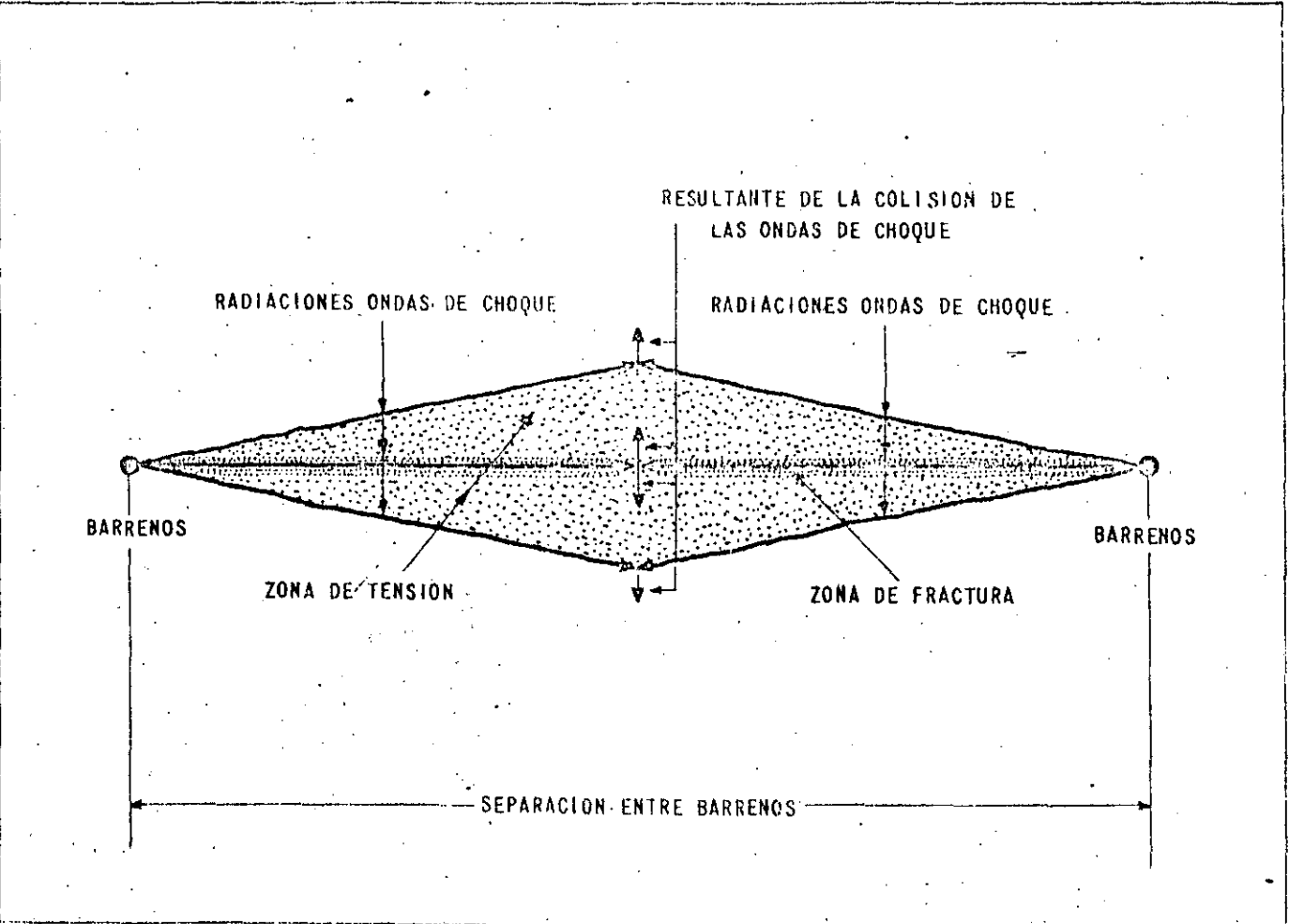
(58)



VOLADURAS PERFILADAS PARA OBTENER  
CONTORNOS SEGUN PROYECTO.

58

Figura 10



PRINCIPIO DEL PREFRACTURADO

N O T A.- Si los barrenos están sobrecargados, la zona de fractura se extenderá hacia los lados y aún mas allá de la zona de tensión.

formaciones no bien consolidadas.

Las figuras 8 y 9 muestran los resultados de la aplicación de la Voladura Perfilada.

VENTAJAS.

La Voladura Perfilada o de Afine ofrece dos ventajas principales:

• Reduce el rompimiento excesivo que produce los métodos convencionales.

Requiere menos ademe.

LIMITACIONES

Hay dos limitaciones básicas para la Voladura Perfilada:

Utiliza más barrenos perimetrales que los métodos convencionales.

No es efectiva para todas las formaciones geológicas. Si el terreno es demasiado débil como para sostenerse así mismo, éste método no eliminará completamente la necesidad de ademes.

P R E F R A C T U R A D O

PRINCIPIO

El Prefracturado, también llamado Precortado o Pre-ranurado comprende una fila de barrenos a lo largo de la línea de excavación. Los barrenos son generalmente del mismo diámetro (2" - 4") y en la mayoría de los casos, todos cargados. El Prefracturado difiere de la Barrenación en Línea, de la Voladura Amortiguada y de la Voladura Perfilada, en que sus barrenos se disparan antes que cualquier barrero de los de alguna sección de la excavación principal inmediata.

La teoría del Prefracturado consiste en que cuando dos cargas se disparan simultáneamente en barrenos adyacentes, la colisión de los ondas de choque procedentes de los barrenos rompe la pared de roca intermedia y origina grietas entre los barrenos. (Ver Fig. 10). Con cargas y espaciamientos adecuados, la zona fracturada entre barrenos se constituirá en una agosta franja que la voladura principal puede romper con facilidad. El resultado es una pared li-

(5)

TABLA III.

CARGAS Y ESPACIAMIENTOS PROPUESTOS PARA  
EL PREFRACTURADO.

DIAMETRO DEL BARRENO EN PULGADAS	CARGA EXPLOSIVA EN LBS./PIE (1) (2)	ESPACIAMIENTO EN PIES. (1)
1 1/2 - 1 3/4	0.08 - 0.25	1 - 1/2
2 - 2 1/2	0.08 - 0.25	1 1/2 - 2
3 - 3 1/2	0.13 - 0.50	1 1/2 - 3
4	0.25 - 0.75	2 - 4

(1).- Dependen de la naturaleza de la roca.

(2).- El diámetro del cartucho debe ser igual o menor que la mitad del diámetro del barreno.

sa que casi no produce sobreexcavación.

El plano prefRACTURADO refleja parte de las ondas de choque procedentes de las voladuras principales inmediatamente posteriores impidiendo que sean transmitidas a la pared terminada, reduciendo al mínimo la fracturación y la sobreexcavación. Esta reflexión de las ondas de choque de las voladuras principales también tiende a reducir la vibración.

### APLICACION

Trabajos a cielo abierto... Los barrenos para prefRACTURAR se cargan de manera similar a los barrenos para voladuras amortiguadas, esto es, se forman cargas "en rosario" de cartuchos enteros o partes de cartucho, de 1" ó 1 1/2" de diámetro, por 8" de largo, espaciados a 1 a 2 pies centro a centro.

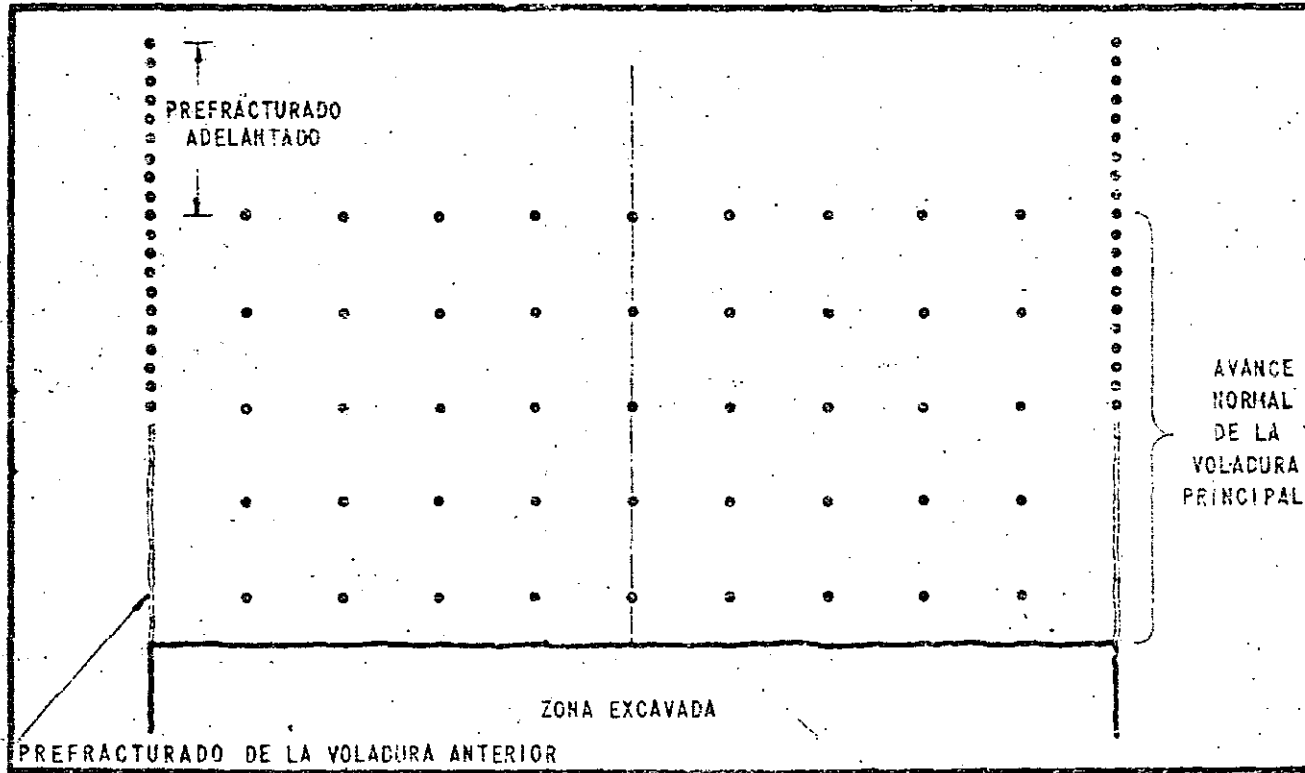
Como en las Voladuras Amortiguadas, los barrenos se disparan generalmente en forma simultánea, usando una línea troncal de Primacord. Si se disparan líneas demasiado largas se pueden retardar algunos tramos con estopines MS a Conectores Primacord MS.

En roca sin consolidación alguna, los resultados se mejoran utilizando barrenos-guía o de alivio (sin carga), entre los barrenos cargados, provocando así el corte a lo largo del plano deseado. Aún en formaciones más consistentes, los barrenos-guía colocados entre los cargados, dan mejor resultado que aumentando la carga explosiva por barreno.

Los espaciamientos promedio y las cargas por pie de barreno se dan en la Tabla III. Estas cargas anotadas son para las condiciones de rocas normales y pueden obtenerse utilizando cartuchos de dinamita convencionales, fraccionados o enteros, espaciados y ligados a líneas de Primacord, ("rosarios"). En una formación sin consolidación alguna se obtuvieron malos resultados hasta que la carga se redujo a una columna formada por Primacord de 400 granos/pié exclusivamente en barrenos a 12" de centro a centro. Existe también un caso en que fue necesario reducir la carga de la columna a dos tramos de Primacord de 50 granos/pié para evitar el exceso de rompimiento en una pared acabada, muy poco consolidada. Por lo tanto, las cargas y espaciamientos dados en la Tabla III pueden utilizarse sólo como una guía y en formaciones extremadamente in-temperizadas. (Debe consultarse a un representante de Du Pont antes de proceder).

Todos los barrenos cargados por PrefRACTURADO se taponan completamente tanto alrededor como entre cargas para evitar la fuga de gases hacia los estratos débiles y que se originen así malos

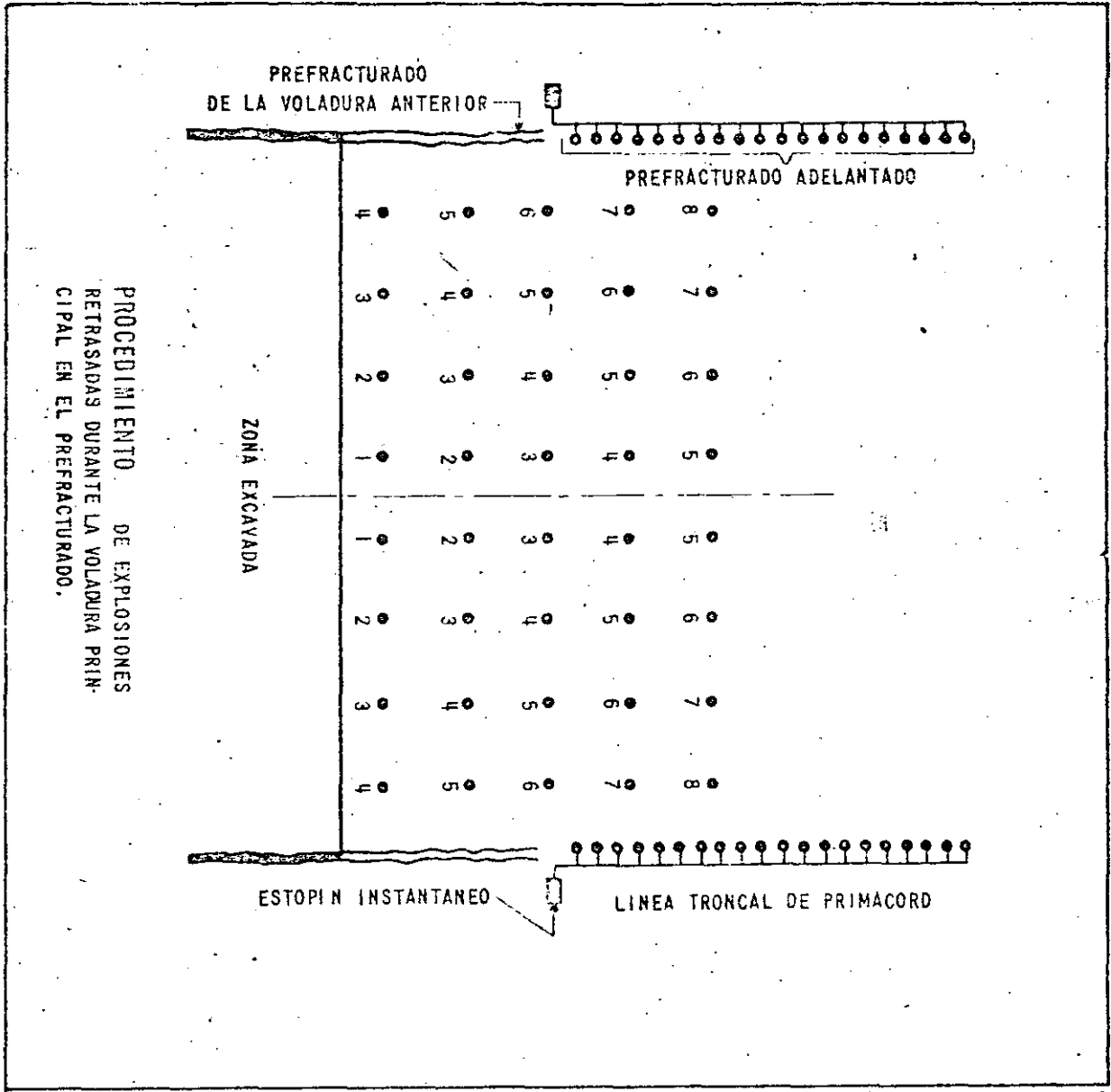
Figura 11



PROCEDIMIENTO RECOMENDADO  
PARA  
EL PREFRACTURADO

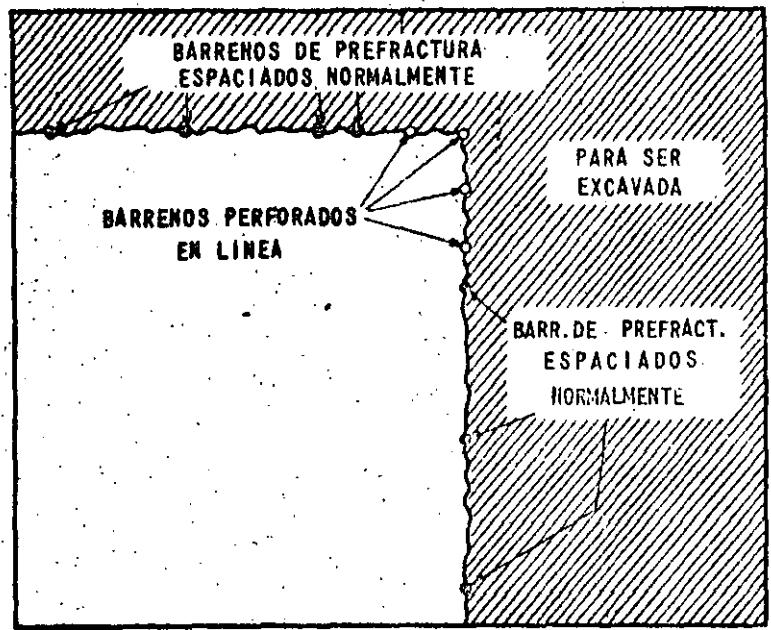
(53)

FIG. 12



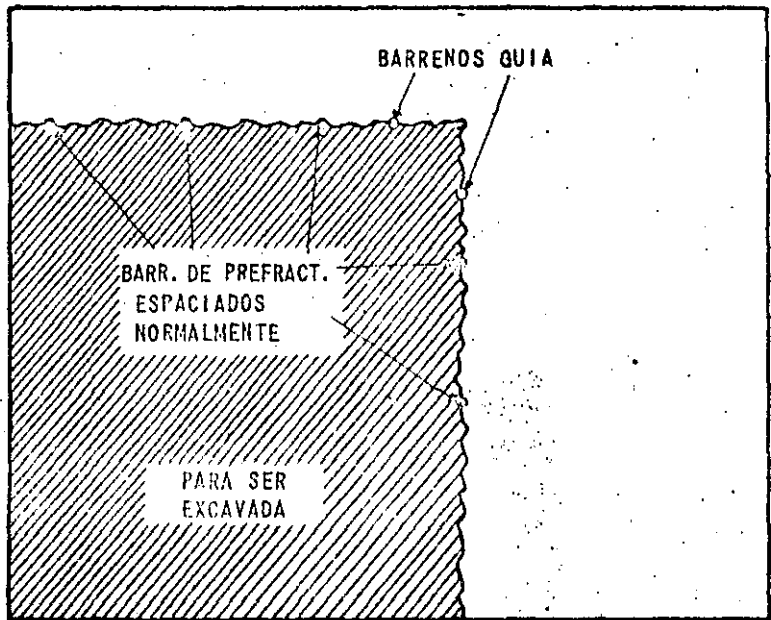
PROCEDIMIENTO DE EXPLOSIONES  
RETRASADAS DURANTE LA VOLADURA PRIN-  
CIPAL EN EL PREFRACTURADO.

Fig. 13



1. - PLANTILLA, CUANDO LA EXCAVACION ESTA FUERA DE LOS PLANOS DE PREFRACTURA.

2. - PLANTILLA, CUANDO LA EXCAVACION ESTA DENTRO DE LOS PLANOS DE PREFRACTURA.



● CARGADOS

○ DESCARGADOS

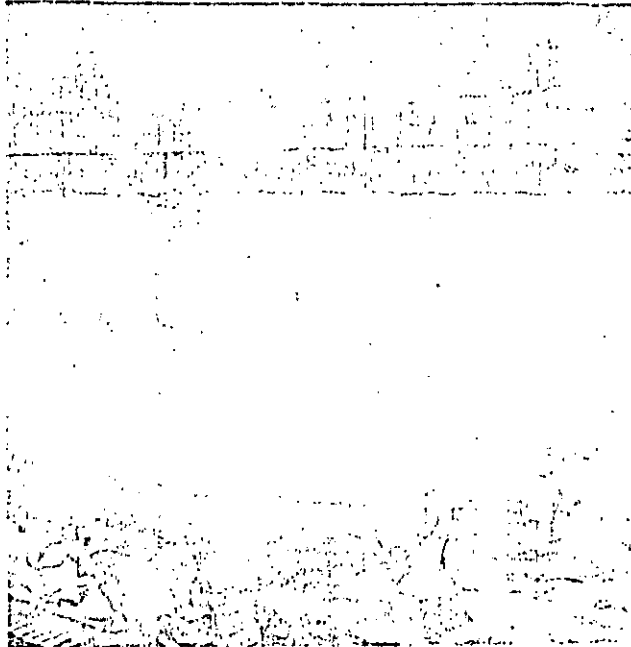


Figura No. 14



RESULTADO DE PREFRACTURA EJECUTADA  
EN UN FRENTE DE ROCA CALIZA.

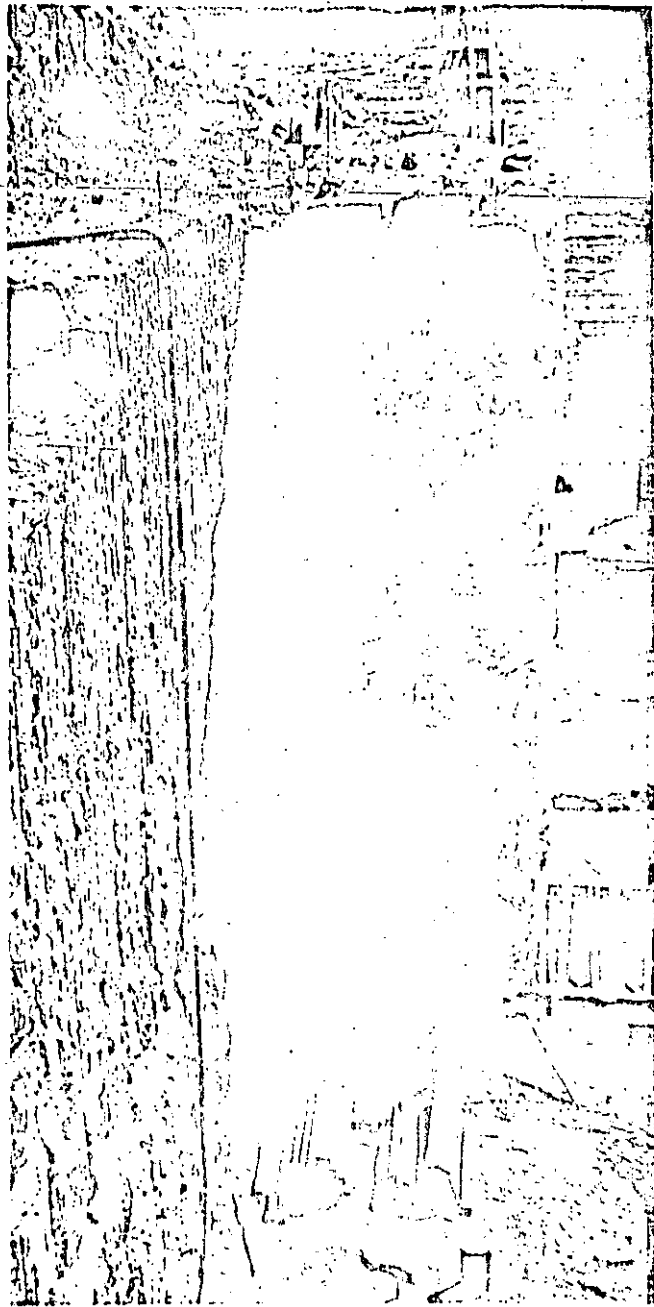
Figura No. 15



RESULTADO DE PREFRACTURADO EN FORMACIONES  
ALTAMENTE ESTRATIFICADAS

Figura No. 16

(63)



PREFRACTURADO A AMBOS LADOS DE UN RINCON.

malos resultados. Sin embargo, al igual que en las Voladuras Amortiguadas, se han obtenido buenos resultados en las formaciones homogéneas más sólidas, colocando el taco solamente en los últimos dos o tres piés del barrenó. También, como en las Voladuras Amortiguadas, es conveniente aumentar la carga en los primeros piés del barrenó hasta cerca de 2 ó 3 veces la utilizada en la porción superior. Esto provoca el corte en el fondo en donde es más difícil obtenerlo.

Las cargas para Prefracturado se colocan y detonan de la misma manera descrita para las Voladuras Amortiguadas. Se recomienda asimismo, colocar las cargas al tresbolillo en barrenos adyacentes para obtener una mejor distribución total de la carga.

La profundidad que puede prefracturarse de una sola vez, nuevamente depende de la habilidad para mantener un buen alineamiento de los barrenos. Las desviaciones mayores a 6" del plano de corte deseado, darán resultados negativos. Generalmente la máxima profundidad que puede utilizarse para barrenos de 2" a 3½" de diámetro sin una desviación considerable en el alineamiento es de 50 piés.

Teóricamente, la longitud de una voladura para Prefracturar es ilimitada. En la práctica, sin embargo, el disparar muy adelante de la excavación primaria puede traer problemas pues las características de la roca pueden cambiar y la carga ser causa de un exceso de fractura en las zonas más débiles. Llevando el Prefracturado adelante únicamente a la mitad de la voladura principal siguiente (Ver Fig. 11) los conocimientos que se van obteniendo con las voladuras principales respecto a la roca, pueden aplicarse a los disparos de prefracturado subsecuentes. En otras palabras, las cargas pueden modificarse si es necesario y se corre un menor riesgo que si se dispara el total de la línea de excavación antes de avanzar con las voladuras principales.

El Prefracturado puede realizarse simultáneamente a la voladura principal retrasando sus barrenos con retardadores MS, de manera que los barrenos de Prefracturado estallen primero que los de la voladura principal. (Ver Fig. 12).

En muchos casos, especialmente si se trata de frentes no lineales, el Prefracturado, en combinación, con la Barrenación en Línea dará buenos resultados v.g. cuando se desea conservar una esquina de roca sólida entonces puede utilizarse la barrenación en líneas en la esquina para evitar el rompimiento a través de ella. (Ver Fig. 13). Los barrenos-guía son tan ventajosos en el Prefracturado como en las Voladuras Amortiguadas para provocar cortes a lo largo de los planos deseados.

Cuando se prefractura en formaciones sin consolidación y además se utiliza la Barrenación en Línea, entre los barrenos espaciados normalmente, la profundidad de la Barrenación en Línea puede ser menor unos cuantos piés, respecto de la profundidad total de los barrenos de la Prefracturación. El rompimiento hacia atrás es más probable en la parte superior de un banco o nivel; en consecuencia, el barrenar en Línea entre barrenos de Prefracturado, a profundidades medias, reduce la posibilidad de rompimiento excesivo en cualquier tipo de formación. El material sin consolidación las cargas de explosivo por pié lineal deberán reducirse en un 50% en la parte superior del barreno, tendiendo a reducir al mínimo el rompimiento excesivo de la pared terminada en las capas superiores. Figs. 14, 15 y 16.

Trabajos Subterráneos. -- Usualmente combinado con el trabajo a cielo abierto, el Prefracturado tiene alguna aplicación en frentes y rebajes subterráneos escalonados para controlar el exceso de excavación y así mejorar la estabilidad del techo y de las paredes, reduciendo los volúmenes de concreto del revestimiento.

Si los barrenos perimetrales de un frente se ejecutan bajo el principio del Prefracturado, se cargan ligeramente y se disparan simultáneamente antes de la voladura principal; el exceso de excavación puede reducirse al mínimo. En barrenos horizontales, sin embargo, no resulta práctico atar los cartuchos de carga fragmentados a líneas de Primacord o colocar taco alrededor de la carga. En consecuencia, en trabajos subterráneos, pueden utilizarse cartuchos de menor diámetro, con espaciadores, para reducir al mínimo la carga por pié. Es necesario utilizar alguna forma de tapón colocado en la boca para evitar que "escepten".

Aunque teóricamente firmes, las técnicas del prefracturado no se emplean con frecuencia en los frentes subterráneos debido a posibles problemas por barrenos sin detonar, a la línea de menor resistencia y a los espaciamientos tan pequeños que se usan en la voladura principal. No obstante se han obtenido buenos resultados utilizando las técnicas del Prefracturado en galerías subterráneas.

Una aplicación del Prefracturado en trabajos subterráneos que ha probado ser satisfactoria, es su utilidad para el control en las operaciones de socavación y derrumbe. Prefracturando hasta los límites de la veta, reduce al límite la pérdida de mineral en la operación de derrumbe. También prefracturando hasta los límites del rebaje facilita el derrumbe inicial del mineral.

(57)

VENTAJAS

El Prefracturado ofrece las siguientes ventajas:

Aumento en el espaciamento de los barrenos - reducción de costos de barrenación.

No es necesario regresar a volar taludes o paredes después de la excavación principal.

LIMITACIONES

Al prefRACTURAR, es difícil determinar sus resultados - -- hasta no haber excavado totalmente hasta la pared terminada. Puesto que el Prefracturado se lleva a cabo antes que las voladuras principales, no es posible aprovechar el conocimiento de las condiciones de la roca que se obtiene con las voladuras principales. - También, los espaciamentos de los barrenos de las Voladuras Amortiguadas y Perfiladas son generalmente mayores que en el Prefracturado, siendo así que los costos de barrenación son menores con este último sistema.

COMBINACIONES .

Como se apuntó en las secciones anteriores, es conveniente a menudo, especialmente en formaciones imperfectamente consolidadas, barrenar en Línea entre los barrenos de voladuras amortiguadas y de Prefracturado para obtener buenos resultados. Es también frecuentemente ventajoso barrenar en Línea o prefRACTURAR esquinas en donde se emplea la voladura amortiguada.

Hay un caso registrado en donde el Prefracturado se hizo dentro de la línea neta de excavación antes de la voladura principal; después de llevar la excavación principal hasta el plano prefRACTURADO, el banco restante se voló usando la técnica de voladura amortiguada. Este procedimiento ofrece la máxima protección para la pared terminada puesto que el plano prefRACTURADO tiende a reflejar las ondas de choque de la voladura primaria. También puede obtenerse un conocimiento completo de la formación al quitar el banco final por medio de Voladura Amortiguada. De esta manera se da protección y un margen de seguridad por errores de cálculo en el caso de que la línea prefRACTURADA sea rebasada.

RESUMEN .

Este informe ha descrito los procedimientos principales para las Voladuras Controladas. Ha definido las ventajas y limitaciones de la Barrenación en Línea, de la Voladura Amortiguada, de la Voladura Perfilada y del Prefracturado.

## TABLA A

TIPOS DE EXPLOSIVOS DUPONT PARA VOLADURAS  
CONTROLADAS A CIELO ABIERTO

(7)

TAMAÑO	GELATINA ESPECIAL C. GELATINA EXTRA		RED CROSS EXTRA C. DIPLOTTA EXTRA	
	CARTUCHOS POR c/50 Lbs.	LIBS./CARTUCHO	CARTUCHOS POR c/ 50. Lbs.	LIBS./ CARTUCHO
1 x 8"	139	0.36	167	0.30
1 1/8" x 8"	114	0.44	137	0.36
1 1/4" x 8"	90	0.56	110	0.45
1 1/2" x 8"	61	0.82	79	0.63
2 x 8"	36	1.40	42	1.20

(2)

La Barrenación en línea, se ha demostrado que dá resulta -- dos imprevisibles excepto en formaciones homogéneas. Los pequeños -- espaciamentos y el gran número de barrenos necesarios, origina que los costos sean altos y la perforación tediosa. La Voladura Amortiguada ofrece ventajas definitivas sobre la barrenación en línea, in -- cluyendo un mayor espaciamiento y obteniéndose mejores resultados.

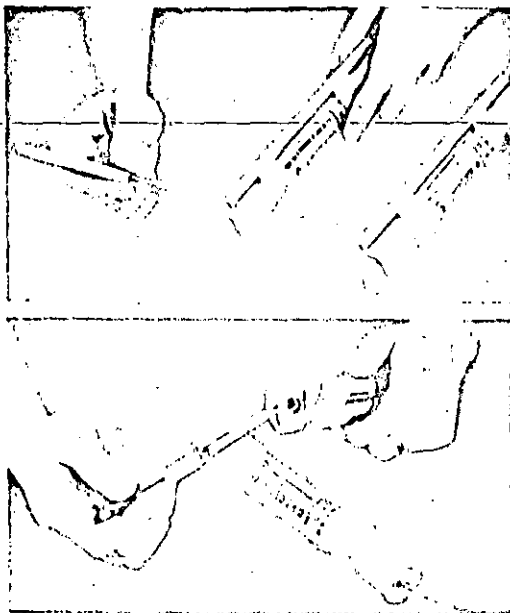
La Voladura Perfilada o de Afine sigue básicamente el mismo principio que la Voladura Amortiguada. Disparando con un mínimo de -- retardo entre barrenos, se obtiene una acción de corte que propor -- ciona paredes más lisas y un mínimo de sobreexcavación. El uso de -- este método, en trabajos subterráneos requiere de ciertas formas -- especiales que ya han sido expresadas en detalle .

El Prefracturado difiere de los otros métodos en que sus ba -- rrenos se disparan antes que cualquiera de los de la voladura prin -- cipal. Es innecesario regresar a volar taludes o paredes después de la voladura principal. Sin embargo, no es posible aprovechar la ex -- periencia o conocimiento de las condiciones de la roca que normal -- mente se obtienen de las voladuras principales.

Es muy conveniente que aquéllos que tienen que ver con el -- trabajo de voladuras conozcan de antemano las ventajas y limitacio -- nes de cada procedimiento. Al utilizar cualquiera de los tipos de -- voladuras controladas, se recomienda efectuar ensayos para determi -- nar las cargas y plantillas más convenientes. Deben tronarse varios barrenos y estudiarse los resultados antes de proseguir. La expe -- riencia y conocimientos que Du Pont ha adquirido en Voladuras Con -- troladas a través de una diversidad de operaciones prácticas, pro -- porciona al consumidor de explosivos una fuente inapreciable de cono -- cimientos. Los representantes técnicos de Du Pont están dispuestos -- a trabajar conjuntamente en la determinación del método más apropia -- do que deba ser aplicado en una situación dada.

Una evidencia más del conocimiento de Du Pont en el campo -- de las Voladuras Controladas, está representada en los tres tipos -- de explosivos especialmente diseñados para Voladuras Controladas.

Los tipos anteriores en diámetros de 1 1/4" y mayores es -- tán pre-perforados a lo largo de todo el cartucho, o bien tienen un tubo de Primacord de 8" insertado para cargar por gravedad en lí -- neas verticales de Primacord. Los tubos de 8" de Primacord se pue -- den utilizar como espaciadores entre cartuchos completos o parcia -- les. (Veáse Tabla A).



(13)

TIPOS DU PONT PARA VOLADURAS  
CONTROLADAS A CIELO ABIERTO



TIPOS DU PONT PARA VOLADURAS  
CONTROLADAS SUBTERRANEAS



TIPOS DU PONT PARA VOLADURAS CONTROLADAS SUBTERRANEAS.

TRIMTEX es un producto de baja densidad, de 7/8" diámetro, por 24" de largo con 100 cartuchos por cada 50 libras o sea 1/4" de lb./pié de cartucho. Los cartuchos están provistos de mangas de acoplamiento para acoplar más de 1 cartucho y asegurar el alineamiento en el barreno. La ligera carga/pié y el anillo de aire entre el cartucho de pequeño diámetro y la pared del barreno contribuyen a obtener un perímetro liso con un sobre-rompimiento mínimo.



**DIVISION DE EDUCACION CONTINUA  
FACULTAD DE INGENIERIA U.N.A.M.**

MECANICA DE ROCAS APLICADA A LA MINERIA

Y A LA CONSTRUCCION

TRATAMIENTO DE MACIZOS ROCOSOS

ING. RAUL CUELLAR BORJA

MAYO 1985.

# EXCAVACIONES A CIELO ABIERTO EN ROCA

①

Raúl Cuéllar Borja

mayo, 1985

## PROPIEDADES GEOMECHANICAS QUE INTERVIENEN PARA EL DISEÑO

### ESTRUCTURA

Masiva . . . . . Granito, caliza, mineral  
Estratificada . . . . . Caliza  
Plegada . . . . . Lutita, pizarra, esquisto  
Fracturada . . . . . (Enfriamiento o tectonismo)  
Discontinua . . . . . Basalto vesicular  
Cavernosa . . . . . Caliza cárstica

### ACTITUD

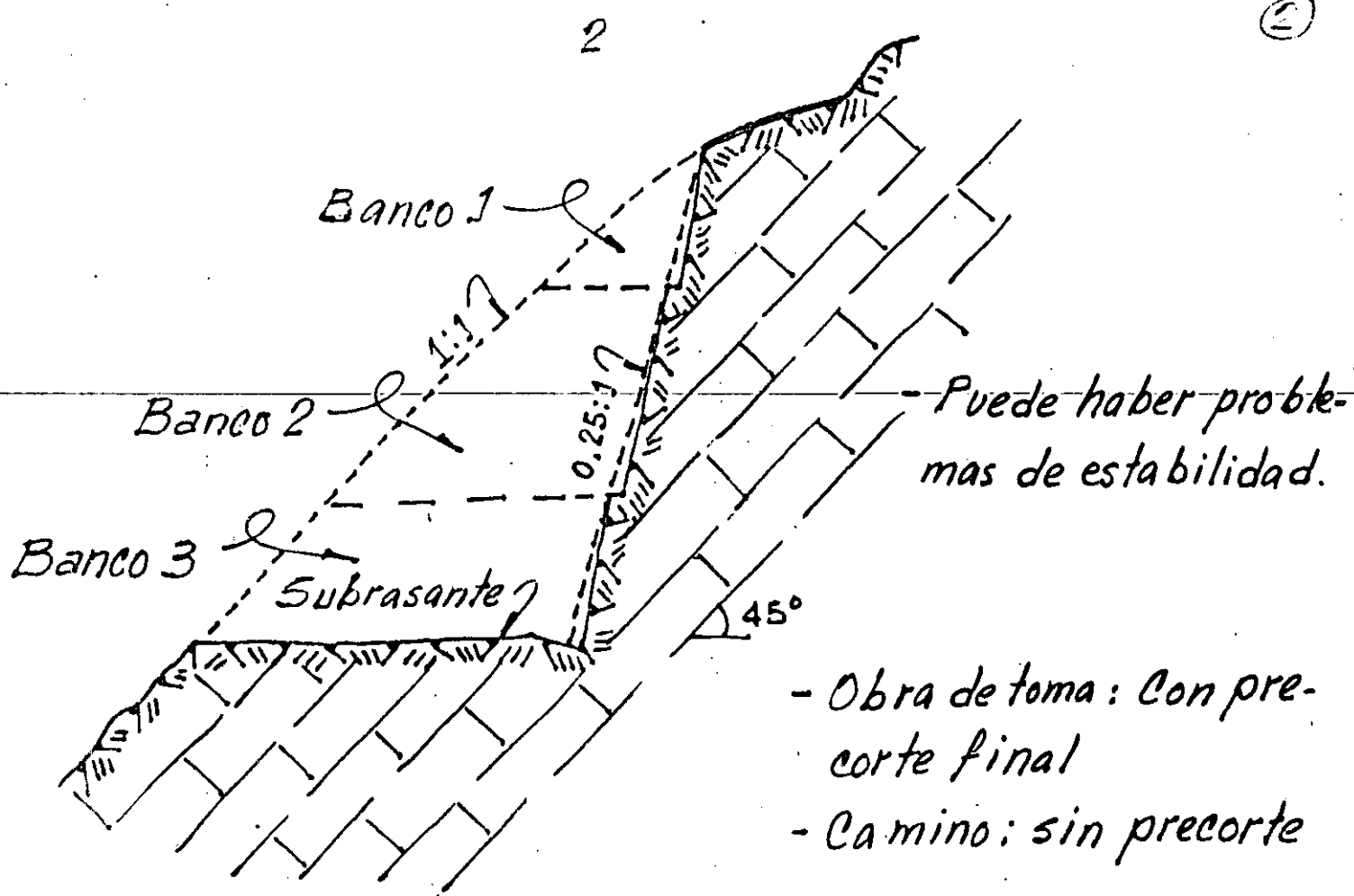
Rumbo y echado . . . . . Capas horizontales, verti-  
cales e inclinadas.

### CALIDAD

Física . . . . . } Sana o alterada  
Química . . . . . }

### PROPIEDADES FISICAS E INDICES

Resistencia  
Densidad  
Porosidad

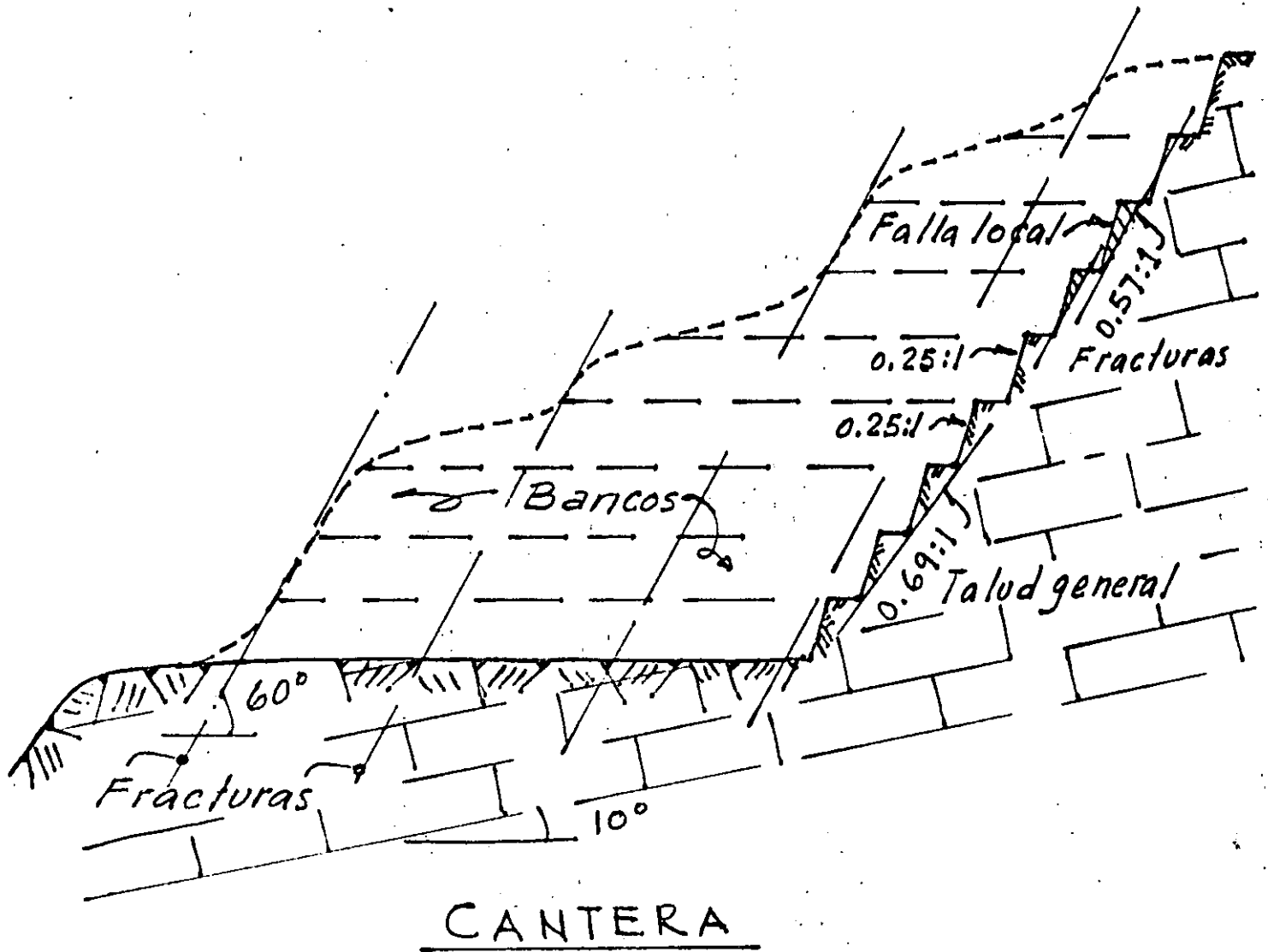


CORTE EN OBRAS DE TOMA Y CAMINOS

Banco 1.. Con perforadora de pierna  
 Bancos 2 y 3.. Con track-drill.

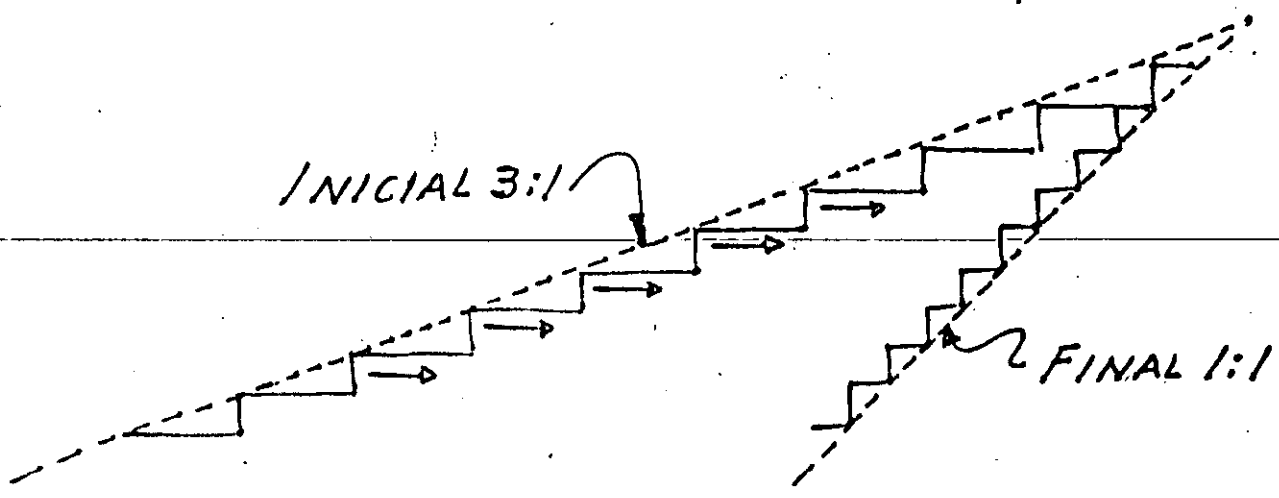
TALUDES USUALES

- Granitos, basaltos y lavas : 1/4:1, 1/2:1
- Areniscas masivas, calizas : 1/4:1, 1/2:1
- Areniscas estratificadas, lutitas y calizas no masivas : 1/2:1, 3/4:1
- Gneiss, esquistos, marmol : 1/4:1, 1/2:1
- Pizarras : 1/2:1, 3/4:1

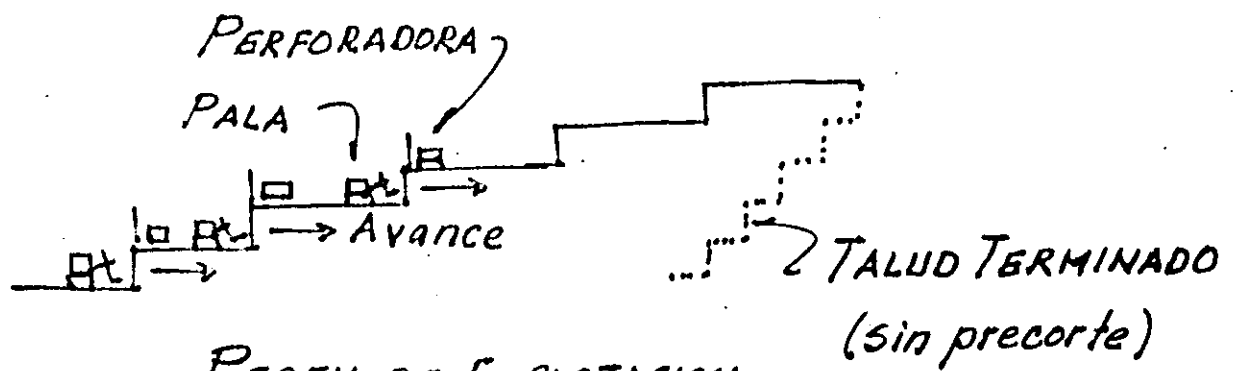


- El talud general tiene menor pendiente que las fracturas con echado de 60°.
- Se presentarán problemas de falla local.
- El talud final no debe llevar precorte.
- Tomando en cuenta los echados de las dos discontinuidades (estratos y fracturas) el talud general deberá ser estable.

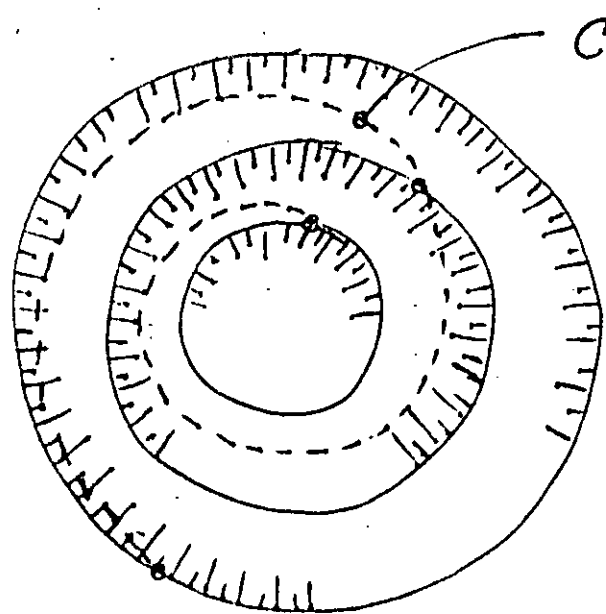
MINAS DE COBRE



TALUDES DE LOS TAJOS



PERFIL DE EXPLOTACION



Camino espiral  
 Pendientes:  
 Uniforme : máx 8%  
 Rampas de acceso : 10%  
 Máxima : 12%

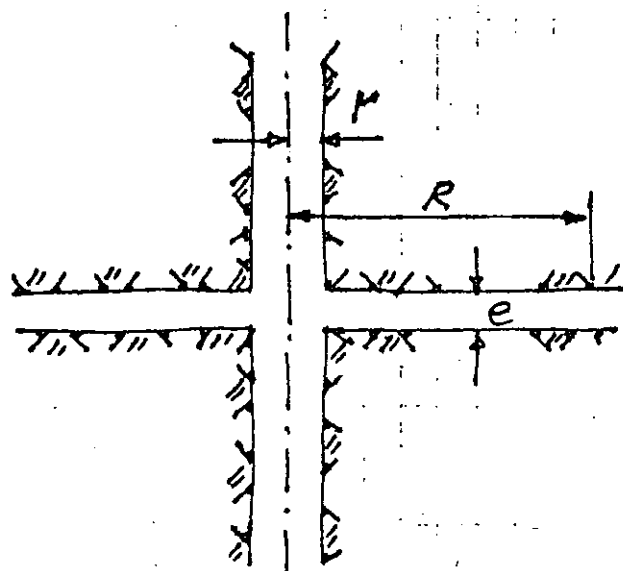
CAMINOS

Raúl Cuéllar Borja

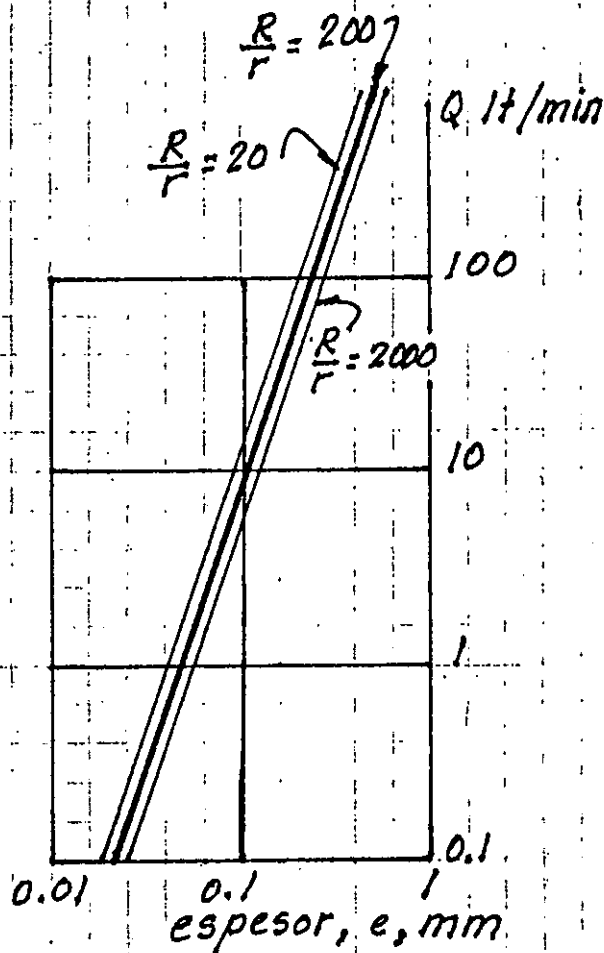
mayo, 1985

1.- MECANISMO DE PENETRACION DE MEZCLAS

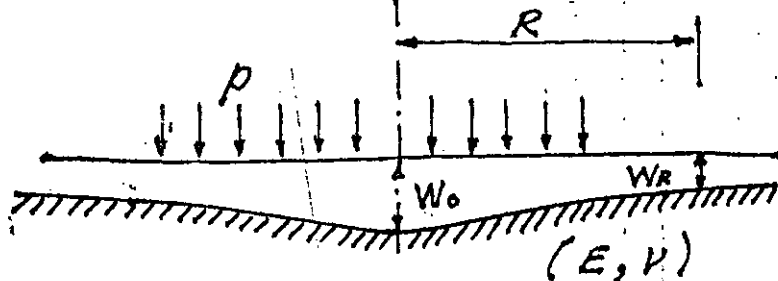
a) Deformabilidad de la roca bajo presión hidrostática semejante al ensaye de placa flexible



GASTO EN lt/min bajo una presión de 10 Kg/cm<sup>2</sup>



Tramo de inyectado = 5m  
 1 UL = 1 lt/min/m  
 a 10 Kg/cm<sup>2</sup> de presión



Centro:

Borde:

$$W_{(0)} = \frac{2(1-\nu^2)Rp}{E}$$

$$W_{(R)} = \frac{4(1-\nu^2)Rp}{\pi E}$$

$$\Delta e = 2W_0 ; \Delta e = 2W_0$$

Si:  $E = 100\,000 \text{ Kg/cm}^2$ ;  $\nu = 0.5$ ;  $R = 10 \text{ m}$  y  $p = 10 \text{ Kg/cm}^2$

$\Delta e = 2W_0 = 0.3 \text{ mm}$  (centro);  $\Delta e = 2W_R = 0.2 \text{ mm}$  (Borde)

1 UL = 5 lt/min para 1 fisura de 0.1 mm

10 UL = 50 lt/min para 1 fisura de 0.2 mm

100 UL = 500 lt/min para 1 fisura de 0.5 mm

Si un tramo de 5 m absorbe un gasto  $Q = 100$  lt/min a  $10$  Kg/cm<sup>2</sup>, corresponde a 1 fisura de 0.25 mm de espesor o a 10 fisuras de 0.12 mm o a 100 fisuras de 0.06 mm.

### PERMEABILIDAD CONTRA APERTURA DE FISURAS

UL.	1 fisura	10 fisuras	100 fisuras
100	0.484 mm	0.225 mm	0.106 mm
10	0.225	0.106	0.048
1	0.106	0.048	0.022

Si un cemento "A" tiene 0.2% de granos  $> 0.25$  mm  $\cong$  20 gramos en 10 Kg de cemento es suficiente para producir sedimentación y taponamiento.

Si inyectáramos a  $30$  ó  $40$  Kg/cm<sup>2</sup> las fisuras se abrirían a  $0.6$  ó  $0.9$  mm y entonces sí pasarían los granos.

Se pueden usar cementos finos a bajas presiones o cementos gruesos a altas presiones.

Como la prueba-Lugeon se hace con agua limpia y a  $10$  Kg/cm<sup>2</sup> de presión no existe correlación con las absorciones de mezclas.



El gasto en una fisura indeformable es:

$$Q = \frac{\pi}{6\eta \log_e(R/r)} p \left( e_0 + \frac{\alpha}{E} p \right)^3 \dots \text{Poiseuille}$$

donde:  $\eta$  = viscosidad del fluido

$r$  = radio del barreno

$R$  = radio de penetración

De los ensayos de deformabilidad:  $\Delta e = \alpha \frac{p}{E}$

La deformación de la fisura es directamente proporcional a la presión e inversamente proporcional con el módulo elástico de la roca.

Durante la aplicación de la presión la fisura  $e_0$  pasa a ser:

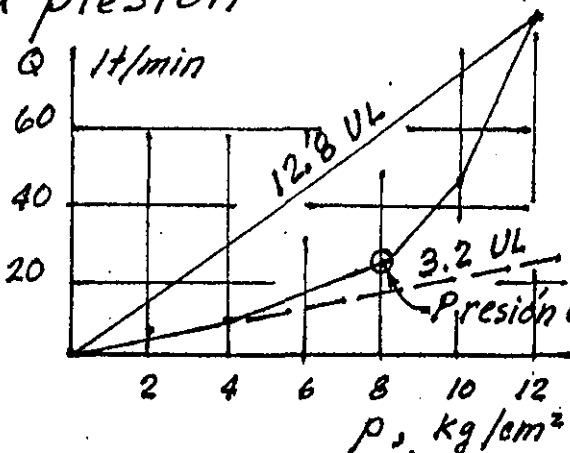
$$e_0 + \alpha \frac{p}{E}$$

Resulta entonces:

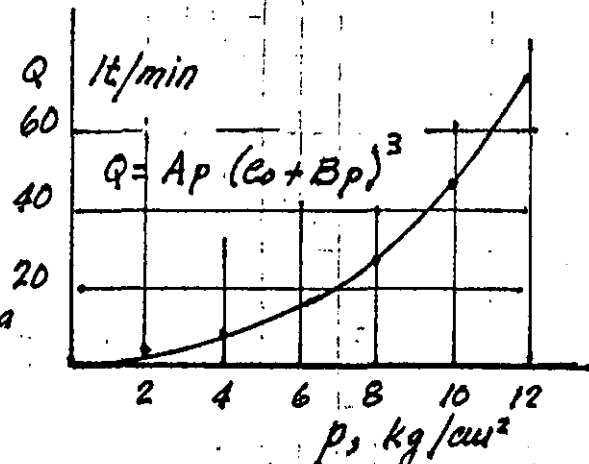
$$Q = A p^4$$

siendo  $A$  una constante

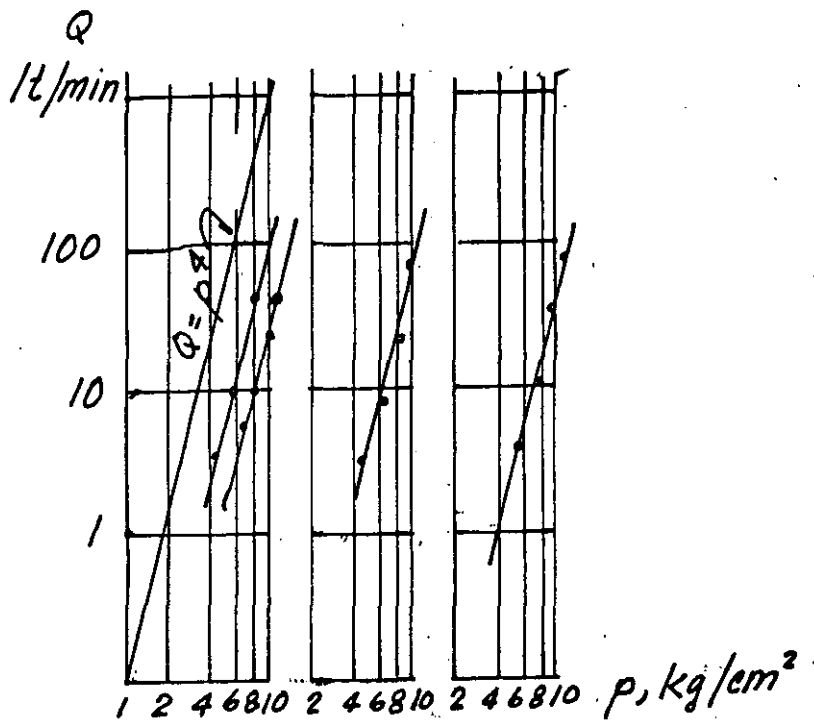
Por tanto el gasto es proporcional con la cuarta potencia de la presión



⊗ Fracturamiento hidráulico



Comportamiento elástico

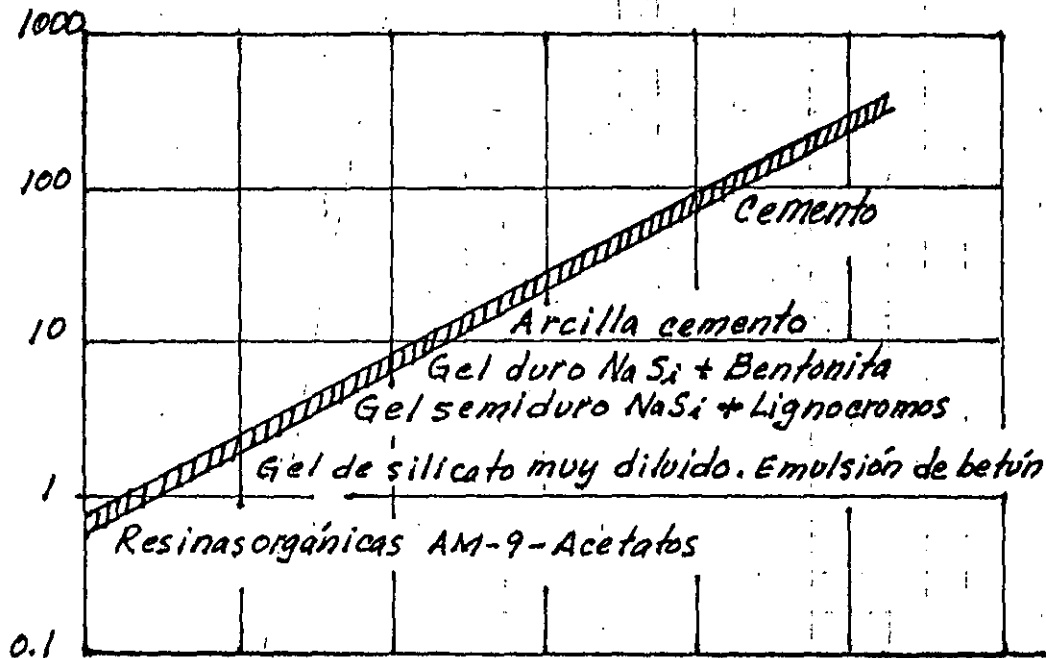


### REPRESENTACION DE ENSAYES LUGEON EN ESCALA LOGARITMICA

- Si la pendiente de las envolventes rectas fuera mayor de 4, se tendrá fracturamiento hidráulico

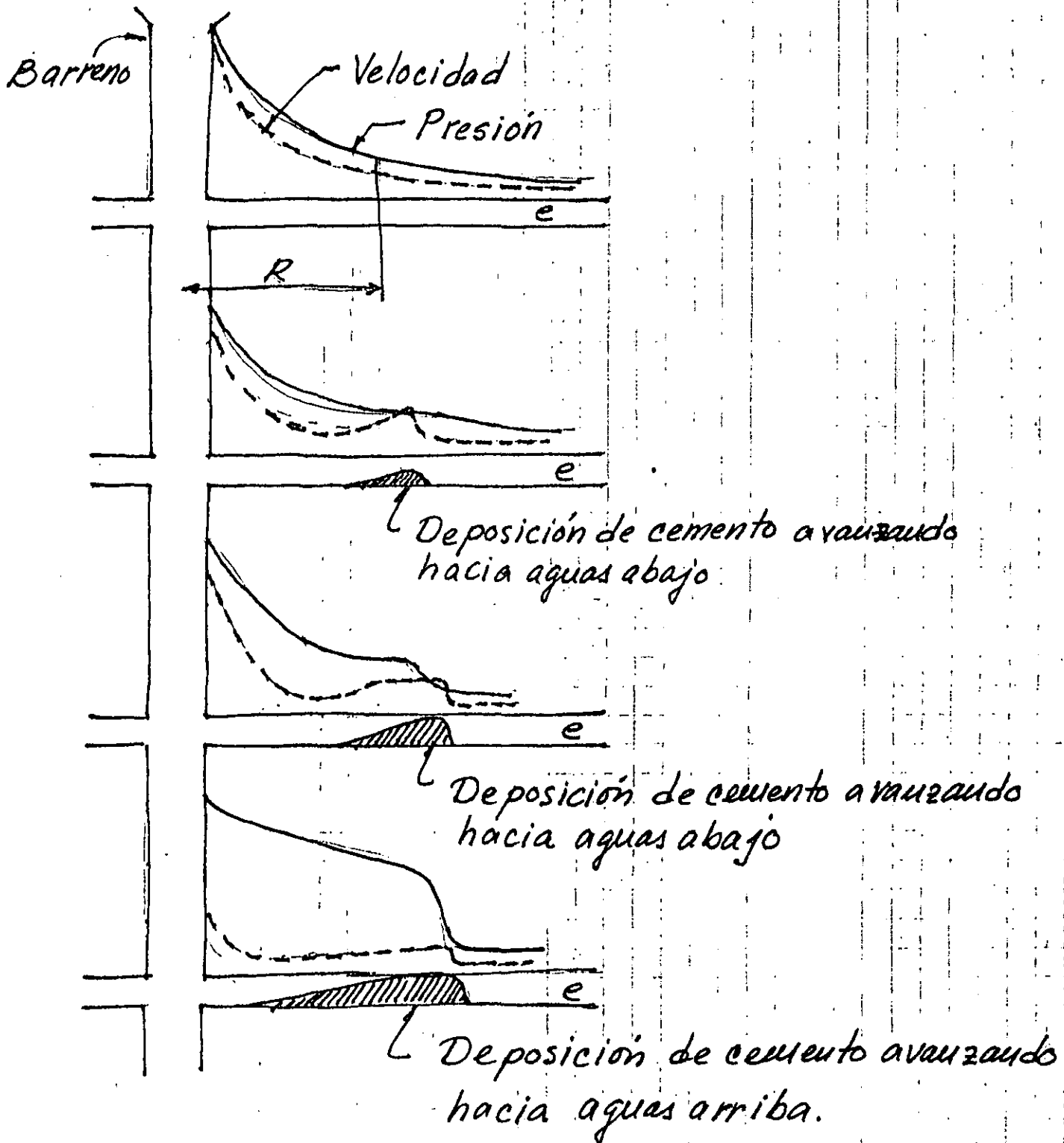
b) Límites de penetrabilidad de las mezclas en función de la permeabilidad del terreno.

Tamaño de los granos en micras.



$10^{-6}$     $10^{-5}$     $10^{-4}$     $10^{-3}$     $10^{-2}$     $10^{-1}$    1   K en m/s  
 $10^{-4}$     $10^{-3}$     $10^{-2}$     $10^{-1}$     $10^0=1$    10    $10^2$  K en cm/s

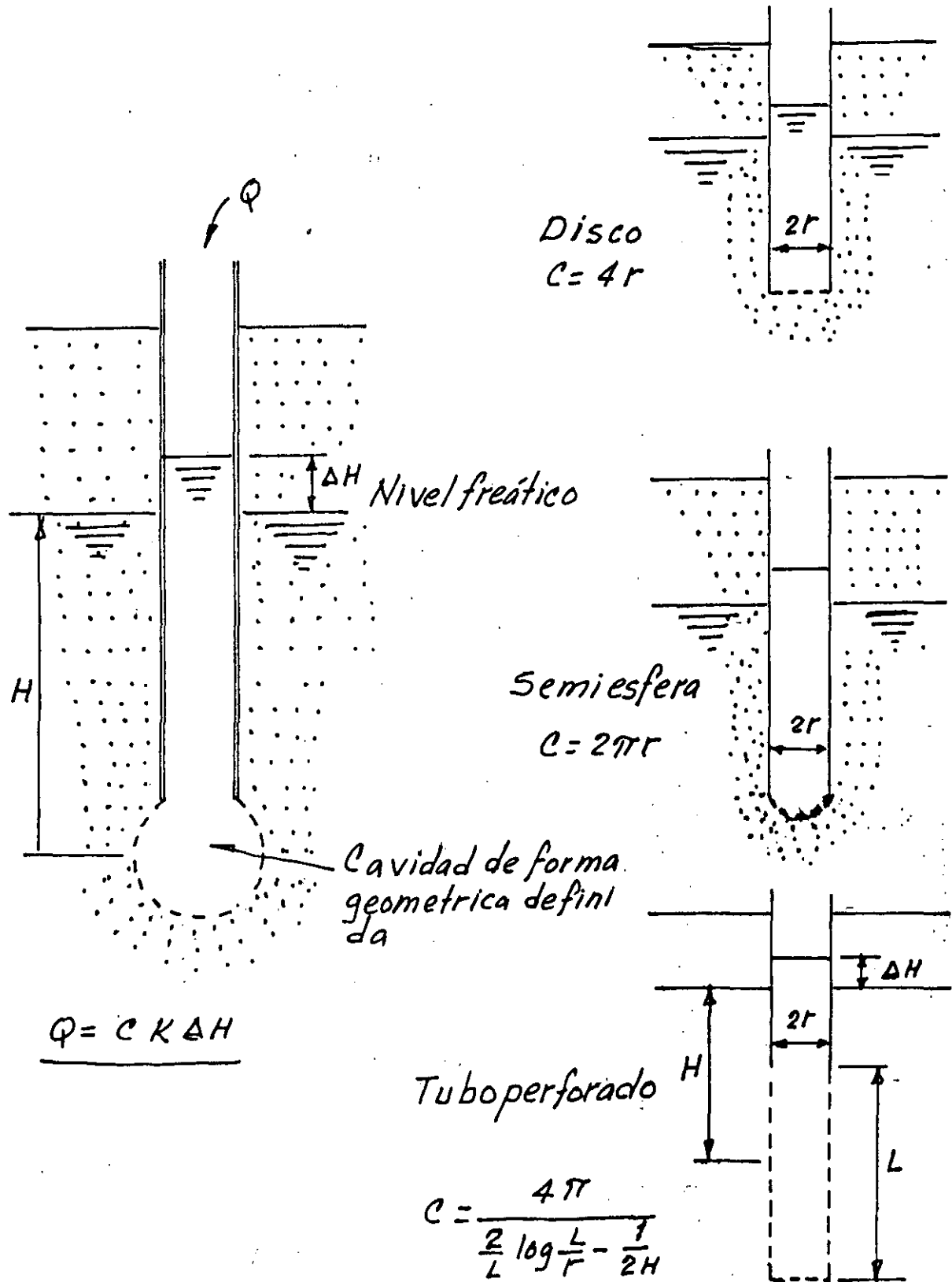
## c) Sedimentación

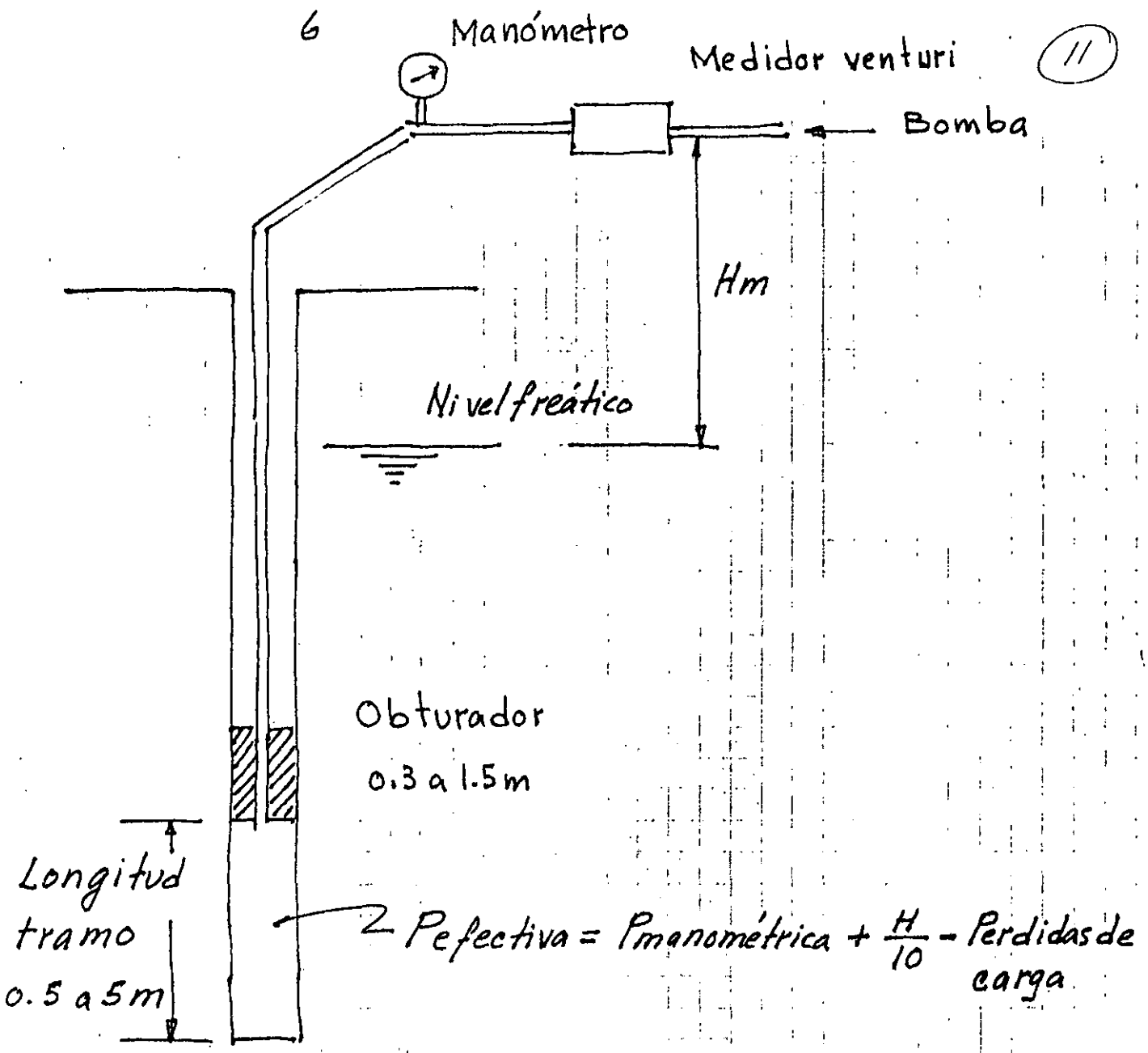


INYECCION DE UNA FISURA CON MORTERO INESTABLE

Para que no se produzca arqueo:  $\frac{e}{\text{diám. partícula}} > 15$

PRUEBA LEFRANC-MANDEL

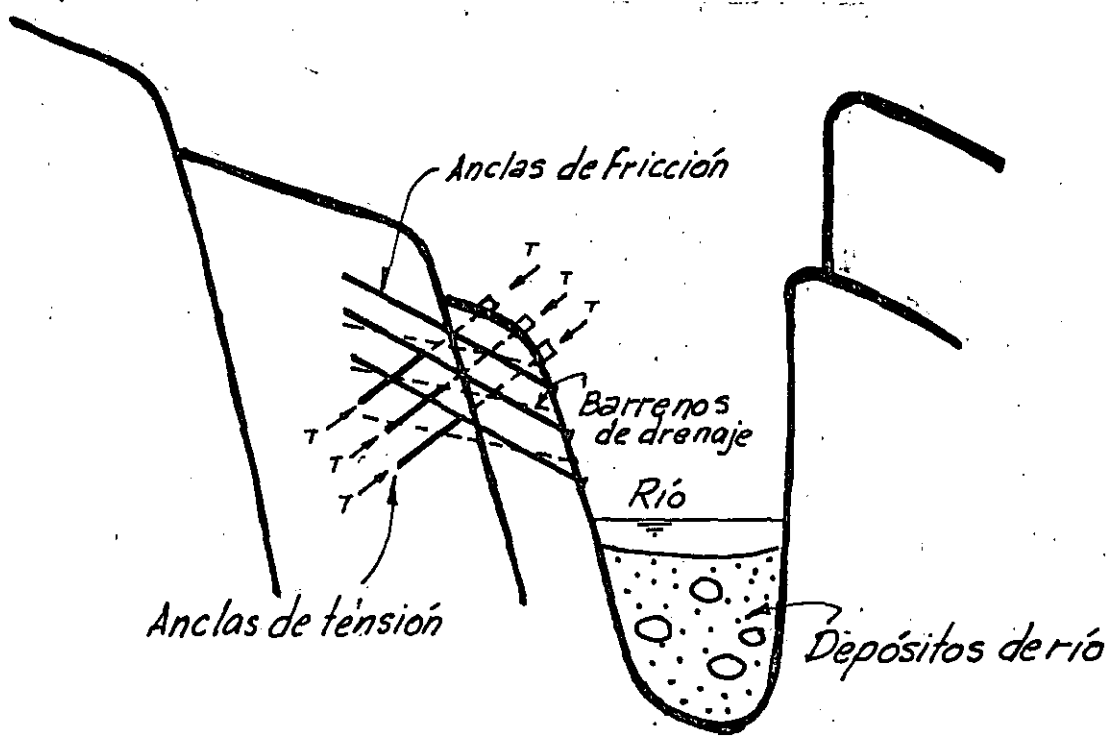




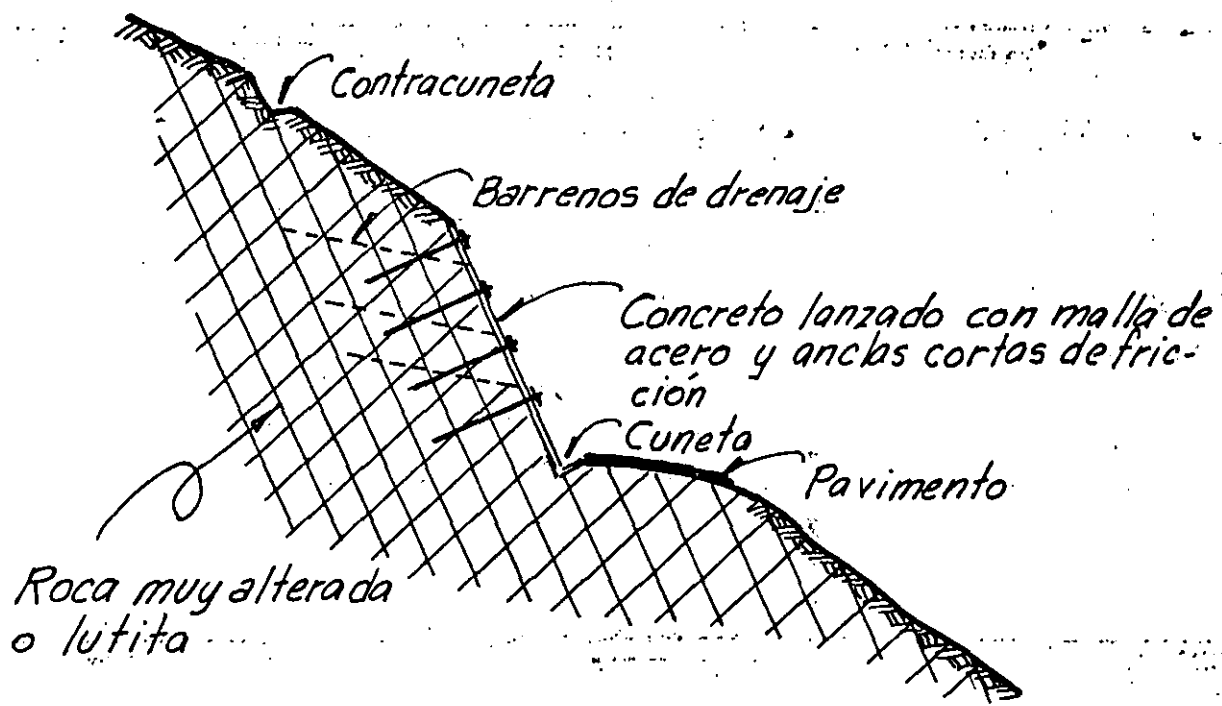
ENSAYE LUGEON

1 Lugeon = 1 lt/min/m bajo  $10 \text{ Kg/cm}^2$  de presión efectiva.

SISTEMAS DE SOPORTE CON ANCLAS Y CONCRETO LANZADO



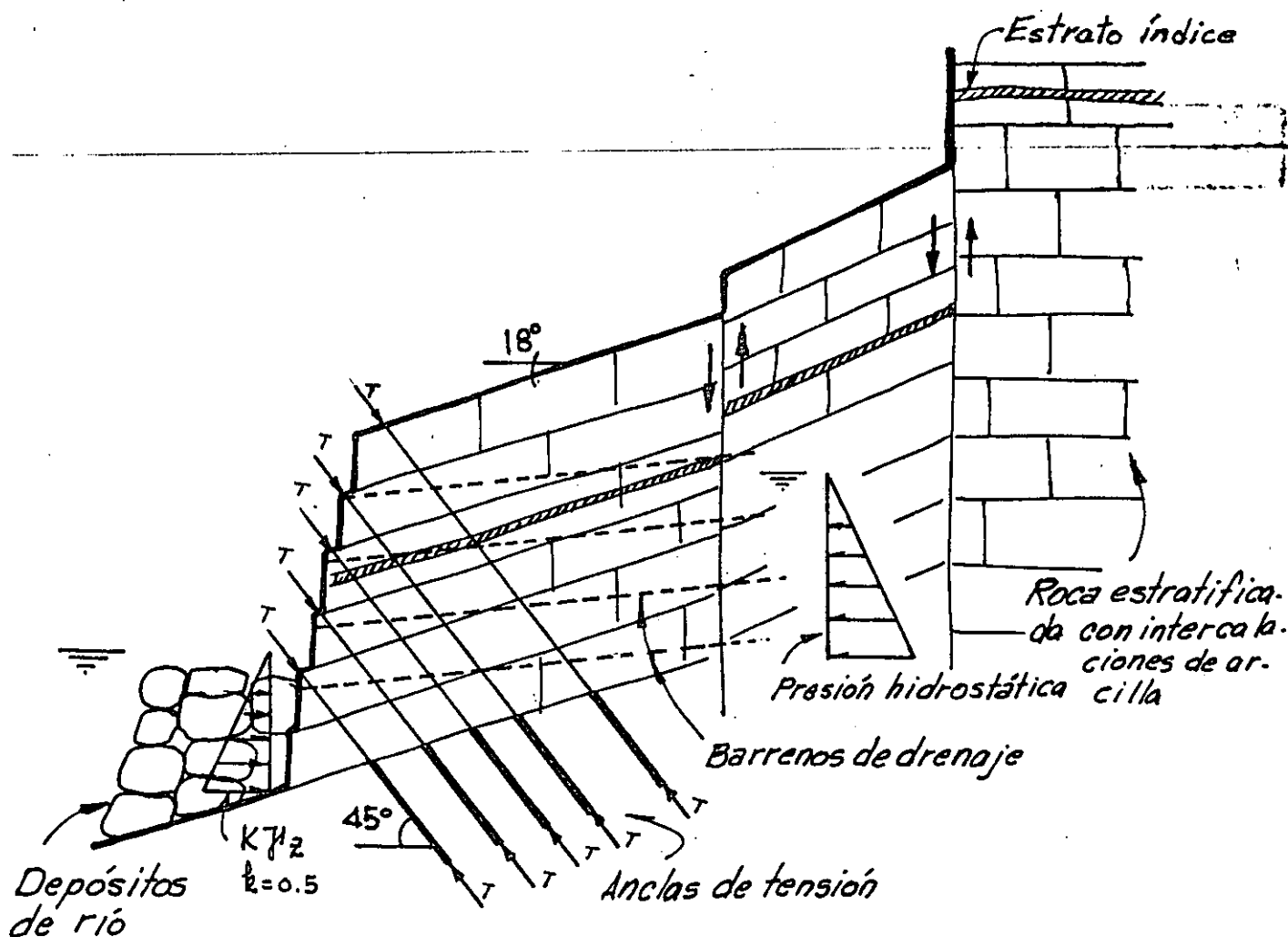
TALUD SOPORTADO CON ANCLAS DE FRICCIÓN Y TENSION



TALUD SOPORTADO CON ANCLAS DE FRICCIÓN Y CONCRETO LANZADO CON MALLA METALICA

ANCLAJE EN TALUDES

A continuación se muestra un sistema de soporte de taludes a base de anclas de tensión postensadas y barrenos de drenaje. En el diseño de este anclaje se ha tomado en cuenta el empuje hidrostático, el efecto de sismo y el soporte de los depósitos del río.



TALUD SOPORTADO CON ANCLAS DE TENSION  
EN ROCA ESTRATIFICADA

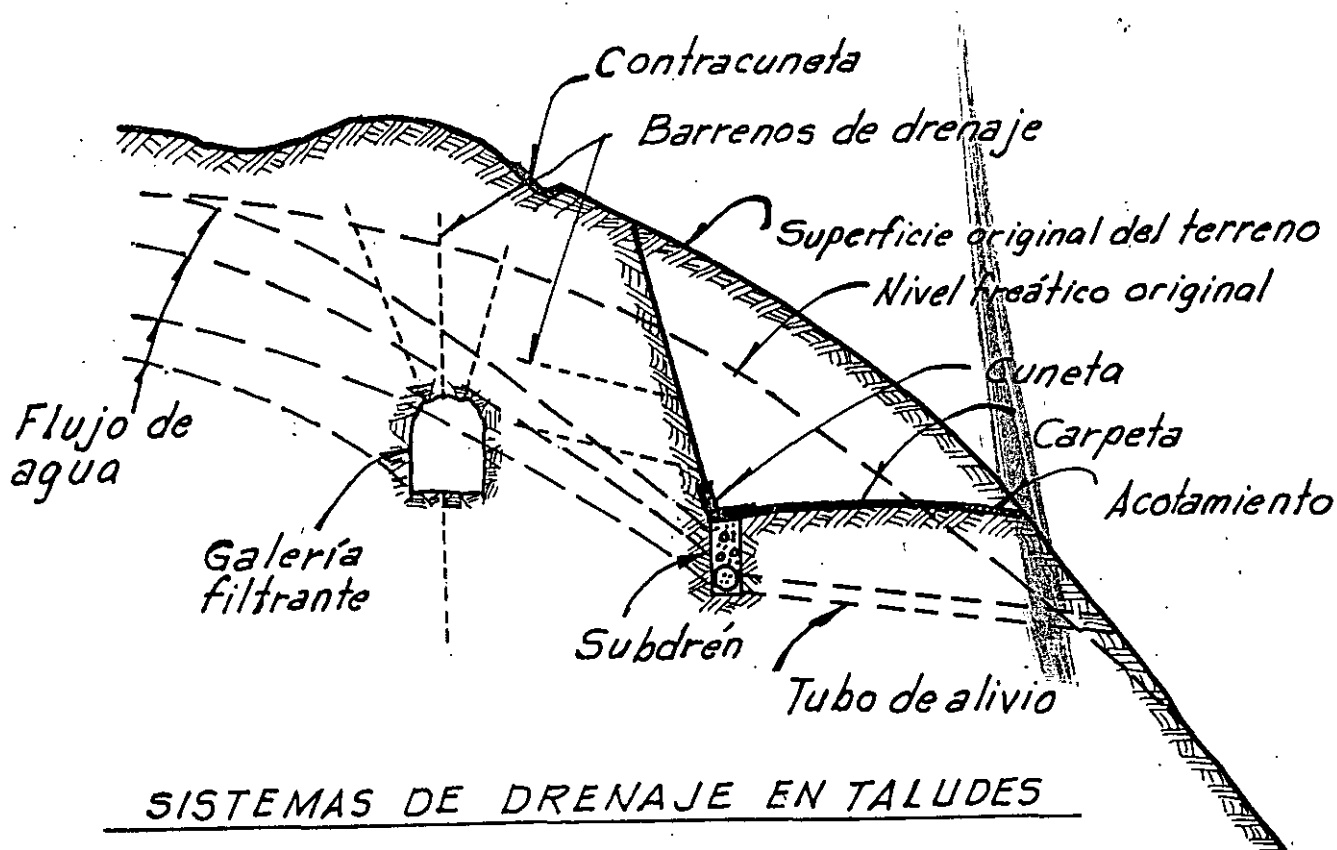


### SISTEMAS DE DRENAJE EN TALUDES

De la relación entre esfuerzos cortantes y normales de Mohr-Coulomb,  $\tau = \sigma \tan \phi$ , puede verse que los esfuerzos cortantes dependen de los esfuerzos normales.

Cuando existe presión hidrostática en forma de subpresión la fuerza normal tiende a disminuir con la consiguiente disminución de la fuerza cortante:  $\tau = (\sigma - u) \tan \phi$ ; en donde  $u =$  subpresión.

De acuerdo con lo anterior, se comprende la importancia del drenaje en la estabilidad de taludes. En la figura de abajo se muestran los sistemas de drenaje usuales.



SISTEMAS DE DRENAJE EN TALUDES

SISTEMAS DE ESTABILIZACION DE TALUDES

DRENAJE

Cunetas y aliviaderos  
Contracunetas  
Alcantarillas  
Subdrenes  
Galerías filtrantes  
Barrenos de drenaje

ANCLAJE

Anclas de fricción  
Anclas de tensión  
Tendones

MUROS DE RETENCION

Concreto  
Mampostería

MOVIMIENTO DE MATERIALES

Cortes o bermas en zonas de  
carga actuante  
Terraplén en zonas de carga  
resistente

CONCRETO LANZADO Y MALLA

Para estabilización local

PERFILAMIENTO DE TALUDES

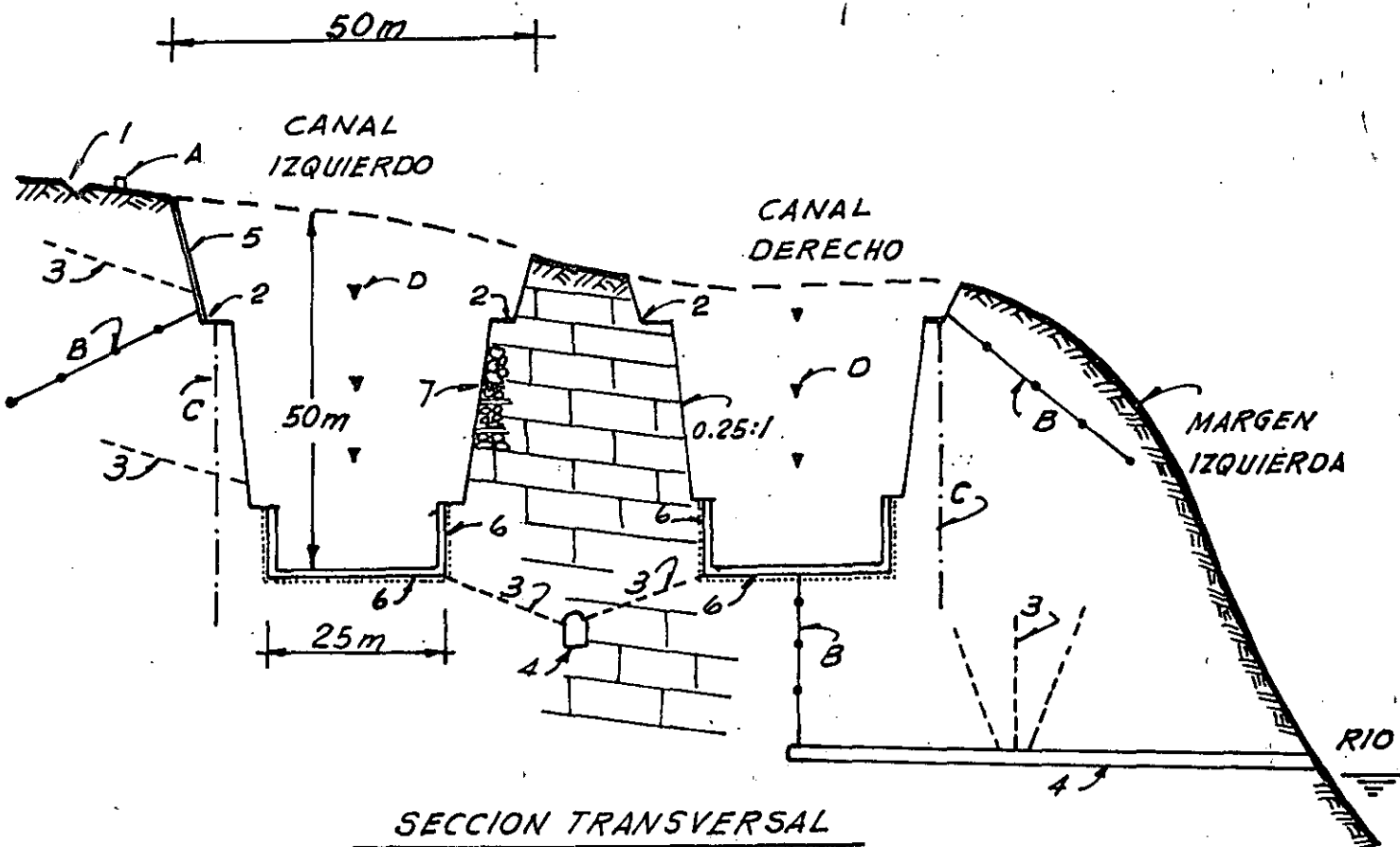
Uso de voladuras de precorte  
para estabilización local

P.H. LA ANGOSTURA, CHIS.

Sistema de drenaje e instrumentación en canales vertedores

Como medida preventiva contra la falla de talud se implementó un sistema de drenaje constituido por canalones en muros y losas en la zona revestida, descargando mediante barrenos a una galería central. Superficialmente se construyeron cunetas y se hicieron barrenos en paredes. A la vez se instaló un sistema de control de desplazamientos mediante instrumentación.

Hasta la fecha no se han presentado problemas de estabilidad y solo durante la construcción se presentaron fallas locales en zonas de fracturas y disolución, resolviéndose mediante rellenos de mampostería.



SECCION TRANSVERSAL

SISTEMA DE DRENAJE Y PROTECCION

INSTRUMENTACION

- 1.. Contracuneta
- 2.. Cunetas
- 3.. Barrenos de drenaje
- 4.. Galería filtrante
- 5.. Gunite
- 6.. Canalones
- 7.. Relleno de mampostería

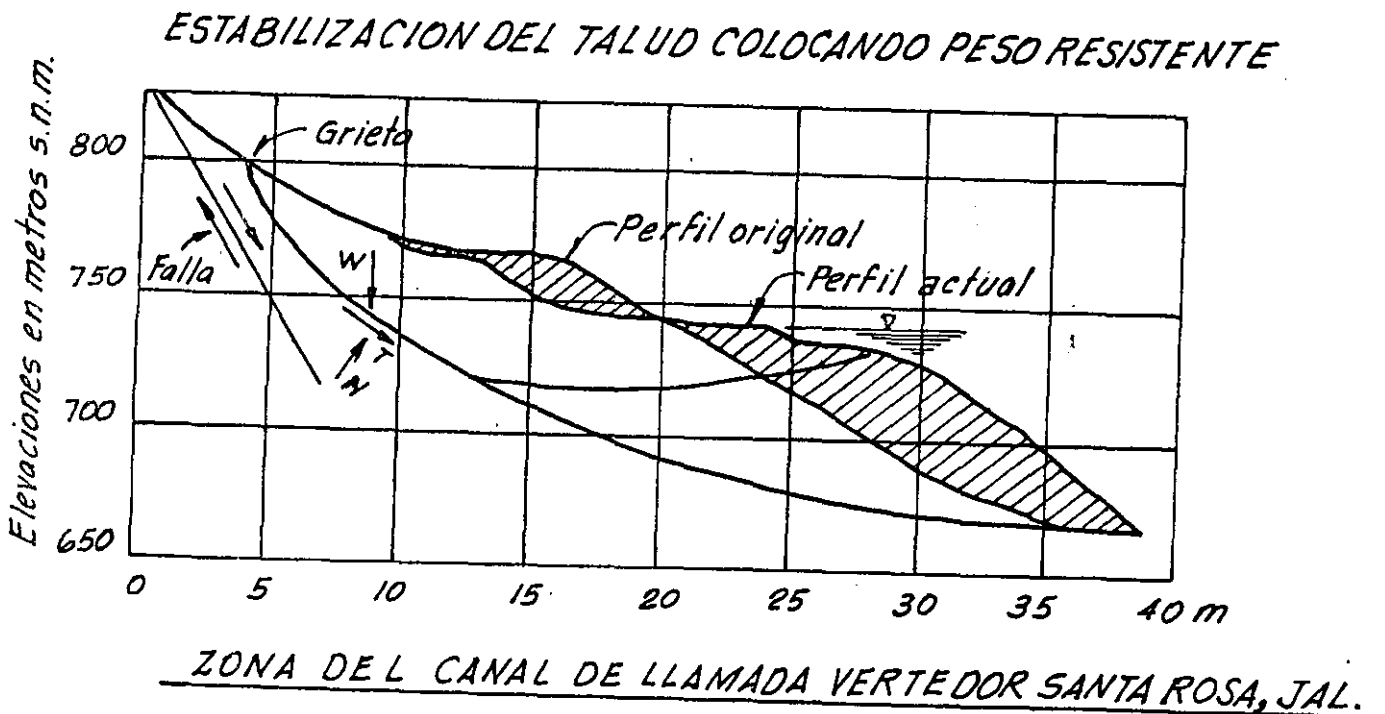
- A.. Majoneras (10)
- B.. Extensómetros longitudinales (8)
- C.. Inclínómetros (6)
- D.. Bancos de nivel profundo (6)

P. H. SANTA ROSA, JAL.

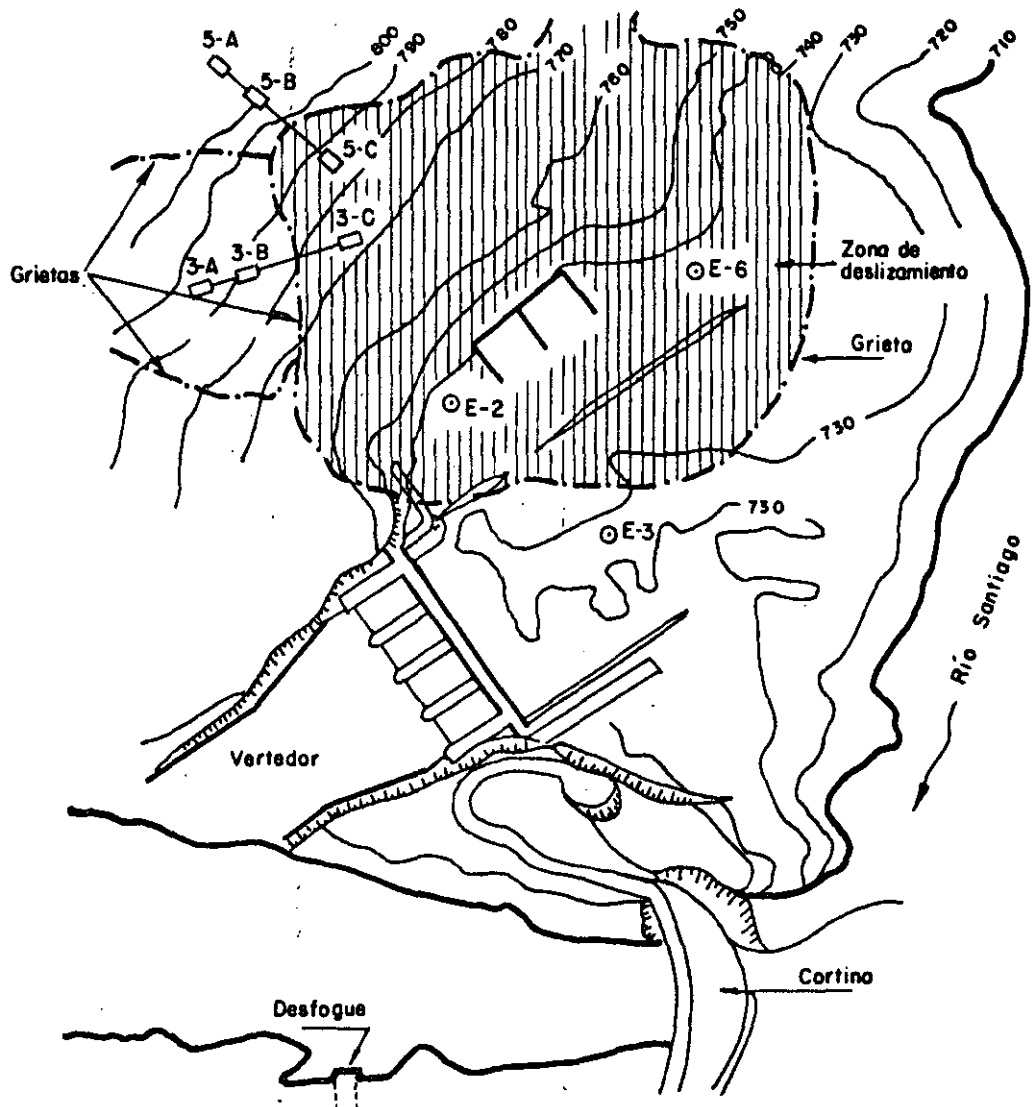
En la zona vecina al canal de llamada del vertedor, sobre la margen derecha, se detectó una zona inestable que cubica aproximadamente 700 000 m<sup>3</sup> hacia el año 1964. La solución que se le dió fué la de colocar material para aumentar el peso al pie del talud. Se colocaron aproximadamente 100 000 m<sup>3</sup>.

Durante el primer llenado los desplazamientos horizontal y vertical fueron del orden de 2.5 m, de entonces a la fecha el desplazamiento ha continuado a una velocidad del orden del centímetro por año. Desde 1965 hasta 1976 la operación de la planta se restringió para que no se presentaran descensos en el embalse mayores de 25 cm/día para evitar problemas de subpresión. A la fecha se ha modificado este criterio sin que se haya acelerado el movimiento del talud.

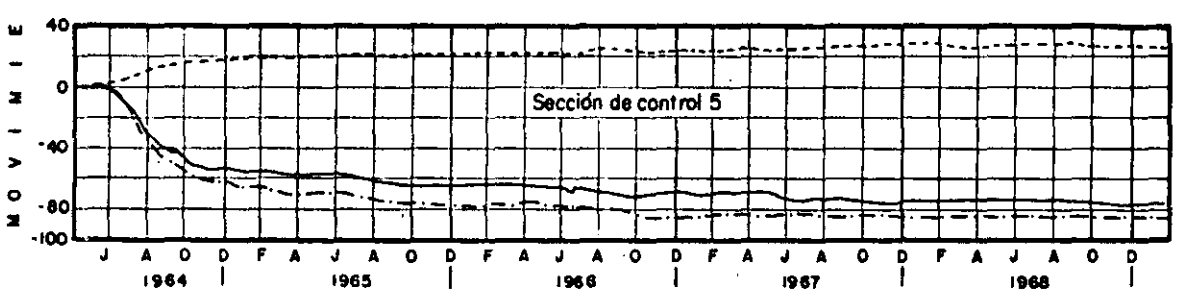
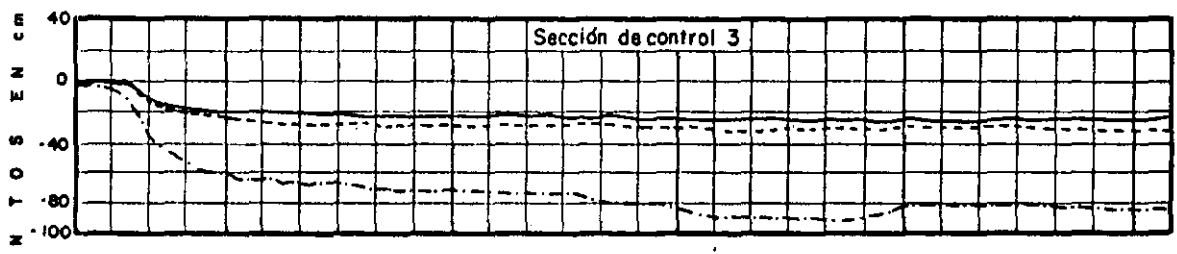
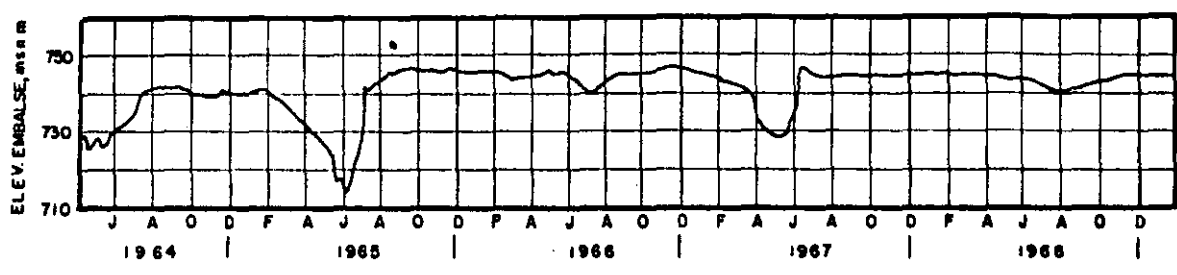
Toda el área tiene un sistema de control de desplazamientos horizontales y verticales a base de extensómetros superficiales eléctricos y mecánicos, bancos de nivel, líneas de colimación, inclinómetros, vertedores y piezómetros.



Se estabilizó el talud colocando 100 000 m<sup>3</sup> de material en la zona resistente.



Zona de deslizamiento cercana al vertedor de la presa Santa Rosa, Jal.  
localización de instrumentos de observación

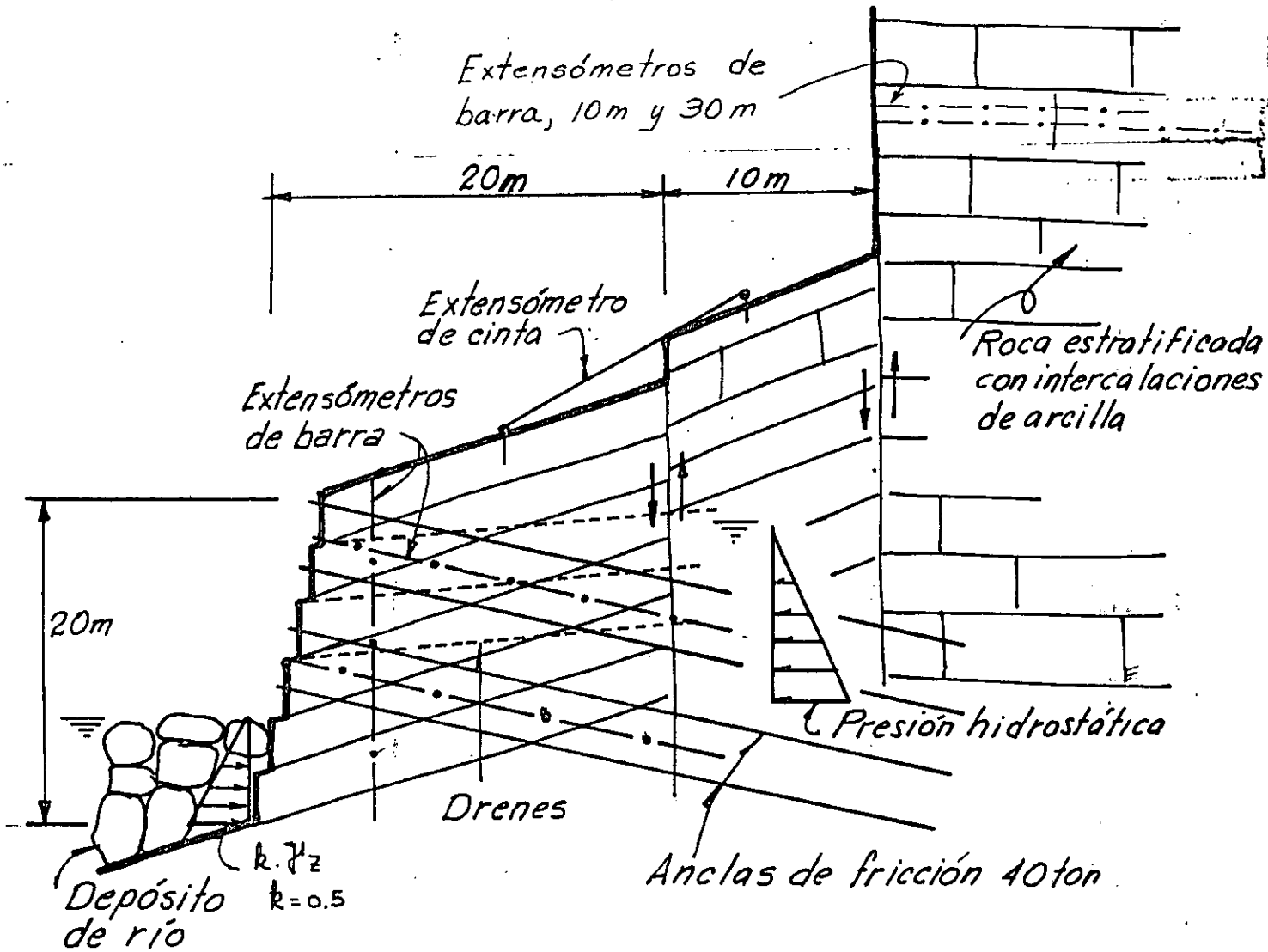


Movimientos verticales - - - - -  
Movimientos // al alineam. ————  
Movimientos ⊥ al alineam. - - - - -

Desplazamientos verticales y horizontales en dos estaciones del vertedor de Santa Rosa

ANCLAJES EN TALUDES EN LA P.H. CHICOASEN, CHIS.

Cauce del río. Caliza estratificada con intercalaciones de arcilla. Se utilizaron 570 anclas de fricción de  $\varnothing 1\ 1/2$ " acero grado duro, con longitud variable entre 24 m y 32 m. Al profundizar la excavación se fueron realizando barrenos de drenaje. El control de desplazamientos se realizó mediante extensómetros mecánicos y superficiales complementados con nivelación de precisión.



TALUD SOPORTADO CON ANCLAS DE FRICCIÓN

ROCA ESTRATIFICADA

- Anclas
- Extensómetros
- Drenes

P.H. IXTAPANTONGO, MEX.

Zona de tubería de presión junto a la casa de máquinas

La conducción a presión está constituida por tres tuberías exteriores. En el tramo de llegada a la casa de máquinas entre los machones 9 y 10 estos conductos están apoyados sobre depósitos de talud constituidos por rocas volcánicas. Desde la época de construcción entre 1945 y 1952 hasta la fecha, se han producido movimientos de tipo "creep" en la zona correspondiente al depósito de talud con una velocidad de desplazamiento del orden de 5 mm/año en dirección diagonal con la tubería .

El movimiento se inicia desde el contacto con la roca fija aproximadamente a la mitad entre los apoyos 9 y 10 hacia abajo, incluyendo el cárcamo de la casa de máquinas que también ha sido alcanzado por este efecto ocasionando desplazamientos verticales diferenciales hasta de 15 mm que llevaron a la necesidad de renivelar la unidad No. 3 en el año 1975.

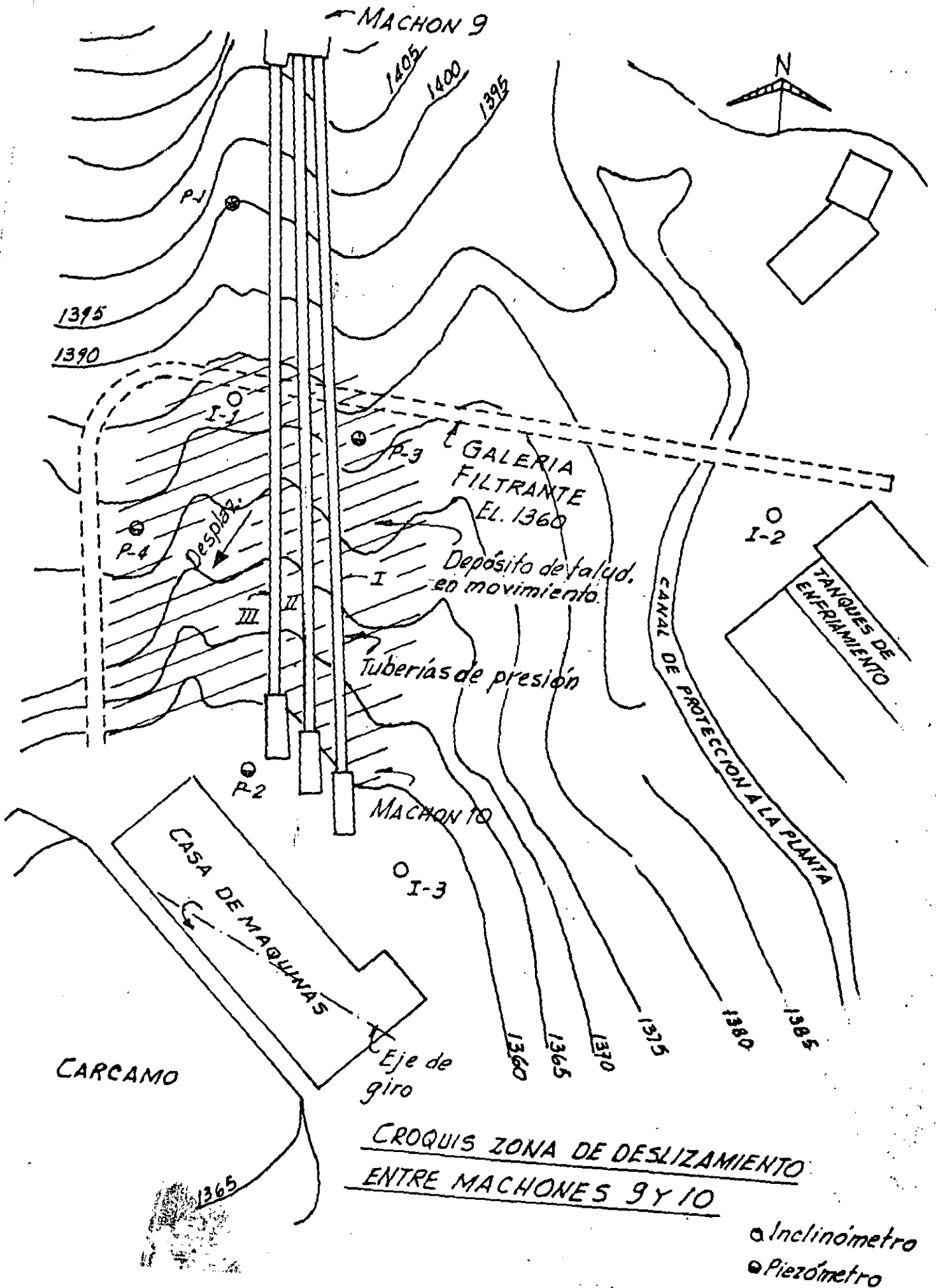
Los movimientos relativos entre el terreno y la tubería han producido empujes horizontales sobre los apoyos de las silletas de soporte que han ocasionado la ruptura de varias de ellas en vista de que no tienen libertad de desplazamiento transversal. Este efecto se ha disminuido eliminando las restricciones de los apoyos al movimiento transversal de la tubería. Se ha considerado que el movimiento del talud es ocasionado por el flujo de aguas subterráneas ya que el material de talud cubre parcialmente el cauce de un arroyo antiguo. Además de que durante las exploraciones geológicas en



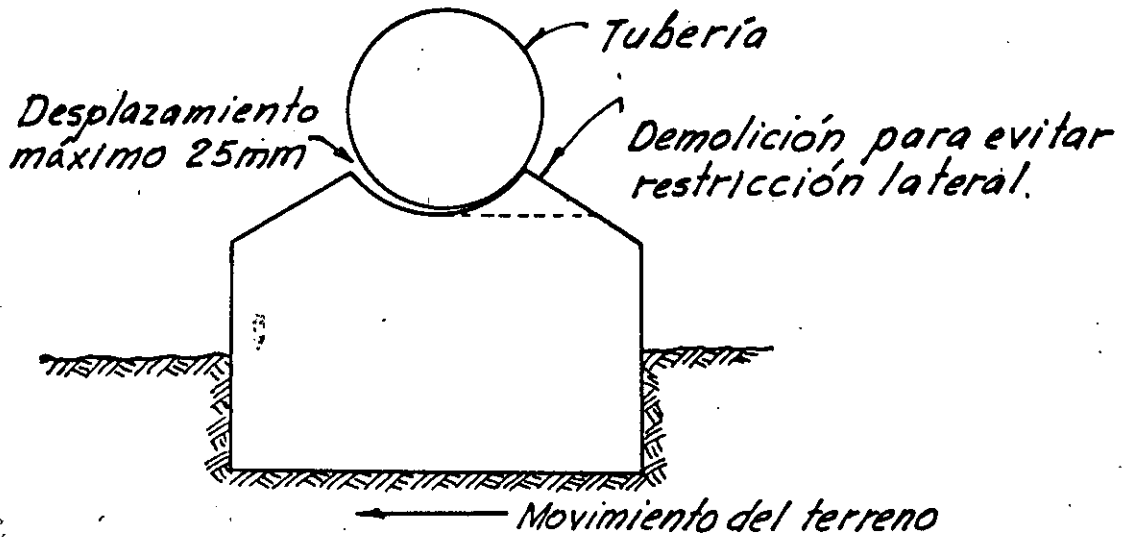
los años 1970 y 1973 se presentó artesianismo en un barreno del talud y en un barreno de la plataforma inferior de casa de máquinas. Con objeto de disminuir el movimiento de este talud en el año 1974 se construyó una galería filtrante a la elevación del pie del talud pasando a unos 25 m por debajo del terreno en la zona de contacto con la roca fija. Esta galería filtra un gasto de 4 lt/seg y faltan aún de ejecutar barrenos radiales habiéndose logrado disminuir la velocidad de movimiento a 1 mm/año.

Se tiene instalado un sistema de control de desplazamientos mediante colimación, extensómetros de cinta y nivelación de precisión, complementados con piezómetros e inclinómetros.

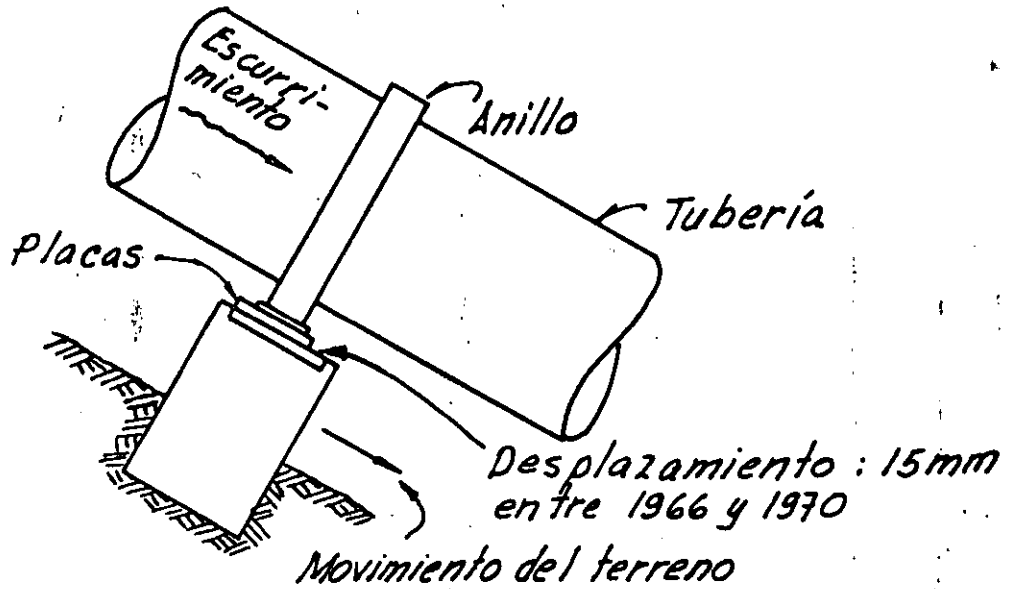
P.H. IXTAPANTONGO, MEX.



P. H. IXTAPAN TONGO, MEX.



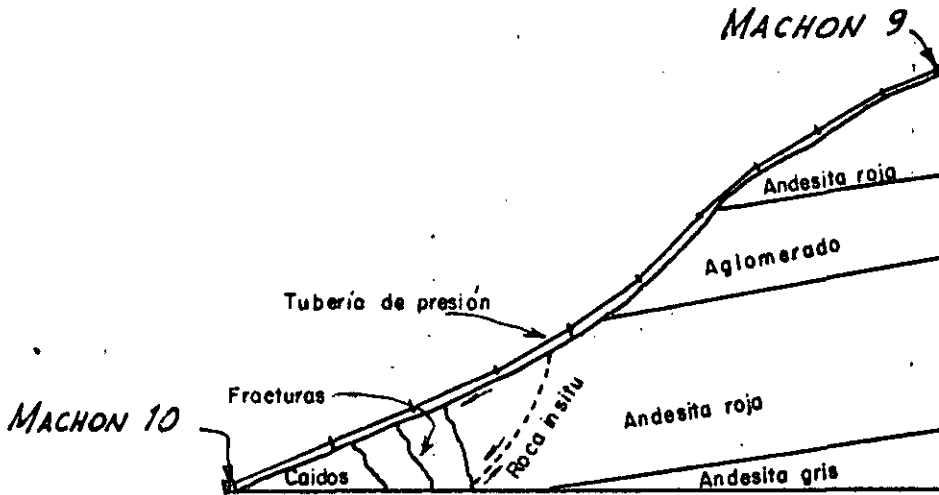
SILLETAS DE APOYO  
PARA TUBERIAS I Y II  
(Vista desde aguas abajo)



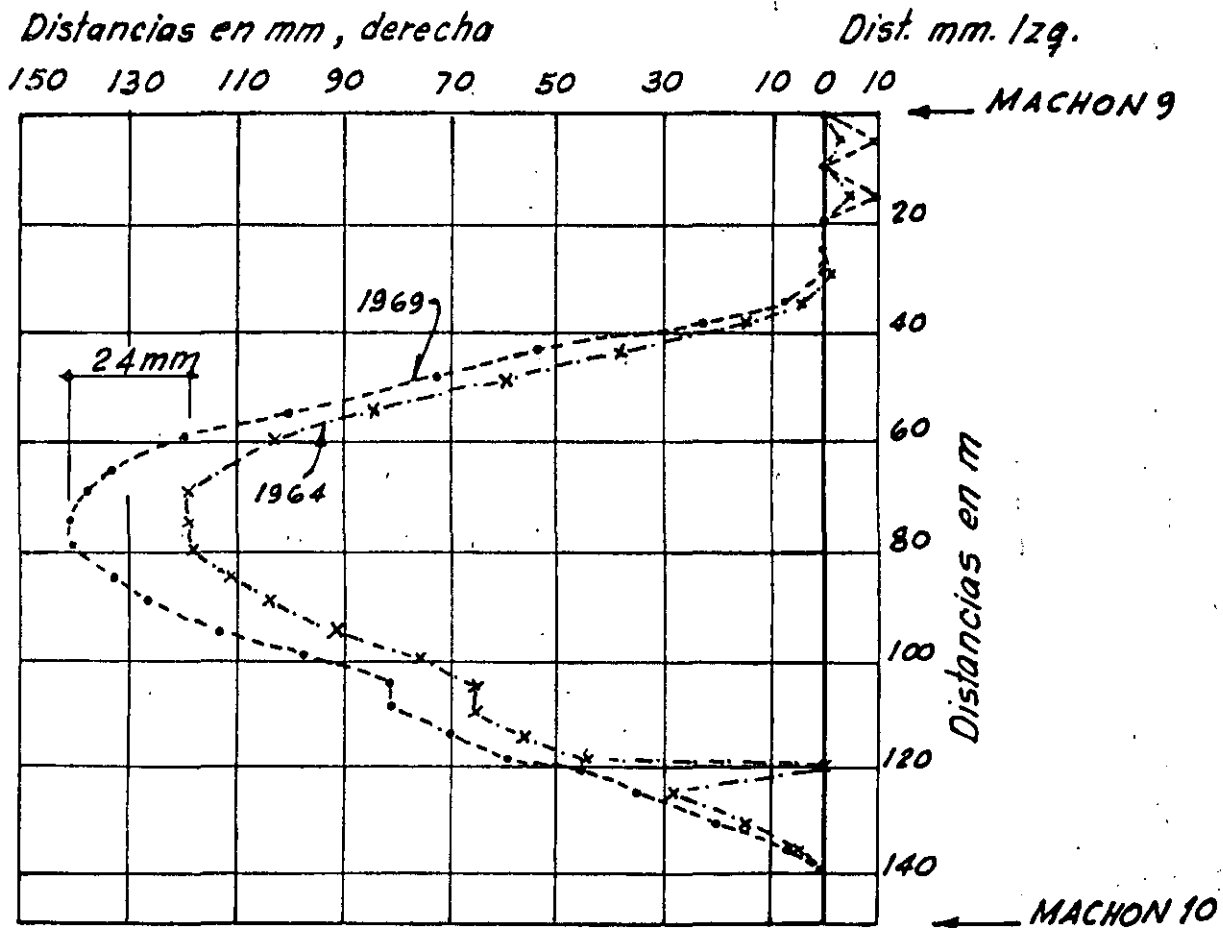
SILLETA DE APOYO  
PARA TUBERIA III

DESPLAZAMIENTOS RELATIVOS ENTRE EL TERRENO Y LAS TUBERIAS

P.H. IXTAPANTONGO, MEX.



Perfil esquematizado mostrando las trazas de los diferentes flujos y la orientación que guardan las fracturas de tensión



TUBERIA I

DESPLAZAMIENTOS HORIZONTALES

P.H. EL INFIERNILLO, MICH.

Zona de vertedores y obra de toma

Los portales de entrada de los túneles vertedores y de toma sobre la margen izquierda, quedaron localizados en la formación del conglomerado silicificado con intenso fracturamiento de origen tectónico. Cuando se excavaron los portales ocurrió un desplazamiento del talud, de 2 a 3 cm, en todo el frente de excavación, a través de uno de los planos de estratificación, con formación de grietas en varias zonas del corte. Se suspendió el trabajo y se excavaron dos galerías de exploración. A 5 m del frente, apareció una franja de roca intensamente fracturada y alterada. El resultado de estas investigaciones fué: 1) desplazar las estructuras del vertedor 12 m hacia el río, con objeto de reducir el volumen de la excavación y 2) aplicar en todos los cortes de esta zona, una poscompresión de 7 ton/m<sup>2</sup> mediante anclajes con inclinación de 45° respecto a los planos de estratificación y de 18 a 25 m de profundidad.

Se utilizaron barras de 1.25 pulgadas de diámetro, espaciadas a 2.5 m tensadas a 42 ton, también se usaron anclajes formados por alambres de acero, de 7 mm de diámetro. Ambos tipos se alojaron en perforaciones de 7.5 cm, fijando a la roca el tramo interior de 4 m con mortero inyectado. Periódicamente se verifica la tensión y a partir de la segunda revisión, la pérdida de carga en las anclas ha resultado menor que 10% por año.

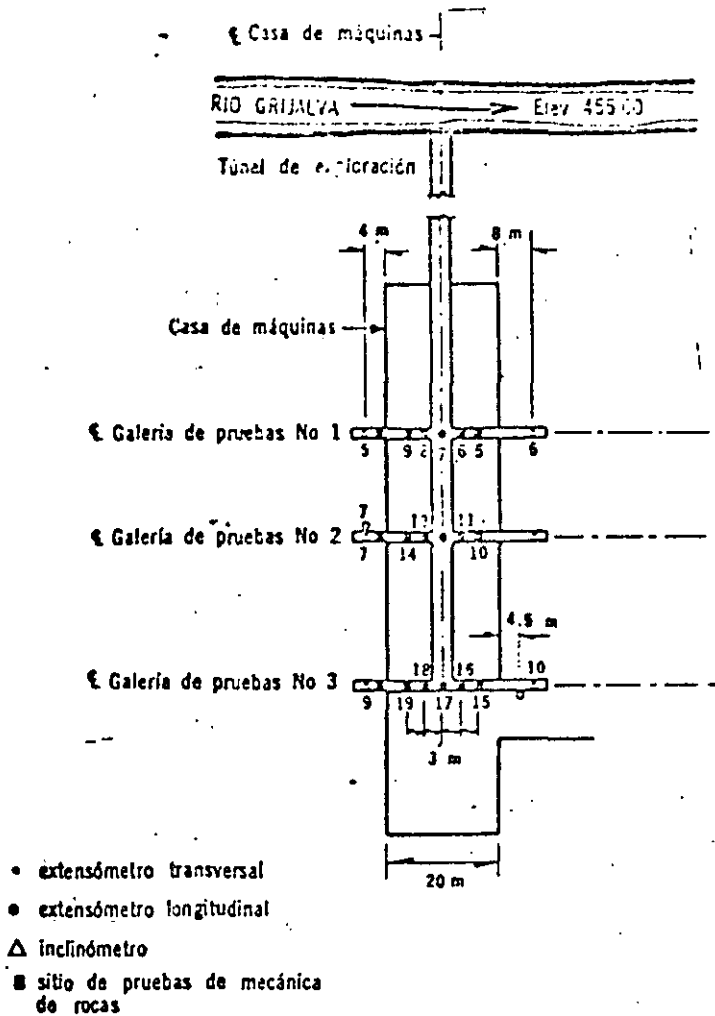


Fig 16.19a Planta de localización en la casa de máquinas, de los aparatos de medición y de los sitios de prueba. Presa La Angostura, Chis.

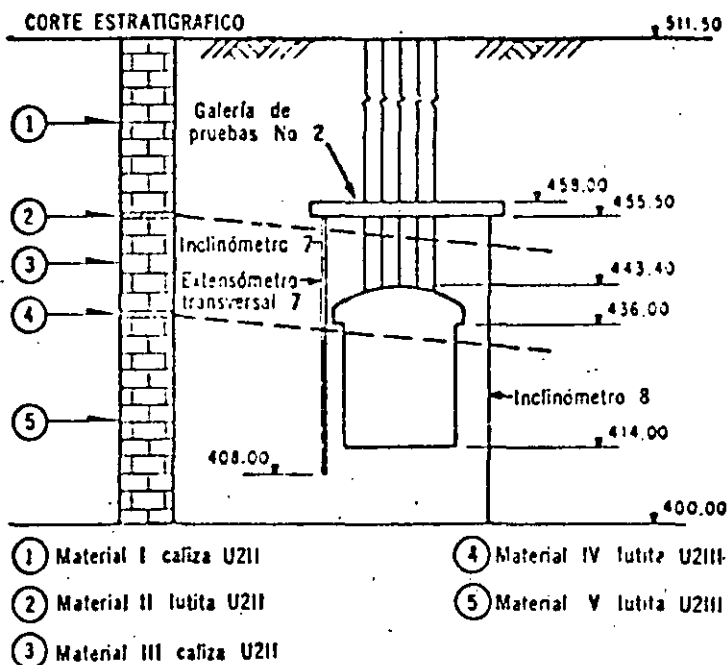
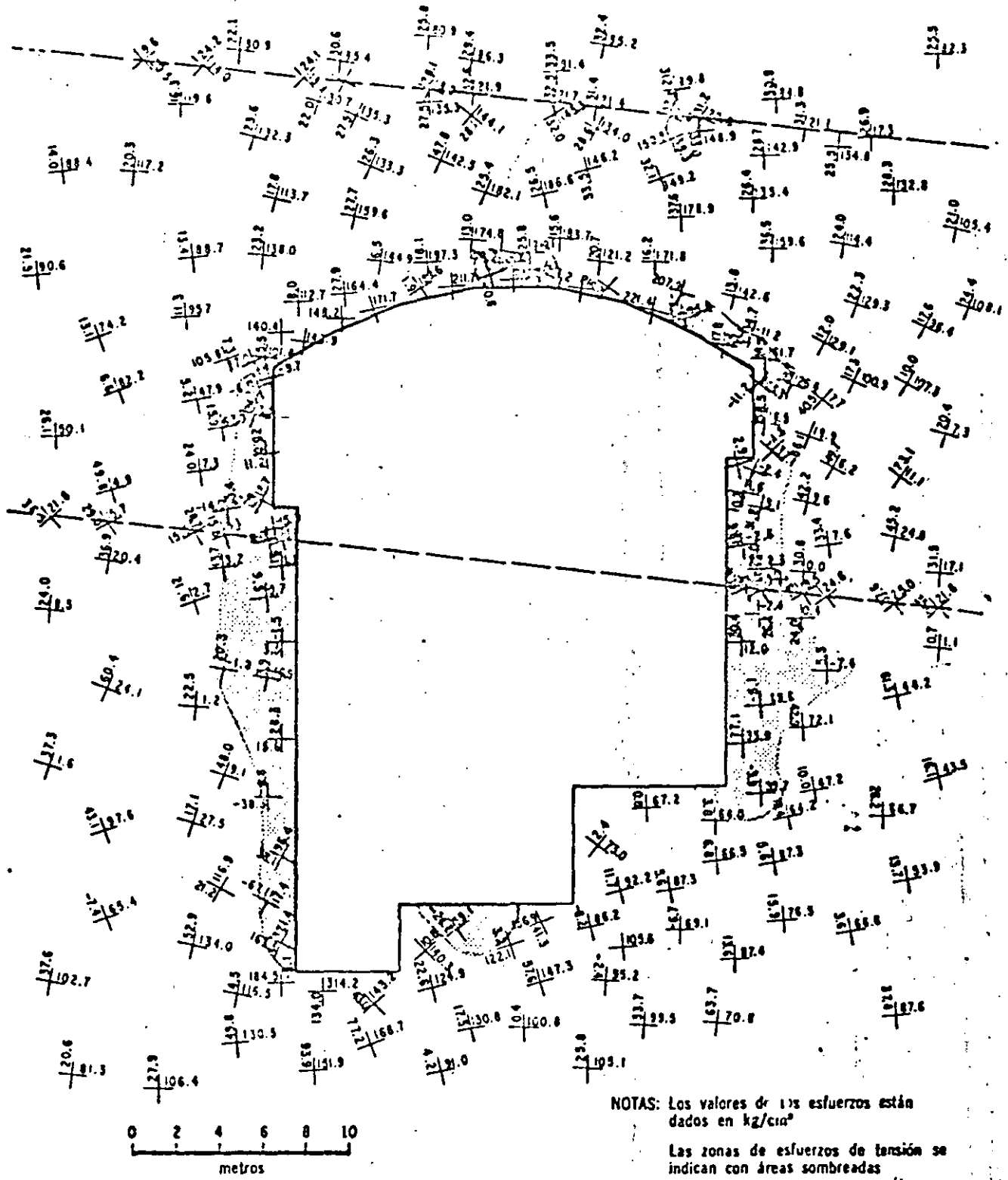
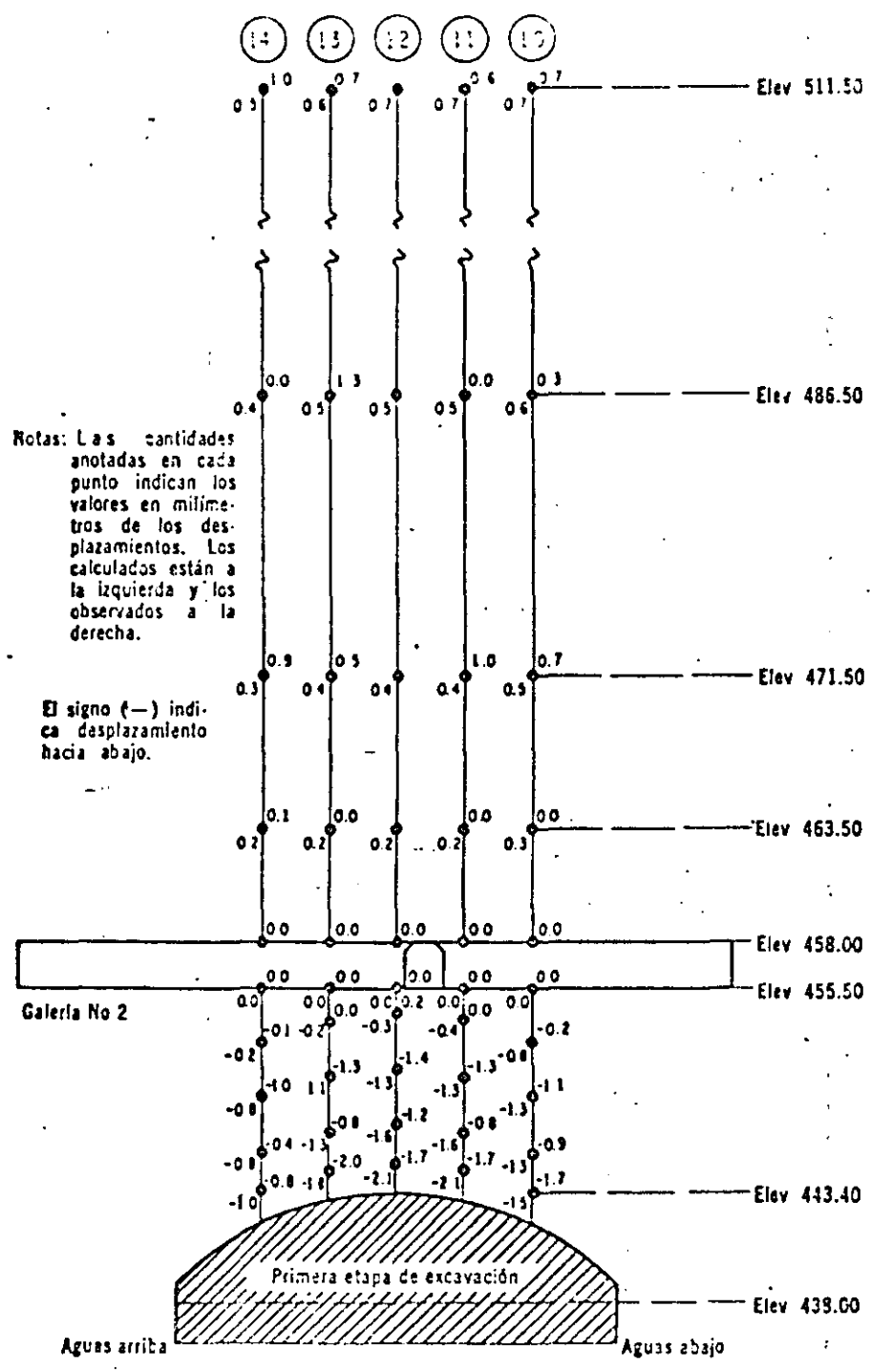


Fig 16.19b Corte en la galería de pruebas No 2. Presa La Angostura, Chis.



F 16.20 Distribución de esfuerzos principales en el contorno de la casa de máquinas, al término de la excavación. Presa La Angostura, Chis.



Notas: Las cantidades anotadas en cada punto indican los valores en milímetros de los desplazamientos. Los calculados están a la izquierda y los observados a la derecha.

El signo (-) indica desplazamiento hacia abajo.

Fig 16.21 Comparación de los desplazamientos calculados, suponiendo que la roca soporta tensión, y observados con extensómetros longitudinales, referidos al techo y al piso de la galería de instrumentación. Presa La Angostura, Chis.

cavación. En la parte central de la bóveda los esfuerzos de compresión son elevados y hasta mayores que la resistencia a la compresión simple de la roca (220 kg/cm<sup>2</sup>, en promedio, para la formación U 2 II). Se presentan, también, concentraciones de esfuerzos de compresión por debajo del piso de la casa de máquinas.

A raíz de ese análisis se recomendó la colocación, a tresbolillo, de anclas de 15 m de longitud en las paredes verticales de la excavación, según hileras distantes entre sí de 2.5 m en la direc-

ción vertical y de 5 m según la dirección horizontal. Como se comprobó analíticamente, a carga de 10 ton impuesta por cada una de estas anclas a la roca, no modifica apreciablemente la magnitud de los esfuerzos en el contorno de la excavación; sin embargo, dichas anclas son útiles para evitar los caídos delimitados por fisuras de tensión. La excavación de la casa de máquinas, hoy día concluida, se pudo efectuar en estas condiciones sin problemas ni demoras.

A fin de comprobar los resultados numéricos



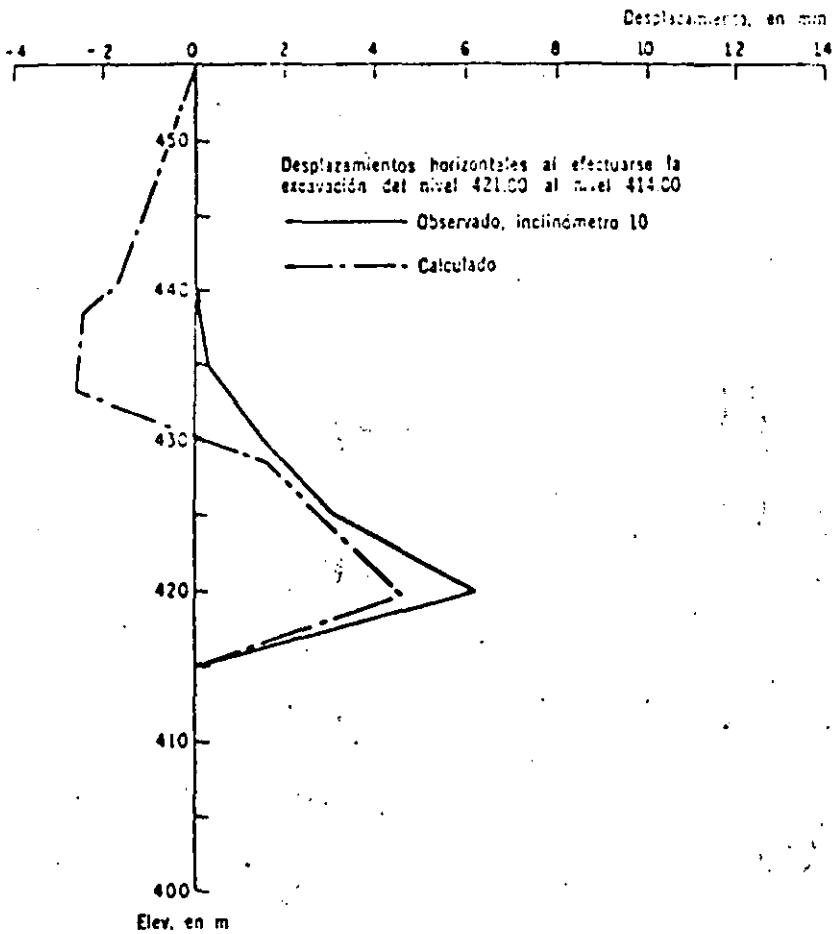


Fig 16.23 Desplazamientos horizontales observados y calculados. Tercera etapa de excavación. Inclinómetro 10. Casa de máquinas de la presa La Angostura, Chis.

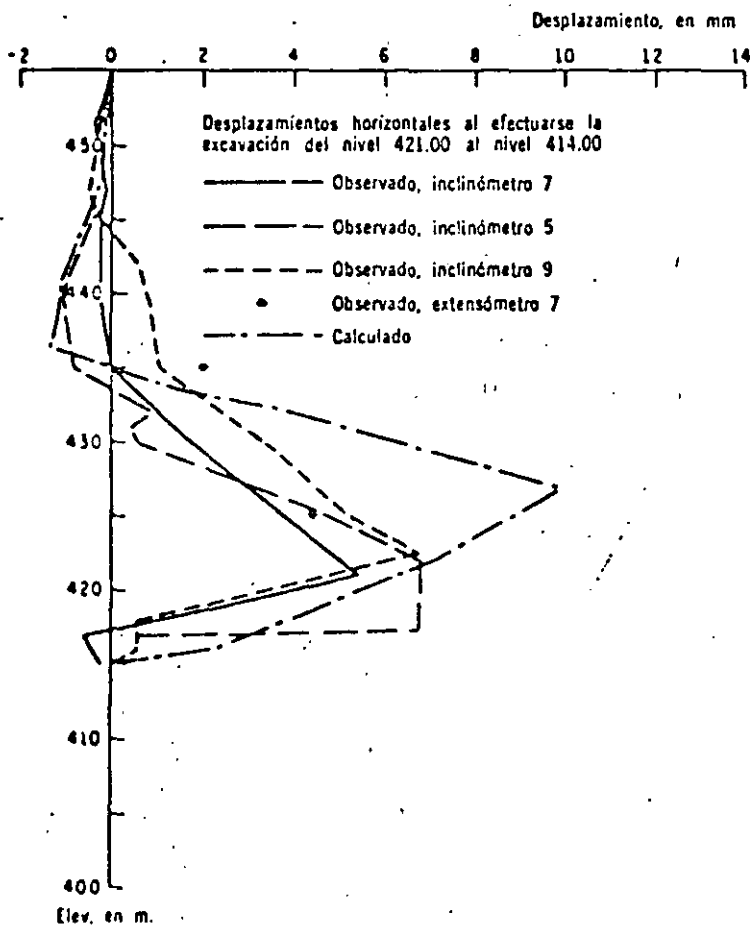
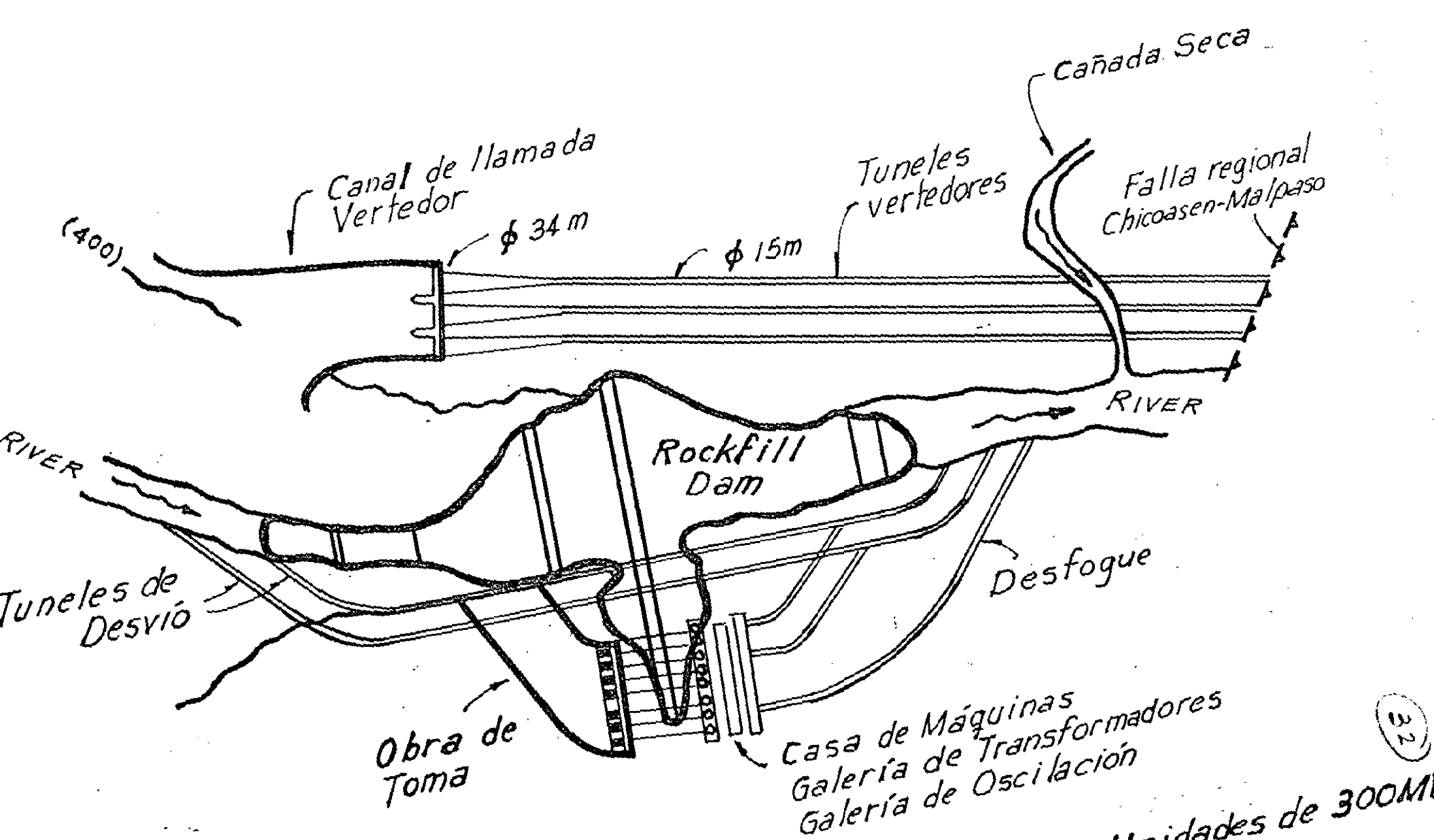
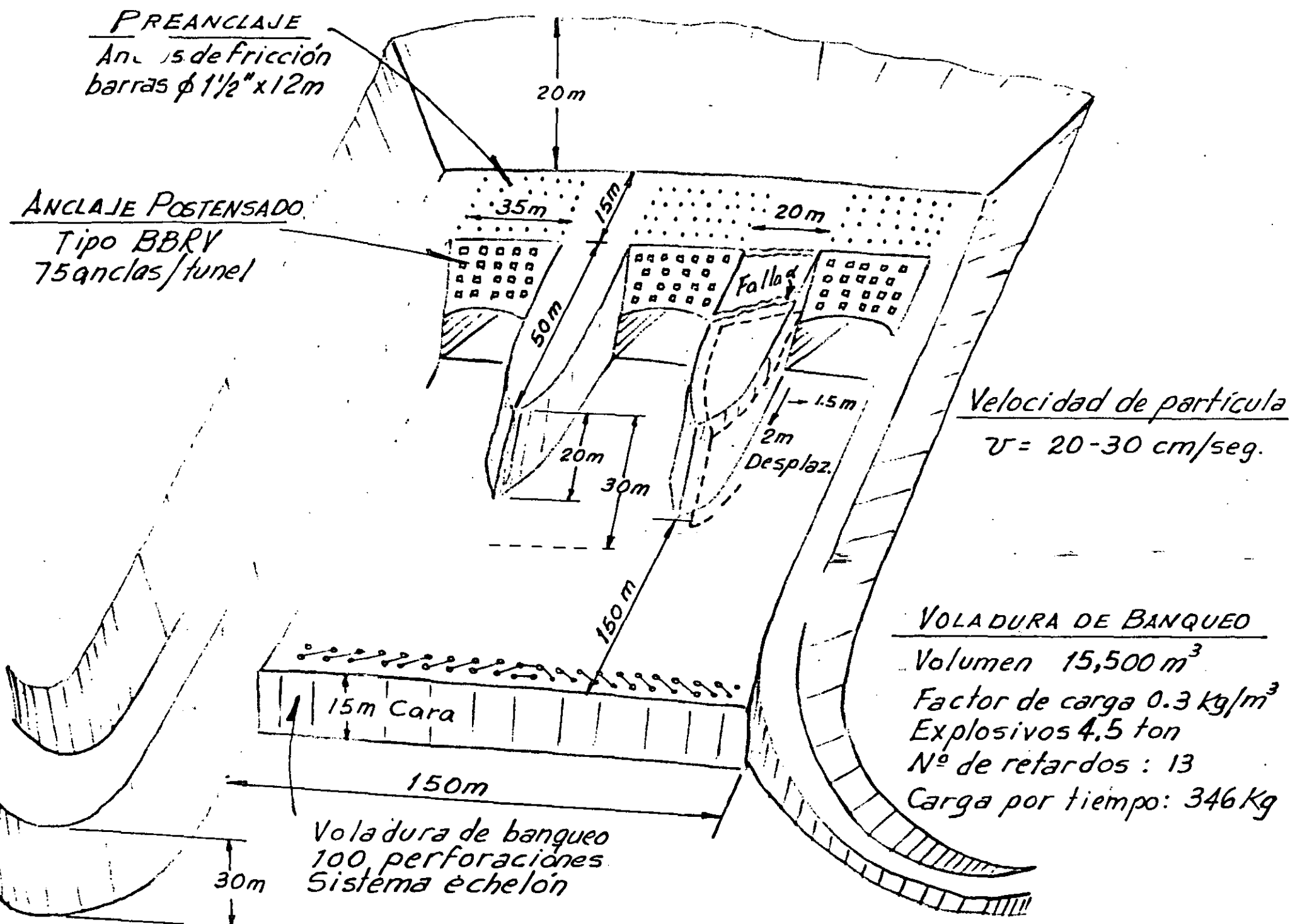


Fig 16.24 Desplazamientos horizontales observados y calculados. Tercera etapa de excavación. Inclinómetros 5, 7 y 9; extensómetro 7. Casa de máquinas de la presa La Angostura, Chis.



PLANTA  
P.H. CHICOASEN

8 Unidades de 300M  
 Altura 264 m  
 Volumen  $14 \times 10^6 m^3$



PREANCLAJE  
Anclajes de fricción  
barras  $\phi 1\frac{1}{2}'' \times 12m$

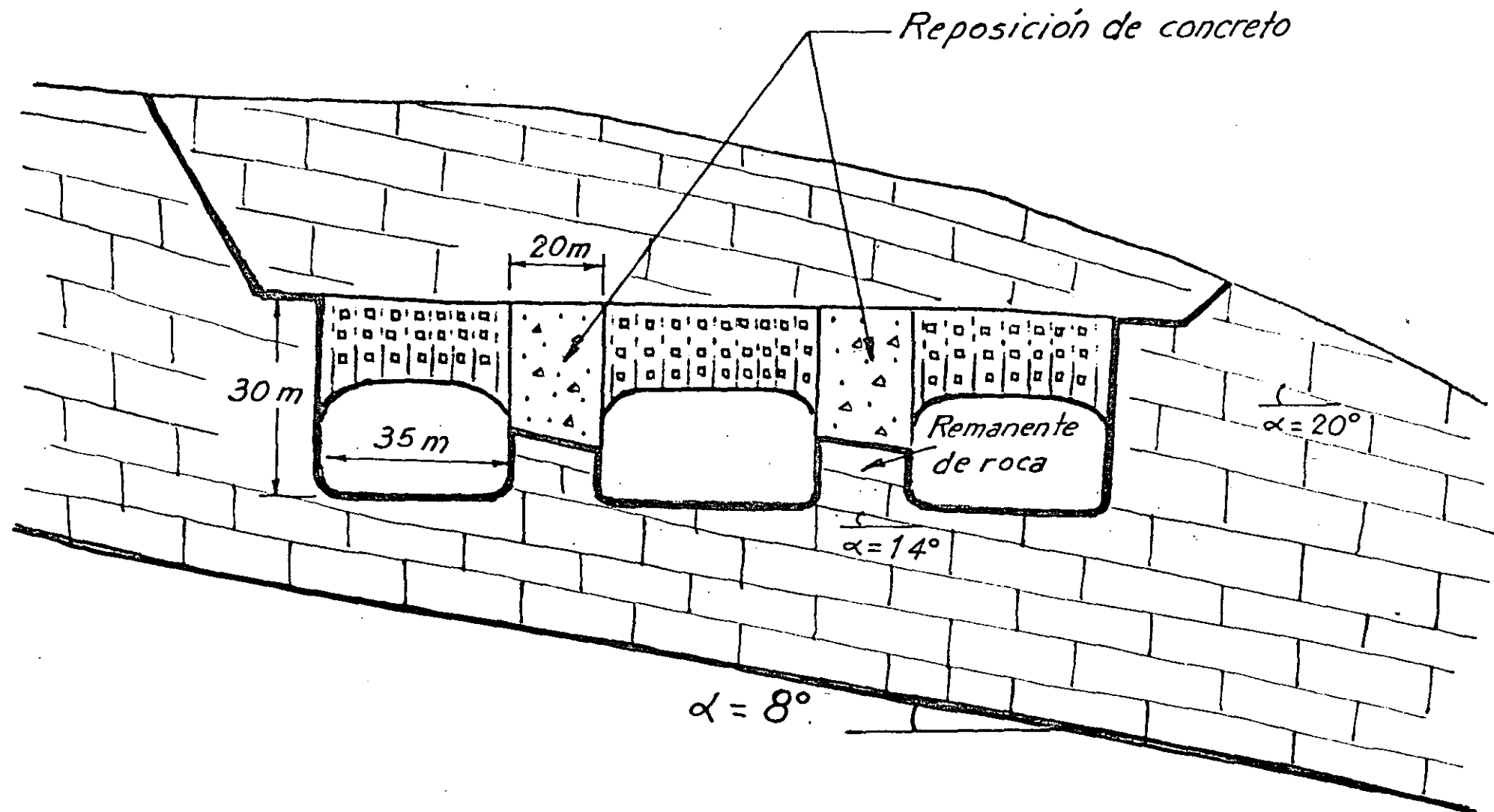
ANCLAJE POSTENSADO  
Tipo BBRV  
75 anclas/tunel

Velocidad de partícula  
 $v = 20-30 \text{ cm/seg.}$

VOLADURA DE BANQUEO  
Volumen  $15,500 \text{ m}^3$   
Factor de carga  $0.3 \text{ kg/m}^3$   
Explosivos  $4.5 \text{ ton}$   
Nº de retardos : 13  
Carga por tiempo:  $346 \text{ Kg}$

Voladura de banqueo  
100 perforaciones  
Sistema échelon

CANAL DE LLAMADA, VERTEDOR

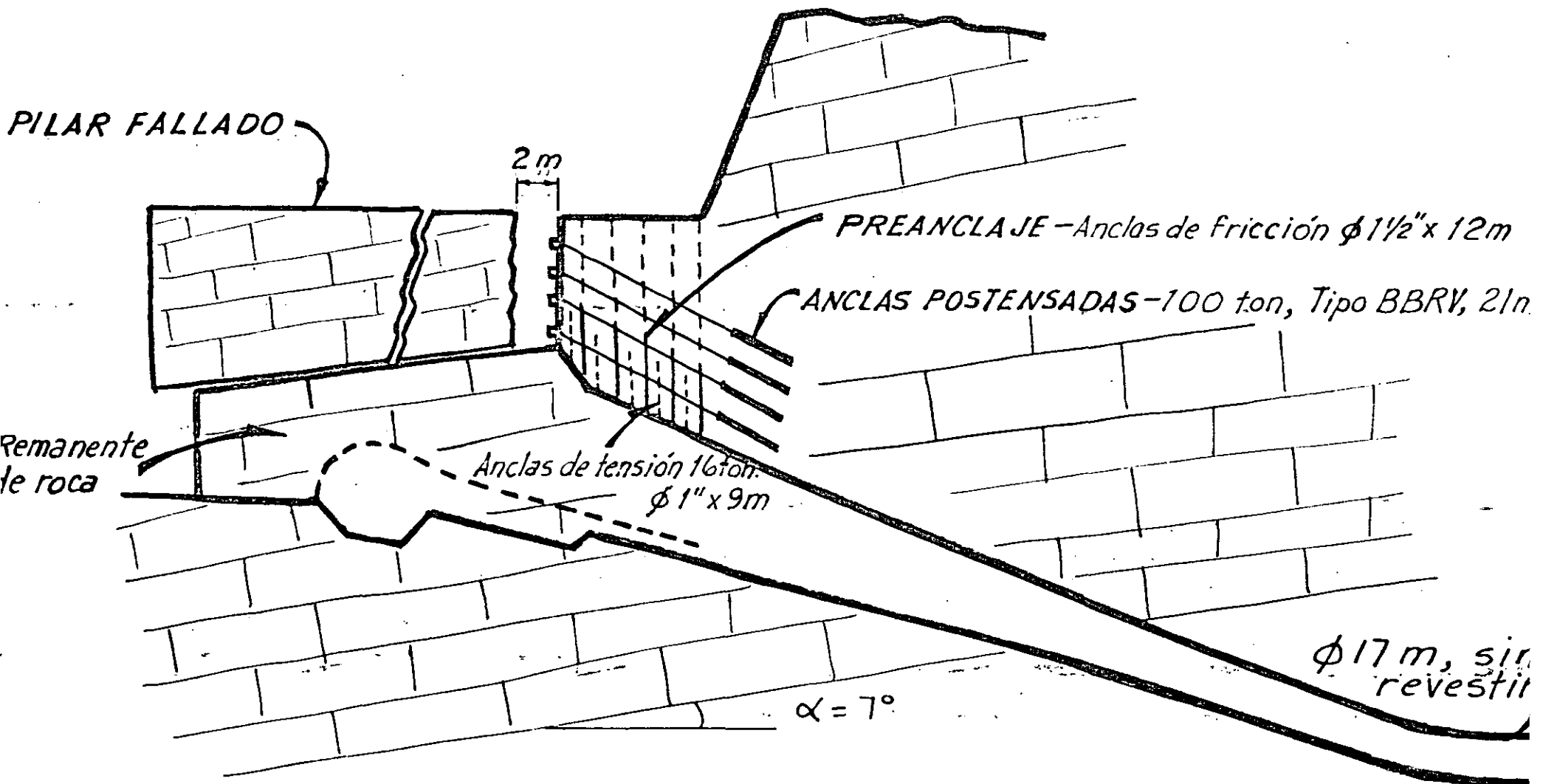


SECCION TRANSVERSAL

CANAL DE LLAMADA, VERTEDOR

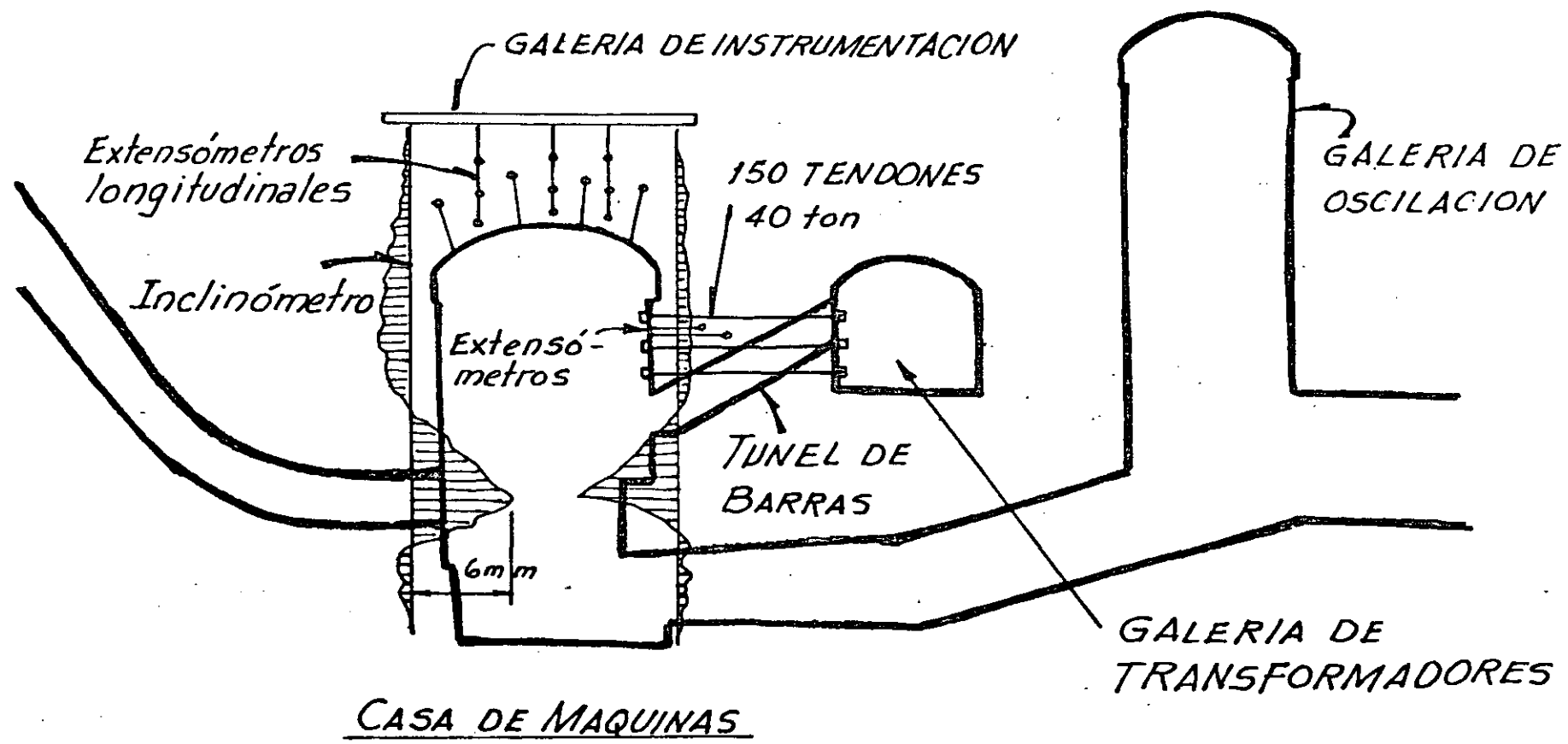
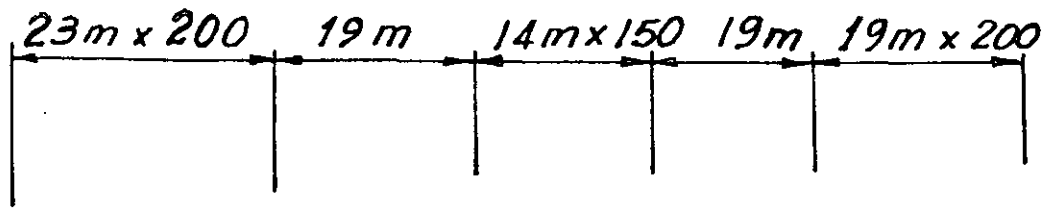
FIG. 3

(34)



SECCION LONGITUDINAL

CANAL DE LLAMADA, VERTEDOR



SECCION TRANSVERSAL  
PLANTA HIDROELECTRICA, CHICOASEN  
(CALIZAS)

EFFECTO DE REFLEXION-REFRACCION

BLOQUE GIRADO

1ª ETAPA - BALCONEO

2ª ETAPA - VOLADURA TRINCHERA

ACUEDUCTO

TREN DE ONDAS

PLANO DE DEBILIDAD

100 m

MONTAÑA

TRINCHERA

PLANTA

SECCION TRANSVERSAL DEL TALUD

ACUEDUCTO RIO COLORADO-TIJUANA

FIG. 6

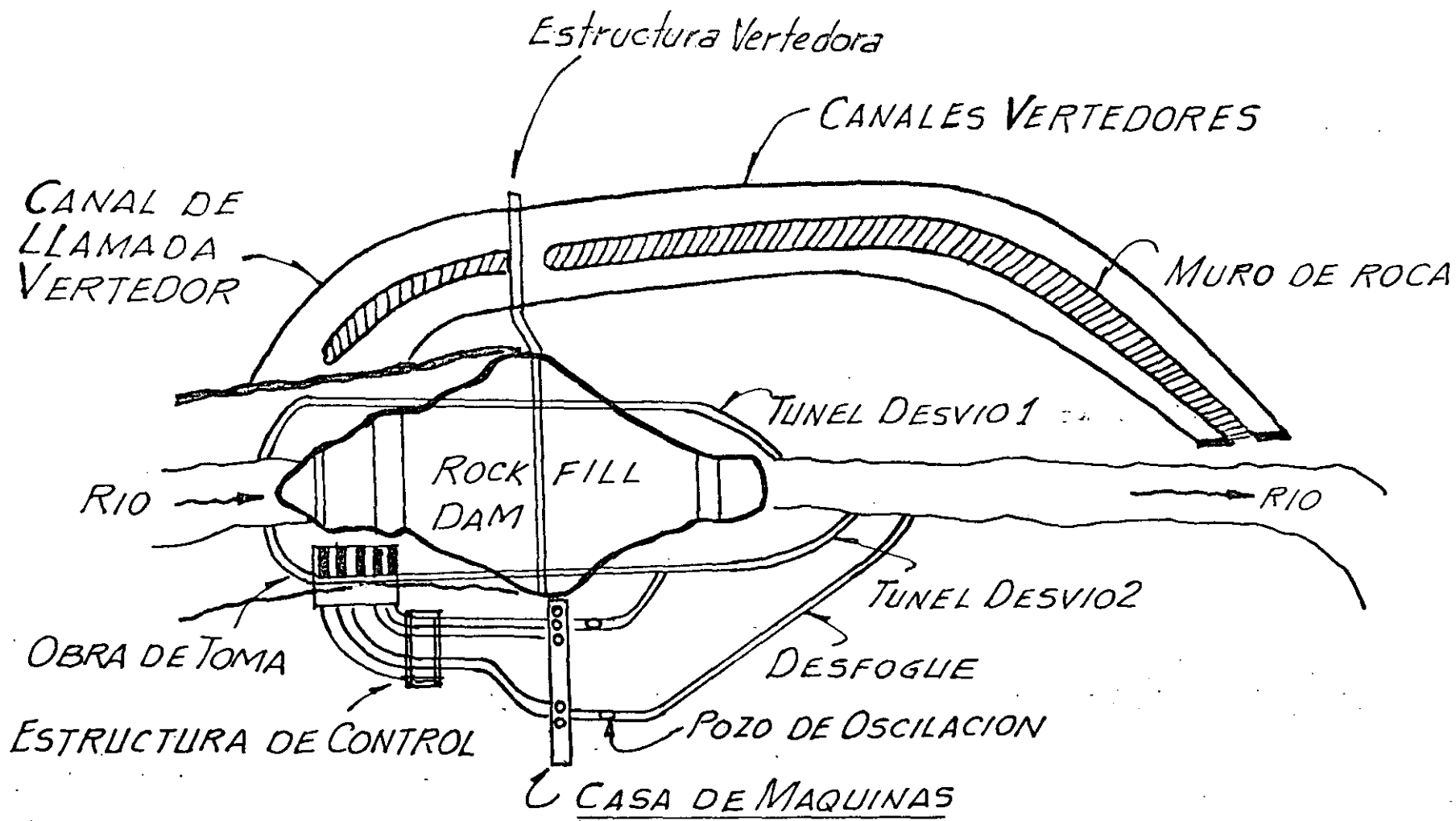
(37)

¿ QUE PODEMOS HACER PARA EVITAR LA FALLA DE UN TALUD ?

- 1.. CALCULAR EL MAXIMO VALOR DE g PARA LA ESTABILIDAD CRITICA
- 2.. DISEÑAR VOLADURAS CONTROLADAS A MODO DE NO ALCANZAR EL g CRITICO.
- 3.. EJECUCION EN EL CAMPO CON PERSONAL ENTRENADO, CONTROL DE CALIDAD Y MONITOREO

13 en total





PLANTA

P.H. LA ANGOSTURA

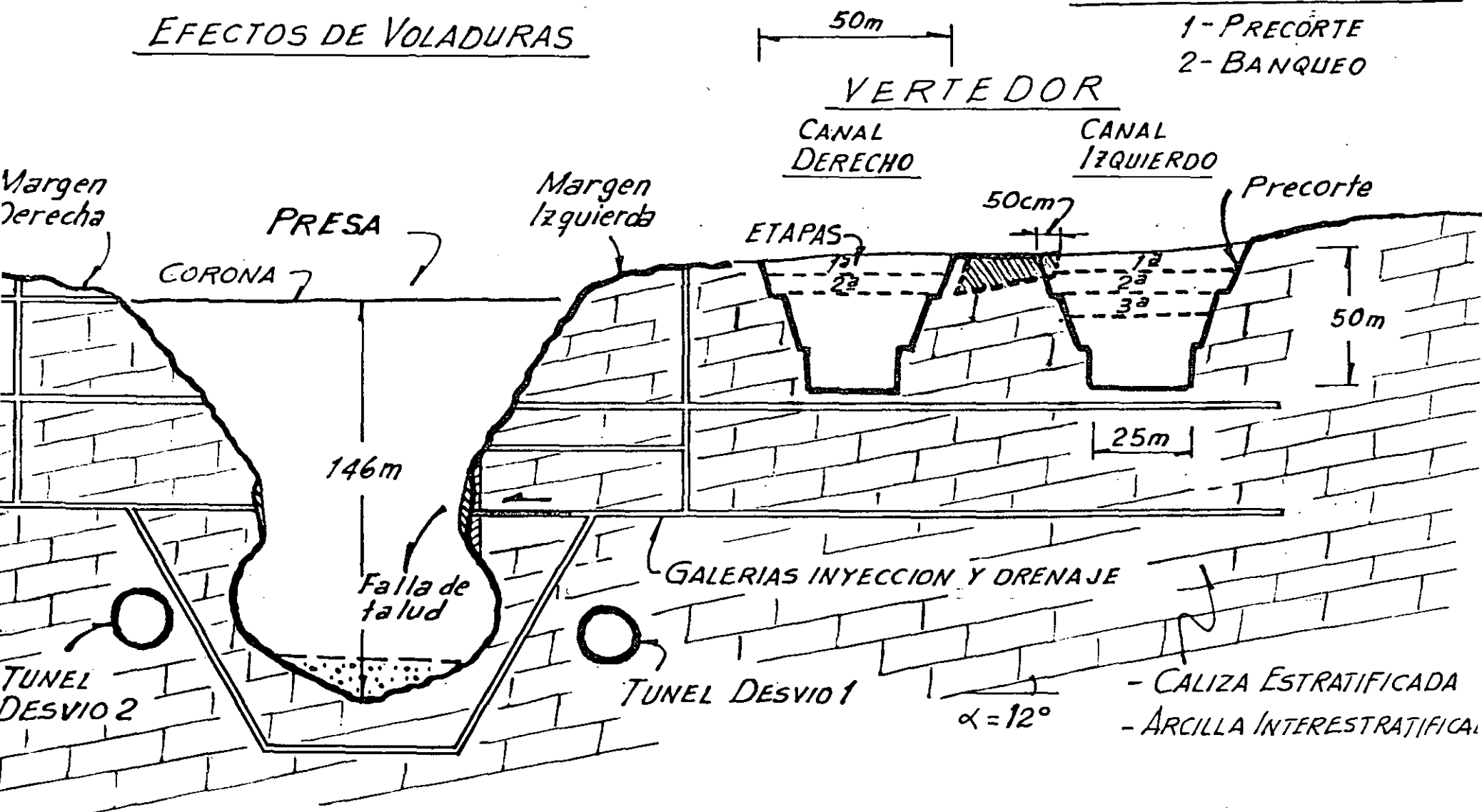
ALTURA PRESA...146m  
 VOLUMEN... $5 \times 10^6 \text{ m}^3$   
 5 UNIDADES DE 180 MW

FIG. 8

EFFECTOS DE VOLADURAS

SECUENCIA DE EXCAVACION

- 1- PRECORTE
- 2- BANQUEO



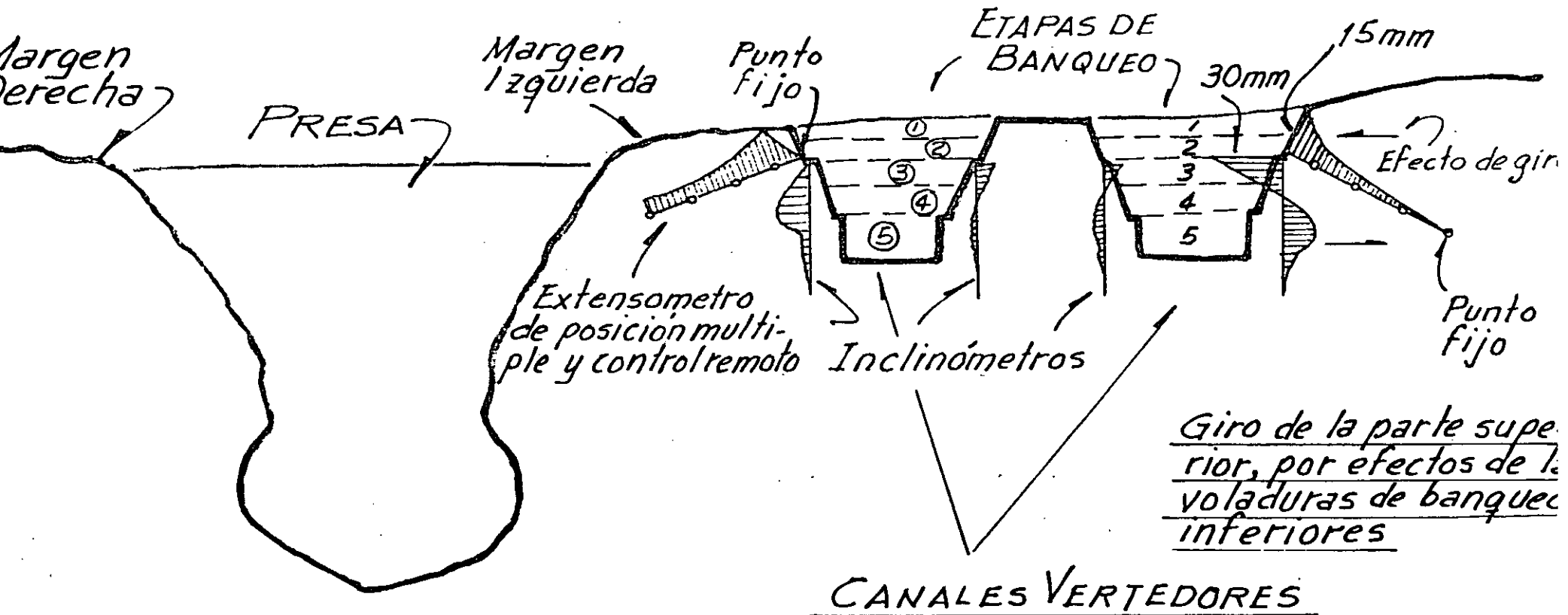
SECCION TRANSVERSAL

PRESA LA ANGOSTURA

Vista de aguas abajo hacia aguas arriba

FIG. 9

EFFECTOS DE VOLADURAS DE BANQUEO EN LOS  
CANALES VERTEDORES

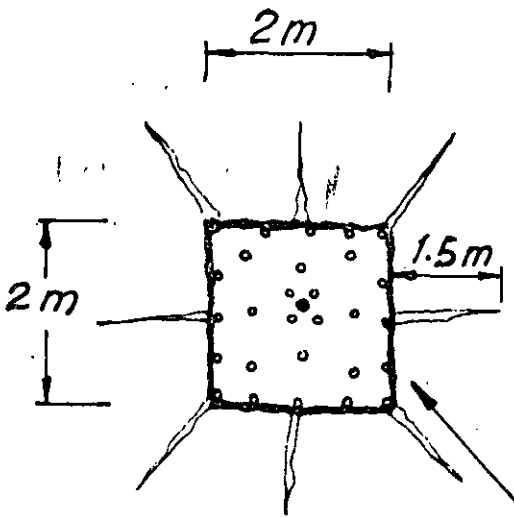


SECCION TRANSVERSAL

Vista de aguas abajo hacia aguas arriba

P. H. LA ANGOSTURA

Los desplazamientos hacia la montaña, en la parte inferior no concuerdan con los calculados.

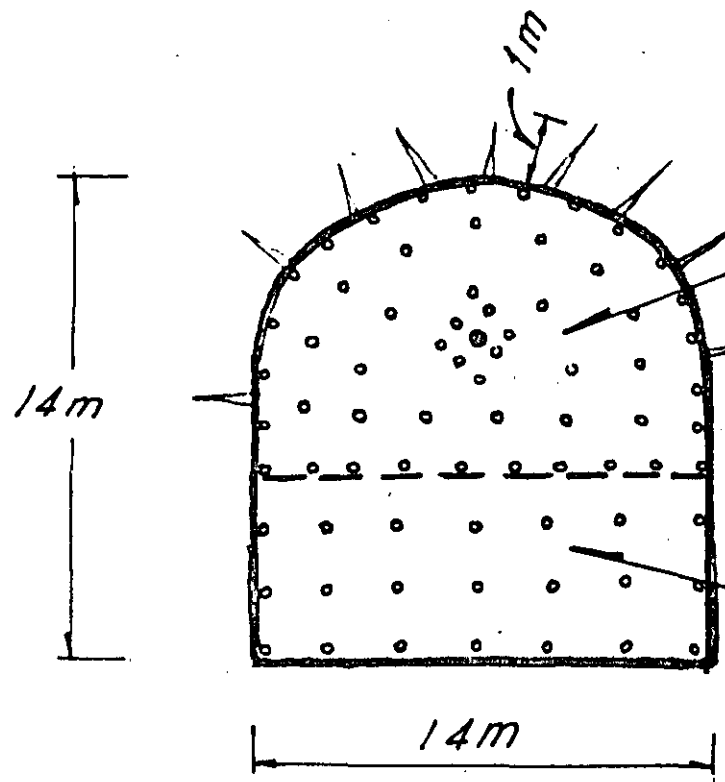


LEVANTAMIENTO GEOFISICO

SMOOTH BLASTING Long. fracturas 1.5m  
 (Efecto de Confinamiento)  
PRESPLITTING Long. fracturas 10cm

El efecto de confinamiento es muy importante en la liberación de energía

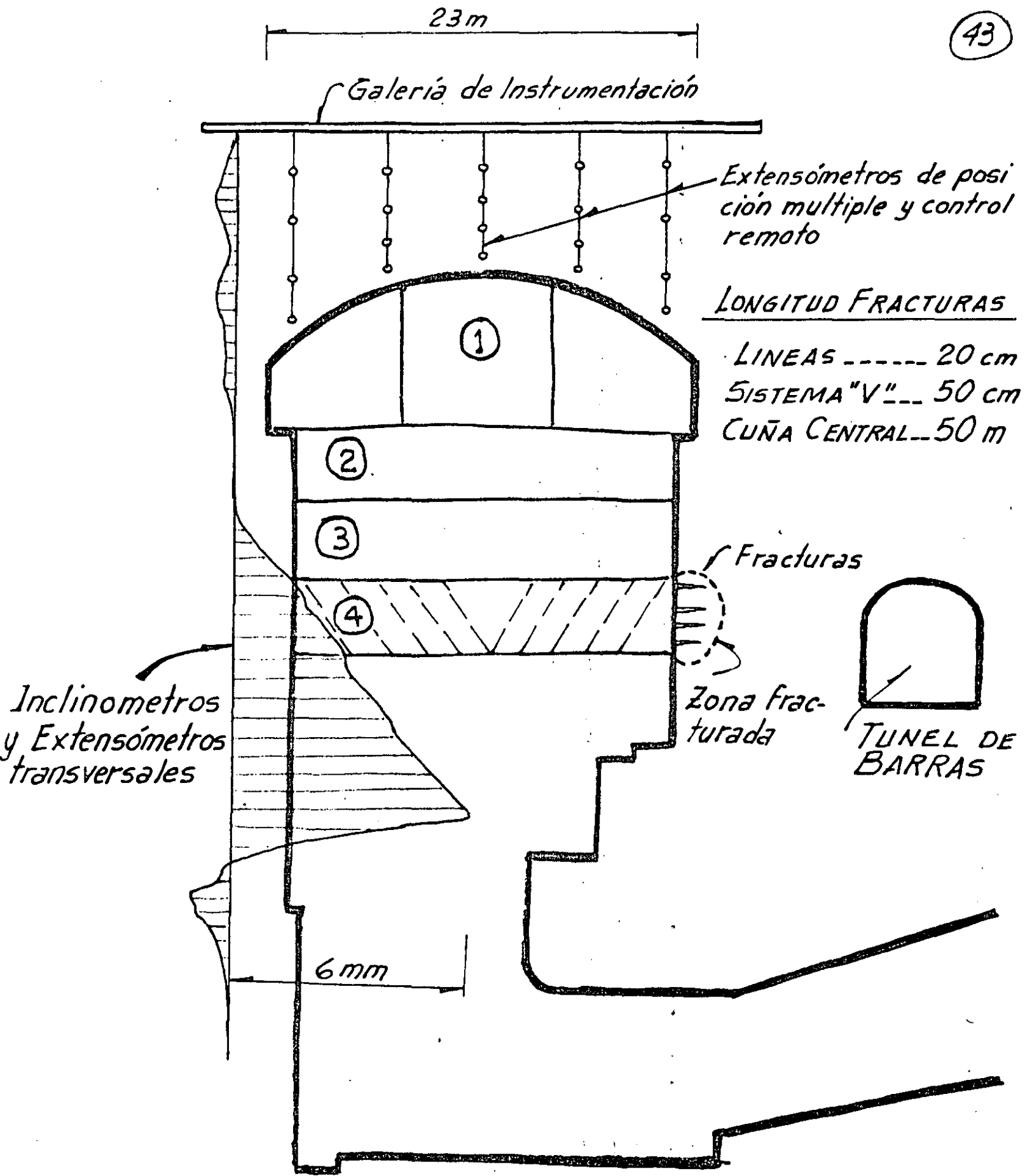
SOCAVONES EXPLORATORIOS (CALIZAS)



1ª ETAPA  
SMOOTH BLASTING  
 Long. fracturas 1.0m  
Efecto importante de confinamiento

2ª ETAPA  
BANQUEO  
No hay confinamiento

SECCION PORTAL TUNEL (Calizas)

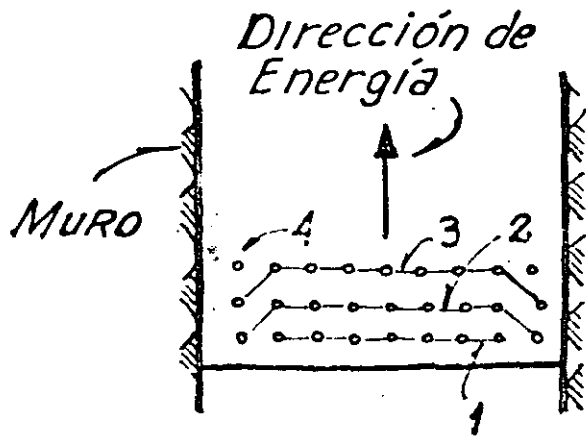


CASA DE MAQUINAS

FIG. 12

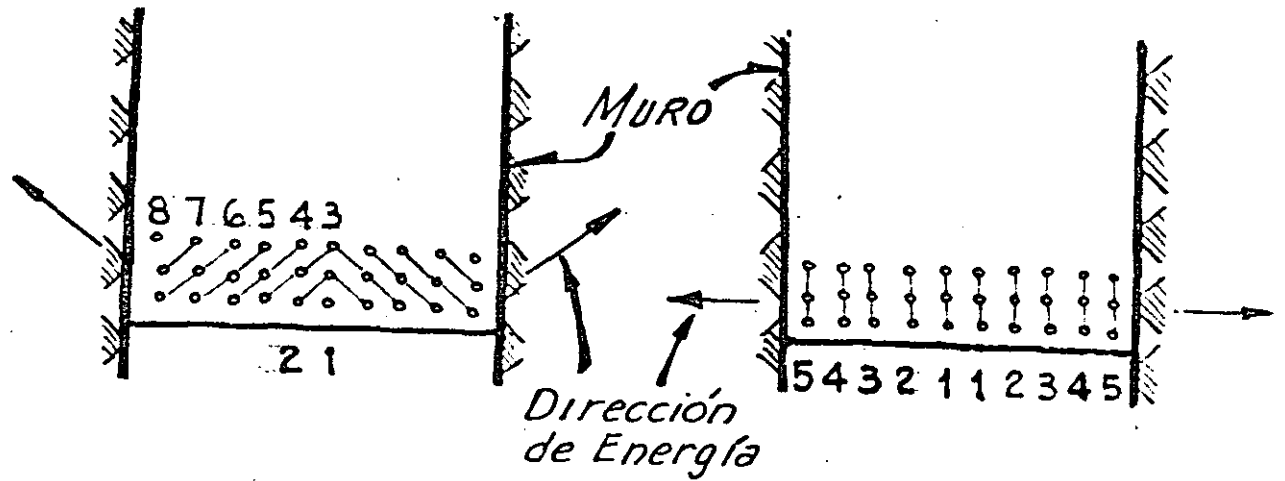
EFFECTOS DE VOLADURAS DE BANQUEO

# TIPOS DE VOLADURAS DE BANQUEO



LINEAS

20 cm



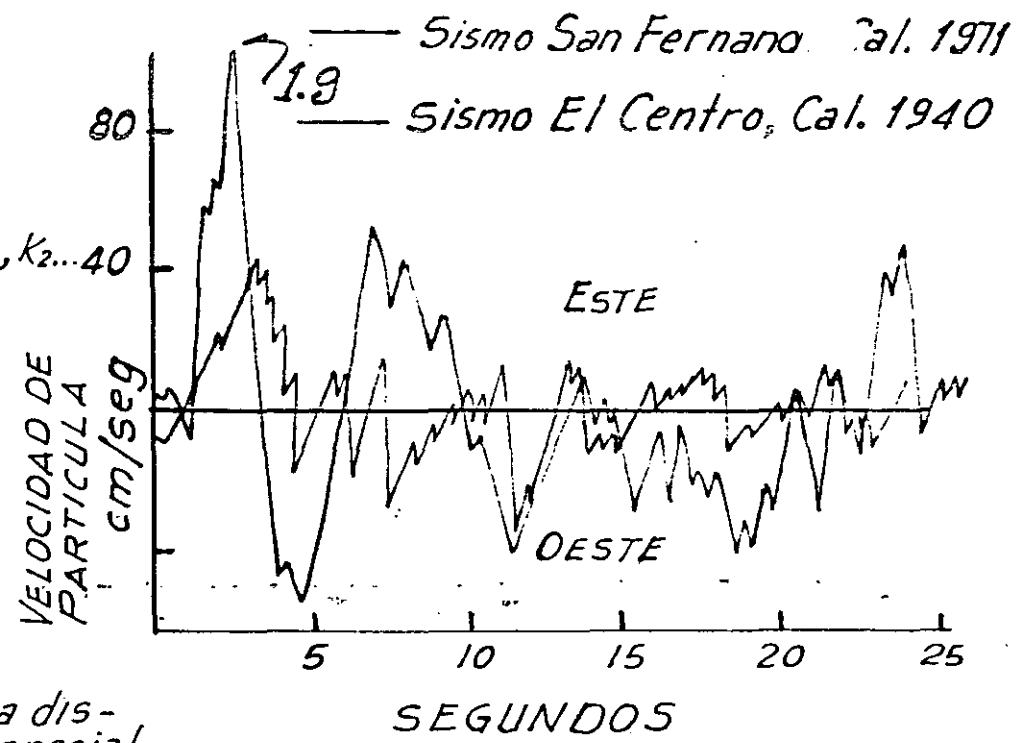
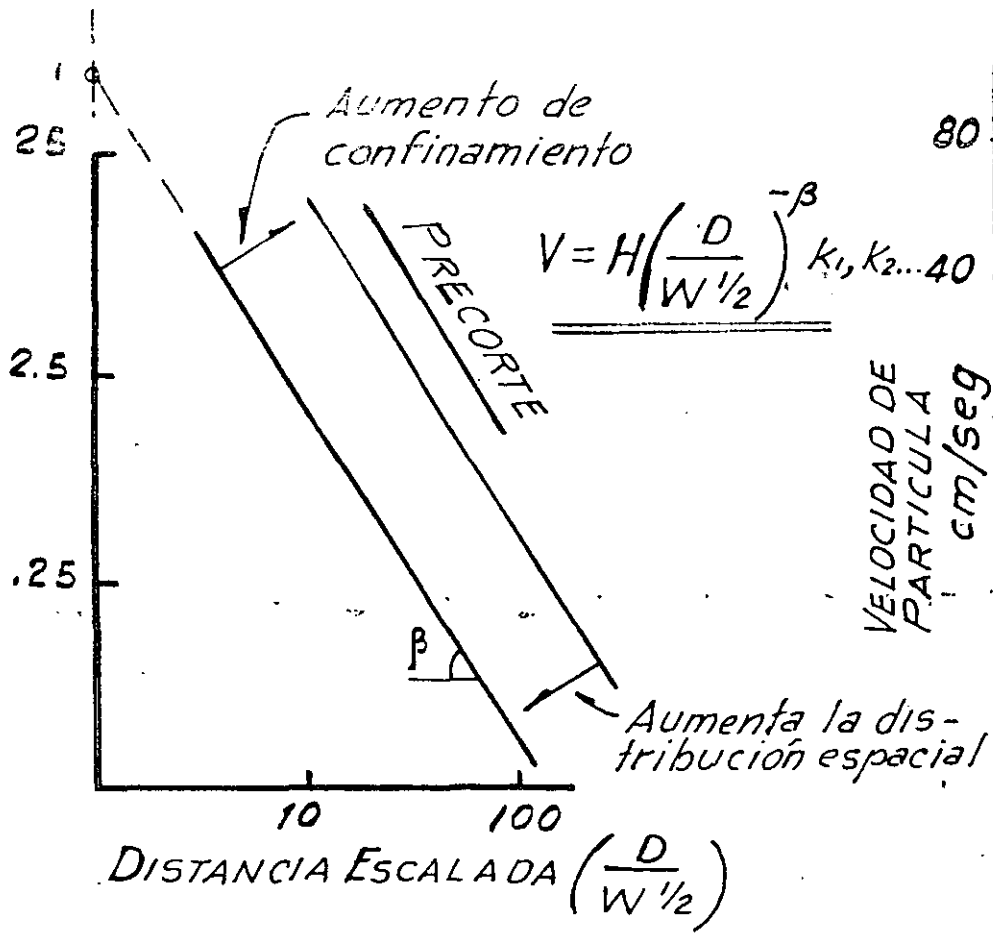
SISTEMA EN "V"

50 cm

CUÑA CENTRAL

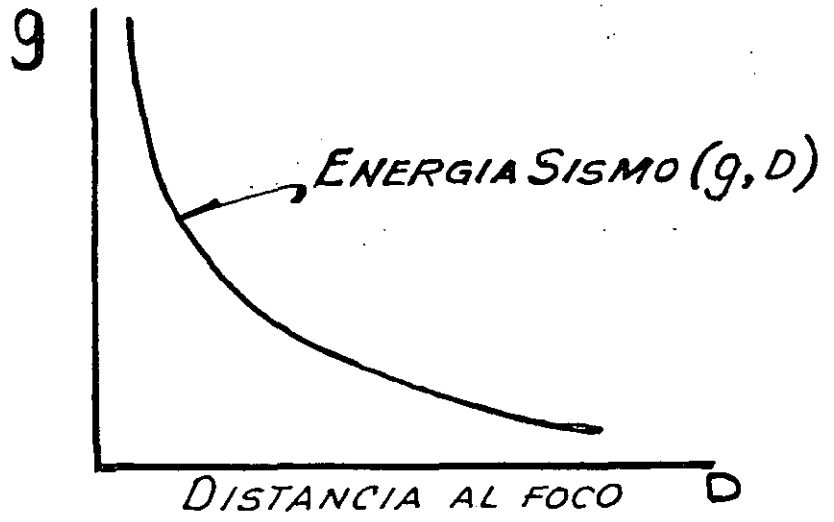
50 cm

VELOCIDAD DE PARTÍCULA  
cm/seg



MOVIMIENTOS DEL TERRENO

VELOCIDAD DE PARTÍCULA  
cm/seg



COMPARACION ENTRE EFECTOS SISMICOS Y DE VOLADURAS

FIG. 14

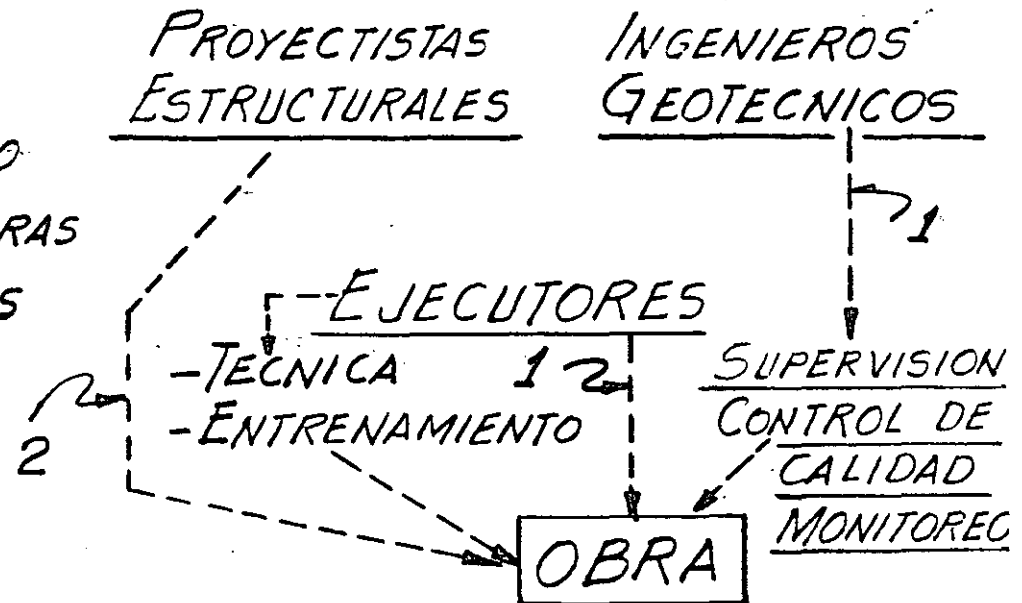
45

# PRODUCCION CONTRA SEGURIDAD

## FACTORES QUE PRODUCEN ACCIDENTES

- CORTO TIEMPO DEL PROGRAMA CONSTRUCTIVO
- DESCONOCIMIENTO DE EFECTOS DE VOLADURAS
- DISEÑO INADECUADO DE VOLADURAS
- AUSENCIA DE MONITOREO
- ERRORES

## ¿QUIEN ES EL RESPONSABLE?



## QUE PODEMOS HACER PARA EVITAR ACCIDENTES?

- 1.. ENSEÑANZA DE TECNICAS SOBRE EXPLOSIVOS EN LA LICENCIATURA DE INGENIERIA CIVIL Y GEOLOGICA
- 2.. EFECTUAR PROGRAMAS DE ENTRENAMIENTO
- 3.. RESPETAR LAS LEYES DE REGULACION SOBRE EL USO DE EXPLOSIVO
- 4.. UTILIZAR SISTEMAS DE MONITOREO

(46)





**DIVISION DE EDUCACION CONTINUA  
FACULTAD DE INGENIERIA U.N.A.M.**

MECANICA DE ROCAS APLICADA A LA MINERIA Y A LA CONSTRUCCION

MISCELLANEOUS TOPICS

Expositor:  
Ing. Lepoldo Espinoza G.

MAYO, 1985

# Chapter 10 Miscellaneous topics

## Introduction

The theoretical models presented in the previous chapters are intended to provide a rational basis for the design of rock slopes. It should, however, be clear to the reader that the successful design of a slope depends not only upon the choice of the correct theoretical model but also upon a number of other considerations which cannot conveniently be quantified. This chapter deals with the following topics :

- The influence of slope curvature upon stability
- Controlled blasting
- Drainage of slopes
- Surface protection of slopes
- Control of rockfalls
- Monitoring and interpretation of slope displacements.

## The influence of slope curvature upon stability

All methods of stability analysis currently in use treat slopes two-dimensionally in that it is assumed that the section of slope under consideration is part of an infinitely long straight slope. It is also generally assumed that the slope face is planar from toe to crest, i.e. the slope face inclination can be defined by a single angle.

Actual slopes are invariably curved in plan and there is no reason why they should not also be curved in elevation. Moffitt, Friese-Greene and Lillico<sup>1</sup> have shown that the pit slope geometry, in both plan and elevation, is important in the economics of an open pit mining operation. It is the task of the rock slope engineer to define a slope geometry which provides for the steepest possible slope angles and a minimum risk of failure and he should be free to incorporate any factor which is likely to improve the stability of the slopes. Experience suggests that the curvature of a slope has a significant influence upon its stability and this factor is discussed on the following pages.



Figure 109 : An extension of an open pit to follow a branch of the ore body results in the formation of convex slopes. These "noses" are invariably less stable than the concave slopes.

The only serious attempt to study the influence of slope curvature, in plan, upon the stability of slopes, as far as the authors are aware, was made by Jenike and Yen <sup>214</sup> in 1962. This study, although giving useful indications of the improvement in stability resulting from decreasing the radius of curvature of a concave slope, was based upon assumptions which the authors do not feel are applicable to rock slopes in which the stability is controlled by structural discontinuities. Although the authors have not attempted a complete analysis of this problem, it is suggested that a useful analogy exists in the wedging action which occurs in the case of a slope containing two intersecting discontinuities - defined by the factor  $K$  given by the graph in figure 94 on page 187.

As the included angle of the wedge ( $\xi$ ) decreases, the horizontal components of the reactions  $R_A$  and  $R_B$  (see page 185) play an increasingly important part in supporting the wedge and the resulting "arching" action gives rise to a significant increase in stability. In the case of a concave slope in which many intersecting discontinuities exist, the lateral support provided by the surrounding rock would have much the same effect. On the other hand, a convex slope would permit lateral relaxation of the rock mass to take place and the beneficial effects of the arching action would be lost.

Figure 109 illustrates an open pit in which a small secondary pit had been created in order to recover a branch of the ore body. The overall slope angles were kept constant around this small pit and the two "noses" were noticeably less stable than the remainder of the pit.

Piteau and Jennings <sup>215</sup> studied the angles of slopes around five large diamond mines in the Kimberley region in South Africa. Because of the method of mining involves a form of block caving, the slopes are all in a condition of limiting equilibrium and their inclination depends, amongst other factors, upon the plan shape of the diamond pipe. After separating out the various factors involved, Piteau and Jennings concluded that the average inclination of concave slopes with a radius of curvature of 200 feet is  $39.5^\circ \pm 9^\circ$  as compared with an inclination of  $27.3^\circ \pm 5^\circ$  for concave slopes of 1000 feet radius. The average slope height for these mines is 320 feet.

These studies by Piteau and Jennings confirm the general conclusions reached by the authors as a result of experience in other parts of the world. This experience can be summed up in the following suggested design procedure :

When the radius of curvature of a *concave* slope is less than the height of the slope, the angle of the slope can be  $10^\circ$  *steeper* than that calculated by two-dimensional theory. When the radius of curvature of a *convex* slope approaches the height of the slope, the angle of the slope should be approximately  $10^\circ$  *flatter* than that indicated by two-dimensional theory.

Obviously, care must be exercised in the application of this suggestion since major changes in the geology or the drainage characteristics of the rock mass can invalidate the assumptions upon which the conclusions are based.

The shape to which a slope fails almost always approaches that of a general curve in which the slope angle decreases with increasing slope height. Since a failure represents an attempt, by nature, to relieve dangerously high stresses, it can be concluded that the shape of the failed slope is more stable than the original planar slope. This reasoning leads to the suggestion that the ideal shape for an open pit mine is that of a bowl, i.e. the slopes should be concave in both plan and elevation.

The authors fully realise that practical considerations related to the shape of the ore body and the layout of haul roads means that this ideal is seldom realised. There is, however, no basic reason why a slope should not be curved in elevation if there is any economic benefit to be gained by making it curved. Moffitt, Friese-Greene and Lillico<sup>1</sup> show that slope curvature can have a significant influence upon mining economics and Rana and Bullock<sup>216</sup> suggested the curved slope face illustrated in figure 110 as a basis for the design of a pit for the Iron Ore Company of Canada. While the authors are not in complete agreement with the method used by Rana and Bullock to derive their design curve (figure 110a), the application of this curve to a slope design is an interesting example of sound engineering.

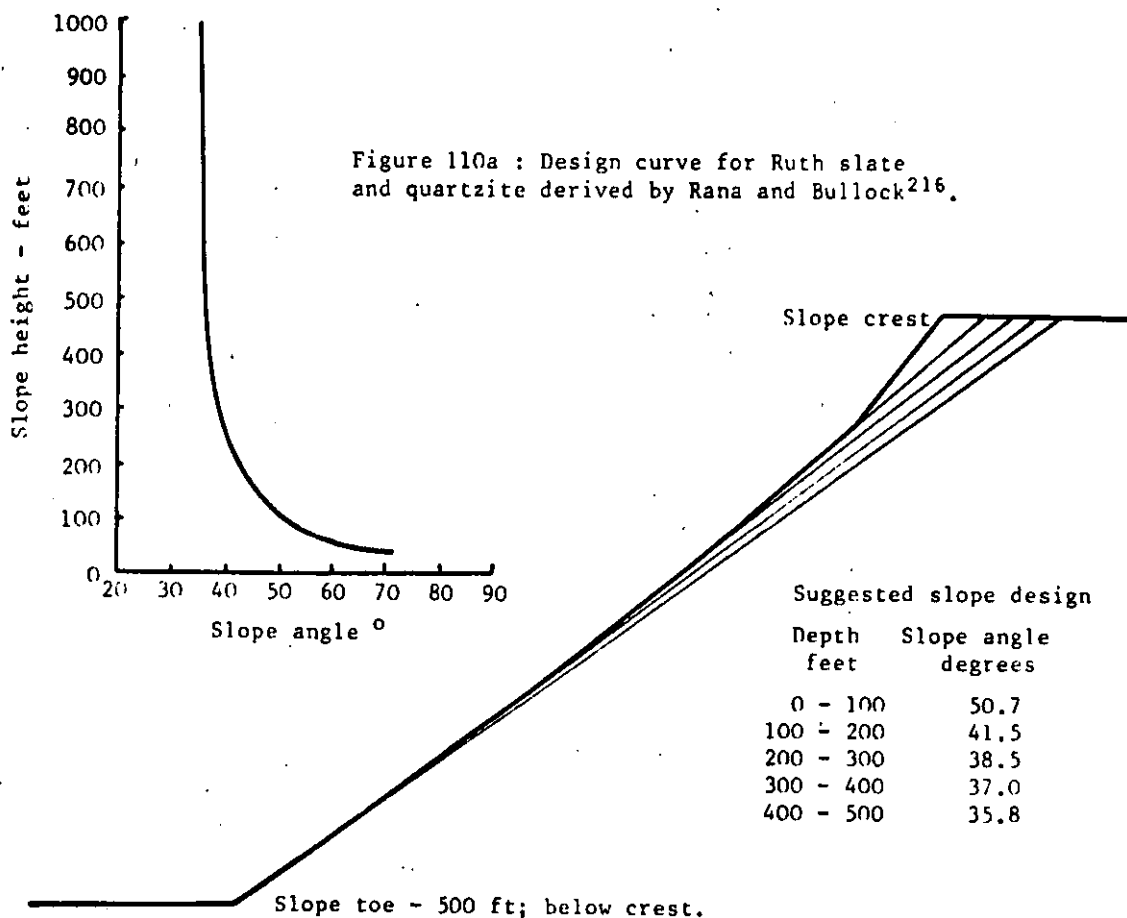


Figure 110b : Rana and Bullock's suggested slope design for the Iron Ore Company of Canada.

Several curves similar to that presented in figure 110a have been given in this book and the interested reader may consider the influence of such typical slope height versus slope angle relationships upon the slopes with which he has been concerned. A word of warning is necessary, however, since over-enthusiastic application of these concepts could lead to trouble.

In some cases, it may prove necessary to *flatten* the upper part of the slope, particularly when this part is to be excavated in soft weathered overburden materials. In other words, the variation of geology with depth may be the controlling factor and should be carefully examined.

It is also important to realise that the increased slope angle which can be used for small slope heights depends upon the cohesive strength of the rock mass and, as has been made abundantly clear in this book, cohesion is the least reliable of material properties. Hence, before proposing a design curve such as that presented in figure 110a, the rock slope engineer should be absolutely convinced about the reliability of his rock strength data.

#### Controlled blasting

Experienced open pit operators will often remark upon the deterioration of slope behaviour which has resulted from the introduction of increasingly large production blasts in the mine. The authors do not dispute the need for such large blasts in order to achieve the tonnages required in large scale modern open pit mining operations but they do wish to enter a plea that a different approach should be adopted for production blasts and for the blasting method used to create the final pit slopes.

Figure 111 illustrates the damage to a slope face resulting from the use of uncontrolled blasting techniques and, in contrast, the appearance of an 18 meter high slope face created by pre-split blasting is illustrated in figure 112. Although these two examples represent the extreme ends of the spectrum of blasting damage, they do illustrate the significant difference which can be achieved by the application of controlled blasting techniques.



Preparation for a large production blast in an open pit mine. The dark coloured mounds are piles of chippings which have been air-flushed from the large diameter holes drilled to accommodate the explosive.



Figure 111 : A hard rock slope face damaged by excessively heavy blasting during the excavation of a road cut.

Figure 112 : An 18 meter high rock face created by pre-split blasting. Note the clean fracture running between the parallel holes in the face, in spite of the variability of the rock through which the holes have been drilled. ( Photograph reproduced with permission of Atlas Copco Ltd, Sweden )



It would exceed the scope of this book to enter into a full discussion on either the detailed techniques or the costs of controlled blasting applied to rock slope engineering. The purpose of this discussion is simply to draw the reader's attention to the benefits to be gained from the use of smooth blasting and pre-split blasting techniques in the creation of the final slopes of an open pit mine or a roadcut. More detailed information on these methods can be obtained from the excellent textbook by Langefors and Kihlström<sup>217</sup> or from papers such as that by Oriard<sup>218</sup>. Much of the material upon which the following discussion is based has been drawn from an unpublished memorandum by Kihlström<sup>219</sup> which was made available to one of the authors (E.H.) by Nitro Nobel AB during a recent visit to Sweden.

*Smooth blasting* is a technique which is used for trimming the face of an excavation which has already been created. Figure 113 shows a smooth blasting operation in progress on the site of a large arch dam site in Tasmania. The purpose of this particular operation was to trim off loose and unstable surface rock from an existing natural slope in order to provide sound stable abutments for the dam. The method involves the drilling of small diameter parallel holes along the line of the desired slope profile. In the example illustrated, the holes were drilled with a normal hand held percussion drill to a depth of approximately ten feet for each blast. The holes are lightly charged and detonated simultaneously and, as can be seen from the photograph reproduced in figure 113, this results in a clean cut face in which the fractures have propagated along planes passing through the parallel holes. Two more examples of smooth blasting are illustrated in figures 114 and 115 which show, in the one case, an air-track machine being used to drill a pattern of holes and, in the other, a tunnel profile created by smooth blasting.

*Pre-split blasting* is similar to smooth blasting except that the line of lightly charged holes is detonated *before* the normal excavation blast and this results in a smooth fracture which protects the rock mass behind the face from the effects of the normal blast. An example of slopes in which pre-split blasting was used on a large scale is illustrated in figure 116.



Figure 113: Smooth blasting being used to trim loose and unstable rock from a natural slope face on the site of the Gordon arch dam in Tasmania.

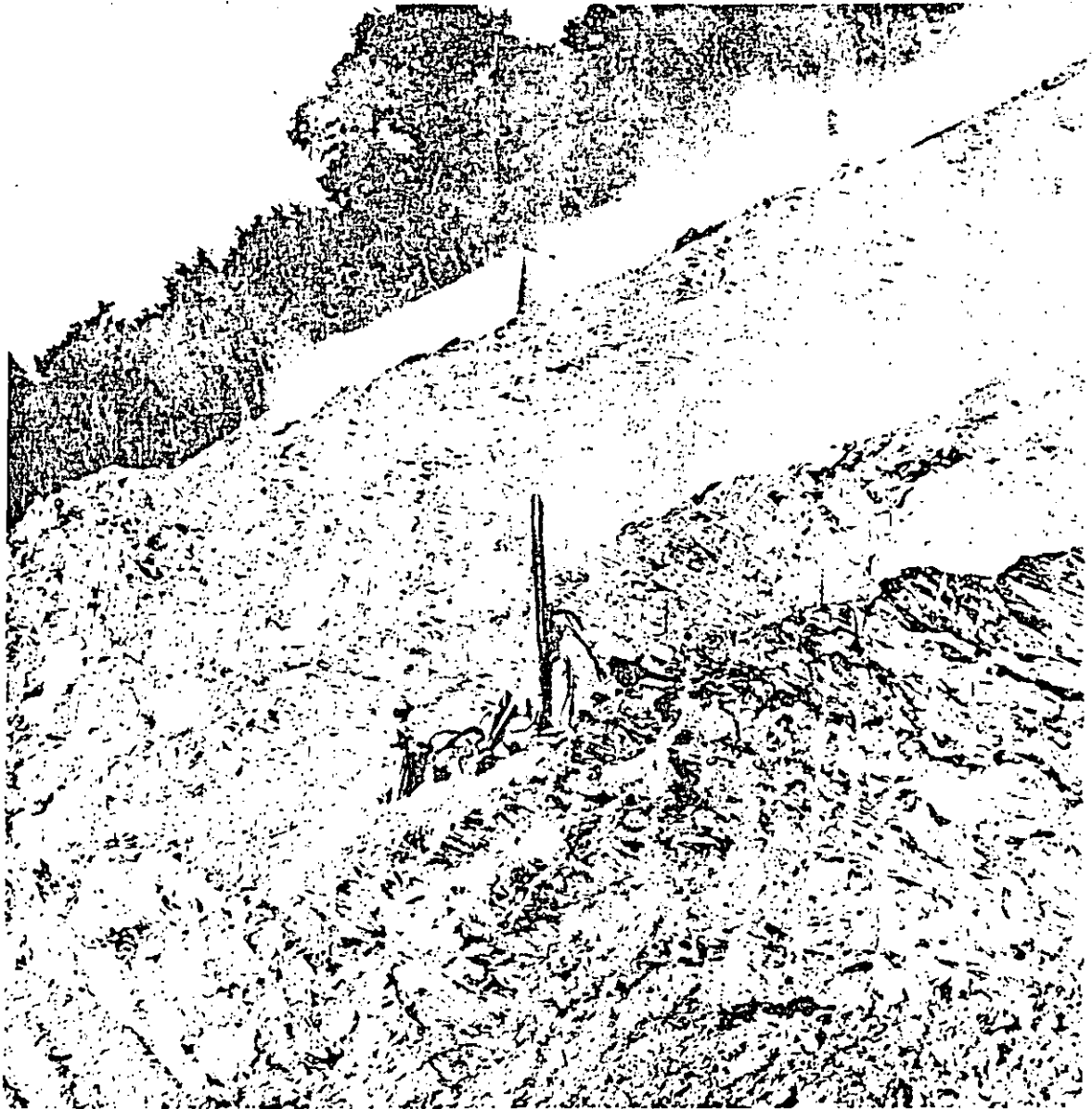


Figure 114 : Drilling a pattern of holes for a smooth blasting operation to trim a rock slope. ( Photograph reproduced with permission of Atlas Copco Ltd, Sweden )



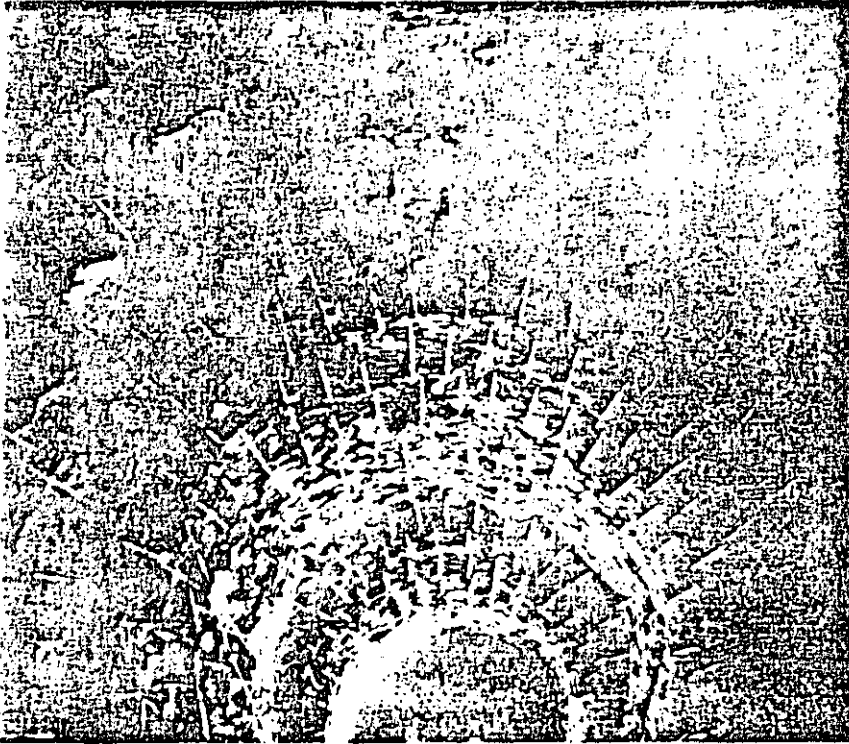


Figure 115 : Tunnel profile trimmed by smooth blasting. (Photograph reproduced with permission of Atlas Copco Ltd. and Nitro Nobel AB, Sweden ).

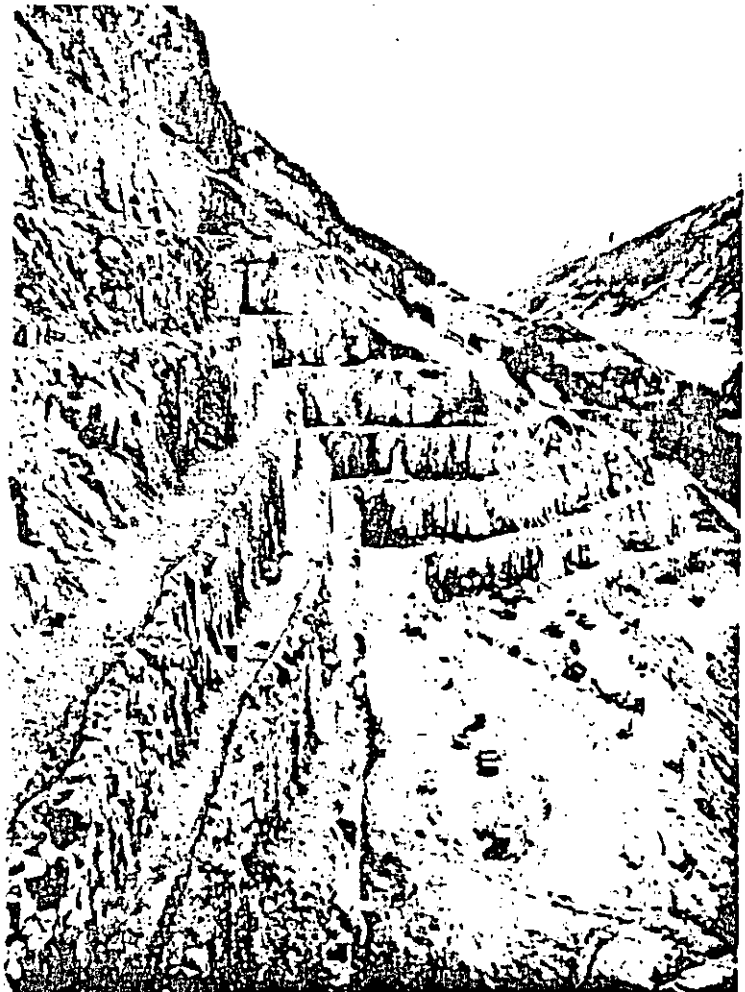
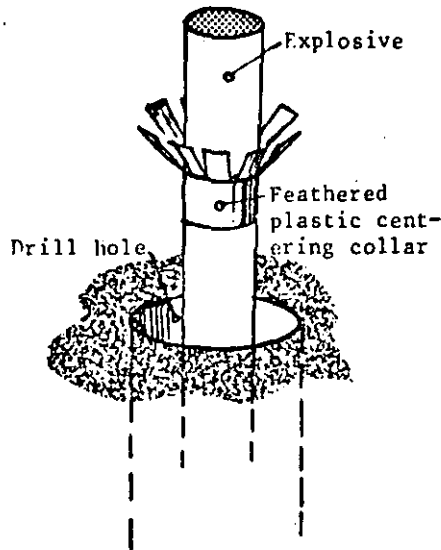


Figure 116 : Slopes excavated after pre-splitting final faces on the site of a hydro-electric project in Austria. (Photograph reproduced with permission of Atlas Copco Ltd, Sweden ).

The factors which are important in a smooth blasting or a pre-split blasting operation are :

- The specific charge (weight of explosive per unit length of hole ),
- Detonation sequence and delay,
- Ratio of hole diameter to charge diameter,
- Burden V ( distance between free face and hole ) and
- Spacing E ( distance between successive holes ).



Typical arrangement of explosive charge in drill hole for smooth or pre-split blasting.

The table given below is taken from the memorandum by Kihlström<sup>219</sup> and lists recommended values for hole diameter, charge diameter, specific charge, burden and spacing for typical hard Swedish rock. This table can be regarded as a guide for both smooth blasting and pre-split blasting and may be varied to suit local rock conditions.

Note that no value for the burden is given for pre-split blasting because the charges in these holes are detonated before the normal blast and hence the burden is either infinite or very large as compared with the spacing between holes.

In both smooth blasting or pre-split blasting, all the charges in a line should be detonated as nearly simultaneously as possible. Best results are obtained using instantaneous detonators or a pentyl fuse but acceptable results can be obtained as long as the delay between detonators does not exceed  $\pm 100$  milliseconds. The purpose of the simultaneous detonation is to allow gas pressures to build up at the same time in all the holes, thereby encouraging the propagation of a planar fracture between successive holes<sup>220</sup>.

Recommended dimension for smooth blasting and pre-split blasting											
Drill hole diameter.		Charge diameter		Specific charge*		Smooth blasting				Pre-split blasting	
mm.	in.	mm.	in.	Kg/m.	Lb/ft	Spacing E		Burden V		Spacing E	
						m.	ft.	m.	ft.	m.	ft.
30	1 1/4	11	1/2	0.07	0.05	0.5	1.6	0.7	2.3	0.25-0.3	0.8 -1.0
37	1 1/2	17	2/3	0.12	0.08	0.6	2.0	0.9	3.0	0.30-0.5	1.0 -1.6
44	1 3/4	17	2/3	0.17	0.11	0.6	2.0	0.9	3.0	0.30-0.5	1.0 -1.6
51	2	22	7/8	0.25	0.17	0.8	2.6	1.1	3.6	0.45-0.75	1.5 -2.5
62	2 1/2	22	7/8	0.35	0.23	1.0	3.3	1.3	4.2	0.55-0.8	1.8 -2.6
75	3	25	1	0.50	0.34	1.2	4.0	1.6	5.2	0.6 -0.9	2.0 -3.0
87	3 1/2	25	1	0.70	0.50	1.4	4.6	1.9	6.2	0.7 -1.0	2.3 -3.3
100	4	29	1 1/4	0.90	0.60	1.6	5.2	2.1	6.9	0.8 -1.2	2.6 -4.0
125	5	40	1 1/2	1.40	0.90	2.0	6.6	2.7	8.8	1.0 -1.5	3.3 -4.9
150	6	50	2	2.00	1.30	2.4	7.9	3.2	10.5	1.2 -1.8	4.0 -5.9
200	8	52	2	3.00	2.00	3.0	9.8	4.0	13.0	1.5 -2.1	4.9 -6.9

\* Based upon Nitro Nobel's Dynamex B

As with all other techniques described in this book, smooth blasting and pre-split blasting techniques should only be applied after due consideration of all the factors involved and after trials of limited extent in the rock mass being worked. Herget <sup>221</sup> reports that, in some preliminary experiments carried out by the Canadian Department of Energy, Mines and Resources, pre-splitting in heavily fractured ore resulted in more damage to the slopes than a normal blast because of the venting of the gasses from the closely spaced holes. On the other hand, the photographs reproduced on the previous pages should have served to convince the reader that, when correctly applied, these techniques can result in considerable improvements in the appearance and the stability of slope faces. Obviously, pre-splitting a slope face will not prevent a deep-seated slide if the slope is inherently unstable but the authors suggest that the slope face itself can probably be cut 10° or more steeper if controlled blasting methods are used. The main benefits which derive from the use of these methods are in the reduced maintenance and the reduced danger of rock falls from a face which has not been shattered by excessively heavy blasting.

**Drainage of slopes**

The very important influence of water pressure upon the stability of a slope has been emphasised time and time again in this book. Since water pressure reduces the stability of a slope, it follows that drainage will increase the stability of that slope. The following discussion is concerned with methods of slope drainage.

The three basic principles to be kept in mind when considering slope drainage are:

- a. prevent surface water from entering the slope through open tension cracks and fissures,
- b. reduce water pressure in the vicinity of the potential failure surface by selective sub-surface drainage and
- c. position the drainage so that only the water in the immediate vicinity of the slope is drained - there is no point in draining the country-side for miles around the pit.

The most common methods of slope drainage are illustrated in the composite sketch presented in figure 117 and the following comments refer to the methods illustrated :

*Surface drains* are designed to collect run-off and to divert it before it reaches the area immediately behind the crest of the slope. This is the area in which the most dangerous tension cracks are likely to occur. Attempts to line these surface drains are usually unsuccessful because of movements in the slope and because of the damage which results from heavy traffic in the area. The authors suggest that the surface drain can be left unlined provided that it is steeply graded to promote rapid water movement and that it is regularly maintained and kept free of blockages. Some of the most effective surface drains are those which are cut by a narrow bladed bull-dozer and where the same machine is run along the drain at fairly regular intervals.

*The slope surface*, immediately behind the slope crest, is an area of considerable potential danger in that water which is allowed to collect in pools in this area is likely to find its way into the slope through open tension cracks

Surface drain to collect run-off before it can enter the top of open tension cracks. This drain should be steeply graded and must be kept clear.

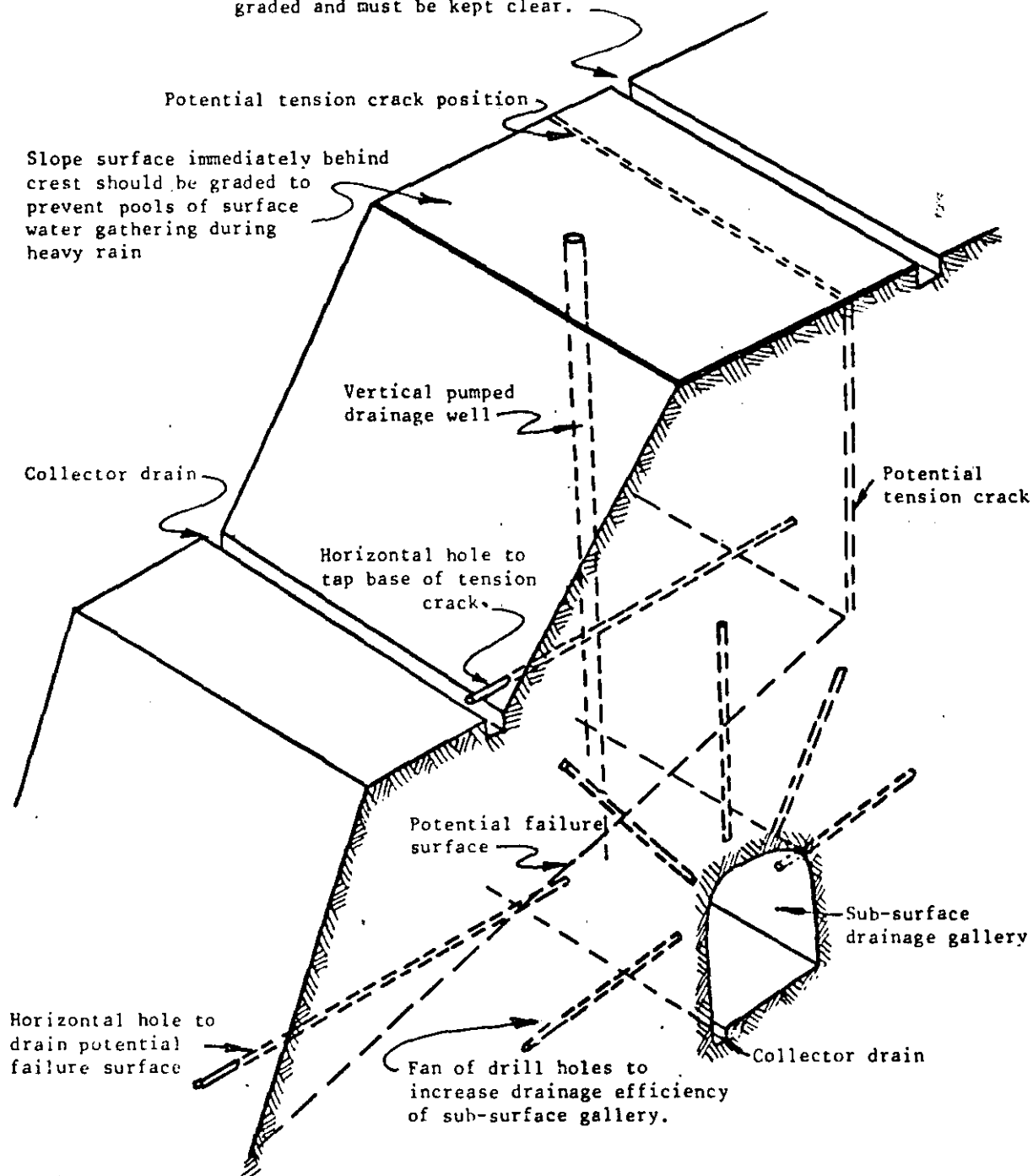


Figure 117 : Slope drainage methods .

and fissures. Grading of this surface and the removal of obstructions which could cause damming of surface water is probably adequate in most cases. Sometimes additional measures are considered necessary and the slope surface is sealed with a flexible layer such as lateritic soil. In one instance, old engine oil from the workshops was used to bind the soil into a surface sealing layer above a particularly important slope.

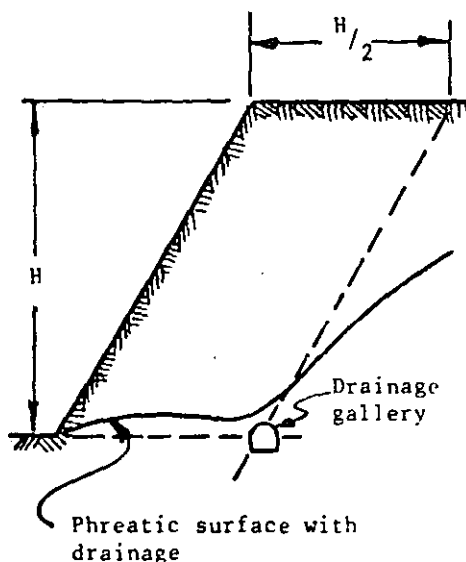
*Open tension cracks* are very dangerous in areas liable to high intensity rain storms since the water forces which are generated if these cracks become full of water are likely to induce violent slope failures (see practical example number 2 on page 158 ). In addition to diverting surface water away from such cracks, it is also advisable to take steps to prevent water entering the crack by sealing the top of the crack with a flexible material such as clay. When the crack is more than a few inches wide it should be filled with gravel or waste rock before the flexible cap is placed. This permeable filling will allow the free passage of sub-surface water while, at the same time, providing support for the surface seal. Under no circumstances should the tension crack be grouted or concrete filled since the creation of an impermeable barrier at this point in the slope could result in the build-up of dangerous water pressures within the rock mass.

*Horizontal drain holes* drilled into the slope face can be very effective in reducing water pressures near the base of a suspected tension crack or along a potential failure surface. The spacing and positioning of these holes depends upon the slope geometry and the structural discontinuities within the rock mass. In a hard rock slope, the water is generally transmitted along joints and the horizontal drain holes will only be effective if they penetrate such features. In the case of a soft rock or soil slope, the drain holes can be regularly spaced but a certain amount of trial and error is necessary in order to determine the optimum spacing. In either case, the installation of *piezometers* before the drilling of the horizontal holes is strongly recommended since, without an indication of the change in water level, the rock slope engineer will have no idea of the effectiveness of the drainage measures which he has implemented.

*Collector drains* to lead the water discharged from horizontal drains are important otherwise this water will simply find its way into the next bench down and the problem will have been transferred from one level to the next.

*Vertical drainage wells* drilled from the slope surface and fitted with down-hole pumps can be effective in slope drainage and they have the advantage that they can be in operation before the slope is excavated. The disadvantage of this method of drainage is the expense of keeping the pumps running and also the danger of power failure during the most critical period - a heavy rain storm. In some cases, vertical wells have been used during the early stages of a drainage programme and these well have later been connected to a sub-surface drainage scheme so that they become gravity drains.

*Drainage galleries*, with or without fans of radial holes, are probably the most effective means of sub-surface drainage



Sub-surface drainage gallery location in a slope.

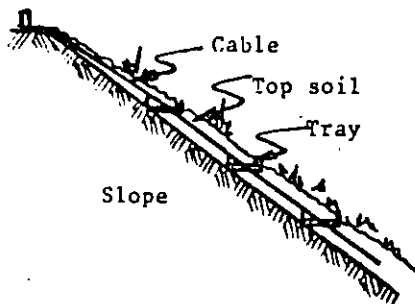
but they are also the most expensive. In many open pit mining situations, such galleries already exist in the form of underground mine workings. In other cases, the excavation of suitable galleries can be justified as part of the ore body exploration programme. The excavation of a gallery for the sole purpose of drainage would only be justified in the case of a very important hard rock slope in which the groundwater flow pattern was known with a reasonable degree of certainty. The optimum location of drainage galleries has been investigated by Sharp<sup>117</sup> and has been discussed by Sharp, Hoek and Brawner<sup>222</sup>. In very general terms, the optimum gallery position is at the corner of the parallelogram defined in the sketch opposite. A sub-surface drainage gallery will effectively drain about 200 feet of over-lying material and, hence, for very large slopes, two or more levels of drainage galleries may be required.

The effectiveness of any slope drainage scheme is very difficult to gauge. Piezometers installed in the slope before the drainage system is brought into operation can give very valuable information on the reduction in water pressure which is brought about by drainage. Knowledge of the overall groundwater flow pattern in the slope is also of considerable help in planning the most effective drainage measures and some of the concepts discussed in chapter 8 may be useful in building up this knowledge. One positive aspect of slope drainage is that it can never do any harm - some drainage, however inefficient, is better than no drainage. The drainage characteristics of most slopes can be improved with relatively little effort or expense and simple precautions such as the diversion of surface run-off should be an integral part of any slope design. More elaborate drainage measures designed to improve the stability of critical slopes are generally more expensive but they are sometimes the only means available for achieving the desired results.

#### Surface protection of slopes

Slopes in soft rock or soil are liable to serious erosion during heavy rain and some rock slopes are prone to severe weathering when exposed. The surface protection of such slopes can be a serious problem and the following comments offer some guidance on this subject although it must be emphasised that local conditions and the availability of suitable materials may be the dominant consideration in many cases.

Vegetation is almost certainly the best form of surface protection against the erosion of soil slopes. A grass mat covering the slope will not only bind the surface material together but will also tend to inhibit the entry of water into the slope. Establishing the grass or other vegetation is the most difficult problem since the rain which is needed to promote the growth of the young plants is also capable of removing these plants from the slope, particularly when the slope is relatively steep and when the rainfall intensity is high. Various schemes for stabilising the surface layer during the initial growing period of the vegetation have been tried but finding the best method for a particular slope is very much a question of trial and error.



Mechanical anchoring of top soil layer on slope.

One system which has proved successful in some applications is to mix grass seed and fertilizer into a liquid rubber or plastic which is then sprayed onto the slope surface and which serves to bind the seeds, soil and fertilizer together until growth has been established. Another system involves mechanically anchoring the top soil in place by means of trays anchored into the slope or suspended from the slope crest by means of wire ropes.

Choice of the correct grass type and deciding upon the best method of establishing growth depends so much upon the local conditions on the site that the authors feel that there is little value in discussing this topic further in this text. Instead, it is recommended that the slope engineer should consult the local agricultural officers who will have experience of local conditions and who would normally be very willing to help in a project which, to them, would be unusual and interesting.

In the case of rock slopes, surface protection is necessary when these slopes are prone to rapid weathering. Materials such as shales and, in some cases, granites have to be treated with care when they are exposed in a slope face and, since it is not normally possible to establish vegetation on such slopes, some form of protective layer must be used. Probably the most common form of surface layer is a cement-sand mortar which is sprayed onto the slope surface. This pneumatically applied mortar, known as "Gunnite" or "Shotcrete", depending upon the moisture content of the mix, is very successful if applied immediately after excavation of the face, before the weathering process has set in. The mortar is sometimes applied by hand, as in the case of the "Chunam" surface layers which are common in Hong Kong.

When a slope surface is to be protected by means of a surface layer, it is essential to remember that this layer may not only keep water out but it may also keep it in the rock mass behind the slope and the resulting water pressure can induce instability in the slope. Shallow drains or weep holes left at regular intervals in the layer will serve to dissipate these potentially dangerous water pressures and should be included in the specifications for the protective surface layer. It is also important that these layers should be inspected at regular intervals and that repairs should be carried out if the layer is damaged since failure to repair a hole in the layer can give rise to progressive damage to the whole layer.

More elaborate, and more expensive, methods of surface protection are sometimes used and figure 118 illustrates a scheme used to protect the surface of a large soil slope in Hong Kong. Interlocking precast concrete members form an open framework into which a layer of no-fines concrete is placed. This porous layer supports a layer of top soil which is then seeded to produce a grass-covered slope.

Another form of surface protection is to use various types of gabions which are wire baskets filled with waste rock. Figure 119 illustrates two typical applications of gabions for the surface protection of slopes. This form of protection is particularly effective when the slope is subjected to wave action or scour from rapidly flowing water.

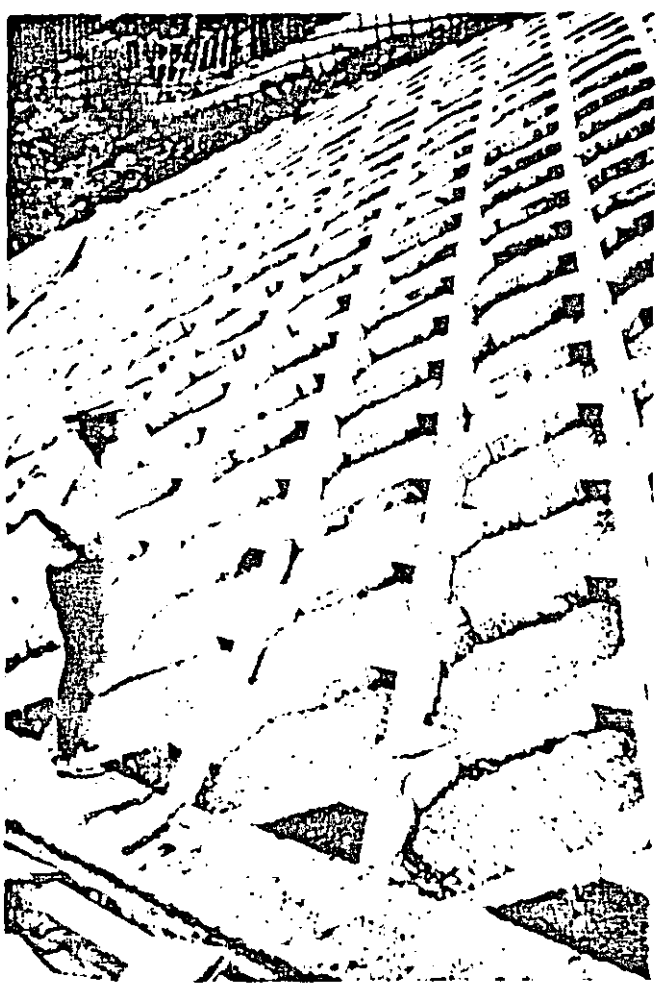


Figure 118 : Protection of the surface of a large soil slope in Hong Kong. Precast concrete members interlock to form a framework into which layers of no-fines concrete are placed. These layers support top soil which is seeded to produce a grass covered slope.

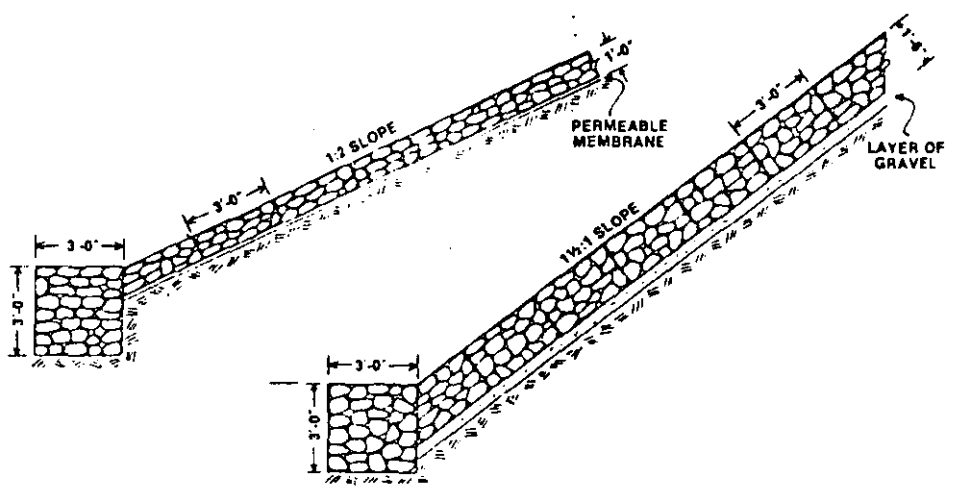


Figure 119 : The use of gabions for the stabilisation and surface protection of slopes. Technical literature on gabions is available from River and Sea Gabions (London) Ltd, Princes Street, London W1R 8SQ and from Terra Aqua Conservation Ltd., 4930 Energy Way, Reno, Nevada 89502.



### Control of rockfalls

One of the dangers associated with rock slopes is that of falls of loose boulders from the top of the slope. Such boulders can fall, bounce or roll down the slope as shown in figure 120 and, unless steps are taken to dissipate the energy which has been acquired by the boulder, considerable damage can be caused. This danger is particularly acute in the case of highway slopes and a study carried out by Ritchie in 1963<sup>223</sup> was aimed at minimising this hazard.

Figure 120, adapted from a drawing in Ritchie's paper, summarises the main recommendations for the control of rockfalls. A ditch at the foot of the slope will contain much of the energy of the fall and a chain link fence on the shoulder of this trench will prevent the rock from bouncing onto the roadway. Unfortunately, to be fully effective, the ditch should be as much as 25 feet wide and 6 feet deep for a 100 foot high slope. The authors suggest that it may be possible to reduce these dimensions by placing a thick layer of gravel in the base of the ditch since recent work has shown that such a layer of gravel is very effective in dissipating the energy of a runaway airplane or truck. However, in most open pit mining situations, the space required for such a ditch could not be made available and these suggestions could only be used for critical haul roads or public roads.

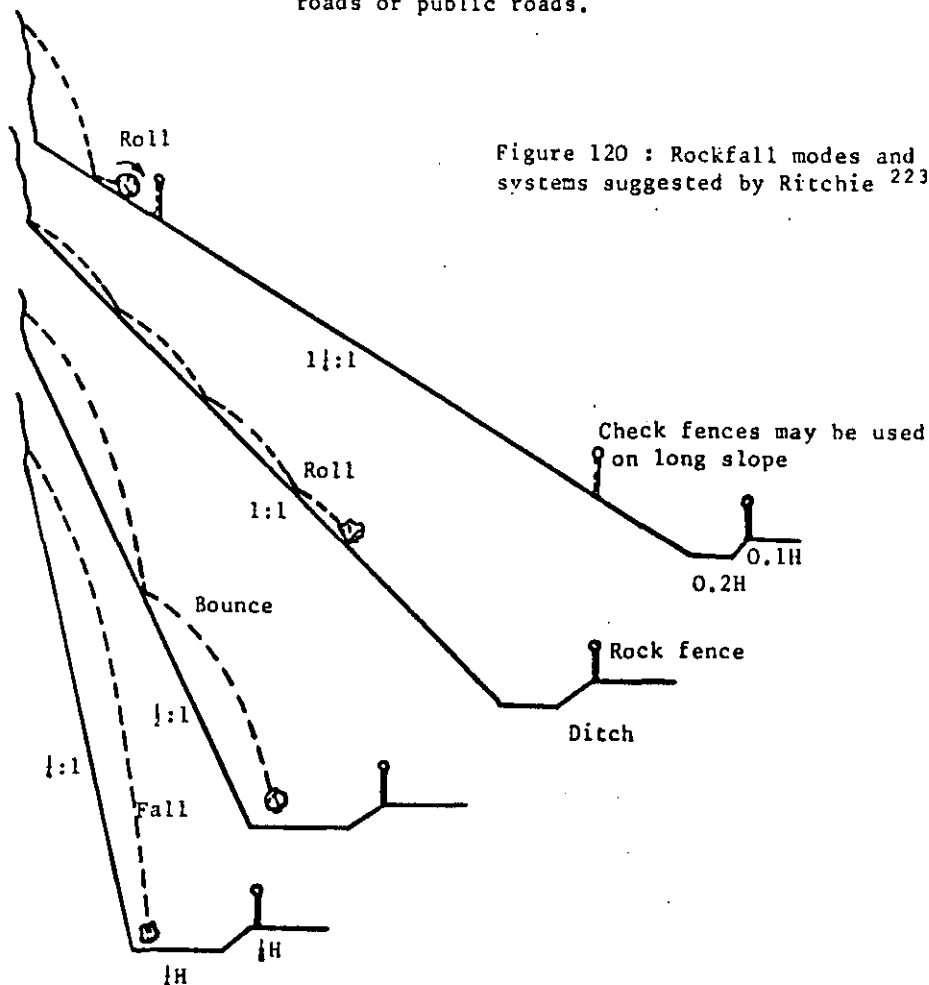


Figure 120 : Rockfall modes and protection systems suggested by Ritchie<sup>223</sup>.

## Monitoring and interpretation of slope displacements

When, in spite of all his efforts to design a stable slope or to improve the stability of a potentially dangerous slope, the engineer finally comes to accept that a major failure is inevitable, what steps, other than catching the next plane, can he take? The answer lies in attempting to provide a reliable prediction of the slope behaviour up to and including the final failure so that appropriate action can be taken to minimise the danger to men and equipment.

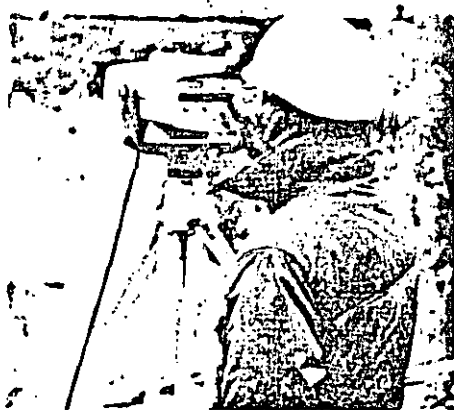
The most spectacular set of predictions of this sort was associated with a major slope failure in the Chuquicamata mine in Chile<sup>224,225</sup>, to be discussed in more detail later in this section. There have, however, been a number of other cases of slope failure prediction which, although less spectacular, have been just as important in preventing the serious consequences which invariably result from an unexpected failure. The lesson to be learned from these cases is that a large slope will almost always give warning of failure, provided that the slope engineer knows what to look for and takes heed of the warning.

Since shear movement on a failure surface within a soil or rock mass will be transmitted into the overlying mass of material, monitoring of the movements of the slope surface will give an indication of overall movements resulting from instability in the slope. Experience has shown that detailed knowledge of the precise movement pattern within the rock mass is not important and that measurement of surface displacement is usually adequate for the prediction of slope behaviour.

Measurement of these surface displacements is basically a survey problem of establishing adequate targets or benchmarks, a stable reference datum and using the correct instruments for the measurements themselves. These problems have been discussed by Kennedy and Niermeyer<sup>225</sup>, Watt<sup>226</sup> and St John<sup>227</sup> and will not be dealt with in detail in this chapter. Most mine survey departments would have adequate equipment for the measurement of slope surface displacements but these departments would almost certainly require assistance in the interpretation of these measurements.

Obviously, the earlier a displacement measuring system is established around an open pit the better since the gradual change in the movement pattern would reveal any anomalous slope behaviour which would identify areas requiring detailed examination. Unfortunately, the cost and the time required to establish and to maintain such a system can seldom be justified, particularly when slope problems are not anticipated. Consequently, a displacement monitoring system is normally only installed when slope instability is evident or when local mining regulations require that a check must be kept on surface movements.

Since the serious instability of a slope is almost always accompanied by the development of one or more tension cracks behind the crest of the slope, one of the best and most reliable methods of displacement monitoring is to measure the opening of the tension crack at regular intervals. Very simple measuring systems, using a steel



An electro-optical distance measuring instrument set up to monitor displacements across a large quarry.

tape stretched between pegs on either side of the crack, have proved very effective and have provided sufficient information for sound decisions to be made in many mines and quarries. More sophisticated systems, using more precise measuring methods, have been used and one such system is illustrated in figure 121. Even more sophisticated systems, using electro-optical distance measuring devices have also been used in certain cases <sup>227</sup>.

The authors do not wish to enter into a discussion on the merits of these different systems of measurement. The choice of the method to be used in a particular situation will depend upon the magnitudes of the anticipated movements, the local site conditions and the availability of staff and equipment. While it may be interesting to measure the displacements in thousandths of an inch, this is seldom necessary and the slope engineer should avoid demanding an unnecessarily high degree of accuracy. In the case of the Chuquicamata slide, movements of the order of 6 meters were recorded and it would certainly not require a micrometer to measure such displacements. It is preferable to get a simple measuring system functioning early than to argue about the required accuracy while the slope falls down.

In some cases, loose overburden on the upper surface of the slope may make it impossible to establish stable bench marks for displacement measurements. Under these conditions, a borehole method of displacement monitoring can be considered. Several systems for this type of measurement are available commercially and most of them depend upon the lowering of some form of borehole survey instrument down a borehole lined with a grooved plastic casing. The casing is left permanently in place and measurements are taken at the same depths at regular intervals. The relative movements with time of different points in the rock or soil mass will give an indication of instability in the slope.

The interpretation of the displacement versus time plot obtained from these measurements poses the most difficult problem for the rock slope engineer. There are no theories which define the movement patterns in slopes and the authors feel that it will be a long time before such theories are developed. Experience does suggest, however, that the rate of movement in an unstable slope will gradually accelerate until the point of failure is reached and that this rate of movement, rather than the magnitude of the movement itself, provides the most sensitive indication of slope behaviour. This is best illustrated by means of the Chuquicamata slide prediction which is discussed on the following pages \*.

Figure 122 illustrates the eastern slopes of the Chuquicamata pit. The overall height of the slope in the failure region, in the centre of the photograph, was 248 meters and the overall slope angle approximately  $43^{\circ}$ . The main rock type in the slide area is unaltered porphyritic granodiorite.

\*The authors claim no credit for this example which has been taken from the papers by Kennedy et al <sup>224, 225</sup>.



a. Four pegs are set into holes drilled into the rock on either side of the tension crack by means of epoxy resin. The measuring heads are protected by grease-filled caps screwed onto the peg. These caps should be left unpainted otherwise they are likely to attract vandals.



b. A large vernier caliper can be adapted to measure the displacements across a tension crack of up to 5 feet wide. The attachments on the caliper are cone seatings which are centred on balls on the top of the measuring pegs.



c. A precision level placed along the caliper bar can be used to determine the change in level of the pegs. Note that measurements are made across the diagonals as well as along the sides of the measuring square in order to detect any shear movement along the tension crack.



d. Precise measurement of movements across a narrow tension crack can be made by means of a mechanical extensometer. Measurements of this accuracy have proved useful for correlation with daily rainfall and blasting records for research purposes.

Figure 121 : Measurement of movements across a tension crack .

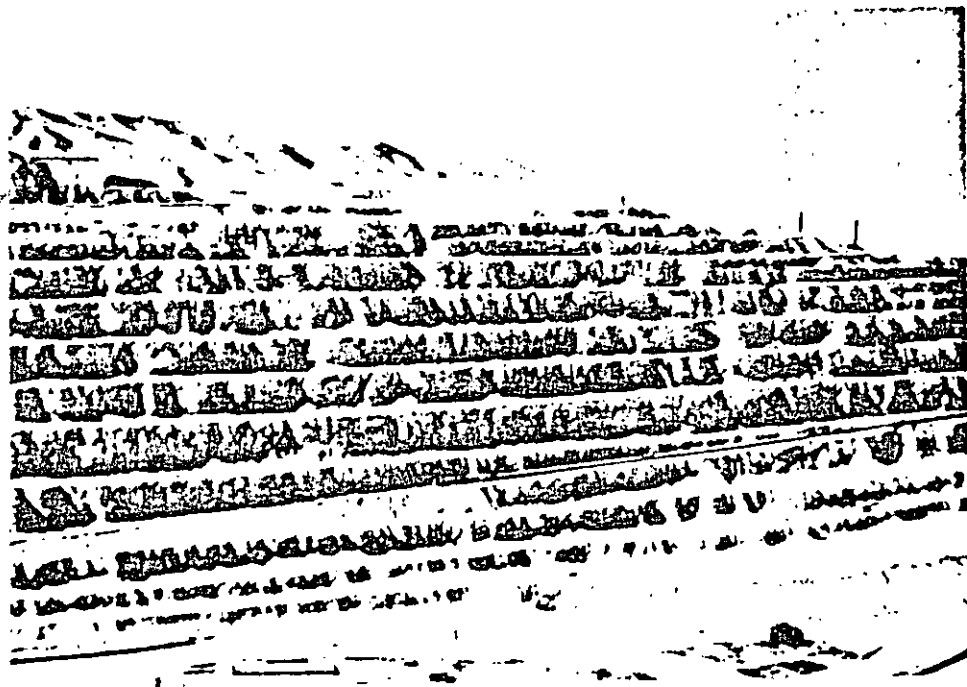
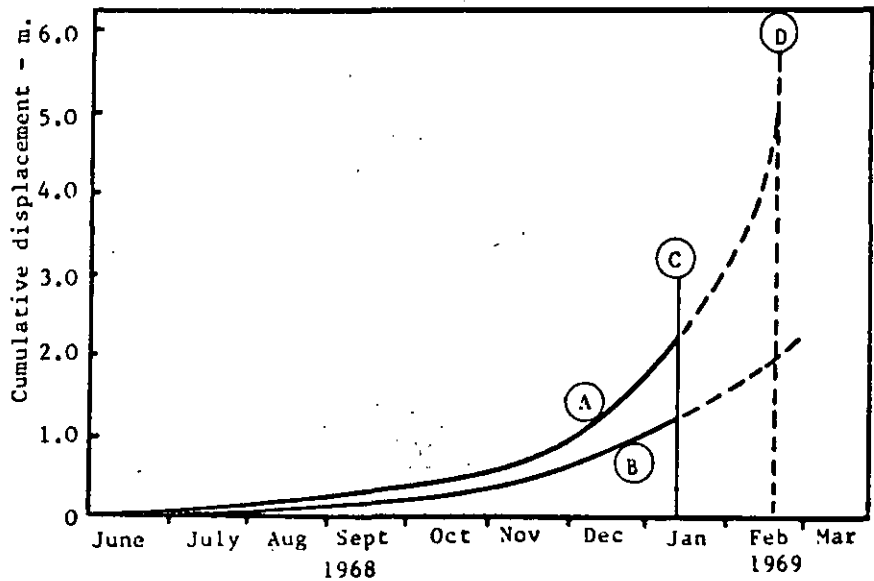


Figure 122 : Eastern slope of the Chuquicamata mine in Chile in late 1968. The area on the top of the slope to the left of the two smelter stacks is where 4½ million tons of material was removed in the unloading programme.

Figure 123 : Plot of slope displacement versus time used for prediction of the Chuquicamata mine slide.

- A - Plot of fastest moving target on slope face.
- B - Plot of slowest moving target on slope face.
- C - Prediction of slope failure date made on the basis of existing data on January 13.
- D - Predicted and actual failure date - February 18, 1969.



Tension cracks were first noticed in this slope in August 1966 and a simple monitoring system was established. Movements were found to be extremely small and eventually ceased so that monitoring was discontinued. An earthquake, on December 20, 1967 of magnitude 5 on the Richter scale, was apparently responsible for reactivating movement. Incidentally, Chuquicamata is in a desert area with extremely low annual rainfall and hence groundwater is not a factor in this slide.

Displacement monitoring commenced in June 1968 when it was evident that movements were taking place in the slope. The monitoring systems, described by Kennedy and Niermeyer<sup>225</sup>, were basically very simple, consisting of tension crack measurements, survey measurements and some extensometer measurements. A three channel, short period siesmograph was also installed on the site and, although the results produced by this instrument were not used in the failure prediction, it is interesting to compare them with the displacement records<sup>225</sup>.

In an effort to stabilise the slope, an unloading programme was started in August 1968 and a total of 4.5 million tons of material was eventually stripped from the top of the slope. This stripping is visible on the top of the slope, to the left of the smelter stacks, in the photograph reproduced in Figure 122. Although the amount of material finally deposited on the pit floor by the slide was probably reduced by this stripping programme, it is unlikely that the unloading of the slope had any significant influence on the slide. The analysis presented in Figure 85 on page 171 shows that a very large reduction in slope height is necessary before the factor of safety of a slope is significantly improved.

By late 1968 it was evident that a major slope failure was inevitable and steps were taken to reroute the haul road system and to stockpile material for the mill. On January 13, 1969, a projection of the displacement data, plotted in Figure 123, was made. The earliest predicted failure data, based upon the fastest moving target on the slope, was given as February 18, 1969.

The failure itself, illustrated in the photograph reproduced in Figure 124, occurred at 6.58 p.m. on February 18 and involved the movement of approximately 12 million tons of material. Figure 125 shows the slide, as seen from the air, and the relocated haul road can be seen in the lower right hand side of the photograph.

Full production resumed on February 19 after a shut-down of the pit of 65 hours. The mill continued working throughout this period on stockpiled material.

The spectacular accuracy of this prediction is not particularly relevant to this discussion since the overall result would have been the same had the prediction been a few days or even weeks out. The point of this example is that by knowing what to look for and by making full use of the available data, a set of sound engineering decisions could be made and the serious consequences which could have resulted from this failure were avoided.



Figure 124 : Failure of the Chuquicamata mine east slope at 6.58 p.m.,  
February 18, 1969.

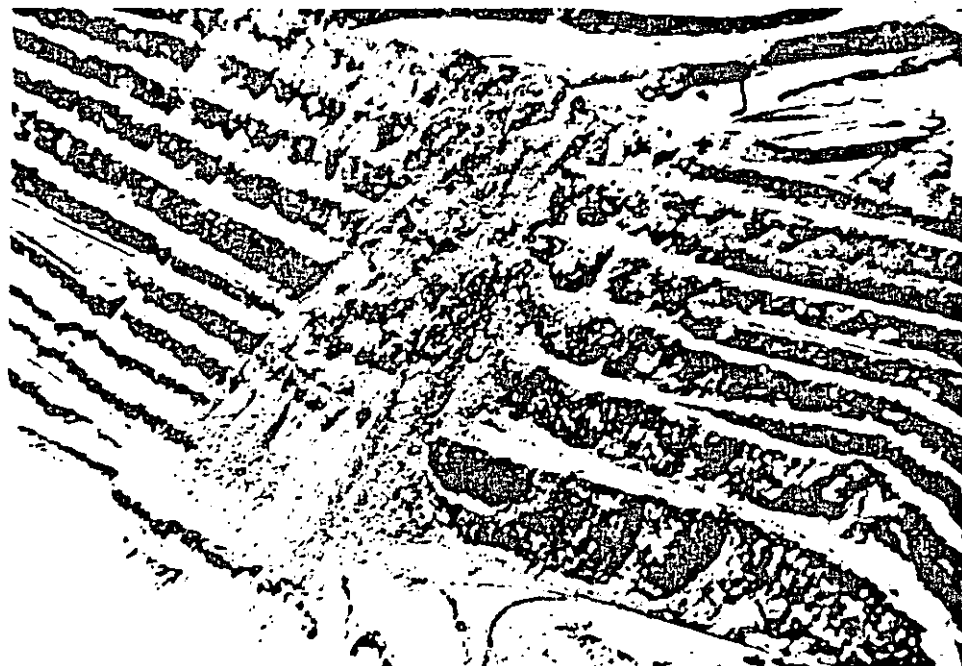


Figure 125 : The Chuquicamata slide seen from the air. Note the  
new haul road position in the bottom right hand side of the photograph.

The photographs reproduced in figures 122, 124 and 125 are prints of colour slides  
released to Imperial College by the Anaconda Company .

## Chapter 10 references

### Selected references

214. JENIKE, A and YEN, B. Slope stability in axial symmetry. *Proc. 5th Symp. Rock Mech.*, Univ. Minnesota 1962. Pergamon Press 1963, pp. 689-711.
215. PITEAU, D.R. and JENNINGS, J.E. The effects of plan geometry on the stability of natural slopes in rock in the Kimberley area of South Africa. *Proc. 2nd Congress Intl. Soc. Rock Mechanics, Belgrade 1970*. Vol. 3, paper 7-4.
216. RANA, M.H. and BULLOCK, W.D. The design of open pit mine slopes. *Canadian Mining Journal*, August 1969, pp. 58-66.
217. LANGEFORS, U. and KIHSTROM, B. *Rock Blasting*. Wiley & Sons, New York 1963, 404p.
218. ORIARD, L.L. Blasting effects and their control in open pit mining. *Geotechnical practice for stability in open pit mining*. Editors Brawner, C.O. and MILLIGAN, V., AIME, New York, 1972, pp. 197-222.
219. KILHSTROM, B. The technique of smooth blasting and presplitting with reference to completed projects. *Nitro Nobel AB Technical Memorandum No. B672*, January, 1972.
220. KUTTEP, H.K. and FAIRHURST, C. On the fracture process in blasting. *Intl. J. Rock Mechanics, Mining Sci.*, Vol. 8, No. 3, 1971, pp. 181-202.
221. HERGET, G. Recent research on rock slope stability by the Mining Research Centre (Ottawa). *Geotechnical practice for stability in open pit mining*. Editors Brawner, C.O. and Milligan, V., AIME, New York, 1972, pp. 47-66.
222. SHARP, J.C., HOEK, E. and BRAUNER, C.O. Influence of groundwater on the stability of rock masses - drainage systems for increasing the stability of slopes. *Trans. Inst. Min. Metall., London. Sect. A*, Vol. 81, No. 786, 1972, pp. 113-120.
223. RITCHIE, A.M. The evaluation of rockfall and its control. *Highway Record*, Vol. 17, 1963, pp. 13-28.
224. KENNEDY, B.A., NIERMEYER, K.E. and FAHM, B.A. Major slope failure at the Chuquicamata Mine. *Mining Engineering*, AIME, Vol. 21, No. 12, 1969. p.60.
225. KENNEDY, B.A. and NIERMEYER, K.E. Slope monitoring systems used in the prediction of a major slope failure at the Chuquicamata Mine, Chile. *Proc. Symp. Planning Open Pit Mines, Johannesburg*, September 1970, A.A. Balkema, Amsterdam, pp. 215-225.
226. WATT, I.B. Control for early warning of potential danger in open pits. *Proc. Symp. Planning Open Pit Mines, Johannesburg*, Sept. 1970, A.A. Balkema, Amsterdam, pp. 103-113.



227. ST. JOHN, C.M. A note on displacement measurement for open pit monitoring. *Proc. Symp. Planning Open Pit Mines, Johannesburg, September 1970.* A.A. Balkema, Amsterdam, pp. 328-330.



**DIVISION DE EDUCACION CONTINUA  
FACULTAD DE INGENIERIA U.N.A.M.**

MECANICA DE ROCAS APLICADA A LA MINERIA Y A LA CONSTRUCCION

USO DE EXPLOSIVOS EN ROCA

ING. RAUL CUELLAR BORJA

MAYO, 1985.



**DIVISION DE EDUCACION CONTINUA  
FACULTAD DE INGENIERIA U.N.A.M.**

MECANICA DE ROCAS APLICADA A LA MINERIA Y A LA CONSTRUCCION

THE LAWS OF ENERGY DIVERGENCE

MAYO, 1985.

## THE LAWS OF ENERGY DIVERGENCE

By Richard L. Ash, P.E.

Energy transmitted through a homogeneous isotropic medium from an explosion-induced confined source is diverged outward equally in all directions. The effect is to reduce the unit energy at any one position within the medium as the distances increase away from the explosion center. This phenomenon as applied to mass, volumetric, or weight considerations is described by what is known as the cube-root law: whereas, the decrease of the effective stress or pressure with distance in any single direction is expressed by the square-root law. Both of the two laws serve as the principle bases for all explosive-energy design criteria. It is most important, therefore, that the laws be clearly distinguished from one another as to their specific applications.

The first assumption made in the use of the laws is that the explosion source consists of a single concentric or point charge, i.e., one that is initiated in its center and whose length-to-diameter ratio ( $L_e/D_e$ ) is not more than 6. However, the laws can be applied equally as well to the long-length cylindrical charge normally used for the bulk of industrial blasting, providing one recognizes that only in the planes of the charge length will the effects differ from those produced by the concentric charge.

To comprehend the unique characteristics of the long-length charge it is convenient to consider that it is essentially no more than a continuous series or succession of individual point charges. Thus, stress energy from each segment normally will be released in a definite sequence or progressive order, from the point of initiation and then preceding to each adjacent portion of the charge remaining in the column. The resultant composite stress-form transmitted into the surrounding medium will vary in shape from that of a sphere to that of a cylinder with hemispherical ends, depending on the method of initiation used and the properties of both the explosives and containing material. For the cylindrical wave to form, for example, all points along the column must be initiated simultaneously. This is highly improbable for most types of blasting except for very short columns that are initiated in the center or moderate length charges that contain closely-spaced primers which are all initiated by means of instantaneous electrical blasting caps. Instead, the composite wave-form usually is either some form of conical shape or spherical. The conical wave results when the reaction velocity through the explosive column exceeds the compressive wave velocity of the surrounding medium. In this instance stresses from the charge ends in each of the planes intersecting the axis of the explosive column will be diverged like those from the spherical charge with changing angles of incidence at free-face planes, while stresses in the planes of the axis from the central portion of the column will be directed with a constant angle of incidence. Stresses in the planes of the charge diameter and perpendicular to the column axis, however, will be diverged much in the same circular manner as those produced from the spherical point charge.

### The Cube-Root Law

For the idealized condition of the single point charge, as would be also the case for each single segment within the long-length column charge, the divergence of energy through a material propagated from an explosion could be considered to be contained within a sphere of influence whose volume would be a function of the cube of the distance of propagation away from the explosion's center or  $V_d = \frac{4}{3}\pi d^3$ . It follows, then, that for the energy to spread out within a volume whose radius is twice that of the charge, the explosive's energy would have been dispersed throughout a volume equal to 8 times that occupied by the explosive. In the event the radius of influence considered in the material is 5 times the charge radius or  $d = 5D_e/2$ , then the volume of the expanded sphere of influence would be 125 times that of the charge. In other words, the ideal magnitude of the energy contained within one unit volume of material at a distance of  $d$  from an explosion center ( $dQ_d$ ) would be equal to the product of the unit energy released initially from the explosion ( $dQ_e$ ) TIMES the specific ratio of the explosive's initial volume to that of the sphere of influence in the material affected. Mathematically, the general relationship would be

$$dQ_d = dQ_e (V_e/V_d).$$

Because the volume of the explosive would be a function of its charge diameter, or  $V_e = (D_e/2)^3$ , and the volume of the sphere of influence in the material being stressed by the explosive is proportional to the distance away from the explosion center, where  $V_d = d^3$ , it can be concluded that the fraction of the explosion's unit energy contained within a unit volume of the material will be equal to

$$dQ_d/dQ_e = (D_e/2d)^3.$$

In similar manner, it can be reasoned that for any specific spherical explosive, its total weight and amount of available energy would depend to a large extent on its unit density ( $SG_e$ ) and charge diameter ( $D_e$ ), providing velocity effects are excluded. Thus, a point charge with a 4-inch diameter could be expected to contain 8 times the energy and weigh 8 times that of a 2-inch diameter point charge of the same explosive. However, the total weights would differ between a concentric point charge and a long-length column charge with identical charge diameters by a factor equal to the ratio of their respective lengths; although the energy concentration PER FOOT OF CHARGE LENGTH would be identical. Therefore, it is generally preferred to use the unit density ( $SG_e$ ) or loading density ( $d_e$ ) of an explosive as the standard for comparison, rather than total charge weight. In the event the explosive's velocity does NOT remain constant, it is then necessary to account for its difference in order to consider the energy quantity for each condition. As a general rule, the relative energy (RE) would be a function of the product of the loading density and reaction velocity squared, or  $d_e v_e^2$ . Therefore, using the concept of relative energies from different explosives and under different blasting

conditions, it is possible to make reasonable approximations of the energy capabilities of various kinds of explosives and the estimated level of the transmitted stresses at any distance  $d$  from the explosion center. With respect to the relative energies of explosives with different densities but having a constant charge diameter and velocity of reaction, the following expression can be used:

$$RE_2 = RE_1 (SG_{e2}/SG_{e1})$$

In the case where explosives' densities, charge diameters, and reaction velocities all differ, the general relationship for making the comparison would be

$$RE_2 = RE_1 (c_{e2} v_{e2}^2 / d_{e1} v_{e1}^2)$$

For all practical considerations, the comparisons would be reasonably valid for all center-initiated 1-ft long charges with diameters that would vary from 2 to 72 inches. This is because the range of values for  $L_e/D_e$  and its reciprocal, or  $D_e/L_e$ , would not exceed 6, which was defined earlier as the limitation for a point charge.

The significance of the foregoing relationships becomes apparent when one considers their application for cratering in materials. The problem, in gist, is one involving the accomplishment of mechanical work, whereby the energy supplied by the explosive ( $Q_e$ ) is used for fracturing the materials by overcoming their strength properties and then displacing the broken particles. In general, the required diverged value of  $dQ_e$ , or  $dQ_e$  at distance  $d$  from the explosion's center, will be unique for any given type of material.

The specific depth of charge burial, which would correspond with the maximum limit for distance  $d$ , at which optimum crater results will be achieved is called the burden,  $B$ . The volume of the developed crater ( $V_c$ ), in turn, will always be a function of  $B$ , as well as the explosive's  $Q_e$ . For example,  $V_c$  for a simple cone-type crater with one free surface is  $\pi r^2 B/3$ , but the value for the crater radius  $r$  is dependent on the material's properties and is related to  $B$ . Thus, as a general rule one can assume that  $V_c = B^3 = Q_e$  for approximation purposes. From the previous discussions it was shown that  $Q_e = RE_e = SG_e = D_e^3$ . Therefore, for any confined explosive charge it can be concluded that

$$B = V_c^{1/3} = RE_e^{1/3} = SG_e^{1/3} = D_e'$$

$$\text{and } B_2 = B_1 (RE_2/RE_1)^{1/3} \text{ or } B_2 = B_1 (D_{e2}/D_{e1})$$

In summation, the cube-root law describes the effect of three-dimensional divergence in reducing the stress energy produced by a confined explosive charge as the energy propagates in all directions

through a material. As a result, the ideal optimum depths of burial (or burden) and the resultant crater volumes produced by confined explosive charges in a given blasting environment will be proportional to the charge diameters and the cube root of their respective relative energies.

### The Square-Root Law

Because the energy of an explosive is released as a pressure or stress, i.e.,  $P_e$  or  $\sigma_e$ , it will exert itself over the entire surface of the charge. For the concentric or point charge the total outer surface at which the pressure acts is equal to  $4\pi r_e^2 = \pi D_e^2$ . Therefore, the total energy from the explosion ( $Q_e$ ) will be equal to  $\sigma_e(\pi D_e^2)$ . By similar analysis, from the explosion center the stress transmitted through a material a distance  $d$  will be distributed over a surface area equaling  $4\pi d^2$ , in which the total energy at that location  $\sigma_d$  times the area would be related in the form of  $Q_d = \sigma_d(4\pi d^2)$ . Assuming there are no losses because of absorption, etc., or  $Q_e = Q_d$ , it follows then that

$$\sigma_e(\pi D_e^2) = \sigma_d(4\pi d^2),$$

$$\text{or} \quad \sigma_d = \sigma_e (D_e/2d)^2.$$

If  $d = B$  for the optimum crater produced, then

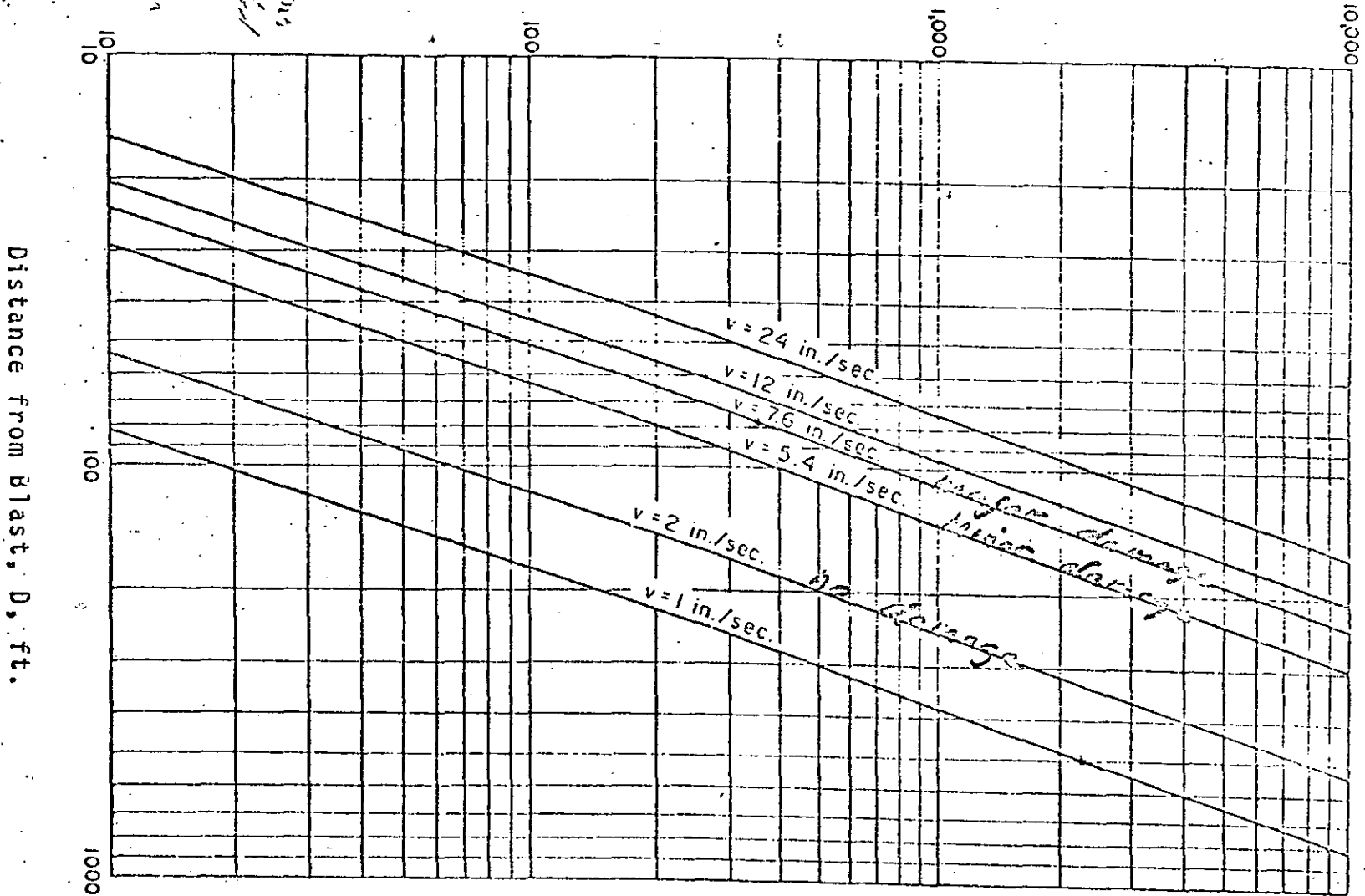
$$B = (D_e/2) (\sigma_e/\sigma_B)^{1/2}$$

Because the stresses transmitted into a material are proportional to the pressure released by the explosion, or  $\sigma_e = P_e$ , the transmitted stresses for the production of a crater must equal or exceed the material's strength properties, or  $\sigma_t$  or  $\tau_s$  depending on which would be the most critical. Thus, one can conclude that

$$B = P_e^{1/2} = \sigma_t^{-1/2} \text{ or } \tau_s^{-1/2}.$$

In brief, then, the square-root law of energy divergence, when used to predict requirements for the production of craters, states that the optimum depths of burial (or burden) and the resultant crater volumes for confined explosive charges in any given blasting environment will vary directly with the square root of their respective explosion pressures and inversely with the square root of the pertinent materials' strengths.

Maximum Weight of Charge Per Delay W, lbs.



42

US monograph

was NOT copied

to USSB III's. Reasons

group can't find

any sub. text

factor - 1150m

reference point

for this graph

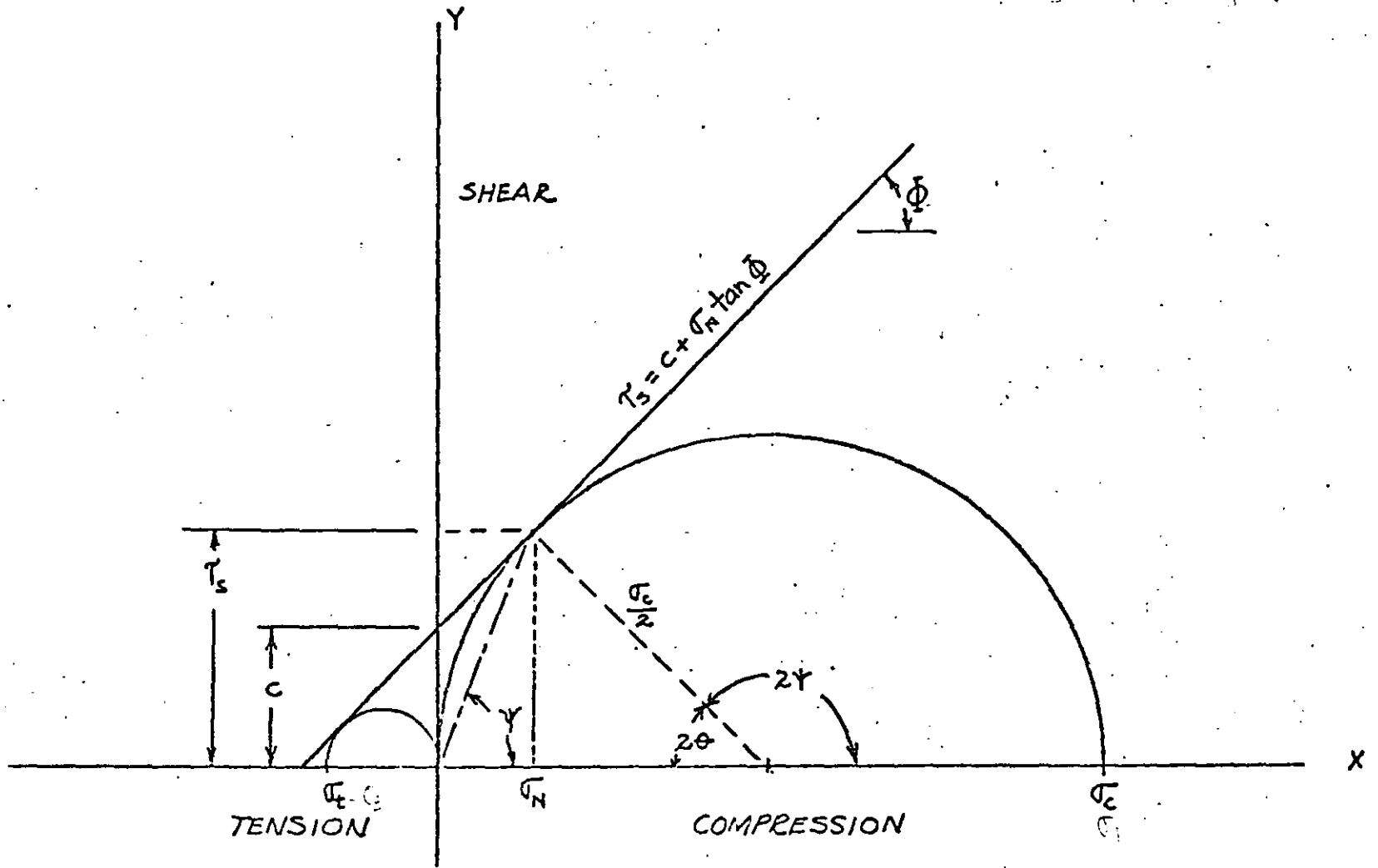
NOT correlated

to Sealed Distances

from which is based upon

Minor damage: fine plastic cracks, opening of old cracks  
 Major damage: serious new cracking, plastic pellets





MOHR'S FAILURE ENVELOPE

NOTE: @  $\phi = 36.8^\circ$ ,  $\tau_s = \sigma_c = \sigma_c / 1.4$ ; AND  $\gamma = (90^\circ + \phi) / 2$

TABLE I. Strength Data For Some Competent Rocks (13).

Rock Type	Compressive Strength psi x 10 <sup>3</sup>	Elasticity Modulus (Compression) psi x 10 <sup>6</sup>	Tensile Strength psi	C psi	$\phi$ deg.	Equation of Mohr's Envelope (ref. Fig. 3)
Chert	29.3	8.15	820	2550	71.5	$Y = 2550 + 3.0 x$
Coal	6.2	-	-	1600	38.5	$Y = 1600 + 0.8 x$
Granite	28.0	3.17	410	1720	76.5	$Y = 1720 + 4.2 x$
Green Stone	29.1	8.82	380	1700	77.5	$Y = 1700 + 4.5 x$
Greywacke	7.9	1.80	700	1200	59.5	$Y = 1200 + 1.7 x$
Limestone	21.3	9.50	350	1320	75.5	$Y = 1320 + 3.9 x$
Marble	30.8	7.15	863	2650	71.0	$Y = 2650 + 2.9 x$
Salt Rock	2.2	1.35	85	210	72.5	$Y = 210 + 3.2 x$
Sand Stone	14.8	2.00	230	900	76.0	$Y = 900 + 4.0 x$
Shale	5.2	1.09	1538	1420	31.0	$Y = 1420 + 0.6 x$
Silt-Stone	5.0	12.60	440	750	59.5	$Y = 750 + 1.7 x$

C - Cohesion

$\phi$  - Angle of Internal Friction

Y - Shear Stress,  $\tau_s$

x - Normal Stress,  $\sigma_n$

TABLE II. Strength Data for Some Altered  
or Fragmented Materials (14, 15).

Rock Type	Cohesion, $c$ , psi	Friction Angle, $\phi$ , deg.	Equation of Mohr's Envelope (Ref. Fig. 3)
Decomposed Limestone	7.0	18	$Y = 7.0 + 0.30 x$
Altered Quartzite	5.0	34	$Y = 5.0 + 0.67 x$
Altered Schist	6.0	40	$Y = 6.0 + 0.84 x$
Dense Sand and Gravel	7.0	32	$Y = 7.0 + 0.61 x$
Medium Clay	7.0	20	$Y = 7.0 + 0.36 x$
Soft Clay	2.8	15	$Y = 2.8 + 0.27 x$
Liquid Clay	0.7	15	$Y = 0.7 + 0.27 x$

$Y =$  Shear stress,  $T_s$   
 $x =$  Normal stress,  $\sigma_n$

## SINGLE BLASTHOLE DESIGN PROBLEM

A deposit is quarried in 30-ft high benches for crushed stone. The rock is quite massive and has the following properties:

$$\begin{aligned} SG_r &= 2.9, & v_p &= 17,000 \text{ fps}, & \mu &= 0.25, & S_f &= 0.7, \\ \gamma &= 45 \text{ deg}, & Q_c &= 25,000 \text{ psi}, & & & Q_t &= 1750 \text{ psi}. \end{aligned}$$

Blasted rock is loaded by a 5 cy front-end loader. The blastholes are drilled vertically and bulk loaded ( $D_o = D_n$ ) with an explosive having an SO = 117,  $D_c = 1$  in., and confined velocities of 12,500 fps at 3 in. and 15,000 fps at 5 in. and larger charge diameters. The relationship between  $v_e$  and  $D_e$  in the 1 to 5 in. range can be assumed to be in the form of

$$v = \frac{cx}{a + bx}$$

Drainage at the operation is such that blastholes generally are always dry, and there is no free parting in the rock available that can serve as a floor. For estimating purposes the average blast area  $A$  of material cratered by a single blasthole would be equal to  $1.4B^2$ .

A.. Considering the foregoing information, find the following properties for the intact rock:

(1)  $\bar{v}_s$ , and (2)  $E_r$ .

B.. For charge diameters  $D_e$  of (a) 2 in., and (b) 4 in., determine each of the following estimates:

(1)  $v_a$ , (2)  $P_d$ , (3)  $P_a$ , (4)  $B_s$ , (5)  $T$ , (6)  $J$ ,  
 (7)  $E$ , (8)  $W$ , (9)  $t_f$ , and (10)  $t_1$ .

C. At the given bench height  $L$  determine the respective  $D_o$  values that define each of the following conditions:

(1) The  $B'$  that insures all of the explosive column will react before any cracks will have propagated to any open face when using a single primer located at (a) Floor level, and at (b) The Center of the charge column.

(2) The  $B''$  at which overbreak quite likely may begin to occur when the primer is place at floor level.

# SOLUTION TO SINGLE BLASTHOLE DESIGN PROBLEM

A (1) From Eq. 21,

$$\sigma_t = \sigma_c \left( \frac{1 - \sin \phi}{1 + \sin \phi} \right)$$

Then

$$\frac{1750}{25,000} = \frac{1 - \sin \phi}{1 + \sin \phi}$$

or

$$0.07(1 + \sin \phi) = 1 - \sin \phi$$

$$0.07 + 0.07 \sin \phi = 1 - \sin \phi$$

$$1.07 \sin \phi = 0.93$$

or

$$\sin \phi = 0.87$$

Thus,

$$\phi = 60 \text{ deg}$$

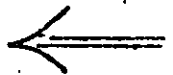
From Eq. 22(b),

$$\tau_s = \frac{\sigma_c}{2} (1 \cos \phi)$$

$$= \frac{25,000}{2} (0.5)$$

or

$$\tau_s = 6250 \text{ psi}$$



A (2) From Eq. 14(b)

$$V_p = \left[ \frac{E_r (1 - M)}{P_r (1 + M)(1 - 2M)} \right]^{1/2}$$

From Eq. 8(b)

$$P_r = 1.941 SGr$$

Thus, substituting given values of  $V_p$ ,  $M$ , and  $SGr$  and squaring both sides of Eq. 14(b),

$$(17,000)^2 = \frac{E_r (1 - 0.25)}{1.941 (2.9)(1 + 0.25)(1 - 2 \cdot 0.25)}$$

Rearranging

$$E_r = \frac{1.7^2 \times 10^8 (1.941)(2.9)(1.25)(0.5)}{0.75}$$

or

$$E_r = 13.5 \times 10^8 \text{ psf} = 9.4 \times 10^4 \text{ psi}$$



## SOLUTION (cont.)

B(1) First determine relationship of  $V_e$  with  $D_e$   
from  $y = \frac{cx}{a+bx}$  where  $y = V_e$  and  $x = D_e - D_c$

$$\text{Then } V_e = \frac{c(D_e - D_c)}{a + b(D_e - D_c)}$$

It is given that  $D_c = 1$  in.,  $V_e = 12,500$  fps @  $D_e = 3$  in.,  
and  $V_e = 15,000$  fps @  $D_e = 5$  in.

$$\text{Then @ } D_e = 3 \text{ in.}, \quad 12,500 = \frac{c(3-1)}{a+b(3-1)} = \frac{2c}{a+2b}$$

Assume  $c = 5000$ ,

$$\text{Then } a + 2b = \frac{2(5000)}{12,500} = \frac{4}{3} = 0.80 \quad (\text{I})$$

$$\text{For } D_e = 5 \text{ in.}, \quad 15,000 = \frac{c(5-1)}{a+b(5-1)} = \frac{4c}{a+4b}$$

$$\text{or } a + 4b = \frac{4(5000)}{15,000} = \frac{4}{3} = 1.33 \quad (\text{II})$$

$$\begin{array}{l} \text{Regrouping} \\ a + 2b = 0.80 \quad (\text{I}) \\ a + 4b = 1.33 \quad (\text{II}) \end{array}$$

Subtracting I from II,

$$2b = 0.53$$

$$\text{or } b \approx 0.27$$

Substituting value of  $b$  in I and II,

$$a + 2(0.27) = 0.80 \quad (\text{I})$$

$$\text{or } a = 0.26$$

$$\text{and } a + 4(0.27) = 1.33 \quad (\text{II})$$

$$\text{or } a = 0.25$$

For all practical purposes, then,  $a = 0.26$  and  $b = 0.27$   
When  $c = 5000$ .

SOLUTION (cont.)

B (1) (cont.)

Therefore, basic velocity equation for the explosive is

$$V_e = \frac{5000(D_0 - 1)}{0.26 + 0.27(D_0 - 1)}$$

with the  $D_0$  range of values from 1 to 5 inches.

Check: @  $D_0 = 3$  in.

$$\begin{aligned} V_e &= \frac{5000(3-1)}{0.26 + 0.27(3-1)} = \frac{10,000}{0.26 + 0.54} \\ &= 12,500 \text{ fps} \quad \underline{\text{OK}} \end{aligned}$$

@  $D_0 = 5$  in.

$$\begin{aligned} V_e &= \frac{5000(5-1)}{0.26 + 0.27(5-1)} = \frac{20,000}{0.26 + 1.08} \\ &= 14,900 \text{ fps} \quad \underline{\text{OK}} \end{aligned}$$

(a)  $D_0 = 2$  in.

$$V_e = \frac{5000(2-1)}{0.26 + 0.27(2-1)} = \frac{5000}{0.26 + 0.27} = 9450 \text{ fps} \leftarrow$$

(b)  $D_0 = 4$  in.

$$V_e = \frac{5000(4-1)}{0.26 + 0.27(4-1)} = \frac{15,000}{0.26 + 0.81} = 14,000 \text{ fps} \leftarrow$$

B (2) From Eq. 4 (a)

$$P_d = \frac{6.06 \times 10^{-3} V_e^2 (S_{hc})}{1 + 0.80 (S_{hc})}$$

From Eq. 1

$$S_{hc} = \frac{141}{3C} = \frac{141}{117} = 1.2$$

Then

$$P_{d_{\max}} = \frac{6.06 \times 10^{-3} \times 1.5^2 \times 10^8 \times 1.2}{1 + 0.80(1.2)} = \frac{6.06 \times 2.25 \times 10^5 \times 1.2}{1.96}$$

or

$$P_{d_{\max}} = 835,000 \text{ psi}$$

SOLUTION (CONT.)

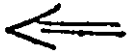
B(2) (CONT.)

(a)  $D_e = 2 \text{ in.}$

$$P_d = P_{d_{\max}} \left( \frac{9450}{15,000} \right)^2 = 835,000 (0.397)$$

or

$$P_d = 331,000 \text{ psi}$$

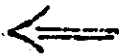


(b)  $D_e = 4 \text{ in.}$

$$P_d = P_{d_{\max}} \left( \frac{14,000}{15,000} \right)^2 = 835,000 (0.87)$$

or

$$P_d = 730,000 \text{ psi}$$

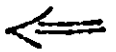


B(3) From Eq. 4 (b),

$$P_e = P_{d_{\max}} / 2$$

Thus, (a)  $D_e = 2 \text{ in.}$ , and (b)  $D_e = 4 \text{ in.}$ ,

$$P_e = 835,000 / 2 = 417,500 \text{ psi}$$



B(4)

From Eq. 35,

$$K_B = 30 \left( \frac{160}{d_r} \right)^{\frac{1}{3}} \left( \frac{S_{6e}}{1.3} \right)^{\frac{1}{3}} \left( \frac{V_e}{12,000} \right)^{\frac{2}{3}}$$

From Eq. 7,

$$d_r = 62.4 (S_{6r}) = 62.4 (2.9) = 181 \text{ psi}$$

Substituting for values of  $d_r$  and  $S_{6e}$ , then

$$\begin{aligned} K_B &= 30 \left( \frac{160}{181} \right)^{\frac{1}{3}} \left( \frac{1.2}{1.3} \right)^{\frac{1}{3}} \left( \frac{V_e}{12,000} \right)^{\frac{2}{3}} \\ &= 30 (0.94)(0.97) \left( \frac{V_e}{12,000} \right)^{\frac{2}{3}} \end{aligned}$$

or

$$K_B = 28 \left( \frac{V_e}{12,000} \right)^{\frac{2}{3}}$$

But from Eq. 34,

$$B = \frac{K_B D_e}{12} = \frac{28}{12} \left( \frac{V_e}{12,000} \right)^{\frac{2}{3}} D_e$$



# SOLUTION (CONT.)

## B(4) (CONT.)

In general form, therefore,  $B = 2.33 D_c \left( \frac{V_c}{12,000} \right)^{\frac{2}{3}}$  ft.

(a)  $D_c = 2$  in.

$$B = 2.33(2) \left( \frac{9450}{12,000} \right)^{\frac{2}{3}} = 4.66 (0.86) = 4.0 \text{ ft} \leftarrow$$

(b)  $D_c = 4$  in.

$$B = 2.33(4) \left( \frac{14,000}{12,000} \right)^{\frac{2}{3}} = 9.32 (1.11) = 10.3 \text{ ft} \leftarrow$$

Also, for  $D_c = 3$  in.

$$B = 2.33(3) \left( \frac{12,500}{12,000} \right)^{\frac{2}{3}} = 7 (1.02) \approx 7 \text{ ft}$$

And for  $D_c = 5$  in. and larger,

$$B = 2.33 D_c \left( \frac{15,000}{12,000} \right)^{\frac{2}{3}} = 2.33 D_c (1.16) = 2.7 D_c$$

Thus, at  $D_c = 5$  in.,

$$B = 2.7(5) = 13.5 \text{ ft}$$

At  $D_c = 6$  in.,

$$B = 2.7(6) = 16.2 \text{ ft}$$

## B(5) From Eq. 33, $T \approx 28.13$

Thus, (a)  $D_c = 2$  in.,

$$T \approx 2(4)/3 = 2.7 \text{ ft} \leftarrow$$

(b)  $D_c = 4$  in.,

$$T \approx 2(10.3)/3 = 6.9 \text{ ft} \leftarrow$$

## B(6) From Eq. 32, $J \approx B/3$

Thus, (a)  $D_c = 2$  in.,

$$J \approx 4/3 = 1.33 \text{ ft} \leftarrow$$

(b)  $D_c = 4$  in.,

$$J \approx 10.3/3 = 3.43 \text{ ft} \leftarrow$$

SOLUTION: (CONT.)

B (7) From Eq. 3 where  $d_c = 0.34 D_o^2 (56_c)$  and combining Eqs. 29 through 33, we obtain when  $L = 30$  ft,

$$E = d_c (PC) = 0.34 D_o^2 (56_c) (L + J - T) \\ = 0.34 D_o^2 (1.2) (30 - B/3) = 0.41 D_o^2 (30 - B/3), \text{ lb.}$$

(a)  $D_o = 2$  in.

$$E = 0.41 (2)^2 (30 - 1.33) = (1.64)(28.7) = 47 \text{ lb} \quad \leftarrow$$

(b)  $D_o = 4$  in.

$$E = 0.41 (4)^2 (30 - 3.43) = (6.56)(26.6) = 174 \text{ lb} \quad \leftarrow$$

B (8) If  $A = 1.4 B^2$  and  $W = \frac{A L d_r}{2000} = \frac{1.4 B^2 (30)(.61)}{2000}$ ,

then  $W = 3.8 B^2$

(a)  $D_o = 2$  in.,  $W = 3.8 (4)^2 = 61 \text{ tons} \quad \leftarrow$

(b)  $D_o = 4$  in.,  $W = 3.8 (10.3)^2 = 402 \text{ tons} \quad \leftarrow$

B (9) From Eq. 19,  $V_f = V_p / 3 = 17,000 / 3 = 5670 \text{ fps}$

If  $t_f = B / V_f$ , sec, (a)  $D_o = 2$  in.,  $t_f = 4 / 5670 = 0.6 \text{ ms} \quad \leftarrow$

(b)  $D_o = 4$  in.,  $t_f = 10.3 / 5670 = 1.5 \text{ ms} \quad \leftarrow$

B (10) If  $t_i = 0.001 B$ , sec.

(a)  $D_o = 2$  in.,  $t_i = 0.001 (4) = 4.0 \text{ ms} \quad \leftarrow$

(b)  $D_o = 4$  in.,  $t_i = 0.001 (10.3) = 10.3 \text{ ms} \quad \leftarrow$

# SOLUTION (CONT.)

C.(1) From Eq. 36,  $K_v = \frac{V_c}{V_p}$ . Thus, from part B and determining  $K_v$  for the respective  $V_c$  values for each  $D_c$  from 1 to 6 inches, inclusive, the following summary table can be prepared:

$D_c$ , in.	$B$ , ft.	$V_c$ , fps	$K_v$
1	0	0	0
2	4	9450	0.56
3	7	12,500	0.74
4	10.3	14,000	0.82
5	13.5	14,900	0.88
6	16.2	15,000	0.88

## (a) Floor Priming

From Eq. 38(a),  $B' = \frac{3L}{9K_v + 2}$

1. At  $D_c = 5$  in.,

$$B' = 3(30) / (9 \times 0.88 + 2) = 90 / 9.9 = 9.1 \text{ ft.}$$

From above Table,  $B = 13.5$  ft.

Thus,  $B > B'$  or  $13.5 > 9.1$ . Diameter can be reduced.

2. At  $D_c = 4$  in.,

$$B' = 3(30) / (9 \times 0.82 + 2) = 90 / 9.4 = 9.6 \text{ ft.}$$

From Table,  $B = 10.3$  ft.

Thus,  $B > B'$  or  $10.3 > 9.6$ . Diameter can be reduced.

3. At  $D_c = 3$  in.,

$$B' = 3(30) / (9 \times 0.74 + 2) = 90 / 8.66 = 10.4 \text{ ft.}$$

From Table,  $B = 7$  ft.

Thus,  $B < B'$  or  $7 < 10.4$ . Diameter too small.

Note that at  $D_c = 4$  in., optimum burden  $B$  and the minimum burden  $B'$  at which misfire might occur are approximately equal. Therefore, use  $D_c = 4$  in.  $\leftarrow$

# SOLUTION (CONT.)

## 3(1) (CONT.)

(b) Primer at center of charge column.

$$\text{From Eq. 38(b), } B' = \frac{3L}{18K_v + 1}$$

1. At  $D_c = 5$  in.,

$$B' = 3(30) / (18 \times 0.88 + 1) = 90 / 16.8 = 5.4 \text{ ft.}$$

From Table  $B = 13.5$  ft.

$B$  is much greater than  $B'$  indicating diameter can be much smaller, i.e.,  $B > B'$  or  $13.5 > 5.4$ .

2. At  $D_c = 3$  in.,

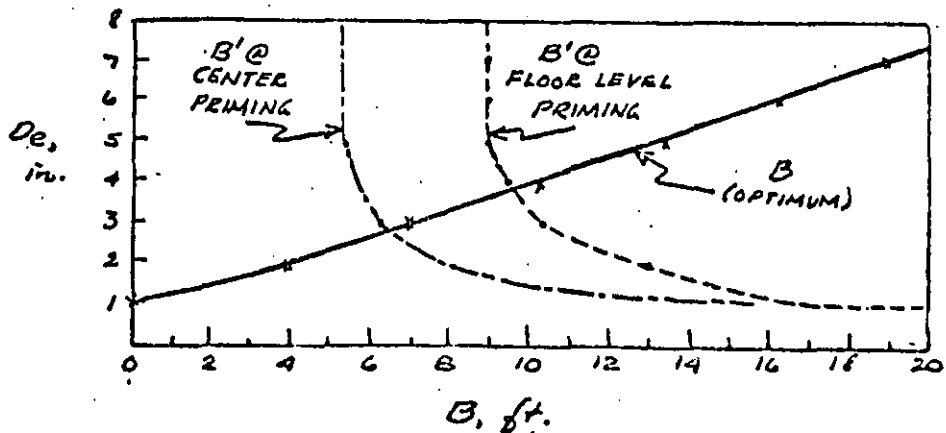
$$B' = 3(30) / (18 \times 0.74 + 1) = 90 / 14.3 = 6.3 \text{ ft.}$$

From Table  $B = 7$  ft.

Values of  $B$  and  $B'$  are approximately equal with  $B > B'$  a small amount, which is desirable.

Therefore, use  $D_c = 3$  in. ←←

NOTE The previous solutions can be solved quite simply by plotting values as shown below:



## C(2)

From Eq. 39,  $B'' = 0.62L = 0.62(30) = 18.6$  ft. ←←

This burden would be for  $D_c = \frac{B''}{2.7} = \frac{18.6}{2.7} = 6.9$  in.



**DIVISION DE EDUCACION CONTINUA  
FACULTAD DE INGENIERIA U.N.A.M.**

**MECANICA DE ROCAS APLICADA A LA MINERIA Y A LA CONSTRUCCION**

**METODOS DE EXCAVACION  
ANEXOS**

**M. EN C. JOSE IBARRA TORRES**

**MAYO, 1985.**

## C O N T E N I D O

PROPIEDADES ELASTICAS DE ALGUNOS TUNELES CON:

- a) Máquina tunelera
- b) Método convencional
- c) Método parcial

ANALISIS ESTADISTICO ENTRE METODOS DE TUNELEO Y RESISTENCIA  
A LA COMPRESION

LINEAS DE CONSTRUCCION DE TUNELES (figura)

CALCULO DE BARRENOS DE CUÑA

NUEVO METODO AUSTRIACO DE TUNELEO

TABLE 1

~~FULL-FACE MACHINE TUNNELING EXAMPLES~~

<u>Tunnel</u>	<u>Rock</u>	<u>Compressive Strength</u> (psi)	<u>Elastic Modulus</u> (psi/uE)	<u>Poisson's Ratio</u>	<u>Advance Rate-Avg</u> (ft/day)	<u>Diameter</u> (ft)	<u>Machine</u>
Nast, CO	Granite, medium to fine grained	18,000	8.50	0.30	22.7	9.75	Wirth TBII-300H
Nast, CO	<del>Granite, fine</del> grained	<del>24,000</del>	<del>8.30</del>	<del>0.33</del>	<del>14.7</del>	9.83	Wirth TBII-300H
Climax, CO	Granite Gneiss Silicified	8,000	9.70	0.35	14.2	13.00	Calweld 40
Mather B, MI	Metamorphic Hematite & Martite	7,000	2.50	0.15	NA	9.96	Calweld Occillator
Geduld, S.A.	Quartzite & Dolerite	14,500 51,000	NA	NA	8.2	11.15	Wirth S11-340H
Richmond, NY	Mica Schist	15,000	12.26	0.17	33	11.00	Jarva 12-1100
Richmond, NY	Mica Schist	13,000	8.50	0.20	28	8.50	Jarva 8-806
Queens Lane NY	Mica Schist	11,000	4.50	0.25	26	11.00	Jarva 11-1100
White Pine MI	Sandstone, fine grained	22,000	5.38	0.25	43	18.10	Robbins 181-122
White Pine MI	Sandstone, Siltstone, Shale	23,000	9.50	0.15	NA	18 x 8.5 Rectangular	Atlas-Copco 4-head

TABLE 1 (Continued)

Tunnel	Rock	Compressive Strength (psi)	Elastic Modulus (psi/μE)	Poisson's Ratio	Advance Rate-Avg. (ft/day)	Diameter (ft)	Machine
Superior AZ	Limestone	29,000	8.70	0.41	70	13.67	Lawrence HRT
Superior AZ	Limestone	20,000	4.61	0.50	58	13.67	Lawrence HRT
Milwaukee WI	Limestone	36,000	10.00	0.30	44	11.17	Jarva 11-1100
Milwaukee WI	Limestone	22,000	7.84	0.46	43	11.17	Jarva 11-1100
Mt. Green	Limestone	26,000	10.63	0.50	85	10.33	Robbins 105-144
Mt. Green	Limestone	30,000	10.82	0.30	105	10.33	Robbins 105-144
Layout, UT	Sandstone, medium grained	10,000	1.80	0.10	130	12.92	Robbins 141-127-1
Layout, UT	Conglomerate, sandstone matrix	22,000	10.80	0.18	79	12.92	Robbins 141-127-1
Currant, UT	Conglomerate, calcareous cement	28,000	6.00	0.18	133	12.92	Robbins 141-127-1
Navajo #3 NM	Sandstone, fine grained	2,000	0.20	0.10	87	20.50	Dresser TB-205
Navajo #1 NM	Sandstone, medium grained	5,000	0.10	0.10	51	20.50	Hughes Betti I

higher E ✓  
 higher Jc ✓

higher V — easier to drill  
 higher E — harder  
 higher Jc —



Table 1 (Continued)

<u>Tunnel</u>	<u>Rock</u>	<u>Compressive Strength (psi)</u>	<u>Elastic Modulus (psi/uE)</u>	<u>Poisson's Ratio</u>	<u>Advance Rate-Avg. (ft/day)</u>	<u>Diameter (ft)</u>	<u>Machine</u>
Rochester NY	Sandstone, fine grained	11,000	4.47	0.24	92	18.33	Lawrence I-R HRT
Starvation, UT	Sandstone, and Shale	NA	NA	NA	64	9.5	Robbins 81-113
Water Hollow, UT	Sandstone, Silt Shale & Cgl.	NA	NA	NA	96	12.92	Robbins 104-121A
River Mtns, NV	Rhyolite and Rhyodacite	16,700	NA	NA	108	12.00	Jarva 11-12
Azotea, CO & NM	Shale and Sandstone	1,400 - 6,000 3,000 - 8,500	NA	NA	153(Sh) 72(Ss)	13.33 12.67	Robbins 104-121A
Blanco, CO	Shale	4,000	NA	NA	154	10.58	Robbins 104-120
Oso, CO	<u>Shale</u>	4,000	NA	NA	<u>198</u>	10.58	Robbins 104-121A
White Pine, MI	Sandstone, Siltstone & Shale	12,000 - 31,000	NA	NA	36	7.00	Hughes
Star, ID	Argillaceous, Quartzite	17,000	8.35	0.13	29	9.00	Jarva VIII
Kermac 33 Grants, NM	Sandstone and Shale (weak)	2,500	NA	NA	16	9.00	Robbins 103
Homer Wauseca MI	Iron Ore	11,000	NA	NA	19.5	7.00	Robbins 71A

NA - Not available.

TABLE 2

Conventional Drill-Blast-Muck Tunneling Examples

<u>Tunnel</u>	<u>Rock</u>	<u>Compressive Strength (psi)</u>	<u>Elastic Modulus (psi/u€)</u>	<u>Poisson's Ratio</u>	<u>Advance Rate (ft/day)</u>	<u>Size (ft)</u>	<u>Shape</u>
Nast, CO	Granite, fine grained	28,000	8.32	0.35	12.6	10x10	Horseshoe
GA-1	<del>Granite, major quartz</del>	<del>35,000</del>	<del>6.40</del>	<del>0.35</del>	NA	10x10	Horseshoe
Hunter,	Granite, fine grained	32,000	8.00	0.31	NA	10x10	Horseshoe
Hunter,	Granite, gneissie	39,000	10.00	0.35	NA	10x10	Horseshoe
Hunter,	Granite Gneiss, jointed	29,000	8.89	0.31	NA	10x10	Horseshoe
San Manuel, AZ	Quartz Monzonite, coarse grained	19,000	7.46	0.20	NA	12x12	Rectangular
Star, ID	Argillaceous Quartzite	21,000	8.53	0.13	NA	9x10.7	Arched Back
Crescent, ID	Quartzite, fractured	13,000	5.72	0.18	NA	10x10	Rounded Rectangular
Homestake, SD	Phyllite Schist Chlorite Schist	19,000	8.62	0.20	NA	7.5x7.5	Arched Back
Mather B, MI	Graywacke	22,000	9.76	0.20	NA	10x10.8	Rectangular

TABLE 2 (Continued)

<u>Tunnel</u>	<u>Rock</u>	<u>Compressive Strength (psi)</u>	<u>Elastic Modulus (psi/uE)</u>	<u>Poisson's Ratio</u>	<u>Advance Rate (ft/day)</u>	<u>Size (ft)</u>	<u>Shape</u>
White Pine, MI	Sandstone, Siltstone, Shale	23,000	9.52	0.15	NA	24x7.5	Rectangular
Superior, AZ	Conglomerate, Limestone Matrix	11,000	7.20	0.25	NA	9x10	Rectangular
Superior, AZ	Conglomerate, Limestone Matrix	25,000	8.70	0.22	NA	9x10	Rectangular
Western Nuc., WY	Sandstone, poorly consolidated	1,000	0.10	0.10	NA	5x9	Rectangular

NA - Not available.

TABLE 3

Partial-Face Machine Tunneling Examples

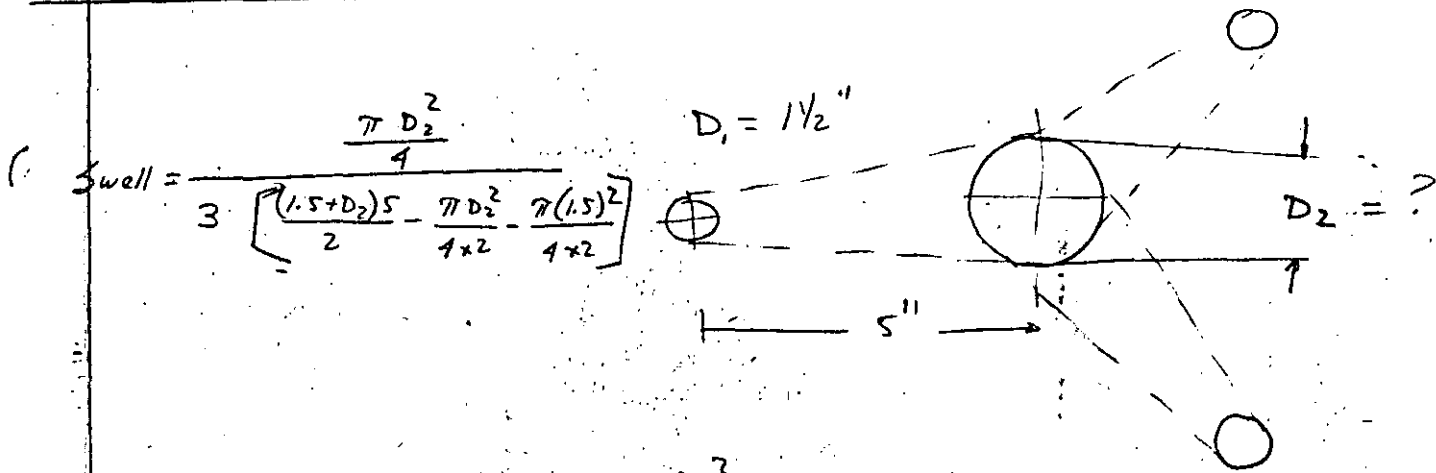
<u>Tunnel</u>	<u>Rock</u>	<u>Compressive Strength (psi)</u>	<u>Elastic Modulus (psi/μE)</u>	<u>Poisson's Ratio</u>	<u>Advance Rate (ft/day)</u>	<u>Size/ Shape</u>	<u>Machine</u>
San Fernando, CA	Sandstone, Arkosic loosely consolidated	1-2,000	0.10	0.10	156	21.0 Circular	Robbins 221S Ripper
Mather B, MI	Metamorphic, Hemzite & Martite	6,000	2.10	0.15	NA	10x9.5 Rectangular	Alpine F-6A
Western Nuc., WY	<del>Sandstone</del> <del>poorly consolidated</del>	<del>15,000</del>	<del>0.10</del>	<del>0.10</del>	13.0	10x8 Rectangular	Alpine F-6A
Kermac, NM	<del>Mudstone</del> <del>massive</del>	<del>41,000</del>	<del>5.0</del>	<del>0.10</del>	NA	10x9 Rectangular	Alpine F-6A
Orchard, CO	Claystone sandy, massive	1,700	1.0	0.37	16	9x9 Horseshoe	Alpine F-6A

NA - Not available.

TABLE 4

**Statistical Analysis of Probable Relationships  
Between Tunneling Methods and Compression Strength**

Tunneling Method	Compression Strength (psi)			Equality of Means - Difference		Equality of Variances - Difference	
	Mean	Std. Dev.	No.	t <sub>calc</sub>	Confidence	f <sub>calc</sub>	Confidence
Conventional D-B-M	22,640	14,240	14	1.778	95.7%	2.12	95.5%
Machine (ALL) Full-Face	16,160	9,780	31	2.659	99.4%	5.22	93.6%
Machine Partial-Face	4,240	4,280	5	2.028	97.1%	6.01	99.5%
Machine (Successes) Full-Face	14,090	10,490	19	1.689	97.1%	1.84	90%
Conventional D-B-M	22,640	14,240	14	2.798	99.3%	11.07	98.1%
Machine Partial-Face	4,240	4,280	5				



$$\text{Swell} = \frac{\frac{\pi D_2^2}{4}}{3 \left[ \frac{(1.5 + D_2)5}{2} - \frac{\pi D_2^2}{4 \times 2} - \frac{\pi (1.5)^2}{4 \times 2} \right]}$$

$$0.60 = \frac{\frac{\pi D_2^2}{4}}{\left( \frac{7.5 + 5D_2}{2} - 0.393 D_2^2 - 0.884 \right) 3}$$

$$0.60 = \frac{0.786 D_2^2}{(11.25 + 7.5 D_2) - 1.179 D_2^2 - 2.65}$$

$$6.75 + 4.5 D_2 - 0.71 D_2^2 - 1.59 = 0.786 D_2^2$$

$$-1.5 D_2^2 + 4.5 D_2 + 5.16 = 0$$

$$D_2 = \frac{-4.5 \pm \sqrt{4.5^2 - 4(-1.5)(5.16)}}{2(-1.5)}$$

$$D_2 = \frac{-4.5 \pm 7.16}{-3.0} = \frac{2.66}{3.0}$$

$$D_2 = \frac{-4.5 - 7.16}{-3.0} = 3.89'' \approx 3\frac{11}{16}''$$

$$D_2 = \frac{-b \pm \sqrt{b^2 - 4ac}}{2a}$$

PADMASTER® Made in U.S.A.

Table 1.- Cohesion (c) and internal friction ( $\phi$ )  
angles for typical rocks.

Intac rock (Farnes, 1963)	(Jaeger & Cook, 1969)	(Wilson, 1962)
	c (psi)	$\phi$ ( $^{\circ}$ )
Shale	2 to 4,300	8 to 33 $^{\circ}$
Granite	2,000 to 7,000	45 to 55 $^{\circ}$
Dolerite (Diabase)	3,500 to 8,500	55 to 60 $^{\circ}$
Basalt	2,800 to 8,500	50 to 55 $^{\circ}$
Sandstone	1,100 to 5,700	27 to 50 $^{\circ}$
Limestone	1,400 to 7,000	35 to 58 $^{\circ}$
Quartzite	2,800 to 8,500	50 to 60 $^{\circ}$
Marble	2,100 to 4,200	35 to 50 $^{\circ}$
Trachyte		45 $^{\circ}$
Coal	800 to 4,600	30 to 40 $^{\circ}$
Rock-on-rock, natural surfaces		
	(Jaeger & Cook, 1969)	(Metcalf, 1965)
	c (psi)	$\phi$ ( $^{\circ}$ )
Shale	5	4 to 10 $^{\circ}$
Granite	45	30 to 35 $^{\circ}$
Gabbro	55	33 to 43 $^{\circ}$
Trachyte	60	29 to 35 $^{\circ}$
Sandstone	40	27 to 35 $^{\circ}$
Marble	160	22 to 36 $^{\circ}$
Rock Salt	---	30
Coke	---	32 to 40 $^{\circ}$
Anhydrite	---	31 to 37 $^{\circ}$

## NÚEVO METODO AUSTRIACO DE TUNELEO (NATM)

### AUXILIAR:

El método provee un sistema de seguridad y soporte económico en cavidades con incapacidad de soporte

### CARACTERISTICAS:

- Reducción del deterioro de roca de baja resistencia.
- Reduce las medidas de protección necesarias en el soporte, permitiendo cierto relajamiento
- Mediciones sofisticadas para confirmar el equilibrio del soporte
- Ausencia de soporte interno
- Record de seguridad establecido

### MEDIDAS DE PROTECCION:

La combinación del concreto lanzado con la malla provee seguridad al personal y estabilidad en la roca

### BASES TEORICAS DEL METODO:

Reajuste de esfuerzos después de la excavación ya sea cuando  $\sigma_o > \sigma_t$  ó  $\sigma_t > \sigma_o$

### BASES PRACTICAS DEL METODO:

Cooperación entre el diseñador, supervisor, contratista y personal de operación

### AVANCES TEORICO-EXPERIMENTALES RECIENTES:

Clasificación de roca

### "DEBILIDAD DEL METODO":

Alta dependencia de ingenieros y personal de operación con gran experiencia y entrenamiento profesional





**DIVISION DE EDUCACION CONTINUA  
FACULTAD DE INGENIERIA U.N.A.M.**

**MECANICA DE ROCAS APLICADA A LA MINERIA Y A LA CONSTRUCCION**

**ESTADO DE ESFUERZOS EN CAVIDADES  
A N E X O S**

**M. EN C. JOSE IBARRA TORRES**

**MAYO, 1985.**

C O N T E N I D O

ESTIMACION DE CONCENTRACION DE ESFUERZOS

- a) Obra subterránea
- b) Tajo abierto

ESTIMACION DE ESFUERZOS Y PRESION DE SOPORTE

P. H. Agua Prieta, Guadalajara, Jal.

Aplicación para diferentes estados de roca

- a) Terzaghi
- b) Talobre
- c) Rabcewicz

ESTIMACION DE ESFUERZOS TANGENCIALES

TAJO ABIERTO

POSICION	r	LINEA	$\sigma_1$	$\sigma_2$
1 - A	1/1		-1.0	+3.0
B	1/4		<u>+1.7</u>	<u>+5.2</u>
			Prom. +0.35	+4.1
2	1/6	2 1/2	+2.5	+1.8
		3	+1.5	+5.2
		3 1/2	<u>+0.0</u>	<u>+4.4</u>
			Prom. +1.3	+3.8
	1/2	2 1/2	-0.4	+4.5
		3	+1.5	+5.2
		3 1/2	<u>+2.4</u>	<u>+3.0</u>
			Prom. +1.2	+4.2
	1/3	2 1/2	+1.2	+3.2
		3	+1.5	+5.2
		3 1/2	<u>+1.2</u>	<u>+3.0</u>
			Prom. +3.3	+3.5
3	1/4	7	+1.4	-0.8
4 - A	1/4		+1.5	+5.2
B	1/4		<u>+1.5</u>	<u>-0.8</u>
			Prom. +1.5	+2.2
5	Si $\frac{R}{CL} = 0.77$			
	$\sigma_t = -0.09$			
	$\sigma_1 = (+1.5) (-0.09) =$		-0.16	
	$\sigma_2 = (+2.2) (-0.09) =$			-0.20

POSICION	r	LINEA	$\sigma_1$	$\sigma_2$
6	1/2		-1.0	+5.0
7	1/2	4 1/2	+0.7	+1.5
8	Si $\frac{R}{CL} = 0.59$			
	$\sigma_c = +3.2$			
	$\sigma_1 = (+0.7) (+3.2) =$		+2.2	
	$\sigma_2 = (+1.5) (+3.2) =$			+4.8
9	1/2	8	+1.7	-0.5
10	Si $\frac{R}{CL} = 0.50$			
	$\sigma_t = -0.1$			
	$\sigma_1 = (+1.7) (-0.1) =$		-0.17	
	$\sigma_2 = (-0.5) (-0.1) =$			+0.05
11 - A	1/2		+2.0	-1.0
B	1/1		+3.0	-1.0
		Prom.	+2.5	-1.0
12	1/1	5 1/2	+1.0	+1.0

EJEMPLO:

Se planea la construcción de una estación quebradora subterránea en forma ovaloide en la parte superior y rectangular en la inferior.

La estación es de 40 ft de ancho, 80 ft de altura y 80 ft de largo a una profundidad de 1 100 ft.

Los esfuerzos *in situ* horizontales son estimados en  $0.5 \sigma_v$  en la dirección NW-SE y  $1.5 \sigma_v$  en la NE-SW

Estime la concentración de esfuerzos en la estación para ambas direcciones a lo largo de los ejes orientados en las zonas indicadas en la Figura.

a) Estime:

$$\sigma_v = \underline{\hspace{10em}} \text{ lb/in}^2$$

$$\sigma_{h_1} = \underline{\hspace{10em}} \text{ lb/in}^2 \quad \text{NW-SE}$$

$$\sigma_{h_2} = \underline{\hspace{10em}} \text{ lb/in}^2 \quad \text{NE-SW}$$

b) Estime los esfuerzos correspondientes:

POSICION	$\sigma_v$	$\sigma_h$	ESFUERZOS TANGENCIALES (lb/in <sup>2</sup> )	
			NE-SW	NW-SE
A	<hr/>	<hr/>	<hr/>	<hr/>
B <sub>1</sub>	<hr/>	<hr/>	<hr/>	<hr/>
B <sub>2</sub>	<hr/>	<hr/>	<hr/>	<hr/>

$B_1, B_2$  (promedio)

\_\_\_\_\_

C

\_\_\_\_\_

c) ¿Qué orientación recomienda?

\_\_\_\_\_

METHODS OF SUPPORT ESTIMATION APPLIED TO  
AGUA PRIETA PROJECT; GUADALAJARA, MEXICO

by

JOSE IBARRA

December, 1983

## CHAPTER II

## CONCRETE SHAFT LINING DESIGN

Depending on the physical and mechanical properties of the rock and the magnitude of the forces acting, the following stress zones can be found around a shaft: elastic, plastic and fractured. In the elastic stress field, the magnitude of the stresses does not exceed the yield point (in compression) of the rock material. Competent rocks, especially under a low degree of confinement, tend to exhibit brittle (clastic) rather than plastic behaviour. Due to brittle properties of most rock material, the clastic state is encountered more often than the plastic state. Weak fractured and soft rock formations which are potentially plastic in their response have also been considered, using both elastic and plastic approaches.

## II.1 TRADITIONAL METHODS

Prior to any shaft lining calculations, an evaluation must be made, taking into account factors as the geologic and structural state, rock properties, the effect of discontinuities and stress state.

The planned Agua Prieta penstock shaft will be located



in soft to hard, competent igneous rock.

The shaft lining requirements are influenced by; 1) the level of confidence in the interpretation of underground conditions which determine the forces acting on the shaft lining and 2) by the function of the shaft and environmental conditions. The importance of the shaft required a conservative safety factor. A concrete shaft lining should be, intimately connected to the adjacent rock walls so that it forms one continuous body with the ground. The mechanical properties of the two materials (rock and concrete) are generally comparable with respect to strength and bonding. The concrete and the rock surface are assumed to be homogeneous.

The lining design, depends on the shaft sinking method, that is, the shaft may be sunk incrementally to a certain level and then immediately concreted, or the shaft may be sunk in stages (10 to 20 ft). The latter shaft sinking method normally necessitates temporary support. Temporary support such as rock bolts allow some relaxation of the rock adjacent to the shaft and out into the rock mass. Relaxation of the adjacent rock reduces the ultimate, or equilibrium thrust, on the concrete lining ( $P_i$ ). Geologic conditions permitting, a concrete lining can be placed before relaxation takes place.

Relaxation of the rock adjacent to a shaft depends on the nature of the rock mass. The intensity of the pressures, dictates the type of temporary support, and the sinking method utilized.

One of the more important aspects to be considered in selecting a lining design are; 1) estimation of the equilibrium thrust ( $P_i$ ), (a function of the radius to the boundary between the elastic-elastic or plastic-elastic zones), and 2) the unconfined compressive strength, (which measures strength with time).

The Agua Prieta penstock shaft lining was designed utilizing traditional methods, i.e. estimating the equilibrium thrust ( $P_i$ ), and calculating the lining pressure on a rigid lining. In a plastic (yielding) rock mass Terzaghi's (1943) equation was used. In the case of a cohesive, rigid (non-yielding), brittle (clastic) rock, Talobre's (1967) equation was employed. In the case of a non-cohesive rock, lining pressure was predicted using Rabcewicz's (1965) equation. Appendix A presents these equations.

Concrete is normally considered to be an elastic material even though it exhibits minor plastic deformation within safe working-load limits. Design of concrete shaft linings should consider the following factors:

- a) Design the concrete lining to support predicted compressive stresses.
- b) Maintain concrete quality by using a low water-cement ratio (Low slump).
- c) Control shrinkage of the concrete by proper curing.
- d) During the concrete curing stage, maintain sufficient moisture to allow the concrete to cure properly.
- e) Deformation of the shaft lining as the concrete creeps (flows plastically) under load and differential stress.
- f) Prevent point loading on the lining which may result in large differential stresses within the lining or potentially, tensile stress.

A temporary shaft support system should, if used, be designed to resist the loads outlined in the following subsection. The final permanent lining, should be designed, to prevent cavitation, erosion/corrosion and to support internal hydraulic pressures.

The thickness of the concrete lining for the Agua Prieta penstock was calculated using the Lamé equation (equation A.15) for each lining pressure predicted by the three theories mentioned. In addition the compressive

strength of the concrete was varied from 3000 psi to 4500 psi. The safety factor varied from 2.0 to 3.0. The Lamé equation does not take into account non-uniformity of applied lining pressure produced by the heterogeneity and anisotropy of rocks. But the use of this particular theory is probably conservative as the concrete is assumed to behave elastically.

Concrete lining thicknesses were calculated for each rock zone at Agua Prieta, considering the concrete design strengths and predicted external pressures. The development of these design lining thicknesses, presented in Tables 2.2 and 2.3, employs the triaxial state of stress condition postulated by Lamé.

The lining thickness must be designed to carry the lining pressure, which develops after sinking has removed the stress shield from ahead of the shaft location (Abel, et. al., 1979).

The radius of the relaxed zone (R) has traditionally been estimated with the Mohr-Coulomb strength criteria. That defines the relationship between confining pressure in the rock and the rock failure strength (See Tables 2.1 to 2.3; Figures 2.1.1 to 2.1.6; and Figures 2.2.1 to 2.2.7).

The results of the lining pressure equations of Terzaghi, Rabcewicz and Talobre, together with the results

Table 2.1 Stress/strength Distribution and Thickness of Over-stressed Rock, including pertinent Rock Properties

Zone	$\sigma_o$ psi	f	$\sigma_h$ psi	Tan $\beta$	C	$l=0.7r$	$\sigma_t$ psi	$\sigma_r$ psi	$\sigma_f$ psi
I-A	170	4	230	21.09	20	0.03	447	13	448
I-B	450	4	280	7.80	80	0.025	547	14	555
I-C'	1250	4	520	18.43	150	0.0			
I-C''	1250	4	570	18.43	150	0.0		$\sigma_t < \sigma_o$	
I-C'''	1250	4	750	18.43	150	0.0			
I-D	260	7	680	7.80	50	0.11	1232	128	1260
II-A'	240	7.5	1020	7.80	45	0.12	1833	207	1853
II-A''	240	7.5	1145	7.80	45	0.12	2058	232	2051
II-A'''	240	7.5	1325	7.80	45	0.12	2381	269	2336
III-B	1010	7.0	710	4.24	245	0.06	1342	78	1341
III-A'	3290	4.0	730	11.50	650	0.0			
III-A''	3290	4.0	820	11.50	485	0.0		$\sigma_t < \sigma_o$	

Table 2.1 (..... continued)

## L E G E N D

- $\sigma_o$  = Unconfined Compressive Strength (Rock Mass), psi
- $f$  = Scale Factor (Selected from Wilson Method. Used to Reduce  $\sigma$  and C)
- $\sigma_h$  = Horizontal Stress, psi
- $C$  = Rock Mass Cohesion, psi
- $l=0.7r$  = Thickness of Relaxed Zone, ft
- $R$  = Radius of the Yielded-Elastic Boundary, ft
- $\sigma_t$  = Tangential Stress, psi
- $\sigma_r$  = Radial Stress, psi
- $\sigma_f$  = Failure Stress, psi
- $r$  = R
- $\tan \beta$  = Passive Pressure Coefficient

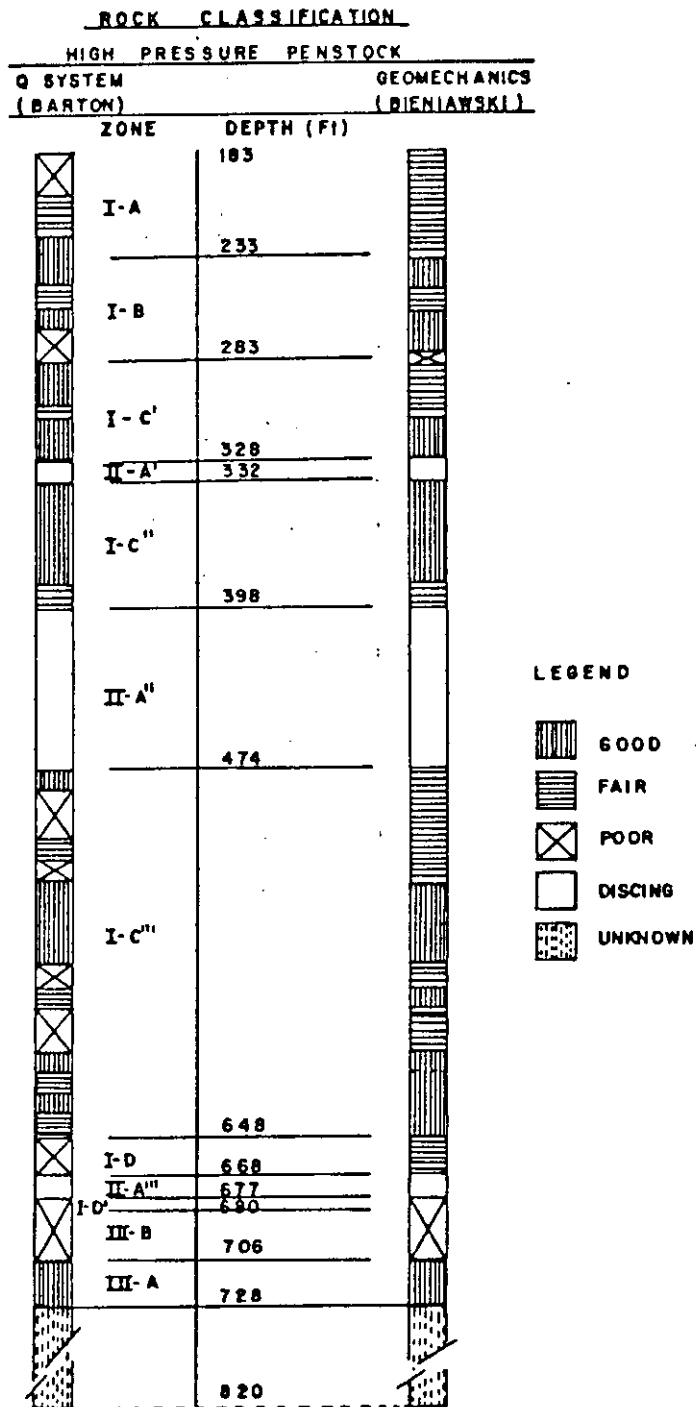


Figure 2.7 Comparison of Rock Mass Classification by the Geomechanics and Q-System for the Penstock Borehole Core

Table 2.2 External Lining Pressure Prediction (Pi) for each Zone of the Agua Prieta Pressure Shaft

	Trial l=0.7r	Stress (psi)			Pi (psi)		
		$\sigma_t$	$\sigma_r$	$\sigma_f$	(Terz)	(Rab)	(Talob)
	0.001	460	1	180	13	20	20
	0.005	457	2	218	11	19	18
Zone I-A	0.010	455	5	266	9	17	16
$\sigma_h = 230$ psi	0.020	451	9	358	6	14	11
Tan $\beta = 21.09$	0.025	449	11	404	5	13	9
$\sigma_o = 170$ psi	0.030	447	13	448	4	12	8
	0.050	439	21	621	0	8	3
	0.100	420	40	1012	0	3	0
	0.200	390	70	1652	0	1	0
	0.001	559	1	454	12	63	63
	0.005	557	3	472	10	62	59
Zone I-B	0.010	555	6	493	7	59	55
$\sigma_h = 280$ psi	0.020	549	11	535	3	56	47
Tan $\beta = 7.8$	0.025	547	14	555	0	54	44
$\sigma_o = 450$ psi	0.030	544	16	575	0	52	40
	0.050	534	26	653	0	46	27
	0.100	511	49	830	0	33	2



Table 2.2 (... continued)

	Trial l=0.7r	Stress (psi)			Pi (psi)		
		$\sigma_t$	$\sigma_r$	$\sigma_f$	(Terz)	(Rab)	(Talob)
	0.001	1359	2	270	124	153	153
Zone I-D	0.005	1353	7	313	120	150	148
$\sigma_h = 680$ psi	0.010	1347	14	365	114	144	142
Tan $\beta = 7.8$	0.050	1297	63	753	79	111	100
$\sigma_o = 240$ psi	0.100	1242	118	1180	47	81	63
	0.110	1232	128	1260	42	76	57
	0.150	1194	166	1553	25	60	36
	0.001	2038	2	256	203	230	230
Zone II-A'	0.005	2030	10	319	197	224	223
$\sigma_h = 1020$ psi	0.010	2020	20	397	189	217	214
Tan $\beta = 7.8$	0.050	1945	95	980	137	166	156
$\sigma_o = 240$ psi	0.100	1863	177	1621	90	121	104
	0.120	1833	207	1854	76	107	88
	0.150	1791	249	2180	57	90	68
	0.200	1728	312	2671	34	67	42

Table 2.2 (... continued)

	Trial l=0.7r	Stress (psi)			Pi (psi)		
		$\sigma_t$	$\sigma_r$	$\sigma_f$	(Terz)	(Rab)	(Talob)
	0.001	2288	2	258	231	258	258
	0.005	2279	11	329	224	252	250
Zone II-A''	0.010	2267	23	416	215	243	241
$\sigma_h = 1145$ psi	0.050	2184	106	1070	157	187	177
Tan $\beta = 7.8$	0.100	2091	199	1790	105	136	119
$\sigma_o = 240$ psi	0.120	2058	232	2051	89	120	101
	0.150	2011	280	2418	68	101	79
	0.001	2647	3	261	272	299	299
Zone II-A'''	0.005	2637	13	343	264	291	290
$\sigma_h = 1325$ psi	0.010	2624	26	444	253	281	279
Tan $\beta = 7.8$	0.050	2527	123	1201	187	216	206
$\sigma_o = 240$ psi	0.120	2381	269	2336	108	139	120
	0.150	2327	323	2760	84	116	95
	0.001	1419	1	1016	77	270	269
Zone III-B	0.005	1413	7	1040	72	267	262
$\sigma_h = 710$ psi	0.010	1406	14	1069	66	262	253
Tan $\beta = 4.24$	0.050	1354	66	1290	21	231	186
$\sigma_o = 1010$ psi	0.060	1342	78	1341	11	224	170
	0.100	1297	123	1532	0	199	116

Table 2.3 External Pressure (Pi) (Talobre) and Design Concrete Thickness (t) (Lame equation)

$f'c = 3000 \text{ psi}$

Zone	Pi (psi)	FS	t (in)	FS	t (in)	FS	t (in)
I-A	8	2.0	0.4	2.5	0.5	3.0	0.6
I-B	44		2.1		2.7		3.3
I-D	57		2.8		3.5		4.3
II-A'	88		4.4		5.7		7.0
II-A''	101		5.2		6.7		8.2
II-A'''	120		6.3		8.1		10.1
III-B	170		9.5		12.5		15.9

$f'c = 3500 \text{ psi}$

Zone	Pi (psi)	FS	t (in)	FS	t (in)	FS	t (in)
I-A	8	2.0	0.3	2.5	0.4	3.0	0.5
I-B	44		1.8		2.3		2.8
I-D	57		2.4		3.0		3.6
II-A'	88		3.8		4.8		5.9
II-A''	101		4.4		5.6		6.9
II-A'''	120		5.3		6.8		8.4
III-B	170		7.9		10.3		13.0

Table 2.3 (... continued)

 $f'_c = 4000$  psi

Zone	Pi (psi)	FS	t (in)	FS	t (in)	FS	t (in)
I-A	8	2.0	0.3	2.5	0.3	3.0	0.4
I-B	44		1.6		2.0		2.4
I-D	57		2.1		2.6		3.2
II-A'	88		3.3		4.1		5.1
II-A''	101		3.8		4.8		5.9
II-A'''	120		4.6		5.8		7.2
III-B	170		6.7		8.8		10.9

 $f'_c = 4500$  psi

Zone	Pi (psi)	FS	t (in)	FS	t (in)	FS	t (in)
I-A	8	2.0	0.2	2.5	0.3	3.0	0.4
I-B	44		1.4		1.8		2.1
I-D	57		1.8		2.3		2.8
II-A'	88		2.9		3.6		4.4
II-A''	101		3.3		4.2		5.2
II-A'''	120		4.0		5.1		6.3
III-B	170		5.9		7.6		9.5

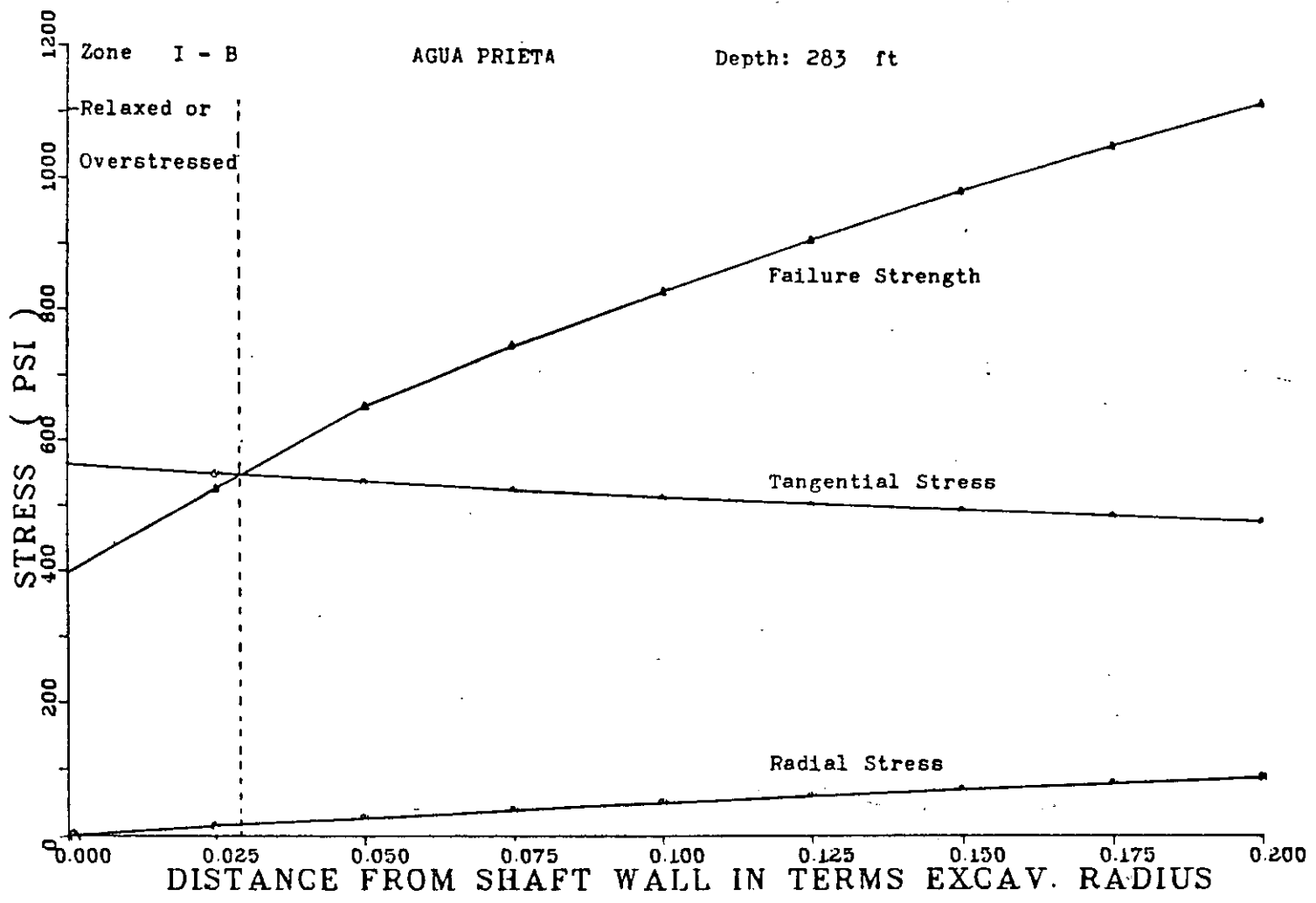


Figure 2.1.1 Stress Distribution for Zone I-B

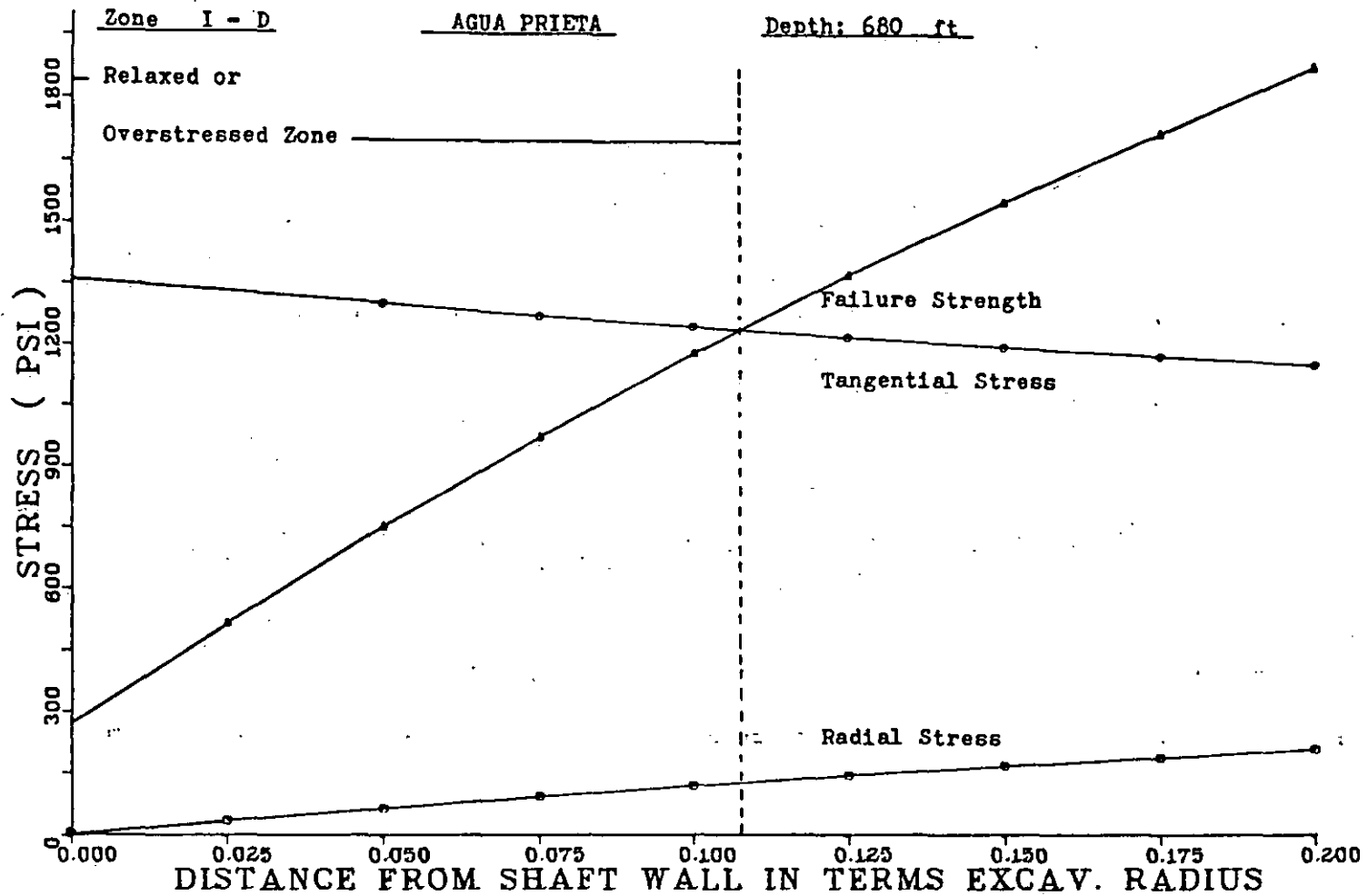


Figure 2.1.2 Stress Distribution for Zone I-D

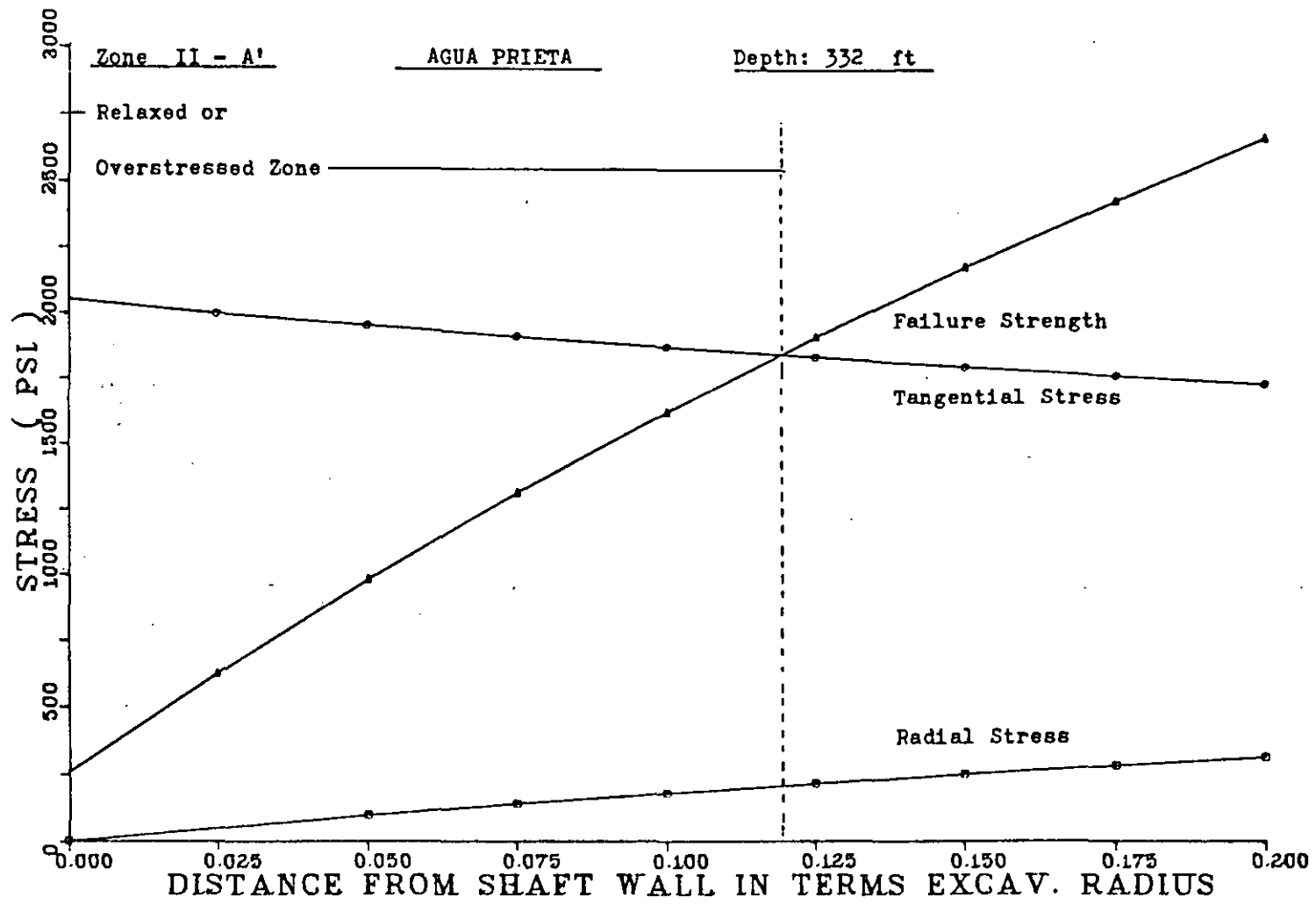


Figure 2.1.3 Stress Distribution for Zone II-A'

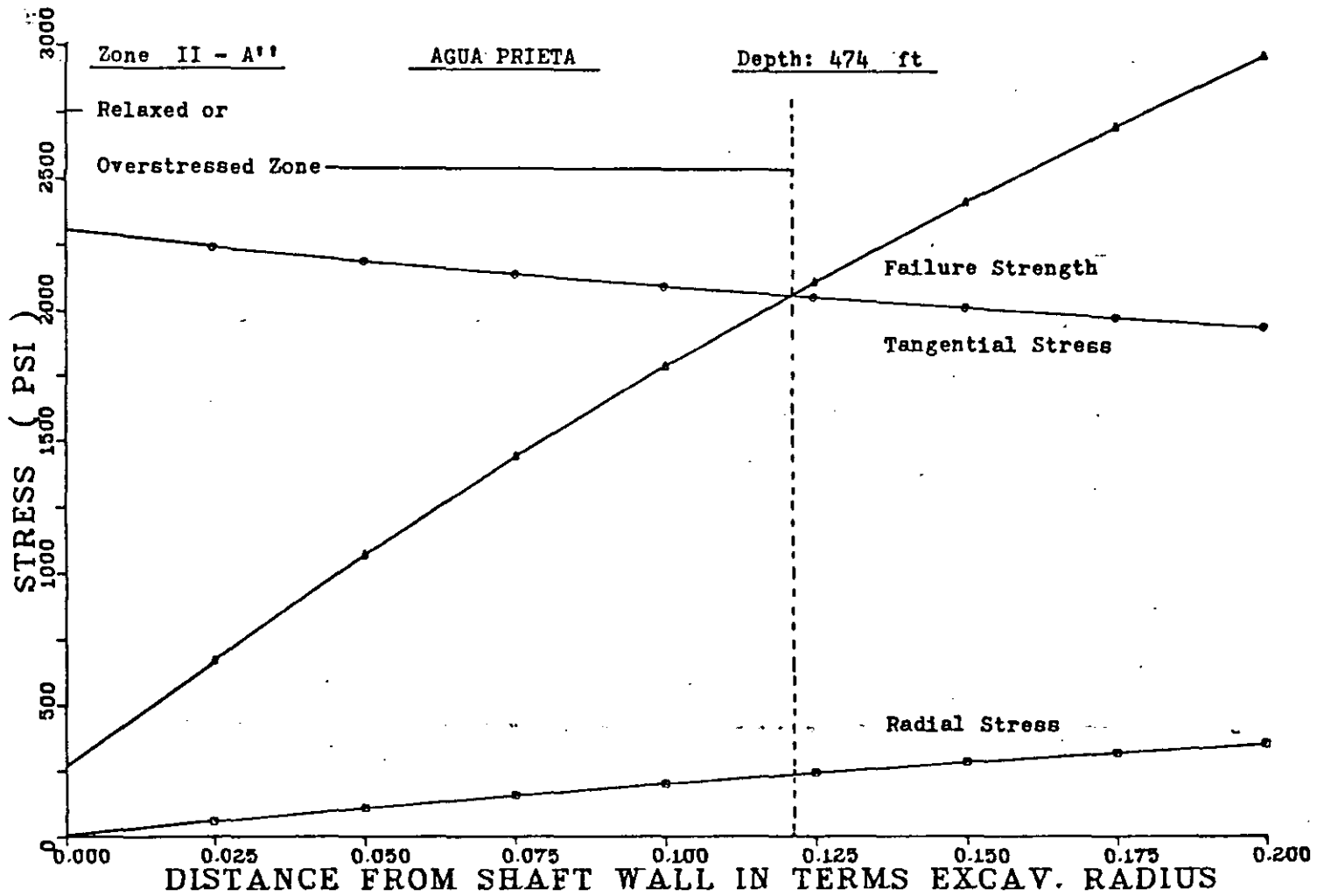


Figure 2.1.4 Stress Distribution for Zone II-A''



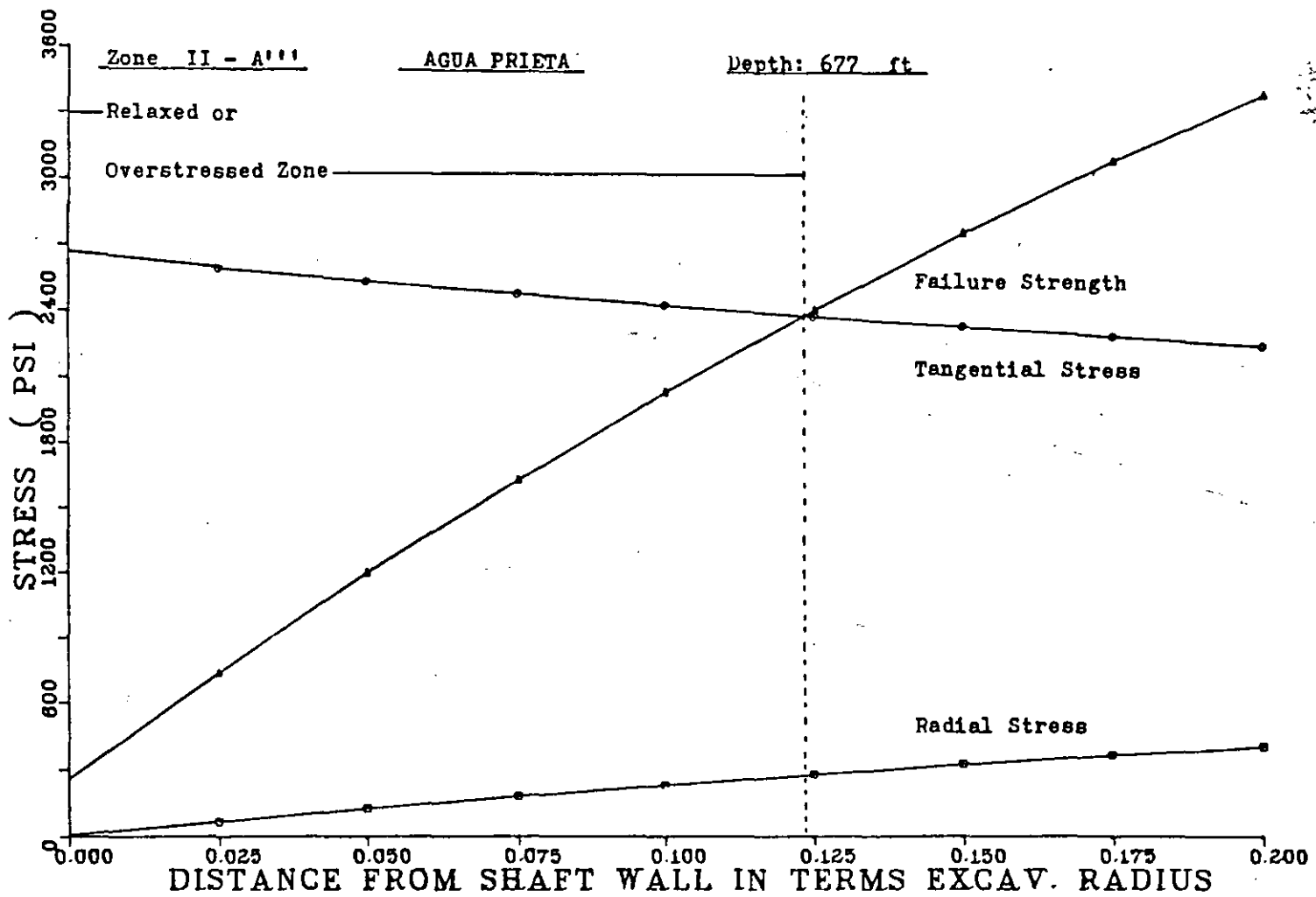


Figure 2.1.5 Stress Distribution for Zone II-A'''

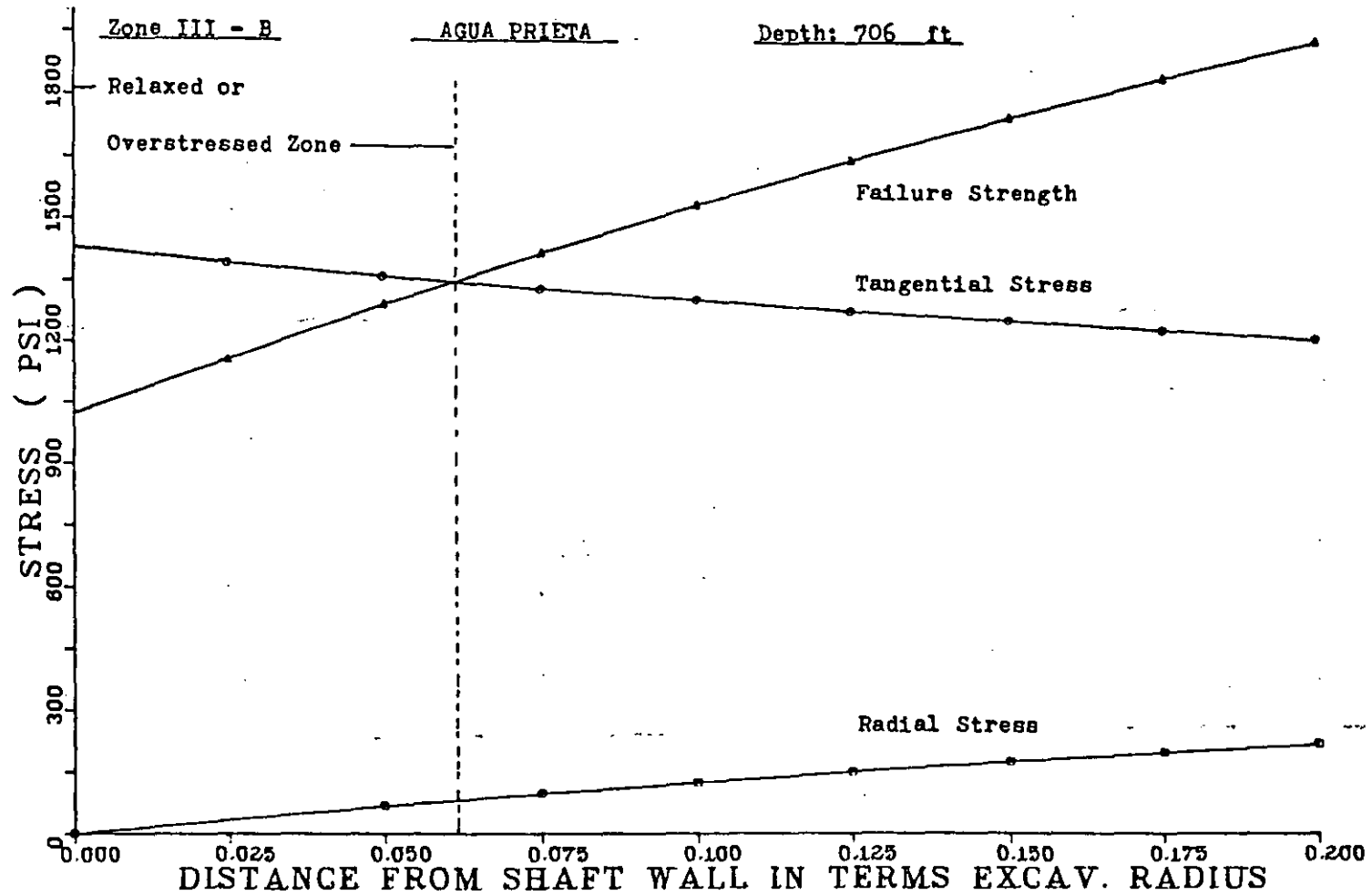


Figure 2.1.6 Stress Distribution for Zone III-B

LINING PRESSURE VS EXTENT OF OVERSTRESSED ZONE  
ZONE I-A SHAFT PRESSURE AGUA PRIETA

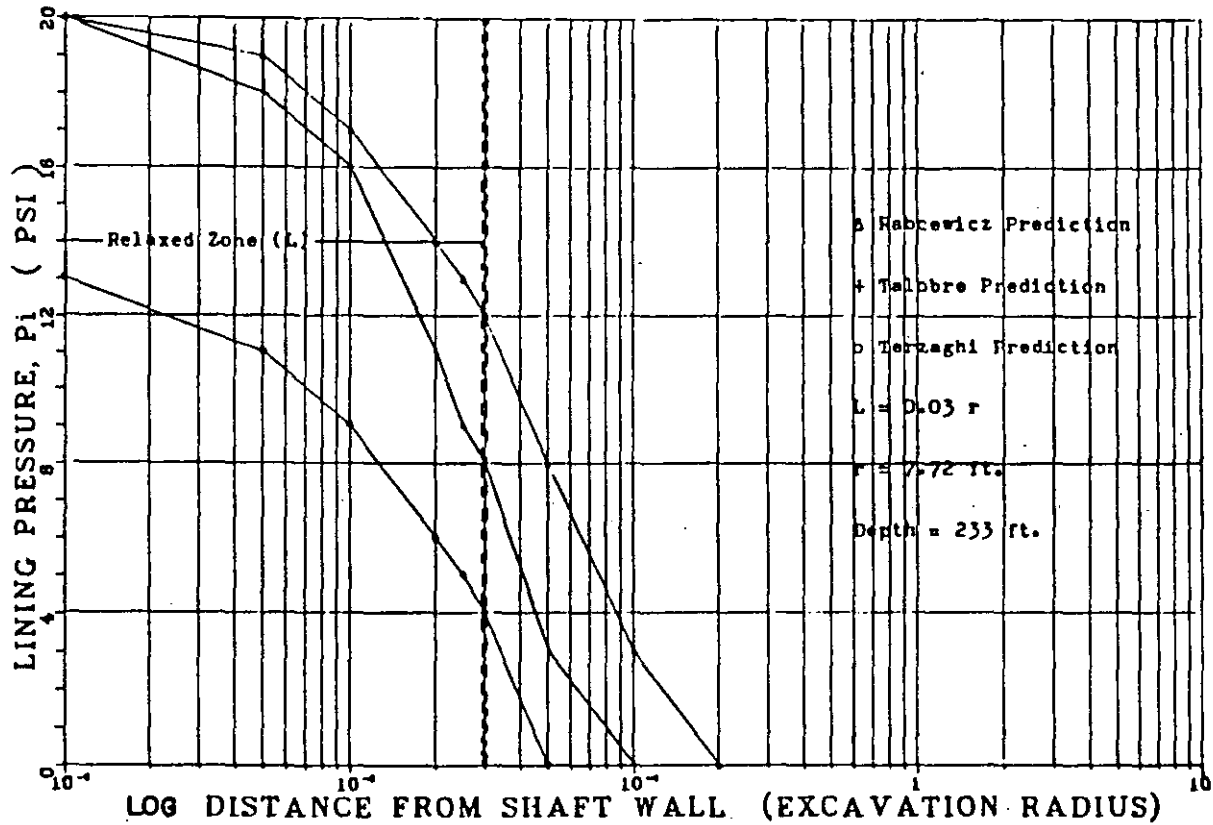


Figure 2.2.1 Lining Pressure vs. Extent of Overstressed Zone. Zone I-A

### LINING PRESSURE VS EXTENT OF OVERSTRESSED ZONE ZONE I-B SHAFT PRESSURE AGUA PRIETA

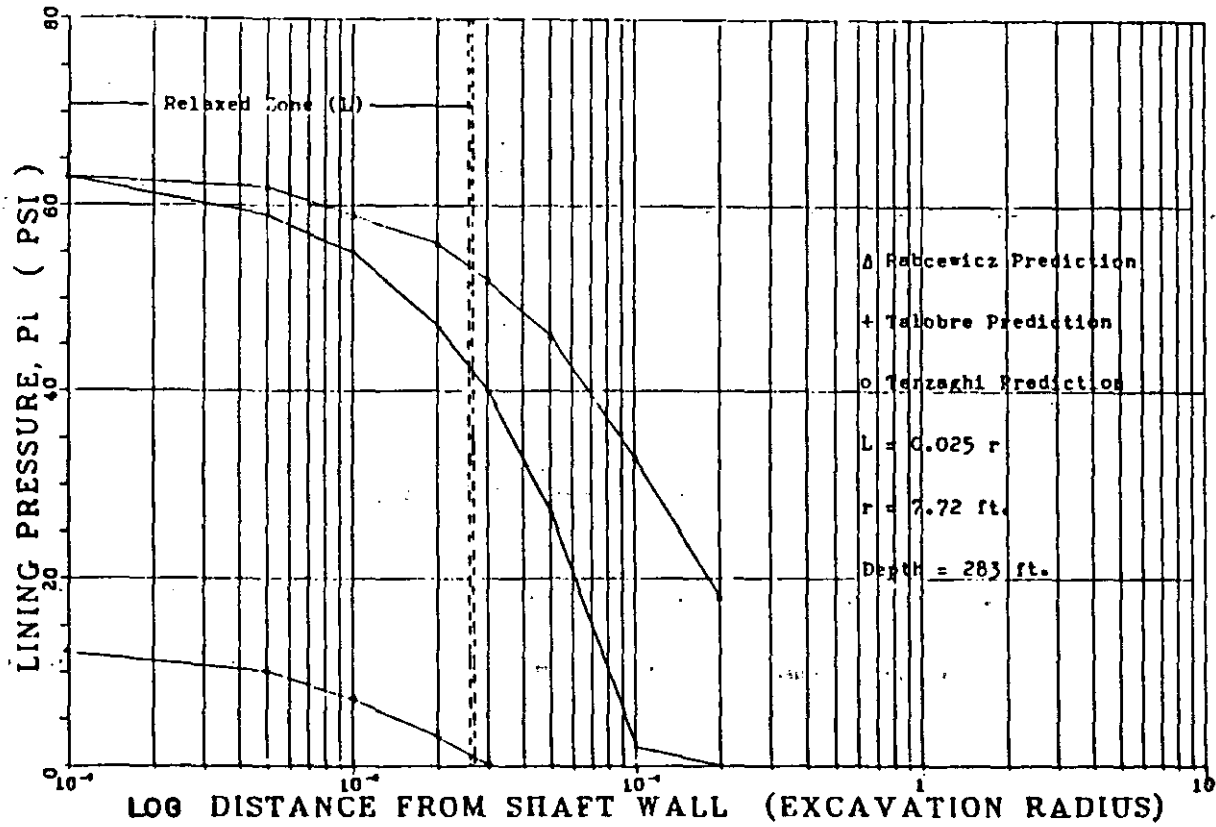


Figure 2.2.2 Lining Pressure vs. Extent of Overstressed Zone. Zone I-B

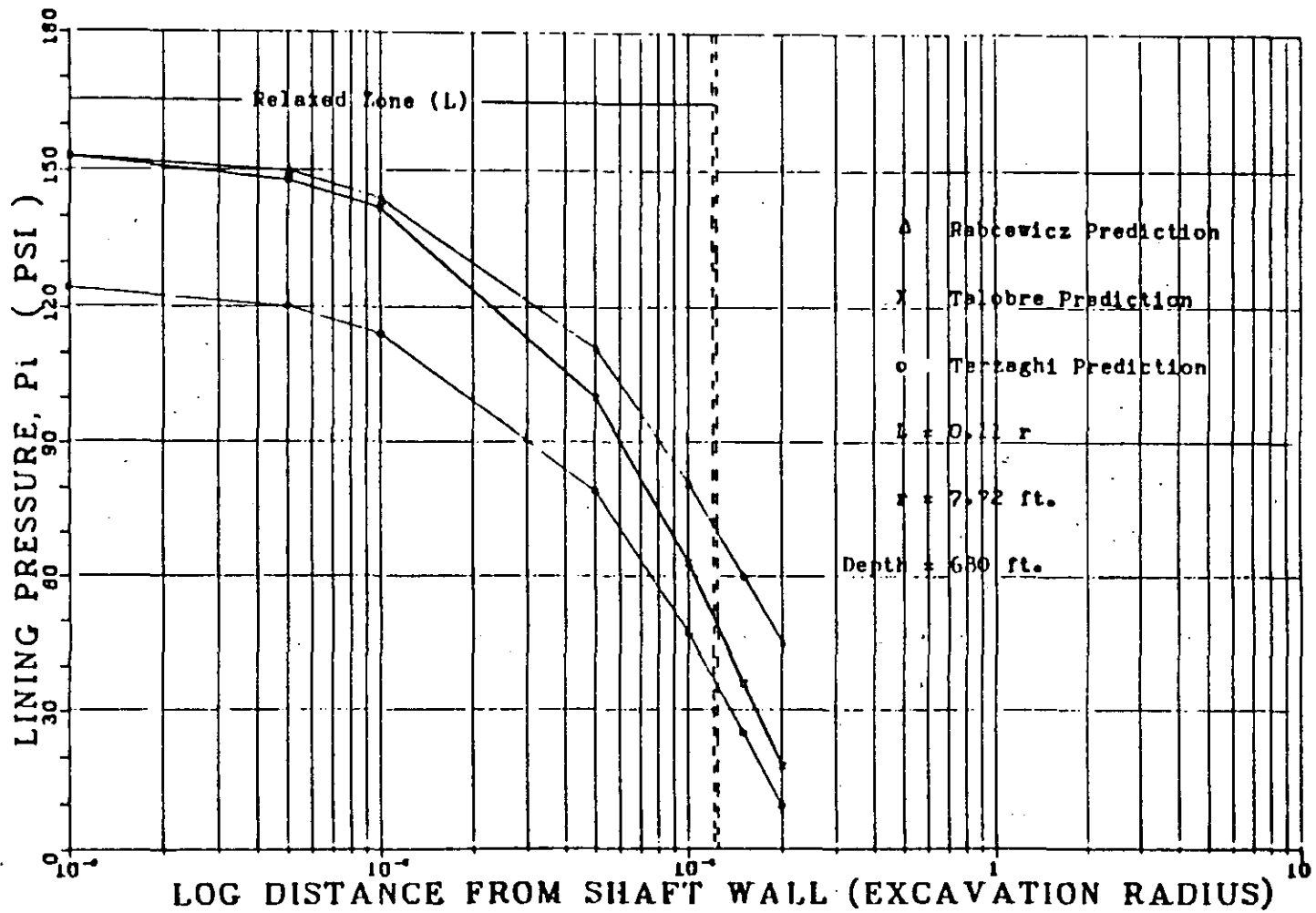


Figure 2.2.3 Lining Pressure vs. Extent of Overstressed Zone. Zone I-D

LINING PRESSURE VS EXTENT OF OVERSTRESSED ZONE  
 ZONE II-A' SHAFT PRESSURE AGUA PRIETA

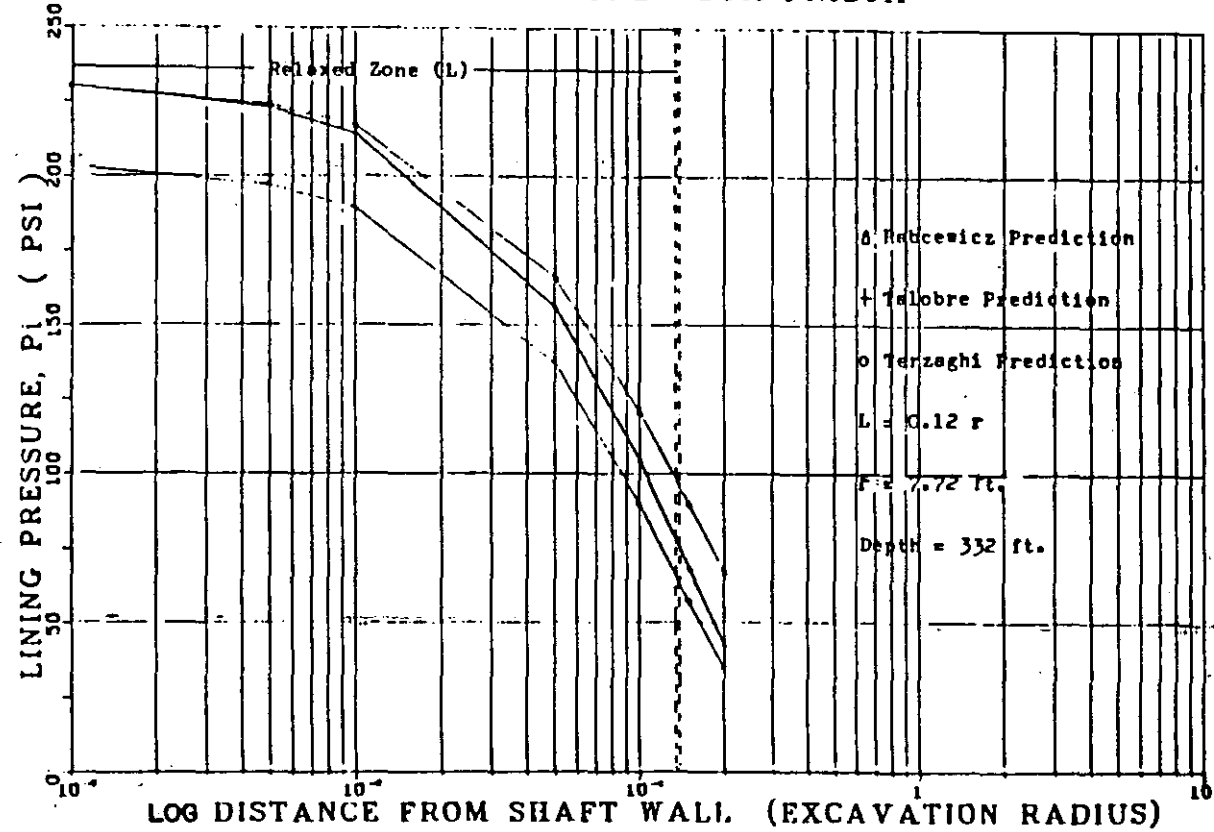


Figure 2.2.4 Lining Pressure vs. Extent of Overstressed Zone. Zone II-A'

LINING PRESSURE VS EXTENT OF OVERSTRESSED ZONE  
ZONE II-A" SHAFT PRESSURE AGUA PRIETA

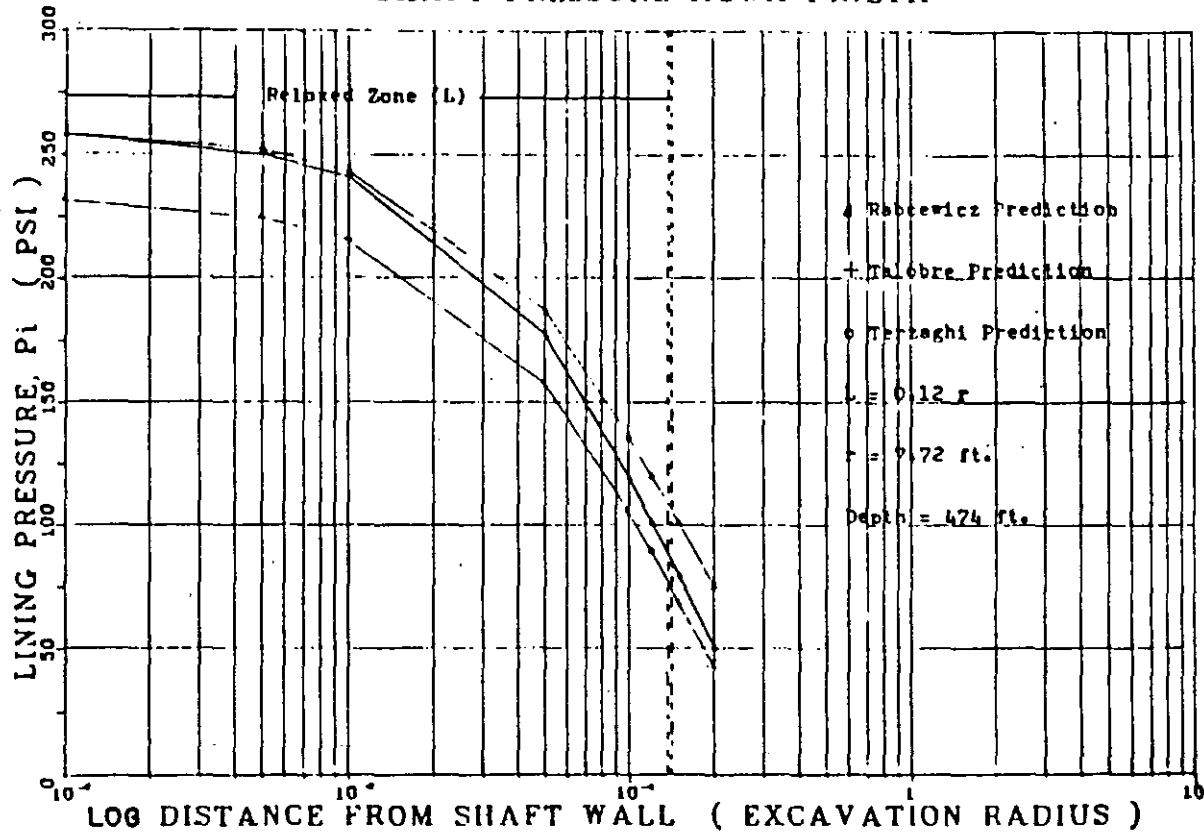
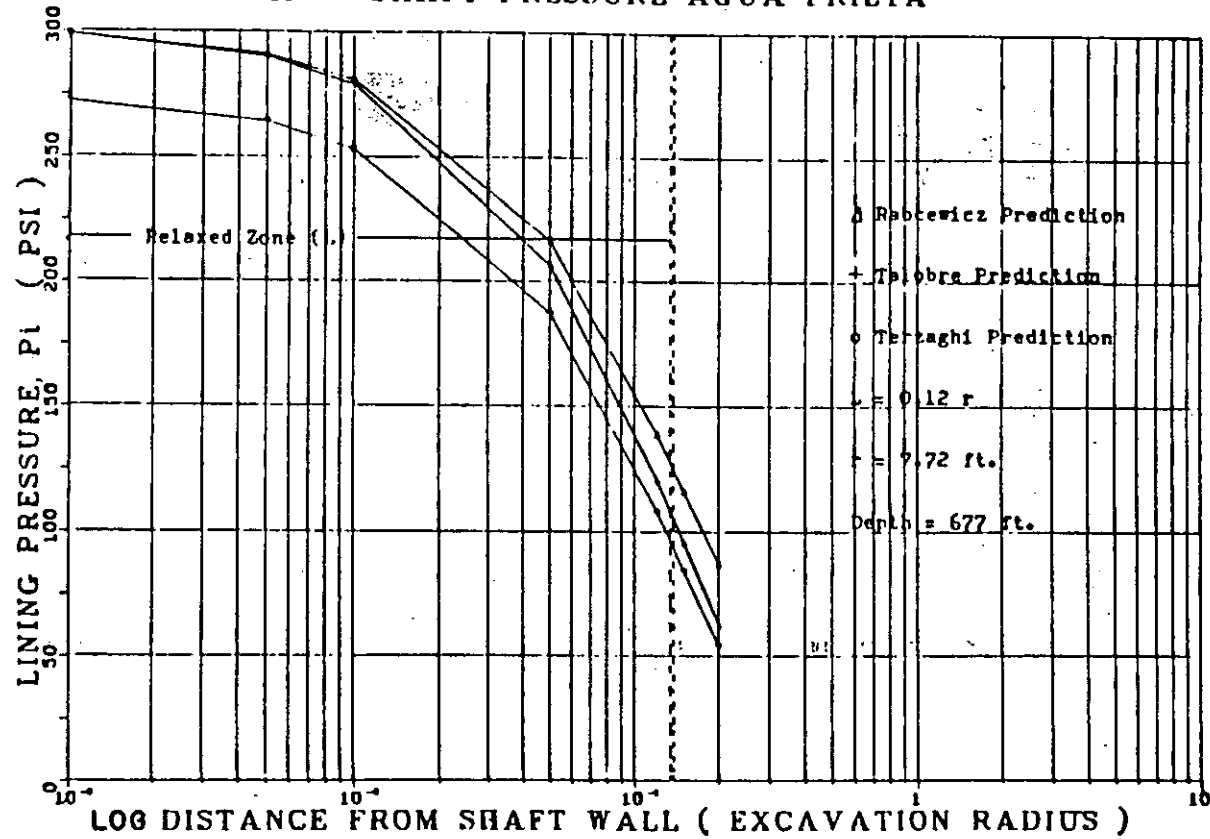


Figure 2.2.5 Lining Pressure vs. Extent of Overstressed Zone. Zone II-A''

LINING PRESSURE VS EXTENT OF OVERSTRESSED ZONE  
 ZONE II-A''' SHAFT PRESSURE AGUA PRIETA



. Figure 2.2.6 Lining Pressure vs. Extent of Overstressed Zone. Zone II-A'''



LINING PRESSURE VS EXTENT OF OVERSTRESSED ZONE  
ZONE III-B SHAFT PRESSURE AGUA PRIETA

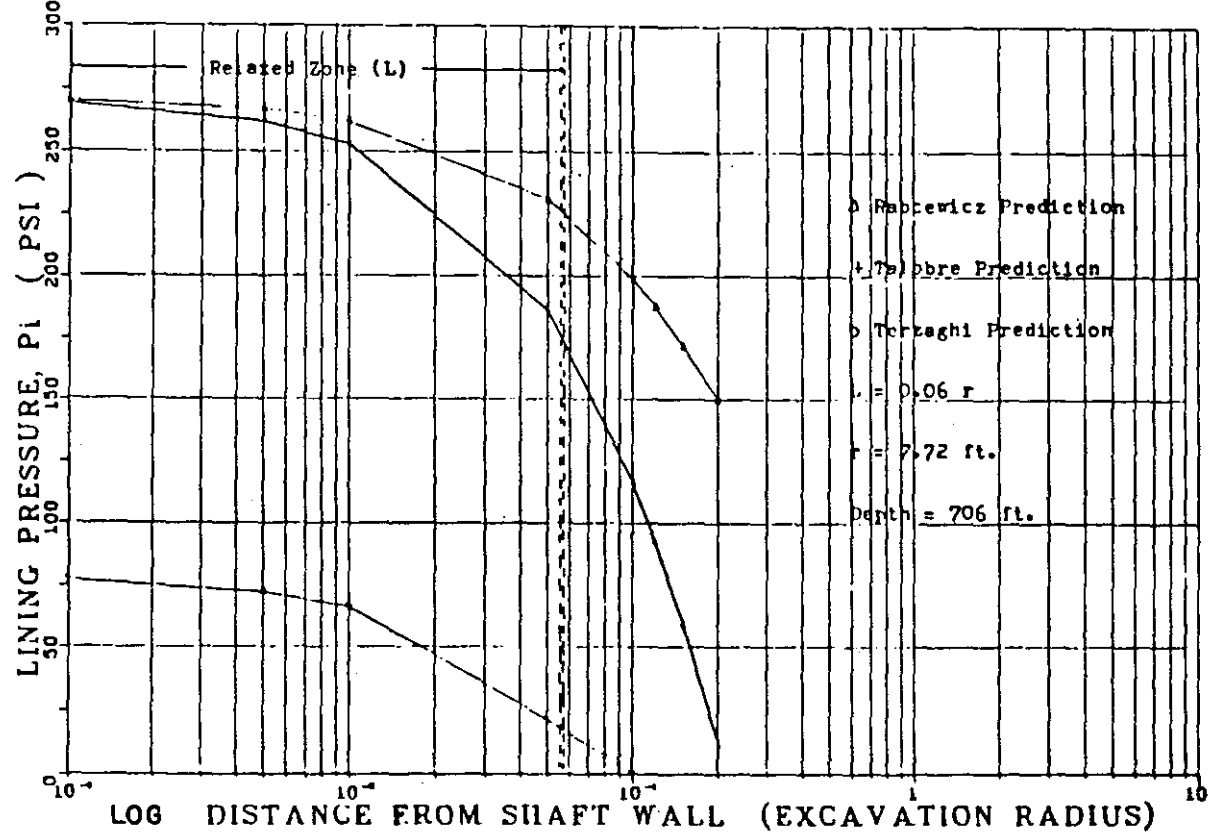


Figure 2.2.7 Lining Pressure vs. Extent of Overstressed Zone. Zone III-B

of the Mohr Coulomb failure criteria were compared with the stress calculations from Carlson strain cells installed in the concrete lining of the 14-ft I.D. shaft at the Mt. Taylor Mine of Gulf Mineral Resources Co. (Abel, et. al., 1979). In that case Talobre's brittle rock lining pressure prediction correlated most closely with the lining pressure measurements.

## II.2 ROCK MASS CLASSIFICATIONS

Tunneling or shaft sinking is not an exact science, therefore theoretical (analytical) methods for predicting support requirements are often lacking. In many cases, empirical formulations based on specific evidence of underground rock behaviour are available, such as the Geomechanics rock mass classification (RMR) method that provides estimates of stand-up time as a function of rock mass rating and unsupported span. This classification was developed by Bieniawski in 1973. Barton (1974) has presented a classification system for rock masses to differentiate between self-supporting openings and those requiring support. The basis of his classification technique is a quality,  $Q$ , representing "Rock Mass Quality".

### 2.2.1 GEOMECHANICS ROCK MASS CLASSIFICATION (RMR)

layers of water-bearing basaltic-tuff. It seems reasonable that the uncored andesite is similar to the andesite on either side and, therefore potentially water bearing.

Above the 675-ft depth high drill water losses were recorded. It would be reasonable to assume that the penstock within the rhyolite will pass through open joints in a permeable rock mass.

The penstock intake tunnel construction is likely to encounter excavation and support problems in the andesite and rhyolite tuff portions of the tunnel, which involve a little more than 2000 ft.

### III.5 DISTRIBUTION OF ROCK MASS RESPONSE ZONES

The response of the Agua Prieta rock mass to excavation depends on quantitative information on the intensity and nature of significant geological features. To calculate that response and evaluate its mechanical properties, the vertical section of the penstock has been divided in seven zones. See Tables 3.1 for the distribution of these zones. A vertical section is presented in Figure 2.7.

### III.6 STATE OF ESTIMATED HORIZONTAL STRESSES

Table 3.5 shows the state of calculated stresses for each lithologic unit at Agua Prieta, Figure 3.1 depicts the

Line	R	Z	$\mu$	Hydrostat.	Conventional			Haimson (1)			Lock & Brown (2)			Haimson (1)			
				$\sigma_h = \sigma_v$	$\sigma_h = \sigma_v \left( \frac{\mu}{1-\mu} \right)$	$\sigma_h = 20 \pm 0.16 (Z)$	$\sigma_v$	$\sigma_h / \sigma_v$	$\sigma_h$	$\sigma_v$	$\sigma_h / \sigma_v$	$\sigma_h$	$\sigma_v$	$\sigma_h / \sigma_v$	$\sigma_h$	$\sigma_v$	$\sigma_h / \sigma_v$
	ft	m															
I-A	233	71	0.16	<u>240</u>	230	0.22	50										
I-B	283	86	0.16	<u>280</u>	280	0.21	60										
I-C <sup>i</sup>	328	100	0.28					<u>330</u>	1.58	<u>520</u>	330	1.30	430				
I-C <sup>ii</sup>	398	121	0.28					<u>400</u>	1.43	<u>570</u>	400	1.13	450				
I-C <sup>iii</sup>	648	197	0.28					<u>650</u>	1.15	<u>750</u>	650	0.82	530				
I-D	668	203	0.39	<u>670</u>	670	0.64	430										
I-D <sup>i</sup>	680	207	0.39	<u>680</u>	680	0.64	435										
II-A <sup>i</sup>	332	101						340	1.54	525	340	1.26	430	<u>340</u>	3.00	<u>1020</u>	
II-A <sup>ii</sup>	474	144						480	1.30	625	480	1.00	480	<u>480</u>	2.39	<u>1145</u>	
II-A <sup>iii</sup>	677	206						680	1.13	770	680	0.77	540	<u>680</u>	1.95	<u>1325</u>	
III-B	706	215	0.37	<u>710</u>	710	0.58	415										
III-A	728	222	0.29	<u>730</u>	730	0.41	300										
III-A <sup>i</sup>	820	250	0.29	<u>820</u>	820	0.41	335										

$\sigma_h = \text{bars, } Z = m \quad (1)$

$\sigma_h = \text{MPa, } Z = m \quad (2)$

Table 3.5 State of Stress (psi) in the Penstock Section

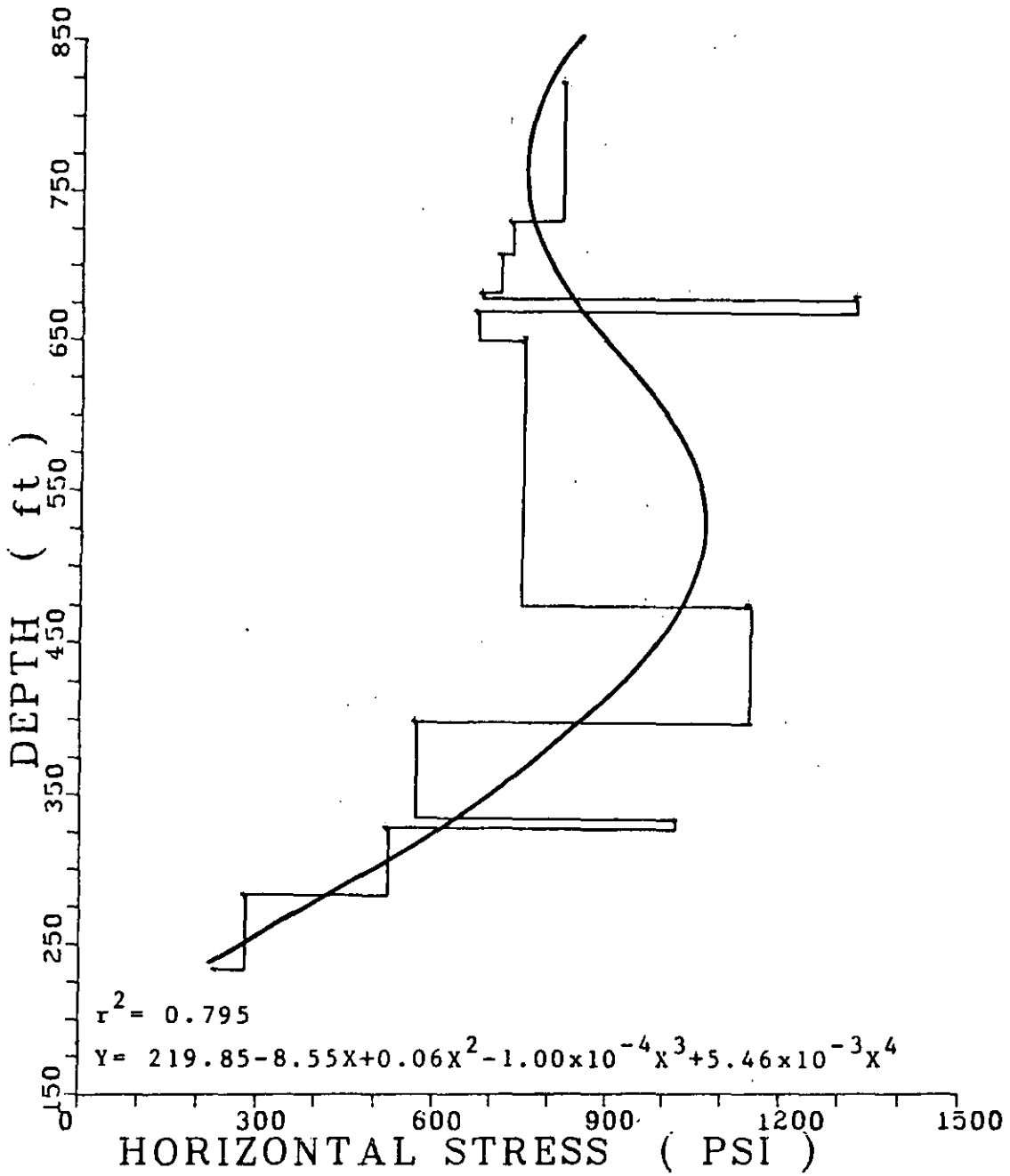


Figure 3.1 Estimation of State of Horizontal Stress in the Pressure Shaft

profile of the calculated horizontal stresses down the axis of the penstock. These results are based on laboratory test results.

The data obtained for this assessment from drilling records, from analysis of drill core and from statistical analysis were as follows:

a) Visual core inspection, describing the lithology and its attendant characteristics, angle of fractures, porosity, partings and fractures, apparent strength, loss of water, sets of fractures, penetration velocity.

b) Percentage core recovery, which is a useful guide in indicating extremely weak rock, zones of sands, clay.

c) Compression tests on samples as a guide to conditions and stability of excavation within the rock mass.

d) Evaluation of the Agua Prieta project elastic rock properties in relation to rock masses with similar structural characteristics.

e) Rock mass classification by more specialized techniques.

### 3.6.1 CONVENTIONAL METHOD

The conventional method used to estimate in-situ stresses involves determining the weight of the overburden

to calculate the vertical stress. Poisson's ratio is then used to calculate the elastic perfect confinement horizontal stresses for the rock. The horizontal stress is an important value needed to estimate the pressure exerted on the shaft lining.

### 3.6.2 HYDROFRACTURING METHOD

Haimson (1968, 1973, 1978) developed equations for horizontal stresses in relation to depth from a number of hydrofracturing in-situ stress determinations made in the U.S.A. These equations are A.9 and A.10 in Appendix A. Haimson's analysis indicated variations of stresses with depth. At shallow depths the mean horizontal stress tends to be higher than the vertical stress. Because of the shallow depth at Agua Prieta the relationship in equation A.10 was used.

The hydrofracturing technique measures average stresses over relatively large areas by recording three hydraulic pressures, one, the pressure to crack open a segment of a section of packer isolated borehole, second, the pressure required to propagate the fracture and the final pressure or the shut-in pressure.

This technique determines stresses directly and is not dependent on knowledge of the elastic rock parameters.

Another feature of this technique is its particular sensitivity to in-situ stress and insensitivity to rock properties.

### 3.6.3 OTHER METHODS

The extensive strain-relief overcoring in-situ stress measurements made since 1969, were used by Hoek and Brown (1978) to develop two equations for horizontal stress, one for maximum and the another for minimum. These equations are presented in Appendix A.

The average minimum horizontal stress method was used for comparison with other methods. See Table 3.5

Modifications of these equations are necessary for density. The average density calculated for the Agua Prieta project rocks is approximately 144.3 lb/cubic foot.

### 3.6.4 STRESS CONDITIONS UNDER DISCING

According to the lithology of the borecore of the penstock area, two minor and one major zone of core discing were found. The former at depths of 328 and 677 ft with thicknesses of 4 and 9 ft, respectively, and the latter between 398 to 474-ft depth, for a 76-ft thickness. See Figure 2.7. Below 474 ft of depth is a low strength lithologic unit, which despite its position adjacent to the



overlying highly stressed rock, exhibits no core discing and has only been affected by the load produced by depth. This underlying unit may well have been shielded from horizontal stress by the overlying stiffer and stronger rock.

Hansagi (1974) experimented in the laboratory with varying pressures applied to core of varying strength rocks. The confining core stress needed to cause discing ranged from 70 psi to 3500 psi in a rock with a 16500 psi compressive strength. He reported heavy core discing rock fragmentation occurs only under higher pressures. The discing has also been reported in core from thin beds of competent anhydrite and sandstone, separated by thick sequences of low strength strata (Abel, 1975).

Thus, it can be inferred that in any area where discing is encountered, stress induced rock failures such as spalling or rock bursting may be experienced in underground excavations.

The state of stress required to produce discing in a core from a vertical hole can be approximated by equation 4 given in Appendix A.

### III.7 LINING DESIGN FOR AGUA PRIETA PROJECT

The concrete lining design method will be demonstrated using rock mass Zone III-B as an example. Zone III-B has

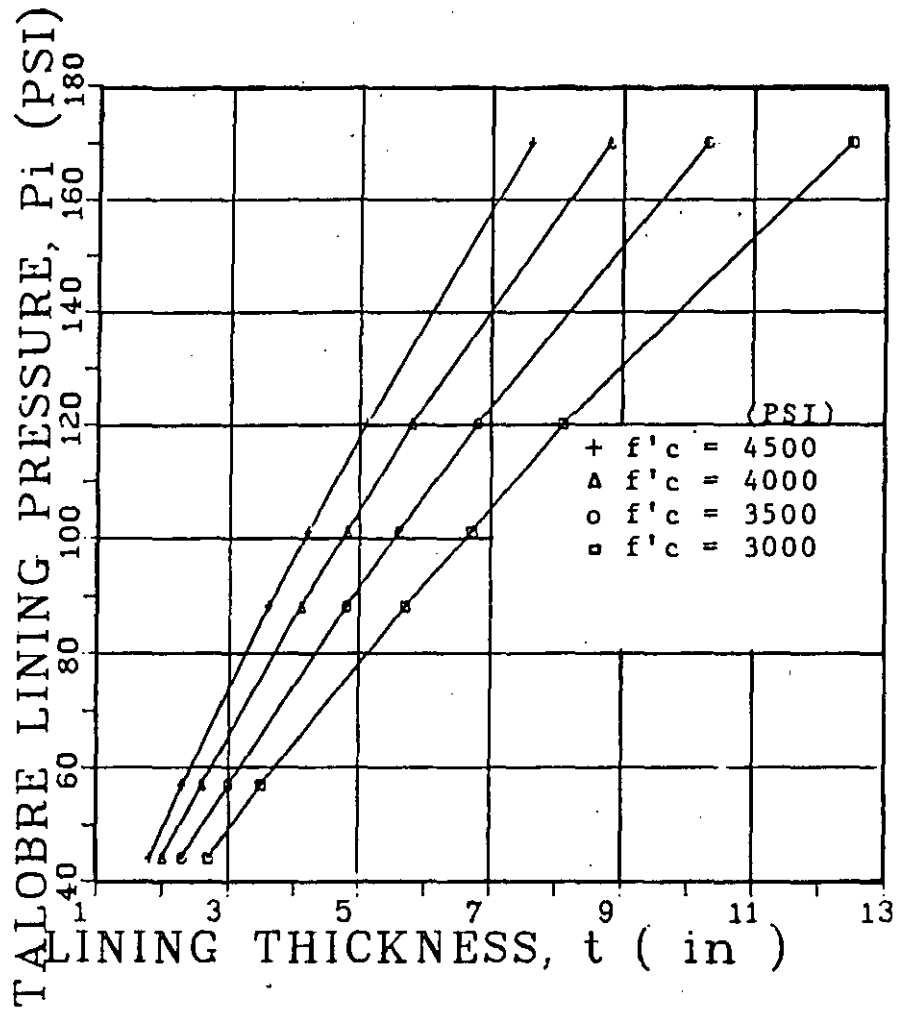


Figure 3.10 Talobre Pressure Predicting ( $P_i$ ) vs. Concrete Lining Thickness ( $t$ ) for various Strengths of Concrete ( $f'_c$ ) and Constant FS (= 2.5)

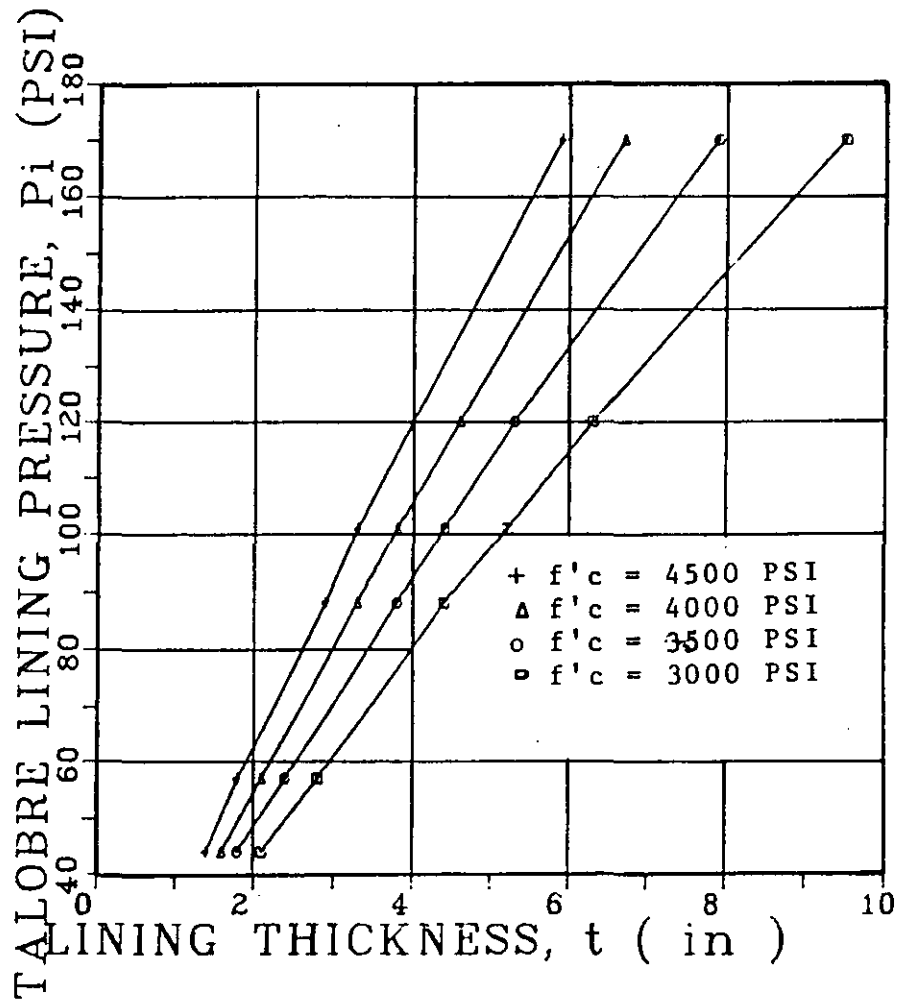


Figure 3.9 Talobre Pressure Predicting ( $P_i$ ) vs. Concrete Lining Thickness ( $t$ ) for various Strengths of Concrete ( $f'c$ ) and Constant FS (= 2.0)

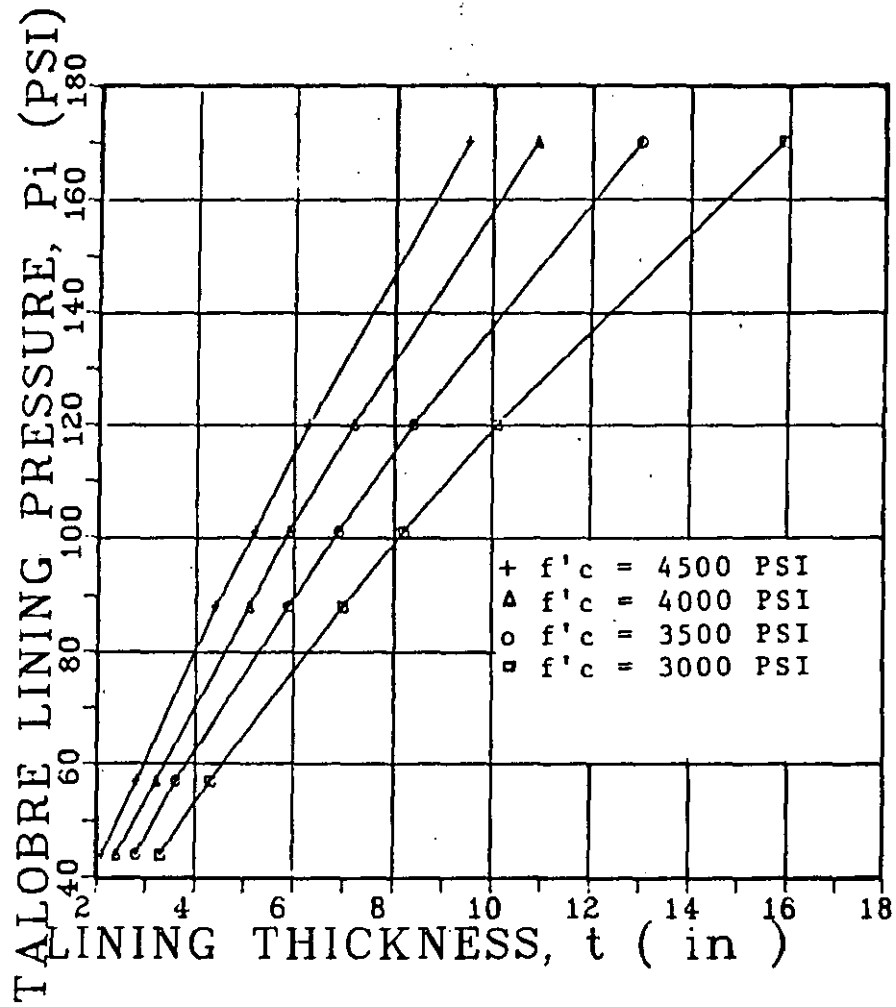


Figure 3.11 Talobre Pressure Predicting ( $P_i$ ) vs. Concrete Lining Thickness ( $t$ ) for various Strengths of Concrete ( $f'_c$ ) and Constant FS (= 3.0)

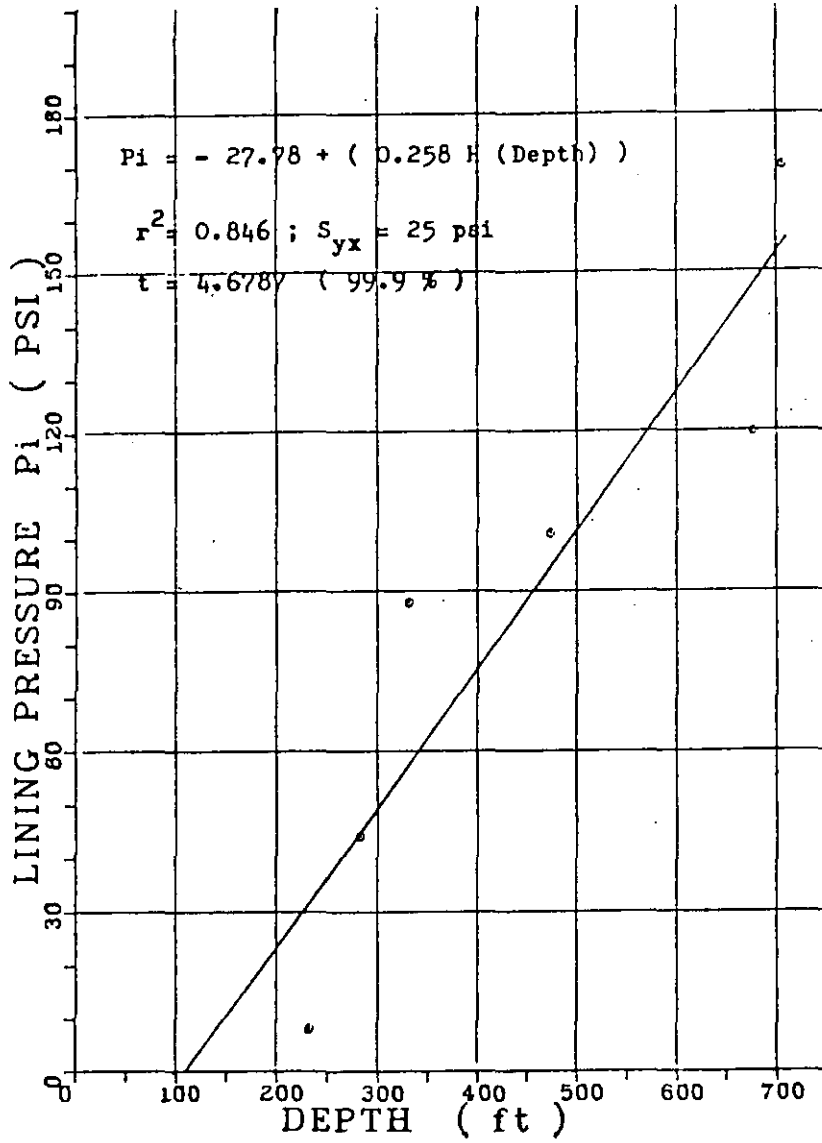


Figure 3.12 Calculated Shaft Lining Pressure ( $P_i$ )

## G L O S S A R Y

a	Internal concrete radius, ft
C	Rock mass cohesion, psi
$C_l$	Average lining circumference, in
$C_{D/L}$	Compressive strength, psi
D	Sample diameter, in
$D_p$	Platen diameter, in
$D_s$	Sample diameter, in
D/L	Ratio of diameter to length of sample
d	External diameter in concrete, in
$d_{new}$	Deformed shaft diameter, in
E	Young's Modulus, psi
$E_x$	Excitation factor, volts
FS	Safety factor
f'c	Compressive strength of the concrete, psi
K	Gage factor
L	Length of the sample, in
l	Core length, cm
$P_i$	External pressure, psi
$P_w$	Internal pressure acting on the steel lining, psi
r	Excavation radius, ft
t	Concrete thickness, in
Tan $\beta$	Passive pressure coefficient
U	Elastic deformation, in

$u$	Displacement, mV
$z$	Depth, m
$\alpha$	Loading factor (proportion of $P_w$ )
$\gamma$	Specific weight of the rock, ton/m <sup>3</sup>
$\Delta d$	Decrease in shaft diameter, in
$\sigma_z$	Tensile strength of the rock, psi
$\Delta C$	Shortening of circumference, in
$\epsilon$	Strain,
$\bar{\epsilon}_{av}$	Average lining strain,
$\theta$	Angle of internal friction, degrees
$\mu$	Poisson's ratio
$\sigma$	Corrected stress, psi
$\sigma_{conf}$	Confined stress, psi
$\sigma_f$	Failure strength, psi
$\sigma_h$	Conventional horizontal stress, psi
$\sigma_{hb}$	Hydrofracturing (minimum horizontal stress), bars
$\sigma_m$	Minimum horizontal stress, psi
$\sigma_o$	Unconfined compressive strength, psi
$\sigma_r$	Radial stress, psi
$\sigma_s$	Tensile stress in the steel lining, psi
$\sigma_t$	Tangential stress, psi
$\sigma_{tc}$	Maximum lining stress developed, psi
$\bar{\sigma}_{tc}$	Average lining stress, psi
$\sigma_v$	Vertical stress, psi

ASTM stress correction for platen-specimen diameter variation under triaxial test:

$$\sigma = \{\text{Load} - \sigma\{n(D_p^2 - D_s^2)/4\}\} / \{D_s^2/4\}n \quad \text{A.1}$$

Modified Bauschinger stress correction for specimen shape (2x1):

$$C_{1/2} = 0.889(C_{D/L}) / \{0.778 + 0.222(D/L)\} \quad \text{A.2}$$

Relationship between the applied strain and voltage in measuring the displacements in the borecore (Vaughan, 1975):

$$\text{Strain level } (\epsilon) = 4ux10^{-3}/E_x K \quad \text{A.3}$$

State of stress to produce discing (Obert and Stephenson, 1965):

$$\sigma_h = \{-3400 - 2\tau\} + \{0.7(-\sigma_v)\} \quad \text{A.4}$$

Moment of resistance of the core (Hansagi, 1974):

$$W = \pi D^3 / 32 \quad \text{A.5}$$

Bending moment (Hansagi, 1974):

$$M = ql^2/2 \quad \text{A.6}$$

$$\text{where } q = D^2 \pi \nu / 4$$

Relevant core length (l) (Hansagi, 1974):

$$l = \sqrt{\{b_z D / 4\nu\}} \quad \text{A.7}$$

State of conventional horizontal stress:

$$\sigma_h = \sigma_v \{ \nu / (1 - \nu) \} \quad \text{A.8}$$

Hydrofracturing (minimum horizontal stress) (Haimson, 1978):

$$\sigma_{hb} = 20 \pm 0.16z \quad \text{A.9}$$

Hydrofracturing at mean horizontal stress (shallow depths) (Haimson, 1978):

$$\sigma_{hb} = 50 + 0.2z \quad \text{A.10}$$

Other methods (minimum horizontal stress) (Hoek and Brown):



$$\sigma_{hm} = 2.2918 + 0.0069z \quad A.11$$

External pressure in the shaft (plastic condition)  
(Terzaghi, 1943):

$$P_i = \left\{ \frac{2}{(\tan \beta - 1)} \right\} \left\{ \sigma_h + \frac{\sigma_o}{(\tan \beta - 1)} \right\} (r/R)^{\tan \beta - 1} - \frac{\sigma_o}{(\tan \beta - 1)} \quad A.12$$

Non-cohesive brittle (clastic) condition (Rabcewicz, 1964):

$$P_i = \sigma_h (1 - \sin \theta) (r/R)^{2 \sin \theta / (1 - \sin \theta)} \quad A.13$$

Cohesive, assuming a rigid (non-yielding) brittle (clastic condition (Talobre, 1967):

$$P_i = \left\{ \frac{C}{\tan \theta} + \sigma_h (1 - \sin \theta) \right\} (r/R)^{\tan \beta - 1} - \frac{C}{\tan \theta} \quad A.14$$

Lame Safety factor for plain concrete shaft lining:

$$FS = \left\{ \frac{f'c - f'c / (t/a + 1)^2}{2P_i} \right\} \quad A.15$$

Tangential stress (Obert and Duvall, 1967):

$$\sigma_t = \sigma_h \{ 1 + (r/R)^2 \} \quad A.16$$

Radial stress (Obert and Duvall, 1967):

$$\sigma_r = \sigma_h \{ 1 - (r/R)^2 \} \quad A.17$$

Failure stress (Mohr-Coulomb Criteria):

$$\sigma_f = \sigma_o + \tan \beta \sigma_r \quad A.18$$

Elastic deformation (shaft unlined) in infinite plate (Obert and Duvall, 1967):

$$U = 4r\sigma_h/E_r \quad A.19$$

Maximum lining stress developed (thick-walled cylinder)  
(Lame, 1852):

$$\sigma_{tc} = 2P_i \{ r^2 / (r^2 - a^2) \} \quad A.20$$

Stiffness of the concrete (ACI, 1971):

$$E_c = 57000 \sqrt{f'c} \quad A.21$$

Average lining strain:

$$\bar{\epsilon}_{av} = \bar{\sigma}_{tc}/E \quad A.22$$

where  $\bar{\sigma}_{tc}$  = average lining stress

Average lining circumference:

$$C_1 = n(a + r) \quad A.23$$

Circumference shortening:

$$\Delta C = C\epsilon = \bar{\sigma}_{tc} C/E \quad A.24$$

Deformed shaft diameter:

$$d_{new} = (C - \Delta C)/n \quad A.25$$

Shaft internal diameter decrease:

$$\Delta d = a + r - d_{new} \quad A.26$$

Overbreak in the shaft (Abel, 1966)

$$\% \text{ overbreak} = 0.0021 \times \text{diameter (ft)} + 11.747 \quad A.27.a$$

$$\text{inches of overbreak} = 0.3364 \times \text{diameter (ft)} + 0.0307 \quad A.27.b$$

Wall thickness of the steel lining (Jacobsen, 1977):

$$t_s = 0.01 P_w / \sigma_s \quad A.28$$



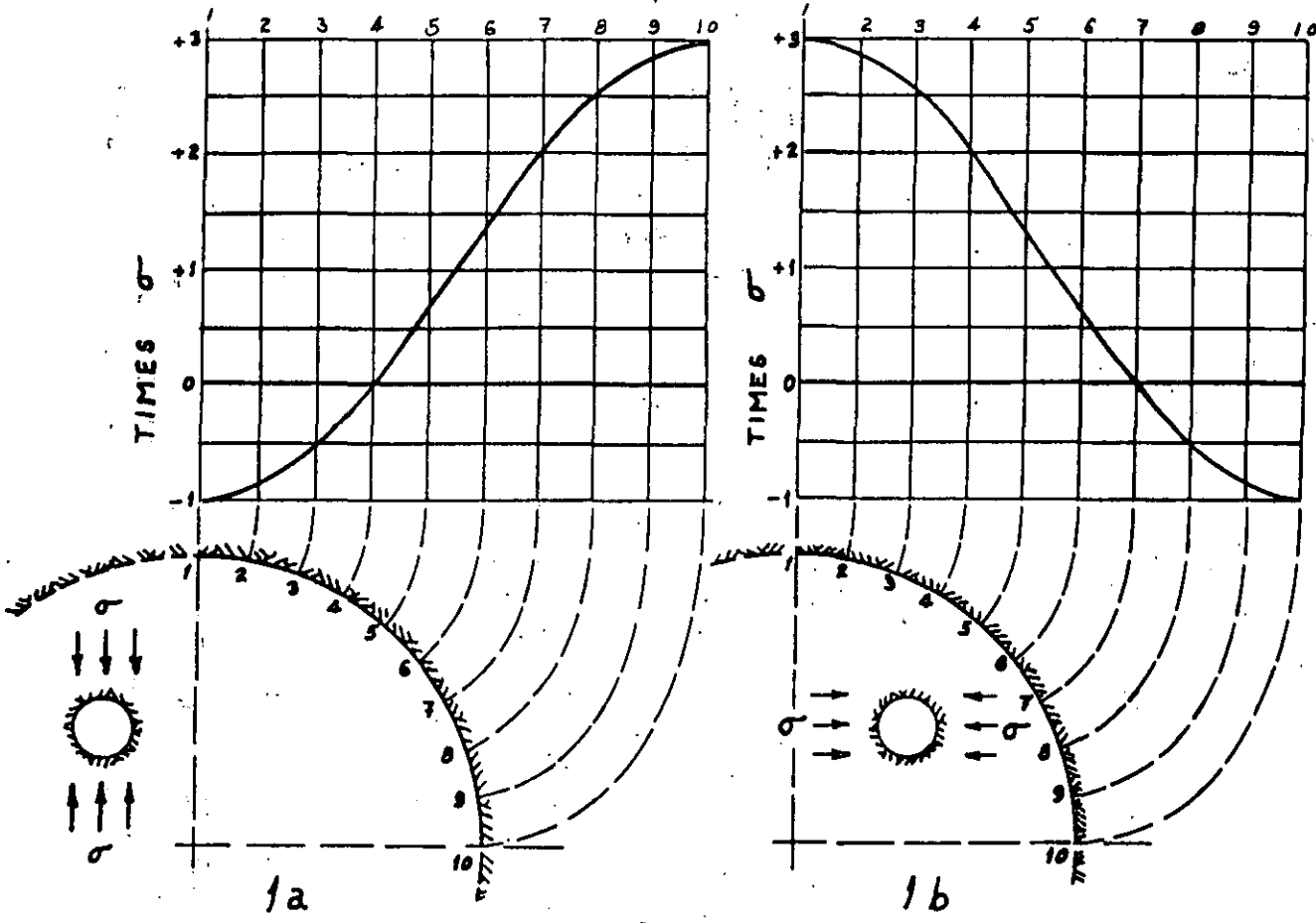
**DIVISION DE EDUCACION CONTINUA  
FACULTAD DE INGENIERIA U.N.A.M.**

MECANICA DE ROCAS APLICADA A LA MINERIA Y A LA CONSTRUCCION

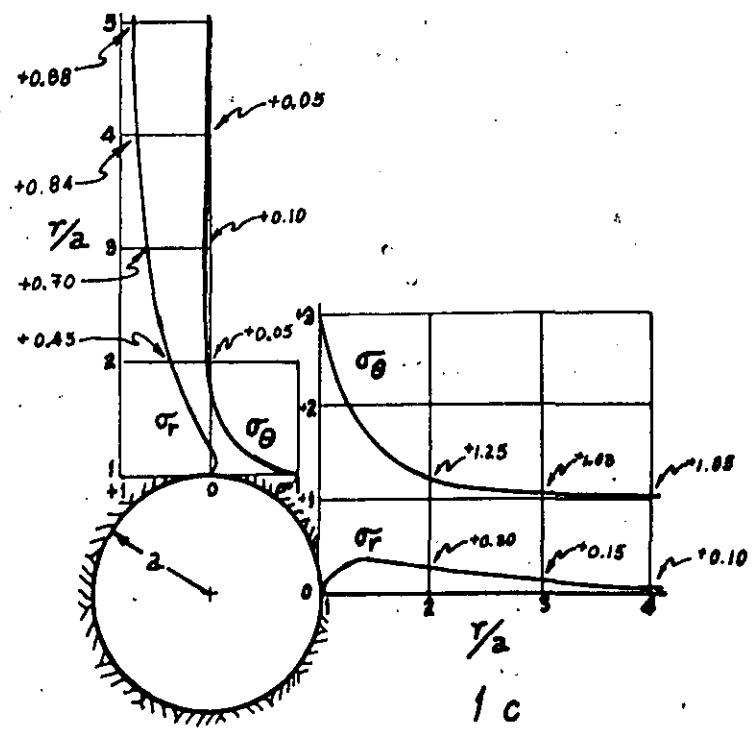
ESFUERZOS EN CAVIDADES

M. EN C. JOSE IBARRA TORRES

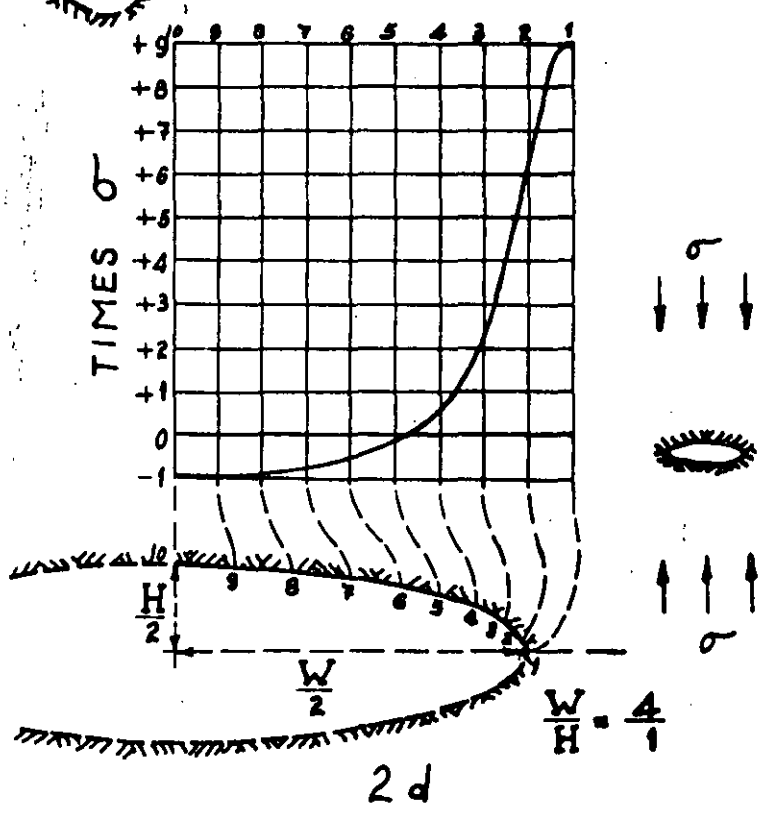
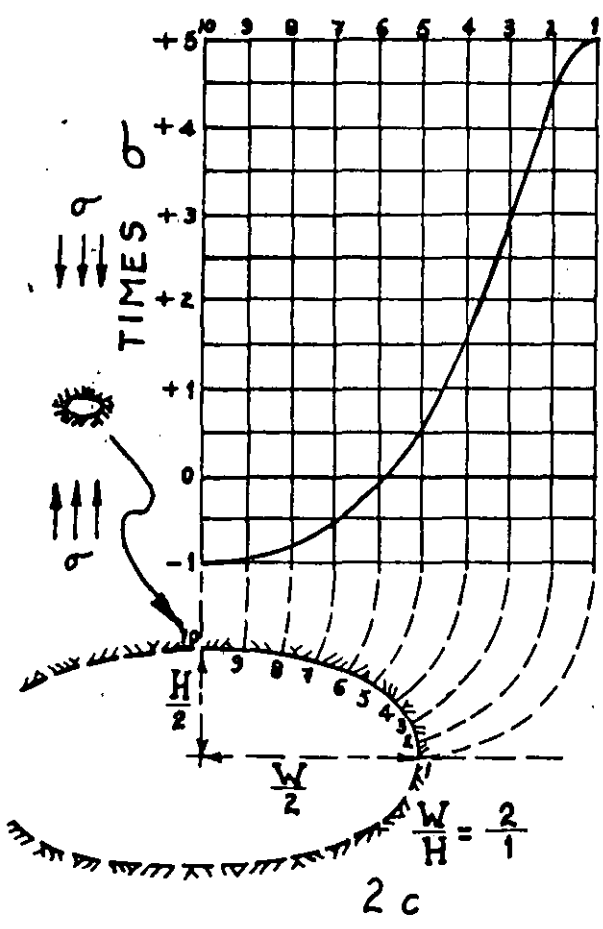
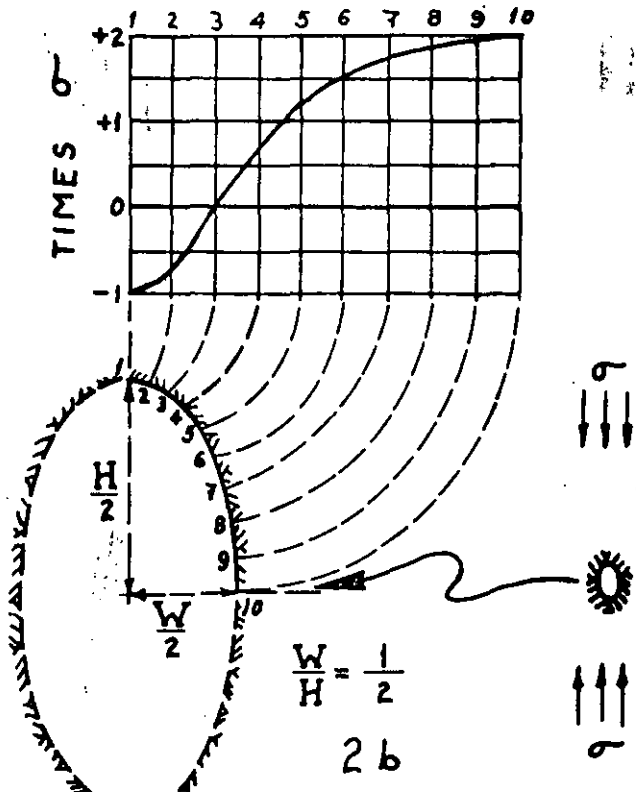
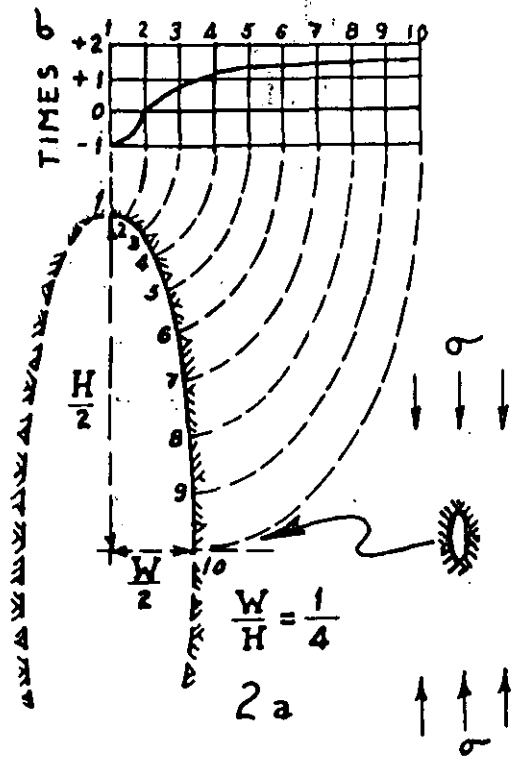
MAYO, 1985.



Boundary Stress Concentration for Circular Openings.  
 (Modified from Obert, Duvall & Merrill, 1960, Bul. 587, USBM)

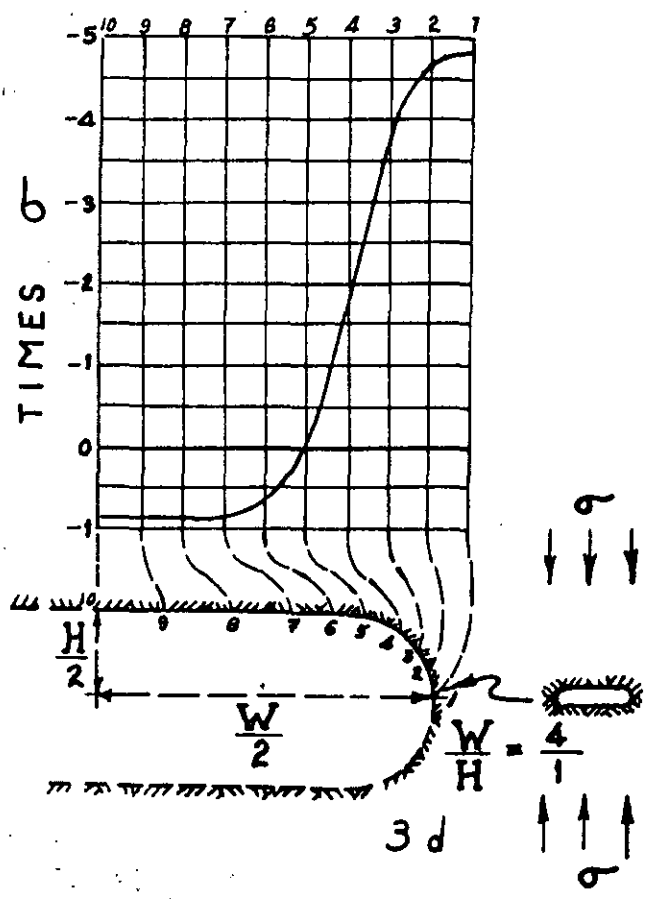
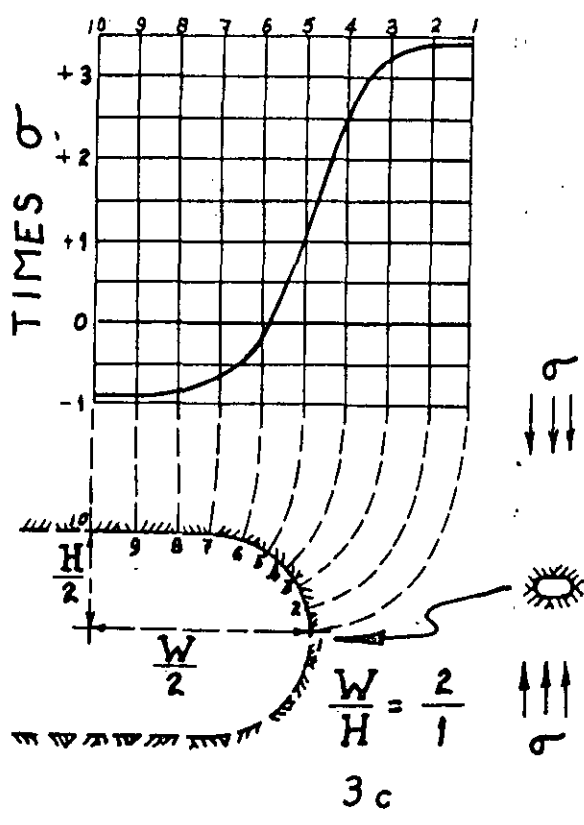
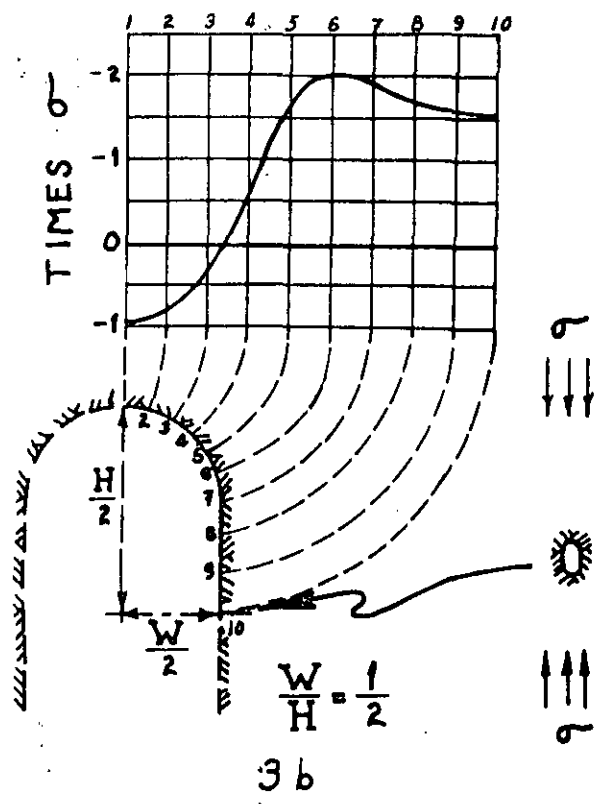
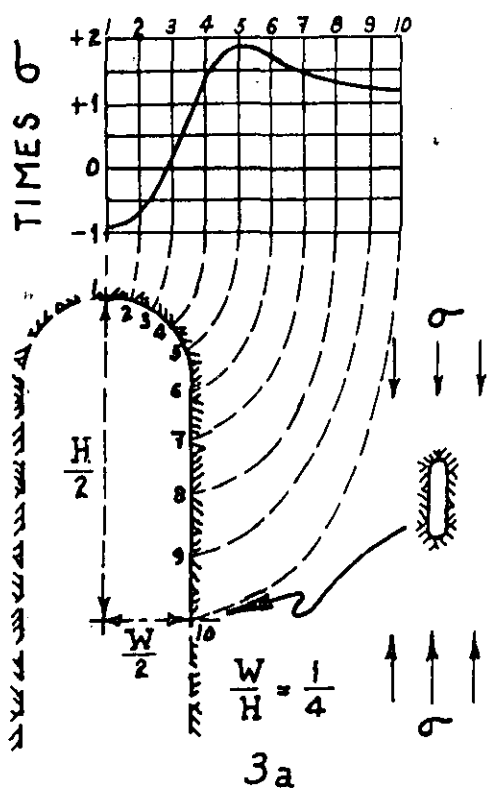


Stress Concentration Along Axis of Symmetry for Circular Openings;  
 Vertical Unidirectional Stress Field. (from USBM Bul 587)

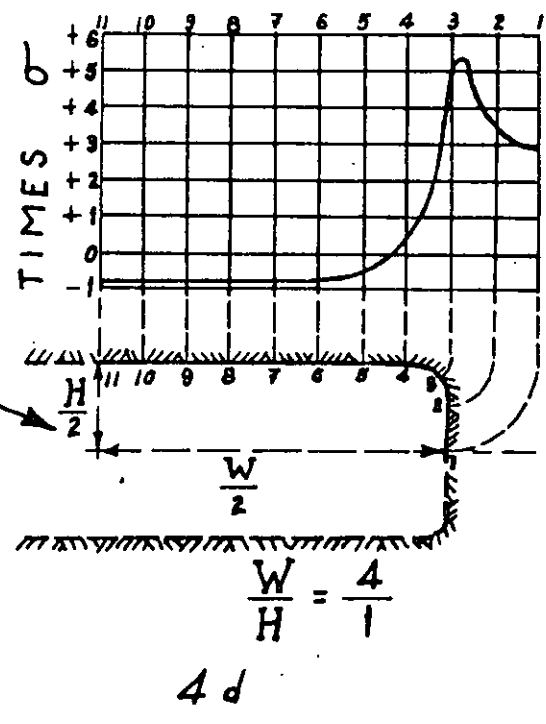
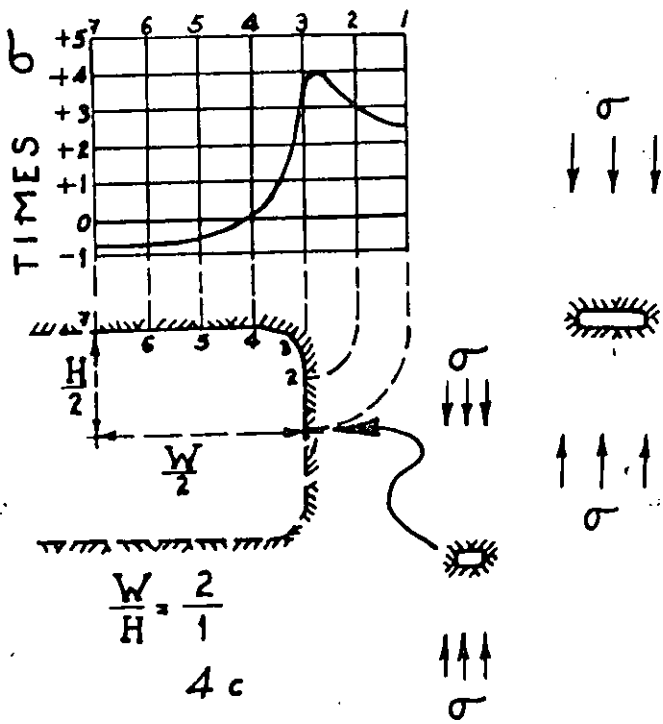
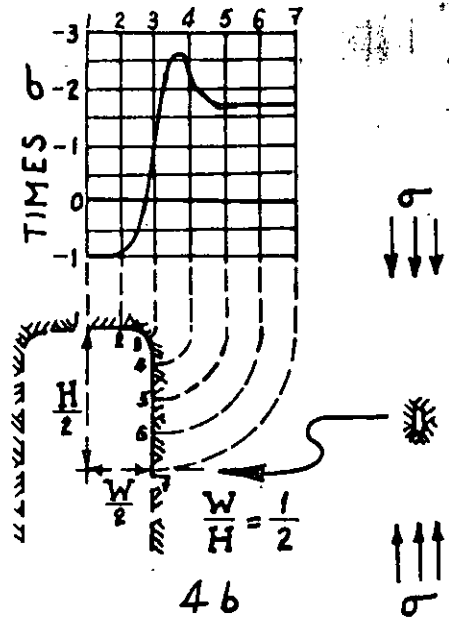
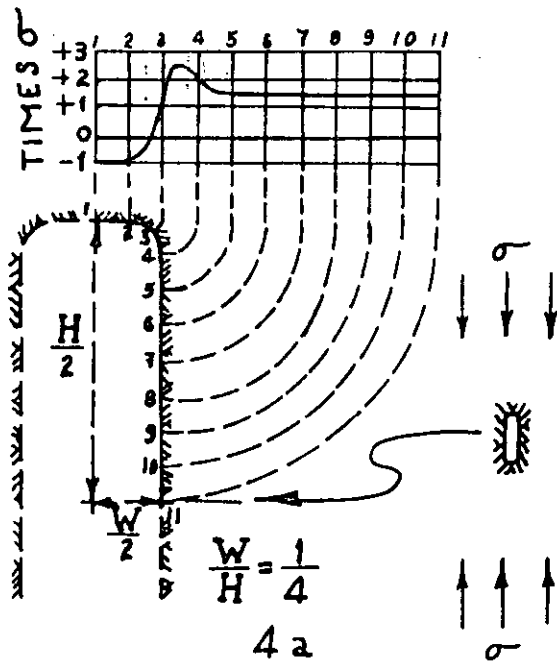


( after Bul. 587, USBM, 1960 )

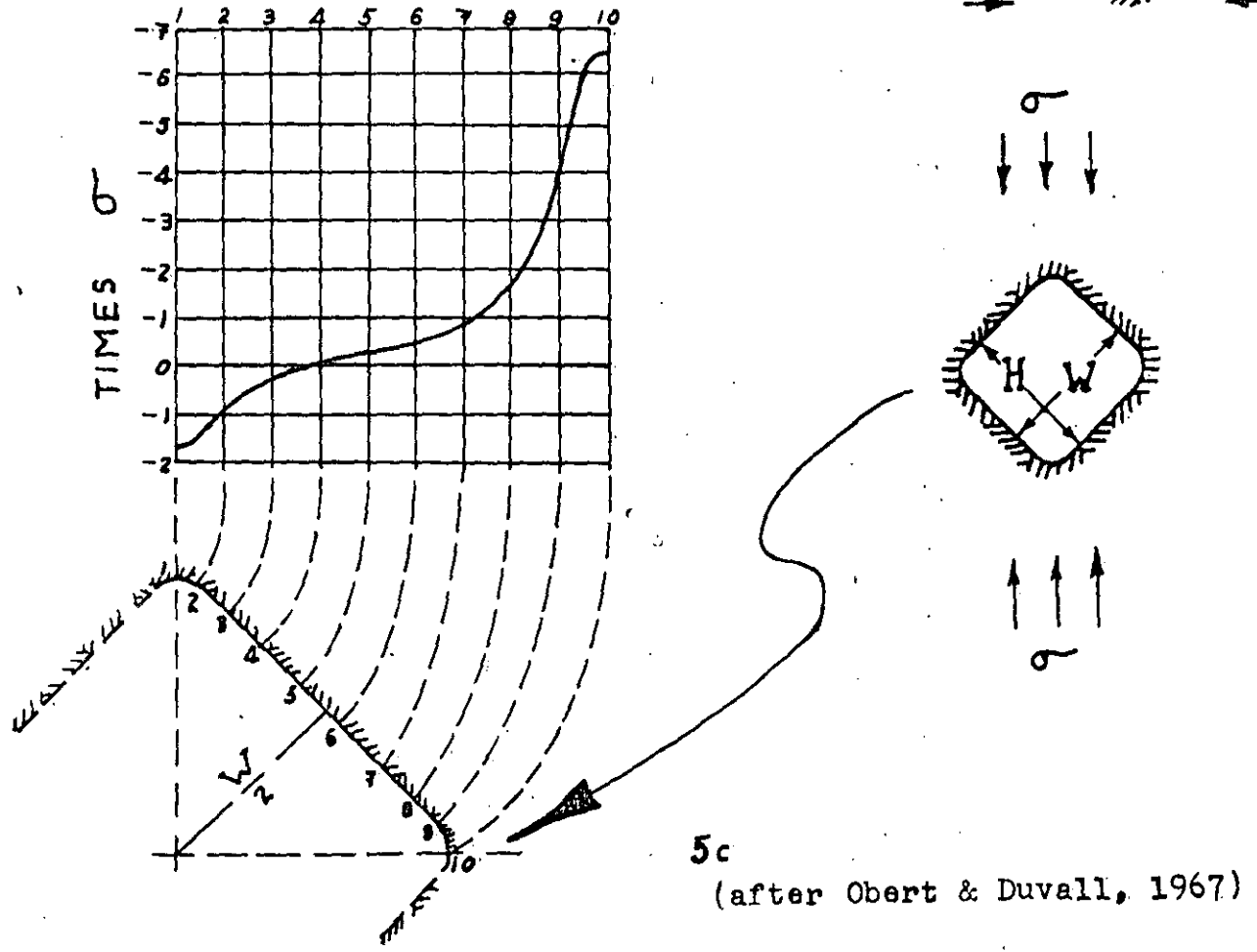
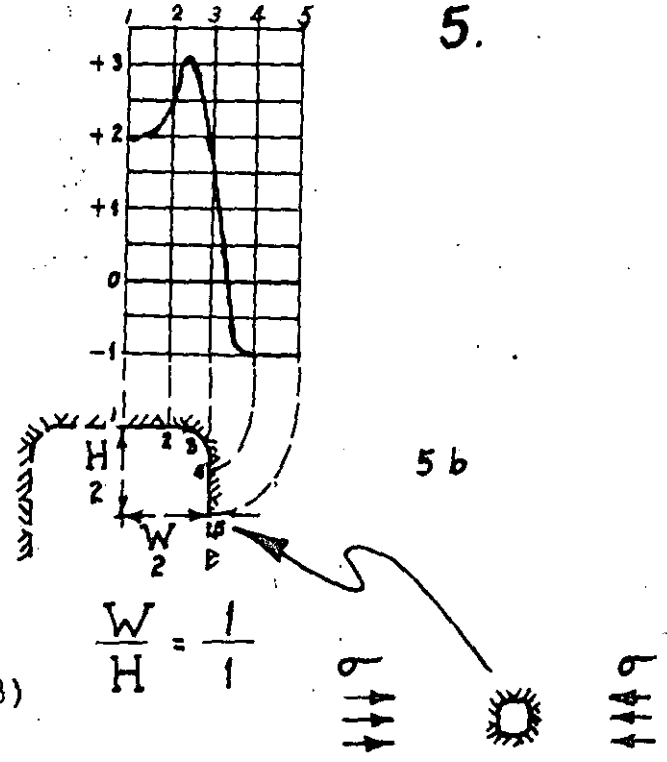
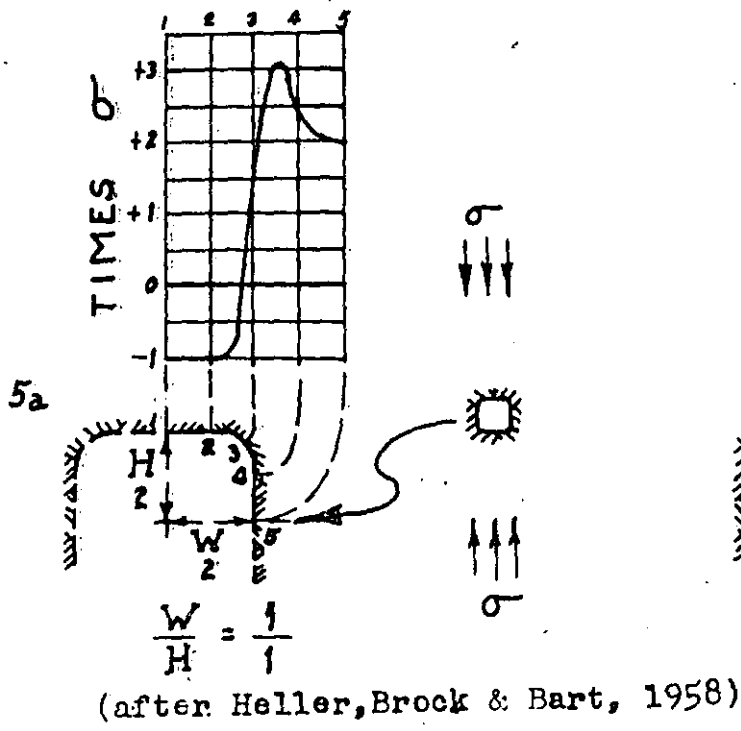
Boundary stress concentrations for ELLIPTICAL openings.



( after Bul. 587, USBM, 1960 )  
 Boundary stress concentration for OVALOIDAL openings.

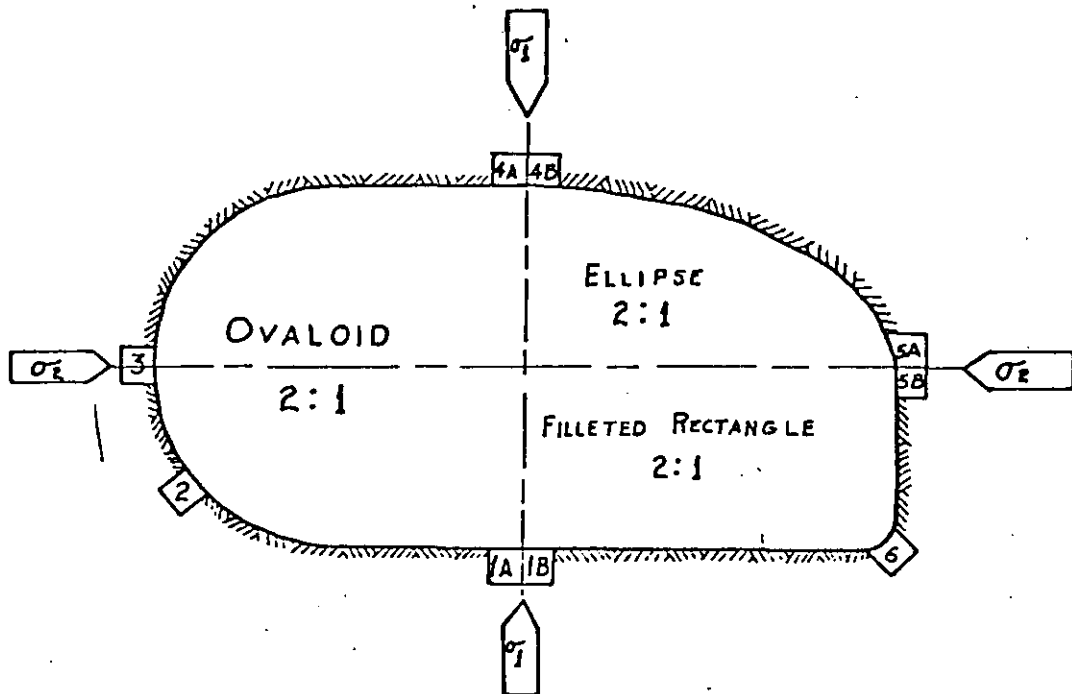


(after Hell, Brock & Bart, 1958)  
 Boundary stress concentration for RECTANGULAR openings with rounded corners; ratio of fillet radius to short dimension, 1 to 6.



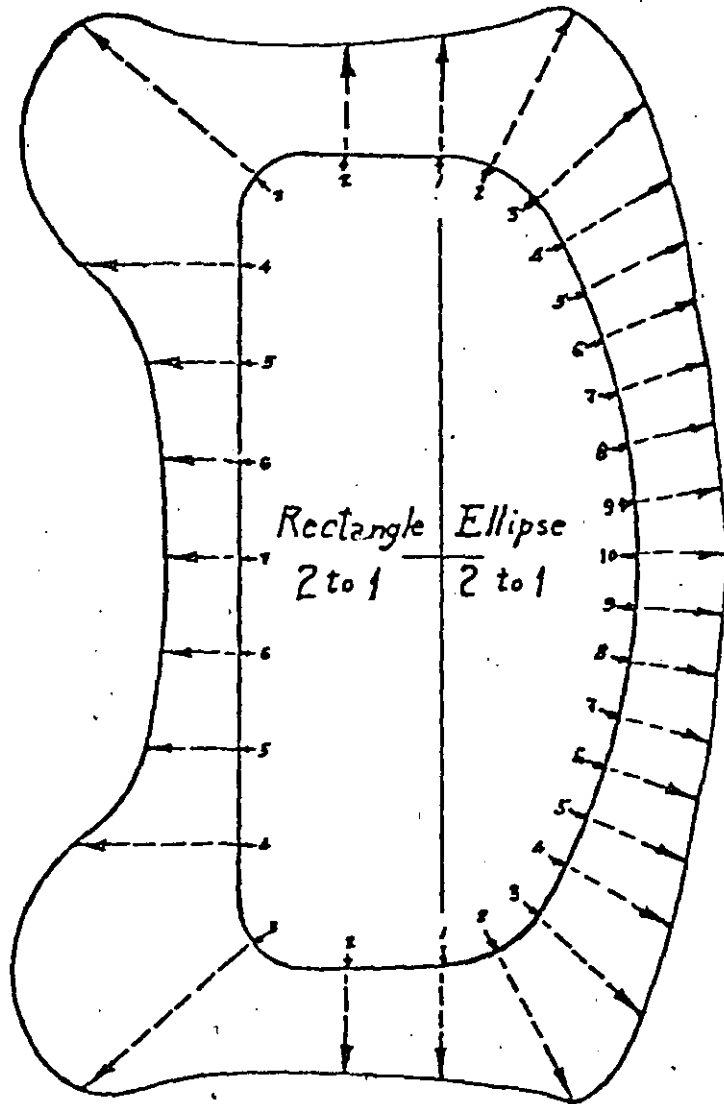
Boundary stress concentration for SQUARE openings with rounded corners; ratio of fillet radius to short dimension, 1 to 6.



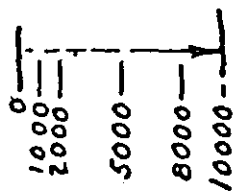


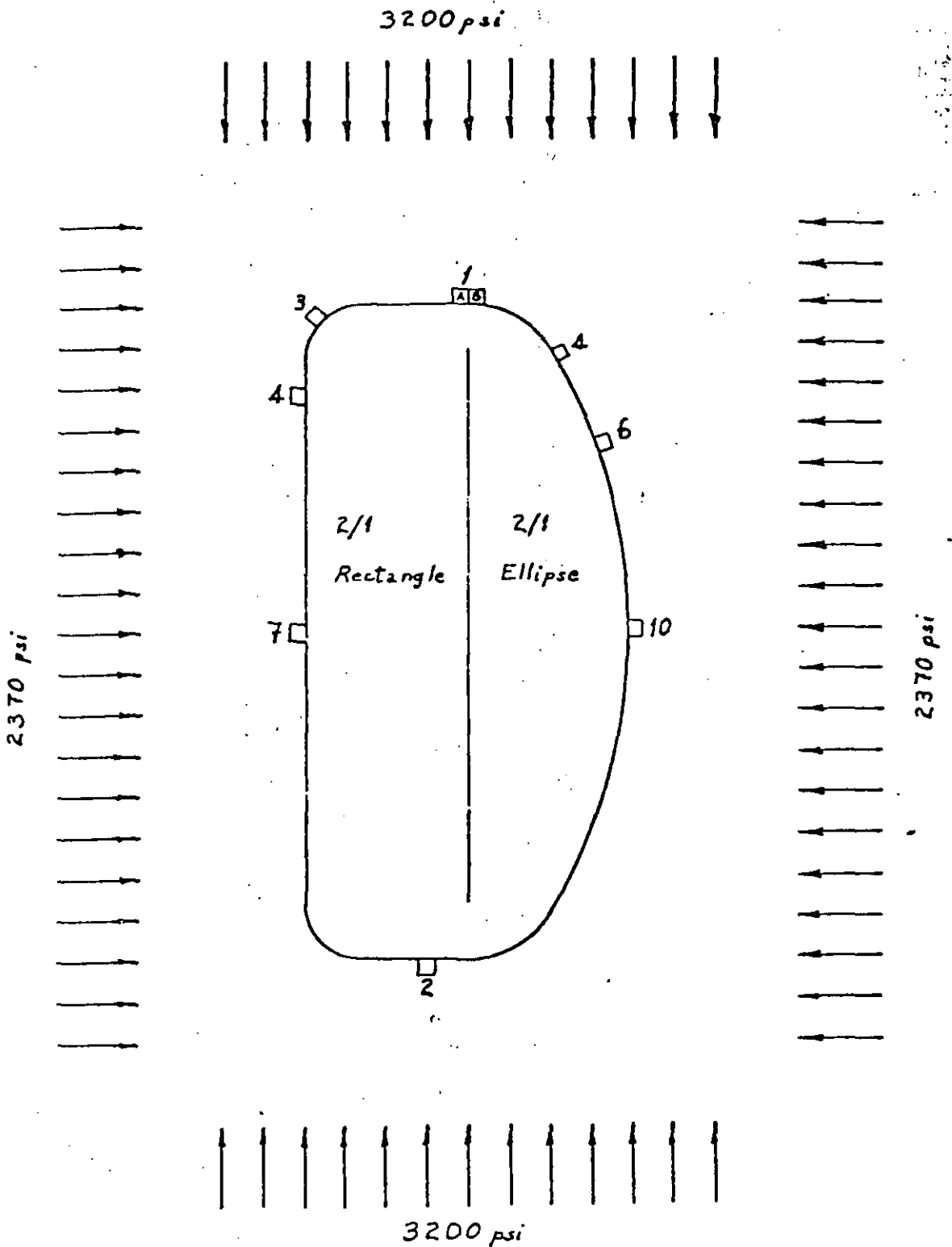
LOCATION		STRESSES FROM $\sigma_1$	STRESSES FROM $\sigma_2$	$\Sigma$ IN $\sigma_1$	AVERAGE
1	A	$-0.9\sigma_1$	$+1.6\sigma_2 \times 4 = +6.4\sigma_1$	$+5.5\sigma_1$	$+5.8\sigma_1$
	B	$-0.7\sigma_1$	$+1.7\sigma_2 \times 4 = +6.8\sigma_1$	$+6.1\sigma_1$	
2	(5 lines)	$-0.2\sigma_1$	$+2.0\sigma_2 \times 4 = +8.0\sigma_1$	$+7.8\sigma_1$	$+7.8\sigma_1$
3		$+3.3\sigma_1$	$-0.8\sigma_2 \times 4 = -3.2\sigma_1$	$+0.1\sigma_1$	$+0.1\sigma_1$
4	A	$-0.9\sigma_1$	$+1.6\sigma_2 \times 4 = +6.4\sigma_1$	$+5.5\sigma_1$	$+6.3\sigma_1$
	B	$-1.0\sigma_1$	$+2.0\sigma_2 \times 4 = +8.0\sigma_1$	$+7.0\sigma_1$	
5	A	$+5.0\sigma_1$	$-1.0\sigma_2 \times 4 = -4.0\sigma_1$	$+1.0\sigma_1$	$-0.3\sigma_1$
	B	$+2.5\sigma_1$	$-1.0\sigma_2 \times 4 = -4.0\sigma_1$	$-1.5\sigma_1$	
6	(2½ lines)	$+1.0\sigma_1$	$+2.6\sigma_2 \times 4 = +10.4\sigma_1$	$+11.4\sigma_1$	$+11.4\sigma_1$

GEOMETRIC TANGENTIAL STRESS ANALYSIS OF SAMPLE PIT PLAN



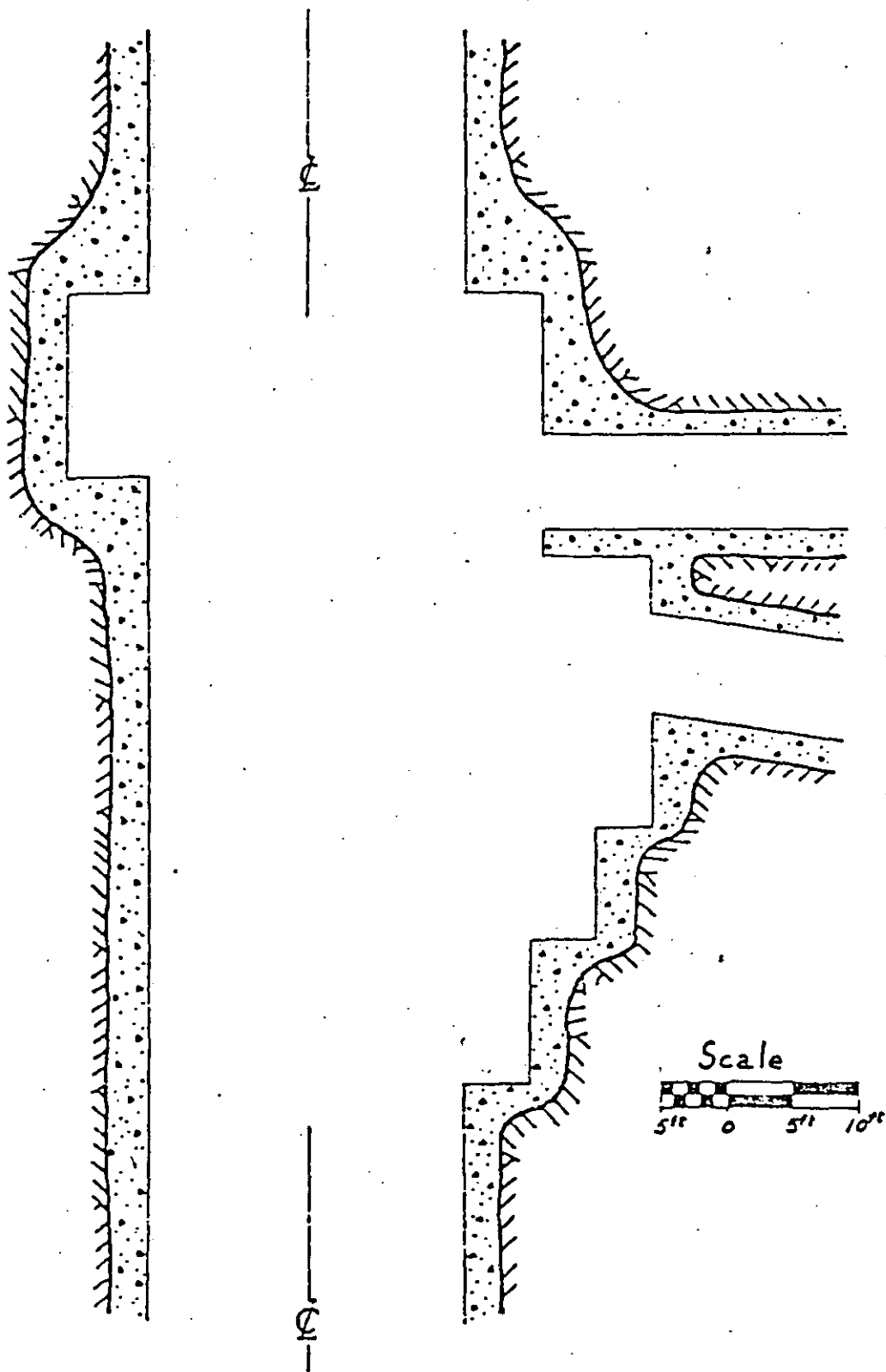
Tangential Stress Magnitude (psi)





Geometric approximation, shaft station  
 3200-ft level, Section view with horizontal  
 and vertical in situ stresses.

Figure



3200-ft level shaft station (24-ft Diameter).

Figure

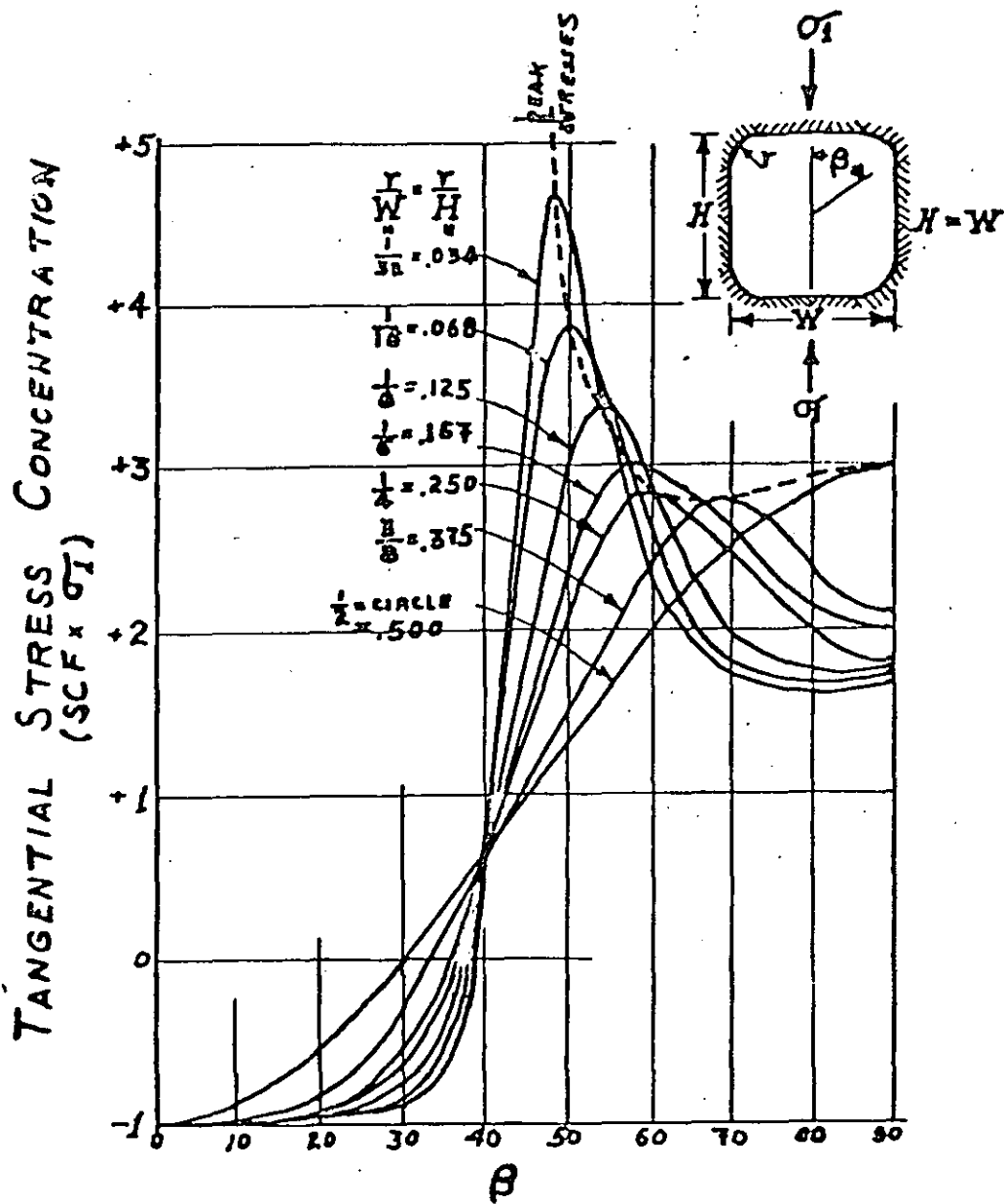


Figure 5

TANGENTIAL BOUNDARY STRESS CONCENTRATIONS (ELASTIC)

FOR SQUARES WITH ROUNDED CORNERS (UNIAXIAL STRESS).

$r$  = fillet radius ;  $\beta$  = angle from uniaxial stress direction ;  $H$  = height ;  $W$  = width ;  $\sigma_1$  = uniaxial stress. (After Brock, J.S., Rpt 1149, D.Taylor Model Basin).

FIGURE - PLATE THEORY -

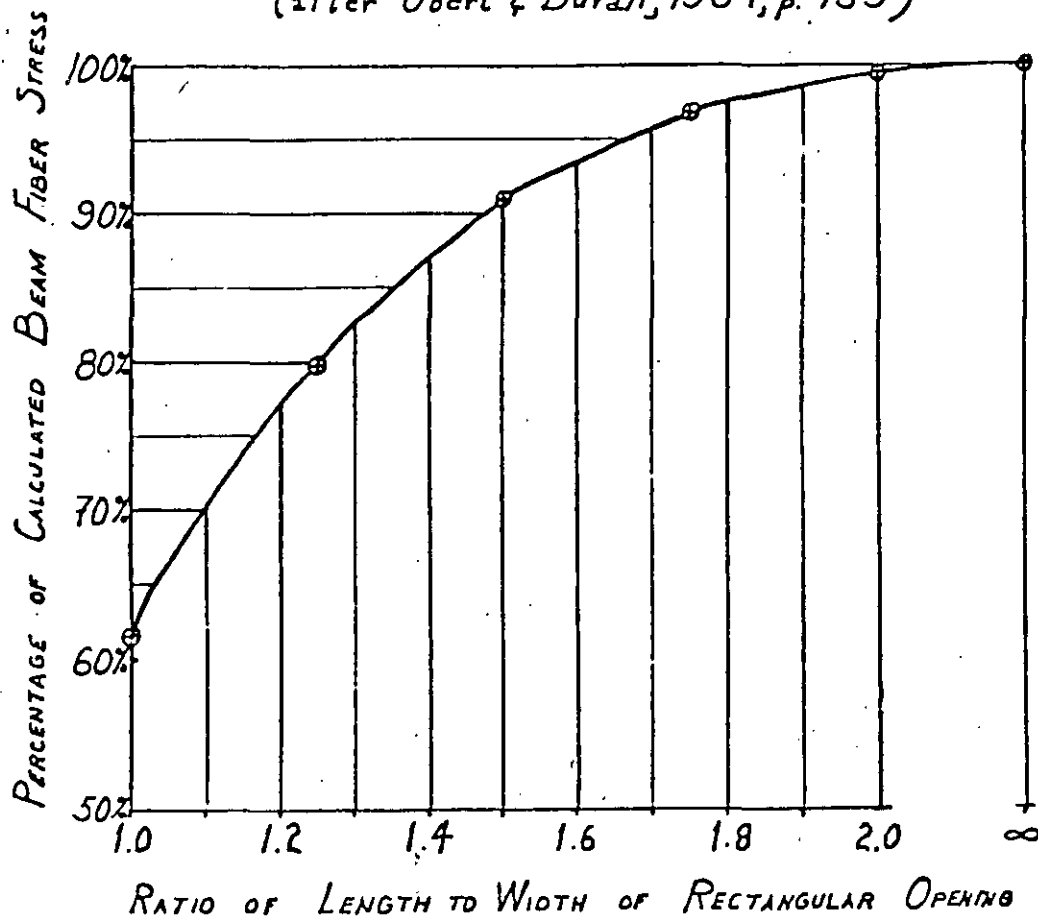
INFLUENCE OF OPENING LENGTH OF RECTANGULAR ROOM

ON MAXIMUM BEAM FIBER STRESS:

Uniformly distributed load, four

built in edges; Poisson's ratio = 0.3

(after Obert & Durrall, 1967, p. 159)



$\sigma_{MAX} = (\%) \sigma_{MAX}$  for uniformly loaded fixed-end beam.



Tertiary intrusives and volcanics with low-grade mineralization.

75° CUSPIDOR FAULT ZONE (Minor-Normal?) 75°

40°

PRINCE CHARMING

Precambrian igneous and metamorphics Barren.

Intense jointing sub-parallel to fault in footwall

Minor vertical faults

Slideface slide ACTIVE

D29 slide ACTIVE

Nosa slump (REMOVED)

11ft of movement STOPPED

Tertiary intrusives and volcanics. (Copper mineralized quartz monzonite to granodiorite.)

FAULT ZONE

T20  
K35  
T20

T20  
K35  
T20

85° DORTMUND FAULT (Minor-Normal?) 85°

40°

FAULT ZONE (Minor-Normal?)

Tertiary intrusives, volcanics, and Conglomerate with low grade mineralization.

Plan view of pit perimeter with major geologic features.

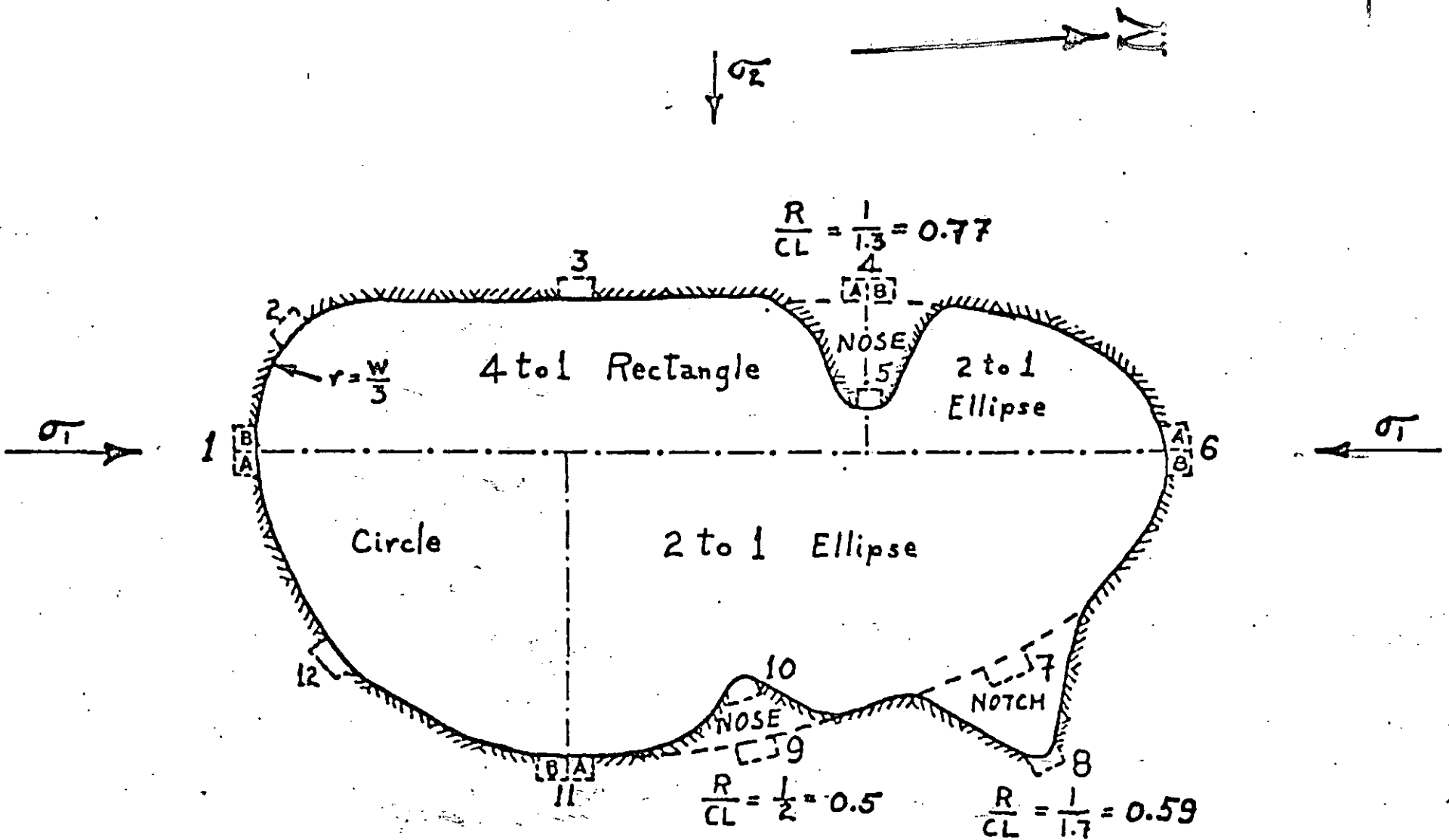
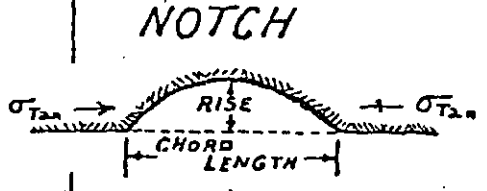
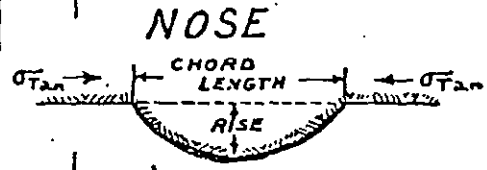
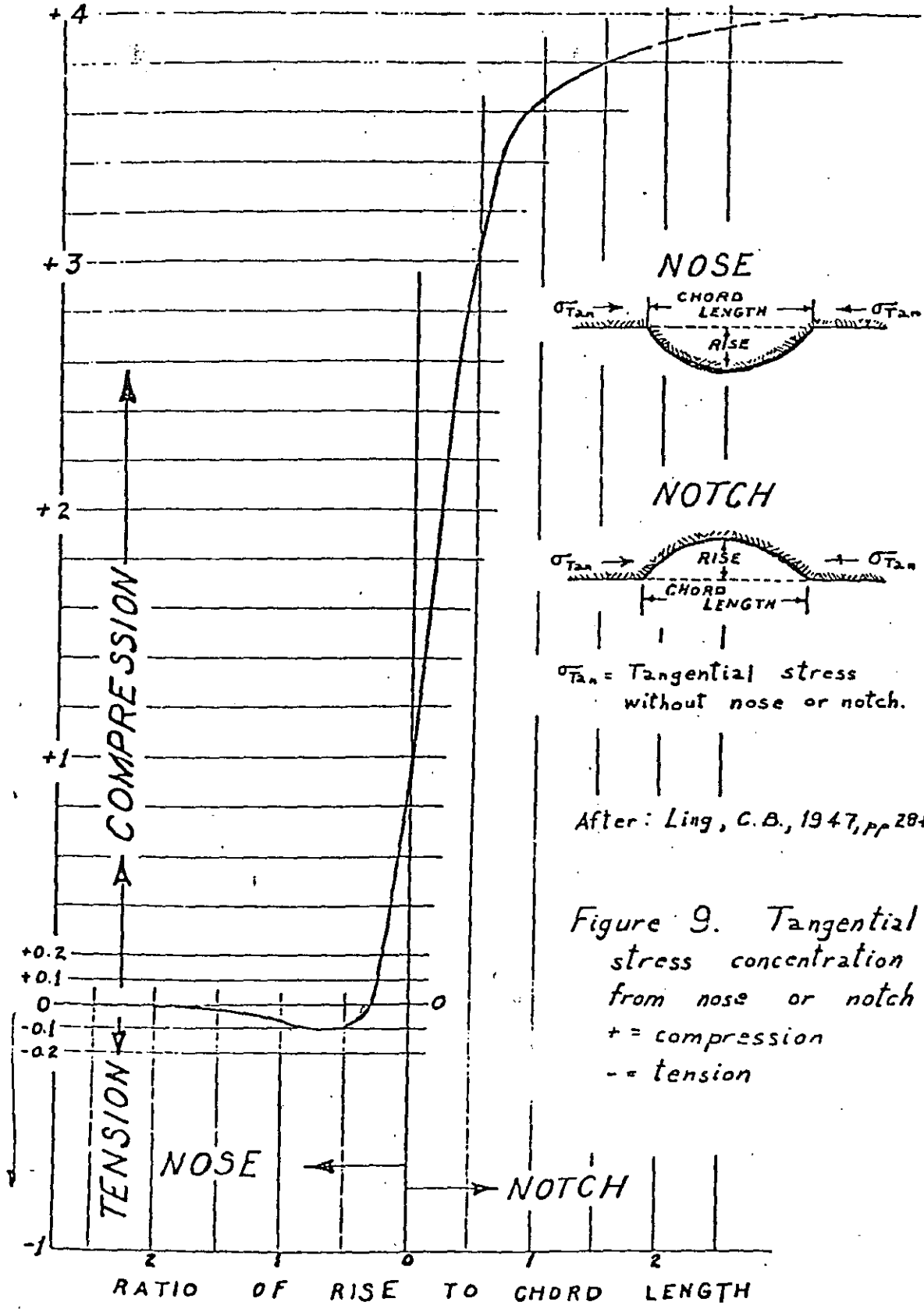


Figure 2. Geometric approximation of pit plan with tangential stress estimation locations.

R = Rise  
 CL = Chord Length



MAXIMUM TANGENTIAL STRESS CONCENTRATION



$\sigma_{Tan}$  = Tangential stress without nose or notch.

After: Ling, C. B., 1947, pp 284-9.

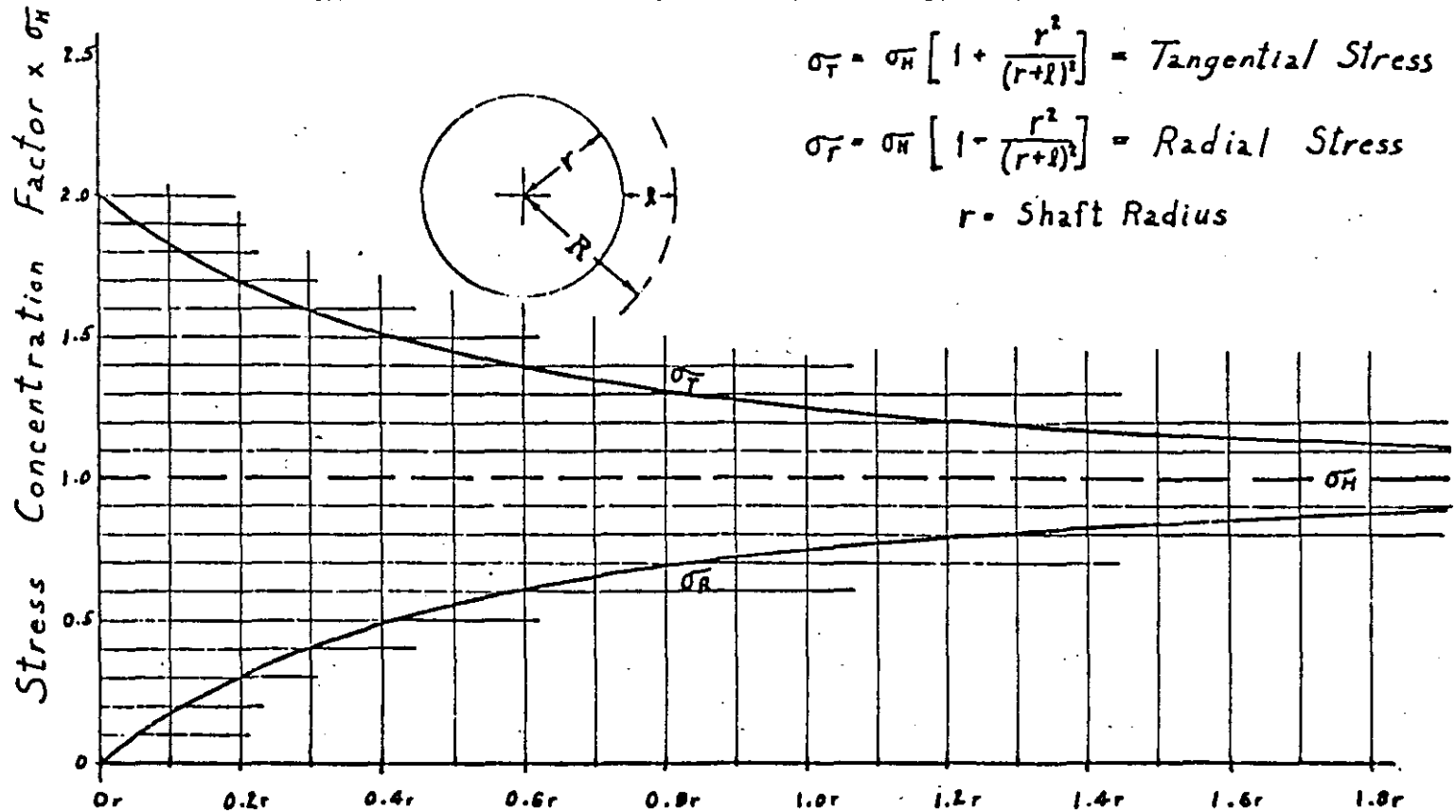
Figure 9. Tangential stress concentration from nose or notch:  
 + = compression  
 - = tension

Tangential and Radial Stress Concentration Factors  
in Terms of a Uniform Horizontal Stress Field

$$\sigma_T = \sigma_H \left[ 1 + \frac{r^2}{(r+l)^2} \right] = \text{Tangential Stress}$$

$$\sigma_r = \sigma_H \left[ 1 - \frac{r^2}{(r+l)^2} \right] = \text{Radial Stress}$$

$r$  = Shaft Radius



$l$  = Distance from Shaft Face, in fractions of  $r$

$r$  = Shaft Radius ;  $R$  = Radius of Relaxed Zone

$l$  = Thickness of Relaxed Zone

Figure



**DIVISION DE EDUCACION CONTINUA  
FACULTAD DE INGENIERIA U.N.A.M.**

MECANICA DE ROCAS APLICADA A LA MINERIA Y A LA CONSTRUCCION

PROCEDIMIENTOS DE EXCAVACION

M. EN C. JOSE IBARRA TORRES

MAYO, 1985.



## THE NEW AUSTRIAN TUNNELING METHOD A ROCK MECHANICS PHILOSOPHY

HAROLD T. WHITNEY  
GILBERT L. BUTLER  
Law/Geoconsult International  
Marietta, GA

A number of technical treatments of the general subject matter regarding the New Austrian Tunneling Method (NATM) approach to tunneling have been published in recent years and have dealt with many facets of the subject. These publications have documented the relatively wide acceptance of the philosophy of NATM throughout the world. However, for a number of reasons that could be considered both technical and philosophical, NATM has been slow to receive much acceptance in the United States. The authors have spent time in recent years trying to understand both the strengths and weaknesses of NATM as a design process and to consider some of the rationale for its relative lack of favor in United States design and construction practice. This paper is an attempt to present our findings and conclusions as to the benefits of NATM as it might be applied to United States practice.

As a starting point of this discussion, we would like to present our definition of what we believe constitutes the NATM philosophy.

We believe it to be a common sense geotechnical approach to the design of underground support systems that can embody a variety of support elements and excavation techniques. It also makes extensive use of monitoring of ground behavior during construction to corroborate design assumptions.

The support elements generally include combinations of shotcrete, wire mesh, rock bolts, and light steel ribs, as applied to construction in rock. These are the most common elements used in relatively poor ground conditions. However, other elements can be used within the context of the general philosophy. Being a geotechnical approach, the design methods incorporate controlled de-

formation to permit mobilization of the inherent strength of the earth medium. This point will be developed further in the discussion. On occasion, the literature has called it a "shotcrete method". It certainly can embody shotcrete as a support method, but it is obviously not restricted to shotcrete alone as a support element. It has also been called an "observational method". Observation during construction is one element of the approach, but this description is also limited.

The philosophy has certain historical negatives, particularly relative to application in the United States. However, we submit that NATM constitutes a valuable tool in the designers' arsenal of design concepts which should be favorably considered on projects where it is advantageous to do so. The authors hope by this discussion to develop the strong points of the philosophy as it applies to United States practice and consider possible limitations. To do so, it is necessary to turn back the clock and examine the philosophical development of the basic concepts.

A convenient point of initial reference to an American engineer, would be to consider the work of Karl Terzaghi. It is understood that part of the early research and study of Terzaghi was accomplished in Europe and that he spent some time at the University of Graz in Austria. His early work in the United States was accomplished in about the late 1920's and early 1930's, when he conducted some of his classical experiments relative to pressures on retaining walls. From this early work, Terzaghi used Rankine theory to evolve an understanding of the nature of stresses on retaining walls. Terzaghi's work demonstrates that movement of a wall, controlled or other-

wise, permits mobilization of the inherent strength of the earth medium behind the wall, such that a stable wall system is reached under conditions where the pressures on the wall are reduced from a state of complete wall rigidity. At the time of this development, this philosophy represented a departure from the historical engineering approach of using theoretically rigid structures to retain the medium.

More adaptations of this philosophical approach are now evident in many aspects of construction that involve support of the earth medium. This is most evident today in highway construction. Twenty years ago, extensive use of massive rock buttresses and/or concrete or steel elements were evident to provide stability to highway cuts and fills in terrain with marked topography. Today, there is extensive use of Gabions and Reinforced Earth construction possibly coupled with drainage systems which are improved ways of helping the earth medium mobilize its own strength through the controlled deformation of flexible support systems.

This adaptation of flexible support systems to permit mobilization of ground strength constitutes the heart of the philosophical approach to tunneling in accordance with NATM theory. An examination of the historic development of NATM shows how well it matches what is really common sense geotechnical engineering.

One of the technical leaders of Europe in this era was, L. v. Rabcewicz. He began his work about the same time as Terzaghi and also spent some time at the University of Graz.

His initial studies also dealt with the concept of mobilization of the strength of the earth medium utilizing controlled deformation of flexible support systems. However, whereas Terzaghi's work dealt with retaining walls, Rabcewicz's work dealt with tunnel lining systems. Rabcewicz also found that tunnel lining systems tended to be more susceptible to shear failure as opposed to failure in bending. The nature of these early investigative techniques involved both model and field case studies as well as more traditional rock mechanics theory and laboratory testing.

Some of the initial research approaches to the understanding as to how the ground medium reacts under load were conducted by field observations in a drift of a large rock tunnel where an initial side drift with complete support had been previously excavated. As the main heading was advanced, careful measurements and observations were made of the

deformation pattern in the ground surrounding the original drift. This was a technique used to understand the movement of the rock mass as the excavation proceeded. This permitted a partial understanding of how the medium had reacted as the initial tunnel was excavated. This approach, coupled with laboratory research led to initial understanding of the mechanism of the ground movement and behavior. Rabcewicz, in his early laboratory modeling tests, developed a load frame to simulate an anchor system similar to what the contribution of rock anchors would be in stabilizing a cobbled ground arch with a thin support membrane. It was discovered that through this relatively simple support concept of simulated rock anchors and thin liner that the cobble arch was capable of carrying significant additional load above what may have been otherwise possible. An example of this load frame is shown in Figure 1.

Through this process of laboratory investigations and field measurements and observations, a significant advance in the understanding of the behavior of the medium under load was possible. It led to the concept of the support mechanism that permits mobilization of the self-carrying capacity of the earth medium.

As the method developed more fully, it became more widely used in practice through value engineering proposals suggested by contractors. Since Europe was undergoing a post-war construction boom during the 1950's, significant underground works were being proposed and developed. Most of the initial design for these facilities used historical engineering concepts. NATM then came into vogue because of its cost effectiveness relative to these historical concepts. Thus, it has evolved from an initial alternative design and construction concept in the 1950's and 1960's such that today it has become a primary design philosophy of European underground practice.

Much of the success that NATM has had in the past two decades can be attributed to its capability of dealing with a variety of ground conditions, its provision for maximum flexibility in choice of ground support and construction methods as applied to tunnels of all sizes and shapes, and its establishment of a mechanism for alternate construction approaches for varying geologic conditions in sensitive areas. NATM does not require unusual tunneling equipment or skill on the part of workmen. But like other tunneling methods it relies heavily on the skill of the tunnel foreman, his tunneling crews, as well as an understanding of basic geotechnical principles by the Engineer in charge.

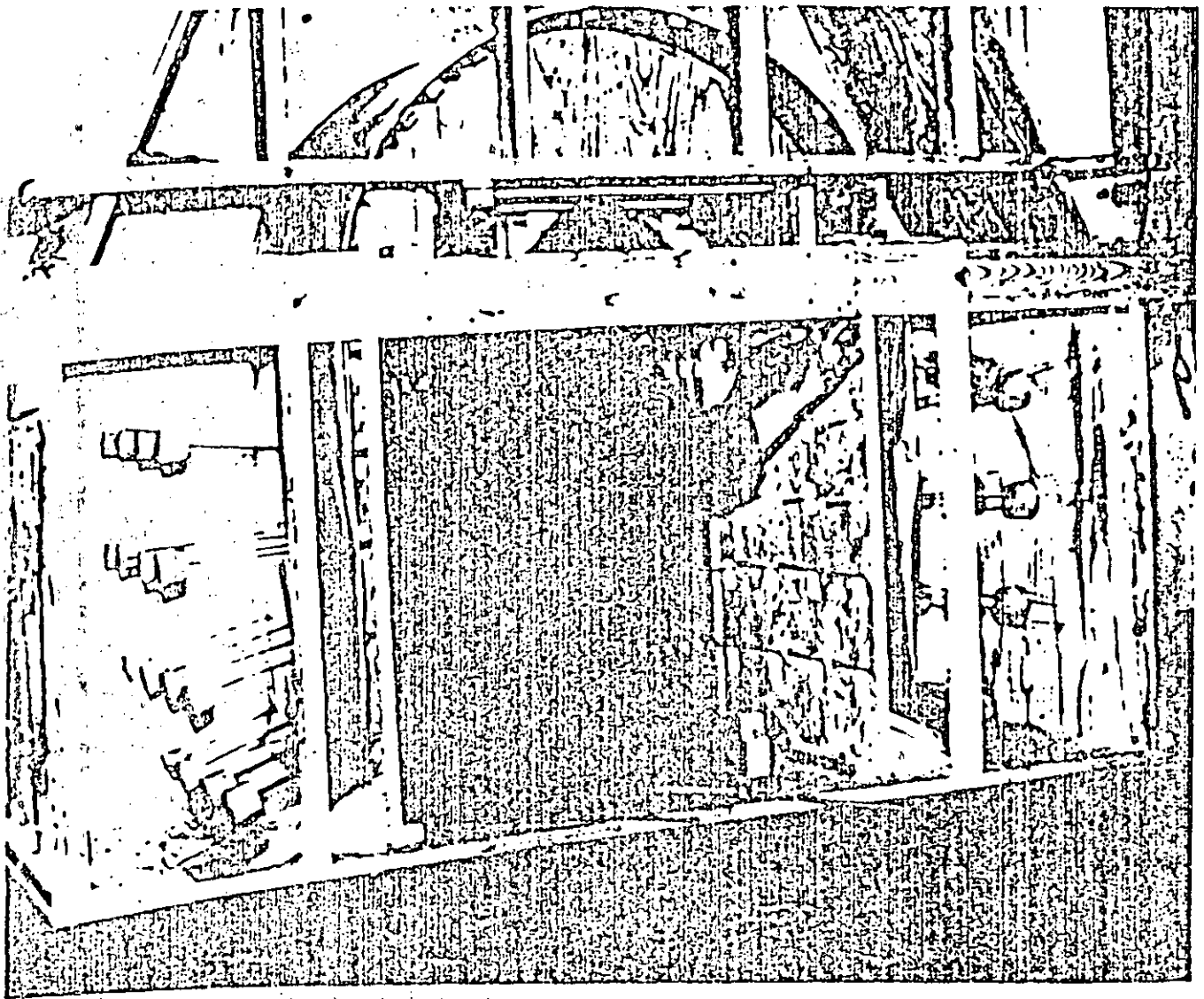


Figure 1. Example of a laboratory load frame used to model an anchor system

The next significant theoretical step in concert with the work of Rabcewicz came in the development of the concept of the ground reaction curve. In Europe, this development came in part from R. Fenner and F. Pacher. An example of a Fenner/Pacher ground reaction curve is demonstrated in Figure 2, with a safety factor analysis as it might apply to a specific support concept. This curve demonstrates the manner in which the radial (i.e., support) stress necessary to stabilize a circular opening in a medium changes as deformation in the medium occurs around the opening. The vertical axis depicts a radial stress relationship and the horizontal axis depicts radial deformation. If deformation does not occur, the radial stress required to

achieve stability of the opening is a maximum. As deformation occurs, the stress required for stability decreases until the deformation reaches a point of theoretical maximum support efficiency. Continued deformation causes irrevocable movements within the medium and resultant loss of strength, such that continued deformation beyond this point requires an increasing amount of radial stress to stabilize the opening. In tunnel design, the optimum interaction between lining and opening is accomplished when stability is reached just prior to deformation reaching the zone of minimum stress. At this stress deformation state, maximum efficiency is achieved relative to the support required to achieve a stable opening.

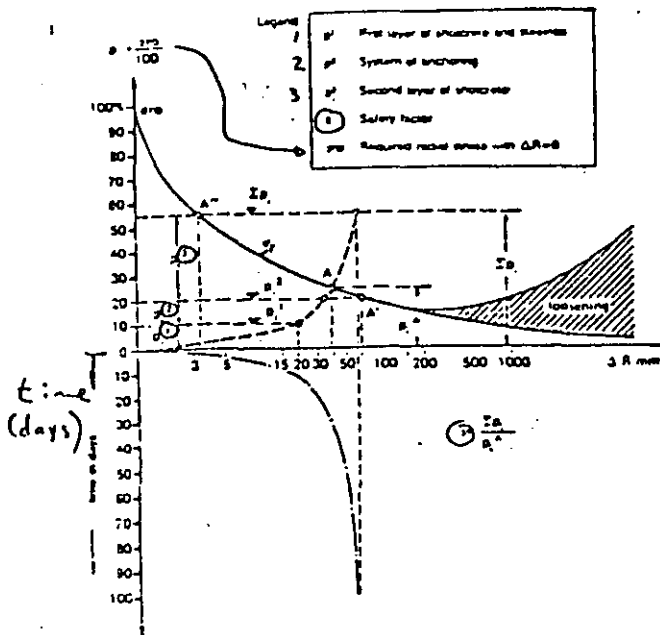


Figure 2. Ground Reaction Curve (after Fenner and Pacher).

It must be pointed out that it is extremely difficult to predict a precise ground reaction curve for a particular medium on a given project site and assumed tunnel support system. Only through a history of construction experience, careful measurement of ground response in tunnels, and an understanding of the nature of various support mechanisms, can this curve be approximated for design purposes for a given site. Different ground conditions obviously yield a family of curves, some of which would have a very steep declining stress with minimum deformation. As Terzaghi pointed out in the development of earth pressure theory, the deformations required to permit the active pressure case to be realized are quite small in an engineering sense. Accordingly, deformations of the medium around an opening necessary to permit strength mobilization such that the optimum design condition of minimal support is realized, are also quite small.

It is a basic principle of NATM to provide initial support at the heading immediately upon excavation to prevent deformation from becoming excessive and causing irrevocable differential loosening of the medium, particularly relative to difficult ground conditions. In this way, NATM attempts to take advantage of the principle expressed by the ground reaction curve such that minimum support is required and the maximum inherent self-carrying capacity of the medium itself is

realized. Too often in United States practice, careful attention is not given by both designer and contractor to the need to prevent excessive deformation at the heading prior to the installation of initial support. The result is that deformations exceed the optimum efficiency of the ground reaction mechanism resulting in the need for a more substantial support system than otherwise would have been necessary.

A further element of this circumstance has to do with the philosophical approach to temporary or initial support. Traditionally in United States practice, the contractor is responsible for temporary support, with safety being the prime motivator. Therefore, it is often the case that the initial support placed in the interest of safety is not integrated into the total support system anticipated for successful project life. Accordingly, no credit is given in the design of the permanent support system to the carrying capacity of the initial support system to be designed by the contractor. Further, because consideration of the ground reaction response is not included in the design of the initial support system, even initial support systems can be quite bulky and wasteful of material. Figure 3 depicts an example of rather massive steel used as initial support which was given no credit as an element of an integrated total support system.

On some projects in the United States, tremendous material quantities are used in initial support systems. Not only is there inefficiency in the design of the initial support system, the initial support system is not included as part of the integrated final support system, and is in effect wasted as far as the long term carrying capacity of the total support required for stability. NATM makes use of an integrated design concept, thereby maximizing the efficiency of the total support system. In this concept, the design engineer lays out the sequencing of each stage of support which becomes incorporated into the permanent support system. An example of a simple staging operation is shown in Figure 4. The initial support is generally developed by shotcrete, anchors, and other supplementary support elements which are usually installed immediately after excavation. In addition to providing initial stability during construction, these elements become incorporated into the permanent support system. Later in the tunneling process, more support elements may be added until complete installation of the total support unit has been accomplished. In this way, maximum efficiency is made of the materials used in the support process. In addition, as much of the inherent strength of the medium as possible is mobilized into a quasi self supporting arch.

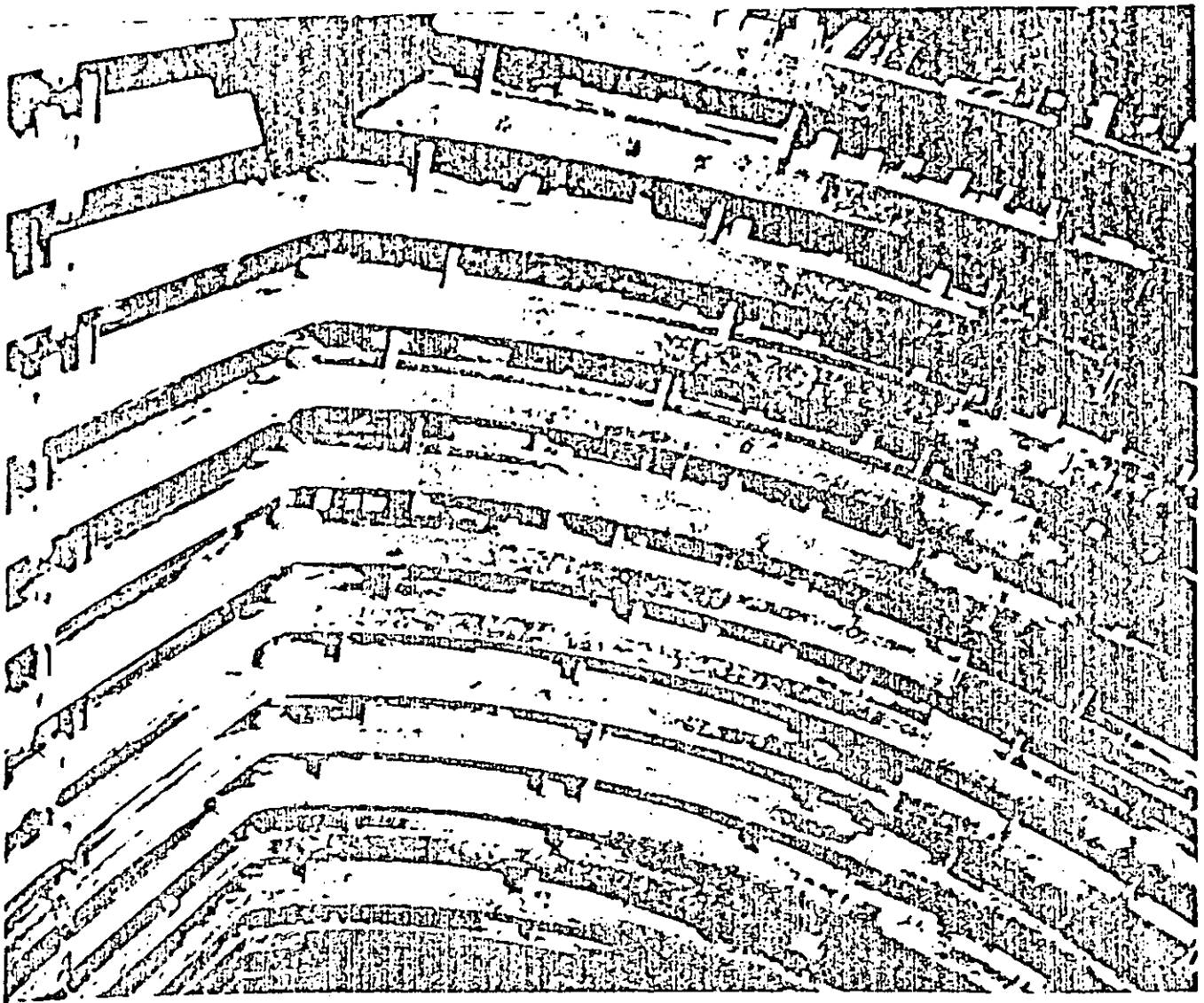


Figure 3. Example of steel sets used as initial support for an underground cavern.

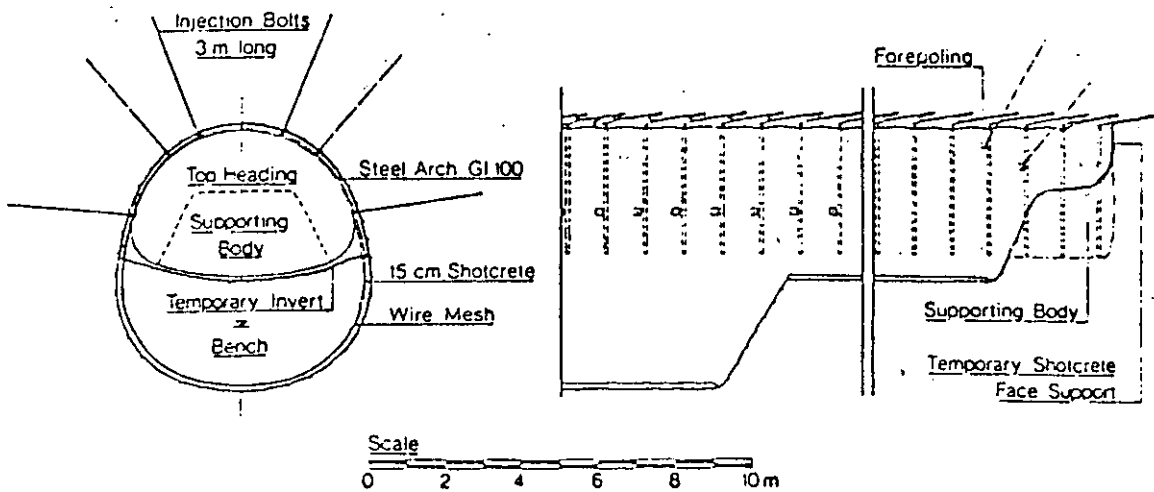


Figure 4. Cross-section and sequence of construction strategy operation.



A more complex staging process is demonstrated in Figure 5 which depicts a mined station. In this case, the construction sequence incorporated a multiple stage excavation process, with installation of initial support occurring immediately after each stage. In this case, the left side gallery was excavated first with the right side gallery following by a distance of approximately 100

feet (30 meters). The third stage involved the excavation of the top heading. At the completion of the installation of the initial support system at the top heading, a complete supporting arch had been achieved which permitted excavation of the central core. NATM frequently makes use of intricate excavation stages, particularly in difficult ground or odd geometry, to permit immediate installation of initial support.

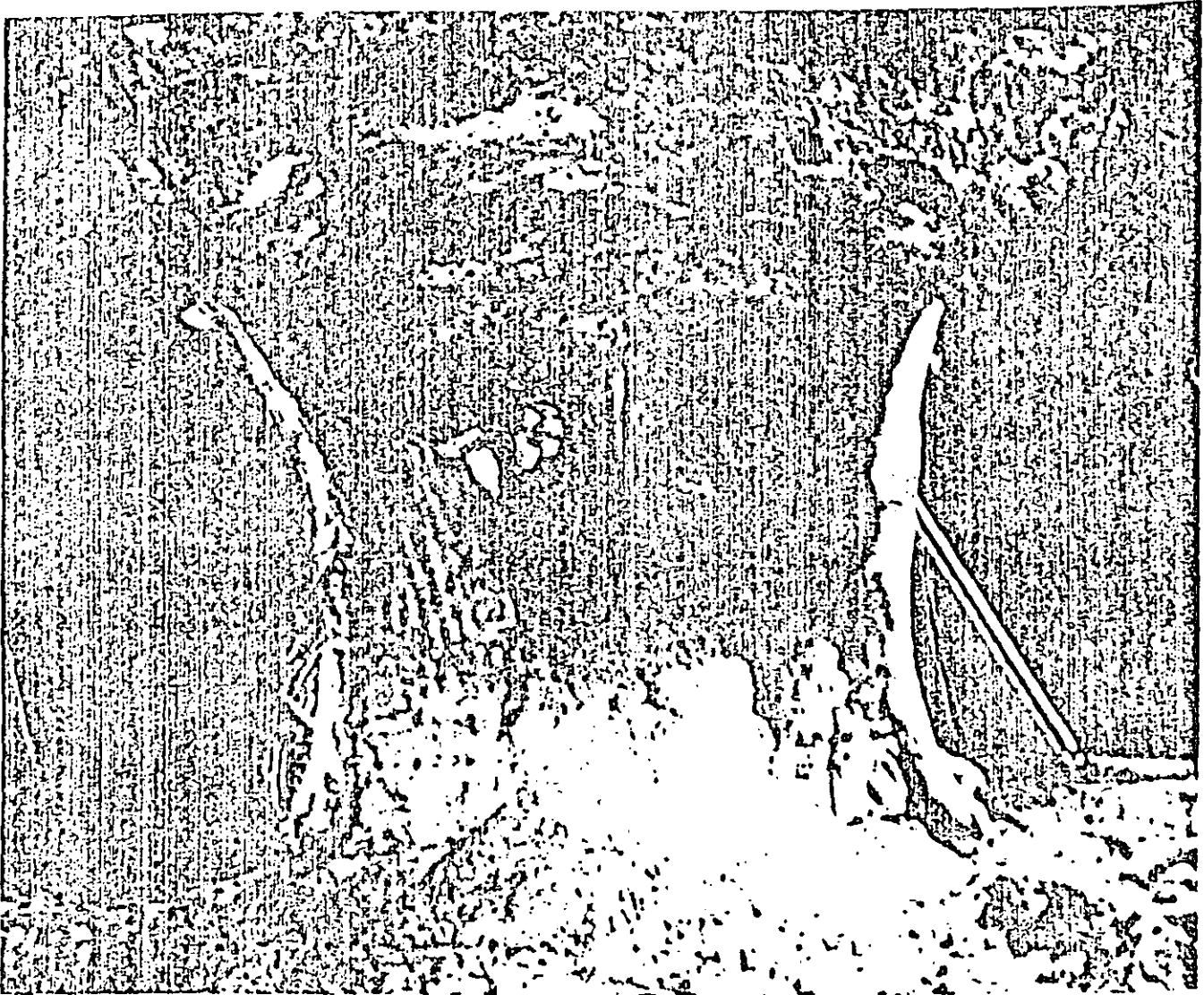


Figure 5. Mined rail transit station constructed with a multiple stage excavation process.

In recent years in Europe, the design process has incorporated finite element techniques as a supplementary mathematical tool. Further, some cases exist where deformations predicted by a finite element analysis have been substantially corroborated by measurement of field performance. Minimal cases of such documentation presently exist in the United States. The European designer using a finite element or other analytical approach, proceeds in the following manner. An initial estimate of support requirements based on experience is made. This is commonly referred to as a predimensioning phase. Mathematical modeling of this assumed ground support system then proceeds. The stability of the ground opening relative to various construction stages is then analyzed. Adjustments are then made in the support system as necessary until a proper stable design for each construction stage is achieved. Inherent in a finite element mathematical model is the capability to mathematically track the mode of failure and also to conduct sensitivity analyses as to the impact on the design of the accuracy of the strength characteristics of the medium. Depending on the knowledge of the strength characteristics of the medium, and the extent to which they can be modelled mathematically, the appropriate safety factors can be incorporated into the design of the support system.

It is also inherent in the NATM design process to prepare a number of proposed support systems in anticipation of varying ground conditions through a particular job site. The exact number of different ground support systems for a particular site is obviously a function of the anticipated variation of ground conditions at that site. Traditionally, three to six different ground support systems are designed for a particular site. These vary between minimal support requirements involving randomly placed rock anchors to a complete integration of several layers of shotcrete, wire mesh, anchors, and light steel ribs. It could also involve subsequent placement of a cast-in-place concrete liner. The bid documents show an estimate of the total linear footage anticipated on the project for each of the support systems. The contractor is then asked to bid on estimated quantities of the anticipated elements of each of the support systems. A field decision is then made during construction between the contractor's representative and the owner's representative where possible change from one support system to another is anticipated. Minor adjustments are generally made in a unilateral decision at the heading by the tunnel foreman.

It has been argued that a greater cooperation exists in Europe between owner and contractor as opposed to the relative adversarial relationship that exists in the United States and that this contracting practice is not tenable in United States practice. The authors believe that some modifications in United States contracting practice are necessary to achieve the full benefit of using a variety of support systems to respond to changing ground conditions. Nevertheless, the authors believe that it is possible to work towards this concept within the basic framework of present United States contracting practice.

Owners must come to understand though that the basic risk of variable conditions at a project site belongs to them and the transfer of this risk is accomplished only through payment of a price relative to the magnitude of the risk.

Construction monitoring is also extensively used to compare predicted stresses and deformations relative to field response. The most commonly used construction monitoring technique involves a network of convergency points to measure deformations and changes in shape of the opening. In addition, some use is made of extensometers and pressure cells. Other devices are also used depending on the nature of the design and the methods of construction. Obviously, timely reading and comparison with predicted response is a major tool to be used during construction to permit understanding of how the ground opening is behaving. This monitoring program, as well as visual observation of changes in geology, ground behavior, etc., plays a major role in decisions regarding the need to change from one support system to another during construction.

In conclusion, the authors believe that NATM as a philosophy has some very important concepts that provide meaningful improvement in the United States tunnel design/construction process. The benefits are maximized in poor ground and/or difficult geometry. It constitutes an important tool for designers to consider as they approach design of a specific project and wish to evaluate the results of a number of design techniques.

#### REFERENCES

Terzaghi, K. and Peck, R.B.: Soil Mechanics in Engineering Practice, John Wiley & Sons, Inc. 1948.

Kabcewicz, L.V., Golser, J., Hackl, E.: Die Bedeutung der Messung im Hohlraumbau, Der Bauingenieur, Heft 7, 8, 1972.

Golser, J., Hackl, E., Jostl, J.: Tunneling in Soft Ground with NATM. International Construction, December 1977.

Mussger, K, and Cavan, B.P.: Dual Lining Procedures Provide Tunneling Economy, Railway Track and Structures, September 1982 pp. 54-56.

Law Engineering Testing Company Project Files.

# The New Austrian Tunnelling Method

After describing the influence of rock-pressure effects on tunnel linings, the author underlines the inadequacy of conventional tunnel driving and lining methods in poor ground and explains the effectiveness and reliability of a new method consisting of a thin sprayed concrete lining, closed at the earliest possible moment by an invert to a complete ring—called an "auxiliary arch"—the deformation of which is measured as a function of time until equilibrium is obtained. Ways are shown to determine the magnitude of active forces, which leads to dimensioning of linings on an empirical basis\*. Further articles describe successful applications of the method

By Prof. Dr.techn. L. v. RABCEWICZ,

## PART ONE

IN the conventional tunnelling practice of the past, masonry in dressed stone or brick was regarded as the most suitable lining material in unstable rock. Concrete was rejected because possible deformation during the settling and hardening process was supposed to cause irreparable damage. The space between masonry lining and rock face was dry packed. Timber lagging, which was subject to decay when left in place, generally could not be removed, particularly from the roof, because of the danger of loosening and rockfalls.

The situation was further aggravated by a very unfavourable time factor. Merely to bring to full section a 9m-long section of a double-track railway tunnel by the old Austrian tunnelling method, after the bottom and top headings had been driven, took about four weeks, and another month was needed to complete the masonry of the section. The amount of timber used in more difficult cases was so enormous that one third and sometimes even more of the excavated space was filled by solid timber.

All these circumstances, together with the tendency of the temporary timber framework to yield, necessarily produced violent loosening pressures, which frequently caused roof settlement up to 40cm and more before the masonry could be closed. Years after construction had been finished a slow decrease in volume of the compressible and sometimes badly executed dry packing often deformed the lining asymmetrically, causing damage and costly repairs. Damage to the surrounding rock as well as to the lining itself was further increased locally by the mechanical and chemical effects of water.

It is evident that in this period of rather inadequate methods and materials for temporary and permanent supports, loosening pressures were a source of the greatest concern to tunnel engineers. All attempts to design a lining during this period were consequently carried out with sole regard to loosening pressures.

Occasional subsequent deformations of linings forcibly led to the erroneous conclusion that the linings designed in this way still lacked the necessary margin of safety, whereas the failures almost without exception were due to incorrect treatment of the surrounding rock and to fundamental shortcomings of the methods.

A typical practical example of the imperfections mentioned† is a double-track railway tunnel in Czechoslovakia, which was driven almost a century ago through a ridge of soft, horizontally stratified sandstone. Although the rock was fairly stable, stratification and jointing caused the corners in the roof on both sides to fall out, leaving a more or less rectangular cavity instead of an arch. The tunnel was supported by an excellent dressed-stone lining, 45cm thick, but it was not backfilled. During the following decades the unsupported layers of sandstone subsided and settled on top of the arch, causing the roof of the lining to bulge downwards (Fig. 1). Had the

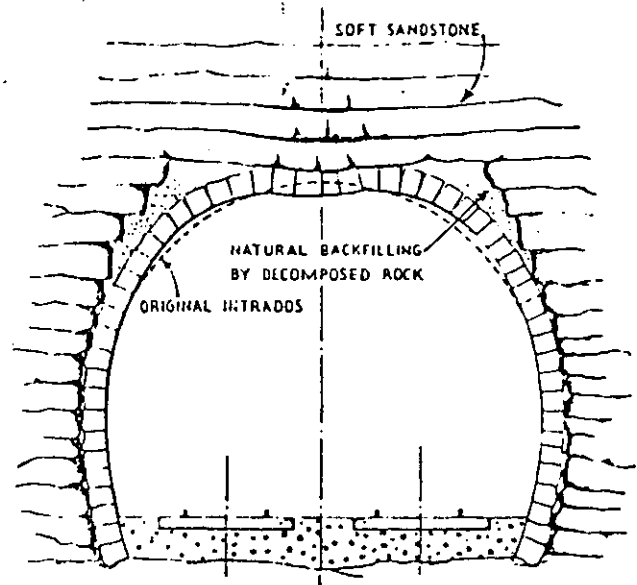


Fig. 1. Deformation of a malconstructed tunnel arch by loosening pressure

\* The substance of this series was originally presented to the XIII Colloquium of the International Society of Rock Mechanics in Salzburg, October 1962, and this English version, which contains additional material, is published by arrangement with Springer-Verlag, Vienna, the publishers of *Felsmechanik und Ingenieurgeologie*.

† References will be collected at the end of the third and concluding article.

cavities at either side behind the lining not been simultaneously filled to a certain degree by pieces of rock falling out of the weathering corners the arch would certainly have failed.

Though methods and means of temporary and permanent support have improved fundamentally since the earlier period, linings are still made as thick as they were about half a century ago. Loosening pressure is still considered by many to be the main active force to be reckoned with in tunnel design, although modern tunnelling methods actually make it possible to avoid loosening almost entirely.

#### Development of Construction and Lining Methods

Shortly after the turn of the century grouting was introduced as an effective means of consolidating the rock surrounding a tunnel. By filling the voids, unsymmetrical local loads on the lining are avoided, and portions of loose or soft rock are strengthened by cementation.

The next stage was the introduction of steel for supports and which, compared with timber, constituted a remarkable improvement as a temporary lining material because of its better physical properties, its higher resistance to weathering, and its reduced tendency to yield. Decreased deformability of the temporary support made it possible to replace masonry as a lining material by concrete. Dry packing then became obsolete, since the concrete filled the spaces outside the theoretical extrados.

One of the most important advantages of steel supports is that they allow tunnels to be driven full face to very large cross sections. The resulting unrestricted working area enables powerful drilling and mucking equipment to be used, increasing the rate of advance and reducing costs. Nowadays, dividing the face into headings which are subsequently widened is used only under very unfavourable geological conditions.

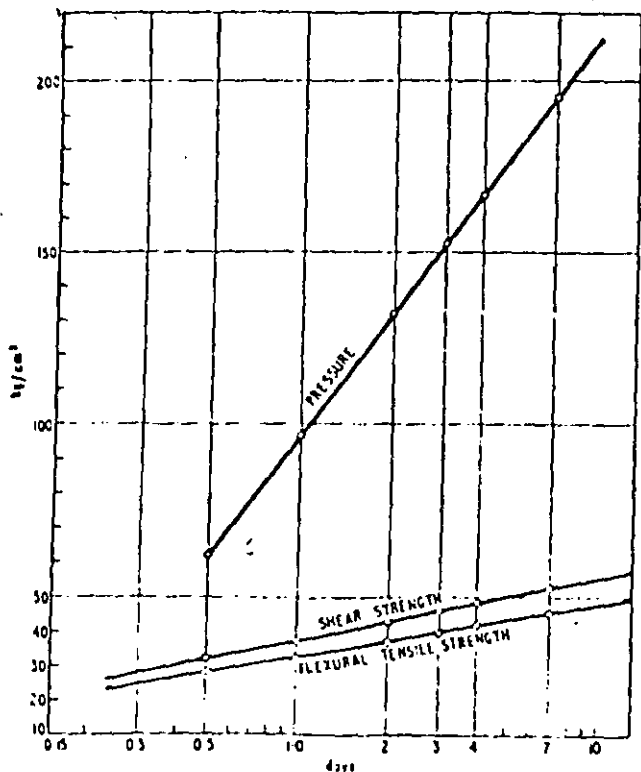


Fig. 2. Results of strength tests on shotcrete carried out in the testing laboratory of the Technische Hochschule, Graz

Remarkable progress in drilling and rock blasting, especially in Sweden, has also helped to reduce damage to the surrounding rock.

#### Modern Tunnelling Methods

Finally, during the last few decades, rockbolting and shotcrete\* were introduced in tunnelling practice. To judge from the results obtained up to now the introduction of these methods of support and surface protection can be considered as a most important event, especially in the field of soft-rock and earth tunnelling†.

The advantages of these methods can best be shown by comparing the rock mechanics of tunnels lined by the new and by older methods. Whereas all the older methods of temporary support without exception are bound to cause loosening and voids by yielding of the different parts of the supporting structure, a thin layer of shotcrete together with a suitable system of rockbolting applied to the rock face immediately after blasting entirely prevents loosening and reduces decompression to a certain degree, transforming the surrounding rock into a self-supporting arch.

A layer of shotcrete with a thickness of only 15cm applied to a tunnel of 10m diameter can safely carry a load of 45 tons/m<sup>2</sup> corresponding to a burden of 23m of rock, which is more than has ever been observed with roof falls. If a steel support structure incorporating No. 20-type wide-flanged arches at 1m centres were used under these conditions, it would fail with 65% of the load carried by the shotcrete lining, and a timber support of the conventional Austrian type would be able to carry only a very small proportion of the same load. If the temporary support deforms or fails the erroneous conclusion is usually drawn that the proposed permanent linings are not strong enough. In this way permanent linings that are already overdesigned become still heavier.

#### Shotcrete as Temporary Support

A temporary support designed to prevent loosening must attain a high carrying capacity as quickly as possible; and it must be rigid and unyielding so that it seals off the surface closely and almost hermetically. The carrying capacity of a temporary support is determined by the material as well as by its structural design. Timber, especially when humid, is by far the worst; it combines low physical properties with a great tendency for the structure to yield. Although steel has much better physical properties the efficiency of steel arching depends mainly on the quality of packing between the arches and the rock face, which is always an unsatisfactory problem. On the contrary, concrete, particularly shotcrete, meets all the requirements for an ideal temporary support.

Shotcrete's high early strength is of the greatest importance in attaining a high bearing capacity rapidly, and this is particularly true of its early flexural-tensile strength, which amounts to 50 and 30% of the compressive strength after one-half and two days (see Fig. 2). A recently introduced hardening-accelerating admixture based on silification gives

\* Pneumatically applied mortar, originally known as "torcrete" or "gunite" became very much improved shortly after World War II by a new type of machine designed to spray a mixture containing aggregates up to 25mm in size. For this new product the term "shotcrete" has become customary. † The first successful application of surface stabilisation by shotcrete for tunnels in unstable ground as an integral part of the driving process instead of using timber or steel as temporary support was carried out at the Lodano-Musagno tunnel of the Maggia hydroelectric scheme, Switzerland, 1931-1955<sup>12</sup>. A patent was granted for this method in Austria in 1956<sup>13</sup>.

still better results. Whereas only a few years ago, even if the water inflow was limited to dripping, efficient drainage had to be achieved before shotcrete could be applied, the new accelerator makes it possible to shotcrete a very wet surface even when dripping heavily. For instance, in one of the tunnels of TIWAG'S Kaunertal hydroelectric scheme, a  $\frac{3}{4}$  in jet of water was plugged off with shotcrete alone without the need to install a relief pipe.

The most conspicuous feature of shotcrete as a support against loosening and stress-rearrangement pressures lies in its interaction with the neighbouring rock. A shotcrete layer applied immediately after opening up a new rock face acts as a tough surface by which a rock of minor strength is transformed into a stable one. The shotcrete absorbs the tangential stresses which build up to a peak close to the surface



Fig. 3. Steel-supported tunnel which failed when reaching a zone of kaolinised gneiss under an overburden of 250m; water inflow 35lit/s

of a cavity after it is opened up. As a result of the close interaction between shotcrete and rock the neighbouring portions of rock remain almost in their original undisturbed state and are thus enabled to participate effectively in the arch action. The statically effective thickness of the zone of arch action is in this way increased to a multiple of that of the shotcrete. In this way, tensile stresses due to bending are diminished and compressive stresses are easily absorbed by the surrounding rock. The zone of arch action can be increased at will by rockbolting.

Disintegration always starts by the opening of a minute surface fissure; if this movement is prevented at the outset by applying a shotcrete layer the rock behind the shotcrete remains stable. This explains why cavities in bad rock lined with a skin of only a few centimetres of shotcrete remain in perfect equilibrium. Shallow tunnels in rock of medium quality, when built by customary methods, need a fairly strong temporary support and concrete lining. When the new method of surface stabilisation is adopted, only a thin layer of shotcrete, possibly locally strengthened by rockbolts, will provide both temporary support and a satisfactory permanent lining.

Experience so far has shown that shotcrete, especially when combined with rockbolting, has proved unexcelled as a temporary support for all qualities of rock with standing times down to less than one hour

and even for ground which normally could only be mastered by careful forepoling. Exceptionally, even almost cohesionless and plastic ground has been

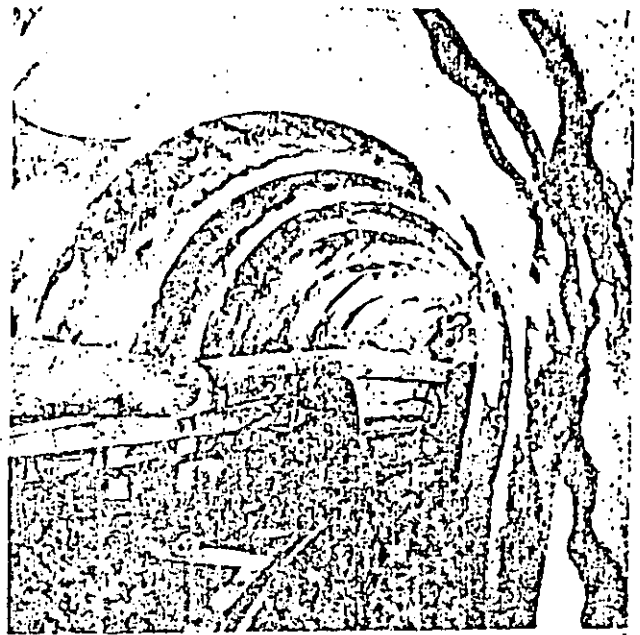


Fig. 4. The tunnel shown in Fig. 3 successfully reconstructed by redriving the deformed portion in steel and strengthening it by shotcrete

successfully handled. In very bad cases of plastic waterbearing ground where steel forepoling failed, shotcrete has been successfully employed as a stabilising reinforcement for steel support, and an example is given in Figs. 3 and 4. For reasons which we shall not discuss here, a tunnel of 8m<sup>2</sup> section for a hydroelectric scheme in the Austrian Alps had originally been driven without shotcrete, using only steel arches and steel lagging. When the tunnel, the overburden of which was 250m, reached a tectonically disturbed zone in a completely crushed kaolinised gneiss with heavy water inflow, the pressure became so heavy that the arches were deformed and their footings forced into the ground. The heavy water inflow could only be relieved slightly as the water discharge pipes became clogged shortly after placing. With the situation as shown in Fig. 3 excavation had to be stopped.

To reconstruct the deformed tunnel the contractor returned to the still undeformed portion and embedded the steel arches in a 30cm lining of shotcrete. After redriving the roof in the deformed portion new steel arches had to be placed at 60cm centres on heavy wooden sills and another arch interposed between each set. As soon as a set was placed the surface was immediately shotcreted to a complete ring (see Fig. 4). This difficult situation, which had been greatly aggravated by unsuccessful attempts at driving, was thus mastered without any further setbacks.

#### Effects of Stress-Rearrangement Pressures

When a cavity is made in undisturbed rock the original stress pattern is disturbed. In the course of time, the duration of which depends on the properties of rock, a new stress situation appears in the neighbourhood of the cavity, and equilibrium is attained either with or without the assistance of a lining

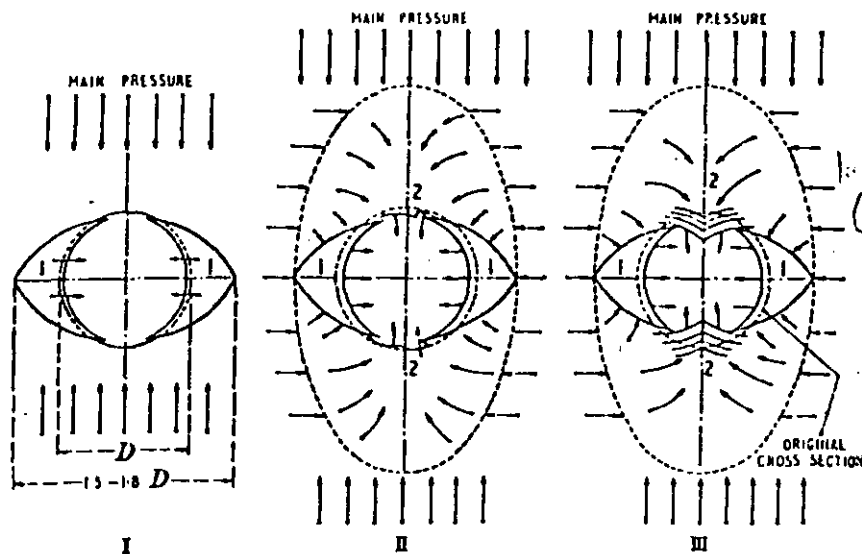


Fig. 5. Sketch of mechanical process and sequence of failure around a cavity by stress rearrangement pressure

according as to whether the shear strength of the rock is or is not exceeded. This stress rearrangement is mechanical and progressive, and generally occurs in three stages (see Fig. 5) provided the rock in the neighbourhood of the cavity has not been disturbed by earlier tunnelling. At first, wedge-shaped bodies on either side are sheared off along the Mohr surfaces and move towards the cavity, the direction of movement being vertical to the main pressure direction (I). The increased span thus produced causes the roof and floor to start converging (II). In the next stage this movement is increased; the rock buckles under continuous lateral pressure and may protrude into the cavity (III).

Pressures arising from this action are correctly termed "squeezing pressures." Stage III, though frequent in mining, is seldom encountered in civil engineering.

During the days of conventional tunnelling practice the effects of stress-rearrangement pressures were not sufficiently well known. Moreover there was no means of clearly recognising the progressive occurrence of pressure phenomena as described above, because, with the obsolete methods then used, the sections were usually not driven full face but divided into headings which were subsequently opened out. Measurement of deformations was most unusual.

#### Behaviour of Linings Subjected to Rearrangement Pressures

Conventional multiple-hinged arches of stone masonry withstood rearrangement pressures in different ways. Frequently the timber lining deformed during construction to such a degree as to allow the appropriate Trompeter zone to be formed, so that permanent equilibrium was attained without any or only significant lining damage such as crushing of mortar in

joints or spalling of the edges of the masonry. However, in many cases linings failed by shearing off after a pattern typical of this kind of strain and had to be rebuilt.

One of the most frequent reasons for these failures—besides many other shortcomings of the customary methods—was the lack of an invert. Not only were inverts provided much too seldom but they were usually placed much too late—generally not until the roof and sidewalls of the entire tunnel had been finished. Given a rock of insufficient strength even linings of mammoth dimensions were bound to deform heavily in the absence of an invert, because they form a shell without any bottom bracing.

With the forming of the Trompeter zone, which we shall call the "protective zone," surface stresses decrease markedly while the surface deforms. The radial stress which must be counteracted by the necessary bearing capacity at the periphery of the cavity, which we shall call "skin resistance," becomes smaller as the peak of tangential stresses moves away from the cavity, the radius of which simultaneously decreases.

These relations are mathematically described by the equations of Fenner-Talobre<sup>7</sup> and Kastner<sup>20</sup>.

$$* p_i = -c \cot \phi + p_o [c \cot \phi + (1 - \sin \phi)] \frac{r^{2 \sin \phi}}{R^{1 - \sin \phi}}$$

and shown schematically in Fig. 6.  $p_i$  = skin resistance,  $c$  = cohesion,  $\phi$  angle of internal friction,  $R$  = radius of the protective zone,  $r$  = radius of cavity,  $p_o = \gamma H$ .  $H$  = overburden. By omitting the cohesion the

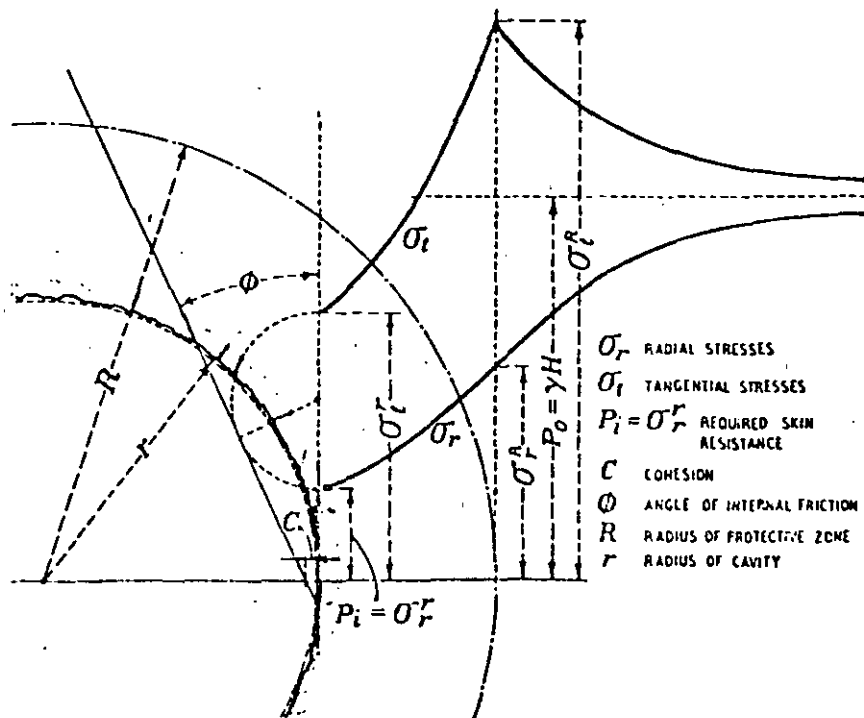


Fig. 6. Schematic representation of stresses around a circular cavity with hydrostatic pressure (after Kastner<sup>20</sup>)

Errata →  $* p_i = -c \cot \phi + [c \cot \phi + p_o (1 - \sin \phi)] \frac{r}{R} \frac{1 - \sin \phi}{2 \sin \phi}$

equation is simplified to  $p_i = p_o (1 - \sin \phi) \frac{r}{R} \frac{2 \sin \phi}{1 - \sin \phi}$

$= np_o$ . In Fig. 7 the values of  $n$  are given as a function of  $p_o$  and  $\phi$ . With  $R=r$ , i.e., without formation of a protective zone,  $p_i = p_o (1 - \sin \phi)$  and the cavity attains equilibrium without any deformation.

The practical interpretation of these theoretical findings is that with a very yielding support structure, having small skin resistance, the protective zone increases but simultaneously the skin zones loosen up, and  $\phi$  decreases. Should loosening eventually become so great that open cracks and seams are formed, the skin zone loses its bearing capacity almost entirely, which has practically the effect of a latent increase of span.

Nevertheless, these theoretical considerations do not altogether explain satisfactorily the extremely high skin resistances actually required in plastic ground when applying obsolete methods of temporary support. The reason must probably be sought in the time element. The formation of the protective zone does not arise simultaneously with the decrease of  $\phi$ , for whereas the latter follows the excavation almost immediately, decrease of stresses due to stress rearrangement (protective zone) needs more time.

A temporary means of support to meet these complicated conditions to the best advantage must first seal the newly exposed rock face as quickly as possible; secondly, it must have sufficient skin resistance to prevent serious loosening; and thirdly it must still be sufficiently yielding to allow a protective zone to be formed.

To comply with these requirements the author tried out during the war a new method called the "auxiliary arch" which consisted of applying a relatively thin concrete lining to the rock face as soon as possible, closed by an invert and intended to yield to the action of the protective zone. Deformations of the auxiliary arch were measured continuously as a function of time. As soon as the observations showed a stabilising trend of the time/deformation curve, another lining called the "inside lining" was constructed inside. The method can be considered as a real predecessor of the "New Austrian Tunnelling Method," as it comprises all its integral features with the exception of the modern means of surface stabilisation.

At that time the method had the great disadvantage that tunnels had to be driven using obsolete methods of temporary support, which necessarily caused far too much loosening before the auxiliary arch could be built. The situation has changed with the introduction of modern tunnelling methods. By applying a layer of shotcrete to the rock face immediately after driving, or if necessary even as an integral part of the driving process, with rockbolts for additional support, an auxiliary arch is formed which complies in every aspect with the requirements for a temporary lining as described above.

There are still some difficulties to be overcome in normal methods of construction, as inverts are still usually built last of all, leaving the roof and sidewalls of the lining to deform at will. In the meantime, experience has taught us that it is by far more advantageous from all points of view, and frequently even imperative, to close a lining to a complete ring at a short distance behind the face as soon as possible.

To comply with this requirement, tunnels should

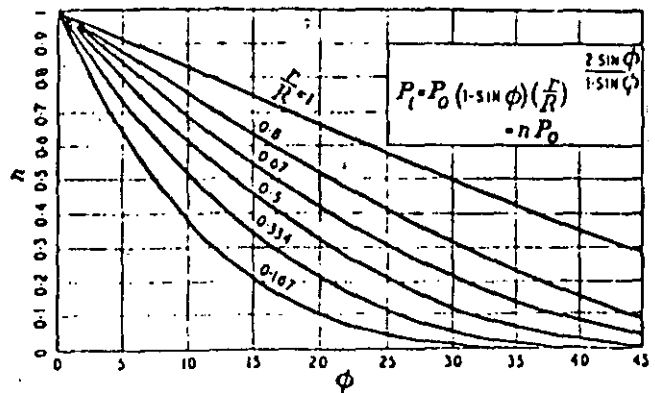


Fig. 7. Skin resistance  $p_i$  required to establish equilibrium of a cavity as a function of  $\phi$  angle of internal friction and  $p_o = \gamma H$

be driven full face whenever possible, although this cannot always be done, particularly in bad ground, where it often becomes necessary to resort to heading and benching. In the most difficult cases it may even be necessary to drive a top pilot heading before opening it out to full section.

An auxiliary arch executed in the upper heading (Belgian roof arch), though fairly effectively preventing roof loosening, represents an intermediate constructional state, which is still subject to lateral deformation. Such instability has to be removed as soon as possible by excavating the bench and closing the lining by an invert.

#### Design of Auxiliary Lining

When designing an auxiliary lining the magnitude of the active forces, the admissible stresses and the safety of the crew have to be considered. Accidents arising from geological causes, invariably brought about by rock falls or slides as a result of loosening or effects of water, can be avoided almost entirely by a conscientious geological survey. Nevertheless, as a general measure of safety, shotcrete linings should be reinforced by light steel sections and relief pipes installed to prevent a build-up of seepage pressure. Deformation resulting from stress rearrangement never occurs in the form of roof falls but as a slow displacement. Such deformations are in no way dangerous to the crew, particularly as the movements are normally very slow.

Under such favourable safety conditions permissible stresses may safely be taken close to the rupture limit, particularly if the auxiliary arch is intended only as temporary support. Should it adopt a permanent character a safety factor of 1.5 to 2 is sufficient.

Active forces can be roughly estimated from the formulae given above, but there seems no danger in adopting rather low values for these forces since a considerable factor of safety results from the interaction of the shotcrete with the neighbouring rock, particularly with higher values of  $\phi$ , a static effect which is not taken into consideration by computing the thickness of the lining.

Though seemingly rather daring at first, these design rules have been tested in practice and proved correct in constructing many kilometres of tunnels, as will be described in the succeeding articles which are devoted to actual examples and to deformation measurements in a test tunnel.



# The New Austrian Tunnelling Method

In this second article the author describes a number of actual tunnels, in various countries, in the construction of which the new Austrian method has been applied successfully

By Prof. Dr. techn. L. v. RABCEWICZ

## PART TWO

**I**NTERESTING practical examples of stress-rearrangement effects, as well as of the soundness of the design rules for auxiliary shotcrete linings enunciated in the first article, have been encountered during the construction of numerous pressure and diversion tunnels for the Tiroler Wasserkraft A.G. (TIWAG) Prutz-Iust and Kaunertal hydroelectric schemes. The author has also had the opportunity to observe the phenomena described in a series of tunnels built abroad in accordance with the new methods. In the Kaunertal scheme alone about 70km of tunnels were built with locally rockbolted auxiliary shotcrete linings as an essential part of the driving procedure (Fig. 8) Amphibolites, schistose gneisses, eye-gneisses and mica slates of all possible qualities down to the worst have been penetrated by tunnels with cross-sectional areas ranging from 10 to 20m<sup>2</sup> and overburdens up to 1,100m.

The working sequence shown in Fig. 10 was used almost without exception. The auxiliary shotcrete lining (stage III), consisting only of roof and sidewalls

of 5-15cm thickness, was as a rule left without an invert for a very long time. In some cases it was a year or more before the invert was placed. The sidewalls were thus bound to deform under pressure to various degrees according to the quality of the rock. Particularly in the sections cutting across mylonites were local deformations up to 25cm observed, causing heavy cracking. In places the sidewalls had to be repeatedly redressed and freshly shotcreted (see Fig. 9). Equilibrium was obtained eventually by the use of additional Perfo rockbolts. Characteristically the roofs showed no signs of pressure anywhere. Roof pressure by loosening the prevailing cause of trouble with the older methods did not arise at all.

In those cases of swelling pressure caused by the increase in volume of tectonically preloaded clayey or marly materials due to water absorption when the pressure is released, systematically applied deep anchoring by Perfo or SN-type rockbolts grouted in place has proved so far to be the sole means of obtaining equilibrium with a minimum of deforma-



Fig. 8. Tunnel wall receiving surface protection by a shotcrete layer immediately after mucking out



Fig. 9. Shotcrete lining failure because Perfo anchors and bottom bracing were not applied in good time

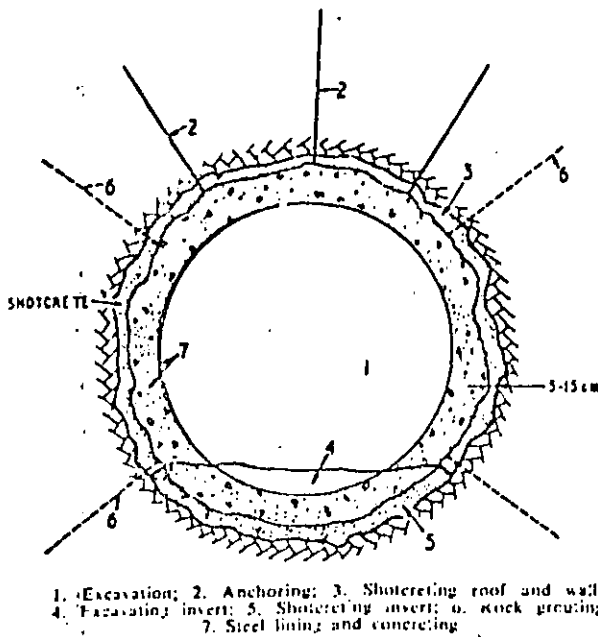


Fig. 10. Construction sequence for the Kaunertal tunnels

tion. To keep the surface from slackening a thin layer of a few centimetres of shotcrete reinforced by a net has best served the purpose. This technique developed many years ago<sup>4</sup> has since been repeatedly confirmed.

For the Kaunertal scheme an inclined pressure shaft of fairly exceptional dimensions was also driven, 1,650m in total length, the lower part, 650m long, inclining at 42° and the upper part at 20°. Its cross section was 16m<sup>2</sup> and the average overburden 150-200m. Geological conditions were rather unfavourable, for the shaft was driven through mica slates and sericite which was partly mylonitised and very wet.

The sequence of operations in the inclined pressure shaft, which differs from that described above for the tunnels, is shown in Fig. 11. The rock was mostly so bad that the top heading could not be driven full face and had to be started by a pilot heading. For safety reasons the roof had to be secured further by a steel-arch segment placed on timber props, together with some channel section as lagging. Immediate shotcreting reinforced by rockbolting had to be carried out not only in the roof but also as the sidewalls and breast of the heading. After widening the heading and extending the steel arches, shotcrete protection was continued up to the centreline, Fig. 12. Two to three weeks after finishing the top heading the bench was excavated in lengths of about 100m. The steel arches were closed and shotcreting was applied immediately after the excavation (Fig. 13).

Though the lining of the top heading remained unbraced for about a month, in spite of very unfavourable geological conditions no visible signs of deformation could be observed. Measurements

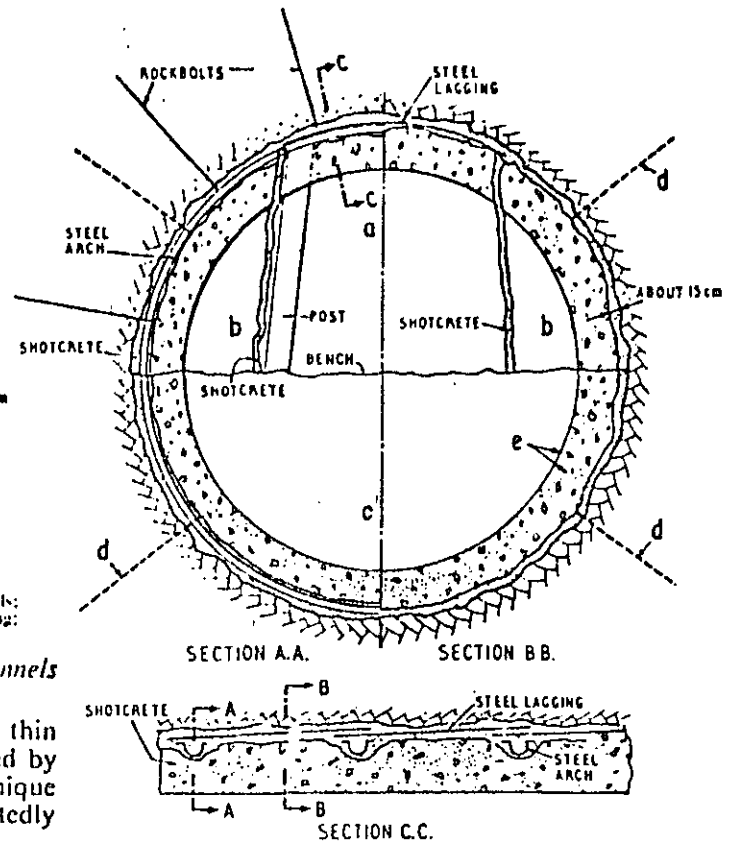


Fig. 11. Construction sequence for the Kaunertal pressure shaft

a. Top heading; b. Widening roof; c. Excavating bench and insert; d. Rock grouting; e. Steel lining and concreting.

made after completion of the auxiliary shotcreting showed that the deformations were decreasing in a range of the order of hundredths of millimetres in several months showing that the rock was practically in equilibrium.

The following conclusions can be drawn from these experiences. When suitably sealed by shotcrete closed to a complete ring, only relatively small deformations



Fig. 12. Driving the top heading in the Kaunertal pressure shaft; protection by steel arches and shotcrete

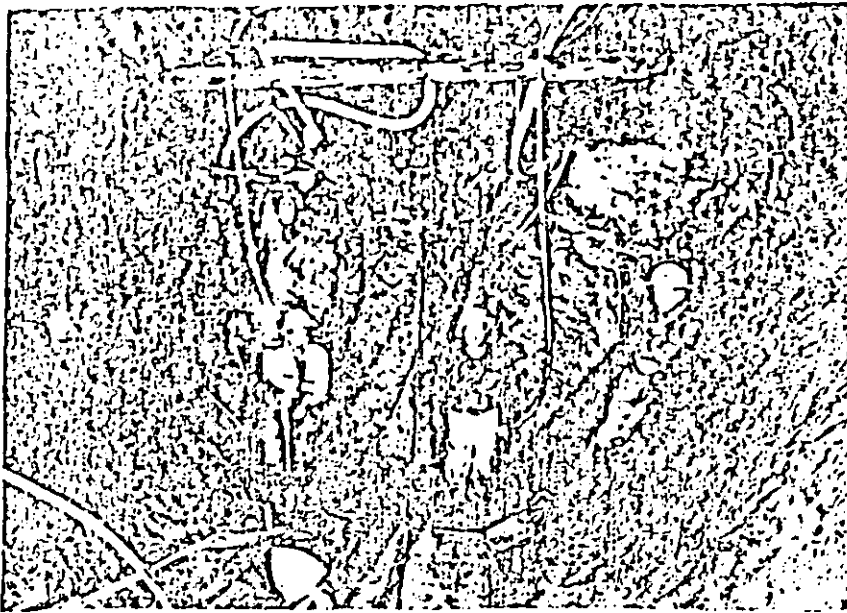


Fig. 13. Benching out the Kaumertal pressure-shaft invert; protection by steel arches and shotcrete

the section a bottom heading was driven followed by a top heading, the latter being subsequently widened to the extent shown in the picture. By the time the masonry of the arch had been closed the roof had settled 40-70-cm. Lateral deformation of the order of 2cm daily not only led to spalling (see Fig. 15) but also caused invisible damage inside the arch, probably similar to the very typical destruction shown in Fig. 16 and the 40cm-diameter timber struts at 1.50m centres were compressed and buckled. Construction was continued by excavating the remaining portion and completing the lining. Movement stopped in the course of time and equilibrium was finally attained. There can be no doubt that by far the greatest part of the distortion of the lining was due to loosening (stage II in Fig. 5) which consequently led

to progressive softening of the rock. In view of the great damage the lining suffered by violent distortion it is obvious that a much thinner lining would have sufficed provided the distortion was kept inside the elastic range.

A similar example is that of the Serra Ripoli 422m super-highway twin tunnel on the Autostrada del Sole Bologna-Firenze in Italy, which was driven through an extensive old slide consisting of chaotic

of the slightly decompressed surrounding zone are sufficient to attain equilibrium. By applying the new methods correctly, even rock of fairly bad quality can be handled successfully by heading and benching provided the auxiliary lining is closed by placing the invert as soon as possible, the actual time being determined by the quality of the rock. An auxiliary shotcrete lining having a thickness of only  $\frac{1}{4}$ m to  $\frac{1}{5}$ m of the diameter suitably reinforced by steel arches and rockbolts is sufficient to allow the lining to be closed without damage by deformation. It is important that the lining be made as thin as possible to allow a relatively large deformation without being damaged to any extent.

We shall now compare these favourable results obtained with the new means of stabilisation with

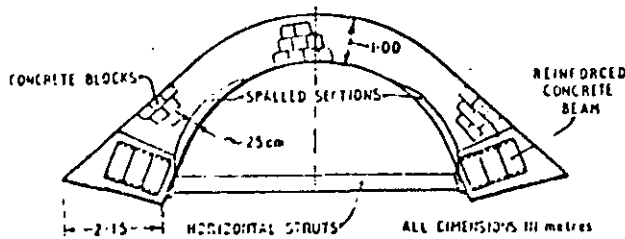


Fig. 14. Roof-arch failure in a clayey-mylonite section of the new Semmering tunnel. The masonry consists of shaped concrete bricks, and high early-strength cement was used for these and for the reinforced-concrete beams

observations made only 15 years ago during the construction of the Semmering tunnel by the Kunz method - a modification of the Belgian method. This is a typical example of the formerly common but erroneous practice of overdimensioning the permanent lining, because of violent deformations that occurred during the intermediate constructional stages as a result of static instability.

A roof arch braced by heavy timber struts in a section of clayey mylonites (Fig. 14) had been constructed in concrete and concrete bricks. To excavate

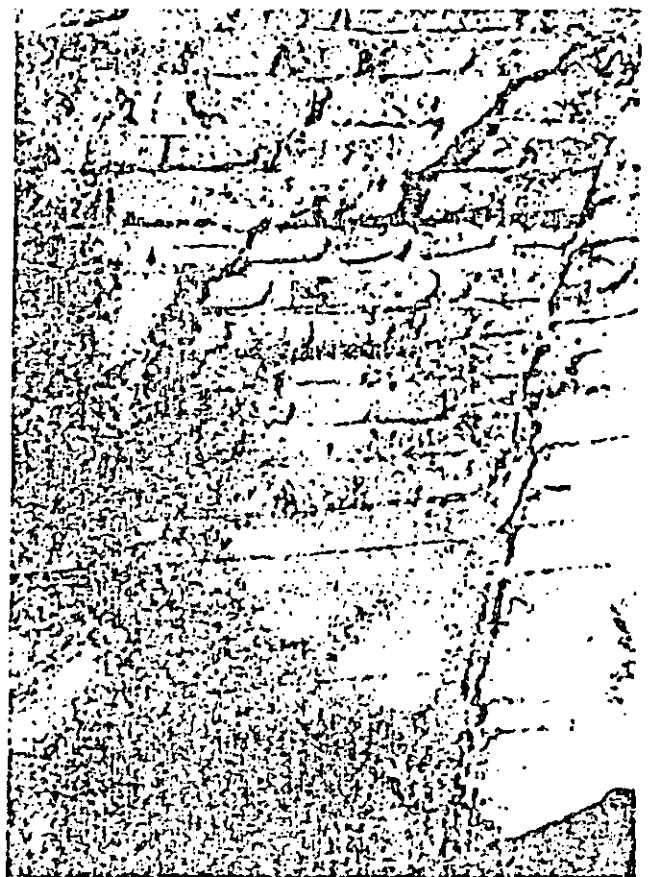


Fig. 15. Spalling of the concrete bricks in the Semmering tunnel as indicated in Fig. 14

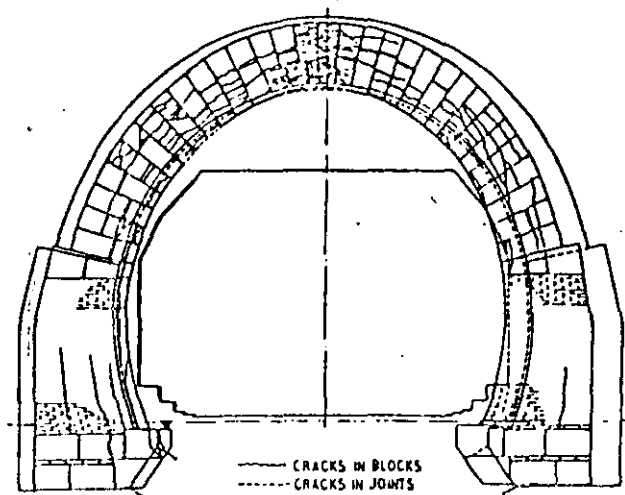


Fig. 16. Destructive deformation of a lining in Karawankeu tunnel by stress-arrangement pressures caused by the absence of an invert

masses of loam and boulders, superposed on layers of black flaky clay with interstratification of more or less compact layers of marl and sandstone. Two sections, each about 90m long, of particularly bad ground consisting of plastic clay, were encountered near the portals. The geological conditions were apparently even somewhat worse than at Semmering.

The twin tunnel was started by driving one tube with a cross section of 110m<sup>2</sup> by the German method of leaving a core in the middle against which the walls were strutted. When opening out the top heading, loosening pressure became locally so great that the timbering settled from 1m to 1.80m (Fig. 17) which necessitated extremely difficult and expensive redressing. Although the tunnel was finally completed by this method, the experience was so discouraging that the management decided to try surface stabilisation by shotcrete for the second tube. Instead of continuously struggling with masses of timber leaving no room for tunnelling equipment, it then became possible to drive the top heading full face, using customary machines for mucking and transport (Fig. 18). The average rate of advance was trebled, no settlement occurred, and an average financial saving of 20% compared with the first tunnel was achieved. It must be mentioned that by taking full advantage of the possibilities of the new method the thickness of both the auxiliary and inside linings could still have been considerably reduced. The Serra Ripoli tunnel was built over the period 1957-1960.

There is no doubt that the difficult section of the new Semmering tunnel described above, as well as any other similar case, could have been executed successfully by applying only a thin auxiliary shotcrete lining reinforced by light steel arches and rockbolts. In very bad ground, however, it would be advisable to protect the roof, walls, face, and exceptionally even the floor, by shotcrete, at intermediate constructional stages.

Another super-highway twin tunnel constructed in 1957-1958 using anchoring and shotcrete was built in Venezuela in thin laminated limestone interleaved with clayey graphitic layers, the maximum overburden being 100m. The originally proposed reinforced-concrete lining, from 60cm thick at the top to 1m at the sidewalls, was changed on the author's advice to a layer of shotcrete with an average thickness of only 20cm for both the auxiliary and permanent linings together, and reinforced by systematically applied prestressed Perfo rockbolts. The final shotcrete closely followed the irregularities of the rock (Fig. 20). Having regard to the overbreak

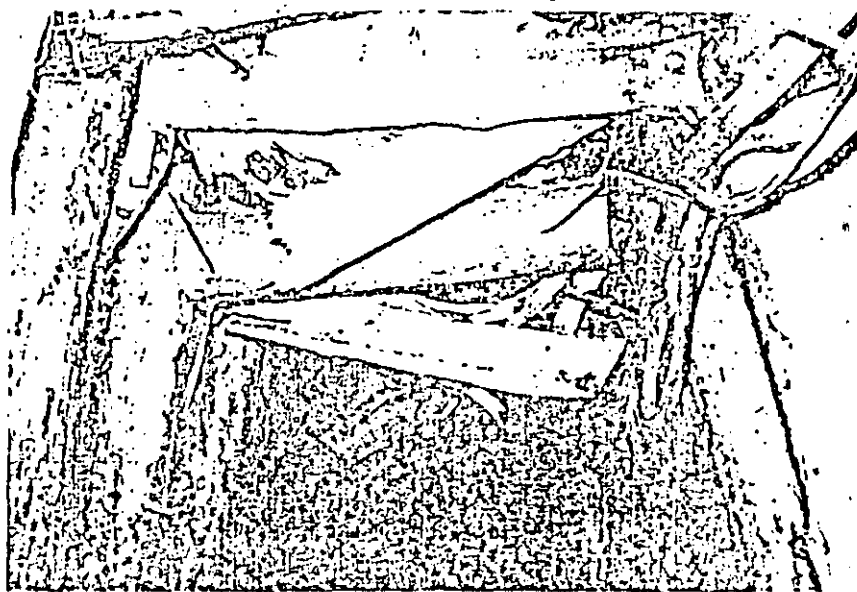


Fig. 17. Failing timber frames in the upper heading in the first tube of the Serra Ripoli super-highway twin tunnel, Italy

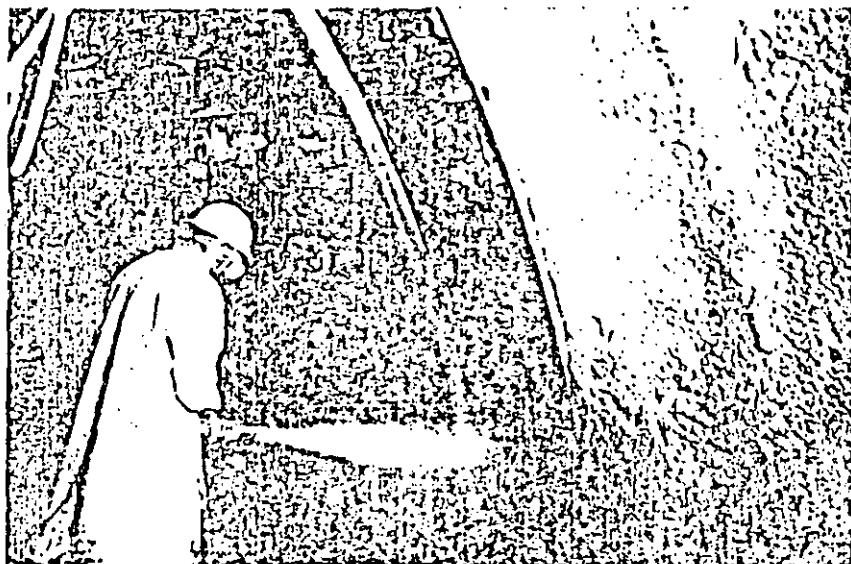


Fig. 18. Full-face driving of the roof section in the parallel tube of the Serra Ripoli tunnel, using shotcrete reinforced by sectional steel. Same geological conditions as in Fig. 17

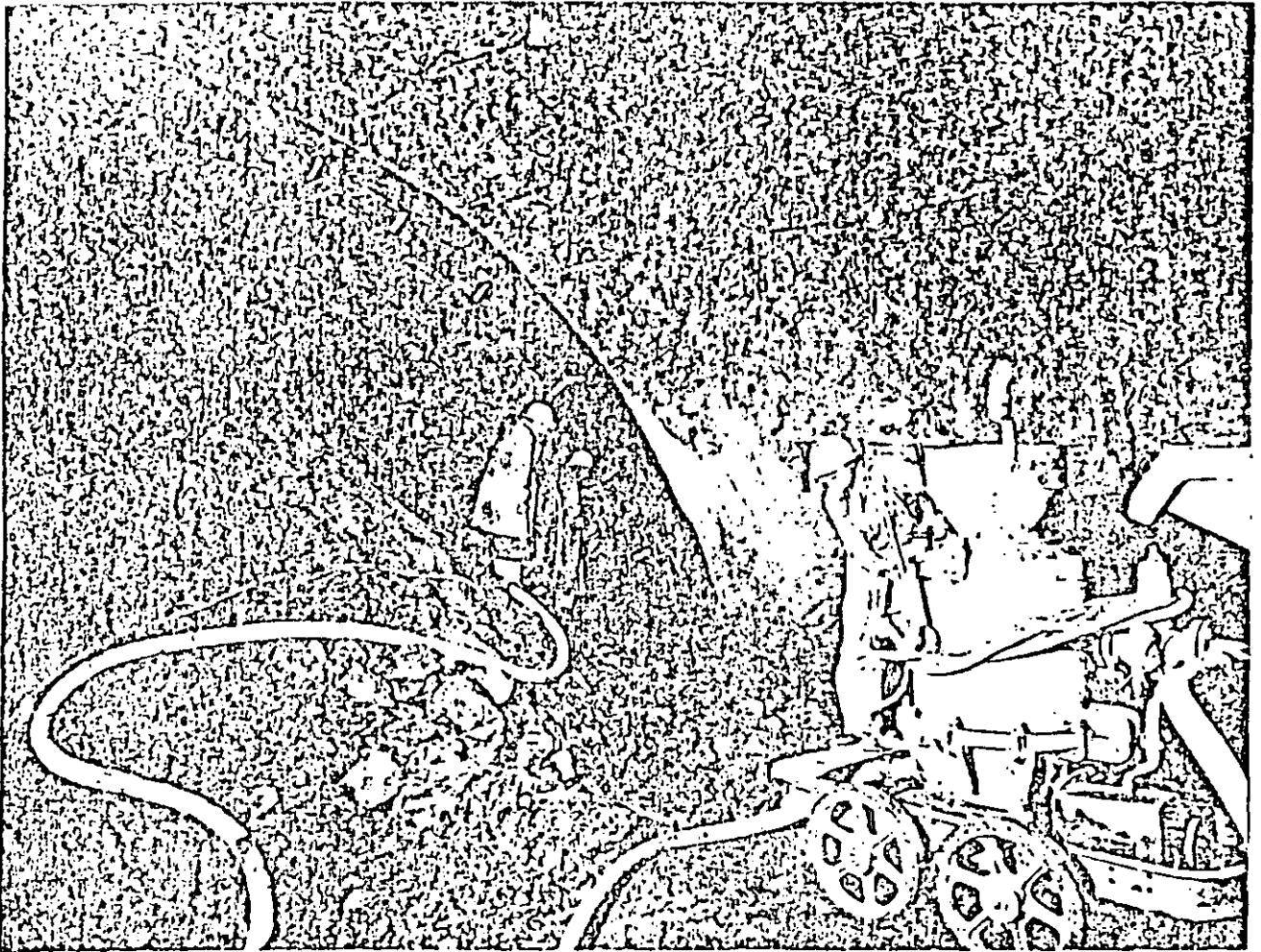


Fig. 19. Super-highway tunnel in Italy south of Firenze. Forming the auxiliary lining of the upper part of the tunnel with shotcrete reinforced by steel netting and steel arches. Contractors: Impresit G. Lodigiani, Milan

together with the low quality of rock, the two tunnels were placed much too close to each other, leaving in places only 6m of poor rock between them. In

spite of this error in design which caused very unfavourable pressure conditions for the intermediate pillar the structure remained in perfect equilibrium. Changing over to modern methods resulted in an economy of about 25%.

In the case of the Venezuelan tunnel just described, Perfo rockbolts were used as the main means of stabilising the shotcrete, which was otherwise left unreinforced. A super-highway tunnel built in 1962 south of Firenze used much the same process of construction as the Serra Ripoli tunnel, and a view inside this tunnel is given in Fig. 19.

In Sweden an equipment has been constructed called "The Robot" which enables the roof of large tunnels to be sprayed with shotcrete immediately after blasting. The equipment incorporates a beam cantilevering over the muck pile, and the operator thus works safely under the portion of roof already protected by shotcrete.

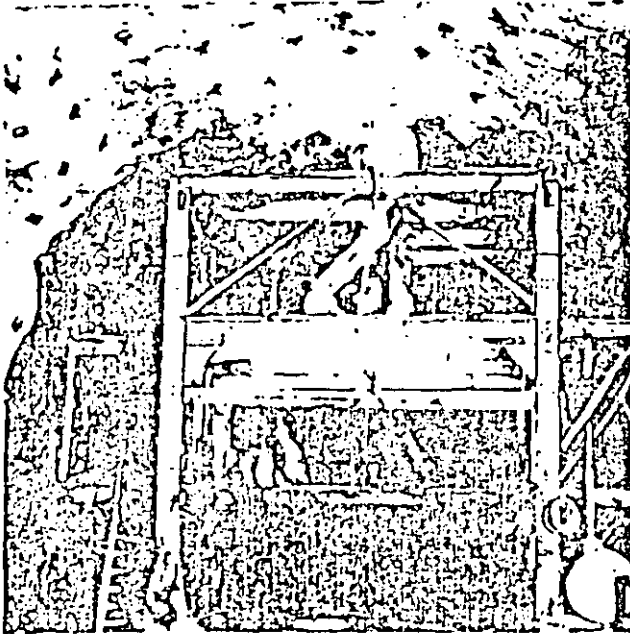


Fig. 20. Full-face driving of a super-highway twin tunnel in Venezuela using shotcrete and prestressed Perfo rockbolts

# The New Austrian Tunnelling Method

In this final article the author stresses the value of rock deformation measurements in determining the thickness of the lining. A test tunnel has been constructed in Austria to investigate this subject. A failed tunnel construction which was rescued by applying the new Austrian technique is described

By Prof. Dr. techn. L. v. RABCEWICZ

## PART THREE

THE fundamental importance of deformation measurements with respect to time was emphasised by the author 20 years ago. A knowledge of the displacement of linings and of the surrounding rock as a function of time, not only makes it possible to determine whether equilibrium will be reached or not, but can also be regarded as a valuable means of ascertaining the magnitude and distribution of the forces around a cavity. Further information, such as checking the formation of the protection zone by geophysical measurements as was done in the case of the Isère tunnel, is naturally extremely valuable.

Based on all this practical experience and theoretical findings a new tunnelling method—particularly adapted for unstable ground—has been developed

which uses surface stabilisation by a thin auxiliary shotcrete lining, suitably reinforced by rockbolting and closed as soon as possible by an invert. For the first time in tunnelling history systematic measurement of deformations and stresses enables the required lining thickness to be evaluated and controlled scientifically. The method has been called "The New Austrian Tunnelling Method," since Austrian engineers have taken a decisive part in its development.

A conspicuous example of an almost complete application of this method is given by a 400m long highway tunnel built recently in the southern part of Austria. With the exception of a small portion in limestone the tunnel is situated in slightly waterbearing graphitic argillaceous schists, partly very soft and

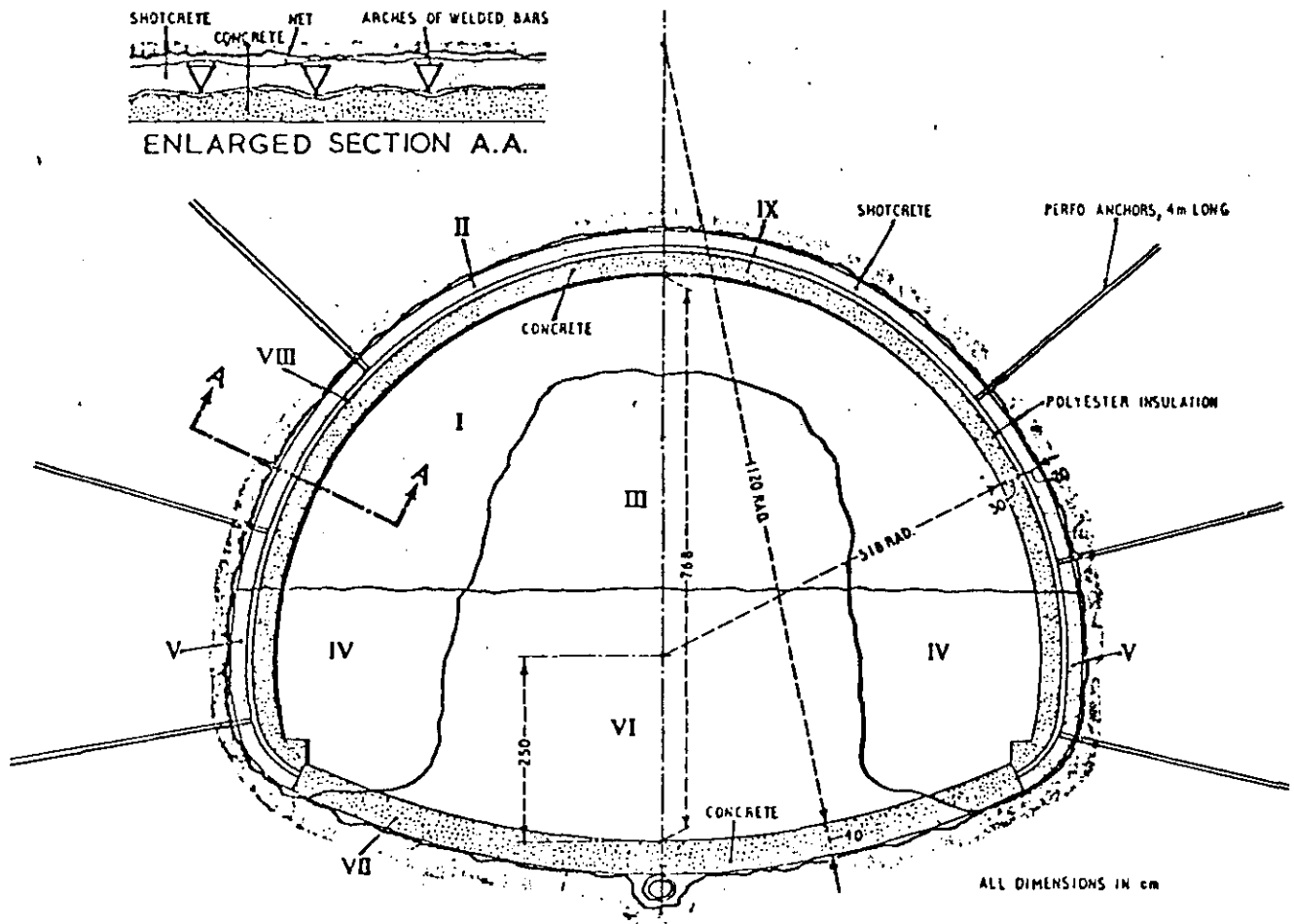


Fig. 21. Construction sequence for road tunnel in southern Austria

in various degrees of disintegration. The maximum overburden was 60m, the strike, though very irregular, was generally about 60° to the axis, with a steep dip of about 60-70°.

The tunnel was started according to the Belgian tunnelling method in very bad ground by driving the upper half of the section at a speed of about 25m a month. As temporary support a very strong auxiliary shotcrete lining 45 to 60cm thick reinforced by arches of welded steel bars and netting had been applied. When the top heading had reached 67m the bench was started by the customary procedure of making a centre trench, but as soon as a small portion of the sidewalls was excavated and shotcrete lined, heavy settlement occurred and the first 27m of the tunnel caved in. Though the top heading had been carried out successfully by immediately lining it by shotcrete, the construction was bound to fail, as not only the method of driving but also the design - which did not even provide an invert - fundamentally violated the principles explained in these articles.

The author, commissioned by the owner to advise on the repair of the damage and on further construction, introduced as soon as possible a system of measuring deformations. After finishing the reconstruction of the collapsed portion a method of driving was carried out as shown in Figs. 21-25. The top heading was excavated in rounds of 0.6-1.20m in the form of a half-ring, leaving the central portion to brace the walls against bulging. Immediately after finishing the excavation I a net was attached to the circumference, which was then protected by a 3.5cm layer of shotcrete (Fig. 22), and after placing the welded arch (Fig. 23), the auxiliary lining was increased to final thickness II. Then the core III was removed, and



Fig. 22. Excavating top heading and forming auxiliary lining (Stages I and II)

the walls were subsequently excavated II' and provided with a shotcrete lining also reinforced by a net and arches I'. Finally the bench II' was excavated and the invert concreted III. While stages I to I' were advanced daily, II' and III were carried out once a week. The platform of the bench was left as short as possible - just enough to give the mucking machine space to turn. In this way the concreted invert followed the face at a distance of 15-25m. The time interval between excavating the face and closing the lining by concreting the invert consequently never exceeded 15 to 25 days.

At a distance of 100-150m behind the face the lining was insulated by spraying glassfibre-reinforced polyester IV (Fig. 25), followed at a short distance by concreting of the inside lining V.

The time interval between operations V and VI, of 3 to 5 months was required to observe the movements of the auxiliary arch and establish deformation-time graphs for it. Measurement was carried out weekly by checking the vertical and horizontal diameters every 15m of tunnel length. In addition, measuring anchors, 6m long, were inserted in both sides, consisting of a steel bar inside a pipe, fastened at the outer end in the rock and provided with a measuring device at the inner end to establish the extension of the rock by measuring the movement of the lining relative to the point of fastening. Further absolute movements were measured geodetically of the top of the auxiliary arch. Diameters and anchor deformations were measured with an accuracy of 0.1mm, and the geodetic measurements of the roof with an accuracy of 0.5mm.

Although the methods of measurement used were rather simple and could be improved upon in many ways they entirely served the intended purpose, which was to prove that in a rock as bad as that in question a shotcrete lining of only 20cm thickness and of a compressive strength of 250kg/cm<sup>2</sup> in 28 days, reinforced as described, sufficed to reach equilibrium in a short time after the arch had been closed by the invert. Fig. 26 gives typical examples of the numerous graphs established for each measuring section, which show throughout almost the same course. Though

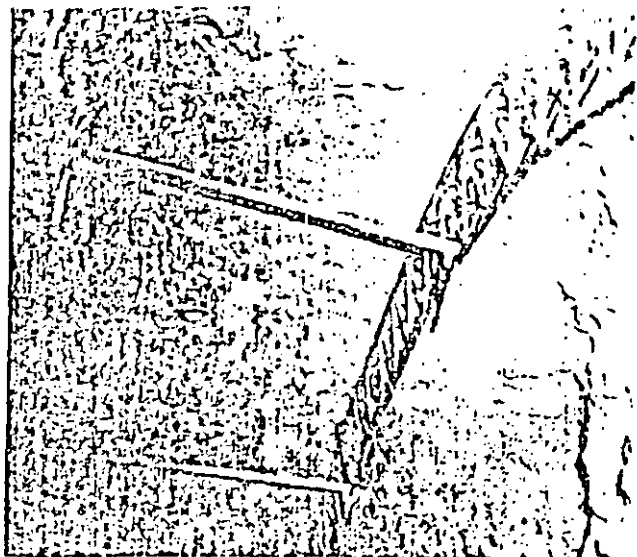


Fig. 23. Placing the welded arch

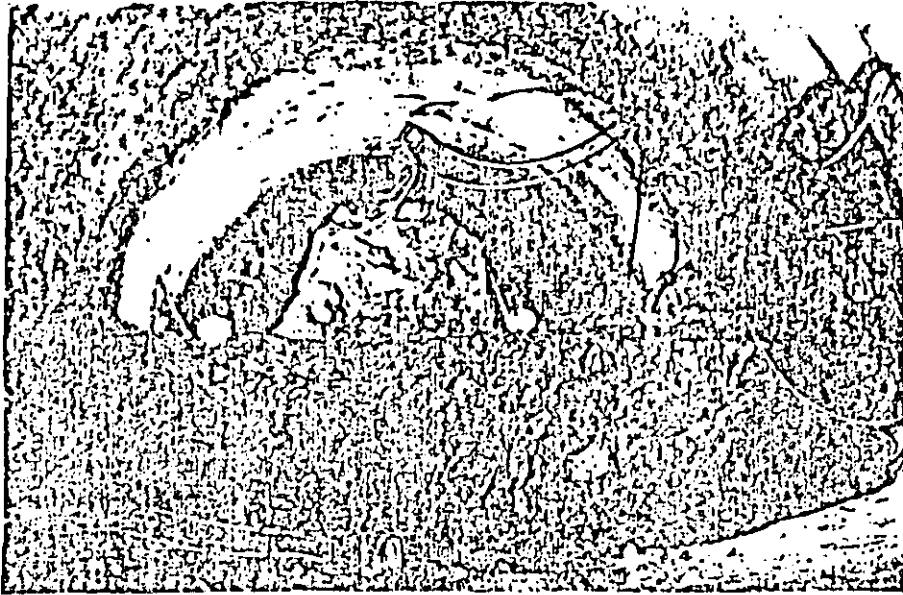


Fig. 24. Benching (Stage VI) and concreting the invert (Stage VII)

frequently the first and—as can be guessed from several observations—considerably greater part of the deformations could not be registered, since the measuring points had to be placed some distance behind the face, the deformation/time graphs clearly show without exception the rapidly tranquillising trend of movements and the obvious reason—the closing of the auxiliary lining.

It was never intended with this simple and cheap way of measurement to gather sufficient data to calculate the actual magnitudes of the active forces. Nevertheless, it has been definitely ascertained that with the present geological conditions a 20cm shotcrete lining provides a certain, though unknown, margin of safety, and that by applying an additional inside lining 30cm thick this safety factor is multiplied correspondingly. By additionally measuring the stresses by decompression slits the actual strains of the auxiliary lining could be established and its required thickness computed.

#### Test Tunnels

Unfortunately measurements of all kinds necessarily cause some trouble to the crews, since they reduce progress somewhat by repeated small losses of time. Experience has shown that carrying out of systematic observations is rather difficult, particularly if great accuracy is called for. Regular observations requiring high exactitude can consequently better be accomplished in proper test tunnels, the purpose of which is only scientific research.

A practical example of the foregoing is afforded by a 1km test tunnel which was driven in southern Austria to provide the basic design data for a twin road tunnel. The most favourable tunnel line was chosen so as to cross deposits of slightly to fairly well cemented sand of medium grain size for three-quarters of its length, while the rest was in fairly stable clay.

The maximum overburden was 80m. The research work in the test tunnel was carried out by Dr. Ing. L. Müller and Dpl. Ing. F. Pacher, the Salzburg consulting engineers, in collaboration with Interfek who provided the instruments.

The actual test section consisted of a circular gallery, 2.5m in diameter, driven in the sand in regular advances of 1m. Immediately after mucking, the freshly exposed rock face was covered with a 2cm layer of shotcrete; then measuring pits were placed at the circumference and the radial and polygonal distances measured by the instrument shown in Fig. 27 at regular intervals. In order to obtain absolute test results, the axis was

centred optically by a precision theodolite before readings were taken, the theodolite being rigidly mounted in a chamber at the entrance to the tunnel. Readings were continued for a year (Figs. 28 and 29.)

Simultaneously the physical properties of the shotcrete with respect to time were tested by measuring the elastic moduli and the compressive strength. The properties of the ground were established by load tests. After deformations had obviously stopped, the ultimate stresses in the shotcrete were measured by three-point strain gauges, of the Electricité de France type, thus providing a check on the final readings. Ultimate stresses in the shotcrete measured in this way were as much as 26kg/cm<sup>2</sup>, and the average proportion of load carried by the shotcrete lining ranged from 0.17 to 0.33//. Load diagrams in which deformations are related to load and time for the shotcrete as well as for the rock (see Fig. 28) were prepared for each test point. The load curve of the shotcrete can be plotted by determining time element, deformation and *E* value for each point, and then computing the load. Since the process of evaluation is still in the development stage it will not be described in greater detail.

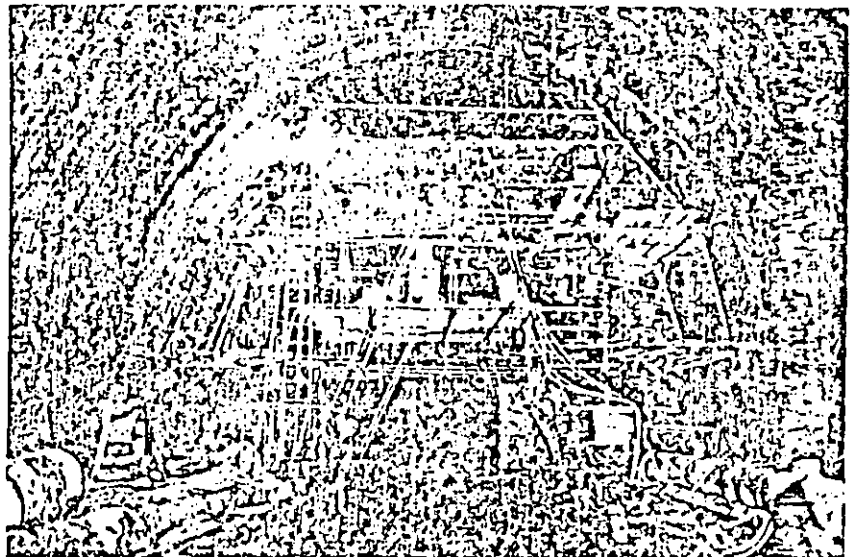
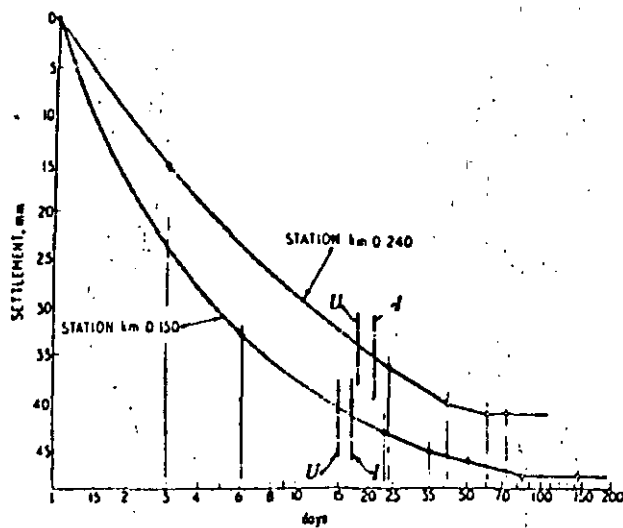
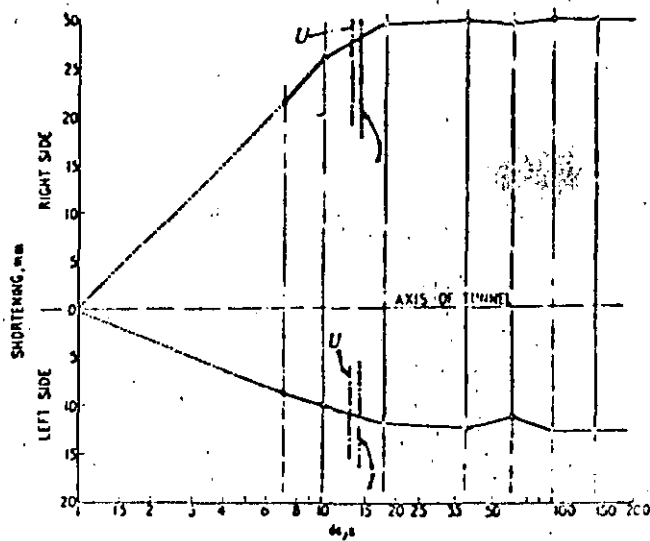


Fig. 25. Placing the polyester insulation, seen completed in the foreground

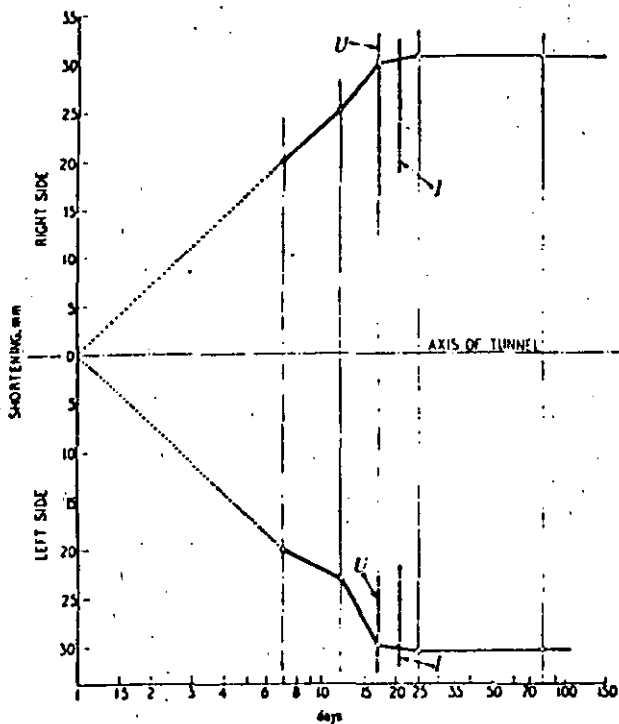




VERTICAL DEFORMATIONS



HORIZONTAL DEFORMATIONS. STATION km 0-150



HORIZONTAL DEFORMATIONS. STATION km 0:240

- ..... ASSUMED SETTLEMENT
- ROOF SETTLEMENT MEASURED GEODETICALLY
- DIAMETER MEASURED BY DIAL GAUGE
- U ——— UNDERPINNING OF ROOF ARCH (STAGE V)
- I ——— CONCRETING OF ROOF ARCH (STAGE VII)

Fig. 26. Curves of horizontal and vertical deformations of the auxiliary lining in respect of time

The Fenner-Talobre formulae were used to compute the forces acting on the full-size tunnel, which was to have a cross-sectional area about 15 times greater than the test tunnel and four times as much overburden. Including a satisfactory factor of safety, the required lining thickness was found to be between one third and one quarter of that assumed for the preliminary design on the basis of experience with customary methods in earlier tunnels in the same region in similar ground. The saving thus made amounts to about 30% of the total cost of the preliminary design.

#### New Waterproofing Techniques

The auxiliary arch can also be used economically to carry a high-quality waterproof layer. After the

rock face has been carefully drained by one of the conventional techniques, such as the Oberhasli method, the auxiliary lining can be sprayed with a film of polyester, which would then be protected by another layer of shotcrete or concrete to prevent the formation of blisters by the water pressure. The fact that insulating agents can now be applied to irregular surfaces by spraying, instead of laboriously bonding bituminous sheets to concrete surfaces which have to be perfectly smooth, is a further important advantage of the new method.

#### Inner Lining

A secondary lining inside the auxiliary lining may be required for structural or for waterproofing reasons. The first case arises if the auxiliary lining has either been overstressed or if the stresses in it are near the elastic limit, so that it does not possess the desired degree of safety. In the second case the inner lining protects the waterproof layer against water pressure and frost.

If the auxiliary lining has actually been overstressed, the inner lining should be designed according to the following principles. Whereas loosening pressure can be left out of consideration as the active force—provided modern methods have been used—rearrangement pressures and possible squeezing pressures have to be considered, and their magnitude and distribution judged by the results of deformation and stress measurement on the auxiliary lining or additionally by results obtained on a test tunnel. Since rearrangement pressures will mostly act laterally, a lining to suit this type of load should properly be elliptical with the longer axis horizontal, and the lining should be thinner at the sides and heavier at the roof; but if it is desired to suit all possible main pres-

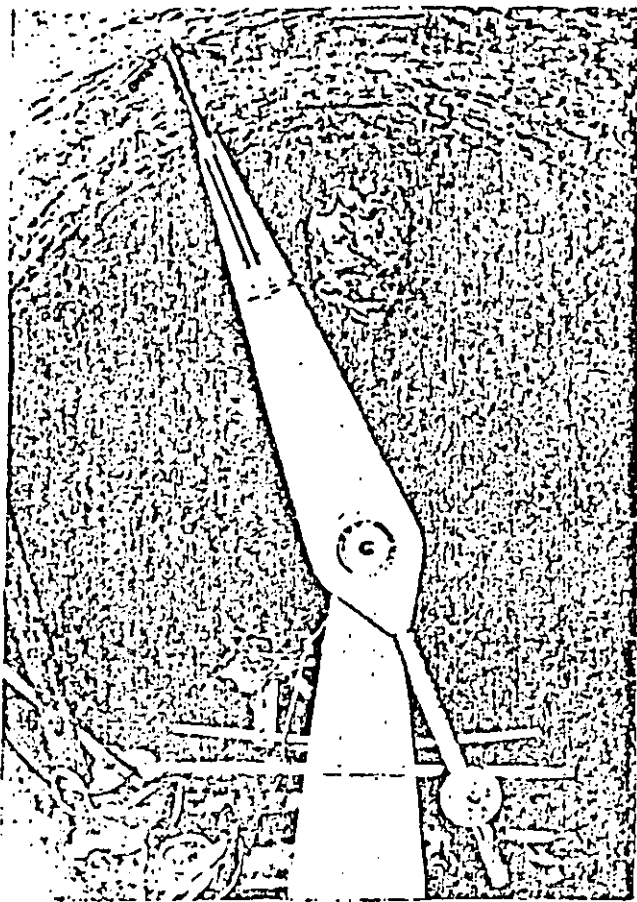


Fig. 27. Deformation measuring apparatus in the Weizawinkel test gallery

sure directions a circular section with a uniform liner thickness should be adopted.

By far the most frequent mode of failure of such a lining in close contact with the rock face and closed by an invert is shearing along planes which continue in the Mohr planes of the surrounding rock. Model

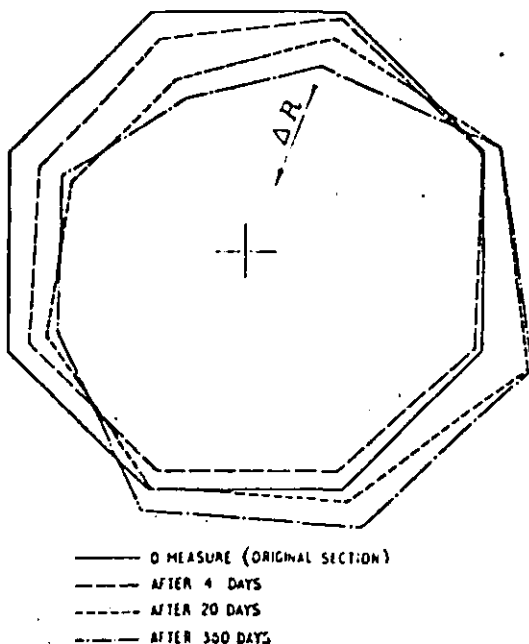


Fig. 28. Deformation of radii with time in test gallery

tests have shown that by eliminating the friction between lining and environment the pressure line remains close to the axis everywhere and results in almost equal compressive edge stresses. This effect is largely obtained by spraying a bituminous layer on the inside of the auxiliary arch or by keeping the  $E$  value of the waterproofing medium relatively low, and the thickness of the separating layers has to be adjusted according to the irregularities of the surface, taking into account the probable amount of tangential movements. In this way the inner lining can be made considerably thinner and thus more economical; simultaneously its deformability increases. If the auxiliary lining has become stable without exceeding its limit of resistance, the inside lining only serves to increase the factor of safety.

If the auxiliary lining fails, its protective zone becomes larger and the skin resistance required to ensure stability decreases. The advantage thus gained is largely counterbalanced by uncertainty in estimating the magnitude of the external forces. It is consequently always preferable from all points of view to build the auxiliary arch so that stability is attained within the limit of resistance.

#### Stability of Linings with Discontinuous Surfaces

One of the conspicuous features of the new method is that the excessive use of shotcrete in overbreak areas is avoided by the fact that the lining approximately follows the irregularities of the rock face. It is often maintained that a lining with a discontinuous surface is a structural impossibility. The error of this opinion has not only been demonstrated in these articles but has clearly been proved in practice (Fig. 30). In sound rock a cavity with discontinuous surface also remains in equilibrium without any reinforcement. Apart from the fact that protruding portions of rock are automatically of better quality, an unstable rock becomes a stable one as a result of the interaction between shotcrete and rock, which transforms the uniaxial state of stress into a triaxial one.

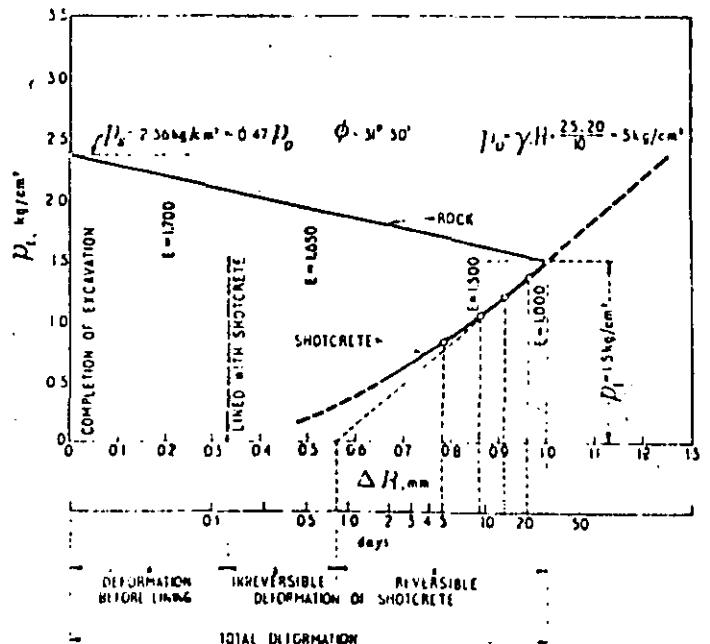


Fig. 29. Determination of skin resistance  $p_s$  after Müller & Racher

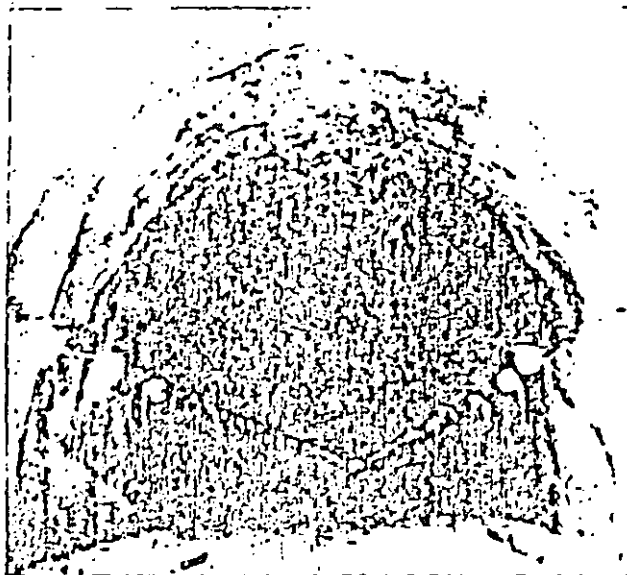


Fig. 30. Permanent shotcrete lining of a super-highway tunnel in Venezuela, following the irregularities of the rock

#### Final Remarks

Shotcrete is unfortunately an expensive construction material, and when used in the wrong way it may not always show a saving compared with concrete placed in shuttering, particularly when unit shuttering costs can be lowered by re-use. As has been explained, shotcrete is not intended to be used like a conventional concrete lining on a fairly good rock far behind the face, where the rock is already decompressed and sufficiently safeguarded by rockbolting. On the contrary the method aims to reduce anchoring to a minimum by preventing initial superficial loosening as a result of the more effective interaction between shotcrete and rock; the worse the rock, the greater the savings that can be made by the new method.

If shotcreting is not introduced as an integral part of the driving process its advantages will not be fully utilised. Further, the new technique is rather difficult in application particularly in soft and possibly waterbearing ground. Applying the method correctly needs as much practical knowledge as, say, forepoling in difficult ground, and it requires in addition much closer collaboration with the engineering geologist. Evaluating forces by measurements with respect to time is the very basis of the method and the sole means of economical design in accordance with the actual properties of rock. The design and dimensioning of auxiliary and inner linings and the associated steel reinforcements should therefore be carried out exclusively by engineers who have not only practical tunnelling experience but also an extensive knowledge of rock mechanics. The handling of the purely practical part of the work can be entrusted to experienced foremen especially trained in the method. Disregard of these rules has already

caused several serious accidents and failures as well as financial loss by overdimensioning. Dimensioning linings on the basis of experience with tunnels built by obsolete methods is entirely out of fashion and is thus no longer acceptable, new experience having superseded what was done in the past. It is a grave blunder to apply obsolete and unscientific methods to expensive modern shotcrete linings.

This causes irresponsible waste and is liable to discriminate against the new method.

#### REFERENCES

1. RABCEWICZ, L.V. "Gebirgsdruck und Tunnelbau," Springer-Verlag, Vienna, 1944.
2. RABCEWICZ, L.V. Patentschrift, Austrian Patent No. 165.573.
3. "Der neue Semmeringtunnel," *Eisenbahn*, Vienna, 1952.
4. RABCEWICZ, L.V. "Bolted Support for Tunnels," *WATER POWER*, April, May 1954; *Mine and Quarry Engineering*, February, March 1955.
5. RABCEWICZ, L.V. "Influence of Constructional Methods on Tunnel Design," *WATER POWER*, December 1955.
6. SONDERIGGER, A. "Spritzbeton im Stollenbau," *Schweiz. Bauztg.*, Jg. 74, 1956, p. 211.
7. TALOIRE, J. "La Mécanique des Roches," Dunod, Paris, 1957.
8. RABCEWICZ, L.V. "Die Ankerung im Tunnelbau ersetzt bisher gebräuchliche Einbaumethoden," *Schweiz. Bauztg.*, Jg. 75, March 1957.
9. RÖTTER, E. "Anwendung von Spritzbeton," *Schriftenreihe des österr. Wasserwirtschaftsverbandes*, 1958, H.35.
10. LAUFER, H. "Gebirgsklassifizierung im Stollenbau," *Geologie und Bauwesen*, Jg. 24, 1958, H.3.
11. Personal communications of TIWAG to the author.
12. RABCEWICZ, L.V. "Spritzbeton und Ankerung als Hilfsmittel zum Vortrieb und als endgültiger Tunnelausbau," *Berg- und Hüttenmännische Monatshefte*, 1961, Jg. 106, H.5-6, Vienna.
13. RÖTTER, E. "Spritzbeton und seine praktische Anwendung im Untertagebau," *Berg- und Hüttenmännische Monatshefte*, Jg. 106, 1961, H.5-6, Vienna.
14. SEEBER, G. "Auswertung von statischen Felsdehnungsmessungen," *Geologie und Bauwesen*, Jg. 24, 1958, H.3, Vienna.
15. ZANON, A. "Ausbruch von Autotunneln in ganz schwierigen Bergarten," *Geologie und Bauwesen*, 1961, Vienna.
16. RABCEWICZ, L.V. "Aus der Praxis des Tunnelbaues. Einige Erfahrungen über echten Gebirgsdruck," *Geologie und Bauwesen*, Jg. 27, H.3-4, 1962, Vienna.
17. Personal communications of "Sika" Plastiment G.m.b.H., Bludenz (Austria), to the author.
18. LAUFER, H., and SEEBER, G. "Die Bemessung von Druckschachtauskleidungen für Innendruck auf Grund von Felsdehnungsmessungen," *Österr. Ingenieurzeitschrift*, H.2, 1962.
19. TERZAGHI, K.V. "Geological Introduction to Tunnelling with Steel Supports," by Proctor and White, The Commercial Shearing and Stamping Company, Ohio, 1946.
20. KASTNER, H. "Statik des Tunnel- und Stollenbaues," Springer, Berlin/Göttingen, 1962.
21. SONDRIGGER, A. "Spritzbeton im Strassenbau," *Strasse und Verkehr*, No. 10, 1956.
22. RABCEWICZ, L.V. "Bemessung von Hohlraumbauten, die 'Neue österreichische Bauweise' und ihr Einfluss auf Gebirgsdruckwirkungen und Dimensionierung," *Felsmechanik und Ingenieurgeologie*, Vol. 3-4, Springer, Vienna, 1963.
23. CLAES, ALBERTS. "Spritzbetong," *Byggnästuren*, No. 1, 1963, Stockholm.
24. MÜLLER, L. "Der Felsbau," Ferdinand Enke Verlag, Stuttgart.



**DIVISION DE EDUCACION CONTINUA  
FACULTAD DE INGENIERIA U.N.A.M.**

MECANICA DE ROCAS APLICADA A LA MINERIA Y A LA CONSTRUCCION

DETERMINACION EN CAMPO DE LAS PROPIEDADES MECANICAS  
DEL MACIZO ROCOSO

ING. ARMANDO RABAGO MARTIN

MAYO, 1985.

# DETERMINACION EN CAMPO DE LAS PROPIEDADES MECANICAS DEL MACIZO ROCOSO

J. Armando Rábago Martín

## OBJETIVO

El objetivo de este tema del CURSO MECANICA DE ROCAS es el de describir los ensayos que se realizan "in situ" para evaluar la Resistencia, Deformabilidad, Permeabilidad y Estado de Esfuerzos Tectónicos del macizo rocoso, estableciendo las ventajas y desventajas de cada método y las diferencias que existen entre los resultados obtenidos con estas pruebas y los obtenidos en laboratorio.

## INTRODUCCION

La determinación de las propiedades mecánicas del macizo rocoso permite al ingeniero predecir el comportamiento futuro de una masa rocosa sometida a fuerzas impuestas por las obras ingenieriles. Los valores de resistencia, deformabilidad, permeabilidad y magnitud de esfuerzos tectónicos obtenidos mediante pruebas de laboratorio y de campo, sirven para alimentar los modelos teóricos o numéricos utilizados para predecir el comportamiento. Es evidente que la validez de los resultados obtenidos con los modelos teóricos o numéricos está en función de la buena determinación que se haga de estas propiedades.

Las pruebas realizadas en campo tienen la particularidad de abarcar un mayor volumen de roca que el ensayado en laboratorio, lo que las hace más representativas ya que involucran a un mayor número de discontinuidades y se hace más evidente la heterogeneidad y anisotropía del medio. Por otro lado la roca ensayada en campo sufre menos alteraciones que las originadas por el muestreo para recuperación de muestras que serán ensayadas en laboratorio.

Una de las más importantes restricciones que imponen los ensayos en campo es su elevado costo respecto al costo de los ensayos de laboratorio. Sin embargo en obras grandes donde el costo de una falla puede ser muy alto (tanto en pérdidas económicas como humanas) justifica plenamente el estudio de las propiedades mecánicas del macizo rocoso en campo.

El conocimiento de las limitaciones que el método de prueba impone y de la representatividad del sitio elegido para hacer la prueba en relación con el resto de la masa rocosa, así como el conocimiento de las hipótesis de la herramienta teórica y numérica de que disponemos (la cual considera, en la mayoría de los casos, al medio rocoso como un medio homogéneo, isótropo y de comportamiento elástico) y la experiencia y buen juicio del ingeniero geotecnista deberán conjuntarse para interpretar adecuadamente los resultados obtenidos de las pruebas y poderlos aplicar racionalmente al diseño ingenieril.

## DETERMINACION DE LA RESISTENCIA AL ESFUERZO CORTANTE

Los problemas de inestabilidad de taludes rocosos, fallas de cimentaciones y, en algunos casos, de movimientos de roca hacia una excavación subterránea, se deben en gran medida a una insuficiente resistencia al esfuerzo cortante de las discontinuidades existentes en la masa rocosa o de la matriz rocosa (roca intacta). Al hacer una excavación o cimentar una estructura se imponen nuevas sollicitaciones a la masa rocosa y se desarrollan fuerzas normales y tangenciales en zonas potenciales de falla del macizo rocoso. Una vez identificados los posibles mecanismos de falla y la(s) discontinuidad(es) crítica(s) por donde puede ocurrir el deslizamiento o falla, debe evaluarse si las fuerzas tangenciales (motoras) inducidas son mayores que las fuerzas resistentes de la roca (fuerzas normales, cohesivas y friccionantes). Si esto ocurre, entonces la masa rocosa comenzará a deslizarse. Es preciso entonces determinar adecuadamente la magnitud de las fuerzas resistentes, es decir, la resistencia al corte de las discontinuidades geológicas y de la roca intacta para diferentes magnitudes de esfuerzo normal actuante en el plano o zona potencial de falla, de tal forma que éstas cubran el intervalo de presiones que se espera actúe sobre la discontinuidad. Conocida la resistencia al corte será posible entonces evaluar si hay condiciones para que la roca falle y deslice y se podrán tomar las acciones correctivas o preventivas que sean pertinentes en cada caso particular.

Identificada la zona o plano potencial de falla debe hacerse un detallado levantamiento de las características de la discontinuidad crítica ya que el espaciamiento entre fracturas, grado de alteración, tipo y espesor de relleno, rugosidad en diferentes sentidos, la presencia de agua, el tamaño y ángulo de las irregularidades, las zonas de contacto roca-roca, tienen una notable influencia en la resistencia al corte.

Los ensayos de resistencia al corte varían de acuerdo a la forma de aplicar la carga lateral al plano de corte y pueden ser de cuatro tipos:

- a. Ensaye aplicando la carga lateral paralela al plano potencial de falla
- b. Ensaye aplicando la carga lateral inclinada respecto al plano de falla
- c. Ensaye aplicando carga radial con cuchillas
- d. Ensaye de torsión

Las figuras 1 a 4 muestran un esquema de cada uno de los ensayos mencionados. Estos ensayos pueden ejecutarse en el interior de un soca-

vón de exploración, o bien en superficie. Cuando se hace en superficie (fig 1) se requiere utilizar marcos de vigas de acero, plataformas de carga y barras ancladas en roca para poder proporcionar apoyo a los gatos hidráulicos que aplican las cargas a las probetas y les permiten transferir sus reacciones. En las pruebas realizadas en socavones la transferencia de las reacciones se hace hacia las paredes y clave (fig 2).

El ensaye de corte consiste en labrar un bloque superior de roca de aproximadamente 0.7 x 0.7 m de sección transversal y 0.35 m de altura (fig 2) sobre la superficie potencial de falla y colocar sobre él los gatos hidráulicos que proporcionaron la carga normal y tangencial. Si el plano potencial de falla es una discontinuidad con relleno arcilloso, se inserta en el relleno una aguja porosa que a su vez se conecta con un transductor de presión para medir las presiones de poro debidas al agua contenida en el relleno. El bloque superior se instrumenta para medir los desplazamientos longitudinales, transversales y la dilatación o movimientos ascendentes. En una primera etapa del ensaye se aplica carga normal al bloque superior para restituir la carga que tenía originalmente antes de que se decomprimiera por el labrado. Posteriormente se mantiene una carga constante, normal al plano potencial de falla y simultáneamente se aplica la carga tangencial en incrementos hasta llegar a la falla. La velocidad de aplicación de la carga tangencial debe ser tal que las presiones de poro generadas durante el proceso de falla sean reducidas. Cuando la carga tangencial se aplica inclinada (aprox. 30° con la horizontal) el centro de carga del gato debe pasar por el centro del área del plano potencial de falla para evitar inducir momentos; por otro lado, conforme la carga tangencial aumenta se adiciona una carga normal de tal manera que resulta necesario ir disminuyendo durante la ejecución de la prueba la carga aplicada con el gato superior, de tal forma de poder mantener la carga normal constante en el plano de falla.

Durante la prueba se construyen gráficas esfuerzo cortante ( $\tau$ )-desplazamiento longitudinal ( $\delta$ ) como la que se observa en la figura 5. De las curvas obtenidas se obtienen un valor máximo de resistencia al corte ( $\tau_{m\acute{a}x}$ ) el cual ocurre para desplazamientos pequeños y un valor residual de la resistencia al corte ( $\delta_{res}$ ) que se presenta después de que ocurre un desplazamiento grande del bloque superior sobre el inferior. En términos generales el valor máximo del esfuerzo cortante normalmente se debe a la ruptura por corte del material rocoso de las caras de la discontinuidad o del relleno y el valor residual a la resistencia por fricción que se desarrolla en conjunto entre el material afallado y las caras de la discontinuidad.

A partir de los valores de  $\tau_{m\acute{a}x}$  y  $\delta_{res}$  obtenidos para cada esfuerzo normal aplicado, se construyen gráficas esfuerzo normal ( $\sigma$ ) - esfuerzo cortante ( $\tau$ ) (fig 6) de las que se obtienen las curvas que representan la ley de resistencia al esfuerzo cortante que en caso de ser rectas, estará dada por la ecuación general:

$$\tau = c + \sigma \tan \phi \quad \text{donde } c = \text{cohesión del material fallado}$$

$$\phi = \text{ángulo de fricción interna del material afollado}$$

que en términos de esfuerzos efectivos será:

$$\tau = c + \bar{\sigma} \tan \phi = c + (\sigma - \mu) \tan \phi$$

donde  $\mu$  = presión de poro actuante en el plano de falla

En la tabla 1 se muestran valores de  $c$  y  $\phi$  obtenidos para distintas rocas. Generalmente se recomienda ejecutar tres pruebas de corte como mínimo para poder trazar la ley de resistencia al corte.

El ángulo  $i$  de las irregularidades existentes en el plano potencial de falla el cual se mide respecto a la superficie media de la discontinuidad (fig 7) también influencia notablemente la resistencia al corte como puede observarse en la figura 7. Para cargas normales bajas (línea OA) la ley de resistencia queda expresada por:

$$\tau = \sigma \tan (\phi_r + i)$$

donde  $\phi_r$  ángulo de fricción residual

En diseño tenemos que predecir la situación más desfavorable posible y la situación más probable. La más desfavorable estará basada en la resistencia residual ( $\tau = \sigma \tan \phi_r$ ). La condición más probable se debería diseñar con la resistencia máxima pero existen una serie de factores que pueden afectarla (desplazamientos previos, falla progresiva, grado de alteración, procedimiento inadecuado de prueba, espaciamiento de discontinuidad, relleno, ángulo  $i$ , etc.). Finalmente, la elección de los parámetros de resistencia para uso en diseño es sobre todo una cuestión de juicio ingenieril basado en el conocimiento de los mecanismos de falla que puedan ocurrir y en la experiencia y observación de casos reales y experimentales.



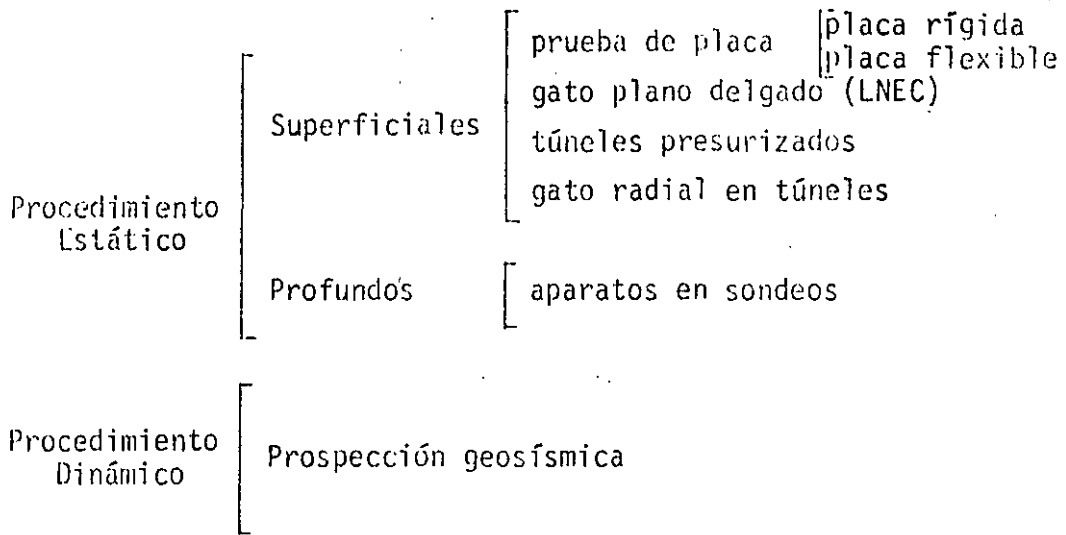
## DETERMINACION DE LA DEFORMABILIDAD DEL MACIZO ROCOSO

La aplicación de cargas impuestas por las obras ingenieriles a la masa rocosa provocan deformaciones en la misma. La magnitud de las deformaciones será función del nivel de esfuerzos aplicado a la masa rocosa, tiempo en que se apliquen estos esfuerzos, espaciamientos y frecuencia de las discontinuidades, características de las discontinuidades y de la roca intacta, grado de alteración de la roca, anisotropía y heterogeneidad de la masa rocosa, tamaño del área cargada en relación al espaciamiento de las discontinuidades y magnitud y dirección de los esfuerzos residuales en la roca. La deformabilidad de la masa rocosa se expresa mediante el Módulo de Deformabilidad que es la relación del esfuerzo aplicado y su correspondiente deformación unitaria durante la aplicación de una carga al macizo rocoso incluyendo su comportamiento elástico e inelástico.

La construcción de excavaciones y cimentaciones en roca requieren definir la deformabilidad del macizo con el propósito de conocer su comportamiento ante cargas y descargas y poder diseñar adecuadamente los revestimientos, estructuras y método de construcción a utilizar.

Las pruebas de campo, por involucrar a un mayor volumen de roca y en consecuencia a un mayor número de discontinuidades, permiten obtener valores más realistas de la deformabilidad de la masa rocosa que los obtenidos mediante ensayos en laboratorio. Los equipos utilizados para las pruebas de campo tienden a afectar volúmenes de roca cada vez mayores y a incrementar la magnitud de los esfuerzos aplicados. El principio de los ensayos es simple y consiste en aplicar una carga al terreno (reproduciendo las condiciones a las que estará sometido) y se miden las deformaciones inducidas mediante aparatos colocados a diferentes profundidades y distancias dentro del volumen de roca afectado por la carga impuesta. Durante el ensayo se registran esfuerzos aplicados ( $\sigma$ ) y deformaciones ( $\delta$ ) las cuales se dibujan en una gráfica esfuerzo-deformación como la que se muestra en la figura 8. El módulo de deformabilidad elegido puede ser secante, tangente o inicial dependiendo del conocimiento del nivel de esfuerzos al que estará sometida la masa rocosa. En algunos casos (p.ej. en excavaciones) es necesario conocer el módulo de deformabilidad a la descarga y en otros (p.ej. cimentación de maquinaria, ciclos de llenado y vaciado de agua en embalses) se requiere conocer el comportamiento de la roca sometida a ciclos de carga y descarga con diferentes tiempos de permanencia para observar la tendencia de la deformabilidad después de cierto número de ciclos y su comportamiento viscoso.

Las pruebas de deformabilidad pueden ser estáticas o dinámicas según el tiempo que dura la aplicación de carga y/o descarga y pueden hacerse en superficie o a profundidad. El siguiente esquema muestra los ensayos que se han realizado para evaluar la deformabilidad de la masa rocosa "in situ".



En general la magnitud del Módulo de Deformabilidad Dinámico es mayor que la obtenida con métodos estáticos de campo. Esto se debe fundamentalmente a que las deformaciones inducidas por la onda que viaja a través del medio son muy pequeñas y se encuentran generalmente dentro del intervalo de comportamiento elástico del medio. En cambio las cargas estáticas\* inducen deformaciones altas que rebasan el intervalo de comportamiento elástico del medio deformable.

En comparación con los módulos dinámicos y estáticos obtenidos en ensayos de laboratorio se puede enunciar la siguiente tendencia.

$$E_{\text{din lab}} > E_{\text{est lab}} > E_{\text{din campo}} > E_{\text{est campo}}$$

### Pruebas Dinámicas

Estas pruebas fueron mencionadas en el tema II y se realizan emitiendo una fuente de ondas al terreno generada por un impulso, estas ondas viajan a través del medio y regresan (por refracción de las mismas) a superficie donde son captadas por geófonos. De esta forma es factible conocer el tiempo y la velocidad de llegada de la onda al geófono el cual capta ondas longitudinales y/o transversales. Los volúmenes de roca involucrados por este tipo de prueba son grandes y dado que la onda se transmite en rocas de litología y grados de alteración diferentes, así como por diversas discontinuidades, el valor del módulo es un valor promedio muy general y se obtiene mediante las expresiones:

---

\*su tiempo de permanencia



**DIVISION DE EDUCACION CONTINUA  
FACULTAD DE INGENIERIA . U.N.A.M.**

MECANICA DE ROCAS APLICADA A LA MINERIA Y A LA CONSTRUCCION

PROBLEMAS EN EL DISEÑO Y CONSTRUCCION DE TUNELES

Ing. Raúl Cuéllar Borja

MAYO, 1985

# DISEÑO Y CONSTRUCCIÓN DE TUNELES

REQUISITO: CARACTERIZACIÓN DEL MACIZO ROCOSO.

ESTUDIOS: GEOLOGICOS Y DE MECANICA DE ROCAS

## GEOLOGIA:

FOTOGEOLOGIA: Imágenes de radar y fotos de vuelos altos y de satélites.

GEOLOGIA REGIONAL. Tectónica. (Plano Caracas).

GEOMORFOLOGIA. Geología estructural. Idem.

GEOLOGIA DETALLADA. Levantamientos superficiales: socavones y barrenos.

GEOHIDROLOGIA. Drenaje superficial (arroyos, manantiales) disolución, flujo subterráneo.

GEOFISICA. Refracción sísmica, resistividad, rayos gamma, flujo térmico, etc.

## MECANICA DE ROCAS:

PROPIEDADES GEOMECANICAS (geométrico-mecánicas)

Propiedades físicas: (Laboratorio)

Compresión, tensión, corte, módulo de ruptura, compresión triaxial, módulo elástico, expansibilidad.

Propiedades índice: (Laboratorio y campo)

Peso volumétrico, densidad, porosidad, relación de vacío, permeabilidad, alterabilidad, mineralogía.

Módulo de deformabilidad, resistencia al corte.

Recuperación, R.Q.D., familias de fracturas, permeabilidad Lugeon

ESTADO DE ESFUERZOS INTERNO (Campo)

Roseta, gato plano, de formación de barrenos

PROBLEMAS EN EL DISEÑO Y CONSTRUCCION  
DE TUNELES.

RAUL CUELLAR BORJA  
JULIO 1982.

LOS PROBLEMAS QUE ENFRENTAN GENERALMENTE -  
SON DEL SIGUIENTE CARACTER:

GEOLOGICOS

TOPOGRAFICOS (DEFINICION DEL TRAZO)

DE CONSTRUCCION

Procedimiento de Excavación

Soporte de la Roca

Tratamiento de la Roca (Gunita. Inyecciones)

Bombeo

DE DISEÑO

Definición de la Carga sobre el Revestimiento

Definición sobre la necesidad del Revestimiento

## TRAZO TOPOGRAFICO

El trazo topográfico siempre deberá basarse en las condiciones geológicas del terreno.

Conforme se conozca mejor la geología sobre el trazo preliminar, este se modificará tratando de evitar atravesar zonas de mala calidad.

### EJEMPLO:

#### TUNEL SAN LUIS RÍO COLORADO - TIJUANA.

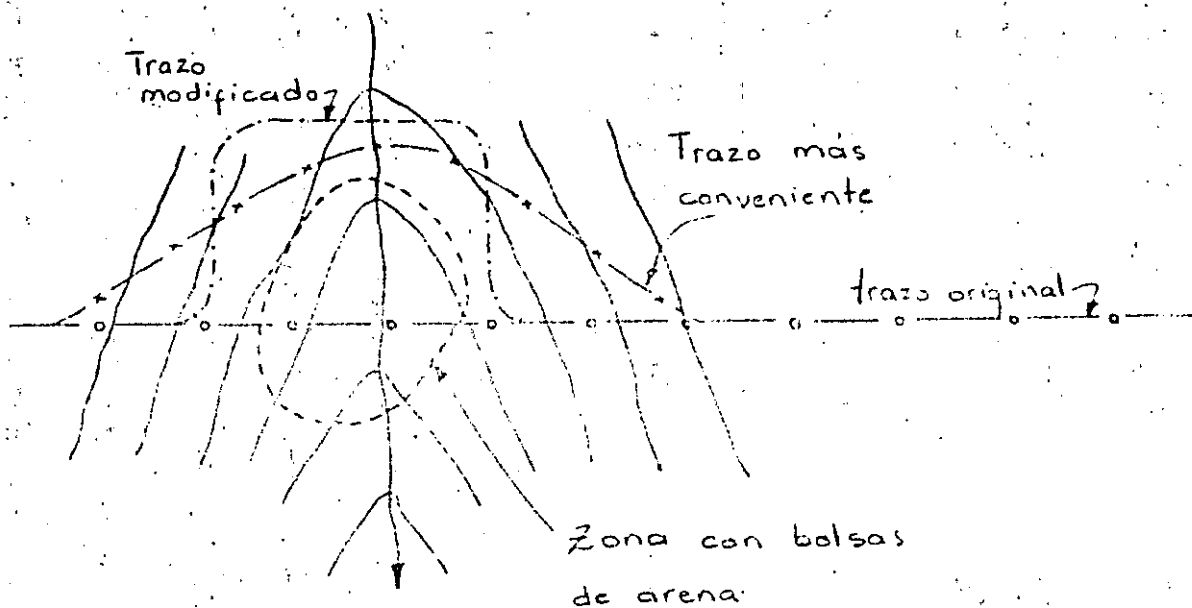
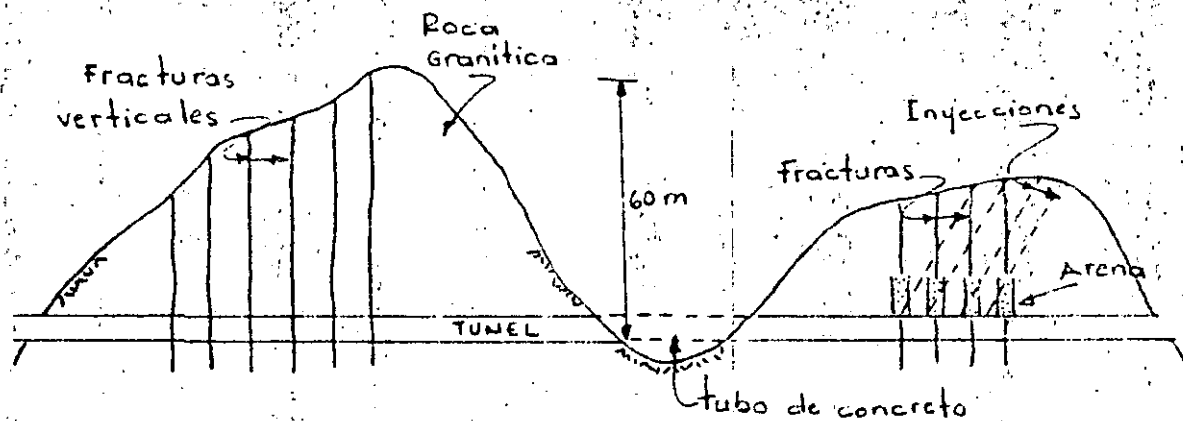
Estos túneles forman parte del <sup>Acueducto</sup> ~~Acuerdo~~ San Luis Río Colorado - Tijuana, B.C. de 125 Km. de longitud construido por la SARH para abastecer de agua potable a Tijuana, durante 1977 a 1980.

Existen dos tramos en túnel, de 3 Km. de longitud cada uno con sección portal de 3.5 m. excavados en granitos de grano fino en la Sierra de La Rumorosa, con cobertura máxima de 60 m.

Los dos túneles se excavaron desde los portales avanzando hacia el centro, en donde por la existencia de arroyos la cobertura es algo menor de 60 m. y el agua se infiltraba por las fracturas de la roca granítica ocasionando su desintegración en arena suelta. Faltando 100 a 150 m. en ambos túneles hubo necesidad de suspender los trabajos al ser expulsada la arena suelta hacia dentro del túnel.

En uno de ellos se cambió el trazo girando el frente 90° para alcanzar mayor cobertura de roca y por tanto roca sana.

En el otro se logró estabilizar mediante inyecciones de cemento.



NOTA: Lo mejor es tener cambios de dirección menos bruscos.

Para el trazo y control se utilizaban  
 y aparatos más avanzados, se utilizaban  
 Se usa la fotogrametría como técnica para  
 para la ubicación de los puntos base de  
 Se usan aparatos como  
 Telurómetros, distanciómetros, nivel  
 precisión, cámaras fotográficas  
 de precisión, cámaras fotográficas



## PROBLEMAS GEOLOGICOS

### TIPO DE EXPLORACION

METODOS INDIRECTOS: FOTOGEOLOGIA  
IMAGEN DE RADAR  
GEOSISMICOS  
RESISTIVIDAD  
RAYOS GAMMA  
FLUJO TERMICO

METODOS DIRECTOS: GEOLOGIA SUPERFICIAL  
PERFORACIONES

### FOTOGEOLOGIA

Sirve fundamentalmente para identificar rasgos estructurales como fallas regionales y locales, arroyos, depósitos de talud, fallas de talud y tipos de rocas, dirección de echados.

En el Anexo 1 se presenta un ejemplo del levantamiento - fotogéologico del Proyecto Coco de Pedro Brand, sobre el Río Haina, Rep. Dominicana.

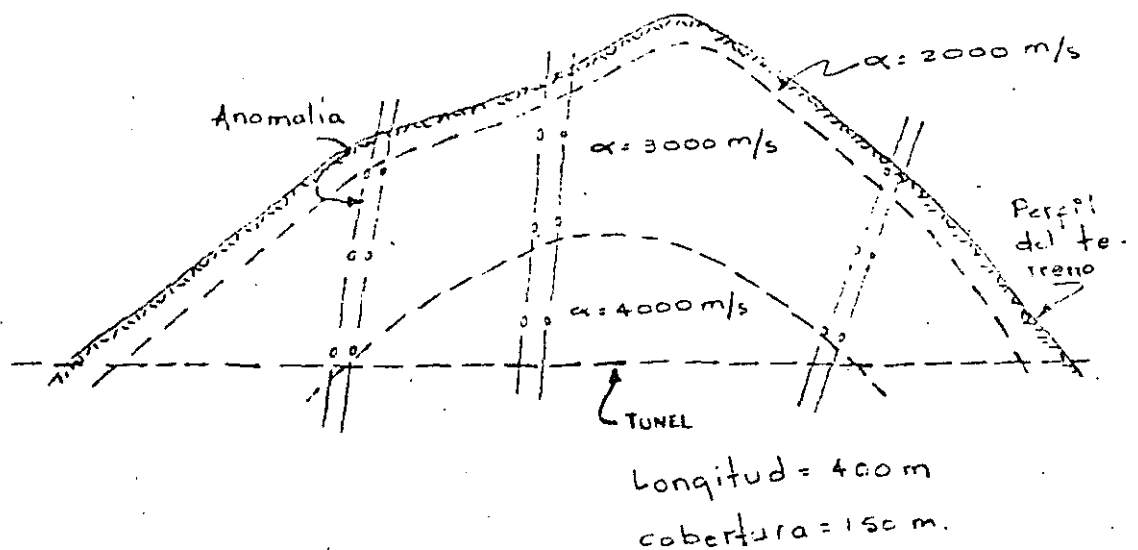
## IMAGEN DE RADAR

Se usa fundamentalmente para identificación de rasgos estructurales como son las fallas regionales ya que en la fotografía se borra la vegetación. Es muy útil para estudios de riesgo sísmico. Ejemplo: Managua, Nicaragua, para estudios del sismo de diciembre 1974 (25 000 muertos).

## GEOSISMICOS

El método de refracción sísmica y microsísmica viene a ser una de las herramientas más importantes en el diseño de túneles. Básicamente se obtiene información fidedigna acerca de la estructura de la roca, así como de su calidad en cuanto a resistencia y deformabilidad de una manera indirecta, con base en la velocidad de transmisión de ondas de choque tanto longitudinales ( $\alpha$ ) como transversales ( $\beta$ ), también se obtiene la relación de Poisson.

Ejemplo: Túneles de Desvío Caracol. Anexo No. 2



Con esta información se puede determinar lo siguiente:

- Extensión de los portales
- Definición del tipo de soporte a lo largo del túnel:
  - a) Temporal.- Anclas, malía, guníta simple o armada, ademes.
  - b) Definitivo.- Anclas, malla, guníta simple o armada, ademes y revestimientos de concreto. Camisa metálica en tuberías de presión.
- Propiedades mecánicas para diseño:

$$E = \alpha^2 \cdot \rho \cdot \frac{(1 + \nu)(1 - 2\nu)}{(1 - \nu)} \cdot \frac{1}{g}$$

E = Módulo de elasticidad dinámico

$\alpha$  = Velocidad de transmisión de ondas longitudinales

$\nu$  = Relación de Poisson ; g = gravedad

$\rho$  = Peso volumétrico del medio de transmisión.

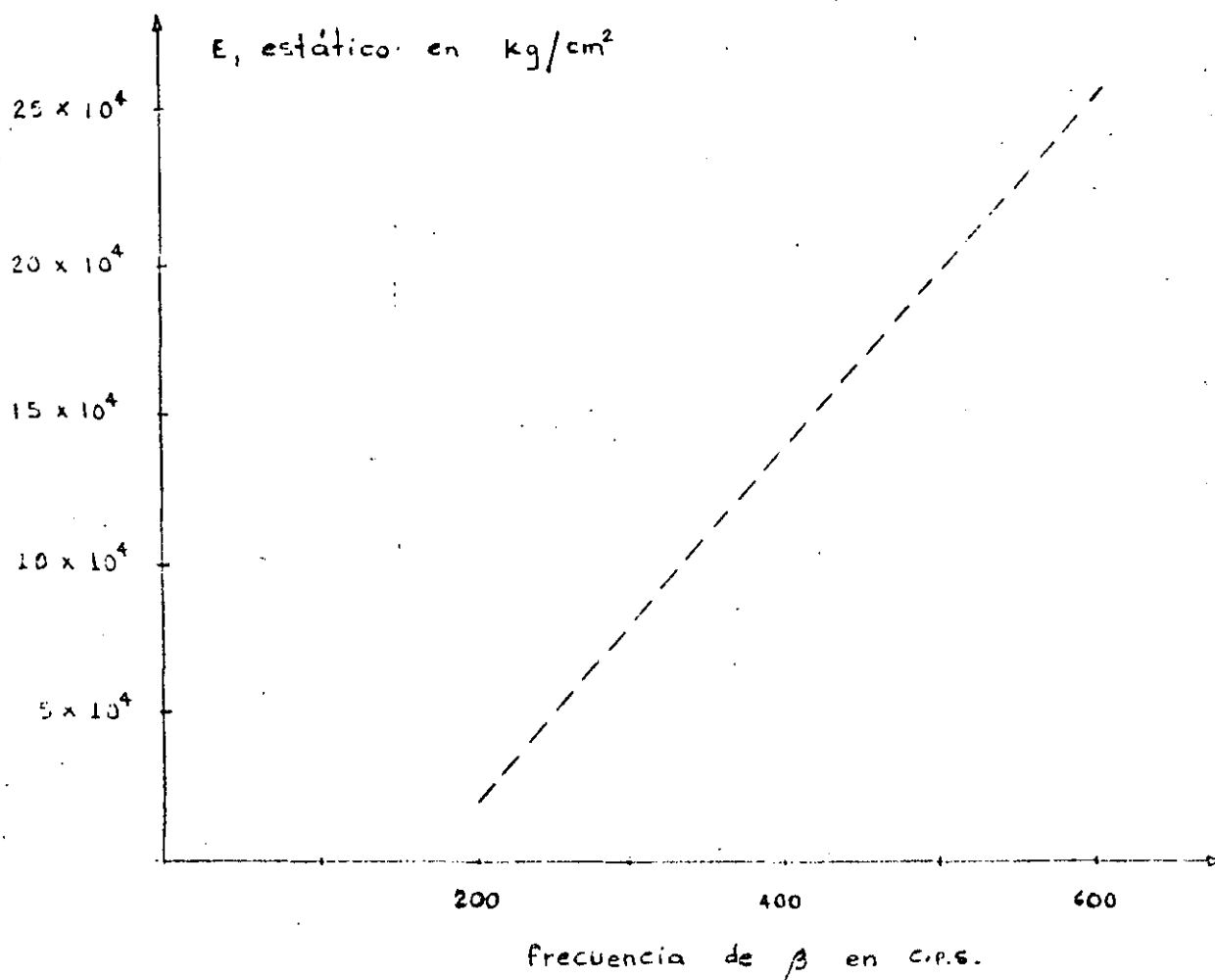
$$E = \beta^2 \cdot \rho \cdot 2(1 + \nu) \cdot \frac{1}{g}$$

$\beta$  = Velocidad de transmisión de ondas transversales

$$\nu = \frac{\frac{1}{2} \left( \frac{\alpha}{\beta} \right)^2 - 1}{\left( \frac{\alpha}{\beta} \right)^2 - 1}$$

- Diseño del revestimiento en función del E, de la roca usando elementos finitos.

-Módulo de elasticidad estático en función de la frecuencia de la onda transversal.



Relación experimental entre el módulo estático en pruebas de placa y la frecuencia de la onda transversal. Referencia:

Moyens nouveaux de reconnaissance des massifs rocheux

Schneider

Annales ITBTP; Julio - Agosto 1967, No. 235-236.

## RESISTIVIDAD

La información mas importante sería la detección de cavernas en rocas calizas y basaltos vesiculares.

También se puede obtener información sobre los niveles de agua.

Ejemplo: Chicoasén, margen izquierda 1974 (Geofimex)

## RAYOS GAMMA

Mediante levantamientos dentro de barrenos pueden localizarse con precisión estratos delgados de lutitas delezna-  
bles que pudieran crear problemas de estabilidad.

Ejemplo: Chicoasén, margen izquierda, 1974, C.F.E. oficina de geofísica.

## FLUJO TERMICO

Mediante mediciones dentro de barrenos puede conocerse la temperatura de la roca y detectar anomalías con temperaturas elevadas, considerando como anomalía las variaciones de temperatura mayores de  $1^{\circ}\text{C}$  por cada 33 m. de profundidad. Los problemas serían que el túnel pasara cerca de zonas hidrotermales con temperaturas mayores de  $60^{\circ}$ . - En el Cañón del Sumidero Chis. y en El Caracol, las mediciones dieron valores normales.

## GEOLOGIA SUPERFICIAL

Reconocimientos a pie efectuando un levantamiento concienzudo de los rasgos estructurales más importantes: echados, fallas, contactos, fallas de talud, litología, cavernas, manantiales, corrientes superficiales, etc.

Los puntos de observación deberán ser controlados por topografía precisa.

Ejemplo: mal control topográfico: Chicoasén margen izquierda donde potencialmente hay problemas de estabilidad en taludes que se extienden a 1.5 Km. desde el río, dificultándose la definición de la geometría del modelo geológico estratigráfico para fines de estabilidad de taludes.

## PERFORACIONES

Este es un medio de exploración caro y por tanto debe seleccionarse la posición y longitud de cada barreno.

Se obtendrá básicamente la estratigrafía y la calidad del macizo rocoso en cuanto a discontinuidades (fracturamiento, fallas, oquedades).

Con las muestras se obtiene la calidad física y química de las rocas (Resistencia, alteración, agresividad al concreto).

Se puede obtener información sobre niveles freáticos y sobre la permeabilidad de la roca.

Conviene que los barrenos tengan dirección e inclinación preferente para atravesar el mayor número de discontinuidades.

Las perforaciones deberán realizarse en tresbolillo a los lados del eje del túnel, digamos a 50 m. La separación entre sondeos a lo largo del eje dependerá siempre de la incertidumbre sobre los cambios importantes ya sea en litología como en la estructura de la roca. La separación máxima podría ser 500 m.

## INFORMACION GEOLOGICA

Con la información obtenida en los estudios y levantamientos geológicos se elaboran planos con plantas y perfiles donde se indique la siguiente información:

GEOMORFOLOGIA.- Topografía superficial, drenaje, manantiales etc..

ESTRUCTURA .- Plantas y perfiles mostrando estratigrafía, fallas, plegamientos, fallas de talud, etc.

TECTONICA .- Fallas regionales, información sísmica (epicentros, profundidad, magnitud).  
Cálculo de desplazamiento de fallas principales y subsidiarias durante eventos sísmicos.

Ejemplo Chicoasén: Se calculó un desplazamiento de 20 cm. en el eje de la boquilla para fallas subsidiarias a 1 km. de distancia de una falla principal de 120 Km. de longitud, para un sismo con magnitud de 7.5.

Ver ejemplo anexo 3.

## GEOHIDROLOGIA

El conocimiento real del flujo hidráulico obtenido de la información del flujo superficial, manantiales y barrenos es de suma importancia para predecir los problemas de manejo del agua de infiltración hacia la excavación, así como para diseñar el drenaje del túnel mediante barrenos, o bien, para estar preparado para evitar la extrusión de la roca por alteración a arenas en granitos y areniscas mediante inyecciones de abanico por delante del túnel. La presión hidrostática también interviene en la determinación de la calidad del macizo rocoso según la clasificación de Barton acerca del tamaño de los bloques y de la resistencia al corte en sus caras.

PROPIEDADES GEOMECANICAS (Geométricas y mecánicas)

Perfiles estratigráficos con los resultados de ensayos de laboratorio practicados en probetas de roca intacta:

Compresión, tensión, corte, porosidad, alteración, peso volumétrico, Módulo elástico, expansibilidad, efecto de creep, efecto de escala.

Lo mismo para ensayos de campo:

Estado de esfuerzos interno, módulo de deformabilidad, resistencia al corte, expansión.

Ver Anexo 4 sobre Pruebas de Campo de Mecánica de rocas.

Ejemplo: Prefactibilidad técnica P.H. Itzantún, Chis. -- C.F.E. 1978.



INTERROGANTES QUE SE PRESENTAN AL CONSTRUIR UN TUNEL:

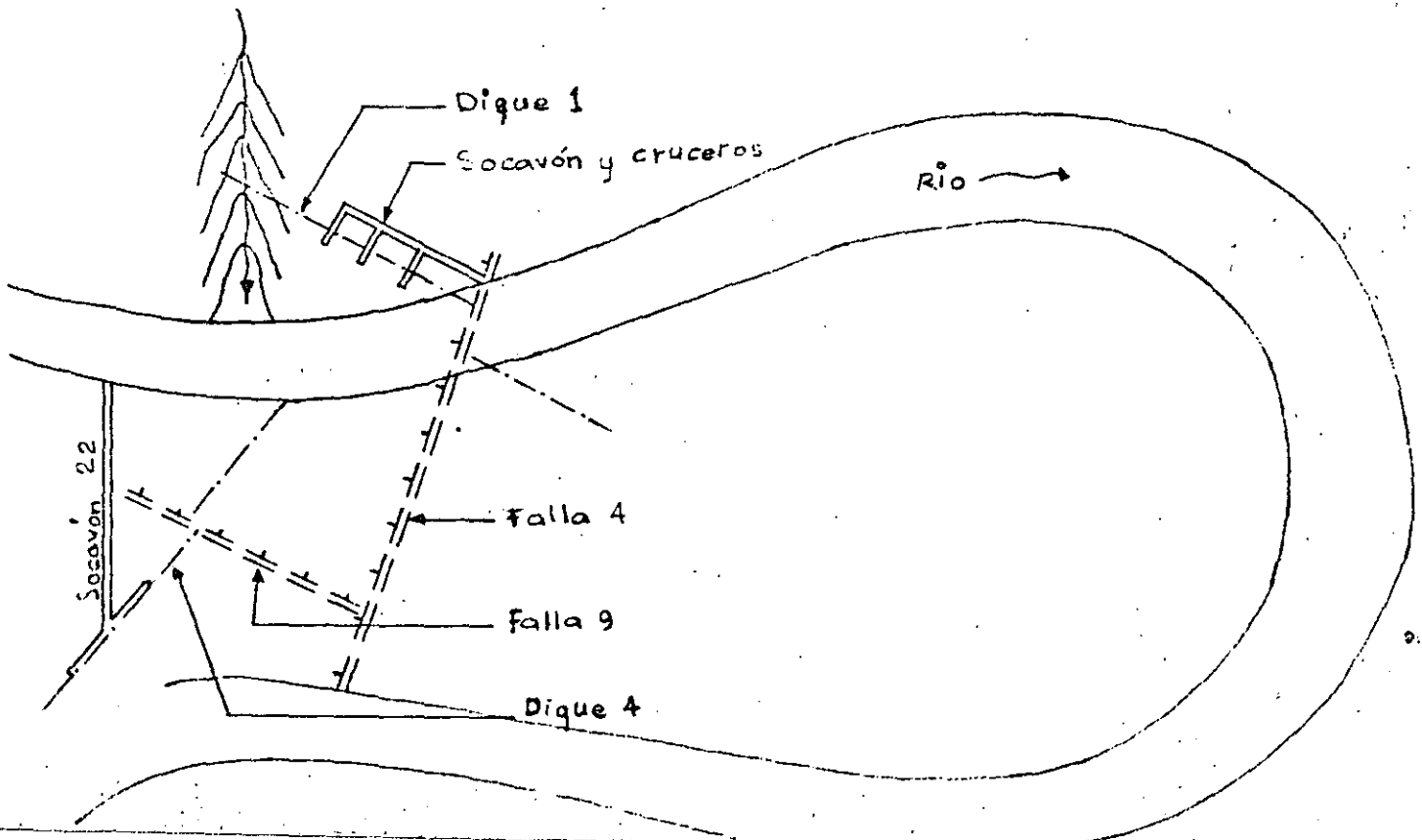
- 1.- FALLAS.- Que posición guardan con el eje del túnel  
 En que longitud afectan al túnel  
 Amplitud de la falla  
 Naturaleza de los materiales en la zona de falla:  
 Milonita (esquistos y calizas)  
 Arcilla expansiva (Montmorilonita)  
 Arena, (alteración de granitos, areniscas, -  
 y rocas antiguas, paleozoicas).

NOTA:

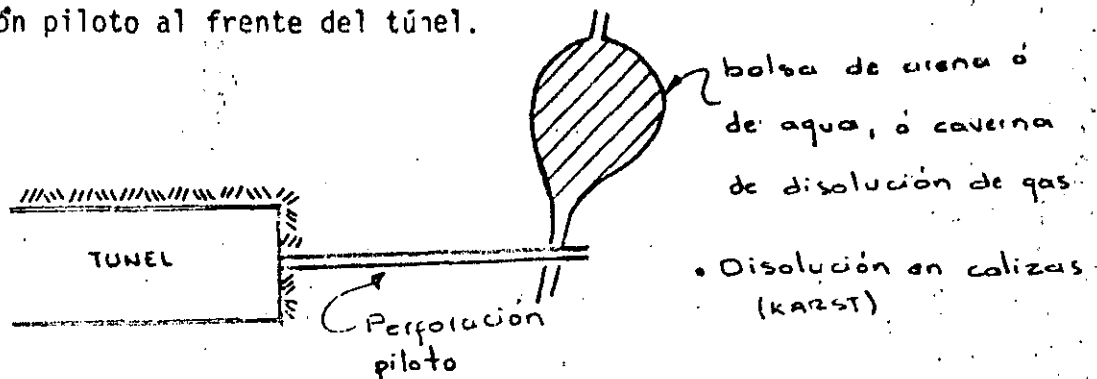
Lo más conveniente es que el túnel atraviese las fallas en dirección perpendicular

Ejemplo: Exploración dique 1 de margen izquierda, en El Caracol, Gro. excavando un túnel paralelo al dique y efectuar cruceros a cada 10 <sup>m</sup> cm.

Mayores dificultades se tuvieron al explorar el dique 4 en El Caracol, Gro., excavando sobre el mismo dique alterado.



La detección de bolsas de arena y/o de agua se realiza mediante una perforación piloto al frente del túnel.



2.-AGUA.-.En que punto se encontrará agua

.En que cantidad

.Con que presión

.De que calidad

.En rocas calizas, anhidritas y yesos se tienen problemas de alteración inmediata y disminuyen en forma notable su resistencia al hidratarse (más del 5%).

.Algunas tobas ígneas de matriz vítreo montmorilonítica se desintegran con la humedad del aire.

Ejemplo: Tobas vítreas blancas en San Juan Tetelcingo, Gro. - margen izquierda.

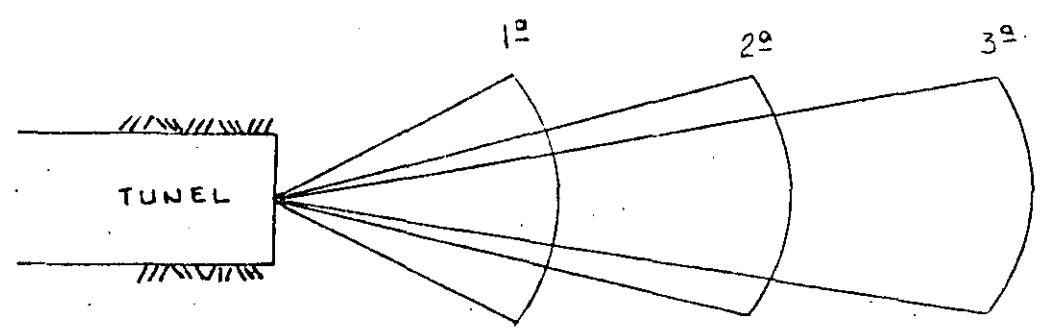
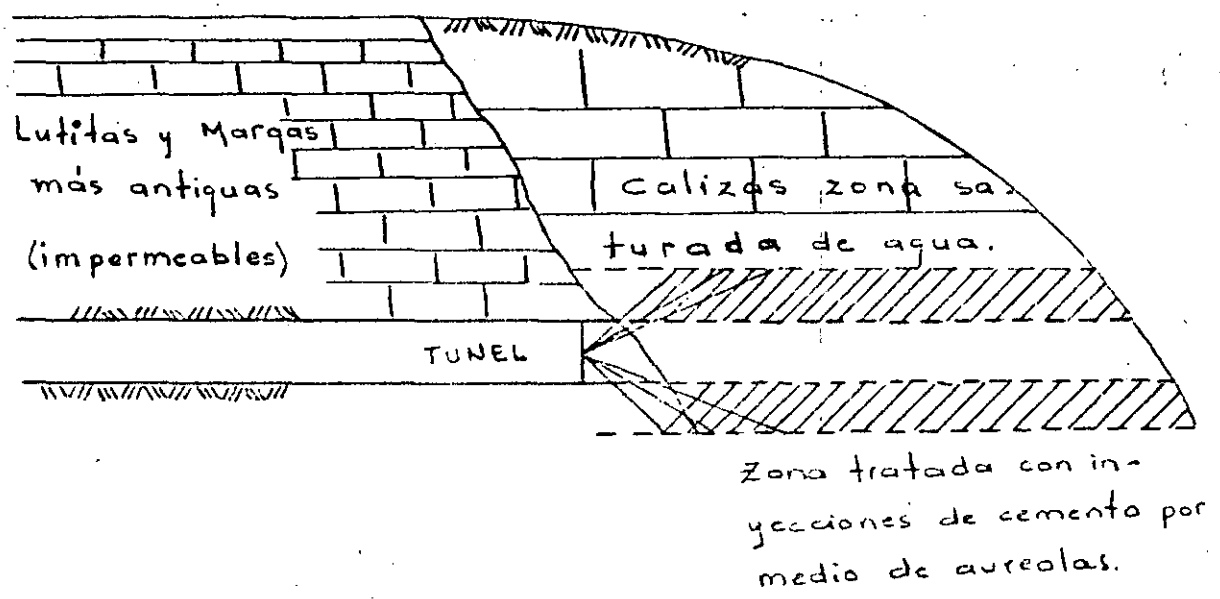
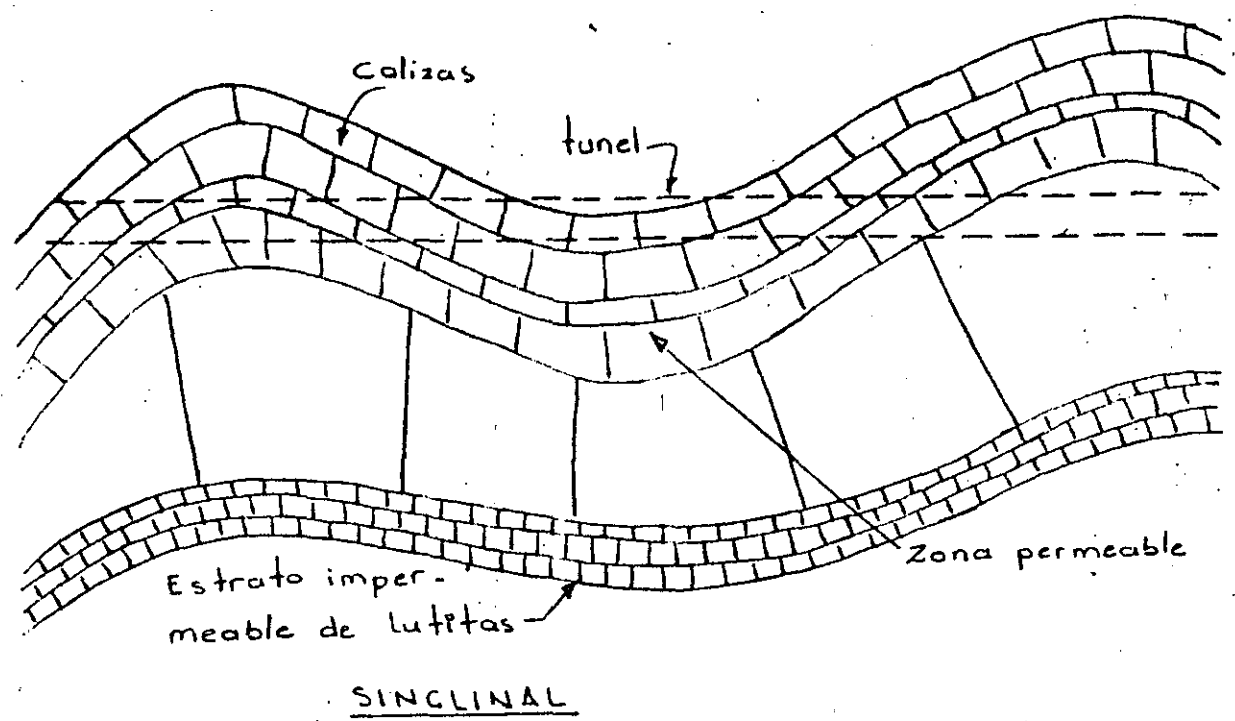
.También la brecha ígnea con matriz vítreo color rosa en la -- misma margen izquierda se expande con la humedad ambiente. -- (Formación Balsas).

.La formación Tuscacuezco en La Presa Las Piedras Gto., de la SARH, esta constituida por areniscas de grano grueso con matriz de arcilla montmorilonítica color café rojizo. Se desintegra en presencia de agua y el material de las excavaciones del vertedor no se pudo usar en la Cortina.

.Las Anhidritas o Lutitas de Río Escondido Suprayacentes al estrato de carbón se expanden y se colapsan con la humedad -- del aire. Se deja una cáscara de carbón de 3" a 4" como protección contra la humedad.

- .Las lutitas interestrificadas con calizas --- en La Angostura y Chicoasén, Chis., dieron valores de  $25 \frac{\text{Kg}}{\text{cm}^2}$  de expansión al saturarlas, -- sin permitir cambios volumétricos.
- .Las calizas, anhidritas, yesos y basaltos producen agua abundante.
- .La estructura de sinclinal produce agua.
- .Los cauces antiguos (paleocanales) también -- producen agua.
- .Las agua zelenitosas (sulfatadas) atacan el - cemento Portland.

NOTA: En El Caracol, Gro., la alteración de los diques ígneos - de composición andesítica (Felsita) ha sido a través de - cientos o miles de años.



AUREOLAS.-  
conos embutidos de inyección

3.- MATERIALES .- ¿Se excavará todo el túnel en roca sana o se encontrarán zonas con rocas deleznales cauces sepultados, etc.?

Desafortunadamente los estudios no son tan completos para conocer con anticipación esta eventualidad.

Con los sondeos geofísicos de microsísmica y resistivos que a veces son los de mayor alcance en profundidad no se logran identificar plenamente estas discontinuidades.

4.- SECCION .- ¿Se obtendrá una sección limpia o habrá sobre excavación?

En rocas con estratificación delgada se produce sobre excavación. Aquí la dirección del echado tiene gran influencia.

Rocas blandas: tobas, morrenas tienen también sobre excavación:

Ejemplo: Túnel de aducción en morrenas en el P.H. Pizayambo, Ecuador, de 4 m. de sección portal y 6 Km. de longitud excavado en morrenas y andesita alterada en la zona de Los Andes.

5.- RESISTENCIA .- Será roca fácilmente excavable o será difícil por su dureza.

Fácil.- Calizas de Angostura, poco consolidadas con resistencias en compresión de  $500 \text{ Kg/cm}^2$  en seco y  $350 \text{ Kg/cm}^2$  en saturado.

Difícil.- Conglomerado silicificado de El Infiernillo con resistencias de 2 500 Kg/cm<sup>2</sup> en compresión. - -  
Muy abrasiva. Produce silicosis.

Gneiss granítico con 20% de cuarzo en la Rumorosa. Túnel San Luis Río Colorado - -  
Tijuana de 3.5 m. de diámetro. Fracaso --  
una máquina topo rascadora tipo Fullface por desgaste excesivo en los cortadores.  
Avance máximo 17 m/día.  
Avance promedio 1 m/día.  
Avance promedio en rocas blandas 35.50 m/día.

#### 6.- ADEMÉS

En función de la calidad de la roca será el ademe que se utilice:

Gunita - Gunita y Malla

Anclas - Preanclajes

Marcos - Simples-colados.

#### 7.- PORTALES

Necesidad de apuntalar la entrada y salida del túnel y en que longitud.

Se determina en función de la calidad estructural del macizo rocoso mas que de la calidad física y resistencia de la roca.

En general la roca superficial esta alterada y es necesario removerla. Tener cuidado de la estabilidad general del talud.

NOTA: Por una falla general de talud se puede obturar toda la toma.

Cerro de Oro-falla portales.

8.- FALLA DEL TUNEL .- Posibilidad en túneles profundos que por relajación de esfuerzos se expanda el material y se presenten desprendimientos violentos. Roca explosiva (Rockburst)

9.- REVESTIMIENTO . ¿Revestimiento en portales zonas de fallas, o en toda la longitud?

¿Revestimiento total en túneles de desvío?

Se ha observado que en general se requiere solo en los portales, para el resto funciona muy bien la protección con gunita. Depende de la calidad estructural de la roca y también de su composición mineralógica y permeabilidad, geometría de la excavación etc.

En general rocas con velocidad de ondas longitudinales  $\approx$  3000 m/seg., son competentes para no revestir.

Depende también de la velocidad del agua y de la energía de la misma.

Velocidades  $>$  15 m/seg., son peligrosas de erosión. Ejemplo: Túneles vertederos Infiernillo.

Las tuberías de presión generalmente se revisten de concreto.

En Noruega y Suecia se han dejado sin revestir en granitos muy sanos sin fracturas.

El revestimiento deberá llevar al menos refuerzo por temperatura cuando se tengan dudas de la colaboración de la roca bajo presión interna del túnel y externa cero.

Ejemplo: Falla conducción a presión en la P.H. El Arenal, Costa Rica, falló un tramo de 600 m. por presión interior en rocas blandas con presión interna de  $6 \text{ Kg/cm}^2$  y externa cero. Se formaron dos fracturas longitudinales en clave y piso con separación hasta de 2 cm.

El túnel tiene 4.6 m. de  $\phi$  interior y 40 cm. de concreto de  $f'_c = 250 \text{ Kg/cm}^2$  y no se colocó acero de refuerzo. Ver anexo 5.

NOTA: Rocas que atacan el concreto: Rocas ígneas o metamórficas con Pirrotita  $\text{Cu Fe So}_4$ .

10.- PRESENCIA DE GASES VENENOSOS.- Se encuentra  $\text{CO}_2$  en terrenos volcánicos recientes, o en rocas que por su composición desprenden gas butano. Antracita, Lignito y Carbón.

Rocas con:  $\text{Fe}_2 \text{SO}_4$ .



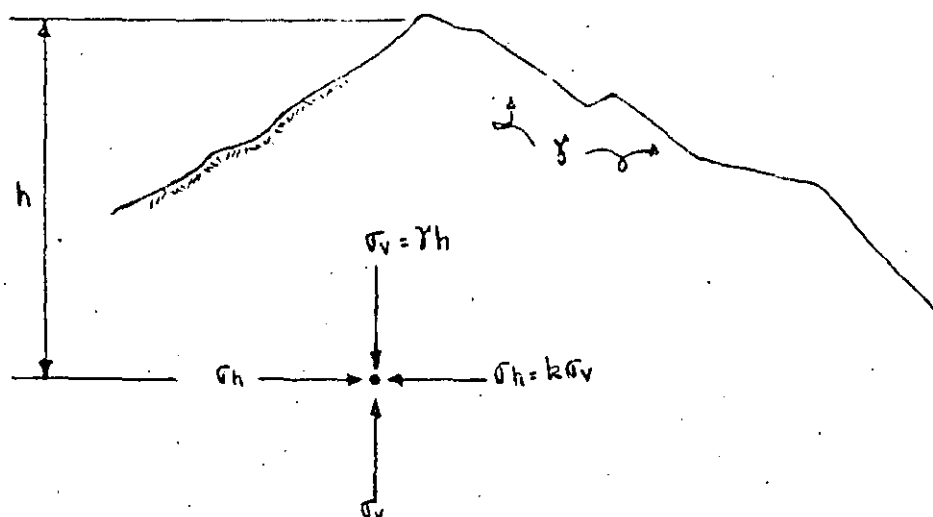
## DISEÑO DE TUNELES

## 1.- ESTADO NATURAL DE ESFUERZOS

Se conoce como "estado natural de esfuerzos" o "esfuerzos residuales" a los esfuerzos existentes en la corteza terrestre previamente a cualquier excavación.

1.1.- Estado de esfuerzos interno en un macizo rocoso. Hipótesis de Heim.

El geólogo Suizo Heim en 1878 observó en los grandes túneles trans-alpinos que la roca estaba fuertemente esforzada en todas las direcciones. Supuso que la componente de esfuerzos verticales  $\sigma_v$  estaba relacionada directamente proporcional al peso de la cobertura de roca, pero que adicionalmente había una componente de esfuerzo horizontal  $\sigma_h$  que probablemente tenía una magnitud similar al de la componente vertical.

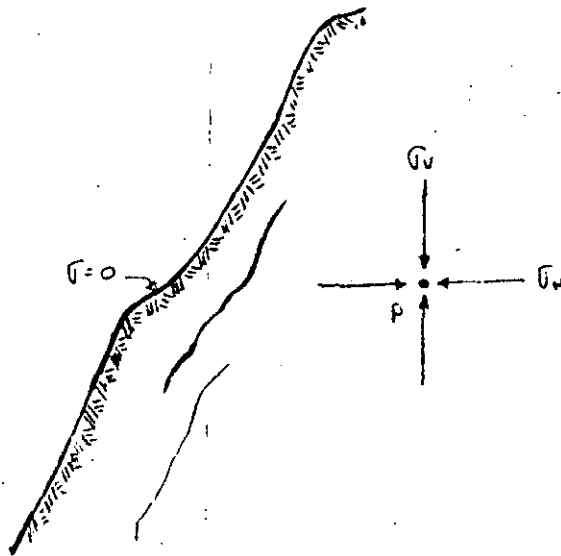


Una hipótesis similar había sido propuesta por el experto en túneles Alemán Rzhia en 1874.

1.2:- Relajación de esfuerzos superficiales en una masa de roca. En un cañón profundo el estado natural tridimensional de esfuerzos debe encontrarse a una gran profundidad (generalmente a profundidades  $\geq 350$  m.) mientras que en dirección normal a la superficie no hay esfuerzos por lo menos en los primeros 50 m.

Se observa que este paso de estado de esfuerzos tridimensional a bidimensional ocasiona fisuras y fracturas paralelas a la superficie del cañón que se les conoce como "foliación".

Son fracturas por relajación de esfuerzos ocasionadas por la falta de confinamiento o de soporte lateral que dan lugar a fracturas perpendiculares al esfuerzo principal menor. Los cambios de temperatura también producen ese fracturamiento.



Relajación de esfuerzos superficiales

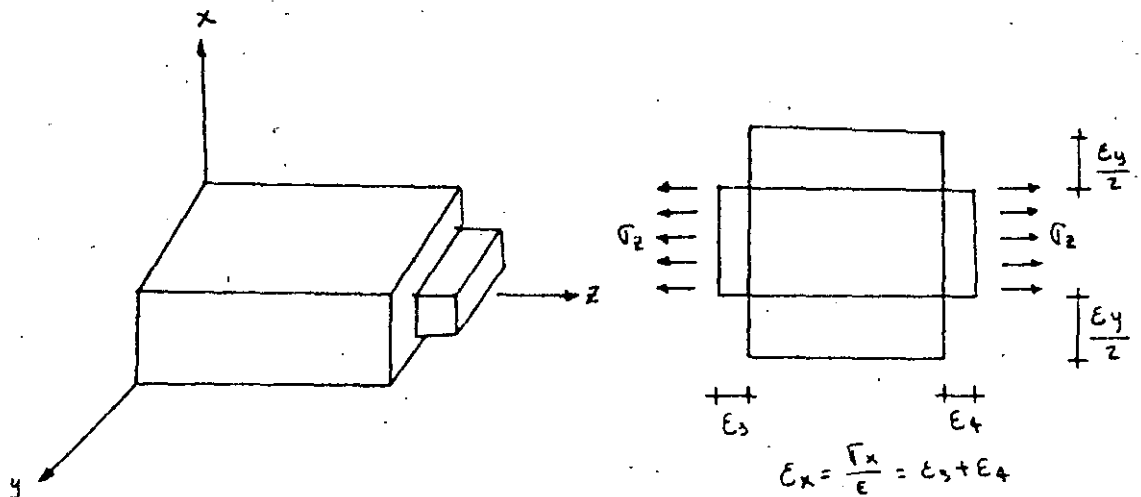
Se deberá poner atención a este fenómeno cuando se apoye la cimentación de una presa en una ladera de estas características en la cual la roca tendría que consolidarse con inyecciones de cemento y anclas postensadas.

### 1.3.- Módulo elástico efectivo y relación de Poisson efectiva en un macizo rocoso.

#### Teoría de Terzaghi

Hemos supuesto que  $k$  es la relación entre los esfuerzos de campo horizontal a vertical;  $k = \frac{\sigma_h}{\sigma_v}$  Terzaghi en 1952 relacionó esta  $k$  con la relación de Poisson como sigue:

#### Ley de Hooke.



La teoría clásica de la elasticidad está restringida a materiales sólidos con las siguientes propiedades elásticas idealizadas:

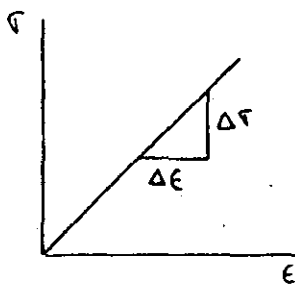
- 1.- Linealidad entre esfuerzos y deformaciones. Ley de Hooke.

Si un cuerpo está sujeto a un esfuerzo, entonces la deformación en la dirección del esfuerzo es directamente proporcional al esfuerzo aplicado.

- 2.- Homogeneidad.- El material de un cuerpo está uniformemente distribuido a través de todo su volumen y las pro-

propiedades elásticas del material son las mismas en todos los puntos del cuerpo.

- 3.- Isotropía.- Las propiedades elásticas del material son las mismas en todas las direcciones.
- 4.- Perfectamente elástico.- Al dejar de actuar las fuerzas deformantes, el tamaño y forma del cuerpo regresan precisamente a su estado original.



$$\epsilon = \frac{\sigma}{E}$$

E = Variación de la deformación con respecto al esfuerzo que actúa en un cuerpo determinado.

E = Módulo de elasticidad.

$\epsilon$  = Deformación unitaria.

$\sigma$  = Esfuerzo principal.

#### 1.4.- Relaciones esfuerzo: deformación.

Suponiendo un paralelepípedo rectangular con sus lados paralelos a los ejes coordenados, actuando sobre él un esfuerzo normal  $\sigma_x$  uniformemente distribuido sobre dos caras opuestas.

La magnitud de la deformación normal  $\epsilon_x$  está dada por

$$\epsilon_x = \frac{\sigma_x}{E}$$

esta extensión del cuerpo es acompañada por una contracción lateral en las direcciones  $y$  y  $z$

esto es:  $\epsilon_y = -\nu \frac{\sigma_x}{E}$  ; y  $\epsilon_z = -\nu \frac{\sigma_x}{E}$

donde  $\nu$  es una constante conocida como relación de Poisson.

La relación de Poisson para muchos de los materiales varía entre 0.15 y 0.35 y a menudo se supone igual a 0.25.

Si al <sup>v</sup> paralelepípedo rectangular se le sujeta a la acción simultánea de esfuerzos normales  $\sigma_x, \sigma_y$  y  $\sigma_z$  uniformemente distribuidas sobre sus caras, las deformaciones normales por el principio de superposición de causas y efectos son las siguientes:

$$\epsilon_x = \frac{1}{E} [\sigma_x - \nu(\sigma_y + \sigma_z)]; \quad \epsilon_y = \frac{1}{E} [\sigma_y - \nu(\sigma_x + \sigma_z)]; \quad \epsilon_z = \frac{1}{E} [\sigma_z - \nu(\sigma_y + \sigma_x)]$$

### 1.5.- Estado plano de esfuerzos.

Si suponemos que en un plano horizontal los esfuerzos son simétricos,  $\sigma_y = \sigma_z$  y que no hay desplazamientos en una dirección horizontal,  $\epsilon_z = 0$

tenemos:

$$0 = \sigma_z - \nu\sigma_y - \nu\sigma_x$$

$$\text{como } \sigma_y = \sigma_z$$

$$0 = \sigma_y - \nu\sigma_y - \nu\sigma_x$$

$$0 = \sigma_y(1 - \nu) - \nu\sigma_x$$

$$\therefore \sigma_z = \sigma_y = \left(\frac{\nu}{1 - \nu}\right) \sigma_x \quad \text{y} \quad k = \left(\frac{\nu}{1 - \nu}\right)$$

Para valores de  $\nu$  entre  $\frac{1}{5}$  y  $\frac{1}{3}$ ;  $\sigma_z = \sigma_y = \frac{\sigma_x}{4}$  a  $\frac{\sigma_x}{2}$  o sea  $k=0.25$  a  $0.5$  con  $k=0.3$  como el valor más probable..

para un estado plano de esfuerzos con  $\sigma_y = \sigma_z \neq 0$  tenemos:

$$\epsilon_x = \frac{1}{E} (\sigma_x - \nu\sigma_z) \quad \text{y} \quad \epsilon_z = 0 = \frac{1}{E} (\sigma_z - \nu\sigma_x)$$

Para  $\sigma_z = \nu\sigma_x$  y  $k = \nu$  tendríamos

$$\epsilon_x = \frac{1}{E} (\sigma_x - \nu^2\sigma_x) = \frac{1}{E} \sigma_x (1 - \nu^2) \quad \text{y} \quad E = \frac{\sigma_x}{\epsilon_x} (1 - \nu^2)$$

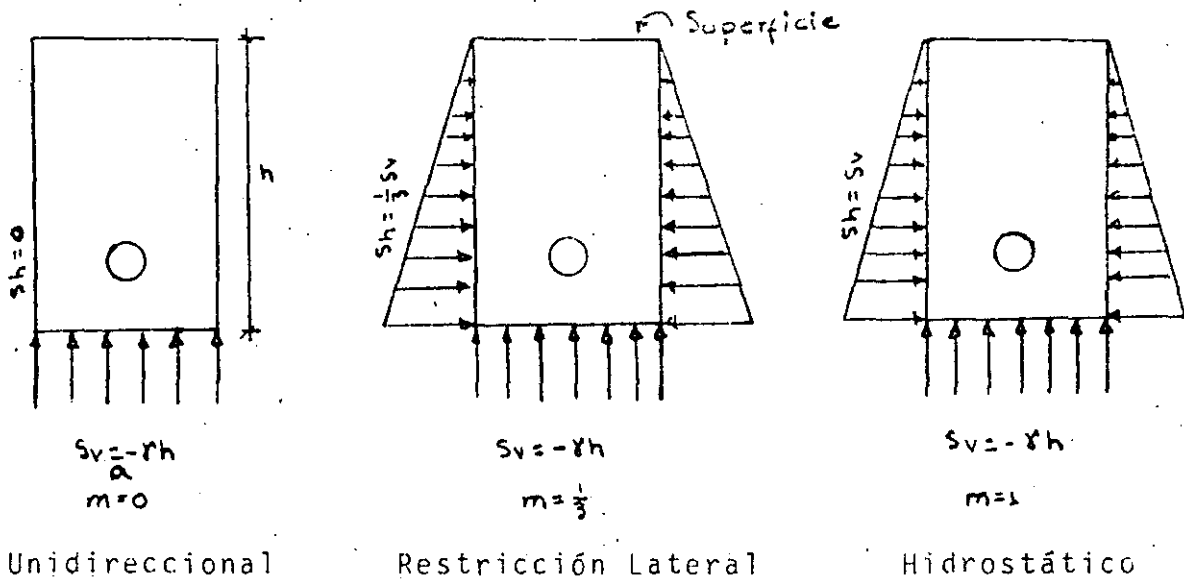
La relación  $(\frac{\nu}{1-\nu})$  de Terzaghi con valores usuales de  $\nu$  para la roca entre 0.3 a 0.25 y 0.2 es contradictoria a las mediciones actuales realizadas en galerías profundas. Los resultados de mediciones favorecen la hipótesis de Heim;  $\sigma_1 = \sigma_2 = \sigma_3$  y  $k=1$  con  $K=1$  se requiere que  $\nu=0.5$  el cual no existen en las mediciones de la roca. Se presenta una paradoja obvia conocida como "paradoja de Terzaghi".

1.6.- Esfuerzos de campo.

Hemos visto que los esfuerzos de campo dependen de las condiciones de confinamiento del material y del comportamiento elástico de la roca, así como, de la magnitud de los esfuerzos de la corteza terrestre.

De esta manera, los esfuerzos alrededor de un túnel pueden compararse con los esfuerzos alrededor de un agujero en una placa siempre y cuando se cumpla (1) que la abertura sea larga en comparación con su sección transversal y (2) que la distribución de esfuerzos a lo largo de la abertura sea uniforme e independiente de su longitud.

Así el problema de un túnel se reduce a un problema de deformación plana y puede ser resuelto considerando un agujero en una placa ancha sujeta a un estado bidireccional de esfuerzos actuando en el plano de la placa.



Suposición de tres estado de esfuerzo de campo.

También deberán considerarse geometrías simples como: círculos, elipses, óvalos o rectángulos con esquinas redondeadas.

Los esfuerzos verticales se considerarán iguales a  $h$  equivalentes al peso de la cobertura de roca en donde  $\gamma$  = peso volumétrico de la roca y  $h$  = la profundidad vertical del túnel.

Por lo tanto:  $S_v$  = Componente del esfuerzo vertical.

$S_h$  = Componente del esfuerzo de compresión horizontal.

y  $m$  = Constante que depende del estado de esfuerzos de campo.

-El estado de esfuerzos para  $m=0$  puede ocurrir a poca profundidad y/o cerca de superficies verticales libres.

-El estado de esfuerzos representado por  $m=\frac{1}{3}$  puede ocurrir para un amplio intervalo de profundidades.

-El estado de esfuerzos para  $m=1$  puede ocurrir a gran profundidad o en macizos con rocas semiviscosas o plásticas (rocas suaves o blandas).

## 2.- ESFUERZOS EN LA VECINDAD DE EXCAVACIONES SUBTERRANEAS

Los esfuerzos que se generan en la vecindad de excavaciones subterráneas, por ejemplo túneles largos profundos son semejantes a los que se producen alrededor de un agujero en una placa infinita. Solamente unas cuantas secciones transversales pueden ser analizadas teóricamente; sin embargo por medio de fotoelasticidad o análisis de esfuerzos, aberturas con cualquier forma de sección transversal pueden ser estudiadas.

Considerando una placa infinita de espesor  $t$  con un agujero circular de radio  $a$  con centro en el origen y sujeta a esfuerzos de tensión  $S_x$  y  $S_y$ . Para una distancia larga desde el agujero, las componentes polares de esfuerzos serán aquellas resultantes solamente de la aplicación de esfuerzos:

## 2.1.- ESFUERZOS EN UNA PLACA CON UN AGUJERO CIRCULAR

Si en una placa sometida a un esfuerzo de tensión uniforme se practica un agujero circular pequeño (diámetro del agujero 5 veces menor que el ancho de la placa) se produce, en los puntos  $n-n$  una gran concentración de esfuerzos. La teoría exacta desarrollada por Kirsh, en 1898 muestra que el esfuerzo de tensión en estos puntos es igual a  $3\sigma$ . Se ve también que esta concentración de esfuerzos es muy local y esta limitada a la vecindad del agujero. Si trazamos una circunferencia concéntrica con el agujero, y de radio  $c$  relativamente grande, -- puede suponerse que el estado de esfuerzos en esta circunferencia no queda afectado por la presencia del agujero.

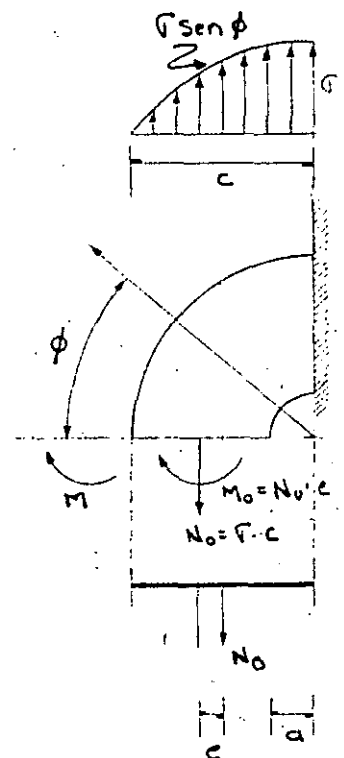
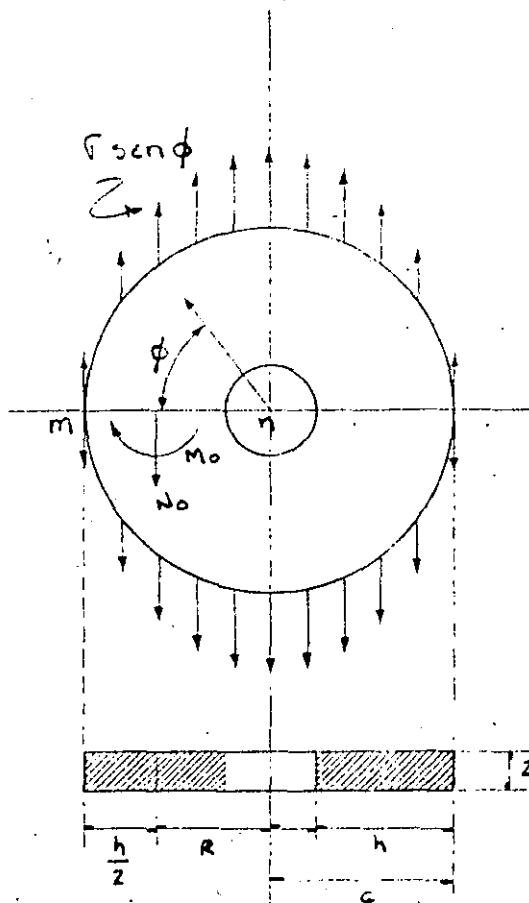
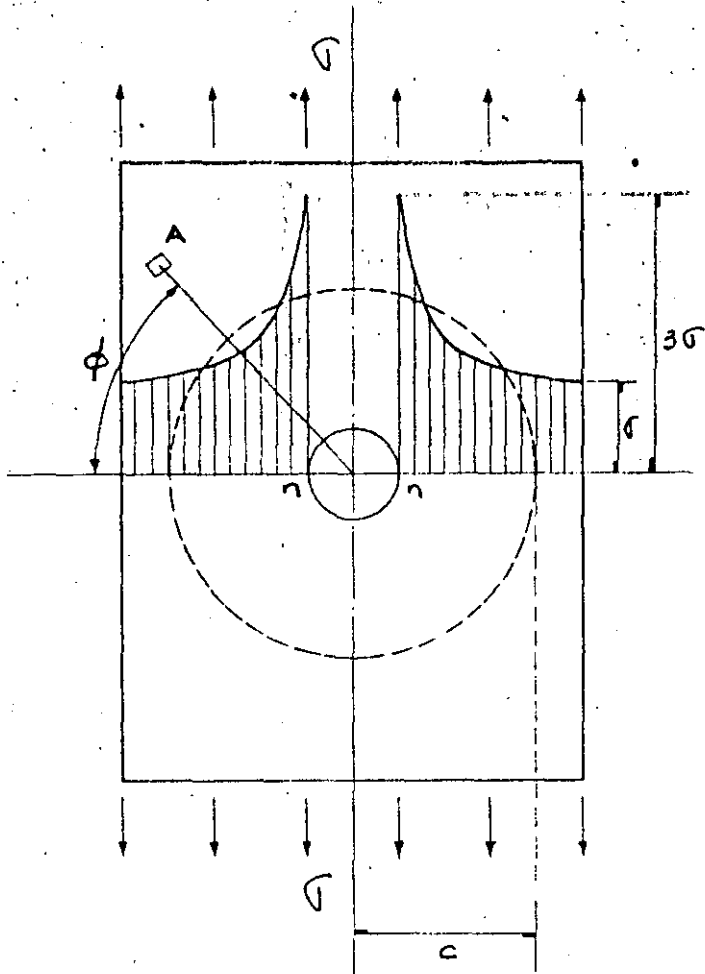
Consideramos por tanto un anillo circular separado de la placa por una superficie cilíndrica circular de radio  $c$ . En cada punto de la superficie exterior de este anillo aplicaremos esfuerzos dirigidos verticalmente y de valor  $\sigma \sin \phi$  es decir, -- iguales al esfuerzo correspondiente en el área elemental  $A$  de la placa.

Por lo tanto, los esfuerzos en el interior del anillo serán -- aproximadamente los mismos que en el trazo de la placa limitado por el círculo de radio  $c$ .

De esta manera el problema de la distribución de esfuerzos en las proximidades del agujero queda reducido al de calcular -- esa distribución en un anillo circular de sección rectangular sollicitado por fuerzas verticales conocidas de intensidad distribuidas en forma continua sobre su contorno exterior.

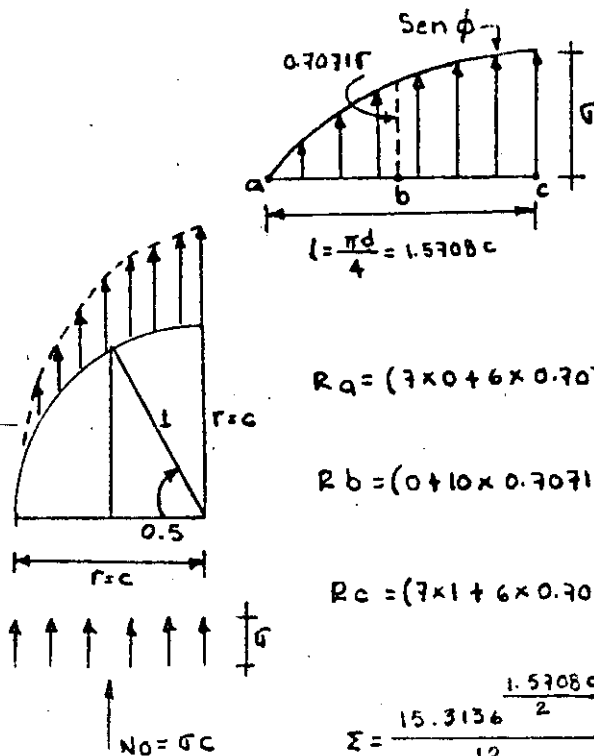


28-A



Este problema puede resolverse considerando un cuadrante de anillo en el cual los esfuerzos ligados a la sección m-n pueden reducirse a una fuerza de tensión longitudinal No aplicada en el centro de gravedad de la sección y a un par flector Mo.

La fuerza longitudinal de tensión se determina por las condiciones de la estática, y es:  $N_0 = \sigma \cdot c$ .



Integral Numérica de los esfuerzos

$$R_a = \frac{h}{24} (7a + 6b - c)$$

$$R_b = \frac{h}{12} (a + 10b + c)$$

$$R_c = \frac{h}{24} (7c + 6b - a)$$

$$R_a = (7 \times 0 + 6 \times 0.7071 - 1) \frac{h}{24} = 1.6213 \frac{h}{12} \times \sigma$$

$$R_b = (0 + 10 \times 0.7071 + 1) \frac{h}{12} = 8.0710 \frac{h}{12} \times \sigma$$

$$R_c = (7 \times 1 + 6 \times 0.7071 - 0) \frac{h}{24} = 5.6213 \frac{h}{12} \times \sigma$$

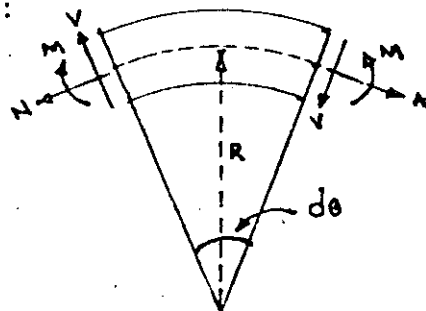
$$15.3136 \frac{h}{12} \times \sigma$$

$$\Sigma = \frac{15.3136 \frac{1.5708c}{2}}{12} \sigma \quad \therefore \Sigma = \sigma \cdot c = N_0$$

El momento  $M_b$  es estáticamente indeterminado (porque no conocemos  $c$ ) y se puede calcular por el teorema del trabajo mínimo -- utilizando la expresión de la energía de la deformación total -- de barras curvas para anillos gruesos, como sigue:

$$U = \int_0^s \left( \frac{M^2}{2AEER} + \frac{N^2}{2AE} - \frac{MN}{AER} + \frac{\alpha V^2}{2AG} \right) ds$$

Anillo grueso:



En esta expresión la fuerza longitudinal y el momento flector para la sección general del anillo caracterizada por el ángulo  $\phi$  son:

$$N = \sigma c \cos^2 \phi \quad y$$

$$M = M_0 + \sigma c (1 - \cos \phi) \left[ \frac{c}{2} (1 - \cos \phi) + \frac{h}{2} \cos \phi \right] - \underbrace{\sigma c \left( c - \frac{h}{2} \right)}_R (1 - \cos \phi)$$

donde  $h$  es la altura de la sección rectangular

La ecuación para el cálculo de  $M_0$  es:

$$\frac{du}{dM_0} = \int_0^{\pi/2} \frac{M d\phi}{AEc} - \int_0^{\pi/2} \frac{NR d\phi}{AE} = 0$$

donde:  $ds = R d\phi$

Después de integrar se tiene:

$$M_0 = \frac{2 \sigma c^2}{\pi} \left[ 1 - \frac{3}{8} \pi - \frac{h}{2c} \left( 1 - \frac{1}{4} \pi \right) + \frac{e\pi}{4c} + \frac{R}{2c} (\pi - 2) \right]$$

en donde  $R$  = radio de la línea media y  $e$  la distancia a la línea neutra desde el Centro de Gravedad de la sección.

El esfuerzo en el punto  $n$  de la sección  $m-n$  del anillo consta de dos partes: 1° el esfuerzo de tensión producido por la fuerza longitudinal  $N_0$  e igual a:

$$\sigma_1 = \frac{N_0}{k} = \frac{\sigma c}{k} \quad (d)$$

y 2° el esfuerzo en el punto de flexión producido por  $M_0$  cuyo valor es:

$$\sigma_2 = \frac{M_0 h_1}{A e a} = \frac{M_0 \left(\frac{h}{2} - e\right)}{A e a} = \frac{M_0}{2 e a} \left(1 - \frac{2e}{h}\right) \quad (e)$$

en donde  $a$  = radio del agujero.

La distancia  $e$  se calcula por la ecuación para diversos valores de la relación  $\frac{c}{a}$  y después  $\sigma_1$  y  $\sigma_2$  se determinan por las ecuaciones (d) y (e). El esfuerzo máximo es:  $\sigma_{\max} = \sigma_1 + \sigma_2$

La distancia  $e$  se calcula por la ecuación  $r = \frac{h}{\log_n \frac{c}{a}}$

Resultados:

c/a	3	4	5	6	8	10
$\frac{2e}{h}$	0.1796	0.2238	0.2574	0.2838	0.3239	0.3536
$\frac{\sigma_1}{\sigma}$	1.50	1.33	1.25	1.20	1.14	1.11
$\frac{\sigma_2}{\sigma}$	2.33	1.93	1.83	1.83	1.95	2.19
$\frac{\sigma_{\max}}{\sigma}$	3.83	3.26	3.08	3.03	3.09	3.30

Comparando los números de la última línea de la tabla anterior con la solución exacta para un agujero pequeño  $\sigma_{\max} = 3\sigma$ ; se vé que para  $5 < \frac{c}{a} < 8$ , los resultados del cálculo aproximadamente están de completo acuerdo con la solución exacta. --- Cuando  $\frac{c}{a} < 5$  el agujero no puede considerarse muy pequeño, -- por lo que tiene una influencia apreciable en la distribución de esfuerzos sobre la circunferencia de radio  $c$  y la hipótesis establecida sobre la sollicitación en el borde exterior -- del anillo no es suficientemente exacta. La discrepancia con la teoría exacta para  $\frac{c}{a} > 8$  se debe a la exactitud insuficiente de la teoría elemental de piezas curvas cuando el radio interior es muy pequeño comparado con el exterior.

Para un punto cualquiera de la sección  $m-n$  a una distancia  $r$  del centro del agujero, el esfuerzo normal es:

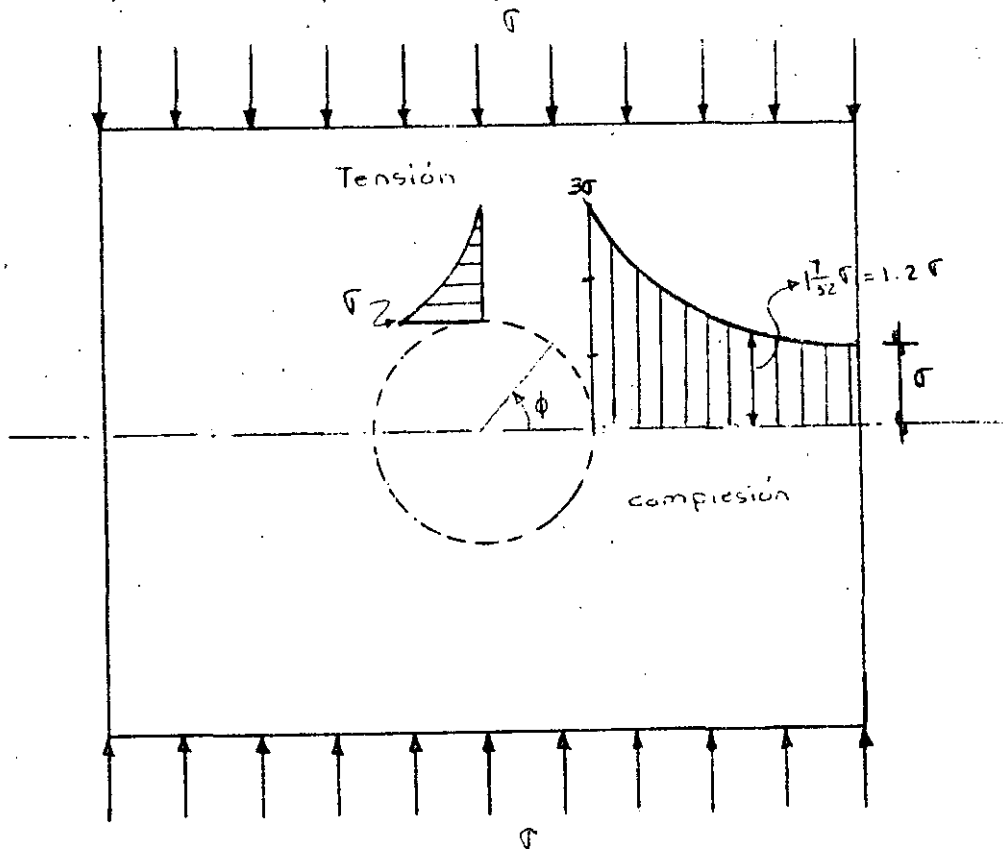
$$\sigma_{\max} = \frac{\sigma}{2} \left( 2 + \frac{a^2}{r^2} + 3 \frac{a^4}{r^4} \right)$$

donde  $\sigma$  es el esfuerzo de tensión uniforme aplicado en los extremos de la placa.

Esta distribución de esfuerzos se presenta en la figura de abajo y se ve que la concentración de esfuerzos esta muy concentrada en los puntos n. El esfuerzo disminuye rápidamente a medida que  $r$  aumenta, y para un punto situado a una distancia del borde del agujero igual al radio del mismo, es decir,  $r=2a$  se tiene un esfuerzo normal  $\sigma_{\theta} = 1\frac{1}{2}\sigma$

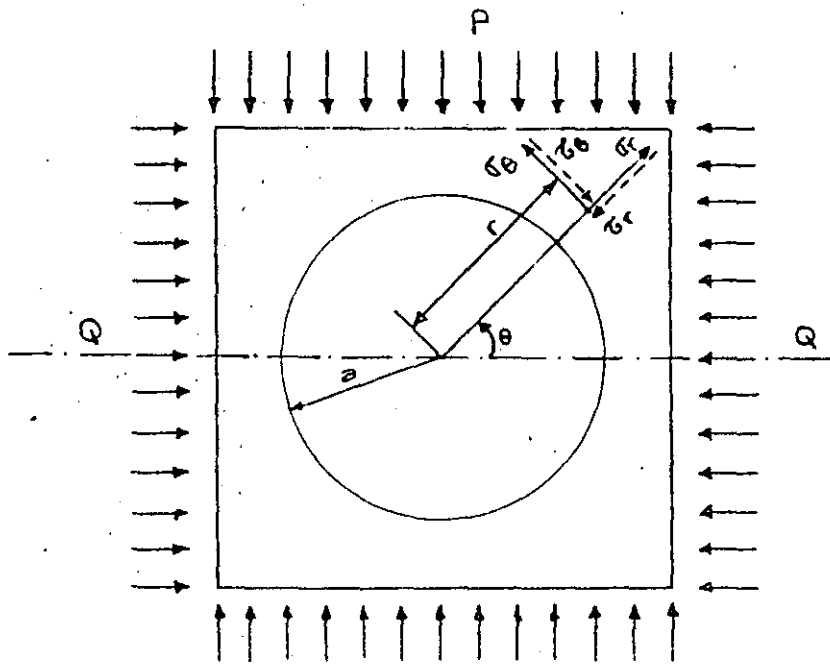
También disminuye rápidamente el esfuerzo al crecer  $\phi$  y para  $\phi = \frac{\pi}{2}$  el esfuerzo normal en el borde del agujero es de compresión e igual a  $\sigma$  o sea  $\sigma_{\theta} = \sigma$

Si los esfuerzos externos fueran de compresión tendríamos un esfuerzo tangencial de tensión  $\sigma_{\phi}$  para  $\phi = \frac{\pi}{2}$  y un esfuerzo de compresión  $\sigma_{\phi} = \sigma$  para los puntos n.



Considerando una placa con una perforación en el centro que se supone de material homogéneo, elástico e isótropo, Kirsh determinó los esfuerzos normales, tangenciales y cortantes en cualquier punto de la placa.

Se supone que las fuerzas externas P y Q corresponden con las transmitidas por la cobertura de roca.



Esfuerzo radial:

$$\sigma_r = \frac{P+Q}{2} \left( 1 - \frac{a^2}{r^2} \right) + \frac{Q-P}{2} \left( 1 - \frac{4a^2}{r^2} + \frac{3a^4}{r^4} \right) \cos 2\theta$$

Esfuerzo tangencial:

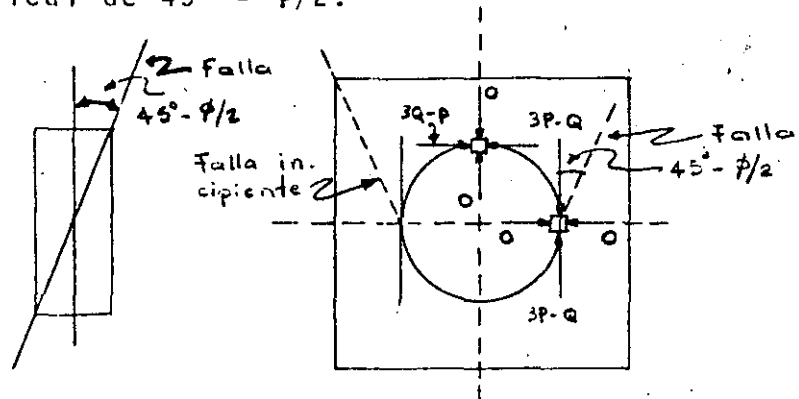
$$\sigma_\theta = \frac{P+Q}{2} \left( 1 + \frac{a^2}{r^2} \right) - \frac{Q-P}{2} \left( 1 + \frac{3a^4}{r^4} \right) \cos 2\theta$$

Esfuerzo cortante:

$$\tau_{\theta} = -\frac{Q-P}{2} \left( 1 - \frac{2a^2}{r^2} - \frac{3a^4}{r^4} \right) \sin 2\theta$$

Se observa que los esfuerzos en la placa no dependen de E y  $\nu$

Para el caso  $r=a$ ,  $\theta=0^\circ$  y  $P > Q$  y tomamos un elemento de roca, el confinamiento horizontal es cero, de manera que si  $(3p-Q) > R_c$  (Resistencia en compresión simple de la roca), entonces se presentarán fracturas con un ángulo de inclinación respecto a la vertical de  $45^\circ - \phi/2$ .



Para el caso  $r=a$ ,  $\theta=90^\circ$  y  $P > Q$  y tomamos un elemento cuyo confinamiento vertical es cero, de manera que  $(3Q-P)$  es negativo se tendrán esfuerzos de tensión en la clave y la roca puede fallar por tensión en caso de que ese esfuerzo de tensión resultara mayor que la resistencia a tensión de la roca.

Resumiendo:

Si  $(3P-Q) > R_c$  } Es la 1ª condición para que se presenten fracturas por compresión en el diámetro horizontal del túnel y fracturas de tensión en la bóveda del túnel.  
 y  $(3Q-P) < 0$  }

Si  $P > \frac{R_c+Q}{3}$  } Es la 2ª condición para que exista tensión en la clave del túnel.  
 y  $P > 3Q$  }

o sea que  $P > \frac{R_c+Q}{3} > 3Q$        $\therefore R_c > 8Q$

Si  $R_c > 8Q$  significa que no se tendrán problemas de falla de la roca ni por compresión ni por tensión.

Para una distribución de presiones externas de tipo hidrostático, o sea  $P=Q$ ; la cual se presenta en túneles con gran cobertura, estudiados por Heim, Suiza 1878, los esfuerzos normales y tangenciales pueden determinarse utilizando las expresiones de Lamé para conductos de pared gruesa sujetos a presión externa  $P$ .

$$\sigma_r = P \left(1 - \frac{a^2}{r^2}\right)$$

Formulas de Lamé.

$$\sigma_\theta = P \left(1 + \frac{a^2}{r^2}\right)$$

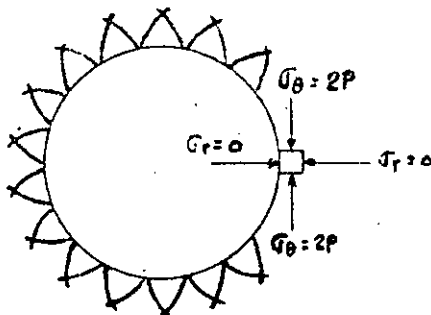
$$\tau_{\theta r} = 0$$

Para  $a=r$ :  $\sigma_\theta = 2P$  y  $\sigma_r = 0$ ; en toda la periferia del túnel.

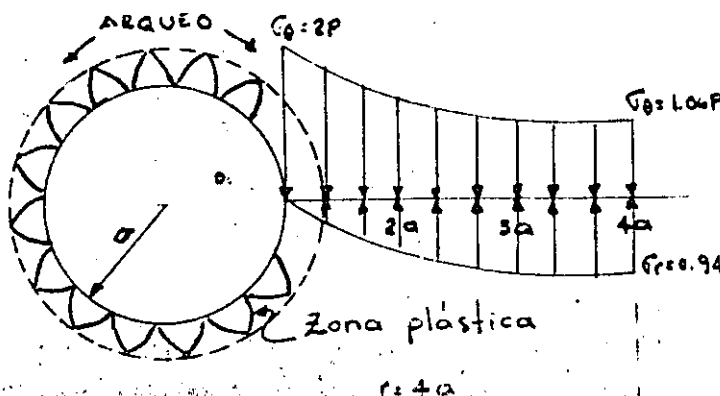
Para  $r=4a$ :  $\sigma_\theta = P \left(1 + \frac{a^2}{16a^2}\right) = 1.06P$  y

$$\sigma_r = P \left(1 - \frac{a^2}{16a^2}\right) = 0.94P$$

De acuerdo con esta hipótesis la distribución de esfuerzos en el túnel será:



2 familias de fallas que delimitan los bloques fallados: cuando  $2P > R_c$  se presenta el fenómeno de roca explosiva ya que el bloque queda suelto y es expulsado (rock-burst). La explosión de estos bloques libera mucha energía.



El comportamiento de la roca es elástico si  $2P < R_c$ , pero si el material se fractura el comportamiento de la roca en la periferia del túnel es plástico, formándose un anillo de material fracturado de propiedades mecánicas muy bajas, de manera que los esfuerzos se "arquean" o "puentean" librándose la zona fracturada apoyándose en la roca más lejana del túnel.



Variación del esfuerzo tangencial para el caso  $Q = \frac{P}{3}$

Para:  $\theta = 0^\circ$  y  $r = a$  ;  $\sigma_\theta = 2.67 P$

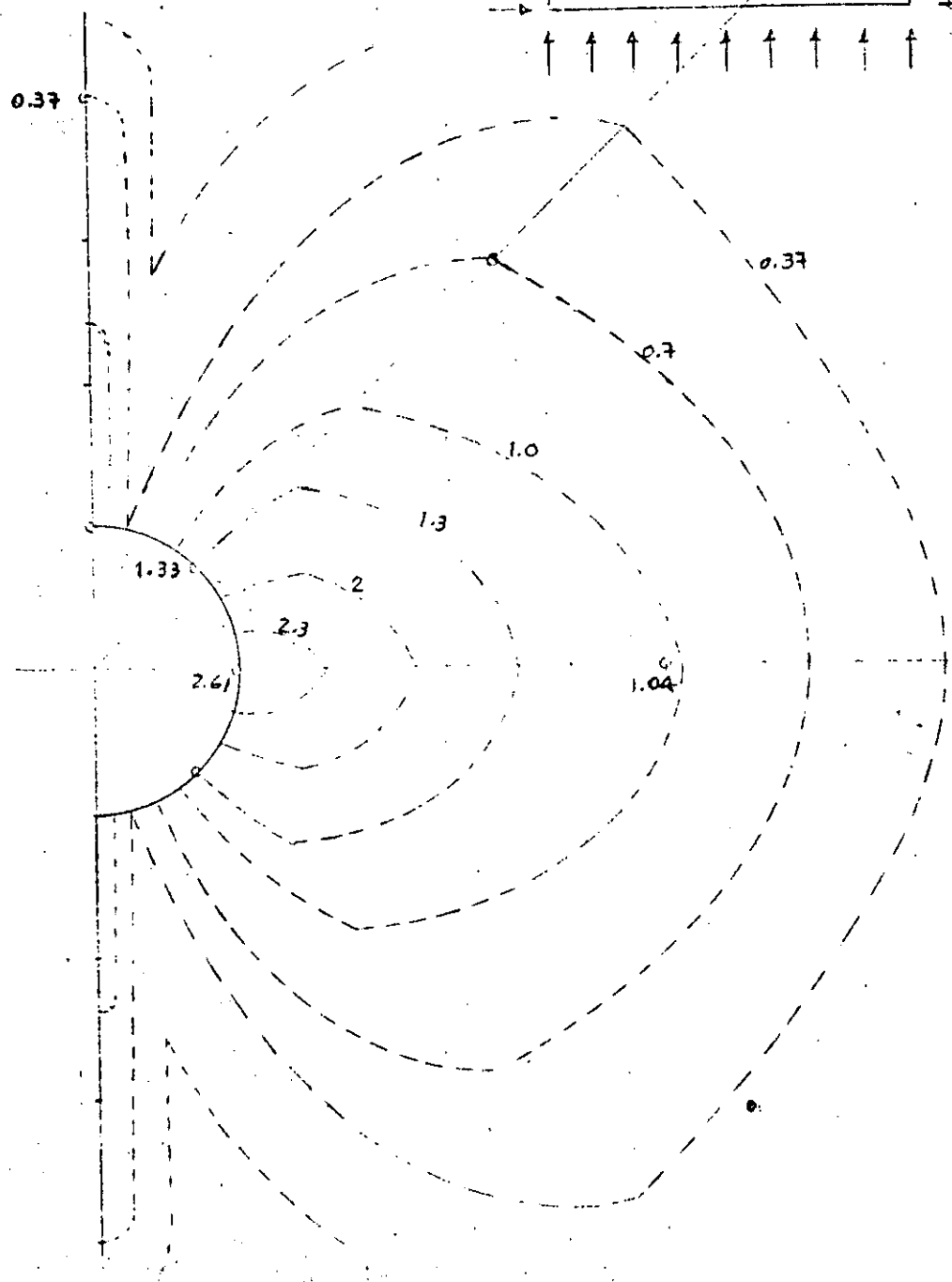
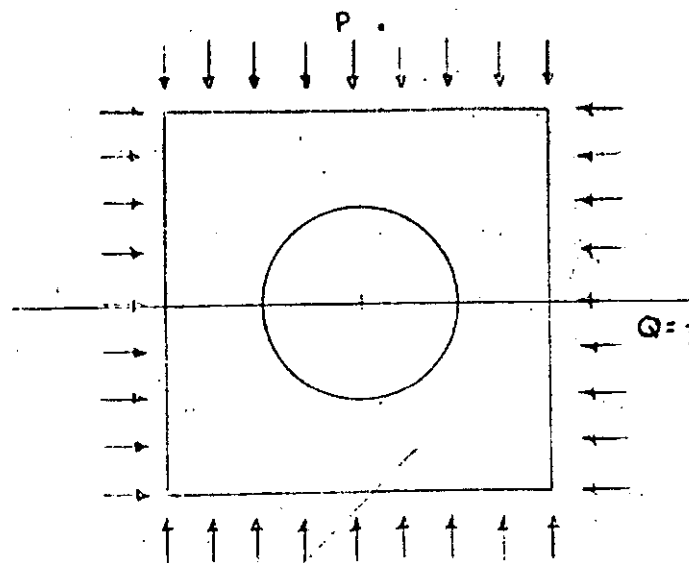
$\theta = 0^\circ$  y  $r = 4a$  ;  $\sigma_\theta = 1.04 P$

$\theta = 90^\circ$  y  $r = a$  ;  $\sigma_\theta = 0$

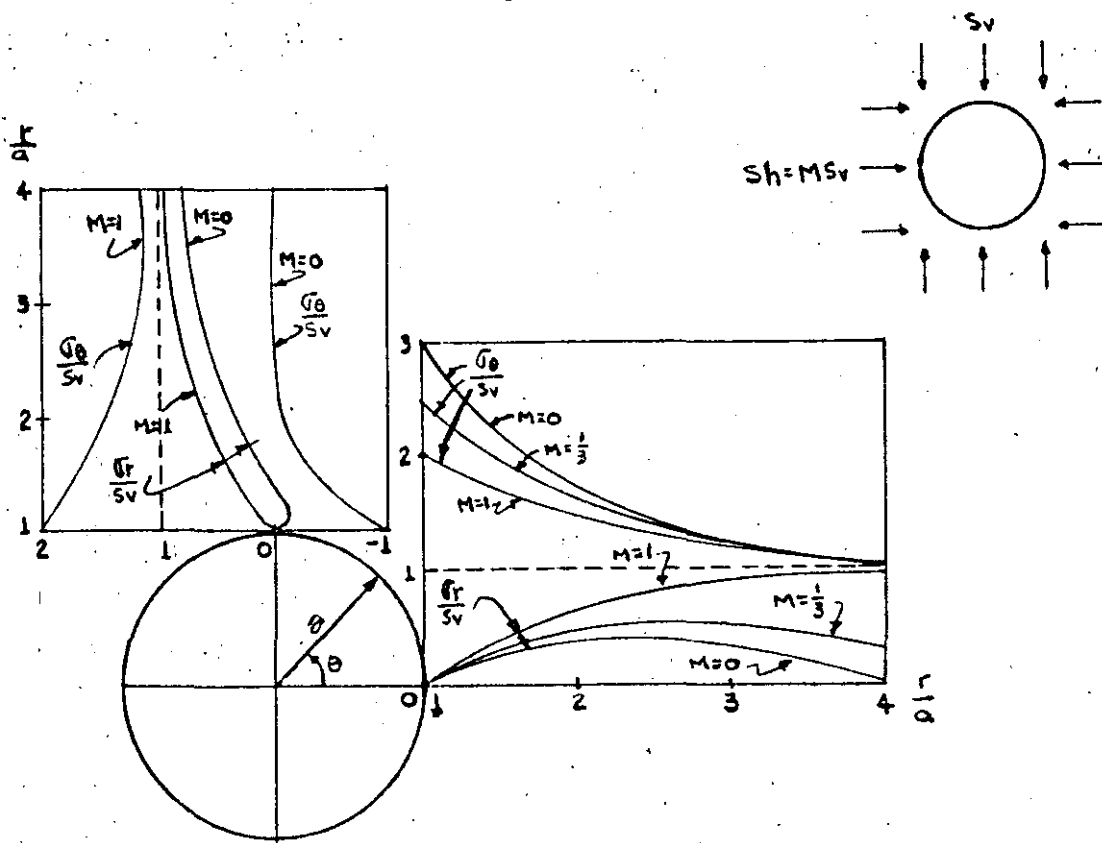
$\theta = 90^\circ$  y  $r = 4a$  ;  $\sigma_\theta = 0.37 P$

$\theta = 45^\circ$  y  $r = a$  ;  $\sigma_\theta = 1.33 P$

$\theta = 45^\circ$  y  $r = 4a$  ;  $\sigma_\theta = 0.71 P$

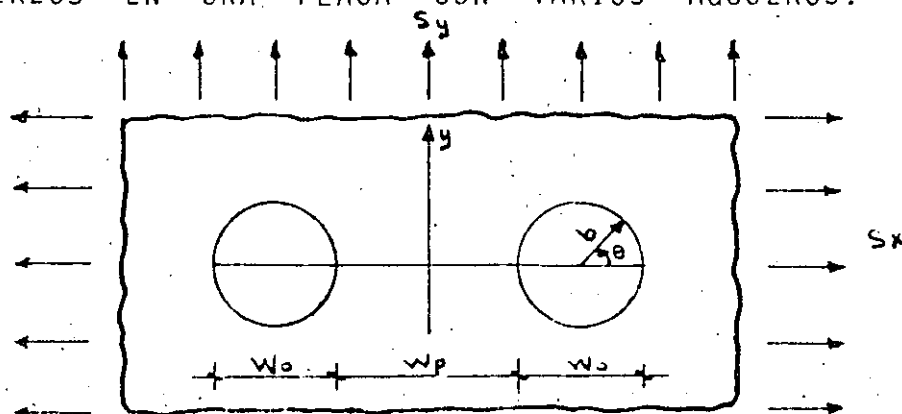


### CONCENTRACION DE ESFUERZOS EN UN AGUJERO CIRCULAR PARA UN ESTADO BIAxIAL DE ESFUERZOS DE CAMPO



Las concentraciones de esfuerzos con signo positivo significa que son del mismo signo que los esfuerzos exteriores aplicados. Cuando las concentraciones de esfuerzos tienen signo negativo significa que son de signo contrario a los esfuerzos exteriores aplicados.

### ESFUERZOS EN UNA PLACA CON VARIOS AGUJEROS.



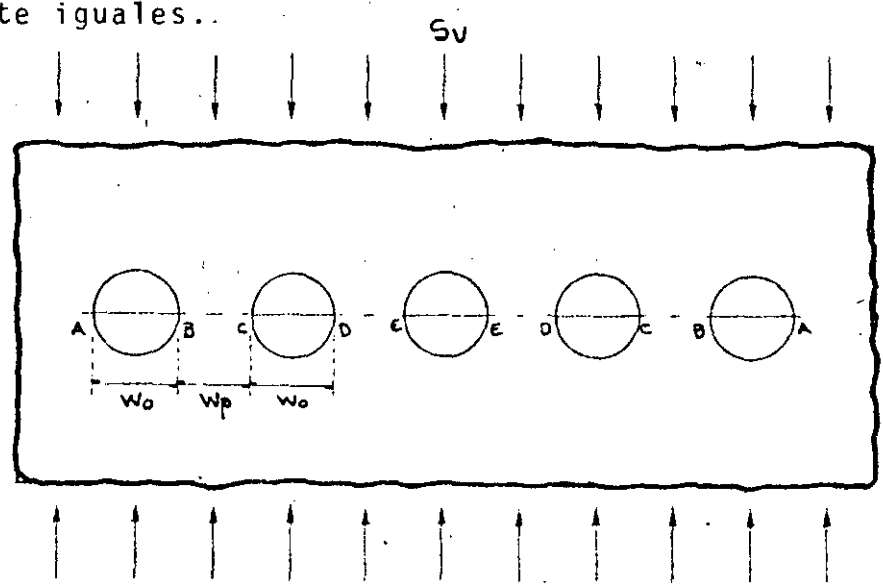
Caso:	$S_x = S_y$		$S_y \neq 0 ; S_x = 0$		$S_y = 0 ; S_x \neq 0$
Esfuerzo	$\frac{\sigma_\theta}{S_y}$		$\frac{\sigma_\theta}{S_y}$		$\frac{\sigma_\theta}{S_y}$
$\frac{W_p}{W_o}$	$\theta = 0^\circ$	$\theta = \pi$	$\theta = 0^\circ$	$\theta = \pi$	$\theta = \pm \frac{\pi}{2}$
0	2.894	0.000	3.859	0.000	2.569
0.5	2.255	2.887	3.151	3.264	2.623
1.0	2.158	2.411	3.066	3.020	2.703
2.0	2.080	2.155	3.020	2.992	2.825
4.0	2.033	2.049	3.004	2.997	2.927
7.0	2.014	2.018	3.001	2.999	2.970
10.0	2.000	2.000	3.000	3.000	3.000

La concentración de esfuerzos para el caso de dos agujeros -- alineados es considerablemente menor que el resultante de un número infinito de agujeros alineados.

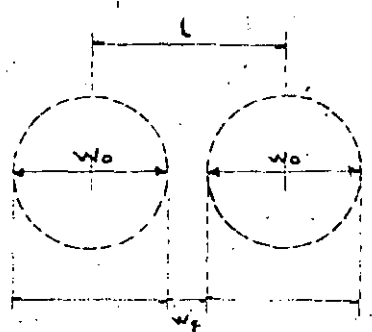
Los esfuerzos en el pilar aumentan a infinito cuando el ancho del pilar disminuye. Por lo tanto, relaciones  $W_p / W_o$  pequeñas deberán evitarse en excavaciones subterráneas. (Resultados de Ling Chih-Bing "On the stresses in a plate containing two circular holes" Journal Applied Physics, January 1948.

### ESFUERZOS EN UNA PLACA CON CINCO AGUJEROS

La distribución de esfuerzos en la periferie de 5 agujeros circulares con igual espaciamiento fue estudiado por Duvall para varias relaciones  $W_o/W_p$ . Las máximas concentraciones de esfuerzos ocurren para los puntos A, B,C,D y E. Obsérvese que las concentraciones de esfuerzos en D y E son prácticamente iguales..



$\frac{W_o}{W_p}$	A	B	C	D	E
1.07	3.29	3.29	3.29	3.29	3.29
2.21	3.63	3.72	3.89	4.03	4.03
2.96	3.53	4.08	4.22	4.39	4.39
4.35	3.96	5.12	5.22	5.28	5.28

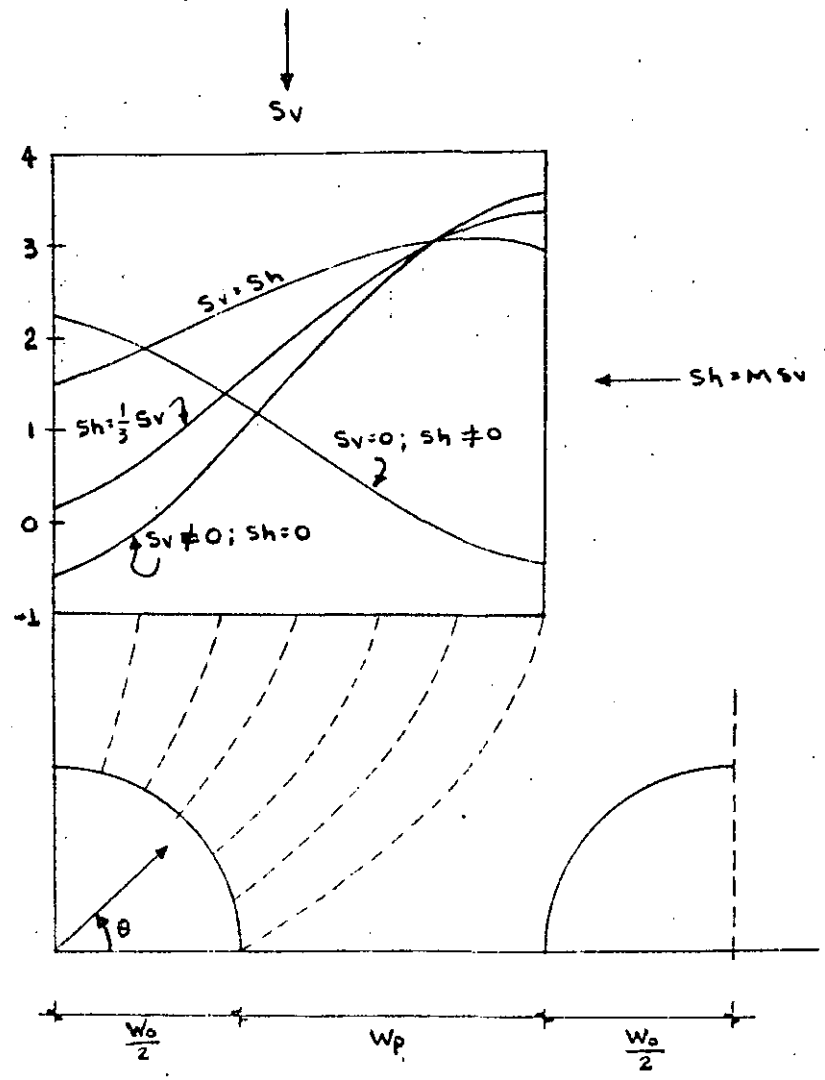


Si  $W_p = \frac{W_o}{4} \quad l = W_o + \frac{W_o}{4} = \frac{5}{4} W_o$   
 La relación de áreas  $\frac{l}{W_p} = \frac{l}{\frac{W_o}{4}} = \frac{5 W_o}{4} = \frac{20}{4} = 5$

Por lo tanto el esfuerzo en  $W_p$  es por lo menos 5 veces mayor que  $S_v$ .

CONCENTRACION DE ESFUERZOS EN DOS AGUJEROS CIRCULARES

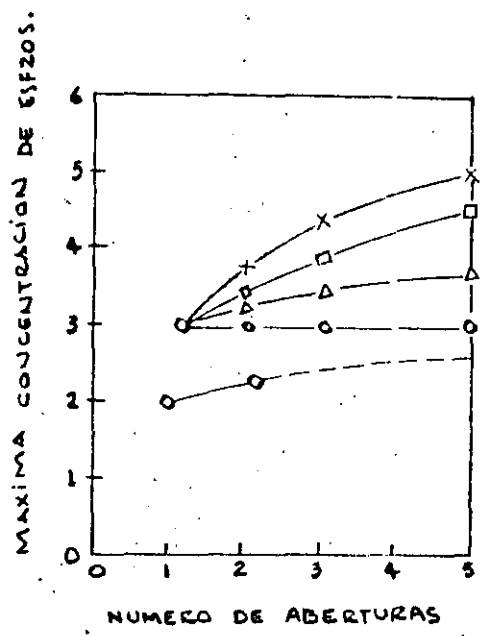
$W_o/W_p = 1$



Para cada uno de los esfuerzos de campo analizados, la concentración de esfuerzos de compresión crítica para  $\theta=0^\circ$  es mayor para el caso de varios agujeros que para un solo agujero, la mayor diferencia ocurre para esfuerzos de campo de tipo hidrostático ( $S_h = S_v$ ).

Una concentración crítica de esfuerzos de tensión ocurre solamente para  $\theta=90^\circ$  para el caso de esfuerzos de campo uniaxial ( $S_x=0$  y  $S_y \neq 0$ ).

CONCENTRACIONES MAXIMAS DE ESFUERZOS PARA VARIAS -  
RELACIONES ANCHO DE ABERTURA A ANCHO DE PILAR RELA-  
CIONADAS TAMBIEN CON EL NUMERO DE ABERTURAS.



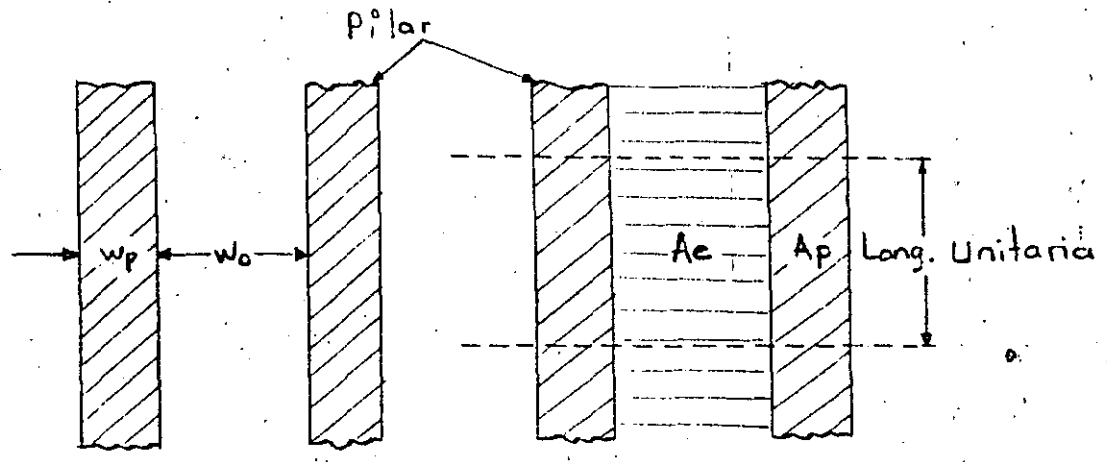
LEYENDA

$\frac{W_o}{W_p}$	SIMBOLO
1	o
2	Δ
3	□
5	x

Obsérvese que cuando el número de aberturas tiende a infinito el valor de la máxima concentración de esfuerzos es solo 15% mayor que para el caso de presión hidrostática ( $S_v = S_h$ ).

DISEÑO DE PILARES

Cuando la longitud de los pilares es grande comparada contra el ancho de la abertura entre los mismos, se considera entonces un estado de esfuerzos de campo bidimensional.



Para un número infinito de pilares con ancho  $W_p$  separados por aberturas con ancho  $W_o$ , el "esfuerzo promedio en el pilar"  $\bar{S}_p$ , se obtiene suponiendo que un pilar soporta uniformemente sobre su plano medio el peso de la roca existentes sobre el pilar más la mitad de la abertura de cada lado del pilar.

$$\bar{S}_p = \frac{W_p + W_o}{W_p} S_v$$

o sea:  $\bar{S}_p \cdot A_p = S_v (A_e + A_p) \quad \therefore \bar{S}_p = S_v \frac{A_t}{A_p}$

en donde:  $\bar{S}_p$  = esfuerzo promedio en el pilar

$A_e$  = área excavada

$A_p$  = área del pilar

$A_t = A_e + A_p$  = área total

Esto significa que el esfuerzo promedio en un pilar para un sistema de aberturas puede obtenerse a partir del área del pilar y el área total dentro de los límites minables.

Para un sistema de aberturas paralelas separadas por  $N$  pilares donde el ancho de la abertura es  $W_o$ , el ancho del pilar es  $W_p$  y la longitud de las aberturas y pilares es  $L_p$ , el área excavada esta dada por:

$$A_e = L_p \cdot W_o \cdot N$$

y el área del pilar esta dada por:  $A_p = L_p \cdot W_p \cdot N$  de donde el esfuerzo promedio en el pilar es:

$$S_p = S_v \frac{W_p + W_o}{W_p}$$

La relación de extracción  $R_a$  se define como la relación entre el área excavada y el área total:

$$R_a = \frac{A_e}{A_t} = \frac{A_t - A_p}{A_t} = 1 - \frac{A_p}{A_t} ; \frac{A_t}{A_p} = \frac{1}{1 - R_a}$$

El esfuerzo promedio en los pilares puede determinarse a partir de la relación de extracción Ra; desde  $\bar{S}_D = S_v \frac{A_t}{A_D}$ .

$$S_p = S_v \left( \frac{1}{1 - R_a} \right) \dots\dots\dots(a)$$

O, bien:

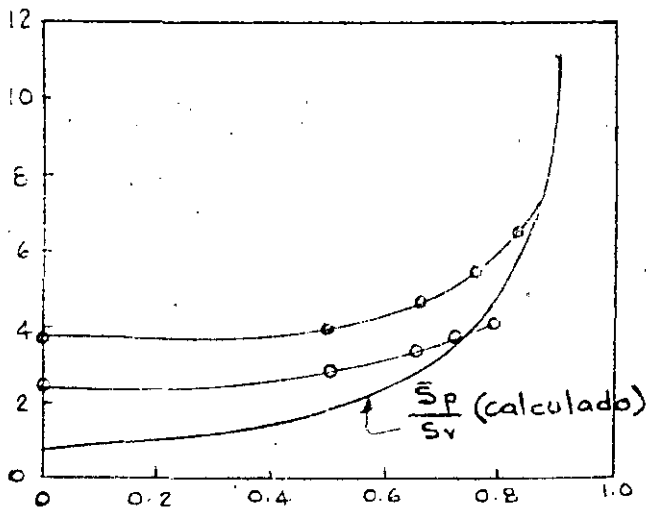
$$R_a = 1 - \frac{S_v}{S_p} \dots\dots\dots(b)$$

Para relaciones de extracción mayores de 75% el esfuerzo promedio en el pilar y la máxima concentración de esfuerzos son iguales, de aquí que la ecuación (b) puede ser reescrita como una ecuación de diseño para pilares sustituyendo  $\frac{S_D}{S_v}$  por  $\frac{C_p}{F_s \cdot S_v}$ ; donde  $\frac{C_p}{F_s}$  es la carga de seguridad del pilar.

esto es:  $R_a = 1 - \frac{S_v}{C_D} \times F_s$

Si la relación de extracción es menor de 75% el esfuerzo promedio y la máxima concentración de esfuerzos en el pilar  $\frac{\bar{S}_p}{S_v}$  puede ser sustituida en (a) por:  $\frac{\sigma_0 \text{ máx}}{S_v}$  y  $\frac{\sigma_0 \text{ máx}}{S_v}$  deberá sustituirse por  $\frac{C_p}{S_v} \times F_s$  para dar la ecuación (b).

El valor de  $\frac{\sigma_0 \text{ máx}}{S_v}$  para cualquier relación de extracción puede obtenerse de la gráfica siguiente:



- Cinco óvalos  $\frac{H_0}{w_0} = 0.5$
- Cinco círculos

Relación de extracción Ra.

Ra	$w_0/w_p$	$w_D/w_0$
0.3	$w_0 = w_p$	$w_D = w_0$
0.5	$w_0 = 2w_p$	$w_D = \frac{1}{2} w_0$
0.67	$w_0 = 4w_p$	$w_D = \frac{1}{4} w_0$
0.71	$w_0 = 5w_p$	$w_D = \frac{1}{5} w_0$



## RESISTENCIA EN COMPRESION DE PILARES

La resistencia en compresión de pilares se determina a partir de la resistencia en compresión simple de especímenes de laboratorio corrigiéndose por esbeltez.

Se utiliza para ello la siguiente expresión que es válida para relaciones de esbeltez  $(\frac{h}{d})$  desde 0.25 a 4.0.:

$$C_s = C_1 [0.778 + 0.222 (\frac{d}{h})] \text{----- (b)}$$

en donde:  $C_1$  = Resistencia en compresión simple para especímenes con  $\frac{d}{h} = 1$ .

$C_s$  = Resistencia en compresión simple de especímenes con  $\frac{d}{h} \neq 1$

$d$  = Diámetro del espécimen

$h$  = Altura del espécimen

La resistencia en compresión de un pilar en roca masiva elástica puede calcularse con la misma expresión substituyendo  $d$  y  $h$  por  $H_p$  y  $W_p$ :

$$C_p = C_1 [0.778 + 0.222 (\frac{W_p}{H_p})] \text{----- (b)}$$

en donde  $W_p$  = Ancho del pilar

$H_p$  = Altura del pilar

El resultado así obtenido deberá estar del lado conservador tomando en cuenta los siguientes aspectos.

- 1.- La resistencia en compresión de un espécimen de sección transversal  $W \times L$  y  $W < L$  como la del pilar es mayor que la de un espécimen de sección circular con diámetro  $W$ .

- 2.- Si las superficies del pilar son cóncavas en caso de que estén formados por aberturas circulares, la resistencia del pilar pudiera ser algo mayor que la resistencia de pilares con paredes rectas.
- 3.- El extremo empotrado de un pilar formado en roca continua pudiera ser mayor que las restricciones laterales que se tienen en una prueba normal de compresión simple.
- 4.- La ecuación (b) no da un aumento tan grande en la resistencia del pilar para diferentes relaciones de  $W_p/H_p$  como las dadas por otras fórmulas P.ej. si  $C_p = C_c \left(\frac{W_p}{H_p}\right)^{\frac{1}{2}}$  -- donde  $C_c$  es igual a la resistencia en compresión de un espécimen cúbico; para un pilar con relación  $W_p/H_p = 4$ . el incremento en la resistencia para un pilar cúbico pudiera ser el doble mientras que con la expresión (b) resulta de 1.66 veces.

#### NOTAS

(1) Habrá que tomar en cuenta para considerar el "ancho efectivo de un pilar" el efecto del fracturamiento producido por los explosivos. Se ha observado y medido que la roca fracturada alcanza hasta 1 m. desde la superficie del pilar.

En el caso de explotación de minerales conviene utilizar voladuras de precorte para preservar la sanidad de la roca y el costo adicional de la voladura por aumento de barrenación y explosivos se compensa con un aumento de explotación de mineral.

En la explotación de minerales usualmente las metas se encaminan a una obtención de mineral tan alta como sea posible y que sea compatible con la seguridad.

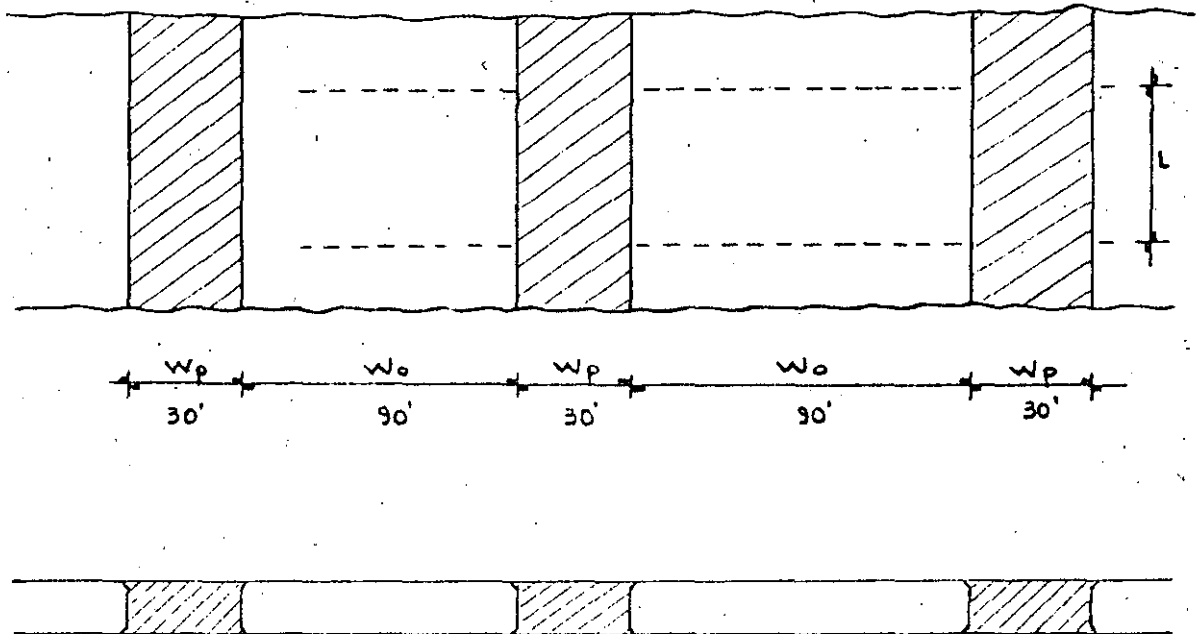
Un sistema de explotación a base de "pilares continuos" pudiera no ser la mejor manera de alcanzar el objetivo anterior.

Por ejemplo: considerando un depósito en forma de un estra

to de 15' de espesor; a causa del fracturamiento de los explosivos el espesor efectivo del pilar pudiera ser de 9'.

Sin embargo, si la relación altura-ancho ( $\frac{H_p}{W_p}$ ) decrece a  $\frac{1}{2}$  haciendo  $W_p=30'$ ; para una relación de extracción de 75% (valor nominal para mineo en roca dura) el ancho del salón deberá tener 90', un claro que pudiera ser minado solamente en roca excepcionalmente competente.

Por otro lado, si se utilizara un arreglo tridimensional de pilares, la relación de extracción de 75% pudiera alcanzarse en el mismo depósito con salones y cruceros con ancho de solo 30'.



$$Ra = 1 - \frac{A_p}{A_t} ; \quad Ra = 1 - \frac{30 \cdot L}{(90+30) L} = 1 - 0.25 = 0.75$$

### Arreglo tridimensional de pilares.

Mientras que en los pilares contínuos la relación longitud a -- ancho del pilar es muy grande, en un arreglo tridimensional de pilares esta relación es de 1 o algo mayor de 1.

El estudio matemático tridimensional de estos pilares es com-- plejo y hay poca información de modelos fotoelásticos tridimen-- sionales. Sin embargo, haciendo ciertas suposiciones este caso tridimensional puede aproximarse a los resultados teóricos y ex-- perimentales del caso bidimensional de pilares contínuos y una ecuación de diseño puede establecerse.

Las suposiciones son las siguientes: (1) en un arreglo tridimen-- sional de pilares, los pilares soportan la carga total de cover-- tura de roca uniformemente en su sección transversal y el es--- fuerzo promedio en el pilar puede ser calculado por la ecuación  $\bar{S}_p = S_v \frac{A_t}{A_p}$  siempre y cuando haya por lo menos 4 pilares en un sa-- lón, con los pilares extremos algo menos esforzados que los pi-- lares centrales, (2). La relación de extracción debe ser algo mayor de 75%, valor que es consistente con la práctica minera. En este caso la concentración de esfuerzos promedio en el pilar puede determinarse por la expresión  $\bar{S}_p = S_v \left( \frac{1}{1 - R_a} \right)$ .

si estas condiciones se satisfacen, el esfuerzo promedio en el - pilar y la ecuación de diseño para pilares contínuos son satis-- factorias para el diseño de pilares con arreglo tridimensional como sigue:

$$S_p = S_r \left( \frac{1}{1 - R_a} \right) \quad \text{y} \quad R_a = 1 - \frac{F_s \times S_v}{C_p}$$

en donde para este caso  $C_p$  es la resistencia en compresión del pilar corregida por esbeltez con la mínima dimensión de la sección transversal como ancho del pilar.

Para un sistema de arreglo aleatorio de pilares y de forma irregular, el área de los pilares  $A_p$  y el área excavada  $A_e$  puede evaluarse por integración gráfica del área total minada.

Para un sistema de pilares con forma regular y con los arreglos que se muestran en la siguiente figura, el área minada total puede considerarse compuesta por  $N$  elementos idénticos de área  $(W_o + W_p) (L_p + W_o)$ , esto es:

$$A_t = N(W_o + W_p) (L_p + W_o)$$

el área total de pilares es:

$$A_p = N(W_p \cdot L_p)$$

Por lo tanto el área excavada será:

$$A_e = N[(W_o + W_p) (L_p + W_o) - W_p \cdot L_p]$$

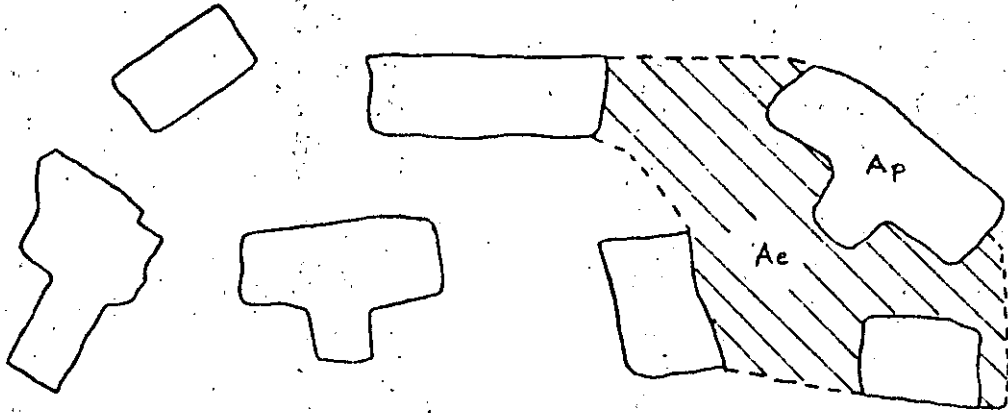
y la relación de extracción:

$$R_a = \frac{A_e}{A_t} = 1 - \frac{W_p \cdot L_p}{(W_o + W_p) (L_p + W_o)} = 1 - \frac{A_p}{A_t}$$

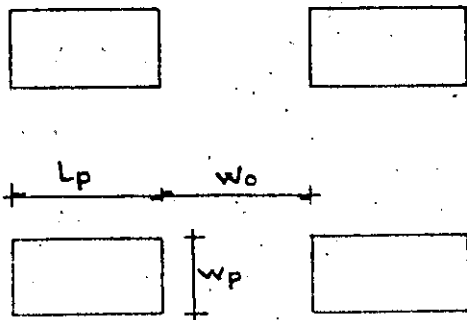
Verificando la expresión para un sistema de pilares con  $W_o = L_p$  se tiene:

$$R_a = 1 - \frac{W_p^2}{4W_p^2} = 0.75$$

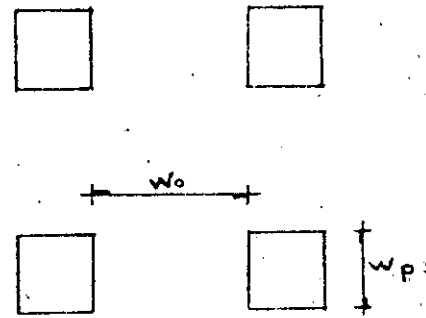
ARREGLO TRIDIMENSIONAL DE PILARES



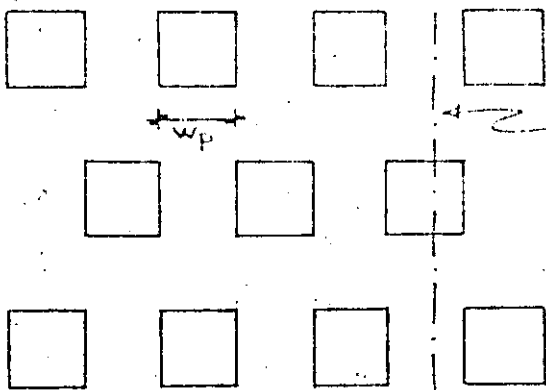
(a) Arreglo Irregular



(b) Pilares rectangulares regularmente espaciados



(c) Pilares cuadrados regularmente espaciados



(d)

Pilares cuadrados, regularmente espaciados con  $W_o = W_p$ .

## DISEÑO DE MÚLTIPLES ABERTURAS EN ROCA COMPETENTE

CONCLUSIONES

Las principales conclusiones pertinentes sobre el diseño de pilares continuos son:

- 1.- La máxima concentración de esfuerzos que se desarrolla sobre las paredes de los pilares de una serie de aberturas horizontales paralelas son dependientes básicamente de la componente vertical de esfuerzos externos.
- 2.- La máxima concentración de esfuerzos de tensión que se desarrolla en el techo y piso de un sistema de múltiples aberturas en un campo de esfuerzo uniaxial, decrece con la aplicación de un esfuerzo horizontal que generalmente es de compresión con  $S_h = \frac{1}{3} S_v$ .
- 3.- Para 5 ó mas aberturas en roca elástica la máxima concentración de esfuerzos de compresión son iguales con excepción -- de las orillas de los agujeros extremos, en las cuales la -- concentración de esfuerzos es menor.
- 4.- En la mayor parte de las operaciones de mineo en las cuales  $m = 1/3$  el problema de diseño de múltiples aberturas se reduce al diseño de pilares de soporte estables.

# TUBERIAS DE PRESION

1.- Esfuerzos alrededor de túneles y galerías ocasionados por presión hidrostática dentro del conducto.

Los esfuerzos analizados serán aquellos inducidos en la masa de roca por la presión hidrostática o hidrodinámica,  $p_i$ , del agua, fluido o gas llenando el túnel, galería o cavidad.

Los análisis de estos esfuerzos usualmente parten de la teoría de esfuerzos en tubos de pared gruesa, la cual es extendida al caso de túneles no revestidos (Jaeger, 1933 y 1949).

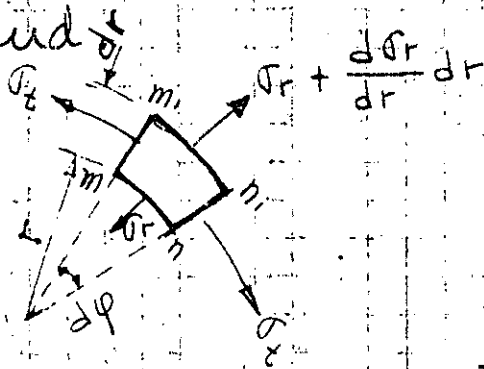
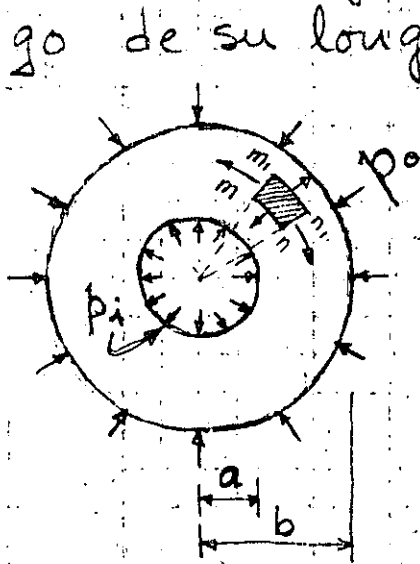
La teoría de esfuerzo-deformación y mediciones en túneles circulares bajo una carga radial (Seeber 1961) aplicada a lo largo de la circunferencia total de un túnel (técnica Austriaca sobre pruebas en roca) puede fácilmente relacionarse a las ecuaciones obtenidas para túneles presurizados.

Similarmente estas ecuaciones pueden ser utilizadas para establecer el techo de roca seguro sobre un túnel bajo presión  $p_i$  (Jaeger 1961). Finalmente, las ecuaciones básicas pueden utilizarse en la teoría de las ondas de ariete hidráulico que se desarrollan en túneles y lumbreras.



## 2. Teoría de tubos elásticos de pared gruesa.

Si un cilindro circular cuya pared tiene un espesor constante está sujeto a la acción de presiones interna y externa, uniformemente distribuidas, la deformación que se produce es simétrica alrededor del eje del cilindro y no varía a lo largo de su longitud.



Consideraremos un anillo separado del cilindro mediante dos planos perpendiculares a su eje y

separados por la unidad de distancia.

Por simetría en las caras de un elemento  $-mm_1, nn_1$  separado por dos planos axiales y dos superficies cilíndricas concéntricas, no existen esfuerzos constantes. Sea  $\sigma_t$  el esfuerzo tangencial normal a las caras  $mm_1$  y  $nn_1$  del elemento, y  $\sigma_r$  el esfuerzo normal radial en la cara  $m, n$ . Este esfuerzo es función del radio  $r$  y varía en  $\frac{d\sigma_r}{dr} dr$  cuando  $r$  varía en  $dr$ . El esfuerzo radial en la cara  $m, n_1$  es por tanto  $\sigma_r + \frac{d\sigma_r}{dr} dr$

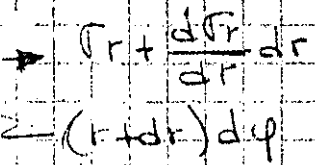
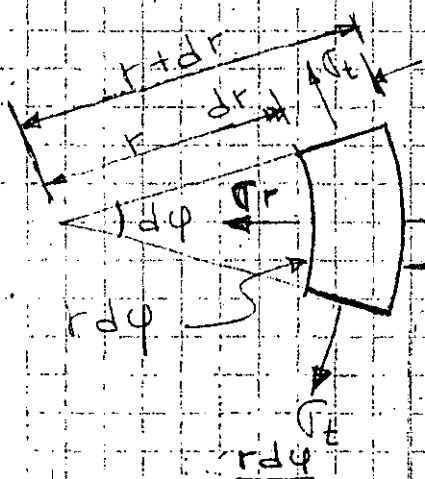
Sumando las proyecciones de las fuerzas que actúan sobre el elemento en dirección de la bisectriz del ángulo  $-d\varphi-$ , se obtiene la ecuación de equilibrio siguiente:

$$\sigma_r \cdot r d\varphi + \sigma_t \cdot dr d\varphi - \left( \sigma_r + \frac{d\sigma_r}{dr} \right) (r+dr) d\varphi = 0 \dots (a)$$

$$\sigma_r \cdot r + \sigma_t \cdot dr - \sigma_r \cdot r - r \frac{d\sigma_r}{dr} - \sigma_r dr - \frac{d\sigma_r}{dr} dr = 0$$

Despreciando cantidades de orden superior:

$$\sigma_t - \sigma_r - r \frac{d\sigma_r}{dr} = 0 \dots (b)$$



Proyección de  $\sigma_t$ :  
 $2 \left( \sigma_t \cdot dr \cdot \sin \frac{d\varphi}{2} \right)$

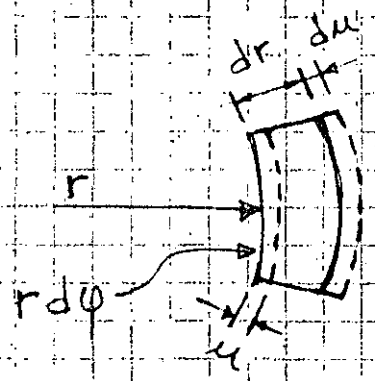
$$2 \left( \sigma_t \cdot dr \cdot \frac{r d\varphi}{r} \right) = \sigma_t \cdot dr \cdot d\varphi$$

Nota: Ver inciso 1, Apéndice 1. (Pág. 77)

Esta ecuación tiene dos incógnitas,  $\sigma_t$  y  $\sigma_r$ .

Es necesaria otra ecuación

y se obtiene considerando la deformación del cilindro.



La deformación es simétrica respecto al eje y consiste en un corrimiento radial de todos los puntos de la pared del cilindro. Este corrimiento es constante en dirección circunferencial, pero varía a lo largo

del radio; es decir, es una función del radio. Representando con  $u$  al corrimiento de la superficie cilíndrica de radio  $r$ , el corrimiento para la superficie  $r+dr$  será:  $u + \frac{du}{dr} dr$

Por consiguiente, un elemento tal como  $mnm, n$ , experimenta en sentido radial un alargamiento total  $\frac{du}{dr} dr$  y un alargamiento unitario en dicha dirección es:  $\epsilon_r = \frac{du}{dr}$   $\frac{du}{dr} dr =$  diferencial total de una función.

El alargamiento unitario del mismo elemento en dirección tangencial es igual al alargamiento unitario del radio correspondiente; es decir  $\epsilon_t = \frac{u}{r}$

Nota: Ver inciso 2 de apéndice 1. (Pag. 77)

Mediante las ecuaciones de esfuerzos para el caso de extensión o compresión en dos direcciones perpendiculares en función de los alargamientos unitarios. (Ecuaciones de compatibilidad elástica):

$$\sigma_y = \frac{E}{1-\nu^2} (\epsilon_y + \nu \epsilon_x) \quad \text{y} \quad \sigma_x = \frac{E}{1-\nu^2} (\epsilon_x + \nu \epsilon_y)$$

Sustituyendo tenemos:

$$\sigma_r = \frac{E}{1-\mu^2} \left( \frac{du}{dr} + \mu \frac{u}{r} \right) \dots (c) \quad \text{y} \quad \sigma_t = \frac{E}{1-\mu^2} \left( \frac{u}{r} + \mu \frac{du}{dr} \right) \dots (d)$$

Los esfuerzos normales  $\sigma_r$  y  $\sigma_t$  dependen por consiguiente del corrimiento  $u$ . Sustituyendo las expresiones (c) y (d) en (b), se obtiene la ecuación siguiente en  $u$ : (Ver inciso 3, Apéndice 1, Pag. 78)

$$\frac{d^2 u}{dr^2} + \frac{1}{r} \frac{du}{dr} - \frac{u}{r^2} = 0 \dots (e)$$

$$\frac{d^2u}{dr^2} + \frac{1}{r} \frac{du}{dr} - \frac{u}{r^2} = 0 \dots (e)$$

La solución general de esta ecuación es:

$$u = C_1 \cdot r + \frac{C_2}{r} \dots (f) \quad \text{Nota: Ver inciso 4, Apéndice 1 (Pag. 79)}$$

lo cual puede comprobarse sustituyendo en la ecuación diferencial (e). Nota: Ver inciso 5, Apéndice 1, Pág 80

Las constantes  $C_1$  y  $C_2$  se determinan por las condiciones de frontera en las superficies interior y exterior del cilindro en las que los esfuerzos normales son conocidos y son iguales a las presiones actuantes.

Sustituyendo (f) en las ecuaciones (c) y (d).

Ver inciso 6, Apéndice 1, Pág. 81

se tiene:  $\sigma_r = \frac{E}{1-\mu^2} \left[ C_1(1+\mu) - C_2 \frac{1-\mu}{r^2} \right] \quad (g)$

y  $\sigma_t = \frac{E}{1-\mu^2} \left[ C_1(1+\mu) + C_2 \frac{1-\mu}{r^2} \right] \quad (h)$

Si  $p_i$  y  $p_o$  representan las presiones interna y externa respectivamente, las condiciones en las superficies exterior e interior del cilindro son:

para  $r=b$ ;  $\sigma_r = -p_o$  y para  $r=a$   $\sigma_r = -p_i$

El signo del segundo miembro de cada ecuación es negativo porque se toman como positivos los esfuerzos normales de tensión.

Si el espesor es pequeño, no hay gran diferencia entre los valores máximo y mínimo de  $\sigma_t$ . Si por ejemplo,  $b = 1.1a$ ,  $\sigma_{t \text{ máx}}$  excede a  $\sigma_{t \text{ mín}}$  en un 10.5%. Se ve, por consiguiente, que no se comete grave error suponiendo que el esfuerzo  $\sigma_t$  se distribuye uniformemente a lo largo del espesor de la pared. Y empleando la ecuación

$$\sigma_t = \frac{p_i a}{b-a}, \text{ coincide con la ecuación para cilindros delgados}$$

El esfuerzo cortante máximo en la superficie interior del cilindro es

$$\tau_{\text{máx}} = \frac{\sigma_t - \sigma_r}{2} = \frac{1}{2} \left[ \frac{p_i (a^2 + b^2)}{b^2 - a^2} + \frac{p_i (b^2 - a^2)}{b^2 - a^2} \right]$$

$$\therefore \tau_{\text{máx}} = - \frac{p_i b^2}{b^2 - a^2} \quad (k)$$

Cuando actúa solamente sobre el cilindro una presión exterior, o sea que  $p_i = 0$  las ecuaciones (i) y (j) dan

$$\sigma_r = - \frac{p_o b^2}{b^2 - a^2} \left( 1 - \frac{a^2}{r^2} \right) \quad (l) \quad \sigma_t = - \frac{p_o b^2}{b^2 - a^2} \left( 1 + \frac{a^2}{r^2} \right) \quad (m)$$

En este caso  $\sigma_r$  y  $\sigma_t$  son ambos esfuerzos de compresión y  $\sigma_t$  es siempre numéricamente mayor que  $\sigma_r$ . El esfuerzo de compresión máximo se presenta en la superficie interior del cilindro donde  $r = a$ ,  $\sigma_{t \text{ máx}} = - \frac{2 p_o b^2}{b^2 - a^2} \quad (n)$

Consideremos ahora la deformación del cilindro. Sustituyendo las expresiones de las constantes arbitrarias  $C_1$  y  $C_2$  en (f) tenemos:

$$u = \frac{1-\mu}{E} \cdot \frac{a^2 p_i - b^2 p_o}{b^2 - a^2} r + \frac{1+\mu}{E} \frac{a^2 b^2 (p_i - p_o)}{(b^2 - a^2) r} \quad (o)$$

Esta ecuación da el desplazamiento radial de cualquier punto de la pared del cilindro.

Para el caso particular de un cilindro sometido solo a presión interna,  $p_o = 0$  y  $r = a$  para el desplazamiento radial en el interior del cilindro: (Ver inciso I, Apéndice 1, Pág 85)

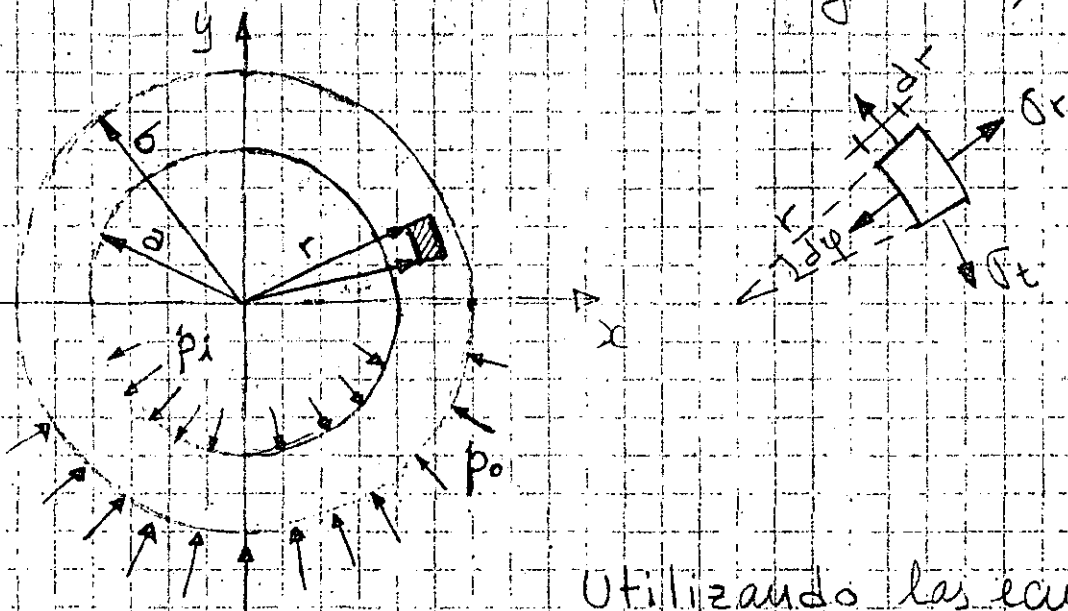
$$r = a \quad u = \frac{a p_i}{E} \left( \frac{a^2 + b^2}{b^2 - a^2} + \mu \right) \dots (p)$$

Cuando el cilindro está sometido a presión externa solamente,  $p_i = 0$ , el desplazamiento radial en la superficie exterior es: (Ver inciso II, Apéndice 1, Pág 86)

$$r = b \quad u = - \frac{b p_o}{E} \left( \frac{a^2 + b^2}{b^2 - a^2} - \mu \right) \dots (q)$$

El signo menos indica que el desplazamiento es hacia el interior del cilindro.

3. Variante en la evaluación de las constantes de integración para la determinación de los esfuerzos normales radiales y tangenciales en cilindros de pared gruesa, según Jaeger:



Utilizando las ecuaciones (g) y (h) que resuelven los esfuerzos normales radiales y tangenciales:

$$\sigma_r = \frac{E}{1-\mu^2} \left( C_1 (1+\mu) - C_2 \frac{1-\mu}{r^2} \right) \dots (g)$$

$$\sigma_t = \frac{E}{1-\mu^2} \left( C_1 (1+\mu) + C_2 \frac{1-\mu}{r^2} \right) \dots (h)$$

$$\sigma_r = \frac{E C_1 (1+\mu)}{(1-\mu)(1+\mu)} - \frac{E C_2 (1-\mu)}{(1-\mu)(1+\mu)} \cdot \frac{1}{r^2}$$

$$\sigma_r = \frac{E C_1}{1-\mu} - \frac{E C_2}{1+\mu} \cdot \frac{1}{r^2} \dots (r)$$

Substituyendo  $\mu$  por  $\frac{1}{m}$

$$\sigma_r = \frac{E C_1}{1 - \frac{1}{m}} - \frac{E C_2}{1 + \frac{1}{m}} \cdot \frac{1}{r^2}$$

$$\sigma_r = \frac{mE}{m-1} C_1 - \frac{mE}{m+1} \cdot \frac{1}{r^2} C_2 \dots (s)$$

$$\sigma_t = \frac{E}{1-\mu^2} \left( C_1 (1+\mu) + C_2 \frac{1-\mu}{r^2} \right) \dots (h)$$

$$\sigma_t = \frac{E C_1 (1+\mu)}{(1-\mu)(1+\mu)} + \frac{E C_2 (1-\mu)}{(1-\mu)(1+\mu)} \frac{1}{r^2}$$

$$\sigma_t = \frac{E C_1}{1-\mu} + \frac{E C_2}{1+\mu} \frac{1}{r^2} \dots (t)$$

Sustituyendo  $\mu$  por  $\frac{1}{m}$  :

$$\sigma_t = \frac{E C_1}{1 - \frac{1}{m}} + \frac{E C_2}{1 + \frac{1}{m}} \frac{1}{r^2}$$

$$\sigma_t = \frac{m E}{m-1} C_1 + \frac{m E}{m+1} \frac{1}{r^2} C_2 \dots (u)$$

Los esfuerzos  $\sigma_r$  y  $\sigma_t$  son ahora :

$$\sigma_r = \frac{m E}{m-1} C_1 - \frac{m E}{m+1} \frac{1}{r^2} C_2 = B' - \frac{C'}{r^2} \dots (s)$$

$$\sigma_t = \frac{m E}{m-1} C_1 + \frac{m E}{m+1} \frac{1}{r^2} C_2 = B' + \frac{C'}{r^2} \dots (u)$$

Las constantes  $C_1$  y  $C_2$  dependen de las condiciones de frontera para  $r=a$  y  $r=b$

Para el tubo de pared gruesa solicitado por presiones estáticas interna  $p_i$  y externa  $p_o$ ; resulta

$$\text{Para } r=a \quad \sigma_r = B' - \frac{C'}{a^2} = p_i$$



Para  $r=a$  ;  $\sigma_r = B' - \frac{C'}{a^2} = p_i$  ;  $B' = p_i + \frac{C'}{a^2} \dots (1)$

Para  $r=b$  ;  $\sigma_r = B' - \frac{C'}{b^2} = p_o$  ;  $B' = p_o + \frac{C'}{b^2} \dots (2)$

Restando (1) de (2):

$$p_o - p_i + \frac{C'}{b^2} - \frac{C'}{a^2} = 0$$

$$(p_o - p_i) a^2 b^2 + C' a^2 - C' b^2 = 0$$

$$\therefore C' = \frac{(p_o - p_i) a^2 b^2}{b^2 - a^2}$$

Sumando (1) y (2)

$$2 B' = p_o + p_i + \frac{1}{a^2} \frac{(p_o - p_i) a^2 b^2}{b^2 - a^2} + \frac{1}{b^2} \frac{(p_o - p_i) a^2 b^2}{b^2 - a^2}$$

$$2 B' = \cancel{p_o b^2} + \cancel{p_i b^2} - \cancel{p_o a^2} - \cancel{p_i a^2} + \cancel{p_o b^2} + \cancel{p_i b^2} + \cancel{p_o a^2} - \cancel{p_i a^2}$$

$$2 B' = \frac{2 p_o b^2 - 2 p_i a^2}{b^2 - a^2} \therefore B' = \frac{p_o b^2 - p_i a^2}{b^2 - a^2}$$

Por lo tanto, para  $r=a$  y sustituyendo en (s) y (u)

$$\sigma_r = \frac{p_o b^2 - p_i a^2}{b^2 - a^2} - \frac{(p_o - p_i) a^2 b^2}{b^2 a^2 a^2} = p_i$$

$$\sigma_t = \frac{p_o b^2 - p_i a^2}{b^2 - a^2} + \frac{(p_o - p_i) a^2 b^2}{(b^2 - a^2) a^2} = \dots (v)$$

$$= \frac{p_o b^2 - p_i a^2 + p_o b^2 - p_i b^2}{b^2 - a^2}$$

$$\sigma_t = \frac{-p_i (a^2 + b^2) + 2 p_o b^2}{b^2 - a^2} = \frac{-p_i \frac{a^2 + b^2}{b^2 a^2} + \frac{2 b^2 p_o}{b^2 - a^2}}{\dots (w)}$$

NOTA: Los valores positivos de  $\sigma_r$  y  $\sigma_t$  son de compresión.

Para;  $r = b$  y sustituyendo en (s) y (u)

$$\sigma_r = \frac{p_0 b^2 - p_i a^2}{b^2 - a^2} - \frac{(p_0 - p_i) a^2 b^2}{(b^2 - a^2) b^2} = p_0 \dots (x)$$

$$y \quad \sigma_t = \frac{p_0 b^2 - p_i a^2}{b^2 - a^2} + \frac{(p_0 - p_i) a^2 b^2}{(b^2 - a^2) b^2}$$

$$\sigma_t = \frac{p_0 b^2 - p_i a^2 + p_0 a^2 - p_i a^2}{b^2 - a^2} = \underline{\underline{-p_i \frac{2a^2}{b^2 - a^2} + p_0 \frac{a^2 + b^2}{b^2 - a^2}}}$$

(y)

En el concreto cuando  $a \leq r \leq b$ , se utilizará el índice '1' para representar sus propiedades.

Para  $r = a$

$$\sigma_{r=a} = \frac{m_1 E_1}{m_1 - 1} F_1 - \frac{m_1 E_1}{m_1 + 1} \frac{G_1}{a^2} = p \quad \dots (1)$$

Para  $r = b$   $\sigma_{r=b} = \frac{m_1 E_1}{m_1 - 1} F_1 - \frac{m_1 E_1}{m_1 + 1} \frac{G_1}{b^2} = \lambda p \quad \dots (2)$

Restando (2) de (1)

$$-\frac{m_1 E_1}{m_1 + 1} \frac{G_1}{a^2} + \frac{m_1 E_1}{m_1 + 1} \frac{G_1}{b^2} = p - \lambda p$$

$$\frac{-m_1 E_1 \cdot b^2 G_1 + m_1 E_1 \cdot a^2 G_1}{a^2 b^2 (m_1 + 1)} = p (1 - \lambda)$$

$$G_1 (m_1 E_1 a^2 - m_1 E_1 b^2) = a^2 b^2 (m_1 + 1) p (1 - \lambda)$$

$$\therefore G_1 = - \frac{m_1 + 1}{m_1 E_1} \frac{a^2 b^2}{b^2 - a^2} p (1 - \lambda)$$

Despejando  $G_1$  de (1) y (2).

$$G_1 = -p \frac{a^2 (m_1 + 1)}{m_1 E_1} + \frac{a^2 (m_1 + 1)}{m_1 E_1} \frac{m_1 E_1}{m_1 - 1} F_1$$

$$G_1 = -\lambda p \frac{b^2 (m_1 + 1)}{m_1 E_1} + \frac{b^2 (m_1 + 1)}{m_1 E_1} \frac{m_1 E_1}{m_1 - 1} F_1$$

Iguando:

$$-p \frac{a^2 (m_1 + 1)}{m_1 E_1} + \frac{a^2 (m_1 + 1)}{m_1 E_1} F_1 = -\lambda p \frac{b^2 (m_1 + 1)}{m_1 E_1} + \frac{b^2 (m_1 + 1)}{m_1 E_1} F_1$$

$$F_1 \frac{a^2}{m_1 - 1} - \frac{b^2}{m_1 - 1} F_1 = p \frac{a^2}{m_1 E_1} - \lambda p \frac{b^2}{m_1 E_1}$$

Multiplicando por (-1)

$$F_1 \frac{b^2 - a^2}{m_1 - 1} = \frac{\lambda p b^2 - p a^2}{m_1 E_1} \therefore F_1 = - \frac{m_1 - 1}{m_1 E_1} \frac{(a^2 - \lambda b^2)}{b^2 - a^2} p$$

Iguando los desplazamientos elásticos :

Para  $r = b$  y recordando  $u = C_1 r + \frac{C_2}{r}$

$$u_{r=b} = F_1 \cdot b + \frac{G_1}{b} = \underbrace{F_2 \cdot b + \frac{G_2}{b}}_{\text{Cero}}$$

$$-\frac{m_1 - 1}{m_1 E_1} \frac{(a^2 - \lambda b^2)}{b^2 - a^2} \cdot p \cdot b - \frac{m_1 + 1}{m_1 E_1} \frac{a^2 b^2}{b^2 - a^2} \frac{p(1 - \lambda)}{b} = -\frac{\lambda p b^2 (m_2 + 1)}{E_2 m_2 \times b}$$

Despejando  $\lambda$  de esta ecuación se tiene:

Ver inciso 12 de Apéndice 1 :

Pág. 87

$$\lambda = \frac{p b}{p} = \frac{\frac{2 a^2}{E_1 (b^2 - a^2)}}{\frac{m_2 + 1}{m_2 E_2} + \frac{(m_1 - 1) b^2 + (m_1 + 1) a^2}{m_1 E_1 (b^2 - a^2)}}$$

Los esfuerzos en el revestimiento de concreto son:

Para  $r = a$  ;  $\sigma_{ra} = p$

Para obtener  $\sigma_{ta}$  tenemos que sustituir las constantes  $F_1$  y  $G_1$  en la ecuación (u), con  $r = a$ .

Con  $r = a$ .

$$\sigma_t = \frac{mE}{m-1} C_1 + \frac{mE}{m+1} \frac{1}{r^2} C_2 \dots (u)$$

$$C_1 = F_1 = -\frac{m_1 - 1}{m_1 E_1} \frac{(a^2 - \lambda b^2)}{b^2 - a^2} p \quad \text{y} \quad C_2 = G_1 = -\frac{m_1 + 1}{m_1 E_1} \frac{a^2 b^2}{b^2 - a^2} p(1 - \lambda)$$

$$\text{Para } r = a \quad \sigma_t = \left( \frac{mE}{m-1} \right) \left( -\frac{m_1 - 1}{m_1 E_1} \frac{(a^2 - \lambda b^2)}{b^2 - a^2} p \right) + \left( \frac{mE}{m+1} \frac{1}{a^2} \right) \left( -\frac{m_1 + 1}{m_1 E_1} \frac{a^2 b^2 (p - \lambda p)}{b^2 - a^2} \right)$$

$$\sigma_{ta} = -\frac{a^2 p - \lambda b^2 p}{b^2 - a^2} - \frac{b^2 p - b^2 \lambda p}{b^2 - a^2}$$

$$\sigma_{ta} = -\frac{a^2 + b^2 - 2\lambda b^2}{b^2 - a^2} p$$

60

Para  $r = b$  ;  $\sigma_{rb} = \lambda p$

Para obtener  $\sigma_{tb}$ , sustituimos las constantes  $F_1$  y  $G_1$  en la ecuación (u):

con  $r = b$

$$\sigma_{tb} = \left( \frac{mE}{m+1} \right) \left( - \frac{m-1}{mE_1} \frac{(a^2 - \lambda b^2)p}{b^2 - a^2} \right) + \left( \frac{mE}{m+1} \frac{1}{b^2} \right) \left( - \frac{(m+1)}{mE_1} \frac{a^2 b^2 (p - \lambda p)}{b^2 - a^2} \right)$$

$$\sigma_{tb} = - \frac{a^2 p - \lambda b^2 p}{b^2 - a^2} - \frac{a^2 p - a^2 p \lambda}{b^2 - a^2}$$

$$\therefore \sigma_{tb} = - \frac{2a^2 - \lambda(a^2 + b^2)}{b^2 - a^2} p$$

---

---

Caso 2.- El revestimiento de concreto esta fisurado

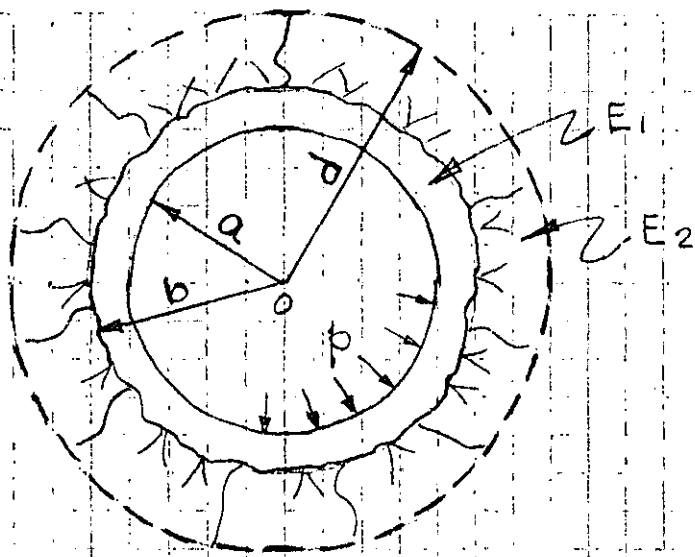
Si las paredes del revestimiento de concreto del túnel estuvieran uniformemente fisuradas en una dirección radial, una presión:

$$p_c = \frac{a}{b} p$$

podría ser transmitida directamente a la roca y los esfuerzos sobre la superficie de roca podrían ser:

$$\sigma_r = - \sigma_t = \frac{a}{b} p$$

Caso 3.- La roca tiene fisuras hasta una profundidad  $d$ .



Túnel revestido en roca radialmente fisurada

Para cualquier profundidad  $r < d$  dentro de la masa de roca fisurada:

$$\sigma_t = 0 \quad \text{y} \quad \sigma_r = \frac{a}{r} p$$

Para el límite de la roca sana la presión es

$$p_d = \frac{a}{d} p$$

Dentro de la roca sana con  $d \leq r < \infty$ :

$$\sigma_r = -\sigma_t = p \frac{a}{d} \cdot \frac{d^2}{r^2} = \frac{ad}{r^2} p$$

A lo largo de la superficie de roca la presión radial es:

$$p_b = \frac{a}{b} p$$

$$\text{y} \quad \sigma_t = 0$$

$$\therefore \sigma_{rb} = p_b = \frac{a}{b} p$$

## 6. Túneles y lumbreras a presión con camisa metálica

a. - En roca sana

La presión hidrostática dentro del túnel es  $p$

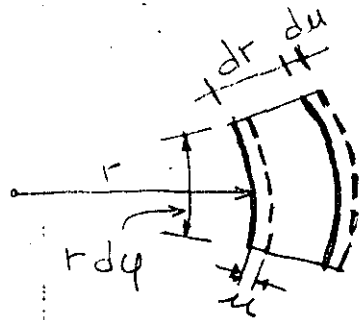
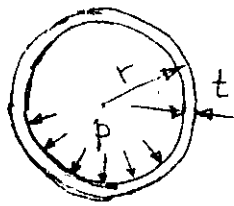
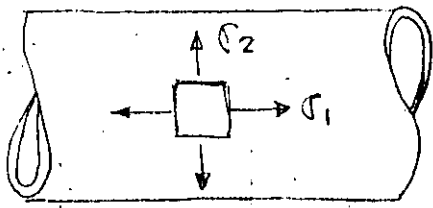
Una presión  $p_b < p$  es transmitida desde la placa metálica al concreto y una presión  $p_c < p_b$  desde el concreto a la roca.

La deformación elástica  $u_b$  del revestimiento de acero es:

$$u_b = \frac{p - p_b}{E} \times \frac{a^2}{e} = p(1 - \lambda_1) \times \frac{a^2}{E e}$$

Donde:  $E$  = módulo elástico de la placa de acero;  $e$  = espesor de la placa y  $p_b = \lambda_1 p$

Esta expresión viene del estudio de tubos de pared delgada.



Las deformaciones unitarias son:

Tangencial: 
$$\delta_t = \frac{2\pi(r+u) - 2\pi r}{2\pi r} = \frac{u}{r}$$

$$\delta_t = \frac{u}{r} = \frac{1}{E} (\sigma_2 - \mu \sigma_1)$$

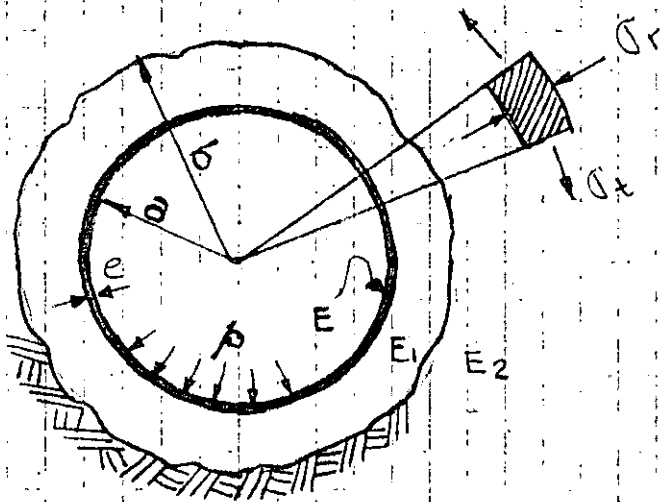
Radial: 
$$\delta_r = \frac{du}{dr} = \frac{1}{E} (\sigma_1 - \mu \sigma_2)$$

De donde: 
$$u = \frac{r}{E} (\sigma_2 - \mu \sigma_1)$$

Como  $\sigma_2 = \frac{pr}{t}$  y  $\sigma_1 = \frac{pr}{2t}$ ; 
$$u = \frac{r}{E} \left( \frac{pr}{t} - \mu \frac{pr}{2t} \right)$$

$$u = \frac{p r^2}{t E} \left( 1 - \frac{\mu}{2} \right) = \frac{p r^2}{t E}$$

La deformación  $u_b$  de la placa de acero debe ser igual a la deformación elástica de la superficie interna del concreto, y la deformación de la cara externa del concreto debe ser igual a la fluencia de la superficie de la roca.



Túnel con camisa metálica

Cálculos de tallados de Jaeger, 1933, demuestran que:

$$\lambda_1 = \frac{p_b}{p_d}$$

$$\lambda_1 = \frac{a^2}{Ee}$$

$$\lambda_1 = \left( \frac{a^2}{Ee} \right) + \left[ \frac{a}{m_1 E_1 (b^2 - a^2)} \right] \left[ (m_1 - 1)(a^2 - \lambda_2^* b^2) + (m_1 + 1)(1 - \lambda_2^*) b^2 \right]$$

$$\lambda_2 = \frac{p_c}{p_b}$$

$$\lambda_2 = \frac{\frac{2a^2}{E_1 (b^2 - a^2)}}{\frac{(m_2 + 1)}{m_2 E_2} + \frac{(m_1 - 1)b^2 + (m_1 + 1)a^2}{m_1 E_1 (b^2 - a^2)}}$$



b. En roca fisurada radialmente

La deformación  $u_b$  de la placa de acero es:

$$u_b = \frac{p - p_b}{E} \frac{a^2}{e} = p(1 - \lambda_3) \frac{a^2}{e} \quad \text{con } p_b = \lambda_3 p$$

y la deformación del revestimiento de concreto y la roca fisurada radialmente hasta una distancia  $d$ .

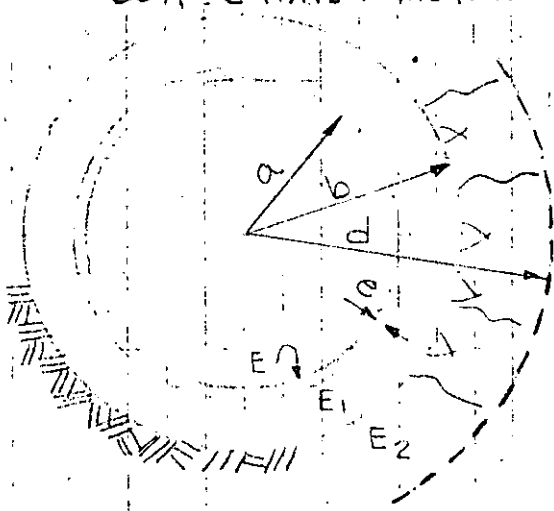
$$u_b = \frac{(p_b + p_d)}{2} \frac{(a-d)}{E_1} + p_d \frac{d(m_2+1)}{m_2 E_2}$$

Igualando los dos valores de  $u_b$  se tiene:

$$\lambda_3 = \frac{\frac{a^2}{Ee}}{\frac{a^2}{Ee} + \frac{d^2 - a^2}{2dE_1} + \frac{(m_2+1)a}{m_2 E_2}}$$

Ejemplo:

Revisión de los esfuerzos que se producen en un túnel con camisa metálica:



$$a = 10' = 304.8 \text{ cm}$$

$$e = 1/2'' = 1.27 \text{ cm}$$

$$b = 10.5' = 320 \text{ cm}$$

$$d = 156'' = 396 \text{ cm}$$

$$p = 216 \text{ psi} = 15.2 \text{ kg/cm}^2$$

$$E_1 = 4 \times 10^6 \text{ psi} = 281,690 \text{ kg/cm}^2$$

$$E_2 = 6 \times 10^6 \text{ psi} = 422,535 \text{ kg/cm}^2$$

$$E = 3 \times 10^7 \text{ psi} = 2,112,676 \text{ kg/cm}^2$$

$$\mu_1 = 0.2 ; \mu_2 = 0.26 ; \mu = 0.28$$

$$f'_c = 350 \text{ kg/cm}^2$$

$$a = 3.048 \text{ m} ; a^2 = 9.29$$

$$b = 3.20 \text{ m} ; b^2 = 10.24 ; b^2 - a^2 = 0.95$$

$$m_2 = \frac{1}{\mu_2} = \frac{1}{0.26} = 3.85 ; E_2 = 4.22 \times 10^6 \text{ ton/m}^2$$

$$m_1 = \frac{1}{\mu_1} = \frac{1}{0.20} = 5 ; E_1 = 2.82 \times 10^6 \text{ ton/m}^2$$

$$m = \frac{1}{\mu} = \frac{1}{0.28} = 3.57 ; E = 21 \times 10^6 \text{ ton/m}^2$$

Obtención de  $\lambda_2$  ;  $\lambda_2 = \frac{p_c}{p_b}$  ;  $\lambda_2 = \frac{2a^2}{E_1(b^2 - a^2)}$

$$\frac{2a^2}{E_1(b^2 - a^2)} = \frac{2 \times 9.29}{2.82 \times 10^6 \times 0.95} = \frac{6.94}{10^6}$$

$$(m_1 - 1)b^2 = (5 - 1)10.24 = 40.96 ; m_1 E_1 (b^2 - a^2) = 5 \times 2.82 \times 10^6 \times 0.95 = 13.4 \times 10^6$$

$$(m_1 + 1)a^2 = (5 + 1)9.29 = 55.74$$

$$\frac{6.94}{10^6} + \frac{55.74}{96.70} = \frac{13.4 \times 10^6}{13.4 \times 10^6 + 96.7 \times 4.22 \times 10^6}$$

$$\lambda_2 = \frac{6.94 \times 4.22 \times 13.4}{13.4 \times 10^6 + 96.7 \times 4.22 \times 10^6} = 0.92$$

Obtención de  $\lambda_1$  :  $\lambda_1 = \frac{p_b}{p}$

$$\lambda_1 = \frac{\frac{a^2}{E_c}}{\left(\frac{a^2}{E_c}\right) + \left[\frac{a}{m_1 E_1 (b^2 - a^2)}\right] \left[ (m_1 - 1)(a^2 - \lambda_2 b^2) + (m_1 + 1)(1 - \lambda_2) b^2 \right]}$$

$$\frac{a^2}{E_c} = \frac{9,29}{21 \times 10^6 \times 0,0127} = \frac{34,64}{10^6}$$

$$\frac{a}{m_1 E_1 (b^2 - a^2)} = \frac{3,05}{5 \times 2,82 \times 10^6 \times 0,95} = \frac{0,23}{10^6}$$

$$(m_1 - 1)(a^2 - \lambda_2 b^2) = (5 - 1)(9,29 - 0,92 \times 10,24) = -0,52$$

$$(m_1 + 1)(1 - \lambda_2) b^2 = (5 + 1)(1 - 0,92) 10,24 = 4,92$$

$$\lambda_1 = \frac{\frac{34,64}{10^6}}{\frac{34,64}{10^6} + \left(\frac{0,23}{10^6}\right) (-0,52 + 4,92)} = \frac{\frac{34,64}{10^6}}{\frac{34,64}{10^6} + \frac{1,01}{10^6}} = \frac{34,64}{35,65}$$

$$\therefore \lambda_1 = 0,97 \quad ; \quad p_b = \lambda_1 p \quad ; \quad p_b = 15,2 \times 0,97 = 14,74 \frac{\text{Kg}}{\text{cm}^2}$$

Por tanto, la presión sobre el concreto es  $p_b = 14,74 \text{ Kg/cm}^2$

y la presión sobre la roca será:  $p_c = \lambda_2 p_b$

$$\therefore p_c = 0,92 \times 14,74 = 13,56 \text{ Kg/cm}^2$$

El esfuerzo en el tubo puede obtenerse de dos maneras

a) Con la fórmula del esfuerzo tangencial de tubos delgados  $\tau = \frac{p r}{t}$  ;  $\tau = \frac{p - p_b}{t} r$

$$\therefore \tau = \frac{15,2 - 14,74}{1,27} \times 305,43 \quad \therefore \tau_t = 110 \text{ Kg/cm}^2$$

b) A través de la deformación tangencial unitaria

$$\mu_b = p(1 - \lambda_1) \frac{a^2}{E_c} = 15,2 (1 - 0,97) \frac{9,29}{21 \times 10^6 \times 0,0127} = 0,000159 \text{ m} = 109 \text{ Kg/cm}^2$$

Los esfuerzos en el concreto son:

Para  $r = a$  :  $\sigma_r = p_b = \underline{14.74 \text{ Kg/cm}^2}$  Compresión

y 
$$\sigma_t = - \frac{a^2 + b^2 - 2\lambda b^2}{b^2 - a^2} p$$

$$\lambda = \frac{\frac{2a^2}{E_1(b^2 - a^2)}}{\frac{m_2 + 1}{m_2 E_2} + \frac{(m_1 - 1)b^2 + (m_1 + 1)a^2}{m_1 E_1 (b^2 - a^2)}} = \lambda_2 = 0.92$$

de donde 
$$\sigma_t = - \frac{9.29 + 10.24 - 2 \times 0.92 \times 10.24}{0.95} \times 14.74 = -10.71$$

$$\sigma_t = \underline{10.71 \text{ Kg/cm}^2} \rightarrow \text{Tensión}$$

Para  $r = b$  :  $\sigma_r = \lambda p_b$  ;  $\sigma_r = 0.92 \times 14.74 = \underline{13.56 \frac{\text{Kg}}{\text{cm}^2}}$   
Compresión

y 
$$\sigma_t = - \frac{2a^2 - \lambda(a^2 + b^2)}{b^2 - a^2} p$$

$$\sigma_t = - \frac{2 \times 9.29 - 0.92(9.29 + 10.24)}{0.95} \times 14.74 = -9.46$$

$$\sigma_t = \underline{9.5 \text{ Kg/cm}^2} \rightarrow \text{Tensión}$$

Los esfuerzos permisibles en el concreto en tensión son igual a aproximadamente a 1/12 de la resistencia en compresión, por tanto:

$$R_t = \frac{f_c'}{12} \quad R_t = \frac{350}{12} ; \quad R_t = 29 \text{ Kg/cm}^2 > \sigma_t$$

que es mayor que los esfuerzos tangenciales de tensión  $\sigma_t$  que se producen para  $r = a$  y  $r = b$ .

## TECHO MÍNIMO SOBRE UN TÚNEL DE PRESIÓN

El problema para la determinación del techo mínimo sobre túneles de presión es muy importante en plantas hidroeléctricas.

Criterios adoptados:  $\gamma_1 = \text{peso volumétrico del agua} = 1 \text{ ton/m}^3$

1. - Regla antigua  $p/\gamma_1 = \frac{1}{2} H$  tiene un factor de seguridad muy alto.  $H = 2p$
2. - Algunos túneles sin revestir en Estados Unidos (Túnel Hass y Nantahala)  $p/\gamma_1 = H$   <sub>$H=p$</sub>  implica que las filtraciones no alcanzan la superficie de roca a través de las fisuras.
3. - Túnel de abastecimiento de agua en Sydney,  $p/\gamma_1 = 2.4 H$ ;  <sub>$H = 0.42p$</sub>   
La cobertura de roca es igual a la presión hidrostática.  
Glen Moriston Tunnel de la Livishie Hydroelectric development diseñado por Sir William Halcrow, sin revestimiento
4. - Terzaghi:  $p/\gamma_1 = 2H$ . La cobertura igual a la mitad de la columna hidrostática.  $H = 0.5p$
5. - Hidroeléctrica Spray en Canadá.  $p/\gamma_1 = 5H$   <sub>$H = 0.2p$</sub>   
El techo es de 216 pies y la presión de agua  $p/\gamma_1 = 1220 \text{ pies}$ .

# APENDICE N° 1

## 1. Reducción de la expresión (a)

$$\sigma_r \cdot r d\varphi + \sigma_t \cdot dr \cdot d\varphi - \left( \sigma_r + \frac{d\sigma_r}{dr} dr \right) (r + dr) d\varphi = 0$$

$$\sigma_r \cdot r d\varphi + \sigma_t \cdot dr \cdot d\varphi - \sigma_r \cdot r d\varphi - \sigma_r \cdot dr \cdot d\varphi - \frac{d\sigma_r}{dr} \cdot dr \cdot r d\varphi - \frac{d\sigma_r}{dr} \cdot dr \cdot dr \cdot d\varphi = 0$$

$$\cancel{\sigma_r \cdot r} + \sigma_t \cdot dr - \cancel{\sigma_r \cdot r} - \sigma_r \cdot dr - \frac{d\sigma_r}{dr} \cdot dr \cdot r - \frac{d\sigma_r}{dr} \cdot dr \cdot dr = 0$$

$$\sigma_t - \sigma_r - r \frac{d\sigma_r}{dr} - \frac{d\sigma_r}{dr} dr = 0$$

→ Se desprecia por ser de segundo orden

$$\boxed{\sigma_t - \sigma_r - r \frac{d\sigma_r}{dr} = 0} \quad (b)$$

## 2. Cálculo de los alargamientos unitarios del cilindro:

- En dirección radial  $r$  se incrementa en  $u$  y pasa a ser  $r+u$  similarmente,  $dr$  se incrementa en  $du$  y pasa a ser  $dr+du = dr \left( 1 + \frac{du}{dr} \right)$ . El alargamiento específico o unitario radial en longitud es:

$$\epsilon_r = \frac{(dr+du) - dr}{dr} \Rightarrow \underline{\underline{\epsilon_r = \frac{du}{dr}}}$$

- En dirección tangencial la circunferencia se incrementa de  $2\pi r$  a  $2\pi(r+u)$  y el alargamiento tangencial unitario es:

$$\epsilon_t = \frac{2\pi(r+u) - 2\pi r}{2\pi r} = \frac{\cancel{2\pi r} + 2\pi u - \cancel{2\pi r}}{2\pi r} \Rightarrow \underline{\underline{\epsilon_t = \frac{u}{r}}}$$

3.- Obtención de la ecuación diferencial en  $u$ , por sustitución de las ecuaciones (c) y (d) en (b)

$$\sigma_t - \sigma_r - r \frac{d\sigma_r}{dr} = 0 \dots (b)$$

$$\sigma_t = \frac{E}{1-\mu^2} \left( \frac{u}{r} + \mu \frac{du}{dr} \right) (d); \quad \sigma_r = \frac{E}{1-\mu^2} \left( \frac{du}{dr} + \mu \frac{u}{r} \right)$$

Sustituyendo:

$$\frac{E}{1-\mu^2} \left( \frac{u}{r} + \mu \frac{du}{dr} \right) - \frac{E}{1-\mu^2} \left( \frac{du}{dr} + \mu \frac{u}{r} \right) - r \frac{d\sigma_r}{dr} = 0$$

$$\frac{E}{1-\mu^2} \cdot \frac{u}{r} + \frac{E}{1-\mu^2} \cdot \mu \frac{du}{dr} - \frac{E}{1-\mu^2} \frac{du}{dr} - \frac{E}{1-\mu^2} \mu \frac{u}{r} - \frac{E \cdot r}{1-\mu^2} \frac{d^2 u}{dr^2} - \frac{E \cdot \mu \cdot r}{1-\mu^2} \frac{r \frac{du}{dr} - u}{r^2} = 0$$

$$\frac{u}{r} + \mu \frac{du}{dr} - \frac{du}{dr} - \mu \frac{u}{r} - r \frac{d^2 u}{dr^2} - \frac{\mu r^2 \frac{du}{dr} - \mu \cdot r \cdot u}{r^2} = 0$$

$$\frac{u}{r} + \mu \frac{du}{dr} - \frac{du}{dr} - \mu \frac{u}{r} - r \frac{d^2 u}{dr^2} - \frac{\mu du}{dr} + \frac{\mu \cdot u \cdot r}{r^2} = 0$$

dividiendo entre  $r$ :

$$\frac{u}{r^2} + \cancel{\mu \frac{du}{dr}} \cdot \frac{1}{r} - \frac{du}{dr} \cdot \frac{1}{r} - \cancel{\frac{\mu \mu}{r^2}} - \frac{d^2 u}{dr^2} - \cancel{\mu \frac{du}{dr}} \cdot \frac{1}{r} + \frac{\mu u}{r^2} = 0$$

$$\frac{u}{r^2} - \frac{du}{dr} \cdot \frac{1}{r} - \frac{d^2 u}{dr^2} = 0$$

Cambiando signos:

$$\frac{d^2 u}{dr^2} + \frac{du}{dr} \cdot \frac{1}{r} - \frac{u}{r^2} = 0$$

4.- Solución de la ecuación diferencial en  $u$

$$\frac{d^2u}{dr^2} + \frac{1}{r} \frac{du}{dr} - \frac{u}{r^2} = 0$$

Se trata de una ecuación lineal de 2º orden con coeficientes variables.

Una de las maneras de resolverla es proponiendo a  $u = r^x$

$$u = r^x ;$$

$$\frac{du}{dx} = x r^{x-1}$$

$$\frac{d^2u}{dx^2} = (x-1)(x) r^{x-2}$$

Sustituyendo en la ecuación:

$$x(x-1)r^{x-2} + \frac{1}{r} x r^{x-1} - \frac{r^x}{r^2} = 0$$

$$x(x-1)r^{x-2} + x \cdot r^{x-2} - r^{x-2} = 0$$

$$r^{x-2} [x(x-1) + x - 1] = 0$$

Alguno de los dos términos del 1º miembro es cero.

$$x(x-1) + x - 1 = 0 ; x^2 - \cancel{x} + \cancel{x} - 1 = 0 \Rightarrow x^2 - 1 = 0 \therefore x = \pm 1$$

$$\text{Para } x=1 ; u_1 = C_1 r$$

$$\text{Para } x=-1 ; u_2 = C_2 r^{-1} = \frac{C_2}{r}$$

Entonces la solución es la suma de las dos raíces.

$$u = C_1 r + \frac{C_2}{r}$$



5.- Comprobación de la solución de la ecuación diferencial en  $u$ .

$$\frac{d^2u}{dr^2} + \frac{1}{r} \frac{du}{dr} - \frac{u}{r^2} = 0$$

Solución: 
$$u = C_1 r + \frac{C_2}{r}$$

Comprobación:

$$\frac{u}{r^2} = \frac{C_1}{r} + \frac{C_2}{r^3}$$

$$\frac{du}{dr} = C_1 - \frac{C_2}{r^2}$$

$$\frac{d^2u}{dr^2} = -\frac{-2rC_2}{r^4} = +\frac{2C_2}{r^3}$$

$$\frac{2C_2}{r^3} + \frac{1}{r} \left( C_1 - \frac{C_2}{r^2} \right) - \frac{C_1}{r} - \frac{C_2}{r^3} = 0$$

$$\frac{2C_2}{r^3} + \frac{C_1}{r} - \frac{C_2}{r^3} - \frac{C_1}{r} - \frac{C_2}{r^3} = 0$$

$0 = 0$

6.- Sustitución de  $u = C_1 r + \frac{C_2}{r}$  ... (f) en los esfuerzos normales radial y tangencial.

$$\underbrace{\sigma_r = \frac{E}{1-\mu^2} \left( \frac{du}{dr} + \mu \frac{u}{r} \right)}_{\text{radial}} \dots (c) \quad \text{y} \quad \underbrace{\sigma_t = \frac{E}{1-\mu^2} \left( \frac{u}{r} + \mu \frac{du}{dr} \right)}_{\text{tangencial}} \dots (d)$$

$$\sigma_r = \frac{E}{1-\mu^2} \left( C_1 - \frac{C_2}{r^2} + C_1 \mu + \frac{C_2 \cdot \mu}{r^2} \right)$$

$$\sigma_r = \frac{E}{1-\mu^2} \left[ C_1 (1+\mu) - C_2 \frac{(1-\mu)}{r^2} \right] \quad (g)$$

---

$$\sigma_t = \frac{E}{1-\mu^2} \left( C_1 + \frac{C_2}{r^2} + \mu C_1 - \mu \frac{C_2}{r^2} \right)$$

$$\sigma_t = \frac{E}{1-\mu^2} \left[ C_1 (1+\mu) + C_2 \frac{(1-\mu)}{r^2} \right] \quad (h)$$

---

7.- Valuación de las constantes de integración, tomando en cuenta las condiciones de frontera.

$$\sigma_r = \frac{E}{1-\mu^2} \left( C_1 (1+\mu) - C_2 \frac{1-\mu}{r^2} \right) \dots (9)$$

Cuando  $p_o$  y  $p_i$  son diferentes de cero; para la superficie interior ( $r=a$ ),  $\sigma_r = -p_i$  por ser  $\sigma_r$  de compresión y para la superficie exterior ( $r=b$ ),  $\sigma_r = -p_o$ , por la misma razón.

$$-p_i = \frac{E}{1-\mu^2} \left( C_1 (1+\mu) - C_2 \frac{1-\mu}{a^2} \right) \dots (1)$$

$$-p_o = \frac{E}{1-\mu^2} \left( C_1 (1+\mu) - C_2 \frac{1-\mu}{b^2} \right) \dots (2)$$

$$-p_i \frac{1-\mu^2}{E} + C_2 \frac{1-\mu}{a^2} = C_1 (1+\mu) \dots (1)$$

$$-p_o \frac{1-\mu^2}{E} + C_2 \frac{1-\mu}{b^2} = C_1 (1+\mu) \dots (2)$$

Restando (2) de (1)

$$-p_i \frac{1-\mu^2}{E} + p_o \frac{1-\mu^2}{E} + C_2 \frac{1-\mu}{a^2} - C_2 \frac{1-\mu}{b^2} = 0$$

$$C_2 (1-\mu) \frac{b^2 - a^2}{a^2 b^2} = \frac{1-\mu^2}{E} (p_i - p_o)$$

$$C_2 = \frac{(1-\mu^2)}{E} \frac{1}{(1-\mu)} \frac{a^2 b^2}{b^2 - a^2} (p_i - p_o)$$

$$C_2 = \frac{1+\mu}{E} \frac{a^2 b^2 (p_i - p_o)}{b^2 - a^2}$$


---

## 8.- Valuación de las constantes de integración (continuación)

$$\sigma_r = \frac{E}{1-\mu^2} \left( C_1(1+\mu) - C_2 \frac{(1-\mu)}{r^2} \right) \dots (g)$$

Para:  $r=a$ ;  $\sigma_r = -p_i$  y para  $r=b$ ;  $\sigma_r = -p_o$

$$-p_i = \frac{E}{1-\mu^2} \left( C_1(1+\mu) - C_2 \frac{(1-\mu)}{a^2} \right) \dots (1)$$

$$-p_o = \frac{E}{1-\mu^2} \left( C_1(1+\mu) - C_2 \frac{(1-\mu)}{b^2} \right) \dots (2)$$

$$-p_i \frac{1-\mu^2}{E} - C_1(1+\mu) = -C_2 \frac{(1-\mu)}{a^2} \dots (1)$$

$$-p_o \frac{1-\mu^2}{E} - C_1(1+\mu) = -C_2 \frac{(1-\mu)}{b^2} \dots (2)$$

Despejando  $C_2$  de (1) y (2) queda:

$$C_2 = \frac{a^2}{1-\mu} \frac{1-\mu^2}{E} p_i + \frac{a^2}{1-\mu} C_1(1+\mu)$$

$$C_2 = \frac{b^2}{1-\mu} \frac{1-\mu^2}{E} p_o + \frac{b^2}{1-\mu} C_1(1+\mu)$$

Iguando:

$$\frac{a^2 p_i (1+\mu)}{E} + \frac{a^2 C_1 (1+\mu)}{1-\mu} = \frac{b^2 p_o (1+\mu)}{E} + \frac{b^2 C_1 (1+\mu)}{1-\mu}$$

$$\frac{(1+\mu)}{E} (a^2 p_i - b^2 p_o) = C_1 \frac{1+\mu}{1-\mu} (b^2 - a^2)$$

$$\therefore C_1 = \frac{1-\mu}{E} \cdot \frac{a^2 p_i - b^2 p_o}{b^2 - a^2}$$


---

9.- Sustitución de las constantes de integración en las expresiones de los esfuerzos normales radial y tangencial.

$$\sigma_r = \frac{E}{1-\mu^2} \left[ C_1(1+\mu) - C_2 \frac{1-\mu}{r^2} \right] \quad (g) \quad \sigma_t = \frac{E}{1-\mu^2} \left[ C_1(1+\mu) + C_2 \frac{1-\mu}{r^2} \right] \quad (h)$$

$$C_1 = \frac{1-\mu}{E} \frac{a^2 p_i - b^2 p_o}{b^2 - a^2} ; \quad C_2 = \frac{1+\mu}{E} \frac{a^2 b^2 (p_i - p_o)}{b^2 - a^2}$$

Sustituyendo  $C_1$  y  $C_2$  en (g)

$$\sigma_r = \frac{E}{1-\mu^2} \left[ (1+\mu) \frac{1-\mu}{E} \frac{a^2 p_i - b^2 p_o}{b^2 - a^2} - \frac{1-\mu}{r^2} \frac{1+\mu}{E} \frac{a^2 b^2 (p_i - p_o)}{b^2 - a^2} \right]$$

$$\therefore \sigma_r = \frac{a^2 p_i - b^2 p_o}{b^2 - a^2} - \frac{(p_i - p_o) a^2 b^2}{r^2 (b^2 - a^2)} \quad \dots (i)$$


---

Sustituyendo  $C_1$  y  $C_2$  en (h)

$$\sigma_t = \frac{E}{1-\mu^2} \left[ (1+\mu) \frac{1-\mu}{E} \frac{a^2 p_i - b^2 p_o}{b^2 - a^2} + \frac{1-\mu}{r^2} \frac{1+\mu}{E} \frac{a^2 b^2 (p_i - p_o)}{b^2 - a^2} \right]$$

$$\therefore \sigma_t = \frac{a^2 p_i - b^2 p_o}{b^2 - a^2} + \frac{(p_i - p_o) a^2 b^2}{r^2 (b^2 - a^2)} \quad \dots (j)$$


---

10. - Desplazamiento radial en la superficie interior del cilindro solo para presión interna.

$$u = \frac{1-\mu}{E} \frac{a^2 p_i - b^2 p_o}{b^2 - a^2} r + \frac{1+\mu}{E} \frac{a^2 b^2 (p_i - p_o)}{b^2 - a^2} \frac{1}{r} \dots (o)$$

Para  $r = a$  y  $p_o = 0$

$$u = \frac{1-\mu}{E} \frac{a^2 p_i}{b^2 - a^2} a + \frac{1+\mu}{E} \frac{a^2 b^2 p_i}{b^2 - a^2} \frac{1}{a}$$

$$u = \frac{(1-\mu) a^3 p_i + (1+\mu) a b^2 p_i}{E (b^2 - a^2)}$$

$$u = \frac{a p_i}{E} \left( \frac{a^2 (1-\mu) + b^2 (1+\mu)}{b^2 - a^2} \right)$$

$$u = \frac{a p_i}{E} \left( \frac{a^2 - a^2 \mu + b^2 + b^2 \mu}{b^2 - a^2} \right)$$

$$u = \frac{a p_i}{E} \left( \frac{a^2 + b^2}{b^2 - a^2} + \frac{\mu (b^2 - a^2)}{b^2 - a^2} \right)$$

$$\underline{u = \frac{a p_i}{E} \left( \frac{a^2 + b^2}{b^2 - a^2} + \mu \right)} \dots (p)$$

# 11. - Desplazamiento radial en la superficie exterior del cilindro solo para presión externa

$$u = \frac{1-\mu}{E} \frac{a^2 p_i - b^2 p_o}{b^2 - a^2} r + \frac{1+\mu}{E} \frac{a^2 b^2 (p_i - p_o)}{b^2 - a^2} \frac{1}{r} \dots (0)$$

Para  $r = b$  y  $p_i = 0$

$$u = \frac{1-\mu}{E} \frac{-b^2 p_o}{b^2 - a^2} b + \frac{1+\mu}{E} \frac{-a^2 b^2 p_o}{b^2 - a^2} \frac{1}{b}$$

$$u = \frac{-b^2 p_o (1-\mu) - a^2 b p_o (1+\mu)}{E (b^2 - a^2)}$$

$$u = - \frac{b p_o}{E} \left( \frac{b^2 (1-\mu) + a^2 (1+\mu)}{b^2 - a^2} \right)$$

$$u = - \frac{b p_o}{E} \left( \frac{b^2 - b^2 \mu + a^2 + a^2 \mu}{b^2 - a^2} \right)$$

$$u = - \frac{b p_o}{E} \left( \frac{a^2 + b^2}{b^2 - a^2} - \mu \frac{(b^2 - a^2)}{b^2 - a^2} \right)$$

$$\therefore u = - \frac{b p_o}{E} \left( \frac{a^2 + b^2}{b^2 - a^2} - \mu \right) \dots (9)$$

12. Despeje de  $\lambda$

$$\frac{m_1-1}{m_1 E_1} \frac{(a^2 - \lambda b^2)}{b^2 - a^2} \cdot p \cdot b + \frac{m_1+1}{m_1 E_1} \frac{a^2 b^2}{b^2 - a^2} \cdot p \cdot (1-\lambda) = \frac{\lambda p b^2 (m_2+1)}{E_2 m_2 \cdot b}$$

$$\frac{m_1-1}{m_1 E_1} \frac{a^2 p b}{b^2 - a^2} - \frac{m_1-1}{m_1 E_1} \frac{\lambda p b^3}{b^2 - a^2} + \frac{m_1+1}{m_1 E_1} \frac{a^2 p b}{b^2 - a^2} - \frac{m_1+1}{m_1 E_1} \frac{a^2 b \lambda p}{b^2 - a^2} = \frac{\lambda p b (m_2+1)}{E_2 m_2}$$

$$\lambda \left( \frac{p b (m_2+1)}{E_2 m_2} + \frac{m_1-1}{m_1 E_1} \frac{p b^3}{b^2 - a^2} + \frac{m_1+1}{m_1 E_1} \frac{a^2 b p}{b^2 - a^2} \right) = \frac{a^2 p b (m_1-1 + m_1+1)}{m_1 E_1 (b^2 - a^2)}$$

Reduciendo  $p$  y una  $b$  queda:

$$\lambda \left( \frac{m_2+1}{E_2 m_2} + \frac{(m_1-1)b^2 + (m_1+1)a^2}{m_1 E_1 (b^2 - a^2)} \right) = \frac{2 a^2}{E_1 (b^2 - a^2)}$$

$$\lambda = \frac{2 a^2}{E_1 (b^2 - a^2)}$$

$$\lambda = \frac{m_2+1}{E_2 m_2} + \frac{(m_1-1)b^2 + (m_1+1)a^2}{m_1 E_1 (b^2 - a^2)}$$



## PANDEO EN TUBERIAS Y LUMBRERAS DE PRESION

Para el estudio de la presión crítica de pandeo en conductos a presión con camisa metálica empacada con mortero o concreto utilizaremos el método de Ernst Amstutz de la Cía. Wartmann de Suiza quien verificó los resultados teóricos mediante dispositivos de prueba, presentado en la revista Water Power de noviembre, 1970

### TEORIA DE PANDEO

El pandeo de un tubo embebido en concreto bajo presión uniforme externa no es un problema clásico de estabilidad como por ejemplo cuando un tubo libre deja su estado de equilibrio cuando alcanza la presión crítica. Una deformación ocurrirá en uno o varios puntos cuando la presión externa exceda el preesforzamiento entre el tubo y el concreto que lo rodea.

La reducción elástica de la circunferencia del tubo resultante de la presión hidrostática externa solamente es posible si el tubo se abolla despegándose del concreto. Si la presión continúa aumentando, las abolladuras se profundizan hasta que se pegan. Unas con otras, por ejemplo, para un comportamiento elástico las deformaciones crecerían permanentemente sin incremento de la carga.

Pero en la práctica la resistencia del tubo queda limitada desde el momento que alcanza la plasticidad. En ese instante las deformaciones aumentan rápidamente, no por causa de las condiciones geométricas, sino por causa de la resistencia límite del material, de tal manera que el contacto de las abolladuras ocurre prácticamente en cuanto se alcanza la plasticidad. Las experiencias demuestran que la extensión mayor de la abolladura ocurre siempre paralela al eje del tubo, a causa de la poca resistencia de la placa contra flexión en esa dirección.

En el caso en que la abolladura tiene la forma de una concha quiere decir que hubo buena resistencia de la placa a la flexión en sentido longitudinal.

Esto significa que es posible delimitar nuestra consideración a un anillo de ancho unitario.

La fricción entre el tubo y el concreto se desprecia ya que su efecto favorable es incierto.

En la Fig. 2 se muestra un elemento infinitesimal de la pared de un tubo con su radio inicial  $r$ , el ángulo central  $d\varphi$  y el desplazamiento radial  $\eta$ . Por otro lado tenemos que la presión externa distribuida uniformemente con un valor igual a  $p$ , el elemento queda

sujeto a una fuerza axial  $N$ , una fuerza cortante  $Q$  y un momento flexionante  $M$ .

Las condiciones de equilibrio del elemento de longitud  $(r-\eta) d\varphi$  son:

haciendo el equilibrio de las fuerzas transversales:

$$dQ - N d\varphi - N \frac{d}{d\varphi} \left( \frac{d\eta}{r d\varphi} \right) + p (r-\eta) d\varphi = 0 \dots (1)$$

el equilibrio de las fuerzas axiales son:

$$Q d\varphi + dN = 0 \dots (2)$$

la ecuación de momentos:

$$Q \cdot r \cdot d\varphi - dM = 0 \dots (3)$$

la ecuación de deformaciones:

$$\frac{d^2\eta}{d\varphi^2} \cdot \frac{1}{r^2} + \frac{\eta}{r^2} + \frac{M}{EJ} = 0 \dots (4)$$

En la expresión (1) los términos que contienen  $\eta$  representan la resultante de la carga adicional a partir de las deformaciones, por tanto  $N$  puede ser sustituida por  $N_0$  en el tercer término, y de acuerdo con la fórmula de esfuerzos para una onda,  $p$  puede ser sustituido por  $N_0/r$  en el cuarto término.

Utilizando la notación de puntos para las derivadas de  $\varphi$  se obtienen las siguientes ecuaciones:

$$Q - N = \frac{N_0}{r} (\eta + \eta'') - pr \quad \dots \quad 1(a)$$

$$Q + N = 0 \quad \dots \quad 2(a)$$

$$Q \cdot r - M = 0 \quad \dots \quad 3(a)$$

$$M = -\frac{EJ}{r^2} (\eta' + \eta''') \quad \dots \quad 4(a)$$

En estas cuatro ecuaciones podemos eliminar las tres variables  $Q$ ,  $N$  y  $M$  a partir de 1(a) y 2(a):

$$Q + Q'' = \frac{N_0}{r} (\eta'' + \eta''') \quad \dots \quad (5)$$

y de 3(a) y 4(a):

$$Q = -\frac{EJ}{r^3} (\eta' + \eta''') \quad \dots \quad (6)$$

La eliminación de  $Q$  en las ecuaciones (5) y (6) nos da la ecuación diferencial que resuelve nuestro problema:

$$\eta \left( 1 + \frac{r^2 N_0}{EJ} \right) + \eta'' \left( 2 + \frac{r^2 N_0}{EJ} \right) + \eta'''' = 0 \quad \dots \quad (7)$$

Utilizando

$$\xi = \sqrt{1 + \frac{r^2 N_0}{EJ}} \quad \dots \quad (8)$$

La ecuación (7) se reduce a:

$$\eta = a \cos(\xi \varphi) + b \cos \varphi + c \quad \dots \quad (9)$$

Esto es suponiendo que el eje de referencia  $\varphi=0$  coincide con el eje de simetría de la abolladura.

El término  $b \cos \varphi$  significa geométricamente una traslación paralela y el término  $c$  significa una contracción (un ensanchamiento si el término es positivo) de la circunferencia del tubo. El término  $a \cos(E\varphi)$  representa las abolladuras alrededor de la línea central ( $b \cos \varphi + c$ ) en la fig. 2. Las constantes de integración  $a, b$  y  $c$  se determinan a partir de las condiciones de frontera. Se denomina con  $\alpha$  el ángulo  $\varphi$  bajo el cual la placa pandeada toca de nuevo el concreto (o sean los extremos de la abolladura) teniendo las siguientes condiciones de frontera.

$$\eta_a = 0 \quad -a \cos(E\alpha) + b \cos \alpha + c = 0 \quad \dots (10)$$

$$\eta'_a = 0 \quad a E \operatorname{sen}(E\alpha) + b \operatorname{sen} \alpha = 0 \quad \dots (11)$$

$$M_a = 0 \quad a(1 - E^2) \cos(E\alpha) + c = 0 \quad \dots (12)$$

de (11) se obtiene:

$$b = -a \frac{E \operatorname{sen}(E\alpha)}{\operatorname{sen} \alpha} \quad \dots (13)$$

de (12) obtenemos:

$$c = +a(E^2 - 1) \cos(E\alpha) \quad \dots (14)$$

sustituyendo (13) y (14) en (10):

$$E \tan \alpha = \tan(E\alpha) \quad \dots (15)$$

La solución de (15) se obtiene por tanteos en la tabla 1 y en la fig. 3. Otras ecuaciones definitivas para las constantes  $a, b$  y  $c$  son las ecuaciones de deformación, cuando la deformación compresional de la circunferencia del tubo es igual a la Fig. 1

Para determinar esta deformación de compresión, necesitamos el valor de la fuerza axial  $N$ .

De (1) y (2) se tiene:

$$N + N'' = pr - \frac{N_0}{r} (\eta + \eta'') \quad \dots (16)$$

sustituyendo (9) en (16):

$$N + N'' = pr - \frac{N_0}{r} [a(1 - \epsilon^2) \cos(\epsilon\varphi) + c] \quad \dots (17)$$

esta solución de acuerdo a (17) es:

$$N = pr - \frac{N_0}{r} [a \cos(\epsilon\varphi) + c] \quad \dots (18)$$

utilizando (12):

$$a = \frac{c}{(\epsilon^2 - 1) \cos(\epsilon\alpha)} \quad \dots (19)$$

Se puede demostrar fácilmente que con dimensiones usuales  $5 < c < 20$ , podemos despreciar el término  $(a \cos \epsilon\varphi)$  en (18) siendo muy pequeño comparado con el término correctivo  $c$  (el cual también es pequeño). Podemos por tanto tomar:

$$N = \text{constante} = pr - N_0 \frac{c}{r} \approx p(r - c) \quad \dots (20)$$

La deformación de compresión  $\Delta$  tomada por la mitad de la circunferencia del tubo es:

$$\Delta = \frac{\pi r (N - V)}{E F} = \pi r \frac{\sigma_N - \sigma_V}{E} \quad \dots (21)$$

en donde  $\sigma_N$  es el esfuerzo normal proveniente de  $N$  y  $\sigma_V$  es un posible presfuerzo proveniente de una fuerza  $V$  resultante de una presión de inyección.

Si tuviéramos un hueco  $k$  entre el acero y el concreto en lugar de un preesfuerzo tendríamos:

$$\sigma_v = -\frac{k}{r} E \quad (22)$$

que viene a ser el esfuerzo de tensión necesario para cerrar el hueco.

La reducción geométrica de la circunferencia consiste de dos partes: La primera  $\Delta_1$  resulta del desplazamiento del centro de línea del tubo hacia el centro:

$$\begin{aligned} \Delta_1 &= \int_0^\alpha \frac{\eta}{r} r d\varphi = \int_0^\alpha [a \cos(E\varphi) + b \cos \varphi + c] d\varphi \\ &= \frac{a}{E} \operatorname{sen}(E\alpha) + b \operatorname{sen} \alpha + c\alpha \dots (23) \end{aligned}$$

Utilizando (13) y (14) se tiene:

$$\Delta_1 = a\beta \quad (24)$$

con el coeficiente:

$$\beta = \left(E - \frac{1}{E}\right) [E\alpha \cos(E\alpha) - \operatorname{sen}(E\alpha)] \dots (25)$$

La segunda parte  $\Delta_2$  resulta de la inclinación de la línea elástica:

$$\Delta_2 = \int_0^\alpha [\sqrt{(r^2 + \eta^2)} d\varphi - r d\varphi] \approx \frac{1}{2r} \int_0^\alpha \eta^2 d\varphi \dots (26)$$

De (9) y (13) obtenemos:

$$\Delta_2 = \frac{a^2}{2r} \int_0^\alpha \left[ -E \operatorname{sen}(E\varphi) + \frac{E \operatorname{sen}(E\alpha)}{\operatorname{sen} \alpha} \operatorname{sen} \varphi \right]^2 d\varphi =$$

$$= \frac{a^2}{2r} \int_0^a \left[ E^2 \operatorname{sen}^2(E\varphi) - 2E^2 \frac{\operatorname{sen}(E\alpha)}{\operatorname{sen}\alpha} \operatorname{sen}(E\varphi) \operatorname{sen}\varphi + E^2 \frac{\operatorname{sen}^2(E\alpha)}{\operatorname{sen}^2\alpha} \operatorname{sen}^2\varphi \right] d\varphi$$

$$\Delta_2 = \frac{a^2}{2r} E^2 \left\{ \frac{1}{2E} [E\alpha - \operatorname{sen}(E\alpha) \cos(E\alpha)] - 2 \frac{\operatorname{sen}(E\alpha)}{\operatorname{sen}\alpha} \frac{1}{E} \left[ \frac{1}{E} \operatorname{sen}(E\alpha) \cos\alpha - \operatorname{sen}\alpha \cos(E\alpha) \right] + \frac{\operatorname{sen}^2(E\alpha)}{2 \operatorname{sen}^2\alpha} [\alpha - \operatorname{sen}\alpha \cos\alpha] \right\} \quad (27)$$

Relacionando con la ecuación (15) el término de en medio puede ser eliminado, esto es reduciendo  $\Delta_2$  a:

$$\Delta_2 = \mathcal{J} \frac{a^2}{4r} \quad (28)$$

con la expresión:

$$\mathcal{J} = E \left[ E\alpha - \operatorname{sen}(E\alpha) \cos(E\alpha) + E\alpha \frac{\operatorname{sen}^2(E\alpha)}{\operatorname{sen}^2\alpha} - E \operatorname{sen}^2(E\alpha) \cot\alpha \right] \quad (29)$$

anotando que:

$$\Delta = \Delta_1 + \Delta_2 \quad (30)$$

obtenemos:

$$\pi r \frac{\sigma_N - \sigma_V}{E} = a\beta + \mathcal{J} \frac{a^2}{4r} \quad (31)$$

En la ecuación (3) solo  $\bar{a}$  debe ser determinada con otra condición. Repitiendo las condiciones mencionadas arriba: que en un punto el esfuerzo de la fibra extrema deberá alcanzar el punto de fluencia  $\sigma_F$ . Como se ve en la fig 1, esto sucede para las partes altas de la abolladura cuando  $\varphi=0$ , ya que allí las curvaturas de la abolladura y lo aplastado del arco se suman.

Los máximos esfuerzos ocurren en la fibra extrema para una distancia  $e$  desde el eje neutro, cuando los esfuerzos axiales y de flexión se suman.



De acuerdo a las ecuaciones (4a), (9) y (14) encontramos que

$$\sigma_F = \sigma_N + \frac{M_0}{r^2} e = \sigma_N - E \frac{e}{r^2} (\eta_0 + \eta_0') \quad \dots (32)$$

y:

$$\frac{\sigma_F - \sigma_N}{E} = \frac{e}{r^2} (a + b + c - a \epsilon^2 - b) = -\frac{e}{r^2} [a(1 - \epsilon^2) + c]$$

$$= \left(\frac{ea}{r^2}\right) (\epsilon^2 - 1) [1 - \cos(\epsilon\alpha)] \quad \dots (33)$$

continuándose que:

$$a = \frac{r^2}{e} \frac{\sigma_F - \sigma_N}{E} \left(\frac{1}{\delta}\right) \quad \dots (34)$$

con el coeficiente:

$$J = (\epsilon^2 - 1) [1 - \cos(\epsilon\alpha)] \quad \dots (35)$$

Combinando (34) y (31) se tiene:

$$\frac{\sigma_N - \sigma_V}{E} = \frac{r}{e} \frac{\sigma_F - \sigma_N}{E} \frac{\beta}{\pi \delta} \left[ 1 + \frac{r}{e} \frac{\sigma_F - \sigma_N}{E} \frac{\gamma}{4\beta} \right] \quad \dots (36)$$

El cociente  $\frac{\beta}{\pi \delta}$  depende fuertemente de  $\epsilon$ . Para hacerlo más constante multiplicaremos ambos términos de la ecuación por  $\epsilon^2$ .

Tomando en consideración la ecuación (8) el término izquierdo queda:

$$\epsilon = \sqrt{\left(1 + \frac{NF^2}{EJ}\right)} = \sqrt{\left[1 + \left(\frac{r}{i}\right)^2 \frac{\sigma_N}{E}\right]} \quad \dots (37)$$

en la cual  $i = \sqrt{\frac{J}{F}}$  que es el radio de giro.

la ecuación final es:

$$\frac{\sigma_N - \sigma_V}{E} \left[ 1 + \left(\frac{r}{i}\right)^2 \frac{\sigma_N}{E} \right]^{3/2}$$

$$= \phi \frac{r}{e} \frac{\sigma_F - \sigma_N}{E} \left[ 1 - \psi \frac{r}{e} \frac{\sigma_F - \sigma_N}{E} \right] \quad \dots (38)$$

con las funciones auxiliares:  $\phi = \frac{\epsilon^{3\beta}}{\pi \delta} \quad \dots (39)$

y  $\psi = -\frac{\gamma}{4\beta \delta} \quad \dots (40)$

Los valores de  $\phi$  y  $\psi$  están en la Tabla 1 y graficados en la Fig. 3. Cuando estas curvas son muy planas, dentro del intervalo de aplicación práctico ( $5 < E < 20$ ) se puede sustituir por el valor mínimo para  $E = 20$  lo cual queda del lado de la seguridad. El error se compensa parcialmente al despreciar el 1 dentro del paréntesis del término izquierdo. La ecuación final por tanto se obtiene:

$$\frac{\sigma_N - \sigma_v}{\sigma_F - \sigma_N} \left[ \frac{r}{\lambda} \sqrt{\frac{\sigma_N}{E}} \right]^3 \approx 1.73 \frac{r}{e} \left[ 1 - 0.225 \frac{r}{e} \frac{(\sigma_F - \sigma_N)}{E} \right] \quad \dots (41)$$

Si  $\sigma_N$  es obtenido de (38) o (41) debemos determinar la presión crítica utilizando la ecuación (20)

$$p_{cr} = \frac{N}{r - c} = \frac{\sigma_N F}{r \left[ 1 - \frac{c}{r} \right]} \quad \dots (42)$$

De (19), (34) y (35) se tiene:

$$\frac{c}{r} = \frac{(\epsilon^2 - 1) \cos(\epsilon \alpha)}{(\epsilon^2 - 1) [1 - \cos(\epsilon \alpha)]} \frac{r}{e} \frac{(\sigma_F - \sigma_N)}{E} \quad \dots (43)$$

y también que:

$$p_{cr} = \frac{\sigma_N F}{r \left[ 1 + \Omega \frac{r}{e} \frac{(\sigma_F - \sigma_N)}{E} \right]} \quad \dots (44)$$

Con el coeficiente:

$$-\Omega = -\cos(\epsilon \alpha) / [1 - \cos(\epsilon \alpha)] \quad \dots (45)$$

$-\Omega$  está calculada en la Tabla 1, y se muestra en el diagrama de la Fig. 3. Si tomamos  $-\Omega_{max}$  para  $E = 20$  ( $-\Omega = 0.175$ ) estaremos del lado de la seguridad y tendremos una nueva ecuación:

$$p_{cr} = \frac{F \sigma_N}{r \left( 1 + 0.175 \frac{r}{e} \frac{\sigma_F - \sigma_N}{E} \right)}$$

$$\approx \frac{F \sigma_N}{r} \left( 1 - 0.175 \frac{r}{e} \frac{\sigma_F - \sigma_N}{E} \right) \dots (46)$$

### TUBO CILINDRICO PLANO.

Para un tubo cilíndrico plano con espesor de pared igual a  $d$ , tomamos  $i = \frac{d}{\sqrt{12}}$  y  $e = \frac{d}{2}$ . A causa de la restricción de la deformación lateral la componente de  $E$  tiene que ser sustituida por:

$$E^* = \frac{E}{\sqrt{1-\nu^2}} \dots (48)$$

$$\text{y } \sigma_F^* = \frac{\mu \sigma_F}{\sqrt{1-\nu+\nu^2}} \dots (49)$$

Siendo la relación de Poisson  $\nu = 0.3$  y  $\mu$  un coeficiente por el efecto soportante, que indica la relación entre el punto de fluencia a la flexión y la deformación de tensión.

$$\mu = 1.5 - 0.5 \left[ \frac{1}{1 + \frac{E}{\sigma_F} \times 0.002} \right]^2 \text{ para secciones rectan-}$$

gulares según

$$\approx 1.5 - 0.5 \left[ \frac{1}{1 + \frac{4}{\sigma_F}} \right]^2 \dots (50)$$

Con  $\sigma_F$  en ton/cm<sup>2</sup>

En la fig 4 se muestra el diagrama esfuerzo-deformación

de una tira de metal de un tubo de prueba para tensión y flexión. El material conserva su elasticidad de flexión bajo el punto de fluencia calculado; esto probablemente ocurre a causa de que la fluencia solo es posible a través del área total de la sección transversal y no en fibras aisladas.

La cuestión salta de si es o no correcto utilizar el incremento de fluencia solamente para flexión y no para fuerza normal. Los ejemplos demuestran que en los casos prácticos, los esfuerzos de flexión son siempre mayores que los esfuerzos normales. Si consideramos el caso crítico de pandeo encontraremos una distribución triangular de esfuerzos.

Podemos poner el caso de dos vigas con igual momento flexionante y fuerzas normales opuestas, una sobre la otra, entonces la condición de esfuerzos es la misma que para una viga sola con doble de peralte pero sujeta solamente a flexión. Por tanto los esfuerzos en las fibras extremas de una viga con diagrama triangular de esfuerzos es el mismo hasta el inicio de la fluencia que aquel de una viga sujeta a flexión pura. Se supondrá que esto es aproximadamente cierto para los diagramas de esfuerzos considerados.

De aquí que la ecuación (41) cambia a:

$$12 \left( \frac{r}{d} \right)^2 \frac{\sigma_N - \sigma_V}{\sigma_F^* - \sigma_N} \left( \frac{\sigma_N}{E^*} \right)^{3/2} = 1 - 0.45 \frac{r}{d} \frac{\sigma_F^* - \sigma_N}{E^*} \dots (51)$$

y la ec (46) cambia a:

$$P_{cr} = \frac{\sigma_N}{\frac{r}{d} \left( 1 + 0.35 \frac{r}{d} \frac{\sigma_F^* - \sigma_N}{E^*} \right)} \dots (52)$$

Ciertamente es posible utilizar las ecuaciones exactas (38) y (44) con los valores auxiliares de  $\phi$ ,  $\psi$  y  $\Omega$  de acuerdo a la fig. 3, pero para casos prácticos esto no es necesario ya que el error es pequeño. Los términos correctivos del miembro derecho son muy pequeños para valores pequeños de  $\epsilon$  cuando el error en  $\psi$  y  $\Omega$  es perceptible, particularmente en las ecuaciones (51) y (52).

Calculos comparativos para un tubo con relación de esbeltez límite  $r/d = 50$  de acero medio  $\sigma_F = 2.4 \text{ ton/cm}^2$  y  $\sigma_F^* = 3.8 \text{ ton/cm}^2$  y  $E^* = 2200 \text{ ton/cm}^2$ ; resulta con las ecuaciones exactas  $\sigma_N = 2.1 \text{ ton/cm}^2$ ,  $e = 5.4 \text{ cm}$ ,  $\phi = 1.97$ ,  $\psi = 0.245$ ,  $\Omega = 0.275$  y  $p_{cr} = 41.5 \text{ Kg/cm}^2$ ; y con la solución aproximada  $\sigma_N = 2.05 \text{ ton/cm}^2$  y  $p_{cr} = 40.5 \text{ Kg/cm}^2$  que representa un error de 2.4% sobre el lado de la seguridad.

Para un tubo delgado con relación de esbeltez límite  $r/d = 250$  de un acero de alta resistencia  $\sigma_F = 6.0 \text{ ton/cm}^2$  y  $\sigma_F^* = 8.8 \text{ ton/cm}^2$  y  $E = 2240 \text{ ton/cm}^2$ ; la ecuación exacta da  $\sigma_N = 0.865 \text{ ton/cm}^2$ ,  $\epsilon = 17$ ,  $\phi = 1.75$ ,  $\psi = 0.225$ ,  $\Omega = 0.175$  y  $p_{cr} = 2.59 \text{ Kg/cm}^2$ .

La ecuación aproximada da  $\sigma_N = 0.855 \text{ ton/cm}^2$  y  $p_{cr} = 2.61 \text{ Kg/cm}^2$  que representa un error de 0.8%.

El diagrama de la fig. 5 muestra en escala logarítmica las relaciones entre la presión crítica y la relación de esbeltez para diferentes límites de fluencia de aceros, resultante de pruebas de tensión para intervalos de  $r/d < 250$  y  $p_{cr} < 100 \text{ Kg/cm}^2$  (1000m de columna de agua)

Las gráficas muestran que el ahorro en espesor de tubo para aceros de alta resistencia no es importante y por tanto no se justifica su precio elevado; la condición es diferente si la presión hidrostática interna es la que gobierna en el diseño. Excepto para zonas de transición el acero con  $\sigma_F = 24 \text{ kg/mm}^2$  deberá usarse en la mayoría de los casos.

Para el intervalo  $60 < r/d < 200$  puede usarse la fórmula empírica:

$$p_{cr} = \left(\frac{r}{d}\right)^{7/4} \quad \dots \quad (54)$$

con un error posible de  $\pm 2\%$

Cuando se utilice la gráfica de la fig. 5 o la expresión (54) deberá utilizarse un factor de seguridad de 1.5.

## PRUEBAS DE PUNDEO

Durante 1962-68 la Wartmann Co. desarrolló ensayos con la idea de determinar las cargas reales de pandeo y comprobar los análisis teóricos.

Para ello desarrollaron un modelo natural a escala como se ve en la fig. 8.

Los resultados de las pruebas realizadas en tubos  $\phi 96 \text{ cm}$  por  $150 \text{ cm}$  de largo, con espesores de 2-5 y 6 mm correspondientes a una escala de  $1/3$  a  $1/4$  se muestran en la Tabla II.

La magnitud del error es  $\pm 2\%$ .

TABLA I

$E$	$E\alpha^\circ$	$\alpha^\circ$	$\tan E\alpha$	$\tan \alpha$	$E \tan \alpha$	$\cos (E\alpha)$	$\sin (E\alpha)$	$\sin \alpha$	$E\alpha$
3	270° 00'	90° 00'	$\infty$	$\infty$	$\infty$	0	-1.00000	-1.00000	4.71239
4	263° 37.2	65° 54.3	8.9446	2.2360	8.9440	-0.11112	-0.99381	0.91287	4.60104
5	261° 11.6	52° 14.3	6.4550	1.2910	6.4550	-0.15310	-0.98821	0.79056	4.55868
10	258° 19.7	25° 50'	4.8409	0.48413	4.8413	-0.20231	-0.97932	0.43575	4.50868
20	257° 40.2	12° 33'	4.5749	0.22873	4.5746	-0.21357	-0.97693	0.22297	4.49719

$E$	$\beta$ (25)	$\gamma$ (29)	$\delta$ (35)	$\phi$ (39)	$\psi$ (40)	$\omega$ (48)
3	-2.6667	28.3	8.00	2.88	0.331	0
4	-1.8095	32.7	16.67	2.21	0.271	0.100
5	-1.3933	38.7	27.67	2.00	0.251	0.133
10	-0.6650	71.4	119.03	1.78	0.226	0.168
20	-0.3286	143.4	484.2	1.73	0.225	0.175

TABLA II

Comparación entre las presiones críticas de pandeo teóricas y medidas en las pruebas

PRUEBA N°		1	2	3	4	5
Radio medio	mm	478	479	480	478	479
Espesor de la placa	mm	2.65	4.28	6.20	3.31	5.38
		—	—	—	152/125	152/250
Módulo elástico E	t/cm <sup>2</sup>	2140	2010	2110	2100	2130
Módulo elastico E*	t/cm <sup>2</sup> (48)	2280	2140	2250	2240	2270
Límite de fluencia $\sigma_F$	t/cm <sup>2</sup>	2.89	2.82	2.98	4.00	4.14
Límite de fluencia $\sigma_F^*$	t/cm <sup>2</sup> (49)	4.53	4.42	4.68	6.14	6.31
Rigidez de cortante	t/cm <sup>3</sup>	—	—	—	0.105	0.052
Factor de reducción k	(61)	—	—	—	0.525	0.763
Esfuerzo axial $\sigma_N$	t/cm <sup>2</sup> (51)	0.94	1.29	1.76	1.58	2.03
Presión crítica de pandeo $p_{cr}$	kg/cm <sup>2</sup> (52)	4.72	10.85	21.9	9.92	21.5
Presión de pandeo medida	Kg/cm <sup>2</sup>	4.73	11.0	22.0	10.0	21.0



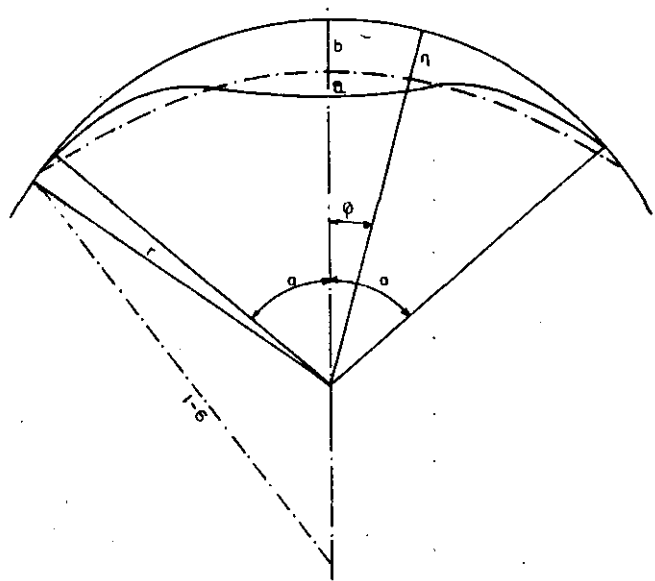


FIG. 1: FORMA DE COMBADURA HACIA ADENTRO DEL TUBO

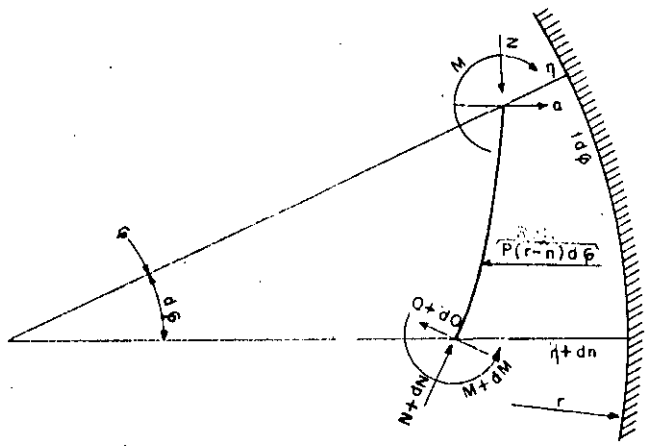


FIG. 2: FUERZAS Y DESPLAZAMIENTOS SOBRE EL ELEMENTO DE TUBO PLANO

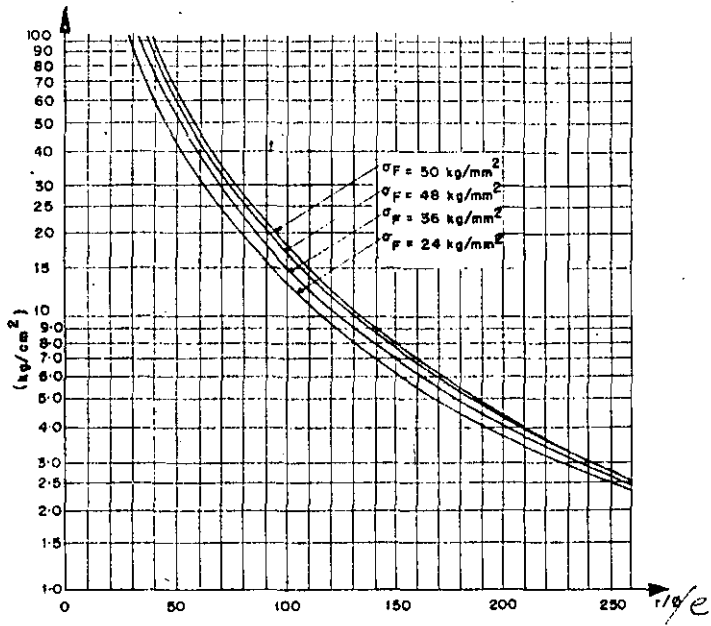


FIG. 5: PRESIONCRITICA DE PANDEO EN FUNCION DE LA RELACION DE ESBELTEZ PARA DIFERENTES RESISTENCIAS LIMITES DE ACEROS.

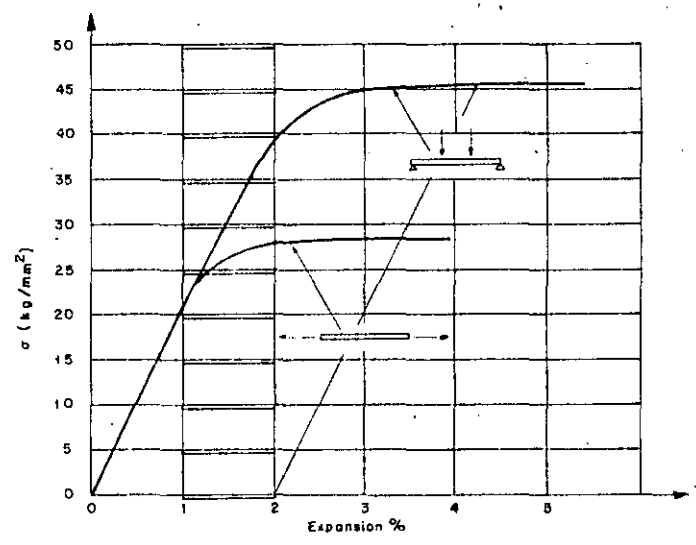


FIG. 4: DIAGRAMA ESFUERZO DEFORMACION PARA TENSION Y FLEXION

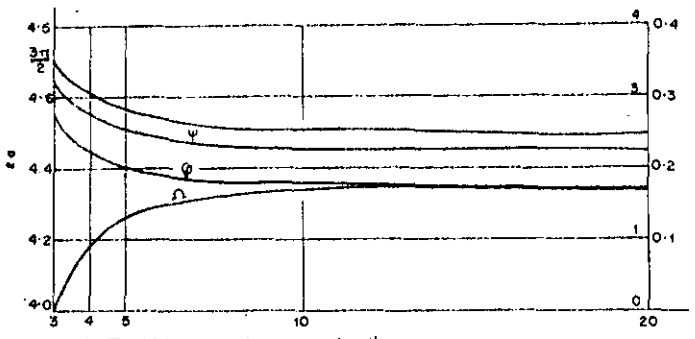


FIG. 3: VALORES DE  $\phi$  y  $\psi$

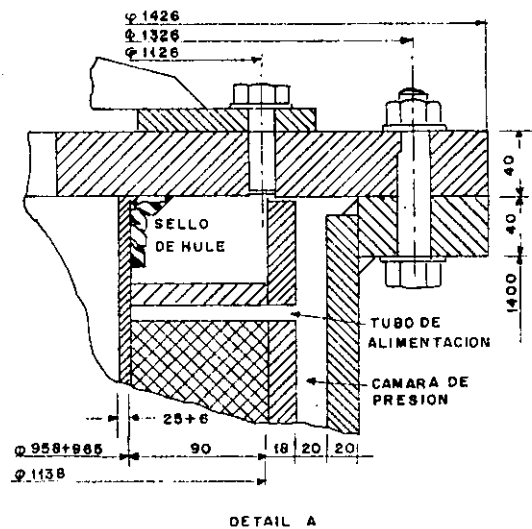
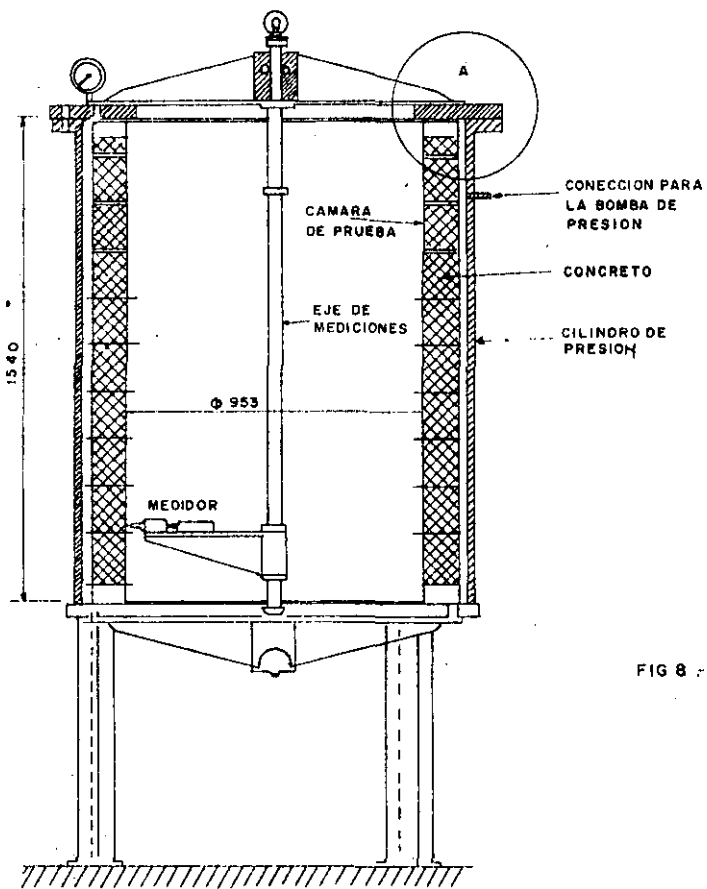


FIG 8 - DETALLES DEL APARATO DE PRUEBAS

## DESARROLLO DE ESFUERZOS RADIALES Y TANGENCIALES ALREDEDOR DE UNA CAVIDAD CIRCULAR EN ROCA ELASTOPLÁSTICA.

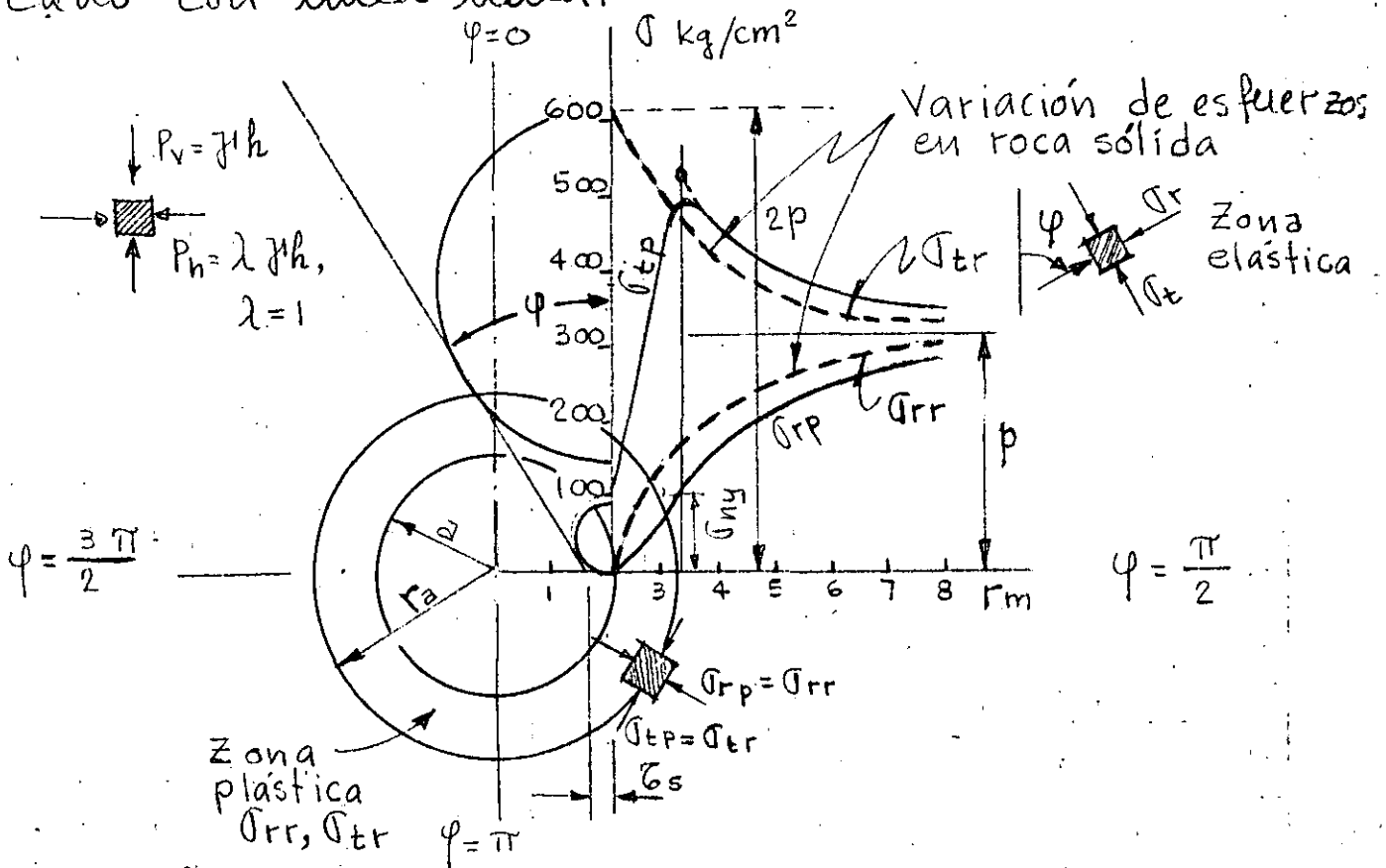
En relación a la extensión de la zona plástica que se desarrolla alrededor de un túnel circular en función de las presiones externas, Kastner (1949) expone lo siguiente:

Considerando el estado de esfuerzos que se desarrolla en la vecindad de un túnel circular, los esfuerzos radiales  $\sigma_r$  son cero por la falta de soporte interno.

Al mismo tiempo los esfuerzos tangenciales  $\sigma_t$  alcanzan su máximo valor y pueden exceder la resistencia de la roca produciéndose una condición plástica de esfuerzos.

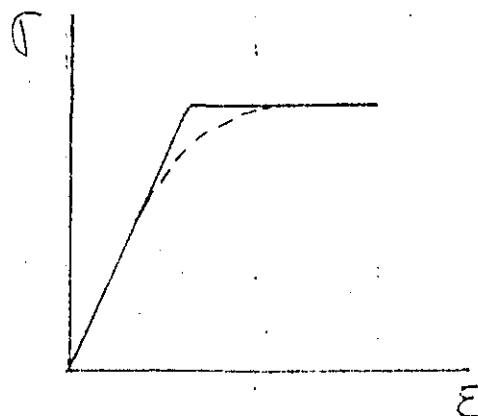
Los esfuerzos tangenciales se propagan hacia el interior de la roca decreciendo en magnitud conforme incrementa el área de la sección transversal afectada hasta que a una cierta distancia caer por debajo de los límites elásticos debajo de la cual la roca queda bajo una condición elástica de esfuerzos. Por otro lado, la magnitud de los esfuerzos radiales dentro de la zona plástica hacia el interior de la roca hasta que las partículas del material plástico bajo la acción de los esfuerzos tangenciales, actuando como una fuerza normal, a través de la fricción, la roca va siendo cada vez más capaz de soportar este esfuerzo radial de cortante.

Para el caso en que los esfuerzos externos  $p$  producen un incremento del doble en los esfuerzos tangenciales internos de un túnel y si este valor es menor que la resistencia en compresión no confinada,  $\sigma_{ny}$ , los esfuerzos radiales  $\sigma_r$  y tangenciales  $\sigma_t$  varían como se indica con la línea discontinua. Este caso se compara con aquel en el cual  $2p > \sigma_{ny}$  indicado con línea llana.



Esfuerzos radiales y tangenciales alrededor de un túnel circular en roca elasto-plástica

Según Kastner:



Relación es fuerza-deformación para un material plástico ideal.



Los esfuerzos elásticos en un disco de longitud infinita perforado por una abertura circular son:

$$\sigma_{rr} = p \left(1 - \frac{r_a}{r^2}\right) + \frac{r_a}{r^2} \sigma_r \quad \text{y} \quad \sigma_{tr} = p \left(1 - \frac{r_a^2}{r^2}\right) - \frac{r_a}{r^2} \sigma_r$$

con  $\tau_r = 0$

En la frontera de la zona elástica y plástica en donde  $r = r_a$  los esfuerzos de arriba adoptan la siguiente forma:

$$\sigma_{rr} = \sigma_r$$

$$\sigma_{tr} = 2p - \sigma_r \quad \text{y} \quad \tau_r = 0$$

Sobre la frontera de las zonas plástica y elástica los esfuerzos calculados por la teorías plástica y elástica deben ser iguales. Desde esta condición de compatibilidad el radio  $r_a$  del círculo frontera es:

$$r_a = a \left[ \frac{2}{\lambda + 1} \frac{\sigma_{ny} + p(\lambda_p - 1)}{\sigma_{ny}} \right]^{\frac{1}{\lambda_p - 1}}$$

La extensión de la zona plástica calculada de esta manera es sin embargo demasiado pequeña comparada con las grandes masas de material extruido que se encuentra en la práctica dentro de túneles en los que se ha encontrado genuina presión de montaña. Recuérdese que la extensión de la zona plástica depende de las relaciones de presiones lateral a vertical ( $\lambda$ ).

Partiendo de la condición de plasticidad completa en la cual:

$$\sigma_{max} = \frac{1}{4} (\sigma_t - \sigma_r)^2 + \tau^2 = \left( \frac{\sigma_{ny}}{2} \right)^2 = k^2 \frac{(\gamma h)^2}{4}$$

una teoría derivada de Kastner para este caso en que los esfuerzos  $\sigma_r$ ,  $\sigma_t$  y  $\tau$  fueron calculados a partir de la teoría elástica. En esta expresión  $\gamma h$  corresponde a la presión geostática y  $k$  es la relación de su resistencia en compresión confinada  $k = \frac{\sigma_{ny}}{\gamma h}$ . La fórmula derivada sobre estas bases para cualquier dirección  $\psi$  es:

$$\cos^2 2\psi + 2 \cos 2\psi \frac{1+\lambda}{1-\lambda} \frac{1-2\alpha^2+3\alpha^4}{4(2-3\alpha^2)} - \left( \frac{1+\lambda}{1-\lambda} \right)^2 \frac{\alpha^2}{4(2-3\alpha^2)} - \frac{(1+2\alpha^2-3\alpha^4)^2}{4\alpha^2(2-3\alpha^2)} + \frac{k^2}{(1-\lambda)^2 4\alpha^2(2-3\alpha^2)} = 0$$

donde  $\alpha = \frac{a}{r}$  = distancia relativa en dirección radial.

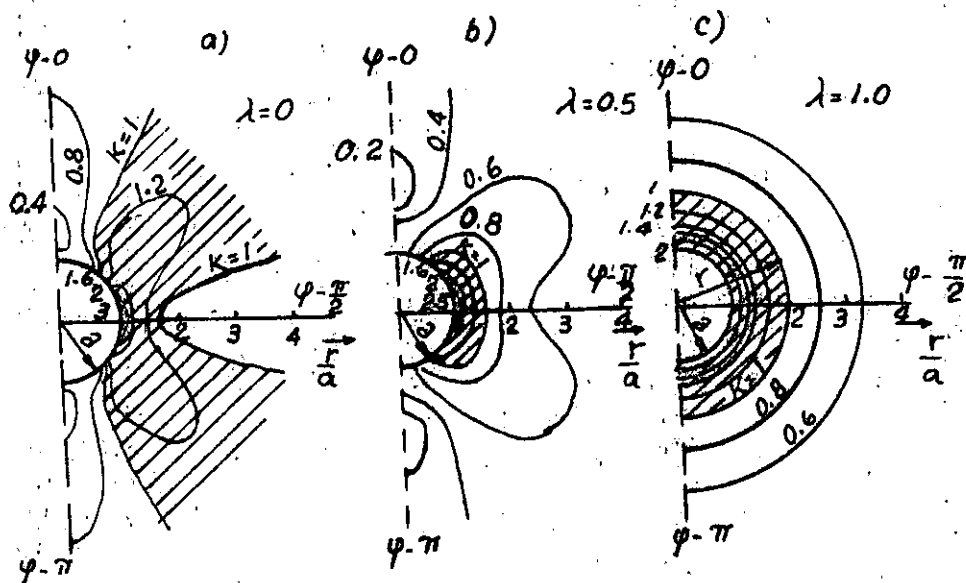
Las fronteras de la zona plástica para valores diferentes de  $k$  y para relaciones de presión lateral  $\lambda=0$ ,  $\lambda=0.5$  y  $\lambda=1$  se muestran en las siguientes figuras.

En esas figuras las áreas sombreadas indican las zonas donde  $k > 1$ , o sea donde la presión geost excede la resistencia en compresión no confinada.

Las fronteras mostradas se obtuvieron para la falla de Mohr en lugar de la fórmula anterior para  $\tau$ .

Los diagramas corresponden a una roca con las siguientes propiedades:  $\phi = 30^\circ$ ,  $c = 25 \text{ kg/cm}^2$ ,  $h = 300 \text{ m}$  y  $\gamma = 2.5 \text{ ton/m}^3$ , para varios valores de  $\lambda$ .

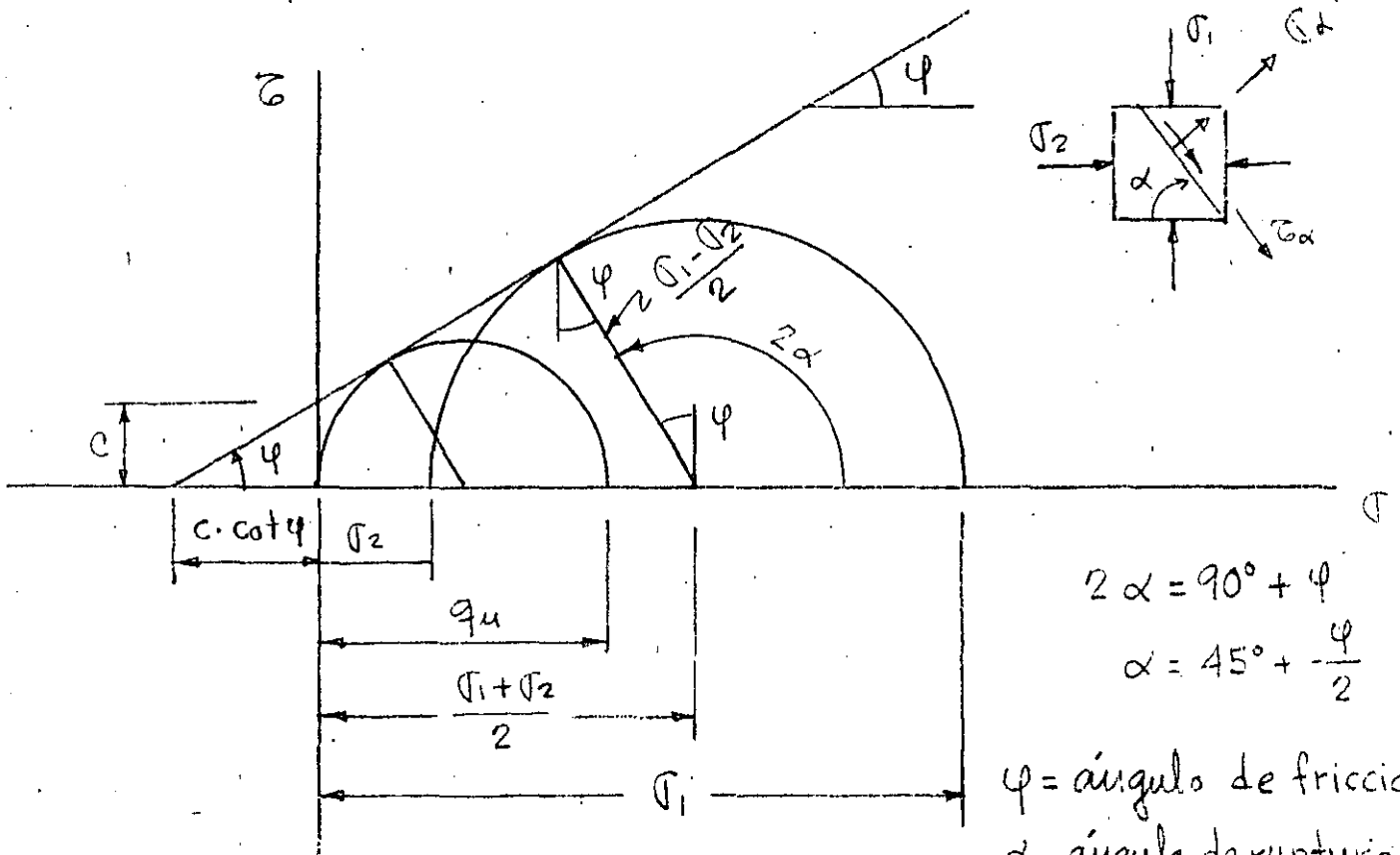




Variación de las isobaras de esfuerzos alrededor de un túnel circular en función del coeficiente de presión lateral del terreno.

La zona plástica queda restringida a un anillo relativamente delgado para el caso de presión externa uniforme tipo hidrostática,  $\lambda = 1$ , mientras que para  $\lambda = 0.5$  la zona plástica permanece relativamente delgada y queda limitada por una curva que regresa al rededor del eje del túnel. Cuando  $\lambda$  disminuye la zona plástica crece en direcciones diagonales a  $45^\circ$ . Para valores de  $\lambda = 0.141$ , la zona plástica se extiende indefinidamente.

# TEORIA A LA FALLA DE MOHR



$$2\alpha = 90^\circ + \varphi$$

$$\alpha = 45^\circ + \frac{\varphi}{2}$$

$\varphi$  = ángulo de fricción

$\alpha$  = ángulo de ruptura

$q_u$  = compresión simple

$$\text{sen } \varphi = \frac{\frac{\sigma_1 - \sigma_2}{2}}{c \cdot \cot \varphi + \frac{\sigma_1 + \sigma_2}{2}}$$

$$\text{sen } \varphi \cdot c \cdot \cot \varphi + \text{sen } \varphi \frac{\sigma_1 + \sigma_2}{2} = \frac{\sigma_1 - \sigma_2}{2}$$

$$2c \cdot \text{sen } \varphi \cdot \cot \varphi + \text{sen } \varphi (\sigma_1 + \sigma_2) = \sigma_1 - \sigma_2 ; \cot \varphi = \frac{\cos \varphi}{\text{sen } \varphi}$$

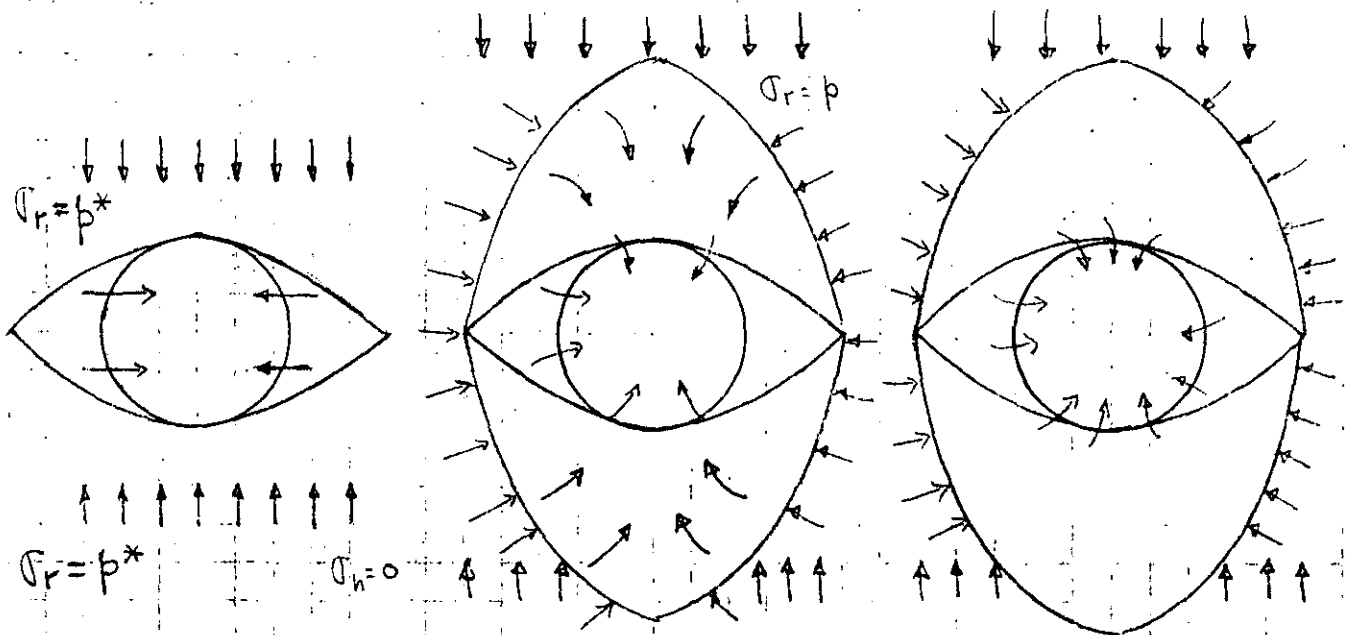
$$2c \cdot \cos \varphi + \sigma_1 \text{sen } \varphi + \sigma_2 \text{sen } \varphi = \sigma_1 - \sigma_2$$

$$\sigma_1 (1 - \text{sen } \varphi) - \sigma_2 (1 + \text{sen } \varphi) - 2c \cdot \cos \varphi = 0$$

$$\sigma_1 - \sigma_2 \frac{1 + \text{sen } \varphi}{1 - \text{sen } \varphi} - 2c \frac{\cos \varphi}{1 - \text{sen } \varphi} = 0$$

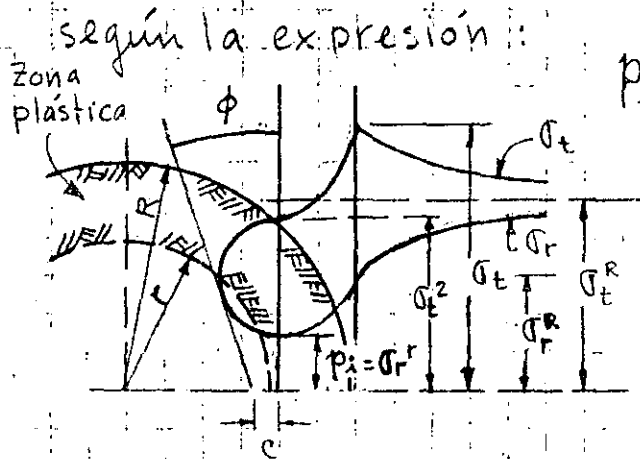
$$\sigma_1 - \sigma_2 \tan^2(45^\circ + \frac{\varphi}{2}) - 2c \tan(45^\circ + \frac{\varphi}{2}) = 0$$

# ESFUERZOS Y DEFORMACIONES ALREDEDOR DE UN TUNEL



REDISTRIBUCION PROGRESIVA DE ESFUERZOS Y DESPLAZAMIENTOS DE LA ROCA HACIA LA CAVIDAD (Rabcewicz, 1964-65).

Talobre y Rabcewicz utilizan la distribución de esfuerzos en la vecindad de una galería excavada en roca sobreesforzada propuesta por Fenner y Kastner (1938), según la expresión:



$$p_i = -c \cdot \cot \phi + [c \cdot \cot \phi + p_0 (1 - \sin \phi)] \left( \frac{r}{R} \right)^{\frac{2 \sin \phi}{1 - \sin \phi}}$$

en donde:

$r$  = radio del túnel

$R$  = radio zona plástica

$p_i = \sigma_t^r$  = resistencia de "piel" requerida (aúdas y concreto)

$p_0$  = esfuerzo primario uniforme

## REPRESENTACION DE FENNER-KASTNER

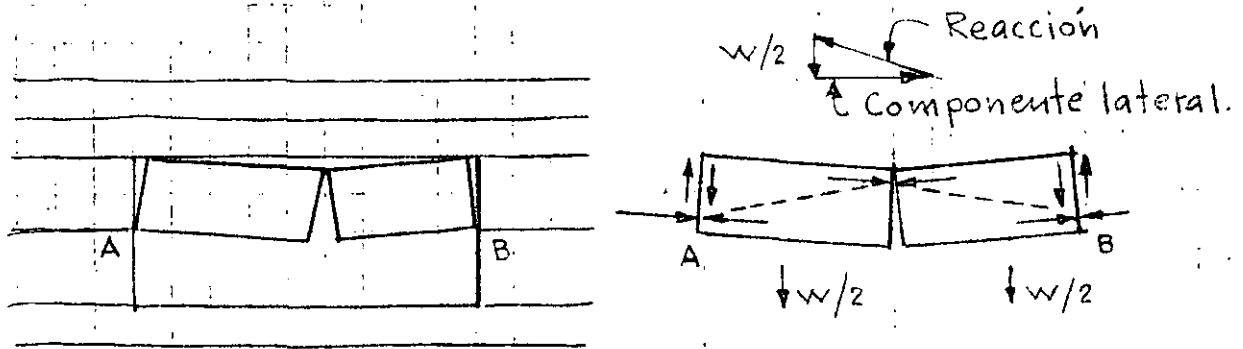
Talobre supone que usualmente  $p_i = 0$ , obteniéndose  $R$  cuando  $c$  y  $\phi$  son conocidos. Para un túnel de 6 m de diámetro y cobertura = 1500 m se tiene  $p_0 = 1500 \times 2.5 = 4000 \text{ ton/m}^2$ ;  $p_i = 0$ ;  $\phi = 30^\circ$ ;  $\sin \phi = 0.5$  y  $c = 28.9 \text{ kg/cm}^2$ .

$$c \cdot \cot \phi = 50 \text{ kg/cm}^2 = 500 \text{ ton/cm}^2; -500 + [500 + 4000 \times \frac{1}{2}] \left( \frac{r}{R} \right)^2 = 0; \frac{r}{R} = \sqrt{\frac{1}{5}}$$

Para  $r = 3 \text{ m}$ ;  $R = 3\sqrt{5} = 6.7 \text{ m} = 3 + 3.7 \text{ m}$ ; Rabcewicz supone que  $p_i$  es la resistencia de concreto y aúdas.

# CLARO MAXIMO PARA EL ARCO DE ROCA AUTOSOPORTANTE

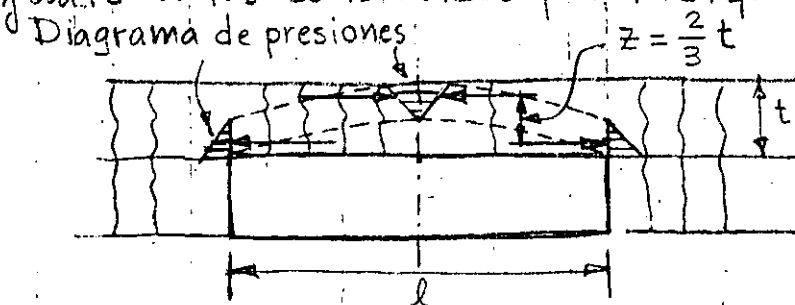
La ecuación obtenida por Evans (1941) da una primera aproximación de la longitud del arco lineal de roca, ya que la longitud final se obtiene por tanteos cuando se presenta la fluencia elástica del arco y de los apoyos



## ACCION DE ARQUEO EN ROCA ESTRATIFICADA

Los dos bloques se sostienen por efecto del giro en A y B. Las fuerzas que restringen el giro son simplemente las reacciones laterales mostradas por las flechas.

Las fuerzas de fricción en los apoyos de los bloques resisten las fuerzas cortantes y evitan que los bloques se muevan verticalmente hacia abajo. Este es el ejemplo más simple de la acción de arqueo. Si este arco simple es cortado por numerosas fracturas verticales se tendrá un arco bóveda semejante a los construidos por tabiques.



ARCO LINEAL O VIGA BOVEDA

Esta claro que en roca discontinua se soporta totalmente por compresión y cortante y que la resistencia del arco lineal no depende de la resistencia a tensión o flexión de la roca o sea resistencia por momento flexionante sino que depende de la resistencia en compresión de la roca que es cuatro a cinco veces mayor que la resistencia en tensión bajo flexión en roca sana y es infinitamente más grande en roca fracturada.

La estabilidad del arco lineal es función de la relación espesor / longitud, así como de la resistencia y módulo elástico de la roca. El módulo elástico es muy importante porque determina la cantidad de deformación del arco.

Evaus utilizó la resistencia en compresión de la roca y la distancia entre centros de presión para calcular aproximadamente el máximo momento resistente de un arco lineal.

Si igualamos el máximo momento resistente con el máximo momento flexionante del arco cargado con su peso propio determinando la máxima longitud de un arco lineal que se auto soporte

La ecuación básica de Evaus es:

$$l = \left( \frac{5Qt}{3\gamma} \right)^{\frac{1}{2}}$$

donde:  $l$  = máxima longitud de auto soporte del arco lineal = pies

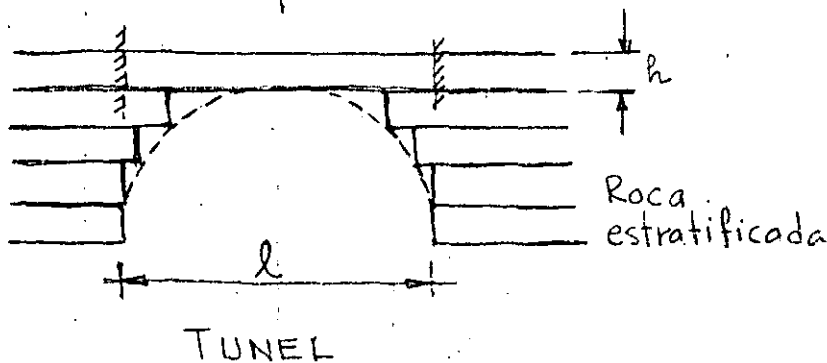
$Q$  = resistencia en compresión simple = lb/pulg<sup>2</sup>

$t$  = espesor del arco = pies

$\gamma$  = peso volumétrico del material = lb/pie<sup>3</sup>

# LOSA AUTOSOPORTANTE

Cuando la roca es competente, o sea que tiene un valor alto de  $E$  y tiene estructura estratificada, con coberturas mayores de 50 m el arco de roca estará muy cercano al comportamiento de una viga empotrada en sus extremos, formándose un estrato de roca con espesor tal que se autosoporta.



Se considera un apoyo semiempotrado por giro en los apoyos, de tal manera que se tengan momentos positivos y negativos iguales.

$$M = \frac{wl^2}{16}; \quad f = \frac{M}{I} y = f_r = \text{esfuerzo de tensión bajo flexión}$$

$$f_r = \frac{wl^2}{16} \cdot \frac{\frac{h}{2}}{\frac{bh^3}{12}} = \frac{3}{2 \times 16} \cdot \frac{wl^2}{bh^2}; \quad \text{como } w = \gamma \cdot bh$$

$$f_r = \frac{3}{8} \frac{\gamma bh l^2}{bh^2} \therefore f_r = \frac{3}{8} \frac{\gamma l^2}{h} \quad \text{de donde } h = \frac{3}{8} \cdot \frac{\gamma l^2}{f}$$

En donde  $h$  = espesor del estrato que se autosoporta.

Ejemplo:

$$l = 13 \text{ m}$$

$$h = \frac{3}{8} \times \frac{2.5 \times 13^2}{150} = 1.06 \text{ m}$$

Cálculo de anclas:

$$R_c = 350 \text{ Kg/cm}^2$$

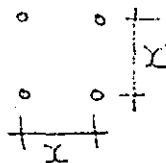
(compresión simple)

$$f_r = 60 \text{ Kg/cm}^2; \text{ F.S.} = 4; \quad f_r = 15$$

(tensión bajo flexión)

$$\gamma = 2.5 \text{ ton/m}^3$$

$$E = 50 \text{ 000 Kg/cm}^2$$



Usando anclas  $\phi = 1''$  con  $Q_{ap} = 10 \text{ ton}$

$$x^2 \times 2.5 \times 1.06 = 10$$

$$x = 1.9 \text{ m}$$

# NUEVO MÉTODO AUSTRIACO DE TUNELEO

Este método para dimensionar el sistema de soporte de túneles fue desarrollado en Austria en la década 1950-1960 por los Ingenieros Rabcewicz, Müller, Pacher y Golser, basado en el principio de que es deseable tomar la máxima ventaja de la capacidad de la roca para soportarse por sí misma. Para ello hay que vigilar cuidadosamente las fuerzas durante el proceso de reajuste que tiene lugar alrededor del túnel y adaptar el soporte en forma concordante.

Generalmente se desarrollan dos métodos para el soporte. El primero es un arco externo flexible o - soporte de protección - diseñado para estabilizar la estructura de roca concordantemente. Consiste en la formación de un arco de roca anclado sistemáticamente en toda su sección, protegiendo la superficie principalmente con concreto lanzado, algunas veces se coloca un refuerzo adicional de marcos metálicos apuntalados en sus patas con tornapuntas.

El comportamiento estructural de este soporte protectorio y de la roca vecina se controla mediante un sistema sofisticado de mediciones.

El segundo método consiste en el revestimiento de concreto el cual generalmente no se coloca hasta que el arco exterior alcance su equilibrio.

## NORMALIZACION DEL DISEÑO DEL SOPORTE

Con el fin de estar en posibilidad de normalizar criterios de diseño es necesario establecer la capacidad de soporte requerido para diferentes tipos de roca. Como se muestra en la figura 2, la capacidad de soporte del arco externo puede determinarse por la relación de la curva  $\sigma_r / \Delta r$ , la cual es característica para cualquier tipo de roca para condiciones iniciales de esfuerzos.

Como es bien conocido, el esfuerzo radial requerido  $p_i a$ , para obtener el equilibrio decrece si la frontera con el túnel tiende a fluir plásticamente. (Fig 1)

La reducción llega a ser principalmente una función de la condición de los esfuerzos primarios  $\sigma_0$  y del ángulo de fricción interna de la roca - como regla disminuye rápidamente. (Fig. 2)

Para cualquier intersección entre  $p_i$  y la curva  $\sigma_r$ , el equilibrio es alcanzado con la correspondiente resistencia del soporte.

Es una característica particular de este método que las intersecciones siempre tienen lugar en la rama descendente de la curva. Por ejemplo, podría fallar parcialmente el soporte por cualquier razón y.



un nuevo equilibrio se desarrolla sin necesidad de esforzamiento adicional del arco externo, mientras no caiga mas abajo del refuerzo mínimo (punto B) en donde puede iniciarse el "aflojamiento detrimental",  $p_i$  min.

Por otro lado, con los métodos convencionales, el punto de intersección queda situado usualmente en la rama ascendente de la curva  $\sigma_r$ . Con cualquier falla, el punto de intersección se mueve a la derecha y el soporte requerido se incrementa, de tal manera que la estructura soportante tiene que ser reforzada por arriba de su capacidad inicial.

El aflojamiento es considerado "detrimental" cuando la apertura de fallas y fracturas es tal que la roca ya no tiene competencia para transmitir los esfuerzos de cortante y de compresión. El peso de la masa de roca aflojada deberá agregarse para ser sostenida por el revestimiento.

Para estar en posibilidad de definir la curva  $\sigma_r/\Delta r$ , deberán conocerse los siguientes parametros: condición de esfuerzos primarios o estado natural de esfuerzos  $\sigma_0$  con la dirección de los esfuerzos principales, el ángulo de fricción interna  $\varphi$ , la resistencia en compresión no confinada  $\sigma_{cd}$  paralela y normal a la estratificación y los correspondientes módulos de elasticidad y de

deformabilidad.

Estos parámetros pueden ser determinados por mediciones y el curso de la curva.  $\sigma_r/\Delta r$  puede ser calculada por el método del elemento finito, tomando en consideración el procedimiento de excavación (con máquina topadora o mediante varias secciones).

Según Kastner el esfuerzo  $\sigma_r^0$  para el caso en que  $\Delta r = 0$  está dado teóricamente por las ecuaciones:

$$\sigma_r^0 = \frac{2\sigma_0 - \sigma_{gd}}{\xi + 1} \quad ; \quad \xi = \frac{1 + \operatorname{sen} \varphi}{1 - \operatorname{sen} \varphi} \quad ; \quad \sigma_{gd} = \frac{2c}{\tan(45^\circ - \varphi/2)}$$

en donde  $c$  = cohesión y  $\varphi$  = ángulo de fricción interna

El establecimiento de  $\sigma_{r \min}$  está influenciado por la magnitud de  $\sigma_r$  por un lado y por las condiciones geológicas por el otro.

Esto puede explicarse fácilmente según el ejemplo siguiente.

Considerando un túnel carretero localizado en roca de regular competencia con techo de roca pequeño para el cual los esfuerzos tangenciales en la frontera exceden ligeramente el valor de la resistencia en compresión no confinada  $p_{t \min}$  será muy pequeño, particularmente si la roca tiene alta capacidad de permanencia debida por ejemplo a una buena trabazón de bloques.

El mismo tipo de roca bajo una gran cobertura de roca está destinada a desarrollar una zona plástica de regular amplitud que ocasionará deformaciones significativas. En este caso la roca llegará a fracturarse hasta una distancia de varios metros requiriendo un  $p_{t \text{ min}}$  más alejado y mayor. El valor de la capacidad requerida del arco exterior  $p_t^a$  debe elegirse de tal manera que se combinen la máxima economía con un grado aceptable de seguridad y  $p_t^a$  deberá por lo tanto quedar tan cercano como sea posible al  $p_{t \text{ min}}$  de tal manera que se obtenga un factor de seguridad suficiente a partir de la resistencia adicional del revestimiento  $p_i^e$  del arco interior.

Para el arco exterior deberá elegirse un tipo de soporte rígido como el señalado con "2" en la Fig 2, la intersección con la curva  $\sigma_r$  está destinada a elevarse, mientras que el factor de seguridad simultáneamente disminuye.

La mínima capacidad de soporte del revestimiento del arco interior quedará definido por el espesor mínimo de revestimiento que permita una adecuada colocación del concreto. En caso de que se requiera un mayor  $p_i^t$ , el espesor puede seleccionarse de acuerdo con el  $p_i^a$  y el factor de seguridad requerido,  $s$ . Una vez que la capacidad de soporte del arco exterior ha sido establecido, el significado de reforzamiento puede elegirse y calcularse conforme a los puntos de vista anteriores.

La resistencia del material de revestimiento, concreto lanzado y concreto colado es como sigue:  
Ver fig. 3.

$$p_t^s \times b = \frac{d}{\text{sen } \alpha} \times 2 \times \tau^s$$

$$\therefore p_t^s = \frac{d \tau^s}{\text{sen } \alpha \left( \frac{b}{2} \right)} ; \text{ Concreto}$$

La resistencia del refuerzo adicional de marcos metálicos es:

$$p_t^{\text{st}} = \frac{F^{\text{st}} \times \tau^{\text{st}}}{\text{sen } \alpha \left( \frac{b}{2} \right)} ; \text{ Marcos}$$

$$\text{con } \tau^{\text{st}} = \frac{\tau^s E^{\text{st}}}{E^s} = 15 \tau^s \text{ para concreto}$$

R

La resistencia del revestimiento es:

$$p_i^R = p_t^s + p_t^{st}$$

Las anclas actúan con una presión radial como sigue:

$$p_t^A = \frac{f^{st} \sigma_p^{st}}{e \cdot t}$$

Con la presión lateral dada por:

$$\sigma_3 = p_t^s + p_t^{st} + p_i^A$$

Y con la envolvente de Mohr, la resistencia al corte de la masa de roca  $\tau^R$  y el ángulo de cortante  $\alpha$  suponiendo que los esfuerzos principales son paralelos al eje del túnel.

La capacidad de soporte del arco externo de roca es:

$$p_t^R \cdot b = 2 \times S \times \tau^R \cos \psi - S \cdot \sigma_n^R \cdot \operatorname{sen} \psi$$

$$\therefore p_t^R = \frac{S \cdot \tau^R \cos \psi}{b/2} - \frac{S \cdot \sigma_n^R \cdot \operatorname{sen} \psi}{b/2}; \text{ Roca}$$

La resistencia de las anclas contra el cortante por el movimiento del cuerpo es:

$$p_t^A \cdot e \cdot t \cdot \frac{b/2}{a \cos \beta} = f^{st} \cdot \sigma_p^{st} \therefore p_t^A = \frac{f^{st} \cdot \sigma_p^{st} \cdot a \cos \beta}{e \cdot t \cdot (b/2)}$$

La capacidad total del arco externo es:  $p_t^W = p_i^R + p_i^R + p_i^A \geq p_{i, \min}$

La experiencia ha demostrado lo siguiente:

1) Con el mismo tipo de roca y cobertura la relación entre el tamaño de los bloques de roca y el área de excavación es decisiva para la movilización de la rezaga.

2) En secciones pequeñas ( $10-16 \text{ m}^2$ ) y roca fracturada en fragmentos de unos cuantos  $\text{dm}^3$ , un sellado de concreto simple con  $d=3 \text{ cm} = 0.017R$  usualmente estabiliza el túnel.

3) En una caverna subterránea de  $400-600 \text{ m}^2$  en el mismo tipo de roca fracturada pudiera no ser estable con un espesor de 19 a 24 cm de concreto lanzado. En este caso es imperativo el uso sistemático del arco de roca anclado, ya que el comportamiento de la masa rocosa se asemeja a un suelo sin cohesión.

Utilizando anclas de tensión con concha de expansión la acción de soporte es realizada por la placa y el ancla estará bajo tensión constante a lo largo del barreno.

Con anclas inyectadas de fricción tipo PERFO o SN el efecto principal de soporte proviene de la adherencia entre el ancla y la roca.

La adherencia consiste principalmente de la fricción ocasionada por los esfuerzos tangenciales alrededor de la roca.

Los esfuerzos de tensión en el ancla se incrementan desde cero hasta un máximo en la placa y cualquier otro esfuerzo radial de frontera puede ser transmitido por el ancla a la placa.

El movimiento de la roca hacia el túnel es contrarrestado de este modo, creándose un efecto de arco en la zona de las anclas como se muestra en la figura 4

La capacidad de soporte de las anclas puede simplificarse como sigue:

$$P_a^B = L d \pi (a + \tan \epsilon \sigma'_m) + F \sigma_r \leq f_e \sigma_e$$

el término  $F \sigma_r$ , puede posiblemente elevarse a  $\sigma_r e t$

Son cuando la capacidad de soporte de las anclas de concha de expansión y las de fricción es la misma y está limitada por la resistencia a la tensión del acero, el efecto de estabilización de las anclas de fricción es mucho mayor que las de tensión.

Como una medida de refuerzo adicional se utilizan marcos ligeros de sección  $\square$  que se sujetan con anclas a la roca.

Los marcos sirven en primer lugar como una protección para la bóveda del túnel contra caídos de roca y como refuerzo local para el puenteo de zonas de debilidad geológica. La resistencia estática de estos marcos es relativamente baja. La rigidez de los marcos contrasta con la relativamente alta capacidad de fluencia del concreto lanzado.

#### DIMENSIONAMIENTO FINAL A TRAVÉS DE LAS MEDICIONES

Indisparablemente conectado con este método y como característica básica del mismo se tiene un programa sofisticado de mediciones. Los esfuerzos y las deformaciones son controlados sistemáticamente permitiendo la definición de la resistencia del soporte elegido correspondiente con el tipo de roca en cuestión y que clase de medidas de refuerzo adicional se requieran, si es que lo amerite.

Las secciones de control se eligen de acuerdo con los diferentes comportamientos estructurales esperados del macizo rocoso.



Una sección de control se compone por extensómetros longitudinales con doble punto de medición y mediciones de convergencia para medir deformaciones y presiones tanto radiales como tangenciales.

Adicionalmente pueden llevarse control de colimación y nivelación en puntos sobre el piso y la bóveda.

La frecuencia de las mediciones serán diarias y se espacian a cada semana y luego a cada mes conforme disminuya la velocidad de deformación.

Este método proporciona un alto grado de seguridad, permitiendo reconocer cualquier situación peligrosa con anticipación.

A veces el proceso de recomado toma un tiempo largo que puede ocurrir alteración de la roca p. ej. expansiones por cambios en el contenido de humedad de manera que se justifica la instalación de celdas de presión radiales y tangenciales para la definición del espesor final del revestimiento.

## CONCLUSION

Este método empírico puede complementarse mas no eliminarse por consideraciones analíticas.

Fig. 1. REPRESENTACION ESQUEMATICA DE REACOMODO DE ESFUERZOS ALREDEDOR DE UN TUNEL (SEGUN KASTNER)  
 $r$  = RADIO DEL TUNEL  
 $R$  = RADIO DE LA ZONA PLASTICA  
 $\Delta r$  = DEFORMACION RADIAL  
 $\sigma_0$  = CONDICION DE ESFUERZOS PRIMARIOS  
 $\sigma$  = ESFUERZOS TECTONICOS  
 $\sigma_r^0$  y  $\sigma_t^0$  = ESFUERZO RADIAL Y TANGENCIAL CUANDO  $\Delta r = 0$   
 $\sigma_r^1$  y  $\sigma_t^1$  = ESFUERZO RADIAL Y TANGENCIAL CUANDO HAY DEFORMACION Y SE TIENE  $r - \Delta r$

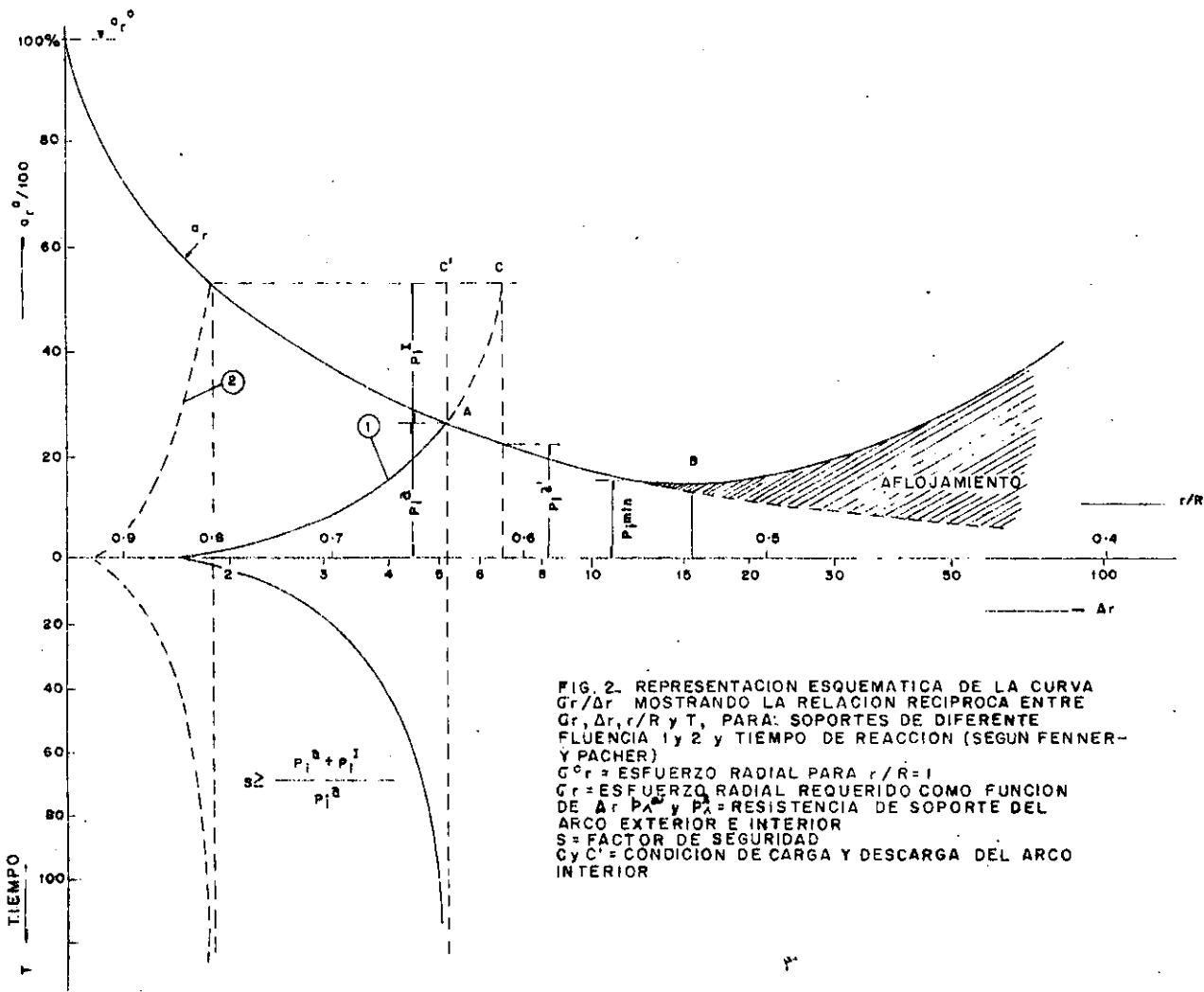
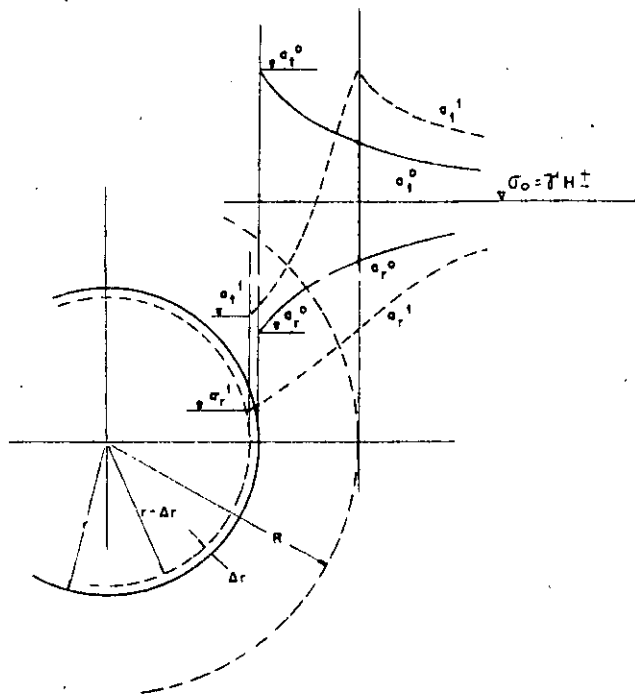
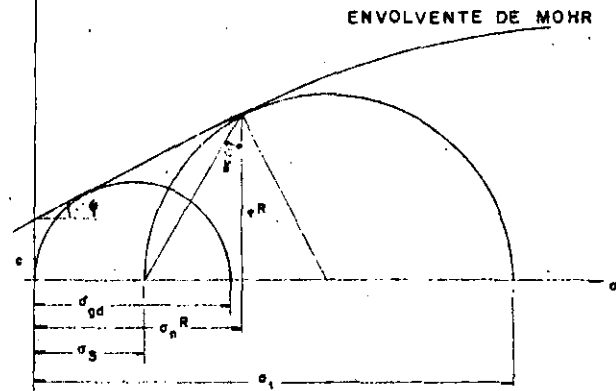
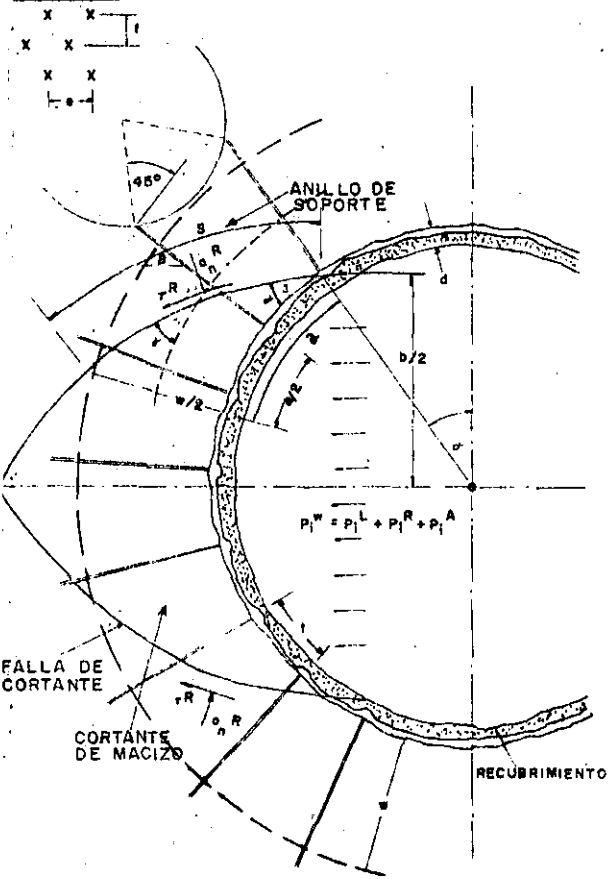


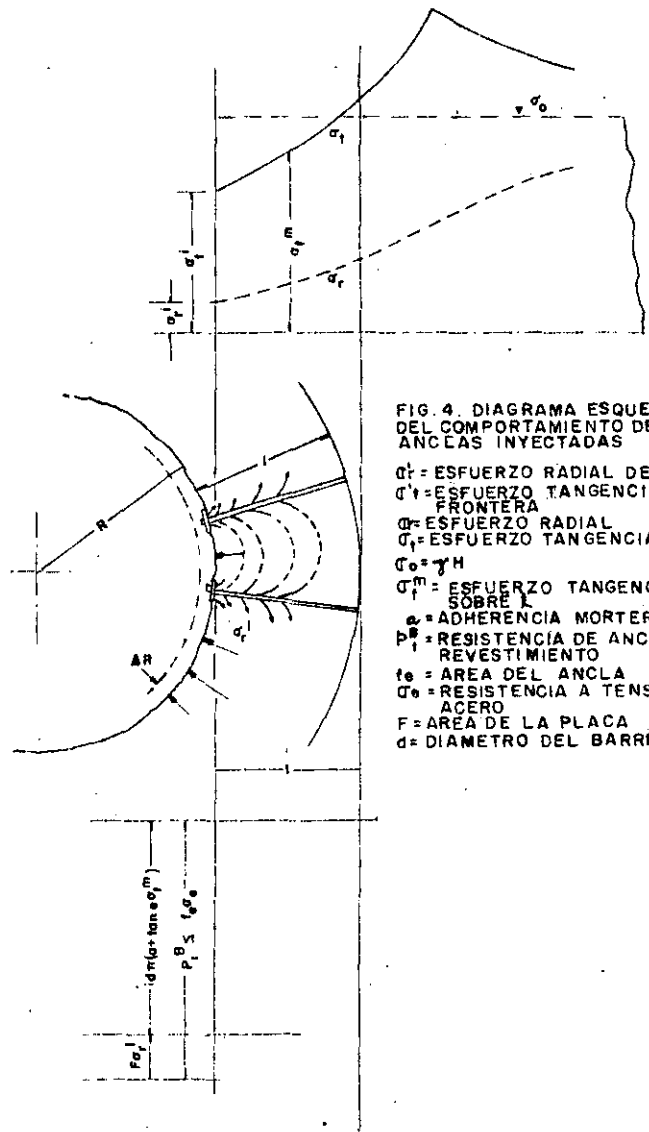
FIG. 2. REPRESENTACION ESQUEMATICA DE LA CURVA  $G_r/\Delta r$  MOSTRANDO LA RELACION RECIPROCA ENTRE  $G_r, \Delta r, r/R$  Y  $T$ , PARA: SOPORTES DE DIFERENTE FLUENCIA 1 y 2 y TIEMPO DE REACCION (SEGUN FENNER-Y PACHER)  
 $\sigma_r^0$  = ESFUERZO RADIAL PARA  $r/R = 1$   
 $G_r$  = ESFUERZO RADIAL REQUERIDO COMO FUNCION DE  $\Delta r$   
 $P_i^B$  y  $P_i^I$  = RESISTENCIA DE SOPORTE DEL ARCO EXTERIOR E INTERIOR  
 $S$  = FACTOR DE SEGURIDAD  
 $C$  y  $C'$  = CONDICION DE CARGA Y DESCARGA DEL ARCO INTERIOR

**PATRON DE ANCLAJE**



**FIG. 3. ESQUEMA DE DISEÑO DEL ARCO EXTERIOR PARA UNA CAPACIDAD DE SOPORTE DADA.**

- $P_A$  = RESISTENCIA DEL CONCRETO, ACERO DE R
- $P_A$  = REFUERZO, ARCO DE ROCA Y ANCLAS.
- $P_A$  = CAPACIDAD TOTAL DEL SOPORTE
- $b$  = ALTURA DE LA ZONA DE CORTANTE
- $d$  = ESPESOR DEL REVESTIMIENTO
- $e, t$  = DISTANCIA SOBRE ANCLAS
- $s$  = LONGITUD DEL PLANO DE CORTE
- $w$  = ESPESOR DEL ARCO DE SOPORTE DE ROCA
- $\sigma_{gd}$  = RESISTENCIA EN COMPRESION SIMPLE DE LA ROCA
- $c$  = COESION DE LA ROCA
- $\beta$  = ANGULO DE FRICCION INTERNA
- $\tau_c$  = RESISTENCIA AL CORTANTE DE LA ROCA
- $\tau_r$  = PROPORCION DE RESISTENCIA AL CORTANTE DEL REFUERZO
- $E^R, E^A$  = MODULO ELASTICO DEL ARCO DE ROCA Y DEL REVESTIMIENTO
- $\alpha_s$  = ANGULO DE CORTE DEL MACIZO ROCOSO
- $F^R$  = AREA DEL ACERO DE REFUERZO POR METRO LINEAL DEL TUNEL
- $f^R$  = AREA DE LAS ANCLAS
- $C$  = LIMITE PROPORCIONAL DE LAS ANCLAS DE ACERO
- $\tau^R$  = RESISTENCIA CORTANTE DE LA ROCA
- $\sigma^R$  = ESFUERZO NORMAL SOBRE EL PLANO DE CORTANTE
- $\alpha^R$  = ANGULO DE CORTANTE EN LA ROCA
- $\psi$  = INCLINACION PROMEDIO DEL PLANO DE CORTANTE
- $\beta^R$  = INCLINACION DE LAS ANCLAS



- FIG. 4. DIAGRAMA ESQUEMATICO DEL COMPORTAMIENTO DE LAS ANCLAS INYECTADAS**
- $\sigma_r^f$  = ESFUERZO RADIAL DE FRONTERA
- $\tau_t^f$  = ESFUERZO TANGENCIAL DE FRONTERA
- $\sigma_r^m$  = ESFUERZO RADIAL
- $\tau_t^m$  = ESFUERZO TANGENCIAL
- $\sigma^m = \tau^m H$
- $\sigma^m$  = ESFUERZO TANGENCIAL PROMEDIO SOBRE L
- $a$  = ADHERENCIA MORTERO-ROCA
- $P^R$  = RESISTENCIA DE ANCLA EN EL REVESTIMIENTO
- $f_e$  = AREA DEL ANCLA
- $\sigma_a$  = RESISTENCIA A TENSION DEL ACERO
- $F$  = AREA DE LA PLACA
- $d$  = DIAMETRO DEL BARRENO

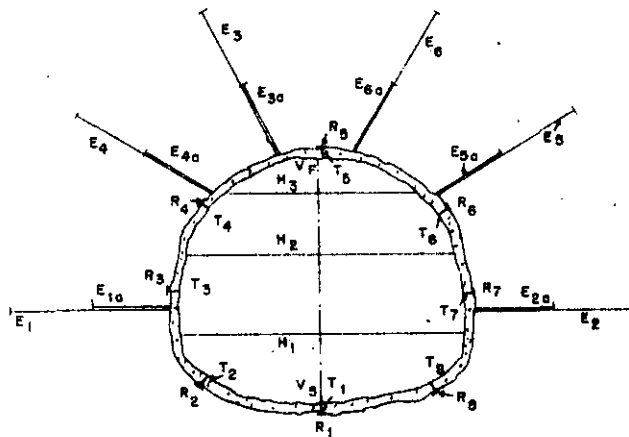


FIG. 5: SECCION NORMALIZADA DE MEDICIONES MAS IMPORTANTES

$R_1 - R_8$  = CELDAS DE PRESION RADIAL

$T_1 - T_8$  = CELDAS DE PRESION TANGENCIAL

$H_1, H_2, H_3$  = LINEAS DE MEDICION DE CONVERGENCIA

$E_1, E_2, E_3, E_4, E_5, E_6$  = EXTENSOMETROS LONGITUDINALES

$E_1a, E_2a, E_3a, E_4a, E_5a, E_6a$  = EXTENSOMETROS CORTOS

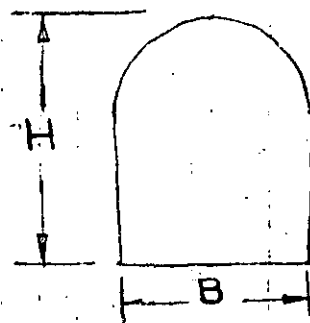
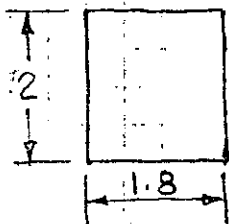
$V_1, V_2$  = PUNTOS DE CONTROL TOPOGRAFICO EN PISO Y TECHO

# PROCEDIMIENTOS DE EXCAVACION DE CAVIDADES SUBTERRANEAS

Los procedimientos de excavación de cavidades subterráneas dependen de los siguientes factores:

- Calidad del macizo rocoso
- Dimensión de la cavidad
- Filtraciones de agua
- Equipo disponible

A continuación presentaremos algunos de los procedimientos más usuales:

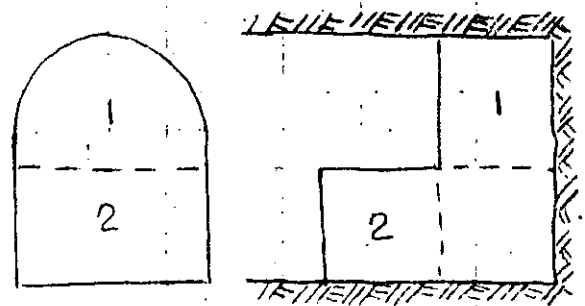
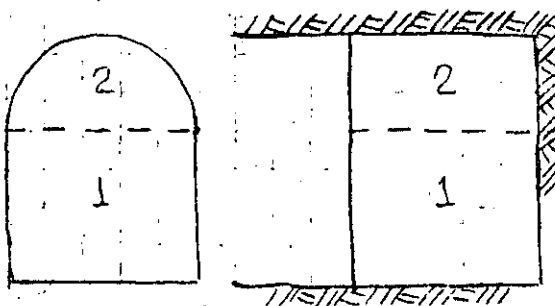


B	H
2.5	3.5 m
6.0	5.0 m
9.0	9.0 m

Sección Portal

## SECCION COMPLETA EN ROCA SANA, CON EXPLOSIVOS

- Socavones de exploración
- Galerías de explotación
- Galerías de inyección y drenaje
- Túneles de acceso

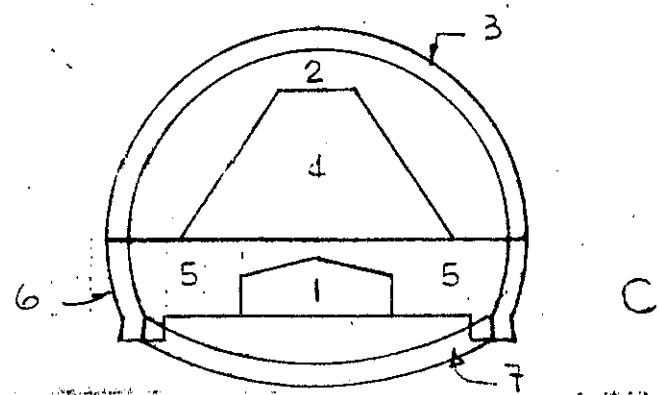
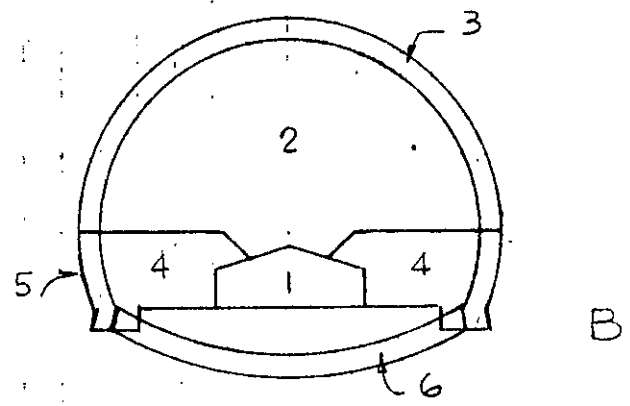
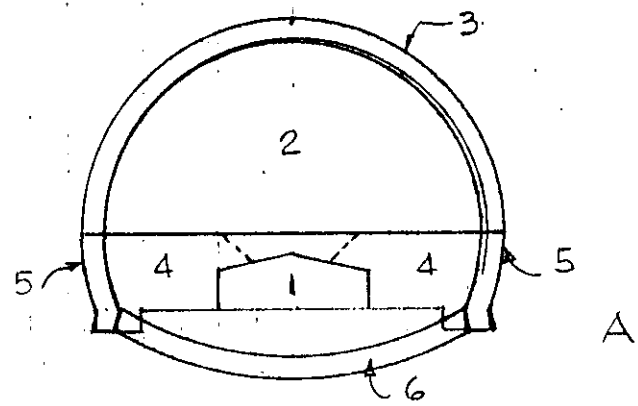


## SECCIONES COMBINADAS

- Cuando hay poco techo (Zona de portales)
- Con perforadora de pierna

### Método de túnel piloto sobre el piso del túnel

Se utiliza en roca blanda con filtraciones. La galería piloto de avance sirve para drenar el agua de infiltración y tiene área entre 9 y 15 m<sup>2</sup>. En las figuras se indican las tres variantes de este método. La galería piloto puede o no ir ademada con marcos y concreto lanzado.

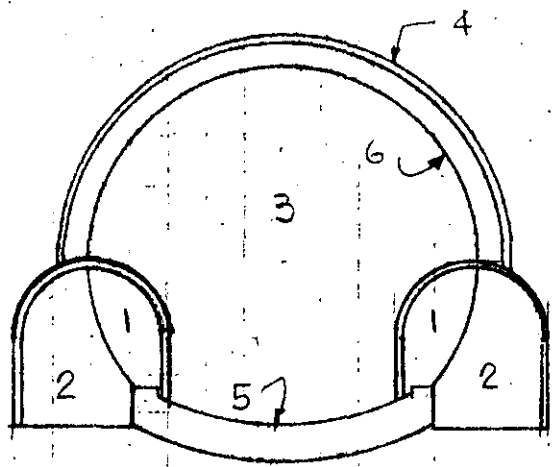


Método de las dos galerías piloto laterales sobre el piso del túnel. Se utiliza en roca blanda.

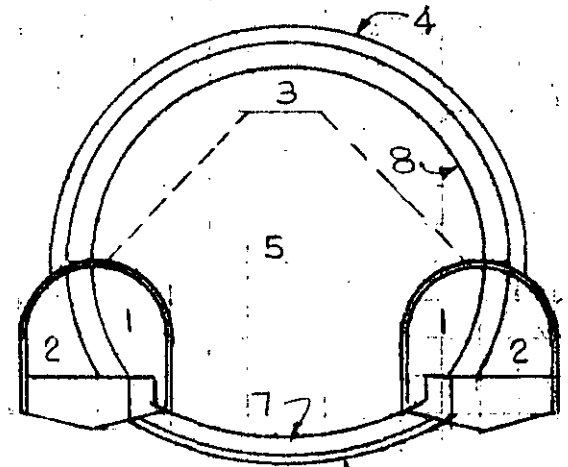
En una primera etapa se excavan los dos túneles piloto los cuales se protegen con marcos metálicos. Se cuelan las guarniciones de piso y arranque de los muros laterales.

En la segunda etapa puede realizarse el resto de la excavación con avances pequeños de 1 ó 2 metros soportando la roca con marcos que se apoyan en los arranques del muro previamente colados.

Cuando la roca no soporta el avance de 1 ó 2 metros, entonces se excava una ranura o corona de 0,75 m a 1 m de longitud que permita la colocación del marco metálico de soporte, continuando con revestimientos de concreto lanzado y finalmente con el núcleo central.



A



B

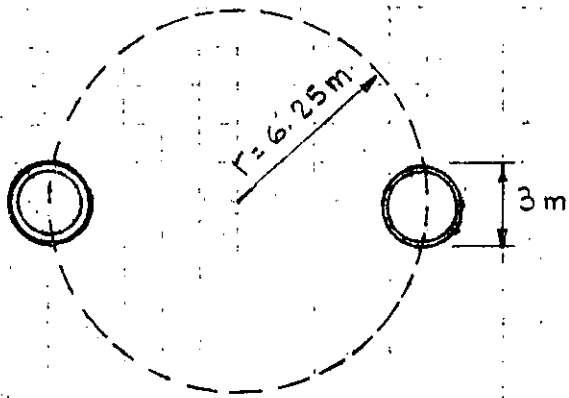
## Método de soportes laterales piloto. (Japón)

Este método se ha utilizado en túneles por debajo del mar en roca deleznable con fuertes filtraciones (1000 a 1500 lt/seg)

- 1.- Perforación de los dos túneles piloto de 3m de diámetro
- 2.- Colocación del ademe metálico del túnel principal, dentro de las dos galerías piloto. Ademe de tubo de acero.
- 3.- Relleno de concreto de las dos galerías piloto
- 4.- Excavación de la mitad superior
- 5.- Colocación de los marcos metálicos tubulares, los cuales se rellenan con mortero para aumentar su resistencia
- 6.- Excavación de la mitad inferior
- 7.- Colocación de los tornapuntas tubulares inferiores
- 8.- Colado del revestimiento de concreto.



# METODO DE SOPORTES LATERALES PILOTO (TUNEL SEIKAN, JAPON)



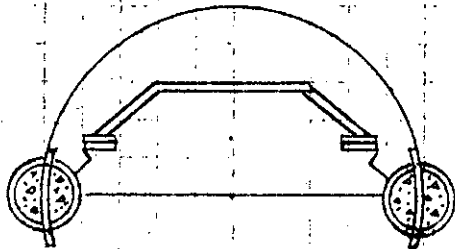
1 PERFORACION TUNELES PILOTO



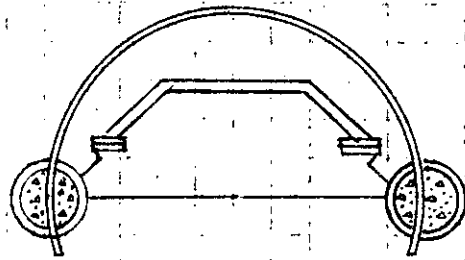
2 COLOCACION ADEME METALICO



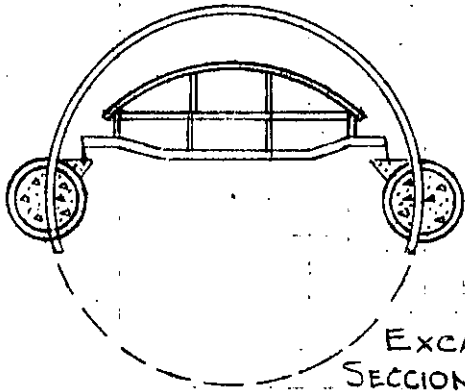
3 CONCRETO TUNELES PILOTO



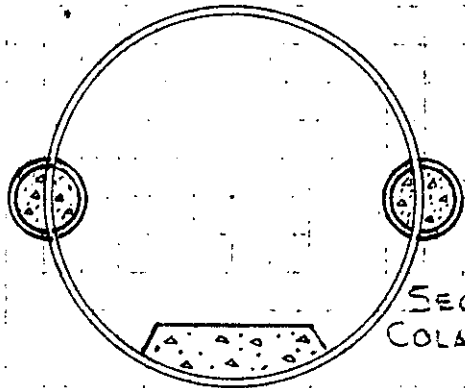
4 EXCAVACION SECCION SUPERIOR



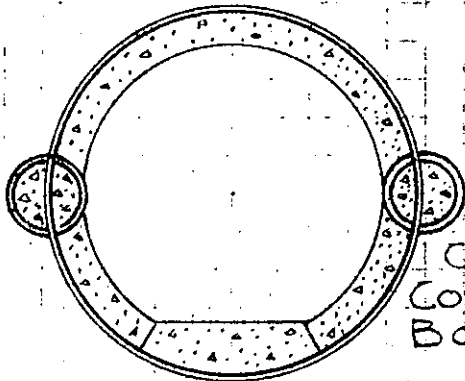
5 ADEME SECCION SUPERIOR



6 EXCAVACION SECCION INFERIOR



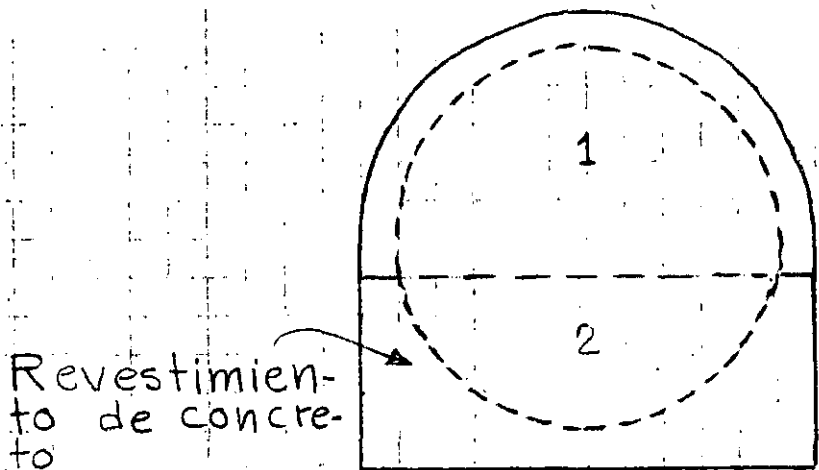
7 ADEME SECCION INFERIOR COLADO CUBETA



8 COLADO COSTILLAS Y BOVEDA

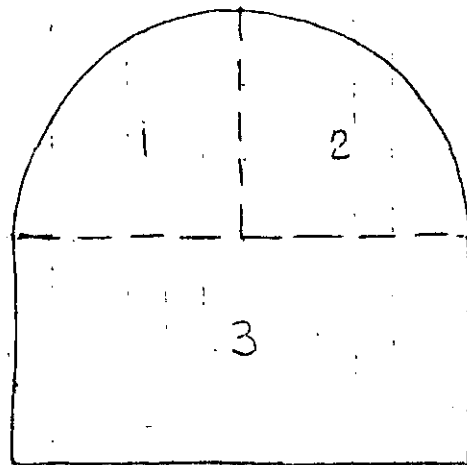
## Método de sección superior y banqueo

Se utiliza en roca sana.



Sección portal  
12 x 12 m

A



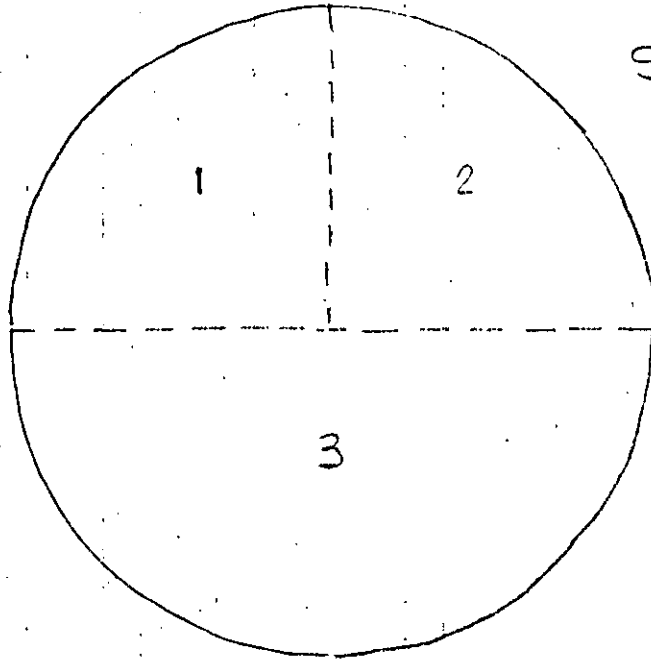
Sección portal  
12 x 12 m

B

- Algunas veces la sección superior es necesario excavarla en dos o tres secciones, como en B.
- La mejor geometría se obtiene mediante voladuras de post-corte perimetral (smooth blasting) con barrenación horizontal tanto en la sección superior como en la inferior.

## Método de sección superior y banqueo.

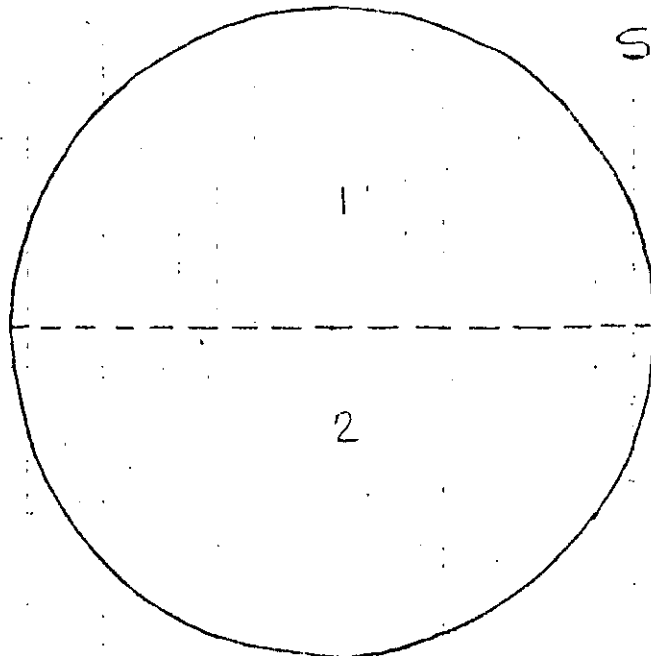
Se utiliza en roca sana



SECCION CIRCULAR

$\phi$  16.5 m

A



SECCION CIRCULAR

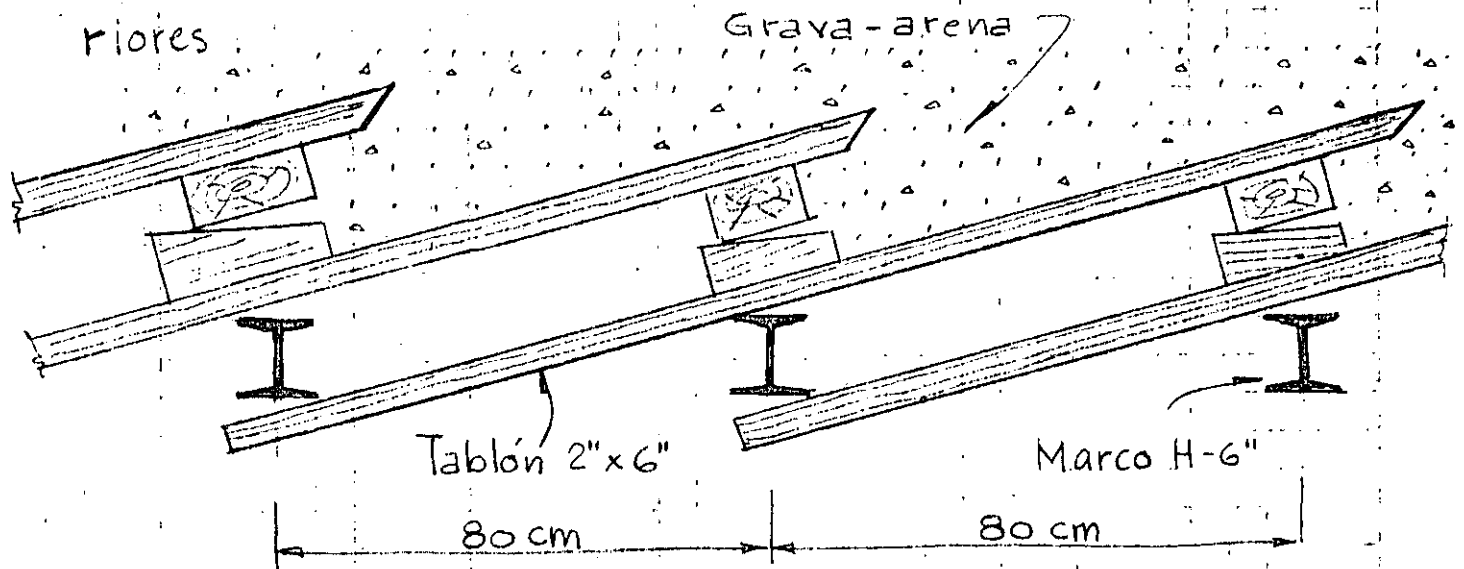
$\phi$  16.5 m

B

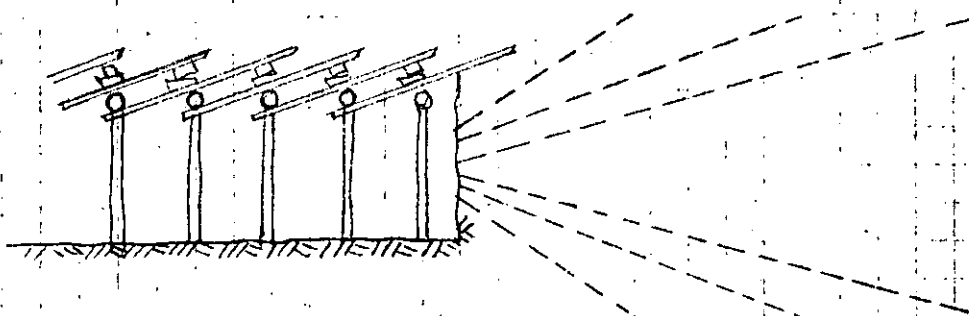
Se deben usar voladuras de post-corte perimetral (smooth-blasting)

# EXCAVACION CON ESTACAS DE AVANCE AL FRENTE

En suelos medianamente compactos como tepetate (toba sedimentaria de origen volcánico, arenas-limo-arcillosas con poca cementación) o rocas deleznales se requiere de soporte adelante del frente del túnel. En estos casos se hincan cuñas de madera o de metal apoyándose en los marcos anteriores.



ESQUEMA DE SOPORTE



ESTACAS DE AVANCE  
MAS AUREOLAS DE INYECCION

# TUNELES EN SUELOS BLANDOS

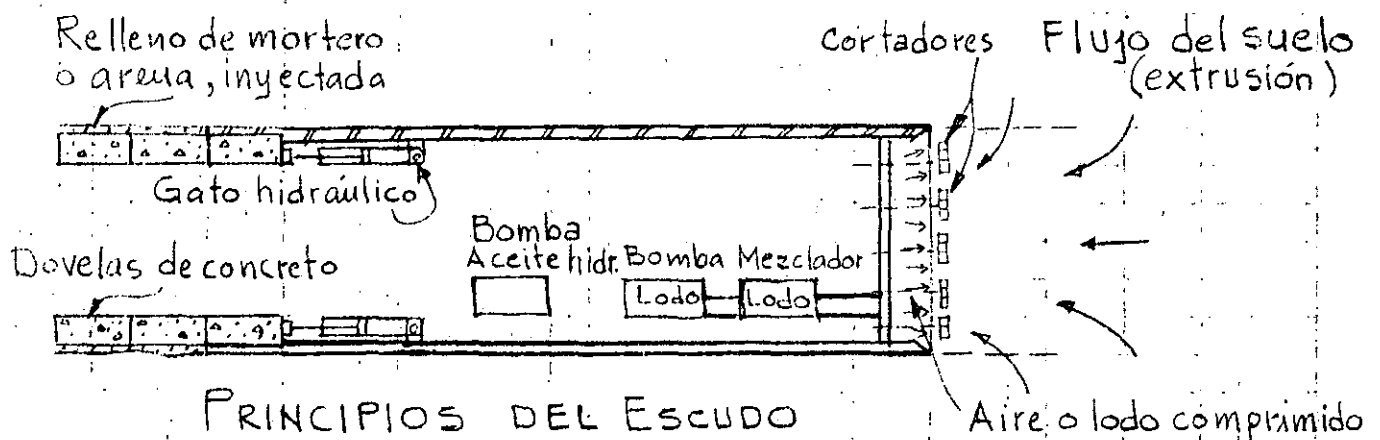
Los procedimientos más usuales son:

- Excavación con escudo
- Cajones hundidos

Los escudos pueden ser abiertos o cerrados según la consistencia del suelo.

Cuando el suelo es muy blando se usan los escudos cerrados con cámara de presión al frente ya sea con aire presurizado o lodo presurizado para evitar la extrusión del suelo hacia el escudo. En algunos casos se ha recurrido a la congelación del suelo para mejorar su consistencia y poderlo excavar.

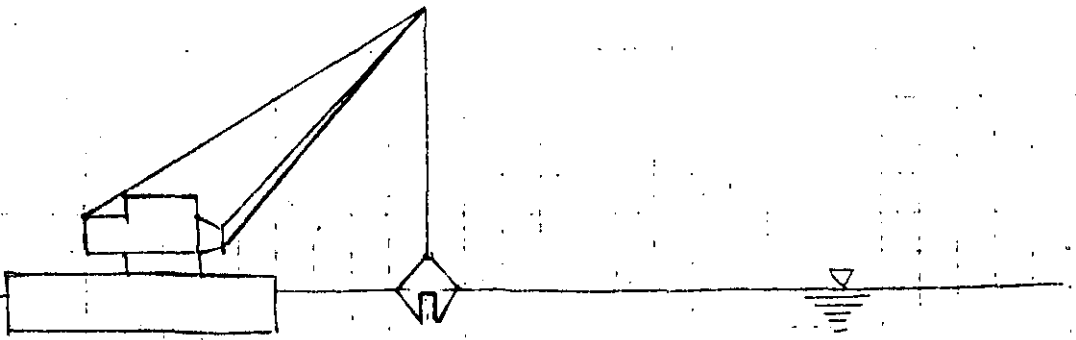
El material excavado se mezcla y se bombea como lodo (slurry) hacia afuera donde se separa el agua de los sólidos para volver a utilizarse.



## PRINCIPIOS DEL ESCUDO

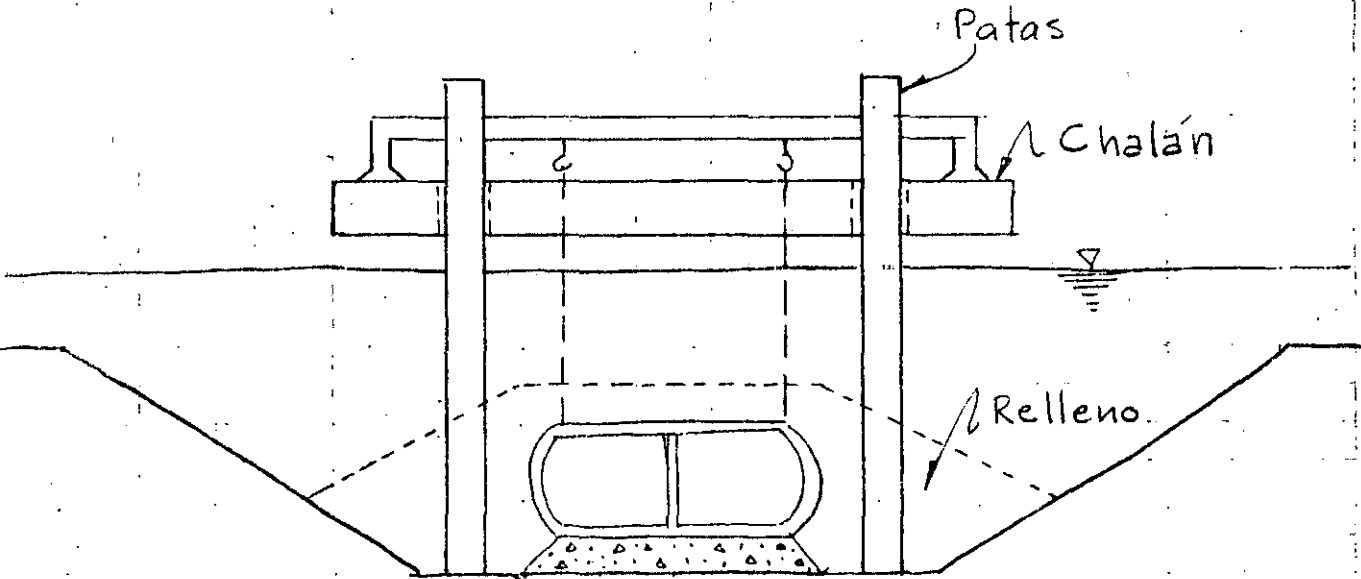
La excavación del frente puede hacerse a mano o con cortadores

# HUNDIMIENTO DE CAJONES

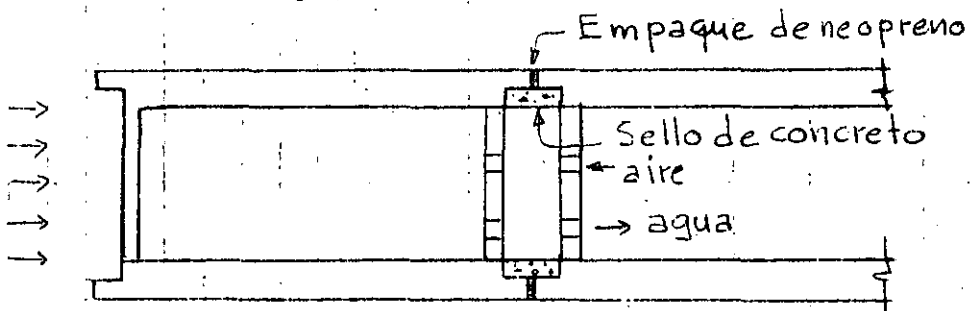


Plantilla de  
grava

## DRAGADO DEL CANAL



## HUNDIMIENTO DE LOS CAJONES

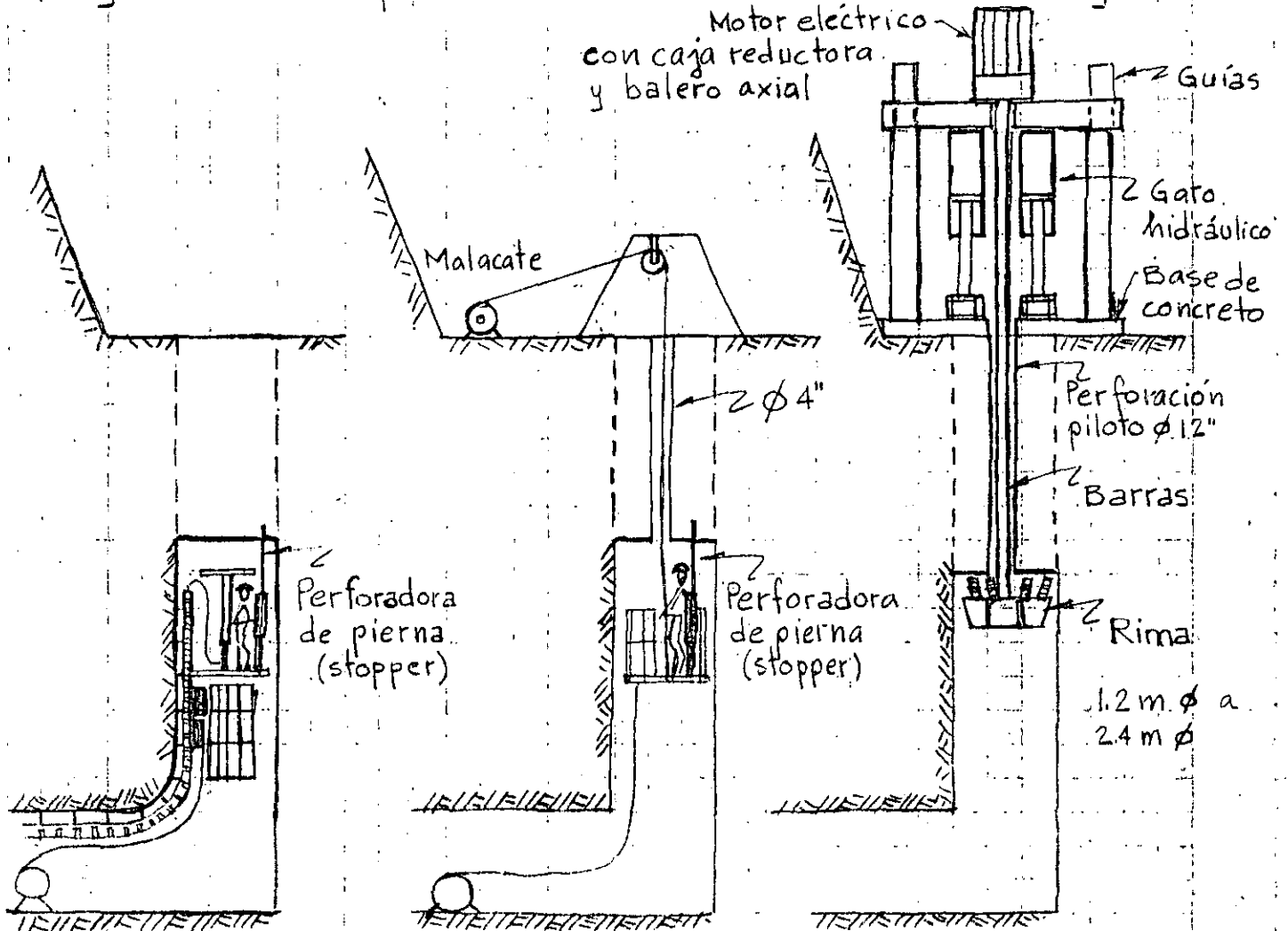


## SELLO DE JUNTAS

# EXCAVACION DE LUMBRERAS

La excavación de lumbreras depende en buen grado del equipo disponible.

Algunos de los procedimientos más usuales son los siguientes:



JAULA TREPADORA

3.6 a 5.4 m/día

JAULA SUSPENDIDA CONTRAPOCERA

3.6 a 5.4 m/día

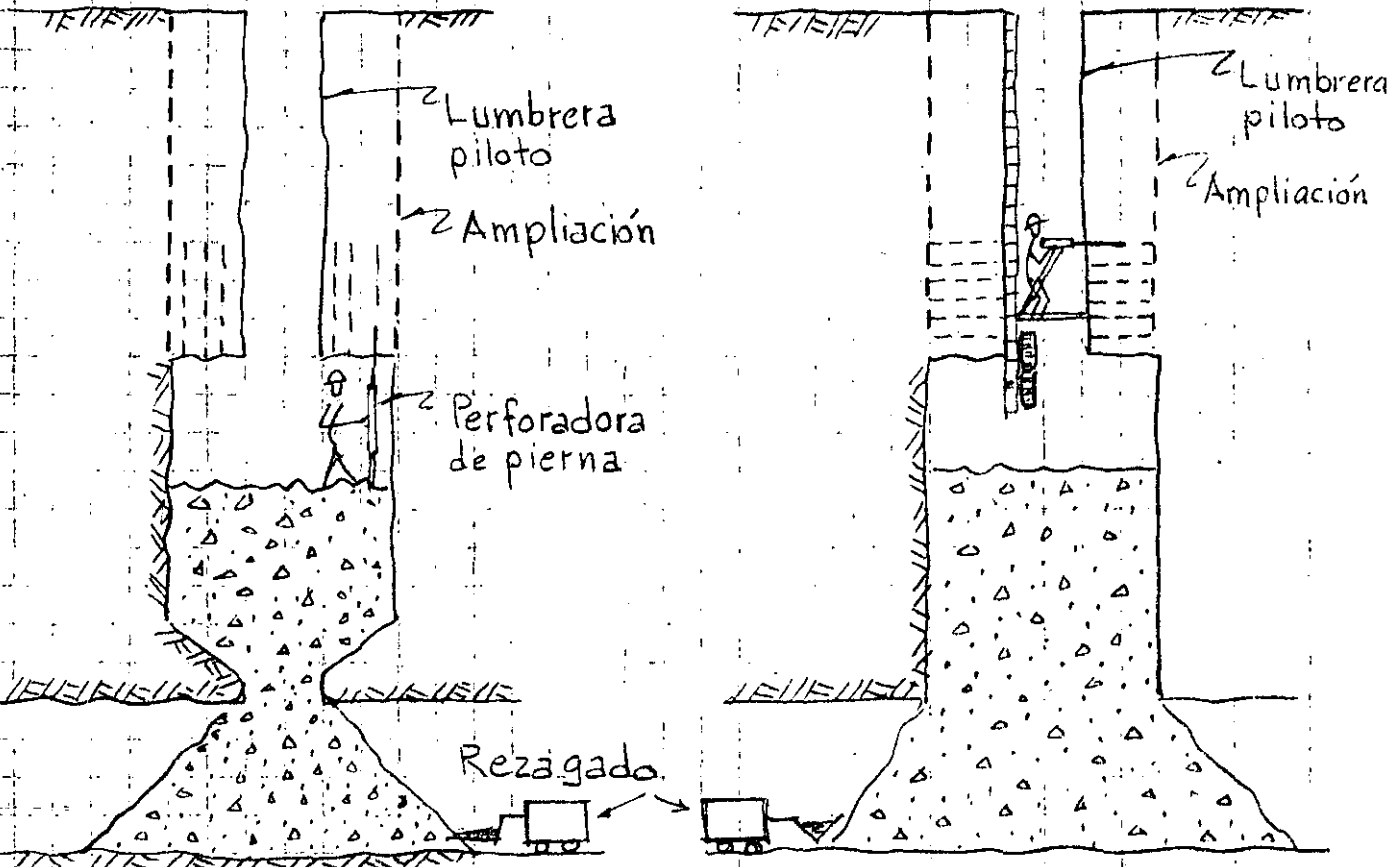
16 a 36 m/día

Ventajas de la contrapocera:

- Menor tiempo.
- Lumbreras más largas
- Mayor producción

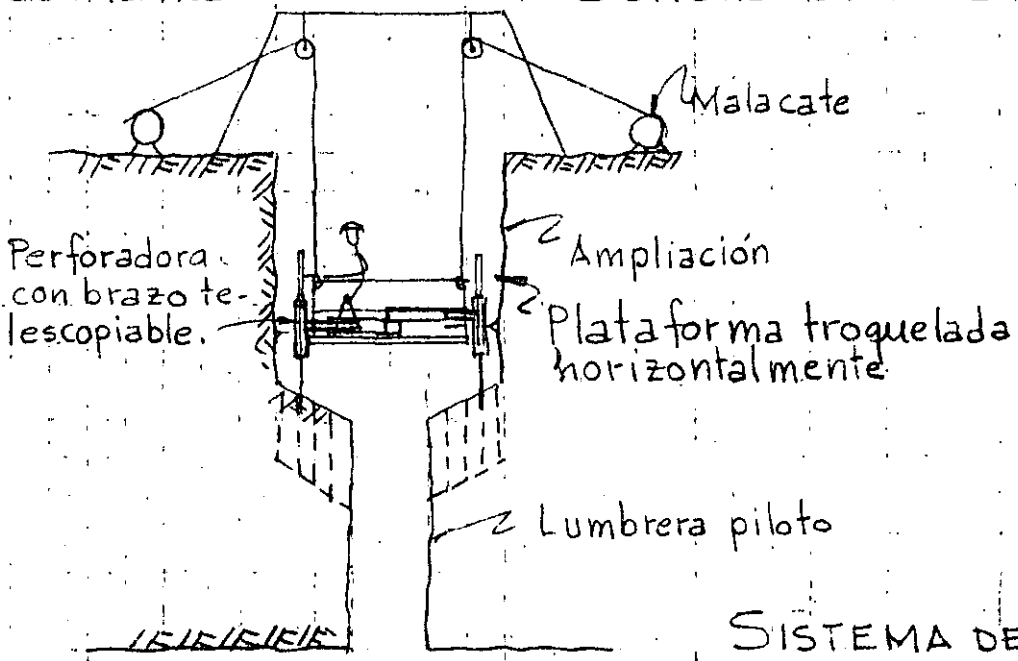
Las jaulas están quedando fuera de uso.

# AMPLIACION DE LUMBRERAS



Barrenación vertical

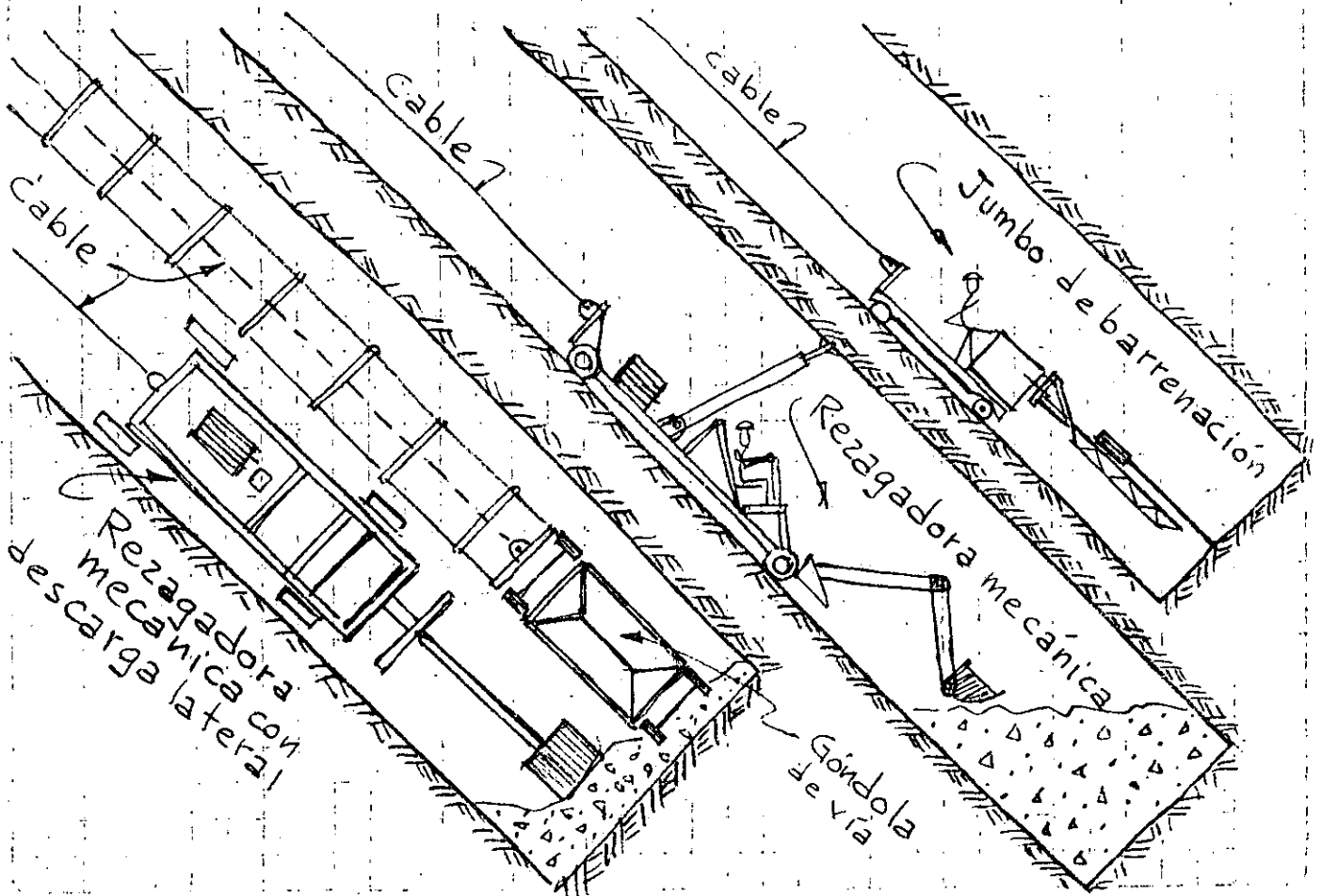
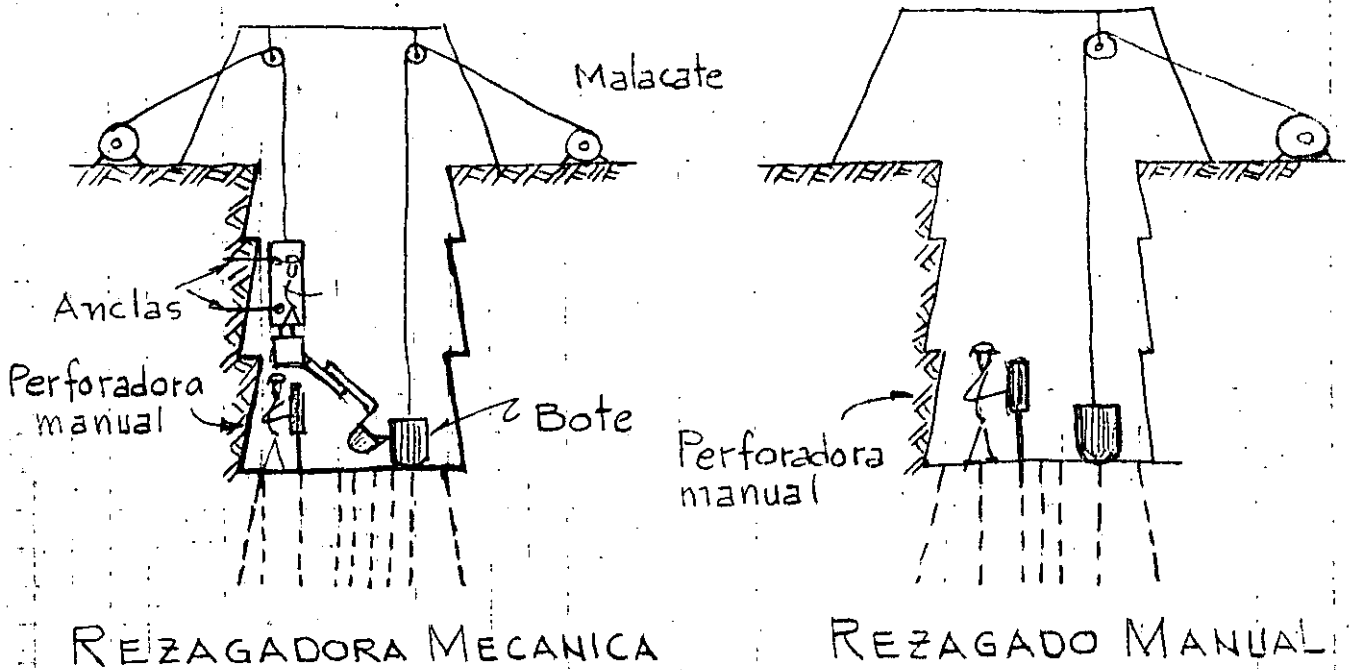
Barrenación horizontal



SISTEMA DE BANQUEO

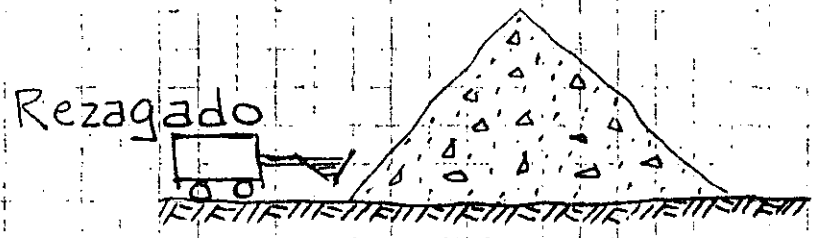
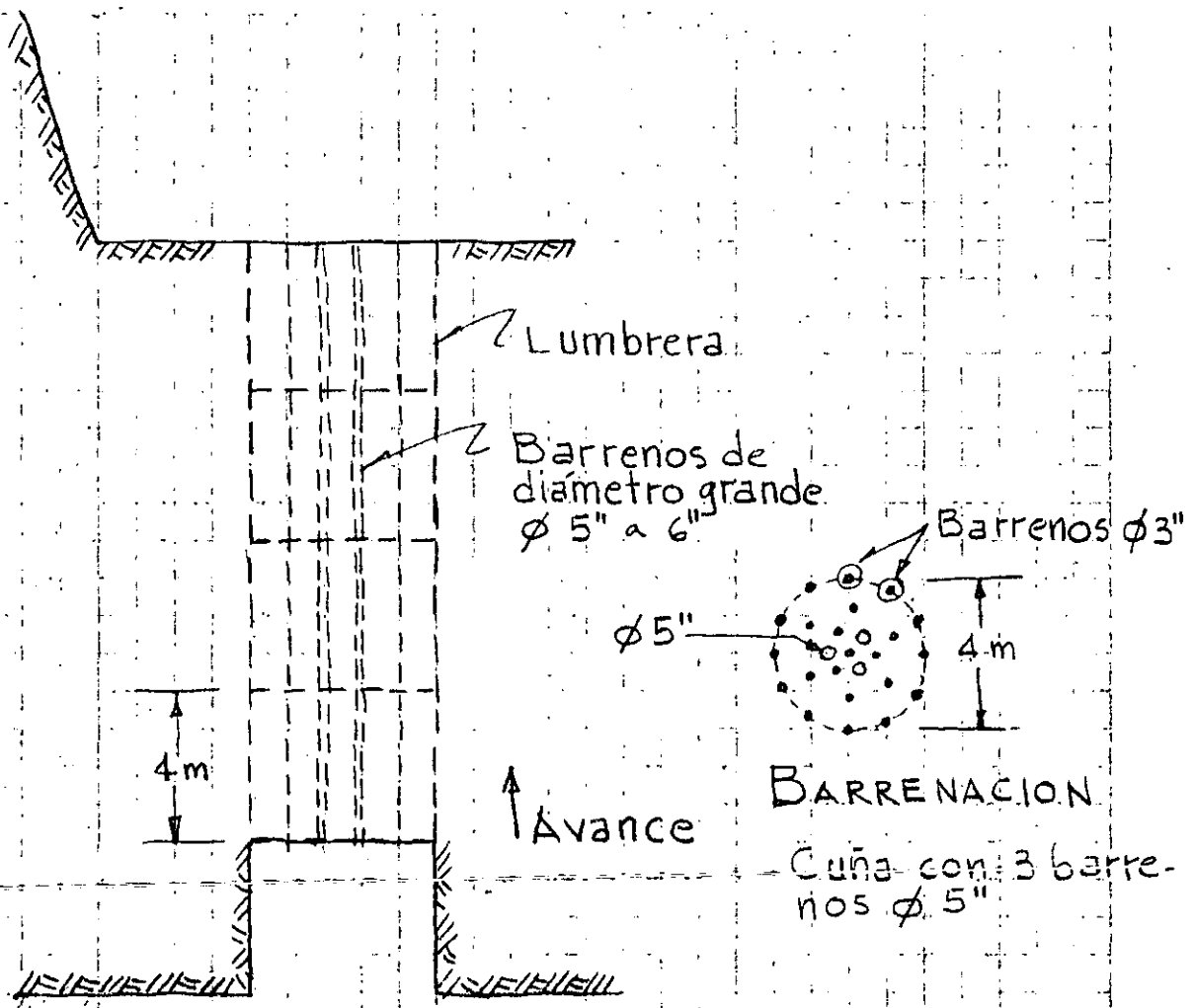


# POZOS VERTICALES E INCLINADOS



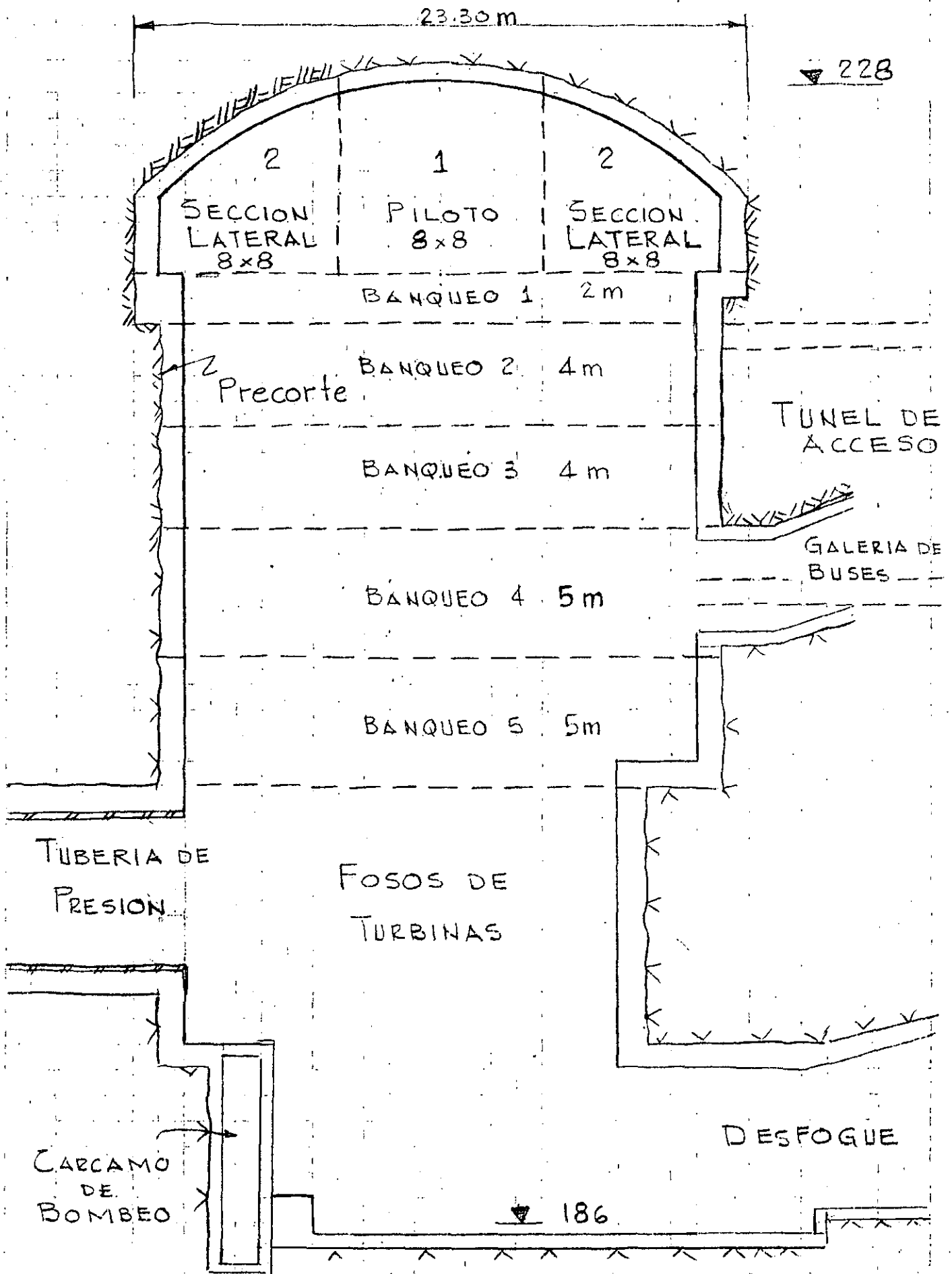
POZO INCLINADO CON EXCAVACION MECANIZADA

# LUMBRERAS CON DETONACION HACIA ARRIBA



AVANCE VERTICAL HACIA ARRIBA

# EXCAVACION DE CASAS DE MAQUINAS



23.30m

228

2  
SECCION LATERAL  
8x8

1  
PILOTO  
8x8

2  
SECCION LATERAL  
8x8

BANQUEO 1 2m

2  
Precorte  
BANQUEO 2 4m

BANQUEO 3 4m

BANQUEO 4 5m

BANQUEO 5 5m

TUNEL DE ACCESO

GALERIA DE BUSES

TUBERIA DE PRESION

FOSOS DE TURBINAS

CARCAMO DE BOMBEO

DESFOQUE

186

ESQUEMA DE EXCAVACION

# BOMBEO EN TUNELES

Las condiciones y características del bombeo de agua en túneles es muy variable.

Dada la importancia que reviste el bombeo para evitar suspensiones de trabajo a causa de inundaciones a continuación presentamos algunos puntos de vista sobre el manejo del agua.

- Tener respaldo de bombas entre 300 y 400 %
- Personal especializado en instalación y mantenimiento.
- Suministro y protección eléctrica adecuado y/o suministro confiable de aire comprimido.
- La bomba debera tener un F.S. = 1.5 para contrarrestar efectos de temperatura y humedad, desgaste y bajas de voltaje. Las pérdidas de carga por fricción son aproximadas al 20%.

## BOMBAS USUALES :

Gasto de 2 a 10 lt/seg.  
con cargas de 15 m.

Bombas de turbina y/o de diafragma accionadas por aire comprimido. Sumergibles

Gasto de 2 a 10 lt/seg  
con cargas de 50 a 75 m

Bombas de pistón, accionadas por bielas acopladas a motor eléctrico. Con pichanicha

Gasto de 25 a 100 lt/seg  
con cargas de 50 a 75 m

Bombas sumergibles de turbina acopladas a motor eléctrico estanco contra el agua.

Gasto de 100 a 1000 lt/seg  
con cargas de 50 a 100 m

Bombas sumergibles y/o de pozo profundo.

Potencia de una bomba  $P = 8QH$ ,  $Q = m^3/seg$ ,  $H = m$ ,  $P = KW$

Si  $Q = 80 lt/seg$  y  $H = 80 m$ ;  $P = 8 \times 0.08 \times 80 \times 1.2 = 61.44 Kw = 82 HP$

Utilizando un F.S. = 1.5.  $P = 105 HP$

# VENTILACION EN TUNELES

## DURANTE LA CONSTRUCCION

### Requerimientos de diseño:

- Calidad del aire fresco: Calidad requerida en las áreas de trabajo.
- Ciclo de trabajo: Número de turnos y horas de ejecución de voladuras.
- Cantidad de aire: Programa de demanda actual y futura, concentración particular de máquinas productoras de gas y polvo.

### CALIDAD DEL AIRE

Máximas concentraciones de impurezas del aire permisibles por el Cuerpo Nacional de Trabajo de Salud y Seguridad de Suecia

SUBSTANCIA	CONCENTRACION PROMEDIO (PPM) DURANTE UNA EXPOSICION DE	
	30 min	8 horas
Monóxido de carbono CO	50	25
Dióxido de carbono CO <sub>2</sub>	15 000	5 000
Dióxido de nitrógeno NO <sub>2</sub>	3	2
Oxidos de nitrógeno NO <sub>x</sub> NO <sub>x</sub> = NO · NO <sub>2</sub>	30	20

La contaminación principal del aire proviene de los vehículos diesel y de los explosivos que producen oxidos de carbono y gases nitrosos y cenizas volantes.

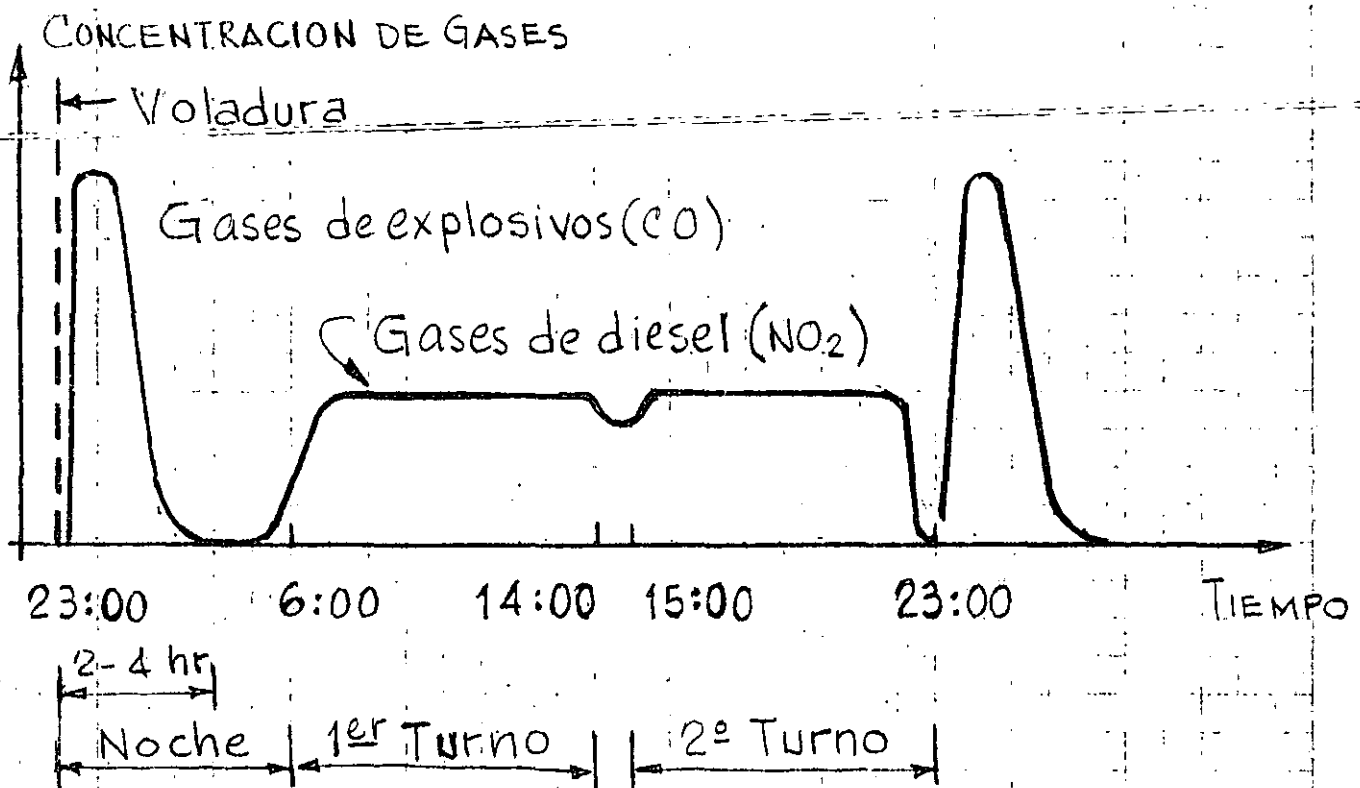
Para el caso de la Mina Kiruna en Suecia, el factor gobernante en el diseño ha sido el bióxido de nitrógeno  $\text{NO}_2$ .

Los vehículos diesel deberían estar normalmente equipados con catalizadores y purificadores.

Con el desarrollo futuro de los sistemas de purificación de gases de los vehículos diesel el factor de diseño será el  $\text{CO}_2$ .

### CICLO DE TRABAJO

A continuación se presenta una gráfica sobre el tipo y concentración de gases medidos en la Mina Kiruna en Suecia durante la operación de dos turnos por día.



### CONCENTRACION DE GASES DURANTE EL DIA

Como se sabe los gases de las voladuras caen hasta un nivel aceptable entre 2 y 4 horas después de la voladura,

siempre y cuando la cantidad de aire de ventilación es igual a la capacidad de aire que se utiliza durante el día. Esto significa que durante la noche en la que solo se tienen los gases de los explosivos se requiere una capacidad de ventilación menor.

Se observa claramente la concentración de gases por combustión del diesel al inicio del primer turno.

## CANTIDAD DE AIRE

Para determinar la cantidad de aire fresco requerida para estar dentro de los límites permisibles de concentración de gases contaminantes es necesario determinar previamente:

- la cantidad de gases producidos para su limpieza
- la eficiencia del sistema de ventilación que se define como:

$$\frac{C_u}{C_d} = \frac{\text{concentración de impurezas en el aire usado}}{\text{concentración de impurezas en el aire de las áreas de trabajo}}$$

- la calidad del aire abastecido

La cantidad de aire puede determinarse mediante la siguiente expresión, basada en los requerimientos de aire por kilogramo de combustible quemado en un metro cúbico de área de trabajo.

$$Q_e = \frac{P \times 0.27 \times Q_s \times k}{3600}, \text{ m}^3/\text{seg.}$$

en donde:

$Q_e$  = cantidad de aire,  $\text{m}^3/\text{seg}$

$P$  = potencia de máquinas, KW

$0.27$  = consumo específico,  $\text{kg}/\text{kWh}$

$Q_s$  = necesidad específica de aire,  $\text{m}^3/\text{kg}$   
recomendación  $Q_s = 3000 \text{ m}^3/\text{kg}$  de combustible quemado, según datos de Kiruna.

$k$  = factor de utilización

= 0.15 para operaciones de transporte

= 0.30 para carga y transporte

= 0.45 para carga

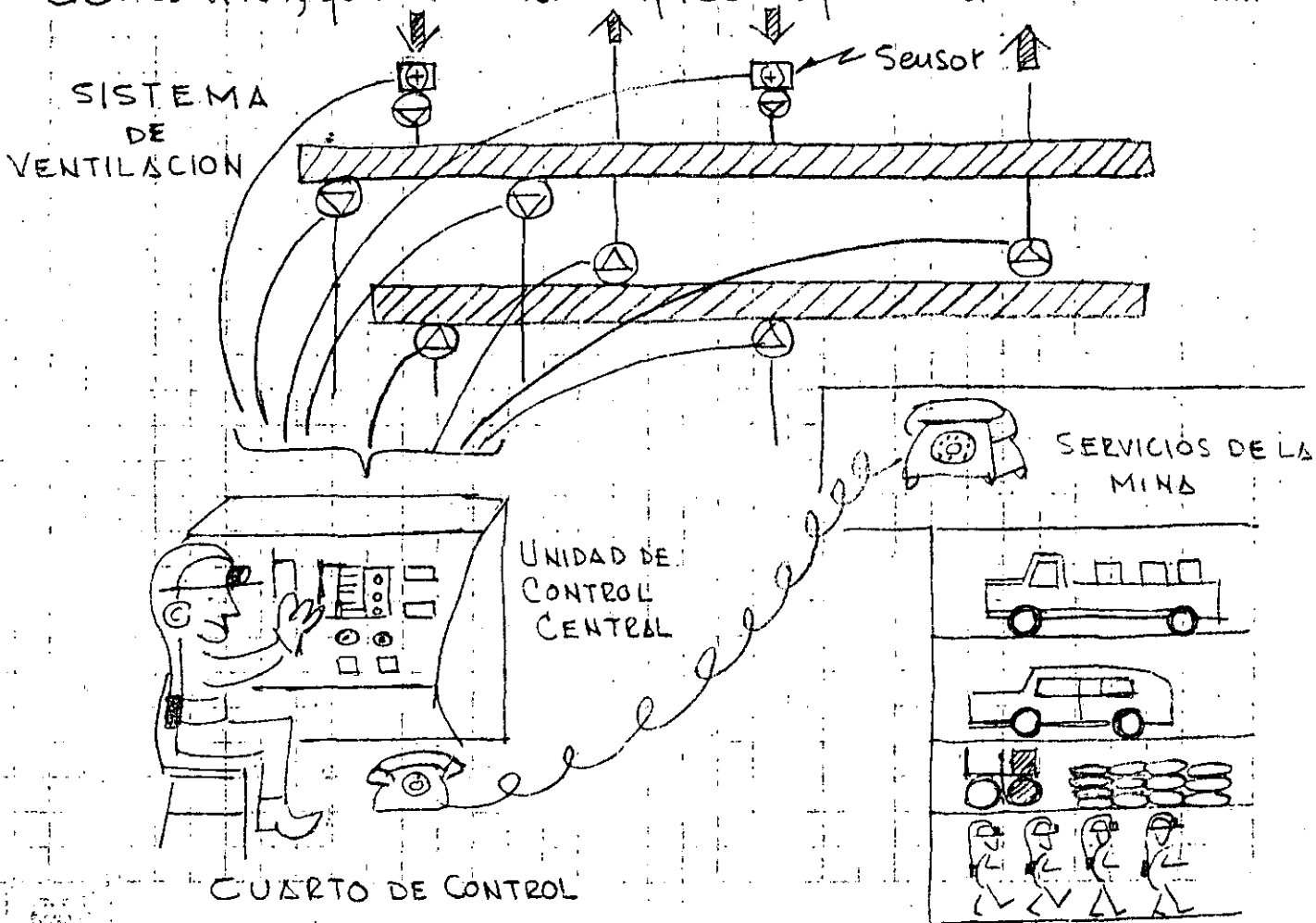


# SISTEMA DE CONTROL

Para estar en mejor posición en el control de la operación del sistema de ventilación fundamentalmente para ahorrar dinero en energía deberá instalarse un sistema de control remoto.

Este sistema está basado sobre una cooperación muy cerrada entre un sistema de señales, un operador y un equipo de mantenimiento.

Si el sistema de ventilación llega a presentarse un defecto por ejemplo: la abertura de una puerta ocasionando fugas, o paro de ventiladores, o temperaturas muy altas, el control unitario manda una señal inmediata al operador del control, quien avisa rápido al personal de mantenimiento



## SELECCION DEL SISTEMA DE VENTILACION

Los arreglos de ventilación pueden hacerse en varias formas. El sistema más adecuado para cada caso dependerá de las condiciones particulares.

INYECCION DE AIRE consiste en soplar el aire a través de los ductos hasta los sitios de trabajo y hasta los frentes de excavación. Se obtiene buena ventilación en el frente, teniendo la desventaja que las fugas de aire pueden arrastrar el humo y los gases a todo lo largo del túnel.

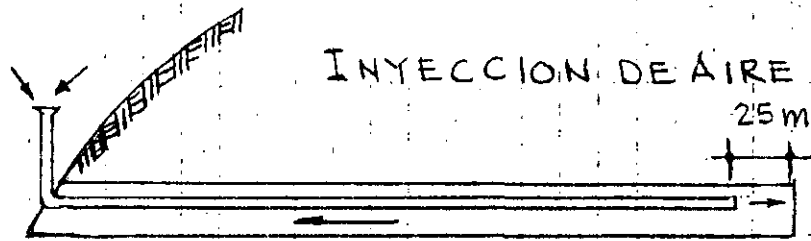
Los ductos de plástico son muy útiles en este caso ya que son fáciles de manejar y ocupan poco espacio.

EXTRACCION FORZADA consiste en lanzar los gases, polvo y humo a la atmósfera a través de un ducto metálico que llega hasta el frente. Para obtener una ventilación más eficiente conviene colocar un abanico auxiliar portátil en el piso del túnel junto al frente.

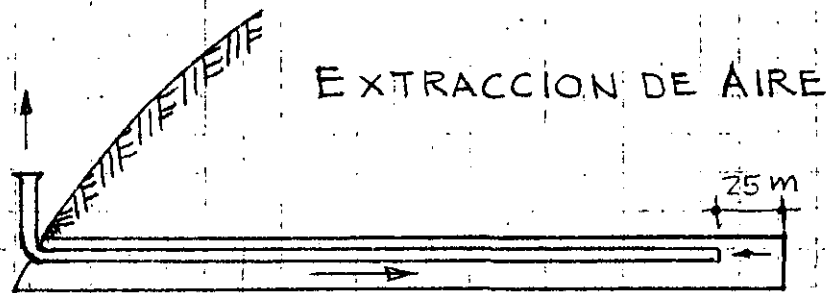
EXTRACCION E INYECCION ALTERNADAS da buenos resultados ya que el tiempo de extracción es suficientemente largo para asegurar que todos los gases han salido antes de invertir el sistema con soplado. El sistema implica el uso de ventiladores reversibles y ductos metálicos.

Los ductos deberán estar a 25 m. del frente para protegerlos de las voladuras. El ventilador auxiliar será de 30 a 70 % de la capacidad del ventilador principal.

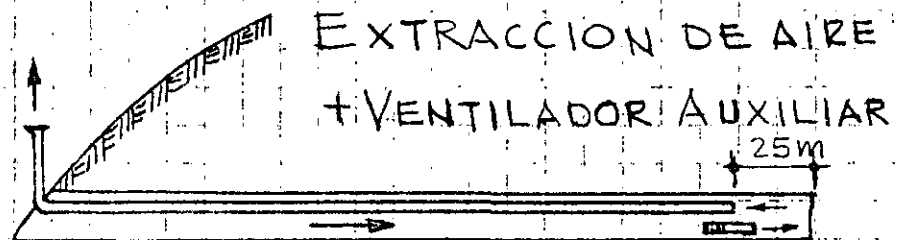
# SISTEMAS DE VENTILACION



Sencillo, se tiene buen control sobre el trayecto del aire. Puede dispersar los gases a lo largo del túnel.



No es muy adecuado. Se tiene pobre ventilación en el frente y en la entrada se produce frío durante el invierno.

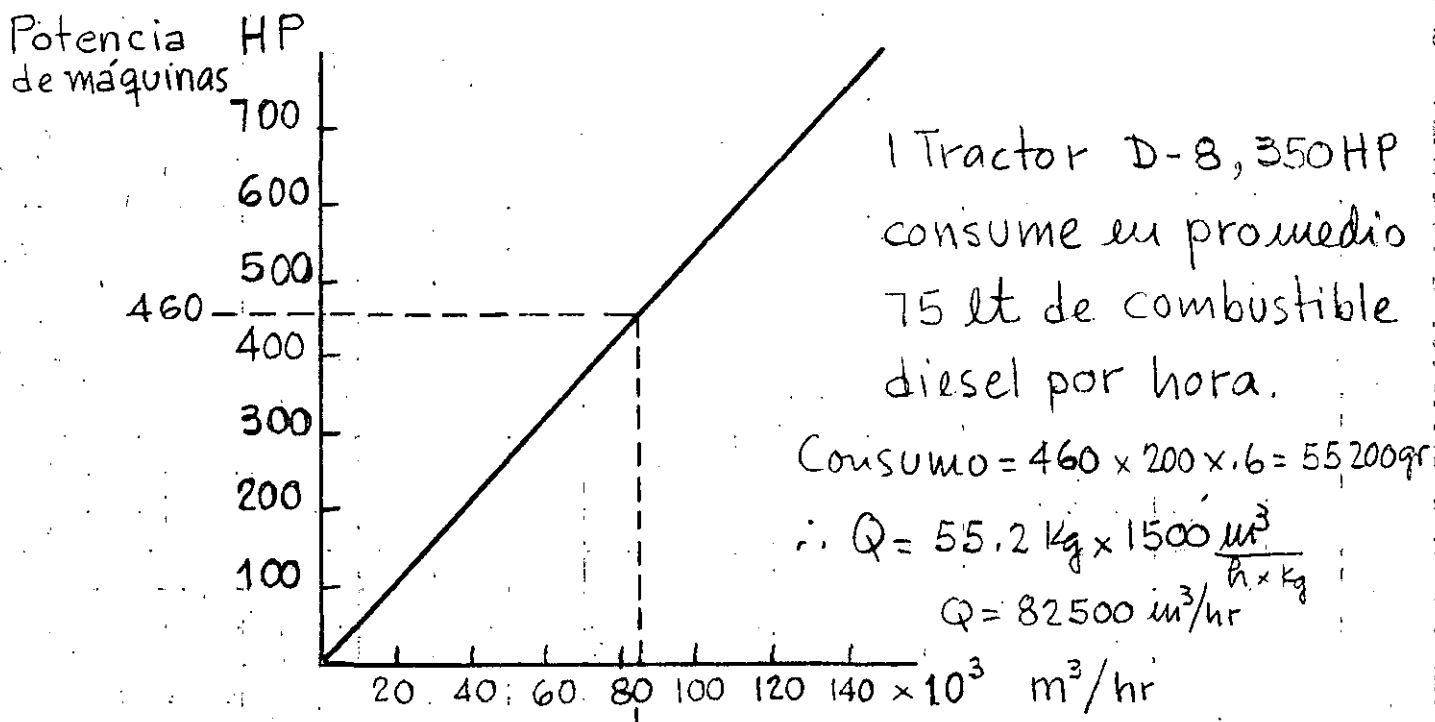


Se obtienen buenos resultados excepto que el enfriamiento en la entrada permanece

Los mejores resultados se obtienen inyectando aire durante la barreración y el rezagado con extracción inmediatamente después de la voladura.

## CALCULO DEL ABASTECIMIENTO DE AIRE

Según el Cuerpo Nacional Sueco de Protección a los Trabajadores publicó en 1969 un método para calcular el abastecimiento de aire de ventilación. Para contrarrestar el efecto de los escapes de gas quemado, deberá abastecerse  $1500 \text{ m}^3/\text{hr}$  por kg de combustible quemado considerando un consumo de diesel de  $200 \text{ gr}/\text{HP}/\text{hr}$ .



82500 Requerimiento de aire fresco.

La gráfica está basada sobre un promedio de 60% sobre los  $200 \text{ g}/\text{HP}/\text{h}$  de consumo de combustible y  $1500 \text{ m}^3/\text{hr}$  por kilogramo de combustible quemado.

Ejemplo: Si tenemos 136HP en cargadores de llantas y 230HP en tractores y 150HP en camiones; estos últimos sobre 40'/hora. tenemos: Total HP =  $136 + 230 + 150 \frac{40}{60} = 460 \text{ HP}$ ; el aire requerido es:  $Q = 82500 \text{ m}^3/\text{h} = 23.7 \text{ m}^3/\text{seg.} \doteq 50000 \text{ p.c.m.}$

# VENTILACION DE GASES POR EXPLOSIVOS

Los valores siguientes se utilizan en Suecia para el cálculo general de requerimiento de aire para la ventilación de gases:

$$q = \frac{A}{t} (L + 120) \text{ m}^3/\text{min}$$

en donde:

A = área del túnel  $\text{m}^2$

t = periodo de ventilación en minutos.

L = longitud del ducto o del túnel.

q = flujo de aire fresco inyectado.

$$q = 180 \frac{A}{t} \text{ m}^3/\text{min} \text{ para extracción de aire}$$

$$\text{y } \frac{2}{3} q \text{ m}^3/\text{min} \text{ para el abanico auxiliar}$$

Ejemplo: Para un túnel de 1200 m de largo con 16  $\text{m}^2$  de área con un tiempo de ventilación de 30', se requiere un gasto  $q = \frac{16}{30} (1200 + 120)$

$$\therefore q = 704 \text{ m}^3/\text{min} = 11.7 \text{ m}^3/\text{seg. de aire inyectado}$$

= 24500 p.c.m.

Para extracción de aire:

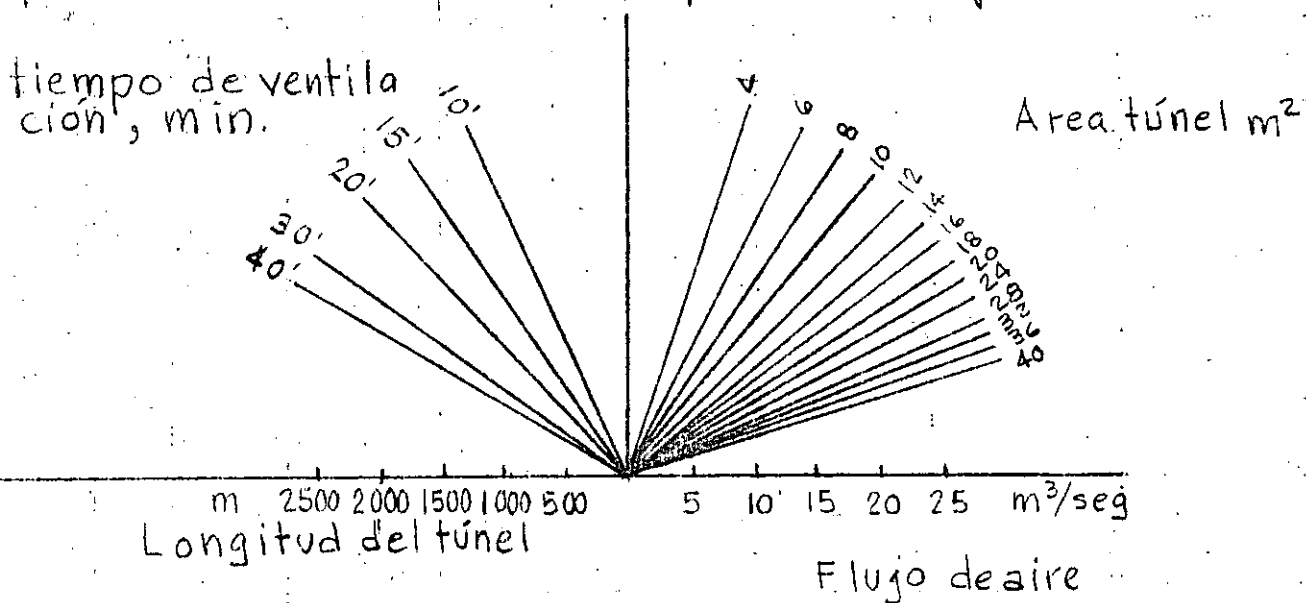
$$q = 180 \times \frac{16}{30} = 96 \text{ m}^3/\text{min} = 1.6 \text{ m}^3/\text{seg}$$

$$+ \text{abanico auxiliar} = \frac{2}{3} \times 1.6 = 1.06 \text{ m}^3/\text{seg}$$

La extracción es aproximadamente 20% de la inyección

# VENTILACION DE GASES POR EXPLOSIVOS EN TUNELES

La expresión  $q = \frac{A}{t} (L + 120) \text{ m}^3/\text{min}$ , en donde  $A = \text{área del túnel en m}^2$ ;  $L = \text{longitud del ducto en metros}$  y  $t = \text{tiempo programado de ventilación}$  se presenta en el nomograma siguiente



Durante la barrenación el flujo de aire deberá ser por lo menos igual al aire consumido por las perforadoras para alcanzar la disolución del aire aceitoso.

La ventilación prevista para la construcción generalmente es suficiente para el arranque de otras actividades como soldadura, pintura, calentamiento, etc.

La velocidad del aire fresco debe variar entre 12 y 18 m/seg.

# USO DE EXPLOSIVOS EN ROCA

## ANTECEDENTES

El uso de los explosivos es más una técnica que una ciencia. Hasta ahora el método más económico para fragmentar la roca es mediante el uso de explosivos.

La teoría está soportada por la práctica de tal manera que el diseño de voladuras se realiza más por la relación entre parámetros que mediante fórmulas teóricas por ejemplo; la relación entre el diámetro y el bordo. Es necesario comprender como trabaja el explosivo en la roca, para lo cual se requiere del conocimiento de las propiedades de los dos elementos, la roca y los explosivos.

En relación a la roca se puede decir lo siguiente:

- Calidad. - Tenemos una gran variedad en la calidad de los macizos rocosos en función de su estructura, y resistencia (caracterización del macizo rocoso). Este término de calidad involucra muchas propiedades del macizo rocoso. p. ej. - velocidad de transmisión de ondas de compresión P, resistencia en compresión simple, densidad, dureza, anisotropía, homogeneidad, flujo de agua, temperatura y estado de esfuerzos interno son algunas de las propiedades más importantes de las rocas para su utilización en el diseño de voladuras.

## Mecanismo de fragmentación:

En todos los tipos de roca tenemos que la resistencia en compresión simple es mucho mayor que la resistencia en tensión, cortante o flexión. (Del orden de 10 veces para tensión y cortante y 4.5 veces para flexión)

De acuerdo con lo anterior los mecanismos de fragmentación están diseñados para romper la roca por tensión, corte y flexión más que por compresión.

Cuando existe una cara libre se produce el fenómeno de reflexión y refracción de las ondas de choque de compresión o primarias. Poniéndose vibraciones de alta frecuencia (150 a 200 c.p.s.) que dan lugar a impactos de tensión intermitentes por razón de la fuerza centrífuga hasta que estas fuerzas de inercia vencen la resistencia a la tensión de la roca y entonces se produce el desprendimiento de fragmentos de roca a partir de la periferie hacia el centro.

Por otro lado, las fracturas de tensión en el cilindro de pared gruesa avanzan y los gases penetran en ellas produciendo el desplazamiento de los fragmentos de roca. También se produce un efecto combinado, semejante a una viga con un apoyo empotrado y otro libre bajo la carga de presión producida por el explosivo.



En relación al explosivo se tiene que la generación de la explosión o voladura ocurre por oxidación o reducción de combustible a alta presión.

Durante esta reacción se producen temperaturas de  $5000^{\circ}\text{C}$  y gases a presiones muy altas que varían entre  $15\ 000$  y  $150\ 000\ \text{Kg}/\text{cm}^2$ .

Esta presión se produce súbitamente en forma de impacto, propagándose las ondas de choque a velocidades entre  $2\ 000$  y  $7\ 000\ \text{m}/\text{seg}$ .

El trabajo realizado por  $1\ \text{Kg}$  de TOVEX es de  $580\ \text{ton}\cdot\text{m}/\text{seg}$  o sea que puede levantar  $1\ \text{ton}$  a una altura de  $580\ \text{m}$  en un segundo, equivalente a  $5800\ \text{KW}$  y  $100\ \text{Kg}$  a  $580\ 000\ \text{KW}$ .

## INGREDIENTES Y COMPOSICION DE LOS EXPLOSIVOS

La mayor parte de los explosivos comerciales son mezclas de compuestos que contienen 4 elementos básicos: Carbono, Hidrógeno, Nitrógeno y oxígeno.

Otros compuestos con elementos tales como: sodio, aluminio y calcio se incluyen para producir ciertos efectos deseados.

Como regla general estos componentes deberán dar un balance de oxígeno correcto.

Esto significa que durante la reacción todo el oxígeno disponible en la mezcla reacciona solamente para formar vapor de agua ( $H_2O$ ) y que con el carbón reacciona para formar únicamente dióxido de carbono ( $CO_2$ ) en forma de gas y el nitrógeno quede libre formando solo gas nitrógeno ( $N_2$ ).

Cuando hay otros elementos además de los cuatro básicos p.ej. sodio, deberá incluirse suficiente oxígeno adicional para lograr una combinación balanceada.

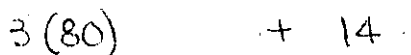
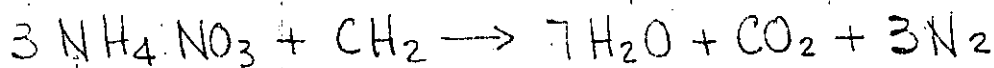
Cuando hay exceso de oxígeno disponible se producen gases altamente venenosos como los gases nitrosos  $NO$  ó  $NO_2$ . (óxidos de nitrógeno). Estos gases son fácilmente detectables por su olor y color café-rojizo.

Por otro lado, si estamos en defecto de oxígeno se forma el mortal gas monóxido de carbono ( $CO$ ) el cual desafortunadamente no es detectado por olor ni color.

Además de la formación de gases venenosos por exceso o deficiencia de oxígeno se produce una disminución de temperatura con una consecuente reducción en la presión de los gases producidos.

Para ilustrar los efectos del balance de oxígeno en el AN-FO (nitrato de amonio - aceite combustible) como agente explosivo tenemos:

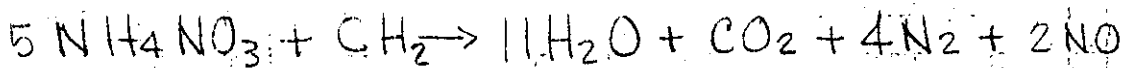
1. Oxígeno balanceado:



$$\frac{240}{254} = 94.5\% \quad ; \quad \frac{14}{254} = 5.5\% \Rightarrow 0.94 \text{ K cal/gr}$$

Nitrato de amonio + Aceite combustible (diesel)

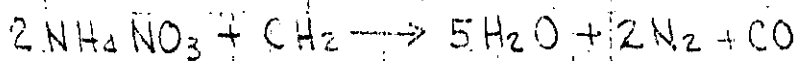
2. Oxígeno en exceso : (positivo)



$$96.6\% + 3.4\% \rightarrow 0.61 \text{ K cal/gr}$$

Además de que se produce menor temperatura y presión se produce gas nitroso (NO) que es un gas venenoso.

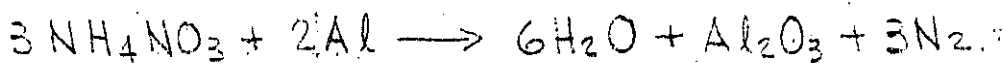
3. Oxígeno deficiente: (negativo)



92%      8% → 0.82 Kcal/gr

Se tiene menor temperatura y presión y se produce monóxido de carbono (CO) que es mortal.

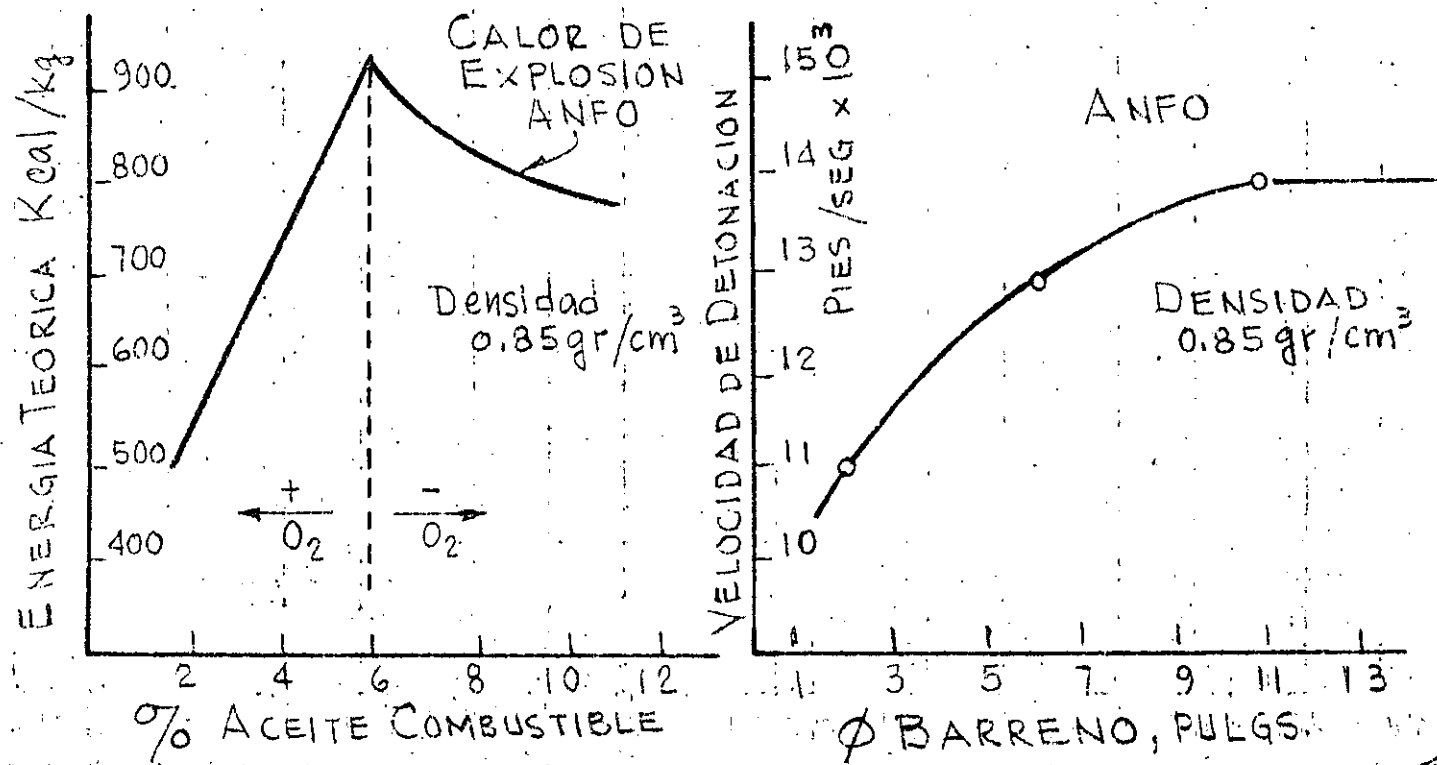
La reacción química más eficiente para el ANFO es, 94% de nitrato de amonio y 6% de aceite combustible diesel. Se pueden producir otros agentes explosivos más potentes p.ej. utilizando aluminio:



240      2(27)

81.5%      18.5% → 1.55 Kcal/gr

La desventaja de este compuesto para uso comercial es su alto costo. Se usa solo para explosivos militares.



## CLASIFICACION DE LOS EXPLOSIVOS

Los ingredientes usados en la fabricación de explosivos se definen como: explosivos bases, oxidantes, antiácidos y absorbentes.

Un explosivo base es un sólido o líquido que bajo la acción de suficiente calor o impacto se transforma en un producto gaseoso con acompañamiento de energía calorífica.

Los combustibles y oxidantes se agregan para lograr el balance del oxígeno.

Un antiácido se agrega para incrementar la estabilidad en almacenamiento y un absorbente se agrega para absorber o proteger los explosivos bases.

Un agente explosivo es cualquier material o mezcla compuesto por un combustible y un oxidante de tal modo que ninguno de sus ingredientes sea explosivo base.

En este caso la mezcla ANFO no puede ser detonado por un estopín N° 8 que contiene 2 gr de una mezcla de 80% de fulminato de mercurio y 20% de clorato de potasio. El ANFO tiene baja resistencia al agua y es defla-

La adición de un ingrediente explosivo como el TNT cambia la clasificación de la mezcla de agente explosivo a explosivo.

Los agentes explosivos pueden ser clasificados como - agentes explosivos secos - o - agentes explosivos

"sturry". El ANFO (agente explosivo seco) se inició en 1950

## Hidrogeles.

Los hidrogeles son los explosivos más recientemente desarrollados y actualmente son los más utilizados. Se fabrican en formulaciones tanto de agentes explosivos como de explosivos.

Contienen alta proporción de nitrato de amonio parte del cual está en solución acuosa y dependiendo del resto de los ingredientes puede ser clasificado como agente explosivo o explosivo.

Los agentes explosivos contienen ingredientes no sensibilizadores como aceite combustible, carbón, azufre o aluminio, y no constituyen cápsulas-sensitivas, mientras que los explosivos hidrogeles si contienen ingredientes como TNT que los transforma en cápsulas-sensitivas, el TNT solo es una cápsula-sensitiva.

Las mezclas del nitrato de amonio y los aceites o los sensibilizadores se espesan o gelatifican con gomas para proporcionar resistencia al agua.

Los hidrogeles son más seguros y no detonan al barrerlos sobre ellos, lo cual no sucede con las gelatinas.

## Dinamita pura

La dinamita pura esta compuesta por: Nitroglicerina (NG) y Silice ( $\text{SiO}_2$ ) en proporción 50% (NG) y 50% ( $\text{SiO}_2$ ) hasta 25% (NG) y 75% ( $\text{SiO}_2$ ). Normalmente se fabrica en 20 a 60% (NG) y 40 a 80% (NS) + C donde NS = Nitrostarch.

TABLA I. - INGREDIENTES USADOS EN LOS EXPLOSIVOS

INGREDIENTE	FORMULA	FUNCION
Nitroglicerina (NG)	$C_3H_5(NO_3)_3$	Explosivo base
Trinitrotolueno (TNT)	$C_6H_2CH_3(NO_2)_3$	Idem
Dinitrotolueno (DNT)	$C_7H_7N_2O_4$	Idem
Glicol de etileno dinitrato (EGDN)	$C_2H_4(NO_3)_2$	Idem, anticongelante
Nitrocelulosa	$C_6H_7(NO_3)_3O_2$	Idem, gelatilizante
Nitrato de amonio (NA)	$NH_4NO_3$	Idem + oxidante
Clorato de potasio	$KClO_3$	Idem + oxidante
Perclorato de potasio	$KClO_4$	Idem + oxidante
Nitrato de sodio (SN)	$NaNO_3$	Oxidante, reduce <sup>ción</sup> congelación
Nitrato de potasio	$KNO_3$	Oxidante
Pulpa de madera	$C_6H_{10}O_5$	Absorbente, combustible
Aceite combustible	$CH_2$	Combustible
Parafina	$CH_2$	Idem
Aceite para lámpara	$C$	Idem
Gis	$CaCO_3$	Antiácido-estabilizador
Oxido de zinc	$ZnO$	Idem
Aluminio (metal)	$Al$	Catalizador
Magnesio (metal)	$Mg$	Catalizador
Kieselgur	$SiO_2$	Absorbente anti-cake diatomeas o infusorios
Oxígeno líquido	$O_2$	Oxidante
Azufre	$S$	Combustible
Sal	$NaCl$	Antiinflamante
Compuestos <sup>nitrosos</sup> orgánicos		Explosivo base, sensibili-

TABLA 2.- ENERGIA CALORIFICA (Q) PARA ALGUNOS EXPLOSIVOS

EXPLOSIVO	DENSIDAD	Q. (cal/gr)
Nitroglicerina (NG)	1.6	1420
PETN	1.6	1400
Pentaeritritetetrinitrato		
RDX	1.6	1320
Compuesto B	1.6	1140
Tetril	1.6	1010
NG, Gelatina 40%	1.5	820
Slurry (TNT-AN-H <sub>2</sub> O) 20-65-15	1.5	770
NG, Gelatina 100%	1.4	1400
NG, Gelatina 75%	1.4	1150
AN, Gelatina 75%	1.4	990
NG, dinamita 40%	1.4	930
AN, gelatina 40%	1.4	800
NG, dinamita 60%	1.3	990
PETN	1.2	1200
Semigelatina	1.2	940
Dinamita extra 60%	1.2	880
Amatol, 50/50	1.1	890
RDX	1.0	1280
DNT	1.0	960
TNT-AN (50-50)	1.0	900
TNT	1.0	870
ANFO (94-6)	0.9	890
AN	0.8	350



Pólvora negra - Es el explosivo comercial más antiguo. Originalmente era una mezcla de nitrato de potasio, carbón vegetal y azufre, ahora se usa nitrato de sodio en lugar del nitrato de potasio.

Composición:

Nitrato de potasio . . . . .	75 %
Carbón vegetal . . . . .	15 %
Azufre . . . . .	10 %

Cuando se usa nitrato de sodio se disminuye un poco su porcentaje aumentando el carbón y el azufre

Tiene propiedades indeseables para su uso razón por la que ha sido sustituida.

Es extremadamente sensible al deflagarse o quemarse explotando a baja velocidad (1300 pies/seg)

Se usa en forma limitada en rocas blandas en canteras

## VELOCIDAD DE DETONACION

La propiedad sola más importante a considerar al evaluar la potencia de un explosivo es su velocidad sónica y puede ser confinada o no confinada.

La velocidad de detonación confinada es una medida de la velocidad con que viaja las ondas de compresión a través de una columna de explosivo dentro de un barreno u otro espacio confinado mientras que la velocidad no confinada se obtiene cuando se detona el explosivo a cielo abierto.

Como los explosivos se usan con cierto grado de confinamiento es más significativa la velocidad confinada.

La velocidad de detonación confinada en los explosivos comerciales varía entre 5 000 y 25 000 pies /seg.

Las velocidades no confinadas son del orden de 70 a 80% de la velocidad confinada.

## PRESION DE DETONACION

La presión de detonación es una función de la velocidad de detonación y de la densidad del explosivo.

Usualmente no se menciona como una propiedad pero es muy importante en la selección del explosivo. Cuando se tiene una cara libre se producen esfuerzos por impulso que son reflejados en la roca y son parte importante del mecanismo de rotura o de fragmentación.

## PRESION DE DETONACION --- Continuación

La relación entre la velocidad de detonación, la densidad y la presión de detonación es compleja.

La siguiente expresión es una de las aproximaciones obtenidas:

$$P = \frac{4.18 \times 10^{-7} DC^2}{1 + 0.8D}$$

en donde:  $P$  = presión de detonación en, kbar

$$1 \text{ kbar} = 14\,504 \text{ lb/pulg}^2$$

$D$  = densidad

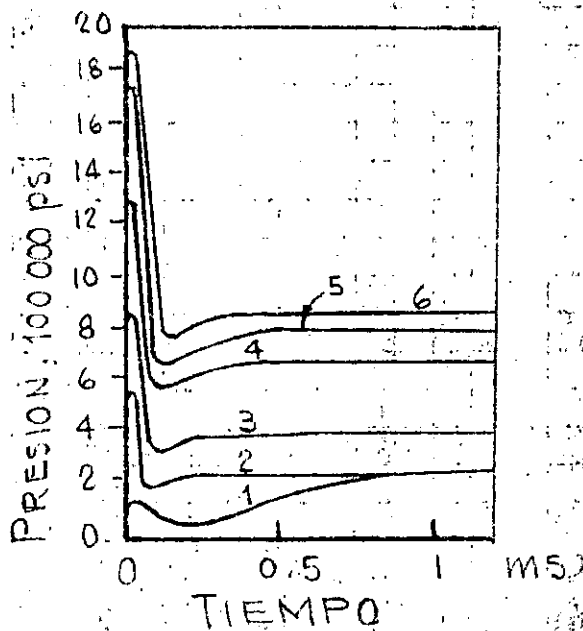
$C$  = Velocidad de detonación en pies/seg

Hay que distinguir entre presión de detonación y presión de ignición o de explosión.

La presión de ignición o explosión es la que produce el choque o impacto y tiene un valor del doble de la presión de detonación. Esta presión de choque o ignición se caracteriza por una onda muy puntiaguda frente a la cual toda la materia es ionizada y pulverizada.

- 1.- ANFO - 94/6 Granulado
- 2.- ANFO - 94/6 Fino
- 3.- AN-Dinamita 60%
- 4.- NG-Dinamita 60%
- 5.- TNT-AN-H<sub>2</sub>O-20/65/15
- 6.- AN-GELATINA, 75%

CURVAS DE PRESION CALCULADA  
BAJO CONFINAMIENTO PERFECTO



## CALIDAD DE GASES

La detonación ideal de los explosivos comerciales deben producir vapor de agua, bióxido de carbono y nitrógeno. Sin embargo gases venenosos como el monóxido de carbono y óxidos de nitrógeno (gases nitrosos) se forman muchas veces. En excavaciones a cielo abierto los gases venenosos no son importantes, por lo contrario en excavaciones subterráneas hay que tener cuidado con ellos.

## CRITERIOS PARA SELECCION DE UN EXPLOSIVO

Para cada sitio habrá un explosivo que proporcione los mejores resultados.

La selección del tipo más adecuado está en función de las propiedades geomecánicas de la roca como son: estructura, dureza, densidad, resistencia, humedad, ventilación, etc. y de la fragmentación obtenida, altura y proyección del banco.

En rocas duras y densas como la Tacueta y los Grautos un explosivo de alta velocidad tendrá buenos resultados sin embargo posiblemente el ANFO también dará buen resultado y es más económico.

En rocas blandas deben usarse explosivos de bajas velocidades. ejemplo: Caliches y basaltos vesiculares.

En general la velocidad de detonación debe ser igual a la velocidad sónica del macizo rocoso. (velocidad de las ondas P de compresión o primarias)

PROPIEDADES DE DINAMITAS PURAS  
DE NITROGLICERINA

PORCIEN TO EN PESO	DENSIDAD	VELOCIDAD CONFINADA pies/seg	RESISTENCIA DEL AGUA	CALIDAD DE GASES
60	1.3	19,000	Buena	Bobre
50	1.4	17,000	Regular	Pobre
40	1.4	14,000	Regular	Pobre
30	1.4	11,000	Pobre	Pobre
20	1.4	9,000	Pobre	Pobre

COMPOSICION DE LAS DINAMITAS PURAS  
DE NITROGLICERINA

COMPONENTES	PORCENTAJE EN PESO				
	20	30	40	50	60
NITROGLICERINA	20.2	29.0	39.0	49.0	56.3
NITRATO DE SODIO	59.3	53.3	45.5	34.4	22.6
ACRILE VULCANIZADO	15.4	13.7	13.8	14.6	15.2
AZUFRE	2.9	2.0	-	-	-
ANTRACENO	1.2	1.0	.8	1.1	1.2
HUMEDAD	.9	1.0	.9	.9	1.2

PROPIEDADES DE DINAMITAS DE AMONIO  
DE ALTA DENSIDAD

FORZAMIENTO EN PESO	DENSIDAD	VELOCIDAD CONTINUA pies/seg	RESISTENCIA DEL AGUA	CANTIDAD DE CARGAS
60	1.3	12,500	Regular	Buena
50	1.3	11,500	Regular	Buena
40	1.3	10,500	Regular	Buena
30	1.3	9,000	Regular	Buena
20	1.3	8,000	Regular	Buena

COMPOSICION DE LAS DINAMITAS DE AMONIO  
DE ALTA DENSIDAD

COMPONENTES	PORCENTAJE EN PESO				
	20	30	40	50	60
NITROGLICERINA	12.0	12.6	16.5	16.7	22.5
NITRATO DE SODIO	57.3	46.2	37.5	25.1	15.2
NITRATO DE AMONIO	11.8	25.1	31.4	43.1	50.3
ACEITE VEGETAL	10.2	8.8	9.2	10.0	8.6
AZUFRE	6.7	5.4	3.6	3.4	1.6
AMILACTO	1.2	1.1	1.1	.8	1.1
HUMEDAD	.8	.8	.7	.9	.7

NUMERO DE CARTUCHOS POR CAJA DE 25 KGS.

DIAMETRO	LONGITUD DE CARTUCHO		
	203 mm (8")	305 mm (12")*	406 mm (16")*
25 mm. (1")	209	139	105
29 mm. (1 1/8")	165	110	83
32 mm. (1 1/4")	137	90	68

\*Longitud optativa

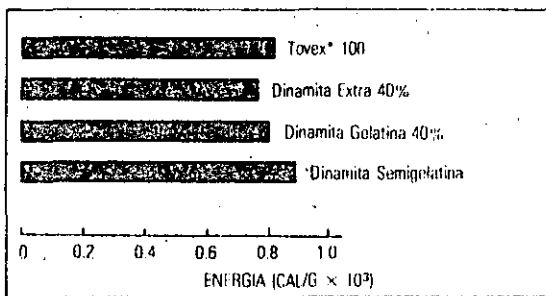
**Gases tóxicos:** Mínimos, clase 1

**Requisitos de cebado:**

Un fulminante ordinario No. 6. Por las características de ruptura del material de la envoltura, para introducir el detonador dentro del cartucho, se recomienda hacer la perforación en un extremo frontal junto al cierre metálico. No se recomienda perforar lateralmente el cartucho. Es indispensable asegurar que en el manejo del cartucho cebado, el detonador no se salga del cartucho.

**Densidad:** 1.10 gms/cc.

**Energía**



**Velocidad**

DIAMETRO	M/SEG	PIES/SEG
32 mm (1 1/4")	4050	13300

**Resistencia al agua:** Excelente. Sin envoltura, sumergido en agua, mantiene sus óptimas velocidad y energía.

**ventajas:**

- Cargado:** TOVEX 100 es sensible a la cápsula. Se ceba y se carga de manera similar a las dinamitas. Su habilidad de compactación proporciona el máximo acoplamiento al barreno y la máxima densidad de carga. Basta un leve empuje del atacador para llenar el barreno.
- Plasteo y Moneo:** Superiormente efectivo para ambas operaciones. Excelentes plasticidad y adherencia.
- Gases Toxicos y Humos:** Mínimos, clase 1.
- Propagación Entre Barrenos:** Los hidrogeles TOVEX están diseñados para minimizar la propagación entre barrenos. Todo sistema de retardo para aumentar la fragmentación y para reducir la vibración funcionará apropiadamente.

Estas informaciones y sugerencias están basadas en la experiencia de Du Pont, S.A. de C.V. y se ofrecen como parte del servicio a sus consumidores. Se presupone que los productos explosivos serán usados por personas con el suficiente conocimiento técnico para poder apreciar el riesgo que acompaña su uso. La compañía Du Pont no garantiza resultados favorables ni asume responsabilidad alguna por cuanto a la interpretación de sus sugerencias. Esta información no se ofrece como autorización para usar o violar cualquier patente existente.

**JUPONT**  
MARCA REGISTRADA

**Tovex® 100**  
(HIDROGEL EN DIAMETRO CHICO)

## propiedades y especificaciones

**Tovex 100** es un hidrogel (explosivo licuado) de diámetro pequeño, sensible al fulminante, diseñado para usos tanto subterráneo (excepto minas de carbón) como a cielo abierto en barrenos desde 25 mm (1") hasta 50 mm (2") de diámetro. Excelente para plasteos y moneos.

**COMPORTAMIENTO:** Adecuada densidad, velocidad y alta energía.

**CUENTA DE CARTUCHOS:**

Los cartuchos son de 203 mm (8") de longitud. Optativamente pueden ordenarse también en 305 y 406 mm (12" y 16"). Se empaican en cajas de cartón de alta resistencia con 25 kgs. netos.



Cebando un cartucho de TOVEX



Cargando en una operación subterránea





# Tovex® 700

(HIDROGEL ENCARTUCHADO)

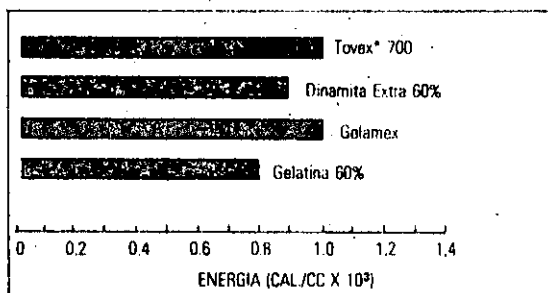
**Tovex 700** es un hidrogel (explosivo licuado) sensible al fulminante. Su diseño está particularmente dirigido para los diámetros de barrenación intermedios desde 50 mm (2") hasta 150 mm (6"). De gran versatilidad, tiene las características y propiedades

requeridas para todo tipo de voladuras de roca y mineral de dura a mediana dureza en minas subterráneas, tajos abiertos, canteras y construcción en general. Muy eficaz en plasteos, con superior plasticidad, consistencia y adherencia.

## propiedades y especificaciones

**Densidad:** 1.18 gms./c.c.

**Energía:**



**Velocidad:** 4800 m/seg (15750 p/seg)

**Gases Tóxicos:** Mínimos (Clase 1)

**Resistencia al Agua:** Excelente

**Cuenta de Cartuchos:**

Diám. del Cartucho mm.	plgs.	Núm de Cartuchos por caja de 25 Kgs.
44	1 3/4	32
50	2	24
64	2 1/2	17
76	3	11

La longitud de los cartuchos es de 406 mm (16 plgs.)

## requisitos de cebado:

Un fulminante ordinario No. 6 (Una vuelta y un nudo de Primacord\* Reforzado de 50 granos, equivalen para el caso con este producto a un fulminante No. 6)

## almacenamiento y transporte:

TOVEX\* 700 es compatible con los altos explosivos (dinamitas y agentes explosivos). Es incompatible con los accesorios detonadores (fulminantes, estopines, etc.) En condiciones adecuadas de almacenamiento, polvorines secos, frescos y bien ventilados, puede conservarse durante 1 año.

## USO:

TOVEX\* 700 es sensible al fulminante. Para iniciarse no necesita ser cebado. Es un extraordinario producto como carga de fondo, carga de columna, como cebo iniciador de otros explosivos o agentes explosivos y como explosivo para plasteos.

## ventajas:

1. **Sensible al fulminante.** No requiere cebo suplementario.
2. **Versatilidad.** Adecuado para uso en barrenaciones de diámetro intermedio, (desde 50 mm hasta 150 mm) en operaciones subterráneas y de superficie. Excelente para plasteo.
3. **Carga.** La variedad de diámetro en que es obtenible permite gran flexibilidad al diseño de voladuras y al cargado de barrenos.
4. **Gases tóxicos.** - Mínima producción de gases tóxicos y humo.
5. **Seguridad incrementada.** Menos sensibilidad al impacto, al golpe y al fuego.
6. **Resistencia al Agua.** Excelente. Superior a la de los explosivos tradicionales.
7. **Propagación entre Barrenos.** Está diseñado para minimizar la propagación entre barrenos en plantillas normales; por lo tanto, todo diseño de retardos con el fin de mejorar la fragmentación y de reducir la vibración, funcionará más apropiadamente.

---

Estas informaciones y sugerencias están basadas en la experiencia de Du Pont, S.A. de C.V. y se ofrecen como parte del servicio a sus consumidores. Se presupone que los productos explosivos serán usados por personas con el suficiente conocimiento técnico para poder apreciar el riesgo que acompaña su uso. La compañía Du Pont no garantiza resultados favorables ni asume responsabilidad alguna por cuanto a la interpretación de sus sugerencias. Esta información no se ofrece como autorización para usar o violar cualquier patente existente.

DU PONT, S.A. DE C.V. DEPARTAMENTO DE EXPLOSIVOS  
HOMERO 206 MEXICO 5, D.F. TEL: 250-90-33

## ACCESORIOS

### Cápsulas de detonación o estopines.

Los estopines eléctricos son los accesorios más utilizados para iniciar o detonar los explosivos potentes. La cápsula puede insertarse directamente en el cartucho o sujetarse fuertemente al cordón detonante.

Una cápsula eléctrica consiste de dos alambres aislados insertados en una cápsula de metal que están conectados por un delgado filamento de alambre que forma un puente. Este alambre de puente a veces se pinta con una mezcla de fósforo que produce flama como los cerillos.

Cuando se le aplica la corriente eléctrica a los alambres el filamento de puente se calienta e inicia una carga instantáneamente de un explosivo altamente sensible al calor. La explosión del alambre detona una primera carga la cual a su vez detona una carga de un explosivo potente en el fondo de la cápsula tal como PETN ó RDX.

Esta carga de fondo tiene potencia suficiente para detonar una cápsula - explosiva sensitiva o cebo (primer) o bien un cordón detonante

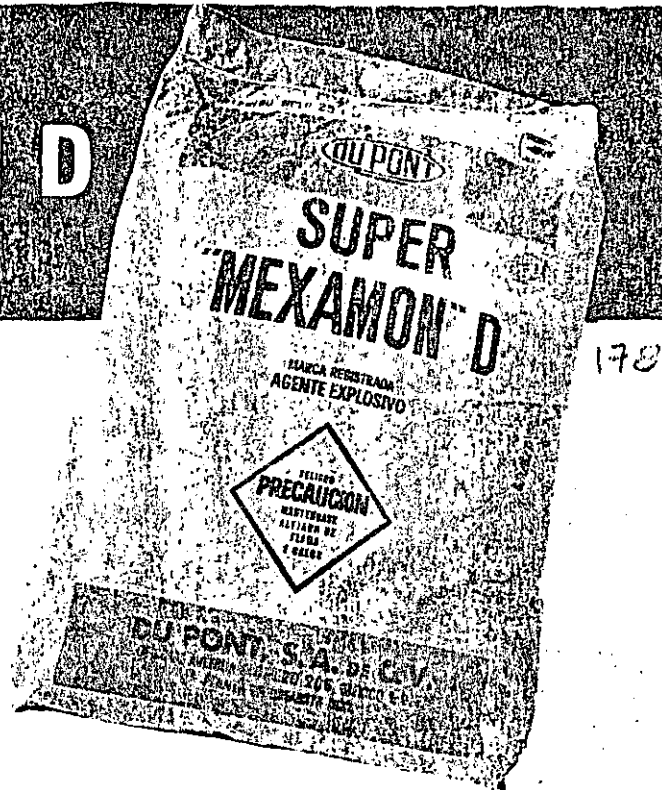
En las cápsulas eléctricas de retardos, un elemento retardante de explosivo en polvo se deposita entre filamento de puente y la carga potente del fondo. Este elemento de retardo está finamente calibrado para dar un intervalo de tiempo específico entre la aplicación de la corriente eléctrica y la detonación de la carga de fondo.

Hay dos series básicas de retardos disponibles: de retardos cortos o milisegundos con incrementos de retardo de 25 ms en el intervalo inferior y 50 ms en el intervalo superior; y retardos largos a menudo llamados retardos lentos o simplemente retardos, con incrementos de retardo de 0.5 seg y 1 seg. Con los estopines de milisegundos se produce mejor fragmentación y se reduce la presión de aire y las vibraciones del terreno.

Los estopines de retardo se usan en lumbreras o túneles para dar tiempo suficiente al movimiento de la roca. Probablemente se produce fragmentación más gruesa que la obtenida con milisegundos.



# SUPER MEXAMON D



Super Mexamon\* D reúne las características principales de los Agentes Explosivos: seguridad, economía y la eliminación de los malestares físicos producidos por las Dinamitas. Conjunta las propiedades principales de trabajo de los altos explosivos potencia y velocidad, pero con dos ventajas: baja densidad, que permite ahorros substanciales y resultados superiores, al hacer posible la mejor distribución de la carga explosiva en el barreno. Además, un mínimo de gases tóxicos que lo hace indicado para uso subterráneo.

## PROPIEDADES

**Potencia:** equivalente a Dinamita Extra 65%  
**Densidad vaciado en el barreno:** 0.65 gms./c.c.  
**Densidad soplado neumáticamente:** 0.75 gms./c.c. (a 4.20 Kg./cm<sup>2</sup> ó 60 lbs./pulg.<sup>2</sup>)  
**Velocidad:** 3,800 mts./seg. (12,500 pies/seg.) aprox.

## USOS

Super Mexamon\* D proporciona buena fragmentación en roca de mediana dureza. Super Mexamon\* D está diseñado para uso en minas bajo tierra. Fluye perfectamente con cargadores neumáticos y se compacta perfectamente aún en barrenaciones de contra-pozo. Super Mexamon\* D es del todo recomendable para ser empleado a cielo abierto. Fluye con toda facilidad en barrenos inclinados.

## VENTAJAS

1. **Versatilidad:** Super Mexamon\* D puede usarse tanto en minas bajo tierra como en operaciones a cielo abierto.

2. **Potencia:** La velocidad de Super Mexamon\* D y la energía que desarrolla por su gran volumen de gases de expansión lo equiparan en potencia a la Dinamita Extra 65%.

3. **Distribución de la carga:** Super Mexamon\* D por su baja densidad permite la mejor distribución del explosivo en el barreno y en consecuencia, una mejor fragmentación.

4. **No requiere mezclas adicionales:** Super Mexamon\* D es un Agente Explosivo cuidadosamente formulado e integralmente elaborado, listo para cargarse directamente de la bolsa, tal como se empaca. Resultado: economía, no hay desperdicio.

5. **Sensibilidad** Super Mexamon\* D ha demostrado ser más sensible a la onda de detonación que cualquier mezcla de Nitrato de Amonio y Aceite Diesel o combustible.

6. **No es aceitoso:** Super Mexamon\* D por su elaboración integral, ofrece las máximas comodidades al usuario. Está libre de migraciones y evaporaciones.

7. **Resultados reproducibles:** Con Super Mexamon\* D los resultados obtenibles, voladura tras voladura, son constantes y reproducibles siempre y cuando se cebe apropiadamente. Los resultados constantes no son posibles en las mezclas de Nitrato de Amonio o fertilizantes con combustibles, debido a las tantas variantes que intervienen en su preparación.

8. **Seguridad:** Super Mexamon\* D no contiene nitroglicerina.

9. **Economías:** Super Mexamon\* D puede en muchos casos sustituir ventajosamente a los otros explosivos, más altos en precio.

## INICIACION

El iniciador o cebo recomendado para detonar el Super Mexamon\* D debe ser un explosivo potente y violento, tal como: 1) Tovex 100 y 2) Tovex 700. El cebo de iniciación debe constituir un 15%.

aproximadamente, en peso, del total de la carga explosiva en el barreno. En barrenos largos es recomendable usar más de 1 cebo de iniciación y cordón detonante "Primacord" o "E-Cord" a lo largo del barreno, distribuyendo los cebos a intervalos máximos de 5 metros; es decir, debe distribuirse el cebo total a intervalos a lo largo del barreno dejando siempre en el fondo la mayor cantidad del cebo iniciador.

## CARGA

En operaciones a cielo abierto, Super Mexamon\* D puede cargarse por gravedad, vaciado. La tabla a continuación muestra aproximadamente los kilos por metro lineal de barrenos de varios diámetros.

Diámetro Barreno cms. (pulgs.)	Kg. por Metro Lineal de Barreno
2.54 (1)	0.329
5.08 (2)	1.318
7.62 (3)	2.964
10.16 (4)	5.270
12.70 (5)	8.234
15.24 (6)	11.857

## ALMACENAMIENTO

Super Mexamon\* D debe almacenarse considerándolo para el caso, como cualquier otro explosivo. Es aconsejable dar rotación a las existencias almacenadas, usando siempre primero el material más antiguo.

## EMPAQUE

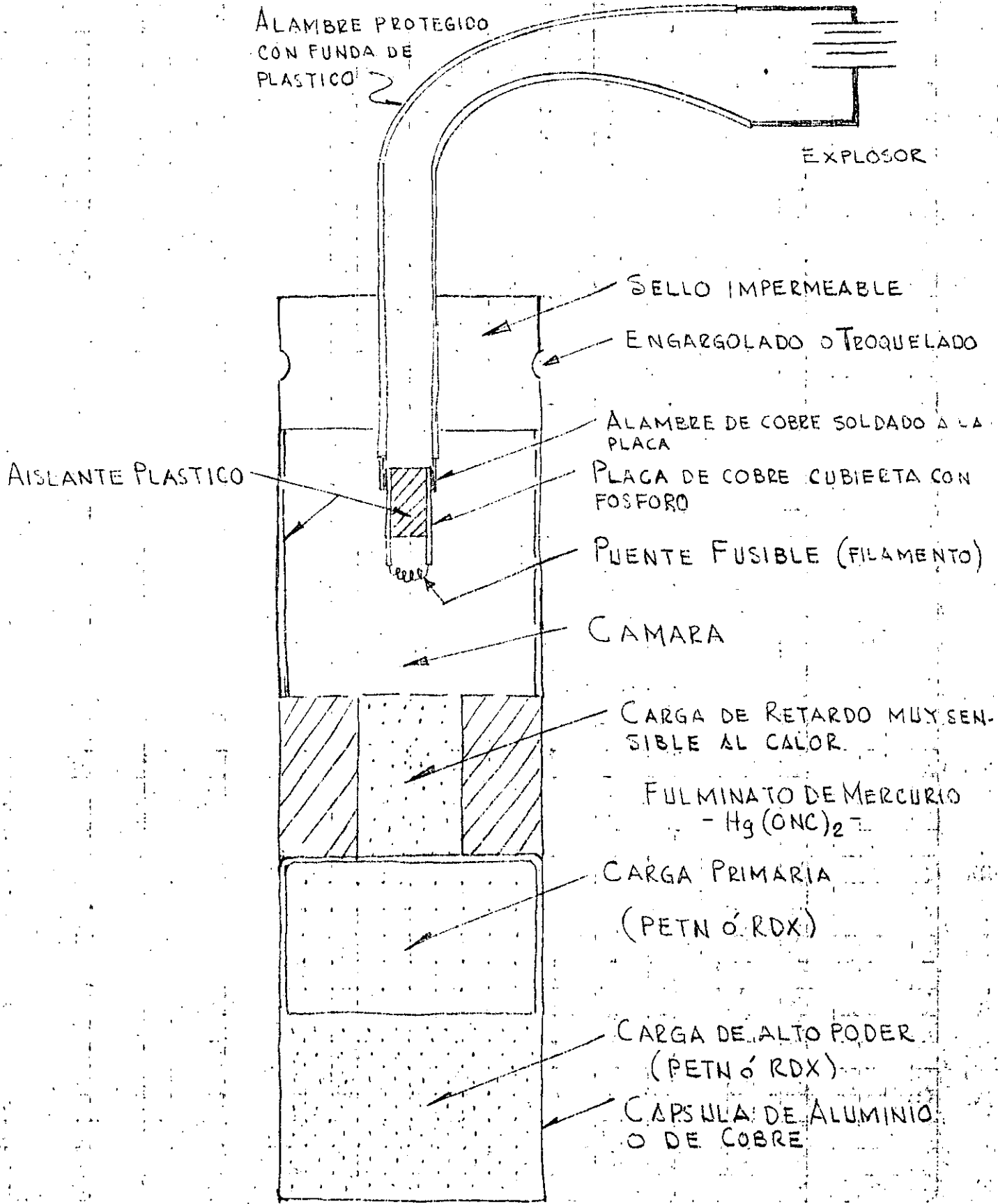
Super Mexamon\* D se envasa en bolsas de papel multicapas con forro interior de polietileno. Cada saco contiene 25 Kgs. netos.

---

Estas informaciones y sugerencias están basadas en la experiencia de Dupont, S.A. de C.V. y se ofrecen como parte del servicio a sus consumidores. Se presupone que los productos explosivos serán usados por personas con el suficiente conocimiento técnico para poder apreciar el riesgo que acompaña su uso. La compañía Du Pont no garantiza resultados favorables ni asume responsabilidad alguna por cuanto a la interpretación de sus sugerencias. Esta información no se ofrece como autorización para usar o violar cualquier patente existente.

**DU PONT, S.A. DE C.V. DEPARTAMENTO DE EXPLOSIVOS**  
**HOMERO 206 MEXICO 5, D.F. TEL: 250-90-33**

# CAPSULA ELECTRICA O ESTOPIN



## Cordón detonante

El cordón detonante consiste de un tubo de plástico resistente al agua que se protege con una cubierta o forro fabricado con una combinación de textiles, plástico y alambre a prueba de agua. Las cubiertas tienen diferentes grados de resistencia a la tensión, abrasión y flexibilidad.

Dentro del tubo de plástico está el núcleo o corazón constituido por un alto explosivo, usualmente PETN. La cantidad de PETN varía entre 1 gramo/pie a 400 gramos/pie y se produce en diferentes potencias.

Todas las potencias de PETN pueden detonarse con una capsula eléctrica y su velocidad de detonación es de 21000 pies/seg.

Su notable insensibilidad contra impacto y fricción es ideal para su uso en la línea de encendido y líneas troncales.

Como los estopines eléctricos se sujetan al cordón detonante hasta el final justamente antes de la voladura, la mayor parte de una falla aleatoria por detonación se elimina.

Usualmente se usa el cordón de 25 gramos/pie y el de 50 gr/pie se usa en trabajos especiales.



## Cordón detonante... continuación.

El cordón detonante es un explosivo de alta potencia que explota con una gran producción de aire. Hay que tener cuidado con este efecto.

Un cordón detonante de 25 a 50 gramos/pie detona cualquier cápsula-sensitiva (primer o cebo y cápsulas de alta potencia como son los boosters).

En barrenos profundos y de gran diámetro se usa mucho el cordón detonante combinado con las cápsulas de alta potencia (boosters)

Un cordón detonante de 50 gramos/pie no detona un agente explosivo como el ANFO.

El cordón detonante tiene amplias aplicaciones bajo el agua. Cuando se usa en ambiente húmedo sus extremos deberán protegerse. PETN absorbe lentamente la humedad y puede detonar si se inicia por el extremo seco.

El cordón detonante se acopla mediante "conectores MS" o de milisegundos. Estos conectores contienen un elemento de retardo constituido por un pedazo de cordón detonante. Los conectores más usuales son de 5, 9 y 17 ms.

Los conectores se acoplan con los extremos del cordón detonante a las líneas troncales y permite el uso ilimitado de periodos de retardo.

Es muy útil para disminuir vibraciones detonando un solo barreno en cada retardo, conectado en serie.

## Cordón detonante Non-electric. (NONEL)

Este es un cordón detonante muy útil para voladoras subterráneas pues se eliminan las fallas por electricidad estática. También se usa en voladoras a cielo abierto para evitar vibraciones detonando barreno por barreno al igual que el cordón detonante y en zonas altas donde se quieren tormentas eléctricas.

El NONEL detona en una sola dirección por lo que hay que tener cuidado en su acoplamiento.

También existen conectores especiales de retardo constituidos por el mismo tubo de NONEL en longitudes de 2 pies con terminales de plástico.

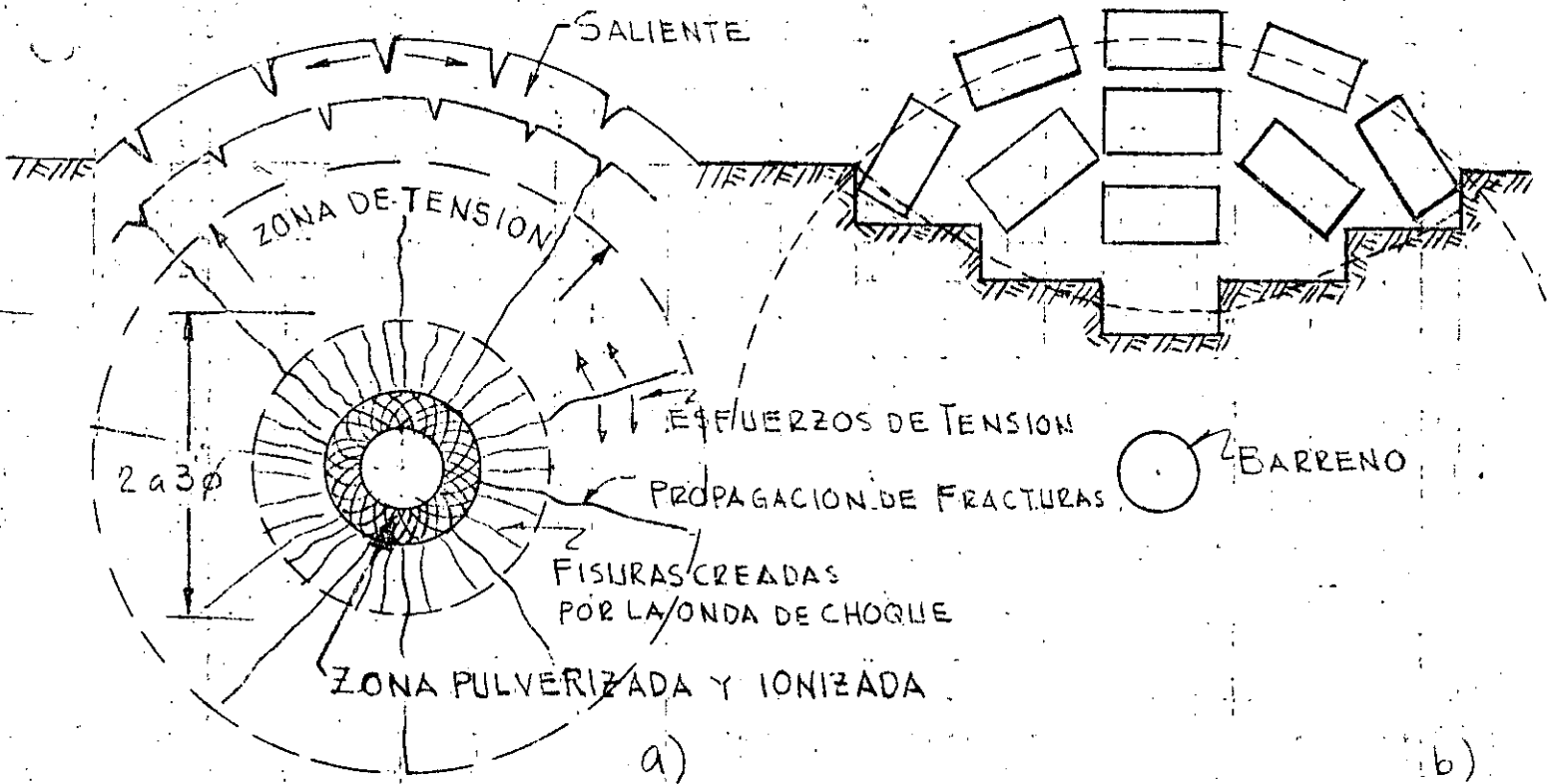
El NONEL tiene una gran resistencia al agua ya que un extremo está sellado contra la cápsula de detonación y el otro está sellado contra una terminal de plástico.

El NONEL no explota, pudiendo sostenerse perfectamente con las manos.

Tiene una velocidad de 9000 pies/seg.

Su composición química es:

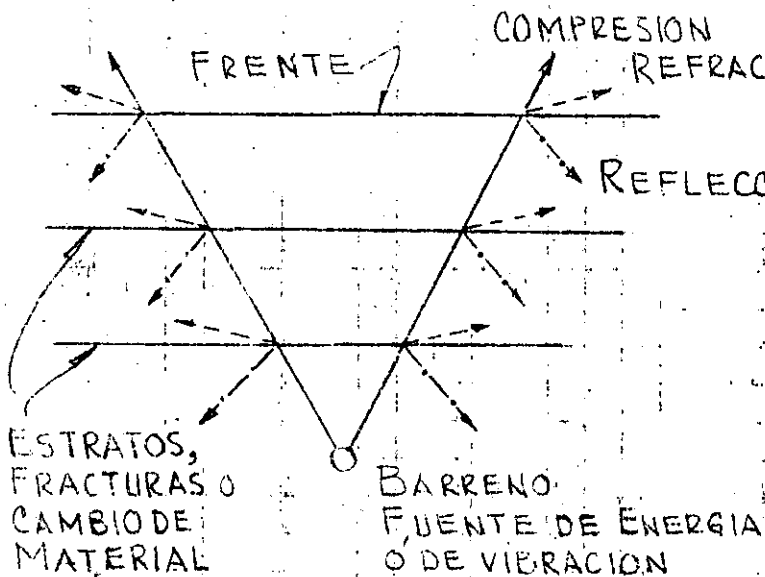
# MECANISMO DE FRAGMENTACION



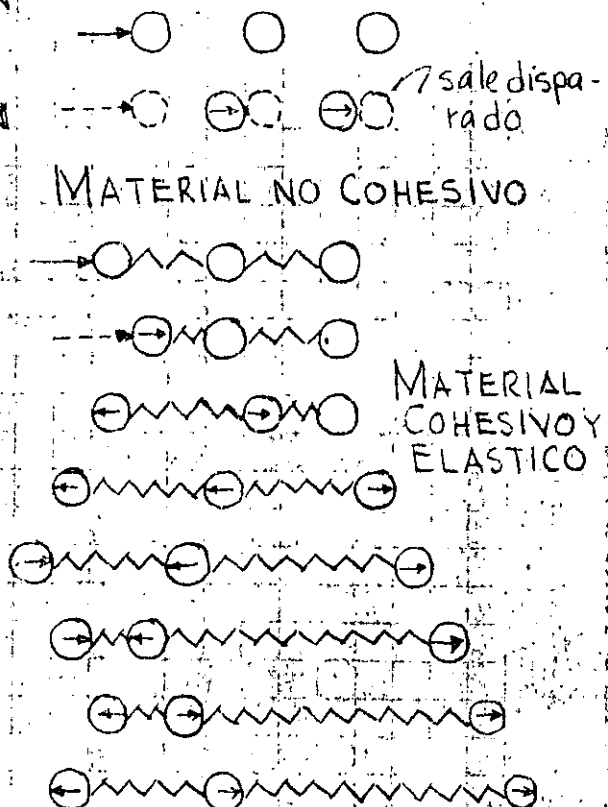
FRAGMENTAS RADIALES

SECUENCIA EN LA FORMACION DEL CRATER

FRAGMENTACION Y DESPLAZAMIENTO = FUERZA-DISTANCIA = TRABAJO

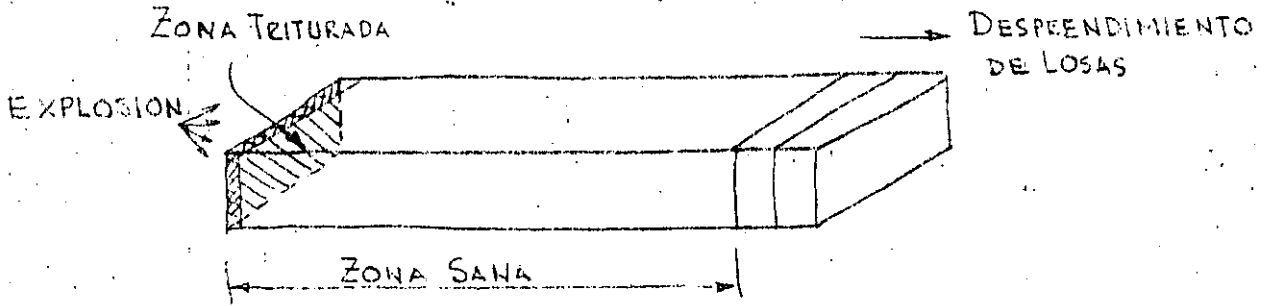


COMPONENTES DE LA ENERGIA POR IMPACTO DEL EXPLOSIVO

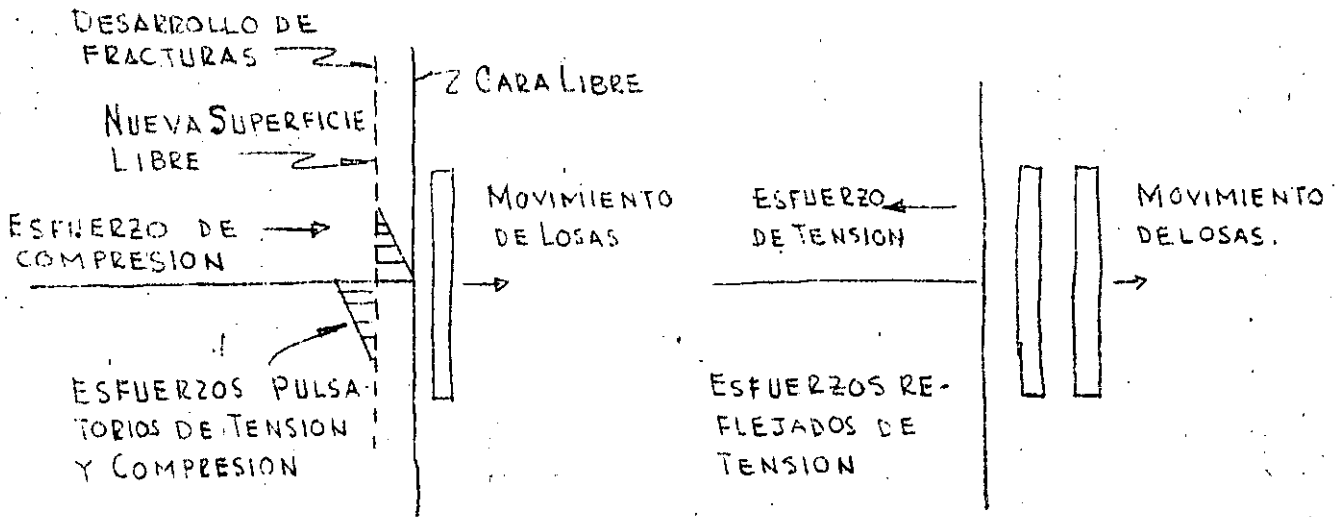


TRANSMISION DE ENERGIA EN MATERIALES BAJO CARGAS DE PULSACION

# MECANISMO DE FRAGMENTACION.... CONTINUA

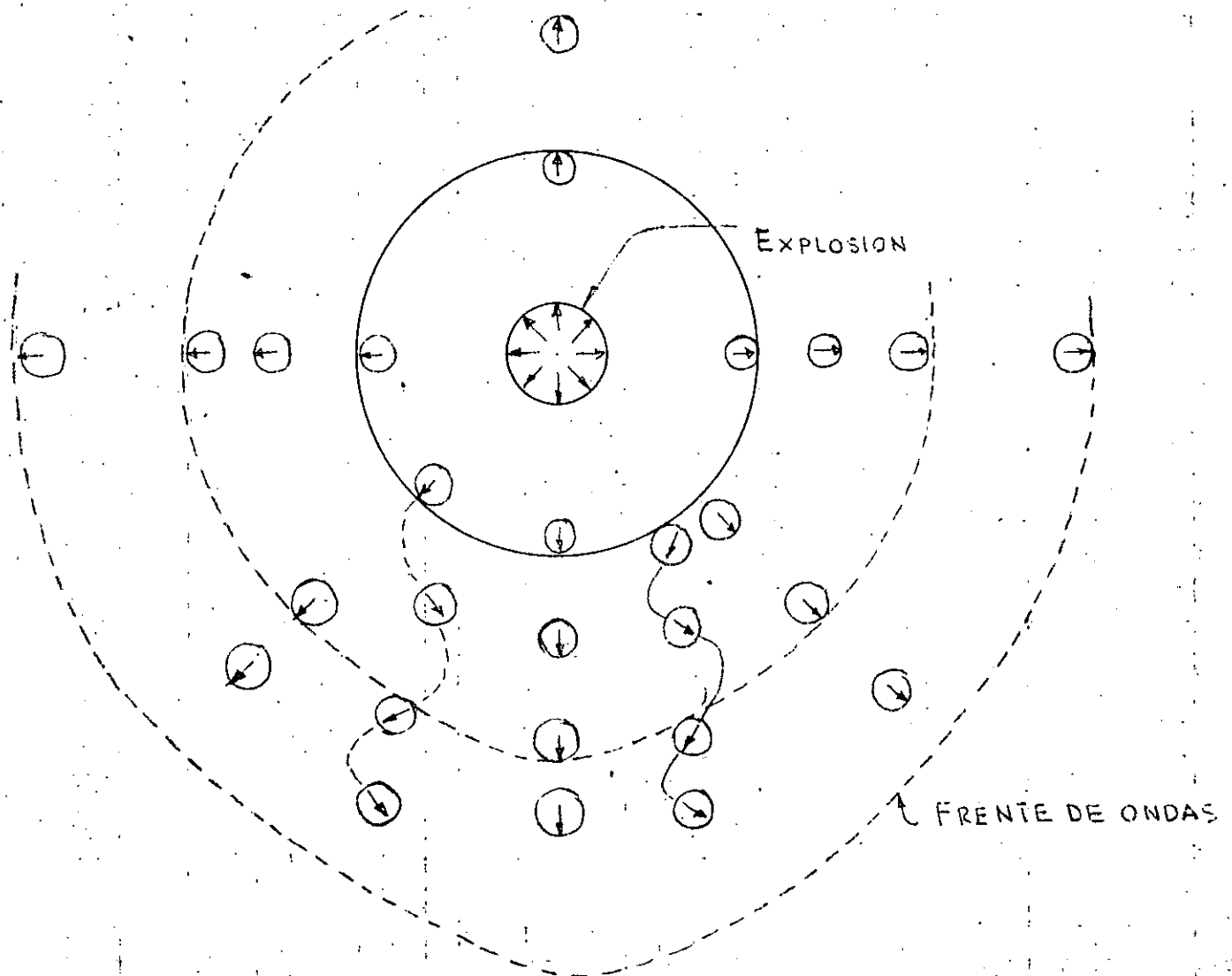


## BARRA EXPERIMENTAL DE CONCRETO

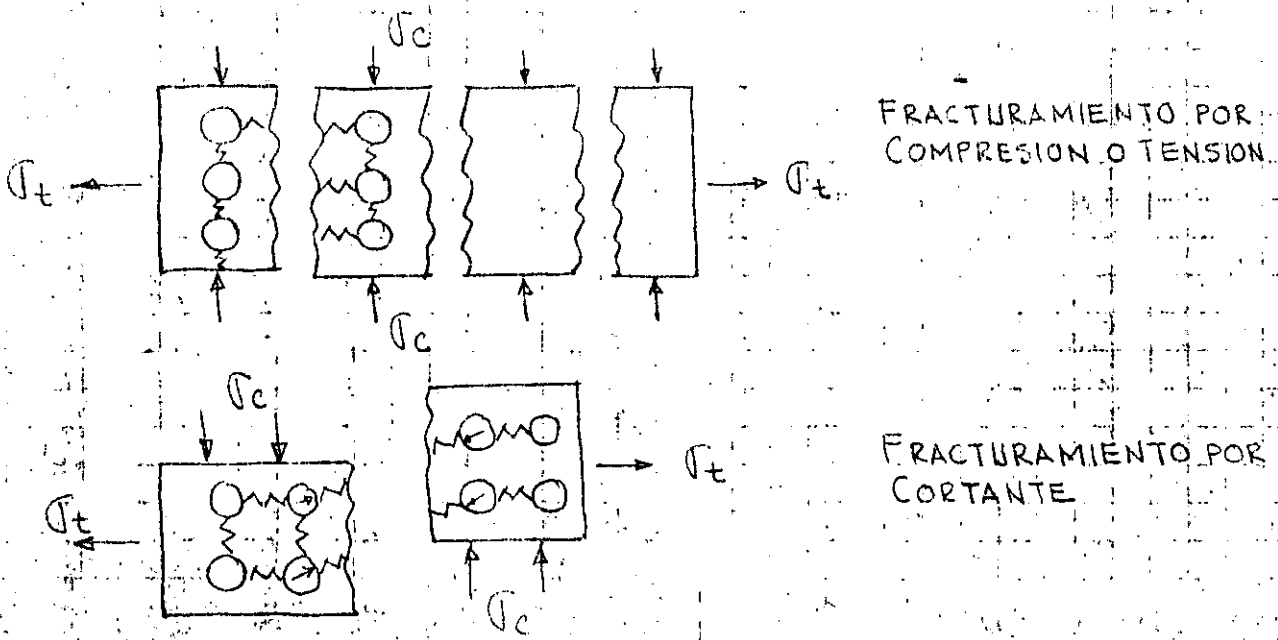


## FRAGMENTAMIENTO DE TENSION POR REFLEXION DE IMPULSOS

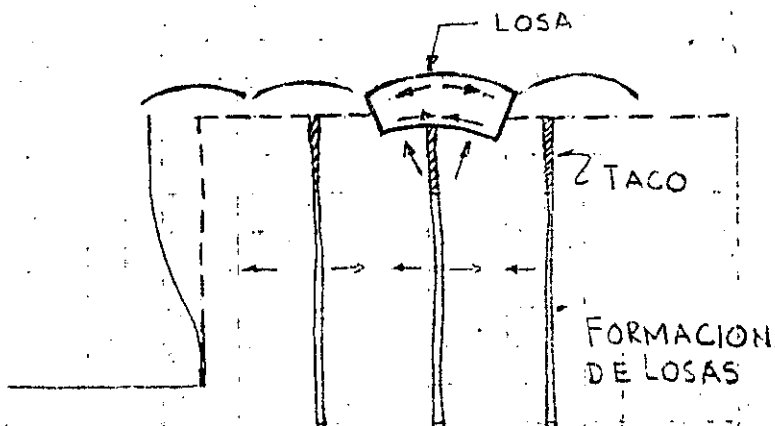
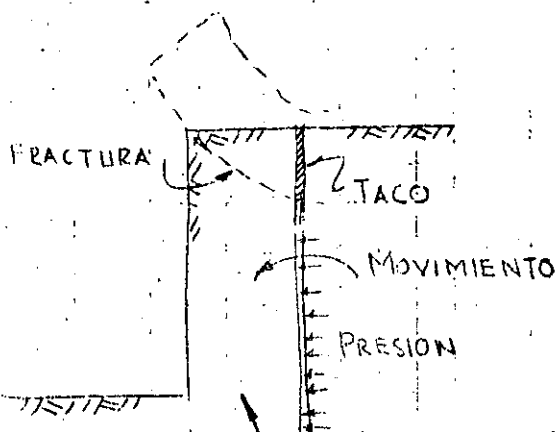
# MECANISMO DE FRAGMENTACION: .... Continúa



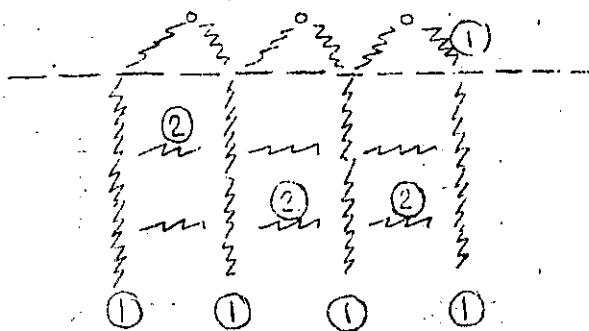
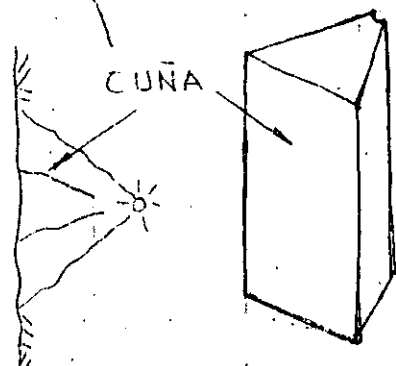
## INFLUENCIA DEL PATRON ESTRUCTURAL DE LAS PARTICULAS



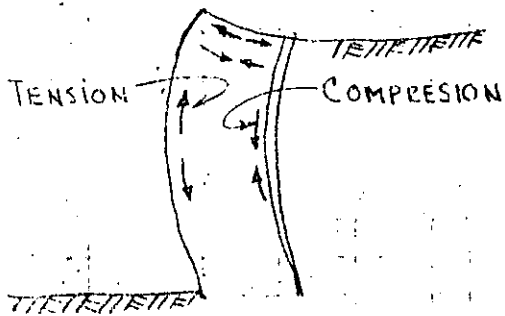
# MECANISMO DE FRAGMENTACION..... Continúa



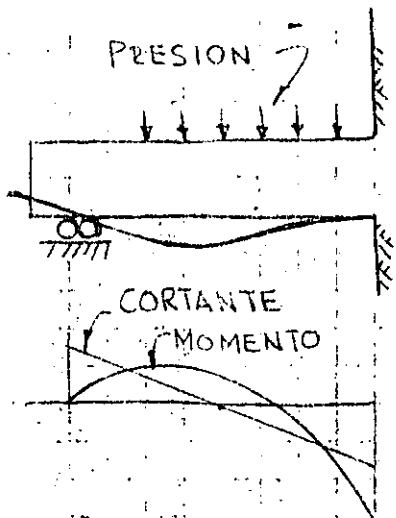
DESPRENDIMIENTO DE CUÑAS VERTICALES



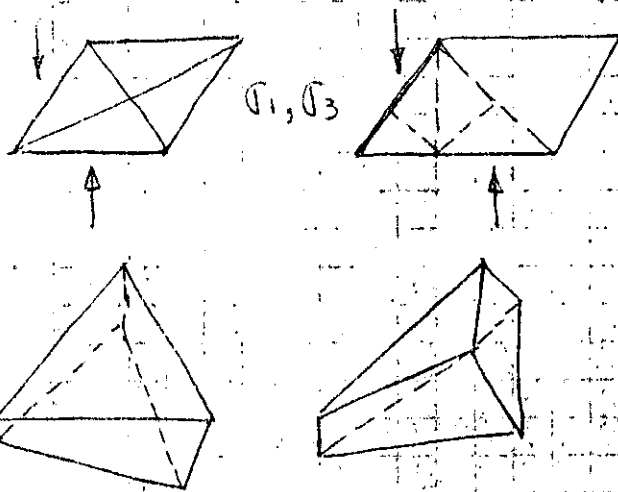
- ① FRACTURAS VERTICALES COMO CUÑAS
- ② FRACTURAS HORIZONTALES
- ③ SALIDA DE GASES



EFEECTO DE VIGA



ANALOGIA DE LA VIGA



FRAGMENTOS EN FORMA DE TRIANGULOS POR EFECTO DE CORTANTE (TORSION) Y FLEXION

## MECANISMO DE FRAGMENTACION... Continúa

### Mecanismos de fragmentación

Las rocas normalmente son más resistentes en compresión y trituración que por tensión. P.ej. algunas calizas tienen resistencias a compresión entre 250 y 1500 Kg/cm<sup>2</sup> y resistencias en tensión tan bajas como 35 a 150 Kg/cm<sup>2</sup>.

Por otro lado los explosivos y agentes explosivos utilizados producen presiones muy altas que reaccionan con velocidades entre 2500 a 8000 m/seg. (5300 a 17.000 mph).

La presión desarrollada súbitamente dentro del barreno alcanza valores desde 18000 hasta 150000 Kg/cm<sup>2</sup> dependiendo del tipo de explosivo y de las condiciones de confinamiento.

El efecto del explosivo que reacciona contra la roca produce un impacto, o impulso, desde un golpe aplicado rápidamente de extremadamente alta intensidad.

Cuando el explosivo está dentro de un barreno circular se ejerce igual presión en todas direcciones a lo largo de todo el perímetro del agujero. La roca en toda esa región es comprimida y pulverizada hasta una distancia limitada del orden de  $\phi/4$ .

La aplicación súbita del impacto es seguida por la producción de alta presión que introduce ondas de esfuerzos compresionales que rápidamente penetran

en forma de abanico a través del macizo rocoso como ondas elásticas. Esta acción se produce aún cuando las rocas son más bien frágiles, pero son algo elásticas. La velocidad con que viajan las ondas de choque a través de la roca es función de la densidad del medio. Las rocas densas dan lugar a altas velocidades y las rocas blandas porosas, o ligeras a bajas velocidades.

Parte de la energía transmitida a través de las ondas compresionales es reflejada y refractada (flexionada) por cambios de densidad o discontinuidades de la estructura. Cualquier frente libre o cambio en el tipo de roca produce este efecto.

El resto de la energía tiende a mantener su dirección original de viaje.

Los ángulos de reflexión son iguales a los que van hacia las fronteras. Los ángulos de refracción dependen de las características de los dos materiales. Esto es que en cada cambio de densidad se produce reflexión y refracción de los impulsos de la energía; al equilibrarse la energía sigue viajando en su dirección original.

Si un golpe es ejercido a una partícula la energía es transmitida en la dirección de aplicación del golpe hacia las partículas adyacentes hasta que la energía



es consumida como resultado del trabajo realizado y por efectos como fricción, amortiguamiento, fragmentación<sup>etc.</sup>. Los suelos granulares no tienen cohesión de modo que tienen poca o ninguna atracción entre partículas, aún cuando cada partícula pueda tener un poco de elasticidad por si mismas.

La mayor parte de las rocas son cohesivas y algo elásticas teniendo diferentes efectos que los producidos en fragmentos sueltos.

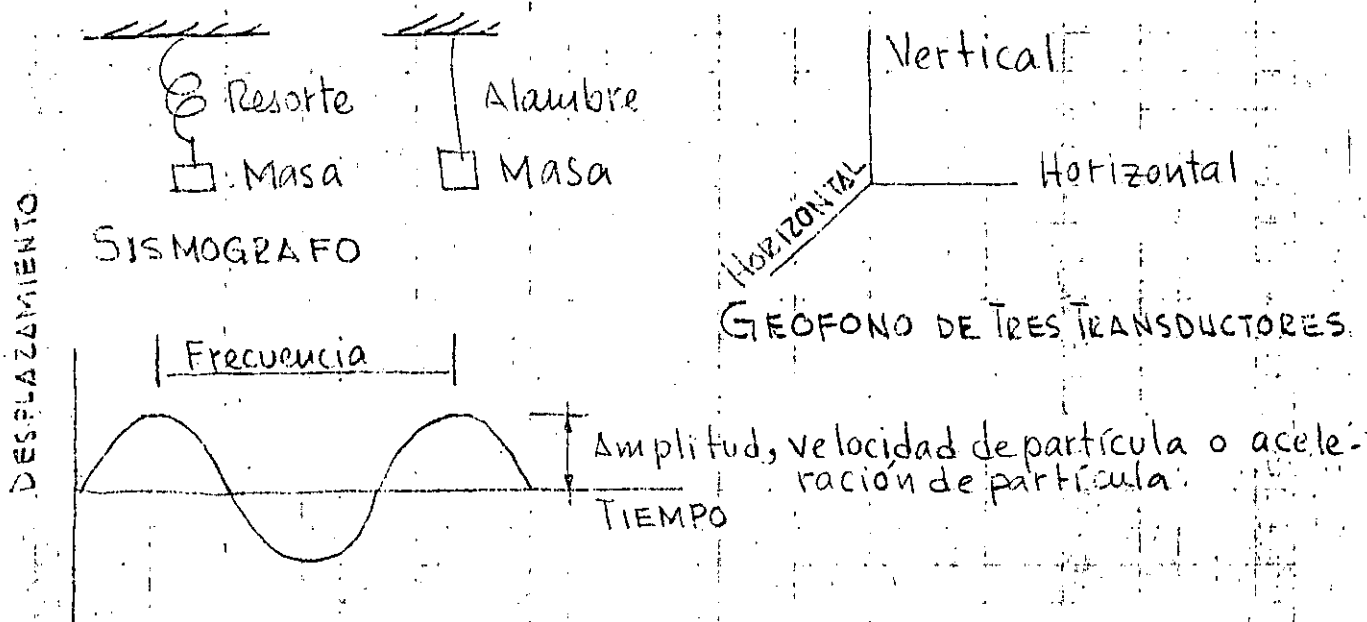
# VIBRACIONES

Las vibraciones del terreno pueden medirse mediante los desplazamientos que se produzcan a una masa sujeta a un resorte o a un alambre. Los impulsos pueden ser proyectados en una pantalla de un osciloscopio en el cual puede determinarse la velocidad de la partícula, su aceleración y la amplitud de su desplazamiento.

Generalmente la masa viene a ser el núcleo de un pequeño transformador lineal en el cual al desplazarse

el núcleo se producen cambios de voltaje y amperaje en el transformador pequeño que significan los desplazamientos de la masa

Estos transformadores (LVDT) constituyen los geófonos y pueden instalarse en tres direcciones dentro de un geófono



# ONDAS SISMICAS

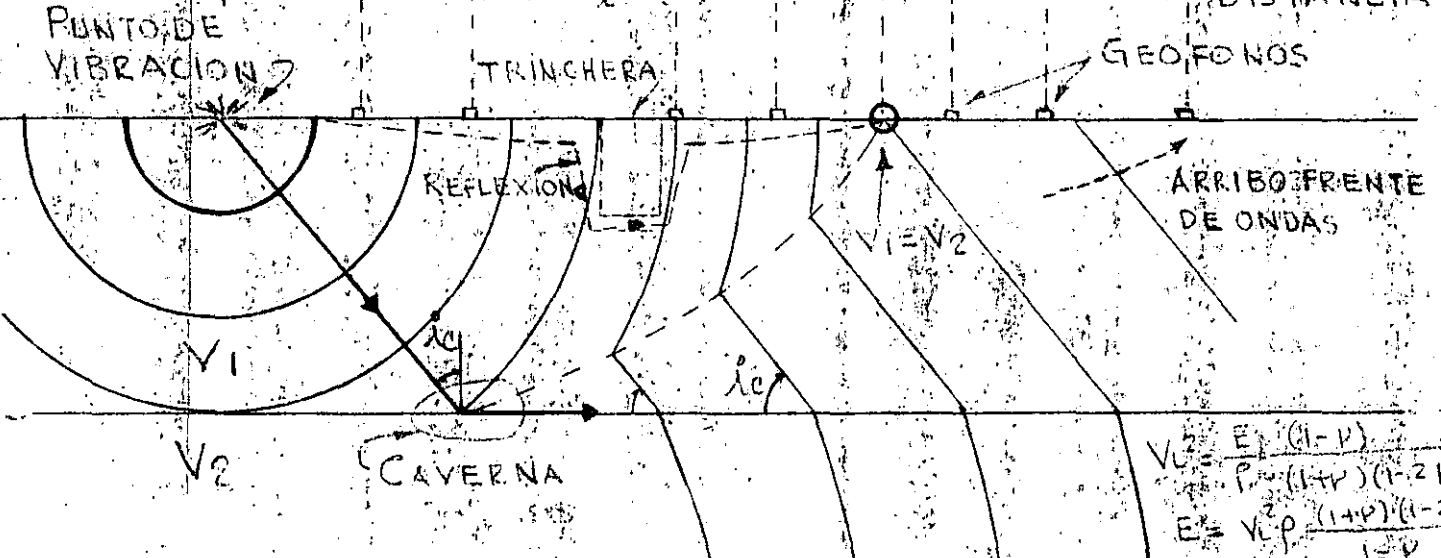
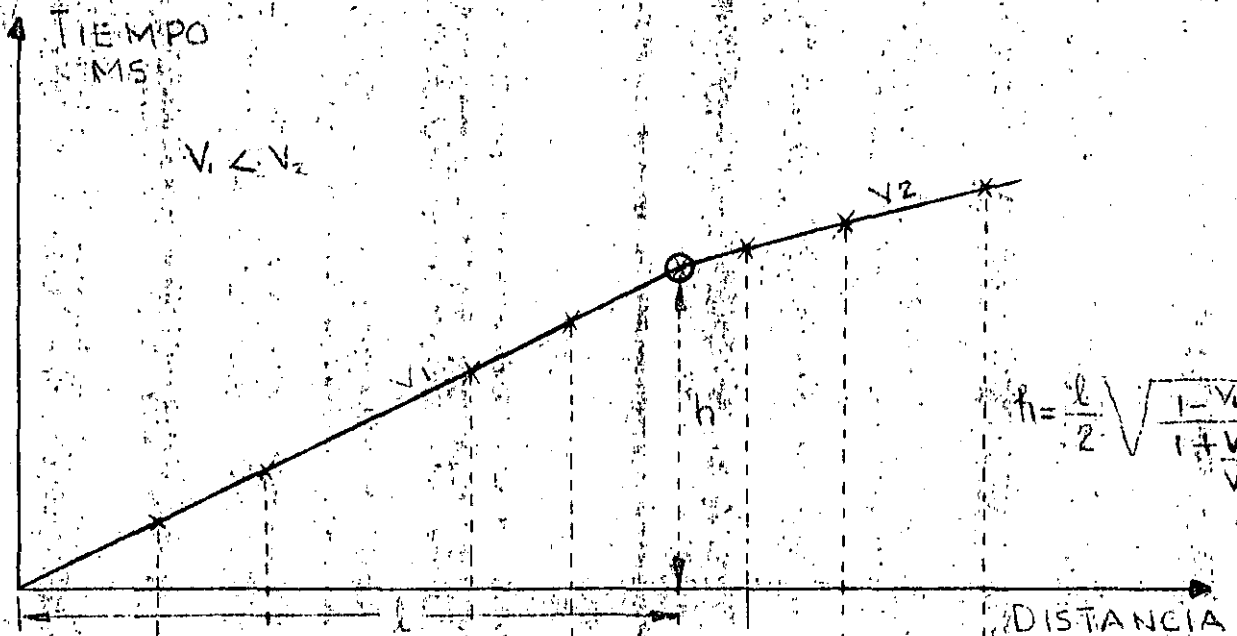
## ONDAS DE CUERPO:

- 1.- Compresional  
Longitudinal  
Primaria - P  
De empuje
- 2.- Corte  
Onda transversal  
Onda secundaria - S

## ONDAS DE SUPERFICIE

- 3.- Love } Igual de peligrosas que  
Rayleigh } las P y S.

En la Fig 1 se presenta la transmisión de ondas de compresión por reflexión y refracción sísmica.



$$V_2 = \frac{E_1(1-\nu)}{\rho_1(1+\nu)(1-2\nu)}$$

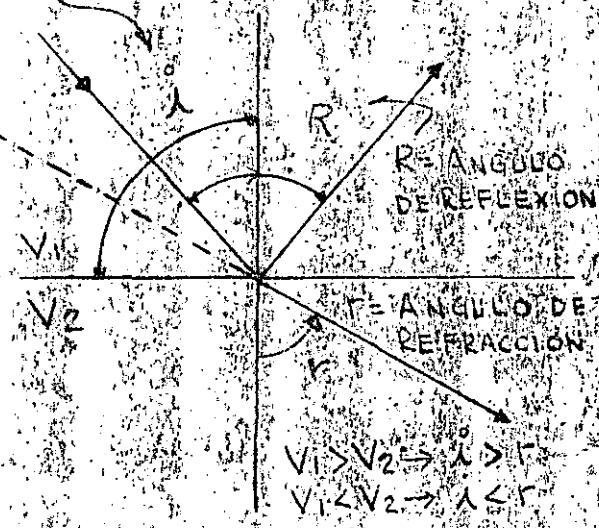
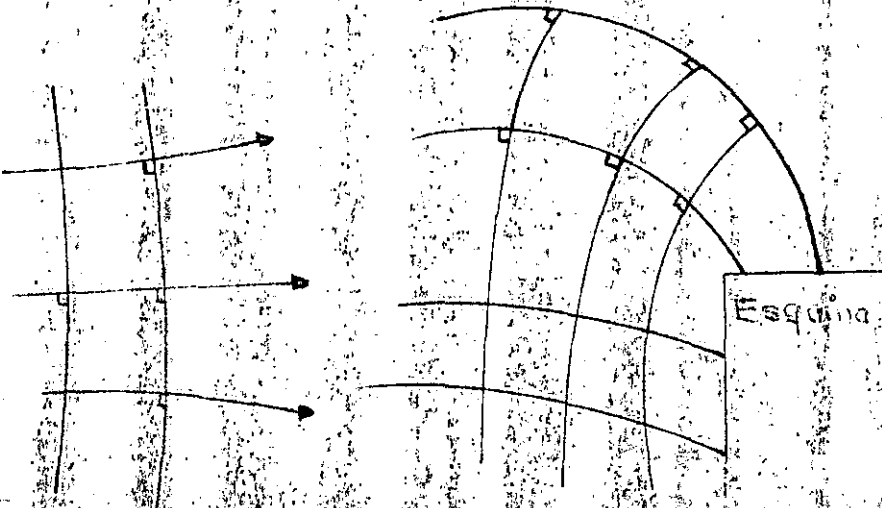
$$E = \frac{V_2^2 \rho_1 (1+\nu)(1-2\nu)}{1-\nu}$$

REFLEXION Y REFRACCION DE ONDAS

$$V_2 = \frac{E}{\rho_2(1+\nu)(1-2\nu)}$$

$$E = V_2^2 \rho_2 (1+\nu)(1-2\nu)$$

$\alpha = \text{ANGULO DE INCIDENCIA}$



PRINCIPIOS DE REFLEXION

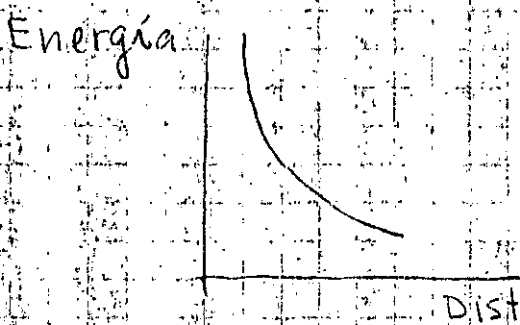
# PROPAGACION DE ENERGIA

La energía se propaga disminuyendo con la distancia. es directamente proporcional con la presión de detonación e inversamente proporcional al cuadrado de la distancia al Bordo.

$$B = k \left( \frac{P_e}{\sigma_t} \right)^{1/2}$$

donde B = bordo, k = constante

P = presión de detonación y  $\sigma_t$  = resistencia a tensión.



$$\sigma_t = \frac{-4p(x^2 + r^2 - B^2)}{(x^2 - r^2 + B^2)} \quad x = (B^2 + r^2)^{1/2}$$

El valor más significativo de la energía es la velocidad de la partícula. El Bureau of Mines usa la siguiente expresión:

$$V = H \left( \frac{D}{W^{1/2}} \right)^{-\beta}$$

Esta expresión puede graficarse en escala logarítmica como se presenta en la Fig. 2. en la cual la distancia escalada es  $SD = \frac{D}{W^{1/2}}$  o sea  $W = \left( \frac{R}{SD} \right)^{1/2}$  en donde

W = máxima carga por retardo

La velocidad de partícula máxima permisible es de 2"/seg

- En las tabla I se presentan las cargas de explosivo máximas permisibles por retardo en Suecia.

En la Fig 3 se presentan los efectos de la velocidad de la partícula en la respuesta humana.



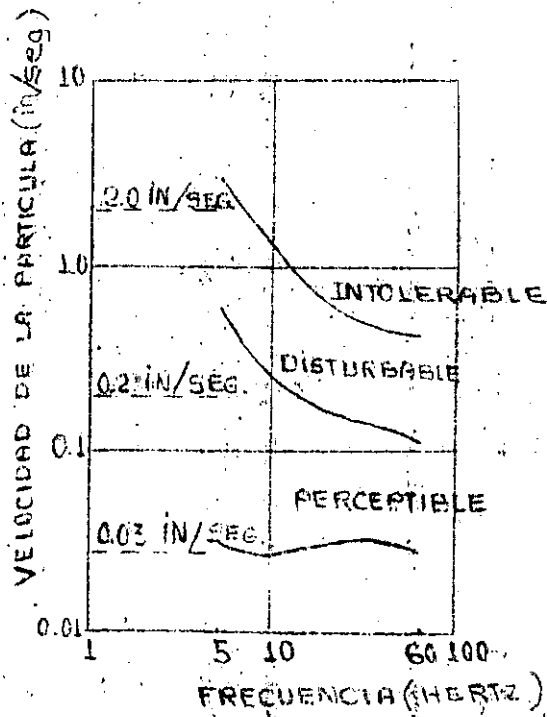
# TABLA I

DISTANCIA m	CARGA EN KG. CON RETARDO						
	GRUPO A	B	C	D	E	F	G
0.5				0,02	0,04	0,08	0,16
1	0,008	0,015	0,03	0,06	0,12	0,25	0,50
2	0,025	0,05	0,09	0,2	0,4	0,7	1,4
3	0,40	0,08	0,16	0,33	0,65	1,3	2,6
4	0,06	0,12	0,25	0,5	1,0	2,0	4,0
5	0,09	0,18	0,36	0,73	1,4	2,8	5,6
6	0,12	0,23	0,47	0,95	1,9	3,8	7,6
7	0,14	0,27	0,57	1,15	2,3	4,6	9,2
8	0,16	0,36	0,72	1,45	2,9	5,8	11,6
9	0,2	0,42	0,85	1,70	3,4	6,8	13,6
10	0,25	0,5	1,0	2,0	4,0	8,0	16,0
12	0,3	0,6	1,3	2,5	5,2	10,5	21
14	0,4	0,8	1,6	3,2	6,4	13,0	26
16	0,5	1,0	2,0	3,9	7,8	15,5	31
18	0,6	1,2	2,4	4,7	9,4	19	38
20	0,7	1,4	2,8	5,6	11	22	44
25	1,0	2,0	4,0	8,0	16,0	32,0	64
30	1,3	2,6	5,2	10,4	21	42	84
35	1,6	3,2	6,5	13	26	52	104
40	2,0	4,0	8,0	16	32	64	128
45	2,4	4,8	9,5	19	38	76	152
50	2,8	5,5	11	22	44	88	176
55	3,3	6,5	13	26	52	104	208
60	3,8	7,5	15	30	60	120	240
65	4,3	8,5	17	34	68	136	272
70	4,8	9,5	19	38	76	152	304
75	5,3	10,5	21	42	84	168	336

TABLE I (Continuation)

DISTANCIA M	GRUPO A	CARGA EN KG. POR RETARDO					
		B	C	D	E	F	G
80	5,8	11,5	23	46	92	184	368
85	6,4	12,8	25,5	51	102	204	408
90	7,0	14,0	28	56	112	224	448
95	7,6	15,2	30	61	122	244	488
100	8,5	16,5	33	66	132	264	528
110	9,3	18,5	37	74	148	296	592
120	10,5	21,0	42	84	168	336	672
130	11,7	23,5	47	94	188	376	752
140	13,2	26,6	52,5	105	210	420	840
150	14,5	29,0	58	116	232	464	928
160	16,0	32,0	64	128	256	512	1024
170	17,5	35,0	70	140	280	560	1120
180	19,0	38,3	76,5	153	306	612	1224
190	20,7	41,5	83	166	332	664	1328
200	22,5	45,0	90	180	360	720	1440





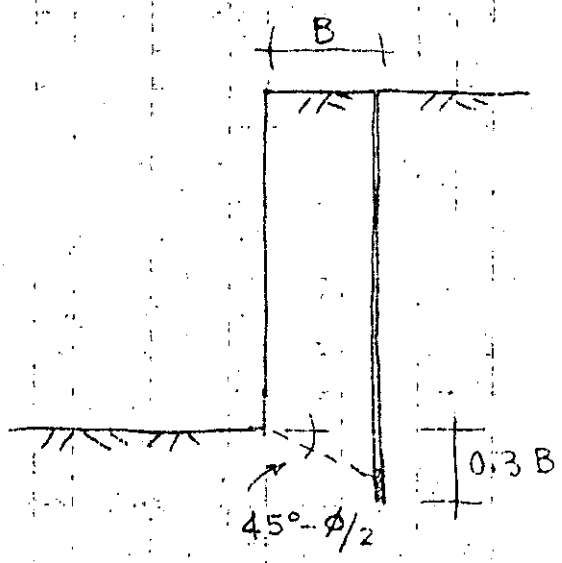
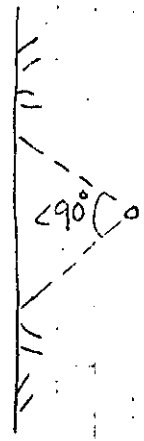
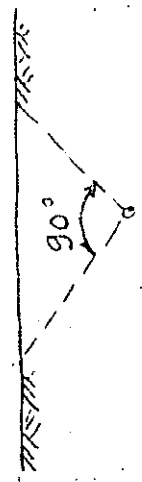
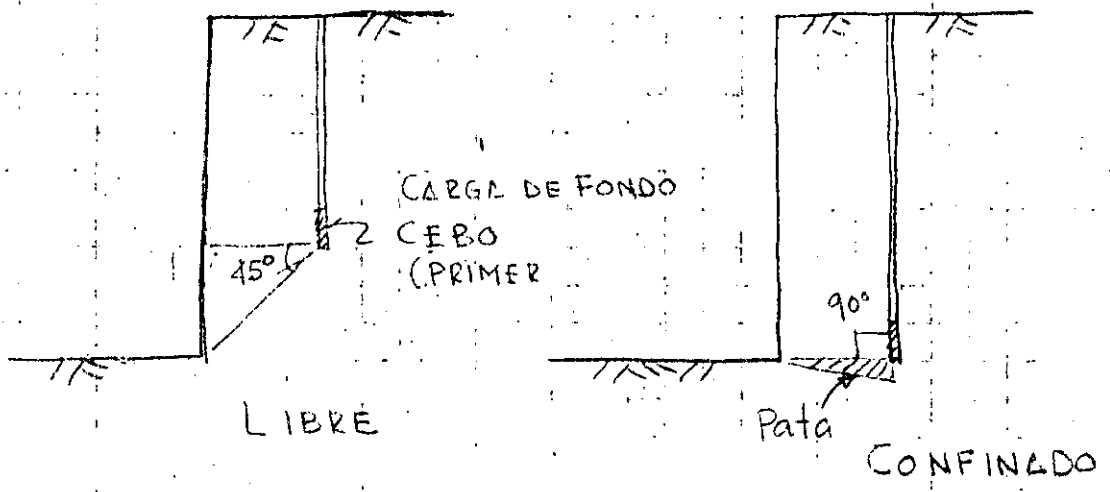
RESPUESTA HUMANA A LA VIBRACION (SEGUN RATHBONE)

## REDUCCION DE EFECTOS DE VIBRACIONES

Para reducir los efectos de las vibraciones las siguientes acciones deberán tomarse :

- 1.- Seccionar la voladura (dividir el banco)
- 2.- Reducir la carga por retardo
- 3.- Cerrar el patrón de barrenación
- 4.- Utilizar dos cargas por barreno.

# ROTURA DE LA ROCA

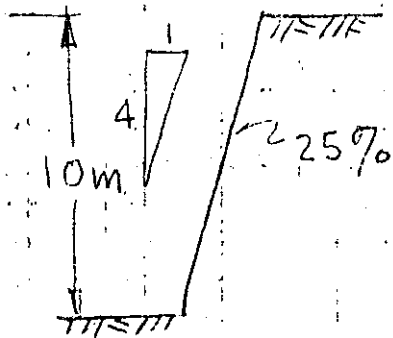


CONFINADO

# EJEMPLO DE CALCULO VOLADURA DE BANQUEO

Banco de 10 m de alto

Constante de roca  $r = 0.33 \text{ Kg/m}^3$



Barrenación  $\phi 3''$

Desviación =  $0.05 + 0.03 \text{ m/m}$

Estopines MS

EXPLOSIVO: TOVEX 700 +

SUPERMEXAMON

Fórmulas:  $B_{\text{máx}} = 45 \times d$

$$F.C. = \frac{d^2}{1000}$$

$$\text{Bordo máximo} = 45 \times 76 = 3420 \text{ mm} = 3.42 \text{ m}$$

Corrección del explosivo:

G.E. 40.9%  $p = 1.00$  Densidad =  $1.25 \text{ Kg/lt}$

TOVEX 700  $p = 0.75$  Densidad =  $1.10$  "

$$B_{\text{máx, TOVEX 700}} = B_{\text{máx}} \sqrt{\frac{0.75 \times 1.10}{1.00 \times 1.25}} = 3.42 \times 0.81 = 2.78 \text{ m}$$

Ajuste por constante de roca:

$$B_{\text{máx } r=0.33} = 2.78 \sqrt{\frac{0.4}{0.33}} = 3.06 \text{ m}$$

$$\text{Bordo práctico} = 3.06 - 0.05 - 10 \times 0.03 = 2.71 \text{ m}$$

$$\text{Espaciamiento práctico} = 2.71 \times 1.25 = 3.39 \text{ m}$$

$$B_i = 2.70 \text{ m} \quad E_i = 3.40 \text{ m}$$

$$\text{Carga de fondo} = 1.3 \text{ B.práct.} = 1.3 \times 3.06 = 4.0 \text{ m}$$

Considerando que se trata de una caliza de resistencia intermedia se puede hacer una reducción de la carga de fondo:

$$1.3 \times 3.06 \times 0.70 = 2.80 \text{ m.}$$

reducción arbitraria

$$\text{Subbarrenación} = 0.3 \times 3.06 = 0.90 \text{ m}$$

$$\text{Profundidad barrenos} = 1.03 \times (10.00 + 0.90) = 11.2 \text{ m.}$$

$$\text{Taco} = 3 \text{ m.}$$

$$\text{Altura carga de columna} = 11.20 - 2.80 - 3.0 = 5.40 \text{ m}$$

Usando Supermexamón con  $d = 65\%$  se ajusta al Tovex 700

$$\text{Carga de columna C.C.} = 5.40 \times \underbrace{4.54}_{\text{lt/m}} \times \underbrace{0.65}_{\text{densidad}} = 16 \text{ Kg}$$

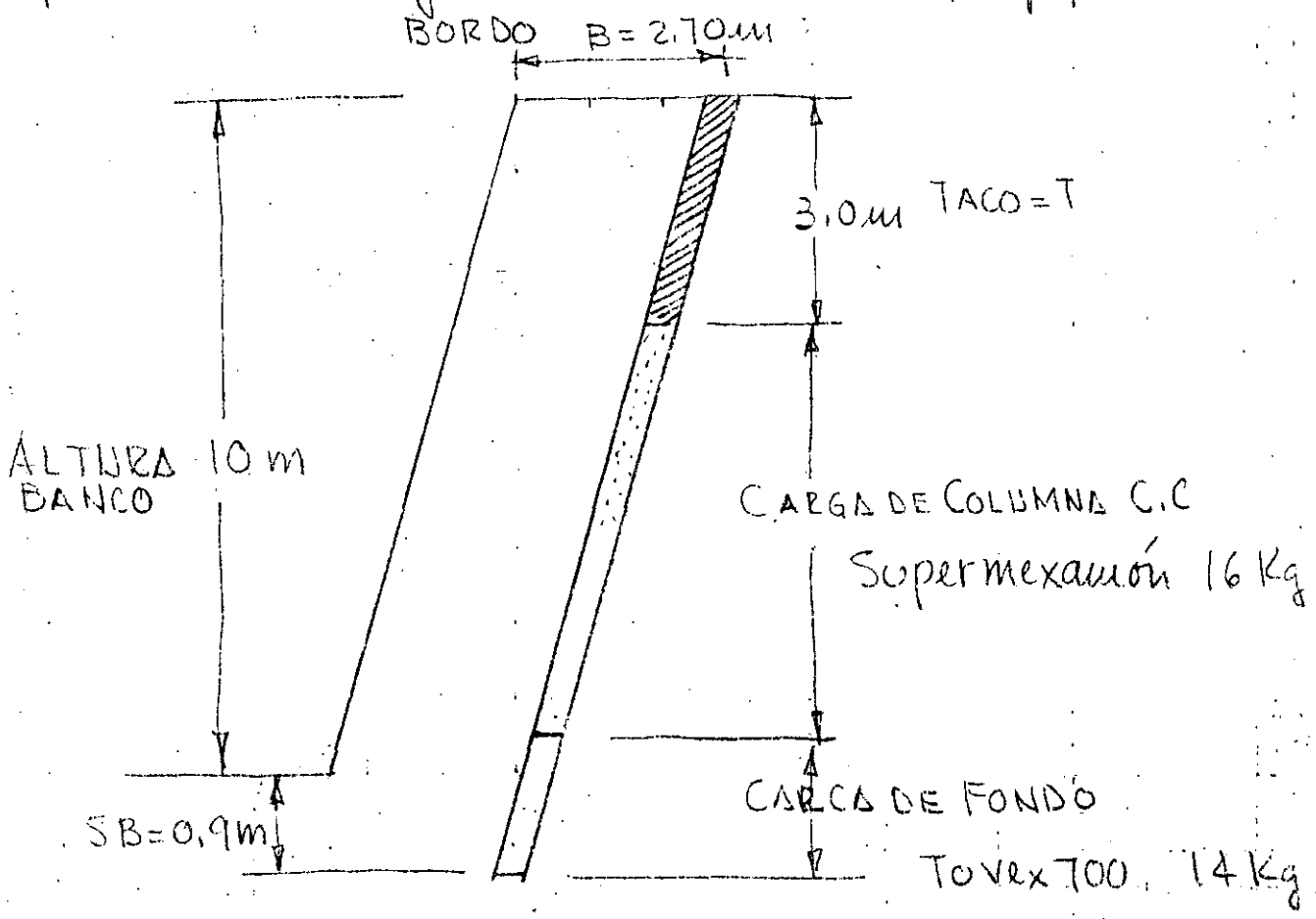
$\phi = 3''$

$$\text{Carga de fondo C.F.} = 2.80 \times \underbrace{4.54}_{\text{lt/m} \rightarrow \phi 3''} \times 1.10 = 14 \text{ Kg.}$$

$$\text{Carga total} = 30 \text{ Kg.}$$

Factor de carga =  $\frac{30}{10 \times 2.70 \times 3.40} = 0.325 \text{ Kg/m}^3$

Haciendo intervenir la potencia del explosivo el factor de carga se reduce a  $\approx 290 \text{ gr/m}^3$



## TIPO DE ROCA

## CONSTANTE DE ROCA

DIAMANTE	0.86
GUARZO	0.62
BASALTO	0.62
HORSTENO	0.59
FELDSPATO	0.57
GNEISS	0.54
ESQUISTOS	0.53
MAGNETITA	0.50
GRANITO	0.46
AARENISCA	0.46
DOLOMITA	0.44
ROCA CALIZA	0.40
PIZARRA	0.36
LUTITA	0.36
CALCITA	0.36
ANTRACITA	0.36
MARMOL	0.36
CARBON BITUMINOSO	0.36
MICA	0.28
YESO	0.24

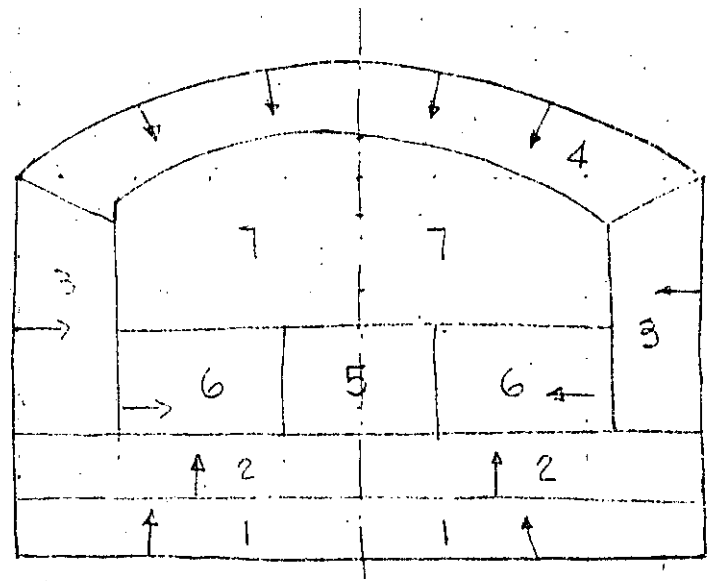
=====

## CONSTANTE DE VOLADURA; ( EXPLOSIVIDAD )

ESTA CONSTANTE TOMA EN CUENTA LA CALIDAD DEL MACIZO ROCOSO.

+ ROCA MUY SOLIDA Y FISURADA	0.60	KG/m <sup>3</sup>
+ ROCA MUY SOLIDA	0.55	KG/m <sup>3</sup>
+ ROCA NORMAL CON GRIETAS	0.50	KG/m <sup>3</sup>
+ ROCA RELATIVAMENTE HOMOGENEA	0.45	KG/m <sup>3</sup>
+ ROCA HOMOGENEA	0.40	KG/m <sup>3</sup>

# DIAGRAMA DE BARRENACION Y CARGA DE UN TUNEL



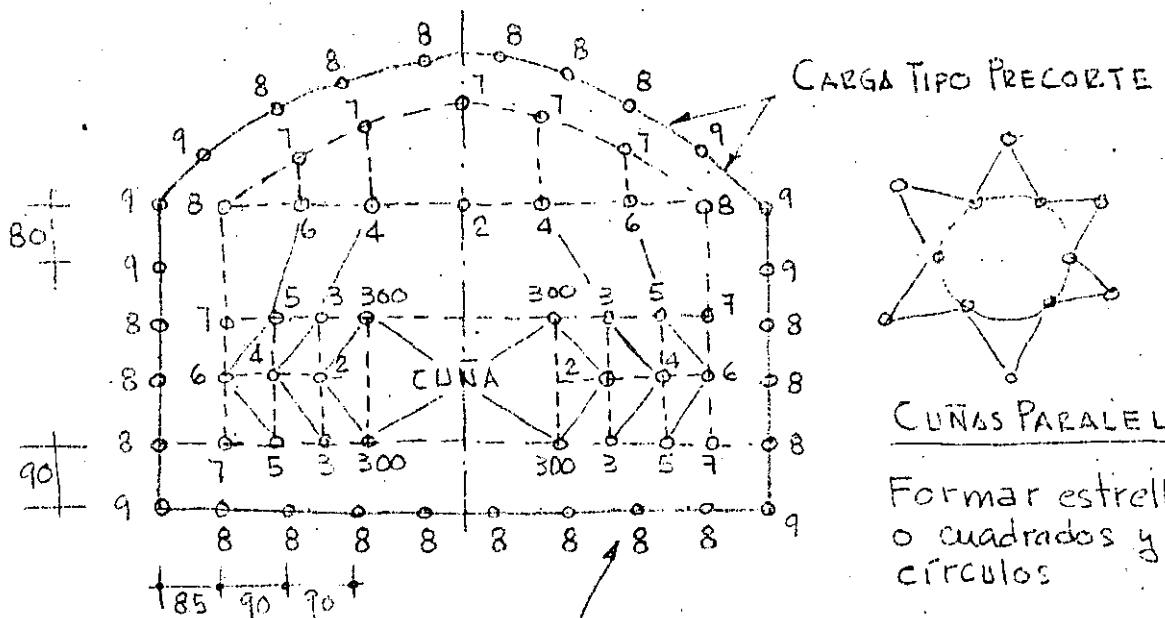
GEOMETRIA PARA EL CALCULO  
(No es diagrama de barrenación)

- 1.- Piso
- 2.- Salida hacia arriba
- 3.- De pared
- 4.- De techo
- 5.- Cuña con ayudantes
- 6.- Salida horizontal
- 7.- Salida hacia abajo

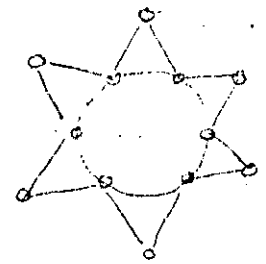
DIRECCION DE SALIDA DE  
LA ROCA



# EJEMPLO VOLADURA EN TUNEL



CARGA TIPO PICORTE



CUÑAS PARALELAS

Formar estrellas o cuadrados y no círculos

Los barroes de piso se cargan completos

C.C = 0.5 a 0.7 CF.

## CALCULO

Ancho = 8 m

Barroes de piso: Bordo = 90 cm.

Altura = 5.65 m

$$B = \frac{\text{Prof} - 0.4 \text{ m}}{2}$$

Bordo real =  $90 - 0.10 = 0.8$   
Picado

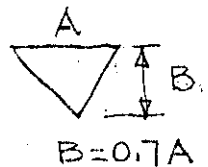
Pared = 4.0 m

$$B_{\text{teor}} = \frac{2.9 - 0.4}{2} = 1.25$$

Es paciamiento:  $E = 1.1 B$

Area =  $40 \text{ m}^2$

$\phi 31 \text{ mm} = \text{Serie II}$



$E = 1.1 \times 8 = 0.88 \rightarrow 0.90$

Hay 9 espacios =  $7 \times 0.9$  y  $2 \times 0.85$

Barreación = 3.20 m

Avance =  $0.9 \times 3.20 = 2.90 \text{ m}$

Explosivo: Gelatina extra 40%

Cuña: Paralela de 2 barroes vacíos grandes

Barreación por picado = 10 cm.

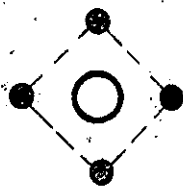
Volumen por tronada =  $40 \times 2.9 = 116 \text{ m}^3$

Factor de barreación =  $\frac{275}{116} = 2.37 \text{ m/m}^3$

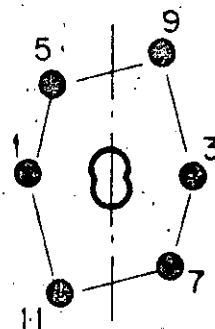
Long. barreación:  
86 barroes  $\times 3.2$   
 $L = 275.2$

Factor de carga F.C. =  $\frac{131}{116} = 1.13 \text{ kg/m}^3$



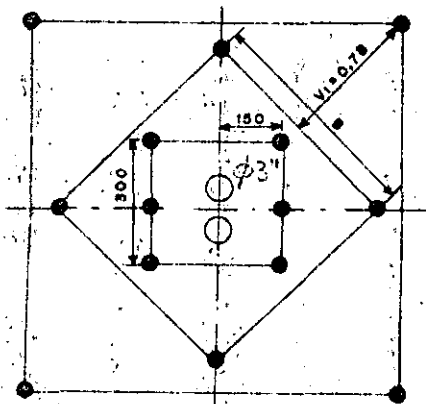


CUÑA "CINCO DE OROS"  
CON UN BARRENO DE GRAN DIAMETRO

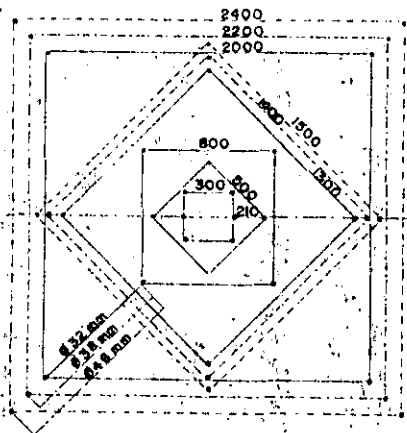


CUÑA COROMANT  
(ADECUADA PARA GALERIA PEQUEÑA)

El dispositivo guía se fija a la roca mediante un expansor.



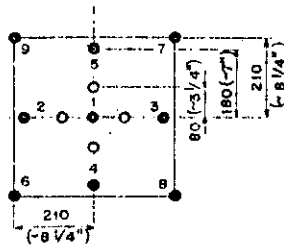
CUÑA DE EXPANSION CON DOS  
BARRENOS QUEMADOS DE  
GRAN DIAMETRO



CUÑA DE EXPANSION PARA UNO  
O DOS BARRENOS QUEMADOS

Avance de 3.9 a 4 m

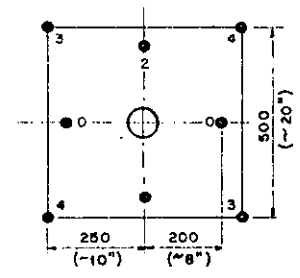
No se debe trabajar con diámetros grandes en todo el frente del túnel.



CUÑA QUEMADA CON CUATRO BARRENOS HUECOS Ø 35 mm (CUÑA GRONLUND)

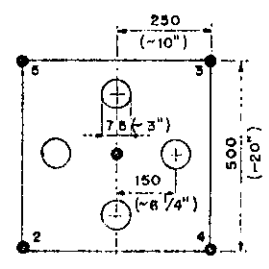
Buena hasta 3.2 m de profundidad.

- En el barreno central el estopín esta en la boca del barrend
- En los ayudantes el estopín esta al fondo.

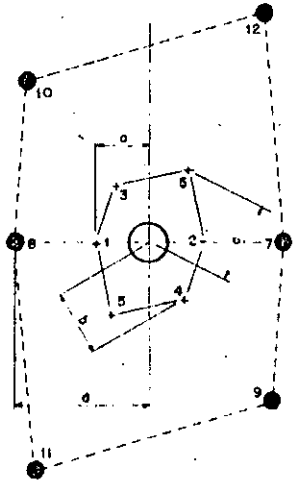


CUÑA QUEMADA MICHIGAN

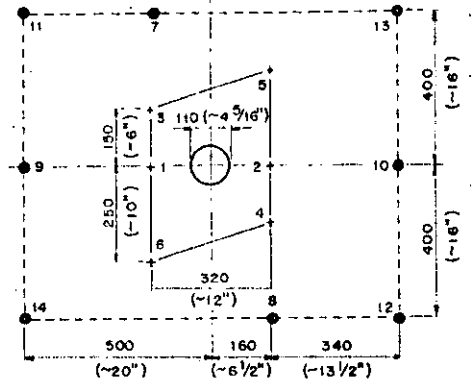
Avance 3.9 m



CUÑA TIPO GATO CON CUATRO BARRENOS VACIOS DE DIAMETRO GRANDE

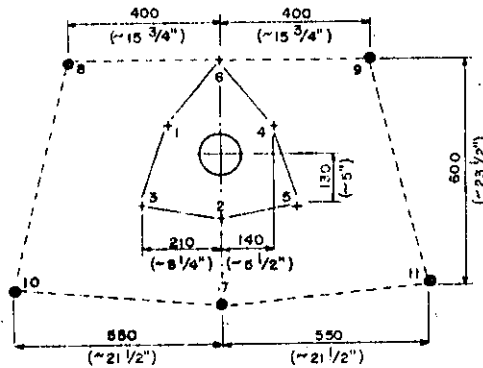


CUÑA EN DOBLE ESPIRAL CON UN BARRENO DE DIAMETRO GRANDE



CUÑA EN DOBLE ESPIRAL MODIFICADO (CUÑA TABY) CON UN BARRENO DE DIAMETRO GRANDE

Más eficiente que la Fagersta



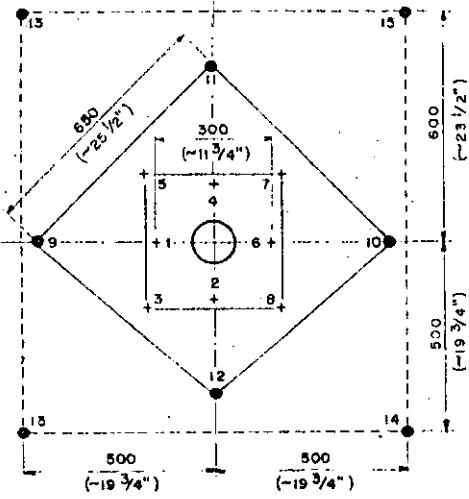
CUÑA DE TRES SECCIONES 25 % MAS EFICIENTE QUE LA TABY

# PATRONES DE BARRENACION USUALES PROMEDIO

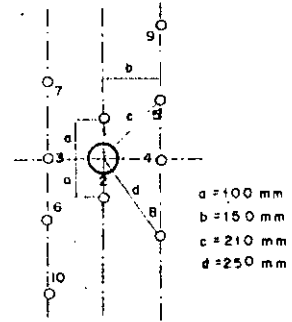
Todos los valores en pies excepto el diámetro del explosivo

D (pulg.)	B	J	T	L <sub>MAX</sub>	Patrones equivalentes	
					Rectangular	Cuadrado
1	2 <sup>1/2</sup>	1	2	10	2 <sup>1/2</sup> x 4	3 x 3
2	5	2	4	20	5 x 9	7 x 7
3	7 <sup>1/2</sup>	2 <sup>1/2</sup>	5	30	7 <sup>1/2</sup> x 13	10 x 10
4	10	3	6	40	10 x 18	13 x 19
5	12 <sup>1/2</sup>	4	8	50	12 <sup>1/2</sup> x 22	16 x 16
6	15	5	10	60	15 x 27	20 x 20
7	17 <sup>1/2</sup>	5 <sup>1/2</sup>	12	70	17 <sup>1/2</sup> x 31	23 x 23
8	20	6	14	80	20 x 36	26 x 27
9	22	7	15	88	22 x 40	29 x 30
10	24	7 <sup>1/2</sup>	16	96	24 x 43	32 x 32
11	26 <sup>1/2</sup>	8	18	106	26 <sup>1/2</sup> x 48	35 x 36
12	29	9	20	116	29 x 59	38 x 39

B = Bordo                      PROMEDIOS : B = 30 Ø ; E = 1/25 B  
 J = Sub-barrenación            J = 0.3 B  
 T = Taco                         T = 0.7 B  
 L = Altura banco                L = 2.6 B



CUÑA EN CUATRO SECCIONES CON UN BARRENO DE GRAN DIAMETRO (ES LA CUÑA CILINDRINCA MAS UTILIZADA)



CUÑA FAGERSTA (ADECUADA PARA GALERIA PEQUEÑA)

# VOLADURAS DE POST-CORTE Y PRECORTE

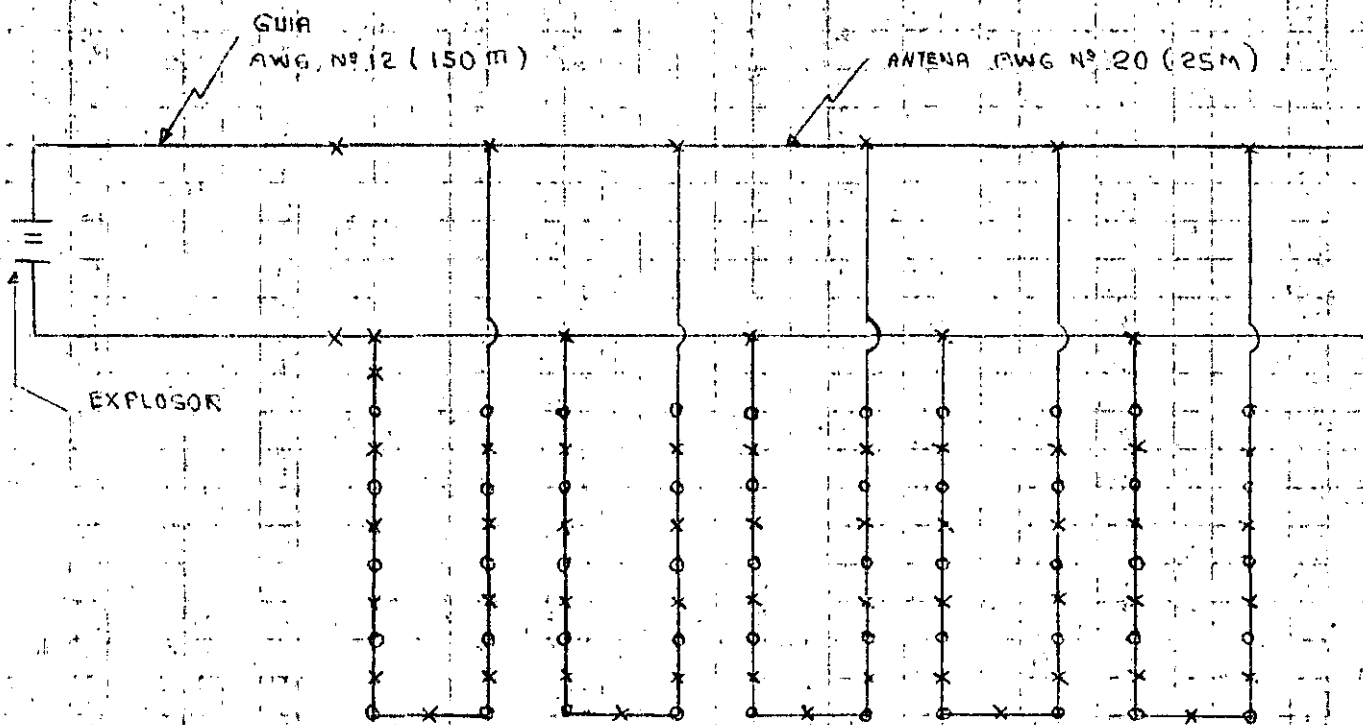
Diámetro del barreno d (mm)	Concentración de carga Kg/m	Post-corte		Precorte
		E <sub>i</sub> m	V <sub>i</sub>	E <sub>i</sub> m
30		0.5	0.7	0.25-0
37	0.12	0.6	0.9	0.30-0.5
44	0.17	0.6	0.9	0.30-0.5
50	0.25	0.8	1.1	0.45-0.70
62	0.35	1.0	1.3	0.55-0.80
75	0.5	1.2	1.6	0.6-0.9
87	0.7	1.4	1.9	0.7-1.0
100	0.9	1.6	2.1	0.8-1.2
125	1.4	2.0	2.7	1.0-1.5
150	2.0	2.4	3.2	1.2-1.8
200	3.0	3.0	4.0	1.5-2.1



# POTENCIA DE UNA RED ELECTRICA: VOLADURA DE CANTERA EN CHICOASEN, CHIS.

## 1).- CARACTERISTICAS ELECTRICAS DEL CIRCUITO UTILIZADO.

CIRCUITO: PARALELO CON 5 CIRCUITOS DE 12 ESTOPINES DE RETARDO.



No. series = 5.

ESTOPINES DE RETARDO DE: 16 pies, alambre de cobre

ANTENA: Alambre de cobre AWG No 20 - 25 M c/u.

GUIA: Alambre de cobre AWG Nº 12 - 150 M c/u.

a) CORRIENTE NECESARIA

$$I = 5 \text{ series} \times 1.5 \text{ A por serie} = 7.5 \text{ A}$$

b) RESISTENCIA DE CADA SERIE

$$R_1 = 12 \text{ estopines} \times 1.65 \Omega = 19.8 \Omega$$

c) RESISTENCIA EN PARALELO DE TODAS LAS SERIES.

$$R_2 = \frac{19.8 \Omega}{5 \text{ series}} = 3.9 \Omega$$

d) RESISTENCIA DE LA ANTENA.

$$R_3 = 25M \times 2 \times \frac{10.15 \Omega}{0.304 M (1000 \text{ pies})}$$

e) - RESISTENCIA DE LA GUIA

$$R_g = \frac{150 \text{ m} \times 2 \times 1.588}{0.307 (1000 \text{ ft})} = 1.567 \Omega$$

f) - RESISTENCIA TOTAL DEL CIRCUITO

$$R_T = 4 \Omega \times 1.67 \Omega \times 1.57 \Omega = 7.24 \Omega$$

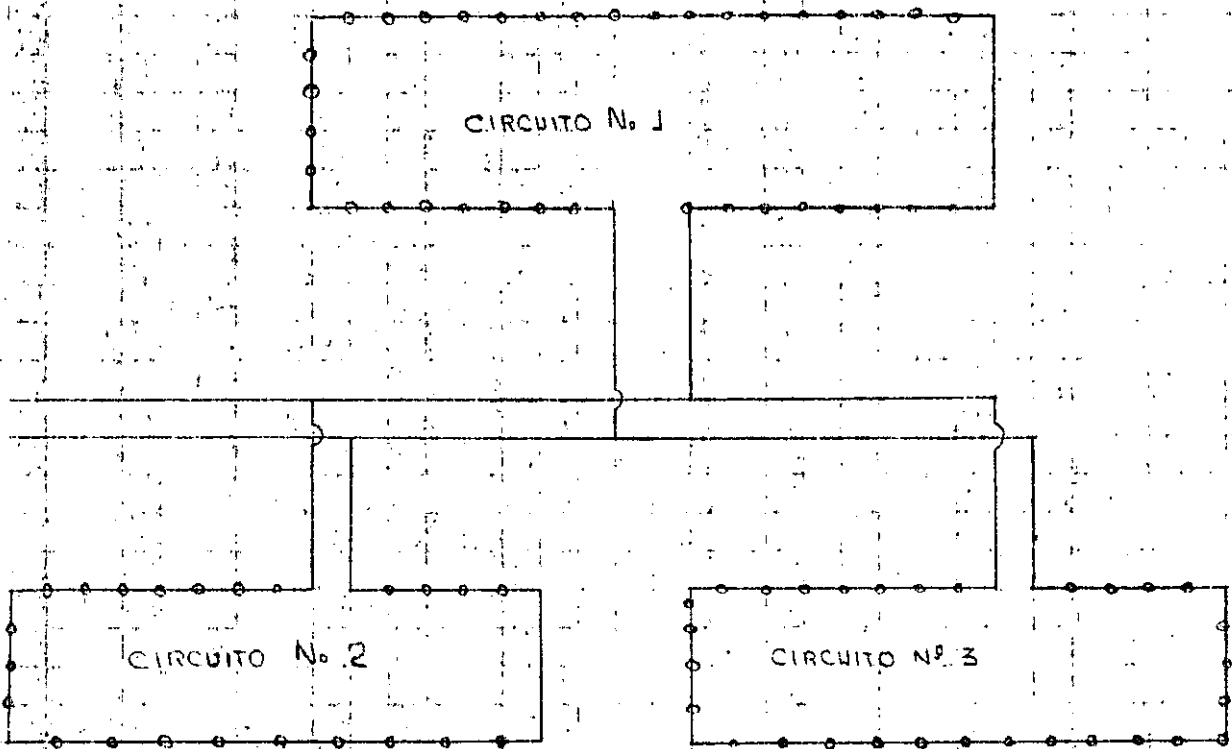
g) - VOLTAJE REQUERIDO

$$E = 7.5 \text{ A} \times 7.24 \Omega = 54.3 \text{ V}$$

h) - POTENCIA REQUERIDA

$$P = I^2 R = (7.5)^2 \text{ A} \times 7.24 \Omega = 407 \text{ Watts}$$

$$P = IE = 7.5 \text{ A} \times 54.3 \text{ V} = 407 \text{ Watts}$$



ESTOPINES

RESISTENCIA DEL CIRCUITO

CIRCUITO No.	DE RETARDO	INSTANTANEOS	RESISTENCIA DEL CIRCUITO
1	57	—	$57 \times 1.32 = 75.24 \Omega$
2	22	9	$22 \times 1.32 + 9 \times 1.42 = 41.82 \Omega$
3	22	5	$22 \times 1.32 + 5 \times 1.42 = 36.14 \Omega$

Se consideró que la longitud de los alambres de los estopines fue de 8ft.

RESISTENCIA DEL ALAMBRE GUIA:

Calib. 20:  $\frac{93 \text{ m} \times 3.28 \times 10.15}{1000} = 3.10 \Omega$

Calib. 14:  $\frac{66 \text{ m} \times 3.28 \times 2.525}{1000} = 0.55 \Omega$

RESISTENCIA DE LOS TRES CIRCUITOS EN PARALELO

$R_e = \frac{1}{\frac{1}{75.24} + \frac{1}{41.82} + \frac{1}{36.14}} = 15.41 \Omega$

$\frac{1}{\frac{1}{75.24} + \frac{1}{41.82} + \frac{1}{36.14}}$

c) - RESISTENCIA TOTAL

$R_t = 15.41 + 3.10 + 0.55 = 19.06 \Omega$

d) INTENSIDAD REQUERIDA

$$I = 3 \text{ Series} \times 1.5 \text{ Amp. por serie} = 4.5 \text{ Amp.}$$

e) VOLTAJE NECESARIO

$$V = IR = 4.5 \text{ A} \times 19.06 \Omega = 85.77 \text{ Volts}$$

f) POTENCIA

$$P = IV = 4.5 \times 85.77 \text{ volts} = 385.97 \text{ Watts}$$

very important, particularly to rock fracturing, is the type and strength of the bonding between individual grains. For example, rock may have pronounced jointing at widely separated distances, but the material between joint planes may be strongly bonded, or massive in character. Large boulders invariably result when blasting is carelessly done under this condition. On the other hand, rocks may be highly laminated or stratified, or the bond between grains may be very weak, so that fragmentation is always easily accomplished by merely moving the material from its original place.

**Resilience** This property, sometimes called sponginess or toughness, refers to the elasticity of a material. It is used to express the capability of a rock to resist shock and recover its original position and shape without being ruptured. If a rock on being dropped, for example, makes a dull thud and does not rebound, it would be very difficult to break by impact. Brittle rocks, however, shatter easily, particularly those types having a high silica (quartz) content. A blaster can generally determine quite easily whether or not a material will break into small sizes or large coarse fragments by conducting a simple drop test. Furthermore, the test provides a clue as to the energy absorption power of the material, which is important for estimating the amount of additional charge, or energy, that would be necessary to overcome expected energy losses.

**Strength** Of the characteristic strengths of materials, blasting is normally concerned only with that of tension. Most rocks are very weak in tension, more resistant to shear, and strongest in compression, having approximately only one-tenth the resistance to tensile rupture that they have to failure by compression (Table 7). However, shear is not actually a force by itself but rather the result of two forces, either two tensile or two compressive forces, or a combination of one of each, which act along different lines and directions.

To know the actual strengths of a material, samples must be tested in a laboratory. (Regular tensile-

Table 7—Properties of Various Selected Materials

Name and Location	Compressive Strength (psi)	Modulus of Rupture (psi)	Specific Gravity (SG)	Density (d.) (ton/cu. ft.)	Longitudinal Velocity (v.) (fps)
Amphibolite (fine grain, India) . . . . .	61,400	7,400	3.12	0.097	19,000
Basalt (New York) . . . . .	46,600	8,000	2.94	0.092	18,700
Basalt (Michigan) . . . . .	33,400	3,800	2.85	0.089	15,200
Basalt glass . . . . .	—	—	2.81	0.088	21,000
Diabase (fine grain, Michigan) . . . . .	44,200	5,300	2.94	0.092	16,700
Dolomite (Missouri) . . . . .	8,800	1,000	2.80	0.087	—
Dolomite (Tennessee) . . . . .	46,700	3,800	2.84	0.089	17,900
Gabbro (altered, New York) . . . . .	40,200	5,400	2.93	0.091	17,600
Granite (Georgia) . . . . .	28,000	2,000	2.64	0.082	8,900
Granite (Vermont) . . . . .	33,200	2,900	2.66	0.083	11,100
Granite (Nevada) . . . . .	39,500	3,900	2.63	0.082	14,500
Granite (North Carolina) . . . . .	30,400	1,600	2.60	0.081	8,000
Greenstone (Michigan) . . . . .	45,500	3,300	3.30	0.103	16,600
Gypsum (Indiana) . . . . .	3,200	1,200	2.32	0.072	—
Limestone (Ohio) . . . . .	28,500	2,900	2.69	0.084	15,400
Limestone (Utah) . . . . .	28,000	2,200	2.78	0.087	15,900
Limestone (fossiliferous, Indiana) . . . . .	10,900	1,600	2.31	0.072	12,400
Limestone (West Virginia) . . . . .	23,000	1,900	2.68	0.084	16,400
Marble (Maryland) . . . . .	30,800	2,800	2.37	0.074	13,700
Marble (New York) . . . . .	18,400	1,700	2.72	0.085	14,500
Obsidian . . . . .	—	—	2.35	0.073	16,100
Quartzite (taconite, Minnesota) . . . . .	91,200	3,400	2.75	0.086	18,200
Rock salt (Louisiana) . . . . .	5,000	Negligible	2.50	0.078	—
Sandstone (Ohio) . . . . .	10,400	500	2.06	0.064	5,600
Sandstone (West Virginia) . . . . .	19,400	3,400	2.50	0.078	12,900
Sandstone (Utah) . . . . .	11,500	620	2.17	0.068	8,400
Sandstone (Alabama) . . . . .	26,800	2,200	2.76	0.086	12,500
Shale (Utah) . . . . .	31,300	2,500	2.81	0.088	14,900
Shale (West Virginia) . . . . .	11,600	4,200	2.40	0.075	13,600
Syenite (New York) . . . . .	34,500	2,800	2.72	0.085	14,500
Alluvium, broken rock, loess . . . . .	—	—	1.3-1.5	0.044	2,300
Clay . . . . .	—	—	2.58	0.081	5,900
Air . . . . .	—	—	0.0012	—	1,080
Water . . . . .	—	—	1.00	0.031	4,750

strength tests are usually difficult to conduct.) However, tests for what is known as the modulus of rupture are much easier to perform; yet they provide information that is just as useful in providing tensile-strength data of equal practical value. In fact, the laboratory test for the modulus breaks samples in tension by bending test slabs until they fracture, much in the same manner that rock is stretched and broken at an open face during blasting (Figure 3).

Quite often it is impossible or quite impracticable for quarry operators to have tests conducted. Also, test results on samples may not necessarily provide information on the over-all strength of a rock deposit, except when the material is homogeneous and very massive. Nevertheless, if tests could be made, the data would aid greatly in determining the stress levels (psi) required for fracture. It is the resistance to tensile rupture that must be exceeded by the energy pulses at

the free faces, and thus, if known, could also give an approximation of the required burden dimension and the explosive pressures needed for proper breakage. In the event specific test data cannot be obtained, the operator may find the information in Table 7 quite useful. From the various moduli listed for many of the representative rock-types, a practical estimate can be made that will approximate the characteristics of his particular deposit.

**Density** Denser materials require greater amounts of work energy to be satisfactorily broken and displaced, and heavier explosives or large charges will therefore be needed. However, from Table 7 it can be concluded that for most rocks there is a very narrow range of density differences, with SG values varying from 2.3 to 3.3 in most instances. The materials generally requiring blasting have densities confined to the 2.5-2.9 SG range. This can be interpreted to mean that the

TABLE 1

## CHARACTERISTICS OF SOME INGREDIENTS USED IN EXPLOSIVE MIXTURES

Compound	Short Name	Freezing Temp., °F	Explosion Temp., °F	Ideal Reaction Products	Available Oxygen Atoms
$4\text{KClO}_3$	Chlorate	695	752 (Decompose)	+ $60\text{O}_2$ + $4\text{KCl}$	12
$4\text{NaNO}_3$	SN	585	712 (Decompose)	$4\text{NO} + 30\text{O}_2 + 2\text{Na}_2\text{O}$	10
$4\text{N}_2\text{H}_4\text{O}_3$	AN	340	460	$8\text{H}_2\text{O} + 3\text{N}_2 + 2\text{NO}_2$	4
$4\text{C}_3\text{N}_3\text{H}_5\text{O}_9$	NG	55	420	$10\text{H}_2\text{O} + 5\text{N}_2 + 12\text{CO}_2 + 2\text{NO}$	2
$4\text{C}_2\text{N}_2\text{H}_4\text{O}_6$	IGDN	- 4	239 (Boils)	$8\text{H}_2\text{O} + 4\text{N}_2 + 8\text{CO}_2$	0
$4\text{CaCO}_3$	Limestone	--	--	$4\text{CO}_2 + 4\text{CaO}$	0
$4\text{C}_5\text{N}_4\text{H}_8\text{O}_{12}$ *	PETN	282	420	$16\text{H}_2\text{O} + 8\text{N}_2 + 12\text{CO}_2 + 8\text{CO}$	- 8
$4\text{C}_3\text{N}_5\text{H}_6\text{O}_6$ *	RDX	252	500	$12\text{H}_2\text{O} + 12\text{N}_2 + 12\text{CO}$	-12
$4\text{C}_6\text{H}_3\text{H}_7\text{O}_{11}$ *	Nitrocellulose, Nitrostarch	212 (Decomp.)	345 250	$14\text{H}_2\text{O} + 6\text{N}_2 + 6\text{CO}_2 + 18\text{CO}$	-18
$4\text{C}_6\text{H}_3\text{H}_3\text{O}_7$	Picric Acid	255	610	$6\text{H}_2\text{O} + 6\text{N}_2 + 22\text{CO} + 2\text{C}$	-26
$4\text{C}_7\text{N}_5\text{H}_5\text{O}_8$	Tetryl	265	495	$10\text{H}_2\text{O} + 10\text{N}_2 + 22\text{CO} + 6\text{C}$	-34
$4\text{C}_7\text{N}_3\text{H}_5\text{O}_6$	TNT	180	888	$10\text{H}_2\text{O} + 6\text{N}_2 + 14\text{CO} + 14\text{C}$	-42
$4\text{C}_6\text{H}_{10}\text{O}_5$	Cellulose, Wood Pulp, or Starch			$20\text{H}_2\text{O} + 24\text{C}$	-48
$4\text{C}_7\text{N}_2\text{N}_6\text{O}_4$	DNT	158	752 (Decompose)	$12\text{H}_2\text{O} + 4\text{N}_2 + 4\text{CO} + 24\text{C}$	-52
$4\text{PbN}_6$	Lead Azide	480 (Decomp.)	660	$12\text{N}_2 + 4\text{Pb}$	-

NOTE: \* - These compounds are used in the water-wet condition. PETN can be initiated by a single #6 blasting cap with up to 35 per cent water content. Nitrocellulose and nitrostarch are very sensitive to initiation when dry.

TABLE 2

HEATS OF FORMATION FOR SELECTED  
CHEMICAL COMPOUNDS

(Rf: Handbook of Chemistry and Physics, 48th Ed., 1967-68)

<u>Compound</u>	<u>Formula</u>	<u>Form</u>	<u>Mol. Wgt.</u>	<u>Qp or Qr Kcal/mole</u>
	AlO	g	43.0	+ 10.7
	Al <sub>2</sub> O	g	70.0	- 31.7
Corundum	Al <sub>2</sub> O <sub>3</sub>	s	102.0	-399.1
	CaCl <sub>2</sub>	s	111.1	-190.0
Calcite	CaCO <sub>3</sub>	s	100.0	-288.5
Lime	CaO	s	56.1	-151.9
	CaO <sub>2</sub>	s	72.1	-158.3
Paraffin	CH <sub>2</sub>	s	14.0	- 7.0
Formaldehyde	CH <sub>2</sub> O	g	30.0	- 27.7
Formic acid	CH <sub>2</sub> O <sub>2</sub>	g	46.0	- 86.7
Methyl alcohol	CH <sub>3</sub> OH	l	32.0	- 57.0
Nitromethane	CH <sub>3</sub> O <sub>2</sub> N	l	61.0	- 21.3
Methane	CH <sub>4</sub>	g	16.0	- 17.9
Urea	CH <sub>4</sub> ON <sub>2</sub>	s	60.0	- 79.9
Acetylene	C <sub>2</sub> H <sub>2</sub>	g	26.0	+ 54.2
Oxalic acid	C <sub>2</sub> H <sub>2</sub> O <sub>4</sub>	s	90.0	-197.6
Ethylene	C <sub>2</sub> H <sub>4</sub>	g	28.0	+ 12.5
Acetic acid	C <sub>2</sub> H <sub>4</sub> O <sub>2</sub>	l	60.0	-116.4
Ethylene glycol dinitrate	C <sub>2</sub> H <sub>4</sub> O <sub>6</sub> N <sub>2</sub>	l	153.0	- 56.0
Ethyl alcohol	C <sub>2</sub> H <sub>5</sub> OH	l	46.0	-66.4
Ethane	C <sub>2</sub> H <sub>6</sub>	g	30.0	- 20.2
RDX	C <sub>3</sub> H <sub>6</sub> O <sub>6</sub> N <sub>6</sub>	s	222.1	+ 18.3
Propane	C <sub>3</sub> H <sub>8</sub>	g	44.1	- 24.8
Glycerine	C <sub>3</sub> H <sub>8</sub> O <sub>3</sub>	l	92.1	+159.7
Nitroglycerine	C <sub>3</sub> H <sub>5</sub> O <sub>9</sub> N <sub>3</sub>	l	227.1	- 82.7
Butane	C <sub>4</sub> H <sub>10</sub>	g	59.0	- 29.8
PETN	C <sub>5</sub> H <sub>8</sub> O <sub>12</sub> N <sub>4</sub>	s	316.1	-123.0
Pentane	C <sub>5</sub> H <sub>12</sub>	g	72.1	- 35.0
Picric acid	C <sub>6</sub> H <sub>3</sub> O <sub>7</sub> N <sub>3</sub>	s	229.0	- 53.5

TABLE 2 (cont.)

<u>Compound</u>	<u>Formula</u>	<u>Form</u>	<u>Mol. Wgt.</u>	<u>Qp or Qr Kcal/mole</u>
Phenol	$C_6H_5OH$	s	94.1	+ 39.2
Benzene	$C_6H_6$	g	84.1	+ 19.8
Nitrocellulose and Nitrostarch	$C_6H_7O_{11}N_3$	s	297.1	- 45.7
Cellulose	$C_6H_{10}O_5$	s	162.2	-170.5
Starch	$C_6H_{10}O_5$	s	162.2	-205.2
Dextrose & Glucose	$C_6H_{12}O_6$	s	180.2	+303.6
Hexane	$C_6H_{14}$	g	86.2	- 40.0
Mannitol	$C_6H_{14}O_6$	s	182.2	+317.3
Trinitrotoluene	$C_7H_5O_6N_3$	s	227.1	- 13.0
Tetryl	$C_7H_5O_8N_5$	s	287.2	+ 9.3
Dinitrotoluene	$C_7H_6O_4N_2$	s	182.1	- 6.9
Toluene	$C_7H_8$	l	92.2	+ 12.0
Heptane	$C_7H_{16}$	g	100.2	- 44.9
Octane	$C_8H_{18}$	g	114.3	- 49.8
Nonane	$C_9H_{20}$	g	128.3	- 54.7
Nicotine	$C_{10}H_{14}N_2$	l	162.2	- 5.2
Camphor	$C_{10}H_{16}O$	s	152.3	+ 79.8
Castor Oil	$C_{11}H_{10}O_{10}$	l	302.2	-
Sucrose	$C_{12}H_{22}O_{11}$	s	342.4	+535.1
	$ClO$	g	51.5	+ 33.0
	$ClO_3$	g	83.5	+ 37.7
	$CO$	g	28.0	- 26.4
	$CO_2$	g	44.0	- 94.1
	$H^+$	ion	1.0	+ 52.1
	$OH^-$	ion	17.0	+ 10.4
Water	$H_2O$	g	18.0	- 57.8
Peroxide	$H_2O_2$	l	34.0	- 47.1
Hydrochloric acid	$HCl$	l	36.5	- 40.0
Carbonic acid	$H_2CO_3$	l	62.0	-167.0
	$HN_3$	g	58.0	+ 70.3
Nitric acid	$HNO_3$	l	63.0	- 49.4
Mercury fulminate	$HgC_2O_2N_2$	s	284.7	+ 64.0



(5)

TABLE 2 (cont.)

10.

<u>Compound</u>	<u>Formula</u>	<u>Form</u>	<u>Mol.Wgt.</u>	<u>Qp or Qr Kcal/mole</u>
Sylvite	KCl	s	75.6	-104.2
Potassium chlorate	KClO <sub>3</sub>	s	122.5	- 93.5
Potassium perchlorate	KClO <sub>4</sub>	s	138.6	-103.6
Salt peter	KNO <sub>3</sub>	s	101.1	-117.8
Caustic potash	KOH	s	56.1	-111.8
	K <sub>2</sub> O	s	94.2	- 86.4
Arcanite	K <sub>2</sub> SO <sub>4</sub>	s	135.2	-342.7
Periclase	MgO	s	40.3	-143.8
Halite	NaCl	s	58.5	- 98.2
Sodium chlorate	NaClO <sub>3</sub>	s	106.5	- 85.7
Sodium perchlorate	NaClO <sub>4</sub>	s	122.5	- 92.2
	Na <sub>2</sub> CO <sub>3</sub>	s	106.0	-270.3
Soda niter	NaNO <sub>3</sub>	s	85.0	-101.5
Caustic soda	NaOH	s	40.0	-102.0
	Na <sub>2</sub> O	s	62.0	- 99.4
	N <sup>+</sup>	ion	14.0	+ 85.1
Ammonia	NH <sub>3</sub>	g	17.0	- 11.0
Sal ammoniac	NH <sub>4</sub> Cl	s	53.4	- 75.4
Ammonium hydroxide	NH <sub>5</sub> O	l	35.1	- 87.6
	NO	g	30.0	+ 21.6
	NO <sub>2</sub>	g	46.0	+ 8.1
Ammonium nitrate	N <sub>2</sub> H <sub>4</sub> O <sub>3</sub>	s	80.1	- 87.3
	N <sub>2</sub> O	g	44.0	+ 19.5
	N <sub>2</sub> O <sub>3</sub>	g	76.0	+ 17.4
	N <sub>2</sub> O <sub>4</sub>	g	92.0	+ 2.3
	N <sub>2</sub> O <sub>5</sub>	g	108.0	+ 3.6
	O <sup>+</sup>	ion	16.0	+ 59.2
Lead azide	PbN <sub>6</sub>	s	291.3	+110.0
	SO <sub>2</sub>	g	64.1	- 71.0
	SO <sub>3</sub>	g	80.1	- 95.1
Quartz	SiO <sub>2</sub>	s	60.1	-205.0
Zincite	ZnO	s	81.4	- 83.2

(6)

11.

TABLE 2 (cont.)

ATOMIC WEIGHTS

Al = 27.00,	C = 12.01,	Ca = 40.08,	Cl = 35.46,	H = 1.01,
Hg = 200.61,	K = 39.09,	Mg = 24.31,	N = 14.00,	Na = 23.00,
O = 16.00,	Pb = 207.21,	S = 32.07,	Si = 28.09,	Zn = 65.37

CONVERSION FACTORS

1 lb = 454 gm,      1 cal/gm = 1403 ft-lb/lb,      1 BTU = 252 cal

TABLE 3.  
HEATS OF EXPLOSION ( $Q_e$ ) FOR SELECTED  
EXPLOSIVE COMPOUNDS AND MIXTURES

A. COMPOUNDS:

<u>Formula</u>	<u>Products</u>	$Q_e$ , <u>cal/gm</u>	$Q_e$ , <u>ft-lb/lb</u>
(Salt peter) $KNO_3$	$K_2O, NO, O_2$	+956	+1,334,950
(SN) $NaNO_3$	$Na_2O, NO, O_2$	+860	+1,206,580
(AN) $N_2H_4O_3$	$H_2O, N_2, NO_2$	-663	- 888,520
(NG) $C_3N_3H_5O_9$	$H_2O, N_2, CO_2, NO$	-1,468	-2,060,170
(EGDN) $C_2N_2H_4O_6$	$H_2O, N_2, CO_2$	-1,620	-2,285,770
$CaCO_3$	$CaO, CO_2$	+420	+ 500,275
(PETN) $C_5N_4H_8O_{12}$	$H_2O, N_2, CO_2, CO$	-1,402	-1,967,570
(RDX) $C_3N_6H_6O_6$	$H_2O, N_2, CO$	-1,220	-1,711,240
(NCENS) $C_6N_3H_7O_{11}$	$H_2O, N_2, CO_2, CO$	-1,402	-1,966,870
(Tetryl) $C_7N_5H_5O_8$	$H_2O, N_2, CO, C$	-1,009	-1,415,210
(Picric Acid) $C_6N_3H_3O_7$	$H_2O, N_2, CO, C$	-779	-1,092,940
(TNT) $C_7N_3H_5O_6$	$H_2O, N_2, CO, C$	-986	-1,383,220
(DNT) $C_7N_2H_6O_4$	$H_2O, N_2, CO, C$	-1,054	-1,478,480
(Cellulose) $C_6H_{10}O_5$	$H_2O, C$	-777	-1,089,710
(Starch) $C_6H_{10}O_5$	$H_2O, C$	-517	-725,770
(Lead ozide) $PbN_2$	$N_2, Pb$	-370	-519,110
(FO) $CH_2$	$H_2, C$	-500	-701,500
$KClO_3$	$KCl, O_2$	-87	-122,480

B. MIXTURES

$2CH_2 + 3O_2$ (23/77)	$H_2O, CO_2$	-2,337	-3,278,950
$C + O_2$ (27/73)	$CO_2$	-2,139	-3,000,600
$C + 2AN$ (7/93)	$H_2O, N_2, CO_2$	-868	-1,217,800
$CH_2 + 2AN$ (8/92)	$H_2O, N_2, CO$	-761	-1,067,960
$CH_2 + 3AN$ (6/94)	$H_2O, N_2, CO_2$	-897	-1,257,790
$CH_2 + 5AN$ (3/97)	$H_2O, H_2, CO_2, NO$	-580	-813,040
Cellulose + 12AN (15/85)	$H_2O, H_2, CO_2$	-911	-1,277,570
$2CH_2 + 9AN + 2Al$ (3/90/7)	$H_2O, N_2, CO_2, Al_2O_3$	-1,160	-1,626,920
$2CH_2 + 9AN + 4Al$ (2/85/13)	$H_2O, N_2, CO_2, Al_2O_3$	-1,398	-1,961,113
$2CH_2 + AN + 2SN$ (10/29/61)	$H_2O, N_2, CO_2, Na_2O$	-693	-971,580

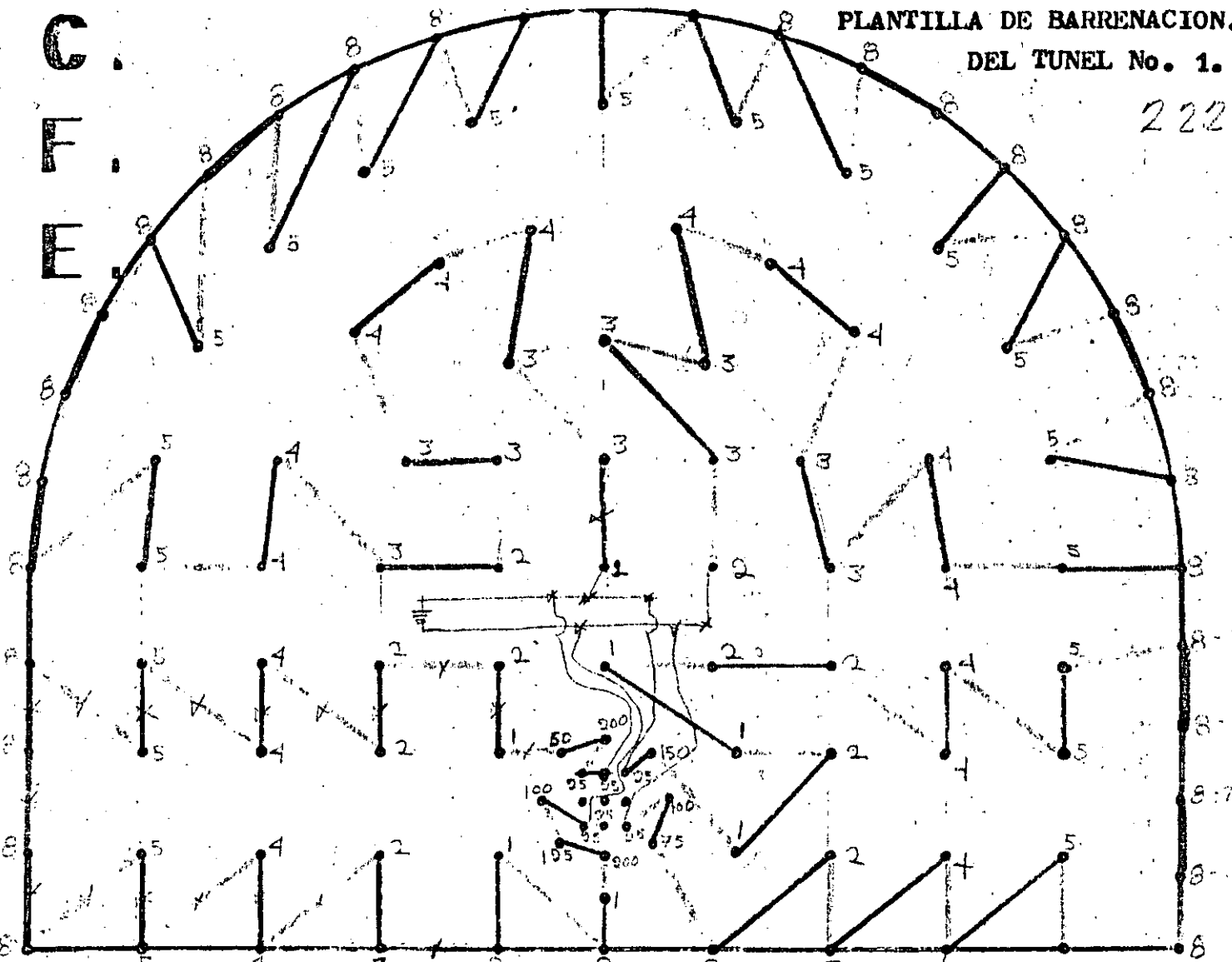
TABLE 3 (Cont.)

<u>Formula</u>	<u>Products</u>	$Q_c$ , cal/gm	$Q_c$ , ft-lb/lb
(Amatol 53AN + 10TNT (65/35)	$H_2O, N_2, CO, C$	-500	-701,500
(AMATOL) 21AN + 2TNT (79/21)	$H_2O, N_2, CO_2$	-1,310	-1,840,000
(TRITONAL) 10TNT + 21A1 (80/20)	$H_2O, N_2, Al_2O_3, CO, C$	-3,938	-5,525,300
(PENTOLITE) 14TNT + 10PETN (50/50)	$H_2O, N_2, CO, C$	-998	-1,400,330
(COMP. B) 70TNT + 10ORDX + 103 Wax + 8 Polyisobutylene	$H_2O, N_2, CO, C$	-1,157	-1,623,270
(COMP. C-4) 10ORDX + 28 Wax + 9 Polyisobutylene + 3 Sebacate	$H_2O, N_2, CO, C$	-1,293	-1,814,080
C + 4NG (1/99)	$H_2O, N_2, CO_2$	-1,598	-2,242,130
Cellulose + 24NG (3/97)	$H_2O, N_2, CO_2$	-1,595	-2,237,080
Cellulose + 12NG + 6AM (5/81/14)	$H_2O, N_2, CO_2$	-1,481	-2,077,420
Cellulose + 2NG + 11AN (11/30/59)	$H_2O, N_2, CO_2$	-1,124	-1,577,390
Cellulose + 4NG + 4SN (12/64/24)	$H_2O, N_2, CO_2, Na_2O$	-1,289	-1,807,770
Nitrocellulose + 9NG (13/87)	$H_2O, N_2, CO_2$	-1,632	-2,290,000
Cellulose + 2NG + 6AM + 2SN (13/36/38/13)	$H_2O, N_2, CO_2, Na_2O$	-1,121	-1,572,623
$CH_4 + 2O_2$ (20/80)	$H_2O, CO_2$	-2,375	-3,332,130

C.  
F.  
E.

PLANTILLA DE BARRENACION.  
DEL TUNEL No. 1.

222



BARRENACION INICIO 12.00 hs / 1<sup>er</sup> Torneo TERMINO 23.00 hs.  
 BARRENACION CON - Jubo - 4 brazos -  
 PROFUNDIDAD Y Ø DEL BARRENO 2.60 mts. 2" Ø  
 TOTAL DE BARRENOS HECHOS. 118 Bar.  
 TOTAL DE BARRENOS CARGADOS 115 Bar.  
 TOTAL DOMBILLOS "TOYEX" 225 Kg.  
 TOTAL KGS. "ANFOSEI" SUPER 100 Kg.  
 TOTAL MTS. "PRILACORD" 24 mts.  
 HORA DE LA TRONADA 0.10 hs.  
 NUMERO DE LA TRONADA 55.  
 AVANCE 12.50 mts.

$F.C = 1.73 \text{ Kg/m}^3$

BARRENACION LADO: Secc. Completa  
 TURNO: 1<sup>o</sup> y 2<sup>o</sup> torneo  
 FECHA: 82-02-17

Guia → 43m calibre calibre 20  
 + 66 m calibre calibre 12  
 + 50 m - - - 20

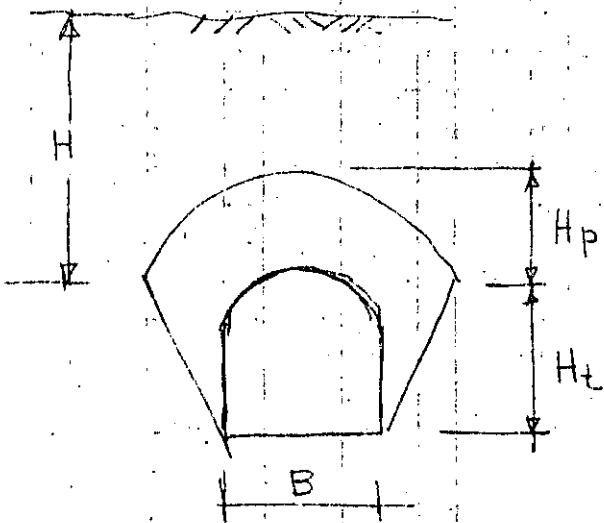
ESTOPIN Nº	CANTIDAD	Explosivo
8	30	
5	21	
4	18	
3	12	
2	14	
1	6	
25	6	
50	1	
75	1	
100	2	
125	1	
150	1	
200	2	

INSPECTOR: C.F.E. Edilberto Domínguez

JEFE DE FRENTE: \_\_\_\_\_

# CARGA DE ROCA

## CRITERIO DE TERZAGUI

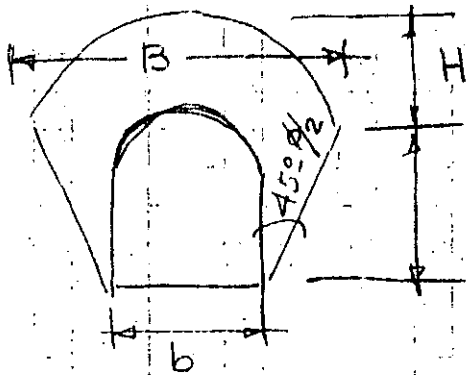


$$H_p = K (H_t + B)$$

Naturaleza de la roca	Carga $H_p$ en m	Observaciones
1.- Dura intacta	0	Ademe ligero si hay caídos.
2.- Estratificada, dura o esquistosa	0 a 0.5B	Ademe ligero con marcos
3.- Maciza con juntas en número moderado	0 a 0.25B	La carga puede variar repentinamente de un punto a otro
4.- Derrumbes moderados	0.25 a 0.35 (B+Ht)	No hay presión lateral
5.- Derrumbes muy frecuentes	0.35 a 1.10 (B+Ht)	Poco o nada de presión lateral.
6.- Totalmente fracturada demolida, pero químicamente sana	1.10 (B+Ht)	Se genera una presión muy importante. Se necesitan zapatas continuas para soportar los pies derechos del marco o cimbras circulares.
7.- Roca compresible a profundidad moderada	1.10 a 2.10 (B+Ht)	Presión lateral importante. necesita retícula para la planilla.
8.- Roca compresible a gran profundidad	2.10 a 4.50 (B+Ht)	Idem.
9.- Roca expansiva	Hasta 7.5m de prof. independiente de (B+Ht)	Cimbras o marcos circulares. En casos extremos usar soporte retráctil (B+Ht)

# CARGA DE ROCA

## CRITERIO DE PROTODIAKONOV



$$H = \frac{B}{2f}$$

f = variable de acuerdo con cada tipo de roca

$$f = 2 \tan \phi$$

TIPO DE ROCA O SUELO	NATURALEZA DEL SUELO O ROCA	f	$\gamma$	$\phi^\circ$	Rc Kg/cm <sup>2</sup>
Muy resis	Más resistentes: cuarcitas, basaltos, otras rocas de resist. excepcional	20	2.8-3.0	87°	2000
	Muy resist.; granitos pizarras silíceas, cuarcita porfídica, areniscas y calizas resistentes	15	2.6 a 2.7	85°	1500
	Areniscas y calizas con conglomerados resistentes	10	2.5 a 2.6	82°	1000
Resistentes	Calizas, granitos alterados areniscos y mármol, dolomitas	8	2.4	80°	800
	Areniscos comunes, mineral de hierro	6	2.4	75°	600
Resistencia media	Pizarra arcillosa, arenisca, caliza más débil, conglomerado poco resist.	4	2.8	70°	400
	Pizarra más débil, margas compactas, lutita	3	2.5	70°	300
	Pizarra blanda, caliza blanda, margas comunes arenisca descompuestas	2	2.4	65°	150-200

$$E_{\text{din campo}} = \frac{v_L^2 \rho (1 + \nu_d)(1 - 2\nu_d)}{1 - \nu_d}$$

donde:

$v_L$  = velocidad longitudinal de onda

$\rho$  = densidad de masa del medio

$\nu_d$  = módulo de poisson dinámico

$v_t$  = velocidad transversal de onda

$$E_{\text{din campo}} = 2v_t^2 \rho (1 + \nu_d)$$

El módulo de poisson puede obtenerse mediante la ecuación:

$$\nu_d = \frac{\frac{1}{2} (v_L/v_t)^2 - 1}{(v_L/v_t)^2 - 1}$$

Estas ecuaciones suponen un medio homogéneo, isótropo y de comportamiento elástico.

## Pruebas Estáticas

### Pruebas de Placa

Existen 2 tipos de placa que pueden utilizarse para determinar la deformabilidad del medio: la placa rígida y la placa flexible. La primera es una placa de acero de aproximadamente 30 cm de diámetro a la cual se aplica carga muerta o con gatos hidráulicos para inducir deformaciones al terreno. Esta placa solo permite medir las deformaciones que se generan en la superficie de apoyo y también en la superficie del terreno lateralmente a la placa. Las figuras 9, 10, 11 y 13 muestran las diferentes formas de ejecutar un ensaye de este tipo. Para una placa infinitamente rígida y considerando al medio rocoso homogéneo, isótropo y elástico, la ecuación siguiente nos permite calcular el Módulo de Deformabilidad estático:

$$E = \frac{Pa}{f\omega a} \left( \frac{1 - \nu^2}{r} \right) \text{sen}^{-1} \left( \frac{a}{r} \right) \text{ para } r > a \quad z = 0$$

$$E = \frac{P}{2\omega_z a} (1 - \nu^2) \text{ para } r > a \quad z = 0$$



donde: P = presión aplicada a la roca

a = radio de la placa

$\omega$  = desplazamiento

$\nu$  = módulo de poisson

r = punto en donde se mide el desplazamiento

z = profundidad del punto de medición de desplazamiento

Lo reducido del área de la placa rígida permite aplicar mayores presiones al terreno, sin embargo, el bulbo de influencia de los esfuerzos en el terreno es muy reducido por lo que se afecta un volumen pequeño.

Por el contrario la placa flexible aunque permite aplicar menores presiones afecta a un mayor volumen de roca y además esta placa es anular y permite medir deformaciones a profundidad en el centro de la placa lo que nos da oportunidad de conocer los desplazamientos máximos generados por la carga aplicada en la zona de influencia de los esfuerzos. Normalmente se colocan deformímetros en el centro de la placa a una profundidad entre 0 y 3 veces el diámetro de la placa. El módulo de deformabilidad se conoce mediante la ecuación siguiente obtenida de la teoría de elasticidad:

$$E = \frac{P}{\pi \omega_z (a_2^2 - a_1^2)} \left\{ [(1 + \nu)z^2] \left[ (a_1^2 + z^2)^{-\frac{1}{2}} - (a_2^2 + z^2)^{-\frac{1}{2}} \right] + [2(1 - \nu^2)] \left[ (a_2^2 + z^2)^{\frac{1}{2}} - (a_1^2 + z^2)^{\frac{1}{2}} \right] \right\}$$

donde:  $a_1$  = radio menor de la placa

$a_2$  = radio mayor de la placa

$\omega_z$  = desplazamiento al centro de la placa

$\nu$  = módulo de poisson

z = profundidad del punto de medición del desplazamiento

Las fig 14, 15 y 16 muestran los equipos utilizados para realizar estos ensayos y la tabla 2 ilustra los datos completos de los ensayos realizados con los equipos correspondientes. Las presiones máximas que se aplican en estas pruebas de placa son hasta de 200 kg/cm<sup>2</sup>.

La selección de uno u otro tipo de placa dependen del espaciamiento entre discontinuidades, del espesor de la capa de alteración de la roca y de la heterogeneidad del medio.

El sitio donde se realizan los ensayos debe estar poco alterado por lo que se recomienda que la medición de desplazamientos superficiales se haga lejos de la placa de carga o a profundidad abajo de la zona de comprimida. Para apegarse a la hipótesis que impone la teoría elástica de semiinfinito es necesario que el diámetro del socavón donde se realice la prueba sea por lo menos cuatro veces el diámetro de la placa de carga.

En la figura 17 se muestra una curva esfuerzo-deformación obtenida de una prueba de placa flexible en roca caliza. Puede observarse que el comportamiento no es elástico y se definen dos módulos y un coeficiente. La relación  $E/\mu$  vale uno en masas rocosas exentas de discontinuidades. El parámetro  $C_p$  crece cuando la plasticidad del relleno de fracturas o fallas o la densidad de fracturamiento aumenta.

### Gato Plano Delgado (LNEC)

Este método consiste en introducir un gato plano en una ranura de aproximadamente 1.2 m de profundidad, 1 m de ancho y 7 mm de espesor. Las paredes del gato quedan en contacto con las de la ranura y el gato posee 4 deformómetros eléctricos en el cuerpo del mismo que permiten medir la deformación de la roca al ocurrir cambios volumétricos en el mismo. La presión se aplica hidráulicamente. Es factible probar áreas mayores si se utilizan más gatos colocados lateralmente. Se han llegado a probar áreas hasta de 4 m<sup>2</sup> y se han aplicado presiones hasta de 100 kg/cm<sup>2</sup>.

La fig 18 muestra la máquina perforadora utilizada para ranurar la roca y los gatos planos. El módulo de deformación se obtiene de la expresión:

$$E = c \frac{P}{\rho}$$

donde:  $p$  = presión aplicada

$\rho$  = desplazamiento de la pared en un punto de medición

$c$  = constante que depende del punto donde se midió  $\rho$ , tamaño del gato y su relación con el tamaño de la ranura y su cercanía a la superficie

Las restricciones a la deformación que imponen los bordes de la ranura y la cercanía a la superficie son limitantes importantes al método ya que los módulos obtenidos son casi siempre bajos. Los módulos obtenidos a partir de los desplazamientos registrados por los deformó-

metros más lejanos a la superficie dan una mayor aproximación al verdadero módulo. Se ha recomendado que la ranura tenga un diámetro de 2 a 3 veces el diámetro del gato para evitar esos problemas de frontera.

Túneles Presurizados

Este método requiere de aislar una cámara en un túnel, colocando tapones en el túnel. Si la roca del túnel en la zona de la cámara es muy permeable requerirá de un aislamiento en las paredes tal como un recubrimiento de concreto o membranas impermeables flexibles. La cámara se instrumenta colocando deformímetros eléctricos (tipo cuerda vibrante) para medir las divergencias o cambios diametrales y también se colocan extensómetros radiales en la roca a diferentes profundidades. La cámara se llena de agua y se aplica presión hidráulica registrando simultáneamente las deformaciones inducidas.

La figura 19 muestra el esquema del equipo utilizado para proporcionar carga y el arreglo de los deformímetros diametrales.

Para obtener el módulo de deformabilidad en un túnel revestido de concreto simple, de diámetro interior, d y espesor de revestimiento, e; se emplea la relación siguiente:

$$E_r = \frac{pd}{\Delta d} - \frac{2e}{d} E_c$$

donde:      p= presión interior  
                  Δd= deformación diametral  
                  E<sub>r</sub> = Módulo de Deformabilidad de la roca  
                  E<sub>c</sub> = Módulo de Elasticidad del concreto  
                  d= diámetro del túnel

Si no hay revestimiento se utiliza la relación:

$$E_r = (1 + \nu) \frac{pd}{\Delta d}$$

donde:      ν= relación de poisson

La longitud de la cámara debe ser mayor a 5d para minimizar los errores provocados por las restricciones que imponen los tapones. Se han ensayado túneles desde 1.5 m de diámetro hasta 4.9 m y la máxima presión aplicada ha sido de 25 kg/cm<sup>2</sup>. En México fue ensayado el túnel de la presa Mazatepec, Pue., de 4 m de diámetro, 500 m de longitud revestido y aplicando 6.8 kg/cm<sup>2</sup>. La figura muestra la gráfica tiempo deformación-presión obtenida en una de las estaciones instrumentadas.

La ventaja de este tipo de ensayos es que pueden medirse deformaciones en varias direcciones poniendo en evidencia la anisotropía del macizo rocoso y el volumen de roca involucrado es muy grande. La desventaja es que el método es muy costoso. En la figura 20 se muestran valores (curva envolvente) de las deformaciones circunferenciales obtenidas con este método.

### Gato radial en túneles

Con este método, al igual que el descrito arriba, es posible aplicar carga en toda la periferia del túnel; solo que en este caso la carga se aplica utilizando varios gatos (almohadillas) metálicos de sección rectangular apoyados en las paredes del túnel y reaccionando contra un marco rígido (de acero o de aluminio) anular como se muestra en la figura 21. Las dimensiones del túnel mostrado en la figura son de 2.7 m de diámetro y la longitud ensayada 2.4 m. La carga máxima aplicada fue de 70 kg/cm equivalente a aproximadamente 1.35 veces la presión que transmitiría el prototipo. La instrumentación se hizo colocando en cada uno de los 8 barrenos radiales de 6 m de profundidad ubicados al centro de la zona de prueba, 7 extensómetros eléctricos LVDT capaces de medir el cierre de grietas cercanas a la excavación y generadas por la apertura de la misma y también el cierre de fracturas preexistentes y las deformaciones elásticas de la roca intacta. Durante la prueba se estudió la deformabilidad de la roca a diferentes niveles de carga y bajo cargas constantes mantenidas durante tiempos hasta de 48 hrs para conocer el comportamiento viscoso de la roca, las deformaciones residuales y las deformaciones a diferentes distancias de las paredes del túnel. La figura 22 muestra las deformaciones obtenidas en diferentes direcciones circunferenciales (nótese la influencia de la anisotropía del medio en la deformabilidad).

Al igual que los ensayos en túneles presurizados estas pruebas involucran un volumen de roca muy grande respecto al involucrado en cualquier otro ensayo de deformabilidad (la influencia de los esfuerzos aplicados en el túnel aquí mencionado llegó hasta una distancia radial de 15 m) sin embargo el ensayo es laborioso y muy costoso y sólo factible de hacer en obras cuyo costo sea considerablemente alto.

### Aparatos en Sondéos

Estos aparatos permiten evaluar la deformabilidad de la masa rocosa a diferentes profundidades sin requerirse la excavación de galerías de prueba. Los aparatos se introducen en un sondeo y pueden ser de dos tipos: los Dilatómetros que se expanden al aplicarles una presión hidrostática interna y presionan a las paredes del barreno deformándolas y los gatos curvos que cargan la pared del barreno con 2 zapatas rígidas curvas diametralmente opuestas. La interpretación de las pruebas efectuadas con dilatómetros es más sencilla y confiable que la correspon-

diente a gatos curvos.

La Tabla 3 presenta un resumen de las características de estos aparatos.

La figura 23 muestra un esquema de un dilatómetro Menard en donde se muestran las 2 partes principales del mismo: la sonda mediante la que se aplica la presión a la pared del barreno (la sonda es presurizada con gas a presión hasta de 60 kg/cm<sup>2</sup>) y el volúmetro mediante el cual se miden los cambios volumétricos que experimenta la sonda. La fig 24 muestra la gráfica presión-deformación volumétrica del terreno mediante la cual es posible calcular el módulo de deformabilidad.

En la fig 25 se muestra un esquema de la sección transversal de un gato goodman (gato curvo) donde se ilustran las zapatas que aplican la presión al barreno en el interior del aparato. Entre las zapatas se encuentra un transductor de desplazamientos LVDT que mide la deformación de las paredes del barreno. La presión sobre las zapatas se aplica hidráulicamente con aceite. El módulo de deformabilidad se determina mediante la expresión:

$$E = \frac{\Delta Q}{\Delta U_d/d} k$$

donde:  $\Delta Q$  = presión aplicada a las paredes de la perforación  
 $\Delta U_d$  = desplazamiento diametral de las paredes  
 $d$  = diámetro de la perforación  
 $k$  = constante función del ángulo  $\beta$  y de la relación de poisson

Con los gatos curvos existe el riesgo de generar fracturas de tensión en las paredes donde las zapatas no están en contacto. Las grietas se desarrollan en sentido perpendicular al de aplicación de la carga con las zapatas y el valor del módulo disminuye.

El uso de aparatos en sondeos tiene la ventaja de ser un método que permite conocer el módulo de deformabilidad de la roca en varios puntos de la masa rocosa y a diferentes profundidades lo que permite, incluso, realizar estudios estadísticos.

La colocación y manejo de los aparatos durante los ensayos es relativamente sencilla y rápida. Sin embargo, su principal desventaja es que afecta a un volumen muy pequeño de roca.

# DETERMINACION DE LA MAGNITUD Y DIRECCION DE LOS ESFUERZOS TECTONICOS RESIDUALES ACTUANTES EN EL MACIZO ROCOSO

## Generalidades

La continua actividad de la tierra hace que las masas continentales se encuentren en movimiento permanente. Como una forma de conservación de energía interna la corteza terrestre se consume en zonas de subducción de placas continentales y se abastece en las zonas o franjas volcánicas también en los límites o contactos de placas continentales. Esta actividad tectónica (tanto la de empuje entre placas como la volcánica) genera fuerzas actuantes en la corteza terrestre que da lugar a cambios estructurales y litológicos (casos de metamorfismo) y provoca la ruptura de las formaciones preexistentes. Los esfuerzos generados durante esta actividad son almacenados por la roca y sólo son liberados en una zona al retirar la roca que confina esta roca lateralmente. La remoción de esta roca confinante puede ser natural (erosión) o artificial (excavaciones superficiales o subterráneas). Al excavar la roca en obras ingenieriles ocurre en el macizo una redistribución de esfuerzos y una tendencia de la roca a desplazarse hacia la zona excavada. Si estas deformaciones son restringidas inmediatamente por algún elemento de contención o soporte, la roca empujará con una fuerza sobre el soporte, equivalente a la magnitud de la fuerza tectónica almacenada en la roca. La determinación de la dirección y magnitud de los esfuerzos tectónicos almacenados por el macizo rocoso nos permite diseñar adecuadamente los elementos de soporte requeridos para la estabilización de excavaciones y además comprender como ocurrió el proceso de fracturamiento local o regional y como estos esfuerzos internos afectan la deformabilidad de la masa rocosa.

Los métodos de liberación de esfuerzos utilizados para conocer la dirección y magnitud de los esfuerzos tectónicos en el macizo rocoso son:

Procedimiento superficial	[	dirección	[ método de la roseta de deformaciones
		magnitud	[ método del gato plano

Procedimiento profundo	[	aparatos en sondeos	dirección	[ método de Merrill
			magnitud	[ método de Hast
		fracturamiento hidráulico		

Los métodos del procedimiento superficial se llevan a cabo en socavones o galerías de prueba. La excavación de esta galería modifica la distribución de esfuerzos en su contorno y por lo tanto los esfuerzos determinados no son los tectónicos sino aquellos modificados por la excavación. El procedimiento profundo también tiene esta limitante, sin embargo, el relajamiento es de menor magnitud.

En algunas regiones donde no ha ocurrido actividad tectónica los esfuerzos en el macizo rocoso únicamente son debidos al peso propio de la roca. En otras (la mayoría) están actuando conjuntamente tanto los esfuerzos tectónicos como los de peso propio. En este último caso, no es válido en estricto rigor, que se calculen esfuerzos verticales por peso propio mediante el peso de la columna de roca actuante en un punto debido a que la presencia de los esfuerzos tectónicos en la masa hace que estos se modifiquen (algunas veces notablemente). En zonas afectadas tectónicamente se han medido magnitudes de esfuerzos horizontales dos veces mayores a las del esfuerzo vertical.

#### Método de la roseta de deformaciones

El procedimiento de ensaye consiste en colocar pijas en la pared o piso de una excavación, diametralmente opuestas y en 3 direcciones radiales a 60° y se mide la distancia inicial entre pijas para cada dirección. Posteriormente se abre una ranura circular (de mayor diámetro que la distancia entre pijas y se registran las deformaciones inducidas al separarse las pijas debido a la relajación de esfuerzos del bloque que contiene las pijas. La figura 26 muestra con detalle como se ejecuta la prueba. La dirección de las deformaciones principales se conoce construyendo un círculo de Mohr de deformaciones como el mostrado en la figura 27. Es necesario hacer por lo menos tres de estas pruebas para conocer espacialmente la dirección de la deformación principal. A partir de las deformaciones principales es posible calcular la magnitud de los esfuerzos principales suponiendo un medio elástico, isótropo, homogéneo y semiinfinito con las siguientes ecuaciones:

$$\sigma_1 = \frac{E}{1 - \nu^2} (\epsilon_1 + \nu\epsilon_2)$$

$$\sigma_2 = \frac{E}{1 - \nu^2} (\epsilon_2 + \nu\epsilon_1)$$

donde: E = módulo de elasticidad

$\nu$  = relación de poisson

$\epsilon_1$  = deformación principal mayor

$\epsilon_2$  = deformación principal menor

$\sigma_1$  = esfuerzo principal mayor

$\sigma_2$  = esfuerzo principal menor

El uso de estas ecuaciones requiere de la determinación de los valores de  $E$  y  $\nu$  por lo que no son utilizadas con frecuencia y en su lugar se prefiere hacer la determinación de la magnitud de los esfuerzos principales mediante el método que se describe a continuación.

### Método del gato plano

El procedimiento de prueba consiste en colocar pijas en la pared o piso de la excavación a ambos lados de una ranura en la cual posteriormente se insertará un gato plano (figura 28). Se mide la distancia entre las pijas antes de perforar la ranura y una vez perforada la ranura y relajados los esfuerzos se miden las deformaciones ocurridas por la diferencia de distancia entre las pijas de referencia. Posteriormente se introduce el gato en la ranura y se aplica presión al gato hasta que todas las pijas vuelvan a su posición original y en ese momento se mide la presión (presión de cancelación) que será equivalente a la magnitud del esfuerzo actuante en esa dirección. Para conocer la magnitud del esfuerzo principal mayor actuante deberán hacerse por lo menos tres ensayos a diferentes direcciones ya que este método solo proporciona el valor del esfuerzo normal actuante en el plano de la ranura.

La figura 29 muestra los resultados de una prueba en el proyecto hidroeléctrico La Angostura, Chis.

### Aparatos en Sondeos

#### Método de relajación de esfuerzos en el contorno de un sondeo mediante el registro de deformaciones (Método de Merrill).

Este método permite efectuar mediciones hasta a 6 m de profundidad y consiste en ejecutar una perforación de  $\varnothing 1\ 1/2"$  (fig 30a) en la cual se introduce un aparato que permite medir deformaciones en tres direcciones ubicadas en una misma sección transversal (fig 30b). Una vez introducido el aparato en la perforación de  $\varnothing 1\ 1/2"$  se perfora con broca anular un barreno de  $\varnothing 6"$  hasta una profundidad mayor a la que se encuentra el fondo del aparato, de esta forma queda aliviado de esfuerzos un cilindro de roca hueco y se miden las deformaciones en los tres sentidos. Suponiendo que el eje del sondeo coincide con la dirección del esfuerzo principal menor  $\sigma_3$ , pueden determinarse las magnitudes y direcciones de los esfuerzos principales  $\sigma_1$  y  $\sigma_2$  que actúan en un plano normal al eje del sondeo, mediante las ecuaciones:



## Método de Merrill

$$e_a = \frac{1}{E} \{(\sigma_1 + \sigma_2) + [2(\sigma_1 - \sigma_2) (1 - \nu^2) \cos 2\phi] - \nu\sigma_3\}$$

$$e_b = \frac{1}{E} \{(\sigma_1 + \sigma_2) + [2(\sigma_1 - \sigma_2) (1 - \nu^2) \cos (\phi + \alpha)] - \nu\sigma_3\}$$

$$e_c = \frac{1}{E} \{(\sigma_1 + \sigma_2) + [2(\sigma_1 - \sigma_2) (1 - \nu^2) \cos^2 (\phi + 2\alpha)] - \nu\sigma_3\}$$

donde  $E$  = módulo de deformabilidad de la roca

$\nu$  = relación de poisson

$\phi$  = ángulo que forma el eje de medición  $a - a'$  con la dirección del esfuerzo principal mayor

$\alpha$  = ángulo formado por la dirección  $b - b'$  con la dirección  $a - a'$

Los valores de  $\sigma_1$ ,  $\sigma_2$  y  $\phi$  determinados, se expresan en función de  $\sigma_3$ . Al efectuar tres mediciones semejantes a lo largo de tres sondeos inclinados entre sí, es posible determinar la magnitud y dirección de los tres esfuerzos principales. Nuevamente la necesidad de determinar  $E$  y  $\nu$  limita el alcance de este método.

Método de relajación de esfuerzos en el contorno de un sondeo en el cual se ha instalado un medidor de esfuerzos (Método de Hast).

En este método se sigue el mismo procedimiento que el utilizado en el método anterior sólo que el medidor de esfuerzos introducido en este caso es de gran rigidez en lugar del aparato medidor de desplazamientos que es de muy baja rigidez. En un caso general en que la rigidez del medidor no se considera infinita los esfuerzos principales actuantes en la roca y en un plano normal al eje del sondeo pueden calcularse con la ecuación:

$$\sigma_1 = \frac{k(x+2) + x_0}{2k(x+1)} S_1 + \frac{x_0 - 2 - k(x-2)}{2k(x+1)} S_2$$

$$\sigma_2 = \frac{x_0 - 2 - k(x-2)}{2k(x+1)} S_1 + \frac{k(x+2) + x_0}{2k(x+1)} S_2$$

donde:

$$S_1 = \frac{1}{2} \{ \sigma' + \sigma'' + \sigma''' + \sqrt{\frac{1}{2} [ (\sigma' - \sigma'')^2 + (\sigma'' - \sigma''')^2 + (\sigma''' - \sigma')^2 ]} \}$$

$$S_2 = \frac{1}{2} \{ \sigma' + \sigma'' + \sigma''' - \sqrt{\frac{1}{2} [ (\sigma' - \sigma'')^2 + (\sigma'' - \sigma''')^2 + (\sigma''' - \sigma')^2 ]} \}$$

$$k = \frac{G_0}{G}$$

$$x = 3 - 4\nu$$

$$x_0 = 3 - 4\nu_0$$

siendo:  $G_0$  módulo de rigidez del dispositivo de medición  
 $\nu_0$  relación de poisson del dispositivo de medición  
 $\sigma'$ ,  $\sigma''$  y  $\sigma'''$  esfuerzos normales medidos según tres direcciones diametrales que forman ángulos de  $63^\circ$  entre sí  
 $G$  módulo de rigidez de la roca  
 $\nu$  relación de poisson de la roca

En el caso en que  $\nu_0 = \nu = 0.25$  las expresiones anteriores se simplifican a:

$$\sigma_1 = \frac{2k + 1}{3k} S_1 \quad \sigma_2 = \frac{2k + 1}{3k} S_2$$

El factor correctivo  $\frac{2k + 1}{3k}$  es poco sensible a las variaciones de la relación de rigideces  $k$ . Si  $k > 5$  el factor correctivo tiende a 0.66 y por lo tanto los esfuerzos registrados con un medidor muy rígido se relacionan directamente con los esfuerzos internos de la roca, casi independientemente del módulo de deformabilidad de la misma. Esta es la gran ventaja de estos medidores que pueden estar constituidos por celdas metálicas con propiedades magnetostrictivas (Hast) o por inclusiones de vidrio con propiedades fotoelásticas (Roberts). Este método parece ser el que más ventajas ofrece sobre los mencionados anteriormente.

### Fracturamiento Hidráulico

Esta técnica originalmente utilizada por los petroleros para estimular la producción de pozos, consiste en inyectar una suspensión de arena,

aditivos y agua en un tramo previamente sellado del pozo e incrementar la presión hasta producir la apertura de las fracturas de la masa rocosa en el contorno del pozo. La fractura creada es normal a la dirección del esfuerzo principal menor actuante y la presión necesaria para lograr la propagación de esta fractura es igual al esfuerzo principal actuante.

Este burdo método ha permitido determinar a gran escala la dirección y magnitud del esfuerzo principal menor actuante en algunos campos petrolíferos. Del mismo modo, es posible inducir fracturamiento hidráulico mediante ensayos de permeabilidad tipo Lugeon en rocas.

## DETERMINACION DE LA PERMEABILIDAD DEL MACIZO ROCOSO

La permeabilidad de un macizo rocoso está fundamentalmente regida por sus discontinuidades debido a que la permeabilidad intrínseca de la roca intacta es muy reducida en la mayoría de los casos. En rocas no fisuradas la permeabilidad está en función de su porosidad absoluta y dependiendo de su grado de alteración o alterabilidad la permeabilidad podrá ir creciendo con el tiempo conforme el fluido intemperiza y erosiona a la roca. En rocas fisuradas está en función del número de familias de fracturas y del espaciamiento y dirección de las fracturas respecto al flujo, así como de la abertura, rugosidad y tipo de material que rellena a las fisuras. En rocas cársticas es función del número de conductos, de su diámetro, rugosidad y trayectoria. En todos los casos la permeabilidad también dependerá de las características del fluido (tipo, viscosidad, temperatura, etc.) que circula a través del macizo rocoso y de la presión o carga hidráulica actuando en el fluido.

La estimación de la permeabilidad en masas rocosas se hace aún considerando a la masa homogénea y flujo laminar a través de la misma, lo que en la mayoría de los casos está alejado de la realidad; sin embargo, esta idealización obedece a la dificultad de expresar matemáticamente el complejo mecanismo de flujo en un medio discontinuo.

El conocimiento de la permeabilidad del medio nos permite estimar los volúmenes de filtraciones esperados - hacia excavaciones tanto superficiales como subterráneas, las posibles fugas de agua a través de la cimentación de una presa, volúmenes de extracción de petróleo, posibilidad de uso de cavidades para almacenamiento de fluidos o desechos, captaciones de agua para diversos usos, niveles de abatimiento de aguas freáticas, etc.

Las pruebas más comunmente usadas para conocer la permeabilidad en roca son:

Arriba del Nivel Freático	[ Pruebas en zanjas
	[ Ensaye Lugeon
	[ Ensaye Lefranc
Abajo del Nivel Freático	[ Pruebas de Bombeo
	[ Trazadores radioactivos
	[ Micromolinetete

En este tema sólo se verán con mayor detalle los ensayos Lugeon y Lefranc que son los de mayor uso.

### Ensaye Lugeon

Este ensaye normalmente se realiza en medios saturados (abajo del nivel de aguas freáticas) pero es factible ejecutarlo en medios no saturados o parcialmente saturados con la condición de que se sature localmente el medio y se pueda establecer el flujo. El ensaye se realiza haciendo primero una perforación en roca (de preferencia en diámetro NX) e introduciendo tubería en la perforación con un empaque al fondo que puede ser de copas de cuero (rocas sanas), mecánico de hule (rocas poco a medianamente fisuradas) o neumático (rocas muy fracturadas y/o blandas) el cual permitirá aislar el tramo de prueba. Los empaques pueden ser dobles si el ensaye se hace del fondo de la perforación hacia la superficie o sencillo si se procede de superficie al fondo, la longitud del tramo de prueba es variable dependiendo de las características del terreno, sin embargo, longitudes de 3 a 5 m son usuales. Una vez fijo el obturador en el tramo de prueba, se inyecta agua al terreno y se mide el gasto de agua en litros por minuto y por metro lineal de perforación hasta una presión máxima aplicada de  $10 \text{ kg/cm}^2$ . La unidad de medición de la permeabilidad se denomina unidad Lugeon y cada unidad Lugeon representa un consumo de un litro por minuto y por metro bajo  $10 \text{ kg/cm}^2$  de presión efectiva. La figura 31 muestra un diagrama donde se observa el equipo utilizado y la forma de calcular la presión efectiva. En términos del coeficiente de permeabilidad,  $k$  utilizado para suelos homogéneos, isotrópicos y para flujo en régimen laminar, una unidad Lugeon equivale a  $k = 10^{-7} \text{ m/seg}$ . Un mismo valor de unidades Lugeon puede obtenerse debido a una fisura grande o a un número grande de fisuras finas y las características de estas fisuras sólo pueden conocerse si se varía la longitud del tramo de prueba.

Para conocer el comportamiento de las fracturas y sus características es necesario variar las presiones de prueba. La secuencia que se sigue es la de incrementos de presión 1, 2, 4, 6, 8 y  $10 \text{ kg/cm}^2$  y luego decrementos a 8, 6, 4, 2,  $1 \text{ kg/cm}^2$  en cada incremento o decremento se inyecta agua durante 10 min al terreno y se miden gastos y presiones efectivas que se grafican obteniendo curvas como las mostradas en la figura 32. La forma de las curvas es muy variable y rara vez es lineal. Estas curvas no permiten detectar si un aumento súbito del gasto a una determinada presión se debe a un destaponamiento y arrastre de material de relleno de una fisura o bien a ruptura de la roca al rebasar las presiones el límite elástico (fracturamiento hidráulico), por lo que es necesario dibujar una gráfica doblemente logarítmica introduciendo valores del gasto y de la presión elevada a la cuarta potencia (fig 33). Un quiebre en la línea recta dibujada indica la ruptura de la roca.

### Ensaye Lefranc

Este ensaye se realiza en rocas ubicadas abajo del nivel freático muy fracturadas o rocas cuyas partículas están débilmente cementadas y se utiliza frecuentemente para medir la permeabilidad de depósitos aluviales. Las presiones que se aplican con este método son bajas y normalmente no mayores de  $0.5 \text{ kg/cm}^2$ . La prueba consiste en inyectar agua en el terreno saturado convirtiendo al pozo en un permeámetro de carga constante (si el terreno es permeable  $k > 10^{-4} \text{ cm/seg}$ ) o bien en inyectar o extraer agua con carga variable si el terreno es poco permeable. En la fig 34 se muestra el dispositivo de ensaye de la prueba Lefranc de carga constante.

Manteniendo la carga constante y conocido el gasto  $Q$  y la sobrecarga  $\Delta H$ , puede calcularse la permeabilidad  $k$  del medio mediante la expresión:

$$Q = c k(\Delta H)$$

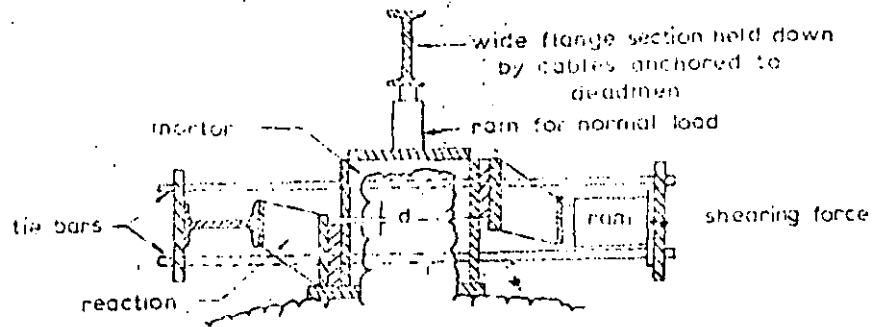
siendo  $k = \frac{Q}{c(\Delta H)}$

$c$  es un coeficiente que depende de la geometría del área de infiltración. Si ésta es cilíndrica de longitud  $L$  y radio  $r$ , entonces:

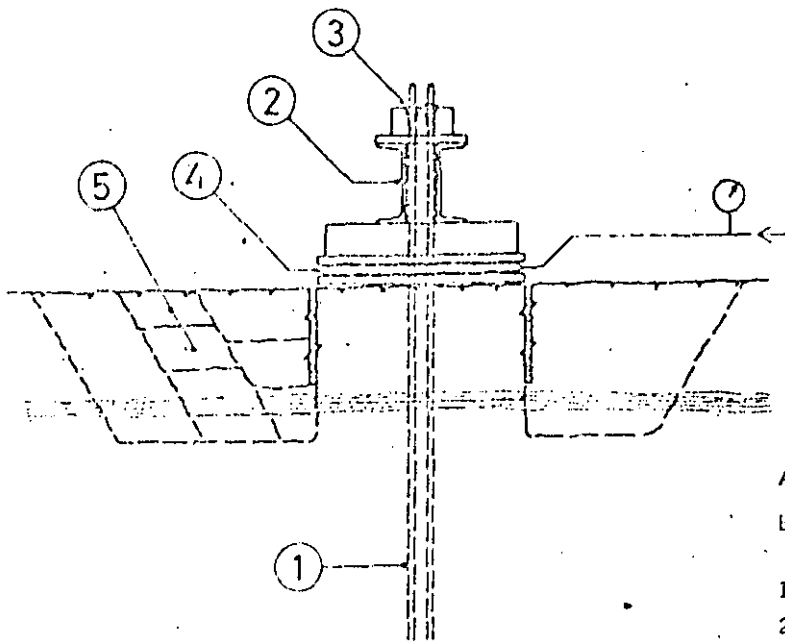
$$c = \frac{4\pi}{\frac{1}{2L} \log \frac{L}{r}}$$

## CLASIFICACION INGENIERIL DEL MACIZO ROCOSO

Dado que estos métodos están orientados a establecer el tipo de soporte requerido en excavaciones subterráneas se considera más adecuado que este aspecto se trate en el tema V del curso, Subtema V.2.4.



(A)



A. - Cutting the block with normal preloading

B. - General arrangement

- 1) Tendons for normal load
- 2) Reaction beam
- 3) Anchor grips
- 4) Flat jack
- 5) Cutting around the block with disc saw
- 6) Base frame
- 7) Jacks for shearing load
- 8) Shear box
- 9) Dial gauges

(B)

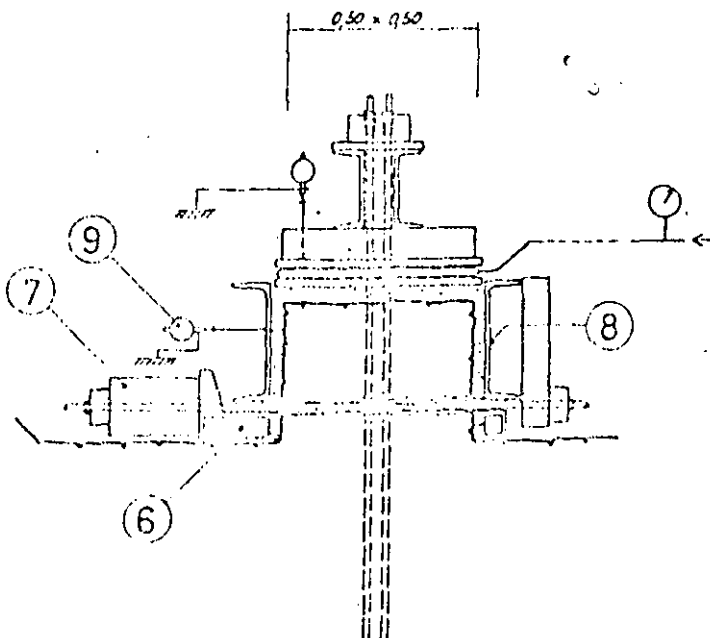
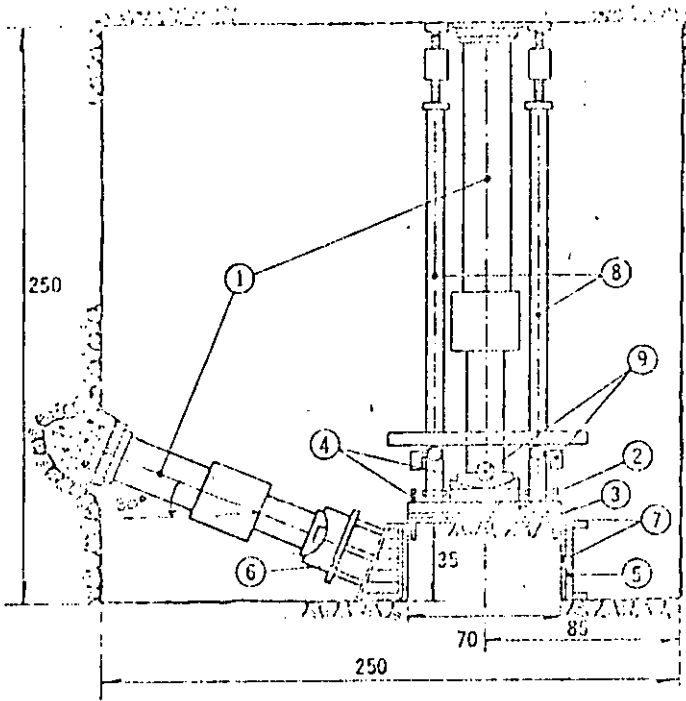


FIG 1

Dos ensayos de corte directo efectuados en superficie y aplicando carga tangencial al plano de falla





- 1 gatos de 100 ton
- 2 placas de asiento
- 3 colchón metálico
- 4 puntos de medición
- 5 marco de cortante
- 6 viga de apoyo
- 7 asiento de mortero
- 8 templete para colocación de medidores.
- 9 deformómetros de carátula

FIG 2

Ensayo de corte directo aplicando carga lateral inclinada

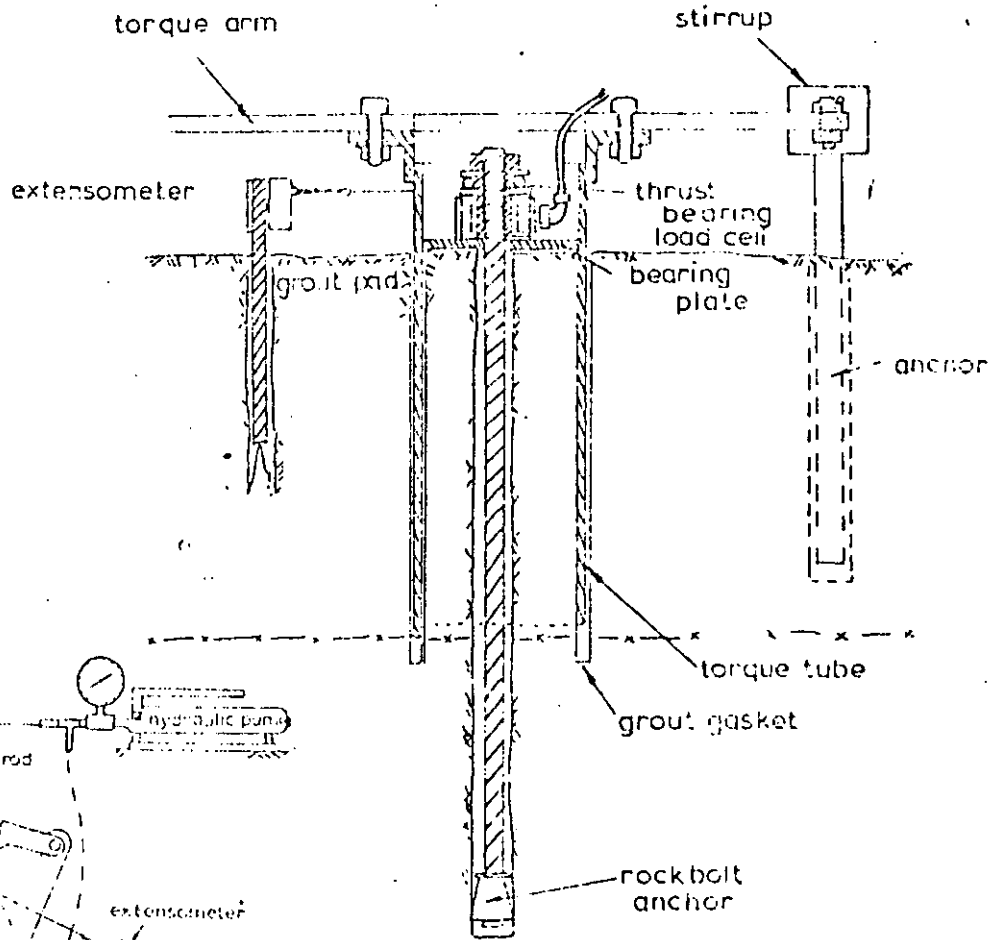


FIG 3

Ensayo de corte directo aplicando torsión a la roca

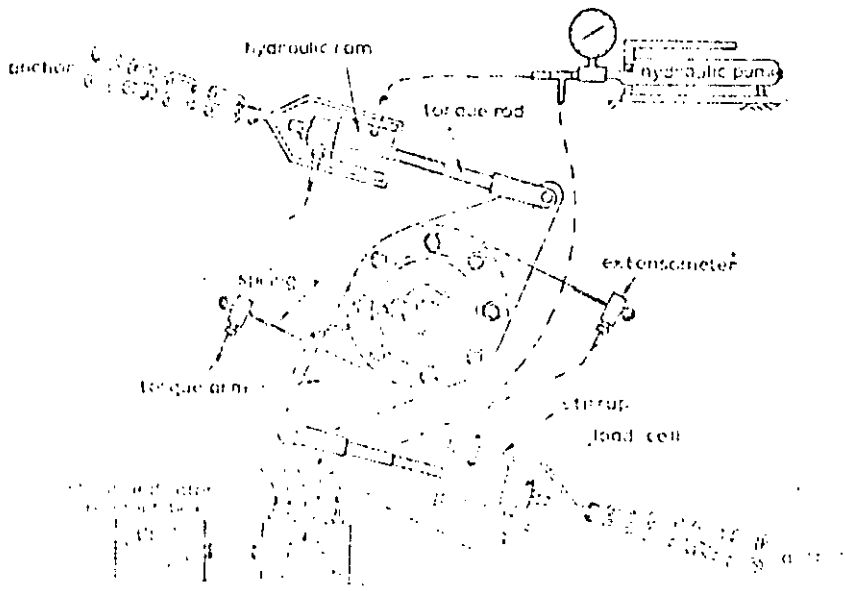
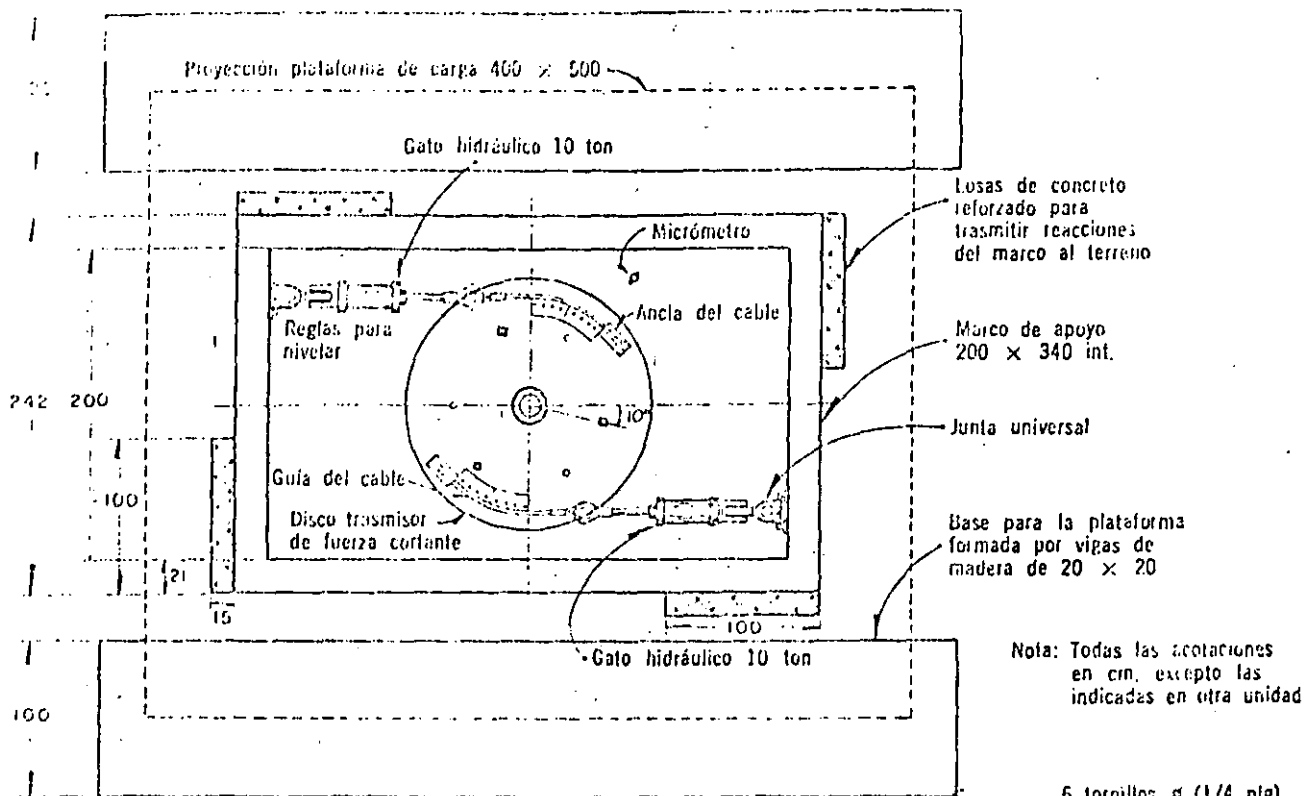
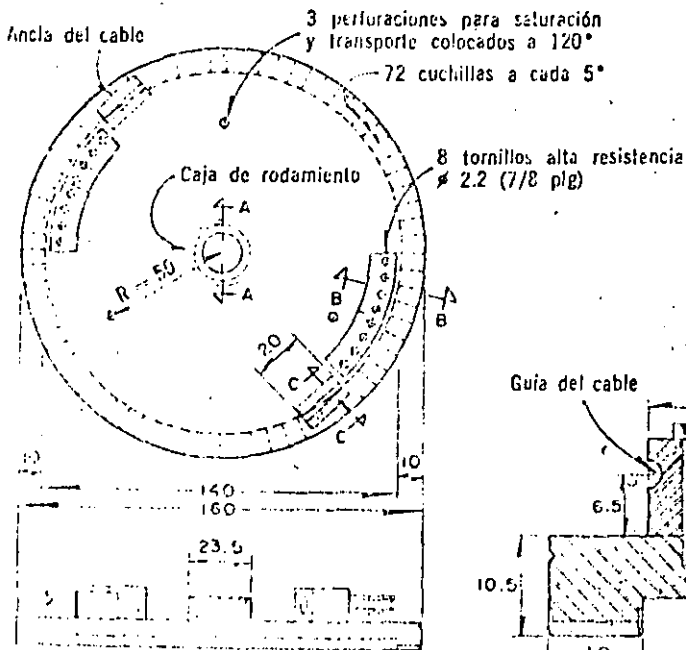


FIG 4

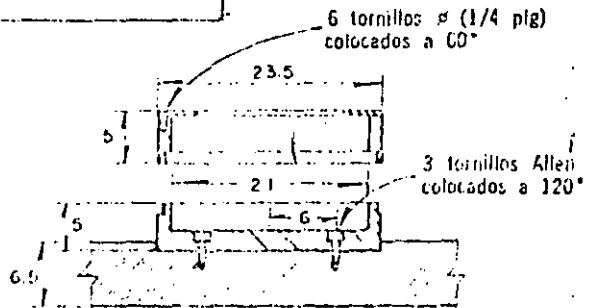
Ensayo de torsión aplicando carga lateral



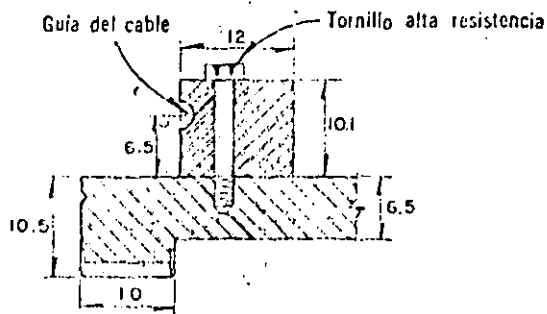
PLANTA GENERAL



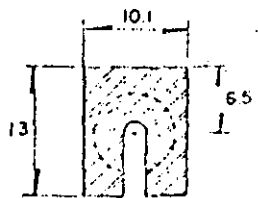
DISCO — PLANTA Y VISTA



CAJA DE RODAMIENTO SKF No 29420  
CORTE A — A



CORTE B — B



CORTE C — C

FIG 4. Ensayo de corte directo aplicando carga radialmente

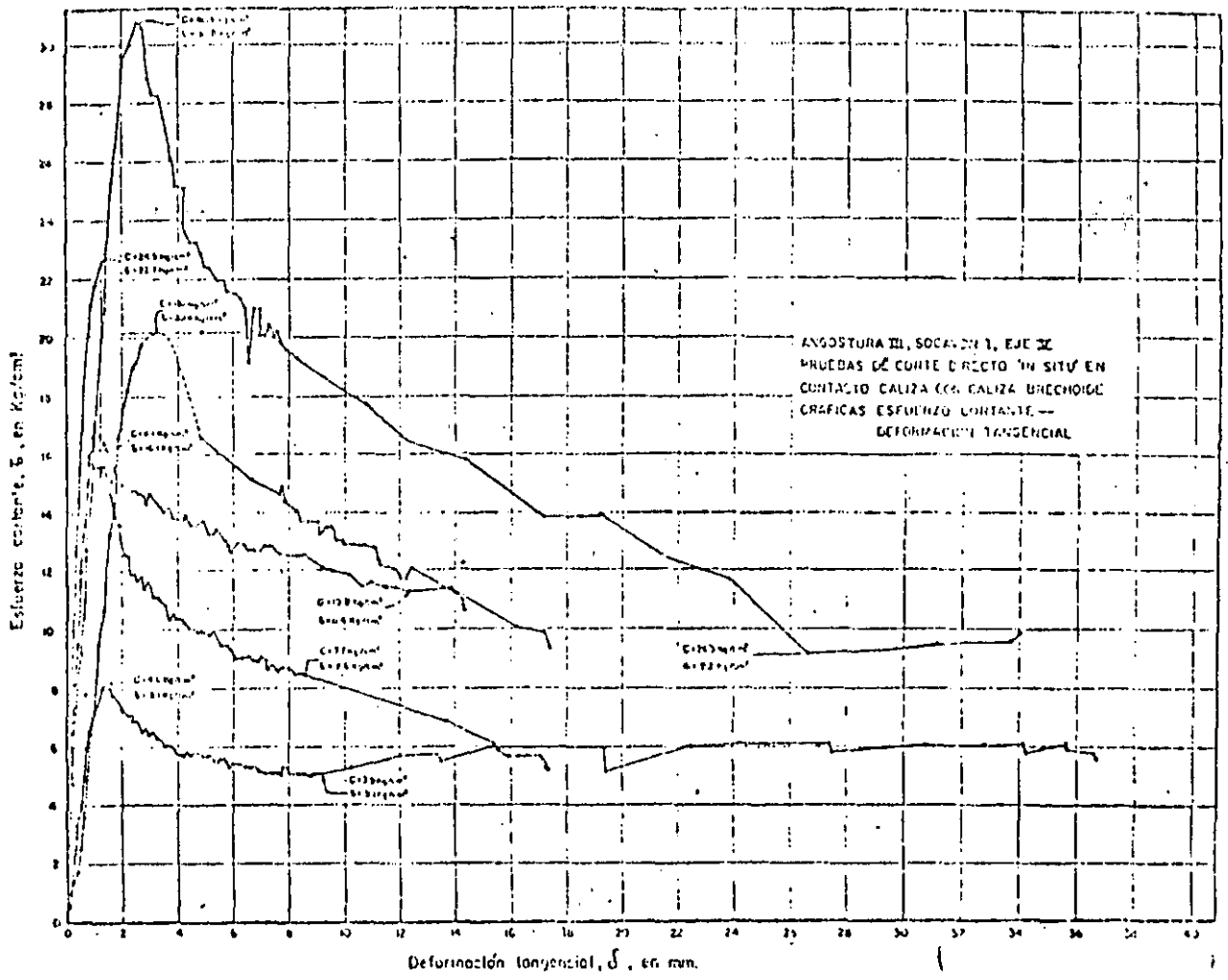


FIG 5. Gráfica Esfuerzo Cortante ( $\tau$ ) - Deformación Tangencial ( $\delta$ )

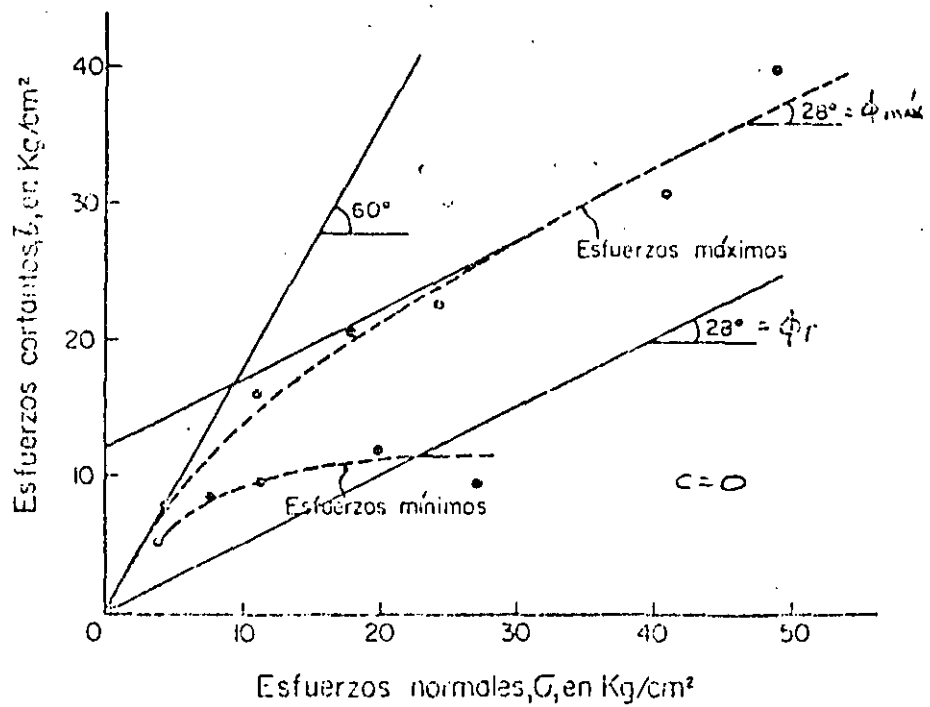


FIG 6. Gráfica Esfuerzo Cortante ( $\tau$ ) - Esfuerzo Normal ( $\sigma$ )

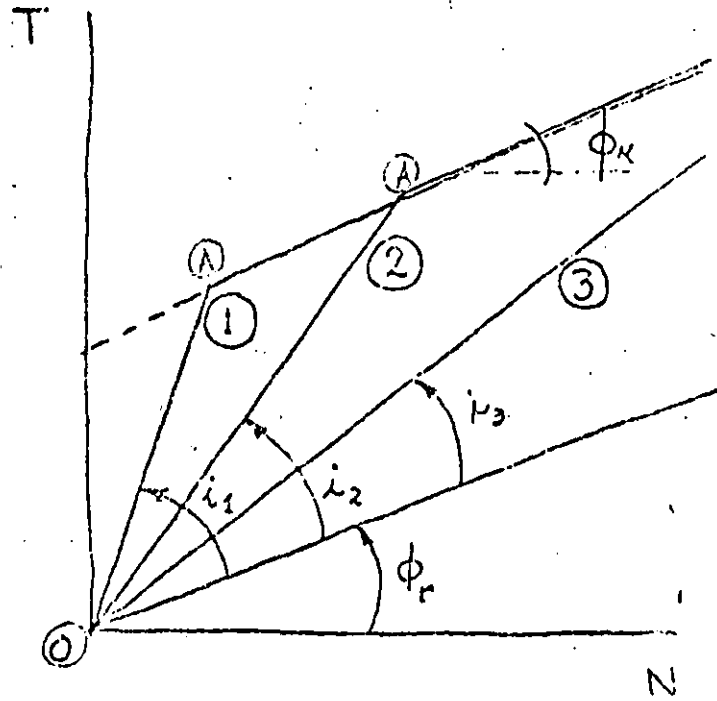
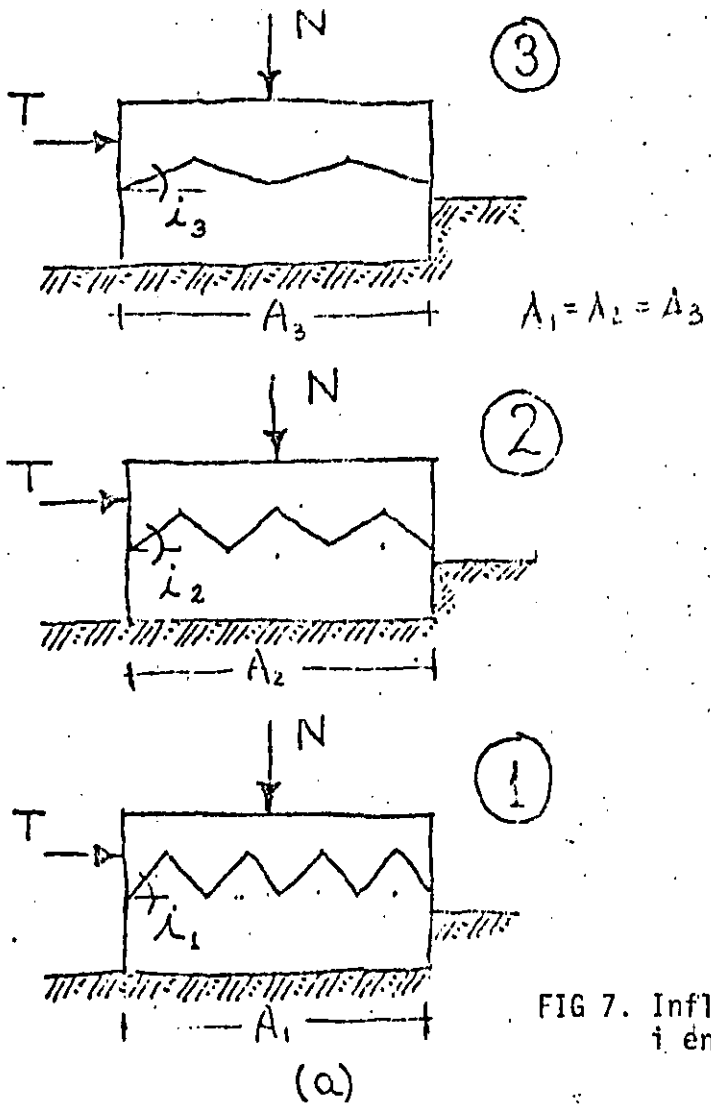


FIG 7. Influencia del ángulo  $i$  en la resistencia al corte (b)

TABLA 1. ESFUERZO CORTANTE DE ROCAS PROBADAS "IN-SITU"

Roca cortada	Tipo de prueba	Índice de calidad de la roca %	Número de pruebas	Cohesión $c$ kg/cm <sup>2</sup>	Ángulo de fricción $\phi$ °	Coefficiente de fricción $\tan \phi$
GRANITOS ALTO RABAGAO (en construcción)	Roca	3	44	13	62	1.9
		5		5	57	1.5
		7		3	52	1.3
		10		2	46	1.0
		15		1	41	0.8
	Concreto-Roca	6.2 a 7.3	8	2	56	1.5
PIZARRAS	Roca normal a la esquistocidad	0.8 a 1.7	9	2	69	2.6
BEAPOSTA (terminada)	Concreto-roca paralelo a la esquistocidad	1.0 a 1.4	5	2	60	1.7
	Concreto-roca paralelo a las juntas	1.3	3	2	63	1.9
PIZARRAS VALDECAÑAS (terminada)	Roca normal a la esquistocidad	0.9 a 1.0	4	29	55	1.3
		1.3 a 2.0	3	7	64	2.0
	Concreto-roca paralelo a la esquistocidad	1.0	3	4	62	1.9
PIZARRAS	Roca paralelo a la esquistocidad	Poco alterada	4	4	59	1.7
	Roca normal a la esquistocidad	Poco alterada	10	6	64	2.0
MIRANDA (terminada)	Concreto-roca paralelo a la esquistocidad	Poco alterada	8	4	62	1.9
	Concreto-roca normal a la esquistocidad	Poco alterada	8	7	60	1.7
PIZARRAS MIRANDA	Roca normal a la esquistocidad	Variable	16	1	70	2.7

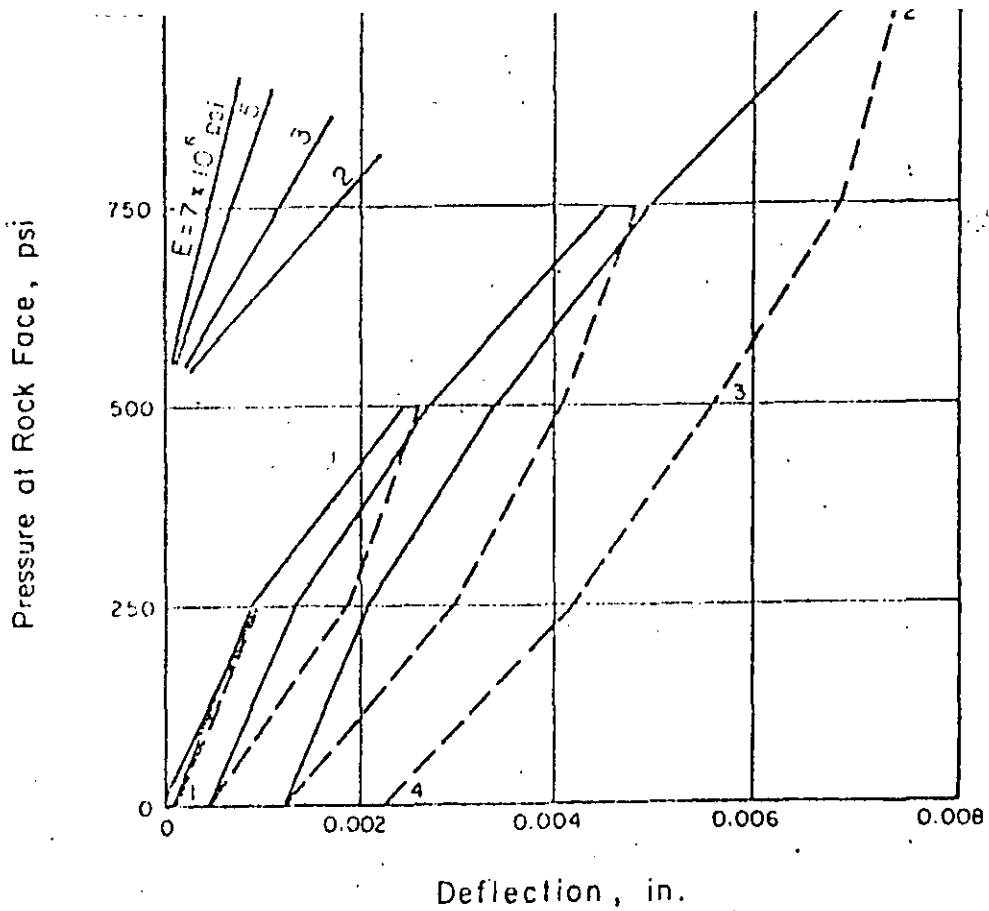


FIG 8. Curva Esfuerzo-Deformación para prueba de placa

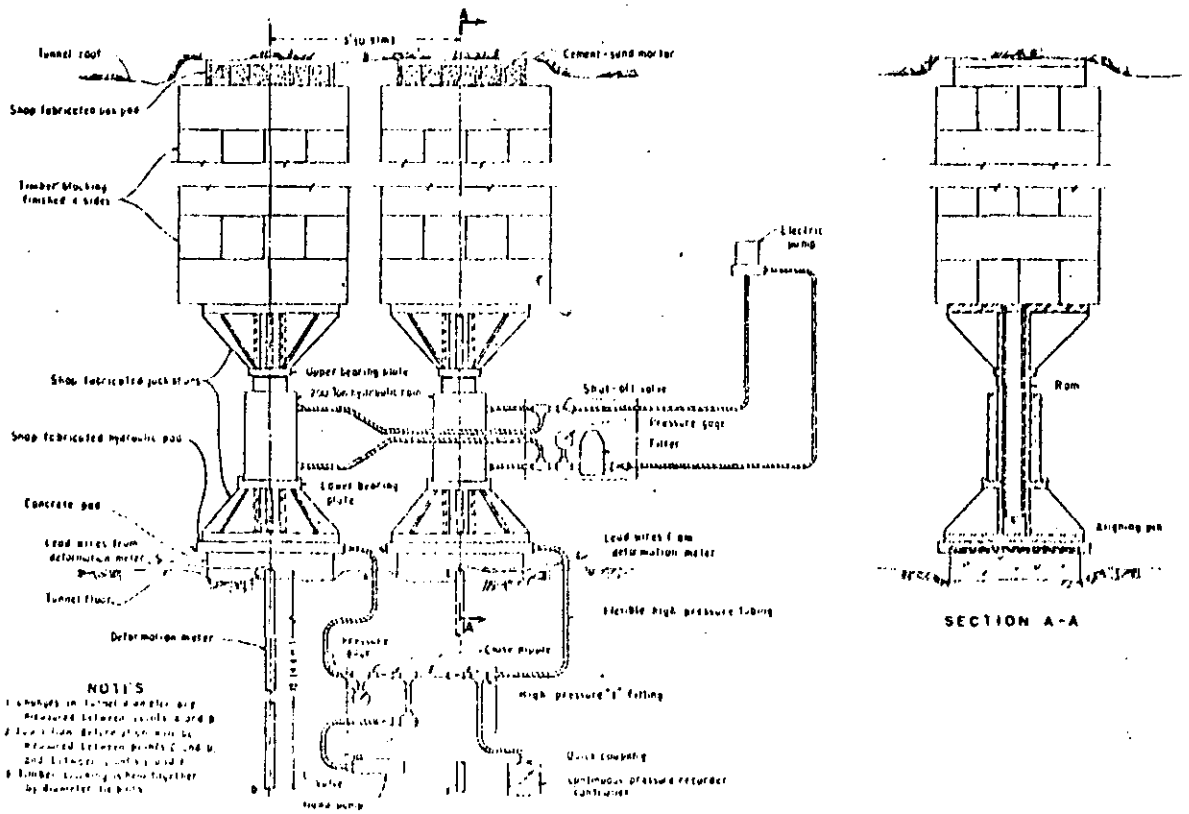
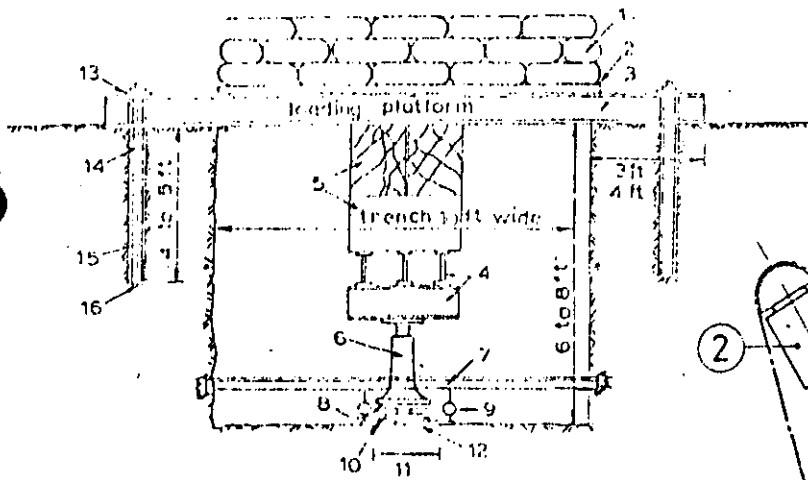


FIG 9. Prueba de placa utilizando 2 placas realizado en socavón



- 1 sand bags
- 2 wooden planks 3ft-8in x 10ft-0in
- 3 R.S.J. 225 mm x 110 mm @ 3.12 kgs/m
- 4 R.S.J. 225 mm x 110 mm @ 3.12 kgs/m
- 5 timber packing
- 6 hydraulic jack 200 tons capacity
- 7 pressure gauge separate pump arrangement
- 8 datum bar suitably anchored
- 9 roller assembly
- 10 dial gauges
- 11 1 1/2 inch thick steel plate 12 in dia.
- 12 surface ground level
- 13 3/4 in thick cement plaster to make the surface even
- 14 3/4 in steel plate 3ft 8in wide 5ft long
- 15 drill hole cement grouted
- 16 pinning rod 1 in dia
- 17 split end and wedge arrangement for anchoring

FIG 10. Prueba de Placa rígida en trinchera

Down-the-hole loading test with extensometric measurement of deformations:

- 1) Tendons
- 2) Hydraulic jack
- 3) Loading column
- 4) Extensometric rod
- 5) Loading plate
- 6) Dial gange

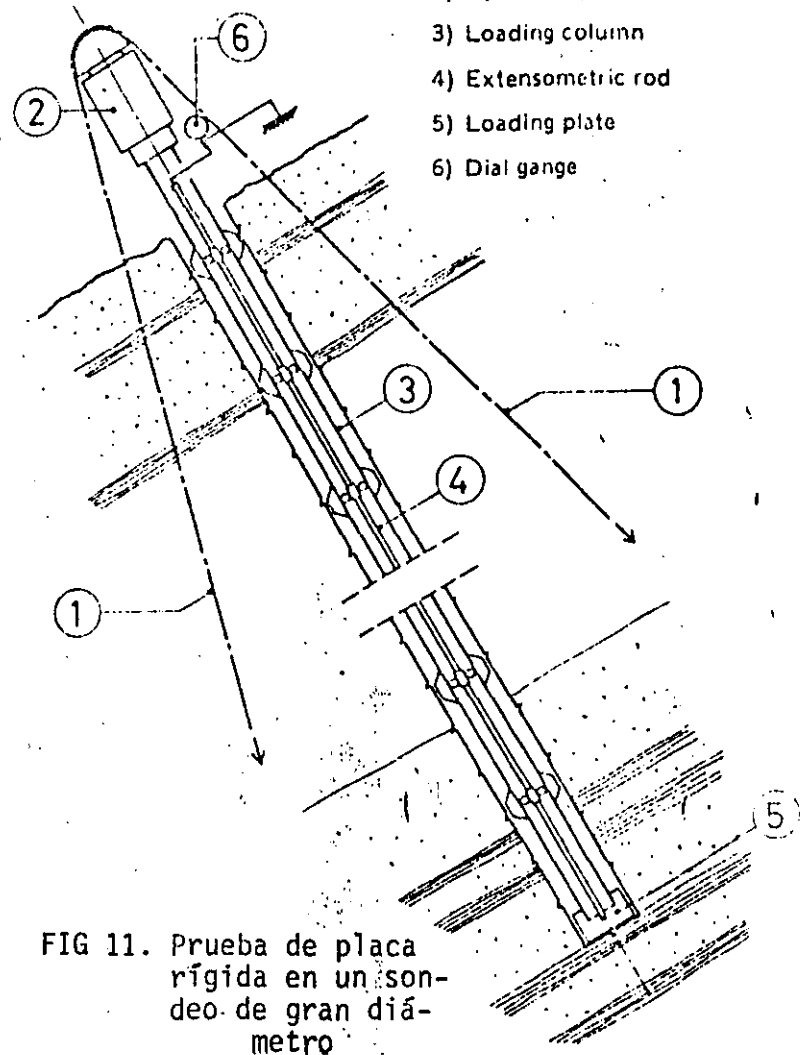


FIG 11. Prueba de placa rígida en un sondeo de gran diámetro

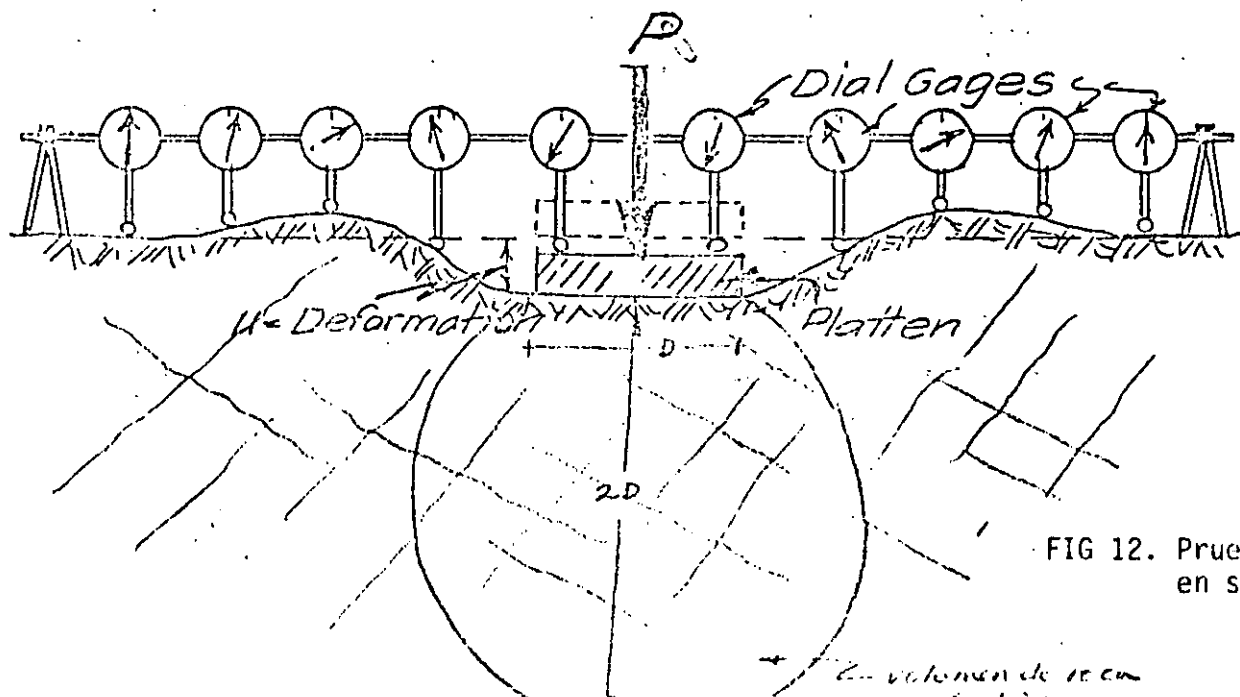
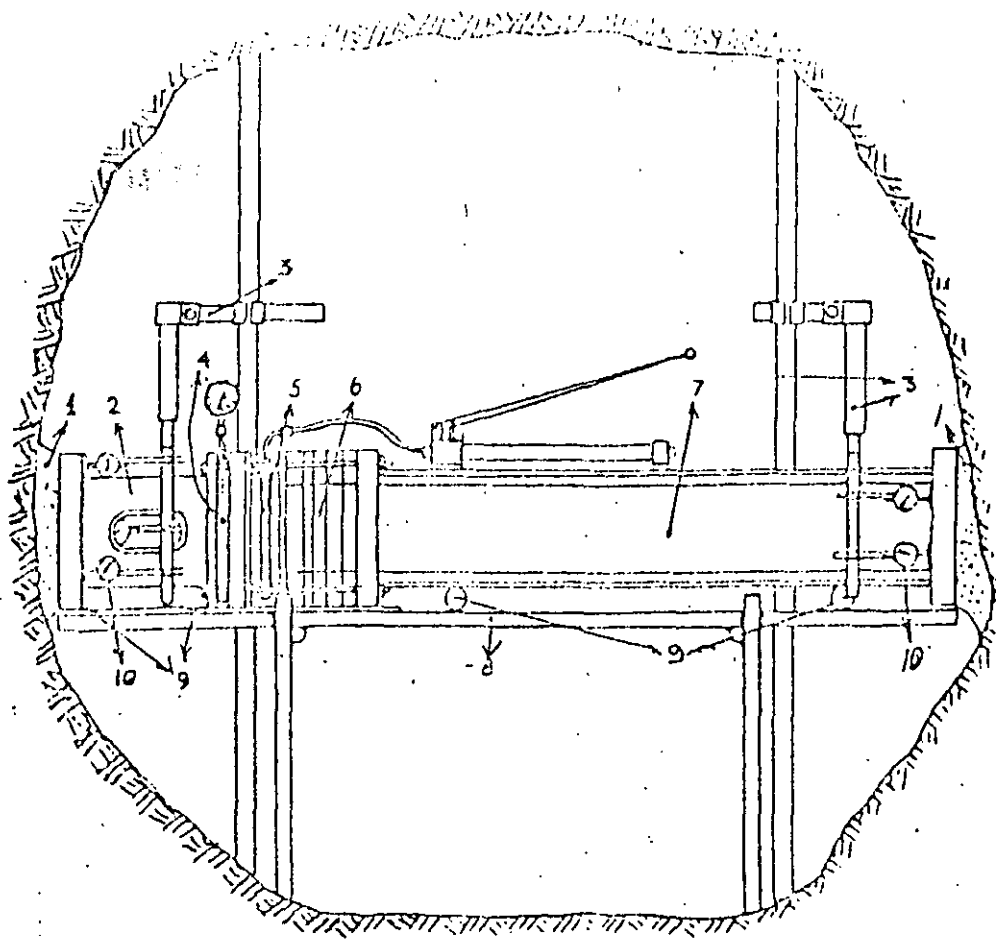


FIG 12. Prueba de placa en superficie



Typical Assembly For Horizontal Test

1. Mortar Pad.
2. Bearing barrel, steel face, circular, 12" diameter.
3. Frame and attachments for dial gauges. 4 dial gauges used per measuring face.
4. Pressure measuring assembly, consisting of flat jack and pressure gauge, sandwiched between two square steel plates.
5. Loading assembly, comprising flat jack, between two circular steel plates + pump.
6. Packing plates octagonal, for adjustment of length of assembly to width of tunnel, thickness ranging from 1/2" to 2".
7. Thrust beam, 10" x 8" x 1/2" I beam, sections of 1, 1-1/2, 2-1/2 and 4 ft. length.
8. Scaffolding frame assembled from 1-3/4" water pipe + scaffolding clamps. It carries the whole assembly, except the reference frames for dial gauges.
9. Rollers, pipe or round rod.
10. Dial gauges, divisions 0.0001".
11. All faces of beams, barrel and packing plates are machined.

FIG 13. Prueba de Placa rígida en paredes de un socavón

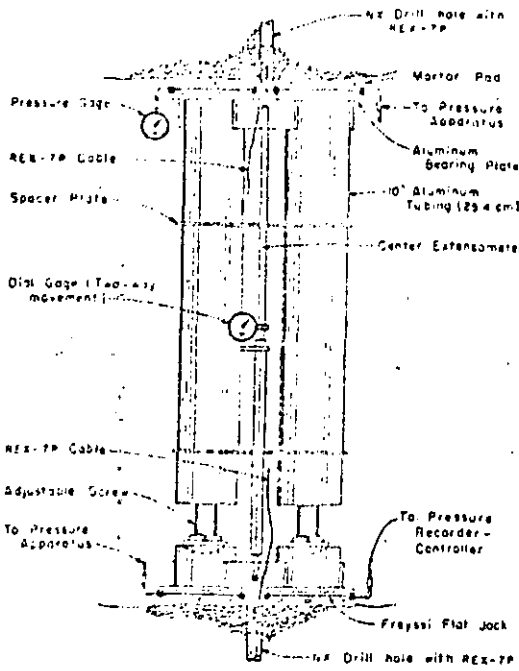


FIG 14. Prueba de Placa Flexible en clave y piso socavón

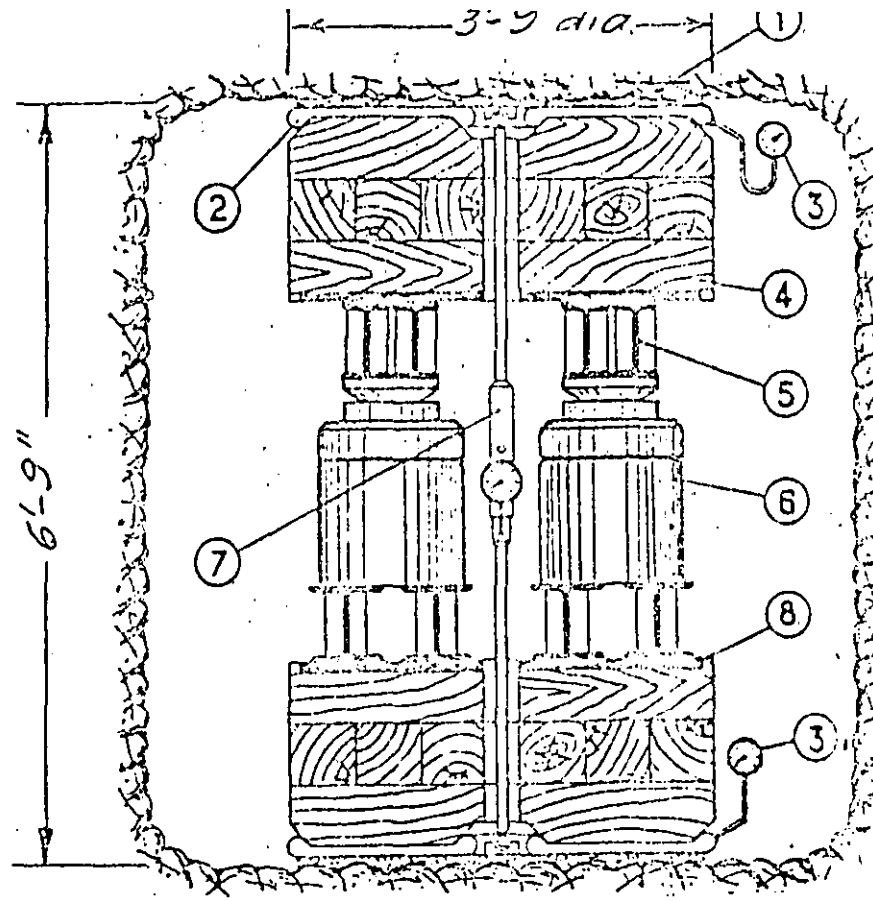
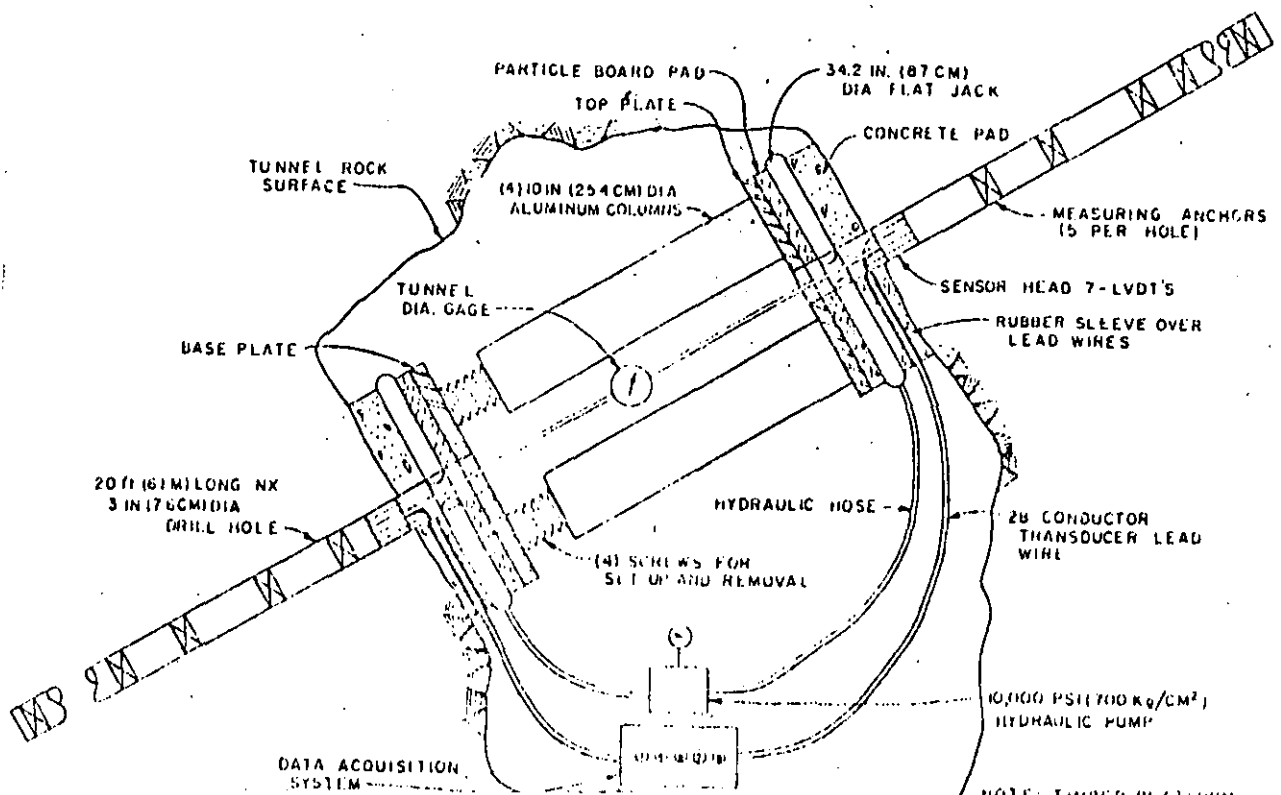


FIG 15. Prueba de Placa Flexible en clave y piso socavón

FIG 16. Prueba de Placa Flexible diagonal en paredes socavón

- (1) Mortar.
- (2) Oil filled metallic cushions..
- (3) Pressure gauges.
- (4) Timber packing.
- (5) H-section irons.
- (6) Hydraulic jack. Total load 300 tons.
- (7) Extensometer for measuring central deformations.
- (8) Iron bearing plate.





FEATURES	DUAL-AXIAL JACKING TEST (Heavyweight Rams, Jointmeters, and Tunnel Diameter Gage)	UNIAXIAL JACKING TEST (A) (Aluminum Columns, Circular Flat Jacks, Jointmeters, and Tunnel Diameter Gage)	UNIAXIAL JACKING TEST (B) (Aluminum Columns, Circular Flat Jacks, REX-7P, and Tunnel Diameter Gage)	RADIAL JACKING TEST (Ring Sets, Rectangular Flat Jacks, REX-7P, Jointmeters, and Tunnel Diameter Gage)
Configuration of loaded rock area	2 - 24 in. (0.61 m) diameter shoes adjacent to each other on 3 ft (0.91 m) centers.	2 - 34.2 in. (0.87 m) diameter flat jacks, diametrically opposite each other.	Same as Uniaxial (A)	Cylinder 8 ft (2.4 m) long and 8 to 8.5 ft (2.4 to 2.6 m) in diameter. 16 each 96 x 16 in. (2.4 x 0.41 m) flat jacks, arranged around ring sets, transmit loads to rock.
Approximate total area rock surface under load	900 in <sup>2</sup> (0.58 m <sup>2</sup> )	1819 in <sup>2</sup> (1.17 m <sup>2</sup> )	Same as Uniaxial (A)	32,500 in <sup>2</sup> (21 m <sup>2</sup> )
Maximum unit load to rock surface	800 psi (56 kg/cm <sup>2</sup> )	1000 psi (70 kg/cm <sup>2</sup> )	Same as Uniaxial (A)	1000 psi (70 kg/cm <sup>2</sup> )
Maximum total load	720,000 lbs. (326,800 kg)	1,810,000 lbs. (821,700 kg)	Same as Uniaxial (A)	32,500,000 lbs. (14,755,000 kg)
Number of drill holes instrumented	2	2	Same as Uniaxial (A)	16
Number measuring points using drill holes only	2	2	14	64
Total measuring points including tunnel diameter gage	3	3	15	66
Testing cycle	200 psi (14 kg/cm <sup>2</sup> ) - 6 days 0 psi - 1 day 400 psi (28 kg/cm <sup>2</sup> ) - 6 days 0 psi - 1 day 800 psi (42 kg/cm <sup>2</sup> ) - 6 days 0 psi - 1 day	200 psi (14 kg/cm <sup>2</sup> ) - 2 days 0 psi - 1 day 400 psi (28 kg/cm <sup>2</sup> ) - 2 days 0 psi - 1 day 600 psi (42 kg/cm <sup>2</sup> ) - 2 days 0 psi - 1 day 800 psi (56 kg/cm <sup>2</sup> ) - 2 days 0 psi - 1 day 1000 psi (70 kg/cm <sup>2</sup> ) - 2 days 0 psi - 1 day	Same as Uniaxial (A)	Same as Uniaxial (A)
Direction of applied load	Horizontal and Vertical	Any angle	Same as Uniaxial (A)	Complete 360° around test bore.
Gage length of measurements	Approximate 15 ft (4.57 m)	Approximate 20 ft (6.10 m) on each side of test adit	14 lengths, varying from 1 to 20 ft (0.3 to 6.1 m) on each side of test adit.	64 lengths, varying from 1 to 30 ft (0.3 to 9.1 m) on each side of test adit.
Instruments measuring deformation	Joint meter Tunnel diameter gage	Same as Dual-axial	Linear variable differential transformer (LVDT) Tunnel diameter gage	Joint meter LVDT Tunnel diameter gage

TABLA 2. Características de las pruebas de placa mostradas en las figuras 9, 14 (A y B) y 21

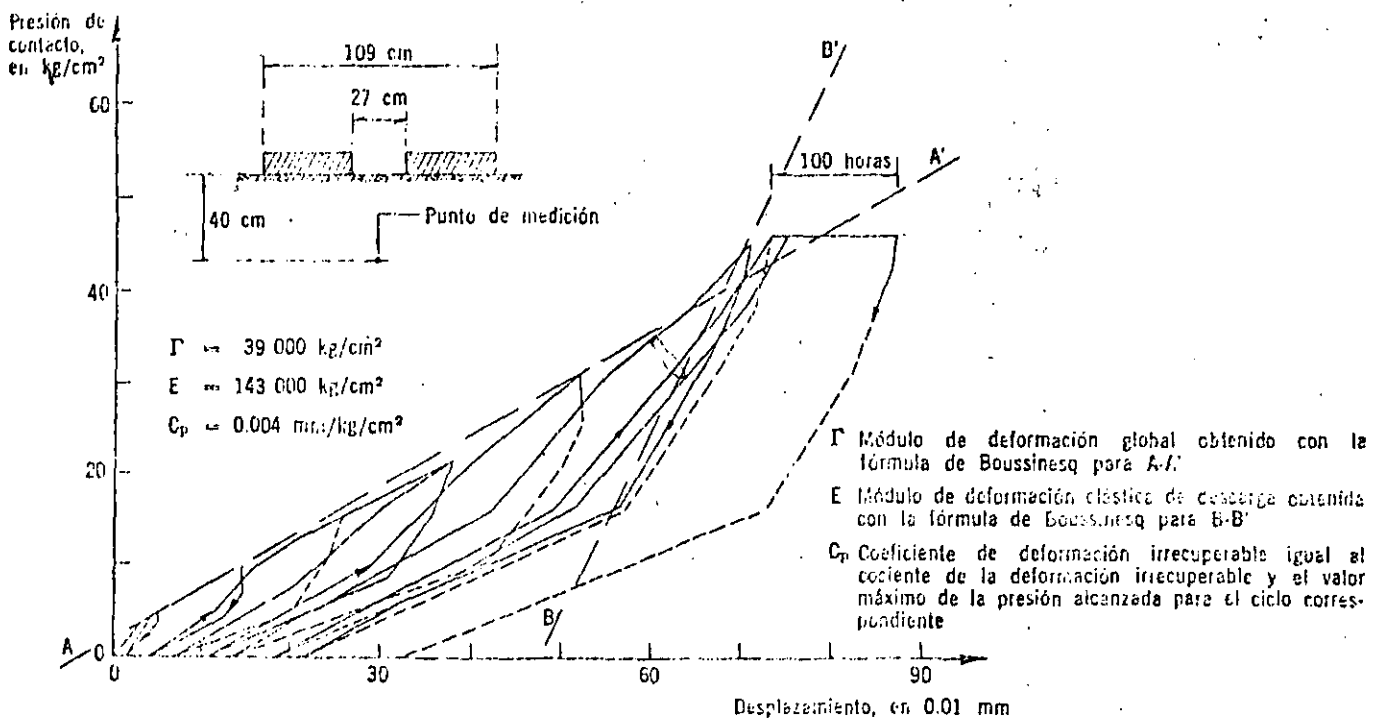


FIG 17. Curva Esfuerzo-deformación obtenida en prueba de placa flexible

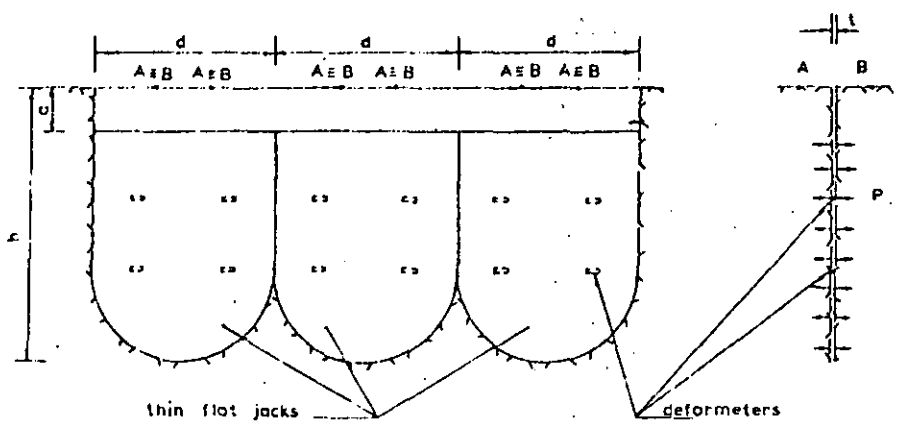
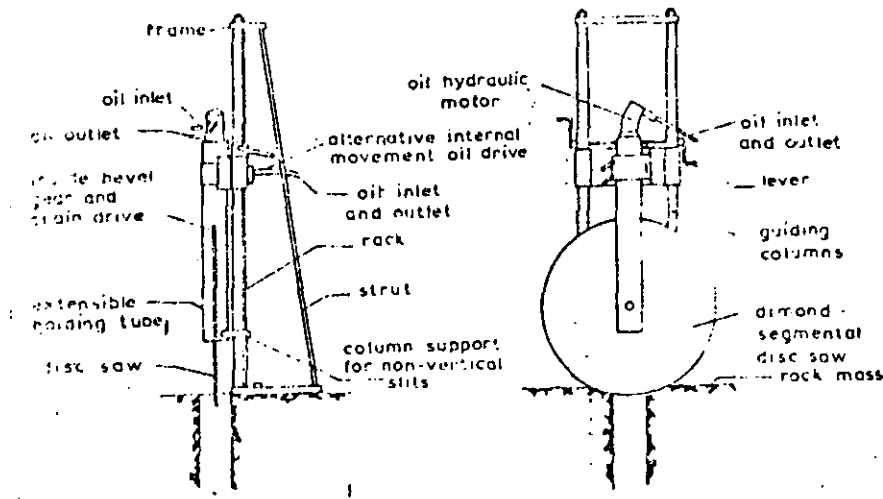


FIG 18. a) Equipo para perforación  
 b) Batería de 3 gatos planos (LNEC)

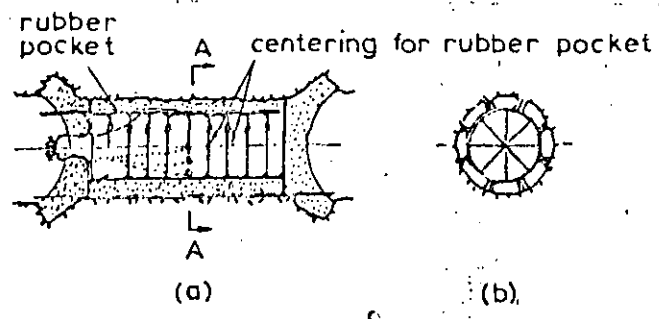
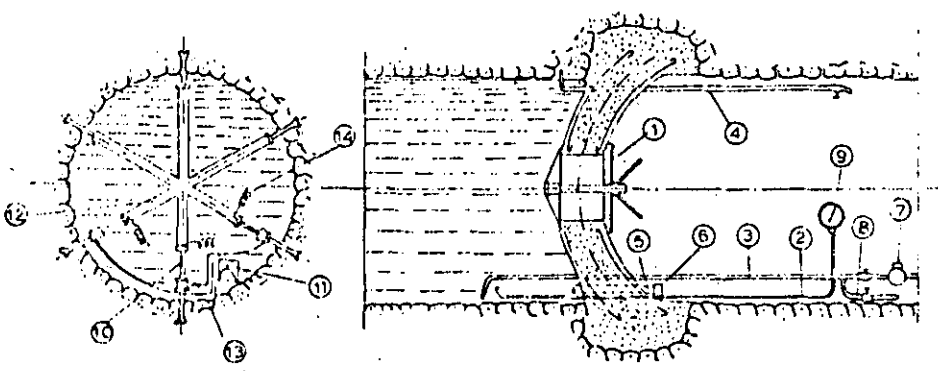
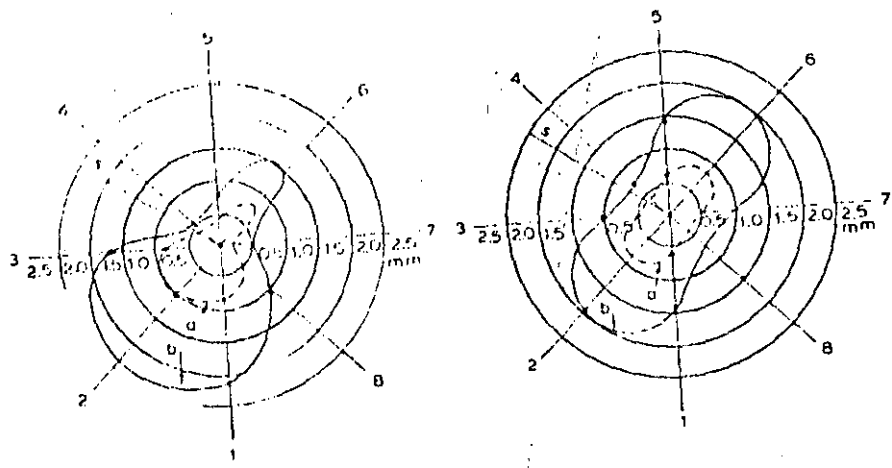


FIG 19. Túnel Presurizado



- |                          |                                      |
|--------------------------|--------------------------------------|
| 1. manhole               | 8. water outlet.                     |
| 2. pressure gauge tube.  | 9. pressure gauge.                   |
| 3. water inlet.          | 10. vibrating meter.                 |
| 4. air outlet            | 11. air pressure equalising chamber. |
| 5. cable admission tube. | 12. invar rods.                      |
| 6. cable tube seal.      | 13. air pressure equalising tube.    |
| 7. water meter.          | 14. cable.                           |



a — elastic deformations.    b — total deformations  
 s — position of the foliation plane of the rock.  
 1 to 8 — measuring points.

FIG 20. Deformaciones circunferenciales alrededor de una galería de prueba ensayada como túnel presurizado

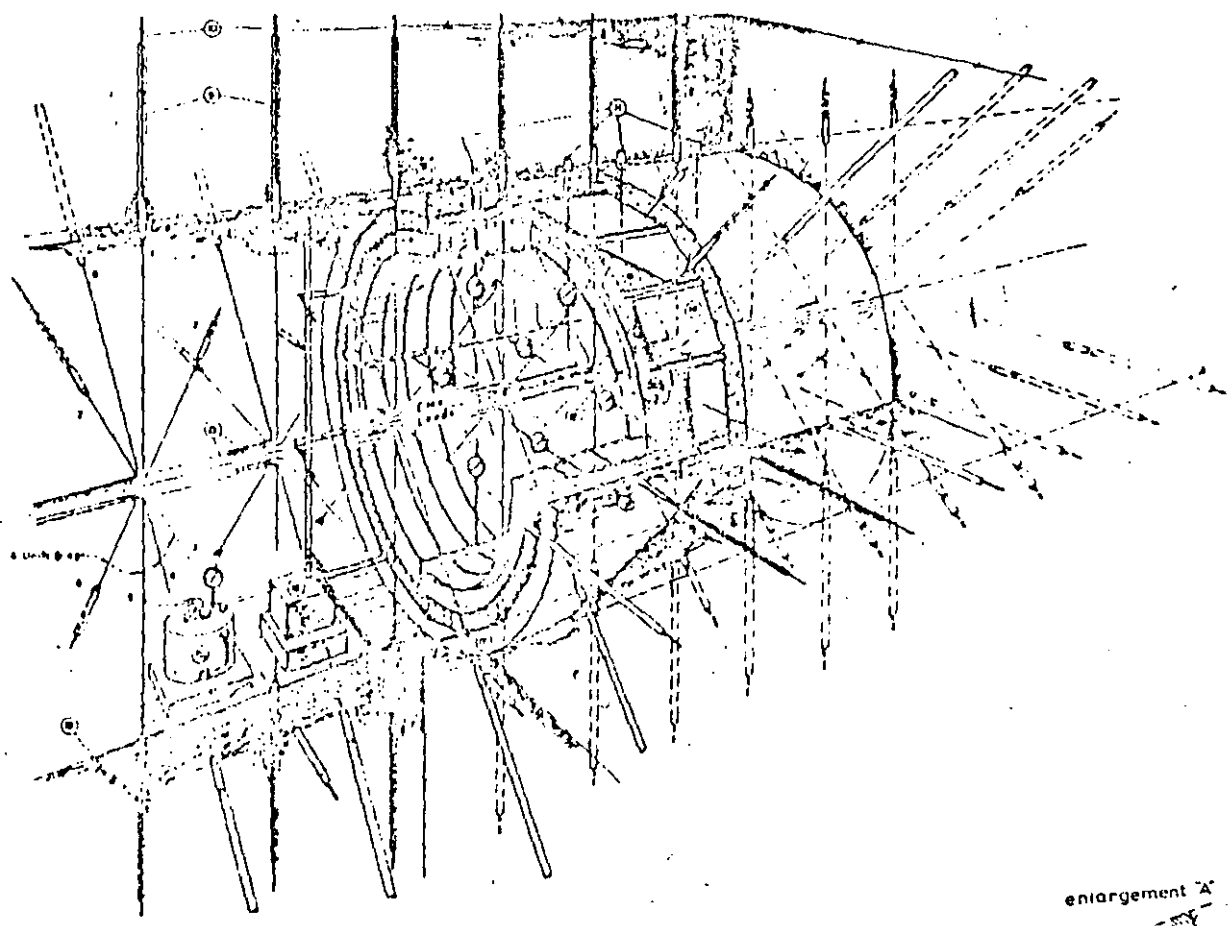
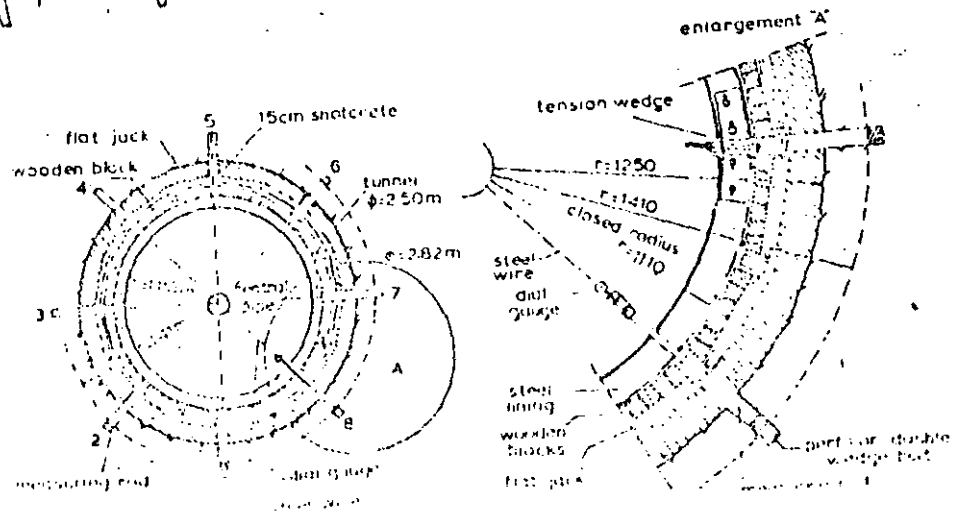


FIG 21. Esquema del arreglo de equipo para prueba de gato radial en un túnel





FOTOGRAFIA  
PRUEBA  
GATO RADIAL

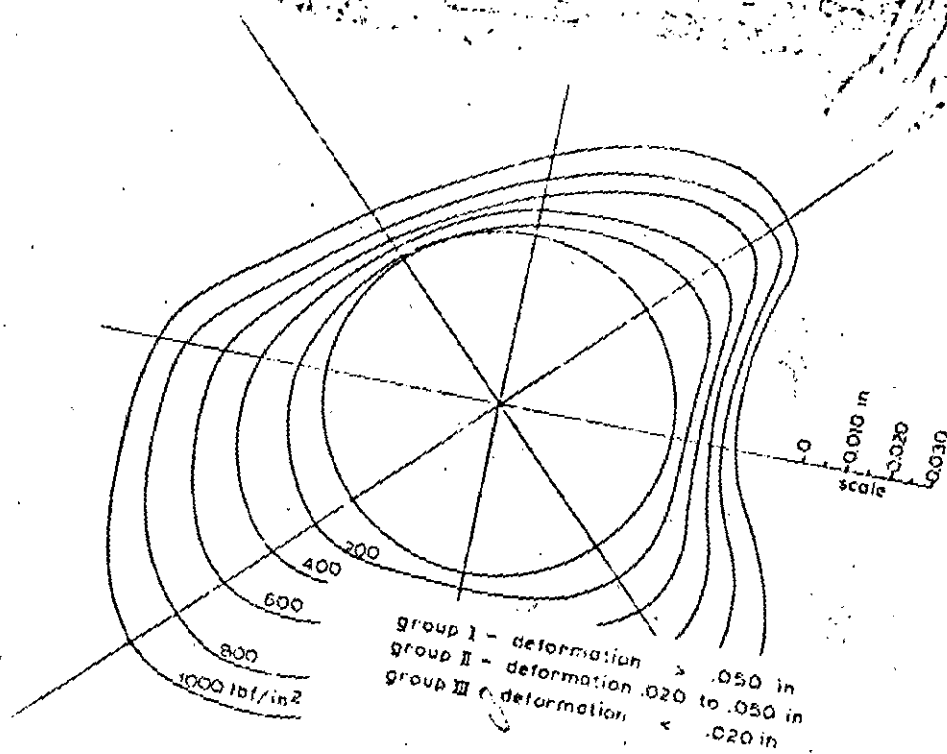
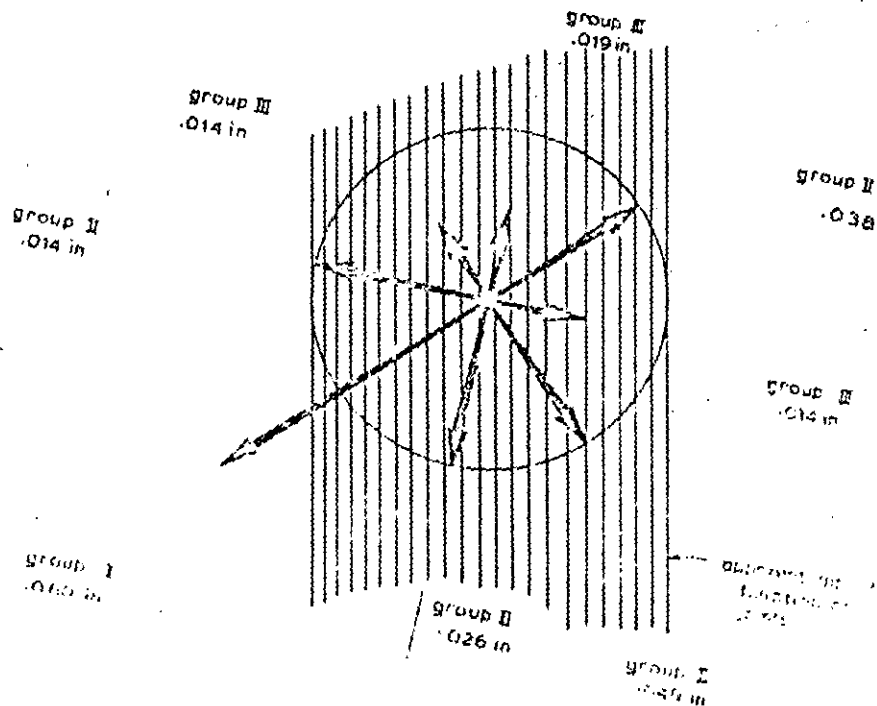


FIG 22.  
Deformaciones circunferen-  
ciales inducidas durante  
la prueba de gato radial



Tipo	Presión	Fórmula	Dispositivo	Fluido de presión	Medición de deformación	Número de diámetros de medición	Diámetro del sondeo, en mm	Longitud, en mm	Presión máxima, en kg/cm <sup>2</sup>	País de origen	Referencia
Dilatómetro	Presión uniforme	$E = \frac{(1 + \nu)}{\Delta d} pd$	Menard	Aire actúa sobre agua	Cambio de volumen		76	515	102	Francia	Menard (1957)
			LNEC	Aceite	4 LVDT	4	76	540	150	Portugal	Rocha (1966)
			Janod Mermin	Aceite	3 LVDT	3	168	770	150	Francia	Janod y Mermin (1954)
			Comes	Aceite	3 LVDT	3	160	1 600	150	Francia	Comes (1965)
			Takaño	Aceite	24 LVDT	4	297	1 300	45	Japón	Takano y Stubbouto (1966)
			Kudjundizic	Aceite	2 MCH	2	300	1 200	68	Yugoslavia	Kudjundizic (1965)
Gatos curvos	Carga aplicada a lo largo de dos sectores diametralmente opuestos	$E = k \frac{pd}{\Delta d}$	Goodman	Aceite	2 LVDT	1	76	204	630	EUA	Goodman y Traub (1967)
			CEBTP	Aceite	2 LVDT	1	76	306	340	Francia	Absi y Seguin (1967)

*E* módulo de Young, en kg/cm<sup>2</sup>  
*ν* relación de Poisson  
*p* presión aplicada, en kg/cm<sup>2</sup>  
*d* diámetro del sondeo, en cm

$\Delta d$  variación del diámetro del sondeo, en cm  
*k* constante del equipo  
 LVDT transformador diferencial variable y lineal

TABLA 3. Aparatos para determinación de deformabilidad de la roca en sondeos

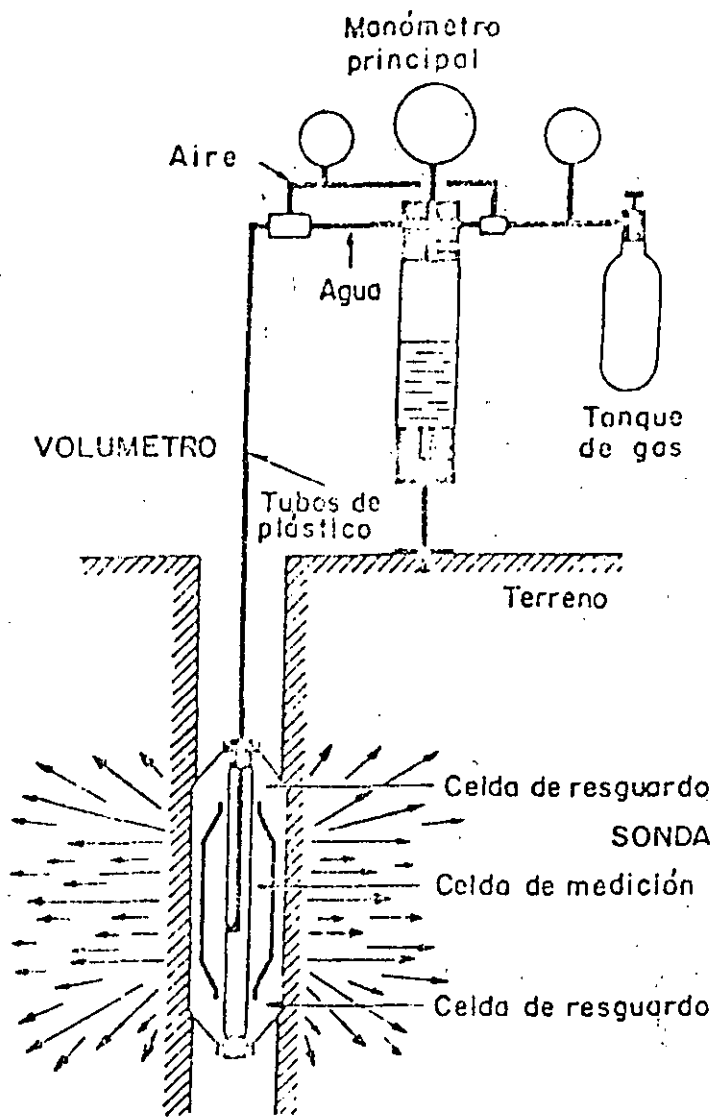
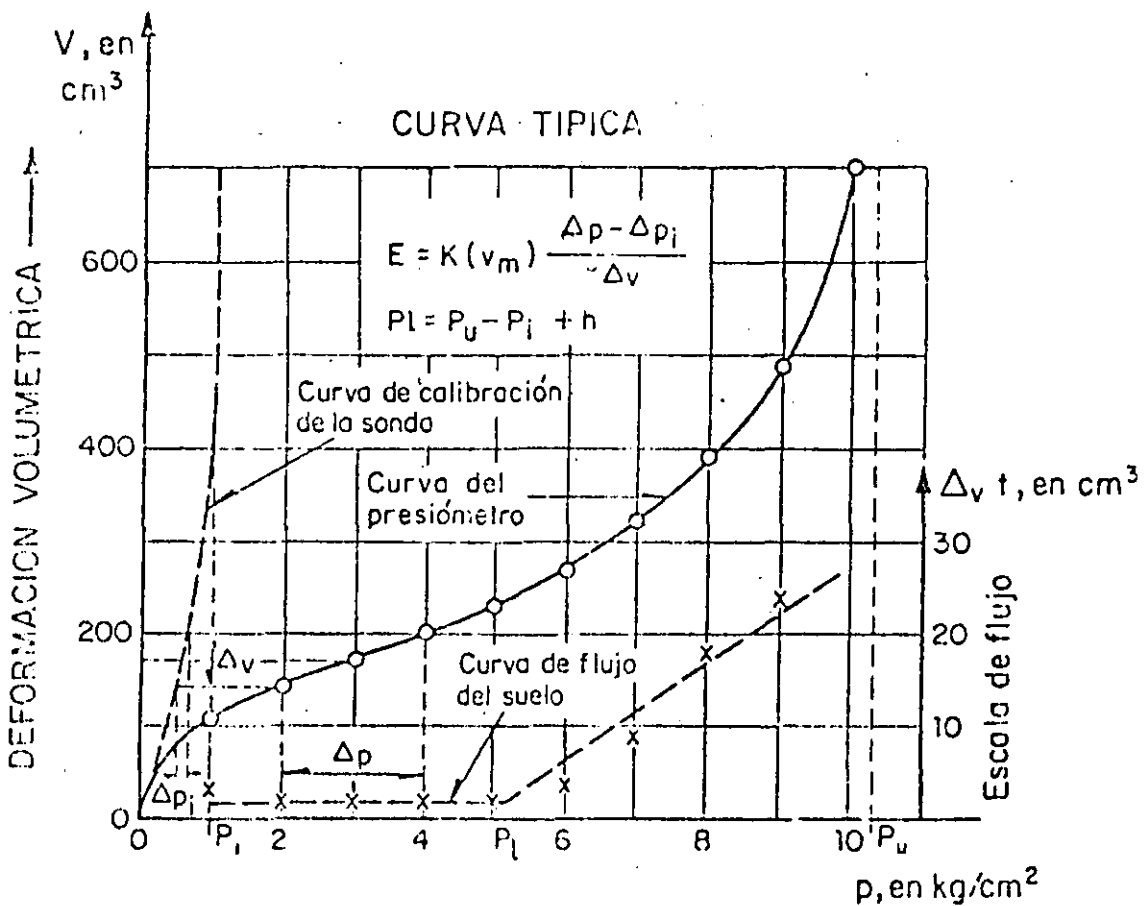
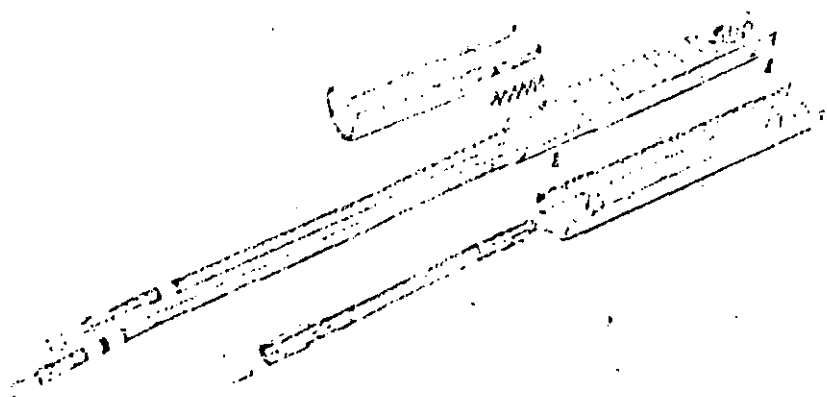


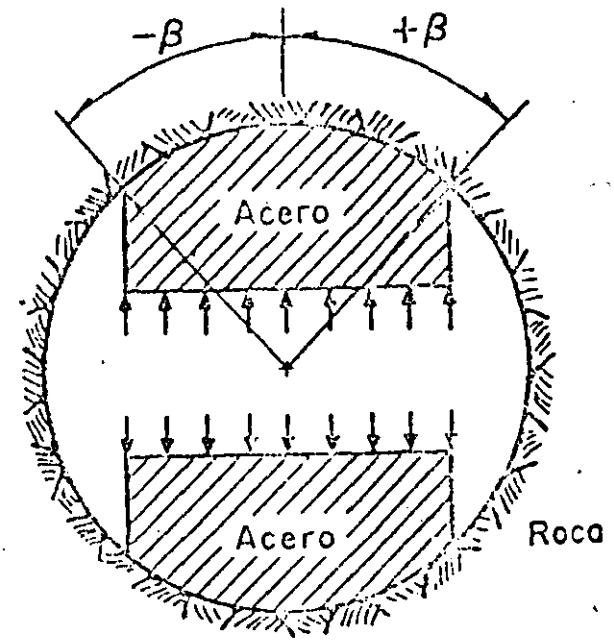
FIG 23. Esquema del equipo del Dilatómetro Menard

FIG 24. Gráfica Deformación Volumétrica-Presión obtenida con un Dilatómetro Menard



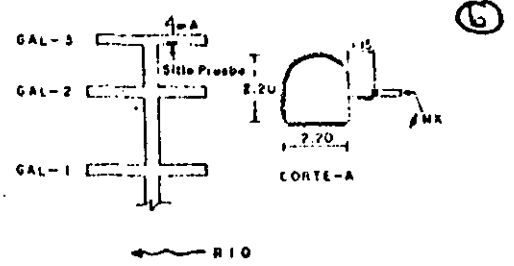


(a)

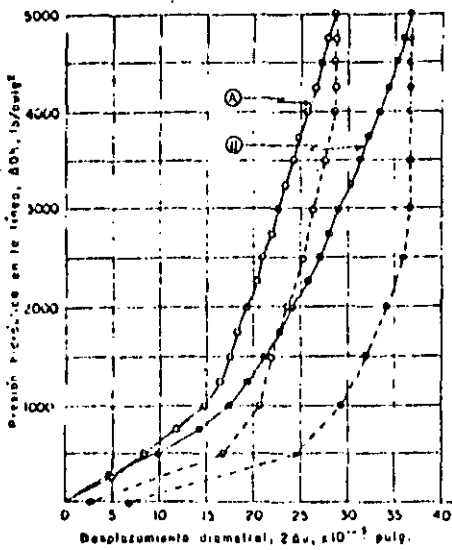


P.H. ANGOŠTUHA, CHIS.

"PRUEBA CON GATO GOODMAN"  
 CASA DE MAQUINAS  
 GAL. 3 PAHED DERECHA  
 PROJ. 1.15 m; HORIZONTAL



GALERIA DE INSTRUMENTACION SOBRE  
 CASA DE MAQUINAS. ELEV. 455



○ — CERCA (NEAR)  
 □ — LEJOS (FAR)  
 "Módulo de Elasticidad"  $E = 300 \frac{\Delta QH}{2 \Delta u}$  (1)

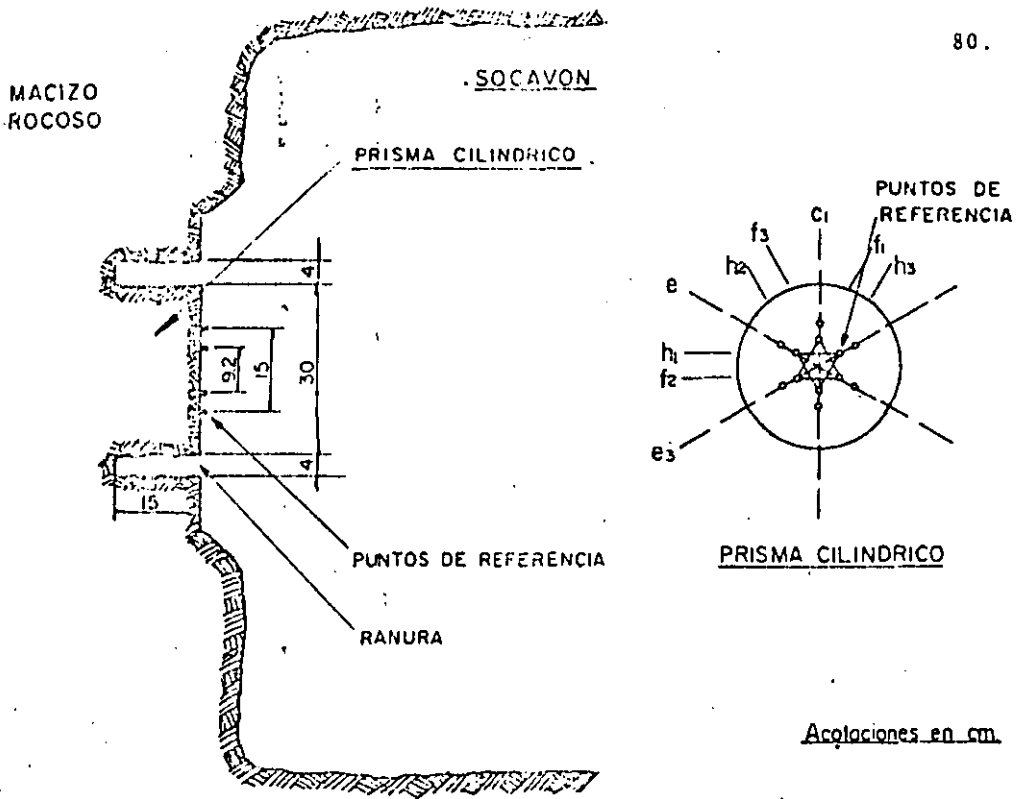
$\Delta QH$ : Intervalo de presión hidráulica en la línea de presión  
 $2 \Delta u$ : Desplazamiento diametral total en el intervalo de presión aplicada

Intervalo de presión [ $\Delta QH$ ] lb/pulg <sup>2</sup>	Desplazamiento ( $2 \Delta u$ ) $\times 10^{-3}$ pulg.	Módulo Elástico, E lb/pulg <sup>2</sup> $\times 10^5$ kg/cm <sup>2</sup> $\times 10^3$	Transductor
CARGA 1000-3000	13.7	0.89	63
DESCARGA 1000-3000	7.8	1.56	110
CARGA 1000-5000	19.1	0.64	45
DESCARGA 1000-5000	7.3	1.67	117

(1) The measurement of rock deformability in bore hole R. E. Goodman, Tzeu K. Yen, and Francoise E. Heuze 10th. Symposium on rock Mechanics, May 1968, University of Texas U.S.A.

Fig. 2-37

FIG 25. a) fotografía mostrando el gato goodman  
 b) sección transversal mostrando las zapatas de carga  
 c) curva esfuerzo-deformación obtenida con este aparato



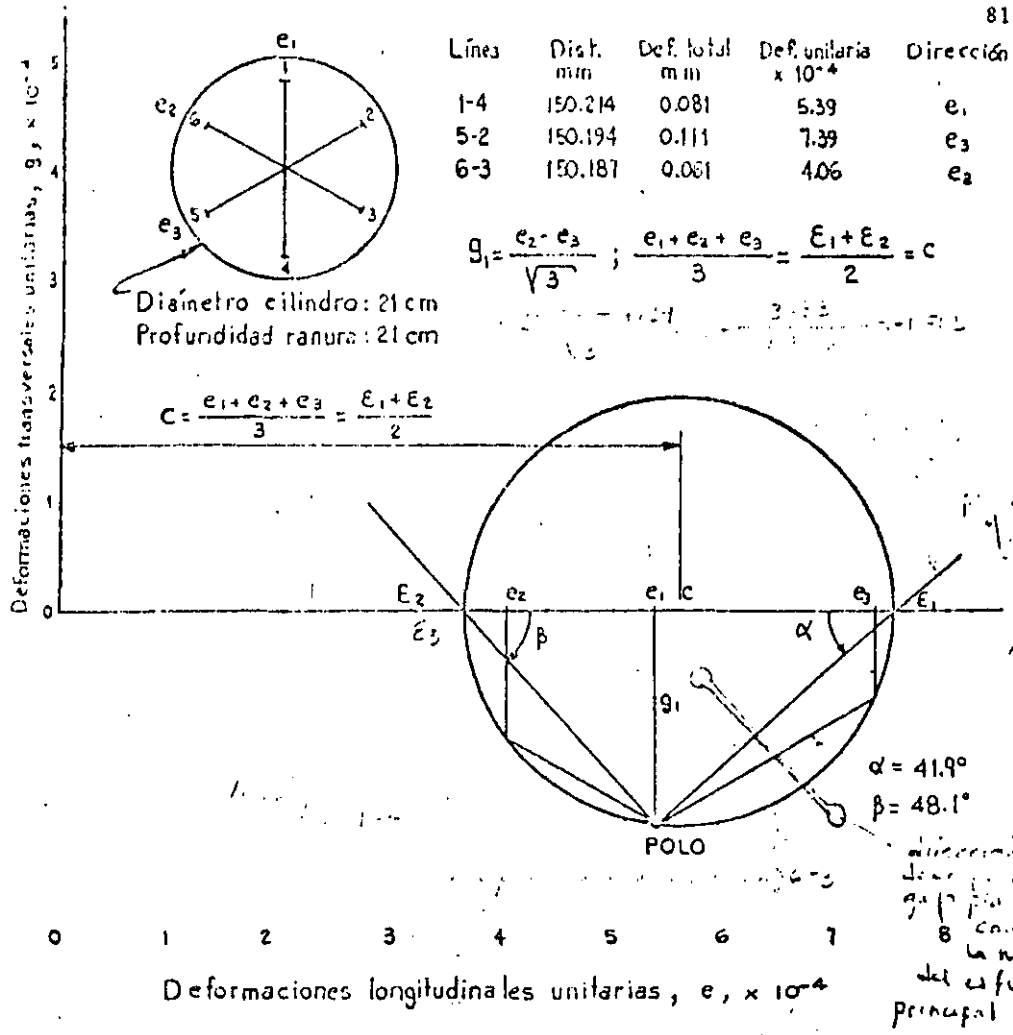
"PRUEBA DE ROSETA"  
 DIRECCION Y MAGNITUD DE ESFUERZOS INTERNOS  
METODO DE LIBERACION DE ESFUERZOS

EJECUCION DE LA PRUEBA

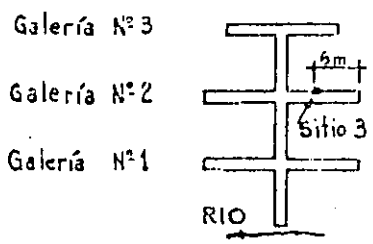
- 1.- Pulido superficie de la roca.
- 2.- Colocación de puntos de referencia, fijandolas con epoxy.
- 3.- Medición inicial de la separación entre los puntos de referencia, con medidor mecánico tipo Whittemore, de cardúla, con precisión de 0.001 mm.
- 4.- Barreración de la ranura de forma circular de 30 cm de diámetro, 15 cm de profundidad y 4 cm de ancho.
- 5.- Proceso de deformación de la roca inducida por rotura de la continuidad de la misma al efectuar la ranura (liberación de esfuerzos que produce deformaciones en el prisma cilindrico de roca).
- 6.- Medición de estas deformaciones en tres direcciones a 60°.
- 7.- Obtención de la dirección de deformaciones principales.

FIG 26. Prueba de Roseta de deformaciones





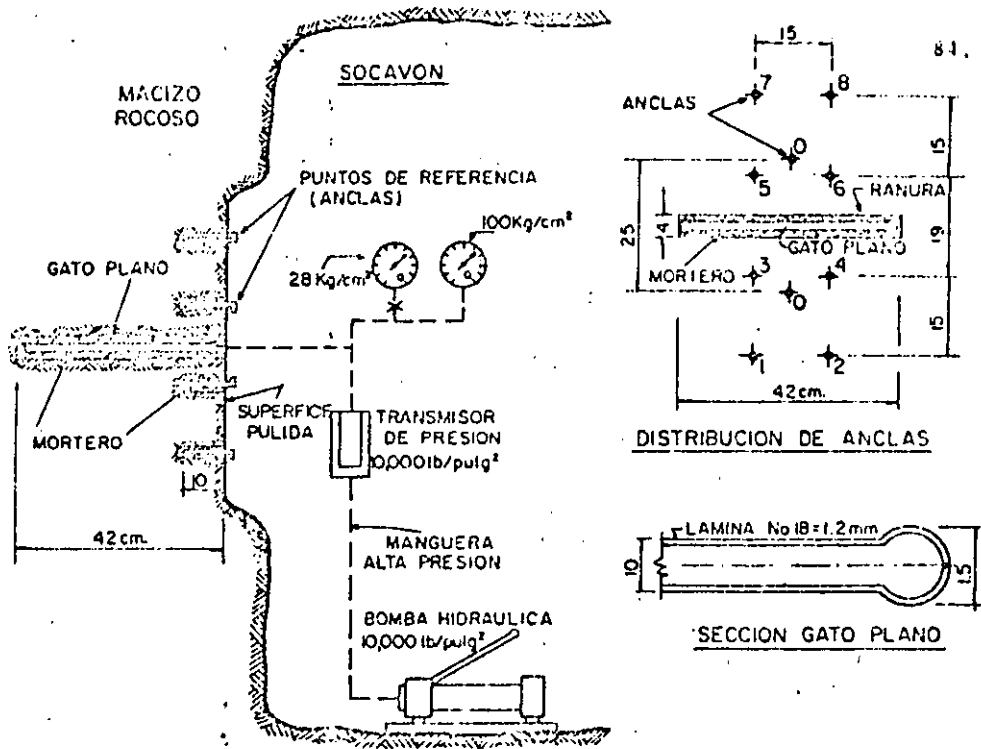
— DIRECCION DE ESFUERZOS PRINCIPALES — "ROSETA DE DEFORMACIONES"



— P.H. ANGOSTURA, CHIS. —  
 — CASA DE MAQUINAS —

FIG. 3-2

FIG 27. Forma de obtención de la Dirección de esfuerzos principales

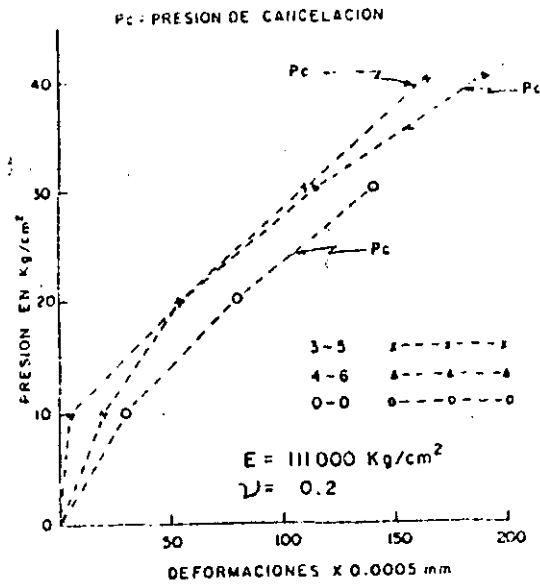


ESQUEMA, PRUEBA DE "GATO PLANO"  
 DETERMINACION DE ESFUERZOS INTERNOS EN ROCA  
 METODO DE LIBERACION DE ESFUERZOS

#### EJECUCION DE LA PRUEBA

- 1- Pulido superficie de la roca.
- 2- Colocación de "puntos de referencia" (anclas), fijándolos a la roca usando mortero con aditivo estabilizador de volumen.
- 3- Medición inicial de la separación entre los puntos de referencia, con medidor mecánico tipo Whittemore, de carátula, con separación mínima de 0.0005
- 4- Barrenación de la ranura de 42x42x4 cm.
- 5- Proceso de deformación de la roca inducido por rotura de la continuidad de la misma al efectuar la ranura (liberación de esfuerzos que produce deformaciones perpendiculares al plano de la ranura).
- 6- Medición de estas deformaciones, tomando lecturas inmediatamente después de ranurar (que son del orden del 90% de la deformación total), y durante un período de tiempo entre 1y3 días después de haber hecho la ranura.
- 7- Inserción del "gato plano" cuadrado en la ranura, ahogándolo en mortero con aditivo estabilizador de volumen, con resistencia de 50Kg/cm<sup>2</sup> a los 7 días.
- 8- Tiempo de fraguado del mortero 3 días.
- 9- Aplicación de presión hidráulica hasta que los "puntos de referencia" regresen a su posición inicial, obteniéndose la "presión de cancelación" que es el valor del esfuerzo interno de la roca en dirección perpendicular al plano de la ranura.

FIG 28. Esquema prueba de gato plano



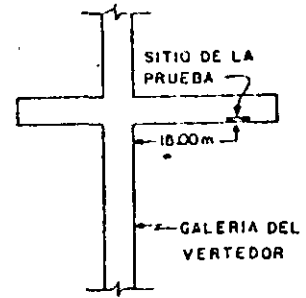
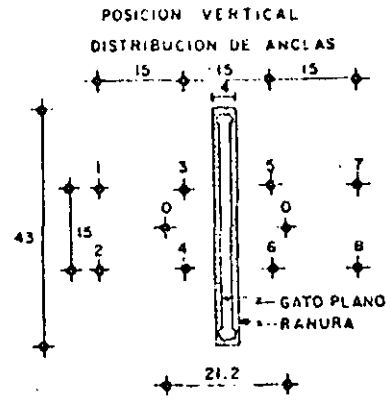
LECTURAS EN EL EXTENSOMETRO \*

LINEA	ANTES DE RANURAR	DESPUES DE RANURAR	PARA PRESIONES DE 30	40 Kg/cm <sup>2</sup>
1-3	410	420		
2-4	70	70		
3-5	970	810	975	
4-6	1010	825	1015	
5-7	390	390		
6-8	480	530		
0-0	1145	1050	1180	

\* EXTENSOMETRO MECANICO 2 UNIDADES/MICRA

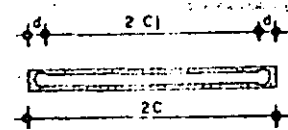
ABRIL 24/1972  
OPERADOR:

VISTA DE FRENTE



CROQUIS DE LOCALIZACION

PRUEBA DE GATO PLANO  
POSICION VERTICAL



$$\sigma_n = P_c(C_j - d) = 24(18.5 - 3)$$

$$\therefore \sigma_n = 17.3 \text{ Kg/cm}^2$$

FIG 29. Forma de obtención de la Magnitud de los Esfuerzos tectónicos principales

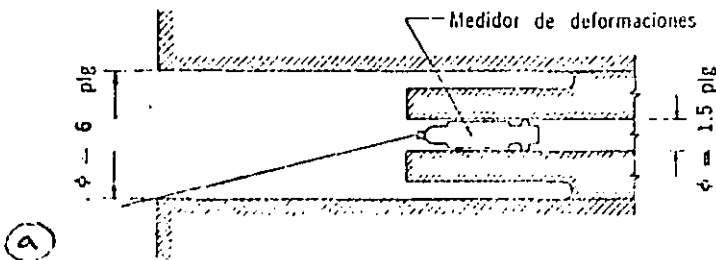
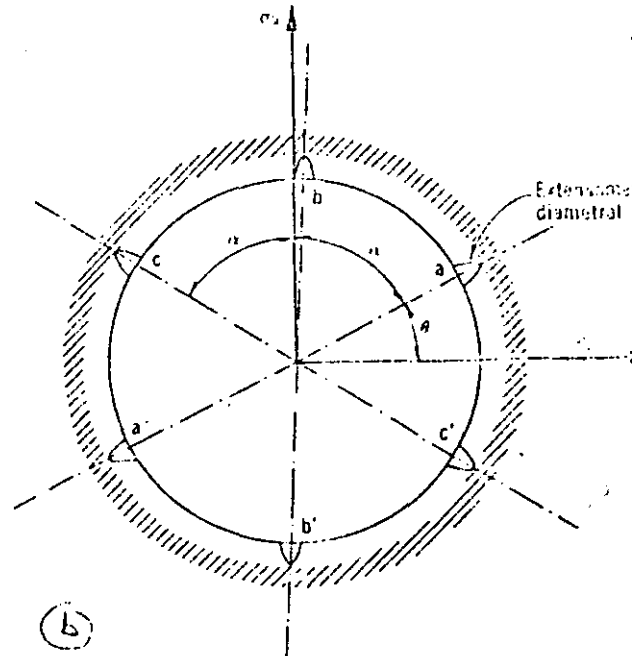


FIG 30. a. sección longitudinal del sondeo en el que se efectúa el alivio de esfuerzos

b. sección transversal del medidor de deformaciones





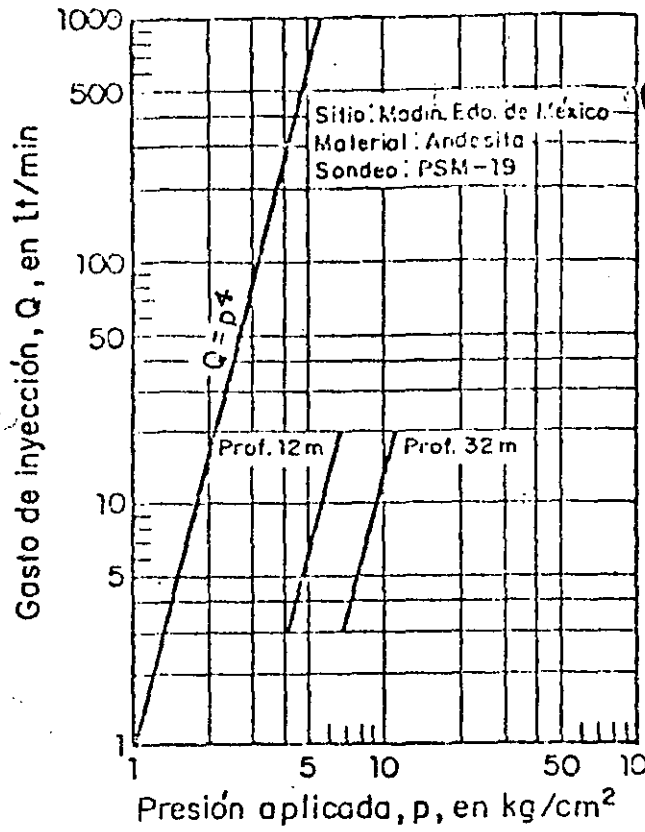
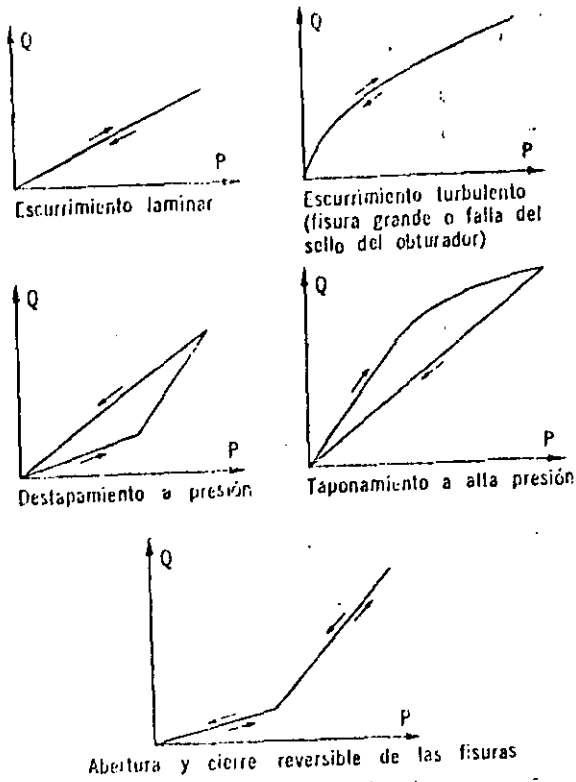


FIG 32. Curvas de comportamiento de fracturas durante un ensaye tipo Lugeon

FIG 33. Curva Doblemente Logarítmica Q

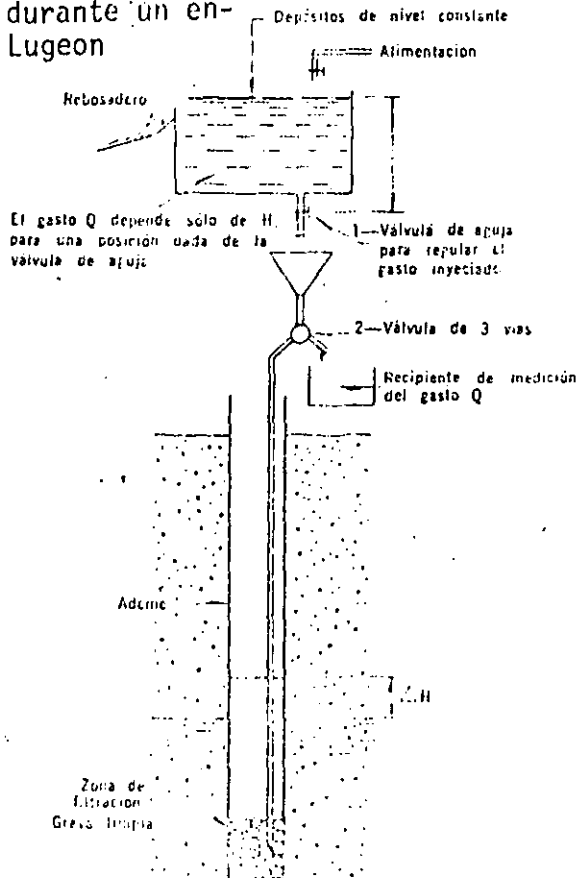
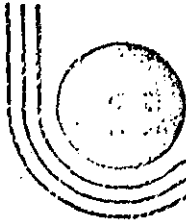


FIG 34. Dispositivo de Ensayo Lefranc



DIVISION DE EDUCACION CONTINUA  
FACULTAD DE INGENIERIA U.N.A.M.

MECANICA DE ROCAS APLICADA A LA MINERIA Y A LA CONSTRUCCION

V A R I O S  
ARTICULOS

ING. TOMAS LUGO IBARRA

MAYO, 1985.

## ANÁLISIS ESTRUCTURAL

## UNA FASE DE PLEGAMIENTO CON FRACTURAS ASOCIADAS (2)

La figura 022 es un mapa de una región de metasedimentos plegados. La forma de la estructura mayor es claramente visible en los afloramientos, además del plegamiento, el área está intensamente fracturada e intrusionada por diques de diferentes composiciones. Este ejercicio sirve básicamente para analizar fracturas, las cuales se pueden clasificar en varios sistemas o grupos, mientras que sus orientaciones se pueden relacionar sistemáticamente con los pliegues mayores.

Describa la estructura de la región especificando la actitud y el estilo de plegamiento, las relaciones del clivaje con los plegamientos mayores y sus trazas.

Distinga los sistemas de fracturas y donde sea posible, relacione sus actividades con el plegamiento. Denomine de manera apropiada los sistemas de fractura.

## PROCEDIMIENTO

Complete la distribución de los afloramientos y coloree el mapa. Prepare una graficación "pi" de la estratificación con los polos de clivaje pizarroso y los ejes de los pliegues menores en el mismo estereograma. No es necesario graficar todos los datos, pero sí un ejemplo representativo de la población.

A partir de este estereograma se puede especificar exactamente la orientación del plano axial y el buzamiento de los pliegues mayores, así como el estilo del plegamiento.

Grafique los polos de los planos de fracturas en otro estereograma y marque la dirección del eje axial mayor, el polo del plano axial y los flancos (círculos grandes).

En el estereograma se ve claramente el agrupamiento de las fracturas, lo que permite determinar la relación de cada sistema de fracturas con los elementos geométricos del plegamiento mayor. Dibuje un esquema de las orientaciones de los sistemas de fracturas con respecto al plegamiento mayor.

¿Qué características sugieren que algunas fracturas son de tensión y no de cizallamiento?

¿Es posible sugerir las razones por las que las fracturas con actitudes particulares deben ser de tensión o de cizallamiento, teniendo en cuenta la manera en las que se forman con respecto a los esfuerzos que originan el plegamiento?





CUARCITA

PIZARRA

CONGLOMERADO



ESTRATIFICACION  
(RUMBO, INCLINACION)



ESTRATIFICACION VERTICAL



CLIVAJE PIZARROSO



FRACTURA



FRACTURA VERTICAL



EJE DE PLEGUE MENOR  
(RUMBO, DIRECTION)



DIQUE DE DIABASA



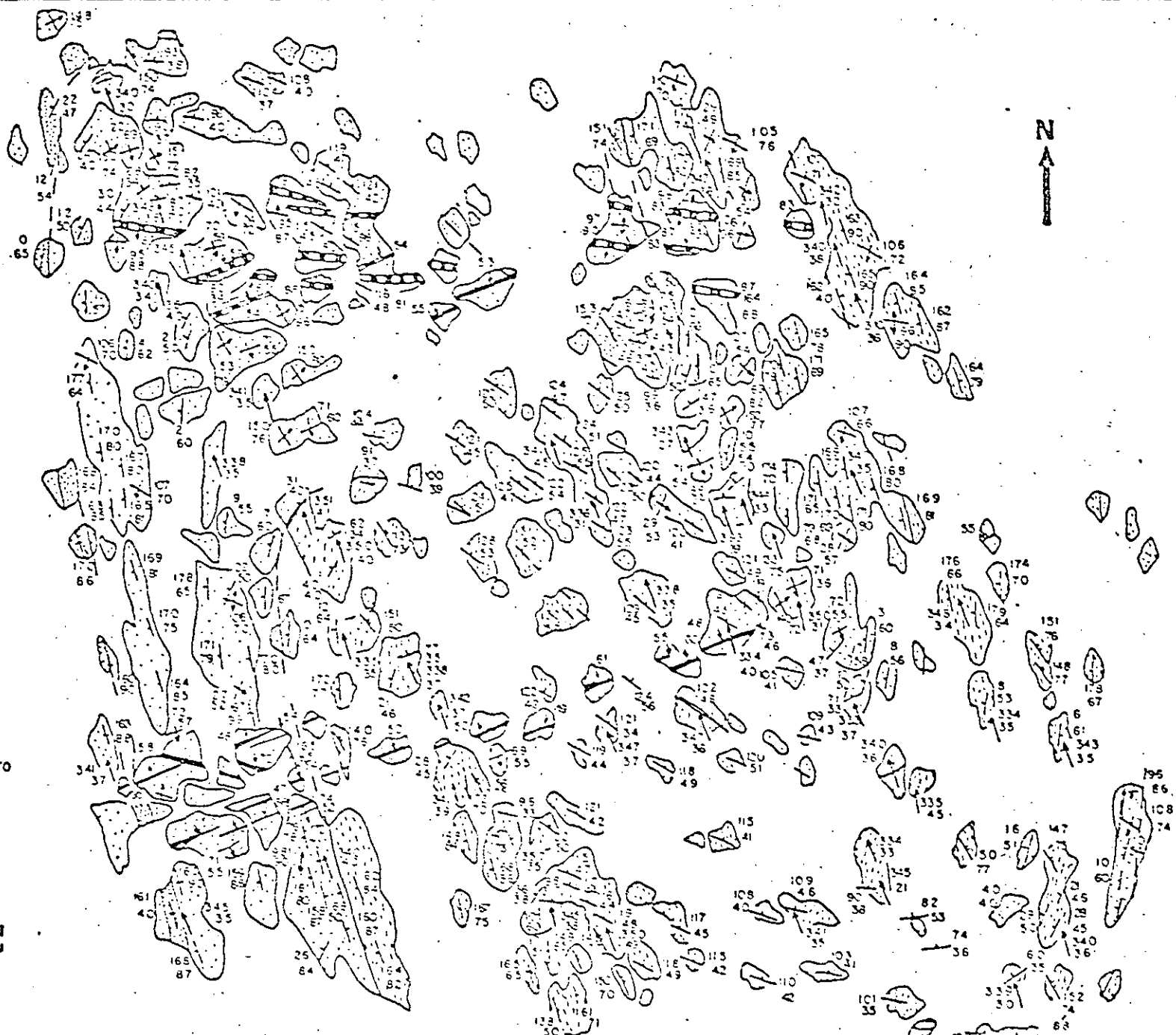
LAMPYRO



INCLINACION DEL CONTACTO  
DEL DIQUE



Km



## ANÁLISIS ESTEREOGRÁFICO DE PLIEGUES (1)

- 1.- Se observa un pliegue en una secuencia de paragneises feldespáticos. Uno de los flancos del pliegue tiene la actitud de  $159^\circ$  SW60° (rumbo-inclinación). El otro flanco no se puede medir directamente pero se observa con una inclinación aparente de  $28^\circ$  a  $277^\circ$  (buzamiento y orientación), en un plano de afloramiento con actitud  $116$  SW58 y con un pitch de  $25^\circ$  al N, en un plano con una actitud de  $0^\circ$  E  $75^\circ$ . En el último afloramiento, la traza axial del pliegue se observa a  $10^\circ$  y  $3^\circ$  (pitch).

Determine la actitud del eje del pliegue, el plano axial y el ángulo entre los flancos del pliegue. Si se observa una traza axial en el plano de afloramiento a  $116^\circ$  SW58°, ¿Cuál sería su pitch?

Dibuje una sección esquemática perpendicular al buzamiento del pliegue (no vertical), en la cual las relaciones angulares sean exactas; marque los dos flancos y la posición del plano axial. Etiquete la sección cuidadosamente.

- 2.- Los siguientes datos son mediciones representativas de la estratificación (rumbo e inclinación) en una región de areniscas calcáreas plegadas.

222 NW 80	256 N 42	237 NW 59	281 NE 33
223 NW 79	314 NE 30	227 NW 72	318 NE 30
224 NW 78	267 N 36	246 N 50	322 NE 31
329 NE 32	225 NW 76	232 NW 65	226 NW 75
297 NE 30	326 NE 32	332 NE 32	

Use un diagrama (pi) para determinar la actitud de los ejes del pliegue en la región. Determine el ángulo entre los flancos y marque el ángulo en el estereograma. Dibuje una sección esquemática perpendicular al buzamiento del pliegue.

Si se asume que el plegamiento es simétrico ¿Cuál es la actitud del plano axial? El plegamiento está acompañado por un fractu -

ramiento (clivaje) convergente en abanico, ligeramente desarrollado, cuyo ángulo dihedral es de  $20^\circ$ . Determine la actitud - aproximada que tendría el clivaje (i.e. planos de clivaje) en capas con actitudes de  $222 \text{ NW } 80$  y  $332 \text{ NE } 32$ . . Dibuje el clivaje en abanico en la sección esquemática.

Los siguientes datos estructurales pertenecen a un levantamiento de fracturas en una roca volcánica fracturada donde se planea construir un canal cuya orientación es  $N20^{\circ}W$  y taludes de corte de 0.25: 1 ( $76^{\circ}$ )

Rumbo	Inclinación	No. Fracturas
N 40 E	60 SE	4
N 37 E	65 SE	3
N 69 W	62 NE	1
N 43 W	60 NE	1
N 43 E	62 SE	4
N 70 W	60 NE	5
N 38 E	66 SE	3
N 35 E	72 SE	1
N 62 W	65 NE	2
N 68 W	63 NE	4
N 21 E	38 SE	1
N 72 E	67 SE	4
N 40 W	65 NE	3
N 46 E	71 SE	2
N 43 E	67 SE	2
N 64 W	72 NE	2

El ángulo de fricción entre los planos de fracturas medido en el laboratorio fue de  $40^{\circ}$ .

Con la ayuda de una proyección estereográfica grafique los polos de las fracturas para determinar lo siguiente:

- Rumbo e inclinación de la tendencia central de los sistemas de fracturas
- Rumbo e inclinación de la intersección de los principales planos de debilidad
- Qué representa esta dirección en términos de esfuerzos principales?
- Angulo dihedro en los sistemas de fracturas
- Para determinar la zona que representa la inestabilidad cinemática, grafique los taludes de corte del canal y el ángulo de fricción entre las discontinuidades.
- Con base al análisis preliminar de estabilidad ¿Qué taludes de corte recomendaría para garantizar la estabilidad de los cortes?

PROYECTO \_\_\_\_\_ LOCALIZACION \_\_\_\_\_  
TIPO DE ROCA \_\_\_\_\_

1) RESISTENCIA-COMPRESION SIMPLE (R)

> 250 MPa	100-250	50-100	25-50	5-25	1-5	< 1
> 2500 kg/cm <sup>2</sup>	1000-2500	500-1000	250-100	50-250	10-50	< 10
(15)	(12)	(7)	(4)	(2)	(1)	(0)

2) RQD-INDICE DE CALIDAD DE ROCA

100-90%	90-75%	75-50%	50-25%	25%
(20)	(17)	(13)	(8)	(3)

3) ESPACIAMIENTO DE FRACTURAS (Js)

> 2 m	2.0-0.6 m	.600-.200 m	.200-.600 m	< 60 mm
(20)	(15)	(10)	(8)	(5)

4) CONDICION DE LAS FRACTURAS (Jc)

Muy rugosa	Poco rugosa	Poco rugosa	Estrías	Arcilla > 5 mm
Discontinua	Abierta < 1 mm	Abierta < 1 mm	Arcilla < 5 mm	Abierta > 5 mm
Cerrada	Poco intemperizada	Muy intemperizada	Abierta, 1-5 mm	Continua
(30)	(25)	(20)	(10)	(0)

5) AGUA (W)

Completamente seca	Húmeda	Húmeda	Goteo incipiente	Flujo continuo
--	< 10 l/min	10-25 l/min	25-125 l/min	> 125 l/min
(15)	(10)	(7)	(4)	(0)

6) AJUSTE POR ORIENTACION (Jo)

	Muy favorable	Favorable	No relevante	Desfavorable	Muy desfavorable
Túneles	0	-2	-6	-10	-12
Cimentaciones	0	-2	-7	-15	-25
Taludes	0	-5	-25	-50	-60

$RMR = R + RQD + Js + Jc + W - Jo$

$RMR = 9 \ln Q + 44$

100-81 macizo rocoso muy bueno

80-61 macizo rocoso bueno

60-41 macizo rocoso regular

40-21 macizo rocoso pobre

-20 macizo rocoso muy pobre

CLASE I

CLASE II

CLASE III

CLASE IV

CLASE V

OBSERVACIONES \_\_\_\_\_

CLASIFICACION NGI  
(Barton, 1976)

TLI

PROYECTO \_\_\_\_\_ LOCALIZACION \_\_\_\_\_

TIPO DE ROCA \_\_\_\_\_

1) RQD %		5) Jw-AGUA	
a) Muy pobre	0-25%	a) Seca	1
b) Pobre	25-50%	b) Flujo medio	0.66
c) Regular	50-75%	c) Flujo grande	0.5
d) Buena	75-90%	d) Flujo más grande	0.33
e) Excelente	90-100%	e) Flujo muy grande	0.2-0.1
Si Jv = No. de fracturas/m <sup>3</sup> entonces		disminuye el tiempo	
RQD = 110.4 - 3.68 Jv		f) Flujo grande constante	0.1-0.5

2) Jn-SISTEMAS		6) SRF-FACTOR DE REDUCCION DE ESFUERZOS	
a) Masiva, sin fracturas	0.5-1.0	a) Múltiples zonas de debilidad. Roca alterada (arcilla)	10
b) Un sistema	2	b) Zonas de debilidad P.<50m Roca alterada (arcilla)	5
c) Un sistema + dispersión	3	c) Zonas de debilidad P.>50m Roca alterada (arcilla)	2.5
d) Dos sistemas	4	d) Múltiples zonas de cizalla Roca competente (sin arcilla)	7.5
e) Dos sistemas + dispersión	6	e) Zonas de cizalla en roca competente (sin arcilla) P.<50m	5
f) Tres sistemas	9	f) Zonas de cizalla en roca competente (sin arcilla) P.>50m	2.5
g) Tres sistemas + dispersión	12	g) Zonas muy fracturadas, abiertas (cualquier profundidad)	5.0
h) Cuatro o más sistemas	15	<i>Problemas de esfuerzos (σ<sub>c</sub>/σ<sub>t</sub>)</i>	
i) Triturada	20	h) Esfuerzos bajos >200	2.5
Nota: para intersecciones Jn x 3		i) Esfuerzos medios 200-10	1.0
para portales Jn x 2		j) Esfuerzos altos 10-5	0.5-2

3) Jr*-RUGOSIDAD		k) Altamente compresibles o expansibles	
<i>Contacto de planos</i>		10-20	
a) Discontinua	4	l) Ligeramente compresibles o expansibles	
b) Rugosa, ondulada	3	5-15	
c) Suave, ondulada	2		
d) Estrías, onduladas	1.5		
e) Irregular, planar	1.5		
f) Suave, planar	1		
g) Estrías, planar	0.5		
<i>Sin contacto de planos</i>			
h) Arcilla	1		
i) Roca triturada	1		
Nota: Si el espaciamiento > 3m sumar 1 al Jr			

4) Ja*-RELLENO			
<i>Contacto de planos</i>			
a) Sellada, dura	0.75		
b) Sin alterar	1		
c) Ligeramente alterada	2		
d) Lijosa, recubrimiento arenoso	3		
e) Recubrimientos minerales (clorita, etc.)	4		
f) Partículas arenosas	4		
g) Arcilla fuertemente consolidada	6		
h) Arcilla medianamente consolidada	8		
<i>Sin contacto de planos</i>			
i) Arcilla expansiva	8-12		
j) Desintegrada	6-8		
k) Bandas de arcilla	13-20		

\* Sistema más desfavorable.

$$Q = \frac{RQD}{Jn} \times \frac{Jr}{Ja} \times \frac{Jw}{SRF}$$

$$Q = \text{---} \times \text{---} \times \text{---}$$

$$Q =$$

OBSERVACIONES \_\_\_\_\_



TABLE 18 - RECOMMENDED SUPPORT BASED UPON HCI TUNNELLING QUALITY INDEX Q

Rock mass quality Q	Span ESR	Block size $\frac{SD}{J_n}$	Inter-block strength $\frac{J_r}{J_n}$	Approx. support pressure p MPa	Spot reinforcement with un- signed grouted dowels	Un-tensioned grouted dowels on grid spacing indicated	Tensioned rockbolts on grid spacing indicated	Chainlink mesh anchored to bolts and intermediate points	Shotcrete applied directly to rock, thickness indicated	Shotcrete reinforced with weld- mesh, thickness indicated	Unreinforced cast concrete arch, thickness indicated	Steel reinforced cast concrete arch, thickness indicated	Notes by Barton, Lien and Lunde	Notes by Hoek and Brown
10 -4	6- 9	<10		0.10		1- 1.5m			20- 30mm				2	
10 -4	<6	<10		0.10					20- 30mm				2	
10 -4	10- 15	>5		0.10			1- 1.5m	/					2,4	a
10 -4	7- 10	>5		0.10		1- 1.5m		/					2	a
10 -4	10- 15	<5		0.10			1- 1.5m		20- 30mm				2,4	
10 -4	7- 10	<5		0.10		1- 1.5m			20- 30mm				2	
10 -4	20- 25			0.10			1- 2m			100- 150mm			2,3,5	c
10 -4	12- 20			0.10			1- 1.5m			50- 100mm			2,3	c
10 -4	35- 52			0.10			1- 2m			200- 250mm			2,6, 7,13	c
10 -4	24- 35			0.10			1- 2m			100- 200mm			2,3, 5,13	c
4-1	2.1- 6.5	>12.5	<0.75	0.15		1m			20- 30mm				2	
4-1	2.1- 6.5	<12.5	<0.75	0.15					20- 30mm				2	
4-1	2.1- 6.5		>0.75	0.15		1m							2	
4-1	4.5- 11.5	>10	<30 >1	0.15		1m		/					2	a
4-1	4.5- 11.5	<10	>1	0.15					25- 75mm				2	
4-1	4.5- 11.5	<30	<1	0.15		1m				25- 50mm			2	c
4-1	4.5- 11.5	>30		0.15		1m							2	
4-1	15- 24			0.15			1- 1.5m			100- 150mm			2,3, 5,8	c
4-1	8- 15			0.15			1- 1.5m			50- 100mm			2	c
4-1	30- 46			0.15			1- 1.5m			150- 300mm			2,6, 7,13	c



TABLE 18 - RECOMMENDED SUPPORT BASED UPON RQI TUNNELLING QUALITY INDEX Q

Rock mass quality Q	Eqivalent dimension ESR	Block size $\frac{RQD}{J_n}$	Inter-block strength $\frac{J_r}{J_n}$	Approx. support pressure p MPa	Spot reinforcement with un- stressed grouted dowels spacing	Unstressed grouted dowels on grid spacing indicated Max. length indicated	Tensioned rockbolts on grid spacing indicated Max. length indicated	Chainlink mesh anchored to bolts and intermediate points spacing	Shotcrete applied directly to rock, thickness indicated	Shotcrete reinforced with weld- mesh, thickness indicated	Weldreinforced cast concrete arch, thickness indicated	Steel reinforced cast concrete arch, thickness indicated	Notes by Barton, Lien and Lunde	Notes by Hoek and Brown
4-1	10-30			0.15			1-1.5m			100-150mm			2,3,5	c
1-0.4	1.5-4.7	>10	>0.5	0.225		1m		✓					2	d
1-0.4	1.5-4.2	≤10	>0.5	0.225		1m				50mm			2	c
1-0.4	1.5-4.2		≤0.5	0.225		1m				50mm			2	c
1-0.4	3.2-7.5			0.225			1m			50-75mm			14,11 12	c
1-0.4	1.2-7.5			0.225		1m			25-50mm				2,10	
1-0.4	1.2-18			0.225			1m			75-100mm			2,10	c
1-0.4	6-12			0.225		1m				50-75mm			2,10	c
1-0.4	12-18			0.225		1m					200-400mm		14,11 12	e
1-0.4	6-12			0.225		1m				100-200mm			14,11 12	c
1-0.4	30-38			0.225			1m			300-400mm			2,5,6 10,13	c, f
1-0.4	20-30			0.225			1m			200-300mm			2,3,5 10,13	c
1-0.4	15-20			0.225			1m			150-200mm			1,3 10,13	c
1-0.4	15-38			0.225			1m				300mm-1m		5,9,10 12,13	
0.4-0.1	1-3.1	>5	>0.25	0.3		1m			20-30mm					
0.4-0.1	1-3.1	≤5	>0.25	0.3		1m				50mm				c
0.4-0.1	1-3.1		≤0.25	0.3			1m			50mm				c
0.4-0.1	2.2-6	≥5		0.3			1m			25-50mm			10	c
0.4-0.1	2.2-6	<5		0.3						50-75mm			10	c
0.4-0.1	2.2-6			0.3			1m			50-75mm			9,11, 12	c
0.4-0.1	4-14.5	>4		0.3			1m			50-125mm			10	c

TABLE 18 - RECOMMENDED SUPPORT BASED UPON RMI TUNNELLING QUALITY INDEX Q

Rock mass quality Q	Equivalent dimension $\frac{RQD}{RMR}$	Block size $\frac{RQD}{J_n}$	Inter-block strength $\frac{J_R}{J_n}$	Approx. support pressure p MPa	Spot reinforcement with untensioned grouted dowels	Untensioned grouted dowels on grid spacing indicated	Tensioned rockbolts on grid spacing indicated	Chainlink mesh anchored to bolts and intermediate points	Shotcrete applied directly to rock, thickness indicated	Shotcrete reinforced with welded mesh, thickness indicated	Unreinforced cast concrete arch, thickness indicated	Steel reinforced cast concrete arch, thickness indicated	Notes by Barton, Lien and Lunde	Notes by Hoek and Brown
0.4 -0.1	4- 14.5	>1.5		0.3						75- 750mm			10	c
0.4 -0.1	4- 14.5	<1.5		0.3			1m				200- 400mm		10, 12	c
0.4 -0.1	4- 14.5			0.3			1m					300- 500mm	9, 11, 12	
0.4 -0.1	20- 34			0.3			1m			400- 600mm			3, 5, 10 12, 13	f
0.4 -0.1	11- 20			0.3			1m			200- 400mm			4, 5, 10 12, 13	c
0.4 -0.1	11- 34			0.3			1m					400mm -1.2m	5, 9, 11 12, 13	
0.1- 0.01	1- 3.9	>2		0.6			1m			25- 50mm			10	c
0.1- 0.01	1- 3.9	<2		0.6						50- 100mm			10	c
0.1- 0.01	1- 3.9			0.6						75- 150mm			9, 11	c
0.1- 0.01	2- 11	>2	≥0.75	0.6			1m			50- 75mm			10	c
0.1- 0.01	2- 11		<0.75	0.6						150- 250mm			10	c
0.1- 0.01	2- 11			0.6			1m					200- 600mm	9, 11, 12	
0.1- 0.01	15- 28			0.6			1m			300- 1m			3, 10, 12, 13	c, f
0.1- 0.01	15- 28			0.6			1m					600mm -2m	3, 9, 11 12, 13	
0.1- 0.01	6.5 -15			0.6			1m			200- 750mm			4, 10 12, 13	c, f
0.1- 0.01	6.5 -15			0.6			1-					400mm -1.5m	3, 9, 11 12, 13	
0.01- 0.001	1- 2			1.2						100- 200mm			10	c
0.01- 0.001	1- 2			1.2			0.5 -1m			100- 200mm			9, 11 12	c
0.01- 0.001	1- 6.5			1.2						200- 600mm			10	c, f
0.01- 0.001	1- 6.5			1.2			0.5 -1-			200- 600mm			9, 11, 12	c, f
0.01 0.001	10- 20			1.2								1m- 3m	10, 14	

TABLE 18 - RECOMMENDED SUPPORT BASED UPON RQI TUNNELLING QUALITY INDEX Q

Rock mass quality Q	Equivalent dimension $\frac{SPAN}{SSR}$	Block size: $\frac{RQD}{J_n}$	Inter-Block strength $\frac{J_r}{J_n}$	Approx. support pressure P, MPa	Steel reinforcement with ungrouted grouted dowels	Ungrouted grouted dowels on grid spacing indicated	Tensioned rockbolts on grid spacing indicated	Chainlink mesh anchored to bolts and intermediate points	Shotcrete applied directly to rock, thickness indicated	Shotcrete reinforced with weld-mesh, thickness indicated	Unreinforced cast concrete arch, thickness indicated	Steel reinforced cast concrete arch, thickness indicated	Notes by Barton, Lien and Lunde	Notes by Hoek and Brown
0.01-0.001	10-20			1.2			1m					1-3m	3,9,11 12,14	
0.01-0.001	4-10			1.2						700mm-2m			10,14	c, f
0.01-0.001	4-10			1.2			1m			700mm-2m			4,9,10 11,14	c, f

Supplementary notes by Barton, Lien and Lunde

1. The type of support used in extremely good and exceptionally good rock will depend upon the blasting technique. Smooth wall blasting and thorough barring-down may remove the need for support. Rough wall blasting may result in the need for a single application of shotcrete, especially where the excavation height exceeds 25m.
2. For cases of heavy rock bursting or "popping", tensioned bolts with enlarged bearing plates often used, with spacing about 1m (occasionally 0.8m). Final support when "popping" activity ceases.
3. Several bolt lengths often used in same excavation, i.e. 3, 5 and 7m.
4. Several bolt lengths often used in same excavation, i.e. 2, 3 and 4m.
5. Tensioned cable anchors often used to supplement bolt support pressures. Typical spacing 2 to 4m.
6. Several bolt lengths often used in same excavation, i.e. 6, 8 and 10m.
7. Tensioned cable anchors often used to supplement bolt support pressures. Typical spacing 4 to 6m.
8. Several older generation power stations in this category employ systematic or spot bolting with areas of chain link mesh, and a free span concrete arch (250 - 400mm) as permanent support.
9. Cases involving swelling, for instance montmorillonite clay (with access of water). Room for expansion behind the support is used in cases of heavy swelling. Drainage measures are used where possible.
10. Cases not involving swelling clay or squeezing rock.
11. Cases involving squeezing rock. Heavy rigid support is generally used as permanent support.
12. According to author's experience (Barton et al), in cases of swelling or squeezing, the temporary support required before concrete (or shotcrete) arches are formed may consist of bolting (tensioned shell-expansion type) if the value of RQD/J<sub>n</sub> is sufficiently high (i.e. > 1.5), possibly combined with shotcrete. If the rock mass is very heavily jointed or crushed (i.e. RQD/J<sub>n</sub> < 1.5, for example a "sugar cube" shear zone in quartzite), then the temporary support may consist of up to several applications of shotcrete. Systematic bolting (tensioned) may be added after casting the concrete (or shotcrete) arch to reduce the uneven loading on the concrete, but it may not be effective when RQD/J<sub>n</sub> < 1.5, or when a lot of clay is present, unless the bolts are grouted before tensioning. A sufficient length of anchored bolt might also be obtained using quick setting resin anchors in these extremely poor quality rock masses. Serious occurrences of swelling and/or squeezing rock may require that the concrete arches be taken right up to the face, possibly using a shield as temporary shuttering. Temporary support of the working face may also be required in these cases.

TABLE 10 - RECOMMENDED SUPPORT BASED UPON NGI TUNNELLING QUALITY INDEX Q

*Supplementary notes by Barton, Lien and Lunde (Continued)*

13. For reasons of safety the multiple drift method will often be needed during excavation and supporting of roof arch. For span/CSR > 15 only.
14. Multiple drift method usually needed during excavation and support of arch, walls and floor in cases of heavy squeezing. For span/CSR > 10 in exceptionally poor rock only.

*Supplementary notes by Hoek and Brown*

- a. In Scandinavia, the use of "Perfobolts" is common. These are perforated hollow tubes which are filled with grout and inserted into drillholes. The grout is extruded to fill the annular space around the tube when a piece of reinforcing rod is pushed into the grout filling the tube. Obviously, there is no way in which these devices can be tensioned although it is common to thread the end of the reinforcing rod and place a normal bearing plate or washer and nut on this end. (See figure 154 on page 328).  
In north America the use of "Perfobolts" is rare. In mining applications a device known as a "Split set" or "Friction set" (developed by Scott<sup>243</sup>) has become popular. This is a split tube which is forced into a slightly smaller diameter hole than the outer diameter of the tube. The friction between the steel tube and the rock, particularly when the steel rusts, acts in much the same way as the grout around a reinforcing rod. For temporary support these devices are very effective. (See figure 153 on page 326).  
In Australian mines, untensioned grouted reinforcing is installed by pumping thick grout into drillholes and then simply pushing a piece of threaded reinforcing rod into the grout. The grout is thick enough to remain in an up-hole during placing of the rod.
- b. Chainlink mesh is sometimes used to catch small pieces of rock which can become loose with time. It should be attached to the rock at intervals of between 1 and 1.5m and short grouted pins can be used between bolts. Galvanised chainlink mesh should be used where it is intended to be permanent, eg in an underground powerhouse.
- c. Weldmesh, consisting of steel wires set on a square pattern and welded at each intersection, should be used for the reinforcement of shotcrete since it allows easy access of the shotcrete to the rock. Chainlink mesh should never be used for this purpose since the shotcrete cannot penetrate all the spaces between the wires and air pockets are formed with consequent rusting of the wire. When choosing weldmesh, it is important that the mesh can be handled by one or two men working from the top of a high-lift vehicle and hence the mesh should not be too heavy. Typically, 4.2mm wires set at 100mm intervals (designated 100 x 100 x 4.2 weldmesh) are used for reinforcing shotcrete.
- d. In poorer quality rock, the use of untensioned grouted dowels as recommended by Barton, Lien and Lunde depends upon immediate installation of these reinforcing elements behind the face. This depends upon integrating the support drilling and installation into the drill-blast-muck cycle and many non-Scandinavian contractors are not prepared to consider this system. When it is impossible to ensure that untensioned grouted dowels are going to be installed immediately behind the face, consideration should be given to using tensioned rockbolts which can be grouted at a later stage. This ensures that support is available during the critical excavation stage.
- e. Many contractors would consider that a 200mm thick cast concrete arch is too difficult to construct because there is not enough room between the shutter and the surrounding rock to permit easy access for pouring concrete and placing vibrators. The US Army Corps of Engineers<sup>244</sup> suggests 10 inches (254 mm) as a normal minimum while some contractors prefer 300mm.
- f. Barton, Lien and Lunde suggest shotcrete thicknesses of up to 2m. This would require many separate applications and many contractors would regard shotcrete thicknesses of this magnitude as both impractical and uneconomic, preferring to cast concrete arches instead. A strong argument in favour of shotcrete is that it can be placed very close to the face and hence can be used to provide early support in poor quality rock masses. Many contractors would argue that a 50 to 100mm layer is generally sufficient for this purpose, particularly when used in conjunction with tensioned rockbolts as indicated by Barton, Lien and Lunde, and that the placing of a cast concrete lining at a later stage would be a more effective way to tackle the problem. Obviously, the final choice will depend upon the unit rates for concreting and shotcreting offered by the contractor and, if shotcrete is cheaper, upon a practical demonstration by the contractor that he can actually place shotcrete to this thickness.  
In north America, the use of concrete or shotcrete linings of up to 2m thick would be considered unusual and a combination of heavy steel sets and concrete would normally be used to achieve the high support pressures required in very poor ground.

TABLE 19 - GEOMECHANICS CLASSIFICATION GUIDE FOR EXCAVATION AND SUPPORT IN ROCK TUNNELS

SHAPE: HORSESHOE; WIDTH: 10 m; VERTICAL STRESS: BELOW 25 MPa;  
CONSTRUCTION: DRILLING AND BLASTING.

Rock mass class	Excavation	Support		
		Rockbolts (20mm dia. fully bonded)	Shotcrete	Steel sets
Very good rock I RMR: 81-100	Full face. 3 m advance.	Generally no support required except for occasional spot bolting.		
Good rock II RMR: 61-80	Full face. 1.0-1.5 m advance. Complete support 20m from face.	Locally bolts in crown, 3m long spaced 2.5m with occasional mesh.	50mm in crown where required	None
Fair rock III RMR: 41-60	Top heading and bench, 1.5-3m advance in heading. Commence support after each blast. Complete support 10m from face.	Systematic bolts 4m long, spaced 1.5-2m in crown and walls with mesh in crown.	50-100mm in crown, 30mm in sidewalls.	None
Poor rock IV RMR: 21-40	Top heading and bench, 1-1.5m advance in heading. Install support concurrently with excavation - 10m from face.	Systematic bolts 4-5m long, spaced 1-1.5m in crown and walls with wire mesh.	100-150mm in crown, and 100mm in sides.	Light ribs spaced 1.5m where required.
Very poor rock V RMR: < 20	Multiple drifts, 0.5-1.5m advance in top heading. Install support concurrently with excavation. Shotcrete as soon as possible after blasting.	Systematic bolts 5-6m long, spaced 1-1.5m in crown and walls with wire mesh. Bolt invert.	150-200mm in crown, 150mm on sides, and 50mm on face.	Medium to heavy ribs spaced 0.75m with steel lagging and forepoling if required. Close invert.

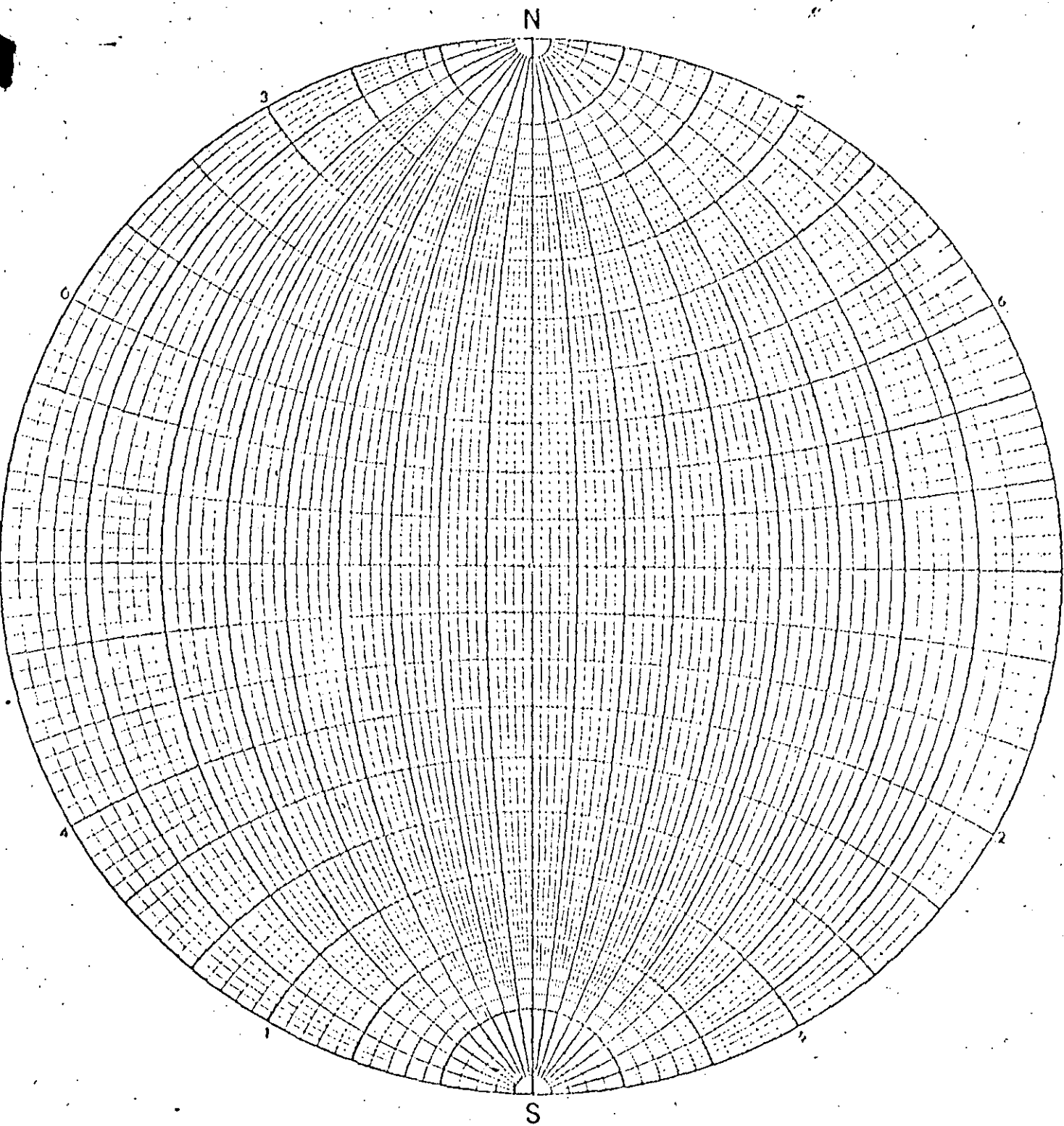
TABLE 20 - MODIFIED GEOMECHANICS CLASSIFICATION GUIDE FOR SUPPORT OF MINING EXCAVATIONS

Adjusted ratings	Original Geomechanics ratings									
	90-100	80-90	70-80	60-70	50-60	40-50	30-40	20-30	10-20	0-10
70-100										
50-60		a	a	a	a					
40-50			b	b	b	b				
30-40				c,d	c,d	c,d,e	d,e			
20-30					g	f,g	f,g,j	f,h,j		
10-20						i	i	h,i,j	h,j	
0-10							k	k	l	l

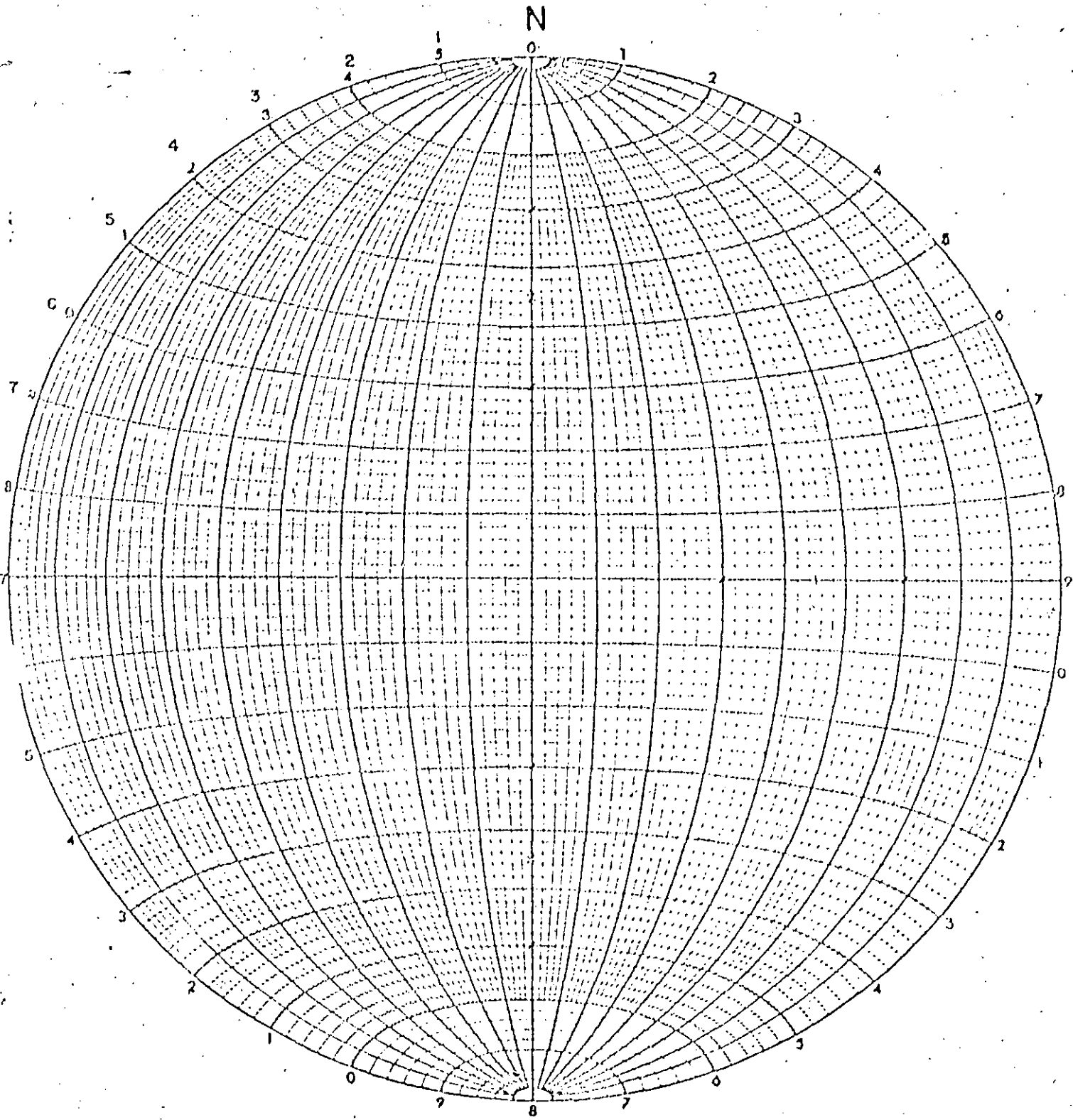
- a - Generally no support but locally joint intersections might require bolting.
- b - Patterned grouted bolts at 1m collar spacing.
- c - Patterned grouted bolts at 0.75m collar spacing.
- d - Patterned grouted bolts at 1m collar spacing and shotcrete 100mm thick.
- e - Patterned grouted bolts at 1m collar spacing and massive concrete 300mm thick and only used if stress changes not excessive.
- f - Patterned grouted bolts at 0.75m collar spacing and shotcrete 100mm thick.
- g - Patterned grouted bolts at 0.75m collar spacing with mesh reinforced shotcrete 100mm thick.
- h - Massive concrete 450mm thick with patterned grouted bolts at 1m spacing if stress changes are not excessive.
- i - Grouted bolts at 0.75m collar spacing if reinforcing potential is present, and 100mm reinforced shotcrete, and then yielding steel arches as a repair technique if stress changes are excessive.
- j - Stabilise with rope cover support and massive concrete 450mm thick if stress changes not excessive.
- k - Stabilise with rope cover support followed by shotcrete to and including face if necessary, and then closely spaced yielding arches as a repair technique where stress changes are excessive.
- l - Avoid development in this ground otherwise use support systems j or k.

*Supplementary notes*

1. The original Geomechanics Classification as well as the adjusted ratings must be taken into account in assessing the support requirements.
2. Bolts serve little purpose in highly jointed ground and should not be used as the sole support where the joint spacing rating is less than 6.
3. The recommendations contained in table 20 are applicable to mining operations with stress levels less than 30 MPa.
4. Large chambers should only be excavated in rock with adjusted total classification ratings of 50 or better.



WULFF NET



SCHMIDT NET



DIRECTORIO DE ALUMNOS DEL CURSO "MECANICA DE ROCAS APLICADA A LA MINERIA Y A LA CONSTRUCCION" IMPARTIDO EN ESTA DIVISION DEL 27 AL 31 DE MAYO 1985.

- 1.- ALVAREZ MEJIA RAUL  
SICARTSA  
PRESIDENTE DEPTO. GEOLOGIA DE MINAS  
LAZARO CARDENAS, MICH.  
CONOCIDO  
COL. VISTA HERMOSA  
LA MIRA, MICHOACAN
  
- 2.- BARBOSA ANAYA HECTOR FDO.  
COMISION DE FOMENTO MINERO  
ANALISTA  
PUENTE DE TECAMACHALCO No. 26  
COL. LOMAS DE CHAPULTEPEC  
DELEGACION MIGUEL HIDALGO  
11000 MEXICO, D.F.  
520-85-07  
GENERAL SOSA No. 12  
COL. PARAJE DE SAN JUAN  
DELEGACION IZTAPALAPA  
09830 MEXICO, D.F.  
520-85-07
  
- 3.- BELMONTE JIMENEZ SALVADOR ISIDRO  
CIA. MEXICANA AEROFOTO, S.A.  
ING. GEOFISICO  
11 DE ABRIL No. 338  
COL. ESCANDON  
DELEGACION MIGUEL HIDALGO  
11800 MEXICO, DF.  
516-07-40 EXT. 148  
HDA. NORIA No. 32  
COL. IMPULSORA  
EDO. DE MEXICO  
37130 MEXICO  
794-10-82
  
- 4.- ESCAMILLA PASILLAS LUIS  
COMISION FEDERAL DE ELECTRICIDAD  
ING. GEOLOGO  
CALZ. H. COLEGIO MILITAR No. 2120  
CULIACAN, SIN.  
28 DE AGOSTO No. 7-1  
DELEGACION BENITO JUAREZ  
516-57-96
  
- 5.- GONZALEZ VILLALVASO PEDRO  
FACULTAD DE INGENIERIA UNAM  
COORDINADOR DE LA CARRERA ING. GEOFISICO  
CIRCUITO INTERIOR FAC. ING.  
590-52-15 ext. 3724  
ANAXAGORAS No. 580-3  
COL. NARVARTE  
DELEGACION BENITO JUAREZ  
03020 MEXICO, DF.
  
- 6.- GURRIA ESQUIVEL GERMAN  
COMISION FEDERAL DE ELECTRICIDAD  
INGENIEROS No. 402  
COL. MARQUES  
QUERETARO, QRO.  
283-79  
M. ARISTA No. 48  
COL. SAN JAVIER  
QUERETARO, QRO.

7.- GUZZY ARREDONDO MA. ELENA A.

NURILLO No. 7  
COL. MIXCOAC  
DELEGACION BENITO JUAREZ  
03910 MEXICO, D.F.  
563-35-15

8.- HERNANDEZ DEHESA JOSE LUIS  
CIA. MEXICANA AEROFOTO  
ING. GEOFISICO  
11 DE ABRIL No. 328  
COL. ESCANDON  
DELEGACION MIGUEL HIDALGO  
11800 MEXICO, DF.  
516-07-40 EXT. 144

HACIENDA DE LA NORIA No. 32  
COL. IMPULSORA  
57130 MEXICO, D.F.  
794-10-82 y 794-30-82

10.- HERNANDEZ VILLANUEVA ALFREDO  
LAS ENCINAS, S.A.  
AV. REY DE COLIMAN No. 268-7o. PISO  
COLIMA. COL. 28000

JOSE MARTI No. 224  
FRACC. SAN PABLO  
COLIMA, COL. 28060

11.- LARA AGUILAR FELIPE  
S. A. R. H.  
JEFE DEPTO. CONTROL CALIDAD  
Y MANEJO DE MATERIALES  
H. COLEGIO MILITAR No. 40  
VILLA CORREGIDORA, QRO.  
6-22-39

HIMIAHUAPAN No. 324  
COL. VISTA ALEGRE  
QUERETARO, QRO.

12.- MANRIQUE GUERRERO JORGE  
S. A. R. H.  
JEFE OFNA. PROTECCION INSTALACIONES  
HIDRAULICAS  
INSURGENTES SUR No. 30-32 PISO 3  
COL. JUAREZ  
DELEGACION CUAUHTEMOC  
266-59-49

BELGICA No. 810  
COL. PORTALES  
DELEGACION BENITO JUAREZ  
03500 MEXICO, D.F.  
532-15-45

13.- MARTINEZ BELLO FLAVIO  
S. C. T.  
DIBUJANTE  
DIREC. GRAL. OBRAS MARTITIMAS  
COL. DEL VALLE  
DELEGACION BENITO JUAREZ  
687-55-10

SAN LUIS POTOSI No. 84  
TLALNEPANTLA, EDO. DE MEXICO

14.- MENDOZA LARA HECTOR  
CIA. MINERA AUTLAN, S.A.